The Malaysian Journal of
ANALYTICAL SCIENCES
ISSN 1394-2506

# Vol 18 No 1 (2014)

# Vol 18 No 2 (2014)

# Vol 18 No 3 (2014)

# 2013

**Malaysian Journal of Analytical Sciences Vol 18 No 1 2014**

**Page**

1.PERBANDINGAN KAEDAH PEMBERUSAN SERBUK CAP JARI DAN PENGWASAPAN SIANOAKRILAT DALAM PENIMBULAN KESAN CAP JARI PENDAM YANG TERDEDAH KEPADA KEADAAN PERSEKITARAN TEMPATAN 1
(Comparison of Powder Dusting and Cyanoacrylate Fuming Techniques in Retrieving Latent Fingerprint Exposed to Environment Conditions)
*Yosmetha Mayalvanan, Sri Pawita Albakri Amir Hamzah, Lee Loong Chuan, Muhamad Hilmi Baba, Amidon Anan*

2. LONG TERM STABILITY OF FARMER TYPE IONIZATION CHAMBER CALIBRATION COEFFICIENT BELONGING TO LOCAL RADIOTHERAPY CENTRES IN MALAYSIA 7
(Kestabilan Jangka Panjang Pekali Tentukuran Kebuk Pengionan Jenis Farmer Kepunyaan Pusat Radioterapi di Malaysia)
*A.M. Mukhtar, S.B. Samat, M.T. Dolah*

3. EFFECTS OF LITHIUM DOPANT ON SIZE AND MORPHOLOGY OF MAGNESIUM OXIDE NANOPOWDERS 15
(Kesan-Kesan Litium Sebagai Pendopan Keatas Saiz dan Morfologi Serbuk Nano Magnesium Oksida)
*Mohd Sufri Mastuli, Siti Nur Hazlinda Hasbu, Noraziahwati Ibrahim, Mohd Azizi Nawawi*

4. SYNTHESIS, CHARACTERIZATION AND CORROSION INHIBITION STUDIES OF o,m,p-DECANOYL THIOUREA DERIVATIVES ON MILD STEEL IN 0.1 M $H_2SO_4$ SOLUTIONS 21
(Sintesis, Pencirian dan Kajian Perencatan Kakisan Keluli Lembut oleh Terbitan o,m,p-Dekanoil Tiourea Dalam 0.1 M Larutan $H_2SO_4$ )
*Noor Khadijah Mustafa Kamal, Adibatul Husna Fadzil, Karimah Kassim, Shadatul Hanom Rashid, Mohd Sufri Mastuli*

5. THE EFFECT OF TEMPERATURE ON MILD STEEL CORROSION IN 1 M HCl BY SCHIFF BASES 28
(Kesan Suhu Terhadap Kakisan Keluli Lembut Dalam 1 M HCl oleh Ligan Bes Schiff)
*Nor Zakiah Nor Hashim and Karimah Kassim*

6. LEAD (Pb) AND ZINC (Zn) CONCENTRATIONS IN MARINE GASTROPOD STROMBUS CANARIUM IN JOHOR COASTAL AREAS 37
(Kepekatan Plumbum (Pb) dan Zink (Zn) di dalam Gastropoda Laut Strombus canarium di Kawasan Perairan Johor)
*Shaikhah Sabri, Mohd Ismid Mohd Said, Shamila Azman*

7. KAJIAN AWALAN TERHADAP KINETIK PENGEKSTRAKAN PEPEJAL-CECAIR DAN ANALISIS KOMPONEN BIO-AKTIF DAUN Hibiscus rosa-sinensis 43
(Preliminary Study on Kinetic Solid-Liquid Extraction and Bio-Active Components Analysis of Hibiscus rosa-sinensis Leaves)
*Saiful Irwan Zubairi, Haizulizam Suradi, Syazwan Aizad Abdul Mutalib, Zetty Shafiqa Othman, Norshahida Bustaman, Wan Ros Maryana Wan Musa*

8. PHOSPHORYLATION OF GELATINE AND CHITOSAN AS AN EXCIPIENT FOR ASIATICOSIDE NANOFIBERS 58

(Pemfosforilan Gelatin dan Kitosan Sebagai Eksipien Bagi Penyediaan Nanofiber Asiatikosida)
*Susana Elya Sudrajat, Khairurrijal, Puspa DN Lotulung, Effionora Anwar*

9. FORENSIC ANALYSIS OF HIGH EXPLOSIVE RESIDUES FROM SELECTED CLOTH 68
(Analisis Forensik Residu Bahan Letupan Berkuasa Tinggi Daripada Kain Terpilih)
*Mohamad Afiq Mohamed Huri and Umi Kalthom Ahmad*

10. A STUDY ON ADSORPTION OF CADMIUM BY USING CHEMICALLY MODIFIED SALVINIA 78
(Kajian Penjerapan Kadmium Dengan Menggunakan Salvinia Yang Diubah Suai Secara Kimia)
*Anies Suhaida Mohd Naspu, Mohd Lias Kamal, Zaini Hamzah, Sharizal Hasan*

11. ESTOLIDE ESTER FROM RICINUS COMMUNIS L. SEED OIL FOR BIOLUBRICANT PURPOSE 85
(Ester Estolida dari Minyak Biji Ricinus Communis L untuk Kegunaan Biolubrikan)
*Nazrizawati Ahmad Tajuddin, Nor Habibah Rosli, Noraishah Abdullah, Mohd Firdaus Yusoff, Jumat Salimon*

12. QUANTIFYING SOIL EROSION AND DEPOSITION RATES IN TEA PLANTATION AREA, CAMERON 94
HIGHLANDS, MALAYSIA USING 137Cs
(Pengiraan Kadar Hakisan Tanah dan Kadar Pemendapan di Kawasan Ladang Teh, Cameron Highlands, Malaysia Menggunakan 137Cs)
*Zaini Hamzah, Che Yasmin Amirudin, Ahmad Saat, Ab Khalik Wood*

13. HYDROGEN PEROXIDE IMPEDIMETRIC DETECTION ON POLY-ORTHO-PHENYLENEDIAMINE 107
MODIFIED PLATINUM DISK MICROELECTRODE
(Pengesanan Hidrogen Peroksida Secara Impedimetrik Di Atas Elektrod Mikro Cakera Platinum Yang Di Ubah Suai Dengan Poli-Orto-Fenilinadiamina)
*Zainiharyati Mohd Zain and Norazreen Zakaria*

14. ANTIOXIDANT ACTIVITY AND BIOACTIVE COMPONENTS OF OXALIDACEAE FRUIT EXTRACTS 116
(Aktiviti Antioksida Dan Komponen Bioaktif Esktrak Buah Oxalidaceae)
*A. Noor Asna and A.Noriham*

15. NATURAL ISOTOPE RADIUM IN MARINE BIOTA AT KAPAR, KLANG COASTAL AREA 127
(Isotop Radium Semulajadi Dalam Biota Marin Di Pesisiran Pantai Kapar, Klang)
*Nik Azlin Nik Ariffin and Che Abd Rahim Mohamed*

16. PENENTUAN TABURAN HARIAN LEVOGLUKOSAN DI UDARA SECARA KOLORIMETRI 140
(Determination of Levoglucosan Diurnal Pattern in Air by Colorimetric Method)
*Mohd Zaidi Mat Satar, Mohd Talib Latif, Mohamed Rozali Othman*

17. SPATIAL DISTRIBUTION OF PHYSICO-CHEMICAL PARAMETER IN UPSTREAM RIVERS AND 148
TIMAH TASOH LAKE, PERLIS: PRELIMINARY STUDY
(Taburan Spatial Parameter Fizikal-Kimia Di Sungai Dan Empangan Timah Tasoh, Perlis: Kajian Permulaan)
*Siti Aesah Abdullah, Sharizal Hasan, Mohd Lias Kamal, Norshahrizan Mohd Hashim*

18. ANALYSIS AND POLLUTION ASSESSMENT OF HEAVY METAL IN SOIL, PERLIS 155
(Analisis dan Penilaian Pencemaran Logam Berat dalam Tanah, Perlis)
*Siti Norbaya Mat Ripin, Sharizal Hasan, Mohd Lias Kamal, NorShahrizan Mohd Hashim*

19. SEASONAL VARIATION OF GRAIN SIZE AND HEAVY METALS CONCENTRATION IN SEDIMENT 162
OF SUNGAI PERLIS
(Variasi Musim Saiz Zarah Dan Kepekatan Logam Berat Di Dalam Sedimen, Sungai Perlis)
*Hanif. H. F., Jamil, T., Lias, K., Norsila, D.*

20. STUDY OF RADIONUCLIDES LINKAGES BETWEEN FISH, WATER AND SEDIMENT IN FORMER TIN MINING LAKE IN KAMPUNG GAJAH, PERAK, MALAYSIA 170
(Kajian Mengenai Hubungan Radionuklid di antara Ikan, Air, dan Sedimen dalam Tasik Bekas Lombong di Kampung Gajah, Perak, Malaysia)
*Ahmad Saat, Norannisak Muhd Isak, Zaini Hamzah, Ab Khalik Wood*

21. DETERMINATION OF MAJOR IONS CONCENTRATIONS IN KELANTAN WELL WATER USING EDXRF AND ION CHROMATOGRAPHY 178
(Penentuan Kepekatan Ion-ion Utama Air Telaga di Kelantan, Dengan Menggunakan Pendaflur Serakan Tenaga Sinar-X dan Ion Kromatografi)
*Zaini Hamzah, Wan Noorhayani Wan Rosdi, Abd Khalik Hj Wood, Ahmad Saat*

22. DETERMINATION OF SUPPORTED 222Rn ACTIVITY CONCENTRATION IN GROUND WATER FROM CAMERON HIGHLANDS AREA USING GAMMA SPECTROMETRY 185
(Penentuan Kepekatan Aktiviti 222Rn Sokongan di dalam Air Tanih dari Kawasan Cameron Highlands Menggunakan Spektrometri Gama)
*Ahmad Saat, Nor Shazlina Zainal, Zaini Hamzah, Abdul Khalik Wood*

23. ASSESSMENT OF HEAVY METAL CONTAMINATION IN SQUID (LOLIGO SPP.) TISSUES OF KEDAH-PERLIS WATERS, MALAYSIA 195
(Penilaian Pencemaran Logam Berat dalam Tisu Sotong (Loligo Spp.) bagi Perairan Air Kedah-Perlis, Malaysia)
*Jamil, T., Lias, K., Norsila, D., Syafinaz, N. S.*

24. EFFECT OF RICE STRAW EXTRACT AND ALKALI LIGNIN ON THE CORROSION INHIBITION OF CARBON STEEL 204
(Kesan Ekstrak Jerami Padi dan Alkali Lignin Terhadap Perencatan Kakisan Keluli Karbon)
*Rabiahtul Zulkafli, Norinsan Kamil Othman, Irman Abdul Rahman, Azman Jalar*

25. DEVELOPMENT OF SPECTROPHOTOMETRIC METHOD FOR ALLOPURINOL IN URINE BASED ON THE DIAZOTIZATION REACTION 212
(Pembangunan Kaedah Spektrofotometrik untuk Penentuan Allopurinol dalam Air Kencing Berdasarkan Reaksi Diazotisasi)
*Edy Agustian Yazid, Ganden Supriyanto, Tjitjik Srie Tjahjandarie*

26. DIGESTION STUDY OF WATER LEACH PURIFICATION (WLP) RESIDUE FOR POSSIBILITY OF THORIUM EXTRACTION 221
(Kajian Penghadaman Residu Pemurnian Larut Resap Air (WLP) Untuk Kebarangkalian Pengekstrakan Torium)
*Wadeeah M. AL-Areqi, Amran Ab. Majid, Sukiman Sarmani*

The Malaysian Journal of ANALYTICAL SCIENCES ISSN 1394-2506

# PERBANDINGAN KAEDAH PEMBERUSAN SERBUK CAP JARI DAN PENGWASAPAN SIANOAKRILAT DALAM PENIMBULAN KESAN CAP JARI PENDAM YANG TERDEDAH KEPADA KEADAAN PERSEKITARAN TEMPATAN

## (Comparison of Powder Dusting and Cyanoacrylate Fuming Techniques in Retrieving Latent Fingerprint Exposed to Environment Conditions)

Yosmetha Mayalvanan, Sri Pawita Albakri Amir Hamzah, Lee Loong Chuan, Muhamad Hilmi Baba, Amidon Anan*

*Program Sains Forensik,*
*Pusat Pengajian Sains Diagnostik & Kesihatan Gunaan, Fakulti Sains Kesihatan,*
*c/o Bilik 10, Tingkat 3, Bangunan Kedekanan FST,*
*Universiti Kebangsaan Malaysia, 43600 UKM Bangi, Selangor, Malaysia*

**Corresponding author: amidon.anan@yahoo.com*

**Abstrak**

Kesan cap jari pendam ialah bahan bukti terbaik untuk membuktikan kehadiran seseorang di tempat kejadian. Terdapat pelbagai teknik yang digunakan untuk penimbulan cap jari pendam. Dua teknik yang kerap digunakan adalah teknik pengwasapan sianoakrilat dan pemberusan menggunakan serbuk cap jari. Kajian ini bertujuan untuk mengenal pasti teknik yang lebih berkesan terutamanya dalam penimbulan kesan cap jari pendam yang telah didedahkan kepada keadaan persekitaran tempatan. Metodologi kajian termasuklah mengambil sampel cap jari daripada 18 orang subjek pada permukaan gelas, perspek dan aluminum. Kesemua sampel didedahkan pada keadaan persekitaran tempatan selama tiga hari. Sampel cap jari ditimbulkan dengan menggunakan dua kaedah di atas. Perbandingan dilakukan antara kesan cap jari sampel dan cap jari rujukan. Hasil kajian menunjukkan penimbulan menggunakan teknik pengwasapan menghasilkan lebih banyak kesan cap jari yang jelas berbanding dengan penimbulan menggunakan teknik pemberusan. Walaupun telah didedahkan kepada keadaan persekitaran yang tidak kondusif, teknik pengwasapan berjaya menimbulkan kesan cap jari pendam. Ini membuktikan yang teknik pengwasapan merupakan teknik yang lebih berkesan untuk menimbulkan cap jari pendam berbanding teknik pemberusan. Faktor permukaan cap jari mempengaruhi kualiti kejelasan cap jari pendam.

**Kata kunci**: Cap jari pendam, wasap sianoakrilat, serbuk cap jari, teknik penimbulan, keadaan persekitaran

**Abstract**

Latent fingerprints are one of the best evidence to prove the presence of an individual's presence at the crime scene. There are many techniques available for a successful fingerprint lifting. Two of the most common ones are fingerprint powder dusting and cyanoacrylate fuming. This research aims to compare both techniques and determine which has a higher success rate in retrieving fingerprints exposed to local environmental conditions for three days. Fingerprint samples were collected from 18 subjects on glass, perspex and aluminium slides. These samples were then exposed to local environmental conditions for three days. The fingerprints were then developed using the aforementioned techniques. Based on the results, it can be safely said that, fuming results in clearer fingerprints and more minutiae can be found from the retrieved fingerprints even with exposure to less than optimum local conditions. This proves that fuming is a better fingerprint lifting method to resolve latent fingerprint compared to powder dusting. Surface on which the fingerprint is retrieved from influences the quality of clarity of a latent fingerprint.

**Keywords**: Latent fingerprint, cyanoacrylate fuming, fingerprint powder, lifting techniques, local conditions

## Pengenalan

Penyiasatan kes jenayah memerlukan bahan bukti yang kukuh untuk membuktikan seseorang itu bersalah. Kesan cap jari adalah bukti yang tidak boleh dinafikan kesahihannya [1]. Hal ini kerana cap jari setiap individu adalah berlainan dan tidak akan berubah sepanjang hayat seseorang. Keunikan cap jari membolehkan pihak berkuasa mengenal pasti pesalah yang bertanggungjawab tanpa sebarang kemusykilan. Ini membuktikan bahawa cap jari merupakan salah satu bahan bukti yang kukuh dan kesahihannya boleh diterima dalam mahkamah.

Walaupun begitu, keutuhan cap jadi di tempat kejadian jenayah berkurangan apabila ia tidak diproses serta merata. Ini menjadikan kemungkinan untuk memperolehi cap jari yang lengkap ditempat kejadian berkurangan dengan peningkatan jangkamasa penemuan tempat kejadian. Pada masa kini, pelbagai kaedah telahpun dicadangkan untuk memperolehi cap jari pendam [2].

Cap jari pendam ialah kesan cap jari yang tidak boleh dilihat menggunakan mata kasar. Secara umum, cap jari manusia dipindahkan pada sesuatu permukaan melalui peluh di permukaan jari [3]. Terdapat pelbagai kaedah yang digunakan untuk menimbulkan kesan cap jari pendam dari permukaan yang keras, licin dan tidak menyerap. Dua teknik yang kerap diaplikasikan adalah teknik pemberusan menggunakan serbuk cap jari dan teknik pengwasapan sianoakrilat. Pelbagai jenis serbuk boleh digunakan termasuklah serbuk cap jari biasa, serbuk pendarflour, serbuk pendarkilau dan serbuk metalik [4].

Serbuk cap jari biasa terdiri daripada polimer yang mengandungi resin untuk lekatan dan pewarna yang kontra bagi memudahkan proses penimbulan kesan cap jari. Fungsi pelekat adalah untuk melekatkan komponen yang lembap dan berminyak pada cap jari melalui tekanan lembut (*soft touch*) [5]. Faktor yang turut menyumbang untuk memaksimumkan daya lekatan antara serbuk cap jari dan kesan cap jari adalah bentuk dan saiz partikel serbuk cap jari. Partikel bersaiz kecil lebih mudah melekat pada sesuatu permukaan berbanding partikel bersaiz besar kerana luas permukaan yang terdedah kepada sisa peluh kesan cap jari adalah lebih besar [6].

Kaedah kimia yang paling mudah dan sering digunakan adalah pengwasapan sianoakrilat. Polimer polisianoakrilat bertindak balas dengan bes, lipid, asid lemak, asid amino dan protein yang ada pada kesan cap jari pendam dan menghasilkan mendakan putih yang jelas kelihatan pada mata kasar. Polimer putih tersebut bukan sahaja meningkatkan kontra antara kesan cap jari pendam dan permukaan, ia juga mengelakkan kerosakan pada kesan cap jari tersebut [7]. Mendakan polisianoakrilat menguatkan integriti kesan cap jari dan menjadikan kesan cap jari yang ditimbulkan lebih berkualiti dan tahan lebih lama [8].

Seperti mana yang telah dibincangkan diatas, tujuan kajian ini dilakukan adalah untuk menentukan kaedah mana yang terbaik untuk memperolehi cap jari pendam. Ini seterusnya membolehkan pakar Sains Forensik tempat kejadian memilih kaedah terbaik pemulihan cap jadi agar peratusan kejayaan melihat cap jari tersebut tinggi.

## Bahan dan Kaedah

Kesemua (18 orang) pelajar Tahun Empat Program Sains Forensik Universiti Kebangsaan Malaysia telah dipilih sebagai subjek dalam kajian ini. Subjek diminta untuk menurunkan kesan cap jari pada slaid kaca yang disediakan. Satu tanda dibuat pada kawasan di mana kesan cap jari diletakkan untuk memudahkan proses pencarian. Selepas 30 minit, proses diulangi pada slaid kaca yang baru. Proses diulangi sehingga lima kesan cap jari diperolehi daripada setiap subjek.

Proses ini telah diulang pada dua hari yang berbeza iaitu satu hari untuk sampel yang dianalisis menggunakan kaedah pemberusan dan satu hari lagi untuk sampel yang dianalisa dengan kaedah pengwasapan. Kedua-dua persampelan dilakukan pada keadaan yang sama walaupun pada hari yang berbeza. Sampel diambil pada slaid kaca, slaid perspek dan kepingan aluminium.

Selepas sampel diambil daripada subjek, kesemua sampel didedahkan ke persekitaran tempatan selama tiga hari sebelum proses penimbulan dilakukan. Selepas tiga hari, lima sampel ditimbulkan dengan menggunakan serbuk cap jari berwarna hitam dan teknik pemberusan. Sepanjang teknik pemberusan dilakukan daya yang diaplikasi sewaktu pemberusan minima supaya tidak merosakkan kesan cap jari.

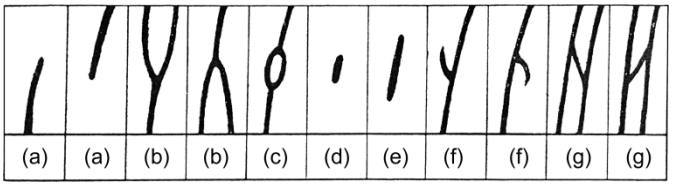
Ini diikuti dengan lima sampel lagi ditimbulkan menggunakan pengwasapan sianoakrilat. Pengwasapan cap jadi tersebut dilakukan menggunakan tiga titik sianoakrilat yang dipanaskan diatas kepingan aluminium selama 5 minit. Proses pengwasapan dilakukan didalam kotak dengan kesemua sampel digantung di siling dalam kotak tersebut. Oleh kerana wap sianoakrilat merbahaya, kesemua proses ini dilakukan dalam kebuk wasap. Bagi mengurangkan lagi risiko tersedut wap sianoakrilat, bilik yang menempatkan kebuk wasap ini dipastikan mempunyai pengudaraan yang optimum.

Selepas cap jadi ditimbulkan oleh salah satu teknik, kesan cap jari akan melalui proses angkat (*lifting*). Proses ini adalah untuk mengabadikan kesan cap jari yang ditimbulkan. Pita angkat digunakan untuk memindahkan kesan cap jari dari sampel ke kad angkat (*lifting card*). Kesan cap jari yang paling jelas kelihatan jalur-jalurnya digunakan untuk mencari titik minuta (Rajah 1). Titik-titik ini kemudiannya dibandingkan dengan kesan cap jari rujukan yang diambil dari subjek menggunakan teknik *single blind*. Pengesanan titik minutia pada setiap cap jari dibuat oleh penyelidik dan disahkan kemudiannya oleh co-penyelidik yang lain.

Keputusan yang diperolehi kemudiannya dianalisis secara diskriptif. Ia juga dianalisiskan menggunakan SPSS 20.0 dengan tahap kemaknaan $p < 0.05$. Aspek yang telah dianalisis termasuklah: (1) Menentukan jika terdapat perbezaan bilangan minuta diantara cap jari segar dengan cap jari yang telah dibiarkan selama 3 hari menggunakan kaedah serbuk hitam atau wasap sianoakrilat, (2) Menentukan jika peratusan minuta yang berjaya diperolehi daripada cap jari yang dibiarkan selama 3 hari dipengaruhi oleh interaksi faktor permukaan dimana cap jari tersebut diletakkan dan kaedah yang digunakan untuk mengesan cap jari tersebut dan (3) Menentukan kaedah pengesanan cap jari yang terbaik setelah dibiarkan selama 3 hari dipersekitaran berdasarkan pelbagai permukaan dimana cap jari tersebut diletakkan. Ujian T-berpasangan telah digunakan untuk analisis pertama, ANOVA dua hala untuk analisis kedua dan ujian T-tidak berpasangan untuk analisis yang terakhir.

## Keputusan dan Perbincangan

Perbandingan dilakukan berdasarkan bilangan minutia (Rajah 1) yang ditemui dari kesan cap jari yang ditimbulkan. Keputusan positif dicapai apabila kesan cap jari subjek berjaya menemui sebanyak 12 atau lebih minutia. Data dikumpulkan dalam jadual yang berasingan untuk setiap permukaan. Teknik pemberusan menggunakan serbuk cap jari mencatatkan 100% keputusan positif (Jadual 1). Permukaan kaca yang licin dan keras membolehkan kesan cap jari ditimbulkan dengan mudah menggunakan serbuk cap jari. Kesan cap jari yang ditimbulkan dari permukaan slaid kaca adalah jelas dan kemas. Hal ini kerana permukaan kaca tidak mempunyai cas dan tidak melekat pada pita angkat semasa proses angkat. Oleh itu, permukaan kaca berupaya menghasilkan penimbulan kesan cap jari yang sempurna dan boleh digunakan untuk perbandingan.




Rajah 1: Pelbagai bentuk *minutiae* cap jar

Walau bagaimanapun, permukaan perspek yang mempunyai cas elektrostatik tidak merekodkan keputusan yang memuaskan. Hanya 5.6% dari sampel menunjukkan keputusan yang positif (Jadual 1). Cap jari yang ditimbulkan menjadi comot apabila melalui proses angkat. Ini mungkin kerana daya lekatan pita angkat adalah lebih baik pada permukaan perspek berbanding permukaan kaca atau aluminium. Permukaan aluminium pula mencatatkan 72% peratus kejayaan. Dijangkakan permukaan logam aluminium yang mempunyai keupayaan tinggi untuk mengalirkan haba telah mempercepatkan proses pemeruapan dan penuaan komponen kesan cap jari.

Jadual 1: Perbandingan antara kaedah penimbulan kesan cap jari menggunakan teknik yang berbeza pada permukaan yang berlainan

| **Permukaan** | **Peratus kejayaan kaedah penimbulan kesan cap jari (%)** | |
|---|---|---|
| | **Serbuk Cap Jari** | **Wasap Sianoakrilat** |
| Gelas | 100 | 100 |
| Perspek | 5.6 | 89 |
| Aluminium | 72 | 100 |

Kami turut mendapati bahawa penimbulan kesan cap jari menggunakan pengwasapan sianoakrilat mempunyai kadar kejayaan yang lebih tinggi bagi ketiga-tiga permukaan yang dikaji jika dibandingkan dengan kaedah serbuk. Aplikasi teknik pengwasapan pada permukaan kaca dan aluminium menunjukkan 100% sampel kesan cap jari adalah jelas dan 12 atau lebih bilangan titik minutia berjaya ditemui. Namun begitu, penwasapan sianoakrilat hanya mencatatkan peratusan kejayaan sebanyak 89% pada permukaan perspek.

Keputusan (Jadual 2) jelas menunjukkan bahawa terdapat kehilangan secara signifikan bilangan minutia setelah cap jari dibiarkan selama 3 hari di persekitaran terbuka. Analisis interaksi permukaan cap jari dan penggunaan kaedah penimbulan menggunakan Anova dua hala menghasilkan keputusan yang menarik. Didapati teknik penimbulan menggunakan serbuk hitam tidak dipengaruhi oleh ketiga-tiga permukaan kajian. Walaupun begitu, kualiti cap jari pendam yang boleh diperolehi menggunakan teknik pengwasapan sianoakrilat bergantung kepada pemukaan dimana cap jari tersebut berada. Ini benar bagi permukaan gelas dan aluminium. Walaupun begitu amat menarik kualiti cap jari teknik pengwasapan sianoakrilat tidak bertambah baik jika cap jari cuba ditimbulkan pada permukaan perspek.

Jadual 2: Perbandingan bilangan minutia yang berjaya diperolehi daripada cap jari segar dan yang dibiarkan terdedah dipersekitaran selama 3 hari berdasarkan pelbagai permukaan dan kaedah penimbulan.

| **Permukaan** | **Gelas** | | **Perspek** | | **Aluminium** | |
|---|---|---|---|---|---|---|
| | **CJS** | **CJP** | **CJS** | **CJP** | **CJS** | **CJP** |
| Serbuk hitam | 25 $\pm$ 1 | 14 $\pm$ 1 | 25 $\pm$ 1 | 6 $\pm$ 1 | 25 $\pm$ 1 | 13 $\pm$ 0 |
| Statistik | $t(17)=7.865, p < 0.01$ | | $t(17)=10.517, p < 0.01$ | | $t(17)=12.310, p < 0.01$ | |
| Wasap sianoakrilat | 25 $\pm$ 1 | 18 $\pm$ 1 | 25 $\pm$ 1 | 13 $\pm$ 0 | 25 $\pm$ 1 | 18 $\pm$ 1 |
| Statistik | $t(17)=14.296, p < 0.01$ | | $t(17)=11.250, p < 0.01$ | | $t(17)=11.250, p < 0.01$ | |

CJS = Cap Jari Segar, CJP =Cap Jari Pendam, t = ujian T, Statistik ANOVA dua hala

Seperti mana yang dijangkakan, teknik pengwasapan sianoakrilat dan serbuk hitam mempunyai keupayaan yang sama untuk menimbulkan cap jari yang segar. Walaupun begitu, teknik penimbulan menggunakan serbuk hitam mempunyai sensitiviti yang rendah untuk menimbulkan cap jari pendam. Kehilangan minutia sebanyak 44 hingga 76% perlu diambil perhatian kerana ia akan menurunkan tahap keyakinan milik sesuatu cap jari kepada tertuduh.

Peratusan kehilangan bilangan minutia didapati amat tinggi pada permukaan perspek berbanding dengan permukaan gelas dan aluminium. Oleh itu, dicadangkan apabila pakar forensik ingin memperolehi cap japi pendam – permukaan perspek perlu dijadikan permukaan pilihan terakhir. Bila perlu memperolehi cap jari pendam pada permukaan perspek, teknik pengwasapan sianoakrilat perlu digunakan kerana ia akan menghasilkan keputusan yang terbaik.

Secara umum, penggunaan serbuk cap jari adalah satu teknik yang berasaskan ikatan mekanikal. Serbuk cap jari melekat pada komponen cap jari seperti minyak dan sebum melalui ikatan mekanikal. Tetapi ikatan ini hanya optimum jika komponen cap jari masih mempunyai komponen-komponen minyak dan sebum [9]. Pengwasapan sianoakrilat menghasilkan polimer polisianoakrilat yang membentuk ikatan kimia dengan komponen kesan cap jari seperti asid amino dan asid lemak. Hal ini kerana ikatan kimia adalah lebih kuat berbanding ikatan mekanikal [10].

Pengwasapan sianoakrilat mampu menambah baik kualiti kesan cap jari yang ditimbulkan. Polisianoakrilat yang terdeposit pada kesan cap jari bertindak sebagai satu lapisan pelindung [8,11]. Proses penuaan yang berlaku selepas didedahkan kepada keadaan persekitaran tidak menghapuskan keseluruhan kesan cap jari tetapi sebahagian komponen kesan cap jari seperti sebum dan asid lemak akan teruap [12]. Selain itu, pendedahan kepada keadaan persekitaran yang kurang kondusif seperti suhu antara 26°C hingga ke 38°C boleh menyebabkan komponen kesan cap jari meruap.

Tambahan pula, keadaan cuaca yang panas, kering, lembap dan sejuk juga mempengaruhi kadar peruapan kesan cap jari. Terdapat sampel yang keseluruhan kesan cap jari tidak dapat ditimbulkan [13]. Malaysia mempunyai keadaan persekitaran yang panas dan lembap. Suhu dan kelembapan adalah tinggi kerana negara kita adalah negara beriklim tropika. Suhu harian adalah berlainan pada setiap hari iaitu sekitar 24°C sehingga 38°C. Kebiasaannya, suhu pada waktu malam adalah lebih rendah berbanding waktu siang [14]. Variasi yang tinggi ini akan menyebabkan komponen penting seperti asid amino dan lemak pada cap jari mengalami denaturasi. Oleh kerana polisianoakrilat akan terikat asid amino dan asid lemak, kemusnahan sebahagian daripada asid amino dan lemak akan secara tidak langsung mengurangkan kualiti cap jadi yang boleh ditimbulkan semula.

Kajian ini berjaya membuktikan bahawa walaupun keadaan persekitaran boleh mempengaruhi kesempurnaan kesan cap jari yang ditimbulkan, teknik yang digunakan untuk menimbulkan kesan cap jari turut memainkan peranan yang penting. Penimbulan dengan serbuk cap jari adalah baik sekiranya kesan cap jari yang ditemui dalam keadaan baik. Namun demikian, teknik ini tidak mengubah kualiti kesan cap jari. Sementara itu, penimbulan dengan teknik pengwasapan mampu menambah baik kualiti kesan cap jari pendam [15].

## Kesimpulan

Secara kesimpulannya, teknik pengwasapan berjaya menghasilkan kesan cap jari yang lebih jelas selepas proses penimbulan. Hal ini kerana pengwasapan sianoakrilat membentuk satu lapisan pelindung pada kesan cap jari pendam dan menjadikan kesan cap jari tersebut lebih tahan lama. Selain itu, proses pengwasapan juga berupaya menambah baik kualiti kesan cap jari yang ditemui. Walau pun teknik penimbulan menggunakan serbuk cap jari adalah salah satu teknik yang popular dan sering digunakan, namun kadar kejayaan teknik ini bagi kesan cap jari yang terdedah kepada keadaan persekitaran Malaysia tidak begitu memuaskan terutamanya permukaan perspek dan aluminium. Justeru, kedua-dua teknik ini boleh digunakan dengan mengambil kira faktor jenis permukaan, kualiti kesan cap jari pendam yang ditemui dan keadaan kesan cap jari yang ditemui.

## Rujukan

1. Fish, J. T., Miller, L. S. and Braswell, M. C. (2010). *Crime Scene Investigation*. Burlington, MA: Anderson/ Elsevier.
2. Shelton, D. (2010). *Criminal Adjudication: The Challenges of Forensic Science Evidence in the Early 21st Century*. Charleston, SC: BaiblioBazaar.
3. Stevenson, S. H. P., V.J. (2010). Analysis of aged fingerprints and enhancement of the cyanoacrylate fuming method. *Identification Canada*, 33(2): 44.

4. Thamnurak, C., Bunakkharasawat, W., Riengrojpitak, S. and Panvisavas, N. (2011). DNA typing from fluorescent powder dusted latent fingerprints. *Forensic Science International: Genetics Supplement Series*, 3(1): e524-e525.
5. Lyle, D. P. (2011). *Forensics for Dummies*. Hoboken, NJ: For Dummies.
6. Daéid, N. N., Carter, S. and Laing, K. (2008). Comparison of three types of white powder suspensions for the recovery of fingerprints on wetted nonporous surfaces. *Journal of Forensic Identification* 58(5): 590-599.
7. Fung, T. C., Grimwood, K., Shimmon, R., Spindler, X., Maynard, P., Lennard, C. and Roux, C., (2011). Investigation of hydrogen cyanide generation from the cyanoacrylate fuming process used for latent fingermark detection. *Forensic Science International* 212(1): 143-149
8. Xanthe Spindler , O. H., Andrew M. Mcdonagh , Claude Roux and Chris Lennard., (2011). Enhancement of latent fingermarks on non-porous surfaces using anti-L-amino acid antibodies conjugated to gold nanoparticles. *Chemical Communications* 47: 5602-5604.
9. Aumeer-Donovan, S., Lennard, C. and Roux, C., (2009). *Friction Ridge Skin: Fingerprint Detection and Recovery Techniques*. Hoboken, NJ: Wiley Encyclopedia of Forensic Science.
10. Bacon, S. R. (2012). *Interactions between Latent Fingermarks, Deposition Surfaces and Development Agents*. Middlesex, UK: Brunel University School of Engineering and Design
11. Girod, A., Ramotowski, R. and Weyermann, C. (2012). Composition of fingermark residue: A qualitative and quantitative review. *Forensic Science International*, 223(1-3): 10-24.
12. Jasuja, O. P., Toofany, M., Singh, G. and Sodhi, G., (2009). Dynamics of latent fingerprints: The effect of physical factors on quality of ninhydrin developed prints—a preliminary study. *Science and Justice* 49(1): 8-11.
13. Osterburg, J. W. and Ward, R. H. (2010). Physical evidence: Development, interpretation, investigative Value. *Criminal Investigation (Sixth Edition)*, Boston, USA: Anderson Publishing Ltd.
14. Hasan, H., Salam, N. and Kassim, S. (2013). Modeling annual extreme temperature using generalized extreme value distribution: A case study in Malaysia. *AIP Conference Proceedings*, 1195.
15. Widjaja, E. (2009). Latent fingerprints analysis using tape-lift, Raman microscopy, and multivariate data analysis methods. *Analyst* 134(4): 769-775.

The Malaysian Journal of ANALYTICAL SCIENCES ISSN 1394-2506

# LONG TERM STABILITY OF FARMER TYPE IONIZATION CHAMBER CALIBRATION COEFFICIENT BELONGING TO LOCAL RADIOTHERAPY CENTRES IN MALAYSIA

## (Kestabilan Jangka Panjang Pekali Tentukuran Kebuk Pengionan Jenis Farmer Kepunyaan Pusat Radioterapi di Malaysia)

A.M. Mukhtar[1], S.B. Samat[1]*, M.T. Dolah[2]

[1]*School of Applied Physics,*
*Universiti Kebangsaan Malaysia, 43600 UKM Bangi, Selangor, Malaysia*
[2]*Secondary Standard Dosimetry Laboratory,*
*Malaysian Nuclear Agency (Nuclear Malaysia),*
*43000 Kajang, Selangor, Malaysia*

**Corresponding author: sbsamat@ukm.my*

**Abstract**

The accuracy of the ionization chambers' calibration coefficient is one of the factors that would contribute to efficient radiotherapy treatment. The IAEA therefore has recommended that an ionization chamber be calibrated every year, with a condition that the deviations between the previous and new calibration coefficients $N_{D,w}$ should not differ by ±1.5%. It has been identified that Farmer type ionization chambers is the most popular ionization chamber among the radiotherapy centres in Malaysia. For this reason, the purpose of this work is to evaluate the calibration coefficients' long term stability of the Farmer type ionization chambers. A total of 33 Farmer type ionization chambers were studied and the mean $\mu$ of the $N_{D,w}$ deviation together with its standard error *SE* were calculated. This $\mu \pm SE$ will be used to measure stability of $N_{D,w}$. Our results showed that most chambers have $\mu \pm SE$ lies within the ±1.5%. It is thus concluded that most of the Farmer type ionization chamber were stable in their $N_{D,w}$ and safe to be used for radiotherapy treatment.

**Keywords:** Farmer type ionization chambers, radiotherapy centres, calibration coefficients $N_{D,w,}$ stability.

**Abstrak**

Ketepatan pekali tentukuran kebuk pengionan merupakan salah satu faktor yang menyumbang kepada keberkesanan dalam rawatan radioterapi. Oleh itu, IAEA mencadangkan supaya kebuk pengionan ditentukur setiap tahun dengan satu syarat bahawa sisihan antara pekali tentukuran baru dan sebelumnya mestilah tidak lebih daripada ±1.5%. Ianya telah dikenalpasti bahawa kebuk pengionan jenis Farmer merupakan kebuk pengionan paling popular dikalangan pusat radioterapi di Malaysia. Oleh sebab itu, tujuan kajian ini adalah untuk menilai kestabilan jangka panjang kebuk pengionan jenis Farmer. Sebanyak 33 buah kebuk pengionan jenis Farmer telah dikaji dan nilai purata $\mu$ untuk sisihan $N_{D,w}$ bersama dengan nilai ketidakpastian piawai *SE* dikira. Nilai $\mu \pm SE$ ini akan digunakan untuk mengukur kestabilan $N_{D,w}$. Keputusan menunjukkan hampir kesemua kebuk pengionan mempunyai nilai $\mu \pm SE$ di dalam julat nilai ±1.5%. Oleh itu dapat disimpulkan bahawa hampir kesemua kebuk pengionan jenis Farmer adalah stabil dalam nilai $N_{D,w}$ dan selamat digunakan untuk rawatan radioterapi.

**Kata kunci:** Kebuk pengionan jenis Farmer, pusat radioterapi, pekali tentukuran $N_{D,w,}$ kestabilan.

## Introduction

Presently in Malaysia, radiotherapy treatment with photon beams can be sought from 24 radiotherapy centres (RC) located at eleven hospitals, ten medical centres and three cancer hospitals. These centres used ionization chambers (IC) for the determination of the dose delivered to the patients. The accuracy of the ionization chambers' calibration coefficient is one of the factors that would contribute to efficient radiotherapy treatment [1]. For the absorbed dose

to water calibration coefficient $N_{D,w}$, it is important that the next value of $N_{D,w}$ lies within the accuracy range of ±1.5% recommended by IAEA [2]. Accurate $N_{D,w}$ can only be obtained if the chambers were calibrated annually by the standard laboratory. For this reason, ICRU [3] and IAEA [4] has recommended an ionization chamber be calibrated every year for the purpose of getting accurate and stable $N_{D,w}$.

In Malaysia the standard laboratory for determining the $N_{D,w}$ is the SSDL Malaysia [5]. Most of the ICs belonging to the radiotherapy centres were calibrated here. Table 1 shows an example of a chamber that has been calibrated eight times (frequency $f$=8) by the SSDL. To calculate the accuracy $\Delta(\%)$ of $N_{D,w}$, this work used the first value of $N_{D,w}$ as the standard. Note that from this accuracy values, the long term stability of the chamber can be evaluated from mean μ, standard deviation $\sigma_{N-1}$ and standard error $SE$ for $\Delta(\%)$. It is clear from the table, the long term stability evaluation requires $f$>2.

Table 1: The accuracy and the long term stability analysis of calibration coefficients of a chamber [1]

| Year of calibration | $f$ | $N_{D,w}$(mGy/nC) | | $\Delta(\%)$[2] | $\mu$[3][4] | $SE$[3][4] | $\sigma_{N-1}$[4] |
|---|---|---|---|---|---|---|---|
| | | First | Consequent | | | | |
| 2004 | 8 | 57.66 ± 1.44% | | | | | |
| 2005 | | | 57.57 ± 1.42% | −0.16 | – | – | – |
| 2006 | | | 57.85 ± 0.94% | 0.33 | 0.09 | 0.35 | 0.35 |
| 2007 | | | 57.73 ± 1.18% | 0.12 | 0.10 | 0.17 | 0.25 |
| 2008 | | | 57.29 ± 1.18% | −0.64 | −0.09 | 0.24 | 0.42 |
| 2009 | | | 57.39 ± 1.18% | −0.47 | −0.16 | 0.20 | 0.40 |
| 2010 | | | 57.58 ± 1.39% | −0.14 | −0.16 | 0.16 | 0.36 |
| 2012 | | | 57.40 ± 1.22% | −0.45 | −0.20 | 0.14 | 0.35 |

1) Will be seen in Table 3 that this chamber is IC22 i.e NE 2581.

2) $\%\Delta = \frac{N_{D,w} - N_{D,w\ standard}}{N_{D,w\ standard}} \times 100\%$. Note that all $\Delta(\%)$ are within ±1.5%.

3) Note that $\mu \pm SE$ *(all in %)* are within ±1.5%.

4) Method of calculation is described by reference [6].

From year 2004 to 2012, the SSDL Malaysia has calibrated 114 chambers. Table 2 shows the chambers' categories, type, model and the frequency of calibration. It can be seen in the table that the most popular type is Farmer type ionization chambers (48.25 %). For this reason, the purposes of the present work are to get the accuracy and to evaluate the long term stability of the Farmer type ionization chambers.

Table 2: The details of the 114 therapy level ionization chambers belonging to 24 radiotherapy centres in Malaysia calibrated at SSDL Malaysia from year 2004-2012.

| **Categories** | **Type** | **Model** | **Chamber Number *N*** | | | |
|---|---|---|---|---|---|---|
| | | | ***f* < 2** | ***f* > 2**[1] | **Subtotal** | **%** |
| Cylindrical | Farmer | FC 65-G | 8 | 14 | 22 | 19.30 |
| | | FC 65-P | 0 | 3 | 3 | 2.63 |
| | | NE 2571 | 6 | 4 | 6 | 5.26 |
| | | NE2581 | 3 | 3 | 10 | 8.77 |
| | | TW 30001 | 2 | 3 | 5 | 4.39 |
| | | TW 30013 | 3 | 6 | 9 | 7.89 |
| | | | 22 | 33 | 55[2] | 48.25 |
| | Pinpoint | TW 31014 | 2 | 1 | 3 | 2.63 |
| | | TW31016 | 0 | 1 | 1 | 0.88 |
| | | | 2 | 2 | 4 | 3.51 |
| | Compact | CC01 | 10 | 1 | 11 | 9.65 |
| | | CC13 | 6 | 2 | 8 | 7.02 |
| | | | 16 | 3 | 19 | 16.67 |
| | Semiflex | TM 31010 | 2 | 5 | 7 | 6.14 |
| | | | 2 | 5 | 7 | 6.14 |
| | Thimble | A1SL-30-361 | 3 | 0 | 3 | 2.63 |
| | | | 3 | 0 | 3 | 2.63 |
| Parallel Plate | Roos | PPC05 | 1 | 1 | 2 | 1.75 |
| | | PPC 40 | 11 | 5 | 16 | 14.04 |
| | | TW 34001 | 2 | 1 | 3 | 2.63 |
| | | | 14 | 7 | 21 | 18.42 |
| | Markus | TW23343 | 2 | 1 | 3 | 2.63 |
| | | TW34045 | 2 | 0 | 2 | 1.75 |
| | | | 4 | 1 | 5 | 4.39 |
| | Total | | 63 | 51 | 114 | 100.00 |

1) The present work will focus on this 33 chambers only, as the long term stability evaluation can only be done for f>2, as shown in Table 1.
2) The calibration frequency is given in Table 3.

## Materials and Methods

### Calibration at SSDL Malaysia

For the calibration purpose of $N_{D,w}$ at SSDL Malaysia, the 1.25 MeV Co-60 beam was obtained from the SSDL Malaysia Eldorado 8(#104) teletherapy machine [7] The standard IAEA substitution method was utilised in determining the chambers' coefficients. The experimental set-up is shown in Figure 1. Reference standard chamber used by SSDL is NE2571 (#1028) with volume 0.6 $cm^3$. Apparatus and set-up used in this study are as follows: PMMA water phantom size 30 cm × 30 cm × 30 cm, Perspex sheath (used to place the ionization chamber inside the phantom), surface to source distance (SSD) = 100 cm, surface to chamber distance (SCD) = 105 cm (with reference point depth = 5 $g/cm^2$) and field size (FS) = 10 × 10 $cm^2$.

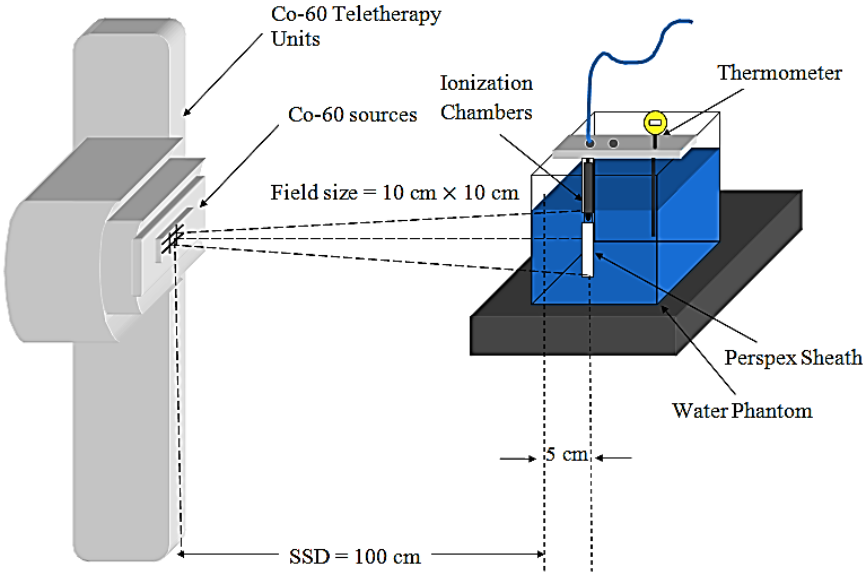



Figure 1: Experimental set-up for the determination of $N_{D,w}$

### Long term stability analysis

Table 3 gives the $N_{D,w}$ calibration frequency record for the 33 chambers since 2004. A total of 178 calibration were performed from 2004-2012 where 3 chambers were calibrated 2 times, 8 chambers 7 times, 4 chamber 6 times, 6 chambers 5 times, 8 chamber 4 times and 4 chambers 3 times. For the purpose of confidentiality, only codes are used to represent the RC and the IC respectively. In this work, $\mu \pm SE$ will be used to measure stability of $N_{D,w}$. The $N_{D,w}$ of a chamber is considered stable if $\mu \pm SE$ (at the 95% confidence intervals) are in the range of ±1.5%.

Table 3: $N_{D,w}$ calibration frequency for 55 Farmer type ionization chambers used in this work.

| Criteria | Chamber's Model | IC | RC | Year of calibration | | | | | | | | | Calibration's frequency, $f$ |
|---|---|---|---|---|---|---|---|---|---|---|---|---|---|
| | | | | 2004 | 2005 | 2006 | 2007 | 2008 | 2009 | 2010 | 2011 | 2012 | |
| $f$ >2 | FC 65-G | 1 | R1 | √ | | √√ | | √ | √ | | | | 5 |
| | ($N$=14) | 2 | R2 | √ | √ | | √ | √ | √ | | √ | √ | 7 |
| | | 3 | R3 | √ | √ | | √ | | | | | | 3 |
| | | 4 | R3 | | √ | √ | √ | √ | √ | | | | 5 |
| | | 5 | R4 | √ | √ | √ | √ | √ | √ | √ | | √ | 8 |
| | | 6 | R5 | √ | | √ | √ | √ | √ | √ | | √ | 7 |
| | | 7 | R5 | | | √ | | √ | √ | √ | √ | √ | 6 |

| | | | | | | | | | | | | |
|---|---|---|---|---|---|---|---|---|---|---|---|---|
| | | 8 | R6 | | | | | √ | √ | √ | | | 3 |
| | | 9 | R6 | √ | √√ | √ | | | | | | | 4 |
| | | 10 | R7 | √ | √ | √ | √ | √ | √ | | √ | √ | 8 |
| | | 11 | R8 | | | √ | √ | √ | √ | √ | √ | √ | 7 |
| | | 12 | R9 | | | | √ | √ | √ | √ | √ | | 5 |
| | | 13 | R10 | | | | | | √ | √ | | √ | 3 |
| | | 14 | R11 | | | | | | | √ | √ | √ | 3 |
| | FC 65-P | 15 | R10 | | | | √ | √ | | √ | | √ | 4 |
| | (*N*=3) | 16 | R12 | √ | | √ | | √ | √ | √ | √ | √ | 7 |
| | | 17 | R12 | √ | | √ | √ | √ | √ | √ | | √ | 7 |
| | NE 2571 | 18 | R8 | √ | √ | √ | √ | √ | √ | | | | 6 |
| | (*N*=4) | 19 | R10 | √ | √ | √ | √ | | | | | | 4 |
| | | 20 | R13 | √ | √ | √ | √ | | | | | | 4 |
| | | 21 | R14 | √ | | √ | √ | √ | √ | | √ | √ | 7 |
| | NE 2581 | 22 | R9 | √ | √ | √ | √ | √ | √ | √ | | √ | 8 |
| | (*N*=3) | 23 | R15 | | √ | √ | √ | | √ | | | | 4 |
| | | 24 | R16 | | √ | √ | √ | √ | √ | √ | | √ | 7 |
| | TW 30001 | 25 | R14 | √ | √ | | √ | √ | √ | √ | | √ | 7 |
| | (*N*=3) | 26 | R14 | | | √ | √ | √ | √ | | √ | √ | 6 |
| | | 27 | R17 | √ | √ | √√ | | | | | | | 4 |
| | TW 30013 | 28 | R17 | | | √ | √ | √ | √ | | √ | | 5 |
| | (*N*=6) | 29 | R18 | | | √ | √ | √ | √ | | | √ | 5 |
| | | 30 | R18 | | | √ | √ | √ | √ | √ | | √ | 6 |
| | | 31 | R19 | | | | √ | √ | √ | | √ | √ | 5 |
| | | 32 | R19 | | | | | | √ | √ | √ | √ | 4 |
| | | 33 | R20 | | | | √ | | √ | √ | | √ | 4 |
| | | | | | | | | | | | | | 178[1] |
| $f < 2^{(2}$ | FC 65-G | 34 | R7 | | | | | | | | | √ | 1 |
| | (*N*=8) | 35 | R11 | | | | | | | √ | | √ | 2 |
| | | 36 | R12 | | | | | | | | | √ | 1 |
| | | 37 | R12 | | | | | | | | | √ | 1 |
| | | 38 | R14 | | | | | | | | | √ | 1 |
| | | 39 | R21 | √ | | | | | | | | | 1 |
| | | 40 | R22 | | | | | | | | | √ | 1 |
| | | 41 | R22 | | | | | | | | | √ | 1 |
| | NE 2571 | 42 | R5 | | √ | | | | | | | | 1 |
| | (*N*=6) | 43 | R6 | | | √ | | √ | | | | | 2 |
| | | 44 | R11 | | | | | √ | | | | | 1 |
| | | 45 | R10 | √ | √ | | | | | | | | 2 |
| | | 46 | R20 | √ | | | | | | | | | 1 |
| | | 47 | R21 | | | | | | | | | √ | 1 |
| | NE 2581 | 48 | R6 | | √√ | | | | | | | | 2 |
| | (*N*=3) | 49 | R15 | √ | | | | | | | | | 1 |
| | | 50 | R21 | | | | | | √ | | | | 1 |
| | TW 30001 | 51 | R5 | | | | √ | | | | | | 1 |
| | (*N*=2) | 52 | R20 | √ | √ | | | | | | | | 2 |
| | TW 30013 | 53 | R1 | | | | | | | √ | √ | | 2 |
| | (*N*=3) | 54 | R6 | | | | | | | | | √ | 1 |
| | | 55 | R23 | | | | | | | √ | | √ | 2 |
| | | | | | | | | | | | | | 29 |

1) The 145 deviations shown in Figure 2 may be calculated from this frequency, i.e. 178−33 = 145.

2) The 22 chambers (IC34 to IC55) under this category were not discussed in this paper. They are included here for two reasons: to justify the details shown in Table 2 and to be used for future references.

## Results and Discussion

Figure 2 shows 145 deviations for the 33 chambers. The $\Delta(\%)$ of $N_{D,w}$ calculated in relation to the first value, are as follows: 2nd calibration (33 deviations) = −2.18 % to 6.55 %; 3rd calibrations (33 deviations) = −2.45 % to 3.41 %;

$4^{th}$ calibrations (29 deviations) = −7.08 % to 1.85 %; $5^{th}$ calibrations (21 deviations) = −1.75 % to 5.81 %; $6^{th}$ calibrations (15 deviations) = −2.77 % to 4.77 %; $7^{th}$ calibrations (11 deviations) = −5.34 % to 6.45 %; $8^{th}$ calibrations (3 deviations) = − 1.15 % to − 0.45 %.

If we see the *Δ(%)* for the calibration coefficients of 33 cylindrical Farmer-type chambers based on the chamber's model, it was found that, the range of *Δ(%)* for; FC 65-G = − 2.77 % to 2.51 %; FC 65-P = − 1.33 % to 0.37 %; NE 2571= − 7.08 % to 6.55 %; NE 2581 = − 1.34 % to 0.62 %; TW 30001= − 0.46 % to 6.45 %; TW 30013= − 1.99 % to 2.29 %. Overall, clear from Figure 2 that most of these deviations lie within the IAEA tolerance value, ±1.5% except for few chambers which have deviations outside the IAEA acceptable limits which will be discussed later.

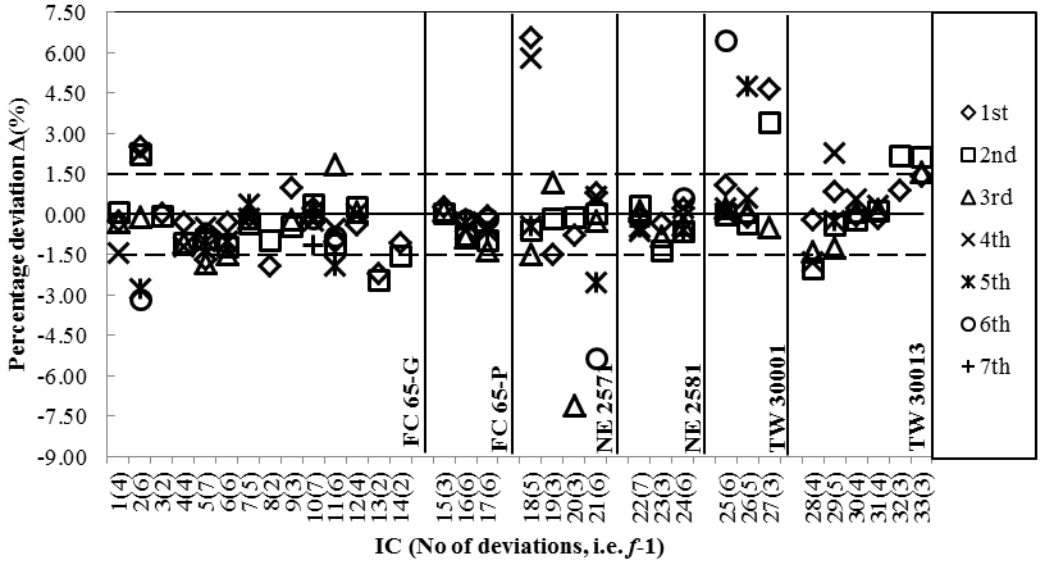



Figure 2: 145 percentage deviations of $N_{D,w}$ for 33 Farmer type chambers. From these deviations, $\mu \pm SE$ were calculated as shown in Figure 3. As an example, for IC22, Table 1 shows the values of $\mu \pm SE$, and Figure 3 shows the plot.

Discussion will mainly focus on $\mu \pm SE$ in particular. It is interesting to see the chambers with most calibration frequency first. Based on Table 2, there are three chambers with 8 calibration frequency in the period of 9 years (2004-2012) namely IC5, IC10 and IC22. All three chambers give a quite good value of $\mu \pm SE$ which are -1.05 ± 0.19, 0.19 ± -0.10 and -0.20 ± 0.13 respectively. The variation of $\mu \pm SE$ for the 33 chambers is shown in Figure 3.

It is interesting to check whether $\mu \pm SE$ include the value of zero for each chamber. If it does, we conclude that the result is satisfactory and no evidence that a systematic error occurred in the measurements. On the other hand, if it does not, the student's t-test [8] needs to be done as shown in Table 4.

On examining Figure 3, it is obvious that $\mu \pm SE$ for 23 chambers do not include the value of zero. This may lean the results towards a systematic error. Thus, a student's-t test is conducted to prove that the results were statistically significance. Upon checking this test (Table 4) it is found 8 out of 23 chamber have evidence that a systematic errors have occurred in the measurement (of calibration coefficients) at 5% significance level. IC5 (which is chambers with most calibration frequency) however also indicated the existence of systematic errors in the $N_{D,w}$ during the long term period of measurements. In terms of chamber's model, 66.67 % from the total amount of FC 65-P chambers give systematic errors. This is then followed with 33.33 % for TW 30013 and 14.29 % for FC 65-P.

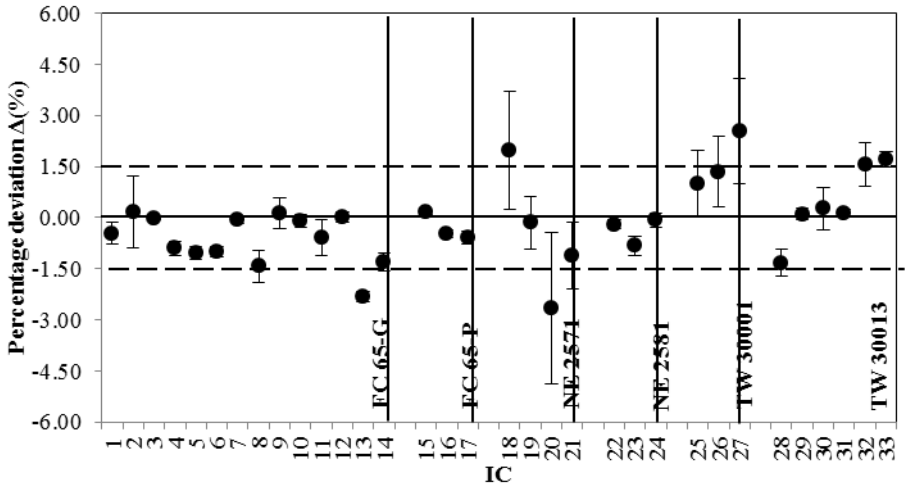



Figure 3: Variation of Δ(%) for μ±SE with chamber number

Table 4: Student's t-test analysis for a selected 23 chambers with μ±SE do not include the value of zero

| Chamber's Model | IC | *f* | μ±SE | T value[1] | T-test[2] | T test < \|μ\|[3] | Systematic Error |
|---|---|---|---|---|---|---|---|
| FC 65-G | 1 | 5 | −0.46±0.33 | 2.776 | 0.916 | N | N |
| | 4 | 5 | −0.90±0.21 | 2.776 | 0.569 | Y | Y |
| | 5 | 8 | −1.05±0.19 | 2.365 | 0.455 | Y | Y |
| | 7 | 6 | −0.07±0.12 | 2.571 | 0.308 | N | N |
| | 9 | 4 | 0.13±0.45 | 3.182 | 1.424 | N | N |
| | 10 | 8 | −0.10±0.19 | 2.365 | 0.458 | N | N |
| | 13 | 3 | −2.32±0.14 | 4.303 | 0.581 | Y | Y |
| | 14 | 3 | −1.30±0.25 | 4.303 | 1.082 | Y | Y |
| FC 65-P | 15 | 4 | 0.15±0.06 | 3.182 | 0.199 | N | N |
| | 16 | 7 | −0.48±0.12 | 2.447 | 0.291 | Y | Y |
| | 17 | 7 | −0.59±0.20 | 2.447 | 0.485 | Y | Y |
| NE 2571 | 19 | 4 | −0.15±0.78 | 3.182 | 2.471 | N | N |
| | 20 | 4 | −2.65±2.22 | 3.182 | 7.069 | N | N |
| | 21 | 7 | −1.10±0.98 | 2.447 | 2.393 | N | N |
| NE 2581 | 22 | 8 | −0.20±0.13 | 2.365 | 0.310 | N | N |
| | 23 | 4 | −0.83±0.29 | 3.182 | 0.921 | N | N |
| TW 30001 | 25 | 7 | 1.01±0.95 | 2.447 | 2.332 | N | N |
| | 26 | 6 | 1.34±1.03 | 2.571 | 2.658 | N | N |
| | 27 | 4 | 2.54±1.55 | 3.182 | 4.921 | N | N |
| TW 300013 | 28 | 5 | −1.33±0.40 | 2.776 | 1.111 | Y | Y |
| | 30 | 5 | 0.26±0.61 | 2.776 | 1.692 | N | N |
| | 32 | 4 | 1.56±0.65 | 3.182 | 2.054 | N | N |
| | 33 | 4 | 1.71±0.21 | 3.182 | 0.680 | Y | Y |

1) from Student's t table [9,10].
2) T test = T value × SE.
3) Y = Yes, N = No.

In Figure 3, it is also can be seen that few chamber (i.e. IC2, IC18, IC19, IC20, IC21, IC25, IC26 and IC27) gives a large value of *SE*. If now we look back again at Figure 2 for these particular chambers, we can see that there is a deviation values which are significantly different from the groups of deviations.

It is also obvious that 5 chambers (i.e. IC13, IC18, IC20, IC27 and IC33) have μ values outside the IAEA tolerance value, ±1.5%. However $\mu \pm SE$ value for these chambers still lies within the IAEA action value, ±3.0%.

## Conclusion

As a conclusion, almost all 33 Farmer type ionization chamber have a stable $N_{D,w}$ calibration coefficients despite 8 chambers that shown a systematic error in their measurements. It is also concluded that all these chambers is safe to be used for radiotherapy treatment.

## Acknowledgement

A.M.M. is thankful for the award of Zamalah UKM from August 2012 to August 2013. We gratefully acknowledged the Ministry of Higher Education for a research grant of UKM-ST-07-FRGS0154-2010 and the Nuclear Malaysia Agency for the cooperation given.

## References

1. Czap, L., Matcheko, G., Andreo, P. 1995. Intercomparison of ionization chamber calibration factors in the IAEA/WHO network of SSDLs. SSDL Newsletter 34:17-25.
2. IAEA. 2000a. *Technical Report Series No. 398: Absorbed Dose Determination in External Beam Radiotherapy.* Vienna: International Atomic Agency.
3. ICRU. 1976. *Determination of Absorbed Dose in a Patient Irradiated by beams of X or Gamma Rays in Radiotherapy Procedures, Rep 24*. Bethesda: International Commissioning Radiation Unit.
4. IAEA 2000b. *Safety Report Series No. 17: Lesson learned from accidental exposures in radiotherapy*. Vienna: International Atomic Agency.
5. Kadni, T. 2004. Calibration of Radiation Instruments Used in Radiation Protection and Radiotherapy in Malaysia. *Australian Physical and Engineering Sciences in Medicine.* 27(2): 79.
6. Samat, S.B. and Evans, C.J. 1992. Statistics and Nuclear Counting – Theory, Problems and Solutions. Serdang: Universiti Putra Malaysia Press.
7. Samat, S.B., Evans, C.J., Kadni, T. & Dolah, M.T. 2000. Accurate measurement of exposure rate from a $Co^{60}$ teletherapy sources: deviations from the inverse square law.
8. Bland, M. 1987. *An Introduction to Medical Statistics*. Oxford: Oxford University Press.
9. Lind, D.A., Marchal, W.G. & Wathen, S.A. 2008. *Basic Statistics for Business and Economics*. Ed. ke-6. New York: McGraw Hill.
10. Spiegel, M.R. and Stephens, L.J. 2011. *Statistics*. 4th ed. United States: McGraw Hill.

The Malaysian Journal of ANALYTICAL SCIENCES ISSN 1394-2506

# EFFECTS OF LITHIUM DOPANT ON SIZE AND MORPHOLOGY OF MAGNESIUM OXIDE NANOPOWDERS

## (Kesan-Kesan Litium Sebagai Pendopan Keatas Saiz dan Morfologi Serbuk Nano Magnesium Oksida)

Mohd Sufri Mastuli[1,2]*, Siti Nur Hazlinda Hasbu[1], Noraziahwati Ibrahim[1], Mohd Azizi Nawawi[1]

[1]*School of Chemistry and Environmental Studies, Faculty of Applied Sciences, Universiti Teknologi MARA, 40450 Shah Alam, Selangor, Malaysia*
[2]*Centre for Nanomaterials Research, Institute of Science, Level 3 Block C, Universiti Teknologi MARA, 40450 Shah Alam, Selangor, Malaysia*

**Corresponding author: mohdsufri@salam.uitm.edu.my*

**Abstract**

Lithium doped of magnesium oxide powders have been synthesized using the sol-gel method with magnesium acetate tetrahydrate, oxalic acid dihydrate and lithium acetate dihydrate used as the starting materials. The dried sol-gel products were calcined at 950 °C for 36 h to form the Li doped-MgO samples. The calcined samples were characterized using X-Ray diffraction (XRD) and field emission scanning electron microscopy (FESEM). The present work is investigated the effect of lithium ion on the band gap energy of studied samples. The band gap energies were obtained from a Tauc plot that drawn based on absorption edge of each sample that measured using a UV-Vis spectrophotometer. It is found that the doped and undoped MgO samples showed a slightly different in their band gap energies. The lithium ion that present in the MgO as a dopant affects the crystallite size and morphology of the final products. Our study shows that the lithium dopant can modified optical properties of the metal oxide which to be beneficial in some industrial applications.

**Keyword**: Magnesium oxide, doping, sol-gel method, band gap energy

**Abstrak**

Magnesium oksida yang didopkan dengan litium telah disintesis menggunakan kaedah sol-gel dengan magnesium asetat tetrahidrat, asid oksalik dihidrat dan litium asetat dihidrat sebagai bahan pemula. Produk-produk sol-gel yang kering telah dipanaskan pada 950°C selama 36 jam untuk pembentukan sampel-sampel MgO yang didopkan dengan Li. Sampel-sampel yang telah dipanaskan dianalisa menggunakan X-Ray pembelauan (XRD) dan bidang pelepasan elektron imbasan mikroskop (FESEM). Kerja terkini ini adalah mengkaji kesan ion litium keatas tenaga jurang jalur untuk bahan-bahan yang diuji kaji. Tenaga jurang jalur telah diperolehi daripada plot Tauc berdasarkan di pinggir penyerapan sampel yang diukur menggunakan UV-Vis spektrofotometer. Didapati bahawa MgO dengan dan tanpa pendopan ion litium menunjukkan sedikit perbezaan dalam jalur tenaga jurang mereka. Kehadiran litium didalam magnesium oksida sebagai pendopan juga memberikan kesan kepada saiz kristalit dan morfologi serbuk tersebut. Kajian ini menunjukkan bahawa ion litium boleh mengubahsuai sifat-sifat optik oksida logam yang memberikan kebaikan kepada beberapa aplikasi industri.

**Kata kunci:** Magnesium oksida, pendopan, kaedah sol-gel, jalur jurang tenaga

## Introduction

Magnesium oxide (MgO) is a versatile metal oxide having numerous applications in many fields such as catalysis [1], toxic waste remediation [2], refractory materials [3], antimicrobial materials [4] and electrochemical biosensor [5]. It is widely accepted that the properties of MgO is depend strongly on the synthesis methods and the processing conditions. Many efforts have been devoted to synthesize MgO nanostructures using various methods such as precipitation [6], sol-gel [7], chemical vapour deposition [8], combustion [9] and many other methods. The

properties of MgO are further improved when it used as nanosized particles compared to bulk MgO. Therefore, the formation of MgO nanostructures with small crystallite size of less than 100 nm and well-defined morphology is a key issue on the nanomaterial research. The crystallite size and morphology of the nanomaterials can be tuned by introducing a secondary metal into crystal structure of metal oxide that can be done *via* doping either interstitial or substitution [10]. This may alter the properties of the materials. The aim of this study is to synthesize MgO and $Li_{0.2}Mg_{0.9}O$ samples using the sol-gel method and studying the effects of $Li^+$ ions on their properties.

## Materials and Methods

All the chemicals were analytical grade and directly used as received without further purification. Both MgO and $Li_{0.2}Mg_{0.9}O$ were synthesized using the sol-gel method with magnesium acetate tetrahydrate, $Mg(CH_3COO)_2.4H_2O$ (Merck, 99.5 % purity); oxalic acid dihydrate, $C_2H_2O_4.2H_2O$ (Merck, > 98 % purity); lithium acetate dihydrate, $LiCH_3COO.2H_2O$ (Merck, 99.9 %) and absolute ethanol, $C_2H_5OH$ (J. Kollin Chemical, 99.9 % purity) used as the starting materials. For MgO, magnesium acetate tetrahydrate was dissolved in ethanol under constant stirring. Then, pH of the solution was adjusted to pH 5 using 1 M of oxalic acid. The mixture solution was continuously stirred until formed a thick white gel. The sol-gel product was left overnight for further gelation process before drying in an oven at 100 ºC for 24 h. The steps above were repeated for the $Li_{0.2}Mg_{0.9}O$ sample with lithium acetate dihydrate was added during the sol-gel reaction. Later on, the dried solids were ground using mortar and pestle to produce fine powder precursors. Each precursor was annealed at 950 ºC for 36 h to form the respective samples.

The two synthesized samples were systematically characterized using various instruments. The XRD patterns of MgO and $Li_{0.2}Mg_{0.9}O$ were obtained by X-Ray diffraction (XRD: PANalytical X'Pert Pro MPD) with $CuK_\alpha$ radiation. The Bragg-Brentano optical configuration was used during the data collection. The size and morphology of the samples were examined using field emission scanning electron microscopy (FESEM: JEOL JSM-7600F). The band gap energies for both samples were measured using UV-Vis-NIR spectrophotometer (Perkin Elmer Lambda 950 UV-Vis-NIR).

## Results and Discussion

The XRD patterns for MgO and $Li_{0.2}Mg_{0.9}O$ are shown in Figure 1. All the diffraction peaks are indexed according to ICDD 01-0178-0430 reference number showing a face-centered cubic phase of periclase MgO with space group Fm-3m. These XRD peaks are assigned to (111), (200), (220), (311), and (222) crystal planes. The XRD pattern of lithium-doped MgO is isostructural to the XRD pattern of MgO. However, all the XRD peaks for $Li_{0.2}Mg_{0.9}O$ are slightly shifted to the right due to the presence of $Li^+$ ions. Figure 2 shows the shifting of (200) peaks and this is true with the other peaks as well. The lithium ion can be said to have been successfully introduced into the cubic crystal structure of MgO. In addition, the sharp and intense XRD peaks are clearly observable for both samples that reflect higher crystallinity. The XRD results also suggest that the obtained samples are also pure and single phase with no impurities present. The doped sample is expected to have a larger crystallite size as compared to the undoped sample and this agrees with its FWHM (full width at half maximum) value that can be obtained from the XRD peak broadening. The smaller FWHM value corresponds to the larger crystallite size, and vice versa. The FWHM values for the (200) peak of MgO and $Li_{0.2}Mg_{0.9}O$ are 0.1506° and 0.1004° respectively. Thus, the crystallite size of MgO is smaller than the $Li_{0.2}Mg_{0.9}O$ crystals. This observation is in a good agreement with the FESEM micrographs for both samples.

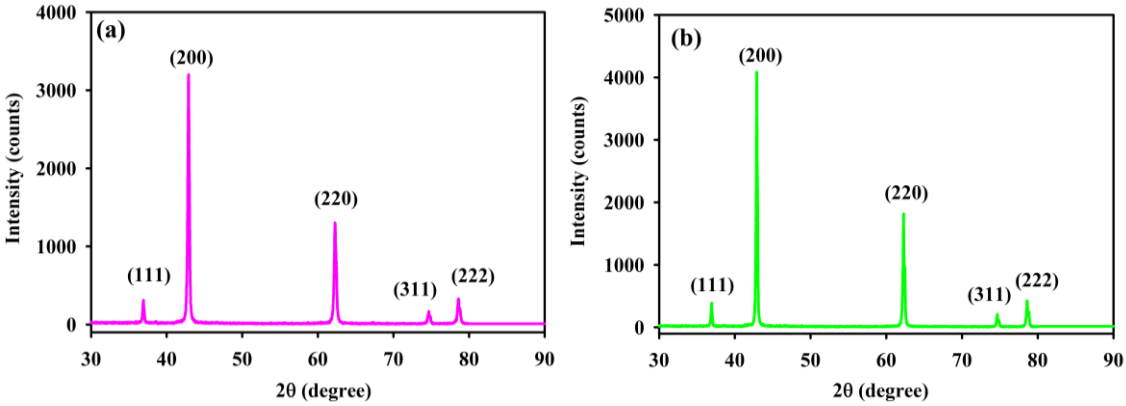



Figure 1: XRD patterns of (a) MgO and (b) $Li_{0.2}Mg_{0.9}O$

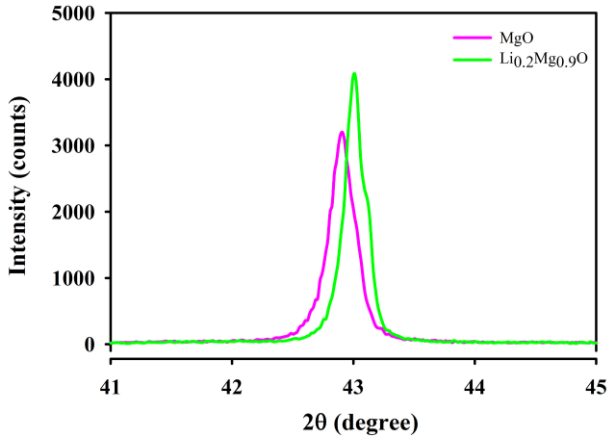



Figure 2: Shifting of (200) peak for both samples

Figure 3 shows the FESEM micrographs for the studied samples. As can be seen, the crystallite size for MgO and $Li_{0.2}Mg_{0.9}O$ are different to each other in which the doped sample exhibited larger crystallites although the annealing temperature and annealing time are identical as for the undoped sample. The MgO sample has crystallite size of average 30 nm which is smaller than of $Li_{0.2}Mg_{0.9}O$ sample which has an average crystallite size of more than 100 nm. The morphology of MgO is cubic crystal while that of $Li_{0.2}Mg_{0.9}O$ is of mixed cube and sphere shaped. These results show that the addition of lithium ion causes the crystal defect in the sample.

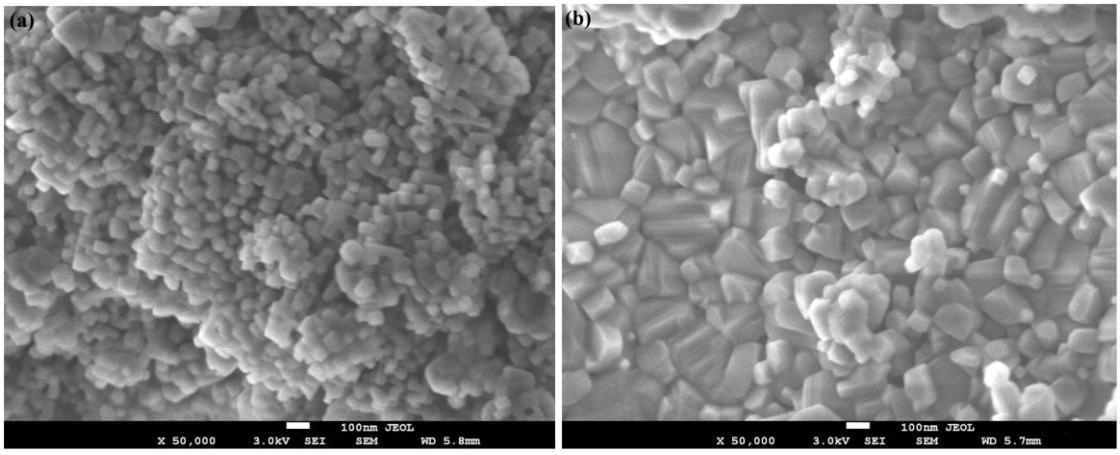



Figure 3: FESEM micrographs of (a) MgO and (b) $Li_{0.2}Mg_{0.9}O$

The UV-Vis spectra for MgO and $Li_{0.2}Mg_{0.9}O$ are shown in Figure 4. It can be seen that the absorption edge for the MgO appeared at a higher wavelength compared to the $Li_{0.2}Mg_{0.9}O$. This reveals that the MgO should have larger band gap energy than the $Li_{0.2}Mg_{0.9}O$. The band gap energies for both samples were estimated using a Tauc equation as shown in Equation (1) [11].

$$\alpha h\upsilon = C(h\upsilon - E_g)^n \quad (1)$$

where, α is the absorption coefficient at a certain value of wavelength (λ), h is the Planck's constant, υ is the frequency of light, C is the proportionality constant, n is the nature of transition and $E_g$ is the band gap energy. MgO is considered as a direct band gap material, thus, its n has the value of ½ indicating the allowed direct transition mode, resulting in Equation (2).

$$(\alpha h\upsilon)^2 = C'(h\upsilon - E_g) \quad (2)$$

From Equation (2), the plot of $(\alpha h\upsilon)^2$ against hυ would gives the value of band gap energy. This plot is also known as a Tauc plot. The Tauc plot is evaluated such that the linear part when extrapolated will give the band gap, $E_g$, as shown in Figure 5. The band gap energies for the MgO and $Li_{0.2}Mg_{0.9}O$ are found to be 6.38 eV and 6.35 eV respectively. These energies are lower than the band gap energy of bulk MgO (7.8 eV) [12]. The reduced in band gap for the MgO nanostructures have been reported by other researchers [13-15] and our results are consistent with theirs. The lower band energy for the nanosized MgO is attributed to the reduced of crystallite size. As the crystallite is scaled down to nano size, its surface area-to-volume (SAV) ratio is increased [16]. The higher SAV ratio would affect the electron binding energy of the material because the number of core atoms in nanosized crystallites seems less than they in micron crystals. This affects the energy levels of the nanocrystals resulting in widening of the bands. When the number of core atoms in a crystallite is much reduced from micron sized crystals, the fraction of atoms at the surface becomes larger. This results in higher average binding energy of the smaller crystallites.

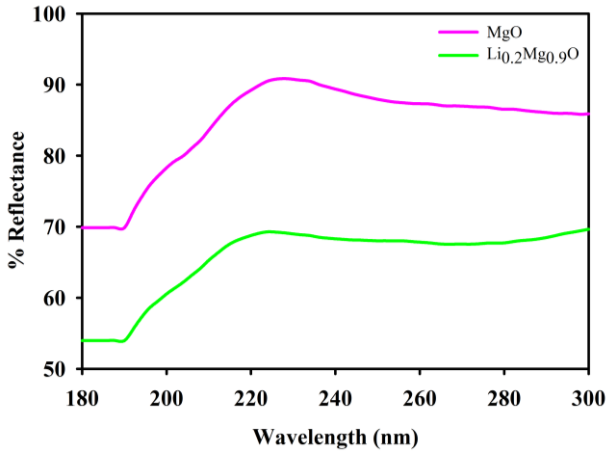



Figure 4: UV-Vis spectra of the samples

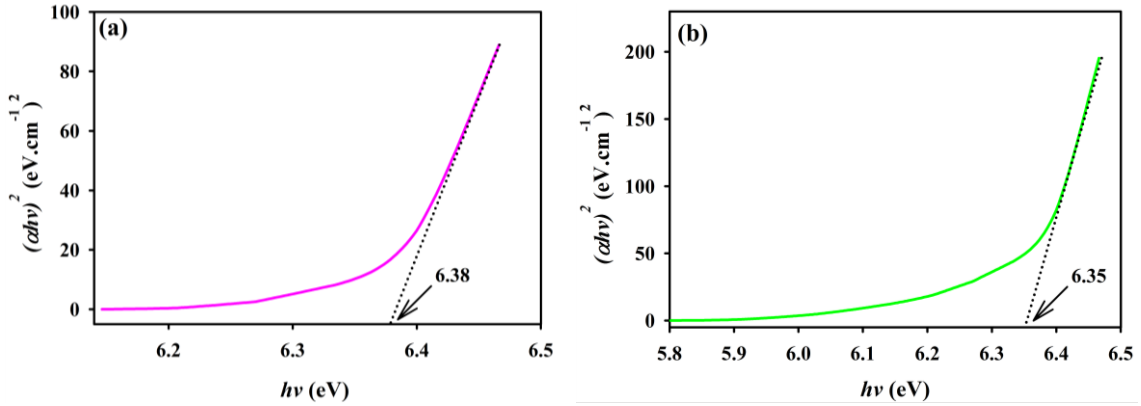



Figure 5: Tauc plots of (a) MgO and (b) $Li_{0.2}Mg_{0.9}O$

## Conclusion

The pure and single phase of MgO and $Li_{0.2}Mg_{0.9}O$ were obtained *via* the sol-gel process. The presence of the lithium ion affects the crystallite size and morphology for both samples. The used of lithium as a dopant has been demonstrated as an important way in tuning the energy levels of the target material.

## Acknowledgement

Authors would like to thank the Ministry of Higher Education, Malaysia for supporting this work through the Fundamental Research Grant Scheme (600-RMI/ST/FRGS 5/3/Fst(200/2010)).

## References

1. Mutreja, V., Singh, S. & Ali, M. (2011). Biodiesel from Mutton Fat using KOH Impregnated MgO as Heterogeneous Catalysts. *Renew Energy*, 36 (8): 2253 – 2258.
2. Rakmak, N., Wiyaratn, W., Bunyakan, C. & Chungsiriporn, J. (2010). Synthesis of Fe/MgO Nano-Crystal Catalysts by Sol-Gel Method for Hydrogen Sulfide Removal. *Chem Eng J*, 162 (1): 84 – 90.
3. Braulio, M.A.L., Brant, P.O.C., Bitterncourt, L.R.M. & Pandolfelli, V.C. (2009). Microsilica or MgO Grain

Size: Which One Mostly Affects the *in-situ* Spinel Refractory Castable Expansion?. *Ceram Int*, 35 (8): 3327 – 3334.
4. Zhang, K., An, Y., Zhang, L. & Dong, Q. (2012). Preparation of Controlled Nano-MgO and Investigation of Its Bactericidal Properties. *Chemosphere*, 89 (11): 1414 – 1418.
5. Umar, A., Rahman, M.M. & Hahn, Y. (2009). MgO Polyhedral Nanocages and Nanocrystals Based Glucose Biosensor. *Electrochem Commun*, 11 (7): 1353 – 1357.
6. Veldurthi, S., Shin, C., Joo, O. & Jung, K. (2012). Synthesis of Mesoporous MgO Single Crystals Without Templates. *Microporous Mesoporous Mater*, 152 (1): 31 – 36.
7. Kumar, A. & Kumar, J. (2008). On the Synthesis and Optical Absorption Studies of Nano-Size Magnesium Oxide Powder. *J Phys Chem Solids*, 69 (11): 2764 – 2772.
8. Li, H., Li, M., Wang, X., Wu, X., Liu, F. & Yang, B. (2013). Synthesis and Optical Properties of Single-Crystal MgO Nanobelts. *Mater Lett*, 102 – 103: 80 – 82.
9. Selvam, N.C.S., Kumar, R.T., Kennedy, L.J. & Vijaya, J.J. (2011). Comparative Study of Microwave and Conventional Methods for the Preparation and Optical Properties of Novel MgO-Micro and Nano-Structures. *J Alloys Compd*, 509 (41): 9809 – 9815.
10. Okuyama, Y., Kurita, N. & Fukatsu, N. (2010). Electrical Conductivity of Calcium-Doped α-Alumina. *Solid State Ionics*, 181 (3 – 4): 142 – 147.
11. Rusdi, R., Abd Rahman, A., Mohamed, N.S., Kamarudin, N. & Kamarulzaman, N. (2011). Preparation and Band Gap Energies of ZnO Nanotubes, Nanorods and Spherical Nanostructures. *Powder Technol*, 210 (1): 18 – 22.
12. Roessler, D.M. & Walker, W.C. (1967). Electronic Spectrum and Ultraviolet Optical Properties of Crystalline MgO. *Phys Rev*, 159 (3): 733 – 738.
13. Al-Gaashani, R., Radiman, S., Al-Douri, Y., Tabet, N. & Daud, A.R. (2012). Investigation of the Optical Properties of $Mg(OH)_2$ and MgO Nanostructures Obtained by Microwave-Assisted Method. *J Alloys Compd*, 521: 71 – 76.
14. Jalili, S. & Majidi, R. (2008). The Effect of Impurities on the Electronic Properties of MgO. *Physica B: Phys Condens Matter*, 403 (19 – 20): 3522 – 3526.
15. Kumari, L., Li, W.Z., Vannoy, C.H., Leblanc, R.M. & Wang, D.Z. (2009). Synthesis, Characterization and Optical Properties of $Mg(OH)_2$ Micro-/Nanostructure and Its Conversion to MgO. *Ceram Int*, 35 (8): 3355 – 3364.
16. Kamarulzaman, N., Yusoff, R., Kamarudin, N., Shaari, N.H., Abdul Aziz, N.A., Bustam, M.A., Blagojevic, N., Elcombe, M., Blackford, M., Avdeev, M. & Arof, A.K. (2009). Investigation of Cell Parameters, Microstructures and Electrochemical Behaviour of $LiMn_2O_4$ Normal and Nano Powders. *J Power Sources*, 188 (1): 274 – 280.

The Malaysian Journal of ANALYTICAL SCIENCES ISSN 1394-2506

# SYNTHESIS, CHARACTERIZATION AND CORROSION INHIBITION STUDIES OF *o,m,p*-DECANOYL THIOUREA DERIVATIVES ON MILD STEEL IN 0.1 M $H_2SO_4$ SOLUTIONS

## (Sintesis, Pencirian dan Kajian Perencatan Kakisan Keluli Lembut oleh Terbitan *o,m,p*-Dekanoil Tiourea Dalam 0.1 M Larutan $H_2SO_4$ )

Noor Khadijah Mustafa Kamal[1], Adibatul Husna Fadzil[1]*, Karimah Kassim[1,2], Shadatul Hanom Rashid[1], Mohd Sufri Mastuli[1]

[1]*Faculty of Applied Sciences,*
[2]*Institute of Science,*
*Universiti Teknologi MARA, 40450 Shah Alam, Selangor, Malaysia*

**Corresponding author: adibatul@salam.uitm.edu.my*

**Abstract**

A series of decanoyl thiourea derivatives, namely *N*-decanoyl-*N'*-2-pyridinethiourea (D1), *N*-decanoyl-*N'*-3-pyridinethiourea (D2) and *N*-decanoyl-*N'*-4-pyridinethiourea (D3) were successfully synthesized and were applied as corrosion inhibitors. The compounds were characterized via elemental analyser, Fourier Transform Infra Red (FTIR) and $^{1}H$ and $^{13}C$ Nuclear Magnetic Resonance (NMR) spectroscopies. The inhibition efficiency of each compound was studied on the corrosion of mild steel in 0.1 M $H_2SO_4$ with different concentrations of the compounds by using weight loss method and linear polarization resistance technique. From both techniques the results indicate that the corrosion process was significantly reduced with the presence of such compounds. It shows that compound D3 has the highest efficiency which is 85.84% compared to D1 and D2. The effects of position of N atom located at *ortho, meta* and *para* in chemical structure of pyridine on the corrosion inhibition efficiencies of the compounds were also investigated.

**Keywords:** Corrosion inhibitor, spectroscopic studies, corrosion studies, inhibition efficiency

**Abstrak**

Siri terbitan dekanoil tiourea, iaitu *N*-dekanoil-*N'*-2-piridinatiourea (D1), *N*-dekanoil-*N'*-3-piridinatiourea (D2) and *N*-dekanoil-*N'*-4-piridinatiourea (D3) telah berjaya disintesis dan digunakan sebagai perencat kakisan. Sebatian tersebut dicirikan dengan penganalisis unsur, spektroskopi infra merah (IR) dan $^{1}H$ and $^{13}C$ resonans magnet nukleus (NMR). Keberkesanan tindakan merencatkan kakisan oleh setiap sebatian telah diuji pada besi keluli di dalam larutan 0.1 M $H_2SO_4$ dengan kepekatan sebatian yang berbeza menggunakan teknik perubahan berat dan kaedah rintangan pengutuban linear. Daripada kedua-dua teknik, ia telah menunjukkan bahawa proses kakisan boleh direncatkan dengan adanya sebatian tersebut. Sebatian D3 mempunyai peratusan perencatan tertinggi sebanyak 85.84% berbanding D1 dan D2. Kajian ini juga termasuk kesan struktur kimia sebatian terhadap kebolehan merencat kerana sebatian yang disintesis mempunyai kedudukan atom N iaitu *orto-*, *meta-* dan *para-* dalam struktur piridina.

**Kata kunci**: Perencat kakisan, kajian spektorskopi, kajian kakisan, keberkesanan perencat.

## Introduction

Corrosion is one of the biggest problems encountered b**y** the industrial sector since it used acid as the main solution in the daily processes. The general aggressively of the acid solutions make it easy for the corrosive attack on the metallic materials [1]. Commonly, acid is widely used in the industry for acid pickling, industrial acid cleaning, acid descaling and oil well acidizing [2-3]. The use of organic inhibitors is the most practical methods to protect metals against corrosion. Organic inhibitors containing nitrogen (N), sulphur (S) and oxygen (O) atoms are capable of retarding metallic corrosion [4]. Thus, thiourea and its derivatives are the potential corrosion inhibitor because it

contains one S and two N atoms [5]. The lone pair presence in these atoms makes it easily adsorbed on the metal surface by forming a protective layer and hence reduces the corrosion attack [6, 7]. Apart from that, the S atom have negative charge and the N atom have positive charge which able to enhance the adsorption of molecules by inducing additional charges of both atoms using electric field [8]. Others investigation states that heterocyclic ring structure which contains nitrogen and oxygen atoms can enhance greater adsorption on metal surface [9]. Therefore, cyclic structure of thiourea is the best organic compound that can be used as the corrosion inhibitor. The aim of this study is to investigate the inhibitory efficiency of decanoyl thiourea derivatives that were synthesized as in Figure 1 via substitution and addition reaction using decanoyl chloride, ammonium thiocyanate and *o*, *m*, *p*-aminopyridine.

## Materials and Methods

### Synthesis of *N*-decanoyl-*N'*-2-pyridinethiourea

5 mmol of decanoyl chloride in acetone was mixed with an equamolar of ammonium thiocyanate and stirred for 10 minutes. Then, an equamolar of 2-aminopyridine in acetone was added to the solution. The solution was refluxed for 3 hours and then poured into a beaker containing ice blocks. The solid product formed was filtered and finally recrystallized by using acetonitrile. Yield 70.7% ; white solid. IR (KBr pellet, $cm^{-1}$): ν(N-H) 3356.2, ν(C=O) 1664.1, ν(C-N) 1160.4, ν(C=S) 768.8. $^1$H NMR δ 0.8 (s, 3H, $CH_3$); 1.2-1.4 (m, 2H, $CH_2$); 6.65-7.90 (m, Ar-H); 10.35, 9.1 (s, 2H, NH). $^{13}$C NMR δ 14.42 ($CH_3$); 22-31 ($CH_2$); 112-156 (aromatic ring); 171 (C=O); 177 (C=S). *Anal*. Calc. (%) For $C_{17}H_{25}N_3OS$: C, 62.50; H, 8.20; N, 9.14; S, 10.43. Found (%) : C, 61.27; H, 8.27; N, 9.07; S, 12.57.

### Synthesis of *N*-decanoyl-*N'*-3-pyridinethiourea

This compound was prepared as above from equamolar of decanoyl chloride, ammonium thiocyanate and 3-aminopyridine. Yield 73.4 % ; brick-red solid. IR (KBr pellet, $cm^{-1}$): ν(N-H) 3354.1, ν(C=O) 1663.2, ν(C-N) 1174.6, ν(C=S) 789.2. $^1$H NMR δ 0.85 (s, 3H, $CH_3$); 1.2-1.35 (m, 2H, $CH_2$); 6.65-8.00 (m, Ar-H); 10.25, 9.15 (s, 2H, NH). $^{13}$C NMR δ 14.41 ($CH_3$); 22-35 ($CH_2$); 126-149 (aromatic ring); 174 (C=O); 178 (C=S). *Anal*. Calc. (%) For $C_{17}H_{25}N_3OS$: C, 62.50; H, 8.20; N, 9.14; S, 10.43. Found (%): C, 62.78; H, 8.99; N, 9.88; S, 12.85.

### Synthesis of *N*-decanoyl-*N'*-4-pyridinethiourea

This compound was prepared as above from equamolar of decanoyl chloride, ammonium thiocyanate and 4-aminopyridine. Yield 74.8%; yellowish-white solid. IR (KBr pellet, $cm^{-1}$): ν(N-H) 3353.7, ν(C=O) 1669.4, ν(C-N) 1187.7, ν(C=S) 796.1. $^1$H NMR δ 0.85 (s, 3H, $CH_3$); 1.2-1.45 (m, 2H, $CH_2$); 6.65-7.95 (m, Ar-H); 10.25, 9.15 (s, 2H, NH). $^{13}$C NMR δ 14.41 ($CH_3$); 29-31 ($CH_2$); 110-165 (aromatic ring); 169 (C=O); 176 (C=S). *Anal*. Calc. (%) For $C_{17}H_{25}N_3OS$: C, 62.50; H, 8.20; N, 9.14; S, 10.43. Found (%): C, 61.45; H, 8.53; N, 9.37; S, 12.61.

.

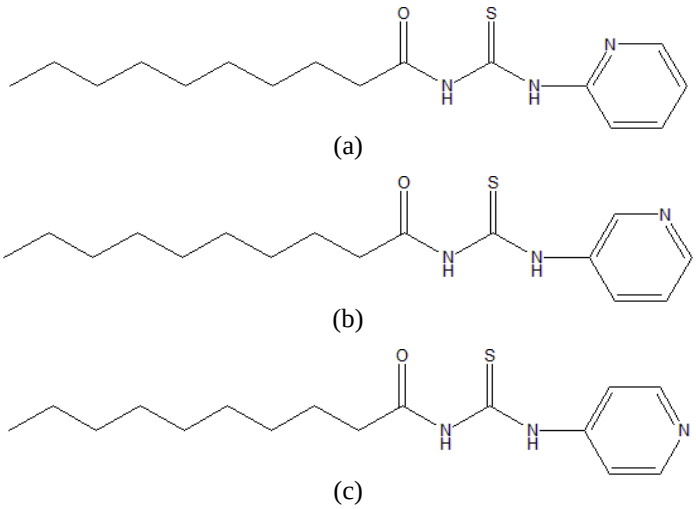



Figure 1: The chemical structure of the investigated compounds: (a) *N*-decanoyl-*N'*-2-pyridinethiourea (D1), (b) *N*-decanoyl-*N'*-3-pyridinethiourea (D2) and (c) *N*-decanoyl-*N'*-4-pyridinethiourea (D3)

**Weight loss method**

The mild steel coupons were used as the specimens with size of 2 x 2 cm. The coupons were abraded with emery paper and double washing using acetone and distilled water and finally dried at room temperature. The dried coupons were immersed in corrosion medium of 0.1 M $H_2SO_4$ solution for 3 days with and without inhibitors. The concentration of the inhibitors was varied from 1 x $10^{-5}$ M, 1 x $10^{-4}$ M to 1 x $10^{-3}$ M. The weight loss of the coupons was recorded.

**Linear polarization resistance technique**

This method was carried out in a three-electrode cells using AUTOLAB instrument equipped with NOVA software. A saturated calomel electrode (SCE) was used as a reference electrode and a graphite electrode as a counter. The working electrode was prepared by embedding a rod with mild steel coupon in epoxy resin, with an exposed surface area of 0.065 $cm^2$. The surfaces were polished with emery paper and washed with distilled water for electrochemical studies.

## Results and Discussion

**FTIR spectroscopy**

The D1, D2 and D3 compounds show important stretching in the FTIR spectra such as ν(C=S), ν(C=$O_{amide}$), ν(C-N) and ν(N-H) which can be observed around 700 $cm^{-1}$, 1600 $cm^{-1}$, 1200 $cm^{-1}$, and 3000 $cm^{-1}$. This observation agrees very well with the values previously reported in [10, 11]. Meanwhile, the functional group related to the pyridine structure was observed at a wavelength range from 1360 to 1250 $cm^{-1}$. The absorption bands for N-H in all three compounds were observed around 3300 $cm^{-1}$ which is supported by the previous study [10], stating that the assymetric and symmetric stretching vibration of the absorption band for N-H bond in thioamide group were found in a range above 3200 $cm^{-1}$. As for the carbonyl band, ν(C=O), it was clearly observed at 1660 $cm^{-1}$. This is due to the presence of aromatic group and the existence of intramolecular hydrogen bonding. For C-N, the absorption band was observed lower than 1200 $cm^{-1}$ because the presence of C-N bond in aromatic ring. The N atom in the ring becomes electron donating group which is also an activating group. It pushes the electron clouds to the ring and increases the electron density in the ring causing the absorption band to be shifted to lower frequency region. The C=S absorption band was observed at a range between 760 $cm^{-1}$ to 796 $cm^{-1}$. This band was in good agreement with the previous study [12].which this type of band was observed at 700 $cm^{-1}$. However, the reading of the C=S band spectra is a bit higher due to the aromatic group which is describe as large double bond character and has lower nucleophilic character of the sulphur atom compared to alkylthioureas.

**$^{1}$H NMR spectroscopy**

For all of the compounds, a resonance was observed at a range of 0.8-0.85 ppm as singlet. This is due to the presence of methyl protons substituent attached to the aliphatic structure of the compounds. As for the methylene, the resonance was observed in the range of 1.2-1.45 ppm. Since the methylene presences in the compounds are in long chains, the absorption observed becomes overlapped in an unresolvable group. The resonance for aromatic group for the compounds was observed at 6.65-7.8 ppm. It was a distinctive multiplet resonance because of the unresolved aromatic protons. As for the N-H, there are two resonances, one for the proton near to the C=O and the other is for the C=S resonance. For C=O, the resonance was observed at a range of 9.1-9.15 ppm. Meanwhile, for the C=S, the $^{1}$H shifts resonance was observed at 10.25-10.35 ppm. Theoretically, the resonance for this type of group should be observed at higher chemical shift which is 12 ppm, but in this experiment, it was observed at lower resonance because the presence of the aromatic group as the substituents in the thiourea compounds. The electrons on the aromatic ring deshield the hydrogen attached to N atom. Besides, the chemical shift of this group is variable. It is depends not only on the chemical environment in the molecule but also on the concentration, temperature and solvent.

**$^{13}$C NMR spectroscopy**

The resonance of methyl and methylene were observed at 14.4 ppm and 22.0 – 35.0 ppm respectively. For aromatic rings, the carbon resonance was found at a range of 110-165 ppm which is corresponding to the pyridine in the compounds. The C=O and C=S carbon resonance were clearly observed in between 169-174 ppm and 176-178 ppm. There is slightly difference in the carbon resonance because they are slightly deshielded due to the formation of

intramolecular hydrogen bonding, increasing electronegativity of oxygen and sulphur atoms and different environment and conformations.

**Weight loss method**

By using the weight loss method, the inhibition efficiency (IE%) of the three compounds synthesized and their respective corrosion rate has been calculated by using the formula equation (1) and (2) below and listed as in Table 1.

$$IE\ \% = \frac{(W_{blank} - W_{inhibitor})}{W_{blank}} \times 100\% \quad (1)$$

where, $W_{blank}$ is the weight loss of mild steel without inhibitor and $W_{inhibitor}$ is the weight loss of mild steel in with inhibitor.

$$\text{Corrosion rate} = \frac{\text{Weight loss of mild steel (g)}}{\text{Surface area of mild steel (cm}^2\text{) x Time (h)}} \quad (2)$$

Table 1: Parameters of mild steel corrosion activities in 0.1 M $H_2SO_4$ solution with and without inhibitors

| Compound | Concentration (M) | Average weight loss (g) | Inhibition efficiency (IE %) | Corrosion rate ($g/cm^{-2}\ h^{-1}$) |
|---|---|---|---|---|
| Blank | - | 0.1399 | - | $4.86 \times 10^{-4}$ |
| D1 | $1 \times 10^{-5}$ | 0.0222 | 84.13 | $7.71 \times 10^{-5}$ |
| | $1 \times 10^{-4}$ | 0.0199 | 85.78 | $6.91 \times 10^{-5}$ |
| | $1 \times 10^{-3}$ | 0.0215 | 84.63 | $7.47 \times 10^{-5}$ |
| D2 | $1 \times 10^{-5}$ | 0.0242 | 82.70 | $8.40 \times 10^{-5}$ |
| | $1 \times 10^{-4}$ | 0.0372 | 73.41 | $1.29 \times 10^{-4}$ |
| | $1 \times 10^{-3}$ | 0.0294 | 78.98 | $1.02 \times 10^{-4}$ |
| D3 | $1 \times 10^{-5}$ | 0.0267 | 80.91 | $9.27 \times 10^{-5}$ |
| | $1 \times 10^{-4}$ | 0.0198 | 85.84 | $6.87 \times 10^{-5}$ |
| | $1 \times 10^{-3}$ | 0.0249 | 82.20 | $8.65 \times 10^{-5}$ |

From Figure 2, it can be observed that all the compounds were able to decrease the corrosion process at any concentration of the inhibitors. This is because there are N, S and O atom present in the chemical structure of the inhibitor which acts as the center for the adsorption to the mild steel. It forms a film on the surface of mild steel via adsorption process by which it decreases the mild steel area from corrosion attack. Among the three concentrations tested for the studies, concentration of $1 \times 10^{-4}$ M shows the best activity for the compounds to inhibit corrosion. This is because that at this concentration, the activity of the synthesized compound to slow down the corrosion rate is optimum. Since the compounds that were synthesized have *ortho-*, *meta-* and *para-* positions of N atom in the pyridine structure, they show different inhibitory activity towards the corrosion of mild steel. N atom in the pyridine structure is an electron donating group and the presence of it in different position of an aromatic structure affects the reactivity of the compound towards the inhibition. The compounds that have higher inhibitory efficiency are both compound D1 and D3 at concentration of $1 \times 10^{-4}$ M in which the inhibitory efficiency is about 85%. This happens because o*rtho-* and *para-* positions are more favoured by N atom due to the N atom can donate electron easily to the system and therefore enhances the stability of the compound. Thus, these two positions of N atom enhance the adsorption of thiourea derivatives compound on the metal surface. On the other hand, the *meta-* position is not favoured by the N atom because this position is favoured to electron withdrawing group or deactivating group. This

is proved by inhibitory activity by compound D2 that shows it has the lowest IE % compared to the other two compounds.

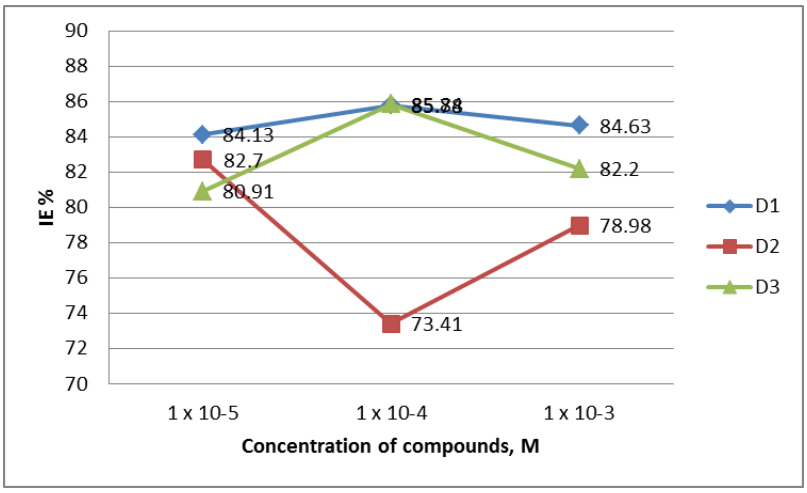



Figure 2: Graph of concentration of inhibitors versus inhibitory efficiency (IE%) by using weight loss method

**Linear polarization resistance technique**

This technique is used for further confirmation of the inhibitory efficiency at the best concentrations of the synthesized compounds. The corrosion of the mild steel was tested with the concentration of compound D1, D2 and D3 at 1 x $10^{-4}$ M in 0.1 M sulphuric acid. The linear polarization curves and its parameters such as current densities ($i_{corr}$), corrosion potential ($E_{corr}$), cathodic and anodic Tafel slopes (bc, ba) and inhibition efficiency (IE %) with the presence and absence of the inhibitors are given in Fig. 3 and Table 2 respectively.

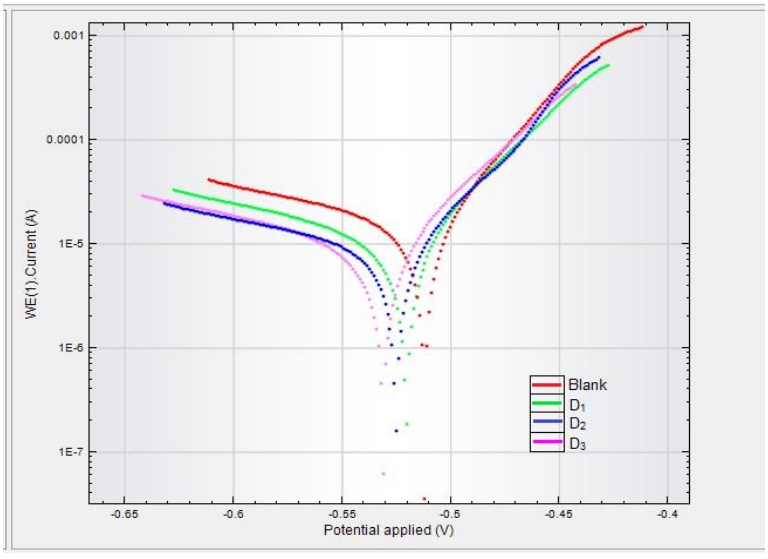



Figure 3: Polarization curves of 1 x $10^{-4}$ M D1, D2 and D3 in 0.1 M sulphuric acid

Table 2: Corrosion parameters for mild steel in 0.1 M sulphuric acid with and without inhibitor

| Compound | $i_{corr}$ ($\mu A\ cm^{-2}$) | $E_{corr}$ (V) | bc (V/dec) | ba (V/dec) | IE % |
|---|---|---|---|---|---|
| Blank | 386.75 | -513.69 | 60.47 | 1.22 | - |
| D1 | 314.91 | -519.91 | 71.90 | 3.46 | 18.6 |
| D2 | 271.80 | -526.40 | 68.11 | -1.47 | 29.7 |
| D3 | 139.46 | -532.43 | 47.51 | 240.08 | 63.9 |

From Table 2 the efficiency of inhibitors was calculated by using the formula (equation 3) below:

$$IE\% = \frac{(i_{corr(blank)} - i_{corr(inh)})}{I_{corr(blank)}} \times 100\% \quad (3)$$

where $i_{corr(blank)}$ is the current densities without inhibitor and $i_{corr(inh)}$ is the current densities with inhibitors either D1, D2 and D3. It was found that the $i_{corr}$ of mild steel in the presence of different type of inhibitor were smaller than without it. This implies that there is an adsorption on mild steel [13] and also the presence of aromatic group that have high electron density which suppressed the reactions [14]. The addition of the inhibitors also resulted in the shift of the corrosion potential ($E_{corr}$) to the left side as compared to corrosion potential without inhibitor. This shows that all inhibitors favour to cathodic reaction. From this technique, compound D3 has the highest IE% which is 63.9%. This results correlate with the weight loss method stating that D3 has is most potential corrosion inhibitor. Meanwhile, for compound D1 it does not shows that the results from LPR technique and weight loss method support each other as the compound to be the second best corrosion inhibitor. This may be due to external factor that affects the linear polarization resistance such as noise or any other factor that may interfere during the measurement.

## Conclusion

*N*-decanoyl-*N'*-2-pyridinethiourea, *N*-decanoyl-*N'*-3-pyridinethiourea and *N*-decanoyl-*N'*-4-pyridinethiourea were successfully synthesized and characterized. The *N*-decanoyl-*N'*-4-pyridinethioureawith N atom located at *para*-position gave the best corrosion inhibition at optimum concentration of 1 x $10^{-4}$ M corrosion inhibitors in 0.1 M sulphuric acid. All the obtained compounds are cathodic type of inhibitors.

## Acknowledgement

The authors are grateful to the Ministry of Higher Education of Malaysia for the research grant no. 600-RMI/RAGS 5/3 (3/2012) and the Faculty of Applied Sciences, Institute of Science and Universiti Teknologi MARA for providing research facilities.

## References

1. Bahrami M.J., Hosseini S.M.A. and Pilvar P. (2010). Experimental and theoretical investigation of organic compounds as inhibitors for mild steel corrosion in sulfuric acid medium, *Corrosion Science*, 5: 2793-2803.
2. Ameer M.A. and Fekry A.M. (2010). Inhibition effect of newly synthesized heterocyclic organic molecules on corrosion of steel in alkaline medium containing chloride. *International Journal of Hydrogen Energy*, 35: 11387-11396.
3. Amin M.A. and Ibrahim M.M. (2011). Corrosion and corrosion control of mild steel in concentrated solutions by a newly synthesized glycine derivative. *Corrosion Science*, 53: 873-885.
4. Benali O., Larabi L. and Harek Y. (2009). Adsorption and inhibitive corrosion properties of thiourea derivatives on cold rolled steel in 1M $HClO_4$ solutions. J Appl Electrochem 39: 769-778.

5. Shetty S.D. and Shetty P. (2008). Inhibition of mild steel corrosion in acid media by *N*-benzyl-*N'*-phenyl thiourea. *Indian Journal of Chemical Technology*, 15: 216-220.
6. Edrah S. and Hasan S.K. (2010). Studies on thiourea derivatives as corrosion inhibitor for aluminium in sodium hydroxide solution. *Journal of Applied Science Research*, 6: 1045-1049.
7. Shetty S.D. and Shetty P. 2008. Inhibition of mild steel corrosion in acid media by *N*-benzyl-*N'*-phenyl thiourea, *Indian Journal of Chemical Technology*, *15*, 216-220.
8. Shetty S.D., Shetty P. and Nayak V.S., (2006). The inhibition of N-furfuryl-N'- phenyl thiourea on the corrosion of mild steel in acid media, J. Serb. Chem. Soc., 71: 1073-1082.
9. Chauhan J.S. and Gupta D.K. (2009). Corrosion inhibition of titanium in acidic media containing fluoride with bixin, *E-Journal of Chemistry*, 6, 975-978.
10. Roslan R., Yusof M.S.M and Zin W.M.K.W.M. (2009). Synthesis and characterization studies of novel thiourea amino acid derivatives. *Prosiding Seminar Kimia Bersama UKM-ITB VIII,* Univsersiti Kebangsaan Malaysia, Bangi, 9-11 Jun.
11. Yang W., Zhou W. and Zhang Z. (2007). Structural and spectroscopic study on *N*-2-fluorobenzoyl-*N′*-4-methoxyphenylthiourea. *Journal of Molecular Structure,* 828: 46-53.
12. Yusof M.S.M., Jusoh R.H., Khairul W.M. and Yamin B.M. (2010). Synthesis and characterization of *N*-(3,4-dichlorophenyl)-*N'*-(2,3 and 4-methylbenzoyl) thiourea derivatives. *Journal of Molecular Structure*, 975, 280-284.
13. Fouda A.E.E. and Hussein A. (2012). Role of some phenylthiourea derivatives as corrosion inhibitors for carbon steel in HCl solution. *Journal of the Korean Chemical Society*, 56(2), 264 – 273.
14. Wang J., Cao C., Chen J., Zhang M., Ye G., Lin H. (1995). Anodic desorption of inhibitors. *Journal Chinese Society Corrosion Protection*, 15: 241-248.

The Malaysian Journal of ANALYTICAL SCIENCES ISSN 1394-2506

# THE EFFECT OF TEMPERATURE ON MILD STEEL CORROSION IN 1 M HCl BY SCHIFF BASES

## (Kesan Suhu Terhadap Kakisan Keluli Lembut Dalam 1 M HCl oleh Ligan Bes Schiff)

Nor Zakiah Nor Hashim[1]* and Karimah Kassim[1, 2]

[1]*Faculty of Applied Sciences,*
[2]*Institute of Sciences,*
*Universiti Teknologi MARA,40450, Shah Alam, Selangor, Malaysia*

**Corresponding author: norzakiah21@gmail.com*

**Abstract**

The temperature effects in the range of 25 to 55°C on the inhibition efficiency of three Schiff bases which were (*E*)-$N^1$-benzylidene-$N^4$-phenylbenzene-1,4-diamine (K1), *N*-[(*E*)-4-chlorobenzylidene-$N^{'}$-phenylbenzene-1,4-diamine (K2), and *N*-[(*E*)-4-methoxybenzylidene-$N^{'}$-phenylbenzene-1,4-diamine (K3) against mild steel in 1 M hydrochloric acid (HCl) solution were studied using polarization method. Thermodynamic adsorption parameter suggests that the inhibitors under study were mixed type inhibitors dominated by anodic reaction and it was found that from all of the three inhibitors, K2 having the highest corrosion inhibition efficiency.

**Keywords:** 1 M HCl, mild steel, Schiff base, temperature, corrosion

**Abstrak**

Kesan suhu dalam lingkungan 25 hingga 55°C kepada kecekapan pengekangan tiga ligan bes Schiff iaitu (*E*)-$N^1$-benzylidene-$N^4$-phenylbenzene-1,4-diamine (K1), *N*-[(*E*)-4-chlorobenzylidene-$N^{'}$-phenylbenzene-1,4-diamine (K2), dan *N*-[(*E*)-4-methoxybenzylidene-$N^{'}$-phenylbenzene-1,4-diamine (K3) terhadap keluli lembut dalam 1 M asid hidroklorik (HCl) telah dikaji dengan menggunakan kaedah polarisasi. Parameter penjerapan termodinamik mencadangkan bahawa perencat di bawah kajian ialah perencat jenis bercampur dikuasai oleh reaksi anodik dan didapati bahawa dari ketiga-tiga perencat, K2 mempunyai tertinggi kecekapan kakisan pengekangan.

**Kata kunci:** 1 M HCl, keluli lembut, bes Schiff, suhu, kakisan

### Introduction

In industrial applications such as acid pickling, the metals are immersed in an appropriate acid media to eliminate unwanted rust and mill scale. After the scales are removed, the surface of the metal is exposed for dissolution of metal due to the attack of the aggressive media. To overcome this problem organic inhibitors are added into the acid pickling bath generally hydrochloric acid solution at elevated temperature to inhibit the corrosion of metal [1]. The acid inhibitors available are mostly organic compounds containing heteroatoms of N, O and S which effectively retarding the dissolution of metal in an acid solution by adsorption on the surface of metal [2]. Schiff base known as a nitrogen bearer (C=N bond) inhibitor was chosen due to the planarity and lone pair of electrons in its molecular structure therefore increase the adsorption on the active sites of metal surface as reported to by several authors [3,4]. These inhibitors have to be chemically stable and provide high protection to the metal from the corrosive media even under high temperature condition. The aim of this work is to study the temperature effect of studied Schiff bases (Table 1) as organic inhibitor in retarding the corrosion of mild steel in 1 M HCl. The investigated Schiff bases are selected based on the analogous molecular area and any distinction in the inhibiting properties attributed mainly due to effect of substituent in the molecular structure of the organic compound.

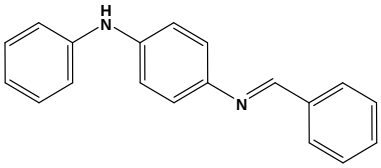
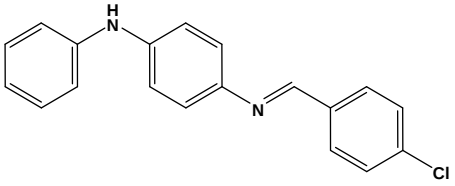
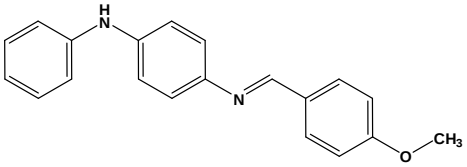
## Materials and Methods

Schiff bases as in Table 1 were synthesized using the established method [5] and structure confirmation was done by elemental analysis, infrared spectroscopy (IR), and nuclear magnetic resonance spectroscopy (NMR). Electrode for polarization measurement was square shaped mild steel specimen embedded in an epoxy resin having exposed surface area of 0.049 $cm^2$. The specimen was mechanically polished using different grades of silica carbide paper then polished to mirror finish using diamond paste. It was degreased with ethanol and cleaned using distilled water and lastly dried before introducing it to the acidic solution. The test was carried out at stagnant open air condition in a 100 ml volume cell using a thermostat controlled waterbath and experiment was conducted at 25, 35, 45 and 55$^oC$. In the conventional three electrode cell system, platinum rod as counter electrode, Gamry instruments silver-silver chloride ($Ag|AgCl|Cl^-$) as reference electrode and mild steel as working electrode were employed. The measurement was done using Gamry 600$^{TM}$ potentiostat/galvanostat potential connected to a personal computer. For polarization method, the working electrode was immersed completely in the acid solution at open circuit potential ($E_{ocp}$) in 30 min. The curves were obtained in the potential sweeping rate of 1 mV/sec from the corrosion potential ($E_{corr}$) in the cathodic followed by anodic direction. Inhibition efficiency ($\eta_{pol}$%) were calculated using equation (1) [6].

$$\eta_{pol}\% = \frac{i_{corr} - i'_{corr}}{i_{corr}} x100 \quad (1)$$

where $i_{corr}$ and $i'_{corr}$ are the corrosion current densities without and with addition of inhibitors, respectively.

Table 1: Schiff base under investigation

| Inhibitor | Structure | Abbreviation | Molar mass (g/mol) |
|---|---|---|---|
| (*E*)-$N^1$-benzylidene-$N^4$-phenylbenzene-1,4-diamine |  | K1 | 272.34 |
| *N*-[(*E*)-4-chlorobenzylidene]-$N'$-phenylbenzene-1,4-diamine |  | K2 | 306.79 |
| *N*-[(*E*)-4-methoxybenzylidene]-$N'$-phenylbenzene-1,4-diamine |  | K3 | 302.37 |

## Results and Discussion

The change in the corrosion rate of mild steel in 1 M HCl at different temperatures was investigated in the presence of 2.0 mM inhibitor and absence of inhibitor. The corrosion parameters extracted from polarization measurements at different temperatures are shown as in Table 2 while the polarization curves are demonstrated in Figure 1. In Figure 1, it is apparent that by increasing the temperature of the solution, the values of $i_{corr}$ in the absence and presence of corrosion inhibitors are increased (Table 2). The increases in $i_{corr}$ indicate increase in hydrogen gas evolution (cathodic reaction) and also iron corrosion (anodic reaction) in the corrosive solution [7]. Furthermore, the corrosion potential ($E_{corr}$) in the inhibited solution shifted to anodic region at higher temperature in comparison to the 1 M HCl. This finding suggests inhibitors are mixed type predominantly anodic.

From Table 2, most of the studied compounds demonstrated decreased in the inhibition efficiency ($\eta_{pol}$%) at higher temperature apart from K2. The results for $\eta_{pol}$% differ slightly at certain temperature for each inhibitor, but sustain the efficiency to protect mild steel from corroded in the acid solution at highest temperature studied compared to the blank of 1 M HCl. At 25$^{o}$C, the highest $\eta_{pol}$% is as follows: K2 > K1 > K3. The K1 inhibitor $\eta_{pol}$% at 25$^{o}$C is 95.1 %, but the value slightly increased at 35$^{o}$C and starting to decrease again until 84.3% at 55$^{o}$C. For K2, the $\eta_{pol}$ % slightly increases up to 97.2% at the highest temperature examined. As for K3, $\eta_{pol}$% illustrate decrease in value but sudden slight increase at 95.0% during 45$^{o}$C then starting to decrease until 81.8% at the highest temperature tested. Thus at 55$^{o}$C only K2 have high $\eta_{pol}$%, and the order for inhibition efficiency at the temperature is as follows: K2 > K1 > K3. The reason is that the effect of temperature in the presence of inhibitor at the metal interface reaction is highly complex since modification at the mild steel surface example as etching at higher rate, inhibitors desorption process at the surface and decomposition at elevated temperature [8].

Table 2: Corrosion parameter values from polarization measurements for mild steel in 1 M HCl at inhibitors optimum concentration (2.0 mM) in different temperatures

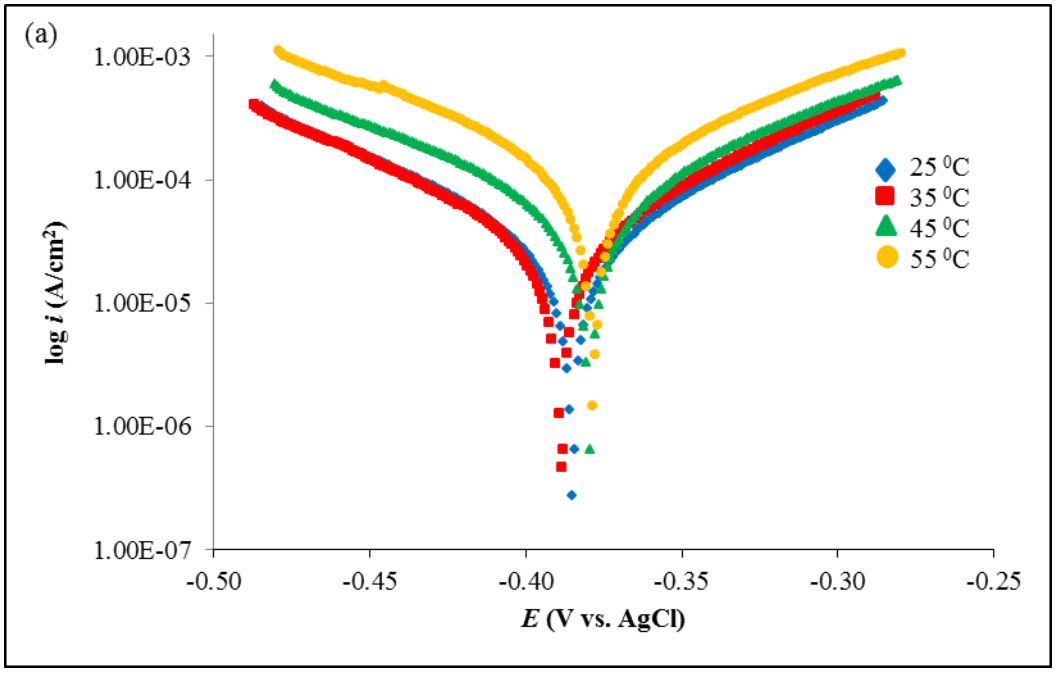
| **Compound** | **Temperature ($^{o}$C)** | **$i_{corr}$ (μA/cm$^2$)** | **$E_{corr}$ (-mV)** | **$\eta_{pol}$ %** |
|---|---|---|---|---|
| 1 M HCl | 25 | 706.1 | 385 | - |
| | 35 | 767.3 | 389 | - |
| | 45 | 1359 | 380 | - |
| | 55 | 1724 | 378 | - |
| 2.0 mM K1 | 25 | 34.63 | 373 | 95.1 |
| | 35 | 38.78 | 343 | 95.0 |
| | 45 | 122.9 | 359 | 91.0 |
| | 55 | 271.4 | 367 | 84.3 |
| 2.0 mM K2 | 25 | 20.86 | 354 | 96.0 |
| | 35 | 22.14 | 343 | 97.1 |
| | 45 | 41.80 | 341 | 96.9 |
| | 55 | 48.71 | 357 | 97.2 |
| 2.0 mM K3 | 25 | 42.61 | 354 | 94.0 |
| | 35 | 45.71 | 387 | 94.0 |
| | 45 | 67.55 | 356 | 95.0 |
| | 55 | 314.3 | 374 | 81.8 |

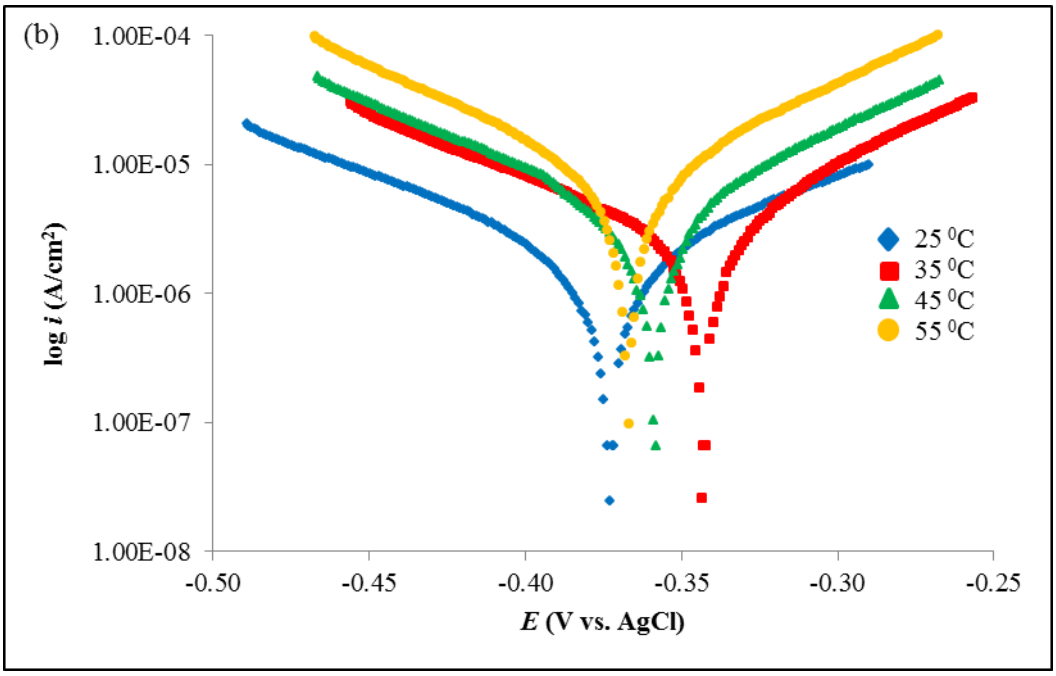
According to the Arrhenius equation to express the activation energy ($E_a$) of corrosion process of mild steel in the blank solution of 1 M HCl and presence of 2.0 mM inhibitors, the calculation involve is as following equation (2) [8]:

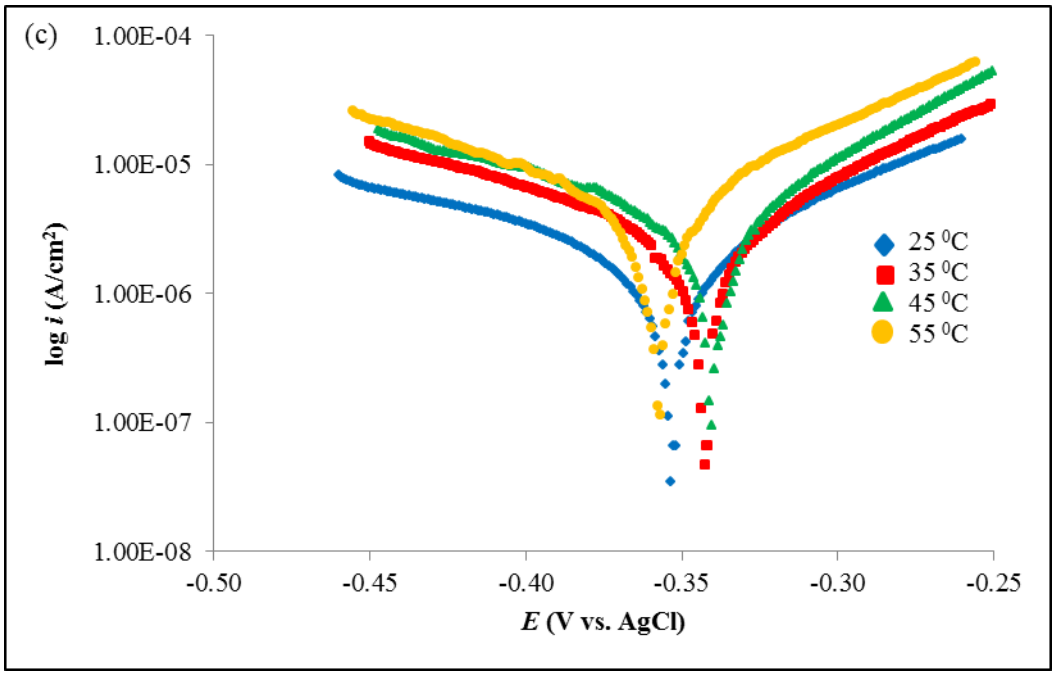
$$i_{corr} = k \exp\left(-\frac{E_a}{RT}\right) \quad (2)$$

where $E_a$ is the activation energy in the corrosion of iron reaction in kJ mol$^{-1}$, $k$ is the pre-exponential constant, $R$ is the gas constant and $T$ is the temperature in Kelvin (K). using the logarithm form equation (3) [9]:

$$\log i_{corr} = \log k - \frac{E_a}{RT} \quad (3)$$




(b)
1.00E-04
1.00E-05
1.00E-06
1.00E-07
1.00E-08
log i (A/cm²)
-0.50
-0.45
-0.40
-0.35
-0.30
-0.25
E (V vs. AgCl)
25 °C
35 °C
45 °C
55 °C


(c)
1.00E-04
1.00E-05
1.00E-06
1.00E-07
1.00E-08
log i (A/cm²)
-0.50
-0.45
-0.40
-0.35
-0.30
-0.25
E (V vs. AgCl)
25 °C
35 °C
45 °C
55 °C

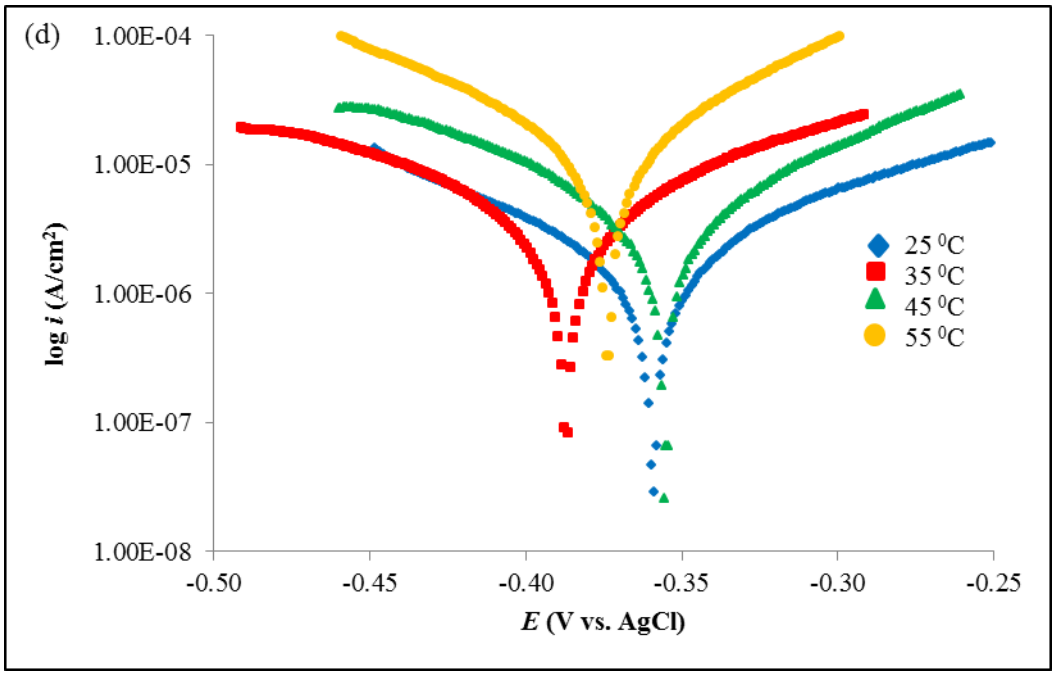



Figure 1: Potentiodynamic curves of mild steel in (a) 1 M HCl, (b) 1 M HCl + 2.0 mM of K1, (c) 1 M HCl + 2.0 mM of K2 and (d) 1 M HCl + 2.0 mM of K3 at different temperatures.

In Figure 2, it demonstrates the Arrhenius plot of mild steel in 1 M HCl as previously discussed in the absence and with addition of 2.0 mM Schiff base inhibitors. The graph of log $i_{corr}$ vs. 1/T in this figure presents linear line having slope of ($-E_a$/R). The calculated $E_a$ presented as in Table 3 demonstrate the values of $E_a$ for K2 is lower compared to the 1 M HCl while for K1 and K3 are higher than the blank solution. The inhibition efficiencies correlate to the activation energies for organic inhibitors are classified into three categories which also related to the temperature effects [10]:

1. Inhibitors in whose presence the inhibition efficiency increases with temperature increased while the value of $E_a$ for the corrosion process is lower than that obtained in the uninhibited solution.
2. Inhibitors whose inhibition efficiency does not change with temperature variation. The apparent activation energy does not change with the presence and absence inhibitors.
3. Inhibitors in whose presence the inhibition efficiency decreases with temperature increased while the value of $E_a$ for the corrosion process is higher than that obtained in the uninhibited solution.

The increase of inhibition properties along with the increase in temperature indicates chemisorption type of adsorption [11] while the decrease in inhibition efficiencies suggests the physical adsorption on the surface of metal [12]. Generally, presence of π electron in the benzene ring and C=N bond in the studied planar Schiff base structure facilitates the adsorption interaction of organic inhibitor as electron donator to the metal surface since iron acts as electron acceptor in the chemisorption bond [13]. Thus, it can be recommended that K2 ligand form strong chemisorptive bond even at 55$^{o}$C hence provide better protection on mild steel surface compared to the other studied Schiff base ligands since K2 have –Cl substitution at the para-position in phenyl ring and the –Cl assist N in formation of this type of bond to the iron surface [14]. The adsorption mechanism for inhibitors depends on the functional group available in that structure molecule, because certain groups adsorbed at different degree [15].

Table 3. Thermodynamic parameters for adsorption of studied inhibitors on the mild steel surface in 1 M HCl

| **Inhibitor** | $E_a$ **(kJ/mol)** |
|---|---|
| 1 M HCl | 26.31 |
| K1 | 59.11 |
| K2 | 25.82 |
| K3 | 51.07 |

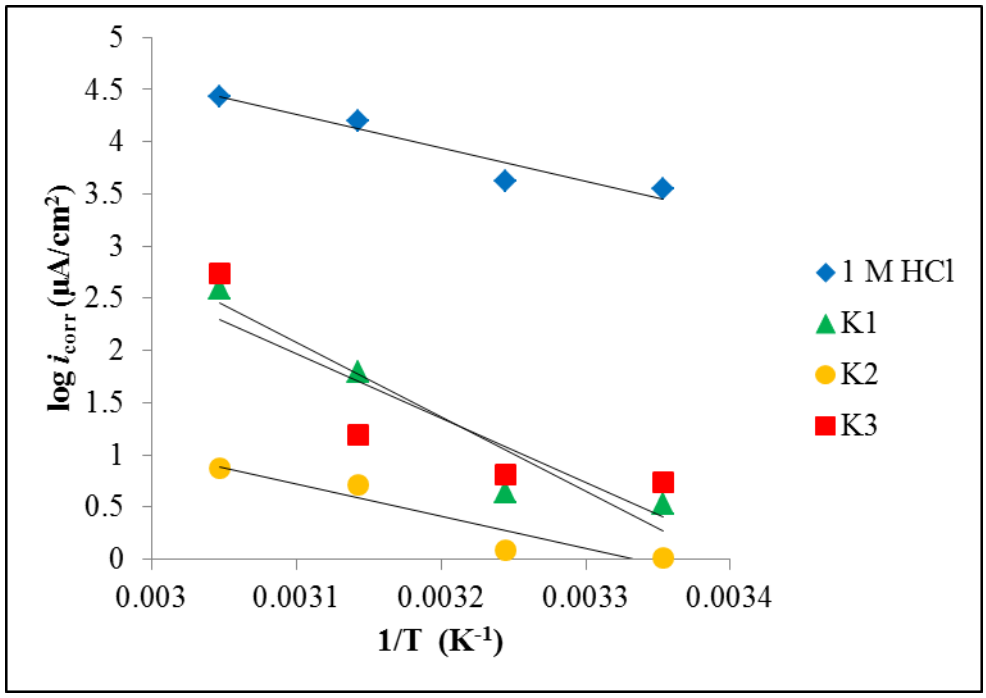



Figure 2: Arrhenius plot obtained from mild steel current density in 1 M HCl

The K1 and K3 organic inhibitors having $E_a$ higher than that found in 1 M HCl suggesting the type of adsorption formed between inhibitor and iron predominantly is physisorption. In an acidic solution, some Schiff bases are protonated and exist in cationic form along with the molecular Schiff base in the solution. The already adsorbed chloride ions from the electrolyte at the iron surface causes the cationic form of the inhibitors of K1 and K3 adsorbed via electrostatic interaction. Generally, methoxy ($-OCH_3$) substituent as in K3 is known to have high inhibition efficiency since it is an electron donating group due to the lone pair of oxygen atom increases the electron density of aromatic ring thus π electrons readily adsorbed to the surface of metal [16,17]. However, the adverse effect from this group it is bulkier compared to K1 and causes steric hindrance thus easily desorp from the iron

surface at highest investigated temperature [18]. This leads to the increase of corrosion of iron due to the attack of aggressive solution to the exposed sites on its surface.

## Conclusion

Studied Schiff base inhibitors are effective corrosion inhibitors for mild steel in the test solution in the presence of optimum concentration of inhibitors compared to the blank solution of 1 M HCl even at elevated temperature. The inhibiting properties of K2 is due to chemisorption of the Schiff base molecule on the iron surface while K1 and K3 physical adsorption is affected by surface charge interaction between adsorbed chloride and the protonated form of inhibitors. The adsorption of these Schiff bases on the iron surfaces contribute to the high inhibition efficiencies of studied inhibitors in 1 M HCl. From the temperature effect, the activation energy parameter is calculated.

## Acknowledgement

Authors would like to thank Ministry of Higher Education Malaysia for the Fundamental Research Grant Scheme (FRGS) in granting financial assistance (600-RMI/FRGS 5/3 (51/2013). The authors are as well thankful to the Faculty of Applied Sciences for financial support as well as Institute of Sciences, Universiti Teknologi MARA in providing synthesis and corrosion researches facilities.

## References

1. Haleem, S.M.A.E., Wanees, S.A., Aal, E.E.A.E. and Farouk, A. (2013). Factors affecting the corrosion behaviour of aluminium in acid solutions. I. Nitrogen and/or sulphur-containing organic compounds as corrosion inhibitors for Al in HCl solutions. *Corrosion Science* 68: 1-13.
2. Goulart, C.M., Souza, A.E., Huitle, C.A.M., Rodrigues, C.J.F., Maciel, M.A.M. and Echevarria, A. (2013). Experimental and theoretical evaluation of semicarbazones and thiosemicarbazones as organic corrosion inhibitors. *Corrosion Science* 67: 281-291.
3. Ju, H., Kai, Z.P. and Li,Y. 2008. Aminic nitrogen-bearing polydentate Schiff base compounds as corrosion inhibitors for iron in acidic media: A quantum chemical calculation. *Corrosion Science* 50: 865-871.
4. Mallaiya, K., Subramaniam, R., Srikandan, S.S., Gowri, S., Rajasekaran, N. and Selvaraj, A. (2011). Electrochemical characterization of the protective film formed by the unsymmetrical Schiff's base on the mild steel surface in acid media. *Electrochimica Acta* 56: 3857-3863.
5. Hashim, N.Z.N., Kassim, K. and Yamin, B.M. (2010). *N*-[(*E*)-4-Chlorobenzylidene]-*N*′-phenylbenzene-1,4-diamine. *Acta Crystallographica* E66: o2039.
6. Hassan, H.H., Abdelghani, E. and Amin, M.A. (2007). Inhibition of mild steel corrosion in hydrochloric acid solution by triazole derivatives Part I. Polarization and EIS studies. *Electrochimica Acta* 52: 6359-6366.
7. Amin, M.A., Ahmed, M.A., Arida, H.A., Arslan, T., Saracoglu, M. and Kandermirli, F. (2011). Monitoring corrosion and corrosion control of iron in HCl by non-ionic surfactants of the TRITON- X series- Part II. Temperature effect, activation energies and thermodynamics of adsorption. *Corrosion Science* 53: 540-548.
8. Bentiss, F., Traisnel, M., Gengembre, L. and Lagrenée. (1999). A new triazole derivative as inhibitor of the acid corrosion of mild steel: electrochemical studies, weight loss determination, SEM and XPS. *Applied Surface Science* 152: 237-249.
9. Aljourani, J. Raeissi, K. and Golozar, M.A. (2009). Benzimidazole and its derivatives as corrosion inhibitors for mild steel in 1M HCl solution. *Corrosion Science* 51: 1836-1843.
10. Radovici, O. (1965). *Proceedings of the Second European Symposium on Corrosion Inhibitors*. Ferrara, p 178.
11. Hasan, B.O. and Sadek, S.A. (2014). The effect of temperature and hydrodynamics on carbon steel corrosion and its inhibition in oxygenated acid-salt solution, *Journal of Industrial and Engineering Chemistry* 20: 297-307.
12. Vračar, L.M. and Dražić, D.M. (2002). Adsorption and corrosion inhibitive properties of some organic molecules on iron electrode in sulfuric acid. *Corrosion Science* 44:1669-1680.
13. Sorkhabi, H.A. Shaabani, B. and Seifzadeh, D. (2005). Corrosion inhibition of mild steel by some schiff base compounds in hydrochloric acid. *Applied Surface Science* 239: 154-164.
14. Antonijevic, M.M. and Petrovic, M.B. Copper Corrosion Inhibitors. A review. *International Journal of Electrochemical Science* 3: 1-28.
15. Obot, I.B., Egbedi, N.O.O. and Umoren, S.A. 2009. Antifungal drugs as corrosion inhibitors for aluminium in 0.1 M HCl. Corrosion Science 51:1868-1875.

16. Emregül, K.C. and Hayvali, M. 2006. Studies on the effect of a newly synthesized Schiff base compound from phenazone and vanillin on the corrosion of steel in 2 M HCl. *Corrosion Science* 48: 797-812.
17. Nasser, A.J.A. and Sathiq, M.A. (2012). Comparative study of *N*-[(4-methoxyphenyl) (morpholin-4-yl)methyl]acetamide (MMPA) and *N*-[morpholin-4 yl(phenyl)methyl]acetamide (MPA) as corrosion inhibitors for mild steel in sulfuric acid solution. *Arabian Journal of Chemistry*. http://dx.doi.org/10.1016/j.arabjc.2012.07.032
18. Kandias, D., Bundjali, B. and Wahyuningrum, D. 2011. Curcuminoid compounds isolated from curcuma domestica val. as corrosion inhibitor towards carbon steel in 1 % NaCl solution. *Sains Malaysiana* 40: 1013-1018.

The Malaysian Journal of ANALYTICAL SCIENCES ISSN 1394-2506

# LEAD (Pb) AND ZINC (Zn) CONCENTRATIONS IN MARINE GASTROPOD *STROMBUS CANARIUM* IN JOHOR COASTAL AREAS

## (Kepekatan Plumbum (Pb) dan Zink (Zn) di dalam Gastropoda Laut *Strombus canarium* di Kawasan Perairan Johor)

Shaikhah Sabri, Mohd Ismid Mohd Said, Shamila Azman*

*Faculty of Civil Engineering,*
*Universiti Teknologi Malaysia, 81310 UTM Skudai, Johor, Malaysia*

**Corresponding author: shamila@utm.my*

**Abstract**

*Strombus canarium* is a popular food source with high commercial value in southern part of Peninsular Malaysia. As a deposit feeder, *Strombus canarium* can accumulate pollutants especially heavy metals in their system. Study on this species was conducted at Teluk Sengat and Mersing, Johor where samples of seawater and *Strombus canarium* were collected during spring low tides around 0 to 0.2 meters. Lead (Pb) and zinc (Zn) concentrations were investigated to determine pollution status in the area. Samples from Teluk Sengat showed that Zn has higher concentration in both water and *S. canarium* with 0.055 mg/L and 20.257 mg/kg wet weight respectively. However the concentrations were within permissible limit of Malaysia Marine Water Quality Criteria and Standard (MMWQS). In contrast, Pb concentration at Teluk Sengat exceeded the MMWQS and its concentration in soft tissues of *S. canarium* also exceeded the permissible limit recommended by Food and Agriculture Organisation (0.5 mg/kg wet weight) and World Health Organisation (0.2 mg/kg wet weight).

**Keywords**: Johor coastal areas, lead, zinc, *Strombus canarium*

**Abstrak**

*Strombus canarium* adalah sumber makanan yang popular dan mempunyai nilai komersil yang tinggi di bahagian selatan Semenanjung Malaysia. Sebagai pemakan mendapan, *Strombus canarium* dapat mengumpulkan bahan cemar terutama logam berat di dalam sistem mereka. Kajian terhadap spesies ini telah dijalankan di Teluk Sengat dan Mersing, Johor di mana sampel air laut dan *Strombus canarium* diambil ketika air surut sekitar 0 hingga 0.2 meter. Kepekatan plumbum (Pb) and zink (Zn) disiasat untuk penentuan status pencemaran kawasan kajian. Sampel air dan *S. canarium* dari Teluk Sengat mengandungi kepekatan Zn paling tinggi iaitu masing-masing 0.055 mg/L dan 20.257 mg/kg berat basah. Walaubagaimanapun, kepekatan berada di dalam had yang ditetapkan oleh *Malaysia Marine Water Quality Standard and Criteria* (MMWQS). Sebaliknya, kepekatan Pb di Teluk Sengat melebihi MMWQS dan kepekatan di dalam tisu lembut *S. canarium* juga melebihi had yang dibenarkan oleh *Food and Agriculture Organisation* dan *World Health Organisation* (0.5 mg/kg berat basah) dan *World Health Organisation* (0.2 mg/kg berat basah).

**Kata kunci**: perairan Johor, plumbum, zinc, *Strombus canarium*

## Introduction

Metals such as zinc, copper and iron are important element and nutritionally essential to living organisms. Some metals also received more attention for example lead, cadmium and tin which is referred as heavy metals due to their high toxicity and effect on environment. Generally metals enter the environment via natural weathering, erosion and volcanic activity [1]. However, their occurrence and distribution especially in coastal ecosystem are often related to anthropogenic activities. The anthropogenic sources of metals normally come from industrial and municipal waste products, urban and agricultural runoff, sediments eroded from catchments and atmospheric deposition [2]. In fact, these pollutants have capability to accumulate in the food chain and could impose adverse effects in marine organisms [3]. Humans who occupy top level of the food chain and consume metal-contaminated seafood may face greater risk of health problem. Previous studies have shown that progressive and irreversible

accumulation of Pb in human bodies can impair the functions of renal and liver [4]. Long-term intake of Zn (150 – 2000 mg/day) will induce sideroblastic anemia, leukopenia and hypochromic microcytic anemia [5].

The present study focus on marine gastropod, *Strombus canarium* which is widely distributed in the coastal waters of Johor and highly associated with sandy mud bottom at seagrass areas [6]. *Strombus canarium* or locally known as 'siput gonggong' is a popular seafood delicacy and have high demand in the market. However, there is limited information regarding metal concentration of this gastropod at coastal area of Johor. *Strombus canarium* are deposit feeder therefore they can accumulate metals from water and sediment. Currently, their habitats are highly exposed to coastal contamination induced by anthropogenic factors, which can also lead to their depletion [7]. Therefore, metal assessment on *Strombus canarium* is important since it could pose a serious threat to human health risk for individuals who consume them.

This study reports on the concentration of Pb and Zn in soft tissues of *Strombus canarium*, seawater and sediment samples from Teluk Sengat and Pulau Setindan, Mersing. The statistical difference of metals concentration between these sites was also investigated since the areas have different type of human interference. Water quality data were compared to Malaysia Marine Water Quality Criteria and Standard (MMWQCS) and World Health Organisation (WHO), whereas Pb and Zn concentrations in the soft tissues of *Strombus canarium* were compared to Food and Agriculture Organisation (FAO) and WHO. Sediments collected at the study areas were also classified according to sediment criteria proposed by U. S. Environmental Protection Agency (U.S.EPA) and New York Sediment Criteria.

## Materials and Methods

Samples of seawater, sediment and *Strombus canarium* were collected in 2011 from two stations located at Johor coastal area. The first sampling station is Teluk Sengat (N 01$^{o}$ 32' 48.3'', E 104$^{o}$ 01' 57.7") located at the estuary of Johor River on the eastern part of Johor Straits. Teluk Sengat is situated approximately 1.30 km to the north of Senai-Desaru Highway. It is a sub-tidal area covered mainly with muddy substrates and dominated by seagrass *Halophila ovalis*. The second station is Pulau Setindan, Mersing (N 02$^{o}$ 30' 11.7", E 103$^{o}$ 50' 26.1") located at the eastern coast of Johor. The main economic activities in Mersing are tourism, agricultural and fishing.

All sampling and experimental apparatus were soaked in 10% nitric acid for 24 hours and double rinsed with Milli-Q (18 MΩ) water. The seawater was sampled using polyethylene bottles (1 L) approximately 10 cm below the water surface. The water samples were filtered using Whatman syringe filter (0.2µm) then preserved with concentrated nitric acid and later kept at 4$^{o}$C prior to analysis. Twenty *Strombus* specimens were collected from each station which were immediately stored in a cool box and later transported to the laboratory for metal analysis. The average specimen shells used for analysis from Teluk Sengat were from 55 to 66 mm and weight 21 to 39 g whereas samples from Mersing were 50 to 56 mm of shell length and 28 to 35 g of weight.

Soft *Strombus* tissues were dissected by removing the specimen body from its shell using sterilized stainless steel equipment. The digestion procedures were carried out according to U.S EPA method 3050 where soft tissues were oven dried at 105°C for 24 hours. After drying, 1 g of samples were weighed and transferred to SMA model ARM6 block digester sample vessels followed by addition of 20 mL of 98% nitric acid (AnaR grade, Merck). The samples were then digested at 95$^{o}$C for 2 hours. The digested samples were later diluted with 100 mL of Milli-Q deionised water and filtered into clean bottles using Whatman syringe filter (0.2 µm). Pb and Zn concentration were then measured by inductively coupled plasma mass spectrometry (ICP-MS) using 6100 ELAN instrument (Perkin Elmer). Metal concentrations in seawater is reported in milligram per liter (mg/L), metal in sediment in microgram per gram dry weight (µg/g) and metal in soft tissues of *Strombus* specimen is reported as milligram per kilogram (mg/kg) dry weight.

The dry weight is then converted to wet weight using a conversion factor of 0.3 for comparison purposes with guidelines recommended by FAO [8] and WHO [9]. The conversion factor used is based on assumption that 70% of mollusk's soft tissue weight is water [10]. Student t-Test with 95% confidence limits was also used to determine the statistical significance of metal concentrations between the stations.

## Results and Discussion

### Metal concentration in seawater

Result of water quality at Teluk Sengat and Mersing is tabulated in Table 1. Water temperature at Teluk Sengat and Mersing were recorded at 29.23 $^{o}$C and 29.80 $^{o}$C respectively. Salinity concentration at Teluk Sengat (22.24 ppt) was lower than Mersing waters (30.0 ppt). Teluk Sengat waters have lower value of salinity since the samples were taken during rainy period and the station located near an estuary. Variable salinity values of estuary are often influenced by tides, weather and other environmental factors [2]. The DO values (4.41 and 5.52 mg/L) at both sampling stations were above the criteria recommended by MMWQS (4 mg/L), whereas pH (7.72 to 8.12) were within the range recommended by WHO (6.5-8.5).

Table 1: Result of water quality at Teluk Sengat and Mersing

| Location | Parameter | | | | | |
|---|---|---|---|---|---|---|
| | **Temp ($^{o}$C)** | **Salinity (ppt)** | **pH** | **DO (mg/L)** | **Pb (mg/L)** | **Zn (mg/L)** |
| Teluk Sengat | 29.80 | 22.24 | 7.72 | 4.41 | 0.032 | 0.055 |
| Mersing | 29.23 | 30.3 | 8.12 | 5.52 | 0.013 | 0.017 |
| MMWQCS | - | - | - | 4 | 0.0085 | 0.05 |
| WHO | - | - | 6.5 - 8.5 | - | 0.01 | 5 |

MMWQCS – Malaysian Marine Water Quality Criteria Standard

The concentration of Pb and Zn in Teluk Sengat water were found to be significantly higher ($p < 0.05$) than Mersing at 0.032 and 0.055 mg/L respectively. The metals concentration also exceeded MMWQC for Class E where the class is applicable to assess water quality at mangrove and estuarine areas. Based on the findings, seawater at Teluk Sengat is polluted by Pb which can cause adverse effect to living organisms.

Higher metals concentration in samples from Teluk Sengat compared to Mersing is expected since the location of Teluk Sengat is adjacent to industrial, urbanisation and port area. It has been reported that intensive dredging, reclamation and shipping activities at the eastern coast of Johor Straits has led to the enrichment of metals in the aquatic environment [11]. However, the results obtained from the study is lower compared to previous studies reported by [12] and [13] in the water column of Johor Straits and Mersing respectively.

### Metal concentration in sediment

Table 2 shows the concentration of metals in marine sediment from each sampling stations. The metals concentration at Teluk Sengat was significantly higher ($p < 0.05$) than metals concentration at Mersing. Both stations recorded high concentration of Zn than Pb, however according to U. S. EPA guidelines; the sediment at Teluk Sengat is classified as slightly polluted with Pb at 45.572 µg/g dry weight. Studies conducted on sediment from Pulau Tekong located approximately 20 km to the south of Teluk Sengat by Cuong et al. [14] shows lower concentration of Pb (29.8 µg/g dry weight) and Zn (49.8 µg/g dry weight) compared with the current study.

Table 2: Mean metal concentration in sediment comparison with EPA sediment quality guidelines and New York Sediment Criteria

| Station/EPA Guidelines and New York Sediment Criteria | Pb(µg/g dry weight) | Zn(µg/g dry weight) |
|---|---|---|
| Teluk Sengat | 45.572 | 54.491 |
| Mersing | 13.624 | 22.530 |
| **EPA Sediment quality proposed** | | |
| Non-polluted | < 40 | < 90 |
| Slightly polluted | 40 - 60 | 90 – 200 |
| Severely polluted | > 60 | > 200 |
| **New York sediment criteria** | | |
| Lowest effect range | 31 | 120 |
| Severe effect range | 250 | 220 |

Previous studies reported enrichment of Pb in sediment along Johor Straits were due to combustion of fuel by vehicles and boat [15, 16]. Yap et al. [17] suggested that Zn contamination in Johor Straits is contributed by mussel processing factory at Kampung Sungai Melayu. Zn was released to the coastal water by direct discharge of water used in the boiling process. The boiling method was used to facilitate the removing of soft tissue from the shell for packaging and freezing purposes. Ong and Kamaruzzaman [18] reported that the present of Pb concentration in sediment at eastern coast of Johor was resulted of natural erosion of earth's surface.

**Metal concentration in soft tissue of *Strombus canarium***

Mean concentration of Pb and Zn in soft tissues of *Strombus canarium* is shown in Table 3. *Strombus canarium* from both sampling stations have higher accumulation of Zn compared to Pb since Zn is one of the essential element required by aquatic organism [19]. McManus and Newton [20] also reported that seafood contained high level of Zn than other food.

Pb and Zn concentrations were lower compared to the permissible limits recommended by FAO and WHO except for Pb in samples from Teluk Sengat. Pb concentration (2.701 µg/g wet weight) exceeded the limit of FAO (1.5 µg/g wet weight) and WHO (0.2 µg/g wet weight). Therefore, consumption of *Strombus canarium* should be controlled since 25% of total Pb intake will remain in human blood and could cause neurotoxic effects [21].

Table 3: Metal concentration in *Strombus canarium*'s soft tissues and guidelines recommended by FAO and WHO

| Station/Food Guidelines | Metal (µg/g wet weight) | |
|---|---|---|
| | Pb | Zn |
| Teluk Sengat | 2.701 | 20.257 |
| Mersing | 0.095 | 12.253 |
| Food and Agriculture Organization (FAO) | 0.5 | 150 |
| World Health Organization (WHO) | 0.2 | 500 |

The results obtained in the present study are comparable to previous studies by [10, 22, 23]. Rizo et al. [22] reported that Pb and Zn concentration in soft tissues of *Strombus gigas* in Cuba were in the range of 0.2 to 2.3 µg/g wet weight and 20.4 to 31.1 µg/g wet weight respectively. The study suggested high value of Pb in *Strombus gigas* was caused by contaminated effluent from sewage, industrial and agricultural. [10] found high values of Pb (2.778 µg/g wet weight) and Zn (30 µg/g wet weight) in *S. canarium* sampled from Pulau Bangka, Indonesia compared to the present study.

## Conclusion

The present study showed that seawater and sediment at Teluk Sengat contain high concentration of Zn and Pb compared with samples from Mersing. Generally, Zn concentrations were higher in seawater, sediment and soft tissues of *Strombus canarium* at both sampling areas. However, Pb concentrations at Teluk Sengat exceeded the permissible limit by Malaysia Marine Water Quality Criteria and Standard and can be classified as slightly polluted based on U. S. EPA sediment criteria. Moreover, the concentration of Pb in soft tissues of *Strombus canarium* from Teluk Sengat could pose toxicological risk to human health since the concentration exceeded the maximum limit recommended by FAO and WHO.

## Acknowledgement

This work was supported by Universiti Teknologi Malaysia Research University Grant Scheme (Vote Number: 06J10) and Ministry of Higher Education (MyBrain15).

## References

1. Valavanidis, A. & Vlachogianni, T. (2010). Metal Pollution in Ecosystems. Ecotoxicology Studies and Risk Assessment in the Marine Environment. Science Advances on Environment. *Toxicology & Ecotoxicology Issues*, 1-14.
2. Thompson, K. C., Wadhia, K. & Loibner, A. P. (2005). Environmental Toxicity Testing, Blackwell Publishing Ltd.
3. Gupta, S. & Singh, J. (2011). Evaluation of Mollusc as Sensitive Indicator of Pollution in Aquatic System: A Review. *The IIOAB Journal*, 2 (1): 49-57.
4. Anim, A.K., Ahialey, E.K., Duodu, G.O., Ackah, M. & Bentil, N.O. (2011). Accumulation Profile of Heavy Metals in Fish Samples from Nsawam, along the Densu River, Ghana. *Research Journal of Environmental and Earth Science*, 3(1): 56-60.
5. Simon-Hettich, B., Wibbertmann, A., Wagner, D., Tomaska, L. & Malcolm, H. (2001). Zinc. (Environmental Health Criteria; 221).World Health Organization. Geneva.
6. Cob, Z. C., Arshad, A., Bujang, J.S. & Ghaffar, M. A (2009). Age, Growth, Mortality and Population Structure of *Strombus canarium* (Gastropoda: Strombidae): Variations in Male and Female Sub-Populations. *Journal of Applied Sciences*, 9 (18):3287-3297.
7. Chim, C. K., Neo, M.L. & Loh, K.S. (2009). The Status in Singapore of *Strombus (Dolomena) Marginatus Sowerbyorum* Visser & Man In'T Veld, 2005 (Mollusca: Gastropoda: Strombidae). *Nature in Singapore*, 2: 379-384.
8. FAO (Food and Agriculture Organization). (1983). Compilation of Legal Limits for Hazardous Substances in Fish and Fishery Products. FAO Fish Circ. 464, 5-100.
9. WHO (World Health Organization) (1989). Heavy Metals – Environmental Aspect. Environment Health Criteria. No. 85. Geneva, Switzerland.
10. Arifin, Z. (2011). Heavy Metals Concentrations in Water, Sediment and Biota in Kelabat Bay, Bangka Island. *Jurnal Ilmu dan Teknologi Kelautan Tropika*, 3(1): 104-114.
11. Zulkifli, S. Z., Ismail, A., Yusuff, F. M., Arai, T. & Miyazaki, N. (2010). Johor Strait as a Hotspot for Trace Elements Contamination in Peninsular Malaysia, *Bulletin Environmental Contamination Toxicology*, 84: 568 – 57.
12. Hadibarata, T., Abdullah, F., Yusoff, A. R. M., Ismail, R., Azman, S. & Adnan, N. (2012). Correlation Study between Land Use, Water Quality and Heavy Metals (Cd, Pb and Zn) Content in Water and Green Lipped Mussels *Perna viridis* (Linnaeus.) at the Johor Straits, *Water Air Soil Pollution*, 223: 3125-3136

13. Bashir, F. A., Shuhaimi-Othman, M. & Mazlan, A. G. (2012). Evaluation of Trace Metal Levels in Tissues of Two Commercial Fish Species in Kapar and Mersing Coastal Waters, Peninsular Malaysia. *Journal of Environmental and Public Health*, 1-10.
14. Cuong, D. T., Karuppiah, S. & Obbard, J. P. (2008). Distribution of Heavy Metals in the Dissolved and Suspended Phase of the Sea-surface Microlayer, Seawater Column and in Sediments of Singapore's Coastal Environment. *Environmental Monitoring Assessment*, 138: 255–272.
15. Wood, A. K.H., Ahmad, Z., Shazili, N.A.M., Yaakob, R. & Carpenter, R. (1997). Geochemistry of Sediments in Johor Strait between Malaysia and Singapore. *Continental Shelf Research*, 17(10): 1207- 1228.
16. Kanakaraju, D., Jios, C. & Long, S. M. (2008). Heavy Metal Concentrations in the Razor Clams (Solen spp) from Muara Tebas, Sarawak. *Malaysian Journal of Analytical Sciences*, 12 (1). 53-58
17. Yap, C. K., Rashiq, M. & Edward, F. B. (2012). Is a Mussel Processing Site a Point Source of Zn Contamination? Evidence of Zn Remobilization from Boiled Mussel, *Perna viridis. Pertanika of Journal Tropical Agricultural Science*, 35 (2): 199-207.
18. Ong, M.C. & Kamaruzzaman, B.Y. (2009). An Assessment of Metals (Pb and Cu) Contamination in Bottom Sediment from South China Sea Coastal Waters, Malaysia. *American Journal of Applied Sciences*, 6(7): 1416-1421.
19. Abdullah, M. H., Sidi, J. & Aris, A.Z. (2007). Heavy Metals (Cd, Cu, Cr and Zn) in *Meretrix Roding*, Water and Sediments from Estuaries in Sabah, North Borneo. *International Journal of Environmental & Science Education*, 2(3): 69-74.
20. McManus, A. & Newton, W. (2011). Seafood, Nutrition and Human Health: A Synopsis of the Nutritional Benefits of Consuming Seafood. Centre of Excellence Science, Seafood & Health, Curtin Health Innovation Research Institute, Curtin University of Technology, Perth.
21. Hounkpatin, A. S.Y., Edorh, A. P., Salifou, S., Gnandi, K., Koumolou, L., Agbandji, L., Aissi, K. A., Gouissi, M. & Boko, M. (2012). Assessment of Exposure Risk to Lead and Cadmium via Fish Consumption in the Lacuscrian Village of Ganvie in Benin Republic. *Journal of Environmental Chemistry and Ecotoxicology*, 4(1): 1-10.
22. Rizo, O. D., Reumont, S. O., Fuente, J. V., Arado, O. D., Pino, N. L., Rodriguez, K. D., Lopez, J. O. A., Rudnikas A. G. & Carballo, G. A. (2010). Copper, Zinc and Lead Bioaccumulation in Marine Snail, *Strombus gigas*, from Guacanayabo Gulf, Cuba, *Bulletin of Environmental Contamination Toxicology*, 85: 330-333.
23. Nasution, S. & Siska, M. (2011). Kandungan Logam Berat Timbale (Pb) pada Sedimen dan Siput *Strombus canarium* di Perairan Pantai Pulau Bintan. *Jurnal Ilmu Linkungan*, 5(2): 82-93.

The Malaysian Journal of ANALYTICAL SCIENCES ISSN 1394-2506

# KAJIAN AWALAN TERHADAP KINETIK PENGEKSTRAKAN PEPEJAL-CECAIR DAN ANALISIS KOMPONEN BIO-AKTIF DAUN *Hibiscus rosa-sinensis*

## (Preliminary Study on Kinetic Solid-Liquid Extraction and Bio-Active Components Analysis of *Hibiscus rosa-sinensis* Leaves)

Saiful Irwan Zubairi*, Haizulizam Suradi, Syazwan Aizad Abdul Mutalib, Zetty Shafiqa Othman, Norshahida Bustaman, Wan Ros Maryana Wan Musa

*Pusat Pengajian Sains Kimia & Teknologi Makanan, Fakulti Sains & Teknologi, Universiti Kebangsaan Malaysia, 43600 UKM Bangi, Selangor Darul Ehsan, Malaysia*

**Corresponding author: saiful-z@ukm.my*

**Abstrak**

*Hibiscus rosa-sinensis* atau nama tradisinya 'pokok bunga raya' adalah sejenis tumbuhan bunga hiasan yang kerap ditanam di negara yang beriklim subtropika. Tumbuhanini kerap digunakan dalam penyediaan perubatan tradisional kerana ia mempunyai ciri-ciri farmakologi yang mampu merawat beberapa masalah kesihatan. Tumbuhan ini mengandungi beberapa bahan bio-aktif dan nutrient penting yang banyak terutama sekali pada bahagian bunga dan daun. Salah satu bahan bio-aktif tersebut adalah β-sitosterol yang banyak terdapat di dalam ekstrak daunnya. Ekstrak air daun bunga raya mengeluarkan lendir atau mukus yang pekat ia banyak digunakan dalam menurukan suhu badan yang tinggi akibat demam panas (antipiretik). Oleh yang demikian, objektif utama kajian ini dijalankan adalah untuk mengenalpasti keberhasilan maksimum dan masa pengekstrakan menyeluruh ekstrak lendir daun segar dan kering menggunakan model matematik Peleq. Di samping itu, beberapa analisis susulan turut dijalankan seperti analisis kualitatif kehadiran bahan bio-aktif menggunakan kaedah kromatografi cecair prestasi tinggi (HPLC) dan penentuan kumpulan berfungsi melalui kaedah tranformasi fourier inframerah (FTIR). Ujikaji sifat fizikal hasil ekstrak dijalankan iaitu analisis tahap keasidan (pH) dan kelikatan bagihasil ekstrak lendir terhadap tegasan ricihan (*shear stress*). Keputusan kajian mendapati sampel daun kering mempunyai kepekatan hasil ekstrak yang tinggi walaupun masa pengekstrakan menyeluruh yang agak perlahan berbanding daun segar ($p$<0.05). Berdasarkan kepada analisis HPLC, kehadiran bahan bio-aktif utama β-sitosterol dilihat hanya wujud pada sampel daun segar. Ketiadaan β-sitosterol di dalam sampel pengekstrakan daun kering mungkin disebabkan oleh kehilangan beberapa bahan bio-aktif penting yang bersifat surfaktan (membantu pengeskstrakan β-sitosterol) akibat daripada degradasi termal semasa proses pengeringan atau ianya terdegradasi akibat daripada suhu yang tinggi semasa proses pengeringan pra-rawatan. Pembuktian lanjutan melalui analisis FTIR menunjukkan komposisi puncak penyerapan yang sama bagi kedua-dua jenis sampel daun dengan nilai puncak penyerapan tertinggi iaitu ikatan O-H dikenalpasti. Ini membuktikan bahawa kandungan β-sitosterol di dalam kedua-dua jenis sampel tersebut adalah terlalu sedikit dan komposisi fitosterol yang lain dilihat mendominasi serta mempengaruhi kehadiran β-sitosterol di dalam hasil ekstrak. Sementara itu, ujian sifat fizikal terhadap ekstrak kedua-dua jenis daun turut dijalankan bagi pembuktian kesan pengeringan terhadap komponen bahan bio-aktif penting. Nilai keasidan yang tinggi bagi sampel daun segar dilihat berpunca daripada kebolehdapatan semua komponen bahan bio-aktif manakala bagi ekstrak daun kering, nilai pH yang agak *neutral* dilihat berpunca daripada penguraian beberapa bahan fitokimia yang bersifat asidik dan sensitif kepada haba.

**Kata kunci**: *Hibiscus rosa-sinensis*, β-sitosterol, pengekstrakan pepejal-cecair, lendir, kelikatan, FTIR, HPLC

**Abstract**

*Hibiscus rosa-sinensis* or commonly known as '*Hibiscus*' is a kind of decorative flowers which often grown in a subtropical countries. This plant is often used in the preparation of traditional medicine because of its pharmacological properties that are capable of treating number of health problems. The plant contains several essential bio-active substances and nutrients especially in its flowers and leaves. One of the bioactive substances is β-sitosterol which is abundant in the leaf crude extract. *Hibiscus* leaves water extract yielded mucilage which is widely used in lowering high body temperature due to fever (antipyretic). Therefore, the main objective of this paper was to determine the maximum concentration of mucilage and time of exhaustive

extraction from fresh and dried leaves using a Peleq's mathematical model. Moreover, several analyses were conducted such as qualitative analysis to determine the presence of bioactive substances using high performance liquid chromatography (HPLC) and determination of functional groups by means of fourier transform infrared method (FTIR). Physical properties of the extracts were evaluated to determine its acididity and viscosity of the mucilage with respect to different shear stress. The result show that the extract of dried *Hibiscus*leaves exhibited high in its concentrations even though the achieved exhaustive extraction was relatively slow as compared to fresh leaves ($p$<0.05). Based on the HPLC analysis, the main bio-active substances of β-sitosterol was only existed in fresh leaves samples. The absence of β-sitosterol in dried leaves extract was caused by the loss of otherimportant bio-active substances which possess surfactantcapability, due to thermal degradation of drying process or the component itself was deteriorated during the pre-preparation drying process. Furthermore, the FTIR analysis shows that the same composition of theabsorption peaks for both extracts with the highest absorption of O-H bonds was observed. This proves that the content of β-sitosterol in both extracts was too small and the composition of other phytosterols was observed to dominate and influence the availability of β-sitosterol in the crude extract. Meanwhile, physical properties analysis of the both extracts was carried to show the effect of drying process on the observed bio-active components. The high acidity of the fresh leaf extract was attributed to the presence of all bio-active ingredients. Meanwhile for the dried leaf extract, a close neutral pH value was observed due to the bio-active decomposition which is acidic in nature and sensitive to heat.

**Keywords**: *Hibiscus rosa-sinensis,* β-sitosterol, solid-liquid extraction, mucilage, viscosity, FTIR, HPLC

## Pengenalan

Bunga raya atau nama saintifiknya *Hibiscus rosa sinensis* merupakan sejenis tumbuhan hiasan yang tergolong dalam famili *Malvaceae*. Ia juga dikenali sebagai Japa dalam bahasa Sanskrit, Jasum (Hindi), Dasananu (Telugu) dan Sembaruthi (Tamil) [1]. Karakteristik pokok bunga raya ini dapat dilihat daripada segi saiz dan warna bunga serta daunnya. Bunga yang berwarna merah mempunyai saiz yang sangat besar dan mampu membesar sehingga 15 cm panjang. Warna daunnya pula boleh menjadi hijau gelap atau hijau muda dengan tompok pudar dan sisi daun bergerigi bagi tujuan memerangkap lembapan udara [2]. Ciri penting yang ada pada pokok ini yang tiada pada kebanyakan pokok lain adalah daunnya yang mengandungi ekstrak cecair mentah bermukus atau berlendir yang berwarna legap. Kewujudan lendir tersebut adalah disebabkan oleh penghasilan dari sel-sel lendir di dalam korteks yang hanya boleh diekstrak setelah ianya dikisar [3].

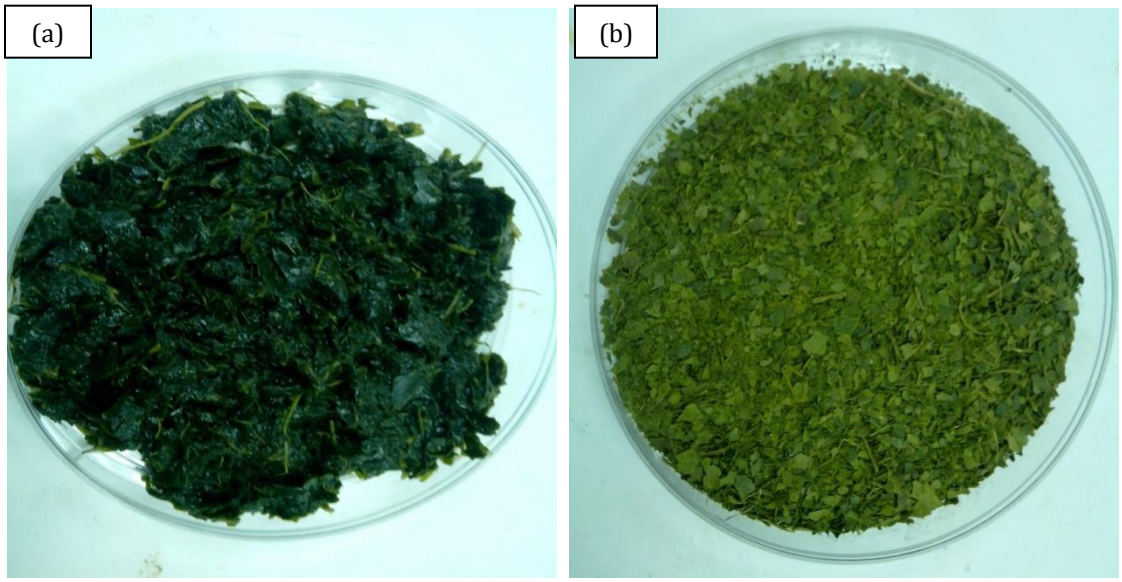
Di samping itu, daun dan pucuknya mengandungi beberapa sebatian fitokimia penting seperti β-sitosterol, stigmasterol, asetat taraxeril dan tiga sebatian saiklopropan [4]. Salah satu daripada bahan bio-aktif penting tersebut yang berperanan penting dalam aktiviti positif biologi adalah β-sitosterol [5]. β-Sitosterol adalah sterol tumbuhan semula jadi. Ia mempunyai struktur yang hampir sama dengan kolesterol. Bahan bio-aktif ini dikatakan mempunyai sifat aktiviti antipiretik yang tinggi dan berfungsi bagi mengurangkan suhu badan yang tinggi ketika demam panas [6]. Selain daripada itu, daun bunga raya kerap kali digunakan dalam perubatan tradisional sebagai *emolien* untuk merawat kesan terbakar, penyakit kulit, sembelit, sakit kepala, kekejangan semasa haid, memudahkan kelahiran anak, penawar racun, ubat sakit mata dan inflamasi [7,8]. Terdapat juga kajian lepas yang membuktikan ekstrak daun bunga raya ini mampu mengawal tahap kolestrol di dalam badan melalui penyediaan minuman *tea* dan ia dilihat berpunca daripada kewujudan komponen-komponen antioksidan yang tinggi [9]. Ini dibuktikan lagi dengan potensi ekstraknya yang mampu memberikan kesan perlindungan peringkat awalan di dalam pembentukan sesuatu tumor (kanser) [10].

Oleh yang demikian, kajian ini dijalankan bagi mengenalpasti tahap keberhasilan menyeluruh lendir dan analisis bahan bio-aktif yang wujud di dalam ekstrak daun bunga raya. Sehingga kini, tiada kajian dijalankan bagi mengenalpasti tahap keberhasilan maksimum ekstrak mentah dan masa optimum bagi mendapatkan nilai kepekatan ekstrak yang tinggi. Secara umumnya, penghasilan maksimum ekstrak mentah adalah berkadar terus dengan kewujudan dan keberhasilan bahan bio-aktif yang tinggi. Bagi mendapatkan parameter tersebut, model matematik Peleg digunakan dengan menjalankan proses pengekstrakan pepejal-cecair (larut resap) [11,12] menggunakan pelarut air dan aseton sehingga terbentuknya keluk fasa logaritma dan *plateau*. Seterusnya, kewujudan/pengesahan bahan bio-aktif dan analisis beberapa ciri fizikal seperti pH dan kelikatan ekstrak mentah daun bunga raya turut dijalankan sepanjang kajian ini.

## Bahan dan Kaedah

**Penyediaan sampel**

Daun bunga raya diperolehi dari kawasan persekitaran kampus Universiti Kebangsaan Malaysia (UKM), Bangi. Daun tersebut dibasuh menggunakan air paip bagi membuang segala kotoran seperti habuk, serangga dan serpihan halus. Terdapat dua jenis sampel daun pra-persediaan pengekstrakan iaitu daun segar dan daun kering. Untuk daun segar, apabila selesai dibasuh, ia akan dilap menggunakan tisu atau kain bersih untuk menghilangkan dan mengeringkan sisa air basuhan pada daun [13]. Manakala untuk mendapatkan daun kering, apabila selesai dibasuh, ia akan diletakkan di atas dulang aluminium dan dikeringkan dalam ketuhar pengering pada suhu 60 $^{o}$C selama 5 hingga 6 jam. Kemudian, kedua-dua jenis daun tersebut dikisar halus dengan menggunakan pengisar elektrik. Rajah 1 menunjukkan hasil kisaran bagi kedua-dua jenis penyediaan daun. Kisaran halus tersebut disimpan di dalam botol kedap udara sebelum proses pengekstrakan dijalankan.




Rajah 1: Hasil kisaran sampel daun bunga raya (a) segar dan (b) kering.

**Penyediaan pengekstrakan pepejal-cecair**

Sebanyak 20 g daun bunga raya segar dan kering masing-masing dimasukkan ke dalam kelalang kon 250 ml berisi 200 ml air suling (nisbah pepejal kepada pelarut - 1:10, w/v) dan ditutup menggunakan kain kapas. Sebelum proses pengekstrakan dijalankan, kedua-dua sampel daun tersebut dibungkus dan dibalut dengan kain muslin (dibentuk sebagai uncang teh atau bunjut sup) bagi mengelakkan pencampuran kisaran halus semasa proses penimbangan hasil ekstrak dijalankan. Kelalang kon yang mengandungi sampel daun kering dan segar bagi pelarut air suling dan aseton dimasukkan ke dalam pengacau inkubator pada suhu 27 $^{o}$C dengan kelajuan 100 rpm. Semua sampel diekstrak selama 24 jam.

Seterusnya, bagi setiap selang 1 jam, 1 ml hasil ekstrak diambil dengan menggunakan mikropipet dan ia ditimbang dengan menggunakan penimbang analitik elektronik bagi mendapatkan kepekatan hasil ekstrak (mg/ml). Langkah ini diulang sehingga ke jam 24 bagi semua sampel ujikaji. Setiap satu set sampel daun segar dan daun kering bagi pelarut air suling dan aseton mempunyai tiga replikasi ujikaji ($n$ = 3) sebelumpembacaan pengiraan hasil kepekatan ekstrak maksimum dan masa pengekstrakan menyeluruh melalui model matematik Peleg diperolehi.

**Model Peleg: Penentuan hasil pengekstrakan lendir maksimum dan masa pengekstrakan menyeluruh**

Proses pengekstrakan fitokimia secara optimum dan perkaitan keberhasilan optimum dengan ciri-ciri biokimianya seperti antioksidan perlu dilakukan bagi mendapatkan parameter-parameter pemprosesan yang optimum bagi penjimatan masa dan kos operasi [14,15]. Oleh yang demikian, model matematik diperlukan sebagai alat kejuruteraan yang berguna yang mana ia akan memudahkan proses pengoptimuman, simulasi, reka bentuk dan kawalan proses dan menyumbang kepada penjimatan penggunaan tenaga, masa dan pelarut. Terdapat beberapa model matematik yang boleh digunakan dalam penentuan nilai keberhasilan dan masa optimum sesuatu proses pengekstrakan *batch* pepejal-cecair seperti model hukum kedua 'Fick'. Namun begitu, model matematik tersebut terlalu kompleks dan memerlukan pengiraan pemboleubah yang banyak. Disebabkan oleh permasalahan tersebut, terdapat satu model matematik yang mudah dan pantas iaitu model Peleg bukan eksponen dua parameter [16]. Model peleg ini melibatkan dua pemalar K iaitu $K_1$ ialah nilai pintasan-*y*, dan $K_2$ ialah nilai kecerunan melalui transformasi keluk kinetik fasa logaritma dan *plateau* ke graf *linear* masa (t)/kepekatan (ρ) versus masa (t) [17]. Daripada hasil pengiraan model Peleg ini, maklumat kadarproses pengekstrakan yang dijalankan ($1/K_1$), hasil kepekatan maksimum ekstrak ($1/K_2$) dan masa penghasilan ekstrak secara menyeluruh ($K_2/K_1$) dapat diperolehi secara tepat.

Di dalam model Peleg, keluk kinetik pengekstrakan (kepekatan (ρ) melawan masa (t)) mempunyai bentuk yang sama dengan keluk penyerapan (kandungan lembapan melawan masa). Oleh yang demikian, di dalam proses pengekstrakan pepejal-cecair, konsep model matematik tersebut diterangkan melalui persamaan (1):

$$\rho\,(t) = \rho_o + t/[K_1 + K_2 \,.\, t] \tag{1}$$

di mana ρ ialah kepekatan hasil ekstrak (g/ml) pada masa t (min), $\rho_o$ ialah kepekatan hasil ekstrak pada masa t = 0 (g/ml), $K_1$ adalah pemalar Peleg 1 (min.mg/ml) dan $K_2$ adalah pemalar kapasiti Peleg 2 (ml/g). Kepekatan hasil ekstrak ($\rho_o$) pada masa t = 0 dianggap sebagai 0, maka persamaan (2) selepas proses penglinearisasi matematik adalah seperti berikut:

$$t/[\,\rho\,(t) - \rho_o] = K_1 + K_2 \,.\, t \tag{2}$$

Pemalar Peleg 1 ($K_1$) berkaitan dengan kadarpengekstrakan ($B_o$) pada masa tertentu proses ($t=t_o$) ditunjukkan di dalam persamaan (3):

$$B_o = 1/K_1 \tag{3}$$

Pemalar tetap Peleg, $K_2$ mempunyai perkaitan dengan hasil ekstrak maksimum. Bila $t \rightarrow \infty$ (keseimbangan pengekstrakan dicapai di antara bahan terlarut di dalam sesuatu sampel dengan isipadu pukal hasil ekstrak), persamaan (4) memberikan hubungan antara keseimbangan kepekatanhasil ekstrak dan pemalar $K_2$:

$$\rho\; t \rightarrow \infty = \rho_e = 1/K_2 \tag{4}$$

**Pengesanan bahan bioaktif bagi ekstrak daun segar dan kering**

Analisis kaedah kromatografi cecair berprestasi tinggi (HPLC) ini dilakukan untuk menentukan kehadiran beberapa bahan bio-aktif terutama sekali β-sitosterol yang terdapat di dalam ekstrak daun bunga raya. Daripada kromatogram yang diperolehi, kewujudan bahan bio-aktif β-sitosterol ditentukan secara kualitatif iaitu membandingkan masa penahanan dan profil kromotogram daripada beberapa kajian lepas [5,18]. Kromotogram kajian lepas digunakan sebagai perbandingan awalan disebabkan oleh faktor kesukaran untuk mendapatkan bahan bio-aktif piawai fitosterol tersebut. Tiada pengiraan kepekatan (mg/ml) dijalankan bagi semua bahan bio-aktif yang diperolehi.

Parameter analisis HPLC bagi pengenalpastian awalan profil bahan bio-aktif ekstrak daun bunga raya adalah seperti berikut: (1) Fasa bergerak disediakan dengan komposisi yang terdiri daripada 20% air dinyah ion dan 80% metanol. (2) Kadar alir fasa bergerak adalah 1 ml/min pada suhu kolum 25 °C. (3) Kolum Chromolith RP-18 (Inertsil 7 ODS-3 4.6 mm ID, 250 mm, Merck®) digunakan mengikut prosedurYe et al. (2010) [5]. (4) Jarak gelombang pengesan UV ditetapkan pada 254 nm. Fasa bergerak dibiarkan mengalir di dalam kolum selama 30 min sehingga garis dasar

(*baseline*) yang stabil diperolehi. Sebanyak 20 µl sampel disuntikkan dan bacaan kromatografi dijalankan sehingga semua puncak terhasil pada masa operasi yang ditetapkan (30 min).

**Kaedah transformasifourier inframerah (FTIR)**

Spektrofotometer Perkin Elmer 2000, model GX digunakan untuk mengetahui kewujudan kumpulan berfungsi yang terdapat di dalam hasil ekstrak air daunbunga raya. Bilangan pengimbas penambah yang digunakan ialah 16 dengan resolusi 4 $cm^{-1}$. Prosedur Keppler dan Rauch (2000) [19] digunakan bagi analisis kuantitatif dan kualitatif di mana sampel diletakkan di antara dua plat sel KBr (*potassium bromide*) dan ditutup dengan kemas agar tiada kontaminasi. Pengrekodan spektrum dilakukan pada kawasan serapan atau julat imbasan adalah di antara 4000-400 $cm^{-1}$. Pada kawasan ini terdapat serapan kumpulan berfungsi selain daripada kawasan cap jari yang memberikan ciri-ciri penting kepada sesuatu sebatian. Hanya sampel daun segar dan kering bagi ekstrak air sahaja yang digunakan untuk analisis FTIR dan spektrum yang diperolehi akan dirujuk kembali kepada maklumat profil bahan bio-aktif yang diperolehi daripada analisis HPLC.

**Ujian sifat fizikal hasil ekstrak**

***Analisis pH***

Nilai bacaan pH diambil dengan menggunakan pH meter (HI 991401-02) *Hanna Instrument* USA. Sampel yang diuji adalah bagi ekstrak air daun segar dan kering pada suhu bilik 28 $^{o}$C. Pembacaan pH dilakukan sebanyak 3 kali bagi mendapatkan purata nilai pembacaan ± *standard error* ($n$ = 3).

***Kelikatan hasil ekstrak***

AST-100® Viskometer Brookfield digunakan bagi analisis kelikatan hasil ekstrak air bagi sampel daun segar dan kering. Tiga jenis saiz gelendung yang berbeza digunakan dengan kelajuan rpm malar iaitu 100 rpm. Pembacaan nilai kelikatan (cP) dilakukan sebanyak 3 kali bagi mendapatkan purata nilai pembacaan ± *standard error* ($n$ = 3).

***Analisis statistik***

Kesemua data hasil ujikaji dianalisa dengan menggunakan perisian SPSS (IBM) versi 17.0. Ujian T-tak bersandar atau 'Student T-test' dijalankan untuk pada aras kebarangkalian signifikan 95% ($p$<0.05) bagi penentuan perbezaan signifikan di antara sampel.

## Hasil dan Perbincangan

**Analisis model Peleg bagi ekstrak air**

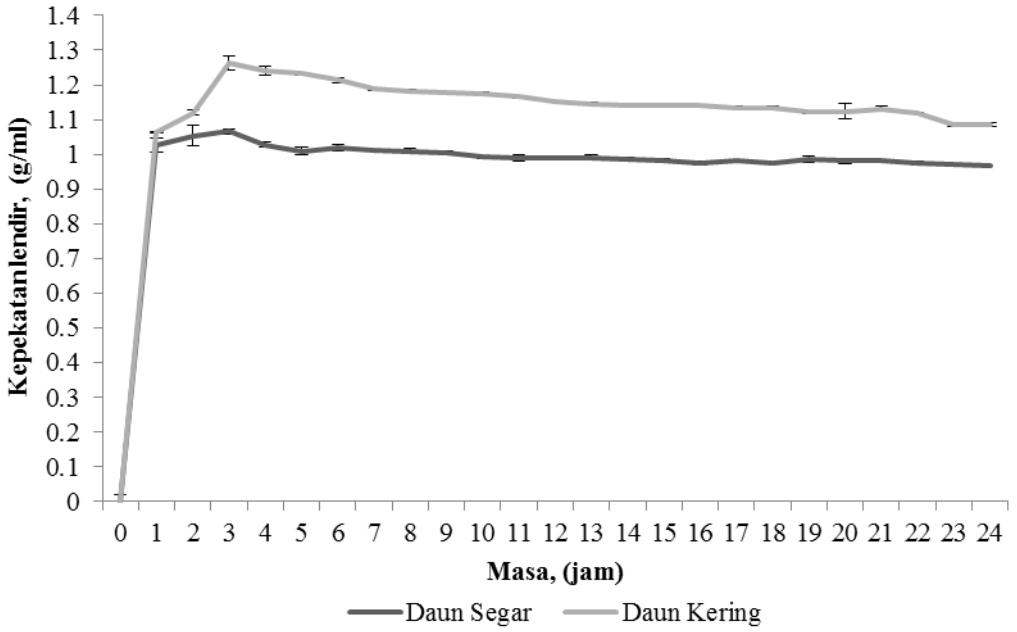
Rajah 2 menunjukkan plot kinetik pengekstrakan kepekatan (g/ml) versus masa (t) di mana sampel daun kering dilihat mempunyai plot kepekatan lebih tinggi secara signifikan ($p$<0.05) berbanding daun segar. Transformasi data keluk kinetik pengekstrakan kepada model matematik Peleg dilakukan bagi penentuan kepekatan (g/ml) dan masa (t) pengekstrakan maksimum melalui persamaan (2), (3) dan (4). Merujuk kepada Jadual 1 dan Rajah 3, sampel daun kering mempunyai kadar pengekstrakan yang lebih rendah (2.21 ± 0.06 g/ml.hr) secara signifikan ($p$<0.05) berbanding sampel segar (3.69 ± 0.36 g/ml.jam) walaupun kepekatan hasil ekstraknya (1.09 ± 0.01 g/ml) dilihat lebih tinggi ($p$<0.05) berbanding daun segar (0.96 ± 0.01 g/ml). Menurut Raymond (2007) [20], fenomena ini dapat dijelaskan oleh faktor kepekatan bahan terlarut yang tinggi menyebabkan kadar pengekstrakan sesuatu bahan ke dalam pelarut pukal akan menurun.

Seterusnya, perbincangan di atas turut dibuktikan dengan masa pengekstrakan menyeluruh bagi sampel daun kering adalah lebih lama (29.68 ± 0.80 min) berbanding sampel daun segar (15.66 ± 1.45 min) ($p$<0.05). Ini boleh dijelaskan dengan lebih terperinci di mana apabila sesuatu sampel daun tersebut dikering terlebih dahulu sebelum proses pengekstrakan dijalankan, sel-sel lendir yang wujud di dalam korteks sel tumbuhan tersebut akan termusnah dan mengecut akibat kehilangan lembapan yang tinggi dan akan meninggalkan gumpalan lendiran yang pekat dan likat [3]. Oleh yang demikian, apabila sampel ini dilakukan proses pengekstrakan, masa yang agak lama diperlukan bagi mencairkan kembali gumpalan likat tersebut sehinggalah wujudnya keseimbangan jisim di antara dua fasapepejal-cecair tersebut.

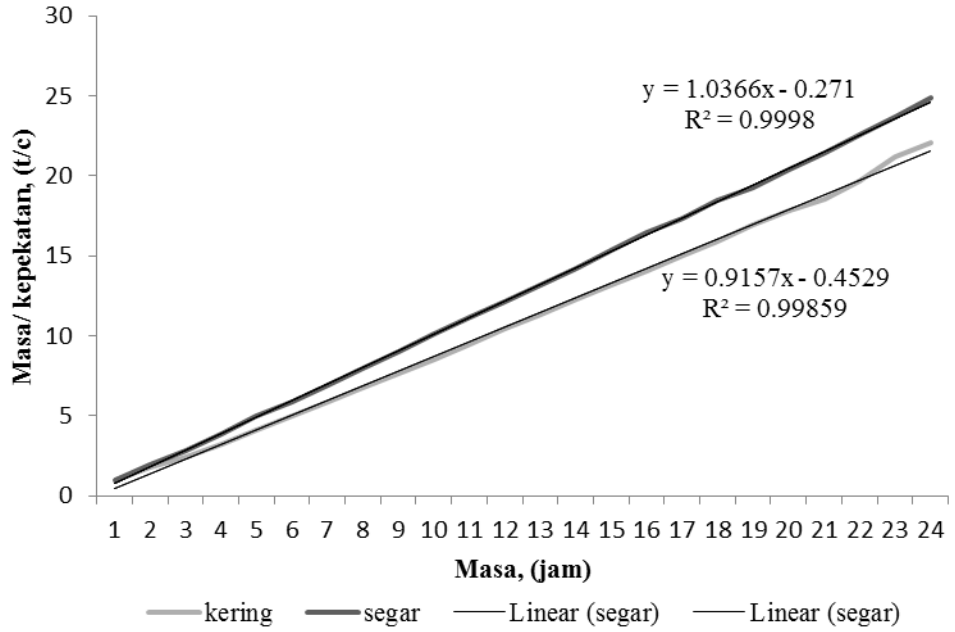
Jadual 1: Nilai kepekatan hasil ekstrak maksimum (g/ml) dan masa pemperolehan keseluruhan ekstrak lendir daun bunga raya (min) bagi pelarut air

| **Parameter pengiraan model Peleg** | **Sampel** | |
|---|---|---|
| | **Daun Segar** | **Daun Kering** |
| *Kadar pengekstrakan (g/ml.jam) | 3.69 ± 0.36 | 2.21 ± 0.06 |
| *Kepekatan hasil ekstrak maksimum (g/ml) | 0.96 ± 0.01 | 1.09 ± 0.01 |
| *Masa pengekstrakan menyeluruh (min) | 15.66 ± 1.45 | 29.68 ± 0.80 |

*$p$<0.05: Perbezaan signifikan di antara daun kering dan segar.




Rajah 2: Graf kinetik pengekstrakan pepejal-cecair daun bunga raya menggunakan pelarut air ($n$ = 3)




Rajah 3: Model pengekstrakan kinetik Peleg bagi pengekstrakan daun bunga raya menggunakan pelarut air ($n$ = 3)

**Analisis model Peleg bagi ekstrak aseton**

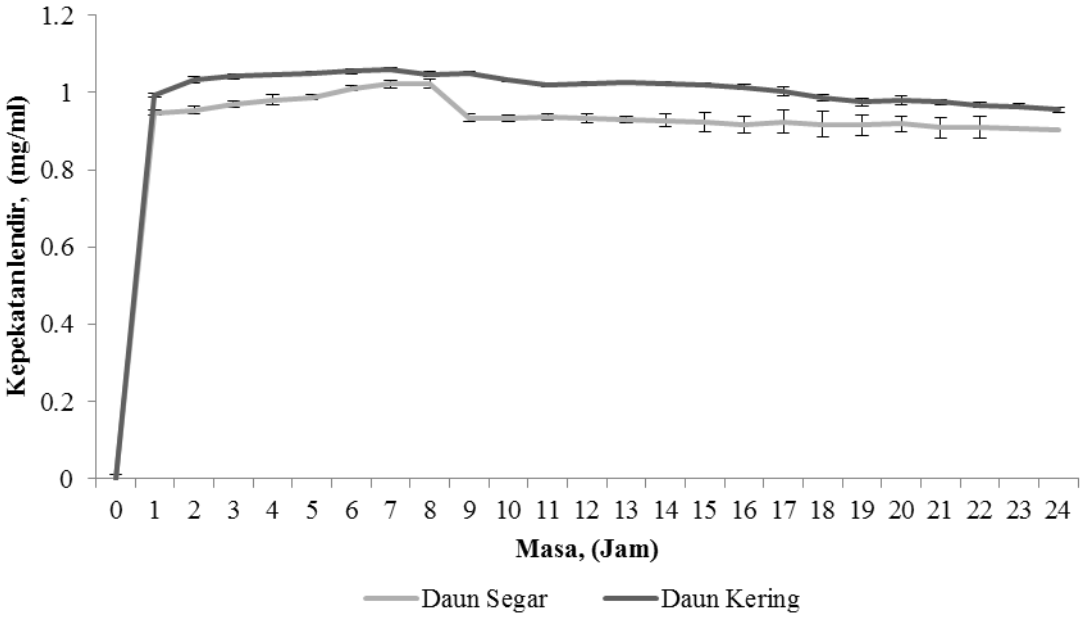
Rajah 4 menunjukkan plot kinetik pengekstrakan kepekatan (g/ml) versus masa (t) di mana sampel daun kering dilihat turut mempunyai plot kepekatan lebih tinggi secara signifikan ($p$<0.05) berbanding daun segar. Transformasi data keluk kinetik pengekstrakan kepada model matematik Peleg dilakukan bagi penentuan kepekatan (g/ml) dan masa (t) pengekstrakan maksimum melalui persamaan (2), (3) dan (4). Merujuk kepada Jadual 2 dan Rajah 5, kedua-dua sampel daun kering dan basah menunjukan kadar pengekstrakan yang sama walaupun kepekatan hasil ekstrak daun kering (0.96 ± 0.01 g/ml) dilihat lebih tinggi ($p$<0.05) berbanding daun segar (0.89 ± 0.03 g/ml).

Jadual 2: Nilai kepekatan hasil ekstrak maksimum (g/ml) dan masa pemperolehan keseluruhan ekstrak lendir daun bunga raya (min) bagi pelarut aseton

| **Parameter pengiraan model Peleg** | **Sampel** | |
|---|---|---|
| | **Daun Segar** | **Daun Kering** |
| Kadar pengekstrakan (g/ml.jam) | 2.005 ± 1.21 | 1.81 ± 0.13 |
| *Kepekatan hasil ekstrak maksimum (g/ml) | 0.89 ± 0.03 | 0.96 ± 0.01 |
| Masa pengekstrakan menyeluruh (min) | 26.72 ± 5.16 | 31.77 ± 2.03 |

*$p$<0.05: Perbezaan signifikan di antara daun kering dan segar.

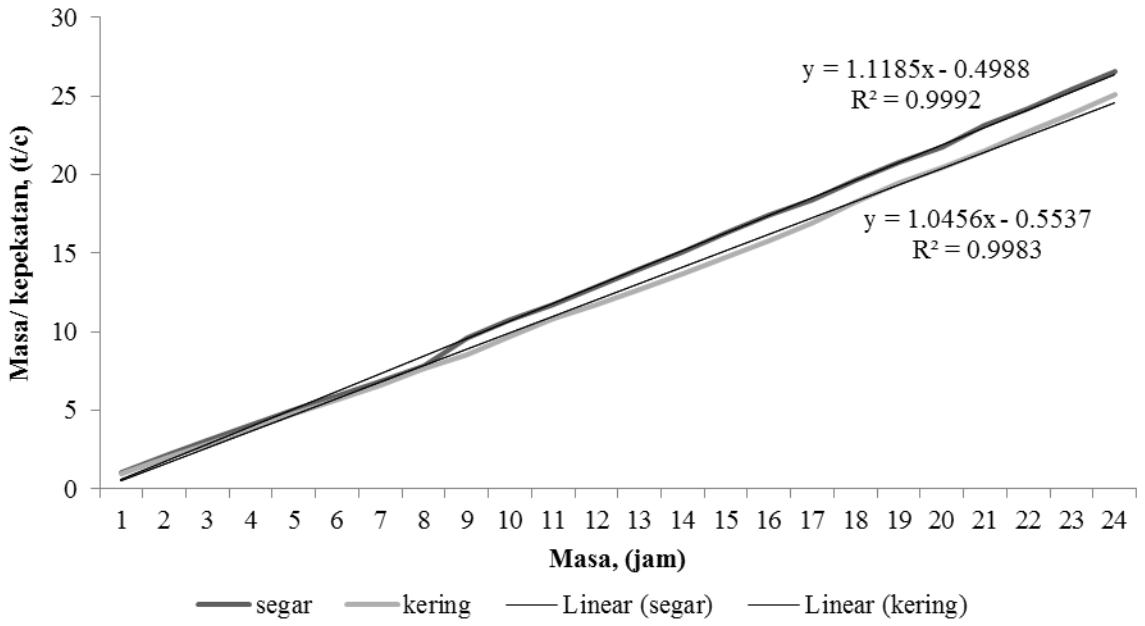
Di samping itu, masa optimum untuk penghasilan hasil pengekstrakan secara menyeluruh bagi kedua-dua jenis sampel daun dilihat tidak memberikan sebarang perbezaan signifikan bagi penggunaan pelarut aseton. Secara keseluruhannya, hasil pengekstrakan menggunakan pelarut air dilihat lebih mesra alam dan ekonomi berbanding penggunaan pelarut organik aseton. Tujuan pelarut organik digunakan adalah untuk melihat sejauhmana keberkesanan lendir dapat diekstrak daripada daun bunga raya. Selain daripada itu, pengekstrakan menggunakan pelarut aseton dilihat mampu dijadikan sebagai *benchmark* tentang keupayaan bahan bio-aktif yang terdapat di dalam sampel daun tumbuhan hijau terhadap aktiviti biokimia penting seperti analisis antioksidan, aktiviti antimikrobiologi dan aktiviti hormon jurvenil [21]. Di samping itu, penggunaan daun bunga raya di dalam penyediaan perubatan tradisional banyak menggunakan pelarut air sebagai cecair pengekstrakan utama. Oleh yang demikian, penggunaan pelarut aseton dilihat kurang sesuai disebabkan oleh penggunaan hasil ekstraknya yang banyak di dalam penjagaan kesihatan tubuh badan manusia.



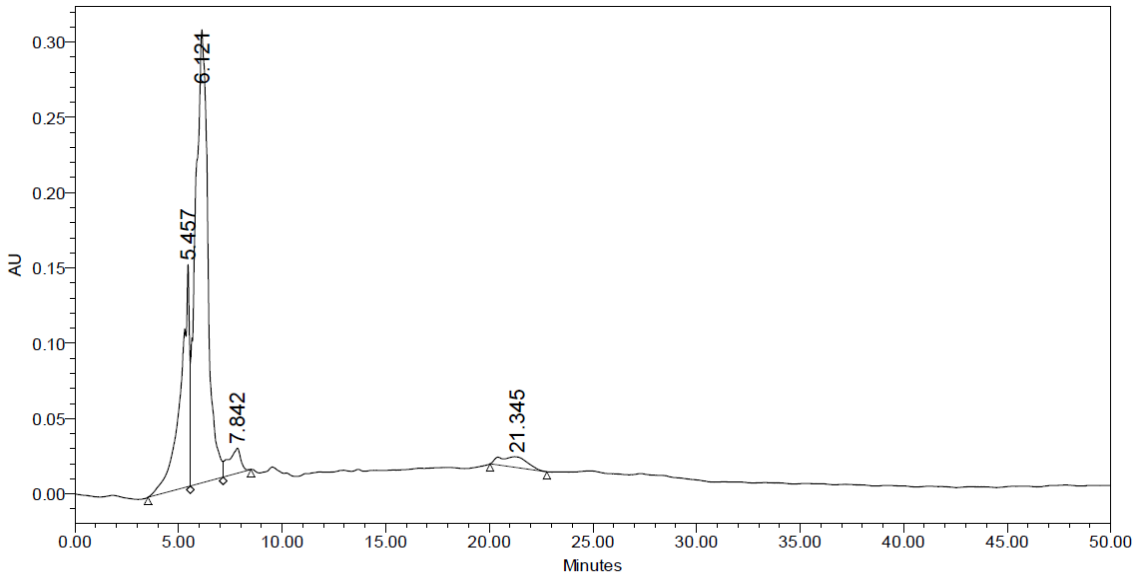

Rajah 4: Graf kinetik pengekstrakan pepejal-cecair daun bunga raya menggunakan pelarut aseton ($n$ = 3)

**Analisis HPLC**

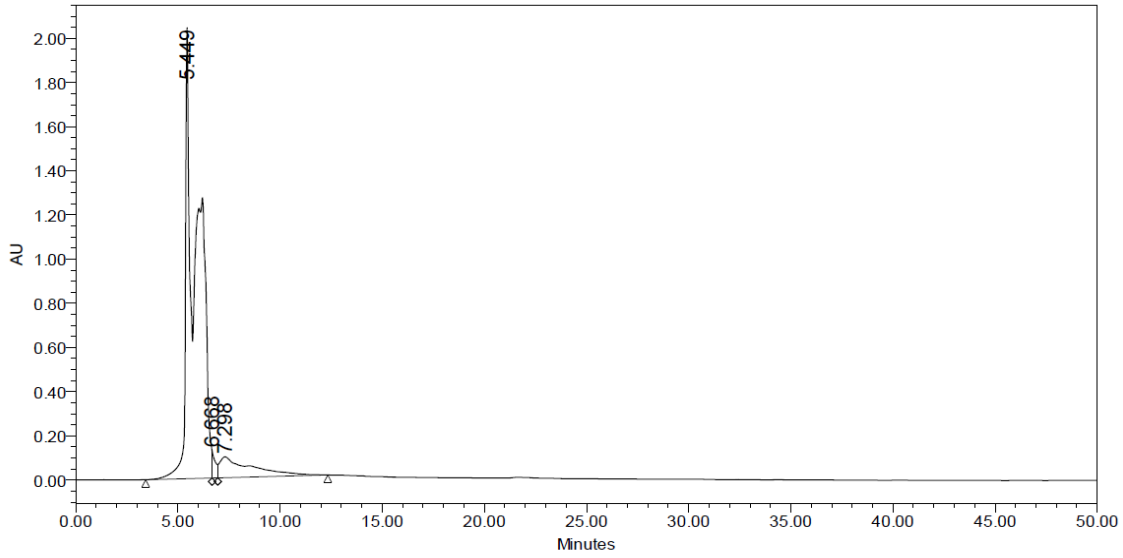
Analisis HPLCdijalankan untuk menentukan kehadiran bahan aktif β-sitosterol secara kualitatif dengan menggunakan kaedah fasa berbalik. Rajah 6 dan 7 menunjukkan profil kromatogram bahan bio-aktif yang terdapat di dalam sampel ekstrak daun bunga raya segar dan daun kering. Sampel daun segar menunjukkan kehadiran 3 puncak penahanan komponen bahan bio-aktif yang tidak diketahui dan 1 puncak β-sitosterol pada masa penahanan 21.35 min. Manakala bagi sampel daun kering, tiada kewujudan puncak penahanan untuk β-sitosterol. Di dalam analisis kualitiatif ini, rujukan masa penahanan paiwaian β-sitosterol dibuat secara perbandingan dengan beberapa kajian lepas [5,18]. Ini disebabkan oleh masalah ketidakbolehdapatan bahan bio-aktif β-sitosterol daripada pembekal bahan kimia piawaian iaitu Sigma Aldrich$^{TM}$. Untuk mengurangkan kesilapan di dalam penentuan bahan bio-aktif β-sitosterol, parameter analisis yang sama digunakan sepertimana di dalam kajian Sheng dan Chen (2009) [18].




Rajah 5: Model pengekstrakan kinetik Peleg bagi pengekstrakan daun bunga raya menggunakan pelarut aseton ($n$ = 3)

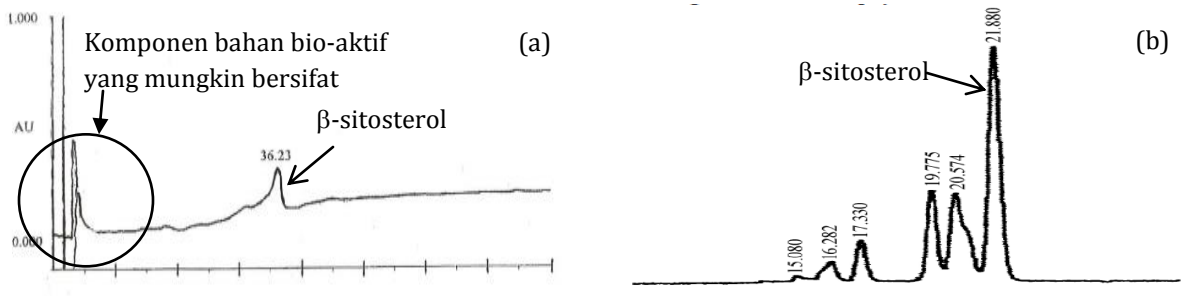



Rajah 6: Profil kromatogram bahan bio-aktif yang terdapat di dalam ekstrak sampel daun bunga raya segar




Rajah 7: Profil kromatogram bahan bio-aktif yang terdapat di dalam ekstrak sampel daun bunga raya kering

Rajah 8(b) menunjukkan rujukan masa penahanan β-sitosterol piawai bagi kajian Sheng dan Chen (2009) [18] iaitu pada masa 21.88 min. Parameter analisis yang digunakan terutama sekali komposisi fasa bergerak (metanol (80%) + air dinyah ion (20%)) adalah yang sama. Masa penahanan β-sitosterol yang diperolehi di dalam sampel daun bunga raya segar (Rajah 6) dilihat hampir sama iaitu pada masa 21.35 min. Manakala sebagai rujukan dan perbandingan yang lain [5], Rajah 8(a) menunjukkan profil puncak penahanan yang hampir sama dengan profil kromotogram sampel daun bunga raya (Rajah 6). Walaubagaimanapun, masa penahanan rujukan piawaian β-sitosterol tersebut adalah lebih kurang 15 min lebih lama berbanding daripada kajian ini disebabkan oleh penggunaan kombinasi fasa bergerak yang berbeza iaitu asetonitril dan etanol.




Rajah 8: Profil rujukan bagi analisis komponen bahan aktif hasil ekstrak daun bunga raya. (a) Penggunaan fasa bergerak yang berbeza dengan kajian Ye et al. (2010) [5] dan (b) penggunaan fasa bergerak yang sama dengan kajian Sheng dan Chen (2009) [18]

Secara teori, masa penahanan yang terhasil untuk sesuatu analit adalah bergantung kepada kepolaran pelarut atau fasa bergerak yang digunakan. Semakin tinggi kepolaran pelarut yang digunakan untuk membawa analit yang bukan polar, semakin kuat interaksinya (daya penyerapan) dengan kolum yang bukan polar. Jadi masa penahananyang

terhasil adalah lebih lama [22]. Di dalam kajian ini, fasa bergerak yang digunakan ialah kombinasi pelarut metanol (80%) dan air (20%). Gabungan dua pelarut tersebut dilihat mengurangkan kepolaran fasa bergerak. Oleh yang demikian, ia mudah membawa analit β-sitosterol yang bukan polar melalui kolum yang bukan polar kerana kekurangan interaksi di antara fasa tetap dan analit. Oleh yang demikian, masa penahanan yang terhasil adalah lebih cepat sepertimana yang ditunjukkan di dalam profil puncak penahanan oleh kajian Sheng dan Chen (2009) [18]. Manakala, kajian yang dilakukan oleh Ye et al. (2010) [5], masa penahanan puncak analit β-sitosterol dilihat lebih lama kerana penggunaan fasa bergerak yang lebih polar iaitu asetoniril dan interaksi yang kuat dengan kolum yang bersifat bukan polar.

Di samping itu, β-sitosterol merupakan komponen fitosterol yang bersifat hidrofobik seperti kolesterol. Namun begitu, kewujudan komponen β-sitosterol di dalam ekstrak air daun bunga raya segar mungkin disebabkan oleh kewujudan komponen bio-aktif yang bersifat surfaktan semulajadi [23]. Surfaktan semulajadi ini berfungsi sebagai bahan yang membolehkan β-sitosterol yang bersifat hidrofobik untuk larut di dalam ekstrak air sepertimana yang dibuktikan di dalam profil kromotogram hasil ekstrak air daun bunga raya segar (Rajah 6).

Selain daripada itu, ketidakhadiran β-sitosterol di dalam ekstrak daun kering berkemungkinan besar disebabkan oleh degradasi terma yang terjadi kepada komponen tersebut. Ia dilihat bersifat sensitif kepada haba jika dibandingkan dengan komponen fitosterol yang lain. Oleh yang demikian, pengekstrakan daun bunga raya segar adalah kaedah yang terbaik bagi mendapatkan bahan bio-aktif penting seperti β-sitosterol walaupun kepekatan hasil ekstrak yang diperolehi agak rendah berbanding penggunaan daun kering ($p$<0.05).

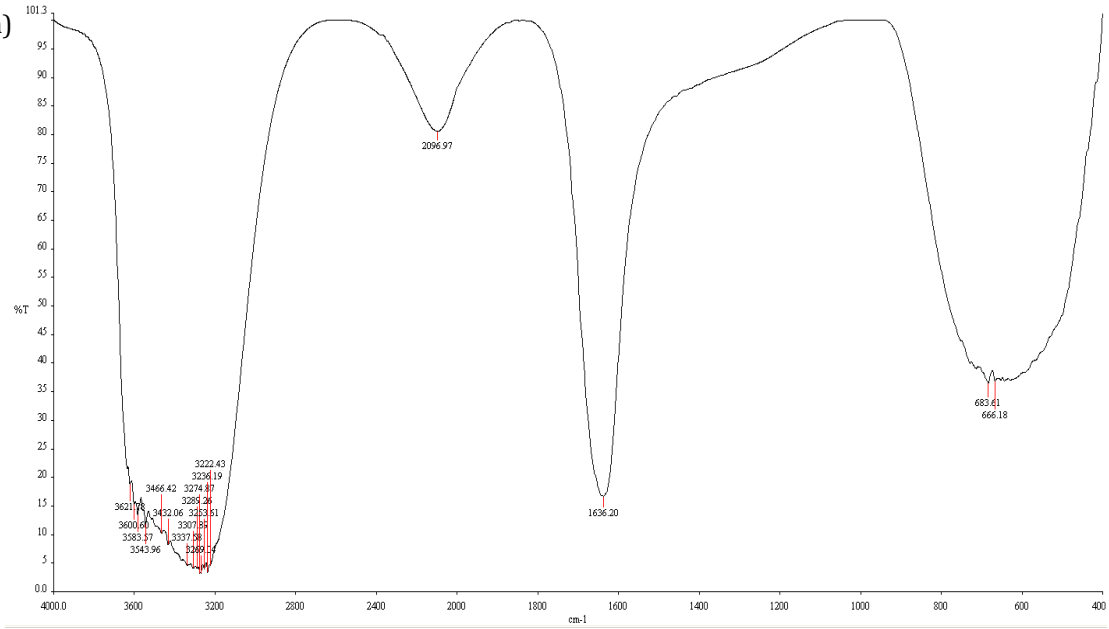
**Analisis kumpulan berfungsi menggunakan FTIR**

Rajah 7 menunjukkan ciri-ciri puncak spektrum FTIR yang hampir setara di antara kedua-dua sampel daun segar dan kering. Manakala Jadual 3 menunjukkan nilai puncak penyerapan dan jenis ikatan yang terdapat di dalam kedua-dua jenis sampel daun.Komposisi nilai puncak penyerapan yang terbanyak adalah bagi ikatan O-H (3400-3700 $cm^{-1}$). Menurut Anil dan Ashatha (2012) [4], daun dan pucuk daun bunga raya mengandungi beberapa sebatian fitosterol seperti β-sitosterol, stigmasterol, asetat taraxeril dan tiga sebatian saiklopropan. Kesemua komponen bahan bio-aktif tersebut kaya dengan kumpulan berfungsi fenolik. Oleh yang demikian, penyerapan gelombang transmisi oleh ikatan O-H yang tinggi membuktikan kebolehdapatan kumpulan berfungsi fenolik yang tinggi di dalam ekstrak kedua-dua daun bunga raya. Ia merupakan ciri penting aktiviti biokimia (antioksidan dan antipiretik) bagi kegunaan perubatan tradisional.

Jadual 3: Nilai puncak penyerapan bagi analysis FTIR bagi ekstrak daun bunga raya segar dan kering

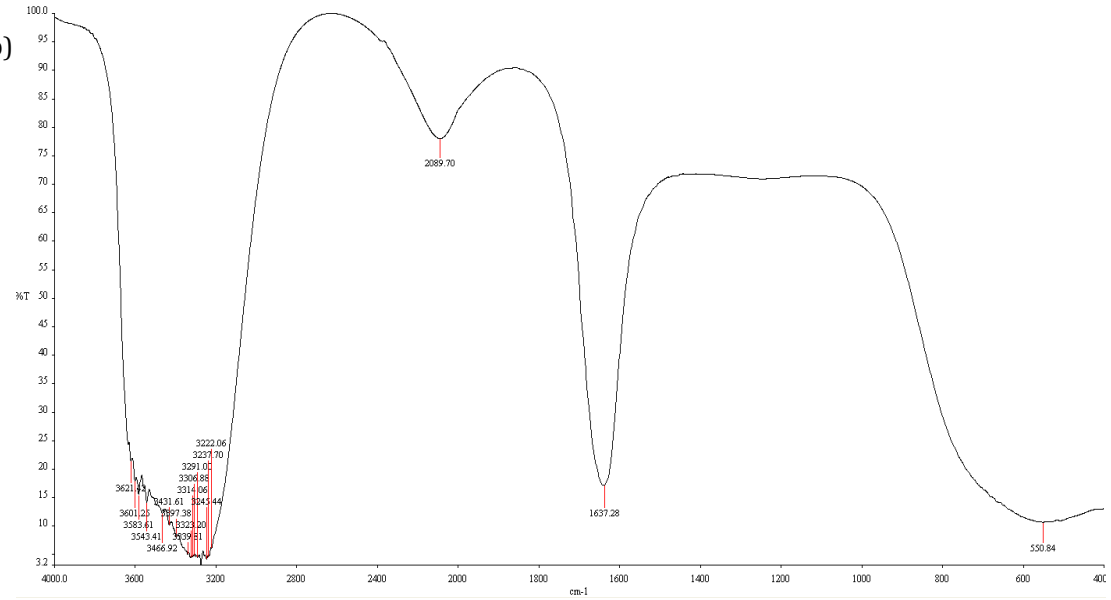
| **Nilai puncak penyerapan ($cm^{-1}$)** | | **Julat penyerapan ($cm^{-1}$)** | **Jenis ikatan spesifik** |
|---|---|---|---|
| **Daun segar** | **Daun kering** | | |
| 3621.42 | 3621.78 | 3580-3650 | O-H (bebas) |
| 3583.61 | 3583.57 | 3580-3650 | O-H (bebas) |
| 3466.92 | 3466.42 | 3200-3550 | O-H (H-diikat) |
| 3222.06 | 3222.43 | 3200-3550 | O-H (H-diikat) |
| 2089.70 | 2096.97 | 1990-2140 | Ikatan C─N |
| 1637.28 | 1636.20 | 1615-1700 | Ikatan C═N |
| 1637.28 | 1636.20 | 1560-1640 | Ikatan N─H |

(a)




No. gelombang ($cm^{-1}$)

(b)

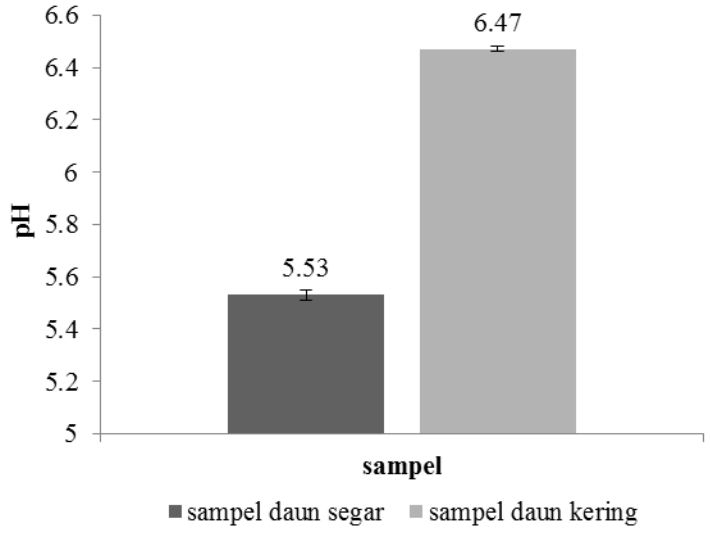



No.gelombang ($cm^{-1}$)

Rajah 9: Spektrum FTIR bagi sampel daun bunga raya (a) kering dan (b) segar

**Analisis pH ekstrak daun bunga raya**

Rajah 10 menunjukkan perbezaan nilai pH di antara kedua-dua jenis sampel daun kering dan basah. Ekstrak air bagi sampel daun kering memberikan nilai pH yang lebih tinggi (6.47 ± 0.01) ($p$<0.05) secara signifikan dan hampir bersifat *neutral* berbanding ekstrak air bagi daun segar (5.53 ± 0.02) yang dilihat bersifat berasid. Daun bunga raya segar yang tidak dikenakan sebarang proses pra-rawatan (pengeringan) dilihat masih mengekalkan beberapa komponen bahan aktif yang bersifat asid dan sensitif kepada haba terutama sekali β-sitosterol. Oleh yang demikian, pendedahan kepada suhu yang tinggi ketika proses pengeringan boleh mengakibatkan penguraian komponen fitokimia penting dan perubahan pada sifat-sifat fizikal hasil ekstrak [24].




Rajah 10: Nilai pH untuk sampel daun bunga raya segar dan kering

Jadual 4: Bacaan kelikatan bagi saiz gelendong yang berbeza pada 100 rpm

| **Saiz gelendong (mm)** | **Bacaan kelikatan (cP)** | |
|---|---|---|
| | **[#]Daun segar** | **[#]Daun kering** |
| *3 | 66.97 ± 2.15 | 120.17 ± 1.48 |
| *4 | 53.77 ± 1.14 | 59.8 ± 2.74 |
| 5 | 40.83 ± 1.12 | 39.87 ± 0.25 |

*$p$<0.05: perbezaan signifikan di antara daun segar dan kering. [#]$p$<0.05: perbezaan signifikan di antara saiz gelendong. cP ialah unit kelikatan *centipoises*.

**Ujian kelikatan**

Jadual 4 menunjukkan bacaan kelikatan (cP) bagi ekstrak daun bunga raya kering dan segar pada kepekatan maksimum berdasarkan kepada penggunaan saiz gelendong yang berbeza. Keputusan menunjukkan sampel daun kering mempunyai bacaan kelikatan yang tinggi ($p$<0.05) secara signifikan untuk saiz gelendong 3 mm dan 4 mm berbanding daun segar. Di samping itu, perbezaan kelikatan yang ketara pada penggunaan saiz gelendong yang berbeza bagi kedua-dua ekstrak daun bunga raya ($p$<0.05) membuktikan sifat kelikatan yang wujud di dalam hasil ekstrak tersebut terhadap tegasan ricihan. Profil penurunan kelikatan menunjukkan semakin besar saiz gelendong yang digunakan, semakin rendah bacaan kelikatan (cP).

## Kesimpulan

Penggunaan model matematik Peleg dilihat lebih berkesan dalam penentuan beberapa parameter pemprosesan penting dengan lebih tepat dan pantas. Hasil analisis model matematik Peleg mendapati, penggunaan daun kering bagi pengekstrakan air dilihat menghasilkan kandungan maksimum hasil ekstrak berlendir dan masa pengekstrakan menyeluruh yang pantas berbanding daun segar ($p$<0.05). Fenomena di atas dilihat berpunca daripada faktor penggunaan pra-rawatan menggunakan haba (proses pengeringan daun) menyebabkan pemecahan dan penguraian pada struktur dinding sel daun. Pemecahan tersebut menyebabkan bahagian sitoplasma yang kaya dengan lendir bergumpal dan menjadi likat semasa proses pengesktrakan. Walaubagaimanapun, berdasarkan kepada analisis HPLC, kehadiran bahan bio-aktif utama β-sitosterol dilihat hanya wujud pada sampel daun segar. Dua punca utama dilihat berkemungkinan yang wujud akibat ketiadaan bahan bio-aktif tersebut: (1) Kehilangan beberapa bahan bio-aktif penting yang bersifat surfaktan semulajadi (pengemulsi β-sitosterol) akibat daripada degradasi termal semasa proses pengeringan dan (2) β-sitosterol dilihat sensitif kepada penggunaan haba semasa proses pengeringan sampel. Analisis FTIR bagi kedua-dua sampel daun segar dan kering dijalankan bagi membuat pembuktian lanjutan berkenaan dengan ketidakhadiran β-sitosterol di dalam sampel ekstrak daun kering. Nilai puncak penyerapan bagi ikatan yang berkaitrapat dengan kumpulan berfungsi fenolik (ikatan O-H) menunjukkan komposisi puncak penyerapan yang sama bagi kedua-dua jenis sampel. Ini membuktikan bahawa kandungan β-sitosterol di dalam kedua-dua jenis sampel tersebut adalah terlalu sedikit dan komposisi fitosterol yang lain dilihat mendominasi kandungan ekstrak tersebut. Sehubungan dengan itu, faktor kehilangan bahan fitosterol yang lain akibat degradasi terma dilihat mempengaruhi kehadiran β-sitosterol kerana komponen tersebut dilihat membantu dalam membawa komponen β-sitosterol ke dalam hasil ekstrak. Ini dapat dijelaskan lagi mengapa berlakunya kesukaran untuk mendapatkan sampel piawai β-sitosterol di pasaran dan juga kemunculan puncak penahanan analit β-sitosterol yang kecil bagi analisis HPLC ekstrak daun segar. Selain daripada itu, ujian sifat fizikal terhadap ekstrak kedua-dua jenis daun turut dijalankan bagi membuktikan bahawa proses pengeringan boleh membawa kepada penguraian beberapa komponen bahan bio-aktif penting. Keasidan yang tinggi bagi sampel daun bunga raya segar dilihat berpunca daripada kebolehdapatan semua komponen bahan aktif manakala bagi ekstrak daun kering, nilai pH yang agak *neutral* dilihat berpunca daripada penguraian beberapa bahan fitokimia yang bersifat berasid dan sensitif kepada haba. Akan tetapi, kajian lanjut seperti ujikaji profil degradasi terma mengikut julat suhu tertentu, penggunaan kaedah *spiking* bagi analisis HPLC dan analisis penguraian kandungan (mg) bahan bio-aktif spesifik perlu dijalankan agar pembuktian yang lebih tepat dapat diperolehi.

## Rujukan

1. Upadhyay, S.M., Upadhyay, P., Ghosh, A.K., Singh, V. & Dixit, V.K. (2011). Effect of ethanolic extract of *Hibiscus rosa sinensis* flowers on hair growth in female wistar rats. *Dermatol Pharmacia Lettre.* 3(4): 258-263.
2. Staples, G.W. & Herbst, D.R. (2005). A Tropical Garden Flora: Plants cultivated in the Hawaiian Islands and other tropical places. Bishop Museum Press, Honolulu, Hawaii.
3. Woolfe M.L., Chaplid, M.F. & Gifty Otchere (1977). Studies on the Mucilages extracted from Okra fruits *(Hibiscus esculentus* L.) and Baobab leaves *(Adansonia digitata* L.). *Journal of the Science of Food and Agriculture.* 28: 519-529.
4. Anil, K. & Ashatha, S. (2012). Review on of *Hibiscus rosa-sinensis. International Journal of Research in Pharmaceutical and Biomedical Sciences.* 3(2): 2229-3701.
5. Ye, J.C., Chang, W.C., Yuan Hsieh, D.Y. & Meen-Woon Hsiao, M.W. (2010). Extraction and analysis of β-sitosterol in Herbal Medicines. *Journal of Medicinal Plants Research.* 4(7):522-527.
6. Bhakuni, O.S., Dhar, M.L., Dhar, M.M., Dhavan, B.N. & Mehrotra, B.N. (1969). Screening of Indian plants for biological activity. *Indian Journal of Experimental Biology*. 7: 250-262.

7. Arullappan, S., Zakaria, Z. & Basri, D.F. (2009). Preliminary screening of antibacterial activity using crude extracts of *Hibiscus rosa sinensis*. *Tropical Life Sciences Research.* 20(2): 109-118.
8. Kirtikar, K.R. & Basu, B.D. (1999). Indian Medicinal Plants (International Book Distributors, Dehradun, India). p335
9. Ghaffar, F.R.A. & El-Elaimy, I.A. (2012). *In vitro*, antioxidant and scavenging activities of *Hibiscus rosa sinensis* crude extract. *Journal of Applied Pharmaceutical Science.* 2(1): 51-58.
10. Sharma, S. & Sultana, S. (2004). Effect of *Hibiscus rosa sinensis* extract on hyperproliferation and oxidative damage caused by benzoyl peroxide and ultraviolet radiations in mouse skin. *Basic & Clinical Pharmacology & Toxicology.* 95(5): 220-225.
11. Ankit, G., Madhu, N. & Vijay, K. (2012). Modern extraction method for preparation of bioactive plant extract. *International Journal of Applied and Natural Science.* 1(1):8-26.
12. Handa, S.S., Khanuja, S.P., Longo, G. & Rakesh, D.D. (2008). Extraction technologies for medicinal and aromatic plants. Trieste: International Centre for Science & Technology (ICS) UNIDO.
13. Abu Bakar, E.M.M. (2009). Antibacterial activity of crude extracts of *Euphorbia hirta* against some bacteria associated with enteric infections. *Journal of Medicinal Plants Research.* 3(7): 498-505.
14. Shi, J., Yu, J., Pohorly, J., Young, J. C., Bryan, M. & Wu, Y. (2003). Optimization of extraction of polyphenols from grape seed meal by aqueous ethanol solution. *Journal of Food Agriculture and Environment.* 1(2): 42-47.
15. Skerget, M., Kotnik, P., Hadolin, M., Rizner Hras, A., Simonic, M. & Knez, Z. (2005). Phenols, proanthocyanidins, flavones and flavonols in some plant materials and their antioxidant activities. *Food Chemistry.* 89: 191-198.
16. Maskan, M. (2002). Effect of processing on hydration kinetics of three wheat products of the same variety. *Journal of Food Engineering.* 52: 337-341.
17. Peleg, M. (1988). An empirical model for the description of moisture sorption curves. *Journal of Food Science.* 53(4): 1216-1219.
18. Sheng, Y. & Chen, X.B. (2009). Isolation and identification of an isomer of β-sitosterol by HPLC and GC-MS. *Health Journal.* 1(3): 203-206.
19. Keppler, H. & Rauch, M. (2000). Water solubility in nominally anhydrous minerals measured by FTIR and 1H MAS NMR: The effect of sample preparation. *Physics and Chemistry of Minerals.* 27: 371-376.
20. Raymond, C. (2007). *Chemistry*. Ed. Ke- 9. New York. McGraw-Hill.
21. Prakash, A.O., Mathur, A., Mehta, H. & Mathur, A. (1996). Concentrations of Na+ and K+ in serum and uterine flushing of ovariectomized, pregnant and cyclic rats when treated with extracts of *Hibiscus rosa sinensis* flowers. *Journal of Ethnopharmacology.* 28:337-347.
22. Wagrowshi-Diehl, D.M., Grumbach, E.S. & Iraneta, P.C. (2002). Development of New HPLC column for the retention and separation of highly polar compound. *Journal of Chromatography.* 2:49-67.
23. Divya, M.J., Sowmia, C., Joona, K. & Dhanya, K.P. (2013). Synthesis of zinc oxide nanoparticle from Hibiscus Rosa-Sinensis leaf extract and investigation of its antimicrobial activity. *Research Journal of Pharmaceutical, Biological and Chemical.*4(2): 1137.
24. Gupta, V., Bansal, P., Garg, A. & Meena, A.K. (2009). Pharmacopoeial Standardization of *Hibiscus rosa sinensis* Linn. *International Journal of Pharmaceutical and Clinical Research.* 1(3): 124-126.

The Malaysian Journal of ANALYTICAL SCIENCES ISSN 1394-2506

# PHOSPHORYLATION OF GELATINE AND CHITOSAN AS AN EXCIPIENT FOR ASIATICOSIDE NANOFIBERS

## (Pemfosforilan Gelatin dan Kitosan Sebagai Eksipien Bagi Penyediaan Nanofiber Asiatikosida)

Susana Elya Sudrajat[1]*, Khairurrijal[2], Puspa DN Lotulung[3], Effionora Anwar[1]

[1]*Faculty of Pharmacy,*
*Universitas Indonesia, Depok, Indonesia*
[2]*Department of Physics,*
*Institut Teknologi Bandung, Indonesia*
[3]*Department of Chemistry,*
*Lembaga Ilmu Pengetahuan Indonesia, Serpong, Indonesia*

**Corresponding author: susanasudrajat_09@yahoo.com*

**Abstract**

Asiaticoside has been widely used and is still studied for topical treatment of wounds, increased fibroblasts and collagen production are noted at the site of injury. Base on getting the optimal effect of wounds' treatment, drug must be released and absorbed from the carrier/drug delivery media. In this research, nanofibers preparation is made using the model drug asiaticoside. The result indicated that gelatine-chitosan phosphorylation can be used as an excipient for asiaticoside nanofibers. In this research 3 formulas with varying concentrations of phosphorus are used. The release of asiaticoside was examined by dissolution in vitro. It was measured by high performance liquid chromatography (HPLC) and nanofibers morphology was measured by scanning electron microscopy (SEM). Phosphorylation chitosan tested by infra red spectrophotometry (FTIR) at wave numbers 1271, 1213, 1157, 1085, 1012 and 954 $cm^{-1}$ where as the phosphorylation of gelatine at 1257, 1026 and 900 $cm^{-1}$ . The characterization result indicates that the formula C was contains sodium tripolyphosphate 0.5% is the best with the release of asiaticoside 51% for 72 hours, compared to formula A(68%) and the formula B(62%). The percentage asiaticoside from nanofibers preparation is between 90%-100%.

**Keywords**: asiaticoside, nanofibers, phosphorylation, sodium tripolyphosphate, electrospinning, dissolution

**Abstrak**

Asiatikosida telah digunakan secara luas dan masih terus dikaji untuk rawatan topikal pengubatan luka dengan cara meningkatkan pembentukan fibroblas dan penghasilan kolagen pada kawasan tercedera. Untuk mendapatkan kesan optimal rawatan luka, ubatnya harus diletakkan dan diserap dari medium pembawa. Penyediaan nanofiber dilakukan dengan mengunakan model ubat asiatikosida. Hasil kajian menunjukkan bahawa kaedah pemfosforilan gelatin dan kitosan dapat digunakan sebagai eksipien nanofiber asiatikosida. Kajian ini mengunapakai variasi 3 formula kepekatan phosphorus. Asiatikosida diuji dengan cara pelarutan in vitro. Ia diukur mengunakan Kromatografi Cecair Prestasi Tinggi (HPLC) dan ujian morfologi nanofiber mengunakan Mikroskopi Elektron Pengimbasan (SEM). Pemfosforilan kitosan diuji dengan *Spektrofotometri Infra Merah* (FTIR) pada nombor gelombang 1271, 1213, 1157, 1085, 1012 dan 954 $cm^{-1}$ manakalan pemfosforilan gelatin pada 1257, 1026 dan 900 $cm^{-1}$. Hasil penyelidikan memperlihatkan bahawa formula C mengandungi sodium tripolifosfat 0.5% adalah yang terbaik dengan pelepasan 51 % asiatikosida selama 72 jam, dibandingkan formula A(68%) dan formula B(62%). Jumlah asiatikosida di dalam penyediaan nanofiber antara 90%-100%.

**Kata kunci**: asiaticoside, serabut nano, phosphorilation, sodium tripolyphosphate, electrospinning, disolusi

## Introduction

Asiaticoside is the most active component of the plant Centella asiatica that can be found in various parts of Indonesia, and it has been proven efficacious in improving wound healing by increasing fibroblast and collagen synthesis [1]. To deliver it, we need a dosage form that can support the release of asiaticoside, so that the work can

be optimal [2]. Drug dosage form for topical wound usually in the form ointment, is generally given twice daily. It is also should be used with wound dressings that are usually change every day. The replacement of wound dressing can cause discomfort to the patient [3]. Therefore, the dosage form needs to be evaluated, to improve the comfort and effectiveness of wound healing. Meanwhile, the development of nanotechnology provides the opportunity to create and characterize drug in the nanometer scale. Biomaterials in the nanoscale have been used to controlled drug delivery and artificial matrices for tissue [4]. Drug delivery system can be engineered by controlling drug release, composition, shape, size and morphology [5]. Topical treatment requires a carrier/drug delivery media to maintain regular release. Carrier should be safe and not inhibit wound healing and will be better if the carrier can also be participate in accelerating wound healing, such as wide surface area, high porosity, interconnected pores, and the active ingredient allows it to enter the nanofibers. Drug release rate depends on the thickness and the degradation rate of polymer fibers, besides the how well the body is able to absorb the drug [3]. Therefore, electrospinning can be used to create nanoscale fibers and degradation rates in order to get the optimal delivery of the drugs into the body. Electrospinning is inexpensive, effective and a simple method to produce non-woven nanofibrous mats, which have intrinsically high surface to volume ratios to improve mechanical performances and have small pores [6]. The necessary components of an electrospinning aparatus include a high power voltage supply, a capillary tube with a needle, and a collector that consist of conducting materials. The solvent is the most important factor in electrospinning operation [7].

Basic selections gelatine and chitosan as a base material of nanofibers because biodegradable, biocompatible and non-toxic. In order to improve the biocompatibility and functions of biomaterials, it is essential for gelatin and chitosan blends to mimic the nanofibrous structure of the native extra cellular matrixs (ECMs) [8]. Chitosan is a natural polysaccharide derived from waste Crustaceae and gelatine is a natural biopolymer that derived from partial hydrolysis of collagen. Cell attachment to chitosan is mainly attributed to electrostatic interactions between the chitosan cationic sites, and the negatively charged carboxylate and sulphate groups found in cell-surface [9]. Gelatine and chitosan nanofiber are soluble in water and they need to be modified with phosphorylation to improve the drug release profile. Sodium tripolyphosphate (TPP) was chosen as the material phosphorylation because it is non-toxic and has simple method to produce that is by dissolving into a gelatine-chitosan solution or dipping the nanofibers into a solution of TPP [10].

In this work, we developed a novel one-step process to fabricate phosphorilated gelatine-chitosan electrospun nano-fibers that was faster and more economical than the two-step method [11]. Phosphorilation of biodegradable polymers potentially is important to control swelling and degradation rates. Phosphorilated electrospun gelatine-chitosan nanofibers was produced by adding sodium tripolyphosphate (TPP) to the gelatine-chitosan solution. SEM morphology and FTIR demonstrated that phosphorilated gelatine-chitosan was succesfully fabricated by electrospinning using acetic acid as a solvent [2]

## Materials and Methods

### Material

Chitosan (degree of acetylation 75-85%, MW 50.000) and gelatin (from bovine skin, type B) was purchased from Sigma-Aldrich USA, sodium tripolyphosphate (TPP) and phosphate buffer solution (PBS pH 7.4) was purchased from Wako Japan, Asiaticoside was purchased from Guanyu China, and acetic acid solution (Merck, Germany).

### Preparation of polymer solution

Solution was prepared by dissolving gelatine 22g, chitosan 50 mg and etylene glycol in 70% acetic acid until the solution 100 ml with constant overnight stirring. Gelatine and chitosan were completely disolved in acetic acid within 24 hours. TPP was then added to gelatine-chitosan solution. Then, the conductivity, viscosity, and pH solution were measured. Asiaticoside was added right before the electrospinning .

### Electrospinning setting

Nanofibers were prepared by electrospinning apparatus as shown in Figure 1 [13]. The solutions were placed in a plastic syringe with 0.8 mm tip diameter. The flow rate of the solutions (0.3 ml/h) was controlled using a syringe pump. The electrospinning voltage (7.5 kV) was supplied directly by a high DC voltage power supply. Aluminum foil located 10 cm away from the tip of the syringe needle was used to collect the nanofibers mats. It takes 10.7

minutes to obtain nanofiber containing 4 mg asiaticoside. The structure of the phosphorilated gelatine-chitosan nanofibers mats containing asiaticoside fabricated with acetic acid as a solvent was observed by scanning electron microscopy (SEM).

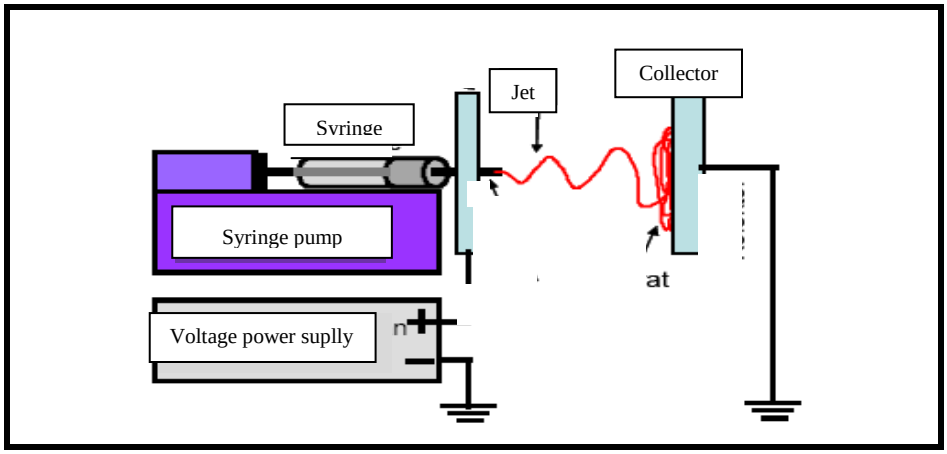



Figure 1: Electrospinning setting

**Characterizations**

***Microstructural Characterizations of Fibers***

Microstructural of the fibers was examined using scanning electron microscopy (JSM, Jeol, Japan). Prior to observation, samples were arranged on metal grids, using double-sided adhesive carbon tape, and coated with gold under vacuum [2].

***Fourier Transform Infrared Chitosan***

The phosphorilated chitosan was characterized by Fourier Transform Infrared Spectra. The infrared spectra of samples were measured over a wavelength range of 4000-500 $cm^{-1}$. The FTIR spectra of pure chitosan, TPP powder, and chitosan TPP were recorded with KBr pellets on a FTIR spectrophotometer (Shimadzu, Japan).

***Fourier Transform Infrared Gelatine***

The phosphorilated gelatine was characterized by Fourier Transform Infrared Spectra. The infrared spectra of the samples were measured over a wavelength range of 4000-500 $cm^{-1}$. The FTIR spectra of pure gelatin, TPP powder, and gelatin TPP were recorded by FTIR spectrophotometer (Shimadzu, Japan).

***Swelling Behavior of Nanofiber Mats***

The swelling behavior of the nanofibers mats was carried out in phosphate buffer solution (PBS pH 7.4) until the fibers reached saturated condition, a constant wet weight. At different time intervals (30 mins, 1h, 2h and 3h), the fibers were weighed after wiping out the surface water with a tissue paper [10]. The degree swelling was calculated using the following formula Equation (1):

$$\text{The degree of swelling } (\%) = \frac{(Ws - Wo)}{Wo} \times 100 \quad (1)$$

where $Ws$ is the weight of each specimen after submersion in the phosphate buffer solution for 30 mins, 1h, 2h, and 3h, and $Wo$ is the initial weight of the specimen in its dry state.

***Water Retention Capacity of Nanofibers***

The nanofibers were allowed to swell for 24 hours in phosphate buffer solution (PBS pH 7.4) and fully swollen fibers were centrifuged at 4000 rpm for 5 minutes to remove excess water among the spaces of the fibers, and weight was taken. The weight was considered as wet weight of the fibers ($W_1$). Then the fibers were dried at 105 $^0$C for 12 hours, then stored in a vacuum container until contant weight is achieved. The weight of fully dry fibers was taken and considered as dry weight ($W_0$). Number of samples was five for each case. Water retention capacity is calculated as follows Equation (2):

$$\text{The water retention capacity } (\%) = \frac{(W_1 - W_0)}{W_0} \times 100 \quad (2)$$

***Measuring Levels of Actual Asiaticoside***

The nanofibers needs to be measured to determine the amount of the asiaticoside in it. The preparation of nanofibers (containing 4 mg asiaticoside) crushed and put into phosphate buffer with 10% methanol, stirring for 30 minutes, then it is added gradually up to 20 ml and dissolved for 24 hours, 2 ml of the solution was filtered through 0.2 µm microphore filter. Asiaticoside that is released was measured by HPLC (Shimadzu, Japan) at 220 nm.

***Asiaticoside Release Assay***

The release of asiaticoside from nanofibers was done by total immersion method . The medium used was phosphate buffer with 10% methanol, because it is more like the body fluids and the addition of methanol is to increase the solubility of asiaticoside. The fibers, that contain, 4 mg asiaticoside, were immersed in 20 ml of medium 37$^0$C within 72 hours. 2 ml of medium were taken out ( the sample solution ) at various intervals of time at 1 hour, 2 hours, 3 hours, 6 hours, 12 hours, 48 hours, 72 hours and was immediately replaced with a new medium with the same amount. The amount of asiaticoside in the sample solution was determined by HPLC. The experiments were carried out in triplicate and the results were reported as average values.

## Results and Discussion

**Optimization of the Preparations of Nanofibers**

In this study, chitosan nanofibers can not be created unless it is added with another polymer. Gelatine copolymer is the best choice, because it is non-toxic, biodegradable and biocompatible. So chitosan and gelatine are used together as polymer and copolymer. The solvent used is 70% acetic acid, because it can be used to produce a homogeneous nanofibers for gelatine-chitosan. Chitosan polymer has a rigid structure, in which the groups of $NH_3^+$ and $OH^-$ formulate the formation of hydrogen bonds. The addition of gelatine in to reduce intermolecular interaction of chitosan with hydrogen bonding.

The mixture of gelatine-chitosan solution obtained by dissolving gelatine and chitosan in 70% acetic acid using a magnetic stirrer. This solution has a slightly yellowish color, rather thick, and the flavor is typical acetic acid. The second solution is a solution obtained by dissolving sodium tripolyphosphate as much as 250 mg in 10 ml of 70% using a magnetic stirrer. The total volume of sodium tripoliphosphate to formulate the formulas of A, B and C respectively was 0.4 ml, 1 ml and 2 ml. This solution has no color and odor, TPP amount used in the solution was 0.1%, 0.25% and 0.5%. If the TPP amounts is more than 0.5%, the insoluble parts will clog the spinerette. It appears that the addition of TPP would increase the degree of the crosslink. The difference between phosphorylation of gelatine-chitosan formula can be seen in Table 1.

Gelatine and chitosan in this study (pH 3-3.4) is cationic polymer that can react with multivalent anions such as sodium tripolyphosphate. Chitosan with a pKa of 6.3 is polycationic when dissolved in acid and presents–$NH_3^+$ sites, because the free amino groups give chitosan its positive charge. Sodium tripolyphosphate ($Na_5P_3O_{10}$) dissolved in water dissociates to give both hydroxyl and phosphoric ions. Since TPP ionization is controlled by the pH solution, whereas at acidic pH only forms ion $P_3O_{10}^{-5}$, it will form a perfect crosslink that is normally used to regulate drug release [11]. Gelatine is cationic polymer because the isoelectric point of gelatin B at pH5. The phosphorylation procedure involves mixing the two solutions, the solution of gelatine-chitosan and TPP solution [12].

Table 1: Phosphorylation formula gelatine and chitosan

| F | Chitosan (b/v) | Gelatine (b/v) | TPP (b/v) | EG (v/v) | AA (70%v/v) | Asiaticoside (b/v) | Conductivity $\mu$S cm$^{-1}$ | Viskosity mPas | pH |
|---|---|---|---|---|---|---|---|---|---|
| A | 0.5 % | 22 % | 0.1% | 5 % | 70% | 7.5% | 2060 | 430 | 3 |
| B | 0.5 % | 22 % | 0.25% | 5 % | 70% | 7.5% | 2260 | 455 | 3.2 |
| C | 0.5 % | 22 % | 0.5% | 5 % | 70% | 7.5% | 2560 | 460 | 3.4 |

F=Formula, EG=etylene glycol, AA=acetic acid

We use 22% gelatine, because the gelatine content of less than 22% lead viscoelastic force can not overcome the electrostatic force and the Coulomb force, forming a non-homogeneous fibers or bead-shaped particles. The mixture solution of gelatine-chitosan has lower viscosity than the solution that consist of chitosan only, that increasing the ability of electric fields to form a Taylor cone and jet polymer in manufacture of good and homogeneous nanofibers.

The addition of ethylene glycol as cosolvent to obtain a homogeneous nanofibers and no particles and its chosen because it has a high dielectric constant compared with acetic acid. The addition of ethylene glycol will increase the conductivity of the solution. The optimal concentration of ethylene glycol is 5% to obtain a clear solution and a homogeneous nanofibers [4]. Addition asiaticoside was done just before electrospinning, by stirring it with magnetic stirrer. Formulating 3 formulas are intended to compare the effectiveness respectively of the testing in vitro.

**Preparation of Nanofibers**

The addition of electric voltage is an important parameter in the electrospinning, because it relates to the speed of the jet stream. When an electric voltage is added, the electrical charge will add to the polymer solution, resulting in the release of the charged jet and form nanofibers. When the applied voltage is to low, it is not enough to overcome the repulsive force between the molecules of the polymer to resist the formulation Taylor cone [13]. While when the voltage is too high, it will cause the jet stream reaches the collector too fast, thus forming a droplet. If the diameter is smaller than 0.8 mm, it will cause the solution to dry quickly and the pinhole will block the flow of the solution. If the diameter is greater than 0.8 mm, it will produce imperfect nanofibers, this is because the solution has not enough time to evaporate the solvent.

The distance of the needle collector should be enough to evaporate the solvent from the Taylor cone to collector. If the flow rate of the solution is too high it will interfere the elongation of polymer and solvent evaporation, resulting in uncharged polymer and reaching the collector in the form of droplets [14].

Table 2: Diameter nanofibers

| Formula | Diameter |
|---|---|
| A | 620±76 nm |
| B | 704± 90 nm |
| C | 760± 85 nm |

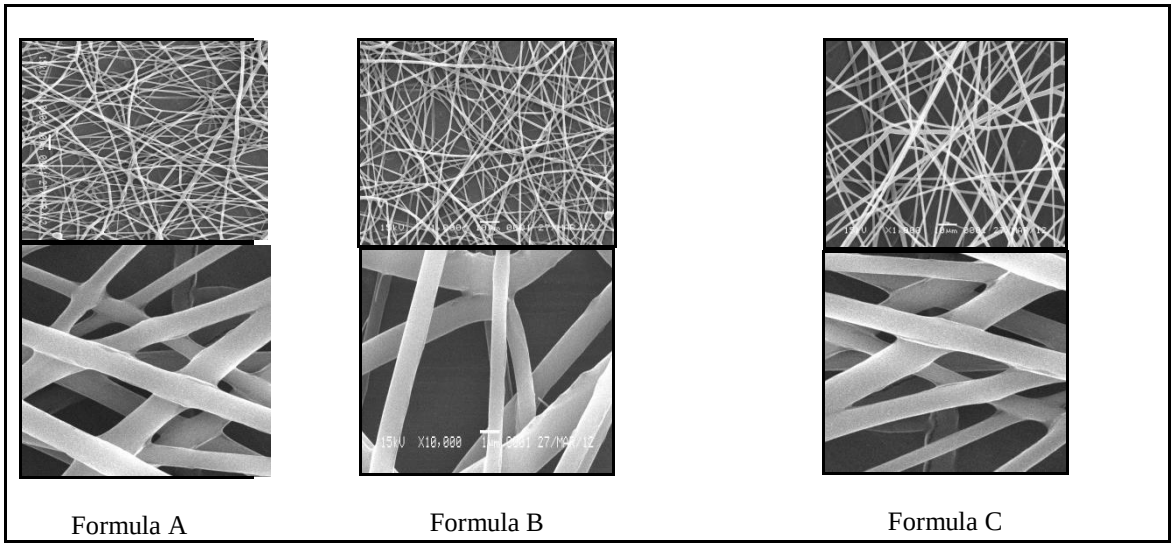



Figure 2: Morphology of nanofibers (1000 x and 10,000 x)

The diameter of the nanofibers produced is determined by the 2 step elongation (streching) during the process, which is at the disposal of Taylor cone and solvent evaporation during the process to reach the collector. The addition TPP to the formula A of 0.1%, formula B 0.25% and the formula C 0.5% turned out to affect the diameter of the fibers. It is because there is an increase of viscosity solution, there by of reducing the fiber elongation during spinning process [15]. Morphology of nanofibers was shown in Figure 2.

**Measurement of the Degree of Swelling**

It can be seen from the graph in Figure 3 that the elongation of the fiber began in the first 30 minutes, then was relatively stable after 90 minutes, where there is a balance solution. This shows the degree of the swelling of fibers ranging from 200% to 500%. Fibers with the addition of TPP 0.5% showed the lowest degree of swelling than others, due to the highest crosslinking density.

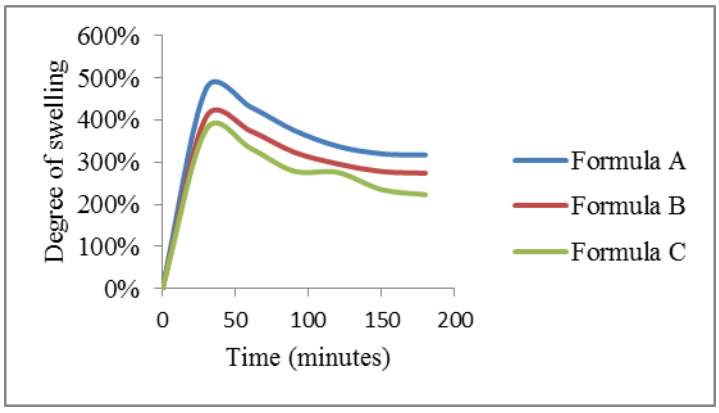



Figure 3. Degree of Swelling

Swelling is mainly influenced by ionic interactions, which depend on the crosslinking density during the formation of the network. An increase in crosslinking density induces a decrease in swelling, by improving the stability of the network, and results in decrease drug release [16].

**Water Retention Capacity of the Nanofibres**

Water retention capacity of fibers was shown in Figure 4. All fibers showed good water retention capacity after removing water by centrifugal force at 25 °C within the range 187 – 238 % of their dry weight. Nanofibers produced 0.5 % TPP showed more water retention capacity than 0.1 % and 0.25 %, may be due to higher crosslinked density in the former case.

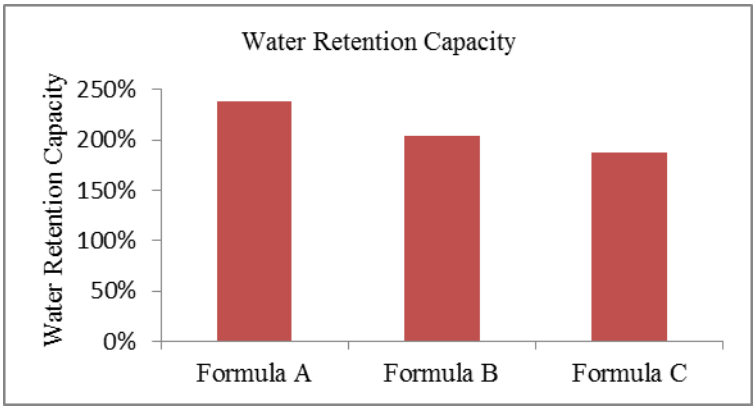



Figure 4: Water Retention Capacity

**Analysis of FT-IR (Fourier Transform Infra Red)**

To compare unknown compounds, it should be done with the standard spectrum in the same condition. The absorbance of infrared radiation changes to the vibrational and rotational energy levels in a covalent bond dipole moment in the molecule. Molecular vibration only occurs when a molecule is composed of two or more atoms.

To be able to absorb infrared radiation, vibration of the molecule must changed dipole moment. There are two types of molecular vibrations which can stretch and bend. Stretching vibration is an organized movement of atoms along the axis of bond between two atoms, so that the distance between atoms can be increased or decreased. The presence of phosphate in the compound can be compared with the absorption in the 1100 – 900 $cm^{-1}$ (P – O stretching) and 1300 – 1150 $cm^{-1}$ (P=O stretching) by using a infrared spectrophotometers [17].

From the results of the spectra as shown in Figure 5, we can see the change in the intensity of the peaks and transmittance chitosan. The peak that appears in the infrared spectra shown in wave numbers 1271, 1213 and 1157 $cm^{-1}$ shows the P = O stretching vibration and the peak at wave numbers 1085, 1012 and 954 $cm^{-1}$ shows the P – O stretching vibration. This is because the bond between the ionic charge of the TPP and the positive amino group (R-$NH_3^+$) of chitosan.

From the results of the spectra as shown in Figure 6, there is a change in the intensity of the peaks and gelatin transmittance. The peak that appears in the infrared spectra shown in wave numbers 1257 $cm^{-1}$ shows the P = O stretching vibration and the peak at wave numbers 1026 and 900 $cm^{-1}$ shows the P – O stretching vibration. This is because the bond between the ionic charge of the TPP and the positive amino group (R-$NH_3^+$) of gelatine.

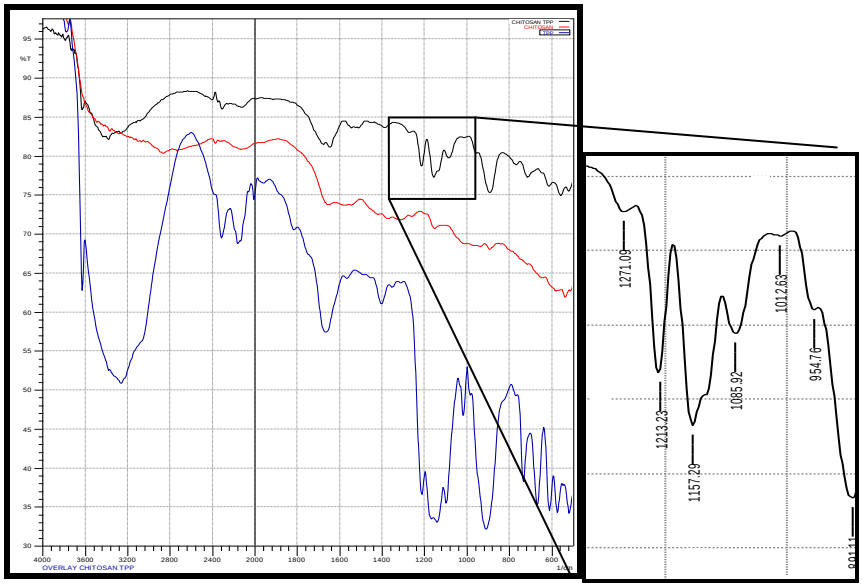



Figure 5: Overlay FTIR Chitosan, TPP and Chitosan TPP

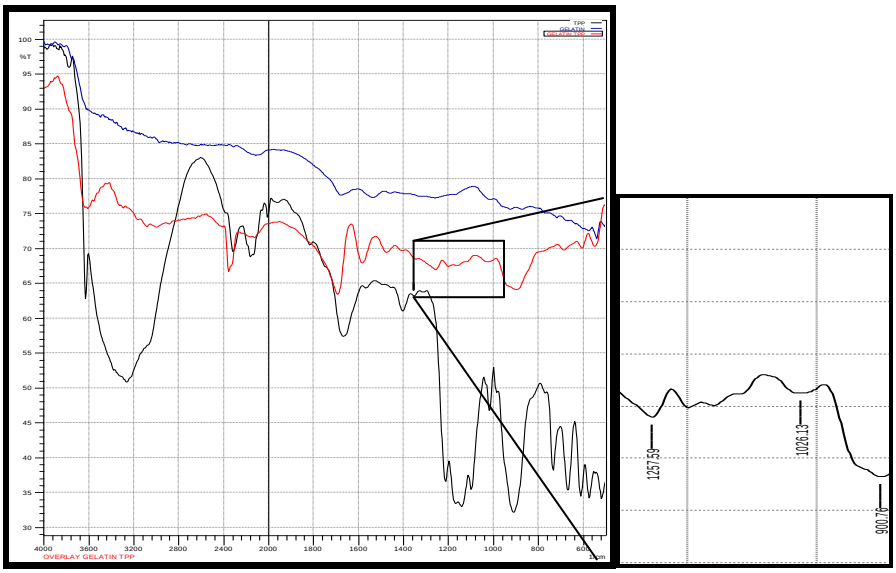



Figure 6: Overlay FTIR Gelatine, TPP and GelatineTPP

**Measurement of the Release Asiaticoside**

The most important thing that is the release of asiaticoside is according to the requirement of wound healing. Asiaticoside has the property to stimulate fibroblasts and synthesize collagen. The phase in which fibroblasts begin to synthesize collagen starts about 72 hours after injury (proliferative phase). Based on the characterization results indicate that the formula C is the best with the release of asiaticoside 51% for 72 hours, compared to formula A

(68%) and formula B (62%). Besides that, formula C has morphology, fiber diameter and the actual content is meet the standard quality requirement of pharmacopoeia.

In this method is used methanol phosphate buffer pH 7.4, which resembles the body fluids. The amount of asiaticoside, obtained from the examination, are formula A 95%, formula B 94% and formula C 94%. From the data obtained, the amount of asiaticoside recovered is sufficiently high, this indicates fairly stable asiaticoside in the process of the manufacturing.

The amount of TPP which were added influences the phosphorylation, in which the degree of swelling, would effected the drug release. Asiaticoside that was release within 72 hours indicates that ph osphorylation gelatine-chitosan can be used to regulate the drug release. The asiaticoside release data can be seen in Figure 7.

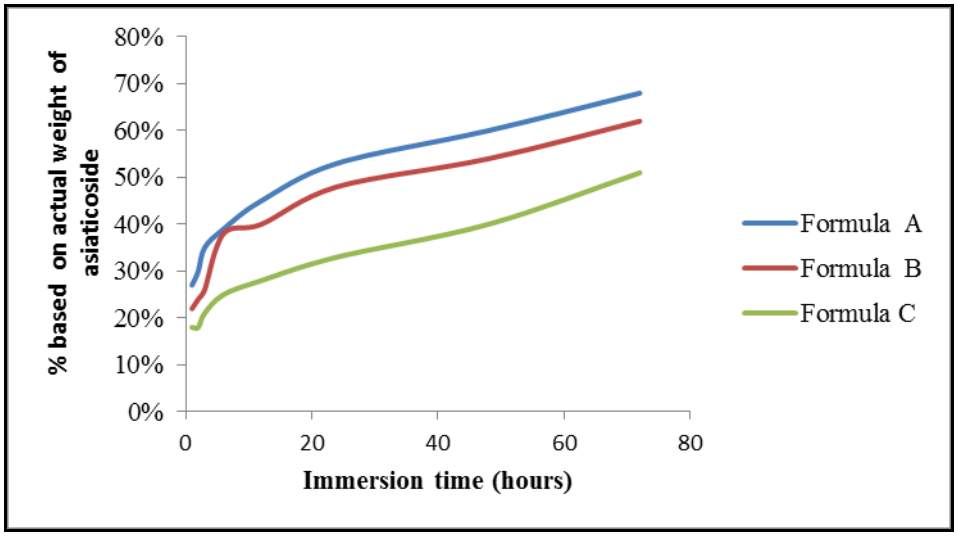



Figure 7: Cumulative release of asiaticoside from nanofibers divided by the actual weight

## Conclusion

Phosphorylation of gelatine and chitosan as an excipient for asiaticoside nanofibers were successfully prepared with the solvent 70% acetic acid using an electrospinning technique. The asiaticoside release from nanofibers in physiological conditions showed a prolonged release profile. The formula C is the best with the release of asiaticoside 51% for 72 hours, compared to formula A (68%) and the formula B (62%). The percentage asiaticoside from nanofibers preparation is between 90% - 100%.

## References

1. Lu, L., Ying, K., Wei, S., Fang, Y., Liu, Y., Lin, H., Ma, L., Mao, Y., (2004). Asiaticoside induction for cell-cycle progression, proliferation and collagen synthesis in human dermal fibroblasts. *International Journal of Dermatology*, 43(11): 801-807.
2. Sikareepaisan, P., Suksamrarn, A., Supaphol, P. (2008). Electrospun Gelatin Fiber Mats Containing a Herbal-*Centella asiatica*- Extract and Release Characteristic of Asiaticoside. *Nanotechnology*, 19(1): 015102.
3. Boateng, JS., Matthews, K., Steven, HE., Eccleston, GM., (2008). Wound Healing Dressings and Drug Delivery Systems. *Journal of Pharmaceutical Sciences*, 97(8): 2892-2923
4. Murugan, R., Ramakrishna, S., (2007). Design Strategies of Tissue Engineering Scaffolds with Controlled Fiber Orientation. *Tissue Engineering*,13(8): 1845-1866.

5. Chew, SY., Wen, Y., Dzenis, Y., Leong, Y., (2006). The Role of Electrospinning in the Emerging Field of Nanomedicine: *Current Pharmaceutical Design*, 12(36): 4751-4770
6. Choktaweesap, N., Arayanarakul, K., Aht-ong, D., Meechaisue, C., Supaphol, P. (2007). Electrospun Gelatin Fibers: Effect of Solvent System on Morphology and Fiber Diameters. *Polymer Journal*, 39(6): 622-631.
7. Vrieze, S., Westbroek, P., Camp,T., Langenhove, L. (2007). Electrospinning of Chitosan Nanofibrous Structures: Feasibility Study. *Journal Materials Sciences*, 42: 8029-8034.
8. Javari, J., Emami, SH., Samadikuchaksaraei, A., Bahar, M A., Gorjipour, F. (2011). Electrospun Chitosan Gelatin Nanofiberous Scaffold: Fabrication and *In Vitro* Evaluation. *Bio-Medical Materials and Engineering*, 21(2): 99-102.
9. Amaral, IF., Granja, PL., Barbosa, MA., (2005). Chemical modification of chitosan by phosphorylation: *J. Biomaterials Science Polymer*, 16(12): 1575–1593
10. Pati, F., Datta, P., Chatterjee, J., Dhara, S. (2010). Development of Chitosan-Tripolyphosphate Fiber for Biomedical Application. *IEEE Students' Technology Symposium*,77-81
11. Schiffman, JD., Schauer, CL. (2007). One-Step Electrospinning of Cross-Linked Chitosan Fibers: *Biomacromolecules*, 8(9): 2665-2667.
12. Bhumkar, Devika R., Varsha B. Pokharkar. (2006). Studies on effect of pH on cross-linking of chitosan with sodium tripolyphosphate: A technical note. *AAPS PharmSciTech*,7 (2) Article 50.
13. Khairurrijal ., Munir, MM., Saehana, S., Iskandar, F., Abdullah, M. (2009). Teknik pemintalan elektrik untuk pembuatan nanoserat dari pemodelan hingga eksperimen. *Jurnal Nanosains & Nanoteknologi*, edisi khusus.
14. M. Pillai, CKS., Sharma, P. (2009). Electrospinning of Chitin and Chitosan Nanofibres. *Trends Biomater. Artif. Organs*, 22(3): 179-201.
15. Suwantong, O., Ruktanonchai, U., Supaphol, P. (2008). Electrospun cellulose acetate fiber mats containing asiaticoside or Centella asiatica crude extract and the release characteristics of asiaticoside. *Polymer,* 49(19): 4239–4247
16. Berger, J., Mayer, JM., Felt, O., Peppas, NA., Gurny, R. (2004). Structure and interactions in covalently and ionically crosslinked chitosan hydrogels for biomedical applications. *European Journal of Pharmaceutics and Biopharmaceutics,* 57(1): 19–34
17. Silverstein, RM., Webster, FX., Kiemle, DJ., *Spectrometric identification of organic compounds,* Wiley, America (2005): 417

The Malaysian Journal of ANALYTICAL SCIENCES ISSN 1394-2506

# FORENSIC ANALYSIS OF HIGH EXPLOSIVE RESIDUES FROM SELECTED CLOTH

## (Analisis Forensik Residu Bahan Letupan Berkuasa Tinggi Daripada Kain Terpilih)

Mohamad Afiq Mohamed Huri and Umi Kalthom Ahmad*

*Department of Chemistry, Faculty of Science,*
*Universiti Teknologi Malaysia, 81310 UTM Johor Bahru, Johor Darul Ta'zi, Malaysia*

**Corresponding author: umi@kimia.fs.utm.my*

**Abstract**

Increased terrorist activities around the Asian region have resulted in the need for improved analytical techniques in forensic analysis. High explosive residues from post-blast clothing are often encountered as physical evidence submitted to a forensic laboratory. Therefore, this study was initiated to detect high explosives residues of cyclotrimethylenetrinitramine (RDX) and pentaerythritoltetranitrate (PETN) on selected cloth in this study. Cotton swabbing technique was employed as a simple and rapid method in recovering analytes from the sample matrix. Analytes were analyzed using Griess spot test, TLC and HPLC. TLC separation employed toluene-ethyl acetate (9:1) as a good solvent system. Reversed phase HPLC separation employed acetonitrile-water (65:35) as the mobile phase and analytes detected using a programmed wavelength. RDX was detected at 235 nm for the first 3.5 min and then switched to 215 nm for PETN. Limits of detection (LODs) of analytes were in the low ppm range (0.05 ppm for RDX and 0.25 ppm for PETN). Analyte recovery studies revealed that the type of cloth has a profound effect on the extraction efficiency. Analytes were recovered better for nylon as compared to cotton cloth. However, no analytes could be recovered from denim cloth. For post-blast samples, only RDX was detected in low concentration for both nylon and cotton cloth.

**Keywords:** high explosive residues, RDX, PETN, HPLC-UV, cotton swabbing, cloth

**Abstrak**

Peningkatan aktiviti keganasan di rantau Asia telah menyebabkan keperluan analisis teknik yang lebih baik dalam analisis forensik. Residu bahan letupan berkuasa tinggi daripada sampel pakaian sering dijumpai sebagai bukti fizikal yang dihantar kepada makmal forensik. Oleh itu, kajian ini telah dimulakan untuk mengesan bahan letupan berkuasa tinggi, siklotrimetilenetrinitramina (RDX) dan pentaeritritol tetranitrat (PETN) pada matriks kain. Kaedah sapuan bebola kapas digunakan sebagai kaedah yang mudah dan pantas dalam mengekstrak analit daripada sampel matriks. Analit dianalisis dengan menggunakan ujian setempat Griess, TLC dan HPLC. Pemisahan TLC menggunakan toluena-etil asetat (9:1) sebagai sistem pelarut. Pemisahan HPLC fasa terbalik dengan menggunakan asetonitril-air (65:35) sebagai fasa bergerak dan analit dikesan menggunakan pengesanan berprogram. RDX dikesan pada panjang gelombang 235 nm dalam masa 3.5 minit yang pertama, dan selepas itu panjang gelombang diubah kepada 215 nm bagi pengesanan PETN. Had pengesanan (LOD) analit berada dalam julat ppm yang rendah (RDX 0.05 ppm dan PETN 0.25 ppm). Kajian pengembalian analit menunjukkan bahawa jenis kain memberi kesan mendalam terhadap kecekapan pengekstrakan. Pengembalian analit bagi nilon lebih baik berbanding dengan kain kapas. Walau bagaimanapun, tiada analit dapat dikesan daripada kain denim. Untuk sampel pasca letupan, hanya RDX telah dikesan dalam kepekatan yang rendah untuk kedua-dua kain nilon dan kapas.

**Kata kunci:** residu bahan letupan berkuasa tinggi, RDX, PETN, HPLC-UV, sapuan kapas, kain

## Introduction

Media reports of bombing incidents in the South East Asian regions have sparked much interest amongst forensic scientists to embark on the study of explosive residue analysis. Post-explosive residues can provide useful information to investigators such as type of explosives used which can be used as the ultimate evidence in the court of law [1-3].

Post-explosion products collected from bombing activities by terrorists have been the main subject of study in forensic investigations. For example, forensic investigations that were made following the bombing incident in Bali, Indonesia on October 2002 has served as crucial evidence in convicting the responsible criminals [4]. A great number of physical evidence such as post-blast samples can be collected at the crime scene in order to link a suspect to the bombing case. Such physical evidence must be collected and kept well for analysis as the evidence itself holds useful information in order to solve the crime [5].

Generally, explosives can be divided into two groups namely high and low explosive. They are divided based on the velocity or rate of the reaction for explosion to occur. According to Mäkinen et al. [6], explosives are usually classified based on their properties and usage. High explosive is a substance that detonates at very high rate. Applications of high explosives included mining, demolition and military use. High explosives are extremely dangerous as they would produce high amount of gases, high temperature and exothermic reactions. The shock waves that are produced from the explosion can have velocities between 1 - 9 km/s.

Cyclotrimethylenetrinitramine (RDX) and pentaerythritoltetranitrate (PETN) are two chemical compounds that can be classified under organic high explosive components. Both compounds (Figure 1) are among the main components of C4 explosive. RDX is toxic and poisonous as it will give adverse effect if it is ingested by the body. RDX is a major component in C-4 explosive comprising of 91% of the total component. In addition, RDX is also used in Semtex explosive and as booster charges. PETN is also known as Penta or Ten. It is usually in the form of white crystalline explosive. PETN is mixed with RDX in Semtex explosive material. It exists as secondary explosive of the high explosive because of its high stability and the need to be initiated by other impact from primary explosive [7].

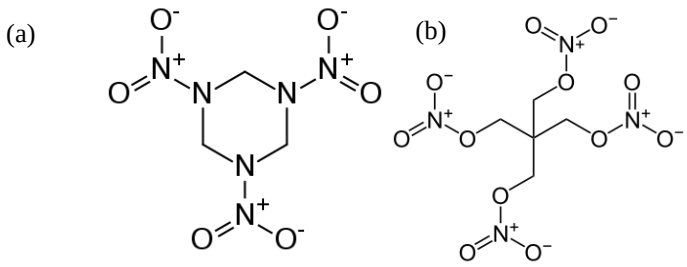



Figure 1**:** Chemical structure of (a) RDX and (b) PETN

Several analytical instrumentations have been used for explosive detection analysis. For inorganic explosive analysis, Varga and Ulbrich employed a combination of gas chromatography (GC) and electron capture detection (ECD) as a highly selective method in trace analysis of organic components of post-blast residues [2]. Furthermore, ECD is more sensitive compared to flame ionization (FID) and thermal conductivity detectors (TCD). Besides, GC-ECD has high sensitivity towards electronegative atoms (nitrogen compounds) and low sensitivity to contaminants as it quite insensitive to hydrocarbons [7]. However, GC-ECD method has a drawback since it is prone to contamination. To overcome this problem, a combination of gas chromatography and solid phase microextraction was employed for removing interfering compounds [8]. Ahmad et al. [9] analysed C4 explosive residue on hair samples by using GC-ECD on a HP5-MS capillary column. RDX and PETN were successfully separated within 10 minutes with good limit of detections (RDX: 10 ppm, PETN: 0.1 ppm). The study concluded that human hairs could be used as important physical evidence to recover explosive residues from post-blast samples.

Micellar electrokinetic chromatography (MEKC) is a modified technique of capillary electrophoresis (CE). This technique has also been widely used for uncharged molecules such as organic explosives. The separation allows a variety of compounds to be separated with high efficiency. In addition, as compared to GC techniques, MEKC has an advantage as the technique permits thermally labile materials to be separated without degradation. Ahmad et al.

[10] successfully employed MEKC coupled to solid phase extraction (SPE) to the analysis of post-blast water samples containing explosive residues. Analyte recoveries of >87 % were obtained. RDX was also detected in the water samples in the range of 51.03 – 156.75 µg/L [10].

High performance liquid chromatography (HPLC) is often used for analysis of explosives because it is ideal for the analysis of high molecular weight, low volatility and thermally unstable compounds [6]. This method will overcome the problem of product decompositions in vapours due to unstable explosive residues properties. Furthermore, the wide range of HPLC detection between 190-800 nm will provide a good range of separation.The most common detector for HPLC is ultraviolet detector (UV). It is because many organic compounds will be detected in the range of UV detection region. Miller et al. reported that RDX, PETN and TNT all have strong absorption wavelengths below 260 nm [11]. Both TNT and RDX peaks were resolved at 205, 235 and 254 nm, while PETN was only resolved at 205 nm. Methanol was used as solvent to extract the analytes.

Forensic analyses typically involve numerous physical evidences that can be found at the crime scene, including debris, soil, water, skin and also cloth or fabric. Cloth of different fiber types can became important physical evidence in forensic investigations. Recovery of fibres at crime scene, either natural or man-made fibers may provide individual identification with a high degree of certainty [12]. However, extraction methods and analytical procedures that are suitable for the analysis of explosive residue on fibres have not been extensively reported. This study was therefore undertaken to extract high explosives of RDX and PETN from several cloth types using cotton swabbing. Extracts were analysed using colour spot test, thin layer chromatography (TLC) and HPLC with UV programmed wavelength.

## Materials and Methods

### Chemical and Materials

Explosive standards of RDX and PETN (1000 ppm solution in acetonitrile) were obtained as gifts from Science & Technology Research Institute for Defense (STRIDE), Batu Arang, Selangor. Cloth samples (denim, nylon and cotton) and cotton balls were obtained from a local store in Taman Universiti, Skudai, Johor. Simulated explosive samples were obtained from a previous sampling exercise made in collaboration with Royal Malaysia Police (RMP).

### Screening Test

As a preliminary test, Griess reagent was employed that was made from two different reagents. First reagent consisted of 0.25 g napthol in 80 mL of 30% acetic acid while the second reagent was prepared by adding 0.5 g sulfanilic acid in 50 mL of 30% acetic acid. An orange color observed indicated the presence of explosive material, nitrite. For TLC analysis, aluminium backed silica gel TLC plate was used. The solvent systems used were mixtures of toluene-cylcohexane with ratio 6:4 and toluene-ethyl acetate with ratio 9:1 [13, 14]. The analyte spots were observed under UV lamp at 254 nm.

### Instrumentation

HPLC analysis utilized an Agilent 1100 series HPLC that was equipped with a variable wavelength detector (VWD), degasser, quaternary pump and computerized data acquisition employing HPLC Chemstation Software g2170AA. The analytical column used was a Purospher C18 (4.6 x 150 mm, 5 µm). A mobile phase consisting of acetonitrile-water mixture with a ratio of 65:35 (v/v) was used at a mobile phase flow rate of 1.0 mL/min. Analyte detection was at 235 nm and 215 nm for RDX and PETN respectively. UV detection was programmed at 235 nm for the first 3.5 minutes, and then switched to 215 nm for the next 6.5 minutes. An aliquot of 20 µL sample was introduced into the system via a Rheodyne six port injection valve fitted with a 20 µL sample loop [15].

### Microscopic Examination

For microscopic examination, a Motic model BA310 stereomicroscope (Xiamen, China) was used. The 30x magnification was used to identify the physical characteristics of both nylon and cotton cloth samples. The thickness of thread and other unique characteristics were also examined.

**Standard Solutions**

A stock solution comprising of 1000 ppm each RDX and PETN was prepared by adding 0.1000 g each of RDX and PETN with acetonitrile in a 100 mL volumetric flask and diluting to the mark. For the standard mixture, the standard solutions were further diluted by mixing both analytes in 5 mL volumetric flask that resulted in concentration of 100 ppm and 500 ppm of RDX and PETN respectively. A series of standard mixture concentration of RDX:PETN from concentration ratio of 100:500 to 1:5 was produced which were used for the construction of calibration curve.

**Sample preparation**

For recovery study on cotton ball, direct spiking of analytes onto the cotton ball was carried out in order to determine the efficiency of swabbing techniques. 1 mL of the standard mixture consisting of RDX (100 ppm) and PETN (500 ppm) was spiked onto a pre-cleaned cotton ball. The cotton ball was then allowed to air dry. Three types of cloth samples used were cotton, nylon and denim. All cloths were pre-washed by soaking in water to reduce contamination arising from impurities. The cloths were dried and then cut into pieces of 7 cm x 8 cm size. Each cloth was then hanged vertically using claw clips and spiked with 1 mL standard mixture by using a micropipette. The cloth was then left to dry for about 10 minutes and later kept in a zip-lock plastic bag and stored in a refrigerator.

**Sample Swabbing and Extraction**

Cotton balls were then subjected to pre-cleaning by soaking the cotton balls overnight in acetone. On the next day, excess acetone was removed by squeezing out the solvent from the cotton balls using a pair of tongs and left to air-dry. The pre-cleaned cotton balls were placed in zip-lock plastic bags and kept in the refrigerator until ready to use. For the swabbing process of the residue, 1 mL of acetone was added to the cotton ball by using a micropipette in order to moisten the cotton ball. By using a rubber glove, the acetone-moist cotton balls were swabbed onto the cloth surfaces in order to extract the residue. The cloth sample was placed on a clean ceramic tile before the cotton ball was swabbed thoroughly across the whole surface of the cloth. Furthermore, the surface of the tile was also swabbed to recover any residual analyte left on the tile. The cotton swabs were then ready for extraction.

The cotton swab was placed in a vial and acetone was added into the vial up to 5-10 mL graduation so as to ensure that the cotton ball was completely covered by the solvent. The vial was then vortex approximately for 1 minute. In order to increase efficiency of filtration process, a filter paper (Whatman, 90 mm) was cut and fitted to the bottom of a 20 mL glass syringe. The extract was then filtered through a syringe that was fitted with filter paper. The extract was poured slowly before the cotton ball was inserted into the syringe. The last few drops were recollected by pressing down the cotton swab tightly to the bottom of the syringe. The extract was collected in a 10 mL vial and then dried gently under a flow of nitrogen gas. Acetonitrile was added to bring the volume to 1 mL [15]. The extract was subjected to color spot test, TLC and HPLC analyses. A blank extraction was also prepared.

## Results and Discussion

**Spot Test Analysis**

Griess reagent provides a visual observation of orange color formation from the reaction between acetic acid vapour, nitrate residues and the chemical content on a filter paper [16]. In this study, explosive standard RDX and PETN of a fixed concentration (1000 ppm) were deposited on a filter paper and then tested with Griess reagent. Both explosives gave a positive orange color spot. Although a positive reaction with Griess test indicated the presence of RDX and PETN, the spot test alone could not differentiate between both explosives. Table 1 shows that the detection limit of Griess spot test on RDX and PETN were both 200 ppm. Lower than this concentration, the orange color could not be positively detected.

**Thin Layer Chromatographic Analysis**

TLC separation employing toluene-cyclohexane (6:4) did not give any significant $R_f$ values. Hence, solvent system employing toluene-ethyl acetate was tested [13]. For standard PETN and RDX, both analytes were well separated and observed. For sample extracts, both extracts for cotton and nylon cloth sample revealed analyte spots on the TLC plate when viewed under UV wavelength. This showed that sample extracts contained both PETN and RDX. By using toluene-ethyl acetate as the best solvent system, standard explosives of decreasing concentration were also

spotted on TLC plate at a fixed volume of 20 µL. This was done to estimate the detection limit of the TLC analysis. Table 2 shows that RDX could be detected using TLC up to 50 ppm, while PETN could only be observed on the TLC plate at concentration of 500 ppm or more.

Table 1: Griess spot test detection limit of RDX and PETN

| Analyte | Concentration (ppm) | * Detectability |
|---|---|---|
| RDX | 1000 | ✓ |
| | 500 | ✓ |
| | 200 | ✓ |
| | 100 | ND |
| PETN | 1000 | ✓ |
| | 500 | ✓ |
| | 200 | ✓ |
| | 100 | ND |

* ✓ : detectable , ND: not detectable

Table 2: Detectability of analytes byTLC analysis using solvent system toluene-ethyl acetate (9:1)

| **Analyte** | **$R_f$** | **Concentration (ppm)** | *** Detectability** |
|---|---|---|---|
| RDX | 0.31 | 1000 | ✓ |
| | | 100 | ✓ |
| | | 50 | ✓ |
| | | 10 | ND |
| PETN | 0.87 | 1000 | ✓ |
| | | 500 | ✓ |
| | | 100 | ND |
| | | 50 | ND |

* ✓ : detectable , ND: not detectable

**HPLC-UV Profile for Standard Mixture**

HPLC conditions used in this study were as suggested by Ahmad *et al.* but with some modifications [10]. UV response for PETN (500 ppm) was found to be much lower than RDX (100 ppm). Thus a mixture of test compounds of unequal analyte concentrations was used. HPLC-UV separation of standard mixture of PETN and RDX gave two resolved peaks that eluted within 5 minutes (Figure 3). RDX eluted earlier than PETN with retention time of 2.5 and 4.3 min respectively. It was not possible to detect both analytes appreciably at a fixed single wavelength. RDX peak gave a good UV response at 235 nm while PETN at 215 nm. Hence UV detection was programmed at 235 nm for the first 3.5 minutes to detect RDX, and then switched to 215 nm for the next 6.5 minutes to detect PETN.

**Calibration Graph and Limit of Detection**

Various concentration of standard mixture was injected to obtained chromatograms, which were used to plot calibration graph. The concentrations of standard mixture of RDX and PETN chosen for this analysis were in the range from 10 to 50 ppm for RDX and 100 to 500 ppm for PETN. Linear calibration graphs were obtained for both RDX and PETN with good correlation coefficients (0.99-1.00). The limit of detection (LOD) of an analyte was assessed from a signal to noise ratio (S/N) of 2:1. In this study, the limit of detection for RDX and PETN were 0.05 µg/g and 0.25 µg/g respectively which gave lower LOD compared to previous studies [9,15] (Table 3).

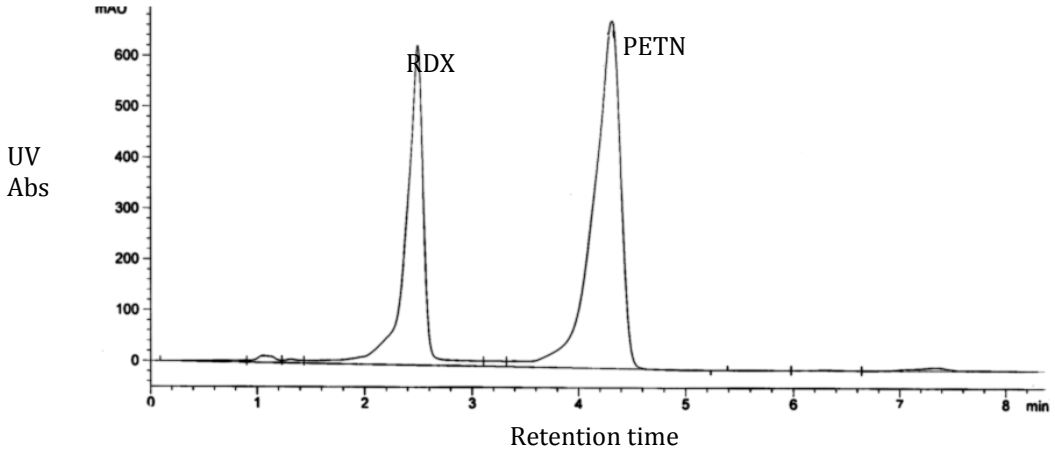



Figure 3: Chromatogram of standard mixture solution containing RDX and PETN, with concentration of 100 ppm and 500 ppm respectively. HPLC conditions: Purospher C18 (4.6 x 150 mm, 5 µm), acetonitrile-water mixtures (65:35, v/v), mobile phase flow at rate of 1.0 mL/min. Analytes detection at 235 nm and 215 nm for RDX and PETN respectively. Programmed UV detection at 235 nm for the first 3.5 minutes, and then switched to 215 nm for the next 6.5 minutes.

Table 3: Detection limit data of each analyte and comparison of LOD with other study.

| Analyte | Limit of Detection (ppm) | | |
|---|---|---|---|
| | **This study** | **Ahmad *et al.* *[9]** | **Ahmad *et al* #[15]** |
| RDX | 0.05 | 10 | NR |
| PETN | 0.25 | 0.1 | 20 |

NR: Not Reported, * Ref 9: GC-ECD, # Ref 15: HPLC-UV, column: Agilent Zorbax Eclipse XDB-C18 (4.6 x 150 mm, 5 µm), mobile phase: acetonitrile-water (55:45), detection: UV at 230 nm.

**Recovery Study**

In order to evaluate the efficiency of extraction, recoveries of analyte from cotton ball and spiked samples were determined. Peak areas of spiked cotton ball and spiked samples measured were used to calculate the percentage analyte recovery. The analyte recovery for extraction using cotton ball swabbing technique was found to be 90.05 % and 89.05 % for RDX and PETN respectively (Table 4). This indicated satisfactory recovery. The result of this technique was comparable to an earlier work done by Ahmad *et al.* who reported recoveries of over 89% for PETN [15]. Meanwhile, recovery for RDX obtained in this study (90.1 %) was much better compared to that in an earlier work by Thompson *et al.*[17].

Table 4: Recovery of analytes from spiked cotton swab

| | | | Percentage Recovery (%) | | |
|---|---|---|---|---|---|
| **Analyte** | **Spiking Level (ppm)** | **Concentration ± SD* (µg/g)** | **This Study** | **Ahmad *et al.* [15]** | **Thompson *et al.* [17]** |
| RDX | 100 | 90.50 ± 3.77 | 90.1 | NR | 70 |
| PETN | 500 | 445.27 ± 22.27 | 89.1 | 89.5 | 63 |

NR: Not Reported, SD: based on triplicate extraction

For spiked sample, the analyte recovery study was done onto three types of cloth which were cotton, nylon and denim. For cotton cloth, mean percentage recovery that has been obtained for RDX and PETN were only 12.7 % and 9.9 % respectively. This shows a very low extraction efficiency was obtained from cotton.This could be due to the physical nature of cotton cloth. Cotton cloths are made up from threads that are spun together causing the analytes to be attached tightly to the threads. Cotton fibres containing cellulose is polar and binds strongly with polar analytes. Cellulose with chemical formula $(C_6H_{10}O_5)_n$, consists of hydroxyl (-OH) groups that would tend to form hydrogen bonds with analytes containing oxygen bond (-O) and nitrogen bond (-N).

For recovery study on spiked nylon cloth, percentage recovery that has been obtained for RDX and PETN were 41.9 % and 34.4 % respectively. Higher percentage recovery obtained for nylon as compared to cotton was possibly due to the smooth nature of the nylon cloth that facilitated the analyte extraction from the matrix. However, no analytes could be recovered from denim. This maybe be due to the thickness of the denim cloth which was thicker compared to other types of cloth analyzed. Table 5 shows the analyte recoveries from cotton, nylon and denim cloth.

Table 5: Analyte recoveries from selected cloth

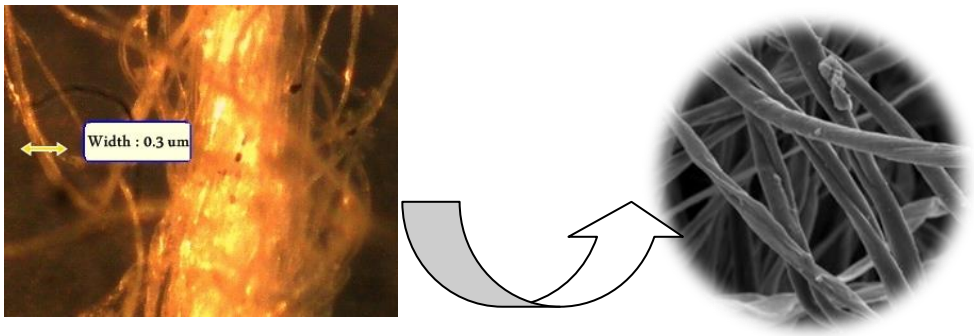
| **Cloth Sample** | **Analyte** | **Concentration ± SD* (µg/g)** | **% Recovery** |
|---|---|---|---|
| Cotton | RDX | 12.71 ± 2.81 | 12.7 |
| | PETN | 49.71 ± 13.16 | 9.9 |
| Nylon | RDX | 41.94 ± 14.34 | 41.9 |
| | PETN | 171.78 ± 69.24 | 34.4 |
| Denim | RDX | ND | ND |
| | PETN | ND | ND |

*ND: Not Detected, SD: Based on triplicate extractions

**Microscopic Analysis of Fibers**

Physical characteristics of the cloth samples were found to have a profound effect on the extraction of explosives analyzed. From the results of HPLC analysis, different types of cloth gave different recovery of analyte. A few threads of fiber from each cloth (cotton and nylon) were removed and examined under a stereomicroscope. Figure 4 shows the microscopic structure of cloth samples.

(a)



(b)

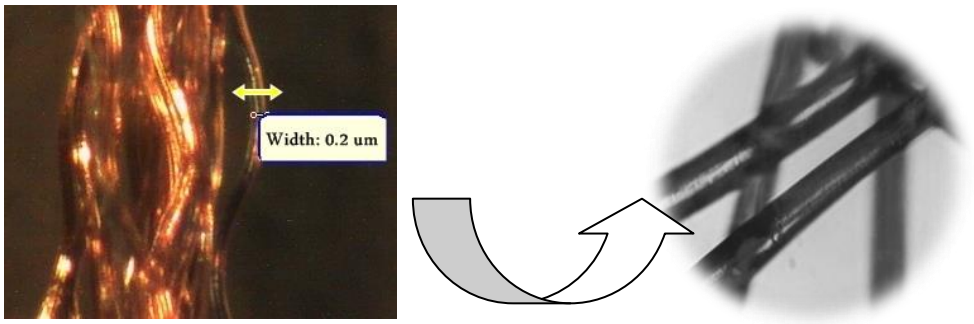



Figure 4: Microscopic structure of (a) Cotton fiber and (b) Nylon fiber using 30X magnifications. Circular inset showing enlarged individual fibers.

Microscopic examination of cotton threads revealed that each thread composed of several strands of cotton fibers that were twisted together to form a thread. Each strand of cotton fiber was observed as highly convoluted and twisted cotton fiber (Figure 4a). Cotton fiber is a natural fiber composed mainly of cellulose that contain hydroxyl (-OH) groups (Figure 5) [18]. In cotton cloth, the fiber matrix is capable of retaining the explosive analytes via ion-dipole and dipole-dipole interactions. Several possible sites within the fiber matrices that can interact with the analytes are depicted in Figure 6.

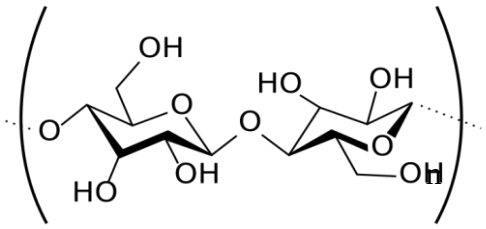



Figure 5: Structural formula of cellulose [18].

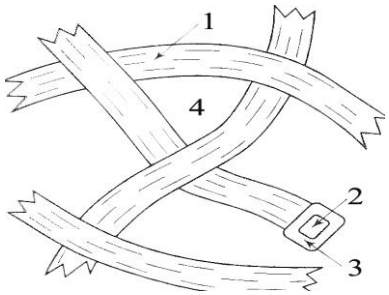



Figure 6: Sites where analyte can interact with cellulose fibers of cotton cloth: (1) on the surface, (2) internally, (3) within the wall of fiber and (4) within spaces between fibers [18].

Nylon fibers are man-made fibers. When these fibers were observed under microscope, they appeared as long strands of fibers and of uniform diameter (0.2 µm). The surface of the nylon fibers appeared smooth and featureless (Figure 4b). The difference in fiber matrix for cotton and nylon accounted for the low analyte recovery from cotton cloth as compared to that from nylon cloth.

**Post Blast Sample Analysis**

Post blast sample analysis was performed on cloth pieces of nylon and cotton that were exposed to explosive using C4 explosives. Results of the study revealed that extraction of analytes were slightly greater for nylon as compared to cotton cloth (Table 5). From the HPLC profiles of the post blast samples, PETN peak was not detected since it is just a minor component of the C4 explosive and that PETN may be present as the propellant [19]. Other factors such as prolong storage in and degradation process may also contribute to the non detectability of PETN. Concentration of RDX that has been recovered from both nylon and cloth samples is listed in Table 5.

Table 5: Concentration of analytes recovered from post blast cloth samples

| | **Concentration ± SD*(µg/g)** | |
|---|---|---|
| **Cloth** | **RDX** | **PETN** |
| nylon | 4.02±0.16 | ND |
| cotton | 3.38±0.29 | ND |

ND: Not Detected, *SD: Based on triplicate extractions

## Conclusion

Simultaneous detection of RDX and PETN explosives have been successfully developed using cotton swabbing technique and HPLC-UV analysis. Reversed phase HPLC separation employed acetonitrile-water (65:35) as the mobile phase and a programmed wavelength for the detection of RDX at 235 nm for the first 3.5 minutes and thereafter for PETN at 215 nm. HPLC separation gave two resolved peaks that eluted within 5 minutes. LODs of analytes were in the low ppm range (0.05 ppm RDX and 0.25 ppm PETN). The extraction of high explosive using cotton swabbing developed in this study shows a relatively high recovery for RDX (90.1 %) and PETN (89.1 %). Analyte recovery studies revealed that the type of cloth has a profound effect on the extraction efficiency. Analytes were recovered better for nylon as compared to cotton cloth. However, no analytes could be recovered from denim cloth. For post-blast samples, only RDX was detected in low concentration (3-4 µg/g**)** for both nylon and cotton cloth.

## Acknowledgement

The authors would like to acknowledge Institut Penyelidikan Sains &Teknologi Pertahanan (STRIDE), Batu Arang, Selangor for their collaboration in providing standard explosives. Thanks are also due to the Department of Chemistry, Faculty of Science, UTM for research facilities and MOHE for financial assistance via FRGS grant R.J130000.7826.4F200.

## References

1. Ahmad, U. K. and Heng, K. K., (2007). Solid Phase Microextraction-Gas Chromatography for the Analysis of Explosives in Post Blast Water Samples, *J. Teknologi C*., **46** (c): 59-74.
2. Varga, R., and Ulbrich, P. (2004). Some Experience with Trace Analysis of Post-explosion Residues, *AARMS* 3 (4): 633-646.
3. Ladham, S., Koehler A. S., Woods P., Huston R., Dominick J., Fotchman W. F., and Wecht H. C. (2005). A Case Of A Death By Explosives: The Keys To A Proper Investigation. *J. Clin. Forensic Med*,. **12**(2): 85-92.
4. Royds, D., Lewis S. W., and Taylor A. M. (2005). A Case Study In Forensic Chemistry: The Bali Bombings. *Talanta*. **67**(2): 262-268.
5. Sharma, M., Khajja B. S.,Vashistha, K. N., Bairwa, T., Sharma, S., Srivastava, S., and Mathur, G. K. (2010). Trace Evidence Crack a Suicide Proved Homicide: A Case Study. *J. Forensic Res*, 1:103.

6. Mäkinen, M., Nousiainen M., and Sillanpää M. (2011). Ion Spectrometric Detection Technologies for Ultra-Traces of Explosives: A review. *Mass Spectrometry Reviews*. 30(5): 940-973.
7. Yinon, J. and Zitrin, S. (1981). The Analysis of Explosives. England: Pergamon Press Ltd. 59-118.
8. Calderara, S., Gardebas, D. and Martinez, F. (2003). Solid Phase Micro Extraction Coupled With On-Column GC/ECD for the Post-Blast Analysis of Organic Explosives. *Forensic Sci. Int.*,**137**: 6-12.
9. Umi Kalthom Ahmad, Noor Hidayat Abu Bakar & Shaikh Abdul Adziz Shaikh Abdullah, Analysis of C4 Explosive Residues On Post Blast Hair Samples (2012). *Jurnal Teknologi*, 57 (Sains & Kej.) Keluaran Khas (1), Mac: 163–171.
10. Ahmad, U. K., Rajendran, S., Ling, L. W., and Hooi, Y. C. (2008). Forensic Analysis of High Explosive Residues in Post-Blast Water Samples Employing Solid Phase Extraction for Analyte Pre-Concentration. *Malays. J. Anal. Sci., 367-374.*
11. Miller, C., Elias G., Schmitt N. C., Rae C. (2010). Identification of Explosives from Porous Materials: Applications Using Reversed Phase High Performance Liquid Chromatography and Gas Chromatography. *Sensing and Imaging*: *An Int. J*. **11**(2): 61-75.
12. Saferstein, R. (2004). Criminalistics: An Introduction to Forensic Science, 9th Ed. New Jersey: Prentice Hall.
13. Nurul Nuwaida Muhammad Salim (2006). Analisis Forensik bagi Bahan Letupan Menggunakan Ujian PetandaWarna dan Kaedah Kromatografi Lapisan Nipis. UniversitiTeknologi Malaysia: Bachelor of Science (Industrial Chemistry) Project Report.
14. Beverige, A. (1998). Forensic Investigation of Explosions. Boca Raton, London: CRC Press.
15. Ahmad, U. K., Rajendran, S., and Hassan A. S. (2008). Forensic Analysis of Explosive Residues from Hand Swabs, *Malays. J. Anal. Sci., 25-31.*
16. James S.H. and Nordby J. J., (2005), Forensic Science – An Introduction to Scientific and Investigative Techniques, Boca Raton, Florida: CRC Press.
17. Thompson, R. Q., Fetterolf, D. D., Miller, M. L. and Mothershead, R. F. (1998) Aqueous Recovery From Cotton Swabs of Organic Explosives Followed by Solid Phase Extraction, *J. Forensic Sci.,* 795-804.
18. Bell, S. (2006). *Forensic Chemistry*, New Jersey, USA: Prentice Hall.
19. Banas, K., Banas, A., Moser, H. O., Bahou, M., Li, W., Yang, P., Cholewa, M., and Lim, S. K. (2010). Multivariate Analysis Techniques in the Forensics Investigation of the Postblast Residues By Means of Fourier Transform-Infrared Spectroscopy. *Anal. Chem*., 82: 3038-3044.

The Malaysian Journal of ANALYTICAL SCIENCES ISSN 1394-2506

# A STUDY ON ADSORPTION OF CADMIUM BY USING CHEMICALLY MODIFIED *SALVINIA*

## (Kajian Penjerapan Kadmium Dengan Menggunakan *Salvinia* Yang Diubah Suai Secara Kimia)

Anies Suhaida Mohd Naspu[1,2]*, Mohd Lias Kamal[2], Zaini Hamzah[1], Sharizal Hasan[2]

[1]*Faculty of Applied Science,*
*Universiti Teknologi MARA, 40450 Shah Alam, Selangor, Malaysia*
[2]*Faculty of Applied Science,*
*Universiti Teknologi MARA, 02600 Arau, Perlis, Malaysia*

**Corresponding author: anies_suhaida@yahoo.com*

**Abstract**

*Salvinia* was collected at the Tasik Melati, Perlis, Malaysia and it was modified using citric acid to increase the performance in removing heavy metals from standard heavy metal solution. Fourier Transform Infrared (FTIR) and Field Emission Scanning Electron Microscope (FESEM) were used to characterize *Salvinia* before and after chemical modification. Cadmium ($Cd^{2+}$**)** removal studies were carried out by using modified *Salvinia* and the effect of various parameters such as contact time, initial heavy metal concentration and biosorbent dosage were studied. The adsorption study was investigated by using Inductively Coupled Plasma Mass Spectrometry (ICP-MS) to determine the removing of heavy metal concentration from the standard $Cd^{2+}$ solution. From the study, FTIR analysis was shown the increasing of intensity on hydroxyl group after modification. A clear and smooth surface morphology of *Salvinia* after treatment were observed by using FESEM. The adsorption of cadmium was increased as contact time and biosorbent dosage increased. In contrast, the percent of adsorption was slightly decreased when initial concentration of $Cd^{2+}$ increased.

**Keywords**: *Salvinia*, biosorbent, citric acid, cadmium and adsorption

**Abstrak**

*Salvinia* diambil di Tasik Melati, Perlis, Malaysia dan diubah suai menggunakan asid sitrik untuk meningkatkan kebolehan dalam membuang cadmium daripada larutan $Cd^{2+}$. Fourier Transform Infrared (FTIR) dan Field Emission Scanning Electron Microscope (FESEM) telah digunakan untuk mencirikan *Salvinia* sebelum dan selepas pengubahsuaian secara kimia. Kajian pengambilan $Cd^{2+}$ telah dijalankan dengan menggunakan *Salvinia* yang telah diubah suai dan kesan terhadap pelbagai parameter seperti masa sentuhan, kepekatan awal $Cd^{2+}$ dan dos dikaji. Kajian penjerapan telah disiasat dengan menggunakan Inductively Coupled Plasma Mass Spectrometry (ICP-MS) untuk menentukan pengambilan $Cd^{2+}$dari larutan $Cd^{2+}$. Analisis FTIR telah menunjukkan peningkatan intensiti pada kumpulan hidroksil selepas pengubahsuaian. Satu permukaan yang jelas dan licin pada *Salvinia* selepas rawatan telah diperhatikan dengan menggunakan FESEM. Penjerapan $Cd^{2+}$ telah meningkat apabila masa sentuhan dan dos meningkat. Sebaliknya, peratus penjerapan telah sedikit menurun apabila kepekatan awal larutan $Cd^{2+}$meningkat.

**Kata kunci:** *Salvinia*, biosorben, asid sitrik, cadmium dan penjerapan

## Introduction

Water pollution can be defined as the introduction of unwanted substances into fresh or ocean waters which changes the quality of water. The growth of the industries such as metallurgy, paper, electronic and food was caused increasing of water pollution level [1]. All these industry produced various types of pollutants such as heavy metals (Cr, Fe, Se, V, Cu, Co, Ni, Cd, Hg, As, Pb, Zn and Al) and being drain away into the rivers as a final outlet.

Cadmium is an element naturally presence in the earth and also come from electroplating, smelting, alloy manufacturing, plastic, mining and refining industries [2]. It is high toxicity and easily accumulates in the

environment [3]. The presence of excess cadmium was result in damaging the human health by accumulating in food chain as well as bringing up harmful effects to the flora and fauna [4]. Due to all these adverse effect, cadmium is necessary to be removed from water system especially drinking water.

Conventional technique such as chemical precipitation, adsorption, electrolysis, ion exchange and reversed osmosis are widely applied previously to remove high concentration of heavy metals [3, 5, 6]. However, these conventional techniques are comparatively high cost to remove heavy metals at low concentration [7]. Therefore, an alternative technique like biosorbent was recommended.

Biosorbent is a biomaterial used to attract metal ions from the polluted area such as water bodies. This process is based on the affinity between biosorbent and the sorbate. This alternative technique has low cost, environmental friendly, high efficiency to remove heavy metals, easy to handle and gaining interest due to relative abundance [8].

Previously, *Salvinia* was used as activated carbon to remove chromium (VI) [9]. In this study, *Salvinia* was used as potential biosorbent to remove $Cd^{2+}$. It was chemically modified with sodium chloride and citric acid in order to increase the performance of biosorbent to remove cadmium from solution. The adsorption process was investigated as function of biosorbent dosage, contact time and initial concentration of $Cd^{2+}$ solution. Furthermore, characteristic of *Salvinia* before and after modification was studied using FTIR and FESEM analysis.

## Materials and Methods

### Preparation of biomaterial

*Salvinia* was collected in the Tasik Melati, Perlis and washed with distilled water to remove dirt. Then, it was oven dried for 24 hours at $60^0$C. The dried *Salvinia* was grounded and sieved between 150-250 μm sizes. Then, it was stored in the desiccators for further analysis.

### Chemically modification of biomaterial

Pre-treatment of biomaterial; The dried *Salvinia* was treating with 1 g/L of sodium chloride (NaCl) for 4 hours. Then, washed with deionized water until neutral (pH: 6.9-7.1) and dried at $70^0$C for 24 hours in a drying oven. The function of pretreatment with NaCl is to remove the pectin and waxy [10]. The modified *Salvinia* (mS) was stored in desiccators before undergo modification using citric acid.

Citric acid; 10g of mS was mixed in 100 mL of citric acid to activate the binding site of biomaterial for heavy metals bind [6, 8, 11]. After that, the modified *Salvinia*-citric acid labeled as (mS-CA) was placed in oven overnight at $60^0$C. After completely dried, the excess citric acid was washed in buncher funnel by using distilled water until citric acid excess is completely removed. Then, mS-CA was dried overnight at $60^0$C again. The final product (biosorbent) was stored in desiccators for the further used. In this study, citric acid acts as chelating agent which is encourages cadmium to bind on the biomaterial. Thus, the adsorption capacity of the biomaterial is expected to be increased.

### Characterization of biosorbent

FTIR was used to verify the chemistry bond and the vibration frequency changes of the functional groups in the biosorbents. FESEM used to observe the morphology of the *Salvinia* before and after modification.

### $Cd^{2+}$ standard solution

$Cd^{2+}$ standard solutions were prepared at desired concentration. The pH range of the solution is in between 3-6 and it was adjusted by adding sodium hydroxide (NaOH) or hydrochloric acid (HCl).

### Adsorption study

$Cd^{2+}$ solution was mixed with biosorbent and the adsorption capacity of $Cd^{2+}$ was studied. The variables was used in this study are contact time, initial heavy metal concentration and biosorbent dosage. The concentration of $Cd^{2+}$ before and after adsorption was measured by using ICP-MS. The uptake capacity of $Cd^{2+}$ was calculated by using equation (1) and (2) below:

$$\text{Uptake capacity} = Ci\text{-}Cf \quad (1)$$

$$\text{Adsorption (\%)} = [(Ci\text{-}Cf)/Ci] \times 100 \quad (2)$$

where Ci (mg/L) and Cf (mg/L) are the initial and final $Cd^{2+}$ concentrations.

## Results and Discussion

### Characterization of biosorbent

#### *Fourier Transform Infrared (FTIR) analysis*

The FTIR spectra of the *Salvinia* samples are shown in the Figure 1 and the characteristic bands of functional groups were obtained. FTIR spectra of raw material, mS and mS-CA showed the presence of characteristic adsorption bands of hydroxyl groups (-OH), amines ($-NH_2$), carboxyl groups (COOH), carbonyl groups (C=O) and alkyl groups (C-H) [12].

From the Figure 1, hydroxyl and amine groups were appeared for all sample of *Salvinia*. mS-CA showed a broad peak and high intensity of hydroxyl and amine group at 3355.42 $cm^{-1}$ compared to raw material and mS. It is due to the reaction of citric acid on the biomaterial [6]. Citric acid treatment was encouraged more –OH group presence and the ability to metal ions to attach is high [13]. The $-CH_2$ peak are appeared in the spectrum at 2919.29-2915 $cm^{-1}$ for the all samples and mS-CA was showed high intensity of absorption compared to others. In contrast, the figure 1 showed mS have a strong stretching of carboxyl group and carbonyl group with 1617.35 $cm^{-1}$ and 1041.63 $cm^{-1}$. The functional groups suggested here were agreed with those reported in other studies on infrared spectra of biomaterial [6, 11, 12, 14].

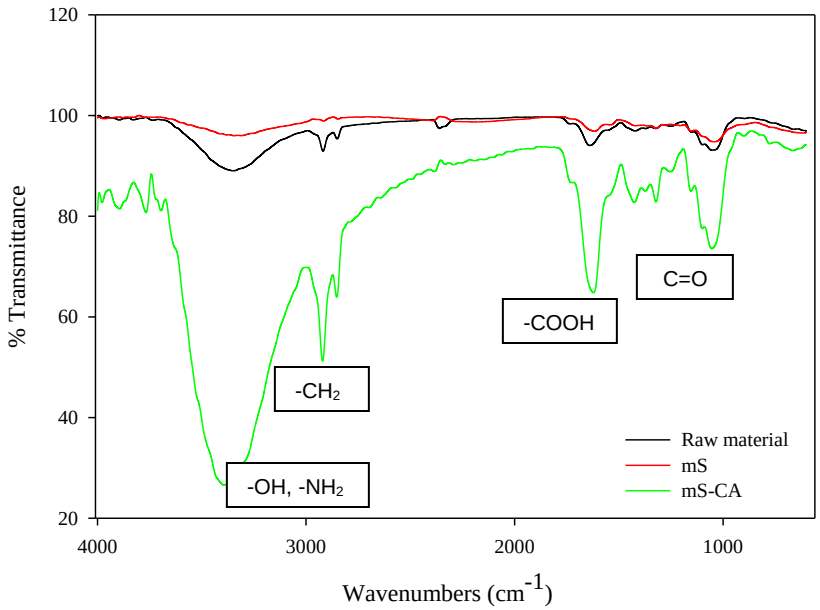



Figure 1: FTIR analysis of raw material, mS and mS-CA

***Field Emission Scanning Electron Microscope (FESEM)***

In this study, FESEM is used to observe the changes in morphological of *Salvinia* before and after modification with citric acid. From the FESEM, it can be seen that there are the changes of *Salvinia* before and after chemical treatment. Figure 2 (a) showed that the surface of *Salvinia* look alike covered by lignin. After pretreatment with NaOH, the surface of *Salvinia* becomes smooth as shown as in Figure 2 (b). Figure 2 (c) was showed that the changes in morphological after citric treatment. The surface of *Salvinia* becomes clear and the pores structure could be seen in the FESEM at 5000x magnification.

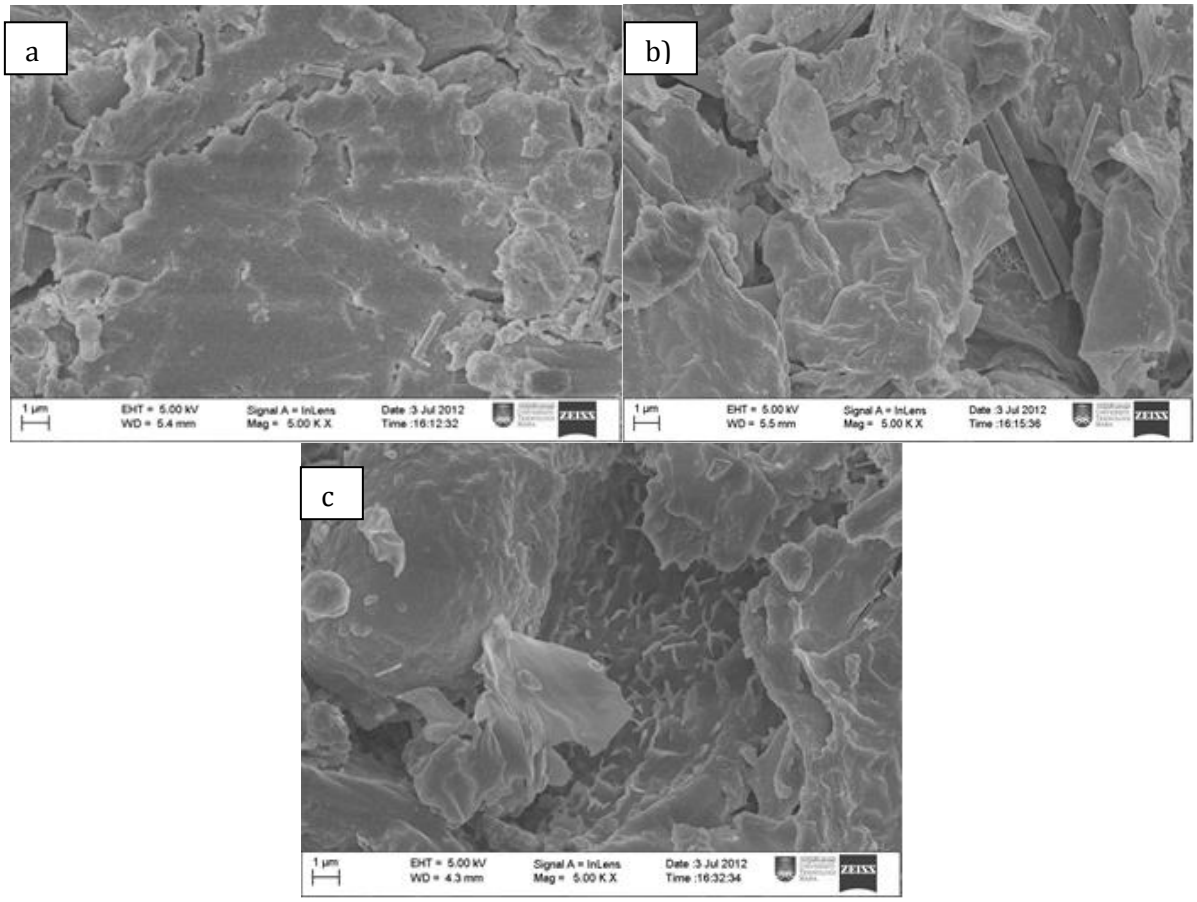



Figure 2: Field Emission Scanning Electron Microscopy of *Salvinia* (a) raw material (b) mS (c) mS-CA

**Absorption towards biosorbent**

***Contact time***

The study on contact time was performed in order to determine the maximum adsorption of $Cd^{2+}$ by biosorbent and Figure 3 was present the percent of adsorption against contact time. From the graph, it can be seen that the adsorption rate of $Cd^{2+}$ increase with the time for mS and mS-CA. The graph also shown the adsorption of mS-CA is greater than mS. From 30 minutes to 90 minutes of contact time, adsorption of mS-CA gradually increased and it is maintain for 30 minutes. After 120 minutes contact time, the adsorption of $Cd^{2+}$ increased until 150 minutes and after 150 to 180 minutes there is no adsorption of $Cd^{2+}$ recorded. Besides that, mS also showed increasing in removing $Cd^{2+}$ in heavy metal solution. After 150 minutes contact time of adsorbent, the removing of $Cd^{2+}$ reached

equilibrium until contact time end. mS-CA showed higher adsorption capacity due to the adsorption site are open to $Cd^{2+}$ interact [6]. Here, citric acid was played their function to activate the site to metal ion to attach on the adsorbent [6, 13].

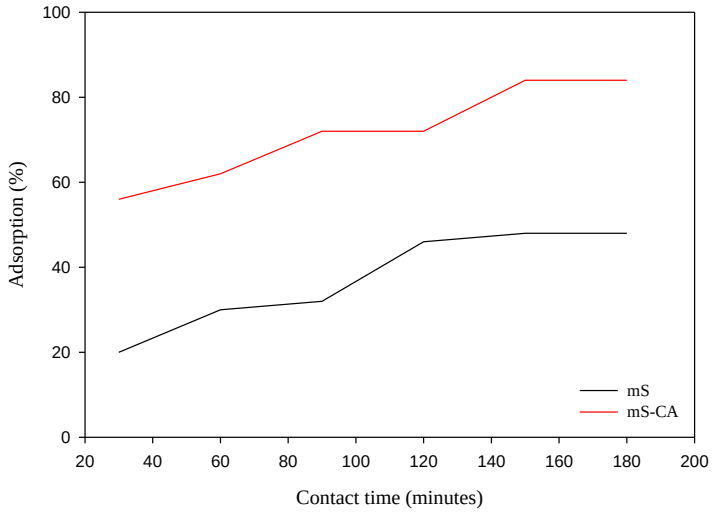



Figure 3: Effect of contacting time on $Cd^{2+}$ adsorption (1.0g adsorbent and 10mL of 0.5 ppb heavy metal solution)

***Biosorbent dosage***

Biosorbent dosage is also an important factor for adsorption of metal ion. The effect of biosorbent dosage of $Cd^{2+}$ was studied by using the different dosage of adsorbent between 0.1g to 1.0g. Figure 4 was showed the adsorption of $Cd^{2+}$ increased as dosage increased and the adsorption of $Cd^{2+}$ by mS-CA is higher compared to mS. The removal of $Cd^{2+}$ from the solution gradually increased when more treated adsorbent was introduced. Figure 4 was showed 1g of mS-CA was removed 0.47ppb (about 98%) of 0.5ppb heavy metal solution. This is due to the greater availability of adsorbent to bind the metal ions and raise the efficiency of metal ions removal [15]. In contrast, the adsorption capacity of mS decreased when 1g of adsorbent used and it was observed in this study. According to Karthikeyan *et. al.*(2007) [16], a partial aggregation of biomaterial at higher adsorbent dose would lead to decrease of biosorption efficiency due to the reduction of effective surface area for biosorption process [16].

***Initial concentration of heavy metal***

The initial concentration of $Cd^{2+}$ was varied from 0.5 ppb to 10.0 ppb to evaluate the effect on the adsorption efficiency. From the Figure 5 above, it was observed that the adsorption capacity of $Cd^{2+}$ by mS-CA is greater than mS. However, the percent removal of $Cd^{2+}$ slightly decreased with the initial concentration of solution as shown as in Figure 5. This is because at low heavy metal concentration, the ratio of surface active sites to the total metal ions in the solution is high. Hence, all $Cd^{2+}$ may interact with the mS-CA and it was removed from the heavy metal solution [17]. In contrast, at higher concentration of cadmium ions was provided more cadmium ions for attached on the biosorbent. As a result, the active sites are not sufficient and the saturation in adsorption process was happened. Therefore, it is resulting reduction in percentage removal.

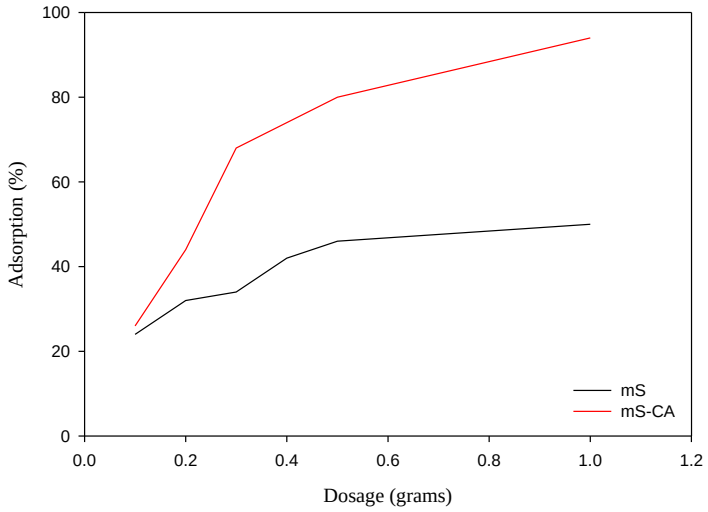



Figure 4: Effect of biosorbent dosage on $Cd^{2+}$ adsorption (180 minutes immersion time and 10mL of 0.5 ppb heavy metal solution)

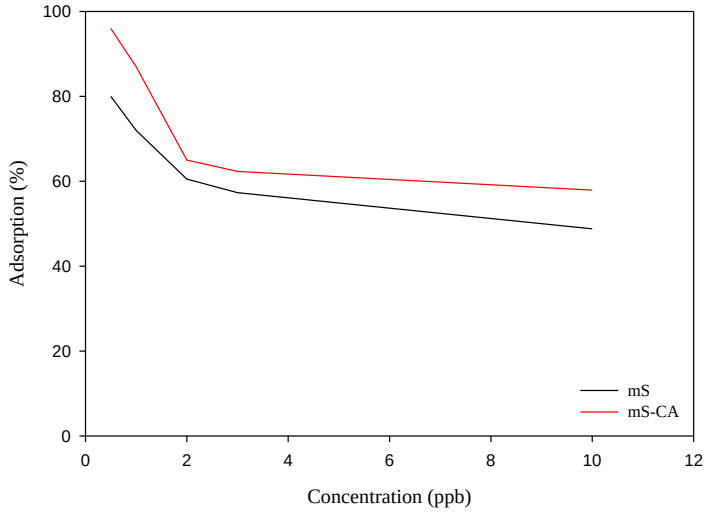



Figure 5: Effect of initial concentration of heavy metal solution on $Cd^{2+}$ adsorption (180 minutes immersion time and 1.0g biosorbent dosage)

## Conclusion

As a conclusion, chemical modification of *Salvinia* by citric acid was enhanced the adsorption of $Cd^{2+}$ ions. The uptake capacity of $Cd^{2+}$ was increased by raising the contact time and biosorbent dosage. However, the adsorption of $Cd^{2+}$ was decreased after varying the initial concentration of heavy metal solution.

## Acknowledgement

This study was supported by the research grant from Dana Kecemerlangan Pendidikan Universiti Teknologi MARA Perlis (600-UiTMPs/PJI&A/ST/DKCP(01/2012)). The authors are thankful to UiTM Perlis for providing the facilities for this research.

## References

1. Vargas, K., Cerro-Lopez, M., Reyna-Tellez, S., Bandala E. R. & Sanchez-Salas, J. L. (2012). Biosorption of heavy metals in polluted water, using different waste fruit cortex.*Physics and Chemistry of the Earth*, 37-39: 26-29.
2. Li, Q., Chai L. & Qin, W. (2012). Cadmium(II) adsorption on esterified spent grain: Equilibrium modeling and possible mechanisms. *Chemical Engineering Journal*, 197: 173-180.
3. Vimala, R. & Das, N. (2011). Mechanism of Cd(II) adsorption by macro fungus *Pleurotus platypus. Journal of Environmental Sciences*, 23(2): 288-293.
4. Espinoza-Quiñones, F. R., Módenes, A. N., Thomé, L. P., Palácio, S. M., Trigueros, D. E. G., Oliveira, A. P. & Szymanski, N. (2009). Study of the bioaccumulation kinetic of lead by living aquatic macro phyte *Salvinia auriculata. Chemical Engineering Journal*, 150(2–3): 316-322.
5. Xiong, C. H. & Yao, C. P. (2009). Study on the adsorption of cadmium (II) from aqueous solution by D152 resin. *Journal of Hazardous Materials*, 166(2–3), 815-820.
6. Zhu, B., Fan T. & Zhang, D. (2008). Adsorption of copper ions from aqueous solution by citric acid modified soybean straw. *Journal of Hazardous Materials*, 153 (1-2): 300-308.
7. Sabdono, A. (2009). An Assessment of Heavy Metal Concentrations in the *Scleractinian* Coral Tisue of Karimunjawa Archipelago, Indonesia. *Journal of Coastal Development*, 13 (1): 9-17.
8. Reddy, D. H. K., Harinath, Y., Seshaiash, K. & Reddy, A. V. R. (2010). Biosorption of Pb(II) from aqueous solutions using chemically modified *Moringaoleifera* tree leaves. *Chemical Engineering Journal*, 162 (2): 626-634.
9. Baral, S. S., Das, S. N., Roy Chaudhury, G., Swamy, Y. V. & Rath, P. (2008). Adsorption of Cr(VI) using thermally activated weed *Salvinia cucullata*. *Chemical Engineering Journal*, 139 (2): 245-255.
10. Chen, Y.-n., Nie, J.-x., Chen, M. & Zhang, D.-c. (2009). Biosorptional removal of lead and cadmium from water by waste material. Paper presented at the International Conference on Management and Service Science:Wuhan.
11. Sajab, M. S., Chia, C. H., Zakaria, S., Jani, S. M., Ayob, M. K., Chee, K. L., Khiew, P. S. & Chiu, W. S. (2011). Citric acid modified kenaf core fibres for removal of methylene blue from aqueous solution. *Bioresource Technology*, 102 (15): 7237-7243.
12. Leyva-Ramos, R., Landin-Rodriguez, L. E., Leyva-Ramos, S. & Medellin-Castill, N. A. (2012). Modification of corncob with citric acid to enhance its capacity for adsorbing cadmium(II) from water solution. *Chemical Engineering Journal*, 180: 113-120.
13. Reddy, D. H. K., Seshaiah, K., Reddy, A. V. R. & Lee, S. M. (2012). Optimazation of Cd(II), Cu(II) and Ni(II) biosorption by chemically modified Moringa oleifera leaves powder. *Carbohydrate Polymers*, 88 (3): 1077-1086.
14. Lasheen, M. R., Ammar, N. S. & Ibrahim, H. S. (2012). Adsorption /desorption of Cd(II), Cu(II) and Pb(II) using chemically modified orange peel: Equilibrium and kinetic studies. *Solid State Sciences*, 14 (2): 202-210.
15. Chubbar, N., Carvolho, J.R. & Correia, M. J. N. (2003). Cork biomass as biosorbent for Cu(II), Zn(II) and Ni(II). *Colloid and Surface A:Physicochemical and Engineering Aspects*, 230 (1-3): 57-65.
16. Karthikeyan, S., Balasubramanian, R. & Iyer, C. S. P. (2007). Evaluation of marine algae *Ulva fasciata*and *Sargassum* sp. for the biosorption of Cu(II) from aqueous solution. *Bioresource Technology*, 98 (2): 452-455.
17. King, P., Srinivas, P., Kumar, Y. P. & Prasad, V. S. R. K. (2006). Sorption of copper(II) ion from aqueous solution by *Tectona grandis* (teak leaves powder). *Journal of Hazardous Material*, 136 (3): 560-566.

The Malaysian Journal of ANALYTICAL SCIENCES ISSN 1394-2506

# ESTOLIDE ESTER FROM *RICINUS COMMUNIS L.* SEED OIL FOR BIOLUBRICANT PURPOSE

## (Ester Estolida dari Minyak Biji *Ricinus Communis L* untuk Kegunaan Biolubrikan)

Nazrizawati Ahmad Tajuddin[1,2,3]*, Nor Habibah Rosli[1], Noraishah Abdullah[2,3], Mohd Firdaus Yusoff[3], Jumat Salimon[3]

[1]*Department of Chemistry, International Education College, Universiti Teknologi MARA (UiTM) Section 17, 40200 Shah Alam, Selangor, Malaysia*
[2]*Department of Chemistry, University of Technology MARA (UiTM), 40450 Shah Alam, Selangor, Malaysia*
[3]*Oleochemistry Programme, School of Chemical Science and Food Technology, Faculty of Science and Technology, Universiti Kebangsaan Malaysia, 43000 UKM Bangi, Selangor, Malaysia*

**Corresponding author: nazriza@salam.uitm.edu.my*

**Abstract**

Product of 2-ethylhexyl estolide ester formed from acid catalyst reaction was characterized by using Fourier Transform Infrared (FTIR) in conjunction to determine the functional groups presence. Meanwhile, Nuclear Magnetic Resonance (NMR) has been used to determine the structure's compounds. The present of ester group at 1738.23 $cm^{-1}$ indicated that the formation of estolide ester has been occurred. The vibration peak of C-O occurred at 1174.60 $cm^{-1}$ and 1117.10 $cm^{-1}$ confirmed the formation of ester. Present of $CH_2$ bending indicated the existence of long-chain compounds. Existent of ester methine signal at 3.8669 ppm indicated the estolide linkage in the $^1$H-NMR spectrum. On the other hand, two signals have been notified in the $^{13}$C-NMR spectrums. One signal appeared at 173.41 ppm indicated the existence of carbonyl acid compound while carbonyl ester's signal appeared at 173.56 ppm. Chemical shift of $^1$H and $^{13}$C for stimulation and experiment were matched with estolide structure. Result of pour point, flash point and viscosity indicated that estolide 2-ethylhexyl ester meet the lubricant criteria as they possesses low pour points (-6 °C), high flash point (246 °C) and optimum viscosity (179 cps).

**Keywords**: Castor oil, estolide ester, biolubricant, pour point, flash point, viscosity

**Abstrak**

Hasil 2-etilheksil ester estolida yang terhasil dari tindakbalas bermangkinkan asid katalis telah dianalisa dengan menggunakan Spektroskopi Infra Merah (SIR) bagi tujuan mengenal pasti kumpulan berfungsi yang hadir. Manakala Resonan Magnetik Nuklear (RMN) digunakan untuk pengecaman formula struktur sebatian. Kumpulan ester telah didapati hadir pada regangan 1738.23 $cm^{-1}$ dan ini menandakan pembentukan ester estolide telah berlaku. Puncak getaran C-O pada 1174.60 $cm^{-1}$ dan 1117.10 $cm^{-1}$ mengesahkan pembentukan ester. Kehadiran bengkokan regangan $CH_2$ menunjukkan kehadiran rantai panjang di dalam kompaun. Isyarat methine ester yang muncul pada 3.8669 ppm melalui spectrum RMN $^1$H menandakan kehadiran rangkaian estolida manakala melalui spektrum RMN $^{13}$C didapati dua isyarat karbonil telah muncul. Isyarat karbonil pada at 173.41 ppm mengesahkan kehadiran karbonil asid manakala isyarat pada 173.56 ppm mengesahkan kehadiran karbonil ester. Spektrum RMN $^1$H dan $^{13}$C telah membuktikan nilai simulasi dan eksperimen berpadanan dengan struktur molekul estolida. Hasil ujian takat tuang, takat kilat dan kelikatan menunjukkan estolida 2-etilheksil ester sesuai digunakan sebagai pelincir kerana mempunyai takat tuang yang rendah (-6 °C), takat kilat yang tinggi (246 °C) dan kelikatan optimum (179 cps).

**Kata kunci**: Minyak jarak, ester estolida, biolubrikan, takat tuang, takat kilat, kelikatan

## Introduction

The development of the petroleum industry over the past few decades has enabled mineral or rather fossil oils to be used as efficient and cost-effective lubricants. Today, most of the lubricants used for industrial needs are made from non-biodegradable materials such as synthetic oils or petroleum derivatives. However, they pose a great deal of

environmental hazards. Bio-lubricants or bio-based lubricants have begun to replace non-biodegradable fossil-based lubricants in industrial purposes [1]. A bio-lubricant can be available in two forms; either as vegetable oil-based or as synthetic esters manufactured from mineral oil-based products. Bio-based lubricants or bio-lubes contain biological materials or renewable domestic agricultural materials such as plant, animal and marine materials or forestry materials. From an environmental perspective, the use of bio-lubricants significantly reduces the carbon footprint than other non-biodegradable mineral oil based sources of crude oil or coal [2]. It is in fact a matter of great concern that millions of tons of hydraulic, machinery and industrial oils are discharged every year into water sources such as rivers and seas, thus leading to groundwater contamination [3]. This can ultimately inhibit the growth of plant life and prove extremely toxic to aquatic life.

The use of bio-based lubricants by industries is still in its infancy stage and there's much left to be done. The development of biolubricants based on estolides derivatives through oleic acid has been studies while only a limited number on ricinoleic acid being studied. Recent study showed *Ricinus communis* (castor bean) possessed high percentage of ricinoleic acid and can be used to produce estolides bio-based products [4]. Estolides are an oligomeric fatty acid produce from condensation of two different fatty acids with the presence of an acid catalyst [5]. Normally, they are found in triglycerides form in vegetable oils. Estolides have potential use as lubricants, plasticizers, cosmetic additives and printing ink components [6]. The aim of this study was to synthesize a new synthetic approach of producing estolide ester from a renewable resource which is later can be used as green-biolubricant.

## Materials and Methods

### Sample and Reagent

Samples of castor oil were collected from four difference areas; Meru-Kapar (Klang); Salak Tinggi(KL); Sungai Chua (Kajang) and Plant House (UKM, Bangi) in Selangor, Malaysia and solely synthesized. 2-ethylhexyl alcohol, lauric acid and percholoric acid were purchased from Sigma-Aldrich (USA). Hexane and potassium hydroxide were obtained from SYSTERM. All other chemicals and reagents were obtained from Aldrich Chemical (Milwaukee, WI). All materials were used without further purification. All organic extracts were dried using anhydrous magnesium sulfate (Aldrich Chemical).

### Synthesis

Samples went under pretreatment of drying (80$^{o}$C, 8 h). Extraction was carried out for 6-12 h at 65°C in order to assure the oil was fully extracted. Collected oil was separated by using rotavapor. Synthesis of estolide 2-ethylhexyl ester were conducted based on Cermak et al., 2003 [7] with modification by using ricinoleic acid as first fatty acid reacted with lauric acid and capped with 2-ethylhexyl alcohol. Ricinoleic acid (50 g, 177 mmol) and lauric acid (17.75g, 88.5 mmol) were combined together and heated to 60 $^{o}$C under vacuum. Once the desired temperature was reached, 11.5 ml perchloric acid was added and stirred for 24 h. All the reactions were conducted in a three-neck round flask, connected to a circulating vacuum in a fume hood. After 24 h, 2-ethylhexyl alcohol (33.75 ml, 228.8 mmol, 29.8 g) was added to the vessel, vacuum was restored and the mixture was stirred for additional 2 h. The complete reaction was quenched by 25 g KOH in 90% ethanol/water (10 ml) solution. Solution was allowed to cool for 30 min. The organic layer was dried over sodium sulphate and filtered. The material was distilled at 105$^{o}$C to remove any excess alcohol and water contents.

### Characterization

NMR spectroscopy been used to detect $^{1}$H proton and carbon $^{13}$C in the estolide structure 1H and 13C NMR spectra were recorded using a JEOL JNMECP 400 spectrometer operating at 400.13MHz and 100.61 MHz, respectively. The spectrometer used a 5-mm broadband inverse Z-gradient probe in DMSO-d6 solvent (Cambridge Isotope Laboratories, Andover, MA) as solvent. Each spectrum was Fourier-transformed, phase-corrected, and integrated using a MestRe-C 2.3a software (Magnetic Resonance Companion, Santiago de Compostela, Spain). FTIR spectra were recorded neat on a Perkin Elmer GX FTIR Spectrophotometer. FTIR spectroscopy analysis was carried out to determine the functional group presence in estolide ester based on the spectrum peaks. Samples which were in liquid form were sandwiches between two sodium chloride (NaCl) plates while samples in solid form were diluted before being placed between two potassium bromide (KBr) plates. The functional group to be monitored for is ester carbonyl (1735 cm$^{-1}$), hydroxyl –OH (2900-3300 cm$^{-1}$), sp$^{3}$ stretching carbon (2800-3000cm$^{-1}$), long chain (720cm$^{-}$

[1]) and other functional groups which may appear as a characteristic of the product. Spectrums for all raw materials (ricinoleic acid and 2-ethylhexyl alcohol) were compared to product's to observe the differences between each spectrum.

**Low temperature operability**

The pour point of a liquid is the lowest temperature at which it becomes semi solid and loses its flow characteristics. This method is routinely used to determine the low temperature flow properties of fluids [8]. Pour point values were measured according to ASTM D5949, a Standard Test Method for Pour Point of Petroleum Products (Automatic Pressure Pulsing Method). It uses automatic apparatus and yields pour point results in a format similar to the manual method (ASTM D97).

The D5949 test method determines the pour point in a shorter period of time than manual method D97. Less operator time is required to run the test using this automatic method. Additionally, no external chiller bath or refrigeration unit is needed. D5949 is capable of determining pour point within a temperature range of -57°C to +51°C. Results can be reported at 1°C or 3°C testing intervals. Generally, materials with low pour point exhibit improved fluidity at lower temperature than those in higher temperature. This test method has better repeatability and reproducibility than manual method D97. Each sample was run in triplicate and the reported average values are rounded to the nearest whole degree.

**Flash point value**

The flash point of a volatile material is the lowest temperature at which it can vaporize to form an ignitable mixture in air. Measuring a flash point requires an ignition source. At the flash point, the vapor may cease to burn when the source of ignition is removed. The flash point is often used as a descriptive characteristic of liquid fuel, and it is also used to help characterize the fire hazards of liquids. "Flash point" refers to both flammable liquids and combustible liquids. The greater the flash point is, the greater the fire hazard [8]. Flash point determination was measured according to ASTM Standard D 56-79 using a Tag Closed Tester. Each sample was run in triplicate and the reported average values are rounded to the nearest whole degree.

**Viscosity index measurement**

Viscosity index (VI) is an arbitrary measure for the change of viscosity with temperature. It is used to characterize lubricating oil in the automotive industry. Viscosity was measured by using automated multi range viscometer tubes HV M472 obtained from Welter Herzog (Germany). Measurements were run in a Temp-Trol (Precision Scientific, Chicago, IL, USA), viscometer bath set at both 40°C and 100°C. The viscosity and viscosity index were calculated using ASTM methods D 445-97 (ASTM D 445-97) and ASTM D 2270-93 (ASTM D 2270-93), respectively. The measurements were taken in triplicate and the average values were reported. The viscosity of liquids decreases as temperature increases. The viscosity of a lubricant is closely related to its ability to reduce friction. Generally, the least viscous lubricant which still forces the two moving surfaces apart is desired. If the lubricant is too viscous, it will require a large amount of energy to move (as in honey); if it is too thin, the surfaces will rub and friction will increase.

## Results and Discussion

**Synthesis of estolide 2-ethylhexyl ester**

Acid-catalyzed transesterification reactions were conducted with solvent 2-ethylhexyl alcohol, in a three-neck round bottom flask under vacuum. Generally, formation of estolide ester is influences by two major factors; acid catalyst and the reaction temperature used. In this reaction, perchloric acid was chosen as catalyst due it provides significantly faster rate (5-8 times) of estolide formation compare to sulphuric acid and produce more yield of estolide [9]. Addition of sulphuric acid to unsaturated fatty acid will produce sulfated oils. The sulfated oil is stable at low temperature (≤ 20°C) in the presence of acid, but at elevated temperature (50°C), the sulphate esters quickly decompose, estolides and lactones are observed.

Estolide esters formation also influences by the temperature. At room temperature (27°C), the rate of reaction catalyzed by perchloric acid becomes slow. However, at higher temperature, the formation become too fast due to the rate is accelerated even though the concentration of perchloric acid is reduced and the side reactions begin to

predominate, chiefly the formation of lactones [9]. Hence, an optimum temperature, 60°C has been applied in this study. Synthesis was carried out within 24 hours in order to assure all the reactions are complete.

Figure 1 shows ricinoleic acid tends to interact with OH group from lauric acid to form ester and capping the chain. Carbonyl group tends to form bonding with OH because carbonyl group are easier to disconnect compared to double bond, which is more stable. By capping the fatty ester, the compounds no longer had the opportunity to undergo either intra- or intermolecular hydrogen bond interaction [5]. Yield produced is about 82.25%.

**FTIR Characterization**

Synthesis of estolide 2-ethylhexyl ester was expected to produce unsaturated estolide as shown in Figure 1. FTIR spectrum in Figure 2 shown there is almost no OH peak appeared at region 3000-3400cm$^{-1}$ as water has been eliminated through hydrolysis process. A strong peak at 1738.23 cm$^{-1}$ indicates the presence of ester group in the compound as ester shows a strong peak at range 1750-1735 cm$^{-1}$ [10]. Precisely, C=O bands appear at 724.20 cm$^{-1}$ and 1738.23 cm$^{-1}$ .This assumption was supported by the presence of two C-O stretch bonds. At 1174.60 cm$^{-1}$ wave number which is more electronegative as the C-O group bonded to the acid backbone while ester with is less electronegative, which is C-O ester bonded to the ester backbone appeared at 1117.10 cm$^{-1}$. CH3 bands appear at range 1378.53-1559.43 cm$^{-1}$.

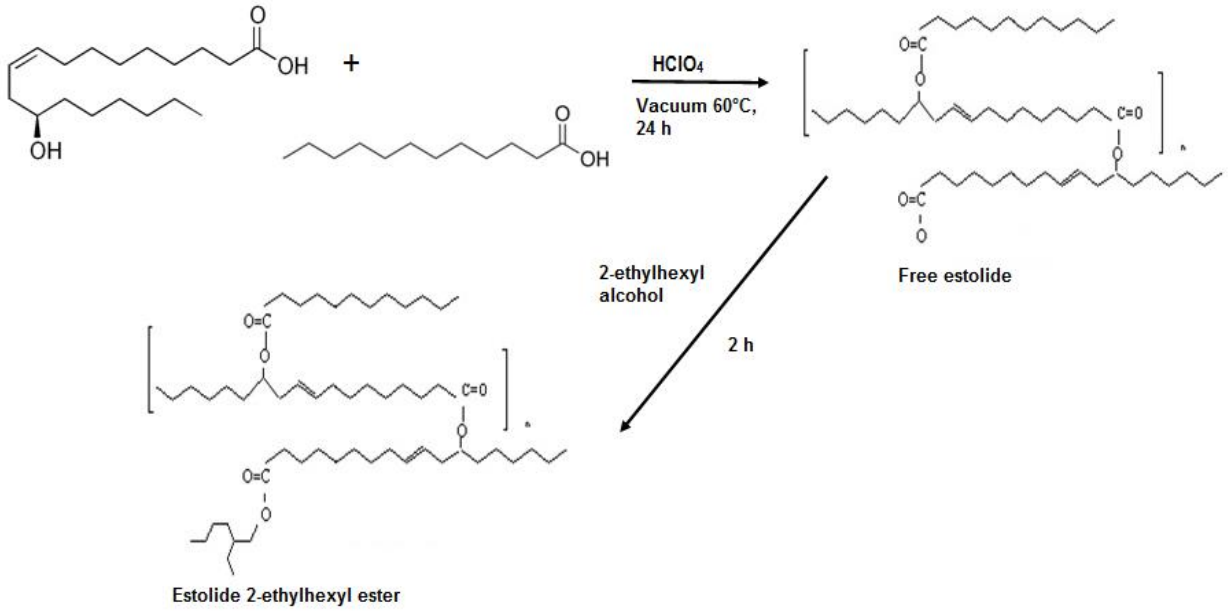



Figure 1: Synthesis of estolide 2-ethylhexyl ester

**NMR Characterization of estolide 2-ethylhexyl ester**

All synthesized compounds were verified by $^{1}$H and $^{13}$C NMR spectroscopy. The $^{1}$H-NMR spectrum for estolide 2-ethylhexyl ester shows in Figure 3 contains the expected estolide signals. The ester methine signal (Hm) at 2.157 ppm indicates the estolide linkage. Another distinctive feature is the α- methelyne proton shift at 4.5438 ppm adjacent to the acid and the α- methelyne proton shift at 3.8669 ppm adjacent to the ester (Table 1). The $^{13}$C NMR spectrum for estolide 2-ethylhexyl ester shows in Figure 4 contains some of the key features for a typical estolide and all the shift data are listed in Table 1. There are two carbonyl signals at 173.4091 ppm (acid) and 173.5697 ppm (ester). Methine carbons were appeared at 76.9122-77.5545 ppm which is common to estolides. Estolide ester is

suggested to have ethylene peak at 130.6 ppm in the spectrum due to double bond from ricinoleic acid. However, spectrum of estolide 2-ethylhexyl ester shows inverse result where there is no ethylene peak or very small signal observed expected cause by the impurity of ricinoleic acid [5]

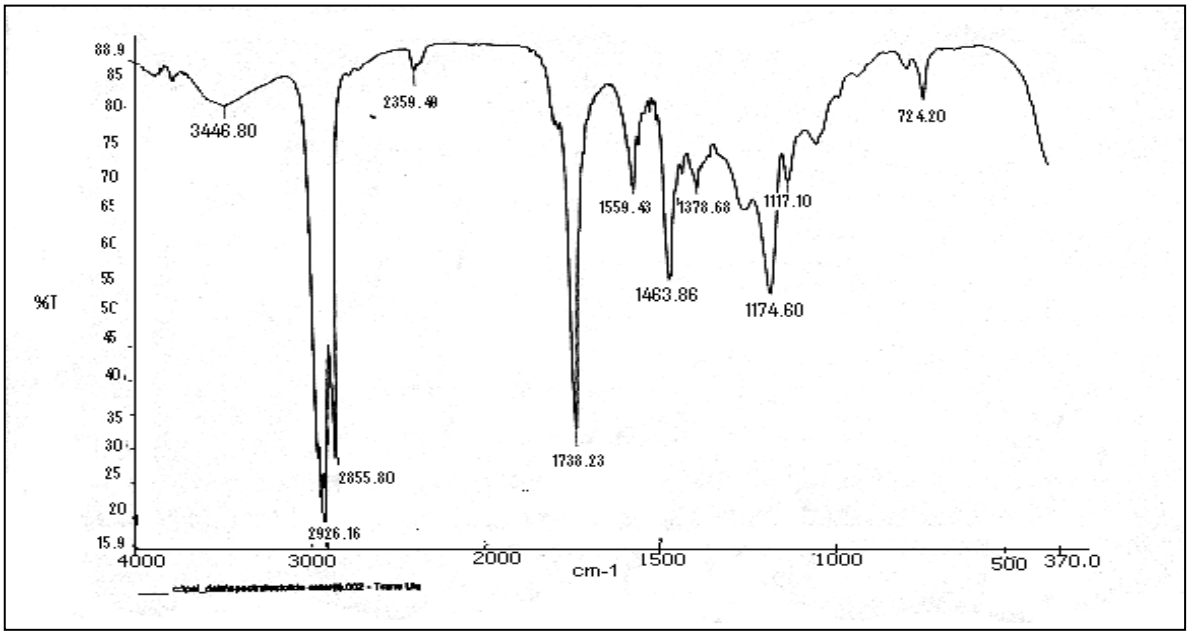



Figure 2: FTIR spectrum of estolide 2-ethylhexyl ester

Table 1: Data elucidation of $^{1}H$ & $^{13}C$ NM

| Node | Shift (ppm) | Group |
|---|---|---|
| **$^{1}H$ NMR** | | |
| $CH_3$ | 0.7710 | Methyl |
| $CH_2$ | 1.1641 | Methylene ($CDCl_3$ peak) |
| | 1.4929 | Methylene |
| | 4.5438 | Methylene (α- acid) |
| CH | 2.1570 | Methine (ester linkage) |
| | 3.8669 | Methine (α-ester) |
| **$^{13}C$ NMR** | | |
| $CH_3$ | 10.8630 - 13.9675 | Methyl |
| $CH_2$ | 22.9137 - 30.4300 | Methylene |
| | 64.7010 - 66.3602 | Methylene |
| CH | 38.7722 | Methine |
| | 76.9122 - 77.5545 | Methine ($CDCl_3$ peak) |
| C-O | 173.4091 | Carbonyl (acid) |
| | 173.5697 | Carbonyl (ester) |

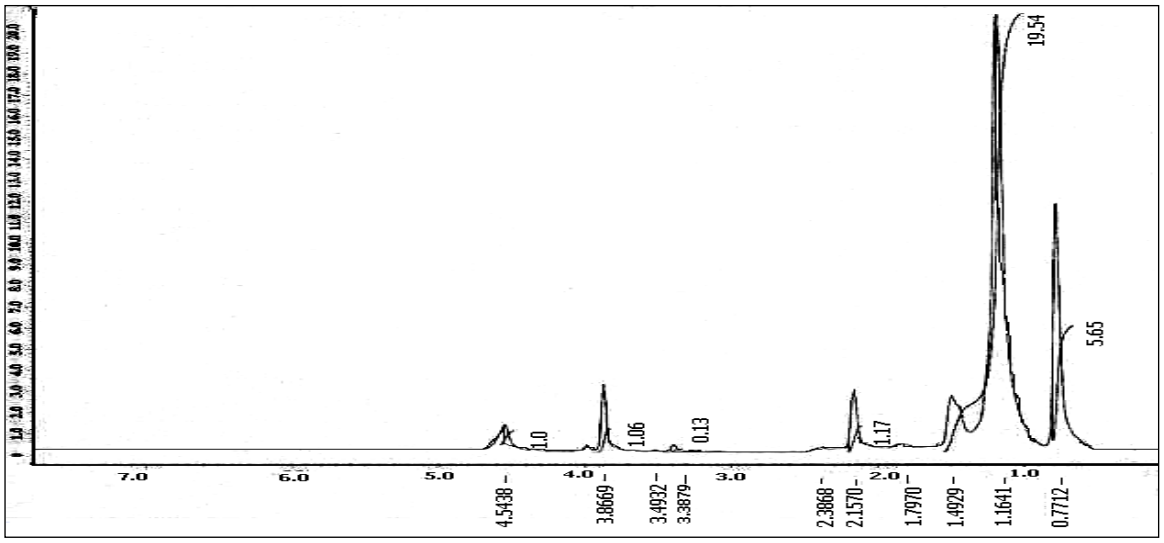



Figure 3: Spectrum of NMR $^{1}$H estolide 2-ethylhexyl ester.

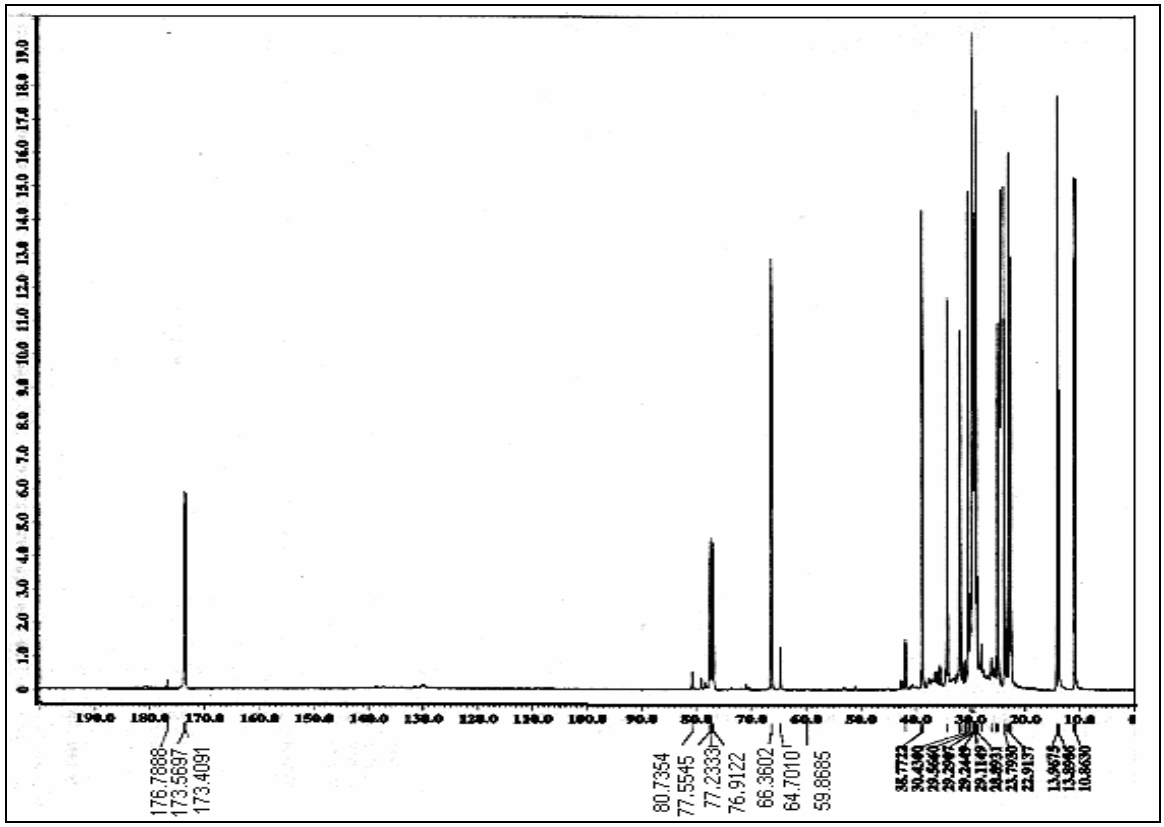



Figure 4: Spectrum of NMR $^{13}$C estolide 2-ethylhexyl ester.

**Biolubricant Parameter**

The ability of a substance to remain as a liquid at low temperatures is an important attribute for a number of industrial materials, such as biolubricant, surfactants and fuels. The cold flow property of plant oils is extremely poor and this limits their use at low operating temperature especially as automotive and industrial fluids [8]. Plant oils have a tendency to form macrocrystalline structures at low temperatures through uniform stacking of the 'bend' triglyceride backbone. Such macrocrystals restrict the easy flow of the system due to loss of kinetic energy of individual molecules during self-stacking [11]. Cold flow properties of these samples were determined using their pour points. In practice, synthetic base stocks are produced from carefully-chosen and well-defined chemical compounds and by specific chemical reactions. The final base stocks are designed to have optimized properties and significantly improved performances features [12].

Even though vegetable based-lubricant possesses effective lubricant and great biodegradation properties, they are failing to meet lubricity need at cold temperature. To ensure quality of estolide lubricant achieve the market standards, pour point, flash point and viscosity test have been done. Lubricity properties of prepared compounds are summarized in Table 2.

Table 2: Pour point, flash point and viscosity of prepared products.

| Parameter | Value of estolide prepared | Reference value | Sources |
|---|---|---|---|
| Pour Point (°C) | -6 | -15 | Ref [13] |
| Flash point (°C) | 246 | 113 - 250 | Ref [14] |
| Viscosity (cps) | 179 | 172 - 196 | Ref [13] |

Pour point has been measured according to method 2.4. Branch chains of 2-ethylhexyl alcohol influenced the pour point value due to it will cause a dramatically decreasing of pour point. The more capping branches are, the higher potential of bond making thus will lowering the pour point value, In contrast, the shorter capping branches used will interrupt the interaction of bond making thus will increasing the pour point value [15]. Result in Table 2 shows pour point value of 2-ethylhexyl alcohol is -6°. This value has been compared with Ref [13] where they synthesized oleic acid with 2-ethylhexyl alcohol and has been capping with ricinoleic acid. At first, the obtained value before been capping with fatty acid was -3 °C and drop to -15 °C once has been capping with new fatty acid.

Ricinoleic acid from *Ricinus communis* oil is a unsaturated fatty acid which once it been capping with new fatty acid, the compound would not have any chances to interact either in inter or intramolecular forces with hydrogen bonds. This make the pour point value become even lower. The higher the unsaturated estolide is, the lower pour point obtained [5]. Estolide 2-ethylhexyl alcohol produced such a lower pour point as it was synthesized from unsaturated fatty acid.

Flash point is one of the important indicators in lubricant quality assurance. According to Ref [5], a good biolubricant posse's higher flash point values as the engine haven't set in fire even in higher flash point. This is an important criterion in major industrial machines as they involving high usage of temperature. Table 2 shows flash point of 2-ethylhexyl ester was 246 °C which is very high. There is no sudden increment has been recorded and this proven a good criteria of biolubricant.

The efficiency of the biolubricant in reducing friction and wear is greatly influenced by its viscosity. Generally, viscosity- temperature charts are available, making a good choice of a biolubricant operation temperature. The viscosity of a biolubricant is its tendency to resist flow. A biolubricant oil of high viscosity flows very slowly. The viscosity must always be high enough to keep a good oil film between the moving parts. Otherwise, friction will increase, resulting in power loss and rapid wear on the parts. The viscosity index, commonly designated as VI, is an arbitrary numbering scale that indicates the changes in oil viscosity with changes in temperature. A low index

means a steep slope of the curve, or a great variation of viscosity with change in temperature; high index means a flatter slope, or lesser variation of viscosity with the same changes in temperature [14].

Result in Table 2 shows a high value of viscosity index (VI). Vegetable oil and synthetic ester possesses way better viscosities compare to mineral oil and they are suitable to be used as lubricant [4]. However, due to the expensive price of derivatives synthetic ester, consumers are tends to choose vegetable oil as new alternative. According to Ref [13], viscosity increased with the increasing of oligomer amounts. In this context, viscosity index of estolide free acid were reported between 122-155 cps while viscosity of 2-ethylhexyl ester were recorded in higher range; 172-196 cps [13]. This is due to the existence of hydrogen bond with carboxylate group.

## Conclusion

Estolide 2-ethylhexyl ester was successfully synthesized between ricinoleic acid from castor oil and lauric acid with addition of 2-ethylhexyl alcohol. Perchloric acid has been used as catalyst. Data elucidation from FTIR and NMR described the characteristic of the product. Result shows significant value with the estimation and matched with the molecular structure, hence possibly been use as biolubricant material. Based on the results obtained, an increase in the chain length of the mid-chain ester had a positive influence on the low temperature properties of the products because they create a stearic barrier around the individual molecules and inhibits crystallization, resulting in lower pour point. The higher the unsaturated estolide is, the lower pour point obtained. Estolide 2-ethylhexyl alcohol produced such a lower pour point as it was synthesized from unsaturated fatty acid.

## Acknowledgement

Thanks to University of Technology MARA (UiTM) for grant sponsored: 600-RMI/ST/DANA 5/3 Dst (238/2011). Thank you to Universiti Kebangsaan Malaysia and supporting staff of Science and Technology Faculty for expert technical assistance. And thank you to International Education College, Universiti Teknologi MARA, Section 17 for accommodation & travelling sponsored.

## References

1. Pearce, F. (2006). Fuels Gold. *New Scientist*, 1: 36-41.
2. Salimon,J., Salih, N. & Yousif, E. (2010). Biolubricants: Raw Materials, Chemical Modifications and Environmental Benefits. *European Journal of Lipid Science and Technology*, 112: 519-530.
3. Bart, J. B. & Larry, P. (2008). Bio-Based Lubricants**:** A Market Opportunity Study Update. *United Soybean Board*, 1: 1-31.
4. Isbell, T.A., Edgcomb, M.R. & Lowery, B.A. (2001). Physical Properties of Estolides Based Function Fluids. *Industrial Crops and Products*, 18: 196.
5. Cermak, S.C., Brandon, K. B. & Isbell, T. A. (2006). Synthesis and Physical Properties of Estolides from Lesquerella and Castor Fatty Acid Esters. *Industrial Crops and Products*, 23:54-64.
6. Cermak, S.C. & Isbell, T.A. (2009). Synthesis and Physical Properties of Mono-estolides with Varying Chain Lengths, *Industrial Crops and Products*, 29:205-213.
7. Cermak, S.C. & Isbell, T.A. (2003). Synthesis Physical Properties of Estolide-based Functional Fluids. *Industrial Crops Products,*18:183-196.
8. Salimon,J., Salih, N. & Yousif, E. (2011). Chemically Modified Biolubricant Basestocks from Epoxidized Oleic Acid: Improved Low Temperature Properties and Oxidative Stability. *Journal of Saudi Chemical Society,* 15: 195–201.
9. Isbell, T.A., Kleiman, R. & Plattner, B.A. (1994). Acid.Catalyzed Condensation of Oleic Acid into Estolides and Polyestolides. *Journal of American Oil Chemistry Society, 1:*71.
10. Pavia, D.L, Lampman, G.M. & Kriz, G.S. (2001). Introduction to Spectroscopy. *America:Thomson Learning,* 3: 124.
11. Salimon, J. & Salih, N. (2009). *European Journal Science Research*, 32: 216.
12. Guzman, D. (2002). Vegetable Oil in Lubricants and Additives Slated for Strong Growth. *Chemical Market Reporter*, 10: 1–2.
13. Cermak, S.C. & Isbell, T.A. (2002). Physical Properties of Saturated Estolides and Their 2-ethylhexyl Ester. *Industrial Crops Products*, 16: 119-127.

14. Salih, N., Salimon,J. & Yousif, E. (2012). Synthetic Biolubricant Base Stocks based on Environmentally Friendly Raw Materials. *Journal of King Saud Universit*y–Science, 24: 221–226.
15. Isbell, T.A., Lowery, B.A., DeKeyser, S.S., Winchell, M.L. & Cermak, S.C. (2006). Physical Properties of Triglyceride Estolides from Lesquerella and Castor Oils. *Industrial Crops and Products*, 23: 256-263.

The Malaysian Journal of ANALYTICAL SCIENCES ISSN 1394-2506

# QUANTIFYING SOIL EROSION AND DEPOSITION RATES IN TEA PLANTATION AREA, CAMERON HIGHLANDS, MALAYSIA USING $^{137}$Cs

## (Pengiraan Kadar Hakisan Tanah dan Kadar Pemendapan di Kawasan Ladang Teh, Cameron Highlands, Malaysia Menggunakan $^{137}$Cs)

Zaini Hamzah[1], Che Yasmin Amirudin[1]*, Ahmad Saat[1,2], Ab Khalik Wood[1]

*[1]Faculty of Applied Sciences,*
*[2]Institute of Science (IOS),*
*Universiti Teknologi MARA, 40450 Shah Alam, Malaysia*

**Corresponding author: cheyasmin07@gmail.com*

**Abstract**

The soil erosion and deposition in the hilly area is a great concern for the planters. In this study, the tea plantation was chosen to quantify the rates of soil erosion and deposition for it will provide information on the improvement of soil conditions and cost reduction of fertilizer consumption. The aims of this research are to determine the rate of soil erosion and deposition using environmental radionuclide, $^{137}$Cs. Soil profile samples were collected by using scrapper plate and two cores soil sample were collected in the undisturbed forests area nearby. The $^{137}$Cs activity concentration was measured using low background coaxial hyper pure germanium detector gamma spectrometer based on $^{137}$Cs gamma energy peak at 661.66 KeV. The highest erosion rate using Proportional Models and Mass Balance Model 1 was found in point HE top area which is 52.39 t ha$^{-1}$ yr$^{-1}$ and 95.53 t ha$^{-1}$ yr$^{-1}$ respectively while the lowest at location HF top which is 4.78 t ha$^{-1}$ yr$^{-1}$ and 4.97 t ha$^{-1}$ yr$^{-1}$. The deposition rate was higher in HF center which is 216.82 t ha$^{-1}$ yr$^{-1}$ and 97.51 t ha$^{-1}$ yr$^{-1}$ and the lowest at HE center which is 0.05 t ha$^{-1}$ yr$^{-1}$ for both models used.

**Keywords:** Soil Erosion, $^{137}$Cs, Cameron Highlands, Gamma spectrometer

**Abstrak**

Hakisan tanah dan pemendapan di kawasan berbukit adalah satu kebimbangan besar bagi peladang. Dalam kajian ini, ladang teh di Cameron Highlands telah dipilih untuk mengira kadar hakisan tanah dan kadar pemendapan kerana ia dapat memberi maklumat mengenai pembaikpulihan keadaan tanah dan pengurangan kos penggunaan baja. Tujuan kajian ini adalah untuk menentukan kadar hakisan tanah dan pemendapan menggunakan radionuklid alam sekitar $^{137}$Cs. Sampel profil tanah dipungut dengan menggunakan plat pengikis dan dua teras sampel tanah tidak terganggu telah diambil dari kawasan hutan yang berdekatan. Kepekatan aktiviti $^{137}$Cs telah diukur dengan menggunakan latar belakang rendah pengesan germanium lampau tulen spektrometer gama berdasarkan tenaga gama $^{137}$Cs puncaknya pada 661,66 keV. Kadar hakisan tertinggi menggunakan 'Proportional Model' dan 'Mass Balance Model 1' didapati di lokasi HE bahagian atas 52.39 t ha$^{-1}$ yr$^{-1}$ dan 95.53 t ha$^{-1}$ yr$^{-1}$ masing-masing manakala yang paling rendah di kawasan HF bahagian atas 4.78 t ha$^{-1}$ yr$^{-1}$dan 4.97 t ha$^{-1}$ yr$^{-1}$ . Kadar pemendapan tertinggi di kawasan HF tengah iaitu 216.82 t ha$^{-1}$ yr$^{-1}$ dan 97.51 t ha$^{-1}$ yr$^{-1}$ dan paling rendah di HE bahagian tengah iaitu 0.05 t ha$^{-1}$ yr$^{-1}$ untuk kedua-dua model.

**Kata kunci:** Hakisan Tanah, $^{137}$Cs, Cameron Highlands, Spektrometer Gama

## Introduction

In hilly regions with swelling topography, the serious problem of soil degradation is the soil erosion that naturally occurred on cultivated lands. The problems not only on-site degradation as resulted from soil erosion but also off-site problems that occurred related to downstream sedimentation as well as surface and ground water pollution [1]. Every year, tones of soil are lost and cause reduction on crop production as well as pollution to rivers, lakes and

other water bodies. Soil erosion that occurred due to natural process is usually does not cause much problem. It becomes a problem when human activity causes it to occur at much faster rate than under natural conditions. The exposure to soil erosion is dependent on a number of factors. The most common factors are the climate conditions of the area, the proportion of sand, silt and clay, sized particles in a particular soil, organic matter level, the length and slope of the field, amount of crop rotation and direction of cultivation. There is a need to explain, predict and quantify the soil erosion at all scales and accurately define the influence of local soil factors for the implementation of appropriate measures to control soil degradation including landslide and erosion. It is also a need to estimate the economic and environmental on-site and off-site impact of in-situ losing of surface soil with its nutrients and potentially polluting constituents [2].

The potential of soil erosion is measured by determination of radionuclide (tracer) content and related the information to the long term history of its formation. The measurement of$^{137}$Cs is to derive soil erosion rates for two reasons, its long live period with regard to human scale, added to a strong advection to soil particles, and has formed a universal soil erosion tracer after precisely known the fallout episode [3].The nuclear weapon tests during the 1950s and 1960s have afforded an effective and valuable means for studying erosion and deposition within the landscape appropriate to it related with the worldwide fallout of $^{137}$Cs which can be used to study the different types of soil erosion and sedimentation in different positions and periods, particularly in the northern hemisphere where atomic deposition was three times as greater as in the southern hemisphere [4]. The Chernobyl accident in 1986 was also another source of radioactive $^{137}$Cs. It provided a new source of $^{137}$Cs deposition in Europe and Western Asia [5].$^{137}$Cs was released into the atmosphere and afterward redeposit on the earth surface via precipitation. Because of its 30 years half life, the relative alleviate of detection of the strong gamma ray that it emit, and its strong adsorption on clay and organic particles, the $^{137}$Cs serves as a useful tracer for determining long term mean annual rates of soil erosion or deposition [6].

The calculations involved conversion of data set of $^{137}$Cs activity concentration into soil erosion or deposition rates unit in tone per hectare per year. In reviewing the variety of models to be used for this study, a vital distinction can be made between cultivated soils and soils under permanent pasture or rangeland, which are uncultivated and effectively undisturbed. The need for this distinction relates to the vertical distribution of the $^{137}$Cs inventory in the soil profile [7]. The $^{137}$Cs method is frequently based on a comparison of calculated inventories (total activity per unit area) at individual sampling points with an equivalent estimate of the inventory representing the cumulative atmospheric fallout input (reference inventory) at the site [8]. From the selected models, the erosion rate values are calculated that relate soil loss with radio-cesium loss and must consequently; show a specific isotope concentration profile at that point. This inherent assumption is, there exist a specific profile of $^{137}$Cs in the soil because erosion itself decreases the overall amount of the radioisotope links to its depth distribution. As a result, application of different models to the same experimental value of total cesium inventory may give very dissimilar erosion rate values [9]. In this paper, the study area was carried out in cultivated soils and the theoretical calibration model selected for data interpretation were Proportional Model and Mass Balance Model 1; which was found to be suited for data interpretation of the generated $^{137}$Cs from this study.

**Study Area**

The study area for this research is in Cameron Highlands, Pahang, Malaysia. It is a small district located at North West of Pahang in the upper left corner inside the Pahang state. The place is situated on the main mountain range of Peninsular Malaysia. Cameron Highlands count roughly 71,000 hectare of lands where 79 percent is still forested which makes 21 percent developed. Specific location is the tea plantation area near Tanah Rata and forest nearby, around 1387 m above sea level. Cameron Highlands is one of the places with the cruel soil erosion in Malaysia. Because of overdevelopment, landslides, soil erosion will occur during heavy raining and lastly river contamination. The specific study area was in agricultural area where it is the second major land used after forestry with 16.4 percent of the total land area [10]. It is one of the areas with high altitude in Malaysia thus; the chance to receive fallout of $^{137}$Cs radionuclide is relatively high. The $^{137}$Cs contamination is positively correlated with altitude, so the upland, most susceptible sites, is mostly contaminated too [11]. This paper presents the study of soil erosion and deposition rates using environmental radionuclide $^{137}$Cs as s tracer. The global positioning system (GPS) as shows in Table 1 was used to record the details information on sampling locations. The sampling locations (three slopes and two forests) are shown in Figure 1.

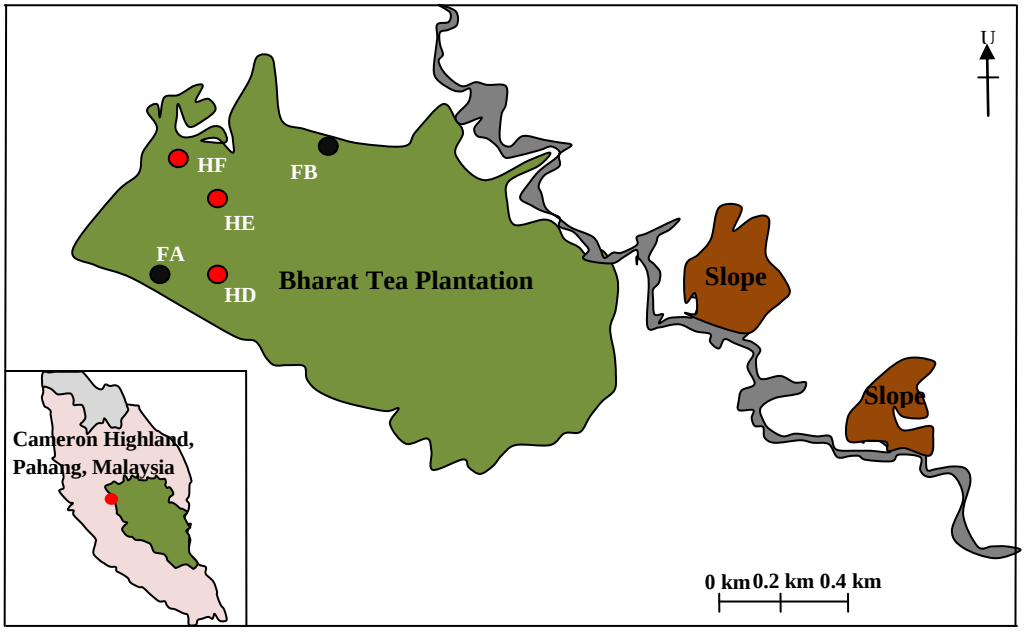



Figure 1: Maps of the study location in the tea plantation area. Inserted map shows the state of Pahang, Malaysia

Table 1: The locations for composite and profile soil samples

| Code | Locations | Elevation (m) | Description |
|---|---|---|---|
| HD | N 04$^0$ 27.145' E 101$^0$ 21.600' | 1340 | Top of the hill |
| | N 04$^0$ 27.139' E 101$^0$ 21.595' | 1329 | Center of the hill |
| | N 04$^0$ 27.205' E 101$^0$ 21.580' | 1322 | Bottom of the hill |
| HE | N 04$^0$ 27.240' E 101$^0$ 21.560' | 1391 | Top of the hill |
| | N 04$^0$ 27.270' E 101$^0$ 21.573' | 1316 | Center of the hill |
| | N 04$^0$ 27.290' E 101$^0$ 21.597' | 1266 | Bottom of the hill |
| HF | N 04$^0$ 27.283' E 101$^0$ 21.441' | 1387 | Top of the hill |
| | N 04$^0$ 27.312' E 101$^0$ 21.487' | 1330 | Center of the hill |
| | N 04$^0$ 27.313' E 101$^0$ 21.514' | 1297 | Bottom of the hill |
| FA | N 04$^0$ 27.064' E 101$^0$ 21.523' | 1330 | Undisturbed flat area |
| FB | N 04$^0$ 27.438' E 101$^0$ 21.728' | 1308 | Undisturbed flat area |

## Materials and Methods

### Sampling and sample preparation

The soil samples were collected from three hilly areas of the tea plantation covering top, center and bottom of each hills-top namely HD, HE and HF, respectively (Figure 1 and Table 1).The soil from two undisturbed forests which are FA and FB were collected for reference inventories. For each of the sampling point, bulk and soil samples of various depth (2 cm each layer) were taken. The specially designed scrapper plate with PVC pipe 40 cm long and 15.2 cm diameter was used for depth profile sampling and this device enable for quantitatively obtaining layer of 2 cm interval of the soil depth profile. Whist a bulk samples were collected using hand auger with 15 cm long for soil basic parameter tests. The soil samples were kept each in polyethylene bags and transported back to the UiTM laboratory in Shah Alam. The samples were taken to the laboratory for oven dried at 60$^{o}$C until constant weight, then ground using Fritsch pulverizer (400 rpm rotational speed, 2 repetitions, 5 minutes) in agate bowl and ball and sieved through 250 µm sieve. About 150 g of samples was kept and sealed properly in the plastic container of 6 cm diameter and 4 cm height.

### Measurements

Gamma spectrometer measurement was carried out using low background hyper pure coaxial germanium (p-type) detector. It is linked to a multi-channel digital analyzer system from EG & G, ORTEC. The gamma peak resolution at 1332 keV$^{60}$Co was 1.82 keV and relative efficiency of 25 % with energy range from 40 keV to 10 MeV. The ORTEC Gamma Vision$^{TM}$ Version 6.07 software was used for the spectra analysis and processing [12]. All the samples were counted at 28800 second live time and the spectrum was analyzed using Gamma Vision software for energy peak at 661.66 keV of $^{137}$Cs. The efficiency calibration of the detector was made using secondary standard made up of $UO_3$ and KCl matrix in the same geometry as the sample [12].The spectrometer efficiency at 661.66 keV obtained from an efficiency calibration curve (12) was used to calculate the absolute activity concentration of $^{137}$Cs in the soil using the Equation 1,

$$A_{Ei} = \frac{N_{Ei}}{\varepsilon_E \times t \times \gamma_d \times M_s} \quad (1)$$

$A_{Ei}$ = Activity concentration (in $Bq/kg$)
$N_{Ei}$ = Net peak area of a peak at energy $E$
$\varepsilon_E$ = Detection efficiency at energy $E$
$t$ = Counting live time
$\gamma_d$ = Number of gammas per disintegratio of this nuclide for a transition at energy E
$M_s$ = Mass in $kg$ of the measured sample

The minimum detectable activity (MDA) of this low background gamma spectrometer at 661.66 keV was 0.03927 Bq/kg calculated using the Equation 2 [13];

$$MDA = \frac{(4.65\sqrt{N+3}}{ET} \quad (2)$$

N = background count
T = counting time
E = counting efficiency

The theoretical calibration model used were the Proportional Model and Mass Balance Model 1 to obtain erosion and deposition rate, Y, t ha$^{-1}$ yr$^{-1}$, as shown in the Equation 3 and 4 below [14];

$$Y = 10\frac{BdX}{100TP} \quad (3)$$

d = depth of the plough or cultivation layer (m)
B = bulk density of soil (kg $m^{-3}$)
T = time elapsed since initiation of $^{137}Cs$ accumulation (yr)
*P* = particle size correction factor
X = percentage reduction in total $^{137}Cs$ inventory (defined as $[(A_{ref} – A)/A_{ref}] \times 100$].
$A_{ref}$ = local $^{137}Cs$ reference inventory (Bq $m^{-2}$)
A = measured total $^{137}Cs$ inventory at the sampling point (Bq $m^{-2}$)

$$Y = 10\frac{dB}{P}\left[1 - \left(1 - \frac{X}{100}\right)^{t-1963}\right] \quad (4)$$

d = depth of the plough or cultivation layer (m)
B = bulk density of soil (kg $m^{-3}$)
t = time elapsed since initiation of $^{137}Cs$ accumulation (yr)
*P* = particle size correction factor
X = percentage reduction in total $^{137}Cs$ inventory

## Results and Discussion

### Properties of soil

Results in Table 2 show that soil in tea plantation study sites are acidic with pH value lower than six with an average of 4.07. The trend shows that higher elevation has lower soil pH. Lower pH will help $^{137}Cs$ ions to move freely and being washed easily by the rain water runoff. Also, low pH level may result in lack of some basic elements such as Ca, Mg, K, N, in the soil [14]. Results on bulk density are in the range between 1.23 – 1.69 $gcm^{-3}$. Bulk density is usually included to evaluate tillage and crop management effects on soil quality. Soil compaction increases bulk density and decreases pore volume. At constant water content, compaction increases the proportion of soil pores filled with water as average pore size decreases. This can lead to aeration stress and changes in biological processes. If bulk density becomes too high, it can limit plant root growth [15]. This density is related to the soil texture in the location itself. Soil texture in the study site is sandy clay loam soil particles. This soil texture directly affects the porosity of soil, which in turn, determined its water-retention, flow characteristic and nutrient-holding capacity. Heavy clay soils normally have higher percentage of smaller pores and higher water holding capacity. On the other hand, sandy soils have relatively higher percentage of larger pores with water holding capacity under relatively dry conditions.

Soil organic matter plays an important role in determining the fertility and productivity of soils. This may be especially true in tropical areas where nutrient poor, highly weathered soils are often managed with few external inputs [17]. Results of organic matter content were in the range of 8.84 – 10.46 % which means lower than 10 %. This organic matter was dependent on the amount of the living organisms in that soil that consumed humus. The highest content of that humus or dead materials, the value of the organic matter also increases.

### $^{137}Cs$ vertical profile

Figure 2 to 5 showed the vertical profile of $^{137}Cs$ activity concentrations in study area. Generally, there are two patterns are observable, one from the depth of 0 cm to about 18 cm and the other from 20 cm until 30 cm. In location HD (Figure 2 (a, b and c)), the upper pattern shows $^{137}Cs$ activity concentrations increase downward to the depth of 15 cm. This is similar to location HE (Figure 3c) and HF (Figure 4c) at the bottom locations. The $^{137}Cs$ activity concentrations increase downward to the depth of up to 20 cm. Zhiyanski and co-workers concluded that 80% of the $^{137}Cs$ from the Chernobyl is located within the upper 15 cm of soils [18]. These would happened because

the surface of soil was wash out by rainfall thus erosion occurs makes the surface soil loss their original $^{137}$Cs fallout as compared the $^{137}$Cs present in the depth profile of soil. Thus, make the $^{137}$Cs measured in the depth was high activity as compared in the surface of soil. The locations itself have more farmers activity such as plough make the soil surface of the study area had low $^{137}$Cs activity concentration. However, in location HE (Figure 2a) and HF (Figure 4b) at top and center of the hills, the $^{137}$Cs activity concentration was high in the surface soil layer but declining in activity level since subsurface soil layer down to the depth of 20 cm. This trend is basically in agreement with the result of study in other countries [19] as reported in literature. This finding signified that the $^{137}$Cs is having characteristic that is strongly adsorbed on the surface of soil particles; thus enable as tracer of soil movement during events such as soil erosion and landslide.

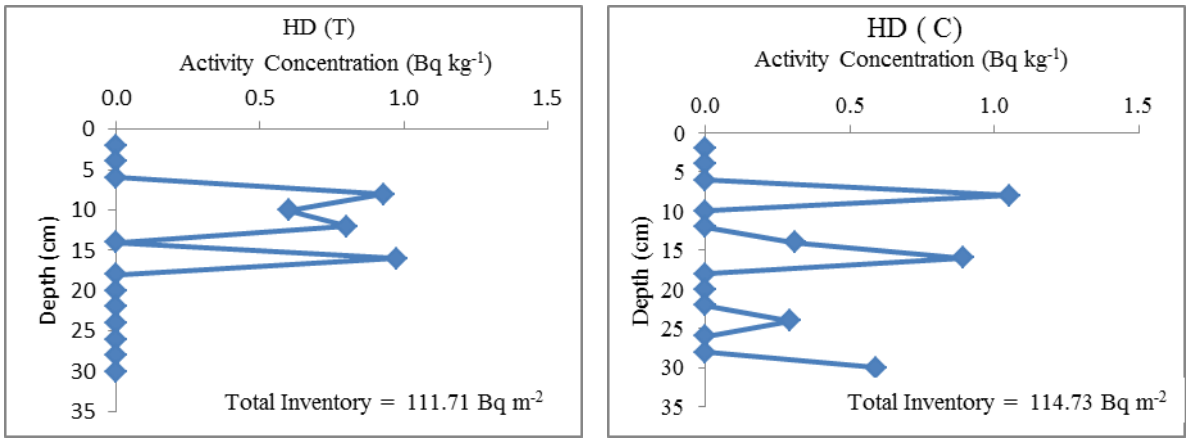
Table 2: Soil basic parameter results in study area

| Location point | Slope position | Bulk density (g/cm$^3$) | Organic Matter Content (%) | pH | Texture (%) | | | Textural Class Name |
|---|---|---|---|---|---|---|---|---|
| | | | | | Clay | Silt | Sand | |
| HD | Top of hill | 1.69 | 10.46 | 4.15 | 26.01 | 18.60 | 55.39 | Sandy Clay Loam |
| | Center of hill | 1.53 | 10.33 | 5.04 | 26.22 | 17.04 | 56.74 | Sandy Clay Loam |
| | Bottom of hill | 1.39 | 9.85 | 4.16 | 27.06 | 19.42 | 53.52 | Sandy Clay Loam |
| HE | Top of hill | 1.64 | 9.63 | 3.38 | 26.66 | 18.46 | 54.88 | Sandy Clay Loam |
| | Center of hill | 1.54 | 9.41 | 4.21 | 27.48 | 19.06 | 53.46 | Sandy Clay Loam |
| | Bottom of hill | 1.62 | 9.77 | 4.25 | 26.80 | 19.65 | 53.55 | Sandy Clay Loam |
| HF | Top of hill | 1.41 | 10.34 | 3.21 | 25.50 | 17.41 | 57.09 | Sandy Clay Loam |
| | Center of hill | 1.55 | 9.97 | 3.50 | 27.45 | 19.90 | 52.65 | Sandy Clay Loam |
| | Bottom of hill | 1.31 | 9.70 | 4.53 | 26.60 | 18.42 | 54.98 | Sandy Clay Loam |
| FA | Undisturbed | 1.23 | 9.49 | 4.63 | 24.80 | 16.20 | 59.00 | Sandy Clay Loam |
| FB | Undisturbed | 1.34 | 8.84 | 3.70 | 22.30 | 18.10 | 59.60 | Sandy Clay Loam |

For the second pattern of $^{137}$Cs activity concentration in soil profile, which is from the depth of 15 cm and 20 cm goes down to 30 cm, all the $^{137}$Cs have initially high activity then change to low in activity. These means, the $^{137}$Cs become loss in the increasing the soil depth. As stated in previous study, $^{137}$Cs will decrease and finally lost in the depth [19]. It was a directly proportional of $^{137}$Cs present highly in soil surface and decreases its value when the depth was increase. The first pattern could be due the $^{137}$Cs that was come from the Chernobyl accidents that occurred in 1986 [20]. It was confirmed by the detection of Chernobyl fallout analysis of individual radionuclide in the air sample which first detected on the filter in 9 May 1986 and reaching a peak on 11 May 1986 [21]. The second pattern source of $^{137}$Cs comes from the above ground nuclear weapon test during the 1950s to 1963s [20].

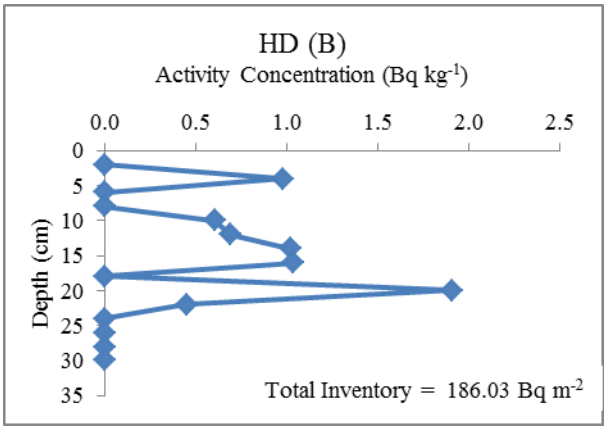
In the reference site, the vertical distribution of $^{137}$Cs at location FA (Figure 5a) was increased in $^{137}$Cs activity concentration which is from the depth of 6 cm to 16 cm. After that, $^{137}$Cs activity concentration began to decrease at the depth of 18 cm until 30 cm. This represents the pattern of $^{137}$Cs decreased exponentially with depth. At the second reference site, location FB (Figure 5b), the $^{137}$Cs activity concentration getting increases its value. The first pattern showed decreased of $^{137}$Cs from the depth of 0 cm until the layer of 14 cm. Then, the second pattern was from the depth of 16 cm that was decreased also its value until the depth of 30 cm. This second pattern which is below 16 cm depth, the $^{137}$Cs activity in the soil decreased rapidly. This shape with subsurface peak reflects both the fallout source of the radionuclide and thus its delivery to the soil surface, slow post-fallout downward migration, thus surface replacement of fallout inputs, in the early 1970s [22].

In the entire core profile soil samples collected in each hills, the $^{137}Cs$ activity concentration showed from top to the center and lastly goes to the bottom, the rising value obtained. The accumulation of this radionuclide clearly showed in this sloping area, where there is a movement of $^{137}Cs$ from the upper site down to lower placed. This reflects the progressive accumulation of soils contains $^{137}Cs$ at the bottom of the slope [22]. In location HD and HE (Figure 2 and 3), the soil containing $^{137}Cs$ can be seen clearly increased down to the lower land of the slopes. That is about 1 Bq $kg^{-1}$ (HD top) to 1.9 Bq $kg^{-1}$ (HD bottom) and 0.5 Bq $kg^{-1}$ (HE top) to 2.5 Bq $kg^{-1}$ (HE bottom). For location HF, there is high value of $^{137}Cs$ in the center location, then decrease again at the bottom low land area. This is due to the location of the sampling point, soil was collected at slightly high of the area with no plantation and erode. Thus, the high accumulation of soil (soil gain) in that location makes the activity of $^{137}Cs$ high.



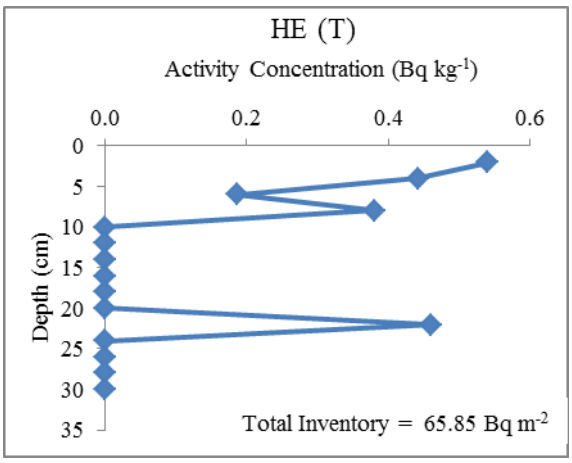

a) Location Hill D Top

b) Location Hill D center

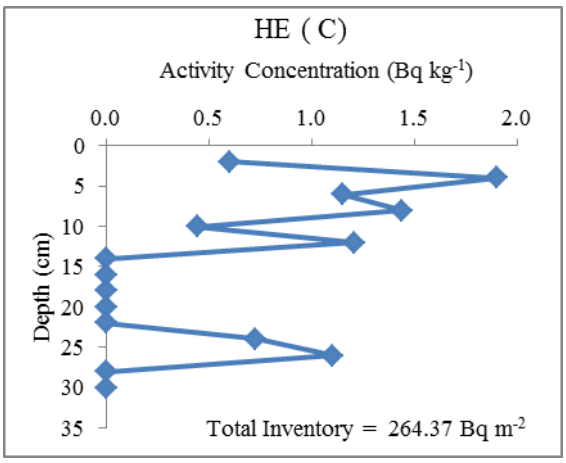



c) Location Hill D bottom

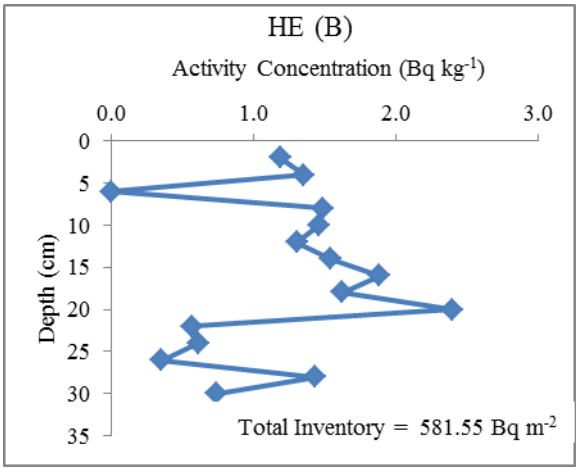
Figure 2: Vertical profile of $^{137}Cs$ in hill HD for top, center and bottom location




a) Location Hill E top

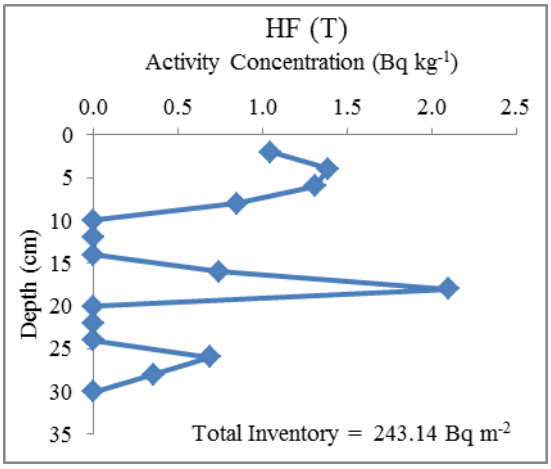



b) Location Hill E center

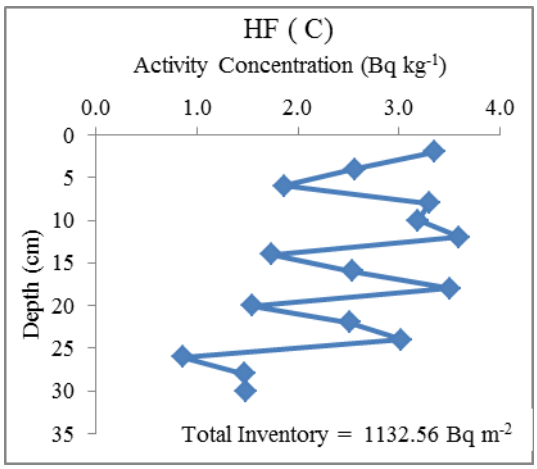



c) Location Hill E bottom

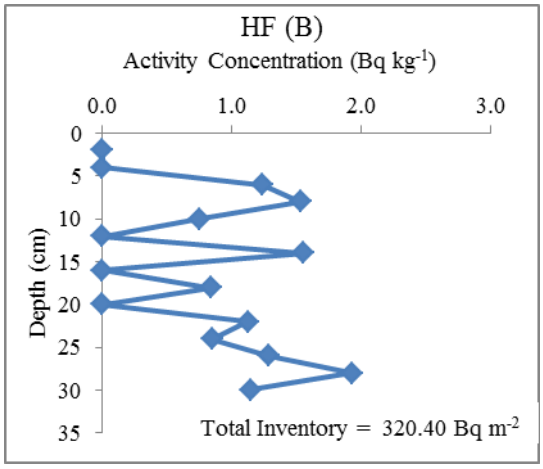
Figure 3: Vertical profile of $^{137}Cs$ in hill HE for top, center and bottom location




a) Location Hill F Top

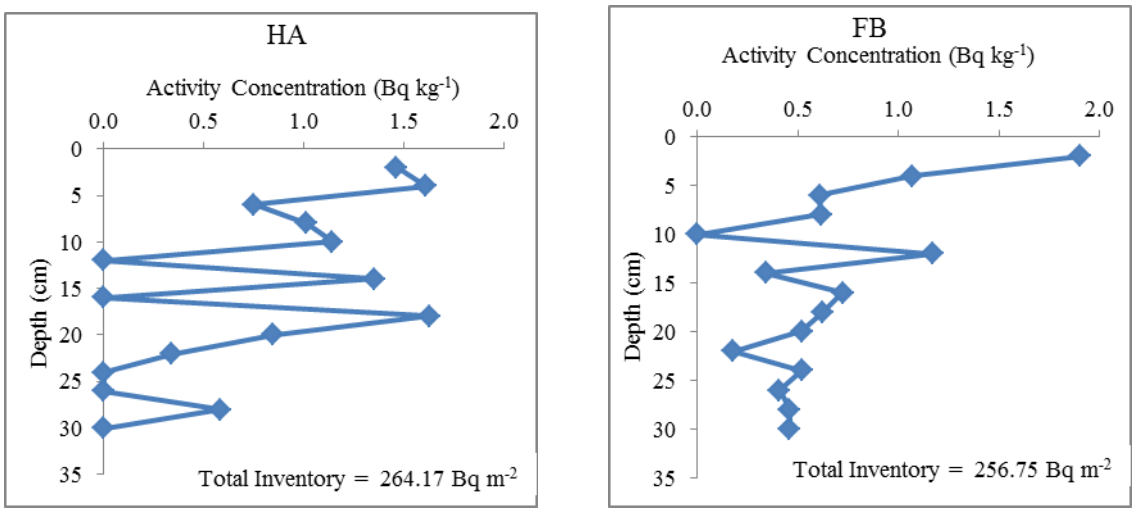



b) Location Hill F center




c) Location Hill F Bottom

Figure 4: Vertical profile of $^{137}Cs$ in hill HF for top, center and bottom location




a) Location Forest A (FA)

b) Location Forest B (FB)

Figure 5: Vertical profile of $^{137}$Cs in the two forests undisturbed area

**Hill slope $^{137}$Cs inventory**

$^{137}$Cs inventories in the unit of Bq m$^{-2}$ was derived from measured $^{137}$Cs obtained by multiplying it with the depth incremental of soil sliced (0.02 m), density (g m$^{-3}$) and sum up with the total core length, 30 cm. Results tabulated in Table 3 shows comparable trends observed in locations HD (Figure 2) and HE (Figure 3) in which the $^{137}$Cs inventories is larger from top to bottom of the hill slope. In location HF, the $^{137}$Cs inventory shows highest in the center location. This may happen due to the location itself at the lower area with most exposed soils, the area without tea trees cover the soil thus, high deposition occurred on that placed. The $^{137}$Cs inventories are one of the main points when determining the soil erosion and deposition rate. The indicator is that, if the $^{137}$Cs inventory measured in reference site, which refers to forest undisturbed flat top area have larger inventory than the sampling site, this mean the soil erosion occurred, and vice versa the soil deposition was occurred. It was assumed that, the reference site which is undisturbed have the $^{137}$Cs from the soil that are not being disturbed since the year of 1964, as known as most fallout occurred of $^{137}$Cs radionuclide [23]. Above ground nuclear weapon testing during the 1950s and 1960s resulted in the release of radioactive $^{137}$Cs to the atmosphere. The passage of the nuclear test ban treaty in 1963 well halted further $^{137}$Cs inputs of the atmosphere level of $^{137}$Cs fell gradually and by the late 1970s, $^{137}$Cs had essentially ceased [23].

In these three sloping hill areas, not all $^{137}$Cs inventory was lower than that of its control field. This signified that in some places, the deposition was occurred and mostly at center and bottom of the hill. These inventory results are consistent with the soil erosion and deposition rate calculated. As shown in Table 3, the average calculated of inventory in the first reference site, was 17.61 Bq m$^{-2}$ and the second reference site was 17.12 Bq m$^{-2}$. The first reference site was chosen as the indicator due to its have more value. The location that greater than this value will form of erosion site, whereas the location that have less than this value will have deposition site.

**$^{137}$Cs derived soil redistribution rates**

The proportional mathematical model and the mass balance 1 mathematical model were used for further data interpretation. Both mathematical models provide difference but comparable soil erosion and deposition rate. The results calculated using the proportional model signified low soil erosion and deposition rate as compared to the results obtained using mathematical mass balance model 1. For the calculation using the proportional model, the same formula was used to determine the soil erosion and deposition rates, except, the value of percentage in reduction of $^{137}$Cs inventory or X (Eq.4). In the calculation of soil deposition, the X' used t was the measured total $^{137}$Cs inventory at sampling point minus $^{137}$Csof reference inventory.

The results are shown in Table 3, the soil deposition signified the soil loss is shown with negative sign and soil gain with positive sign. The overall observations showed, in the top of the hill, soil erosion occurred in almost all top of the hill, confirmed for both models used. The highest erosion rate occurred in hill-top HE, which were -52.39 t ha$^{-1}$ yr$^{-1}$ (Proportional Model) and -95.53 t ha$^{-1}$ yr$^{-1}$ (Mass Balance Model 1). It can be explained that, based on the slope gradient in this hill, which is 61$^{o}$ was the steepest area. Thus, high erosion rate is attributed on that soil resulted in high soil loss. In location HD, the hill-top, hill-center and hill-bottom location showed the soil erosion occurred without the deposition of soil. This could be due to the slope gradient which is only 26$^{o}$ thus avoids the deposition of eroded soil to the low lying area. Since the values obtain for the measured basic soil parameter quiet similar for every location, the only influence of soil erosion and deposition on the study area is the slope gradient factor. The calculated soil erosion was lowest at the top location of hill HF which was -4.78 t ha$^{-1}$ yr$^{-1}$ (Proportional Model) and -4.97 t ha$^{-1}$ yr$^{-1}$ (Mass Balance Model 1). In location HF hill- top area, same reason can be explained due to it slope gradient which was 34$^{o}$. This location was one of the steepest sloping areas, from top to the center location. The slope gradient was 34$^{o}$, thus the retention time for $^{137}$Cs radionuclide retained in soil is very short.

Table 3: Soil erosion and soil deposition in the study area

| Location point | Slope position | Slope gradient ($^{o}$) | $^{137}$Cs activity concentration (Bq/kg) | $^{137}$Cs inventory ( Bq m$^{-2}$ ) | Net erosion rate (tha$^{-1}$yr$^{-1}$) | |
|---|---|---|---|---|---|---|
| | | | | | PM | MBM1 |
| HD | Top of hill | 26 | 0.22 | 7.45 | -41.50 | -61.33 |
| | Center of hill | | 0.21 | 7.65 | -44.05 | -64.37 |
| | Bottom of hill | | 0.45 | 12.40 | -17.49 | -20.66 |
| HE | Top of hill | 61 | 0.13 | 4.39 | -52.39 | -95.53 |
| | Center of hill | | 0.57 | 17.62 | 0.05 | 0.05 |
| | Bottom of hill | | 1.28 | 38.77 | 82.82 | 54.86 |
| HF | Top of hill | 34 | 0.57 | 16.21 | -4.78 | -4.97 |
| | Center of hill | | 2.44 | 75.50 | 216.82 | 97.51 |
| | Bottom of hill | | 0.82 | 21.36 | 11.87 | 10.78 |
| FA | Undisturbed Area | - | 0.77 | 17.61 | - | - |
| FB | Undisturbed Area | - | 0.68 | 17.12 | - | - |

The result of soil deposition shows that the highest deposition was at location HF hill center. As explained above, the soil sample taken at this location consists of the wash out the upper soil immediately above the location which is not covered with any plantation. The calculated results of soil deposition using proportional model was 216.82 t ha$^{-1}$ yr$^{-1}$ and 97.51 t ha$^{-1}$ yr$^{-1}$ using Mass Balance Model 1. The soil deposition also occurs in location HE and HF center and bottom of the hills. The observed small deposition at HE center is consistent with the fact that the hills is at higher sloping angle, hence shorter retention time for loose soil.

## Conclusion

The anthropogenic $^{137}Cs$ radionuclide was present at measurable concentration in tea plantation soil in Cameron Highlands, Pahang. The $^{137}Cs$ tracer technique is applicable for the estimation of the soil erosion and soil deposition rates. The Proportional Model and Mass Balance Model 1 were applicable for data interpretation, the highest erosion rate was in location HE top which are -52.39 t $ha^{-1}$ $yr^{-1}$ and -95.53 t $ha^{-1}$ $yr^{-1}$ respectively and the lowest are at location HF top which is -4.78 t $ha^{-1}$ $yr^{-1}$ and -4.97 t $ha^{-1}$ $yr^{-1}$. For deposition rate, HF top location has the highest value which is 216.82 t $ha^{-1}$ $yr^{-1}$ using the proportional model whereas 97.57 t $ha^{-1}$ $yr^{-1}$ using the mass balance model 1. The lowest deposition was at location HE center which is 0.05 t $ha^{-1}$ $yr^{-1}$ for both models used. The patterns in all three locations were different depending on the hill sampling site conditions and sloping gradient. The high sloping area has more potential to have the greater deposition and low slope tend to have less deposition rate.

## Acknowledgement

The authors would like to thank the District Officer of Cameron Highlands and Authorities of Tea Plantation for giving us the permission to carry out this research in their areas. Thank you also to the Research Management Institute (RMI), Institute of Science (IOS), Faculty of Applied Sciences and INTEC Universiti Teknologi MARA (UiTM) for providing research facility and fund.

## References

1. Afshar, F, A., Shamsollah, A. and Ahmad, J., (2010). Soil redistribution rate and its relationship with soil organic carbon and total nitrogen using $^{137}Cs$ technique in a cultivated complex hill slope in western Iran. *Journal of Environment Radioactivity*, 101, 606-614.
2. Theocharopoulos, S, P., H, Florou., D, E, Walling., H, Kalantzakos., M, Christou., P, Tountas. and T, Nikolaou., (2003). Soil erosion and deposition rates in a cultivated catchment area in central Greece, estimated using the $^{137}Cs$ technique. *Soil & Tillage Research*, 69, 153-162.
3. Perrin, J., Carrier, F. and Guillot, L., (2006). Determination of the vertical distribution of radioelements (K, U, Th, Cs) in soils from portable HP-Ge spectrometer measurements: A tool for soil erosion studies. *Applied Radiation and Isotopes*, 64, 830-834.
4. Chen, Z., Ye, Z., Jie-juan, Q., Qing, Z., Yu-en, Z. and Cui-hua, X., (2009). Retrospection of recent 30 year changes in the process of soil wind erosion in the Luanhe River Source Area of North China using Cesium-137. *Applied Radiational Isotopes*, 67, 1785-1789.
5. Pelt, R, S, V., Ted, M, Z., Jerry, C, R. and Thomas, E, G., (2007). Validating the use of $^{137}Cs$ measurements to estimate rates of soil redistribution by wind. *Catena*, *70*, 455–464.
6. Zou, X., Yang, P., Dong, Y., Li, S., Wei, X., Yang, S. and Pan, X., (2007). Wind tunnel test and $^{137}Cs$ tracing study on wind erosion of several soils in Tibet. *Soil & Tillage Research*, 94, 269-282.
7. Walling, D, E., He, Q. and Appleby, P, G., (2002). Conversion models for use in soil erosion, soil redistribution and sedimentation investigations. *Handbook for the assessment of soil erosion and sedimentation using environmental radionuclide*, 111-164.
8. Kato, H., Onda, Y. and Tanaka, Y., (2010). Using $^{137}Cs$ and $^{210}Pb_{ex}$ measurements to estimate soil erosion redistribution rates on semi-arid grassland in Mongolia. Geomorphology, 114, 508-519.
9. Soto, J. and A, Navas., (2004). A model of $^{137}Cs$ activity profile for soil erosion studies in uncultivated soils of Mediterranean environments. *Journal of Arid Environments*, *59*, 719–730.
10. Fortuin, R., (2006). Soil erosion in Cameron highlands; an erosion rate study of a highlands area. *Regional environmental awareness Cameron Highlands.*
11. Lettner, H., Griesebner, A., Peer, Thomas., Hubmer, A, K. and Pintaric, M., (2006). Altitude dependent $^{137}Cs$ concentrations in different plant species in alpine agricultural area. *Journal of environmental radioactivity*, 86, 12-30.
12. Saat, A., Hamzah, Z., Yusop, M, F. and Zainal, A., (2010). Experimental Determination of the HPGe Spectrometer Efficiency Calibration Curves for Various Sample Geometry for Gamma Energy from 50 keV to 2000 keV. *AIP Conference Proceedings, 1250,* 39-42.
13. Taha, T, M. and Morsi, T, M., (2009). Calibration of single high purity germanium detector for whole body counter. *Proceedings of the 7th conference on nuclear and particle physics*, 485-492.

14. Mupenzi, J, P., Li, Lanhai., Ge, Jiiwen., Varenyam, A., Habiyaremya, G., Theonesta, N. and Emmanuel, Kamanzi., (2011). Geoscience frontiers 2 (4), 599-607.
15. Logdon, S, D. and Karlen, Douglas, L., (2004). Bulk density as a soil quality indicator during conversion to no-tillage. *Soil & Tillage Research*, 78, 143-149.
16. Feller, C. and Beare, M, H., (1997). Physical control of soil organic matter dynamics in the tropics. *Geoderma*, 79, 69-116.
17. Zhao, Z., Chow, T, L., Rees, H, W., Yang, Q., Xing, Z. and Meng, F., (2009). Predict soil texture distributions using an artificial neural network model. *Computers and electronics in agriculture*, 65, 36-48.
18. Zhiyanski, M., Bech, Jaume., Sokolovska, M., Lucot, Eric., Bech, J. and Badot, P., (2008). Cs-137 distribution in forest floor and surface soil layers from two mountainous regions in Bulgaria. *Journal of Geochemical Exploration*, 96, 256 – 266.
19. Hamzah, Z., Saat, A., Riduan, S, D. and Amirudin, C, Y., (2012). Assessment of $^{137}$Cs activity concentration in soil from tea plantation areas in Cameron Highlands. Journal of nuclear and related technologies, 9, 1-5.
20. Hamzah, Z., Amirudin, C., Y. and Saat, A., (2012). Depth profile of $^{137}$Cs fallout in soil in Cameron Highlands. *Malaysia Journal of fundamental & Applied Sciences*, 8, 18-23.
21. Lee, B, Y. and Tsui, K, C., (1999). Retrospective analysis of radiation fallout in Hong Kong after the Chernobyl accident in 1986. *Technical Report No.6, Environment Radiation Monitoring in Hong Kong*, 1-48.
22. Junge, B., Mabit, L., Dercon, G., Walling, D, E., Abaidoo, R., Chikoye, D. and Stahr, K., 2010. First use of the $^{137}$Cs technique in Nigeria for estimating medium-term soil redistribution rates on cultivated farmland. *Soil & Tillage Research*, 110, 211-220.
23. Pelt, R, S, V., Zobeck, T, M., Ritchie, J, C. and Gill, T, E., (2007). Validating the use of $^{137}$Cs measurements to estimate rates of soil redistribution by wind. Catena, 70, 455-464.

The Malaysian Journal of ANALYTICAL SCIENCES ISSN 1394-2506

# HYDROGEN PEROXIDE IMPEDIMETRIC DETECTION ON POLY-ORTHO-PHENYLENEDIAMINE MODIFIED PLATINUM DISK MICROELECTRODE

## (Pengesanan Hidrogen Peroksida Secara Impedimetrik Di Atas Elektrod Mikro Cakera Platinum Yang Di Ubah Suai Dengan Poli-Orto-Fenilinadiamina)

Zainiharyati Mohd Zain* and Norazreen Zakaria

*Faculty of Applied Sciences,*
*Universiti Teknologi MARA, 40450 Shah Alam, Selangor, Malaysia*

**Corresponding author: zainihar@salam.uitm.edu.my*

**Abstract**

This work describes the development of hydrogen peroxide detection based on Poly-ortho-phenylenediamine modified Platinum disk microelectrode (50 µm in diameter). The electrochemical performances of $H_2O_2$ detection were studied using Chronoamperometry, Cyclic Voltammetry (CV) and Electrochemical Impedance Spectroscopy (EIS) techniques in Phosphate Buffer Solution (PBS) pH 7.4. Effect of potential, electrode size, and various concentrations of $H_2O_2$, among others, were investigated by tracking the impedance changes at a specific perturbation frequency. To obtain the Charge transfer resistance ($R_{ct}$) values, a modified Randles Equivalent Circuit was modelled and fitted to Nyquist Plot. Then, this sensor was further applied in the detection of $H_2O_2$ in antiseptic mouthwash with percent recovery of 97% ± 0.14 ($x10^3$ kΩ).

**Keywords:** Electrochemical Impedance Spectroscopy, Platinum microelectrode, hydrogen peroxide, poly-ortho-phenylen-diamine

**Abstrak**

Kajian ini menerangkan pembangunan pengesanan Hidrogen Peroksida berasaskan modifikasi poli ortho- fenilinadiamina di atas mikro elektrod cakera Platinum pada diameter 50 µm. Prestasi elektrokimia bagi pengesanan Hidrogen Peroksida di kaji menggunakan teknik Kronoamperometri, Voltammetri berkitar, Spektoskopi Rintangan Elektrokimia di dalam larutan penimbal fosfat, pH 7.4. Kesan potensial, saiz elektrod dan kepekatan Hidrogen Peroksida di kaji dengan mengenal pasti perubahan rintangan pada frekuensi tetap. Bagi mendapatkan nilai pemindahan cas rintangan, litar Randles terubah suai di padankan bersama plot Nyquist. Kemudian, sensor ini diaplikasikan untuk mengesan Hidrogen Peroksida di dalam ubat kumur antiseptik dengan peratus pemulihan sebanyak 97% ± 0.14 ($x10^3$ kΩ).

**Kata kunci:** : Spektroskopi Rintangan Elektrokimia, mikroelektrod cakera platinum, hidrogen peroksida, poliorthofenilin-diamina

## Introduction

An impedimetric analysis of hydrogen peroxide ($H_2O_2$) has been intensively investigated due to the fact that $H_2O_2$ has wide significance in medicine, food investigation, biological pathway, and industries such as disinfectant, antiseptic, oxidizer and often used in personal usage such as hair dye, conditioner and cosmetics [1]. Detection of $H_2O_2$ plays crucial role as it is an essential mediator in pharmaceutical, clinical, and environmental research. In addition, it is also a byproduct of highly selective oxidase and an important contaminant in several industrial products and wastes [2]. Many other analytical methods such as UV-Vis [3-4] titrimetry [5] as well as electrochemical techniques have been applied for this purpose [6]. However, electrochemical techniques provide simpler, speed, high sensitivity and stability of the sensing element. Electrochemical impedance spectroscopy (EIS) technique is an interesting alternative because it provides more information about the electrochemical system, for example, envision the true condition that passes from the bulk solution towards the surface of electrode [7].

Nyquist plot is resulted from graphing the real (Z') versus the imaginary (-Z") impedance values. Some information can be well-read about the electrochemical system from the Nyquist Plot [8] as such the spectrum is usually present in a semicircle and a straight line. The semicircle reflects the charge transfer resistance ($R_{ct}$) which describes the properties of interface electrode at higher frequency. While the straight line describes the diffusion process on the electrode at lower frequency [9]. Impedance data on $H_2O_2$ detection can be analyzed and determined using the components of the Randles circuit. From this circuit, the a value of charge transfer resistance can be exploited, hence, a calibration graph of $1/R_{ct}$ versus concentration is obtained. A similar study by Zhang *et al.* [10] reported on modified glassy carbon by poly dopamine-hyaluronic acid (PDA-HA) was able to detect $H_2O_2$. They interpreted that detection of $H_2O_2$ was observed by degradation of HA on active oxygen material which is observed by the decrement in the semicircle diameter.

Previously, studies on permselective membrane such as Poly-ortho-phenylenediamine (PPD) on sensor application have been investigated [11-14]. Therefore the efficiency of PPD as a coating polymer on this sensor was undoubted to be useful in this work, not only towards $H_2O_2$ detection, but also 'blocking' other interferences such as ascorbic acid (AA), uric acid and acetaminophen [13-15]. The objective of this study is to examine the characteristics of $H_2O_2$ detection on Platinum microelectrode deposited with PPD using EIS technique. In addition, in order to evaluate the efficiency of the sensor towards the presence of $H_2O_2$, this sensor was also practically applied in antiseptic mouthwash which contain of $H_2O_2$ as one of the ingredients.

## Materials and Methods

Reagents and chemicals- Ortho-phenylenediamine (o-PD), Hydrochloric acid (HCl) 37%, and Sodium Phosphate monobasic ($NaH_2PO_4$) were purchased from Sigma Aldrich (Germany). Sodium Hydroxide (NaOH) was purchased from Merck (Germany). All chemicals were used without further purification. Antiseptic mouthwash brand PolyLab was purchased from a pharmacy outlet. Autolab PG STAT302 potentiostat/galvanostat (Eco Chemie, Netherlands) controlled by Nova 1.7 electrochemical software was employed in this study. The three electrode cell comprised of Ag/AgCl (0.3 KCl) as reference electrode, PPD modified 99.9% Teflon-coated Pt micro (i.d. 25 µm and 50 µm, purchased from Advent Material, UK) electrode as working electrode as described elsewhere [16] and Pt rod as the counter electrode.

Electropolymerization of Pt was done in o-PD solution (10 mM) at constant potential + 0.7 V . The oxidation potential of $H_2O_2$ was investigated at a constant scan rate 10 $mVs^{-1}$ with potential ranges between -1.0 to +1.0 V using CV. Impedance measurements were performed at voltage perturbation of 10 mV over a wide frequency range from 0.1 Hz to 100 kHz at 30 to 50 numbers of frequencies.

## Results and Discussion

### Impedimetric characterization of PoPD electropolymerized on Pt surface

Figure 1 showed Nyquist spectra in comparison of bare Pt and modified Pt/PPD in pH 7.4 PBS solution. Pt bare showed a straight line which is further supported by Miao et al [17]. This is due to the diffusion limiting step of the electrochemical process. Meanwhile, modified Pt/PPD showed a small semicircle indicated that the appearance of impedance caused by PPD polymerization on the surface of the electrode. Moreover, the large difference in charge transfer resistance ($R_{ct}$) value between the presence of PPD on electrode (92.2 kΩ) compared to bare electrode (9.51 kΩ) confirmed that the PPD was successfully electropolymerized on Pt surface.

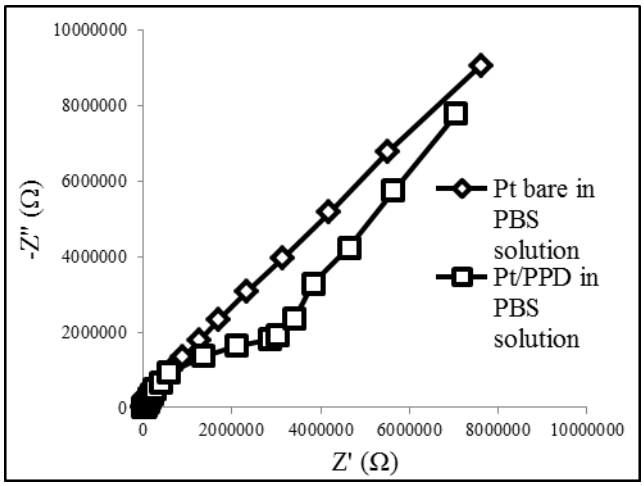



Figure 1: Comparison between Pt bare and Pt/PPD in PBS solution. The appearance of semicircle indicates the formed layer of PPD polymer on Pt surface.

**$H_2O_2$ and AA Amperometric responses**

Current response from chronoamperometric oxidation of $H_2O_2$ at constant +0.7 V potential is shown in Figure 2. This was to determine the efficiency of sensor's behavior towards $H_2O_2$. From the calibration curve, it produced a linear $H_2O_2$ calibration in the range from 5 to 100 µM in PBS (pH 7.4) with $R^2$= 0.9919. The response time ($t_{90\%}$) of the increment $H_2O_2$ spiked was in 0.3 s which is lower than previously reported work [12, 18] and the lowest detection limit (S/N x 3) was about 3 µM. Meanwhile, Equation (1) was used to define the percentage permeability of sensor (100% ± 1.1 n=4), which was close to the ideal values of 100% [13]. $\%P_{H2O2}$ is other important parameters in sensor fabrication to ensure acceptable $H_2O_2$ oxidation on the electrode. While, the sensitivity of electrode towards $H_2O_2$ was represented by the slope of linear calibration graph of $H_2O_2$ which is 188.1 µAcm$^{-2}$ ± 8.5, n= 4 [15].

$$\% \, P_{H_2O_2} = \frac{\text{Slope Pt/PoPD}}{\text{Slope Pt Bare}} \times 100\% \quad (1)$$

In order to exclude the nonspecific species adsorption on surface electrode, the amperometric measurement was carried out with AA [19-20] and resulted in no response of AA spiked into a PBS solution for up to 30 minutes. The percentage permeability of sensor towards AA was 0.08% ± 7.4, n=5, further indicated that this sensor is acceptable at blocking the interference species.

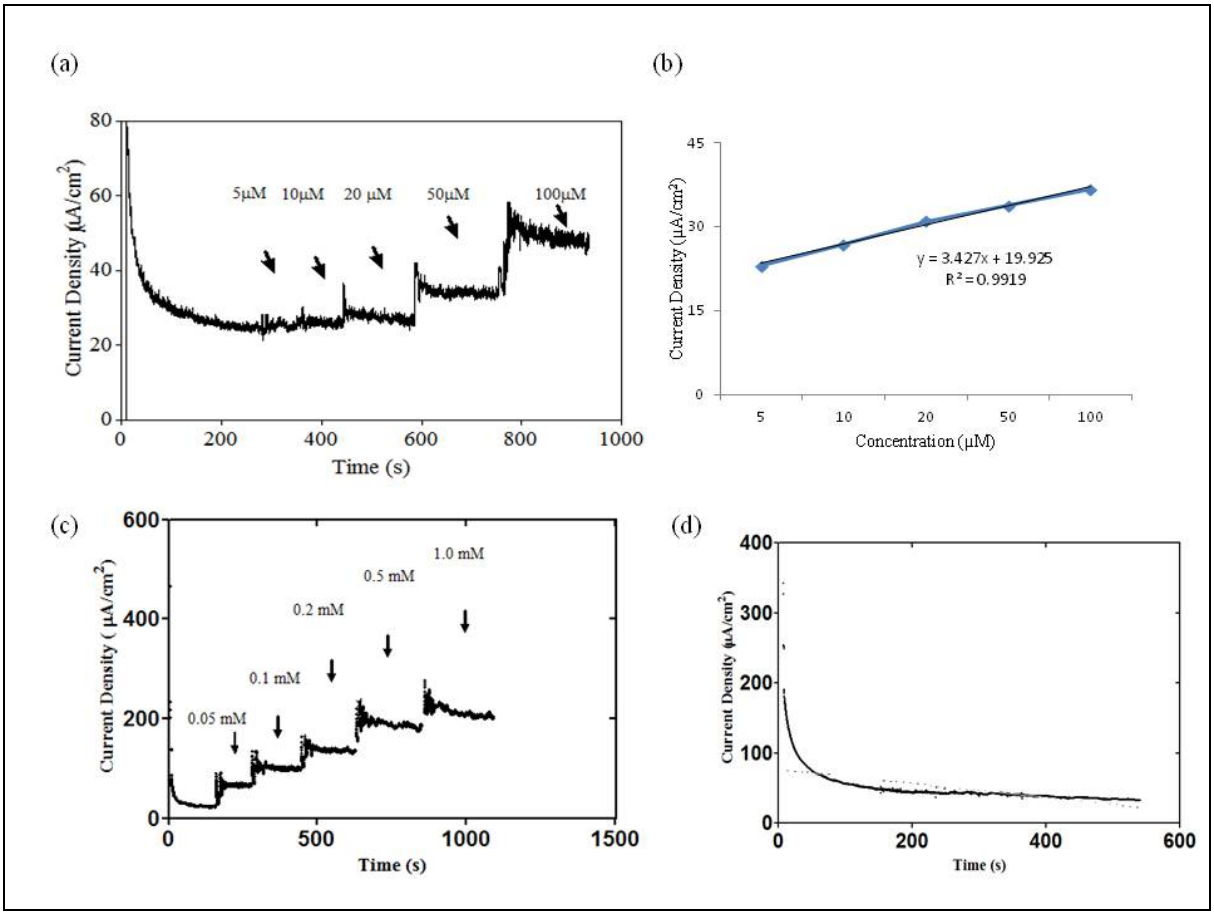



Figure 2: Chronoamperometry of $H_2O_2$ and AA were added in PBS solution with different range of concentrations.
(a) increasing the current density with increasing the $H_2O_2$ concentrations (5-100 μM),
(b) linear calibration of Pt/PPD with concentrations of $H_2O_2$,
(c) different AA concentrations were spiked on bare Pt, and
(d) graph showed there is no signal being detected when AA was spiked in solution after the Pt microelectrode was insulated with PPD.

**Effect of potential**

The dependent of $H_2O_2$ oxidation towards applied potential was at +0.4V as shown in Figure 3 and was supported by the others [21- 22]. The trend was also exhibited by EIS result. Hence, the potential of oxidation peak, which is +0.4V was further applied in performing EIS, which is in line with other literature [23].

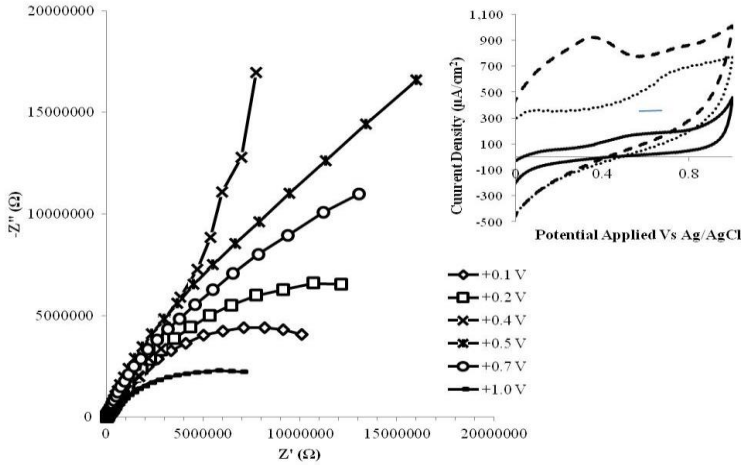



Figure 3: Nyquist plots resulted from the effect of applied potential on EIS measurement by using $Pt_{50}$/PPD in 5 µM $H_2O_2$. Inset: CV voltamogram of Pt bare in PBS solution (-),Pt/PoPD in PBS solution(…) and Pt/PPD (- -) spiked in 5 µM $H_2O_2$ showed the oxidation peak at +0.4 V vs. Ag/AgCl.

**Effect of electrode size**

Two different electrode sizes were studied in this work. The efficiency of Pt/PPD with internal diameter of 50 µm ($Pt_{50}$/PPD) and 25 µm ($Pt_{25}$/PPD) were calibrated with the standard addition of $H_2O_2$ in PBS solution (pH 7.4) at 30 number of frequency measurement. Figure 4 showed $Pt_{25}$/PPD gave a straight line in the Nyquist spectrum while $Pt_{50}$/PPD showed the appearance of a small semi circle which indicates the charge transfer resistance occurred after 5µL of standard $H_2O_2$ was spiked in solution. This observation is in line to Daniels and Pourrmand [8] which discussed on the reduction of electrode area will increase the capacitor behavior at higher frequency and further resulted in lack of analyte oxidation. Thus, on $Pt_{25}$ /PPD it is difficult to measure $H_2O_2$ due to higher resistance of the solution ($R_s$) value (1.1 x $10^8$ Ω) as compared to $Pt_{50}$ /PPD (2.4 x $10^7$ Ω) and supported by Kartika et al [24] whereby the oxidation of $H_2O_2$ on $Pt_{25}$/PPD surface could not be detected. This can be proven by referring to the equation (2),

$$Z_{re} = R_s + \frac{R_{ct} d^2}{d^2 + \omega^2 R_{ct}^2 (\varepsilon_r \varepsilon_o A)^2} \quad (2)$$

whereby, $Z_{re}$ is the real impedance, $R_s$ is the resistance of solution and A is the active surface area that is in contact with the electrolyte. From Figure 4, the impedance decreases as the effective area is in the electrolyte increases. Thereby, the active surface area does not play an appreciable role and electrolyte resistance ($R_s$) is only responsible for impedance response. Hence, $Pt_{50}$ was used as a working electrode throughout this work [25].

**Effect of concentration**

A range of concentrations from 5 mM to 30 mM of standard $H_2O_2$ were prepared. The Nyquist plot in Figure 5 was observed, which gave lower detection of standard $H_2O_2$ [12]. At higher frequency, 10 0000 kHz this electrode behaved as capacitor due to the phase angle from the bode phase was more than 55°. However, at frequencies less than 10 kHz on bode phase the diffusion process was controlled on electrode surface since the angle of the bode phase was at 40°. In order to interpret the charge transfer resistance, $R_{ct}$ the impedance spectrum was fitted into a modified equivalent circuit (Figure 6). From the best fitted model we have calculated the charge transfer resistance ($R_{ct}$) values. Equation (3), gives the relationship between $R_{ct}$ and the concentration of bulk species as below [7]

$$R_{ct} = \frac{RT}{(n^2 F^2 A K_{ct} [S])} \quad (3)$$

where, $K_{ct}$ is the potential dependent charge transfer rate constant, [S] is the concentration of the redox species and the other symbols have their usual meanings. We found that as the concentration of $H_2O_2$ increased, the value of $R_{ct}$ was decreased (583 to 126 kΩ).

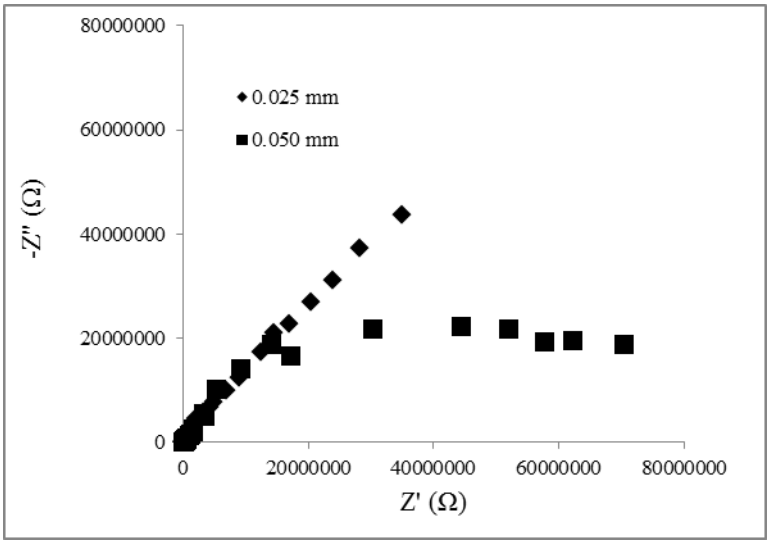



Figure 4: Nyquist spectrums of 5 µM $H_2O_2$ detected on the electrode diameter of (♦) 25 µm and (▪) 50 µm in PBS solution pH 7.4.

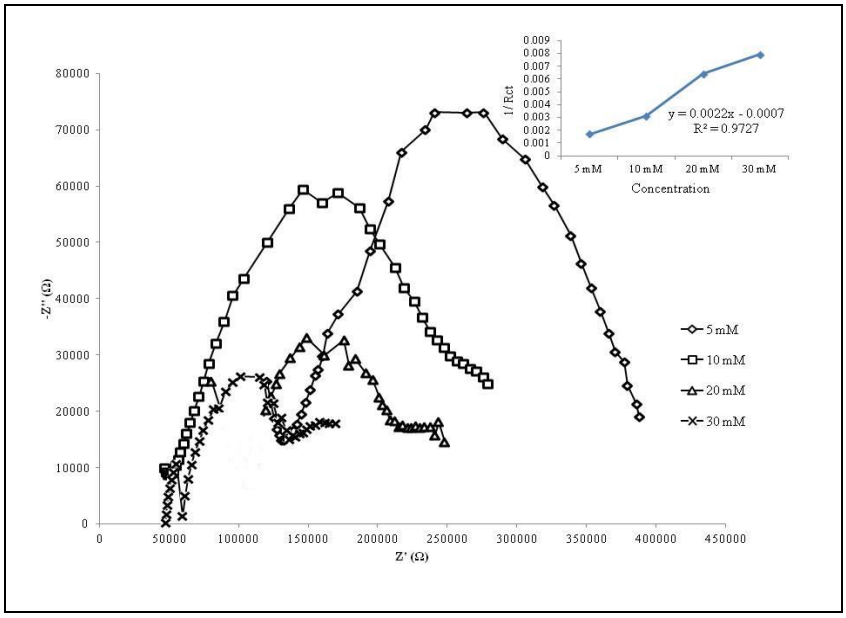



Figure 5: Nyquist plot with corresponding to various concentrations of the standard $H_2O_2$; inset: Calibration graph of $1/R_{ct}$ Vs Concentration (mM).

**Equivalent circuit**

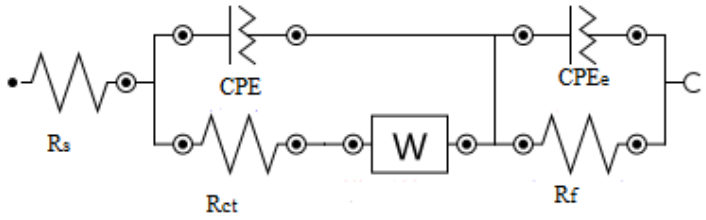



Figure 6: Modified equivalent circuit model for fitting EIS spectra dealing with Pt/PPD micro-electrode immersed in $H_2O_2$.

$R_S$ is the solution resistance. The constant phase element, CPE is then related to the space charge capacitance at the surface electrode–electrolyte interface. $R_{ct}$ is related to the charge transfer resistance at the surface electrode-electrolyte interface. The Warburg impedance (W) is the mass transfer to the electrode surface.

We proposed this modified Randless circuit in order to fit the impedance spectrum. The equivalent circuit in Figure 6 consisted of a constant phase element (CPE) that is parallel to a resistance and was found to give the best fit to the experimental data. The surface of Pt/PPD was non-homogenous as the crater look feature was described from the previous study [16], therefore standard $C_{dl}$ could not describe the charge properties of the interface sufficiently. In addition, element of Q or CPE was commonly applied to the polymer coating system in real application even this is still not clearly understood [6,25]. The other $CPE_e$ and $R_f$ elements are the CPE values of the electrode and resistance of the film respectively, and as an additional to fit with the Nyquist spectrum. [26-27]. Frequency Resonance Analyzer (FRA) software was used to obtain the chi-square goodness-of-fit ($\chi^2$) which authorized the fitted circuit ($\chi^2$= 0.06) obtained. The lowest figure obtained demonstrating the most fitted circuit for the system.

**Sensor Performance**

This sensor was practically used in determination of $H_2O_2$ in antiseptic mouthwash which contains 6% w/v $H_2O_2$ with original concentration, 1.96 M for study purposes. Various concentrations of sample (0.2 – 1.2 M) was calibrated before the samples were spiked in 300 mM PBS solution at pH 7.4. From the trends of the Nyquist plot (Figure not shown), it can tell that similar characteristics happened with standard $H_2O_2$ whereby at higher frequency the interaction between the electrode-analyte interfaces behaved as capacitor while at lower frequency the diffusion behavior was taken control on the electrode. Then, the linear calibration of 1/ $R_{ct}$ was plotted with $R^2$= 0.9566. To evaluate the accuracy of the sensor applicability, standard addition analysis was carried out by using CV technique. As the results found, the concentration of $H_2O_2$ found in real sample was 1.8 M which is close to the original concentration as tabulated in Table 1.

Table 1: The results of the $H_2O_2$ in real sample analysis obtained using Pt/PPD microelectrode assembly by the oxidation peak of CV in pH 7.4 PBS, with n (number of replicates) = 4

| | |
|---|---|
| Concentration founded (M) | 1.8 ≈ 1.9 M (original concentration of $H_2O_2$ in antiseptic mouthwash) |
| % Recovery | 97 % ± 0.14 |

**Stability and repeatability**

The electrode was kept at 4$^{o}$C when not in used. The response time of this sensor decreased 43 % towards 10 µM $H_2O_2$ after continuous usage for 4 weeks. This is due to the degradation of the PPD layer on the platinum surface. Nevertheless, even though the response time was decreased, but the stability of the sensor is in agreement with other reported work [1,2,28].

## Conclusion

The PPD modified Platinum microelectrode of 50 µm in diameter ($Pt_{50}$/PPD) has been successful characterized on its electrochemical performance towards $H_2O_2$ using CV, Chronoamperometry and EIS. This electrode was successfully applied in $H_2O_2$ detection at a lower operating potential (+0.4V) as well as succeeds in brain implantable needle type microelectrode [29]. Interestingly, with several more developments, this electrode is suggested to be applicable as an enzymatic biosensor in future planning.

## Acknowledgement

This study was funded by FRGS Grant (600-RMI/FRGS 5/3 (12/2013)). The authors also like to thank to MyBrain15 scholarship under Ministry Of Education, Malaysia granted to Norazreen Zakaria.

## References

1. Chiu, M. H., Kumar, A. S., Sornambikai, S., Chen, P.Y., Shih, Y. & Zen, J. M. (2011). Cosmetic Silver Electrode. *Int. J. Electrochem. Sci*, 6: 2352- 2365.
2. Li,G. Wang, Y. & Xu, H. (2007). A Hydrogen Peroxide Sensor Prepared by Electropolymerization of Pyrolle based on Screen printed Carbon Paste Electrodes. *Sensors*, 7: 239-250.
3. Ansari, A. A., Solanki, P. R. & Malhotra, B. D.( 2009). Hydrogen peroxide sensor based on horseradish peroxidase immobilized nanostructured cerium oxide film. *Biotechnology*, 142: 179- 184.
4. Chai, X.S., Hou, Q. X., Luo, Q. & Zhu, J.Y. (2004). Rapid determination of hydrogen peroxide in the wood pulp bleaching streams by a dual-wavelength spectroscopic method. *Analytica Chimica Acta*, 507: 281-284.
5. Shamsipur, M., Asgari, M., Maragheh, M. G. & Moosavi-Movahedi A. A. (2012). A novel impedimetric nanobiosensor for low level determination of hydrogen peroxide based on biocatalysis of catalase. *Bioelectrochemistry*, 83: 31-37.
6. C.F. Sanchez, C. J. McNeil, and K. Rawson, *Trends. Anal. Chem.*, **2005**, 24, 37.
7. Shervedani, R. K., Mehrjardi, A. H. & Zamiri, N. (2006). A novel method for glucose determination based on electrochemical impedance spectroscopy using glucose oxidase self-assembled biosensor. *Bioelectrochem*,69: 201- 208
8. Daniels, J. S. & Pourmand, N. (2007). Label-Free Impedance Biosensors: Opportunities and Challenges. *Electroanalysis*, 12: 1239- 1257.
9. Bard, A. J. & Faulkner, L. R. (2001). Electrochemical Methods: Fundamentals and Applications, Second edition. John Wiley and Sons, New York, Chichester, Brisbane, Toronto.
10. Zhang, L., Yin, H. B., Luo, J. J., Yang, P. H. & Cai, J. Y. (2013). Construction of Electrochemical Impedance Sensor Based on Poly Dopamine- Hyaluronic Acid Composite Membrane for Detection of Hydrogen Peroxide. *Chinese Journal of Analytical Chemistry*, 41(4): 534-539.
11. Aziah, A. A., O' Neill, R .D., Yahya, M. Z. A. & Zainiharyati, M. Z. (2012). Electropolymerization of ortho-Phenylenediamine and its Use for Detection on Hydrogen Peroxide and Ascorbic Acid by Electrochemical Impedance Spectroscopy. *International Journal of Electrochemical Science*, 7:10154-10163.
12. Rothwell, S. A., Killoran, S. J. & O'Neill**,** R. D. Enzyme Immobilization Strategies and Electropolymerization Conditions to Control Sensitivity and Selectivity Parameters of a Polymer-Enzyme Composite Glucose Biosensor. *Sensor*, 10: 6439- 6462.
13. Zhou, D. M., Dai, Y. Q. & Shiu, K. K. (2010). Poly(phenylenediamine) film for the construction of glucose biosensors based on platinized glassy carbon electrode. *J. Appl. Electrochem*, 40: 1997-2003.
14. Rothwell, S. A., . Killoran, S. J., Neville, E. M. A., Crotty, M. & O'Neill, R . D. (2008). Poly(o-phenylenediamine) electrosynthesized in the absence of added background electrolyte provides a new permselectivity benchmark for biosensor applications. *Electrochemistry Communications*, 10: 1078-1081.

15. Rothwell, S. A., McMahon, C. P. & O'Neill, R. D. (2010). Effects of polymerization potential on the permselectivity of poly(o-phenylenediamine) coatings deposited on Pt–Ir electrodes for biosensor applications. *Electrochimica Acta*, 55: 1051-1060.
16. Han, J. H., Boo, H., Park, S. & Chung, T. D. (2006). Electrochemical oxidation of hydrogen peroxide at nanoporous platinum electrodes and the application to glutamate microsensor. *Electrochimica Acta.,* 52: 1788-1791.
17. Miao, X. M., Yuan, R., Chai, Y. Q., Shi, Y. T . & Yuan, Y. Y. (2008). Direct electrocatalytic reduction of hydrogen peroxide based on Nafion and copper oxide nanoparticles modified Pt electrode. *Journal of Electroanalytical Chemistry,* 612: 157- 163.
18. Upadhyay, A. K., Chen, S. M., Ting, T . W. & Peng, Y. Y. (2011). A Biosensor for Hydrogen Peroxide Based on Single walled Carbon Nanotube and Metal Oxide Modified Indium Tin Oxide Electrode. *International Journal of Electrochemical Science*, 6: 3466- 3482.
19. Zainiharyati, M. Z., O'Neill, R. D., Lowry, J. P., Pierce, K. W., Tricklebank, M., Dewa, A. & Sulaiman, A. G. (2010). Development of an implantable d-serine biosensor for in vivo monitoring using mammalian d-amino acid oxidase on a poly (o-phenylenediamine) and Nafion-modified platinum–iridium disk electrode. *Biosensors and Bioelectronics 25*, 1454 – 1459.
20. Wahnono, N., Qin, S., Oomen, P., Cremers, T. I. F., Vries, M. G. D. & Westerink, B. H. C.(2012). Evaluation of permselective membranes for optimization of intracerebral amperometric glutamate biosensors. *Biosensors and Bioelectronics 33*, 260- 266.
21. Aldeen. E. (1999). The Electrochemical Oxidation Of Hydrogen Peroxide On Platinum Electrodes At Phosphate Buffer Solutions. Massey University, Palmerston North New Zealand.
22. Jacabson. T (2002) Complex impedance method for AC circuits. Supplement, Phy273. University of Marylan.
23. Ghica, M. E., Brett, M. A. & Goncalves, A. R. (2010). Preparation and characterisation of poly(3,4-ethylenedioxythiophene) and poly(3,4-ethylenedioxythiophene)/poly(neutral red) modified carbon film electrodes, application as sensor for hydrogen peroxide. *Electrochimica Acta,* 10: 1016.
24. Kartika, S. H., Zainiharyati, M. Z., Mohamed, H. I. A., Jafri, M. A. & O'Neill, R. D. (2013). Development of a Brain Glutamate Microbiosensor. *World Academy of Sciences, Engineering and Technology*, 78.
25. Ahmed, R. & Reifsnider, K. (2011). Study of Influence of Electrode Geometry on Impedance Spectroscopy. *International Journal of Electrochemical Science*. 6: 1159 – 1174.
26. Orazem, M. & Tribollet, B. (2008). Electrochemical Impedance Spectroscopy. John Wiley and Sons, Inc., Hoboken, New Jersey.
27. Katz, E. & Willner, I. (2003). Probing Biomolecular Interactions at Conductive and Semiconductive Surfaces by Impedance Spectroscopy: Routes to Impedimetric Immunosensors, DNA-Sensors, and Enzyme *Biosensors. Electroanlysis*, 15: 11.
28. Babaei, A., Garret, D. J. & Downard, A. J. (2012). Electrochemical Investigations on a Third Generation Biosensor for Determination of Hydrogen Peroxide Based on Immobilization of Myoglobin on a Novel Platinum Nanoparticle/Carbon Nanotube/Ionic Liquid/Nafion Composite. *International Journal of Electrochemical Science*, 7: 3141- 3154.
29. Kirwan, S. M., Rocchitta, G., McMahon C. P., , Craig, J. D., Killoran, S. J., O'Brien, K. B., Serra, P. A., Lowry, J. P. & O'Neill, R. D. (2007). Modifications of Poly(o-phenylenediamine) Permselective Layer on Pt-Ir for Biosensor Application in Neurochemical Monitoring. *Sensors*, 7: 420-437.

The Malaysian Journal of ANALYTICAL SCIENCES ISSN 1394-2506

# ANTIOXIDANT ACTIVITY AND BIOACTIVE COMPONENTS OF OXALIDACEAE FRUIT EXTRACTS

## (Aktiviti Antioksida Dan Komponen Bioaktif Esktrak Buah Oxalidaceae)

A. Noor Asna and A.Noriham*

*Faculty of Applied Science,*
*Universiti Teknologi MARA, 40450 Shah Alam, Selangor, Malaysia*

**Corresponding author: noriham985@salam.uitm.edu.my*

**Abstract**

The study was conducted to evaluate the Antioxidant Activity (AA), Total Flavonoid Content (TFC), and Total Phenolic Content (TPC) of Oxalidaceae fruit extracts. Two types of *Averrhoa carambola* L. and two types of bilimbi fruits were used in this study. Bilimbi fruits selected were Averrhoa *bilimbi* L. and *Averrhoa bilimbi* cv. while *Averrhoa carambola* L. selected were *Averrhoa carambola* L. (honey type) and another type of *Averrhoa carambola* L. which is known as tart type. The maturity stage for both *Averrhoa carambola* L. fruits (honey and tart type) were selected at commercial maturity stages which were stage 3 and stage 4. Antioxidant estimation of oxalidaceae fruit extracts were evaluated by using Total Flavonoid Content (TFC) and Total Phenolic Content (TPC), while antioxidant activity were evaluated using scavenging of 2,2-diphenyl-1-picrylhydrazyl radical (DPPH), β-carotene Bleaching (BCB) and Ferric Reducing Antioxidant Power (FRAP) assays. Phytochemical screening of alkaloids, flavonoids, terpenoids, steroids, tannins and saponins were also performed on all samples. *Averrhoa carambola* L. indicated positive results for all phytochemical screening conducted and similar results were observed from bilimbi fruits, except for alkaloids. *Averrhoa carambola* L. (tart type) of stage 4 possessed higher TPC and TFC followed by *Averrhoa carambola* L. (honey type) of stage 4. *Averrhoa carambola* L. (tart type) of stage 4 also exhibited high scavenging effect (74 %) as determined by DPPH assay with the value of $EC_{50}$ 72.36 mg/ml while *Averrhoa carambola* L. (honey type) of stage 3 showed significantly lower percentage of scavenging effect. The results also demonstrated that FRAP values of *Averrhoa carambola* L. (honey type) of stage 4 and *Averrhoa carambola* L. (tart type) of stage 4 were higher than other samples (5.1023 mmol TE/g and 5.0759 mmol TE/g) and similar trends were observed for β-carotene Bleaching (BCB) assay, where *Averrhoa carambola* L. (honey type) of stage 4 had the highest value. There were strong positive correlations between antioxidant activity assays and TPC or TFC, hence indicating that the four types of Oxalidaceae fruits used in this study have the potential as natural antioxidant.

**Keywords**: antioxidant activity (AA), *Averrhoa carambola* L., *Averrhoa bilimbi* L., Total Flavonoid Content (TFC), Total Phenolic Content (TPC)

**Abstrak**

Kajian ini dijalankan untuk mengkaji aktiviti antioksida (AA), Jumlah Kandugan Flavonoid (TFC) dan Jumlah Kandungan Fenolik(TPC) pada ekstrak buah Oxalidaceae. Dua jenis *Averrhoa carambola* L. dan dua jenis belimbing buluh telah digunakan dalam kajian ini. Jenis belimbing buluh yang terpilih adalah *Averrhoa bilimbi* L. dan *Averrhoa bilimbi* cv. Manakala, *Averrhoa carambola* L. yang terpilih adalah *Averrhoa carambola* L. (jenis madu) dan *Averrhoa carambola* L. yang dikenali sebagai jenis masam. Tahap kematangan untuk kedua-dua jenis buah *Averrhoa carambola* L. (jenis madu dan masam) adalah mengikut tahap kematangan komersial iaitu tahap 3 dan tahap 4. Anggaran antioksida pada ekstrak buah Oxalidaceae diuji menggunakan TFC dan TPC, manakala aktiviti antioksida pula di tentukan dengan menggunakan esei radikal 2,2-diphenyl-1-picrylhydrazyl (DPPH), pelunturan β-karotena dan ujian kuasa penurunan ferik. Penyaringan fitokimia alkaloid, flavonoid, terpenoid, steroid, tanin dan saponin juga dijalankan ke atas semua sampel. *Averrhoa carambola* L. menunjukkan keputusan positif bagi semua pemeriksaan fitokimia yang dijalankan dan keputusan yang sama diperhatikan daripada buah belimbing buluh kecuali alkaloid. *Averrhoa carambola* L. (jenis masam) dari tahap 4 memiliki jumlah kandungan fenolik dan flovonoid tertinggi diikuti oleh *Averrhoa carambola* L. (jenis madu) dari tahap 4. *Averrhoa carambola* L. (jenis madu) dari tahap 4 turut menunjukkan pencarian radikal tertinggi (74%) melalui ujian DPPH dengan jumlah $EC_{50}$ 72.36 mg/ml sementara *Averrhoa carambola* L. (jenis madu) dari tahap 3 menujukkan jumlah peratus yang jauh lebih rendah. Keputusan turut menunjukkan bahawa jumlah FRAP bagi *Averrhoa carambola* L. (jenis madu) dari tahap 4 dan *Averrhoa carambola* L. (jenis tat) dari tahap 4 adalah lebih tinggi

daripada sampel yang lain (5.1023 mmol TE/g and 5.0759 mmol TE/g) dan tren yang sama turut ditunjukkan oleh ujikaji pelunturan β-karotena , di mana *Averrhoa carambola* L. (jenis madu) dari tahap 4 memiliki jumlah tertinggi. Terdapat korelasi positif yang kuat antara ujian aktiviti antioksida dan TPC atau TFC, dengan itu menunjukkan bahawa keempat-empat jenis buah Oxalidaceae yang digunakan dalam kajian ini mempunyai potensi sebagai antioksida semula jadi.

**Kata kunci:** antioksida aktiviti (AA), *Averrhoa carambola* L., *Averrhoa bilimbi* L., Jumlah Kandungan Flavonoid, Jumlah Kandungan Fenolik

## Introduction

*Averrhoa bilimbi* L. has been widely used in traditional medicine as a cure for cold, itches, boils, cough, diabetes, whooping cough, hypertension, syphilis and rheumatism [1]. There are two types of bilimbi; *Averrhoa bilimbi* L. that is green in colour while another type is known as *Averrhoa bilimbi* cv. that is yellow in colour as reported by Saidin [2]. According to Carolino et al. [3], *Averrhoa carambola* L. or known as star fruit is thermogenic, febrifuge, antipyretic, tonic, antiscorbutic, sweet and sour. There are two types of *Averrhoa carambola* L., where type one (tart type) is smaller in size, sour taste, richly flavoured and contain more oxalic acid content. The second type is larger in size, mild-flavoured with less oxalic acid and known as honey type. *Averrhoa carambola* L. are used to treat vomiting, headache and restlessness, and also as traditional medicine in Malaysia and China. Oxalidaceae family show high antioxidants activity and antioxidants play an important role especially in preventing the formation of free radicals. There are two types of antioxidants which are natural antioxidant and synthetic antioxidant. Synthetic antioxidant is man made antioxidant through chemical process while natural antioxidant is produce by human body or plant and normally regarded as safe. In fruits and vegetables, the examples of antioxidants are ascorbic acid, hydroxycarboxylic acids, flavonoids and caratenoids [1]. Besides showing antibacterial, anticarcinogenic, antiinflammatory, antioxidants that are isolated from plants also exhibit antiviral, antiallergic, estrogenic and immune-stimulating effects [1]. Shahidi et al. [4] claims that antioxidants have a few characteristics which are capable of reducing, delaying or preventing auto-oxidation where the antioxidants bind together with free radicals to decrease their destructive power, hence, reduce the harmful effect of oxidants.

## Materials and Methods

### Chemicals

Concentrated hydrochloric acid, 95% methanol, ferric chloride, ammonium chloroform, concentrated sulphuric acid, folin-ciocalteu reagent, sodium carbonate, Mayer‘s reagent, 2,4,6-tri(2-pyridyl)-1,3,5-triazine (TPTZ), 2, 2-diphenyl-2-picrylhydrazyl radical scavenging (DPPH), ethanol, trolox, β-carotene, linoleic acid, Tween 20, chloroform, acetic acid, ascorbic acid (AA), Butylated hydroxyltoluene (BHT), and Butylated hydroxylanisole (BHA).

### Fruits (*Averrhoa bilimbi* and *Averrhoa carambola* L. )

Both types of *Averrhoa carambola* L. were taken from Malaysian Agricultural Research and Development Institute (MARDI), Serdang, while both types of bilimbi were collected from Kampung Alai, Melaka.

### Preparation for extraction process

The fruits were washed under running tape water, for about one minute before the fruits were sliced and dried using cabinet oven. About 100g of the fruits were ground and 20g of the ground sample was extracted with boiling water (600 ml) for 10 minutes before being blended and filrated with filter paper, Whatman No.4. The water was removed by using Rotary Evaporator at 70°C and the extracts were stored in amber bottles at 4$^{o}$C prior to further analysis [5].

### Phytochemical screening : Test for flavonoids

The presence of flavonoids was detected by the colour changes from orange to magenta red colouration [6]. Two milligram of crude extract was mixed with 2 ml of distilled water and left for 10 minutes. After that, metallic magnesium and concentrated hydrochloric acid (about five drops) were added.

### Test for steroids

According to Ciriaco et al. [7], the colour changed from violet to blue or green in samples indicated the presence of steroids. Two millilitre of sulphuric acid was added to 0.5g of crude extract. Then, 2 ml of acetic anhydride was added to the mixture and the changes were observed.

**Test for saponins**
Approximately 5 ml of distilled water was added to the 0.5g crude extract in a beaker before filtered into the test tube and the filtrate was shake vigorously for a stable persistent froth. The stable persistent froth was regarded as positive for the presence of saponins [7].

**Test for tannins**
According to Karumi et al. [8], a green precipitate or blue-black precipitate proved the presence of gallic tannin or catechol tannis. Around 10 mg of extract was added with distilled water until all the extract was immersed in the distilled water. One millilitre of extract was mixed with ten millilitre of distilled water before being filtered. Three drops of ferric chloride were added to the filtrate and the changes were observed for the presence of tannins.

**Test for alkaloids**
Ten millilitre of ammonium chloroform and five milligram of crude extract were mixed in the test tube, stirred and filtered into capped test tube. Ten drops of concentrated sulphuric acid was added and shake well. Acidic phase at the top layer and organic phase at the bottom layer were formed. Mayer's reagent was used to test the titrated acidic phase and a white precipitate indicates the presence of alkaloids [7].

**Total phenolic content (TPC)**
Total phenolic content was determined according the method of Singleton and Rossi [9]. Approximately 100 µl were mixed with 0.5 ml of Folin-Ciocalteu reagent and allowed to stand at room temperature for 5 minutes, and 1.5 ml of sodium carbonate solution (7.5%) was added to the mixture. After two hours, absorbance was read at 765 nm. Results were expressed as gallic acid equivalents.

**Total flavonoid content (TFC)**
The flavonoid content in extracts was determined according to Zhishen et al. [10], using a method based on the formation of a complex flavonoid–aluminium, having the maximum absorbanceat 510 nm. Quercetin was used as a standard. One millilitre of diluted samples/standards was separately mixed with 4ml of distilled water, 0.3ml of $NaNO_2$ (10%) and was incubated at dark place for 5 minutes. Then, 0.3ml of aluminium chloride ($AlCl_3$) and 2ml of sodium hydroxide was added and the solution was made up to 10 ml with distilled water. Reaction mixture was measured at 510 nm with UV–Vis spectrophotometer.

**Ferric reducing antioxidant power (FRAP) assay**
The ferric reducing antioxidant power assay was determined according to method of Oyaizu et al. [11]. Two hundred millilitre of buffer (3.2 ml of acetic acid mixed with 196.8 ml of distilled water and 0.62g of sodium acetate) (pH 3.6) was added with 20 ml of TPTZ (2,4,6-tri(2-pyridyl)-1,3,5-triazine) (0.063g of TPTZ in mixture of 78.8µl of hydrochloric acid) and with 20 ml of $FeCl_3$ in the ratio of 10:1:1. The mixture of buffer, TPTZ and also ferum chloride is called FRAP reagent. 0.3 ml of samples/standards were added with 8.7ml of FRAP reagent and were make up until 9 ml. After that, the mixtures were incubated for 1 hour and the absorbance was measured by using UV-Vis spectrophotometer at 593 nm against the blank. Increasing in reducing power will show increasing in absorbance. Trolox was used as a standard for comparison.

**2, 2-diphenyl-2-picrylhydrazyl radical scavenging (DPPH) assay**
The scavenging activity was estimated according to the method of Tang et al. [12]. Six hundred microlitre of samples were added to 4.5ml of 0.1 mM DPPH in 95% of ethanol. The mixtures were shaken vigorously using vortex and left to stand for 20 minutes at room temperature in a dark room. Absorbance was read using spectrophotometer at 517 nm. The scavenging effects on the DPPH radical were calculated using the following equation (1):

$$\text{Scavenging effect (\%) (SE)} = \left[1 - \frac{\text{Absorbance of sample at 517nm}}{\text{Absorbance of control at 517nm}}\right] \text{x } 100 \quad (1)$$

Triplicate measurements were carried out and their scavenging effects were calculated based on the percentage of DPPH scavenged.

**β-carotene-linoleate bleaching (BCB) assay**

β-Carotene-linoleate bleaching assay was conducted according to method of Velioglu et al. [13]. β-carotene solution (2 mg in 10 ml chloroform), 60 µL of linoleic acid and 600µL Tween 20 were transferred into a round bottom flask and the mixture were evaporated at 40ºC for 10 minutes to remove the chloroform. 300 ml of distilled water was added to the mixture, and then shaken vigorously to form emulsion. 5 ml emulsion was then transferred to test tube containing 200µL samples/standards separately and immediately placed in a water bath at 50ºC. The absorbance was read at 20 minutes intervals for 2 hours at 470 nm. Degradation rates (DR) were calculated using the following equation (2)[14]:

$$\left(\ln \frac{a}{b}\right) \times \left(\frac{1}{t}\right) = DR_{\text{sample}} \text{ or } DR_{\text{standard}} \quad (2)$$

where In is natural log, a is the initial absorbance (470 nm) at time 0, b is the absorbance (470 nm) at 20, 40, 60, 80, 100 or 120 minutes and t is the time.

Antioxidant activity (AA) was expressed as percent of inhibition relative to the control, using the following formula equation (3):

$$AA = \left[\frac{DR_{\text{control}} - DR_{\text{sample or standard}}}{DR\text{control}}\right] \times 100 \quad (3)$$

**Statistical analysis**

All data were expressed as mean ± standard deviation. Data were analysed using one-way ANOVA using SAS 15.0. Duncan's multiple-range test was used to measure the difference between means. Pearson's correlation test was used to assess correlations between means. A significant difference was considered at the level of $p < 0.05$.

## Results and Discussion

**Phytochemical Screening**

From the result, it was observed that *Averrhoa bilimbi* L. and *Averrhoa bilimbi* cv. showed negative result for alkaloids and positive result for other phytochemical while all extracts from *Averrhoa carambola* L. indicated positive results for the presence of phytochemicals. (Table 1). For saponin test, all samples showed positive result. Blue-black precipitate proved the presence of gallic, tannin or catechol, which can be seen at all of the extracts. The presence of flavonoids will be detected by the colour changes to magenta red or orange colouration according to Mojab et al. [6]. Light colour of red magenta from the screening of *Averrhoa bilimbi* L. , *Averrhoa bilimbi* cv., stage 3 *Averrhoa carambola* L. ( honey type) and stage 4 *Averrhoa carambola* L. (tart type) indicate the presence of flavonoids. The stage 4 *Averrhoa carambola* L. (honey type) and stage 4 *Averrhoa carambola* L. (tart type) illustrated the high presence of flavonoids. Reddish brown precipitate explained the presence of terpenoids for all extracts.

According to Ciriaco et al. [7], if the filtrate turns red or pink in colour, the presence of steroids will be observed as shown by the positive results of all extracts. All results shown complies to the preliminary phytochemical screening on the bilimbi fruits extracts (bilimbi) reported by Wong et al. [15] who revealed the presence of flavonoids, saponins and terpenoids but no alkaloids. A study conducted by Vasconcelos et al. [16] and Shinu Thomas et al. [17], demonstrated the presence of tannins, alkaloids, flavonoids, saponins, and also steroids in the *Averrhoa carambola* L. Krishnaiah et al. [18] postulated that phytochemical is a natural bioactive compound found in plant that can be divided into two groups which are primary compounds (for examples; amino acid, sugars, protein and chlorophyll) and secondary compounds (for examples; alkaloids, terpenoids, phenolic). These two groups are divided based on the compounds functions in plant metabolism.

Table 1: Phytochemical screening of Oxalidaceae fruit extracts

| **Samples** | **Alkaloids** | **Saponin** | **Tannin** | **Flavonoids** | **Terpenoids** | **Steroids** |
|---|---|---|---|---|---|---|
| *Averrhoa bilimbi* L. | - | + | + | + | + | + |
| *Averrhoa bilimbi* cv. | - | + | + | + | + | + |
| Stage 3 Averrhoa carambola L. (Honey type ) | + | + | + | + | + | + |
| Stage 4 Averrhoa carambola L. (Honey type) | + | + | + | + | + | + |
| Stage 3 Averrhoa carambola L. (Tart type ) | + | + | + | + | + | + |
| Stage 4 Averrhoa carambola L. (Tart type) | + | + | + | + | + | + |

+ = presence; - = absence

**Total Phenolic Content (TPC)**

Ikram *et al.,* [19] stated that different phenolic compounds have different responses in the Folin-Ciocalteau method. Reducing agents for example ascorbic acid may interfere with the results, thus, the Folin-Ciocalteau reagent method may overestimate TPC. Depending on their chemical structure, the molecular antioxidant response of phenolic compounds in methyl linoleate varies remarkably. A proper characterisation of individual phenolic compounds has to be done in order to predict the antioxidant content of an extract, not only depends on the basis of its phenolic content. Total phenolic assay is simple, precise and sensitive [20] as it measures the reducing capacity of sample. However, it may not suitable for measuring the antioxidant activity of every sample [21]. Table 2 showed the TPC for *Averrhoa bilimbi* and *Averrhoa carambola* L. Extract of *Averrhoa bilimbi* L. showed lowest phenolic content than other extracts. TPC for previous study on *Averrhoa bilimbi* done by Ikram *et al.,* [19] reported that the TPC of *Averrhoa bilimbi L* for methanol extract was 12.61mg GAE/g of sample. However, finding exhibited higher value of TPC. Narain *et al.,* [22] reported 67.13mg GAE/g of TPC presence in *Averrhoa carambola* L. extract which is slightly lower than the result obtained. Extrinsic factors (such as agronomic, environmental, handling and storage), different plants, procedures and standards used to express TPC will absolutely give different level of TPCs [23].

Table 2: Total Phenolic Content (TPC) of Oxalidaceae Fruit Extracts

| **Samples** | **TPC (mg GAE/g )** |
|---|---|
| *Averrhoa bilimbi* L. | 41.00±2.75E |
| *Averrhoa bilimbi* cv. | 53.01±4.36D |
| *Averrhoa carambola* L. Stage 3 (honey type) | 72.42±2.98C |
| *Averrhoa carambola* L. Stage 4. (honey type) | 87.65±2.57B. |
| *Averrhoa carambola* L. Stage 3 (tart type) | 79.38±1.53A |
| *Averrhoa carambola L.* Stage 4 (tart type) | 89.50±0.76A. |

Flavonoids are the most common and widely distributed group of plant phenolic compounds, which are characterised by a benzo-pyrone structure which is ubiquitous in fruits and vegetables. According to Chang et al. [24], this method determines flavones and flavonols. The $AlCl_3$ forms acid stable complexes with either keto group (C-4) or hydroxyl group (C-3 or C-5) of flavones and flavonols. In this study, water extract of stage 4 *Averrhoa carambola* L. (honey type) and stage 4 *Averrhoa carambola* L. (tart type) samples showed the highest amount of flavonoid content as compared to other samples with the values of 41.63 mg quercetin equivalent/gram and 48.61 mg quercetin equivalen/gram. These values are slightly higher as compared to TFC of *Averrhoa carambola* L. reported by Narain et al. [22]. Higher antioxidant activity observed may be due to synergistic activity between phenolic compounds found in the samples.

Iker et al. [25] reported that flavonoid accumulates after slight heat treatment in plant in many different species. Actually, flavonoid content appeared to be closely connected with colour. Herb honey with strong red or green colours such as raspberry and black chokeberry have high flavonoid content while those with pale yellow or pale green colours such as camomoli and mint contained a small amount of flavonoid content [26]. As *Averrhoa bilimbi* has pale green colour so it has lower amount of TFC while stage four of *Averrhoa carambola* L. has yellow colour, so it is expected to posses higher amount of TFC. According to Harris [27], maturity and weather condition will affect the physicochemical characteristics of bilimbi.

Table 3: Total Flavonoid Content (TFC) of Oxalidaceae Fruit Extracts

| **Samples** | **TFC (mg QE/g )** |
|---|---|
| *Averrhoa bilimbi* L | 23.32±3.50DE |
| *Averrhoa bilimbi* cv. | 19.62±1.44E |
| *Averrhoa carambola* L. Stage 3 (honey type) | 26.60±0.82D |
| *Averrhoa carambola* L. Stage 4 (honey type) | 41.63±0.25B |
| *Averrhoa carambola* L. Stage 3 (tart type) | 34.26±1.73C |
| *Averrhoa carambola L.* Stage 4 (tart type) | 48.61±0.25A |

**Antioxidant activity**: **Ferric reducing antioxidant power (FRAP)**

For the measurements of the reductive ability, ferric oxide ($Fe^{3+}$) to ferrous oxide ($Fe^{2+}$) transformation in the presence of Oxalidaceae fruit extracts samples were investigated using FRAP assay developed by Oyaizu [11]. The reducing power ability of $Fe^{3+}$ was carried out by varying the concentration of extracts. The result of this analysis as shown in Figure 1 showed that reducing activity increases as the amount of extracts increased.

By reducing ferric ion to give more active ions, the common metal ions such as $Fe^{3+}$ can be reduced by the antioxidant that provokes the antioxidant to behave as prooxidant [14]. The reaction results in a change of colour from brownish to dark green corresponding to the reduction of $Fe^{3+}$complex to $Fe^{2+}$complex. The FRAP assay is inexpensive, reagents are simple to prepare, results are highly reproducible, and the procedure is straightforward and speedy. The FRAP assay offers a putative index of antioxidant, or reducing, potential of biological fluids within the technological reach of every laboratory and researcher interested in oxidative stress and its effects [28].

The FRAP values obtained from this finding are slightly lower than values reported by Yan et al. [29] and Wong et al. [15], where bilimbi and *Averrhoa carambola* L. extracts had FRAP values of 1.76 ± 0.87 mmol TE/g and 4.86 ±

0.57 mmol TE/g respectively. The difference may be due to the types and the quantity of phytochemical and the food matrix presence in the sample [30]. Environmental factors such as climatic growth condition, ripening stage, temperature, duration of storage and thermal treatment may have influenced the antioxidant activity [31,32].

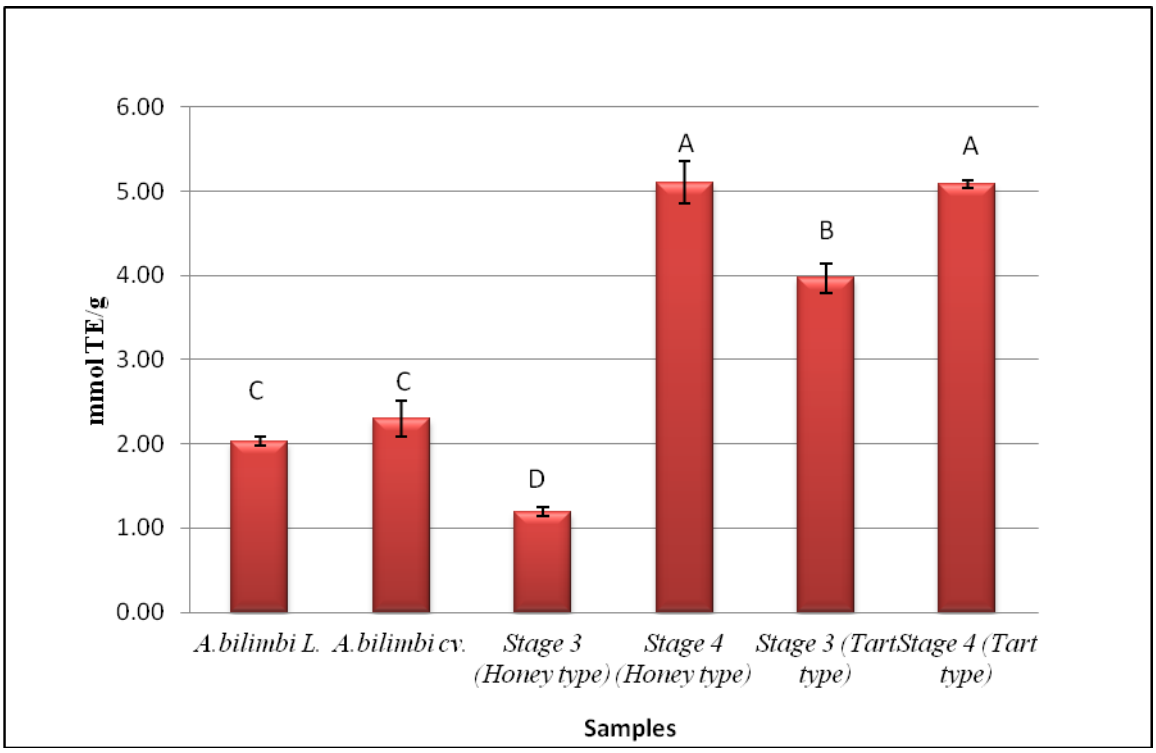



Figure 1: The values of Ferric reducing antioxidant power (FRAP) of Oxalidaceae fruit extracts

**2, 2-diphenyl-2-picrylhydrazyl radical scavenging assay (DPPH)**

DPPH assay is one of the most widely used methods for screening antioxidant activity of sample extract. The assay is based on the measurements of the antioxidant ability to scavenge the stable radical DPPH. DPPH is a stable nitrogen centred free radical which produces violet colour in methanol solution [33]. DPPH radicals react with suitable reducing agents, during which electrons become paired off and the solution losses colour stoichiometrically depending on the number of electrons taken up [34]. In this assay, the solution progressively reduced to yellow coloured product diphenylpicryl hydrazine with the addition of the extracts in a concentration dependent manner. The absorbance was measured at 517 nm.

The DPPH free radical scavenging activity of *Averrhoa bilimbi* and *Averrhoa carambola* extracts are shown in Table 4. *Averrhoa bilimbi* cv. and stage 3 Averrhoa carambola L. (honey type) showed the lowest DPPH free radical scavenging activity. Water extract of *Averrhoa bilimbi* showed significantly higher in radical scavenging activity than methanol extract according to Ikram et al. [19]. They also stated that DPPH free radical scavenging activity for water extraction of sample was 38.09 ± 1.87% for raw *Averrhoa bilimbi* respectively. Narain et al. [22] reported that 66.37 ± 2.44% value of DPPH assay for *Averrhoa carambola* L. extracts. Higher phenolic content especially in stage 4 *Averrhoa carambola* L. (honey type) could be the main reason for its higher antioxidant activity towards DPPH radicals.

The higher the antioxidant activity of the extracts, the more the DPPH bleaching will occur. Thus, the greater the bleaching action of DPPH, the higher the percentage of scavenging effect [19]. Percentage scavenging of Oxalidaceae fruits extracts in this study were in descending order of ascorbic acid (AA) > BHA/BHT > Stage 4 *Averrhoa carambola* L. (honey type) > Stage 4 *Averrhoa carambola* L. (tart type )> Stage 3 *Averrhoa carambola* L. (tart type) > *Averrhoa bilimbi* L. > *Averrhoa bilimbi* cv. > Stage 3 *Averrhoa carambola* L. (honey type).

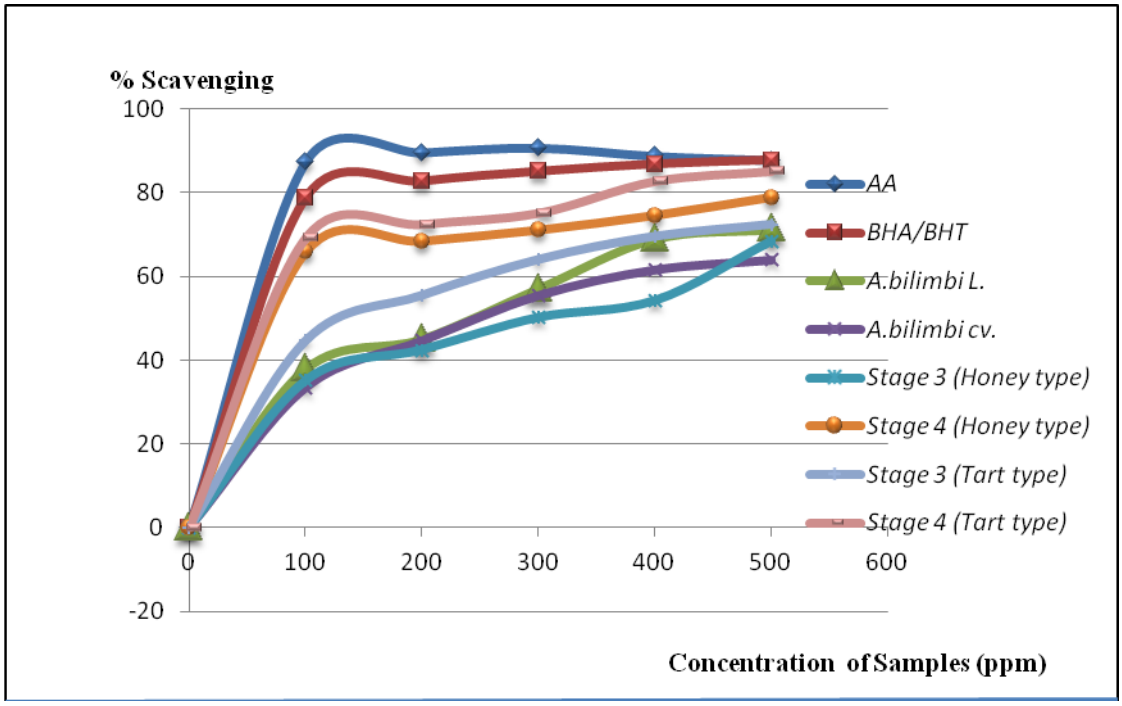



Figure 2: Percentage (%) scavenging of Oxalidaceae fruit extracts

**β-carotene-linoleate bleaching assay (BCB)**

Antioxidant activity of extract is strongly dependent on the solvent, due to different antioxidant potential of compound with different polarity [35]. In the β-carotene bleaching assay, oxidation of linoleic acid release linoleic acid peroxide as free radicals during incubation at 50ºC that will oxidize beta-carotene resulting in discolouration, hence decreasing the absorbance value [36]. A linear relationship was found between the ability of the sample extract to inhibit oxidation and antioxidant activity. Thus, the degradation rate of β-carotene depends on the antioxidant activity of the extracts. There was a correlation between degradation rate and the bleaching of β-carotene, where the extract with the lowest β-carotene degradation rate exhibited the highest antioxidant activity. However, in this study, extracts showed lower antioxidant activity than the standard BHA/BHT combination. The antioxidant activity of standard BHA/BHT was 92.43 ± 0.01%. The antioxidant activity of samples were in decreasing order of BHA/BHT > *Averrhoa carambola L.* (Stage 4- honey type) > *Averrhoa carambola* (Stage 4- tart type) >*Averrhoa bilimbi* cv. > *Averrhoa bilimbi* L.> *Averrhoa carambola* (Stage 3-honey type) > *Averrhoa carambola* (Stage 3- tart type). Ikram et al. [19] reported that antioxidant activity of methanolic extract of *Averrhoa bilimbi* is about 91.89%. However, our findings showed lower activity and this may be due to different extraction method used or due to the difference in species of *Averrhoa bilimbi* used.

Previous study on *Averrhoa carambola* L. as reported by Mishra et al. [37] showed a moderate antioxidant activity. In this fruit, as both types of *Averrhoa carambola* L. from stage 3 illustrated the lower antioxidant activity, which means have lowest β-carotene degradation rate among all the extracts while both types of *Averrhoa carambola* L. from stage 4 exhibited the highest β-carotene degradation rate. Ikram et al. [19], proved that antioxidant activity of methanolic extract of *Averrhoa carambola* L. is higher, which about 95.89%. Othman et al. [38] stated that water extracts had higher antioxidant activity than methanolic extracts in cocoa beans study. Antioxidant activity of *Averrhoa bilimbi* and *Averrhoa carambola* extracts also depends on the type and polarity of the extracting solvent, the isolation procedures and purity of active compounds as well as the assay techniques and substrate used [39].

Table 4: The antioxidant activity of Oxalidaceae fruit using BCB assay

| **Samples** | **BCB (%)** |
|---|---|
| BHA/BHT | 97.43 ± 0.01%A |
| *Averrhoa bilimbi* L | 67.65 ± 2.12%D |
| *Averrhoa bilimbi* cv. | 87.65 ± 3.12%C |
| *Averrhoa carambola* L. (Stage 3- Honey type) | 57.65 ± 4.42%E |
| *Averrhoa carambola* L. (Stage 4- Honey type) | 90.34 ± 1.65%B |
| *Averrhoa carambola* L. (Stage 3- Tart type) | 47.35 ± 1.97%E |
| *Averrhoa carambola* L. (Stage 4- Tart type) | 94.28 ± 1.42%A |

Values are expressed as mean ± standard deviation. Means within column (A-E) marked with different letters were not significantly different at the level of $p>0.05$

**Correlation between antioxidant activity (AA) with TPC and TFC**

The Pearson correlation coefficient between antioxidant assays with TPC and TFC of Oxalidaceae fruit extracts showed positive correlations except for BCB assays and is shown in Table 5. The correlation ($r= 0.432$) for β-carotene indicate that it has moderate positive relationship with TPC. DPPH and FRAP assay showed strong positive relationship with TPC. From this correlation, it can be suggested that, although the plant may contain other antioxidants such as ascorbate, proteins and carotenoids, these antioxidants do not contribute significantly to the antioxidant activity. Hence, it can be postulated that the phenolic compounds may be a major contributor to the antioxidant activity of the Oxalidaceae fruit.

Previous study done by Soong and Barlow [40], suggested that there was a strong correlation between antioxidant assay and TPC. However there are findings indicates that antioxidant assay and TPC do not correlate to each other [41]. There are several reasons that caused variation in the correlations between assays such as due to high content of reducing agents such as ascorbic acid, minerals and carotenoids in fruit [42], and also high protein content or genetic and agronomic and environmental influences such as varieties (cultivar/sub-species) and agronomic and environmental factors (climate, soils and light exposure) [43].

Table 5: Correlation matrix showing relationship between antioxidant assays (DPPH, FRAP and BCB assays)

| | **TPC** | **TFC** |
|---|---|---|
| **DPPH** | 0.8368 | 0.9576 |
| **FRAP** | 0.9344 | 0.8884 |
| **BCB** | 0.432 | 0.173 |

## Conclusion

Antioxidant content of fruits is most probably due to the presence of high phenolic compounds in the Oxalidaceae fruits. Most fruits gave positive results in all phytochemical screening conducted. TPC and TFC were found to be highest in stage 4 of *Averrhoa carambola* L. (tart type). Antioxidant activity from the 3 assays also indicated stage 4 of *Averrhoa carambola* L. (tart type) possessed highest antioxidant activity in all the antioxidant assays conducted. Pearson correlation between the assays indicated that the antioxidant might be contributed by the phenolic compounds presence in Oxalidaceae fruits.

## Acknowledgement

The authors would like to thank the Faculty of Applied Science, Universiti Teknologi MARA for the facilities and Research Cluster fund 600-RMI/DANA 5/3/CG (18/2012) for the fund.

## References

1. Abas, F., Lajis, N.H., Israf, D.A., Khozirah, S. & Kalsom, Y.U. (2006). Antioxidant and nitric oxide inhibition activities of selected Malay traditional vegetables. *Food Chemistry*: 566–573.
2. Saidin, I., (2000). *Sayuran tradisional ulam dan penyedap rasa*, Vol.1, *University kebangsaan Malaysia Publication*, 42.
3. Carolino, R.O.G., Beleboni, R.O., Pizzo, A.F., Flavio, D.V., Norbert, G.C., Miguel, M.N., Wagner , D.S. & Joaquim, C.N. (2005). Convulsant activity and neurochemical alterations induced by a fraction obtained from fruit *Averrhoa carambola* L. (Oxalidaceae: Geraniales). *Neurochemistry International*, *46*: 523–531.
4. Shahidi, F. & Wanasundra, P.K.J.P.D. (1992). Phenolic antioxidants, *Critical Reviews In Food Science and Nutrition*, *32*: 2017-2021.
5. Duh, P.D. & Yen, G.C. (1997). Antioxidative activity of three herbal water extracts. *Journal of Food Chemistry*, *60*: 639-645.
6. Mojab, F., Kamalinejad, M., Ghaderi, N. & Vahidipour, H.R. (2003). Phytochemical screening of some species of Iranian plants. *Iranian Journal of Pharmaceutical Research*, 2: 77-82.
7. Ciriaco, P.O.P. (1978). Phytochemical,Microbiological and Pharmacological Screening of Medicinal Plants: A supplement of the ACTA MANILANA. Philipines. *GMS Publication Corporatio:* 233-256.
8. Karumi, Y., Onyeyili, P. A. & Oyuybuaja, V.O. (2004). Identification of active principles of *M. Balsamia* (Balsam Apple) leaf extract. *Journal Medical Sciences*, 4: 179-182.
9. Singleton, V.L., Orthofer, R. & Lamuela-Raventos, R.M. (1999). Analysis of total phenols and other oxidation substrates and antioxidants by means of Folin- Ciocalteu reagent. *Methods in Enzymology*, *29*: 152–178.
10. Zhishen, J., Mengcheng, T. & Jianming, W. (1999). The determination of flavonoid contents in mulberry and their scavenging effects on superoxide radicals. *Food Chemistry, 64:* 555-559.
11. Oyaizu, M. (1986). Studies on products of browning reactions: Antioxidants activities of products of browning reaction prepared from glucosamine, *Japanese Journal of Nutrition*, *44*: 307-315.
12. Tang, S. Z., Kerry, J.P., Sheehan, D. & Buckley, D.J. (2002). Antioxidative mechanism of tea catechins in chicken meat systems. *Journal Food Chemistry, 76:* 45-51.
13. Velioglu, Y.S., Mazza, G., Gao, L. & Oomah, B.D. (1998). Antioxidant activity and total phenolics in selected fruits, vegetables and grain products. *Journal of Agricultural and Food Chemistry*, *46*: 4113–4117.
14. Thaipong, K., Boonprakob, U., Crosby, K., Zevallos, L.C. & Byrne, D.H. (2006). Comparison of ABTS, DPPH, FRAP, and ORAC assays for estimating antioxidant activity from guava fruit extracts. *Journal of Food Composition and Analysis*, 19: 669-675.
15. Wong, K.C., & Wong, S.N. (1995). Volatile constituents of *Averrhoa bilimbi* L. fruit.*Journal of Essential Oil Research* ,7: 691-693.
16. Vasconcelosa, C.M.L. & Conde-Garciaa, E.A. (2006). Electrophysiological effects of the aqueous extract of *Averrhoa carambola L*. leaves on the guinea pig hearts. *Phytomedicine*, *13*: 501–508.
17. Shinu, T., Patil, D.A., Patil, A.G. & Chandra, N. (2008). Pharmacognostic Evaluation and physicochemic analysis of *Averrhoa Carambola* L. fruit. *Journal of Herbal Medicine & Toxicology, 2- 51-54.*
18. Krishnaiah, D., Devi, T., Bono, A. & Sarbathly, R. (2009). Studies on phytochemical constituents of six Malaysian medicinal plants. *Journal of Medicinal Plants Research, 3(2):* 067-072.
19. Ikram, E.H.K., Khoo, H.E., Jalil, A.M.M., Ismail, A., Idris, S., Azlan, A., Nazri, H.S.M., Dito, N.A.M. &

Mokhtar, R.A.M. (2009). Antioxidant activity and total phenolic content of Malaysian underutilized fruits. *Journal of Food Composition and Analysis, 22*: 388-393.
20. Stratil, P., Klejdus, B. & Kubán , V. (2006). Determination of total content of phenolic compounds and their antioxidant activity in vegetables—Evaluation of spectrophotometric methods. *Journal of Agricultural and Food Chemistry, 54*: 607–616.
21. Huang, D., Ou, B. & Prior, R.L. (2005). The chemistry behind antioxidant activity assays. *Journal of Agricultural and Food Chemistry*, 53: 1841–1856.
22. Narain, N., Bora, P.S., Holschuch, H.J. & Vasconcelos, M.A.D.S. (2001). Physical and chemical composition of carambola fruit (*Averrhoa carambola* L.) at three stages of maturity. *Cienc.Technol.Aliment, 3:* 144-148.
23. Huda-Faujan, N., Noriham, A., Norrakiah, A.S. & Babji, A.S. (2007).Antioxidative activities of water extracts of some Malaysian herbs. *ASEAN Food Journal. 14(1*): 61-68.
24. Chang, C.C., Yang, M.H., Wen, H.M. & Chern, J.C. (2002). Estimation of total flavonoid content in propolis by two complementary colorimetric methods. *Journal of Food and Drug Analysis, 10(3)*: 178-182.
25. Iker, H., Leonor, A., Frank, V.B. & Sergi, M.B. (2005). Opinion: How relevant are flavonoids as antioxidants in plants? *The Avi Publishing Company*, 970
26. Cao, G., Sofic, E. & Prior, R.L. (1997). Antioxidant and prooxidant behavior of flavonoids: Structure–activity relationship. *Free Radical Biology and Medicine, 22:* 749 -760.
27. Harris, R.S. (1996). Effects of agricultural practices on foods of plant origin**.** *The Avi Publishing Company*, 670.
28. Benzie, I.F.F. & Strain, J.J. (1996). The Ferric reducing ability of plasma (FRAP) as a measure of Antioxidant Power‘. *Analysis of Biochemistry, 23:* 70-76.
29. Yan, L.Y., Teng, L.T. & Jhi, T.J. (2006).Antioxidant Properties of Guava Fruit: Comparison with Some Local Fruits. *Sunway Academic Journal, 3:* 9-20.
30. Prior, R.L. & Cao, G. (2000). Antioxidant phytochemicals in fruits and vegetables: diet and health implications. *Horticultural Science, 35(4):* 588–592.
31. Gazzani, G., Papetti, A., Massolini, G. & Daglia, M. (1998). Anti and prooxidant activity of water soluble components of some common diet vegetables and the effect of thermal treatment. *Journal of Agricultural and Food Chemistry, 46*: 4118–4122.
32. Mathew, L., George, S. T., Babylatha, A. K. & Geetha, C. K. (1993) Flowering and fruit development in bilimbi (*Averrhoa bilimbi* L.). *Journal Food Science and Agriculture*, 41: 41-42.
33. Prior, R.L., Wu, X. & Schaich, K., (2005). Standardized methods for the determination of antioxidant activity and phenolics in foods and dietary supplements. *Journal of Agricultural and Food Chemistry, 53*: 4290–4302.
34. Subhasree, R.B., Laxmi, K.R., Lijina, S.R. & Rajasekaran, P. (2009). Evaluation of antioxidant potential in selected green leafy vegetables. *Journal Food Chemistry, 115*: 1213–1220.
35. Lee, W.Y., Emmy, H.K.I. & Amin, I. (2007). Antioxidant activity and phenolic content of selected commercially available cruciferous vegetables. *Malaysian Journal of Nutrition*, 13: 71-80.
36. Talcott, S.T., Howard, L.R. & Brenes, C.H. (2000). Antioxidant changes and sensory properties of carrot puree processed with or without periderm tissue. *Journal ofAgricultural and Food Chemistry, 48*: 1315–1321.
37. Mishra, N., Dubey, A., Singh, N. & Gupta, P. (2010). Antimicrobial, antioxidant and chemopreventive potential of vitamin c rich fruits. *International Journal of Applied Biology and Pharmaceutical Technology, 3:* 915-920.
38. Othman, A., Amin, I., Nawalyah, A.G. & Ilham, A. (2007). Antioxidant activity and phenolic content of cocoa beans. *Food Chemistry, 100:* 1523-1530.
39. Amin, I., Zamaliah, M.M. & Chin, W.F. (2004). Total antioxidant activity and phenolic content in selected vegetables. *Journal Food Chemistry, 87*: 581–586.
40. Soong, Y.Y. & Barlow, P.J. ( 2004). Antioxidant activity and phenolic content of selected fruit seeds. *Journal Food Chemistry, 88 (3):* 411–417.
41. Amin, I. & Lee, W.Y. ( 2005). Effect of different blanching times on antioxidant properties in selected cruciferous vegetables. *Journal of the Science of Food and Agriculture, 85*: 2314–2320.
42. Deepa, N., Kaur, C., Singh, B. & Kapoor, H.C. ( 2006). Antioxidant activity in some red sweet pepper cultivars. *Journal of Food Composition and Analysis, 19*: 572–578.
43. Kaur, C., & Kapoor, H.C. ( 2001). Review: antioxidants in fruits and vegetables the millennium health. *International Journal of Food Science and Technology, 36*: 703–725.

The Malaysian Journal of ANALYTICAL SCIENCES ISSN 1394-2506

# NATURAL ISOTOPE RADIUM IN MARINE BIOTA AT KAPAR, KLANG COASTAL AREA

## (Isotop Radium Semulajadi Dalam Biota Marin Di Pesisiran Pantai Kapar, Klang)

Nik Azlin Nik Ariffin[1]* and Che Abd Rahim Mohamed[2]

*[1]Fakulti Sains Gunaan,*
*Universiti Teknologi MARA, 40450 Shah Alam, Selangor Darul Ehsan, Malaysia*
*[2]Fakulti Sains dan Teknologi,*
*Universiti Kebangsaan Malaysia, 43600 UKM Bangi, Selangor Darul Ehsan, Malaysia*

**Corresponding author: azlin_ariffin@salam.uitm.edu.my*

**Abstrak**

Kepekatan aktiviti $^{226}$Ra dan $^{228}$Ra dalam biota marin di pesisiran pantai Kapar berdekatan dengan Stesen Janakuasa Sultan Salahudin Abdul Aziz Shah (SJSSAAS) telah di analisis. Teknik yang digunakan untuk penentuan kepekatan aktiviti $^{226}$Ra dan $^{228}$Ra ialah teknik pemisah radiokimia dengan menggunakan turus pemisah penukar kation dan Pembilang Sintilator Cecair (LSC). Hasil kajian menunjukkan taburan isotop-isotop radium yang dicerap bergantung pada masa pensampelan dan lokasi kajian. Kepekatan aktiviti-aktiviti $^{226}$Rai dan $^{228}$Rai dalam isi ikan masing-masing mempunyai julat 11.82 ± 5.23 Bq/kg – 17.67 ± 6.81 Bq/kg dan 40.42 ± 16.20 Bq/kg – 67.86 ± 23.11 Bq/kg. Purata kepekatan aktiviti isotop radium dalam bivalvia seperti kerang (*anadara granosa*) adalah 61.73 ± 24.15 Bq/kg ($^{226}$Raag) dan 232.62 ± 119.44 Bq/kg ($^{228}$Raag). Manakala kupang (*perna viridis*) pula, purata kepekatan dalam $^{226}$Rapv dan $^{228}$Rapv masing-masing adalah 38.24 ± 14.19 Bq/kg dan 99.59 ± 44.91 Bq/kg. Faktor kepekatan (CF) bagi biota marin adalah lebih rendah daripada 1 x $10^4$ dan ini adalah kerana isotop radium yang terkumpul adalah rendah dan mempunyai afiniti yang tinggi terhadap bahan organik. Kajian ini juga menunjukkan dos keberkesanan dalam isotop radium telah diukur bagi memastikan tahap keselamatan terhadap pengguna dan ianya masih dibawah had yang telah dibenarkan Malaysia iaitu 1 mSv/tahun.

**Kata kunci:** Isotop radium, biota marin, faktor kepekatan, dos keberkesanan

**Abstract**

The activities concentration of $^{226}$Ra and $^{228}$Ra in marine biota at Kapar coastal area nearby Sultan Salahudin Abdul Aziz Shah Power Station (SJSSAAS) had been analyzed. The techniques that had been used to determine the activities concentration of $^{226}$Ra dan $^{228}$Ra are radiocnhemistry procedures and liquid scintillation counter (LSC). Results shows that the distribution of radium isotopes depend on the location and during sampling periods. The activities concentration of $^{226}$Rai and $^{228}$Rai in tissue were ranged 11.82 ± 5.23 Bq/kg – 17.67 ± 6.81 Bq/kg and 40.42 ± 16.20 Bq/kg – 67.86 ± 23.11 Bq/kg, respectively. The mean activities concentration of radium isotopes in bivalvia such as cockles (*anadara granosa*) are 61.73 ± 24.15 Bq/kg (226Raag) and 232.62 ± 119.44 Bq/kg (228Raag). Meanwhile for green mussles (*perna viridis*), the mean activities concentration of $^{226}$Rapv dan $^{228}$Rapv are 38.24 ± 14.19 Bq/kg dan 99.59 ± 44.91 Bq/kg, respectively. Concentration Factor (CF) in marine biota is higher than 1 x $10^4$ and it is because of the accumulated radium isotopes is low and has a high affinity for organic matter. The study also shows the effectiveness of dose in radium isotopes were measured to ensure the safety of users and it is still below the limit allowed Malaysia which is 1 mSv / year.

**Keywords:** Radium isotopes, marine biota, concentration factor, effective dose

## Pengenalan

Pada masa kini, tidak dapat dibuktikan bahawa radium secara semulajadi boleh membahayakan kepada kesihatan orang awam [1]. Akan tetapi menurut U.S. Environmental Protection Agency, dalam setiap satu juta orang yang menggunakan air yang mengandungi 5 pCi L-1 radium, sebanyak 44 orang akan mati akibat kanser. Risiko ini akan berganda kepada 88 per juta pada 10 pCi L-1 dan tripel kepada 132 per juta pada 15 pCi L-1 dan sebagainya [2].

Bivalvia seperti kima, tiram, kerang, remis dan keluarga mereka adalah di antara kumpulan dari moluska. Semua bivalvia dicirikan oleh dua injap yang bertaut, supaya melindungi binatang perisian di dalamnya. Dalam bivalvia, dua injap adalah bentuk yang serupa dalam profil tapi satu injap di sebelah kanan dari binatang, dan yang lain di sebelah kiri. Kesemua bivalvia adalah akuatik, dengan majoriti jenis yang hidup di perairan laut yang cetek. Namun ada satu kumpulan dalam air tawar iaitu *unionoidea*. Sebahagian besar bivalvia ini hanya seret dan duduk di bawah permukaan sedimen, atau bersembunyi ke dalam pasir dan lumpur sementara yang lain boleh beberapa menembusi kayu dan melekat pada batu.

Kerang adalah sejenis sumber makanan yang murah dan sedap berbanding dengan kerang-kerang lain dan sangat popular di kalangan penduduk Malaysia [3,4]. Jumlah pengeluaran kerang pada tahun 2007 yang melebihi 49,000 tan metrik menyumbangkan 25% daripada jumlah pengeluaran akuakultur air payau [5]. Penternakan kerang dijalankan di kawasan pantai Barat Semenanjung Malaysia di kawasan estuari berlumpur dan dikelilingi oleh hutan bakau [3].

Pembiakan kerang terhasil daripada beberapa faktor seperti keadaan dasar yang semulajadi, kehadiran makanan, ketumpatan dan julat dari saliniti air [6]. Kitar hayat bagi kerang dari pada pensenyawaan sehinggalah menjadi kerang yang matang bersaiz lebih kurang 31.8 mm. Seperti organisma yang lain, kerang juga menghadapi serangan dari pemangsa. Benih kerang ditabur secara rawak di kawasan penternakan yang mana kebiasaannya diserang oleh ikan dan kerang pula diserang oleh tapak sulaiman [7]. Organisma lain seperti teritip juga biasanya dijumpai melekat pada injap dan akhirnya akan menjadi pesaing untuk kerang tersebut. Selepas sepuluh hingga limabelas hari, benih kerang akan terbentuk [8].

Di Malaysia, kerang merupakan salah satu sumber protein yang tinggi, mudah didapati dan murah. Kini, penternakan kerang telah menjadi satu perusahaan yang penting terutamanya di pantai barat Semenanjung Malaysia disebabkan keuntungan yang lumayan dan kos pengurusan yang rendah. Walau bagaimanapun, masalah yang paling ketara yang dihadapi adalah berlakunya pencemaran. Ini disebabkan oleh kawasan penternakan kerang biasanya terletak berhampiran dengan muara sungai yang menerima pelbagai hasil buangan atau sisa dari industri dan kilang serta akuakultur. Kerang-kerang ini boleh menyerap segala bahan kotoran dan akan menjejaskan kesihatan pada manusia.

Kupang atau nama saintifiknya *Perna viridis* [9,10] berada secara meluas di perairan cetek di sepanjang pantai barat Semenanjung Malaysia [11,12,13]. *Perna viridis* dikenali di perairan pesisir laut di kawasan-kawasan Indo-Pasifik, sepanjang Teluk Arab ke wilayah selatan Guangdong dan Fujian di China dan Jepun selatan [9]. Dalam beberapa tahun ini, *Perna viridis* diperkenalkan ke Australia, Caribbean, Amerika Utara dan Amerika Selatan [14,15]. Kegiatan budaya spesies ini di Malaysia terutama terhad pada Johor selatan pada awal tahun 1980.

Saat ini, penternakan kupang telah dipanjangkan dari utara Malaysia, Kedah sehingga ke selatan iaitu Johor dan timur Semenanjung Malaysia kerana penternakan benih remis. Masyarakat pesisir Sebatu, Melaka terlibat dalam kegiatan nelayan dan kupang dari pelbagai jenis, untuk memasukkan pengambilan dan penjualan *Perna viridis*. Kupang diiktiraf sebagai sumber makanan yang berharga di banyak bahagian Asia [10,16,17]. Di seluruh dunia, eksploitasi kupang memainkan peranan penting dalam perekonomian nasional [18]. Namun ada ada laporan tentang dinamik penduduk dan status eksploitasi perikanan moluska di Malaysia.

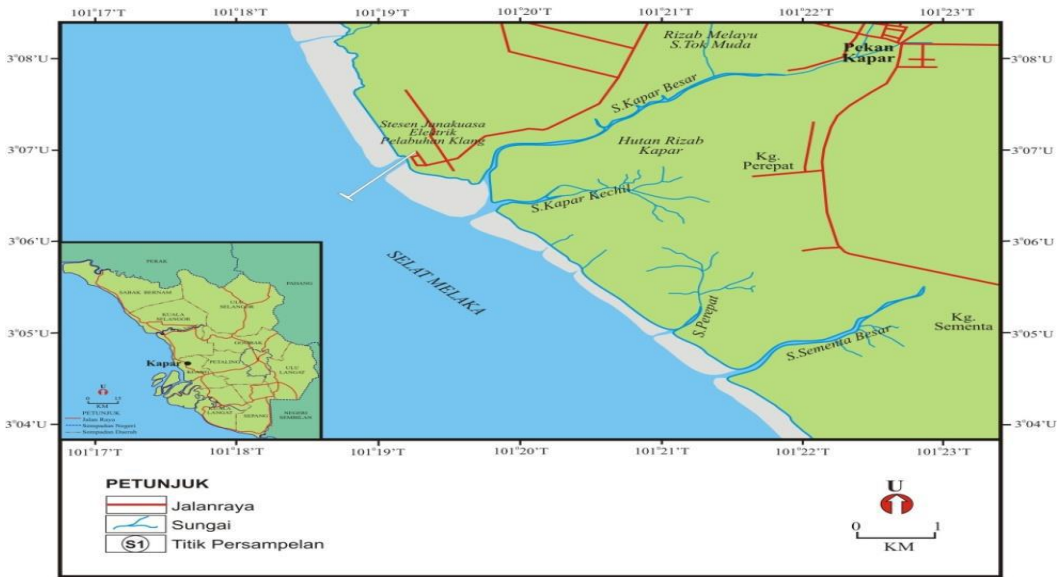
Di Malaysia, makanan laut merupakan makanan yang penting terutamanya ikan kerana kelebihan proteinnya maka kajian keatas kualiti tahap kepekatan radionuklid dan unsur-unsur logam dalam organisma-organisma marin adalah penting. Ini bagi mengenalpasti bahawa dos-dos radiasi yang diambil adalah tidak melebihi tahap yang ditetapkan atau dibenarkan. Objektif kajian ini adalah menentukan dan menilai tahap kepekatan isotop radium terhadap dos dalam makanan laut di pesisran pantai Kapar.

## Bahan dan Metodologi

### Kawasan persampelan

Kapar terletak kira-kira 56 km dari Kuala Lumpur, pantai barat Semenanjung Malaysia berhadapan dengan Selat Melaka serta beberapa kilometer sahaja dari Pelabuhan Klang. Pantai Kapar dipilih adalah kerana ianya merupakan

kawasan pesisir pantai dan untuk melihat kesan daripada operasi Stesen Janakuasa Elektrik Sultan Salahuddin Abdul Aziz (SJSSAAS) terhadap aktiviti radionuklid khususnya radium dan logam berat terhadap perairan marin di sekitarnya. Stesen janakuasa ini berorientasikan bahan bakar seperti arang, gas dan minyak yang diuruskan oleh Kapar Energy Ventures Sdn Bhd.




Rajah 1: Lokasi pensampelan di pesisir pantai Kapar

Sampel yang dibersihkan akan ditimbang untuk mendapatkan berat basahnya. Kemudian, sampel dikeringkan dalam ketuhar pada suhu $60^0$C selama 24 jam dan berat kering ditimbang selama beberapa hari untuk mendapatkan berat malar. Timbang 0.5g tisu biota marindan letakan kedalam bikar teflon. Cernakan sampel dengan menggunakan $HNO_3$, $HClO_4$ dan $H_2O_2$. Selepas itu, tambahkan 1% $HClO_4$ kedalam Teflon dan sedia melalui kolum pemisah.

Dalam kajian ini, kolum berdiameter 1cm digunakan dan pada hujung kolum sedikit kapas kaca disumbat untuk mengelakan resin daripada keluar. Resin yang digunakan dalam turus pemisah kation (cation exchange column) sebanyak 35 ml AG 50W-X4 Resin 200-400 mesh, Bio-rad). Turus pemisah kation perlu dilakukan pada suhu $70^0$C supaya kadar pembawaan ditingkatkan. Pencucian dan pembiasan turus dilakukan sebelum sampel dimasukkan. Langkah pencucian turus ini dilakukan mengikut tertib iaitu 100 ml air suling, 100 ml 2M HCl, 100 ml 7M $HNO_3$ dan 100 ml air suling dan disusuli dengan 20 ml 1% $HClO_4$ (pre-condition) untuk mewujudkan satu keadaan yang sesuai bagi pengaliran sampel. Pengaliran sampel dilalukan melalui turus pemisah kation diikuti dengan 200 ml 1M HCl untuk mengeluarkan ion plumbum, ferum dan uranium. Kesemua efluan ini dibuang. Kemudian lalukan 200 ml 2M HCl kedalam turus pemisah kation yang mana efluen ini disimpan untuk analisis lanjutan. Efluen dipanaskan sehingga kering diatas piring pemanas. Hasil pengeringan dilarutkan dengan 20 ml 0.5M HCl dan 2 ml $H_2SO_4$. Mendakan bewarna putih ($BaRaSO_4$) akan terbentuk. Pembilang sintilator cecair (LSC) digunakan bagi pengeluaran radium dan radioaktif lain yang dilakukan di makmal Oceanografi di UKM Bangi dan makmal teknologi persekitaran Fakulti Sains Gunaan, Uitm Shah Alam.

**Menentusah kaedah analisis pengukuran aktiviti isotop radium**

Kaedah analisis dan pengiraan yang digunakan dalam ujikaji ini adalah sama seperti kaedah yang digunakan keatas sampel. Tujuannya adalah untuk menentukan kebolehgunapakai sesuatu kaedah yang dipilih bagi ketepatan dan kepersisan keputusan sesuatu analisis. Penentusahan kaedah mestilah dilaksanakan sebelum analisis pengukuran

dilakukan keatas sampel sebenar. Sekiranya, nilai hasil kimia dan perolehan semula adalah tinggi dalam lingkungan 50-100 peratus, kaedah ini boleh digunapakai untuk sampel sebenar. Jadual 1 menunjukan keputusan penentusahan bagi isotop radium dan kepekatan unsur.

Dalam kajian ini, penentusahan kaedah terdiri dari pelbagai bentuk bagi memperolehi keputusan yang baik. Bahan rujukan yang diakui seperti bahan rujukan piawai (standard reference material; SRM) digunakan. SRM ini dikeluarkan dan diakui oleh Agensi Tenaga Atom Antarabangsa (IAEA) untuk pengukuran aktiviti radionuklid.

Penentusahan kaedah bagi pengukuran isotop radium, $^{226}$Ra dan $^{228}$Ra, dengan menggunakan bahan rujukan IAEA-315 (*Radionuclides in marine sediment*). Sebanyak 5 replikat bahan rujukan digunakan dalam ujian penentusahan kaedah dan nilai aktiviti dan kepekatan yang diperolehi dibandingkan dengan nilai yang diperakui dalam sijil yang disertakan. Perolehan semula dikira berdasarkan persamaan (1) berikut dan hasil analisis seperti Jadual 1:

$$\text{Perolehan semula (\%)} = (A_M / A_{SRM}) \times 100\% \quad (1)$$

dimana, $A_M$ adalah nilai aktiviti radionuklid atau kepekatan unsur yang dianalisis di makmal (Bq/kg atau µg/g atau %), dan $A_{SRM}$ adalah nilai aktiviti radionuklid atau kepekatan unsur yang dilaporkan dalam sijil SRM (Bq/kg atau µg/g atau %)

Jadual 1: Hasil analisis $^{226}$Ra dan $^{228}$Ra dalam sampel piawai IAEA-315

| **Replikat** | **$^{226}$Ra (Bq/kg ± σ)** | **$^{228}$Ra (Bq/kg ± σ)** |
|---|---|---|
| 1 | 11.79 ± 3.91 | 25.90 ± 8.79 |
| 2 | 11.20 ± 3.87 | 21.98 ± 8.25 |
| 3 | 10.30 ± 3.83 | 24.66 ± 8.72 |
| 4 | 10.90 ± 3.78 | 21.76 ± 8.08 |
| 5 | 10.83 ± 3.81 | 23.98 ± 8.48 |
| Purata | **11.01** | **23.66** |
| Nilai cadangan* | **13.8** | **26.7** |
| Perolehan semula (%) | **79.75** | **88.60** |

## Hasil dan Perbincangan

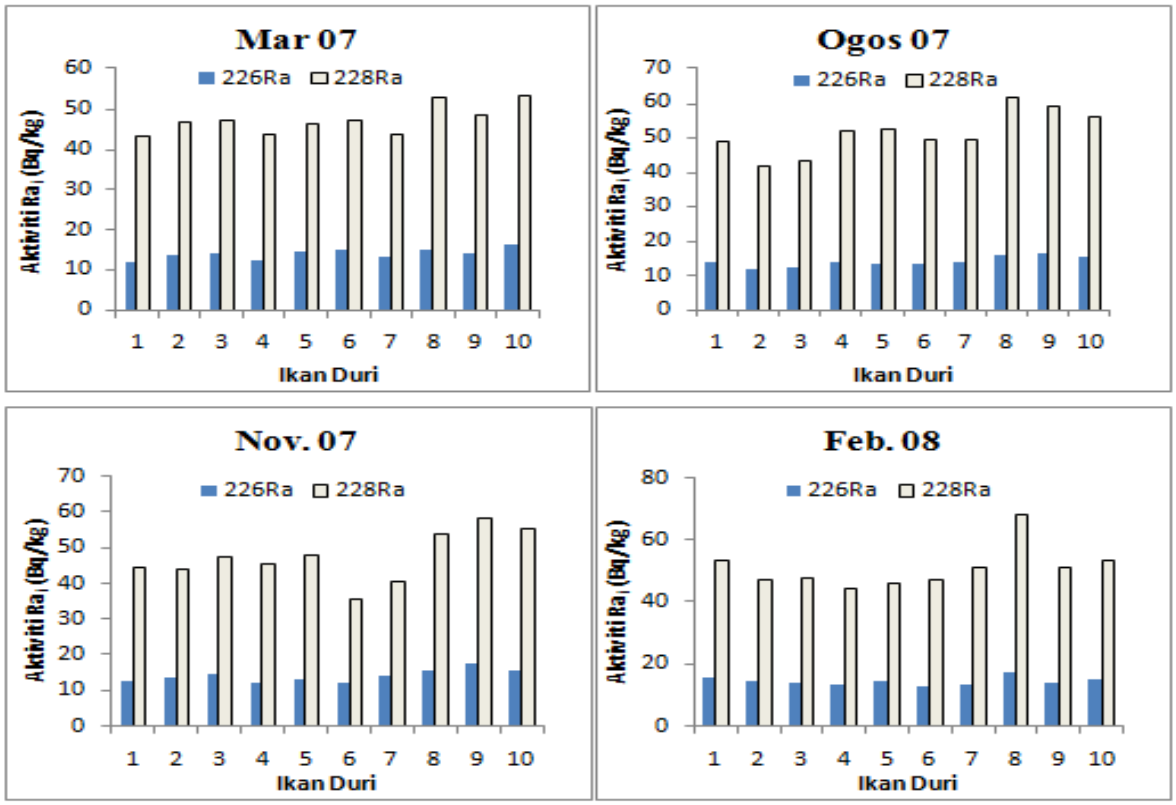
### Taburan aktiviti $^{226}$Ra dan $^{228}$Ra dalam ikan

Kajian terhadap $^{226}$Ra$_i$ dan $^{228}$Ra$_i$ dalam tisu spesies ikan duri di pesisiran pantai Kapar adalah antara yang paling awal dijalankan di Malaysia. Ikan diambil secara rawak dengan bilangan ikan komersil telah diperolehi pada bulan Mac 2007, Ogos 2007, November 2007 dan Februari 2008. Spesies–spesies ikan yang dikaji adalah untuk mendapatkan data asas bagi aktiviti $^{226}$Ra dan $^{228}$Ra di kawasan ini.

Julat keaktifan $^{226}$Ra$_i$ dan $^{228}$Ra$_i$ dalam ikan duri (*Arius sumatranus sp.*) dalam tisu otot ikan duri ditunjukkan dalam Rajah 2. Julat keaktifan $^{226}$Ra$_i$ dalam tisu ikan duri di Kapar berada dalam julat 11.82 Bq/kg hingga 17.67 Bq/kg. Pensampelan pada bulan Ogos 2007 menunjukan keaktifan $^{226}$Ra$_i$ yang paling tinggi dikalangannya manakala keaktifan $^{226}$Ra$_i$ yang paling rendah adalah pada bulan Februari 2008 di Kapar.

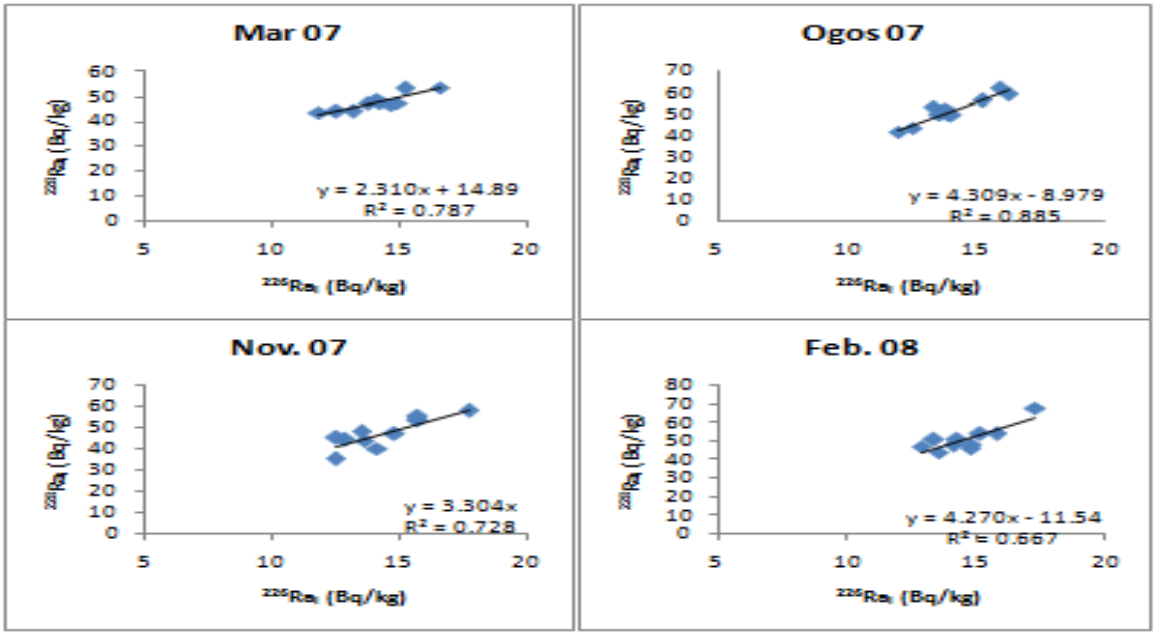
Catatan keaktifan $^{228}$Ra$_i$ di Kapar menunjukkan perbezaan bagi setiap masa pensampelan yang diambil. Ini menunjukkan bahawa pensampelan yang pertama pada bulan Februari mempunyai nilai keaktifan $^{228}$Ra$_i$ yang paling tinggi iaitu 67.86 Bq/kg berbanding pada bulan November menghasilkan nilai yang paling rendah dengan catatannya ialah 40.42 Bq/kg.

Kenyataan yang diambil menyatakan bahawa lebih 97% radionuklid yang berada dalam ikan adalah pengambilan makanan terus dari air laut sebagai medium hidupnya [25]. Selepas polonium, radium adalah yang kebiasaannya akan mempunyai kepekatan yang tinggi berbanding radionuklid yang lain di dalam organisma akuatik dan terlibat dalam rantaian makanan yang diiambil secara terus dari air laut.




Rajah 2: Taburan $^{226}Ra_i$ dan $^{228}Ra_i$ dalam isi ikan di pesisiran pantai Kapar
(*1-3 = 25 sm, 4-6 = 30 sm dan 7-10 = 35 sm)

Antara ketiga-tiga saiz ini, didapati aktiviti $^{226}Ra_i$ dan $^{228}Ra_i$ yang tertinggi telah dicatatkan dalam ikan bersaiz 35 sm dengan nilai 17.67 ± 6.81 Bq/kg dan 67.86 ± 23.11 Bq/kg, masing-masing. Manakala, nilai aktiviti radium yang paling rendah di tunjukkan dalam saiz 25 sm dengan nilai 11.82 ± 5.23 Bq /kg bagi$^{226}Ra_i$ dan 30 sm bagi $^{228}Ra_i$ dengan nilai 35.31 ± 14.85Bq/kg. Perbezaan yang ketara dalam saiz ikan ini adalah disebabkan oleh kadar metabolisma yang berbeza dalam setiap individu ikan [26]. Kolerasi yang ditunjukkan dalam Rajah 3 menerangkan bahawa terdapatnya hubungan yang kuat diantara $^{226}Ra_i$ dan $^{228}Ra_i$ pada setiap masa pensampelan. Ini dapat dibuktikan dengan analisis kolerasi Pearson dengan nilai r = 0.887 (Mac 2007), r = 0.941 (Ogos 2007), r = 0.853 (November 2007) dan r = 0.817 (Februari 2008), ($p < 0.01$). Ikan yang mengambil makanan dari dasar iaitu sedimen dijangka akan mengandungi keaktifan yang tinggi berbanding dalam air [27,28].




Rajah 3: Memaparkan hubungan diantara $^{226}Ra_i$ dan $^{228}Ra_i$ dalam isi ikan di pesisir pantai Kapar.

**Taburan aktiviti $^{226}$Ra dan $^{228}$Ra dalam bivalvia**

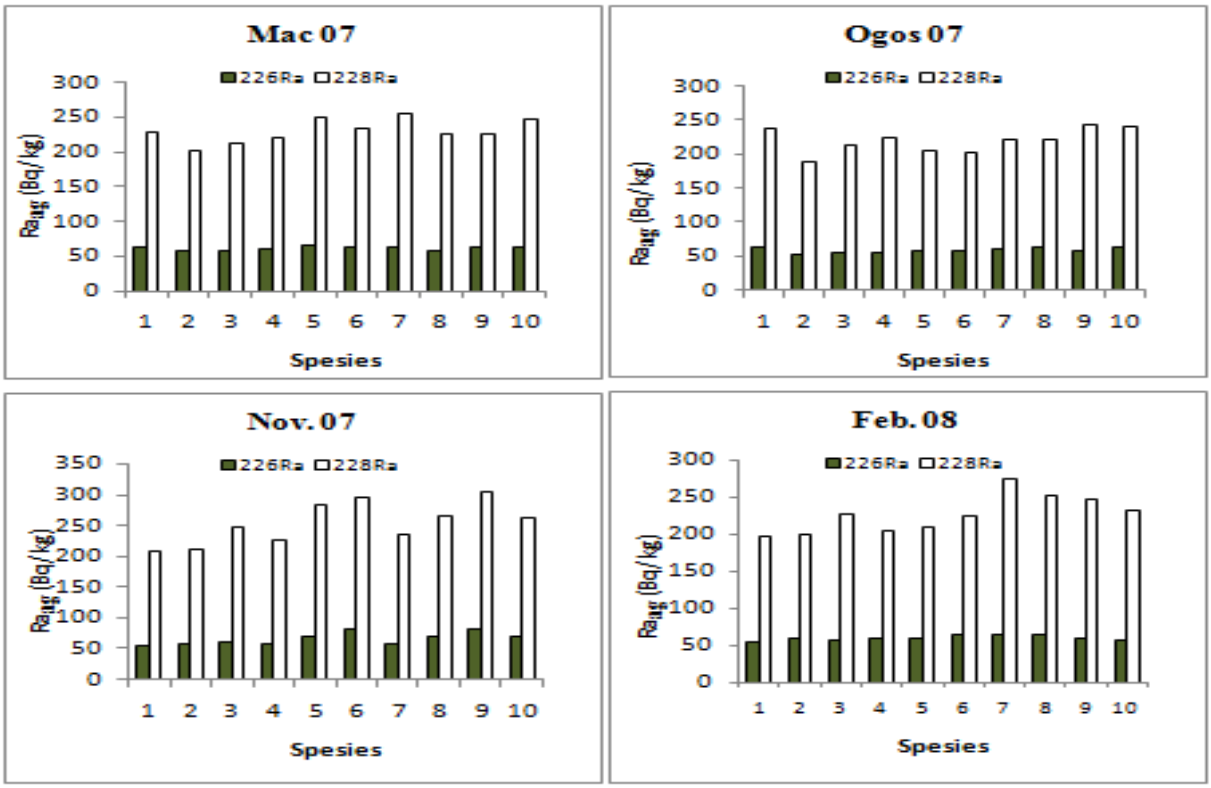
Hasil kajian bagi aktiviti $^{226}Ra_{ag}$ dan $^{228}Ra_{ag}$ dalam tisu lembut *Anadara granosa* dapat dilihat dalam Rajah 4 mengikut masa pensampelan. Secara keseluruhan, aktviti $^{226}Ra_{ag}$dan $^{228}Ra_{ag}$ dalam tisu lembut Anadara granosa adalah rendah berbanding dengan tahap yang telah ditetapkan. Dalam kajian ini, aktiviti $^{226}Ra_{ag}$ dalam tisu lembut *Anadara granosa* adalah dalam julat, 57.89 ± 22.29 Bq/kg - 65.22 ± 25.91 Bq/kg, 51.16 ± 23.27 Bq/kg - 63.63 ± 24.16 Bq/kg, 54.03 ± 21.56 Bq/kg - 81.18 ± 30.28 Bq/kg dan 51.83 ± 25.83 Bq/kg - 65.31 ± 26.91 Bq/kg, masing-masing bagi Mac, Ogos, November 2007 dan Februari 2008. Manakala julat aktiviti bagi $^{228}Ra_{ag}$ adalah 200.86 ± 58.35 Bq/kg - 254.18 ± 70.97 bagi Mac 2007, 188.96 ± 119.08 Bq/kg - 243.35 ± 150.48 Bq/kg bagi Ogos 2007, 207.27± 128.89 Bq/kg - 304.76± 168.01 Bq/kg bagi November 2007 dan 197.04 ± 123.95 Bq/kg - 274.37 ± 174.58 Bq/kg bagi Februari 2008.

Hasil yang diperolehi adalah konsisten yang mana kebanyakan $^{228}Ra_{ag}$ yang terkumpul dalam biota marin adalah $^{228}$Ra tidak tersokong iaitu hasil daripada pengumpulan dan bukan dari reputan. Dalam kajian ini mendapati bahawa aktiviti nisbah $^{228}Ra_{ag}/^{226}Ra_{ag}$ adalah tinggi yang mana melebihi 1 (>1). Ini adalah disebabkan juga daripada cara pengambilan makanan kerang terhadap persekitaran habitatnya. Selain daripada kawasan penternakan kerang di situ terdapat juga kawasan pertanian yang berhampiran.

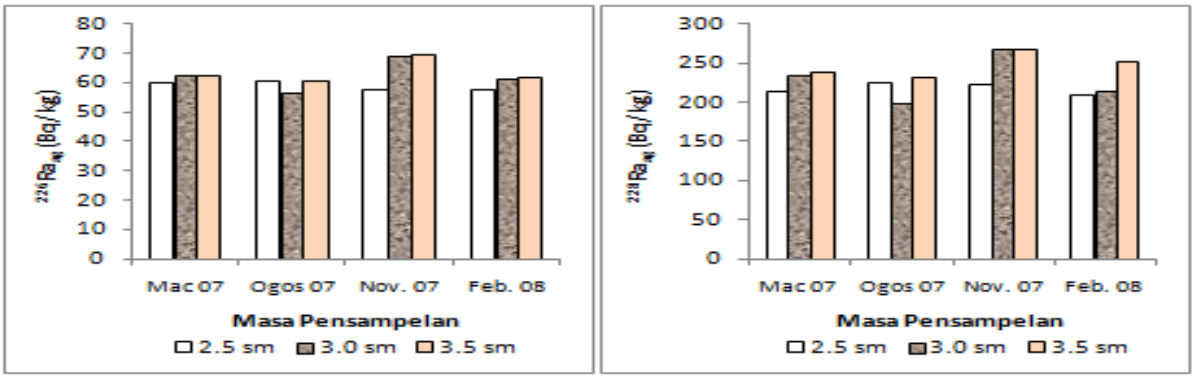
Purata aktiviti $^{226}Ra_{ag}$ dan $^{228}Ra_{ag}$ terhadap saiz kerang bagi setiap masa pensampelan telah diplotkan (Rajah 5). Secara amnya, daripada rajah tersebut didapati bahawa purata aktiviti $^{226}Ra_{ag}$ dan $^{228}Ra_{ag}$ dalam kerang mengikut saiz adalah tidak sekata kecuali bagi saiz 2.5 sm berkurangan dari masa ke semasa. Pengurangan ini adalah berkaitan dengan aktiviti dalam bahan terampai dan terdapat hubungannya dengan kerang disebabkan *Anadara granosa* adalah pemakan secara menuras.

Secara keseluruhan, hasil kajian mendapati bahawa aktviti $^{226}Ra_{ag}$ dan $^{228}Ra_{ag}$ adalah paling rendah pada bulan Ogos 2007 adalah tercatat pada kerang bersaiz 2.5 sm dengan nilai 51.16 ± 23.27 Bq/kg dan 188.96 ± 119.08 Bq/kg, masing-masing. Manakala paling tinggi adalah didapati dalam kerang yang bersaiz 3.5 sm dengan bacaan 81.18 ±

30.28 Bq/kg bagi $^{226}Ra_{ag}$ dan 304.76± 168.01 Bq/kg bagi $^{228}Ra_{ag}$ yang mana masing-masing adalah pada bulan November 2007 (Rajah 5). Secara amnya, didapati bahawa aktiviti $^{226}Ra_{ag}$ dan $^{228}Ra_{ag}$ dalam *Anadara granosa* adalah bertabur secara tidak sekata dan tiada perbezaan yang ditunjukkan ($p>0.05$) dalam setiap masa pensampelan.

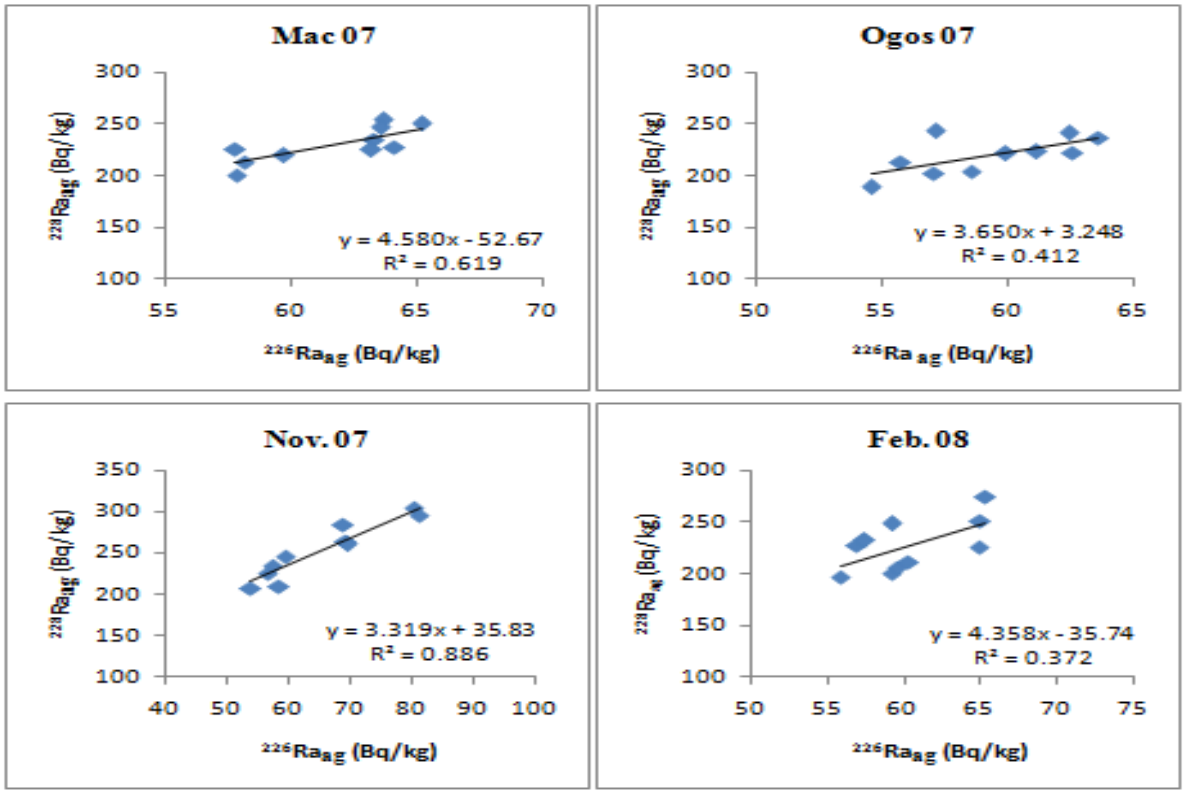



Rajah 4: Taburan aktiviti $^{226}Ra_{ag}$ dan $^{228}Ra_{ag}$ dalam kerang di pesisir pantai Kapar



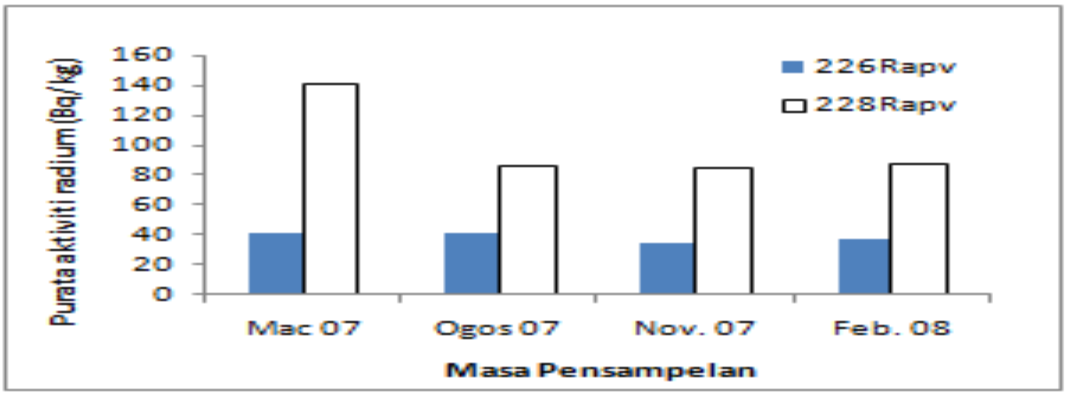

Rajah 5: Taburan aktiviti $^{226}Ra_{ag}$ dan $^{228}Ra_{ag}$ dalam kerang mengikut saiz di setiap masa pensampelan

Rajah 6 memperlihatkan kolerasi diantara $^{226}Ra_{ag}$ dengan $^{228}Ra_{ag}$ dalam *Anadara granosa* di kawasan kajian. Bulan Mac, Ogos dan November menunjukkan kolerasi yang sangat kuat diantara kedua-dua isotop radium. Ini dapat dibuktikan dengan menggunakan kolerasi Pearson ($p<0.05$) dengan nilai r = 0.785, r = 0.646 dan r = 0.942 pada Mac, Ogos dan November 2007. Secara keseluruhan kajian ini mendapati bahawa kolerasi diantara kerang dengan isotop radium ini mempunyai kekuatan yang kuat dengan menggunakan kolerasi Pearson, di mana r = 0.842; p = 0.00 ($p<0.01$).



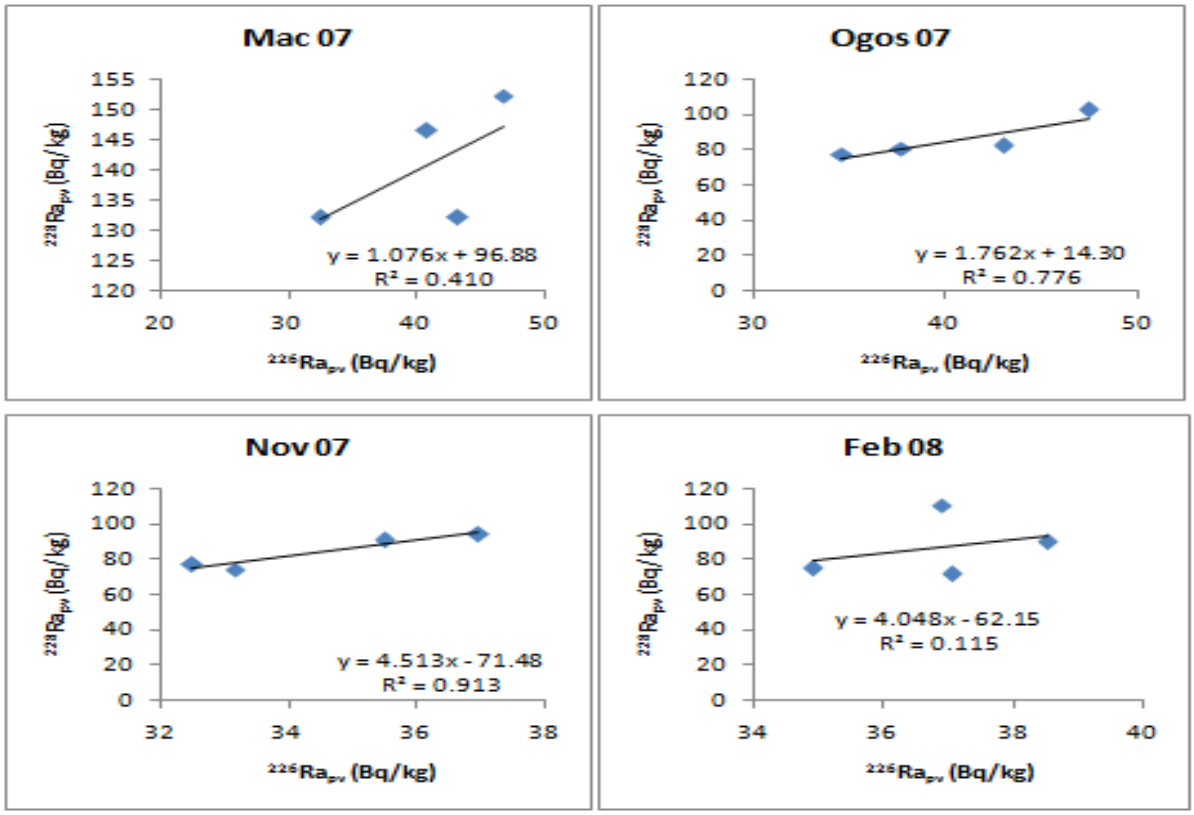

Rajah 6: Kolerasi diantara $^{226}Ra_{ag}$ dan $^{228}Ra_{ag}$ di dalam anadara granosa

Rajah 7 menunjukkan keputusan aktiviti $^{226}Ra_{pv}$ dan $^{228}Ra_{pv}$ dalam kupang (*Perna viridis*). Aktiviti $^{226}Ra_{pv}$ dan $^{228}Ra_{pv}$ yang tertinggi adalah diperolehi dengan nilai 47.47 ± 16.98 Bq/kg dan 152.38 ± 44.76 Bq/kg, masing-masing. Manakala nilai yang paling rendah adalah 32.47 ± 12.35 Bq/kg bagi $^{226}Ra_{pv}$ dan 72.03 ± 21.84 Bq/kg bagi $^{228}Ra_{pv}$. Berdasarkan Rajah 4.9 pula, di dapati bahawa purata aktiviti $^{226}Ra_{pv}$ adalah dalam julat 34.54 Bq/kg – 40.84 Bq/kg dan $^{228}Ra_{pv}$ julatnya adalah 84.39 Bq/kg – 140.86 Bq/kg.




Rajah 7: Purata aktiviti $^{226}Ra_{pv}$ dan $^{228}Ra_{pv}$ dalam kupang (*Perna viridis*) di Kapar

Hubungan diantara $^{226}Ra_{pv}$ dan $^{228}Ra_{pv}$ pada setiap masa pensampelan ditunjukkan dalam Rajah 8. Nilai-nilai $R^2$ menyarankan hubungan linear yang menyakinkan di setiap masa pensampelan. Nilai-nilai $R^2$ untuk setiap masa pensampelan masing-masing adalah $R^2$= 0.410 (Mac), $R^2$= 0.776 (Ogos), $R^2$= 0.913 (Nov.) dan $R^2$= 0.115 (Feb.). Nilai-nilai $R^2$ yang diperolehi adalah tidak kosisten, hanya pada bulan Ogos dan November sahaja yang melebihi 0.70 yang mana menunjukkan terdapatnya hubungan yang kuat antara $^{226}Ra_{pv}$ dan $^{228}Ra_{pv}$ di sekitar pesisir pantai Kapar. Ini juga ada kaitannya dengan pasang surut air laut di stesen janakuasa kerana lokasi pengambilan adalah di stesen 4 (jeti) tempat berlabuhnya kapal-kapal dalam penghantaran arang batu.




Rajah 8: Kolerasi diantara $^{226}Ra_{pv}$ dan $^{228}Ra_{pv}$ dalam kupang di Kapar

Kehadiran pasang surut air laut memberikan sedikit sebanyak impak kepada pesisiran pantai Kapar. Ini juga dapat dilihat dalam bahagian yang seterusnya dalam keaktifan radium dalam air laut dan bahan terampai. Kupang-kupang yang diambil adalah yang melekat di tiang-tiang di stesen 4. Di stesen 4 ini mengalami pasang surut yang ketara kerana apabila terjadinya air surut, maka kawasan ini hanya kawasan berlumpur dan air yang begitu cetek. Kupang-kupang ini akan terdedah kepada dua keadaan iaitu pada air pasang dan air surut.

**Faktor kepekatan (CF) bagi organisma marin**

Jadual 2 menunjukan nilai purata CF yang diperolehi selama setahun daripada setiap organisma marin mengikut spesies masing-masing. Julat CF bagi $^{226}$Ra dalam spesies *Arius sumatranus*, *Anadara granosa* dan *Perna viridis* masing-masing adalah $5.04 \times 10^2 – 11.21 \times 10^2$, $11.83 \times 10^3 – 21.60 \times 10^3$ dan $5.50 \times 10^3 – 12.71 \times 10^3$. Manakala julat CF bagi $^{228}$Ra dalam organisma marin adalah $3.95 \times 10^2 – 9.12 \times 10^2$ bagi *Arius sumatranus*, $8.75 \times 10^3 – 17.89 \times 10^3$ bagi *Anadara granosa* dan $4.50 \times 10^3 – 6.91 \times 10^3$ bagi *Perna viridis*. Jadual 2 juga menunjukkan bahawa bivalvia iaitu *Anadara granosa* diikuti dengan *Perna viridis* mempunyai nilai purata CF yang tinggi berbanding *Arius sumatranus*. Walaubagaimanapun, nilai ini adalah lebih rendah daripada nilai yang dicadangkan oleh IAEA (1985) iaitu $1 \times 10^4$. Ini adalah kerana isotop radium yang terkumpul dalam tisu organisma ini adalah rendah dan persekitaran terutama habitatnya juga adalah rendah.

Organisma marin yang mempunyai nilai CF diantara $1 \times 10^3$ hingga $1 \times 10^4$ dianggap mempunyai afiniti yang tinggi bagi radium terhadap bahan organik. Manakala julat CF untuk radium bervariasi dari $1 \times 10^1$ hingga $1 \times 10^3$ adalah khas untuk pelbagai kumpulan organisma. Secara amnya, organisma yang lebih rendah adalah peringkat trofik seperti plankton menumpukan tahap lebih tinggi radium darikomponen biotik lain dan juga, radium dalam rangkaian keras seperti cenkerang dan tulang dari banyak organisma relatif adalah lebih tinggi. *Anadara granosa* adalah merupakan salah satu penunjuk biologi yang baik bagi menentukan isotop radium.

Jadual 2: Purata faktor kepekatan (CF) bagi isotop radium dalam setahun di pesisir pantai Kapar

| **Organisma Marin** | **Faktor Kepekatan** | |
|---|---|---|
| | $^{226}$Ra | $^{228}$Ra |
| ***Arius Sumatranus*** | $7.98 \times 10^2$ | $5.82 \times 10^2$ |
| ***Anadara granosa*** | $16.46 \times 10^3$ | $13.16 \times 10^3$ |
| ***Perna viridis*** | $9.55 \times 10^3$ | $5.28 \times 10^3$ |

Berbeza dengan nilai yang telah dikaji oleh pelbagai negara sebelum ini yang mempunyai nilai CF yang lebih rendah. Ini adalah disebabkan kepekatan dalam air adalah tinggi berbanding dengan kawasan kajian di Kapar. CF terhadap hidupan bercenkerang yang telah di kaji oleh Iyengar et al. 1980 dan 1984 menunjukkan CF bagi $^{226}$Ra berjulat 44 – 50 manakala $^{228}$Ra dalam linkungan 130 – 170. Kawasan kajian ini merupakan sistem tertutup yang mana berdekatan dengan pelantar sunda menyebabkan kepekatan aktiviti organisma adalah tinggi.

**Dos keberkesanan terhadap pemakanan manusia**

Jadual 3 menunjukkan dos keberkesanan yang telah hitung secara anggaran dalam isotop radium. Walaupun data yang diperolehi masa kini agak terhad kajian ini dapat memberikan data asas dengan mengira anggaran $^{226}$Ra dan $^{228}$Ra dalam organisma bagi dos keberkesanan tahunan untuk pengguna-penggunadi kawsan kajian ini. Dengan andaian makanan mingguan tentang 375g yang diambil adalah (ambilan oleh pengguna = 375 x 52 x aktiviti radium) [30]. Sebagai perbandingan, had dos umum yang ditetapkan oleh Badan Kawalan Tenaga Atom (Atomic Energy Control Board) adalah 5mSv/tahun dan 1mSv/tahun bagi dos yang ditetapkan oleh Malaysia.

Dalam penemuan ini, wujudnya tahap pemindahan yang rendah dalam isotop radium terhadap tisu lembut organisma marin (ikan dan bivalvia). Ini menunjukkan bahawa radionuklid yang hadir dengan tahap penghasilan nilai yang kecil tetapi taburannya diukur untuk pengambilan pengguna. Terdapat juga radionuklid yang lain hadir dalam sedimen atau air dari kawasan kajian dan terhadap sampel tisu lembut yang telah dikaji, namun pengukuran terhadap tahap radionuklid dalam tisu lembut ini boleh digunapakai dalam kajian ini.

Jadual 3: Isotop radium dalam pengambilan tahunan dan dos keberkesanan terhadap pemakanan manusia

| **Organisma (n = 40)** | **Aktiviti Radium (Bq/kg)** | | **Diambil oleh Pengguna (Bq/thn)** | | **Dos Keberkesanan (mSv/thn)** | |
|---|---|---|---|---|---|---|
| | **$^{226}$Ra** | **$^{228}$Ra** | **$^{226}$Ra** | **$^{228}$Ra** | **$^{226}$Ra** | **$^{228}$Ra** |
| **Arius Sumatranus** | 1.43 | 4.93 | 27.80 | 96.04 | 0.01 | 0.03 |
| **Anadara Granosa** | 29.51 | 111.65 | 575.45 | 2177.18 | 0.16 | 0.61 |
| **Perna Viridis** | 18.35 | 47.80 | 357.83 | 923.10 | 0.10 | 0.26 |

Faktor penukaran dos = $2.8 \times 10^{-4}$mSv/Bq

Kajian ini menunjukan bahawa dos keberkesanan isotop radium dalam organisma masih rendah tetapi perlukan pemonitoran secara berkala bagi memastikan tahapnya masih lagi dalam keadaan yang baik. Jadual 4.10 menunjukkan *Anadara granosa* mempunyai dos keberkesanan yang tinggi dalam organisma yang dikaji. Ini menunjukkan bahawa kadar pemakanan kerang terhadap pemakanan manusia adalah mempunyai permintaan yang tinggi. Walaupun fungsi kerang sebagai penambahbaikan hemoglobin dalam badan tetapi ia seharusnya mengambil dalam kuantiti yang sederhana dan berpatutan dalam setiap hidangan.

## Kesimpulan

Dalam kajian ini, biota marin yang terpilih telah mempunyai nilai penumpukan yang tinggi dan ini menunjukkan bahawa organisma berkenaan mempunyai afiniti yang tinggi terhadap $^{226}$Ra. Keaktifan isotop radium dalam tulang adalah lebih kurang tiga kali ganda melebihi daripada tisu ikan duri (*Arius sumatranus sps.*) pada masa pensampelan yang sama di pesisir pantai Kapar. Ini adalah kebiasaan yang didapati dari tempat-tempat lain. Disamping itu, habitat ikan adalah di kawasan demersal maka makanannya banyak bergantung kepada suapan bawah iaitu terhadap sedimen, bentik dan juga humus-humus yang memberikan kesan dinamik radionuklid ke dalam badan. Namun, kerang mempunyai kepekatan $^{226}$Ra dan $^{228}$Ra adalah jauh lebih tinggi berbanding dengan spesies ikan dan kupang di pesisiran Kapar.

Kerang (*Anadara granosa*) adalah spesies paling dominan di kawasan muara Kapar dan merupakan sumber makanan protein utama yang mudah diperolehi di kawasan estuari yang menerima kesan yang paling jelas dari daratan seperti buangan industri yang berhampiran dan dari lautan juga. Kerang mempunyai nilai CF yang tinggi berbanding ikan dan kupang. Organisma marin yang mempunyai nilai CF diantara $1 \times 10^3$ hingga $1 \times 10^4$ dianggap mempunyai afiniti yang tinggi bagi radium terhadap bahan organik. Anadara adalah yang paling sesuai digunakan sebagai penunjuk biologi marin untuk mengawal tahap kepekatan $^{226}$Ra dan $^{228}$Ra. Kajian ini menunjukkan bahawa dos keberkesanan isotop radium dalam organisma masih rendah tetapi perlukan pemonitoran secara berkala bagi memastikan tahapnya masih lagi dalam keadaan yang baik. Walaupun fungsi kerang sebagai penambahbaikan hemoglobin dalam badan tetapi ia seharusnya mengambil dalam kuantiti yang sederhana dan berpatutan.

## Penghargaan

Kajian ini telah biayai oleh Geran Penyelidikan Universiti 600-RMI/DANA 5/3/RIF/66/2012. Pengarang ingin merakam jutaan terima kasih kepada LAOI, Fakulti Sains Teknologi, UKM kerana membantu semasa penyampelan dan penggunaan makmal disana.

**Rujukan**


1. Lentech Water treatment & air purification (2008). Radium: Health effects of radium (atas talian) http://www.lenntech.com/Periodic-chart-elements/Ra.htm. (15 Disember 2008).
2. Damgaard, M. (2008). Frequently asked questions about radium in drinking water. (atas talian) http://www.dnr.state.wi.us/org/water/dwg/radium.htm (15 Disember 2008).
3. Bardach, J.E., Ryther, J.H. & McLarney, W.O. (1972). *Aquaculture: the Farming and Husbandary of Freshwater and Marine Organisms*. Canada: John Wiley & Sons, Inc.
4. Lokman, Shamsudin (1992). *Akuakultur pinggir laut*. Kuala Lumpur: Penerbitan Dewan Bahasa dan Pustaka.
5. Jabatan Perikanan Malaysia (2007). Perangkaan Perikanan Tahunan. http://www.dof.gov.my/224 [15 Mac 2012].
6. Noorddin Ibrahim(1995). Trace element content of Malaysian cockles (*Anadara granosa*). *Food Chemistry* 54: 133-135.
7. McCoy, E. W. & Chongpeepien, T. (1988)**.** *Bivalve mollusk culture research in Thailand*. Department of Fisheries, Bangkok, Thailand; International Center for Living Aquatic Resources Management, Manila, Philippines; and Doutsche Gesellschaft for Technische Zusanmenarbeit (GTZ), GmbH, Eschborn, Federal Republic in Germany.
8. Broom, M. J. (1985). *The biology and culture of marine bivalve mollucs of the genus Anadara*. Manila Filippines: ICLARM Studies and Reviews 12:37 Manila: International Center for Living Aquatic Resources Management.
9. Siddall S.E. (1980). A clarification of the genus *Perna* (*Mytilidae*). *Bulletin of Marine Science* 30: 858-870.
10. Vakily, J. M. (1989). The biology and culture of mussels of the genus *Perna*. ICLARM *Stud. Rev*. 17: 63.
11. Ismail, A., Yap, C. K., Zakaria, M. P., Tanabe, S., Takada, H. & Ismail, A. R. (2000). *Green-Lipped Mussel Perna viridis (L.) as a Biomonitoring Agent for Heavy Metals in the west coast Of Peninsular Malaysia*. Malacca Straits Research and Development Centre (MASDEC), University Putra Malaysia, Serdang, Malaysia: 553-559.
12. Yap, C. K., Ismail, A., Tan, S. G. & Omar, H. (2002). Correlations between speciation of Cd, Cu, Pb and Zn in sediment and their concentrations in total soft tissue of green-lipped mussel *Perna viridis* from the west coast of Peninsular Malaysia. *Env. Int.* 28 (1–2): 117–126.
13. Al-Barwani, S. M., Arshad, A., Amin, S. M. N., Japar, S. B., Siraj, S. S. & Yap, C. K. (2007). Population dynamics of the green mussel *Perna viridis* from the high spat-fall coastal water of Malacca, Peninsular Malaysia. *Fish. Res.* 84: 147-152.
14. Benson, A. J., Marelli, D. C., Frischer, M. E., Danforth, J. M. & Williams, J. D. (2001). Establishment of the green mussel, *Perna viridis* (Linnaeus 1758), (Mollusca: Mytilidae) on the west coast of Florida. *Journal of Shellfish Research* 20(1): 21-29
15. Chapman, J. W., Miller, T. W., & Coan, E. V. (2003). Live Seafood Species as Recipes for Invasion. *Conservation Biology* 17(5): 1386-1395.
16. Angell C. L.(1986). The biology and culture of tropical oysters, International Center for Living Aquatic Resources Management, Manila, Philippines. ICLARM *Study Review* 12: 42.
17. Chonchuenchob, P., K. Chalayondeja and K. Mutarasint, (1980) Hanging culture of the green mussel (*Mytilus smaragdinus* Chemnitz) in Thailand. ICLARM *Transl.* 1: 14.
18. Vakily, J. M. (1992). Determination and comparison of bivalve growth, with emphasis on Thailand and other tropical areas, International Center for Living Aquatic Resources Management, Manila, Philippines, ICLARM. *Technical Report* 36: 125.
19. Sivalingam, P.M. (1977). Aquaculture of the green mussel, *Mytilus viridis* Linnaeus, in Malaysia. *Aquaculture* 11: 297-312.
20. Sivalingam, P. M. & Bhaskaran, B. (1980). Experimental insight of trace metal environmental pollution problems in mussel farming. *Aquaculture* 20: 291-303.
21. Choo, P. S. & Speiser, G.(1979). An estimation of the growth parameters and mortality of *Mytilus viridis* cultured in a suspended plastic cage in Jelutong, Penang, Malaysia. *Malaysian Agriculture Journal* 52(1): 9-16.
22. Kamal Zaman, M.,( 1995). Development in mollusk seed production in Malaysia. In: Siraj, S.S., Saidin, T. (Eds.), Advance in Seed Production Technologies. *Proceedings of Seminar Organized Jointly by Malaysian Fisheries Society*. Department of fisheries, Malaysia and University Pertanian Malaysia, April 12–13: 68.

23. Yap, C. K., Ismail, A., Tan, S. G. & Rahim, I. A., (2003). Can the shell of the green lipped mussel *Perna viridis* from the west coast of Peninsular Malaysia be a potential biomonitoring material for Cd, Pb and Zn? *Estuar. Coast. Shelf Sci.* 57 (4): 623–630.
24. Yap, C. K., Ismail, A. & Tan, S. G. (2004). Biomonitoring of Heavy Metals in the West Coastal Waters of Peninsular Malaysia Using the Green-lipped Mussel *Perna viridis:* Present Status and What Next? *Pertanika J. Trop. Agric. Sci.* 27(2): 151- 161.
25. Kim, Y. J., Kim, C. K., & Lee J. I., (2001). Simultaneous determination of 226Ra and 210Pb groundwater and soil samples by using liquid scintillation counter – suspension gel. *Journal of Radiation and Isotopes*, 54*:* 275-281.
26. Al-Masri, M.S., Mamish, S., Budeir, Y., Nashwati., A. (2000). Po-210 and Pb-210 concentrations in fish consumed in Syria. *Journal of Environmental Radioactivity* 49: 345-352.
27. Shaheed, K., Somasundaram, S. S. N., Shahul Hameed, P. & Iyengar, M. A. R. (1997). A study of Po-210 distribution aspects in riverine ecosystem of Kaveri, Tiruchirappalli, India. Environmental Pollution 95(3): 371-377.
28. Yu, K. N., Mao, S. Y., Young, E. C. M. & Stokes, M. J. (1997). A study of radioactivities in six types of fish consumed in Hong Kong. *Appl. Radiat. Isot*. 48 (4): 515-519.
29. Iyengar, M. A. R. (1990). The natural distribution of radium. Dlm. Editorial Staff IAEA (pnyt). *The environmental behaviour of radium*. Jilid 1. Hlm. 59-128. Vienna: International Atomic Energy Agency.
30. Chulow, F. V., Dave, N. K. & Lim, T. P. (1998). Radium-226 in water, sediments and fish from lakes near the city of Elliot Lake, Ontario, Canada. *Environmental Pollution*, 99: 13-28.

The Malaysian Journal of ANALYTICAL SCIENCES ISSN 1394-2506

# PENENTUAN TABURAN HARIAN LEVOGLUKOSAN DI UDARA SECARA KOLORIMETRI

## (Determination of Levoglucosan Diurnal Pattern in Air by Colorimetric Method)

Mohd Zaidi Mat Satar[1], Mohd Talib Latif[2], Mohamed Rozali Othman[1]*

[1]*Pusat Pengajian Sains Kimia dan Teknologi Makanan,*
[2]*Pusat Pengajian Sains Sekitaran dan Sumber Alam,*
*Fakulti Sains dan Teknologi,*
*Universiti Kebangsaan Malaysia, 43600 UKM Bangi, Selangor Darul Ehsan, Malaysia*

**Corresponding author: rozali@ukm.my*

**Abstrak**

Levoglukosan (1, 6-anhidro-β-D-gukopiranosa) berpotensi dijadikan sebagai pengesan spesifik bagi partikel yang terbebas daripada pembakaran biojisim disebabkan kestabilannya di atmosfera serta wujud dalam komposisi yang banyak. Kaedah yang tepat bagi penentuan kandungan levoglukosan di udara adalah penting bagi mengkaji pelbagai kesan levoglukosan terhadap atmosfera. Kajian ini bertujuan mengkaji dan membangunkan satu kaedah pensampelan optimum yang berpotensi dalam menyerap kandungan maksimum levoglukosan yang hadir di udara. Pensampelan udara dijalankan dengan menggunakan sistem penjerap udara yang mengandungi air nyahion. Sampel yang diperolehi kemudiaanya dianalisis menggunakan kaedah kolorimetri Anthrone-Asid Sulfurik di mana serapan analit diukur menggunakan spektrometer ultra lembayung-nampak pada panjang gelombang 620 nm. Hasil kajian menunjukkan bahawa keadaan yang optimum bagi pensampelan levoglukosan di udara adalah dengan menggunakan air nyahion sebagai larutan penyerap pada kadar alir 1.0 L/min. Kepekatan levoglukosan didapati tidak dipengaruhi oleh tempoh penyimpanan menunjukkan levoglukosan di dalam larutan penyerap adalah stabil. Penutupan tiub penyerap semasa pensampelan didapati mampu mempengaruhi kepekatan levoglukosan di udara.

***Kata kunci**: Kolorimetri, Levoglukosan (1,6-anhidro-β-D-glukopiranosa), udara persekitaran*

**Abstract**

Levoglucosan (1,6-anhydro-β-d-gucopyranose) in the atmosphere a major constituent of biomass burning smoke was able to be used as a specific indicator due to their stability during atmospheric transport and present at expected levels. Therefore, accurate determination of levoglucosan is crucial in order to investigate the possible effects of levoglucosan on the atmosphere. The aim of this study was to identify the optimum sampling method for measuring the maximum quantity of levoglucosan present in ambient air. Air samples were collected using an air absorbing system containing deionised distilled water. Samples obtained were analysed by colourimetry anthrone-sulphuric acid method where absorbance of analyte was measured at 620 nm using UV-visible spectrophotometer. Results obtained found that the optimum sampling method consisted of deionised water as an absorbent solution with the flow rate of 1.0 L/min. The concentration of levoglucosan in all sampling methods remained constant regardless of the storage period (1 day and 4 days), indicating that levoglucosan in the absorbing solution are quite stable. Covering the impinger tube with aluminium foil was shown to influence the amount of levoglucosan detected.

**Keywords**: colorimetry, Levoglucosan (1, 6-anhydro-β-d-gucopyranose), ambient air

## Pengenalan

Levoglukosan telah digunakan sebagai penunjuk untuk menganggarkan pembebasan partikel daripada pembakaran biojisim kerana daya ketahanannya daripada terdegradasi di atmosfera [1, 2]. Levoglukosan adalah stabil di atmosfera dan tidak terurai selepas lapan jam terbebas ke udara [3]. Levoglukosan terhasil daripada pembakaran biojisim melalui penguraian terma selulosa yang wujud di dalam tumbuhan dan telah dikenalpasti wujud di atmosfera dalam kuantiti yang agak tinggi [4, 5]. Levoglukosan berada pada fasa pertikel seni di dalam asap pembakaran biojisim dan kadar penghasilannya berada dalam julat antara 2–18 mg/min [2]. Levoglukosan di

atmosfera boleh digunakan sebagai pengesan pencemaran udara yang mudah, murah serta tersedia bagi mengesan penghasilan asap pembakaran kayu [6].

Selain daripada levoglukosan, sebatian manosakarida lain yang boleh dikesan di dalam atmosfera adalah seperti mannosan (1,6-anhidro-β-D-mannopiranosa) dan galaktosan (1,6-anhidro-β-D-galaktopiranosa) [7]. Keadaan suhu yang berbeza semasa pembakaran menyebabkan proses penguraian dan pertukaran sebatian organik boleh berlaku. Keamatan pembakaran, penganginan, tempoh pembaraan dan tempoh nyalaan akan mempengaruhi komposisi dan nisbah terhadap produk yang terhasil [8]. Penguraian terma selulosa berlaku melalui dua keadaan, pertamanya pada suhu kurang daripada 300°C yang melibatkan proses nyahpempolimeran, penguraian air, fragmentasi dan pengoksidaan dan diakhiri dengan penghasilan bahan yang hangus. Manakala pada suhu lebih daripada 300°C pula melibatkan pemecahan pada ikatan [8]. Penguraian pada keadaan kedua ini akan menghasilkan molekul yang berpotensi menjadi sebagai pengesan pembakaran biojisim terutamanya 1, 6 anhidrida glukosa yang juga dikenali sebagai levoglukosan [9]. Molekul lain yang terbentuk pada suhu ini adalah seperti isomer furanosa dan dianhidrida.

Sehingga kini kajian yang berkaitan dengan paras levoglukosan di udara adalah melibatkan penentuan levoglukosan dalam zarahan terampai di udara, oleh itu penentuannya hanyalah pengutipan zarahan terampai di udara untuk ditentukan kandungan levoglukosan di dalamnya [10, 11], dimana tiada kajian yang dilakukan untuk menentukan paras levoglukosan di udara dengan menyerap secara terus sampel udara ke dalam larutan penyerap tertentu. Kajian ini bertujuan bagi mengoptimumkan kaedah analisis levoglukosan di udara. Oleh yang demikian, parameter yang menyumbang kepada keefisiennan pam udara untuk menyerap levoglukosan di udara dikaji.

## Bahan dan Kaedah

### Penyediaan larutan piawai

***Levoglukosan***

Larutan piawai levoglukosan disediakan dengan menimbang dengan tepat kira-kira 0.1624 g serbuk levoglukosan dan dilarutkan dalam air nyahion dalam kelalang isipadu 1L yang akan memberikan kepekatan larutan levoglukosan kira-kira 1 mM. Lengkuk kalibrasi dengan kepekatan 0-2.5 µM disediakan dari larutan piawai berkenaan.

***Anthrone (9,10-dihydro-9-oxoanthracene)***

Sebanyak kira-kira 200 mg serbuk anthrone dilarutkan dengan 100 ml asid sulfurik pekat, $H_2SO_4$ di dalam bikar. Campuran berkenaan kemudiaannya dikacau dengan menggunakan rod kaca bagi memastikan semua serbuk anthrone terlarut. Larutan anthrone yang segar perlu disediakan sebelum analisis kerana warna larutan ini akan berubah mengikut masa. Larutan anthrone yang segar berwarna kuning keemasan.

### Kaedah penentuan kepekatan levoglukosan

Kepekatan levoglukosan dalam sampel dikesan dan diukur dengan menggunakan kaedah Kolorimetri-Anthrone-Asid Sulfurik seperti yang telah dicadangkan sebelum ini [12]. Sebanyak 10 mL larutan anthrone segar dimasukkan ke dalam kelalang isipadu yang mengandungi 5 mL larutan sampel. Percampuran ini dijalankan pada suhu bilik. Percampuran ini akan menghasilkan larutan yang berwarna hijau cair (campuran yang menggunakan larutan anthrone yang tidak segar akan memberikan warna keperangan ataupun coklat). Larutan ini kemudiannya dipanaskan di dalam kukus air pada suhu 100 ºC selama 10 minit sebelum disejukkan dalam air ais selama 5 minit. Akhirnya, serapan larutan diambil menggunakan Spektrometer UV-nampak pada panjang gelombang 620 nm.

### Pengoptimumam keadaan persampelan

Kaedah untuk menentukan keadaan optimum penentuan levoglukosan di udara dibahagikan kepada dua langkah. Langkah pertama adalah untuk menentukan larutan penyerap yang paling baik diikuti dengan keadaan optimum analisis levoglukosan untuk menentukan kepekataanya di udara. Persampelan dilakukan di kawasan tepi jalan di sekitar Dewan Canselor Tun Abdul Razak (DECTAR), Universiti Kebangsaan Malaysia pada waktu pagi bagi memastikan terdapat sumber-sumber kehadiran levoglukosan melalui pembakaran biojisim menggunakan tiga pam La Motte yang dijalankan serentak bagi mendapatkan data triplikat. Secara prinsipnya, kaedah penentuan levoglukosan di udara adalah melalui peyerapannnya ke dalam larutan penyerap (air nyahion atau 0.1 M asid sulfurik) di dalam tiub penyerap yang berupaya menyerap partikel levoglukosan di udara. Penentuan tahap

kandungan levoglukosan di udara ditentukan melalui kepekatan levoglukosan dalam larutan penyerap ini setelah diekstrak menggunakan larutan anthrone.

***Pemilihan larutan penyerap terbaik***

Langkah pertama kajian ini adalah dengan menentukan larutan penyerap terbaik bagi penentuan levoglukosan di udara. Untuk itu, dua larutan penyerap telah diuji iaitu air nyahion dan larutan 0.1 M asid sulfurik. Larutan penyerap berbentuk pewarna tidak diuji di dalam kajian ini memandangkan penggunaan pewarna hanya akan menyebabkan sampel rosak di mana percampuran antara larutan anthrone segar dengan larutan penyerap pewarna akan menghasilkan pemendakan. Jadi, serapan oleh spektrometer UV-VIS akan memberikan bacaan yang sangat tinggi yang berada di luar julat kepekatan levoglukosan yang sebenar di udara.

***Kadar alir dan masa penyimpanan***

Selepas larutan penyerap optimum ditentukan, kajian diteruskan dijalankan bagi menentukan keadaan optimum bagi prosedur dan peralatan untuk persampelan seperti parameter kadar alir pada pam udara dan keadaan tiub penyerap sama ada berbalut ataupun tidak iaitu dibiarkan terdedah kepada cahaya matahari. Kesan tempoh penyimpanan sampel (sehari atau lebih) terhadap kandungan levoglukosan yang diserap oleh larutan penyerap juga dikaji. Bagi menentukan kadar alir yang optimum, pam udara telah diselaraskan kepada beberapa kadar yang berbeza (0.5 L/min, 1.0 L/min and 2.0 L/min) terhadap udara selama 1 jam. Untuk parameter tempoh penyimpanan sampel, larutan penyerap yang mengandungi sampel disimpan di makmal selama sehari sehingga empat hari.

***Pemilihan keadaan optimum bagi keadaan tiub penyerap***

Untuk mengkaji pengaruh cahaya matahari terhadap tindak balas antara larutan penyerap dan levoglukosan pula, tiub penyerap dibalut dengan kerajang aluminium. Parameter untuk mengoptimumkan kaedah analisis levoglukosan di uadara diringkaskan seperti dalam Jadual 1. Untuk kerja-kerja pengoptimuman ini persampelan perlu dilakukan pada waktu yang sama untuk setiap parameter yang sama tetapi berbeza nilai atau bahan.

## Hasil dan perbincangan

**Pengoptimuman keadaan persampelan**

Purata kepekatan levoglukosan yang diperolehi bagi setiap faktor yang dikaji adalah seperti yang diringkaskan dalam Jadual 1.

Jadual 1: Purata kepekatan (n=3) levoglukosan bagi setiap faktor yang diuji

| **Faktor** | **Elemen** | **Purata kepekatan (µmol/m$^3$)** |
|---|---|---|
| **Larutan penyerap** | Air suling | 0.182±0.185 |
| | Asid sulfurik (0.01M) | 0.144±0.127 |
| **Keadaan tiub penyerap** | Berbalut-alluminium | 0.532±0.091 |
| | Tidak berbalut | 0.232±0.098 |
| **Kadar alir** | 0.5 L/min | 0.158±0.039 |
| | 1.0 L/min | 0.313±0.264 |
| | 1.5 L/min | 0.027±0.006 |
| **Tempoh simpanan** | Sehari | 0.145±0.059 |
| | 4 hari | 0.174±0.011 |

Hasil kajian mendapati air suling merupakan larutan penyerap yang paling baik dengan nilai kepekatan di udara setinggi 0.182 ±0.185 µmol/m$^3$ berbanding dengan larutan 0.01M $H_2SO_4$ yang menunjukkan bacaan lebih rendah

iaitu 0.144 ±0.127 μmol/$m^3$. Ini memandangkan levoglukosan merupakan satu sebatian yang sangat polar. Oleh itu sebatian ini sangat mudah diekstrak ke dalam fasa akuas [13]. Walau bagaimanapun ujian statistik yang dijalankan menggunakan ujian t-berpasangan antara kedua-dua larutan ini menunjukkan perbezaan yang tidak bererti ($p>0.05$) diperolehi. Dengan ini, dapat disimpulkan bahawa jenis larutan penyerap tidak begitu mempengaruhi kepekatan levoglukosan di udara. Walau bagaimanapun, air suling dipilih sebagai larutan penyerap yang paling sesuai untuk digunakan semasa persampelan udara memandangkan ia mencatatkan bacaan yang tertinggi dan penggunaannya yang lebih mudah.

Tiub penyerap yang berbalut mencatatkan bacaan kepekatan levoglukosan yang lebih tinggi iaitu sebanyak 0.532 ± 0.09 μmol/$m^3$ berbanding tiub penyerap yang tidak berbalut iaitu sebanyak 0.232±0.098 μmol/$m^3$. Keadaan tiub penyerap yang berbalut mencatatkan kepekatan purata yang lebih tinggi mungkin kerana larutan penyerap tidak didedahkan dengan cahaya matahari akibat dilindung oleh kerajang aluminium. Suhu yang tinggi mungkin menyebabkan molekul levoglukosan akan terurai terlebih dahulu di dalam larutan penyerap. Ini menunjukkan bahawa levoglukosan yang telah diserap masuk ke dalam larutan penyerap tidak sesuai didedahkan kepada cahaya matahari. Walau bagaimanapun, partikel levoglukosan di udara sangat dipengaruhi oleh suhu. Keadaan suhu yang berbeza menyebabkan proses penguraian dan pertukaran sebatian organik boleh berlaku [9]. Dapat disimpulkan di sini bahawa faktor suhu hanya memainkan peranan ke atas komposisi levoglukosan di udara sahaja dan bukannya ke atas larutan penyerap.

Sementara itu, tiub penyerap yang terdedah dengan sinaran matahari juga masih dapat mencatatkan purata kepekatan yang agak tinggi. Ini adalah kerana levoglukosan merupakan molekul yang amat stabil di udara dan hadir dalam kuantiti yang banyak berbanding molekul yang lain [1]. Oleh itu, kebarangkalian untuk menyerap levoglukosan adalah tinggi. Walau bagaimanapun tiub penyerap yang berbalut dipilih kerana ia menunjukkan bacaan yang lebih tinggi. Perbandingan menggunakan ujian t-berpasangan antara tiub penyerap yang berbalut dengan kerajang aluminium dengan yang tidak berbalut menunjukkan bahawa perbezaannya adalah bererti ($p<0.05$). Ini menunjukkan bahawa perbezaan keadaan tiub penyerap yang digunakan semasa persampelan menunjukkan perbezaan secara bererti terhadap kepekatan levoglukosan yang dikaji.

Kadar alir 1.0 L/min menunjukkan bacaan purata levoglukosan yang tertinggi iaitu sebanyak 0.313±0.264 μmol/$m^3$ manakala kadar alir 0.5 dan 1.5 L/min masing-masing menunjukkan bacaan sebanyak 0.158±0.039 μmol/$m^3$ dan 0.027±0.006 μmol/$m^3$ . Pam penyedut udara LaMotte yang telah diselaraskan dengan kadar alir yang rendah menyebabkan udara yang disedut juga adalah rendah. Oleh yang demikian, levoglukosan yang dijerap oleh larutan penyerap juga adalah rendah. Pelarasan kadar alir yang terlalu tinggi pula menyebabkan kemungkinan berlakunya tindak balas lain yang seterusnya menyebabkan kepekatan levoglukosan yang dapat dikesan adalah rendah. Disamping itu juga mungkin disebabkan kelarutan levoglukosan yang agak perlahan sehingga menyebabkan sebahagian daripadanya akan terbebas semula tanpa diserap oleh larutan penyerap yang digunakan.

Perbandingan menggunakan ujian ANOVA yang dilakukan ke atas ketiga-tiga kadar alir di atas menunjukkan perbezaan yang tidak bererti ($p>0.05$). Ketiga-tiga kadar alir yang digunakan tidak menunjukkan perbezaan yang bererti. Walau bagaimanapun, kadar alir 1.0 L/min dipilih kerana mencatatkan bacaan kepekatan leoglukosan yang lebih memuaskan. Oleh yang demikian, dapat disimpulkan di sini bahawa kadar alir 1.0 L/min merupakan kadar alir yang paling sesuai digunakan semasa persampelan udara dijalankan. Kepekatan levoglukosan dapat dikesan dengan nilai yang tinggi pada kadar alir ini.

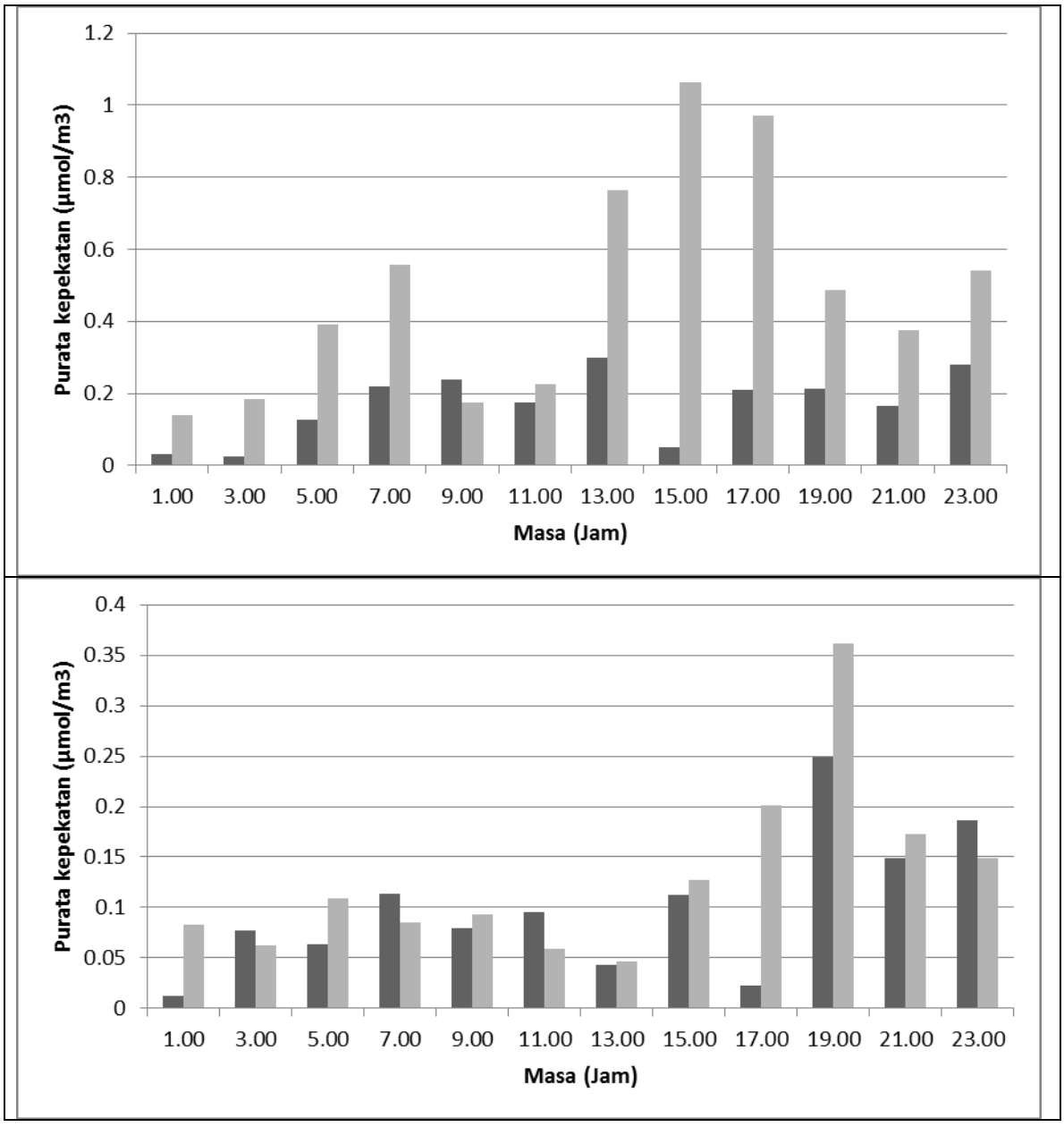
**Taburan Harian Levoglukosan Di Udara**

Dengan menggunakan keadaan persampelan yang telah dioptimumkan, kajian telah dilakukan untuk menentukan corak taburan levoglukosan di dua kawasan berbeza iaitu kawasan pinggir jalan dan kawasan perumahan di sekitar Kajang, Selangor.

***Kepekatan purata levoglukosan di udara kawasan pinggir jalan***

Kepekatan levoglukosan pada waktu cuti adalah lebih tinggi berbanding waktu bekerja (Rajah 1). Ujian ANOVA satu hala yang dijalankan menunujukkan bahawa perbezaan kepekatan levoglukosan antara hari bekerja dan hari cuti adalah bererti ($p<0.05$). Aktiviti pembakaran yang dilakukan oleh penduduk menghasilkan asap yang

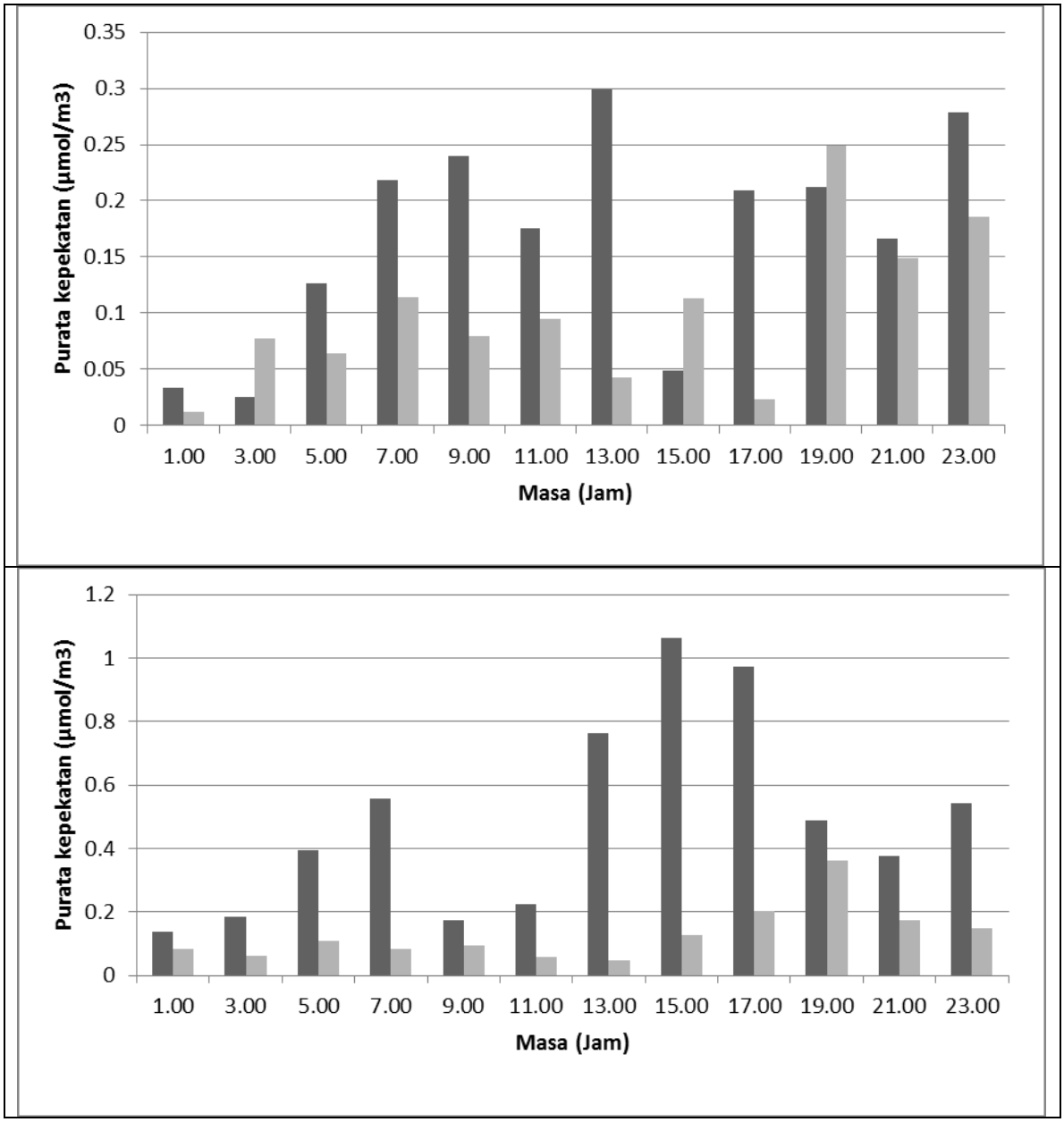
seterusnya menyebabkan penguraian terma selulosa boleh berlaku. Kepekatan levoglukosan dalam partikel asap pembakaran tumbuhan, kayu, unggun api, asap rokok dan bahan api adalah tinggi [2, 6, 8]. Kepekatan levolukosan di udara adalah tinggi pada waktu penduduk bercuti mungkin kerana banyak aktiviti pembakaran tumbuhan yang berlaku pada waktu ini.




Rajah 1: Perbandingan kepekatan levoglukosan pada waktu bekerja (■) dan cuti (□) di kawasan pinggir jalan (atas) dan di kawasan perumahan (bawah)

***Perbandingan kepekatan purata levoglukosan di udara di kawasan perumahan***

Corak taburan kepekan levoglukosan yang hamper sama juga diperolehi di kawasan perumahan (Rajah 2) dan ujian ANOVA yang dijalankan mendapati perbezaan kepekatan levoglukosan antara hari bekerja dan hari cuti adalah bererti ($p<0.05$). Jika dibandingkan antara kedua-dua keadaan, kepekatan levoglukosan dapat dikesan dalam julat yang tinggi pada waktu petang. Keamatan cahaya yang berbeza-beza antara jam-jam tersebut menyebabkan berlakunya corak taburan levoglukosan yang tidak sekata. Pendedahan kepada sinaran ultra lembayung (UV) akan mempercepatkan kadar pemutusan ikatan antara ikatan karbon dalam molekul levoglukosan.




Rajah 2: Perbandingan kepekatan levoglukosan di udara pada hari bekerja (atas) dan hari cuti (bawah) di kawasan pinggir jalan (■) dan kawasan perumahan ( □)

***Perbandingan kepekatan levoglukosan di udara pada hari bekerja dan hari cuti***

Kepekatan levoglukosan di udara pada hari bekerja adalah tinggi di kawasan pinggir jalan berbanding kawasan perumahan (Rajah 2A). Hasil ujian ANOVA mendapati bahawa perbezaan kepekatan levoglukosan antara kedua-dua hari berkenaan adalah bererti ($p<0.05$). Jika dibandingkan antara kedua-dua keadaan, kepekatan levoglukosan dapat dikesan dalam julat yang tinggi pada waktu petang. Walau bagaimanapun, kepekatan levoglukosan di udara semakin menurun selepas jam 1900 petang mungkin kerana faktor cuaca yang menyebabkan asap daripada pembakaran biojisim tidak dapat bertahan lama di sesuatu kawasan kerana tiupan angin berupaya membawa hasil pembakaran biojisim ini ke tempat yang lebih jauh.

***Kepekatan levoglukosan di udara pada hari cuti antara kawasan pinggir jalan dan kawasan perumahan***

Terdapat perbezaan yang agak ketara antara kepekatan levoglukosan di kawasan pinggir jalan dan perumahan pada hari cuti (Rajah 2B). Kepekatan levoglukosan pada hari cuti adalah tinggi di kawasan pinggir jalan berbanding di kawasan perumahan. Ujian ANOVA menunjukkan bahawa perbezaan bagi kedua-dua kawasan ini ini adalah bererti ($p<0.05$).

## Kesimpulan

Levoglukosan (1, 6-anhidro-β-D-gukopiranosa) berpotensi dijadikan sebagai pengesan spesifik bagi partikel yang terbebas daripada pembakaran biojisim disebabkan kestabilannya di atmosfera serta wujud dalam komposisi yang banyak. Kaedah yang tepat bagi penentuan kandungan levoglukosan di udara adalah penting bagi mengkaji pelbagai kesan levoglukosan terhadap atmosfera. Kajian ini bertujuan mengkaji dan membangunkan satu kaedah pensampelan optimum yang berpotensi dalam menyerap kandungan maksimum levoglukosan yang hadir di udara. Pensampelan udara dijalankan dengan menggunakan sistem penjerap udara yang mengandungi air nyahion. Sampel yang diperolehi kemudiaanya dianalisis menggunakan kaedah kolorimetri Anthrone-Asid Sulfurik di mana serapan analit diukur menggunakan spektrometer ultra lembayung-nampak pada panjang gelombang 620 nm. Hasil kajian menunjukkan bahawa keadaan yang optimum bagi pensampelan levoglukosan di udara adalah dengan menggunakan air nyahion sebagai larutan penyerap pada kadar alir 1.0 L/min. Kepekatan levoglukosan didapati tidak dipengaruhi oleh tempoh penyimpanan menunjukkan levoglukosan di dalam larutan penyerap adalah stabil. Penutupan tiub penyerap semasa pensampelan didapati mampu mempengaruhi kepekatan levoglukosan di udara.

Kaedah optimum untuk menentukan levoglukosan di udara yang menggunakan pam LaMotte adalah dengan menggunakan larutan penyerap air suling dan udara disedut masuk pada 1.0 L/minit. Selain itu, keadaan tiub penyerap yang berbalut juga dipilih semasa persampelan udara dilakukan ini bagi mengelakkan daripada levoglukosan yang telah terperangkan terdedah kepada sinaran matahari. Sampel yang telah diambil pula boleh dianalisis pada pada bila-bila masa memandangkan tempoh simpanan sampel tidak memberikan perbezaan secara bererti terhadap kepekatan levoglukosan. Kaedah penentuan levoglukosan di udara yang telah dibangunkan ini telah berjaya diapplikasikan dalam penentuan kepekatannya di udara dan hasil yang diperolehi adalah memberansangkan.

## Penghargaan

Pengarang ingin mengucapkan ribuan terima kasih kepada Universiti Kebangsaan Malaysia melalui geran penyelidikan DLP-2012-024 yang membolehkan kerja-kerja dalam kajian ini dapat dilakukan dengan jayanya.

## Rujukan

1. Fraser, M. P. and Lakshmann, K. (2000). Using levoglucosan as a molecular marker for the long range transport of biomass combustion aerosols. *Environ. Sci. Technol.* 34, 4560-4564.
2. Simoneit, B. R. T. (2002). Biomass burning: A review of organic tracers for smoke from incomplete combustion. *Appl. Geoche.* 17, 129-162.
3. Locker, H.B. (1988). The used of levoglocosan to assess environmental impact of residential wood burning on air Quality. PhD thesis Dartmouth Colledge, Hanover NH.
4. Dixon, R. W. and Baltzell, G. (2006). Determination of levoglucosanin atmospheric aerosols using High Performance Liquid Chromatography with aerosol charge detection. *J. Chrom. A* .1109, 214-221.

5. Dos Santos, C. Y. M., Azevedo, D. D. A. and De Aquino Neto, F. R. (2002). Selected organic compounds from biomass burning in the atmospheric particulate matter over sugarcane plantation areas. *Atmos. Environ.* 36, 3009-3019.
6. Jordan T. B., Seen, A. J. and Jacobsen. (2006). Levoglucosan as an atmospheric tracer for woodsmoke. *Atmos. Environ.* 40:5316-5321.
7. Nolte, C. G., Schauer, J. J., Cass, G. R. and Simoneit, B. R. T. (2001). Highly polar organic compounds present in wood smoke and in the ambient atmosphere, *Environ. Sci. Technol.* 35, 1912–1919.
8. Simoneit, B. R. T., Schauer, J. J., Nolte, C. G., Oros, D. R., Elias, V. O., Fraser, M. P., Rogge, W. F. and Cass, G. R. 1999. Levoglucosan, a tracer for cellulose in biomass burning and atmospheric particles. *Atmos. Environ.* 33, 173-182.
9. Elias, V. O., Simoneit, B. R. T., Cordeiro, R. C. and Turcq, B. (2001). Evaluating levoglucosan as an indicator of biomass burning in Carajas, Amazonia: A comparison to a charcoal record. *Atmos. Environ.* 65, 267-272.
10. Fuzi Mohamed Fartas, Mohamed Rozali Othman, Faraj Ali Rajeb and Mohd Talib. Latif. (2009). Determination of Levoglucosan in PM10 and Biomass Close Burning Residue Samples Using Anthrone-sulfuric Acid Colorimetric Method. *J. Appl. Sci. Res.* 5(10), 1663-1667.
11. Michihiro Mochida, Kimitaka Kawamura, Pingqing Fu, Toshihiko Takemura. (2010). Seasonal variation of levoglucosan in aerosols over the western North Pacific and its assessment as a biomass-burning tracer. *Atm. Environ.* 14( 29): 3511-3518.
12. Laurentin, A. and Edwards, C. A. (2003). A microtiter modification of the anthrone-sulfuric acid colorimetric assay for glucose-based carbohydrates. *Anal. Biochem.*315, 143-145.
13. Qi Li, Philip H. Steele, Brian Mitchell, Leonard L. Ingram, and Fei Yu. (2013). The addition of water to extract maximum levoglucosan from the bio-oil produced via fast pyrolysis of pretreated loblolly pinewood. *BioResources,* 8(2), 1868-1880.

The Malaysian Journal of ANALYTICAL SCIENCES ISSN 1394-2506

# SPATIAL DISTRIBUTION OF PHYSICO-CHEMICAL PARAMETER IN UPSTREAM RIVERS AND TIMAH TASOH LAKE, PERLIS: PRELIMINARY STUDY

## (Taburan Spatial Parameter Fizikal-Kimia Di Sungai Dan Empangan Timah Tasoh, Perlis: Kajian Permulaan)

Siti Aesah Abdullah[1,2]*, Sharizal Hasan[2], Mohd Lias Kamal[2], Norshahrizan Mohd Hashim[3]

[1]*Faculty of Applied Sciences,*
*Universiti Teknologi MARA, 40450 Shah Alam, Selangor, Malaysia*
[2]*Faculty of Applied Sciences,*
[3]*Faculty of Architecture, Planning and Surveying,*
*Universiti Teknologi MARA, 02600 Arau, Perlis, Malaysia*

**Corresponding author: sa.abdullah26@gmail.com*

**Abstract**

Rivers located in the northern part of Perlis which are used as a source of fresh water for Tasoh Dam are exposed to heavy metals pollution since all industrial and agricultural waste were directly discharge into rivers. In order to determine the distribution pattern of heavy metals in rivers and dam, the physico-chemical parameter forms of metals were investigated. Surface water sample were collected randomly from selected sampling site and were analysed for lead (Pb), copper (Cu), chromium (Cr), arsenic (As) and manganese (Mn) using Inductive Coupled Plasma Mass Spectrometry (ICP-MS). The concentration range of the metals were; 0.37-2.37 ppb, 0.23-3.27 ppb, 0.57-6.8 ppb, 0.27-12.60 ppb and 7.00-383.83 ppb respectively. All measured metals were found to be below the permissible limit set by Department of Environment Malaysia except for manganese. The sources of Mn were come from industrial activities such as textiles, chemical, food industry which directly discharged waste water into river.

**Keywords:** heavy metals, pollution,distribution,spatial,anthropogenic

**Abstrak**

Sungai yang terletak di bahagian utara Perlis yang digunakan sebagai sumber air tawar untuk Empangan Tasoh terdedah kepada pencemaran logam berat kerana semua sisa industri dan pertanian terus dilepaskan ke dalam sungai. Untuk menentukan corak taburan logam berat dalam sungai dan empangan, parameter fiziko-kimia logam telah dikaji. Sampel air dipermukaan telah diambil secara rawak dari kawasan pensampelan yang dipilih dan dianalisis bagi plumbum (Pb), kuprum (Cu), kromium (Cr), arsenik (As) dan mangan (Mn) menggunakan *Inductively Coupled Plasma-Mass Spectrometry* (ICP-MS). Julat kepekatan logam; 0,37-2,37 ppb, 0,23-3,27 ppb,,57-6,8 ppb,,27-12,60 ppb dan 7,00-383,83 ppb masing-masing. Semua logam yang diukur didapati berada di bawah had yang dibenarkan oleh Jabatan Alam Sekitar Malaysia kecuali mangan. Sumber-sumber bagi Mn datang daripada aktiviti industri seperti tekstil, kimia, industri makanan yang terus dilepaskan sisa ke dalam sungai.

**Kata kunci**: logam berat, pencemaran, taburan,spatial,antropogenik

## Introduction

Water is the most vital resources in all aspects of human, ecosystem, survival and health. However with the rapid growth in urbanization and industrialization, water can be easily contaminated [1]. Among of various pollutants exist on earth, heavy metals are the most toxic pollutants present in surface waters, tend to accumulate in organisms and become persistent due to their chemical stability and readily soluble [2]. Those metals are environmentally mobile and may enter human food chain which in turn give a harmful effect to human and living things [3].The most toxic metals are Cr, Ni, Pb, Cd and As while metals such as Mn, Co, Cu, and Zn act as the essential micronutrients for flora and fauna, but they are still dangerous at high levels. In addition, environmental factor such

as temperature, pH dissolved oxygen, salinity can influence the toxicity of metals in solution [2].These metals enter and distributed into water bodies by weathering and erosion or anthropogenic activities such as industrial processing, agricultural runoff and sewage disposal [4].

Timah Tasoh Dam located in Northern part of Perlis is the major source of drinking water, industrial, agricultural and also used for irrigation and flood control [5]. Rivers that supply freshwater into the Dam are Pelarit and Jarum Rivers. The influence of human activities in the upstream until downstream catchments area of both rivers such as agriculture, housing, recreation contributes to the degradation of water quality of the lake [5].These activities resulting in large scale deterioration of the water quality in dam. To date, there have been no systematic studies on this river in upstream and downstream as well as in dam although well planned monitoring programmed has been conducted by Department of Environment [6]. Therefore, it is important to investigate the spatial distribution of physico-chemical parameter in order to control the water quality of upstream rivers and dam, since they are mainly use for drinking, industrial and agricultural purpose. The objective of this study was to investigate the spatial distribution of physico-chemical parameter in Upstreams Rivers and Timah Tasoh Lake.

## Materials and Methods

### Description Of Study Area

TimahTasoh Lake, Perlis ($6^o$ $36^o$N and $100^o$ 14'E) located approximately 13 km north of the Kangar town near the Thailand boarder. The average surface area is about 13.33 $km^2$ and able to store capacity up to 40 million meter cube.Two main river which are Jarum (64.4 $km^2$) and Pelarit River (42.7 $km^2$) are the most important sources of freshwater for dam where the upstream of these river is located at Perlis State Park (st4) and Post Razi(st 1) as showed in figure 1 [5]. Water from upstream will flow through another six rivers namely Rimba Mas (st 2), Jarum River (st 3), Wang Kelian River (st 5), Gua Kelam (st 6), Gua Wang mo ( st 7), Wang Mo River (st 8), Pelarit River (st 9) and lastly its enter Tasoh Lake (st 10). Based on the observation, there was an agricultural area in upstream catchments such as rubber, paddy, sugar, cane, timber plantation and livestock surrounding Dam [5]. Those activities were identified as non-point source pollution. Meanwhile, domestic and industrial zone was categorized as point source pollution to the Tasoh Lake [5.] Both sources of pollutions may contribute to the depletion of water quality. Figure 1 below illustrates the location of sampling site.

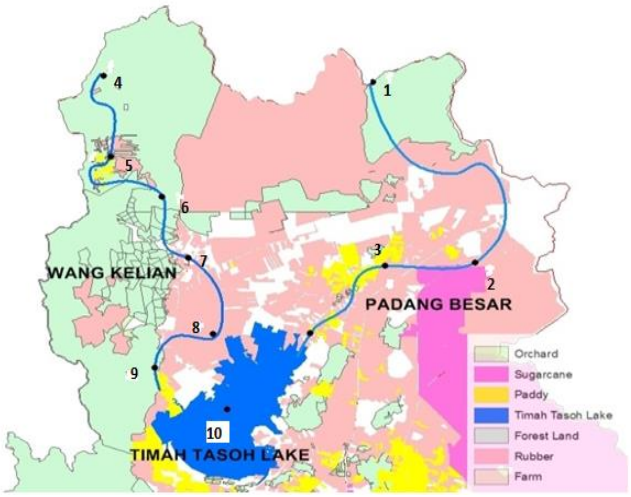



Figure 1: Location map for sampling site

**Sampling and pre-treatment**

About 30 surface samples were collected using Niskin water sampler from 10 sampling points with the help of Global Positioning System (GPS Map 76Cx) on May and June 2012 during dry season. Water sample was kept in 500ml polyethylene sample bottle and was acidified with concentrated $HNO_3$ to pH <2. All preserved water samples were kept in coleman box using ice cubes and transported to the Green Environmental Research Laboratory at Unversiti Teknologi MARA Arau, Perlis. All preserved samples were transferred into incubator at 4$^{o}$C before used in analysis. Six of *in-situ* parameter such as temperature, salinity, dissolves oxygen, conductivity, pH and total dissolved solid were measured directly at each station using HYDROLAB DataSonde

**Water Analysis**

All preserved water samples were filtered through pre-washed 0.45 µm Milipore nitrocellulose filters and the initial portion of the filtration was discarded to clean the membrane. 1 mL filtered samples was then transferred into a pre-cleaned centrifuge tube and adjusted with deionised water from Mili-Q water system to 10 mL. Samples were then ready to be analyzed with ICP-MS. Mili-Q water system and analytical grade reagents were used throughout the work. Standard Reference Material 1643e (SRM) for fresh water and reagent blank were used for quality control sample during analysis. The percent recovery of metals is acceptable which is within 85-120%. The standard solution used for calibration was prepared by diluting stock solution of 1000 mg/L of multi element standards.

## Results and Discussion

Table 1 revealed that the temperature was varied from 24.0-33.6 $^{o}$C; mainly because of different timing during sampling as well as the effect of atmospheric temperature [7]. The TDS values of the study area lies between 0.033 – 0.452 g/L. This varied value was due to the increase of various kinds of minerals such as ammonia, nitrite and metallic ion which comprised of dissolved solid in water [8]. The lowest value of salinity observed was 0.02% meanwhile the highest value is 0.34%. The possible reason salinity give varied values is because of the presence of ionic substance that come from the reaction occur between metals and acid in water [8]. The range of DO obtained was from 9.93 -16.48 mg/L. High value of DO at Station 3 located at Jarum River possibly to the increase of temperature during dry season lead to acceleration of the photosynthesis which utilizing carbon dioxide and giving off oxygen [9]. The pH value varied from 7.0 – 8.5 which is within the permissible limit for diverse uses such as water supply, fishery set by DOE (pH 6.5-8.5). The electrical conductivity (EC) obtained is in the range from 0.051-0.395 mS/cm. The highest values of EC were found at Station 3. This may come from the addition of waste water from residential area near the river as well as from industrial activities such as textile, chemical and rubber made industries which are located at Padang Besar Town [10]. Beside that, EC may naturally come from the origin of the river water and due to inert stream bank material [10].

In term of spatial distribution pattern of heavy metals, overall result show all reading give the same graph pattern between May and June samples (as shown in Figures 2(a)-2(e). However, the level of heavy metal's concentration of in this two month is different. This may caused by a prolonged summer occurred causing the water to recede and shallow. When depth, temperature and river flow change, it will result in changes of the equilibration between sediment and water. This will result in the oxidation of solid metals compounds and resuspension of sediments would release entrapped soluble metals in sediment into the water [11].

However, this pattern was occur due to the influence of anthropogenic activities for example in Fish Temple at Station 7 there was an illegal dumping wastes which accumulated at the end of the stream. Diesel and plaster ceiling factories found in Station 2 located at Padang Besar also give significant bad impact and contamination to the river. But the major sources of pollutant in Jarum River (Station 3) is due to the existing of residential area that generate solid waste and sewage which were directly discharge into the river [5].

Table 1: Mean value for physical parameter in May and June*

| Sampling station | Location | Mean value for physical parameter in May (June) | | | | | |
|---|---|---|---|---|---|---|---|
| | | T ($^{o}$C) | TDS (g/L) | Salinity (%) | DO (mg/L) | pH | EC (mS/cm) |
| 1 | N $6^{0}$ 41.411' | 26.67 | 0.4333 | 0.32 | 13.00 | 7.3 | 0.360 |
| | E $100^{O}$ 16.853' | (27.3) | (0.452) | (0.34) | (12.03) | (7.3) | (0.353) |
| 2 | N $6^{0}$ 38.213' | 29.57 | 0.229 | 0.17 | 10.21 | 7.3 | 0.384 |
| | E $100^{0}$ 17.531' | (30.4) | (0.129) | (0.17) | (12.71) | (7.4) | (0.214) |
| 3 | N $6^{0}$ 36.843' | 28.83 | 0.239 | 0.17 | 11.15 | 7.0 | 0.395 |
| | E $100^{0}$ 14.697' | (33.6) | (0.286) | (0.21) | (16.48) | (7.9) | (0.395) |
| 4 | N $6^{0}$ 41.052' | 24.6 | 0.033 | 0.02 | 15.68 | 7.1 | 0.051 |
| | E $100^{O}$ 11.334' | (24.9) | (0.034) | (0.02) | (16.16) | (7.6) | (0.052) |
| 5 | N$6^{o}$ 39.511' | 26.74 | 0.194 | 0.14 | 14.17 | 7.2 | 0.308 |
| | E$100^{O}$ 11.026' | (27.8) | (0.221) | (0.16) | (13.25) | (7.7) | (0.359) |
| 6 | N $6^{0}$ 38.746' | 26.55 | 0.236 | 0.17 | 14.81 | 7.5 | 0.374 |
| | E $100^{0}$ 12.023' | (26.50) | (0.236) | (0.17) | (14.81) | (7.5) | (0.374) |
| 7 | N$6^{0}$ 38.746' | 26.43 | 0.227 | 0.17 | 14.46 | 7.7 | 0.359 |
| | E $100^{0}$ 12.366' | (26.5) | (0.237) | (0.17) | (13.94) | (8.1) | (0.375) |
| 8 | N$6^{0}$ 36.811' | 26.62 | 0.223 | 0.17 | 14.42 | 7.6 | 0.327 |
| | E $100^{0}$ 12.251' | (26.3) | (0.245) | (0.18) | (14.55) | (7.7) | (0.387) |
| 9 | N$6^{0}$ 35. 512' | 27.21 | 0.224 | 0.16 | 12.77 | 7.0 | 0.361 |
| | E $100^{0}$ 12.432 | (27.1) | (0.238) | (0.17) | (12.59) | (8.0) | (0.375) |
| 10 | N $6^{O}$34.509' | 30.18 | 0.218 | 0.09 | 13.58 | 7.6 | 0.217 |
| | E $100^{0}$ 12.237' | (29.20) | (0.145) | (0.10) | (12.37) | (8.6) | (0.209) |

*in bracket is refer to value in June

Table 2: Concentration of metals in surface water in ppb unit

| Sampling station | Actual Concentrations in ppb May and June* | | | | |
|---|---|---|---|---|---|
| | Pb | Cu | Cr | As | Mn |
| 1 | 0.43 (0.60) | 0.23 (0.30) | 3.63 (6.87) | 0.27(0.30) | 26.77(31.83) |
| 2 | 0.80 (0.37) | 0.57 (1.07) | 3.70 (4.67) | 7.73(4.40) | 383.83 (78.24) |
| 3 | 0.90 (1.07) | 0.57 (1.30) | 3.33 (4.27) | 2.07(2.90) | 119.13(191.27) |
| 4 | 1.40 (0.53) | 0.43 (0.27) | 0.60 (0.80) | 7.07 (5.97) | 43.63(11.37) |
| 5 | 3.70 (0.17) | 1.33 (0.23) | 1.87 (0.57) | 7.27(6.63) | 165.50(121.90) |
| 6 | 0.83 (0.73) | 0.83 (1.50) | 1.97 (1.27) | 4.17(5.03) | 67.80(94.97) |
| 7 | 0.87 (0.57) | 0.43 (0.50) | 2.43 (3.93) | 9.27(10.10) | 7.00(39.83) |
| 8 | 0.90 (0.73) | 0.47 (0.93) | 2.60 (3.30) | 8.40(12.60) | 46.27(66.80) |
| 9 | 2.27 (2.00) | 6.77 (2.07) | 2.27 (1.37) | 10.00(11.20) | 91.17(105.50) |
| 10 | 1.80 (1.30) | 1.53 (2.07) | 1.37 (0.97) | 10.97(9.57) | 132.03(128.43) |
| **SRM Recovery (%)** | 110 (111) | 100 (103 ) | 110 (106) | 84 (96) | 94 (99) |
| **INWQS (Class III)** | 14 | 12 | 2530 | 40 | 100 |

*in bracket is refer to value in June

The mean concentrations of metals in water are shown in Table 2. The range of metals during both month are Pb 0.37-2.37 ppb, As 0.27-12.60 ppb, Cu 0.23-3.27 ppb, Mn 7.00-383.83 and Cr 0.57-6.8 ppb, ppb respectively. As shown in Figure 2(a), the source of high concentration Pb in Station 5 on May was come from Hi-Clean Sewage Treatment Plant from nearest base camps which create wastewater into the stream [5]. Moreover, an illegal dumping waste directly into the river was found at this station.

The concentration of As in water ranged between 0.27-12.60 ppb as illustrated in Figure 2(b). The anthropogenic sources of high concentration of As at Station 8 is may come from wastewater discharged from factory producing mineral water and domestic wastes. However, As might occur naturally from the extensive evaporation of water due to high temperature and low rate of rain falls [12]. As in nonessential for plants but is an essential trace element in several animal species. Severe poisoning of As can arise from the ingestion of as little as 100 mg arsenic trioxide, chronic effects may result from the As compounds, in body at low intake levels. Carcinogenic properties also have been imputed to arsenic compounds depend on chemical forms [13].

The highest concentration of Cu in Station 9 as shown in Figure 2(c) is may come from the used Cu salts are in water supply system to controlled biological growth in reservoir and distribution pipe since this river is an important source of freshwater in Tasoh Dam [13]. Corrosion of copper that contain alloys in pipe fitting may introduce measureable amounts of Cu into water in pipe systems. Besides that, other possible sources of Cu is due to automobile activity such as the usage of copper in brake particles transportation in residential area [14].

Based on result in Table 2, the high level of Mn on May located at Station 2,3,5 and 10 as shown in Figure 2(d). Meanwhile on June, located at Station 3,5,9 and 10. River water at all of these stations were classified under Class III based on Interim National Water Quality Standard (INWQS) set by Department of Environment Malaysia due to the exceed limit of Mn in river water which is more than 100 ppb. The possible source of this highest concentration of Mn at Padang Besar area (Station 1-3) might come from industrial activities factories located at Padang Besar town such as textile, fiberglass, chemical, food and rubber made industry. The waste water from these industries was directly discharges into river [5]. There is no industrial activity reported at Wang Kelian area which is at Station 4-9 but extensive rubber and paddy cultivation as well as animal's livestock were reported at this area [5]. The used of fungicides and livestock feeding supplements in agricultural and livestock area may contain Mn compound could be the reason why Mn is exist in water bodies (WHO). Besides that, Mn may occur naturally in river since it's very essential for plants and animal growth but elevated Mn can give bad influence to those who consumed it [13].

Based on the Figure 2(e), highest concentration of Cr was found at Station 1 which is control area. This element can occur in natural water based on water hardness, the harder the water, the high level of Cr naturally exists in water. However, Cr is nonessential for plant but essential trace element for animals. Hexavalent of Cr such as $CrO_4^{2-}$, $Cr_2O_7^{2-}$ (absorbed by clay mineral) has been shown to be carcinogenic by inhalation and is corrosive to tissue [13]. In addition, based on INWQS the baseline value for Cr in water under Class III was 2530 ppb which is too high when compared with obtained result with the highest value was only 6.87 ppb recorded at Station 1.This can support that the existing Cr in water was come from natural sources.

The overall results obtained were compared with the Interim National Water Quality Standard for Malaysia set by DOE. The concentration of all metals remained below the permissible limit except for Mn which is above 100 ppb. These metal fall into Class III that is set by DOE which means an extensive treatment is required for the drinking water purposed as well as for fishery, livestock and drinking.

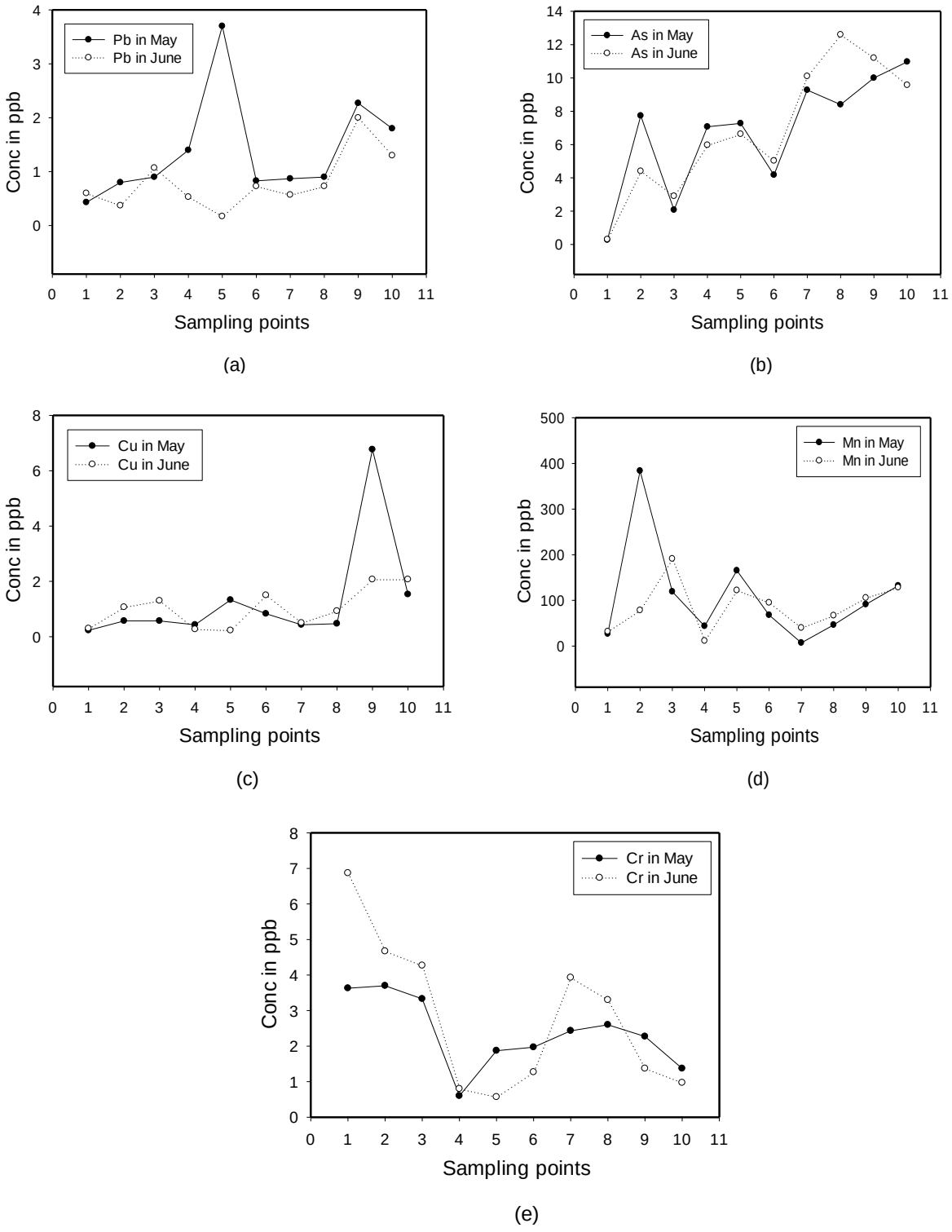



Figure 2: Distribution pattern of metals during May and June ; (a) lead , (b) arsenic, (c) copper, (d) manganese, (e) chromium

## Conclusion

From the result, the preliminary study of distribution pattern of metals was varied through rivers and Lake. This indicates that there is unregulated discharge of contaminated effluent into water bodies without earlier treatment by responsible industries and communities within the study area. Results of this study provide baseline data which can be used for expanding this research. For the future work, statistical analysis and geographical information system (GIS) will be use in determination the sources of heavy metal contents in water within different areas as well as for modelling metals concentration distribution pattern in large scale area.

## Acknowledgement

This study was funded by Dana Kecermelangan Pendidikan UiTM Perlis Fasa 1/2012 with the project code 600 UiTMPs/PJIM&A/ST/DKCP 5/5 (02/2012).

## References

1. Oyewale, A. O and Musa, I. (2006). Pollution assessment of the lower basin of Lakes Kainji/Jebba, Nigeria:heavy metal status of the waters, sediments and fishes. *Environ. Geochem. Health*, 28, 273-281.
2. Emoyam, O. O., Ogban, F. E., Akarah, E., (2006). Evaluation of Heavy Metals Loading of River Ijana in Ekpan – Warri, Nigeria. *J. Appl. Sci. Environ. Mgt. June*, 10 (2) 121 – 127.
3. Bhaskar, C. B., Kumar, K.., G. Nagendrappa. (2010) Assessment of Heavy Metals in Water Samples of Certain Locations Situated Around Tumkur, Karnataka, India.*E-Journal of Chemistry*, 7(2): 349 - 352
4. Kaushik, A., Kansal, A., Meena, A., Kumari, S., Kaushik, C. P. (2009). Heavy metal contamination of river Yamuna, Haryana, India: Assessment by Metal Enrichment Factor of the Sediments. *Journal of Hazardous Materials*, 164 265–270.
5. Kamarudzaman, A.N ., Feng, V. K.., Aziz, R. A., Jalil, M. F. (2011). Study of Point and Non Point Sources Pollution – A Case Study of Timah Tasoh Lake in Perlis, Malaysia**.** *International Conference on Environmental and Computer Science IPCBEE* ,19.
6. DOE., Malaysia Environmental Quality Report. (2006). Department of Environmental Ministry of Science, Technology and Environment Malaysia.
7. Sharma , R., Capoor, A. (2010). Seasonal Variations in Physical, Chemical and Biological Parameters of Lake Water of Patna Bird Sanctuary in Relation to Fish Productivity. *World Applied Sciences Journal*, 8 (1): 129-132.
8. Lutfor, A. K. M., Islam, M., Hossain, M. Z., Ahsan, M. A. ( 2012). Study of the Seasonal Variations in Trag River Water Quality Parameters. *African Journal of Pure and Applied Chemistry*,. 6(10) : 144-148.
9. Lawson, E. O. (2011). Physico-Chemical Parameters and Heavy Metal Contents of Water from the Mangrove Swamps of Lagos Lagoon, Lagos, Nigeria. *Advances in Biological Research*, 5 (1): 08-21.
10. Eisakhani, M., Malakahmad, A.( 2009). Water Quality Assessment of Bertam River and its Tributaries in Cameron Highlands, Malaysia.*World Applied Sciences Journal*, 7 (6) :769-776.
11. Chon, H. S., Ohandja D., Nikolaos, V. (2012). The Role of Sediments as a source of metals in River Catchments.*Chemosphere* 88(10):1250-6.
12. Jameel, B. A., Tasneem, K. G., Muhammad A. B., Hassan, A. H. (2009). Evalutation of arsenic and other physic-chemical parameters of surface and ground water of Jamshoro, Pakistan.*Journal of Hazardous Materials*, 166, 662-669.
13. APHA .(2000) Standard Methods for Examination of Water and Wastewater. 21st Edition. Washington, DC. American Public Health Association.
14. Davis, A.P., Shoukouhian, M., Ni, S. (2000). Loading estimates of lead, copper, cadmium and zinc in urban runoff from specific sources. *Chemosphere*, 44 :997-1009.

The Malaysian Journal of ANALYTICAL SCIENCES ISSN 1394-2506

# ANALYSIS AND POLLUTION ASSESSMENT OF HEAVY METAL IN SOIL, PERLIS

## (Analisis dan Penilaian Pencemaran Logam Berat dalam Tanah, Perlis)

Siti Norbaya Mat Ripin[1,2]*, Sharizal Hasan[2], Mohd Lias Kamal[2], NorShahrizan Mohd Hashim[3]

[1] *Faculty of Applied Sciences,*
*Universiti Teknologi MARA, Malaysia 40450 Shah Alam, Malaysia*
[2]*Faculty of Applied Sciences,*
[3]*Faculty of Architecture, Planning and Surveying,*
*Universiti Teknologi Mara Perlis, 02600 Arau Perlis, Malaysia*

**Corresponding author: norbaya24@gmail.com*

**Abstract**

Concentration of 5 heavy metals (Cu, Cr, Ni, Cd, Pb) were studied in the soils around Perlis, to assess heavy metals contamination distribution due to industrialization, urbanization and agricultural activities. Soil samples were collected at depth of 0-15cm in eighteen station around Perlis.The soil samples (2mm) were obtained duplicates and subjected to hotblock digestion and the concentration of total metal was determined via ICP-MS. Overall concentrations of Cu, Cr, Ni, Cd and Pb in the soil samples ranged from 0.38-240.59, 0.642-3.921, 0.689-2.398, 0-0.63 and 0.39-27.47 mg/kg respectively. The concentration of heavy metals in the soil display the following decreasing trend: Cu>Pb>Cr>Ni>Cd. From this result, found that level of heavy metal in soil near centralized Chuping industrial areas give maximum value compared with other location in Perlis. The Pollution index revealed that only 11% of Cu and 6% of Cd were classes as heavily contaminated. Meanwhile, Cu and Pb showed 6% from all samples result a moderately contaminated and the others element give low contamination. Results of combined heavy metal concentration and heavy metal assessment indicate that industrial activities and traffic emission represent most important sources for Cu, Cd and Pb whereas Cr, Ni mainly from natural sources. Increasing anthropogenic influences on the environment, especially pollution loadings, have caused negative changes in natural ecosystems and decreased biodiversity.

**Keywords**: Contamination, Heavy metals, Distribution, ICP-MS, Pollution index

**Abstrak**

Kepekatan 5 logam berat ( Cu , Cr , Ni, Cd, Pb ) telah dikaji dalam tanah di sekitar Perlis , untuk menilai taburan pencemaran logam berat akibat perindustrian , perbandaran dan aktiviti pertanian. Sampel tanah telah dikumpulkan pada kedalaman 0 -15cm dalam lapan belas stesen sekitar Perlis. Sampel tanah ( 2mm ) telah diperolehi dua salinan dan melalui kaedah penghadaman hotblock dan kepekatan jumlah logam ditentukan melalui ICP- MS. Kepekatan keseluruhan Cu , Cr , Ni , Cd dan Pb dalam sampel tanah masing-masing antara ,38-240,59 , 0,642-3,921 , 0,689-2,398 , 0-0,63 dan 0,39-27,47 mg / kg. Kepekatan logam berat dalam tanah mengikut urutan menurun adalah : Cu > Pb > Cr > Ni > Cd. Daripada keputusan ini, didapati bahawa tahap logam berat dalam tanah berhampiran kawasan perindustrian Chuping berpusat memberi nilai maksimum berbanding lokasi lain di Perlis. Indeks Pencemaran mendedahkan bahawa hanya 11% Cu dan 6 % daripada Cd berada dalam kelas sebagai banyak tercemar. Sementara itu, Cu dan Pb menunjukkan 6 % daripada semua sampel dalam kelas sederhana tercemar dan logam berat lain menunjukkan pencemaran yang rendah. Gabungan keputusan antara logam berat dan penilaian logam berat menunjukkan bahawa aktiviti perindustrian dan pelepasan trafik mewakili sumber yang paling penting bagi Cu, Cd dan Pb manakala Cr dan Ni terhasil daripada sumber semula jadi . Peningkatan pengaruh antropogenik kepada alam sekitar, telah menyebabkan perubahan negatif dalam ekosistem semula jadi dan menurunkan biodiversiti Malaysia.

**Kata kunci:** Pencemaran, Logam berat, Taburan, ICP-MS, Indeks pencemaran

## Introduction

Heavy metals contamination of soils becomes a severe issue around the world as a result of anthropogenic activities that been emitted into atmosphere as aerosols and distributed in soil [1, 2, 3, 4]. They are distributed by atmosphere

within a distance and transported up to several kilometers away from their sources and transferred to the soil through wet or dry deposition [1, 5].

Heavy metals in soils have been considered as powerful tracers for monitoring impact of anthropogenic activity such as industrial emission (cement plant, fossil fuel and coal combustion chemical plants), vehicular emission, and atmospheric deposited. These lead to emission of heavy metals into the air and their subsequent deposition into soils [6, 7, 1]. Heavy metal is the most dangerous pollutant of anthropogenic environmental pollutants due to their toxicity and persistence in the environment [6, 8].

Past studies have revealed that human exposure to high concentrations of heavy metals will lead to their accumulation in the human body [9]. Heavy metal exposure to human occurs through three primary routes namely inhalation, ingestion and skin absorption. The threat that heavy metals pose to human and animal health is aggravated by their low environmental mobility, even under high precipitations, and their long term persistence in the environment [10]. Rising metal concentration in soil is serious and current concern for governmental and regulatory bodies for environmental and human risk assessment [11]. Therefore, the use of simple and accurate methods for monitoring heavy metals has a great importance among the environmental studies [12]. The assessment of heavy metal contamination can be conducted using various methods such as total heavy metal concentration [4]. The present study assessed heavy metal pollution in soils employing Pollution index (PI).

In this study, determination of total concentrations of heavy metal in soil was carried out around Perlis. Based on the result, heavy metal assessment index (Pollution Index) was calculated. The result can then be used as a basis for improving the situation and guide environmental planners and government in reducing pollution in Malaysia.

## Materials and Methods

### Study Area

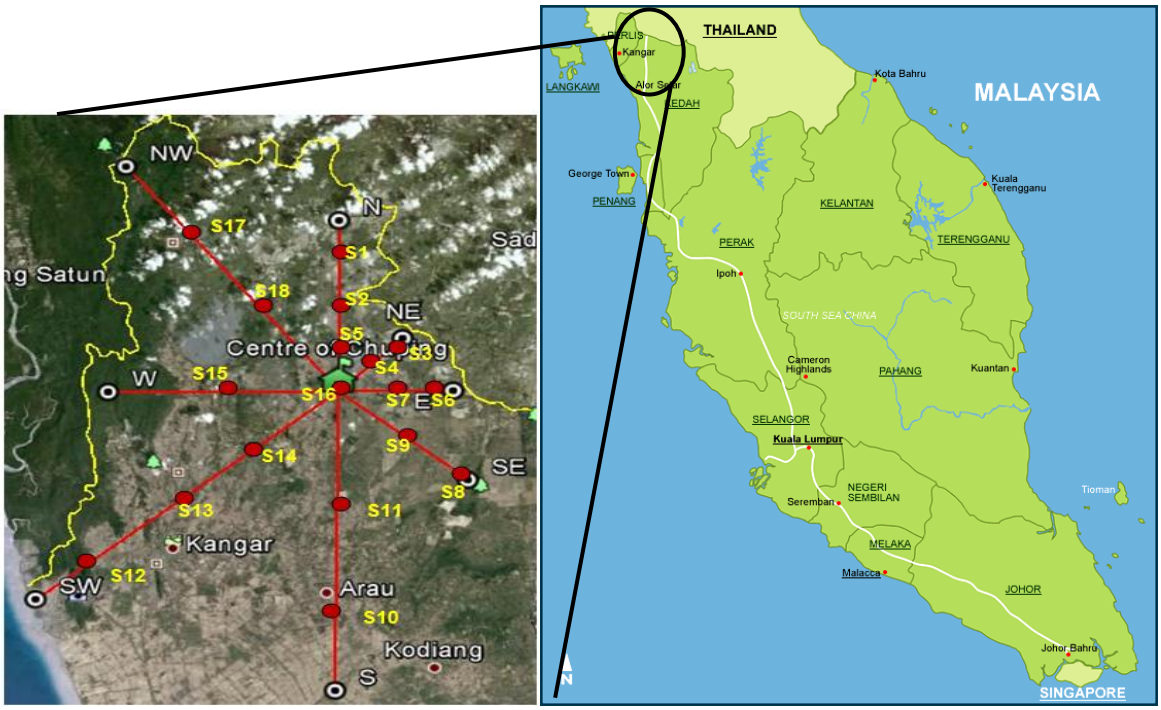



Figure 1: Location sampling site of soil

The study of heavy metal concentration has been performed in the whole Perlis state with 8 directions and Chuping as a centre according to GPS coordination as shown in Table 1. This area undergo various anthropogenic activities such as cement, chemical, quarry, power plant, transportation and agriculture activities that might contribute to heavy metal contamination. Figure 1 show a map of sampling points in the study area.

Table 1: Coordination of Sampling Site

| **Station Code** | **Location** | **Coordinates** |
|---|---|---|
| S1 | 12KM N | N 6°38’ 50.5” E 100°17’ 37.8” |
| S2 | 6KM N | N 6°35’ 57.3” E 100°17’ 34.3” |
| S3 | 10KM NE | N 6°36’ 42.3” E 100°17’ 35” |
| S4 | 5.4KM NE | N 6°34’ 39.6” E 100°16’ 31.2” |
| S5 | 2KM N | N 6°33’ 27.9” E 100°18’ 15.5” |
| S6 | 7KM E | N 6°32’ 39.2” E 100°21’ 11” |
| S7 | 4KM E | N 6°32’ 40.5” E 100°19’ 37.5” |
| S8 | 10KM SE | N 6°29’ 15.5” E 100°19’ 32.3” |
| S9 | 5KM SE | N 6°30’ 51.5” E 100°19’ 35.7” |
| S10 | 20KM S | N 6°27’ 13.1” E 100°17’ 18.5” |
| S11 | 10KM S | N 6°27’ 10.4” E 100°16’ 31.4” |
| S12 | 25KM SW | N 6°21’ 33.4” E 100°8’ 52” |
| S13 | 20KM SW | N 6°23’ 57.2” E 100°10’ 49.7” |
| S14 | 10KM SW | N 6°28’ 12.2” E 100°14’ 44.8” |
| S15 | 7KM W | N 6°32’ 47.4” E 100°13’ 41.5” |
| S16 | CENTER CHUPING | N 6°32’ 40.9” E 100°17’ 45” |
| S17 | 20KM NW | N 6°40’ 59.5” E 100°11’ 17.5” |
| S18 | 10KM NW | N 6°37’ 00.5” E 100°14’ 13.2” |

**Soil sampling and chemical analysis**

A total 18 samples were collected at depth of 0-15cm using hand auger, stored in polyethylene bags and were oven dried at 60°C for 2days, followed by grinding with mortar and pestle and sieved using a 2 mm sieve. The soil samples were digested with the mixture of $HNO_3$ and $H_2O_2$ using EPA method 3050B [13]. The solution obtained was filtered through a 0.45µm cellulose membrane filter and diluted to 10mL with miliQ water then stored at 4° before analysis. Concentration of in the digestion solution was determined by inductively couple plasma mass spectroscopy (ICP-MS). Analysis of the samples including soils digests and blanks was set up in duplicates.

**Heavy metal pollution assessment**

To assess contamination level of heavy metals, a pollution index (PI) of each metal was attributed to each metal using Equation 1 [14] below:

$$PI = C_n / B_n \quad (1)$$

where Cn (mg/kg) is the measured concentration of each heavy metal and Bn is background value for each metal. The PI of each metal was classified as either low ($P \leq 1$), moderate ($1 < PI \leq 3$) or high contamination ($PI > 3$).

## Results and Discussion

### Heavy metal in soil

The concentration of heavy metals in the soil of Perlis is listed in Table 2. All data in Table 2 were compared with allowable limit from Netherlands and China (Table 3) proposed by (Wang et al 2012, ECDGE 2010) since there are no information available in Malaysia on soil background values for heavy metal concentration [15, 16, 17]. The maximum concentration of Cu (240.59 mg/kg) and Cd (0.63mg/kg) level were higher compared with limit from Netherlands and China. Thus, attention has to be taken in order to control the level because it may results a dangerous effect for future. Meanwhile, Pb, Cr and Ni relatively below limit from other country (Table 3). Thus, we can summarized that, most of the Perlis state is still in save level, except on certain location that contribute high value of Cu and Cd which exceed allowable limit.

The result showed that all 5 elements (Cu, Pb, Cr, Ni, Cd) were highly distributed on centralized of sampling location which is on Station 2,4,5,7 and 16. This centralized area was located near the Chuping industrial area and near major road that loads a heavy traffic. Cu generally has the highest value while Cd generally has the least and the order observed for this study is Cu>Pb>Cr>Ni>Cd. The high concentration of copper was obtained at Station 2, 7 and 16 with 240.59, 110.25 and 33.46 mg/kg respectively. Cr was high at Station 4 and 5 with 3.92 and 2.69 mg/kg respectively. Meanwhile, high concentration of Ni were recorded at Station 5 (2.40 mg/kg) and 2 (2.08 mg/kg). Pb and Cd high at Station 16 with 27.47 mg/kg and 0.63 mg/kg respectively. According to previous report found that, heavy metal emit from cement industry which undergo process and production require energy from burning fossil fuel [5,18, 19] and vehicle emission [5, 6, 20]. This activity considered as major emission sources in atmosphere and soil [6, 18].

Table 2: Heavy metal concentration in soil (mg/kg)

| Sample No. | Heavy metal concentration (mg/kg) | | | | |
|---|---|---|---|---|---|
| | Cu | Pb | Cd | Cr | Ni |
| S1 | 3.58 | 0.68 | 0.02 | 1.05 | 1.98 |
| S2 | 240.59 | 0.82 | 0.02 | 1.05 | 2.08 |
| S3 | 1.16 | 0.88 | 0.02 | 2.01 | 1.62 |
| S4 | 0.38 | 0.66 | 0.05 | 3.92 | 1.09 |
| S5 | 1.82 | 1.74 | 0.08 | 2.69 | 2.40 |
| S6 | 0.71 | 0.79 | 0.02 | 0.74 | 0.69 |
| S7 | 110.25 | 2.37 | 0.02 | 1.32 | 1.59 |
| S8 | 0.66 | 0.39 | 0.02 | 1.28 | 1.29 |
| S9 | 0.52 | 0.44 | ND | 0.95 | 1.03 |
| S10 | 1.18 | 1.10 | 0.02 | 1.58 | 1.72 |
| S11 | 0.53 | 0.7 | 0.01 | 0.83 | 2.09 |
| S12 | 1.82 | 1.75 | 0.06 | 1.63 | 2.22 |
| S13 | 0.89 | 1.22 | 0.03 | 1.36 | 1.75 |
| S14 | 2.91 | 0.80 | 0.03 | 0.91 | 1.37 |
| S15 | 0.98 | 0.76 | 0.02 | 1.35 | 0.82 |
| S16 | 33.46 | 27.47 | 0.63 | 1.38 | 1.54 |
| S17 | 1.16 | 1.00 | 0.02 | 0.64 | 1.33 |
| S18 | 0.86 | 2.90 | 0.06 | 0.93 | 1.72 |
| Max | 240.59 | 27.47 | 0.63 | 3.92 | 2.40 |
| Min | 0.38 | 0.39 | 0.01 | 0.64 | 0.69 |
| SD | 60.46 | 6.25 | 0.14 | 0.85 | 0.48 |

ND – no data (heavy metal not detected)

Besides that, some element elevated on opposite side of centralized stations such as Ni at station 11 (2.09 mg/kg) and station 12 (2.22 mg/kg). Station 12 located near power plants at Kuala Perlis that having high traffic density from that plant. In addition, ferry transportation at station 12 also gives contribution in elevated of Ni. As reported by A. Mandal et al., [5] heavy vehicular give large contribution through traffic emission. But Ni are mainly originated from natural sources, thus the concentration not greatly vary from each station [7]. Thus from the overall result, we can state that contamination level in Perlis is still in control level, just on certain location that located near industrial areas and major road that produce high level of heavy metal. For further view on contamination level in this study area, heavy metal assessment index will be carried out and explain further detail below.

Table 3: Allowable limits of heavy metal concentrations in soil (mg/kg).

| Heavy metal | Netherlands[b] | Environmental Quality Std of Soils GB15618-1995[a] | This study |
|---|---|---|---|
| Cu | 0.5 | 0.6 | 0.63 |
| Pb | 40 | 100 | 240.59 |
| Cd | 40 | 350 | 27.47 |
| Cr | 15 | 60 | 2.40 |
| Ni | 30 | 250 | 3.92 |

[a] Wang et al. 2012, [b]ECDGE 2010

**Heavy metal assessment**

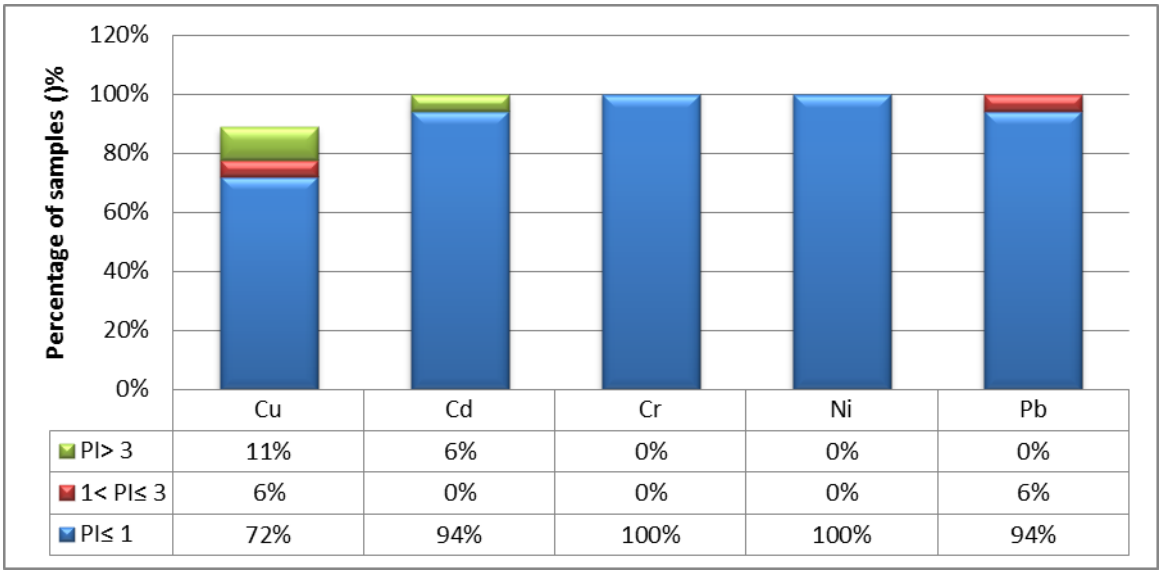
The concentration of heavy metal in soil in each station influence by various sources such as anthropogenic and naturally. Thus, a pollution index (PI) was applied to the data set to discover possible sources that might influence different distribution of elements over study area around Perlis state. The Pollution index calculated relative to the background values of heavy metals in the soils and the result as shown in Table 4.

High PI values (higher than 3) were observed in 11% of the samples for Cu, 6% for Cd (Fig 2). These indicate that Cu and Cd pollution relatively serious in Perlis soil when compare with other elements. The PI values higher generally in centralized station which is at station 2,4,5,7 and 16 where there are heavy traffic and many industrial activities than in other districts, indicating the presence of serious heavy metal pollution [21,22]. Therefore, highly contaminated samples clearly been polluted by anthropogenic emission [7]. The PI value of Cu, Pb, Cd, Cr, and Ni ranged from 0.01 to 9.01, 0.02 to 1.4, 0 to 5.25, 0.01 to 0.08 and 0.03 to 0.09 respectively. For Pb about 6% are classified as moderately or heavily contaminated (Fig 2) indicating there is potential the area been polluted by Pb if no remediation effort been implement. Besides that, Cr and Ni are 100% at low contamination level (Fig 2) indicating no obvious pollution for Cr and Ni. From figure 2, generally majority of study area is still in secure state where more than 70% of all study area for each elements give PI$\leq$ 1 indicate low contamination. Meanwhile, less than 15% of Cu, Pb and Cd give moderately and high contamination level.

Table 4: Heavy metal concentrations (mg/kg) Pollution index (PI) of soil

| Heavy metal | No. of samples | Background values[a] | Concentration | | | Pollution index values | | |
|---|---|---|---|---|---|---|---|---|
| | | | Min | Max | Mean | Min | Max | Mean |
| Cu | 18 | 26.7 | 0.38 | 240.59 | 22.42 | 0.01 | 9.01 | 0.84 |
| Pb | 18 | 19.4 | 0.39 | 27.47 | 2.58 | 0.02 | 1.40 | 0.13 |
| Cd | 18 | 0.12 | ND | 0.63 | 0.06 | ND | 5.25 | 0.52 |
| Cr | 18 | 49.3 | 0.64 | 3.92 | 1.43 | 0.01 | 0.08 | 0.03 |
| Ni | 18 | 26.6 | 0.69 | 2.40 | 1.57 | 0.03 | 0.09 | 0.06 |

ND – not detected, [a]CNEMC,1990[23]




| | Cu | Cd | Cr | Ni | Pb |
|---|---|---|---|---|---|
| PI> 3 | 11% | 6% | 0% | 0% | 0% |
| 1< PI≤ 3 | 6% | 0% | 0% | 0% | 6% |
| PI≤ 1 | 72% | 94% | 100% | 100% | 94% |

Figure 2: Heavy metal percentage based on Pollution index.

## Conclusion

Eighteen soil samples collected from whole Perlis state were analyzed for Cu, Cr, Ni, Cd and Pb. Cr, Ni and Pb concentrations in soil were lower than allowable limit, whereas Cu and Cd concentration exceeded their corresponding values. Heavy metal concentrations were assessed using pollution index (PI). In respect of Pollution index only Cu (11%) and Cd (6%) were classes as heavily contaminated. Meanwhile, Cu and Pb showed 6% from all station result a moderately contaminated and the others element give low contamination. From this result, found that level of heavy metal in soil near centralized Chuping industrial areas give maximum value compared with other location in Perlis. Results of combined heavy metal concentration and heavy metal assessment indicate that industrial activities and traffic emission represent most important sources for Cu, Cd and Pb whereas Cr, Ni mainly from natural sources. Increasing anthropogenic influences on the environment, especially pollution loadings, have caused negative changes in natural ecosystems, decreased biodiversity, simplified structure and lowered productivity. Consequently, it is imperative to continually assess and monitor the levels of heavy metals in the environment due to anthropogenic activities for evaluation of human exposure and for sustainable environment.

## Acknowledgement

We would like to thank to Faculty of Applied Sciences, Universiti Teknologi MARA and Dana Kecemerlangan (600-UiTMPs/PJIM&A/ST/DKCP 5/3 (03/2012)) for financing this study.

## References

1. Soriano, A., Pallarés, S., Pardo, F., Vicente, A.B., Sanfeliu, T. & Bech, J. (2012).Deposition of heavy metals from particulate settleable matter in soils of an industrialised area. *Journal of Geochemical Exploration*, 113: 36-44.
2. Hernandez-Soriano, M.C. & Jimenez-Lopez, J.C. (2012). Effects of soil water content and organic matter addition on the speciation and bioavailability of heavy metals. *Science of the Total Environment*, 423: 55–61.
3. Zeng, F., Ali, S., Zhang, H., Ouyang, Y., Qiu, B., Wu, F. & Zhang, G. (2011). The influence of pH and organic matter content in paddy soil on heavy metal availability and their uptake by rice plants. *Environmental Pollution*, 159: 84-91.
4. Zhao, H., Xia, B., Fan, C., Zhao, P. & Shen,S. (2012). Human health risk from soil heavy metal contamination under different land uses near Dabaoshan Mine, Southern China. *Science of the Total Environment*, 417–418:45–54.

5. Mandal, A. & Voutchkov, M. (2011). Heavy metals in soils around the Cement Factory in Rockfort, Kingston, Jamaica. *International Journal of Geosciences*, 2:48-54.
6. Guo, G., Wu, F., Xie, F. & Zhang, R. (2012).Spatial distribution and pollution assessment of heavy metals in urban soils from southwest China. *Journal of Environmental Sciences*, 24(3): 410–418.
7. Lu, A., Wang, J., Qin, X., Wang, K., Han, P. & Zhang, S. (2012). Multivariate and geostatistical analyses of the spatial distribution and origin of heavy metals in the agricultural soils in Shunyi, Beijing, China. *Science of the Total Environment*, 425: 66–74.
8. Koz, B., Cevik, U. & Akbulut, S. (2012). Heavy metal analysis around Murgul (Artvin) copper mining area of Turkey using moss and soil. *Ecological Indicators*,20: 17–23.
9. Lee, C.S., Li, X., Shi, W., Cheung, S.C. & Thornton, I. (2006). Metal contamination in urban, suburban, and country park soils of Hong Kong: A study based on GIS and multivariate statistics. *Science of the Total Environment*, 356: 45-61.
10. Adelekan B. A & Abegunde. K. D. (2011). Heavy metals contamination of soil and groundwater at automobile mechanic villages in Ibadan, Nigeria. *International Journal of the Physical Sciences* 6(5): 1045-1058.
11. Maas, S., Scheifler, R., Benslama, M., Crini, N., Lucot, E., Brahmia, Z., Benyacoub, S. & Giraudoux,P. (2010). Spatial distribution of heavy metal concentrations in urban, suburban and agricultural soils in a Mediterranean city of Algeria. *Environmental Pollution*, 158: 2294-2301.
12. Guven, D.E. & Akinci, G. (2011). Comparison of acid digestion techniques to determine heavy metals in sediment and soil samples. *Gazi University Journal of Science*, 24 (1): 29-34.
13. E. Lutz & M. I. Thompson (2012). Hot block digestion of soil, sediment, waste, and tissue samples for total recoverable Metals, 2012.
14. Wei, B., Jiang, F., Li, X. & Mu, S. (2009). Spatial distribution and contamination assessment of heavy metals in urban road dusts from Urumqi, NW China. *Microchemical Journal*, 93:147–152.
15. Fong, F.T., Chee, P.S., Mahmood, A.A. & Tahir, N.M.(2008). Possible source and pattern distribution of heavy metals content in urban soil at Kuala Terengganu Town Center. *The Malaysian Journal of Analytical Sciences*, 12 (2): 458-467.
16. European Commission Director General Environment, ECDGE (2010). Heavy Metals and Organic Compounds from Wastes Used as Organic Fertilizers. Final Rep., July. WPA Consulting Engineers Inc. Ref. Nr. TEND/AML/2001/07/20, pp. 73-74.http://ec.europa.eu/environment/waste/compost/pdf/hm_finalreport.pdf
17. Wang, M., Bai, Y., Chen, W., Markert, B., Peng, C. & Ouyang, Z. (2012). A GIS technology based potential eco-risk assessment of metals in urban soils in Beijing, China. *Environmental Pollution*, 161: 235-242.
18. Martley, E., Gulson, B.L. & Pfeifer, H.R. (2004). Metal concentrations in soils around the copper smelter and surrounding industrial complex of Port Kembla, NSW, Australia. *Science of the Total Environment*, 325: 113-127.
19. Li, X. & Feng, L. (2012). Multivariate and geostatistical analyzes of metals in urban soil of Weinan industrial areas, Northwest of China. *Atmospheric Environment*, 47: 58-65.
20. Cai, L., Xu, Z., Ren, M., Guo, Q., Hua, X., Hua, G., Wand, H. & Peng, P.(2012). Source identification of eight hazardous heavy metals in agricultural soils of Huizhou, Guangdong Province, China. *Ecotoxicology and Environmental Safety*,78: 2–8.
21. Yang, Z., Lu, W., Long, Y., Bao, X. & Yang, Q. (2011). Assessment of heavy metals contamination in urban topsoil from Changchun City, China. *Journal of Geochemical Exploration*, 108: 27–38.
22. Wang, Y., Qiao, M., Liu, Y. & Zhu, Y.(2012). Health risk assessment of heavy metals in soils and vegetables from wastewater irrigated area, Beijing-Tianjin city cluster, China. *Journal of Environmental Sciences*, 24(4): 690–698.
23. CNEMC (China National Environmental Monitoring Centre) (1990), The background values of Chinese soils, Environmental Science Press of China, Beijing.

The Malaysian Journal of ANALYTICAL SCIENCES ISSN 1394-2506

# SEASONAL VARIATION OF GRAIN SIZE AND HEAVY METALS CONCENTRATION IN SEDIMENT OF SUNGAI PERLIS

## (Variasi Musim Saiz Zarah Dan Kepekatan Logam Berat Di Dalam Sedimen, Sungai Perlis)

Hanif. H. F[1]*., Jamil, T.[1], Lias, K[2]., and Norsila, D[1].

[1]*Marine Technology Program,*
[2]*Applied Chemistry Program*
*Faculty of Applied Science*
*Universiti Teknologi MARA (Perlis), 02600 Arau, Perlis, Malaysia*

**Corresponding author: hanifharif@yahoo.com*

**Abstract**

Heavy metals concentration (As, Co, Cu, Pb, Zn, Cr) and grain size analysis were determined in sediment collected from Sungai Perlis during Southwest and Northeast monsoon. Ten sampling areas of the Sungai Perlis were selected based upon anthropogenic activities which resulted in elevated metals load into the river. Heavy metals concentration in the sediments show average decreasing trend of Zn>Cr>Pb>Cu>As>Co during Southwest monsoon and Cr>Zn>Pb>As>Cu>Co on Northeast monsoon which can be related by the impact of the anthropogenic activities. Most of the sampling areas were dominated by silt sediments while sand and clay sediment were poorly present. Result of grain size showed that the average mean size, sorting and skewness are 7.32 ± 0.44 phi, 1.55 ± 0.14 phi and -0.16 ± 0.19 phi for Southwest monsoon and 7.14 ± 0.27 phi, 1.56 ± 0.12 phi and -0.08 ± 0.17 phi during Northeast monsoon. The analysis of heavy metals and grain size fractions of sediments indicated that the distributions of metals and grain size in upstream and downstream river sediments were affected by monsoon seasons.

**Keywords**: grain size, metals, sediment, Sungai Perlis, seasonal variation

**Abstrak**

Kepekatan logam berat (As, Co, Cu, Pb, Zn, Cr) dan saiz zarah telah ditentukan di dalam sedimen yang diperolehi daripada kuala Sungai Perlis ketika musim monsun barat daya dan timur laut. Sepuluh kawasan telah ditentukan di kuala Sungai Perlis berdasarkan aktiviti manusia yang akan menyumbang kepada kepekatan logam berat di dalam sungai. Kepekatan logam berat di dalam sungai menunjukkan gaya penurunan Zn>Cr>Pb>Cu>As>Co ketika musim monsun barat daya dan Cr>Zn>Pb>As>Cu>Co ketika musim monsun timur laut di mana ia mungkin dipengaruhi oleh aktiviti manusia. Kebanyakan kawasan sampel diambil menunjukkan dominasi lumpur yang halus tetapi pasir jarang sekali dijumpai. Keputusan saiz zarah menunjukkan purata nilai min, susunan dan skewness adalah 7.32 ± 0.44 pai, 1.55 ± 0.14 pai dan -0.16 ± 0.19 pai untuk monsun barat daya dan 7.14 ± 0.27 pai, 1.56 ± 0.12 pai dan -0.08 ± 0.17 pai ketika musim monsun timur laut. Keputusan analisis logam berat dan saiz zarah di dalam sedimen menunjukkan taburan logam dan saiz zarah di muara sungai adalah dipengaruhi oleh musim monsun.

**Kata kunci:** saiz zarah, logam berat, sedimen, Sungai Perlis, variasi musim

## Introduction

The increasing growth of human population has lead to the land development alongside of the river basin. Most of the rivers which were affected by the industrialization and urbanization become the end point where all of the effluents are discharge directly from the factories and municipal waste. This phenomenon gives stress to aquatic ecosystem which soon giving rise to water pollution and environmental deterioration. Pollutant such as heavy metals usually being carried by the runoff from the primary sources and spread to other part of the aquatic ecosystem [1].

Elemental concentrations in sediments were not only depending by natural and anthropogenic sources but also upon the organic matter content, mineralogical composition and textural characteristic of the sediment [2]. Heavy metals are usually enriched in the smaller grain size fractions [3]. Smaller particles have a large surface area over volume ratio which is associate to co-precipitation and complexation of metals on particles surfaces. Thus, the adsorption process of metals are higher in fine grain size which result in high metals concentration [4].

There is not much data available on the heavy metals and grain size analysis in the sediment in North Western Part of Peninsular Malaysia especially in Sungai Perlis area. Contamination from anthropogenic sources such as domestic sewage, boat activities, agriculture and aquaculture run off can possess a serious threat to the food chain system in aquatic environment. Moreover, bioavailability of metals in sediment can be influenced by several factors including sediment characteristics such as grain size distribution, mineral composition and organic content [5].

Comparison of heavy metals distribution with grain size allowed the identification of the area where the sediment fine fraction appears affected by heavy metal anthropogenic contamination [6]. Therefore, it is important to study the distribution of the potentially toxic metals and its factors that can contribute to the increasing load of metals in the sediment. This research was carried out to illustrate the distribution of selected heavy metals (Co, Cu, Zn, Pb, As and Cr) and grain size distribution in Sungai Perlis during Southwest and Northeast monsoon seasons.

## Materials and Methods

### Sampling Areas and Sample Collection

Sampling was carried out in Sungai Perlis in Perlis which is located at the Northern West of Peninsular Malaysia. The location of Kuala Perlis Jetty at the edge of ocean plays an important role in attracting local people and tourist since it is one of the gateway to the Langkawi Island. This hectic river also serves as fish landing sites and anchorage for hundreds of fishing boats mainly at the upstream of river. Furthermore, there are various sources of effluent being dump straight to the river such as runoff from urban areas, agriculture and aquaculture practice and municipal waste. Generally, the river basin is approximately 310 km with the length is about 11 km which is connected from Kangar city to Kuala Perlis.

Samples were collected during Southwest and Northeast Monsoon season. Ten sampling stations were chose based upon the anthropogenic sources nearby the location. Figure 1 shows the location of the ten sampling stations and Table 1 are coordinates of each sampling station which were determined by using the Global Positioning System (GPS) device. The surface of sediments in each station was collected by using Van Veen Grab. Sediment samples were placed in clean Polypropylene (PP) plastic bags all samples were properly labeled to avoid any cross contamination.

### Heavy Metals Analysis

The samples were dried in oven at 80˚C and grounded by using mortar and pestle. Then the samples were sieved through a 63 µm mesh size. For the analysis of total heavy metals, sediment samples were digested by following the published methods with some modifications [7, 8]. Before digestion, fine powdered samples were heat to get a constant weight. After that, a mixed acid solution (concentrated HF, $HNO_3$ and HCl) was added into the Teflon vessel along with the samples and heated at 150˚C. After cooling, a mixed solution of EDTA and boric acid were added and once again the vessel was heated in the oven 150˚C. After cooling, the digested samples were transferred into a clean polypropylene test tube and analysis using inductively-coupled plasma mass spectrometer (ICP-MS).

### Grain Size Analysis

Mean, sorting and skewness in sediment samples were determined by using laser diffraction method. Firstly, all carbonates were dissolved by using 4 M Hydrochloric acid solution (HCl). Then the organic components from sediment samples were removed by adding 50% hydrogen peroxide ($H_2O_2$). Subsequently, the flocs of finer particles were break up by adding a dispersing agent (5% calgon solution). Then, the samples were analyzed by using Particle Size Analyzer (PSA) system. Percentage of silt, clay and sand were calculated to determine the texture of sediment using classification standard proposed by Nichols and Biggs (1985) [9].

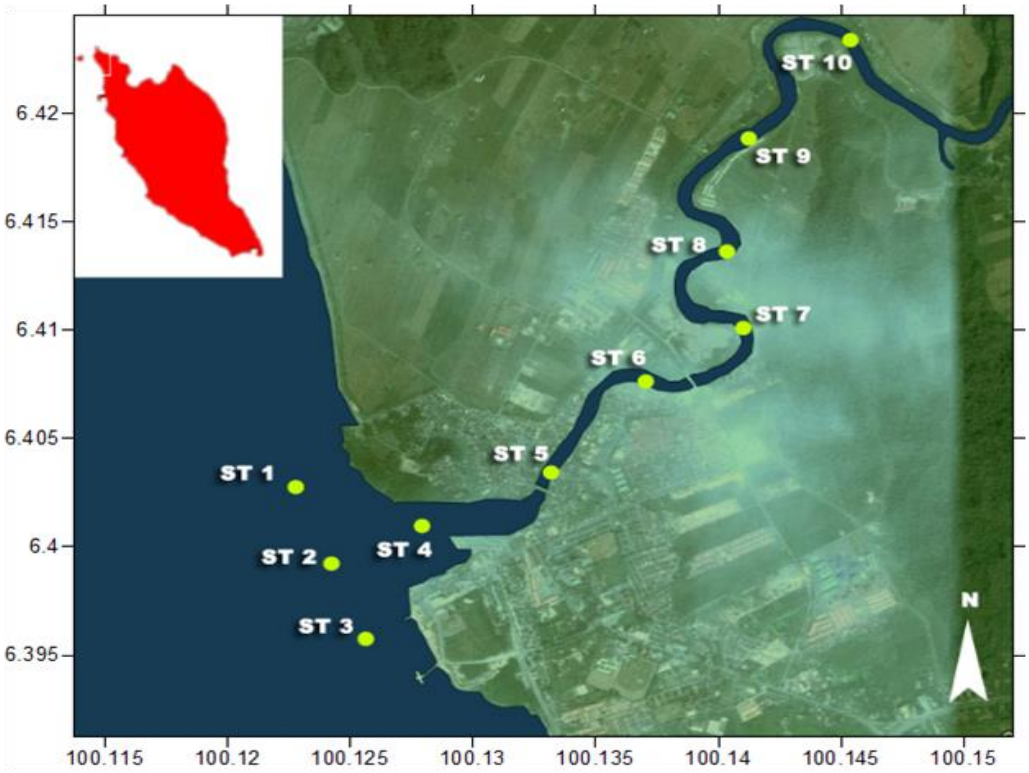



Figure 1: Sampling areas in Sungai Perlis

Table 1: The coordinates for each sampling station

| Station | Latitude | Longitude |
|---|---|---|
| 1 | 6°24'27.72"N | 100° 6'56.46"E |
| 2 | 6°24'2.04"N | 100° 7'6.72"E |
| 3 | 6°23'42.00"N | 100° 7'20.22"E |
| 4 | 6°24'1.62"N | 100° 7'34.92"E |
| 5 | 6°24'10.68"N | 100° 7'58.44"E |
| 6 | 6°24'26.22"N | 100° 8'15.30"E |
| 7 | 6°24'38.10"N | 100° 8'22.02"E |
| 8 | 6°24'53.70"N | 100° 8'22.32"E |
| 9 | 6°25'7.20"N | 100° 8'27.72"E |
| 10 | 6°25'26.10"N | 100° 8'34.08"E |

## Results and Discussion

### Sediment Grain Size

Characteristics of sediment such as mean size, sorting and skewness are given in Table 2. Current and seasonal changes tend to affect the distribution of sediment characteristics in Sungai Perlis. The sampling points extend from downstream to upstream river which cover approximately 7 km of the river. Since the study areas were affected by several human activities such as boating and land reclamation, sediment composition and grain size may fluctuate overtime. Thus, grain size analysis may indicate the impact of different activities to the sediment in the aquatic environment [11].

Table 2: Characteristics of sediments during Southwest and Northeast Monsoon seasons

| Stations | Southwest Monsoon | | | Northeast Monsoon | | |
|---|---|---|---|---|---|---|
| | Mean | Sorting | Skewness | Mean | Sorting | Skewness |
| 1 | 7.04 | 1.79 | 0.02 | 6.70 | 1.77 | -0.07 |
| 2 | 7.27 | 1.59 | -0.29 | 6.84 | 1.63 | -0.04 |
| 3 | 8.50 | 1.37 | -0.43 | 6.94 | 1.57 | 0.05 |
| 4 | 7.16 | 1.56 | -0.21 | 6.99 | 1.53 | -0.04 |
| 5 | 7.27 | 1.54 | -0.37 | 7.18 | 1.54 | -0.07 |
| 6 | 7.32 | 1.53 | -0.19 | 7.48 | 1.31 | 0.08 |
| 7 | 7.27 | 1.43 | 0.02 | 7.29 | 1.57 | -0.39 |
| 8 | 7.21 | 1.45 | -0.14 | 7.14 | 1.69 | -0.37 |
| 9 | 7.34 | 1.78 | -0.19 | 7.39 | 1.46 | 0.02 |
| 10 | 6.86 | 1.45 | 0.19 | 7.48 | 1.52 | 0.00 |
| Average | 7.32 | 1.55 | -0.16 | 7.14 | 1.56 | -0.08 |
| Std Dev | 0.44 | 0.14 | 0.19 | 0.27 | 0.12 | 0.17 |
| Classification | Fine silt | Poorly soorted | Symmetrical | Fine Silt | Poorly sorted | Symmetrical |

The average mean size of sediment along Sungai Perlis during Southwest (SW) and Northeast (NE) monsoons was 7.32 ± 0.44 phi and 7.14 ± 0.27 phi, classified as fine silt for both season. The dominating of high percentage of fine silt may result from the low velocity depositional in the river [12]. Apparently, the mean size reach a maximum value of 8.50 phi (Station 3) and minimum value at Station 10 (6.86 phi) during SW monsoon. However, during NE monsoon, maximum value was obtained at Station 6 and Station 10 (7.48 phi) and the minimum value is 6.70 phi at Station 1. SW monsoon which characterized by strong wind mainly affect the western coastal which can be explained by the difference on the mean size on both season. Generally the mean size gives a simple indication of the magnitude of the force, applied by water or wind which will affect the mean size of the grains [13].

Most of sampling sites during these two seasons were poorly sorted which also indicate that little selection of grains size had taken place during transport or deposition. The fluctuation of sorting values on each sampling sites reflected the unstable condition of the environment in the estuary which may be due to human activities and natural constituent [6].

The skewness of Sungai Perlis sediment reach a maximum value of 0.19 phi at Station 10 during SW monsoon and a minimum value at Station 3 (-0.43 phi). About 60% of the samples were negatively skewed (i.e. coarsely skewed), while 40% of the sediments were positively skewed (i.e. finely skewed) during NE monsoon. Based on Table 2, the average skewness during NE monsoon show negatively skewed data compare to SW monsoon but still this two seasons indicate symmetrical skewness which could probably be associated with sediments erosion in environments dominated by strong current actions. Some of sampling sites on both seasons show tendency for sediment to become coarser, due to increasing transport capacity and current within the river [12].

Accordingly, SW monsoon had finely silt compare to NE monsoon which explain the role of the wind on the distribution patterns of sediments in the study area. Besides, influence from natural activities (i.e. transport capacity and current) and human activities (boating and land reclaimation) around the study area might be effected the distribution pattern of sediment in the study area.

**Heavy Metals Analysis**

The concentrations of heavy metals in sediment of Sungai Perlis estuary during Southwest (SW) and Northeast (NE) monsoon are shown in Table 2. Heavy metals concentration in the sediments show average decreasing trend of Zn>Cr>Pb>Cu>As>Co during SW monsoon and Pb>Cr>Zn>Cu>As>Co on NE monsoon season. The average concentration of Cr was slightly higher during NE monsoon compare to SW monsoon. The maximum value of Cr was found at Station 8 (158.23 mg/kg) and the minimum value was at 70.92 mg/kg (Station 3) during NE monsoon. Primarily Cr was used in paints especially on boat's hull in order to slow down the growth of organisms that attach to the hull [3]. The dumping of municipal and industrial waste materials can significantly increase chromium concentration in soil and is usually accompanied by groundwater contamination [15]. Since SW monsoon bring a heavy rainfall in the Perlis, Cr concentration was diluted which explained the slightly lower concentration compare to NE monsoon.

The average concentration of Zn (94.45 mg/kg) obtained was slightly higher during SW monsoon compare to NE monsoon that only has a value of 90.49 mg/kg. Based on Table 2, concentration of Zn reach a maximum value at Station 10 (121.00 mg/kg) and minimum value of 62.20 mg/kg at Station 4 during SW monsoon. During SW monsoon, a slightly high humidity affect the weather condition and approximately 35%-110% above average of rain was received in Perlis [18]. During this rainy season, runoff from the industrial areas and the main city of Perlis (Kangar) were carried to the Sungai Perlis which can be explained the elevated level of Zn in the river. This result was in the line with the finding by Fortune (2006) where storm water from urban areas has increase the Zn loads to 60 times higher than background levels [12]. Besides, other sources of Zn alongside the Sungai Perlis include residential and domestic waste may also contribute to the load of Zn in the river. The calculation for household products includes laundry detergents, general purpose cleaners, shampoos, bar soaps and toilet tissue could account for a portion of Zn load from these sources [16]. Furthermore, lower salinity in the estuary river due to the rainfall might also affect the mobility and availability of metals the sediment. According to Laing et al., (2009) the binding of Zn in the sediment was affected by salinity where decrease in salinity might increase the mobility of Zn in the river [17]. On the other hand, Perlis received a minimum rainfall which is below average level during NE monsoon season [18]. The difference in between these monsoons might explain the high level of Zn in the sediment of Sungai Perlis estuary.

In contrast, average concentrations of Pb (52.30 mg/kg) during NE monsoon was slightly higher compare to SW monsoon with the value of 39.23 mg/kg. The maximum value of Pb was obtained at Station 9 which has a value 76.88 mg/kg during NE monsoon and the minimum value of 32.46 mg/kg at Station 3. Elevated concentrations were found at a number of sites mostly at downstream areas. Due to the location of Perlis at the west coast of Peninsular Malaysia, NE monsoon do not really affect the western coastal area [18] which, by this time, high number of fishing and boating activities were spotted compare to SW monsoon season. Oil leakage from boats may be contributed to the Pb source which originates from leaded fuel use by fishing boat [12]. Besides, due to the fact that Sungai Perlis is the main river that carry waste from urban and industrial areas, there is no doubt that Pb was accumulated in the sediment. Unsal (2001) reported that local industries can cause lead pollution in the aquatic environment and a notable amount of lead has been transported in particulate form contained in riverbed [21].

Table 3: Heavy metals concentration (mg/kg) in the sediment during Southwest and Northeast Monsoon

| Stations | Monsoon | Heavy Metals Concentration (mg/kg) | | | | | |
|---|---|---|---|---|---|---|---|
| | | Cr | Zn | Pb | As | Cu | Co |
| 1 | SW | 77.01±2.23 | 84.12±2.84 | 33.34±4.51 | 11.88±1.25 | 34.47±4.46 | 6.01±0.47 |
| | NE | 76.73±3.02 | 62.82±1.25 | 39.71±1.70 | 15.52±1.12 | 10.22±0.25 | 6.78±0.88 |
| 2 | SW | 82.34±1.54 | 73.99±4.33 | 31.19±2.15 | 13.98±2.73 | 14.49±6.02 | 6.69±0.95 |
| | NE | 105.27±5.14 | 86.16±2.31 | 46.83±1.69 | 23.65±1.79 | 16.76±1.77 | 10.26±1.35 |
| 3 | SW | 90.85±4.02 | 89.08±6.34 | 38.42±4.21 | 18.98±1.32 | 19.74±2.36 | 8.18±2.00 |
| | NE | 70.92±2.98 | 61.29±2.33 | 32.46±1.21 | 26.48±1.68 | 7.32±1.49 | 8.12±1.96 |
| 4 | SW | 56.67±3.17 | 62.20±2.68 | 23.54±4.73 | 11.47±0.96 | 8.01±5.51 | 4.74±0.43 |
| | NE | 114.47±4.69 | 95.33±4.41 | 52.16±4.00 | 32.87±3.37 | 18.13±4.44 | 11.97±1.85 |
| 5 | SW | 113.17±5.65 | 107.63±6.66 | 45.87±1.70 | 20.19±3.59 | 22.74±3.09 | 9.19±2.72 |
| | NE | 103.54±3.04 | 78.48±2.75 | 43.47±1.36 | 26.41±3.75 | 15.16±2.20 | 9.80±1.04 |
| 6 | SW | 100.76±3.11 | 109.69±6.86 | 45.62±2.96 | 24.98±3.44 | 29.03±4.62 | 10.75±1.70 |
| | NE | 115.34±5.30 | 89.53±4.92 | 48.32±0.56 | 29.59±2.46 | 23.34±4.21 | 10.73±1.02 |
| 7 | SW | 109.38±2.98 | 111.04±3.48 | 45.97±1.84 | 26.36±4.42 | 30.57±6.60 | 10.70±1.67 |
| | NE | 124.44±6.08 | 96.64±1.46 | 48.57±6.24 | 26.27±0.11 | 28.53±2.37 | 10.58±1.59 |
| 8 | SW | 96.52±6.11 | 100.34±4.40 | 42.66±3.86 | 21.47±0.97 | 21.43±5.35 | 9.74±0.99 |
| | NE | 158.23±7.23 | 117.37±.40.09 | 63.99±2.72 | 35.72±1.85 | 20.73±3.52 | 14.41±4.11 |
| 9 | SW | 87.52±5.20 | 85.35±3.70 | 36.19±3.00 | 19.94±0.12 | 19.86±4.26 | 7.50±0.59 |
| | NE | 126.75±3.15 | 110.03±1.90 | 76.88±4.43 | 77.50±7.02 | 26.4±2.46 | 24.17±6.91 |
| 10 | SW | 116.64±4.58 | 121.10±4.09 | 49.44±1.15 | 28.13±1.43 | 35.91±2.56 | 11.70±2.38 |
| | NE | 132.60±2.55 | 107.30±3.02 | 70.62±1.73 | 59.12±2.13 | 35.29±3.14 | 17.89±2.51 |
| Average | SW | 93.09 | 94.45 | 39.23 | 19.74 | 23.63 | 8.52 |
| | NE | 112.83 | 90.49 | 52.3 | 35.31 | 20.19 | 12.47 |
| Std Dev | SW | 18.35 | 18.57 | 8.18 | 5.86 | 8.87 | 2.28 |
| | NE | 25.81 | 18.95 | 14.01 | 18.72 | 8.51 | 5.17 |

It was found that concentration of As was slightly higher during NE monsoon (35.31 mg/kg) compare to SW monsoon (19.74 mg/kg). The sources of As was possibly byproduct from agriculture and aquaculture activities that uses As in pesticides and as additives in fish/shrimp food [22]. Furthermore, Cu concentration shows a maximum value at Station 10 (35.91 mg/kg) during SW monsoon and a minimum value of 7.32 mg/kg at Station 3 during NE monsoon season. Municipal waste and boating activities alongside the river may increase Cu load since the major source of Cu were from vehicles (brakes, tires, protective paint on boats, petrol, car washing) and building materials such as drinking water pipes and corrosion from steel material [23]. Sometimes, a lot of rubbish can be seen visible at the river such as plastic, tires, and even corroded steel which being lift during grabbing the sediment. On the other hand, Co concentration shows a maximum value at St 10 (11.70 mg/kg) and a minimum value of 4.74 mg/kg during SW monsoon. Improper sewage from squatter and residential areas alongside the river may possibly contribute to the Co load in the sediment [24].

## Conclusion

From the data obtained, mean size and skewness during SW monsoon shows slightly higher compare to NE monsoon season and for sorting is vice versa. However, classification of mean, sorting and skewness were the same for both monsoon seasons. For heavy metals, Cr concentration was lower during SW monsoon which bring a heavy rainfall in the Perlis and cause Cr concentration diluted. On the other hand, rainy season during SW monsoon tend to carry runoff from the industrial areas and the main city of Perlis (Kangar) and elevate the level of Zn in the river. The old dumping sites, aquaculture, anchorage and residential areas were the possible source of various metals to the river. The main reason behind the seasonal variation of heavy metals is dilution of metal ions in the sediment during rainy season and it tends to accumulate free movement of the metal ion in the next seasons.

## Acknowledgement

This research was conducted with funding from the FRGS research grant. The author thank to the Centre of Ocean Research, Conservation and Advances (ORCA) teams for their invaluable assistance throughout the sampling period.

## References

1. Phiri, O., Mumba, P., Moyo, B.H.Z., & Kadewa, W. (2005), Assessment of the Impact of Industrial Effluents on Water Quality of Receiving Rivers in Urban Areas of Malawi. *International Journal Environment Science and Technology*, 237–244.
2. Filgueiras, A.V., Lavilla, I. & Bendicho, C. (2004). Evaluation of Distribution, Mobility and Binding Behaviour of Heavy Metals in Surficial Sediments of Louro River using Chemometric Analysis: A Case Study. *Science Total Environment*, 330: 115-129.
3. Ozkan, E.Y. (2012). A New Assessment of Heavy Metal Contaminations in an Eutrophicated at Inner Izmir Bay, Turkey. *Turkish Journal of Fisheries and Aquatic Sciences*, 12: 135-147.
4. Jain, C.K., Singhal, D.C. & Sharma, M.K. (2005). Metal Pollution Assessment of Sediment and Water in the River Hindon, India. *Environmental Monitoring Assessment*. 105: 193-207.
5. Bartoli, G., Papa, S., Sagnella, E., & Fioretto, A. (2011). Heavy Metal Content in Sediments along the Calore River: Relationships with Physico Chemical Characteristics. *Journal of Environmental Management*. 1-6.
6. Lotfy, I. H. (2002). Studies on the Particle Size Distribution and Both Light and Heavy Minerals of Recent Sediments at Rosetta Nile branch, Egypt. *Bulletin of National Institute Oceanography and Fish*, 28: 367 -384.
7. Noriki, S. K. T., Nakanishi, M., Fukawa, T., Uematsu, H., Uchida & Tsunogai, S. (1980). Use of a Teflon Vessel for the Decomposition Followed by Determination of Chemical Constituents of Various Marine Samples. *Bulletin Faculty Fish*. 31: 354- 465.
8. Jamil, T. (2006). Physico- Chemical and Sediment Characteristics of the Bottom Sediment of Terengganu River, Terengganu, Malaysia. Thesis, MSc. Faculty of Science and Technology, Kolej Universiti Sains & Teknologi Malaysia, Terengganu.
9. Nicholas, M.M. & Biggs, R.B. (1985). Coastal Sedimentary Environment.*Springer-Verlag*. 77-186.
10. Lim, W. Y., Aris, A.Z., & Zakaria, M.P. (2012). Spatial Variability of Metals in Surface Water and Sediment in the Langat River and Geochemical Factors that Influence their Water-Sediment Interactions. *The Scientific World Journal.* 10*:*1-14.
11. Shata, M. A. (2000). Sedimentological Characteristics of Subsurface Sediment in Burg El-Arab Region, Northwestern Coast Of Egypt. *Bulletin National Institute of Oceanography & Fish*. 26: 1-26.
12. Fortune, J. (2006). The Grain Size and Heavy Metal Content of Sediment in Darwin Harbour. *Environmental Protection Agency*.
13. Kamaruzzaman, B.Y., Shazili N.AM., & Lokman, H. (2002). Particle Size Distribution in the Bottom Sediments of the Kemaman River Estuarine System, Terengganu, Malaysia. *Pertanika Journal of Tropical Agricultural Science*, 25(2): 149 - 155.
14. Idris, A.M., Eltayeb, M. A. H., Potgieter, S. S., R., Van, G., & Potgieter J. H., (2007). Assessment of Heavy Metals Pollution in Sudanese Harbours along the Red Sea Coast. *Microchemical Journal*, 87 (2): 104 - 112.
15. Bielicka A., Bojanowska, I. & Wiśniewski, A, (2005). Investigation of Heavy Metals Mobility in Industrial Waste Polluted Soils. *Polish Journal of Environmental Study*. 14(2): 151.
16. Agency for Toxic Substances and Disease Registry-ATSDR, (2005). Zinc Toxicity. *Case Studies in Environmental Medicine (CSEM)*. 148- 150.

17. Laing, G.D., Rinklebeb J., Vandecasteelec, B., Meersa, F. & Tacka F.M.G., (2009). Trace Metal Behaviour in Estuarine and Riverine Floodplain Soils and Sediments: A Review. *Science of the Total Environment*. 3972-3985.
18. Malaysian Meteorological Department Ministry of Science, Technology & Innovation (2012). Agroclimatic Analysis & Outlook. 9 (3): 1-10.
19. Wedepohl, K. H., (1995). The Composition of the Continental Crust. *Geochimica et Cosmochimica Acta.* 59 (7): 1217– 1232.
20. Canadian Councils of Ministers of the Environment (CCME) (2002). Canadian Water Quality Guidelines for the Protection of Aquatic Life. Canadian Water Quality Index Technical Report. 1: 29-36.
21. Unsal, M., (2001). Lead Pollution and its Sources along the Turkish Coast of the Black Sea. *Mediterranean Marine Science.* 33-44.
22. Jain, C.K., (2003). Metal Fractionation Study on Bed Sediments of River Yamuna, India. *Water Research.* 38: 569–578
23. Ho, H. H., Swennen, R. &Van Damme, A., (2010). Distribution and Contamination Status of Heavy Metals in Estuarine Sediments near Cua Ong Harbor, Ha Long Bay, Vietnam. *Geologica Beligica*. 13 (1): 37-47.
24. Agency for Toxic Substances and Disease Registry-ATSDR, (2004). Toxicological Profile for Cobalt. *Case Studies in Environmental Medicine (CSEM).* 207- 212.

The Malaysian Journal of ANALYTICAL SCIENCES ISSN 1394-2506

# STUDY OF RADIONUCLIDES LINKAGES BETWEEN FISH, WATER AND SEDIMENT IN FORMER TIN MINING LAKE IN KAMPUNG GAJAH, PERAK, MALAYSIA

## (Kajian Mengenai Hubungan Radionuklid di antara Ikan, Air, dan Sedimen dalam Tasik Bekas Lombong di Kampung Gajah, Perak, Malaysia)

Ahmad Saat [1,2], Norannisak Muhd Isak[1]*, Zaini Hamzah[1], Ab Khalik Wood[1]

[1]*Faculty of Applied Sciences,*
[2]*International Education Centre (INTEC),*
*Universiti Teknologi MARA, 40200 Shah Alam, Selangor, Malaysia*

**Corresponding author: nysa_chy@yahoo.com*

**Abstract**

Tin mining activities not only released metal contaminants into environment, but also radionuclides into the native soil and sediment. There is a possibility that radionuclides be transferred between sediment, water and biota as a result of exchanges between them through biological, physical and chemical processes. Fishes from former tin mining lakes in Kampung Gajah, have become main sources of protein supplies and economic profit to the local resident. The present study is to determine linkages between activity concentrations of natural radionuclides in biota (fish), water and sediment in one of the former tin mining lake. The study involved analysis of radionuclides in water, edible part of fish and sediment. Filtered and unfiltered water samples collected from the study area were filled into marinelli beakers, sealed and count using gamma spectrometry. Fish and sediment samples prior to measurement were dried, grind and sieved through 250 µm and kept in special container for measurement of radionuclides activity concentration using gamma spectrometry. The range of transfer ratio of $^{226}$Ra, $^{228}$Ra and $^{40}$K from unfiltered water samples to fish are 1.95 to 3.42, 0.86 to 2.70 and 12.63 to 18.69, while, for sediment to fish are from 1.30 to 2.27 x $10^{-2}$, 0.43 to 1.13 x $10^{-2}$ and 9.08 to 13.45 x $10^{-2}$ , respectively. Transfer ratio of $^{226}$Ra, $^{228}$Ra and $^{40}$K from sediment to unfiltered water is 7.00 x $10^{-3}$, 4.26 x $10^{-3}$ and 7.30 x $10^{-3}$, respectively. This present study shows that there is transfer for radionuclides from water to fish, sediment to fish and lastly sediment to water column.

**Keywords**: radionuclides, sediment, water, fish, tin mining lake, gamma spectrometry

**Abstrak**

Aktiviti perlombongan bijih timah bukan sahaja mengeluarkan pencemaran logam kepada alam sekitar, tetapi juga radionuklid ke dalam tanah dan sedimen. Radionuklid mungkin dipindahkan antara sedimen, air, dan biota akibat pertukaran antara mereka melalui proses biologi, fizikal dan kimia. Ikan dalam tasik bekas lombong bijih timah di Kampung Gajah menjadi bekalan sumber utama protein dan sumber kewangan kepada penduduk tempatan. Kajian ini menentukan hubungan antara kepekatan aktiviti radionuklid tabii dalam sedimen, air dan biota (ikan) dalam satu tasik bekas lombong bijih timah. Kajian ini melibatkan radionuklid analisis dalam air, ikan dan sedimen .Sampel air yang dituras dan tidak dituras yang diambil dari tempat kajian diisi di dalam bekas marinelli yang ditutup rapi dan diukur menggunakan spektrometri gama. Sampel ikan dan sedimen dikeringkan, dikisar dan diayak dengan 250 µm dan disimpan di dalam bekas khas untuk mengkaji kepekatan aktiviti menggunakan spektrometri gama. Julat nisbah pindahan masing-masing daripada sampel air yang tidak dituras kepada ikan ialah 1.95 hingga 3.42, 0.86 hingga 2.70 dan 12.63 hingga 18.69 dan bagi sedimen kepada ikan ialah 1.30 hingga 2.27 x $10^{-2}$, 0.43 hingga 1.13 x $10^{-2}$ dan 9.08 hingga 13.45 x $10^{-2}$. Nisbah pindahan masing-masing bagi $^{226}$Ra, $^{228}$Ra and $^{40}$K daripada sampel sedimen kepada air yang tidak dituras ialah 7.00 x $10^{-3}$, 4.26 x $10^{-3}$ dan 7.30 x $10^{-3}$. Kajian ini menunjukan bahawa terdapat pemindahan bagi radionuklid daripada air ke ikan, sedimen kepada ikan dan akhirnya sedimen ke air.

**Kata kunci**: radionuklid, sedimen, air, ikan, tasik lombong bijih timah, spektrometri gama

## Introduction

Malaysia was once been the world's largest tin producer by the end of the 19$^{th}$ century [1]. The factors that contributed to the success were discovery of rich tin fields in Perak and Selangor as well as high demand in market at that time [1]. However, depletion in tin deposits and decreasing in demand of tin in the world market, the tin mining activities has ceased operation about 30 to 40 years ago [2] which lead Malaysia nowadays to produce less than 1.5% of total world production [1]. As a result, the mining areas now are left with many abandoned lakes, which later have found secondary land uses in the form of aquaculture and vegetable cultivation plots [2, 3, 4]. The abandoned areas are also naturally rich with varies fresh water fish species that become the main sources of protein to local residents. However, some of them have still left abandoned.

The tin mining activities had left tin ores residue, quartz sand and certain minerals such as monazite, ilmenite, zircon and xenotime in the industry byproduct in the form of 'amang' (tin tailings) [5]. Monazite and xenotime are two minerals rich in natural radionuclides, particularly uranium, thorium and potassium [3, 5]. The natural radionuclide can be accumulating into the environment. The hyper-accumulation may become toxic and will affect the surrounding living organisms [6].

According to Suresh *et al*., [7], sediment is a basic indicator of radiological contamination as it plays a dominant role and also can plays role in accumulating and transporting contaminants within the geographic area. Hence it is useful in aquatic radioecology study. The water and biota in the former tin mining lake also can contain natural radionuclides due to interaction of chemical, physical and biological processes with sediments, in which the amount of the natural radionuclides in materials determined by their respective exchanges processes.

Fishes from this mining lake can pose health risk to human due to the natural radionuclides that have been accumulated in fish' body via food chain [4, 8]. The present study was carried out to determine the activity concentration of $^{226}$Ra, $^{228}$Ra and $^{40}$K in some of fish species (biota). The activity concentration in water and sediment samples from the area were also determined in the representative sites of the lake with the final aim to determine the radionuclide linkage in water, sediment and fish.

## Materials and Methods

### Sampling site

The study area is located at Kapal 7 Lake. It is one of the former tin mining lakes in Kinta Valley in the State of Perak, Malaysia. The size of lake is about 0.5 km x 1.5 km. The deepest part is about 40 m near the center of the lake. There are four small islands located near the centre of the lake. The uniqueness of this lake is the water in Kapal 7 Lake is connected to Sungai Kampar on the west side and Air Hitam Lake on the east side via water channel which allowed the water to flow in and out in two ways under certain condition. Besides, there are palm oils that have planted along east side of the lake. Table 1 shows the latitude, longitude (measured by using global positioning system (GPS)) and water depth of sampling locations for water and sediment. The water depth at most locations ranged between nearest 9 to 10 m.

Table 1: The coordinate for sampling locations

| Location | Latitude | Longitude | Water depth (m) |
|---|---|---|---|
| KT1 | N 04º 12.537' | E 101º 02.631' | 9 |
| KT2 | N 04º 12.527' | E 101º 02.517' | 10 |
| KT3 | N 04º 12.568' | E 101º 02.339' | 10 |
| KT4 | N 04º 12.556' | E 101º 02.215' | 10 |
| KT5 | N 04º 12.419' | E 101º 02.179' | 10 |

Physical and chemical water quality was measured *in situ* for some parameters (temperature, specific conductivity, total dissolved solid, salinity, dissolved solid and pH) using calibrated YSI multi sensor probe, while, the turbidity (Table 2) was measured using calibrated turbidity meter.

**Sampling collection and preparation**

Eight species of fish were collected as representative of biota sample including Jelawat (*Leptobarbus hoevenii*), Lampam (*Puntius schwanenfeldii*), Patung (*Pristolepis fasciatus*), Raja (*Cichla monoculus*), Terbui (*Osteochilus hasselti*), Tilapia (*Oreochromis mossambicus*), Toman (*Channa micropeltes*) and Tongsan (*Aristichthys nobilis*). As far as possible, for each species samples of the same size were used. Before analysis, the edible flesh of fish samples were separate from the non-edible parts and oven dried at 60°C until constant weight was obtained. Then the samples were pulverized and sieved through 250 μm sieves. About 500 g were packed into special container (height (~90 mm) and diameter (~83 mm)) and sealed properly.

The water samples were collected 1 meter below the water surface using grab sampler and transferred into plastic container that have been rinsed with acid nitric and distilled water, respectively. Water samples were acidified using 6 M nitric acid to pH 2 to stabilize the water [9]. Then samples were divided into two portions which are filtered and unfiltered water samples in order to determine the dissolved and suspended solid. Cellulose membrane nitrate filter 0.45 μm was used for filtering the samples [9]. The water samples (filtered and unfiltered) were transferred into the marinelli beaker and sealed properly prior to gamma counting using gamma spectrometer system.

Sediment cores were collected by using manual gravity corer with PVC core tube of 45 mm inner diameter. Sediment samples in PVC core tube were left air-dried in vertical position for about 3 to 4 weeks to obtain the shape of PVC column [10]. To form homogenous sample for each locations, the cores were sub-sampled by slicing it into 2 cm and mixed with other cores of the same depth. The first two top layers were used for analysis of radionuclides in surface sediments. The aggregates were oven dried at 60˚C until constant mass, pulverized and sieved through 250 μm sieves and seal properly into a special plastic container (height ~20mm and diameter ~50 mm) [10]. All samples were kept for 21 days, to establish secular equilibrium between $^{226}$Ra and $^{228}$Ra and their respective radioactive progenies prior to gamma counting.

**Measurement of $^{226}$Ra, $^{228}$Ra and $^{40}$K**

The measurement of activity concentrations of radionuclides for all samples were done by using ORTEC® gamma rays spectrometer with HPGe detector with resolution 1.84 keV, 25% relative efficiency at 1332 KeV $^{60}$Co gamma ray and couple to Multi Channel Analyser (MCA) [11]. The measurement is possible by assuming secular equilibrium between parents and various daughters were achieved after about 21 days [11]. Since $^{226}$Ra is an alpha emitter with weak gamma line, the measurements of $^{226}$Ra are based on radon daughters of either $^{214}$Bi or $^{214}$Pb [11]. In this study, $^{214}$Bi were selected for measurement of $^{226}$Ra activity concentration due to higher intensity compared with $^{214}$Pb. Meanwhile the $^{228}$Ra was measured by determining the activity of $^{228}$Ac [11]. The $^{226}$Ra, $^{228}$Ra and $^{40}$K activity concentration were determined based on 609, 911 and 1460 KeV gamma ray, respectively. The fish and sediment samples were counted for 4 hours (14400s) while, 8 hours (28800s) for filtered and unfiltered water samples. The efficiency calibration was made by using secondary standard prepared by mixing known amount $UO_3$ and KCl in the same container of the same geometry as samples [11].

## Results and Discussion

The data generated in this research include water quality parameters, activity concentrations of $^{226}$Ra, $^{228}$Ra and $^{40}$K in edible part of the selected biota (fish), water and sediment. From these results, the radionuclides linkages in fish-water-sediment system were determined. The physical and chemical water quality parameters that have been measured on-site during the sampling are shown in Table 2. Generally in all sampling locations, the temperature is in the ranged of 29.89°C to 31.67°C [12]. It is important to note that the water temperature is varies depending on the weather at a particular time. The pH values are in general close to neutral and its comparable with others study as Samudi *et al.,* [4] which stated that the pH ranged is 7.21-7.92 in former tin mining water at Puchong, Malaysia. Specific conductivity value is ranged from 155 to 225μS/cm. The total dissolved solid and turbidity are in the range from 0.090 to 0.134 mg/L and 2.50 to 6.89 NTU respectively, which indicated that the amount of suspended solid in water is low. Total suspended solid is in the range of 1.92 to 8.40 mg/L which is 0.45 μm. Meanwhile, dissolved

oxygen is ranged from 6.96 to 11.15 mg/L which allowed the aquatic organisms and plants to live. The reading of salinity is low which is on average of 0.08 mg/L. According to Zaini *et al*., [9], in low salinity environments radium is strongly adsorbed on water molecules of surfaces water. Generally, the physical water quality parameters in this study are comparable with other studies by Samudi *et al*., [4] and Zaini *et al*., [12]. The *in-situ* parameter in Table 2 shows that most of the parameter falls into Class I (practically no treatment necessary) while certain parameter falls into Class IIA (conventional treatment required) based on National Water Quality Standard, NWQS (DOE, 2008) [13].

Table 2: Water Quality Parameters measured in Kapal 7 Lake

| Location | Temp (°C) | Sp C (µS/cm) | TDS (mg/L) | Salinity (mg/L) | DO (mg/L) | pH | Turbidity (NTU) | TSS (mg/L) |
|---|---|---|---|---|---|---|---|---|
| KT1 | 29.9 | 225 | 0.13 | 0.10 | 6.96 | 7.10 | 4.24 | 1.92 |
| KT2 | 30.0 | 187 | 0.11 | 0.08 | 8.61 | 7.21 | 4.55 | 2.83 |
| KT3 | 30.0 | 193 | 0.11 | 0.08 | 11.15 | 6.98 | 6.89 | 7.00 |
| KT4 | 31.6 | 190 | 0.11 | 0.08 | 10.94 | 7.81 | 3.16 | 2.85 |
| KT5 | 31.7 | 155 | 0.09 | 0.06 | 10.36 | 7.16 | 2.50 | 8.40 |
| *NWQS | - | I | I | IIA | IIA | I | IIA | I |

*National Water Quality Standard (NWQS)

The activity concentrations of radionuclides in edible part of fish flesh samples in Jelawat (*Leptobarbus hoevenii*), Lampam (*Puntius schwanenfeldii*), Patung (*Pristolepis fasciatus*), Raja (*Cichla monoculus*), Terbui (*Osteochilus hasselti*), Tilapia (*Oreochromis miloticus*), Toman (*Channa micropeltes*) and Tongsan (*Aristichthys nobilis*) are shown in Table 3. The results, the $^{226}$Ra, $^{228}$Ra and $^{40}$K activity concentration are higher in Tongsan, Patung and Toman species which is 5.67 ± 0.47, 4.48 ± 0.63 and 239.7 ± 8.6 Bg/kg, respectively. Meanwhile, the lowest activity concentrations of $^{226}$Ra, $^{228}$Ra and $^{40}$K are in Jelawat, Toman and Tongsan species which is 3.24 ± 0.36, 1.42 ± 0.37 and 161.9 ± 6.9 Bg/kg, respectively. The differences between activity concentrations of radionuclides in various edible fish flesh samples from the same lake indicate that there are different amount of radionuclides uptake depending on fish species. In addition, the water chemistry, the physiology of fish which included the feeding behavior and their digestion of food may also affect the amount of radionuclides accumulated in their body [13]. In all fish species, activity concentrations of radionuclides is of the order $^{228}$Ra < $^{226}$Ra < $^{40}$K. This may due to the amount of $^{238}$U parent of $^{226}$Ra is higher than $^{232}$Th parent of $^{228}$Ra in edible parts of fish.

Table 3: Activity concentrations of radionuclides in fish samples

| Fish (local name) | Activity concentrations of radionuclides (Bg/kg) | | |
|---|---|---|---|
| | $^{226}$Ra | $^{228}$Ra | $^{40}$K |
| Jelawat | 3.24 ± 0.36 | 1.71 ± 0.39 | 172.9 ± 7.1 |
| Lampam | 4.66 ± 0.42 | 2.08 ± 0.42 | 169.4 ± 6.9 |
| Patung | 3.48 ± 0.37 | 4.48 ± 0.63 | 178.1 ± 7.1 |
| Raja | 4.13 ± 0.40 | 3.93 ± 0.59 | 184.3 ± 7.3 |
| Terbui | 4.70 ± 0.43 | 3.26 ± 0.54 | 209.1 ± 7.9 |
| Tilapia | 3.84 ± 0.40 | 3.70 ± 0.59 | 216.8 ± 8.2 |
| Toman | 3.80 ± 0.40 | 1.42 ± 0.37 | 239.7 ± 8.6 |
| Tongsan | 5.67 ± 0.47 | 3.51 ± 0.56 | 161.9 ± 6.9 |

Table 4 shows the activity concentrations of radionuclides in water samples for filtered and unfiltered water. The average of activity concentration of $^{226}$Ra, $^{228}$Ra and $^{40}$K in all locations is 1.66 ± 0.30, 1.66 ± 0.46 and 12.82 ± 2.26

Bg/kg for unfiltered water samples, while, for filtered water samples is 1.25 ± 0.26, 0.73 ± 0.32 and 10.63 ± 2.04 Bg/kg, respectively. The activity concentration of radionuclides in filtered water samples is less than in unfiltered water samples. This may explain that some of the radionuclides had been adsorbed to the surface of suspended solid in water. The amount of $^{228}$Ra attached to suspended solid is higher than $^{226}$Ra may due to the residence time. Results obtain in Table 3 and Table 4 of filtered water samples shows the same trend of radionuclides. This may explain that uptake of radionuclides by fish depends on the concentration and on the speciation of the radionuclides in dissolved water [14]. In addition, the concentration of radionuclides in water may possibly used to predict accumulation in fish [14].

Table 4: Activity concentrations of radionuclides in water samples

| **Water sample** | **Activity concentrations of radionuclides (Bg/kg)** | | | | | |
|---|---|---|---|---|---|---|
| | **$^{226}$Ra** | | **$^{228}$Ra** | | **$^{40}$K** | |
| | **Filtered** | **Unfiltered** | **Filtered** | **Unfiltered** | **Filtered** | **Unfiltered** |
| **KT1** | 1.07 ± 0.11 | 2.19 ±0.15 | 0.46 ± 0.11 | 1.33 ± 0.18 | 7.89 ± 0.79 | 13.29 ± 1.03 |
| **KT2** | 1.18 ± 0.11 | 1.55 ± 0.13 | 0.48 ± 0.11 | 2.48 ± 0.24 | 10.44 ± 0.82 | 11.73 ± 0.96 |
| **KT3** | 1.31 ± 0.12 | 1.34 ± 0.12 | 0.98 ± 0.15 | 1.21 ± 0.17 | 12.94 ± 1.01 | 14.04 ± 1.06 |
| **KT4** | 1.46 ± 0.12 | 1.56 ± 0.13 | 0.99 ± 0.15 | 1.47 ± 0.19 | 12.32 ± 0.99 | 12.47 ± 1.00 |
| **KT5** | 1.24 ± 0.11 | 1.67 ± 0.13 | 0.73 ± 0.13 | 1.79 ± 0.21 | 9.58 ± 0.87 | 12.57 ± 1.00 |
| **Average** | 1.25 ± 0.26 | 1.66 ± 0.30 | 0.73 ± 0.32 | 1.66 ± 0.46 | 10.63 ± 2.04 | 12.82 ± 2.26 |

Table 5 shows the activity concentration of radionuclides in surface sediment samples. The surface sediment were sampled and analyzed because the major water-sediments interaction by the chemical and biological processes occurred on the surface of benthic sediments layer. From Table 5, the average of sediment samples for $^{226}$Ra, $^{228}$Ra and $^{40}$K activity concentration are 249.8 ± 19.5, 397.9 ± 42.1 and 1782.2 ± 201 Bg/kg, respectively. In sediment sample, activity concentration of radionuclides is of the order $^{226}$Ra < $^{228}$Ra < $^{40}$K. This may due to the present of monazite which contained $^{232}$Th and $^{40}$K [14]. In the surrounding of study area (Kapal 7 Lake) there have planted palm oil which may results in high amount of $^{40}$K in fish-water-sediment due to runoff of the fertilizers into the lake. Generally, the activity concentrations of radionuclides are higher in sediment than in fish and in water due to the characteristics of sediment that better in accumulating of radionuclides [7] than fish and water.

Table 5: Activity concentrations of radionuclides in sediment samples

| **Sediment sample** | **Activity concentrations of radionuclides (Bg/kg)** | | |
|---|---|---|---|
| | **$^{226}$Ra** | **$^{228}$Ra** | **$^{40}$K** |
| KT1 | 258.0 ± 8.5 | 434.7 ± 20.2 | 1647 ± 88 |
| KT2 | 152.6 ± 7.1 | 344.2 ± 17.0 | 1905 ± 90 |
| KT3 | 266.0 ± 8.3 | 373.5 ± 17.9 | 1731 ± 87 |
| KT4 | 289.8 ± 9.1 | 422.7 ± 20.0 | 2095 ± 101 |
| KT5 | 282.4 ± 8.5 | 414.9 ± 18.9 | 1533 ± 80 |
| Average | 249.8 ± 19.5 | 397.9 ± 42.1 | 1782 ± 201 |

Radionuclides maybe transferred between biota and reference media (water and sediment) in freshwater ecosystem. Referring to bioaccumulation models, the aquatic organisms are assuming in equilibrium with water and sediment in their surroundings [14]. The accumulation of radionuclides in biota can be represented in simplified ratio by relating radionuclides concentration in biota to radionuclides concentration in water and sediment [14]. The transfer radionuclides in fish-water-sediment can be calculated using Concentration Factor (CF) and Distribution

Coefficient, $K_d$ as in Equation 1 and 2 [14]. In addition, the dissolved and particulate phase also been assumed to be equilibrium with exchanges of nuclides between particles and water being wholly reversible [16].

$$CF = \frac{\text{Activity concentration in biota (Bg/kg) (dry weight)}}{\text{Activity concentration of reference medium (Bg/kg)}} \quad \text{(Equation 1)}$$

$$K_d = \frac{\text{Activity concentration in sediment (Bg/kg)(dry weight)}}{\text{Activity concentration in unfiltered water (Bg/kg)}} \quad \text{(Equation 2)}$$

The Concentration Factor, CF from unfiltered water to fish samples as fish represent receiving medium, while, water as transfer medium which are shown in Table 6. The higher CF of $^{226}$Ra, $^{228}$Ra and $^{40}$K activity concentration are Tongsan (*Aristichthys nobilis*), Patung (*Pristolepis fasciatus*) and Toman (*Channa micropeltes*) which is 3.42, 2.70 and 18.69, respectively. From this results, the transfer ratio, CF of $^{226}$Ra are generally higher than $^{228}$Ra while $^{40}$K showed nearly 11 times the value of $^{226}$Ra and $^{228}$Ra. This may show that physicochemical factors of the water from which fish were caught also determining factors that vary from one location to others as shown in Table 2.

Table 6: The Concentration Factor (CF) of radionuclides from unfiltered water samples to fish samples

| **Fish (local name)** | **Distribution coefficient, $K_d$** | | |
|---|---|---|---|
| | **$^{226}$Ra** | **$^{228}$Ra** | **$^{40}$K** |
| **Jelawat** | 1.95 | 1.03 | 13.49 |
| **Lampam** | 2.81 | 1.25 | 13.21 |
| **Patung** | 2.10 | 2.70 | 13.89 |
| **Raja** | 2.49 | 2.37 | 14.38 |
| **Terbui** | 2.83 | 1.96 | 16.31 |
| **Tilapia** | 2.31 | 2.23 | 16.91 |
| **Toman** | 2.29 | 0.86 | 18.69 |
| **Tongsan** | 3.42 | 2.11 | 12.63 |

Table 7 shows Concentration Factor, CF from sediment to fish samples. The higher ratio of $^{226}$Ra, $^{228}$Ra and $^{40}$K activity concentration are Tongsan (*Aristichthys nobilis*), Patung (*Pristolepis fasciatus*) and Toman (*Channa micropeltes*) which is $2.27 \times 10^{-2}$, $1.13 \times 10^{-2}$ and $13.45 \times 10^{-2}$, respectively. The observable results in Table 6 and Table 7 had shown the same species of fish have higher transfer ratio, CF for $^{226}$Ra, $^{228}$Ra and $^{40}$K, respectively. However, the CF in unfiltered water to fish is higher than in sediments to fish. The observable difference may explain that fish received high amount of radionuclides in water than sediment.

The distribution coefficient, $K_d$ from sediments to unfiltered water is shown in Table 8. The average ratio for all locations for $^{226}$Ra, $^{228}$Ra and $^{40}$K are $7.00 \times 10^{-3}$, $4.26 \times 10^{-3}$ and $7.30 \times 10^{-3}$, respectively. Location KT2 showed highest transfer ratio of $^{226}$Ra and $^{228}$Ra, while, $^{40}$K shows highest at KT5. The highest transfer ratio of $^{226}$Ra and $^{228}$Ra at KT2 indicated that there is abundance of U and Th which is parents of $^{226}$Ra and $^{228}$Ra, respectively, at KT2 compared to other locations. Meanwhile, there is slightly difference in transfer ratio of $^{40}$K at all location even though transfer factor of $^{40}$K is highest at KT5.

Table 7: The Concentration Factor (CF) of radionuclides from sediment samples to fish samples

| Fish (local name) | Distribution coefficient, $K_d$ ($x10^{-2}$) | | |
|---|---|---|---|
| | $^{226}Ra$ | $^{228}Ra$ | $^{40}K$ |
| **Jelawat** | 1.30 | 0.43 | 9.70 |
| **Lampam** | 1.87 | 0.52 | 9.51 |
| **Patung** | 1.39 | 1.13 | 9.99 |
| **Raja** | 1.65 | 0.99 | 10.34 |
| **Terbui** | 1.88 | 0.82 | 11.73 |
| **Tilapia** | 1.54 | 0.93 | 12.17 |
| **Toman** | 1.52 | 0.36 | 13.45 |
| **Tongsan** | 2.27 | 0.88 | 9.08 |

Table 8: The Distribution Coefficient ($K_d$) of radionuclides from sediment samples to unfiltered water samples according to locations

| Location | Distribution coefficient, $K_d$ ($x10^{-3}$) | | |
|---|---|---|---|
| | $^{226}Ra$ | $^{228}Ra$ | $^{40}K$ |
| KT1 | 8.49 | 3.06 | 8.07 |
| KT2 | 10.16 | 7.21 | 6.16 |
| KT3 | 5.04 | 3.24 | 8.11 |
| KT4 | 5.38 | 3.48 | 5.96 |
| KT5 | 5.91 | 4.31 | 8.20 |
| **Average** | 7.00 ± 2.23 | 4.26 ± 1.72 | 7.30 ± 1.14 |

Generally, the results (Tables 4, 5 and 6) shown that there are linkages between biota-water-sediment in the ecosystem. However, transfer ratio shows very low from sediment to unfiltered water and fish samples compared to transfer ratio from water to fish. This may indicated that the major transfer of radionuclide happen between unfiltered water with fish. The distribution of these radionuclides in fish can occur through solid suspensions as well involved of their food chain which may included the aquatic plants, plankton and etc. The transfer ratio is less in sediment to unfiltered water may due to the solubility and mobility of these radionuclides in water. In addition, solid particles from water can settle to the bottom of the lake thus be removed from the water column [14]. Besides, radionuclides dissolved in water can also be absorbed by the bottom sediment [14]. However, the absorbed of radionuclides by bottom sediment can be remobilized and available for uptake by biota [14]. This may indicate that there may possibly high transfer ratio from water to sediment compared transfer ratio from sediment to water.

## Conclusion

There is linkage of radionuclides between fish-water-sediments samples in former tin mining lake in Kampung Gajah, Perak, Malaysia. The sequence of radionuclides activity concentration is; sediment > fish > water. While, transfer ratio is in the sequence of; water to fish > sediments to fish > sediments to water. The higher transfer ratio was found in Tongsan, Patung and Toman that could be attributed to their habitat, dietary and species.

## Acknowledgement

The authors would like to thanks the Universiti Teknologi MARA, especially Faculty of Applied Sciences for the facilities provided during this study. Thank you also to the research management institute (600-Dana 5/3/RIF (1/2012)) for financial support for this study.

**References**


1. Yap, K., M., (2007). Tin Mining in Malaysia- Is There any Revival?. *Bulletin Jurutera*. 12-18.
2. Hamzah, Z, Saat, A., Abu Bakar Z and Wood, A. K. (2011). Anthropogenic Heavy Metals, U-238 and Th-232 Profiles in Sediments from an Abandoned Tin Mining Lake in Malaysia. Proceeding of 2011 3rd International Conference on Chemical, Biological and Environmental Engineering, Singapore. **20**: 75-79.
3. Yusof , A., M., Mahat, M., N., Omar A, N. and. Wood A., K., H. (2001). Water Quality Studies in an Aquatic Environment of Disused Tin-Mining Pools and in Drinking Water. *Ecological Engineering*; **16**: 405–414.
4. Yasir, M. S. Ahmad Kabir, N., Yahaya R. and Majid, A. A. (2008). Kandungan logam berat dan radionuclide tabii di dalam ikan, air, tumbuhan dan sedimen di bekas lombong. *The Malaysia Journal Analytical Science.* **12** (1): 172-178.
5. Hamzah, Z., Saat, A., Mashuri, N. H., and Redzuan, S. D. (2008). Surface Radiation Dose and Radionuclide Measurement in Ex-Tin Mining Aerea, Kg. Gajah, Perak. *The Malaysian Journal of Analytical Science*. **12** (2): 419-431.
6. Marlinda Musa, (2008). Thesis of Metals and Radionuclides Uptake by *Ottelia Alismoides* Collected from the Ex-Mining Area in Kg. Gajah, Perak. 1-13.
7. Suresh G., Ramasamy V., Meenakshisundaram V., Venkatachalapathy R.and Ponnusamy V., (2011). Influence of mineralogical and heavy metal composition on natural radionuclide concentrations in the river sediments. *Applied Radiation and Isotopes*. 69: 1466-1474.
8. Nwabueze A., A., (2010). Levels of Some Heavy Metals in Tissues of Bonga Fish, *Ethmallosa fimbriata*(Bowdich, 1825) from Forcados River. *Journal of Applied Environmental and Biological* Sciences. **1** (3): 44-47.
9. Hamzah, Z., Saat A. and Kassim, M. (2011). Determination of Radon Activity Concentration in Hot Spring and Surface Water using Gamma Spectrometry Technique. *The Malaysian Journal Of Analytical Sciences*. **15** (2): 288–294.
10. Hamzah, Z., Redzuan S. D. and Saat A. (2011b). Determination of Sediment Profile for $^{210}$Pb, Pb, U and Th from Sultan Abu Bakar Dam Due to Soil Erosion from Highland Agriculture Area, Cameron Highlands, Malaysia. *American Journal of Environmental Sciences.* 7(3): 263-268.
11. Hamzah, Z., Redzuan S. D. and Saat A. (2011). Assessment of Radiation Health Risk in Cameron Highlands Tea Plantations. *The Malaysian Journal of Analytical Sciences* 15: 130 –137.
12. Hamzah, Z., Alias, M., Saat, A. and Ishak, A. K. (2011). Measurement of Some Water Quality ParametersRelated to Natural Radionuclides in Aqueous Environmental Samples from Former Tin Mining Lake. *Journal of Nuclear and Related Technologies.*8 (2): 49-59.
13. DOE (2008). *National Water Quality Standards for Malaysia.* Retrieved November 3, 2013, from http://www.nahrim.gov.my.
14. Handbook of Parameter Values for the Prediction Of Radionuclide Transfer in Terrestrial and Freshwater Environments International Atomic Energy Agency Vienna, (2010).Technical Reports Series No. 472: 117-131.
15. Ramasamy, V., Suresh, G., Meenakshisundaram, V. and Gajendran, V. (2009). Evaluation of Natural Radionuclide Content in River sediments and Excess Lifetime Cancer Risk Due to Gamma Radioactivity. **1** (1): 6-10.
16. Sediment Distribution Coefficients and Concentration Factors for Biota in the Marine Environment. Technical Reports Series No.422: 8-25.

The Malaysian Journal of ANALYTICAL SCIENCES ISSN 1394-2506

# DETERMINATION OF MAJOR IONS CONCENTRATIONS IN KELANTAN WELL WATER USING EDXRF AND ION CHROMATOGRAPHY

## (Penentuan Kepekatan Ion-ion Utama Air Telaga di Kelantan, Dengan Menggunakan Pendaflur Serakan Tenaga Sinar-X dan Ion Kromatografi)

Zaini Hamzah[1]*, Wan Noorhayani Wan Rosdi[1], Abd Khalik Hj Wood[1], Ahmad Saat[2]

[1]*Faculty of Applied Sciences*
[2]*Institute of Science (IOS)*
*Universiti Teknologi MARA, 40450 Shah Alam, Selangor, Malaysia*

**Corresponding author: zaini648@salam.uitm.edu.my*

**Abstract**

Well water is a renewable natural resources and one of the drinking water sources for many areas in Kelantan. The assessment of well water quality is very important in evaluating the suitability of the water for drinking and other domestic purposes. Major ions such as $K^+$, $Ca^{2+}$ and $Na^+$ in well water may originated from dissolved mineral composition of the underground rocks and soil mainly granitic in origin. The objective of this study is to determine the concentration of $K^+$ and $Ca^{2+}$ using Energy Dispersive X-ray Fluorescence (EDXRF), whereas $F^-$, $Cl^-$ and $SO_4^{2-}$ were determined by ion chromatography (IC) in the well water collected from various districts of Kelantan. The well water samples were collected from Gua Musang, Jeli, and Tanah Merah districts. In situ measurement of water quality parameters such as temperature, pH, salinity, dissolve oxygen (DO), conductivity, turbidity and total dissolved solids (TDS) were conducted using YSI portable multi-probes meter. The concentrations of K+ and $Ca^{2+}$ were measured and found in the range of 227.89 – 691.44 and 0 – 36.71 ppm respectively. The concentration of $Cl^-$, $SO_4^{2-}$ and $F^-$ were measured and found on the ranged of 2.08-17.0, 0.71-13.10 and 0 – 3.54 ppm respectively.

**Keywords**: well water, cations, anions, EDXRF, ion chromatography

**Abstrak**

Air telaga adalah sumber alam yang dapat diperbaharui dan salah satu daripada sumber air minuman untuk beberapa kawasan di negeri Kelantan. Penilaian kualiti air telaga adalah sangat penting dalam menilai kesesuaian air ini sebagai air minuman. Ion-ion utama seperti $K^+$, $Ca^{2+}$ dan $Na^+$ dalam air telaga berasal daripada komposisi mineral terlarut dalam batuan bawah tanah dan tanih yang kebanyakannya bercirikan granit. Kajian ini dijalankan untuk menentukan kepekatan $K^+$, $Ca^{2+}$ dan $Na^+$ dengan menggunakan Pendaflur Serakan Tenaga Sinar-X, manakala $F^-$, $Cl^-$ dan $SO_4^{2-}$ telah diukur menggunakan ion kromatografi. Sampel air telaga di dalam kajian ini telah diambil dari daerah Gua Musang, Jeli dan Tanah Merah. Parameter in situ kualiti air telah diukur dengan menggunakan multi probe YSI mudah alih. Julat kepekatan untuk $K^+$ dan $Ca^{2+}$, masing-masing adalah dalam lingkungan 227.89 – 691.44 dan 0 – 36.71 ppm. Julat kepekatan untuk $Cl^-$ , $SO_4^{2-}$ dan $F^-$ masing-masing adalah di antara 2.08-17.0 , 0.71-13.10 dan 0 – 3.54 ppm

**Kata kunci:** air telaga, kation, anion, EDXRF, ion kromatografi

## Introduction

Groundwater issues have become great interests among researchers recently due to strong possibility of being anthropogenically contaminated by various types of pollutants. It is a public knowledge that human activities such as mining, agriculture as well as an increase in population may directly affected the groundwater system. Well water categorize as ground water is an important source of domestic, agricultural and industrial activities in some countries and remains one of usable water in fast growing countries [1]. Generally, groundwater is less polluted than surface water because when it flows through soil and rocks, they filters most of the pollutants presents in groundwater [2, 3]. Groundwater also contains higher mineral concentration than surface water since minerals in

groundwater come from earth subsurface system. Major ions such as $K^+$, $Ca^{2+}$, $Cl^-$, and $SO_4^{2-}$ are normally applied in classifying and assessing groundwater quality [3]. It plays a significant component of the total dissolved solids present in groundwater [4]. It is important to have continuously groundwater quality monitoring program especially if the fresh groundwater is used as the major source of urban water supply for domestic and industrial [4]. Continuous monitoring is also needed because the quality of the groundwater may vary due to various factors such as season, climate and other factors which include anthropogenic and domestic activities. This groundwater quality will reflects inputs from the atmosphere and soil, as well as the level of activities that is source of pollutant such as mining, land clearance, agriculture, acid precipitation, domestic and industrial waste [5].

Major and minor ions in drinking water are very crucial to human health. These ions are very important to serve several functions in human body. It can have a significant effect on human health either through deficiency due to inadequate intake or toxicity due to excessive intake of the nutrients [6]. Potassium which present in our daily diet and ground water is vast and widely distributed and is an essential element in human, animal and plant tissues. Potassium and sodium are very important in maintaining normal osmotic pressure in cells. It is a cofactor for many enzymes and is required for the secretion of insulin, carbohydrate metabolism and protein synthesis [6]. Calcium can be found in all natural waters and it can contribute to the water hardness. Calcium is an essential element for human diet as it needed for many body functions such as bone structure, muscle contraction, nerve impulses transmission as well as blood clotting.

Many studies on the determination of major ions in the groundwater had been conducted to assess the concentration of major and minor ions as well as heavy metals. Those studies concluded that these ions are varies from place to place, depending on the chemical composition of the rocks through which the groundwater move and also based on the human activities at that place. The objectives of this study is to determine the concentration of major ions which are, $Ca^{2+}$ and $K^+$, $F^-$, $Cl^-$ and $SO_4^{2-}$ in well water collected from different locations in Kelantan and to compare the results with WHO permissible limit.

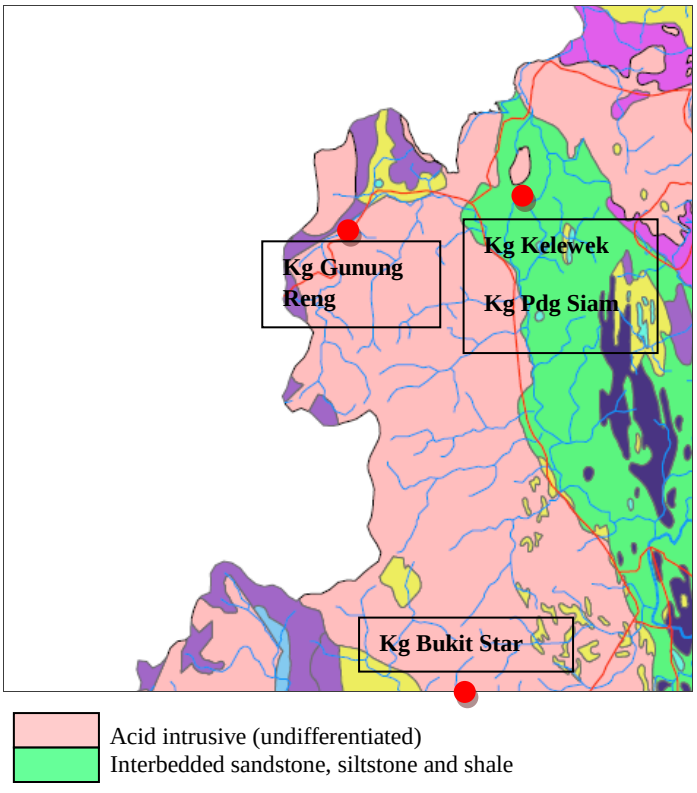



Figure 1: The geological map of the sampling area

**Study Area**

The State of Kelantan with the total area of 15,099 $km^2$ still relies on well water and boreholes for drinking and domestic purposes were chosen for this study. It is located in the north-east of Peninsular Malaysia, bordered with Narathiwat Province of Thailand in the north and Terengganu to the south-east, while the west is adjacent to the Perak and Pahang in the south. Figure 1 shows the geological formation of the sampling sites. In general the geology of the sampling sites consists of acid intrusive rock; which is mainly granites and sandstone [7].

Table 1: Sampling points and depth of the well

| Location | Location code | Depth of the well (m) | Sampling Depth (m) | Latitude(N) | Longitude(E) | Altitude (m) |
|---|---|---|---|---|---|---|
| Kg Baru Star, Gua Musang | KBS | 1.5 | 1 | 05°00.009’ | 101°58.601’ | 132 |
| Kg Gunung Reng, Jeli | KGR | 1.5 | 1 | 05°43.056’ | 101°44.683’ | 93 |
| Kg Banggol Jenerih, Tanah Merah | KBJ | 5 | 1,2,3,4,5 | 05° 49.265’ | 102°08.629’ | 61 |
| Kampung Kelewek, Tanah Merah | KKL | 3.5 | 1,2,3 | 05° 58.387’ | 102°05.888’ | 44 |
| Kg Padang Siam, Tanah Merah | KPS | 1.5 | 1 | 05° 43.175’ | 102° 07.753’ | 39 |

## Materials and Methods

Well water samples were collected from five locations in Kelantan. The sampling locations were selected based on the availability of the well in that area. Sampling coordinates and elevation were obtained using Global Positioning System (GPS). Water sampling was performed by taking the samples at every 1 meter interval from water surface. The samples were taken using water sampler and transferred to the polyethylene bottles which were previously washed with nitric acid and thoroughly rinsed with deionized water. YSI portable multi probes water quality equipment were used for in situ measurement of pH, specific conductivity, DO, temperature, salinity, TDS and turbidity. Table 1 shows the sampling points and the depth of the wells.

The water samples were preserved by adding nitric acid 6 M to pH 2 before filtering using 0.45 µm cellulose nitrate membrane filter prior to analysis. The concentration of $K^+$, $Ca^{2+}$ in both filtered and unfiltered samples were determined using Minipal4 Energy Dispersive X-ray Fluorescence (EDXRF) and $F^-$, $Cl^-$ and $SO_4^{2-}$ (for filtered samples) using ion chromatography (IC). For EDXRF measurement, 5 mL of filtered and unfiltered samples were pipette into the sample cups fitted with 1.5 µm thin mylar film beneath the cups. For Ca measurement, helium gas was applied to enhance the stability of air pressure for good precision of measurement. 1000 ppm stock single element standard solutions were used for calibration. It was diluted to several concentrations to obtain linear calibration plot.

In ion chromatography analysis, the filtered samples were injected in the column with running time 12 minutes. Triplicate measurements were done for each sample to ensure constant results obtained. The calibration was done using series of anion concentration 0 to 10 ppm; prepared from stock solution of 1000 ppm to obtain linear calibration with $r^2 = 0.998$, $r^2 = 0.986$ and $r^2 = 0.992$ for Cl, $SO_4$ and F respectively.

## Results and Discussion

Table 2 shows the values of in situ water quality parameters from 5 sampling locations. The values in the table below only differ slightly for different levels of well water samples. There is little variation in the temperature range

which is between 26.11 to 27.38$^{o}$C. The result indicates that the pH of well water samples is slightly acidic which is 4.6 to 5.82. The lower pH is probably due to the acidic type of rock of the well location, in which most of the sampling sites are located on granite rocks which consist of acid intrusive rocks. Generally, it may also be attributed to the interaction of surface water and the carbon dioxide in the atmosphere and gain entry into the well. When the groundwater from open dug well is exposed to the air, the carbon dioxide that present in the air gets dissolved in the water and results in decreasing of pH. This lower pH value is beyond the WHO recommended ranged for drinking purposes which is between 6.5-8 [8]. Conductivity is a numerical expression of ability of an aqueous solution to carry electric current. It also indicates the amount of total dissolved solids (TDS) in water. TDS consist of inorganic salts such as calcium, magnesium, potassium, sodium, bicarbonates, chloride and sulphate [8]. Salinity is an indicator of the concentration of the amount of dissolved salts, including calcium, magnesium, sodium and potassium [9]. KGR water sample has the highest value for TDS, conductivity and salinity which is 0.33 g/L, 523 μS/cm and 0.25 mg/L respectively.

Table 2: Physical and chemical properties of water from the ground water system studied

| Loc Code | Sampling Depth | Temp ($^{o}$C) | DO (mg/L) | Salinity (mg/L ) | TDS (mg/L) | pH | Conductivity (μS/cm) | Turbidity (NTU) |
|---|---|---|---|---|---|---|---|---|
| KBS | 1 m | 26.8 | 2.40 | 0.07 | 0.10 | 5.58 | 157.0 | 43.10 |
| KGR | 1 m | 26.1 | 2.72 | 0.25 | 0.33 | 4.83 | 523.0 | 2.54 |
| KBJ | 1 m | 27.3 | 0.81 | 0.08 | 0.11 | 4.65 | 172.0 | 2.41 |
| | 2 m | 27.3 | 0.86 | 0.08 | 0.11 | 4.60 | 172.0 | 2.53 |
| | 3 m | 27.3 | 0.75 | 0.08 | 0.11 | 4.70 | 172.0 | 2.46 |
| | 4 m | 27.3 | 0.68 | 0.08 | 0.11 | 4.80 | 172.0 | 2.94 |
| | 5 m | 27.3 | 0.67 | 0.08 | 0.11 | 4.87 | 172.0 | 97.90 |
| KKL | 1 m | 26.7 | 1.66 | 0.03 | 0.05 | 5.08 | 80.0 | 0.62 |
| | 2 m | 26.7 | 1.62 | 0.03 | 0.05 | 5.17 | 80.0 | 1.02 |
| | 3 m | 26.7 | 1.60 | 0.03 | 0.05 | 5.58 | 79.0 | 2.70 |
| KPS | 1 m | 27.3 | 1.44 | 0.07 | 0.10 | 5.82 | 159.0 | 1.45 |

The concentrations of $Ca^{2+}$ and $K^{+}$ for both filtered and unfiltered samples are presented in Figure 2 and 3. These results are the average of triplicate analysis measurement. Table 3 shows a wide variation in the concentration of the major ions. This variation may be closely related to the geological formation and human activities around the wells [10]. The concentrations of calcium for all collected samples are below the permissible limit by WHO which is 75 to 200 mg/L [2]. KGR that were taken from Jeli shows the highest concentration for $Ca^{2+}$ and $K^{+}$. The concentration of ions in well water is closely related to the specific conductivity and TDS of the samples. From Table 2, we can see that KGR has the highest value for both specific conductivity and TDS. The other reason is it might be due to geological formation of that area. $Ca^{2+}$ is mainly associated with carbonate minerals like calcite ($CaCO_3$ ) and dolomite $(CaMg)(CaCO_3)_2$ which is occurs in the secondary minerals residual boulders of igneous granite [2]. The concentration could also be attributed by dissolved limestone found in that area, which is Gunung Reng. The concentration of $K^{+}$ for filtered and unfiltered samples are varies between 272.02 to 619.58 ppm respectively. The concentration of $K^{+}$ is higher than the WHO permissible limit 250 mg/L.

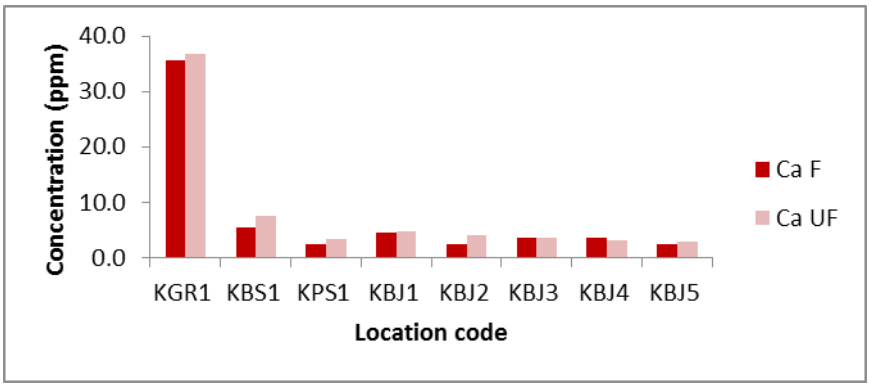



Figure 2: Concentration (ppm) of $Ca^{2+}$ in Kelantan well water




Figure 3: Concentration (ppm) of $K^{+}$ in Kelantan well water

Figure 4 shows the concentration of $Cl^{-}$, $SO_4^{2-}$, and $F^{-}$ for filtered samples. Sulphate is important in groundwater quality assessment because it is part of naturally occurring minerals in some soil and rock formation. Over time, this mineral will dissolve and release into groundwater. Chloride normally present in low concentrations in surface water while groundwater will contain varying amounts of chloride depending on the weathering and leaching of sedimentary rocks and soils and the dissolution of salts deposits. Generally, chloride is not harmful to human beings unless high concentration is reached [11]. Fluoride is an important criterion for groundwater quality with an acceptable limit of 1.5 mg/L [1, 12] [13]. The potential sources of fluoride in the groundwater include various minerals in rocks and the weathering of process of these rocks. It is considered as dominant source of fluoride in groundwater [14]. Fluoride is important for oral health. However high concentration can cause dental and skeletal flourosis [1]. The variations in the results below are mainly due to the different geological formation and anthropogenic sources like agricultural practices. The surrounding area of the wells also plays an important role in determining the concentration of these ions.

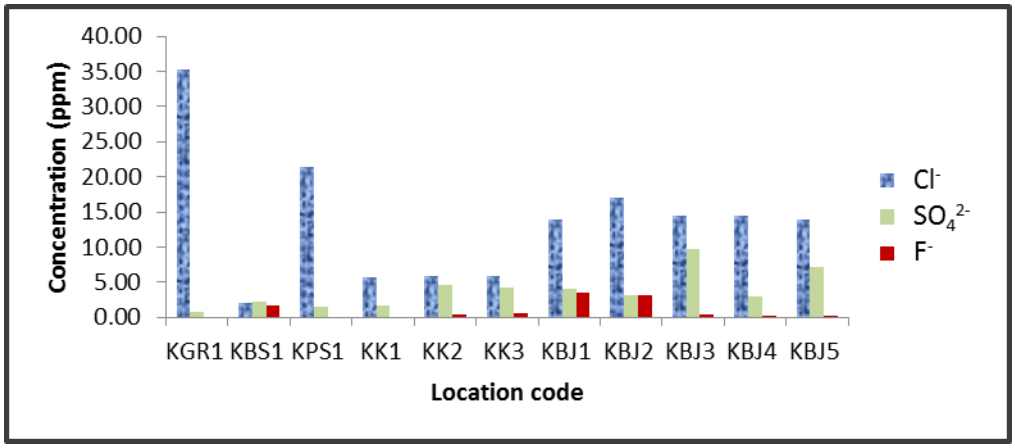



Figure 4: Concentrations of $Cl^-$, $SO_4^{2-}$ and $F^-$ (ppm) in water from ground water system in Kelantan

## Conclusion

The concentrations of $K^+$ and $Ca^{2+}$ were measured and found in the range of 227.89 – 691.44 and 0 – 36.71 ppm respectively, while the concentration of $Cl^-$, $SO_4^{2-}$ and $F^-$ are ranged of 2.08-17.0, 0.71-13.10 and 0 – 3.54 ppm respectively. Generally the concentrations of cations and anions in Kelantan well water is not within the WHO permissible levels, consumption of the water for drinking may require treatment. We have found that pH values are slightly acidic and below than with WHO permissible limit which is 6.5 – 8. This is possibly due to acidic type of rock in Kelantan which is acid intrusive rocks.

## Acknowledgement

The authors would like to express their thanks and gratitude to UiTM's Research Management Institute (RMI) for grant Research Excellence Fund 600-RMI/DANA 5/3/RIF (1/2012) and other support bestowed to our research group for the success implementation of the project program. The help and cooperation of other member of the ESCAN research group are also appreciated.

## References

1. Ishaya, S. and I.B. Abaje, (2009). Assessment of bore wells water quality in Gwagwalada town of FCT. *Journal of Ecology and Natural Environment*. 1(2): 32-36.
2. Sharma, P. and H.P. Sarma, (2011). Groundwater quality assessment of Pachim Nalbari block of Nalbari district Assam based on major ion chemistry. *International Journal of ChemTech Research*. 3(4): 1914-1917.
3. Khodapanah, L., W.N.A. Sulaiman, and N. Khodapanah, (2009). Groundwater Quality Assessment for Different Purposes in Eshtehard District, Tehran, Iran. *European Journal of Scientific Research*. 36(4): 543-553.
4. Nwankwoala, H.O. and G.J. Udom, (2011). Studies on Major Ion Chemistry and Hydrogeochemical Processes of Groundwater in Port Harcourt City, Southern Nigeria. *Journal of Spatial Hydrology*. 11(1).
5. Ackah, M., Agyemang, O., Anim, A. K., Osei, J., Bentil, N. O., Kpattah, L, (2011). Assessment of groundwater quality for drinking and irrigation: the case study of Teiman-Oyarifa Community, Ga East Municipality, Ghana. *Proceedings of the International Academy of Ecology and Environmental Sciences*,. 1(3-4): 186-194.
6. Satyanarayanan, M., Balaram, V., Hussin, M. S. A., Jemaili, M. A. R. A., Rao, T. G., Mathur, R., Ramesh, S. L. (2006). Assessment of Groundwater Quality in a Structurally Deformed Granitic Terrain in Hyderabad, India.
7. Zaini Hamzah, Siti Afiqah Ahmad Saat, Siti Shahrina Agos, and Zaharudin Ahmad, (2010). Measurement of $^{226}Ra$ in Water Using Liquid Scintillation Counting Technique.
8. WHO Guidelines for Drinking Water Quality, (2004). 1.

9. Zaini Hamzah, Ahmad Saat, and Mohammed Kassim, (2011). Determination of Radon Activity Concentration in Hot Spring and Surface Water Using Gamma Spectrometry Technique. *The Malaysian Journal of Analytical Sciences*, **15**(2): 288 - 294.
10. Soltan, M.E., (1997). Evaluation of Groundwater Quality in Dakhla Oasis (EgyptianWestern Desert). *Environmental Monitoring and Assessment*, (57): 157–168.
11. Bacha, A.A., M.I. Durrani, and P.I. Paracha, (2010). Chemical Characteristics of Drinking Water of Peshawar. *Pakistan Journal of Nutrition*. **9**(10): 1017-1027.
12. Sivasankar, V. and R. Gomathi, (2009). Fluoride and other Quality Parameters in the Groundwater Samples of Pettaivaithalai and Kulithalai Areas of Tamil Nadu, Southern India. *Water Qual Expo Health,* (1): 123–134.
13. Pritchard, M., T. Mkandawire, and J.G. O'Neill, (2008). Assessment of groundwater quality in shallow wells within the southern districts of Malawi. *Physics and Chemistry of the Earth,* (33): 812–823.
14. Chae, G. T., Yun, S.T, Kwon, M.J., Kim, Y.S., & Mayer, B. (2005). Batch dissolution of granite and biotite in water: Implication for fluorine geochemistry in groundwater. *Geochemical Journal,*. 40: 95-102.

The Malaysian Journal of ANALYTICAL SCIENCES ISSN 1394-2506

# DETERMINATION OF SUPPORTED $^{222}$Rn ACTIVITY CONCENTRATION IN GROUND WATER FROM CAMERON HIGHLANDS AREA USING GAMMA SPECTROMETRY

## (Penentuan Kepekatan Aktiviti $^{222}$Rn Sokongan di dalam Air Tanih dari Kawasan Cameron Highlands Menggunakan Spektrometri Gama)

Ahmad Saat[1,2], Nor Shazlina Zainal[1]*, Zaini Hamzah[1] and Abdul Khalik Wood[1]

[1]*Faculty of Applied Sciences,*
*Universiti Teknologi MARA, 40450 Shah Alam, Selangor, Malaysia*
[2]*International Education College (INTEC),*
*UiTM Kampus Seksyen 17, 40200 Shah Alam, Selangor, Malaysia*

**Corresponding author: elinshazlinazainal89@gmail.com*

**Abstract**

Humans may be exposed to the emission of energetic alpha particle from supported radon decaying process in ground water when it is consumed. Cameron Highland's water supply was chosen as study area since it coming from hilly area of Gunung Pass, Gunung Brinchang and Gunung Cantik whose geological formations made from mainly igneous rocks (intrusive rocks, mainly granite with minor granodiorite) that flows into Sungai Terla, Sungai Ulu Bertam and Sungai Jasar. Determination of supported radon in this ground water was carried out using eighteen ground water samples collected from Cameron Highlands. Water samples (filtered and unfiltered) were poured into Marinelli beaker and closed tightly. These samples were kept at least for three weeks to allow the equilibrium between $^{226}$Ra and $^{222}$Rn. The measurement was accomplished by measuring water samples using low background gamma spectrometry (ORTEC) using a hyper pure coaxial germanium detector linked to a multi-channel digital analyzer system. $^{222}$Rn was measured at its daughter's photo peaks: $^{214}$Pb (352 keV) and $^{214}$Bi (609 keV). Results of the study show the supported $^{222}$Rn activity concentration ranges from 0.19 to 0.66 Bq/L for unfiltered, filtered and untreated samples, 0.32 to 0.39 Bq/L of $^{222}$Rn for treated water at water treatment plant and 0.26 to 0.55 Bq/L of $^{222}$Rn for domestic water. These values are lower than the activity concentration of radon in drinking water as proposed by USEPA (11 Bq/L).

**Keywords:** Ground water, supported radon, natural radioactivity, gamma spectrometry

**Abstrak**

Manusia mungkin terdedah kepada pancaran zarah alfa bertenaga tinggi dari proses penyepaian 'supported radon' dalam air ini apabila digunakan. Sumber air Cameron Highlands dipilih sebagai tempat kajian kerana air tanih mengalir daripada Gunung Pass, Gunung Brinchang dan Gunung Cantik di mana keadaan geologinya adalah kebanyakannya daripada batuan igneous (batuan intrusive (batuan yang terhasil daripada pengkristalan magma di dalam bumi), granit dengan sedikit granodiorite (batuan kecil mengandungi kandungan silika yang tinggi) yang mengalir ke Sungai Terla, Ulu Sungai Bertam dan Sungai Jasar. Pengukuran radon sokongan dalam air tanih dijalankan menggunakan lapan belas sampel air tanih dari Cameron Highlands. Sampel air dimasukkan ke dalam bikar Marinelli dan ditutup dengan ketat. Sampel ini disimpan sekurang-kurangnya selama tiga minggu untuk membenarkan keseimbangan di antara $^{226}$Ra dan $^{222}$Rn. Pengukuran terlaksana dengan mengukur sampel air menggunakan spektrometri gama berlatar belakang rendah (ORTEC) menggunakan pengesan *coaxial* germanium berketulenan tinggi bersambungan kepada sistem digital analisis pelbagai-haluan. $^{222}$Rn diukur pada its daughter's photopeaks: $^{214}$Pb (352 keV) dan $^{214}$Bi (609 keV). Keputusan daripada kajian menunjukkan bahawa kepekatan aktiviti $^{222}$Rn sokongan dalam lingkungan dari 0.19 sehingga 0.66 Bq/L bagi sampel air tidak bertapis,bertapis dan air tidak dirawat, 0.32 sehingga 0.39 Bq/L $^{222}$Rn bagi air terawat di loji rawatan air dan 0.26 sehingga 0.55 Bq/L $^{222}$Rn bagi lokasi pengagihan air dirawat. Nilai kepekatan aktiviti radon sokongan lebih rendah daripada kepekatan aktiviti radon dalam air minuman yang dianjurkan oleh USEPA (11 Bq/L).

**Kata kunci:** Air bawah tanah, radon sokongan, radioaktiviti tabii, spektrometri gama

## Introduction

In the last decades, radon and its decay product in water has become a great deal of concern to the public since it can pose health hazard to humans and environment [1, 2, 3]. Radon is a naturally occurring radioactive inert gas, partially soluble in water, colorless, odorless with a half-life of 3.84 days which a progeny of uranium and thorium decay series [1, 4, 5, 6]. Radon is an alpha emitter that decays into a chain of progenies of alpha emitters such as $^{218}$Po (6.0 MeV), $^{216}$Po (6.7 MeV), $^{214}$Po (7.7 MeV) and $^{212}$Po (8.8 MeV) [1, 4]. It is produced continuously by the alpha decay of radium with some atoms escaping to the surrounding fluid phase, such as ground water when the water moves through granitic rocks containing natural uranium and thorium that released radon to the water [7]. Thus, this gas found in various concentrations in ground water [8].

Cameron Highlands used ground water as its own fully water supply. It was chosen as study area since the ground water is coming from Gunung Pass, Gunung Brinchang and Gunung Duri whose geological formations mainly made from igneous rocks (intrusive rocks, mainly granite with minor granodiorite) that flows into its specific rivers of Sungai Terla, Sungai Habu and Sungai Jasar [9,10]. This ground water is sufficiently large volume to induce an appreciable spread in dissolved supported radon concentration [11]. The ground water was collected from source, river, diverted upstream to the treatment plant and distributed treated water for domestic purposes. The geology and local in nature of Cameron Highlands are ideal for such study since public water sources are used for services and drinking purposes.

Normally, radon-in water activity concentrations are measured by means of liquid scintillation counting (LSC) as recommended by USEPA [1,12, 13]. However, alternative method such as gamma spectrometry has been used as alternative method to quantify radon-in-water [1, 12, 13, 14]. The quantification of $^{222}$Rn-in-water after at least three weeks to allow the secular equilibrium between $^{226}$Ra, $^{222}$Rn and its progenies is known as supported $^{222}$Rn [15].The aim of the study is to determine supported $^{222}$Rn activity concentration in untreated and treated ground water from Cameron Highlands area using gamma spectrometry technique.

## Materials and Methods

### Sampling Site and Samples

Ground water sampling location in Cameron Highlands, Malaysia is shown in Figure 1. The sampling was carried out on 25$^{th}$ until 27$^{th}$ of November 2011. Nine ground water samples were collected comprises of water source intake, treated water treatment plant and domestic water from houses in Cameron Highlands, Pahang. The exact sampling point was determined using global positioning system (GPS). Sampling points is shown in Table 1. From each sampling point, 10 liter samples were collected and kept in containers. The containers was cleaned with 6 M nitric acid ($HNO_3$) and rinsed with distilled water in order to remove any contaminants, prior to use.

As shown in Table 1, there were three types of samples collected which were untreated ground water from Sungai Terla and Kuala Terla water Treatment Plant (LAKT), treated water from LAKT and domestic water from houses. At intake, water samples taken at surface and at 0.5 m below surface. Aerated sample taken at surface and below surface water (0.5 m) at LAKT aeration pond and treated water sample was collected from water output of LAKT. The domestic water was collected from domestic pipes at houses. The altitude for intake sampling point was higher than LAKT results the untreated river water was transferred to the LAKT due to gravity. The treated water was distributed to KRA, TKP, KTS and TRA using buffer pumps since their altitude were higher than LAKT.

On the same sampling point, seven water quality parameters were measured in-situ using YSI multi probe water quality meter. The parameter measured were dissolved oxygen (DO), pH, turbidity, temperature, total dissolves solid (TDS), salinity and oxidation reduction potential (ORP). Total suspended solid (TSS) was determined in the laboratory [16].

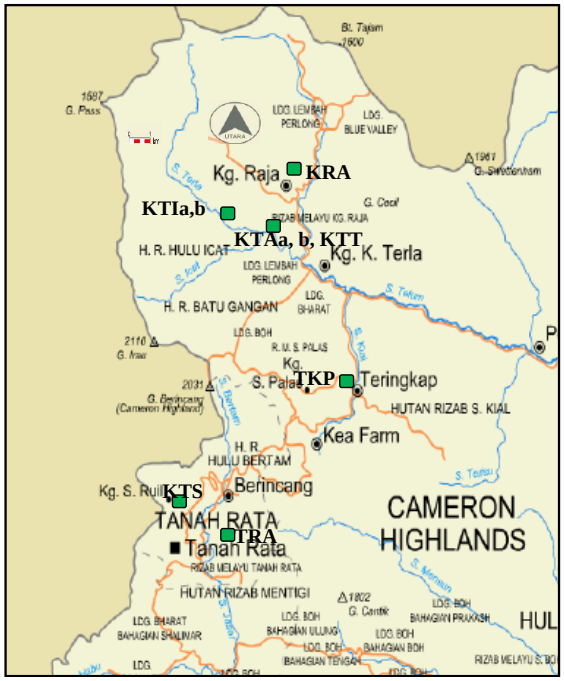



Figure 1: Locations of ground water sampling in Cameron Highlands, Malaysia (Note: ■ Sampling Location).

Table 1: Description of Sampling point

| Location | Sample | Type of Water Samples | Latitude (N) | Longitude (E) | Altitude (m) |
|---|---|---|---|---|---|
| Intake Kuala Terla | KTIa | Terla River (surface) | 04° 33.500’ | 101° 23.873’ | 1286 |
| | KTIb | Terla River (below surface) | 04° 33.500’ | 101° 23.873’ | 1286 |
| Water Treatment Plant Kuala Terla (LAKT) | KTAa | Aerated untreated water (surface) | 04° 32.796’ | 101° 24.562’ | 1269 |
| | KTAb | Aerated untreated water (below surface) | 04° 32.796’ | 101° 24.562’ | 1269 |
| Water Treatment Plant Kuala Terla (LAKT) | KTT | Treated water (in water tank) | 04° 32.796’ | 101° 24.562’ | 1269 |
| Kampung Raja | KRA | Domestic water | 04° 34.122’ | 101° 24.608’ | 1298 |
| Tringkap | TKP | Domestic water | 04° 30.842’ | 101° 25.646’ | 1433 |
| Kampung Taman Sedia | KTS | Domestic water | 04° 28.620’ | 101° 22.922’ | 1454 |
| Tanah Rata | TRA | Domestic water | 04° 28.014’ | 101° 23.083’ | 1464 |

**Sample Preparation**

In laboratory, the pH of the water samples were adjusted to below 2 using 6 M nitric acid in order to stabilize the water, to avoid the loss of radionuclides fractions via adsorption on the wall of the containers and to prevent any biological activities [1, 4]. Each water samples were divided into two portions; one portion represented for unfiltered samples and another portion was for filtered water samples. The filtered samples were filtered using cellulose membrane filters (0.45 μm, Whatman) on Buchner funnel attach to pump to filter away suspended solid and impurities from water samples. This will enable the suspended solids to be determined.

The filtered and unfiltered water samples were then filled into 600 ml Marinelli beaker to brim and closed tightly. The beaker was sealed using silicon glue, to avoid the leakage of radon gas [14]. The beakers were kept for at least three weeks to allow the secular equilibrium between $^{226}$Ra, $^{222}$Rn and its progenies ($^{214}$Pb and $^{214}$Bi) and ready for measurement using gamma spectrometry.

**Measurement of Supported $^{222}$Rn**

The samples were counted using low background gamma rays spectrometry (ORTEC) using a hyper pure coaxial germanium detector with resolution 1.84 keV, 25% relative efficiency at 1332 KeV $^{60}$Co gamma ray linked to a multi-channel digital analyzer system. The efficiency calibration of gamma spectrometry was done using secondary standard made up by mixing known amount of uranium trioxide ($UO_3$) and KCl in the same container geometry as samples to cover energy from 63 keV to 1001 keV and 1460 keV for $^{40}$K [17]. The standard and samples were counted for 8 hours (28800s). Figure 2 shows the efficiency of the gamma rays spectrometer used for calculation of individual radionuclides activity in water samples. Since, the energy of radionuclides interested is higher than 200 keV, Equation (A); Efficiency = $1.143x^{-0.67}$ were used to calculate the detection efficiency at energy of each radionuclides [18].

Since $^{222}$Rn is an alpha emitter, the measurement of $^{222}$Rn in water samples was based on $^{222}$Rn progenies which were $^{214}$Pb and $^{214}$Bi with gamma energy peak at 352 keV and 609 keV respectively. This approach is possible for $^{222}$Rn that is equilibrium with its progenies [15, 19]. The spectra obtained were analyzed using Gamma Vision-32 version 6.07 software provided by ORTEC®. After analyzing the peak in the spectra, the activity concentration of the individual radionuclide was calculated using Equation 1.

$$A_V = \frac{C_\gamma}{\xi_\gamma \times P_\gamma \times M_s} \quad (1)$$

where:

$C_\gamma$ = Net peak area per counting time (count/sec)
$\varepsilon_\gamma$ = Detector efficiency at the specified energy
$P_\gamma$ = Transition probability of gamma radiation
$M_s$ = Volume of sample (L)

The activity concentrations for both progenies ($^{214}$Pb and $^{214}$Bi) where then averaged to represent the supported $^{222}$Rn activity concentration [19]. The gamma spectrometry method for determination was validated earlier and precision of 10 measurements was found to be 2.15% and the minimum detectable activity (MDA) for 609 keV was 0.12 Bq/L [15].

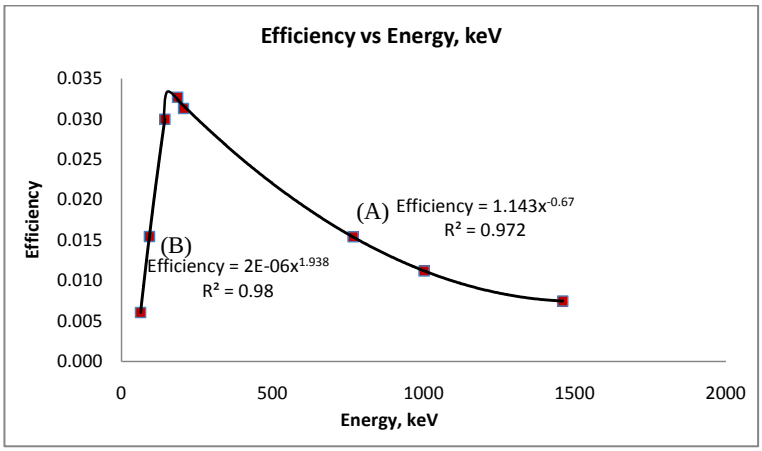



Figure 2: Efficiency Calibration using $UO_3$ and KCl by Gamma Spectrometry

## Results and Discussion

### Water Quality Parameter Measurement

Table 2 shows various water quality parameters measured for each sample together with NWQS individual value for Class I and Class IIA Water [20] for comparison purpose. High concentration of DO indicates good water quality [1] because it will reduce the activity of microbial reduction of nitrate to nitrite and sulfate to sulfide and reduced the concentration of ferrous iron [3]. However, DO do not affect $^{222}$Rn activity concentration [15]. The pH of KTS is slightly acidic due to the origin of river water, tannin and leaves that released from forest floor [21]. Leaves decay and react with water, forming humic acid and released from forest to the river [21].

KTA has highest turbidity value since the sample was aerated untreated sample at aeration pond. Particulate matter that may be present from water source as a result from inadequate filtration or from re-suspension of sediment and the presence of inorganic particulate matter in some ground waters within the distribution system can cause turbidity [3]. The suspended solid was attributed to soil erosion due to opening up lands around the areas for agriculture and other activities [22]. The effect was extremely significant during rain [22].

The low temperature for all samples due Cameron Highlands elevation of more than 1500 m above sea level, resulting the temperature to be less than 25°C year-around and rarely falls below 12°C [23]. This low temperature slows down the water-rock interaction processes and consequently radon emanation to the ground water [9]. Since this ground water is used for drinking water purposes, it should be at least in Class IIA or better [20].

### Supported $^{222}$Rn Activity Concentration

Activity concentrations of supported $^{222}$Rn in nine ground water samples (unfiltered and filtered) were presented in Table 3. The uncertainty in the measured activity concentration estimated from the peak area determination and the background [24]. The filtered samples activity concentration of supported $^{222}$Rn were lower than unfiltered samples due to removal of non-dissolve suspended solid that contains a small amount of radionuclides from ground water samples [4, 14, 15]. However, the F-value (0.91) shows no significance difference in variance between both types of samples. This was due to small amount of radionuclides that contains in a small amount TSS in samples as shown in Table 2.

Unfiltered samples from Sungai Terla (KTIa and KTIb) contained highest amount of $^{222}$Rn due to the raw water was coming from underground. This ground water source of LAKT, is coming from Gunung Pass which is located on the backbone of Peninsular Malaysia that flows into Sungai Terla [10]. Based on the geological map, the geological formation of the area is mainly made from igneous rocks (intrusive rocks, mainly granite with minor granodiorite)

[9]. Igneous rocks normally contain high amount of natural uranium and thorium which natural source of radon [4, 5]. Unfiltered samples of KTAa and KTAb contain lower $^{222}$Rn than KTIa and KTIb due to samples were aerated at aeration pond. The aeration process enhances the degassing of $^{222}$Rn from water samples.

Table 2: Some of Water Quality Parameters Measured and NWQS Individual Value for Class I and Class IIA

| **Sample Code** | **DO (mg/L)** | **pH** | **Turbidity (NTU)** | **Temperature (°C)** | **TDS (mg/L)** | **Salinity (mg/L)** | **TSS (mg/L)** |
|---|---|---|---|---|---|---|---|
| KTI | 9.25 | 7.40 | 6.46 | 19.47 | 0.010 | 0.010 | 3.83 |
| KTA | 9.28 | 7.16 | 8.73 | 18.77 | 0.011 | 0.010 | 8.40 |
| KTT | 8.55 | 7.17 | 6.04 | 19.69 | 0.020 | 0.010 | 3.54 |
| KRA | 10.88 | 7.07 | 7.22 | 19.84 | 0.012 | 0.010 | 5.94 |
| TKP | 7.99 | 7.00 | 6.95 | 20.18 | 0.022 | 0.010 | 4.73 |
| KTS | 8.87 | 6.98 | 4.75 | 20.04 | 0.009 | 0.007 | 4.91 |
| TRA | 9.51 | 7.13 | 6.20 | 20.62 | 0.031 | 0.020 | 5.06 |
| Class I [19] | ≥7 | 6.5 – 8.5 | ≤5 | - | ≤500 | ≤0.05 (0.5 %) | ≤25 |
| Class IIA [19] | 5 -7 | 6-9 | ≤50 | (27 ± 2) °C | ≤1000 | ≤0.1 (1%) | ≤50 |

For KTT, the slightly elevated supported $^{222}$Rn in treated water was due to the fact that it was kept in enclosed treated water tank. The increases in supported $^{222}$Rn activity concentration possibly due to the accumulation of radon gas in the enclosed tank and back diffused into the water. Domestic water contained 0.26 to 0.55 Bq/L of supported $^{222}$Rn. TKP contained higher $^{222}$Rn concentration than LAKT. This may be due to the particulate matters such as sand inside the piping system as shown by higher TSS of TKP than KTT in Table 2. For unfiltered samples, the untreated and treated shows appreciable difference of variance with an F-value of 0.37. The same observation prevails for filtered samples where the F-value is 0.11. Since both shows significance differences, the water supply need to be treated before received by the consumer in order to reduce the $^{222}$Rn activity concentration.

High activity concentration of supported $^{222}$Rn was observed from samples (KTIa and KTAa) taken at water surface compared to below surface samples. This possibly due to the $^{222}$Rn was easily moves from below to the river water surface during water movement, geology of the area and bottom sediment of the river [4,14].

The farthest location up to north from LAKT was only KRA while the nearest location to the south from LAKT was TKP followed by KTS and TRA. Based on Table 3, there was no trend in supported $^{222}$Rn activity concentration from KTI to KTT where the water transportation occurs from intake to LAKT. These mainly due potential changes occurring in the water distribution, the oxidation state of the water and the concentration of suitable complexing agents which can increase the solubility of uranium or thorium [24]. However, there was a decreasing trend of

supported $^{222}$Rn activity concentration from TKP to the TRA due to some of supported $^{222}$Rn may loss during water distribution to the higher altitude of KTS and TRA [4].

Table 3: Supported radon activity concentrations in ground water samples

| Sample | **Supported $^{222}$Rn Activity Concentration (Bq/L)** | |
|---|---|---|
| | Unfiltered sample | Filtered sample |
| KTIa | 0.66 ± 0.07 | 0.59 ± 0.07 |
| KTIb | 0.43 ± 0.06 | 0.32 ± 0.05 |
| KTAa | 0.36 ± 0.05 | 0.29 ± 0.05 |
| KTAb | 0.29 ± 0.05 | 0.19 ± 0.04 |
| KTT | 0.39 ± 0.05 | 0.32 ± 0.05 |
| KRA | 0.40 ± 0.06 | 0.31 ± 0.05 |
| TKP | 0.55 ± 0.07 | 0.44 ± 0.06 |
| KTS | 0.36 ± 0.05 | 0.32 ± 0.05 |
| TRA | 0.28 ± 0.05 | 0.26 ± 0.04 |

**Pearson Correlation of Supported $^{222}$Rn and Water Quality Parameter Measurement**

Table 4 presents Pearson correlation coefficient, between supported $^{222}$Rn activity concentration in ground water samples and water quality parameter. A strong correlation observed between supported $^{222}$Rn activity concentration for unfiltered and filtered samples (r = 0.94) due to some radionuclides may attach to the non-dissolved suspended solids in samples [14, 15]. Moderate correlation observed between $^{222}$Rn with temperature. This was due to low temperature slows down the water-rock interaction processes and the releasing of radon to the ground water [8, 15]. Besides that, there was inversely correlation between $^{222}$Rn with pH, DO, salinity, and TSS. pH may influence the solubility and mobility of radionuclides in water as the solubility is increasing with decreasing in pH as radium is more soluble in pH less than 5 than at higher pH [15]. DO and salinity does not affect the emanation of $^{222}$Rn to the ground water [14, 15]. TSS contained very low amount of $^{222}$Rn [15]. In this study, supported $^{222}$Rn activity concentration shows inversely very weak correlation with turbidity (r = -0.08 and 0-0.38) and very weak correlation with TSS (r = 0.15). However, another study showed good correlation between $^{222}$Rn activity concentration with TSS and turbidity [15].

The study was extended to explore the correlation between various water quality parameters. A strong correlation between TDS and salinity (r = 0.83) possibly due to the dissolved solids in the samples was the dissolved salts such as calcium, magnesium, sodium and potassium that indicate salinity [14, 15]. Moderate correlation can be observed between turbidity and TSS (r = 0.74), temperature with TDS (r = 0.68) and salinity (r = 0.52). Suspended solids such as soils and particulate matters can affect the turbidity of the water samples [3, 22]. Since TDS and salinity has strong correlation between each other, higher temperature possibly can enhance the dissolving salts and solids in the water samples. The other parameters show no significant correlation between each other.

Table 4: Pearson correlation coefficient, between supported $^{222}$Rn activity concentration in ground water samples and water quality parameter

| | **$^{222}$Rn(UF)** | **$^{222}$Rn(F)** | **DO** | **pH** | **Turbidity** | **Temp** | **TDS** | **Salinity** | **TSS** |
|---|---|---|---|---|---|---|---|---|---|
| $^{222}$Rn (UF) | 1 | | | | | | | | |
| $^{222}$Rn(F) | **0.94** | 1 | | | | | | | |
| DO | **-0.43** | **-0.47** | 1 | | | | | | |
| pH | **-0.23** | **-0.31** | 0.13 | 1 | | | | | |
| Turbidity | **-0.08** | **-0.38** | 0.25 | 0.19 | 1 | | | | |
| Temp | **0.21** | **0.48** | -0.08 | -0.43 | -0.63 | 1 | | | |
| TDS | **0.00** | **0.15** | -0.23 | -0.16 | -0.09 | **0.68** | 1 | | |
| Salinity | -0.41 | -0.29 | 0.19 | 0.13 | 0.05 | **0.52** | **0.83** | 1 | |
| TSS | **-0.43** | **-0.64** | 0.36 | -0.21 | **0.74** | -0.53 | -0.25 | -0.01 | 1 |

UF – unfiltered samples, F – filtered samples

**Comparison with other studies**

Table 5 shows comparison of supported $^{222}$Rn of the present study with other studies. The measured supported $^{222}$Rn activity concentrations in ground water samples were lower than study in India [2] and Korea [25] but similar with studies in Malaysia [14, 15]. Generally, the supported $^{222}$Rn activity concentrations in this present study were lower than the activity concentration limit of radon in drinking water as proposed by USEPA (11 Bq/L) [6, 26]. As a consequence from this, by drinking this water does not cause health hazard risk to the user since the dietary intake ($D_{ing}$) of $^{222}$Rn in this water vary from 0.48 to 1.68 μSv/yr. This $D_{ing}$ is lower than $1x10^2$ μSv/yr (0.1 mSv/yr) of the world limit [27].

Table 5: Comparison of the supported $^{222}$Rn activity concentration obtained in the present study with other studies

| **Place** | **Type of water** | **Supported $^{222}$Rn activity concentration (Bq/L)** |
|---|---|---|
| Punjab, India[2] | Ground water | 2.56 - 7.75 |
| Kelantan, Malaysia [14] | River water | 0.51 - 1.41 |
| Jeju Island, Korea [25] | Ground water, coastal waters and river water | 0.15 to 1.28 |
| Taman Negara Pahang, Malaysia[15] | River water | 0.32 – 1.06 |
| Cameron Highlands, Malaysia (present study) | Ground water | 0.19 – 0.66 |

## Conclusion

The supported $^{222}$Rn activity concentration for unfiltered, filtered and untreated samples ranged from 0.19 to 0.66 Bq/L, the treated and domestic water samples supported $^{222}$Rn activity concentration ranged from 0.32 to 0.39 Bq/L and 0.26 to 0.55 Bq/L. All samples contain lower supported $^{222}$Rn activity concentration than11 Bq/L as proposed by USEPA. The variations are possibly or mainly due to the potential changes occurring in the water distribution, the oxidation state of the water and the concentration of suitable complexing agents. The decreasing trend only observed from TKP to KTS and TRA. The correlation between supported $^{222}$Rn activity concentration and physicochemical parameters could be different from place to place and depends on geological locations.

## Acknowledgement

The authors would like to thank Research Management Institute of Universiti Teknologi MARA for DANAKEP grant (54/2010) and (27/2011), Faculty of Applied Sciences and Environmental Studies using Conventional and Nuclear Method (ESCaN) members for their help in this research works. Thanks also to Pengurusan Air Pahang Berhad (PAIP) for facilitating this sampling process. We also acknowledge everyone who is involving directly or indirectly into this project.

## References

1. Zaini Hamzah, Ahmad Saat and Mohammed Kassim, (2011). Determination of Radon Activity Concentration in water using Gamma Spectrometry and Liquid Scintillation Counter Techniques. In: 3rd *International Symposium and Exhibition in Sustainable Energy and Environment - ISESEE 2011*, 1st-3rd June 2011, Melaka, Malaysia. 191 - 193.
2. Badhan, K, Mehra, R. and Sonkawade, R. G., (2010). Measurement of radon concentration in ground water using RAD7 and assessment of average annual dose in the environs of NITJ, Punjab, India. *Indian Journal of Pure and Applied* Physics, 44: 508 - 511.
3. Guidelines for Drinking Water Quality; in corporating first addendum, (2006). World Health Organization, 1, Recommendation, 3rd ed, 20 Avenue Appia, 1211 Geneva 27, Switzerland. 595 pp.
4. Ahmad Saat, Nor Shazlina Zainal and Zaini Hamzah, (2012). Assessment of Supported Radon in Ground Water from Highland Area Using Portable Continuous Radon Monitor. *Journal of Nuclear and Related Technologies*, 9 (1): 22 - 33.
5. Ahmad Saat, Zaini Hamzah, Wan Muhammad W. A. Kadir, Zaharidah Abu Bakar, Zuraidah A Munir, Siti Mariam Sumari and Misbah Hassan, (2010). Some Remarks on Radon Concentration at Various Locations in Peninsular Malaysia. *Journal of Nuclear and Related Technologies*, 7 (1): 49 - 57.
6. US Environmental Protection Agency, (1999). Radon in Drinking Water Health Risk Reduction and Cost Analysis; Notice. *Federal Register, USEPA 1999*, 5th January, Washington, DC, US. 64 (38): 9560 – 9599.
7. Walia, V., Bajwa, B. S. and Virk, H. S., (2003). Radon monitoring in groundwater of some areas of Himachal Pradesh and Punjab states, India. *Journal of Environmental Monitoring*, 5: 122 - 125.
8. Alessandro, W. D. and Vita, F., (2003). Ground water radon measurements in the Mt. Etna area. *Journal of Environmental Radioactivity*, 65: 187 - 201.
9. Geological Map of Peninsular Malaysia, (2007). Director General of Minerals and Geoscience Malaysia.
10. E-map Pahang, (2008). Director of National Mapping, Malaysia.
11. Abdallah, S. M., Habib, R. R., Nuwayhid, R. Y., Chhatila, M. and Katul, G., (2007). Radon Measurement in Well and Spring Water Lebanon. *Radiation Measurement*, 42: 298 - 303.
12. Osman, A. A. A., Salih, I., Shaddad, I. A., Din, S. E., Siddeeg, M. B., Eltayeb, H., Idriss, H. Hamza, W. and Yousif, E. H., (2008). Investigation of Natural Radioactivity Levels in Water around Kadugli, Sudan. *Applied Radiation and Isotope*, 66: 1650 - 1653.
13. López, R. N., Segovia, N., Cisniege, M. G., López, M. B. E., Armienta, M. A., Seidel, J. L., Peña, P., Godínez, L. and Tamez, E., (2002). Determination of radon, major and trace elements in water samples from springs and wells of northern Mexico State, Mexico. *Geofisica Internacional*, 41: 407- 404.
14. Zaini Hamzah, Ahmad Saat and Mohammed Kassim, (2011). Determination of radon activity concentration in hot spring and surface water using gamma spectrometry technique. *The Malaysian Journal of Analytical Sciences*, 15 (2): 288 - 294.

15. Mohammed Kassim, (2012). *Method Development and Determination of Radon Activity Concentration in Water using Gamma Spectrometry Technique*. MSc Thesis, Universiti Teknologi Mara, Malaysia. 104 pp.
16. APHA, (1998). Standard Methods for Examination of Water and Wastewater (20th). Washington, DC: American Public Health Association.
17. Ahmad Saat, Zaini Hamzah, Mohammad Fariz Yusop and Muhd Amiruddin Zainal, (2010). Experimental Determination of the HPGe Spectrometer Efficiency Calibration Curves for Various Sample Geometry for Gamma Energy from 50 keV to 2000 keV. *Progress of Physics Research in Malaysia – PERFIK, 2009.*
18. Zaini Hamzah, Seh Datul Riduan and Ahmad Saat, (2011). Assessment of Radiation Health Risk in Cameron Highlands Tea Plantations. *The Malaysian Journal of Analytical Sciences*, 15 (2): 130 - 137.
19. Talha, S.A., Lindsay, R., Newman, R.T, de Meijer, R.J., Maleka, P.P., Hlatshwayo, I.N., Mlwilo, N.A. and Mohanty, A.K., (2008). γ-Ray spectrometry of radon in water and the role of radon to representatively sample aquifers. *Applied Radiation and Isotopes*, 66: 1623 – 1626.
20. National Water Quality Standard for Malaysia, (2010). Malaysia Environmental Quality Report. Department of Environment Malaysia (MDOE). 6 pp.
21. Chau, K.W., and Jiang, Y.W., (2002). Three-dimensional pollutant transport model for the Pearl River Estuary. *Water Research*, 36 (8): 2029 – 2039.
22. Makalahmad, A., Eisakhani, M. and Isa, M.H., (2008). Developing MIKE-11 Model for Water Quality Simulation in Bertam River, Cameron Highlands. In: *International Conference on Construction and Building Technology – ICCBT 2008*, 16th – 20th June 2008, Kuala Lumpur, Malaysia. 8 pp.
23. Eisakhani, M. and Makalahmad, A., (2009). Water Quality Assessment of Bertam River and its Tributaries in Cameron Highlands, Malaysia. *World Applied Sciences Journal*, 7 (6): 769 - 776.
24. Lydie, R. M. and Nemba, R. M, (2008). Quantitative Determination of $^{226}$Ra and $^{228}$Ra in Reservoir and Tap Water in Yaounde Area, Cameroon. *Global Journal of Environmental Research*, 2 (3): 110 - 113.
25. Lee, J. M. and Kim, G., (2006). A simple and rapid method for analyzing radon in coastal and ground waters using a radon-in-air monitor. *Journal of Environmental Radioactivity*, 89: 219 - 228.
26. Radium, Radon and Uranium: Health Information Summary, (2007). Department of Environmental Services, New Hampshire (NHDES). 4 pp.
27. Guidelines for Drinking-water Quality, (2011). World Health Organization, 4th ed, WHO Press, 20 Avenue Appia, 1211 Geneva 27, Switzerland. 564 pp.

The Malaysian Journal of ANALYTICAL SCIENCES ISSN 1394-2506

# ASSESSMENT OF HEAVY METAL CONTAMINATION IN SQUID (*LOLIGO SPP*.) TISSUES OF KEDAH-PERLIS WATERS, MALAYSIA

## (Penilaian Pencemaran Logam Berat dalam Tisu Sotong *(Loligo Spp.)* bagi Perairan Air Kedah-Perlis, Malaysia)

Jamil, T.*, Lias, K., Norsila, D., Syafinaz, N. S.

Center of Ocean Research, Conservation & Advances (ORCA)
Division of Research, Industrial Linkage, Community Network & Alumni
Universiti Teknologi MARA (Perlis), 02600 Arau, Perlis, Malaysia

**Corresponding author: jamiltajam@perlis.uitm.edu.my*

**Abstract**

This study was carried out to determine the concentration of selected heavy metals (Cd, Cu, Pb and Zn) in three different tissues collected from the ink-sac, head, and muscle of the squid. Squid samples were caught off the coastal waters of Kedah-Perlis, where only mature squids within the maturity size-range of 13 to 15 cm were used. From this study, the concentration of Zn (35.06±4.06 mg/kg in dry weight) was found significantly higher in all of the tissues, followed by Cu (15.10±13.28 mg/kg in dry weight), Cd (4.76±3.77 mg/kg in dry weight), and Pb with an average value of 4.01±0.08 mg/kg in dry weight. From this study, it was discovered that Zn and Cu concentrations in the tissues were lower than the maximum limit recommended by the Food and Agriculture Organization, Malaysian Food Regulation (1985), as well as other countries. Meanwhile, both non-essential elements namely Cd and Pb recorded higher values than that of the recommended concentrations. According to the Metal Pollution Index (MPI), the ink-sac indicated medium-range contamination, while the head and muscle tissues showed low contamination levels.

**Keywords :** Heavy Metal, Squid (Loligo spp) and Metal Pollution index

**Abstrak**

Kajian ini telah dijalankan untuk menentukan kepekatan logam berat terpilih (Cd, Cu, Pb dan Zn) dalam tiga tisu sotong yang berbeza iaitu kantung dakwat, kepala, dan otot. Sampel sotong telah dikumpulkan dari sekitar Perairan Kedah-Perlis. Hanya sotong yang bersaiz matang sahaja dipilih, iaitu sotong yang bersaiz di antara 13 - 15cm bagi tujuan analisis ini. Daripada kajian ini, kepekatan Zn (35.06 ± 4.06 mg/kg berat kering) telah didapati jauh lebih tinggi di dalam kesemua tisu, diikuti dengan Cu, Cd dan Pb dengan nilai purata masing-masing adalah 15.10 ± 13.28 mg/kg berat kering, 4.76 ± 3.77 mg/kg berat kering dan 4.01 ± 0.08 mg/kg berat kering. Kajian ini telah menunjukkan bahawa kepekatan Zn dan Cu dalam tisu sotong adalah lebih rendah daripada had maksimum yang disyorkan oleh Pertubuhan Makanan dan Pertanian (FAO), Peraturan Makanan Malaysia (1985), dan lain-lain negara. Sementara itu, kedua-dua elemen Cd dan Pb telah menunjukkan nilai kepekatan yang lebih tinggi daripada nilai yang telah disyorkan. Menurut Indeks Pencemaran Logam (MPI), kantung dakwat sotong telah menunjukkan tahap pencemaran pada julat sederhana, manakala tisu dari bahagian kepala dan otot menunjukkan terdapat pencemaran pada peringkat yang rendah.

**Kata kunci:** Logam Berat, Sotong (Loligo Spp), Indek Pencemaran Logam

## Introduction

Nowadays, seafood especially squid *(Loligo Spp.)* from the Cephalopoda class (Figure 1) has a high demand due to their nutritional values. According to Guerra et al. [1], cephalopod resources increase continuously because of their importance and short life cycle. Squids have good-tasting flesh and that makes them commercially favourable among people since the early 80's [2]. Apart from that, they play an important role in the marine ecosystem as they become prey to some marine mammals [3].

Lourenço et al. and Hannalore et al. have stated that squids may provide some of the heavy metals required by the human body [3, 4]. However, humans are also indirectly more susceptible to heavy metal poisoning by consuming this organism [1, 6]. According to Paolo et al. [7], this species is said to be vulnerable to heavy metal contaminants because of their feeding habits. Meng et al.[8] has stated that contamination from heavy metals may occur due to the marine environment being continuously polluted by human activities. Heavy metals may then transfer to and accumulate in marine organisms through the food chain [9].

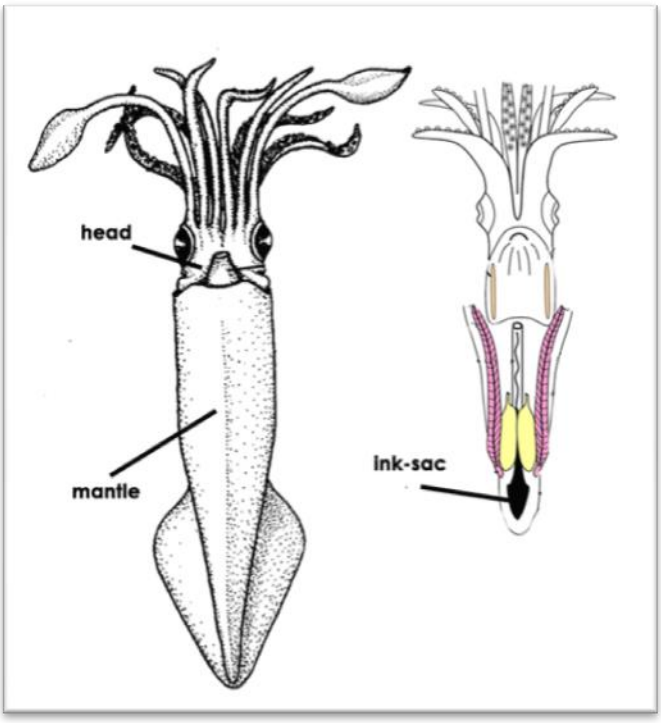



Figure 1: Squid *(Loligo Spp.)* from the Cephalopoda class

In this study, copper (Cu), cadmium (Cd), lead (Pb) and zinc (Zn) have become the main focus due to the fact that all of these elements are found accumulated excessively in squids [4, 10, 11, 12]. This phenomenon occurs because squids need Cu and Zn for their metabolic reaction [13, 14], while the concentration of Cd could be present due to the by-product of the reaction between Zn, Cu and Pb. According to Paolo et al. [7], Cd is also released from biogenic detritus in order to regenerate phosphate and nitrate. Pb, on the other hand, is present in the marine environment through atmospheric deposition and soil erosion, as well as vehicle exhaust, and industrial discharge [15].

According to Aaron et al. [16], these four elements have their own role in the human body, but they may become harmful if the amount taken is high. The imbalance of Cu consumption will lead to chronic diseases, such as Wilson disease, Alzheimer disease and Menkes Syndrome [17], while Cd, Pb and Zn may cause chronic kidney damage and even cancer [18]. Therefore, the amount taken should be minimized in order to avoid being adversely affected. In this regard, the assessment of heavy metals in seafood is needed in order to ensure the safety of the foods for the sake of human health.

## Materials and Methods

### Sample collection and preparation

Fresh squid samples were purchased directly from fishermen with their commercial catches landed at the fisheries harbours of Kuala Kedah. The samples were randomly selected according to their maturity size, where the average length of the samples ranged from 13 to 15 cm. This was in the range of commercial grades. Samples were then immediately iced and brought to the laboratory in insulated boxes. These were either analyzed fresh or kept frozen (-20$^{o}$C) until further analysis. At the laboratory, squid samples were carefully dissected in order to separate the ink-sac, head and mantle tissues. The samples were then dried in the oven at 80°C until a constant weight was obtained. This step should be carefully monitored as to avoid losses of volatile elements such as As, Cd, and Pb during analysis. When the samples have reached a constant weight, they were allowed to cool in the desiccators before they were crushed into a fine powder by using a porcelain mortar and pestle afterwards.

### Sample analysis

In this study, the digestion and analytical procedures were adopted and applied from the Milestone Microwave Digestion Method (DG-FO-17). For this analysis, 0.5 g of the homogenized squid sample was weighed and put into the Teflon vessel. After that, 7 ml of $HNO_3$ (65%) and 1 ml of $H_2O_2$ (30%) were added into the Teflon vessel using a single channel pipette, 100-1000 microlitre (µl) of the brand CappAero which was ISO 9001; 2000 certified. Afterwards, the Teflon bombs were placed into the oven at 200˚C for 30 minutes. The samples were then poured into centrifuge tubes and filled-up to 10 ml with Mili-Q water. These procedures were later repeated for the DORM-3 (Fish Protein Certified Reference Material for Trace Metals). The analysis of Heavy metals concentration was then carried out by using Inductively Coupled Plasma Mass Spectrometer (ICP-MS) (Perkin Elmer model Nexion 300X).

For method validation purpose, a certified reference material for trace metals, DORM-3 (Fish Protein Certified Reference Material for Trace Metals) was digested and heavy metal levels were determined in the same manner as our samples. The limit of detection for each heavy metal was calculated from three standard deviations of eight method blanks.

### Heavy Metal Assessment Index

Metal Pollution Index (MPI) equation is used in order to identify the degree of pollution of both squid and cuttlefish samples [19]. The equation (1) is as shown below:

$$MPI = (Cf_1 \text{ X } Cf_2 \text{ ……..} Cf_K)^{1/K} \quad (1)$$

where $Cf_1$ is concentration value of the first metal, $Cf_2$= concentration value of the second metal and $Cf_k$= concentration value of the $k^{th}$ metal. The MPI index values are then tabularised according to what is shown in Table 1.

Table 1: MPI index value with the corresponding pollution criteria

| Index Value | Degree of Pollution |
|---|---|
| **MPI > 2** | Not impacted |
| **2 < MPI < 5** | Very low contamination |
| **5 < MPI < 10** | Low contamination |
| **10 < MPI< 20** | Medium contamination |
| **20 < MPI < 50** | High contamination |
| **50 < MPI < 100** | Very high contamination |
| **MPI > 100** | Extreme contamination |

## Results and Discussion

### Validity of Methods

For method validation, a certified reference material (DORM-3; National Research Council, Canada) was determined as a precision check. The percentage of recoveries (n = 4 for each metal) for certified and measured concentration of those metals was satisfactory, with the recoveries being 93.10 – 105.07%. Table 2 shows the recovery test results for SRM (1646a) analysis.

Table 2: Determined value, certified value and percent (%) recovery of heavy metal contents of the DORM-3 as validation for analytical technique

| Heavy Metal | Measured Value (mg/kg) | Certified value (mg/kg) | % Recovery |
|---|---|---|---|
| **Cd** | 0.27±0.04 | 0.290±0.02 | 93.10 |
| **Cu** | 14.6±0.21 | 15.5±0.63 | 94.42 |
| **Pb** | 0.401±0.32 | 0.395±0.05 | 101.52 |
| **Zn** | 53.9±2.10 | 51.3±3.10 | 105.07 |

### Accumulation of heavy metals in squids

According to the results shown in Table 3 and Figure 2, there were significant differences ($p<0.05$) among the concentrations of heavy metals in the three parts of squid tissues (mantle, head, and ink-sac). The average concentrations of heavy metals in squids were 35.06 ± 4.06 mg/kg for Zn, 15.10 ± 13.38 mg/kg for Cu, 4.76 ± 3.77 mg/kg for Cd and 4.01 ± 0.08 mg/kg for Pb. Generally, the trend of heavy metals' mean concentration in squids can be seen as Zn>Cu>Cd>Pb. In regard of the accumulation of heavy metals in specific parts of the squid, the most potential part seemed to be the ink-sac, followed by the head and the mantle, with the following trend: ink-sac>head>mantle. From this study, Zn and Cu were found to be abundant in major tissues of the squid. In a previous study done by Craig and Overnell [20], it was also found that Zn and Cu concentrations were significantly high in squids.

Table 3: Heavy metal concentrations (mg/kg) in squid tissues

| Squid Tissue | Metal | | | |
|---|---|---|---|---|
| | **Zn** | **Cu** | **Cd** | **Pb** |
| **Mantle** | 30.6 | 4.29 | 1.39 | 3.93 |
| **Head** | 36.01 | 10.96 | 4.07 | 4.09 |
| **Ink-sac** | 38.56 | 30.06 | 8.83 | 4.02 |
| **Average** | 35.06 ± (4.06) | 15.10 ± (13.38) | 4.76 ± (3.77) | 4.01 ± (0.08) |

Figure 2 indicates that the ink-sac was the most contaminated tissue compared to head and mantle. From the observation, Zn concentration was found to be extremely high in the ink-sac with the value of 38.56 mg/kg. This might be due to the composition of melanin contents in the ink. According to Luçero et al. [21], melanin pigment is the main composition of the ink-sac of squids and other cephalopods. Furthermore, Slominski et al., [22] has stated that melanin in squid ink-sac is the derivation of oxidized L-DOPA (L-3,4-dihydroxyphenylalanine). The oxidation process of L-DOPA involves metal cations such as Cu, Zn, Mn and Fe [22, 23]. Therefore, the characteristic of melanin which enables it to bind with this element was one of the reasons why the ink-sac accumulates higher concentrations of heavy metals compared to muscle and head tissues [4, 22, 24].

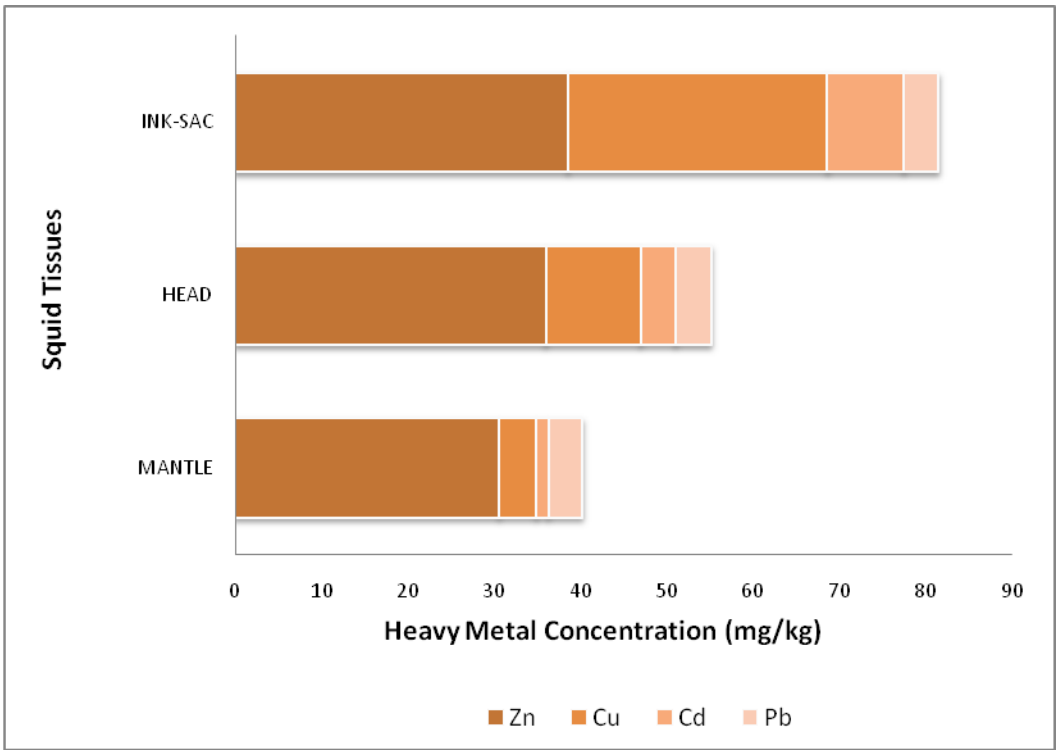



Figure 2: Accumulation of heavy metals in squid tissues

Meanwhile, Zn concentrations in the head tissues were slightly lower compared to the ink-sac with the value of 35.06 ± 4.06 mg/kg. This might be due to the eyes of squids which also contain melanin components. According to Daw and Pearlman [25], and Fox and Crane [26], the retina of the squid eye also contains melanin, but the amount is still little compared to that of the ink-sac. In general, among other heavy metal elements, Zn was found in higher values in squid tissues. According to Tukimat et al. [27], Zn element is always found abundant in marine organisms. Furthermore, Zn is one of the essential elements required by aquatic organisms for their metabolic processes [28].

Cu displayed the second highest in heavy metal content in squid tissues with a mean concentration of 15.10 ± 13.38 mg/kg. Just like Zn, metal cation of Cu is also one of the essential elements in the oxidation process of L-DOPA in producing melanin in the ink-sac and eye tissues of squids [22]. However, the mantle tissue revealed the lowest concentration of Cu, with the value of 4.29 mg/kg. This is due to the movement of oxygen through the mantle via haemocyanin. Squids and other cephalopods use haemocyanin protein in transporting oxygen in their bodies [29]. The accumulation of Cu in muscle tissues of squids still occurs even at low concentrations. This is due to the transportation of oxygen that takes place in the muscle. According to Mommsen et. al. and Ballantyne, muscle tissues of squids consist of both white and red muscle but majorly are white [30, 31]. Both of these muscles have different characteristics. White muscles lack mitochondria, low in blood supply but high in levels of glycolytic enzymes and do anaerobic respiration [30, 32]. Meanwhile, red muscles are high in myoglobin, mitochondria, and oxidative enzymes and do aerobic respiration [30, 32]. The lack of mitochondria can be the answer to why muscle tissues of squids accumulate the lowest levels of Cu.

Meanwhile, Cd recorded lower concentrations with a mean value of 4.76 ± 3.77 mg/kg. This is because generally all of the three squid tissues have a low ability to carry the accumulation of this element compared to the other tissues of the squid body. In a previous study done by Koyama et al. [33], it was stated that muscle, head and ink-sac tissues of squids were accumulated with Cd at the lowest concentration compared to the digestive tract, liver and gills. According to Kojadinovic et al. [34] and Bustamante et al. [35], Cd is found abundant in marine animals

including cephalopods because Cd is required for their physiological and detoxification processes that occur in the squid body. Squids and other cephalopods need Cd for their homeostasis and detoxification processes.

Last but not least, the concentration of Pb was the lowest among the other heavy metals in squid tissues, with the value of 4.01±0.08 mg/kg. From the observation, the distribution of this metal was constant in all squid tissues. Koyama et al. [33], and Bustamante et al. [35] have stated that Pb will accumulate in squid tissues by means of seawater absorption through their skin. The low value of Pb concentration in the present study may indicate that the mantle of the squid is not the target organ for Pb accumulation [36].

**Safety Issues for Human Consumption**

Contamination levels of heavy metals in marine organisms including squids are usually compared with the permissible limits set by Food and Agriculture Organization (FAO), World Health Organization (WHO) and other countries. Malaysian Food Regulation [37] has also set a limit for contamination levels of heavy metals. Table 4 presents the comparison between a set of four selected heavy metal concentrations obtained from this study (Zn, Cu, Cd, Pb) and the recommended permissible limit set by several countries.

Table 4: Comparison of heavy metal concentrations with recommended permissible limit[1-6]

| Heavy Metal | Present Study (mg/kg) | Permissible Limits (mg/kg) | References |
|---|---|---|---|
| **Zn** | 35.06 ± 4.06 | <100 | 1,2 |
| **Cu** | 15.10 ± 13.38 | <30, <20 | 1,2 |
| **Cd** | 4.76 ± 3.77 | 1, 2, 3, 2 | 1,3,4,6 |
| **Pb** | 4.01 ± 0.08 | 2, 0.5, 1.5, 0.5 | 1,2,4,5 |

[1]Malaysian Food Regulation [37], [2]Minsitry of Public Health, Thailand [38], [3]Australia and New Zealand Food Authority Amendment No. 53 [39], [4]US Food and Drug Administration [40], [5]FAO. Report of the Codex Committee on Food Additives and Contaminants [41], [6]FAO. Report of the Codex Committee on Food Additives and Contaminants [42]

From Table 4, the average concentrations of Zn and Cu were within the permissible limits. However, for the non-essential metals, both Cd and Pb concentrations were found higher compared to the values of the recommended permissible limits. According to Castro González and Méndez-Armenta [43], Cd toxicity in humans may affect some organs such as kidney, lung, bones, brain, as well as the central nervous system. Meanwhile, Pb poisoning in humans may lead to diseases like gout, kidney problems and autistic offspring [44]. Furthermore, huge amounts of Pb accumulation in marine organisms can cause genetic alteration and reduce metabolic reactions, therefore reducing the quality of the flesh of commercial organisms, such as squids [45]. Therefore, due to Cd and Pb contamination, squids inhabiting the Kedah-Perlis coastal waters may not be a proper food source for humans.

**Metal Pollution Index (MPI)**

In order to evaluate the degree of heavy metal contamination in squid tissues, Metal Pollution Index (MPI) was applied. The contamination levels in squids taken from the Kedah-Perlis waters are displayed in Table 5. From the observation, the contamination in each tissue ranged from low contamination to medium contamination.

Table 5: The MPI values for squids in the Kedah-Perlis waters

| Sample | MPI | Index Value | Degree of Pollution |
|---|---|---|---|
| **Squid mantle** | 5.15 | 5 < MPI < 10 | Low contamination |
| **Squid head** | 9.01 | 5 < MPI < 10 | Low contamination |
| **Squid ink-sac** | 14.24 | 10 < MPI < 20 | Medium contamination |

The concentrations of heavy metals in mantle and head tissues were within the range of low contamination (5<MPI<10), where the MPI values are 5.15 and 9.01, respectively. However, the MPI value for ink-sac tissues was within the range of medium contamination (10<MPI<20).

## Conclusion

The accumulations of heavy metals are significantly high in the ink-sac tissues compared to head and muscle tissues, except for Pb. The order of heavy metal content in squids is as follows: Zn > Cu > Cd > Pb. Compared to the recommended permissible limits, the concentration of Zn and Cu in squid tissues are still lower than that of safety standards. Meanwhile, the concentration of Cd and Pb are higher than that of safety standards. However, the average value of MPI has shown that the heavy metal concentration in squid tissues is at a low contamination level (5 < MPI < 10). Further research and close monitoring are therefore necessary to follow changes in contamination levels. Further investigation may also provide a better view of contaminant sources, particularly for cadmium and lead.

## Acknowledgement

This research was conducted under the funding of Malaysia Ministry of Higher Education (MOHE) and University Teknologi MARA (UiTM), through the Fundamental Research Grant Scheme (FRGS) -600-RMI/ST/FRGS 5/3/Fst (284/2010). The authors wish to express their gratitude to the Oceanography Laboratory team members for their invaluable assistance and hospitality throughout the sampling period.

## References

1. Guerra, A., L. Allcock & J Pereira. (2010). Cephalopod life history, ecology, and fisheries: an introduction. *Fish. Res.* 106: 117-124.
2. Clyde (1984). FAO Species Catalogue. Volume 3: Cephalopods of the World. Rome: Food and Agricultural Organization of the United Nations.
3. Bustamante, R., Wellington, J. & Troya, R. (2001) In Galapagos, clashes between fishers and managers jeopardize conservation efforts. *MPA News* 2, 1–3
4. Lourenço, H.M., P. Anacleto, C. Afonso, V. Ferraria, M.F. Martins, M.L. Carvalho, A.R. Lino & M. L. Nunes, (2009). Elemental composition of cephalopods from Portuguese continental waters. *Food Chemistry*, 113: 1146-1153.
5. Hannelore, W., Seolwon, K., Guebuem, K., Mi Ran, K.& Beum, K. (2008). Distribution patterns of chalcogens (S, Se, Te, and 210Po) in various tissues of a squid, Todarodes pacificus. *Sci. Total Environ.* 392, 218–224.
6. Domingues P., Sykes A., Sommerfield A., Anto´nio Lorenzo E. & Andrade J. P. (2004). Growth and survival of cuttlefish (sepia officinalis) of different ages fed crustaceans and fish. Effects of frozen and live prey. *Aquaculture* 229, 239–254.
7. Dorneles P. R., Lailson-Brito, J., Aguiar dos Santos, R., Alberto Silva da Costa, P., Malm, O., Azevedo, A. F., & Torres J. P. M. (2007). Cephalopods and cetaceans as indicators of offshore bioavailability of cadmium off central south brazil bight. *Environmental Pollution* 148, 352-359.
8. Meng W, Qin Y. W, Zheng B. H & Zhang L. (2008) Heavy metal pollution in Tianjin Bohai Bay, China. *J Environ Sci* 20(7) :814–819
9. Tulonen T., Pihlström, M. Lauri Arvola and Martti Rask (2006), concentration of heavy metals in food wed components of small, boreal lakes. Boreal Environment Research 11: 185-194
10. Zienab I. Soliman (2006). A Study of Heavy Metals Pollution in Some Aquatic Organisms in Suez Canal in Port- Said Harbour. *Journal of Applied Sciences Research*, 2(10): 657-663
11. Lihan, T., Ismail, N., Mustapha M. A. & Abd Rahim S. (2006). Kandungan Logam Berat Dalam Makanan Laut Dan Kadar Pengambilannya Oleh Penduduk Di Tanjung Karang, Selangor. *Malaysian Journal of Analytical Sciences*: 10 (2): 197-204
12. Bustamante, P., Teyssié, J-L., Fowler, S.W., Cotret, O., Danis, B., Miramand, P., & Warnau, M. (2002). Biokinetics of zinc and cadmium accumulation and depuration at different stages in the life cycle of the cuttlefish Sepia officinalis. *Marine Ecology Progress Series* 231: 167-177.
13. Stephen, C., & Julian, O., (2002) Metals in squid, loligo forbesi, adults, eggs and hatchlings. No evidence for a role for Cu- or Zn-metallothionein. *Comparative Biochemistry and Physiology Part C.* 134 (3): 311-318.

14. Decleir, W., A. Vlaeminek, P. Geladi, & R. Van Grieken, (1978). Determination of protein - bound copper and zinc in some organsl 20 of the cuttlefish Sepia officinalis L. *Comparative Biochemistry and Physiology 60B*: 347 - 350.
15. Yunchao H., Zhigang G., Zuosheng Y., Dejiang F., Ming F., & Xiangdong L. (2008). Tracking historical lead pollution in the coastal area adjacent to the Yangtze river estuary using lead isotopic compositions. *Environmental Pollution* 156: 1325–1331.
16. Aaron J. B., Tsukamoto, Y, Tovar-Sanchez, A., Huerta-Diaz, M., & Bokuniewicz, S. A, (2007). Importance of geochemical transformations in determining submarine groundwater discharge-derived trace metal and nutrient fluxes. *Applied geochemistry* 22 (2), 477-490
17. Sergi P. & Dennis J T., (2002). Molecular mechanisms of copper uptake and distribution. *Bioinorganic chemistry*: 171-180.
18. Ahmed K. S. & Mohamed A. R. (2005). Heavy metals (Cd, Pb) and trace elements (Cu, Zn) contents in some foodstuffs from the Egyptian market. Emir. *J. Agric. Sci.* 17 (1): 34-42
19. Usero, J., Gonzales-Regalado, E. & Gracia, I. (1997). Trace metals in bivalve molluscs Ruditapes decussatus and Ruditapes philippinarum from the Atlantic Coast of southern Spain *Environ. Int.* 23: 291 - 298.
20. Craig, S., & J. Overnell, (2003). Metals in squid, Loligo forbesi, adults, eggs and hatchlings. No evidence for a role for Cu- or Zn-metallothionein. *Comparative Biochemistry and Physiology C* 134: 311-317.
21. Lucero M. T., Farrington, H & Gilly W. F., (1994). Qualification of L-dopa and dopamine in squid ink: implication for chemoreception. *Biol. Bull* 187: 55-63
22. Slominski A., Desmond J. T., Shigeki S., & Jacobo W. (2004). Melanin pigmentation in mammalian skin and its hormonal regulation. *Physiol Rev* 84: 1155–1228.
23. Schetz John A., Alice Chu, & David R. Sibley (1999). Zinc modulates antagonist interactions with D2-like dopamine receptors through distinct molecular mechanisms. *The American Society for Pharmacology and Experimental Therapeutics* 289: 956-964.
24. Bustamante, P., F. Caurant, S.W. Fowler & P. Miramand, (1998). Cephalopods as a vector for the transfer of cadmium to top marine predators in the north-east Atlantic Ocean. *Science of the Total Environment*: 220:71-80.
25. Daw N. W & Pearlman L. (1974). Pigment Migration and Adaptation in the Eye of the Squid, *Loligo pealei. The journal of general physiology* 63: 22-35.
26. Fox, D. L & Crane, S. C, (1942). Concerning the pigments of the Two spotted octopus and the *Opalescent squid. Biol Bull* 82: 284-291.
27. Tukimat, L., R Abu Bakar, C.C. Zaidi & A.R Sahibin. (2002). Determination of heavy metals in seafood and intakes by the populations of Kuala Kemaman, Terengganu. Paper presented at Regional symposium on Environment and Natural Resources, 10-11 April, Hotel Renaissance, Kuala Lumpur, Malaysia
28. Vasconcelos Rita P., Patrick Reis-Santos, Anabela Maia, Miguel Ruano, Maria J.Costa & Henrique (2011). Cabral Trace metals (Cu, Zn, Cd and Pb) in juvenile fish from estuarine nurseries along the Portuguese coast. *Scientia Marina* 75(1): 155-162.
29. Seibel, B. A., Chausson, F., Lallier, F. H., Zal, F. & Childress, J. J. (1999). Vampire blood: respiratory physiology of the vampire squid (Cephalopoda: Vampyromorpha) in relation to the oxygen minimum layer. *Exp. Biol. Online* 4 (1): 1 – 10..
30. Mommsen T. P., Ballantyne J., Macdonald D., Gosline J., & Hochachka P. W. (1981). Analogues of red and white muscle in squid mantle. *Proc. Natl. Acad Sci. USA* 78 (5): 3274-3278.
31. Ballantyne James S. (2004). Mitochondria: aerobic and anaerobic design lessonsfrom molluscs and fishes. *Comparative Biochemistry and Physiology*, Part B139: 461-467.
32. Bartol Ian K. (2001). Role of aerobic and anaerobic circular mantle muscle fibers in swimming squid: electromyography. *Biol. Bull*. 200: 59–66.
33. Koyama J., Nobuyuki N. & Susumu S. (2000). Bioaccumulation of waterborne and dietary cadmium by oval squid, *Sepioteuthis lessoniana*, and its distribution among organs. *Marine Pollution Bulletin* 40 (11): 961 - 967.
34. Jessica, K., Jackson, C. H., Cherel, Y. Jackson, G. D. & Bustamante P. (2011). Multi-elemental concentrations in the tissues of the oceanic squid *Todarodes filippovae* from Tasmania and the southern Indian Ocean. *Ecotoxicol. Environ. Saf*. 74(5):1238-49.

35. Bustamante, P., J.L. Teyssié, B. Danis, S.W. Fowler, P. Miramand & O. Cotret, (2004). Uptake, transfer and distribution of silver and cobalt in tissues of the common cuttlefish Sepia officinalis at different stages of its life cycle. *Marine Ecology Progress Series*, 269: 185-95.
36. Saleh Al Farraj, Amel H. El-Gendy, Hamad Alyahya & Magdy El-Hedeny (2011). Heavy Metals Accumulation in the Mantle of the Common Cuttlefish *Sepia pharaonis* from the Arabian Gulf. *Australian Journal of Basic and Applied Sciences* 5(6): 897-905,
37. Malaysian Food Regulations (1985). In Food Act 1983 & Regulations. International Law Book Services.
38. Ministry of Public Health. (1986). Notification No. 98. Standard Contamination Level in Food. Ministry of Public Health, Thailand.
39. Australia and New Zealand Food Authority. (2000). Provisional Regulation Limitation of Contamination in Food, Specifications and Standards for Foods, Food Additives, etc. Under The Food Sanitation Laws, April 2004, Standard 1.4.1, Contamination and Natural Toxicants, Maximum level of metal contaminates in food, Australia and New Zealand Food Authority Amendment no.53 to Food Standard Code, Commonwealth of Australia, 2000.
40. US. Food and Drug Administration. (2001). Fish and Fisheries Products Hazards and Controls Guidance. 3rd edition. Appendix 5. FDA & EPA Safety Levels in Regulations and Guidance. Available Source:
41. FAO. Report of the Codex Committee on Food Additives and Contaminants.(2011) Draft Guideline level for Cadmium in Food .
42. FAO. Report of the Codex Committee on Food Additives and Contaminants.(2001). Draft Maximum level for Lead. Available Source:
43. Castro-Gonzalez, M. & Mendez-Armenta ,M. (2008) Heavy metals: Implications associated to fish consumption. *Environmental Toxicology and Pharmacology* 26: 263–271.
44. Rosin A. (2009) The long-term consequences of exposure to lead. *Israel Med Assoc J.* 11(11):689–694
45. Svobodova A., Lloyd R., Machova J., & Vykusova B. (1993). Water quality and fish health – EIFAC Tech Pap 54 Rome, FAO 59.

The Malaysian Journal of ANALYTICAL SCIENCES ISSN 1394-2506

# EFFECT OF RICE STRAW EXTRACT AND ALKALI LIGNIN ON THE CORROSION INHIBITION OF CARBON STEEL

## (Kesan Ekstrak Jerami Padi dan Alkali Lignin Terhadap Perencatan Kakisan Keluli Karbon)

Rabiahtul Zulkafli[1], Norinsan Kamil Othman[1]*, Irman Abdul Rahman[1], Azman Jalar[2]

[1]*School of Applied Physics, Faculty of Science and Technology,*
[2]*Institute of Micro Engineering and Nanoelectronics (IMEN),*
*Universiti Kebangsaan Malaysia, 43600 UKM Bangi, Selangor, Malaysia*

**Corresponding author: insan@ukm.my*

**Abstract**

A paddy residue based corrosion inhibitor was prepared by treating finely powdered rice straw with aqueous ethanol under acid catalyst (0.01M $H_2SO_4$). Commercial alkali lignin was obtained from Sigma-Aldrich. Prior to the corrosion test, the extraction yield and alkali lignin was characterized via FTIR to determine the functional group. The effect of paddy residue extract and commercial alkali lignin on the corrosion inhibition of carbon steel in 1M HCl was investigated through the weight loss method, potentiodynamic polarization technique and scanning electron microscopy (SEM). The corrosion inhibition efficiency of the extract and alkali lignin at different immersion times (3h, 24h and 42h) was evaluated. The results show that the paddy waste extract exhibited lesser weight loss of carbon steel in the acidic medium in comparison to the commercial alkali lignin, suggesting that the paddy residue extract is more effective than the commercial alkali lignin in terms of its corrosion inhibition properties. The results obtained proves that the extract from paddy residue could serve as an effective inhibitor for carbon steel in acidic mediums.

**Keywords:** Rice straw extract, corrosion, carbon steel, inhibition

**Abstrak**

Perencat kakisan dari sisa padi disediakan dengan merawat serbuk halus jerami padi dengan akues etanol di bawah pengaruh pemangkin asid (0.01M $H_2SO_4$), sementara alkali lignin komersial diperolehi daripada Sigma-Aldrich. Sebelum ujian kakisan dijalankan, hasil ekstrak dan alkali lignin komersial telah dicirikan melalui FTIR untuk mengetahui kumpulan berfungsi bahan-bahan tersebut. Kesan ekstrak dari sisa padi dan alkali lignin komersial terhadap perencatan kakisan keluli karbon dalam 1M HCl ditentukan dengan kaedah kehilangan berat, teknik pengkutuban potensiodinamik dan mikroskopi pengimbasan elektron (SEM). Kecekapan perencatan kakisan ekstrak dan alkali lignin ditentukan untuk masa rendaman yang berbeza (3j, 24j dan 42j). Keputusan menunjukkan bahawa ekstrak sisa padi mempamerkan kurang kehilangan berat keluli karbon dalam media asid berbanding alkali lignin komersial. Ekstrak dari sisa padi didapati lebih berkesan berbanding alkali lignin komersial dari segi sifat perencatan kakisan. Keputusan yang diperolehi membuktikan bahawa ekstrak dari sisa padi boleh bertindak sebagai perencat yang berkesan bagi keluli karbon dalam media asid.

**Kata kunci:** Ekstrak jerami padi, kakisan, keluli karbon, perencatan

## Introduction

Recently, researchers have been focusing their efforts in the pursuit to replace synthetic corrosion inhibitors with inhibitors obtained from natural substances. This interest has been in high demand due to the fact that naturally sourced corrosion inhibitors are safe, readily available, cheap, ecologically friendly, biodegradable and sourced from renewable materials [1-2]. Various studies have reported that extracts of natural ingredients can slow down and inhibit corrosion, due to the presence of oxygen compounds, sulphur and nitrogen that can help in the process of corrosion inhibition [3-5]. Previous literature has shown that natural material such as Henna leaf extract [6], *Aloe Vera* extract [7], mangrove bark [8], natural honey and black radish juice [9] are effective inhibitors for metal in aggressive solutions.

This study focuses on comparing the corrosion inhibition properties of rice straw extract and commercial alkali lignin. Rice straw was chosen because it is a waste management issue in Malaysia, causing problems such as pollution that can affect human health. This represents a huge missed oppurtunity, especially when these residues can be converted into substances that are beneficial to the community. The inhibition behaviour of both materials on carbon steel was determined in a 1M HCl solution, via the weight loss method and potentiodynamics polarization technique.

## Materials and Methods

Rice straw samples were obtained from a private paddy field in Kedah, Malaysia. The rice straw was dried for 16 hours in an oven at 60°C and ground into powder. The dried and ground rice straw was extracted by a solvent extraction method in a aqueous ethanol (ethanol/water, 60/40) with stirring acid catalyst (0.01M $H_2SO_4$) at 50-60°C for 12h. The ethanol used was then evaporated, leaving behind a black liquor. This black liquor was then transferred into a petri dish and dried in the oven at 100°C for 6 h to obtain an extract product. The extract left in the petri dish was then scraped of the petri surface, producing the final product in the form of a black powder. Meanwhile, the commercial alkali lignin obtained from Sigma-Aldrich was used as received. The powder extracted from rice straw and the commercial alkali lignin was analysed using a Perkin Elmer Spectrum 400 FT-IR/ FT-NIR & Spotlight 400 Imaging System in a wavelength range of 400 to 4000 $cm^{-1}$, to recognize the functional groups present in the extract powder and the commercially obtained alkali lignin. To study the corrosion inhibition behaviour of the rice straw extract and commercial alkali lignin, an arsenal of analytical methods were employed. The weight loss method was used in the corrosion test. Carbon steel SAE 1045 samples with the following composition (C=0.45%, Mn=0.75%, P=0.04% max, S=0.05%) were used. This carbon steel was mechanically cut into smaller test pieces with a diameter of 16mm and thickness of 1mm. Prior to the weight loss test, the specimens were abraded with a series of silicon carbide papers (grade 400, 600, 800 and 1200) before being washed with distilled water, degreased with acetone, dried and weighed.

For the preparation of the corrosion inhibitor solution, a 1M hydrochloric acid solution was first prepared by dilution of analytical grade 37% HCl with distilled water. A corrosion inhibitor solution containing the rice straw extract and commercial alkali lignin was prepared in a 100ml of 1 M hydrochloric acid. Both inhibitors were dissolved at a concentration of 1500ppm. The 1M HCl solution without inhibitors was used as the blank for comparison. Weight loss of the carbon steel test pieces were determined at varying immersion times (3h, 24h and 42h) at room temperature. At each specified time interval, the specimens were taken out of the test solution, rinsed with distilled water, dried and weighed again. The weight loss was measured in milligrams. The test was carried in triplates to obtain accurate results and the mean of weight loss was recorded [10].

Polarization measurements were carried out using a computer-controlled potentiostat (model K47 Gamry framework). Three different types of electrodes were used a saturated calomel electrode (SCE) as reference, the working electrode was carbon steel and platinum wire was the counter electrode. The working electrode surface area used in this study was 1 $cm^2$. The surface of carbon steel was abraded successively using silicon carbide paper 400, 600, 800 and 1200 grade. The ground surface was degreased with acetone and washed with distilled water before being used in the experiment. Before each polarization measurement, the working electrode was left idle for 30 minutes to achieve a steady state. The experiments were performed using a scanning rate of 1.0 mV $s^{-1}$. All the measurements were done at room temperature.

Scanning electron microscopy SEM analysis was carried out to study surface morphology of the untreated and treated carbon steel with the rice straw extract and commercial alkali lignin corrosion inhibitors.

## Results and Discussion

### FTIR analysis

FTIR spectroscopy displays interesting features such as high signal-to-noise ratio, high sensitivity and selectivity, accuracy, mechanical simplicity, short analysis time and small amount of sample required for the analysis [11]. Figure 1 illustrates the FTIR spectra obtained for the rice straw extract and commercial alkali lignin. Table 1

displays the chemical bonds assigned to the FTIR absorption bands of the rice straw extract and commercial alkali lignin. The observed peaks for the extract exhibited signal peaks for functional groups such as hydroxyl (-OH), methoxyl (-$OCH_3$), methyl ($CH_3$) and aromatic rings that can retard the corrosion process. Organic compounds such as hydroxyl (-OH), methoxyl (-$OCH_3$) and methyl ($CH_3$) are known to be electron donating groups that can play a role as a good inhibitor for metal corrosion in acidic media [12]. The compound will adsorb onto the metal surface. As a result, it reduces the exposed surface area from being attacked by the aggressive acidic media [1]. The typical signal peaks of lignin for both the extract and commercial alkali lignin was also present at wavelengths of 1514 $cm^{-1}$ and 1500 $cm^{-1}$, respectively. The cellulose peak can be observed at a wavelength of 1419 $cm^{-1}$ for commercial alkali lignin, but was absent in the rice straw extract. The presence of hemicellulose at 1237 $cm^{-1}$ for the extract and 1210 $cm^{-1}$ for commercial alkali lignin as reported by others [13-14]. As can be seen from Table 1, the rice straw extract shows an observable peak at a wavelenghts numbers of 1324.00 $cm^{-1}$, which indicates the presence of syringyl compound. However, the commercial alkali lignin does not show any peaks in this range of wavelengths. The existence of syringe could be the reason for the capability of the corrosion inhibitor solution to reduce the corrosion rate of metals by strongly attracted to the positively charged electrode surfaces [15].

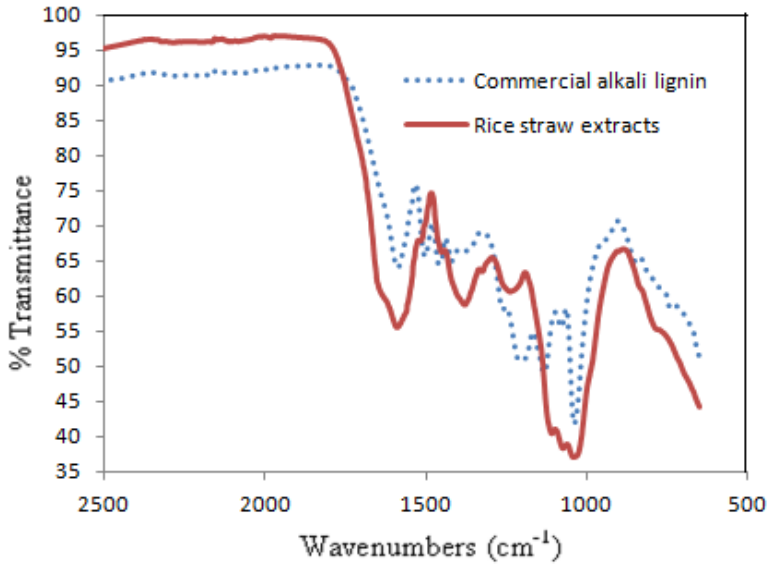



Figure 1: The FT-IR spectrum for rice straw extract and commercial alkali lignin

**Weight loss measurements**

Corrosion process can be investigated by using the simplest and long-established method that called weight loss analysis. The differences in weight of specimens before treated and after treating with inhibitor can be expressed as corrosion rate [19-20]. The corrosion rate and inhibition efficiency can be calculated by the formula Equation 1 and 2 given below:

$$Corrosion\,rate\,(CR, mpy) = \frac{534W}{DAT} \quad (1)$$

$$Inhibition\ efficiency\ \ (IE, \%) = \left(1 - \frac{CR2}{CR1}\right) x\,100 \quad (2)$$

where W = weight loss in mg, D = density of the specimen in unit g/cm$^3$, A = area of specimen in inch$^2$, T = exposure time in hour meanwhile $CR_1$ and $CR_2$ are the corrosion rate in the absence and presence of inhibitors.

Table 1: Peak FTIR spectrum for rice straw extract and commercial alkali lignin

| **Wavenumber range (cm$^{-1}$)** | **Observe peak (cm$^{-1}$)** | | **Peak assignment** |
|---|---|---|---|
| | **Rice straw extract** | **Commercial alkali lignin** | |
| 1600-1550 | 1590.34 | 1587.50 | Aromatic skeletal vibrations [16-17]. |
| 1550-1500 | 1514.31 | 1500.59 | C=C stretching of aromatic ring in lignin. |
| 1500-1450 | 1450.88 | 1459.43 | Assymmetric C-H deformations, C-H and C-O bending or stretching frequencies [18]. |
| 1450-1400 | - | 1419.92 | C-H bending of methyl and methylene groups. |
| 1400-1350 | 1379.84 | 1373.56 | Weak C-O stretching, C-H symmetric and asymmetric deformation. |
| 1350-1300 | 1324.00 | - | C-O stretching, Syringyl ring breathing with C=O stretching [18]. |
| 1250-1200 | 1237.52 | 1210.68 | Pure hemicellulose |
| 1150-1050 | 1107.92 | 1131.59 | Aromatic C-H deformation of syringyl unit β(1-3) polysaccharide. |
| | 1072.24 | 1079.70 | |
| 1050-1000 | 1040.50 | 1038.80 | C-O, C=O, C-C-O vibrational stretching C-OH bending, primary –OH group. |
| 800 | - | 848.23 | C-H bending of syringyl units. |
| 700 | 786.78 | 739.20 | Asymmetric bending of HCCH group. |

The data obtained for the corrosion behaviour of carbon steel in 1M HCl containing rice straw extract and commercial alkali lignin with various immersion times are presented in Table 2. It represents that the weight loss percentage in the absence and presence of the rice straw extract. At the time of carbon steel being exposed to the HCl media increased, the weight loss increases. Compare with commercial alkali lignin, the extract solution from rice straw produced the lowest weight loss. The lowest weight loss indicates that the rice straw extract could be served as an effective inhibitor of carbon steel in acidic medium. The inhibition process is the result of an adsorption of the inhibitor molecule on the carbon steel surface where rice straw extracts solutions act as an adsorptions inhibitor. The reaction between inhibitor and carbon steel surface could limit the occurring of corrosion processes. The comparative value of weight loss of carbon steel can be seen clearly in Figure 2.

Table 2: The percentage of weight loss for rice straw extract and commercial alkali lignin in 1M HCl with different immersion time

| **Corrosion inhibitor solution** | **Weight loss percentage (%)** | | |
|---|---|---|---|
| | **3 hour** | **24 hour** | **42 hour** |
| 1M HCl | 9.9 | 57.8 | 95.8 |
| 1M HCl + 1500ppm Commecial alkali lignin | 4.1 | 24.5 | 46.7 |
| 1M HCl + 1500ppm rice straw extracts | 0.3 | 0.6 | 0.7 |

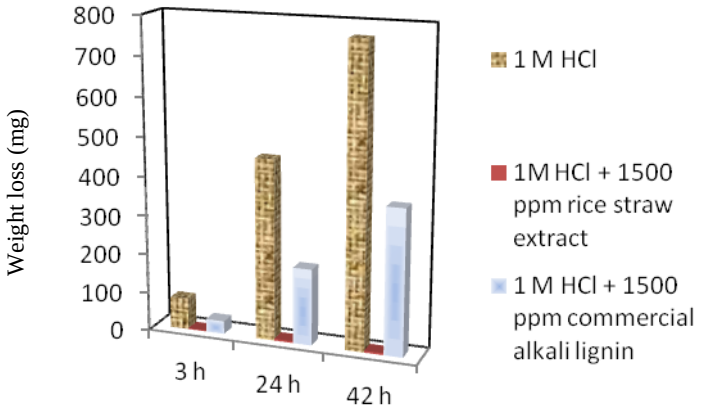



Figure 2: The weight loss of carbon steel in 1M HCl solution for rice straw extract and commercial alkali lignin at different immersion time

**Potentiodynamics polarization technique**

Polarization behaviour for carbon steel in 1M HCl in the absence and presence rice straw extract and commercial alkali lignin are shown in Figure 3. The values of corrosion of corrosion current ($I_{corr}$), corrosion potential ($E_{corr}$), cathodic Tafel slope $b_c$, anodic Tafel slope $b_a$ and inhibition efficiency (E%) are collected in Table 3. From Table 3, the corrosion potential for 1M HCl is -404mV. When carbon steel is immersed with the presence of 1500ppm commercial alkali lignin, there is no changed in corrosion potential value. It reveals that the addition of commercial alkali lignin may not give an influence into corrosion potential. Meanwhile, the corrosion potential for extract of rice straw shifts to -414mV. It is clearly shown that there is a shift towards cathodic region in the values of corrosion potential. In the literature, it has been reported that if the displacement in $E_{corr}$ is >85V with respect to $E_{corr}$, the inhibitor can be seen as a cathodic or anodic type, and if the displacement in *E*corr is <85, the inhibitor can be seen as mixed type. In our study the maximum displacement in Ecorr value was 10mV towards cathodic region, which indicates that rice straw extract is mixed type inhibitors [21-22].

Table 3: Tafel polarization parameters for the corrosion of carbon steel in 0.5 M HCl solution for rice straw extract and commercial alkali lignin

| System/ Inhibitor | $I_{corr}$ (A $cm^2$) | $E_{corr}$ (mV) | $b_c$ ($mVdec^{-1}$) | $b_a$ ($mVdec^{-1}$) | Rp (kΩ $cm^2$) | CR (mmpy) |
|---|---|---|---|---|---|---|
| 1M HCl | $3.0 \times 10^{-3}$ | -404 | 183 | 140 | $1.2 \times 10^{1}$ | 34.43 |
| 1500 ppm commercial alkali lignin | $1.9 \times 10^{-3}$ | -404 | 197 | 124 | $1.7 \times 10^{1}$ | 22.85 |
| 1500 ppm rice straw extract | $6.5 \times 10^{-5}$ | -414 | 101 | 74 | $2.8 \times 10^{1}$ | 0.76 |

**Surface analysis on the corroded coupons**

Scanning electron microscopy **(**SEM) of the polished surface of carbon steel exposed for 24 hours in 1M HCl solution in the absence and presence of 1500ppm rice straw extract and commercial alkali lignin are shown in Figure 4. By comparison of SEM images at the same magnifications, there was a rough surface of carbon steel in the presence of commercial alkali lignin and smooth surface with deposits extract in presence of the rice straw extract. Protective layer can be observed on the corroded surface. The rice straw extract forms a protective layer by

physical adsorption process. It proved again the inhibiting rice straw extract against corrosion of carbon steel in 1M HCl solution is better than commercial alkali lignin.

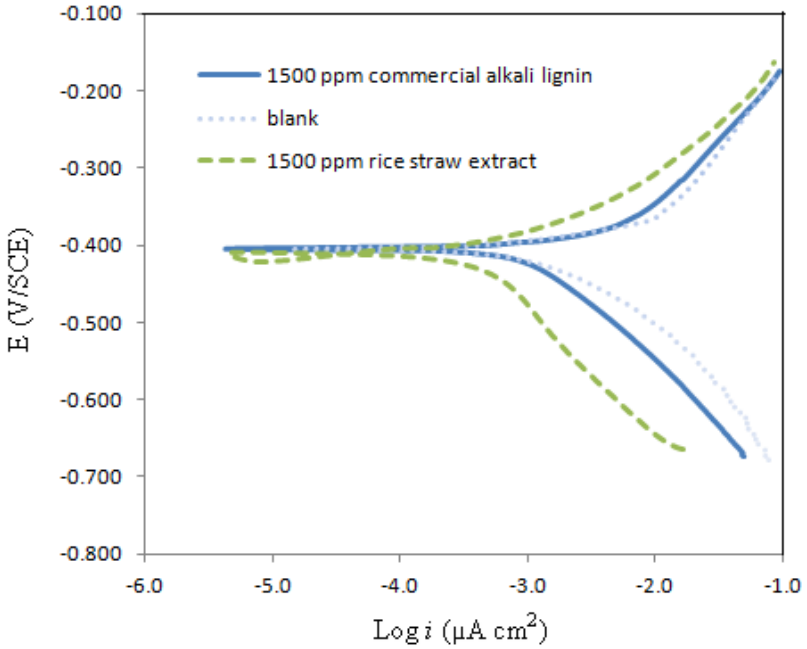



Figure 3: Tafel polarization curves for carbon steel in 1M HCl solution containing rice straw extract and commercial alkali lignin

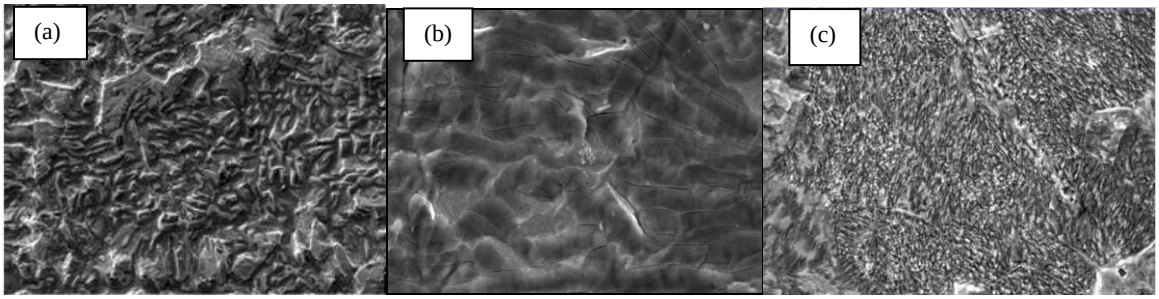



Figure 4: SEM morphology of carbon steel sample, (a) absence inhibitor, (b) in presence of commercial alkali lignin (c) in presence of rice straw extract in 1M HCl solution for 24h

## Conclusion

Both commercial alkali lignin corrosion inhibitor and extract yields from rice straw can prevent carbon steel from corrosion attack but rice straw extract showed a better efficiency as corrosion inhibitor. This behaviour may occur due to the existence of syringyl compound that obtained from FT-IR results.

**Acknowledgement**

The authors would like to thank the Ministry of Science, Technology & Innovation, Malaysia (MOSTI) for the financial support given through the Sciencefund Grant Scheme (03-01-02-SF0734), ERGS/1/2012/STG05/UKM/02/2 and Ministry of Higher Education, Malaysia (MOHE) with their support through MyBrain15 scholarship.

**References**

1. Satar, M. Z. M., Noor, M. F. M., Samsudin, M. W., & Othman, M. R. (2012). Corrosion Inhibition of Aluminum by Using Nipah (Nypa Fruticans) Extract Solutions in Hydrochloric Acid (HCl) Media. *Int. J. Electrochem. Sci.*, 7: 1958 – 1967.
2. Obot, I. B.,Umoren, S. A Umoren & Obi-Egbedi N.O. (2011). Corrosion Inhibition and Adsorption Behaviour for Aluminuim by Extract of *Aningeria Robusta* in HCl Solution: Synergistic Effect of Iodide Ions. *J. Mater. Environ. Sci.* 2 (1): 60-71.
3. Anvar, U., Buranov, & Mazza, G. (2008). Review-Lignin in Straw of Herbaceous Crops. *Industrial Crops and Products* 28: 237–259.
4. Dafalla, S.B., Mukhtar, H., & Shaharun, M.S. (2010). Characterisation of Adsorbent Developed from Rice Husk: Effect of Surface Functional Group on Phenol Adsorption. *J. Appl. Sci.* 10 (12): 1060-1067.
5. Sastri, V.S. (1998). Chemical Aspects of Corrosion Inhibition in Corrosion Inhibitors. Principles and Applications. *John Wiley & Sons, Ltd. Exerter* : 110.
6. El-Eltre, A.Y., Abdallah, M. & El-Tantawy, Z.E. (2005). Corrosion Inhibition of Some Metals using *Lawsonia* Extract. *Corrosion Science* 47: 385 - 395.
7. Olusegun K. A. & James A.O (2010). The Effects of *Aloe vera* Extract on Corrosion and Kinetics of Corrosion Process of Zinc in HCl Solution. *Corrosion Science* 52: 661–664.
8. Afidah A. R., Emmanuel R., Jean Steinmetz, M. Jain K., & M. Sani Ibrahim. (2007). Mangrove Tannins and their Flavonoid Monomers as Alternative Steel Corrosion Inhibitors in Acidic Medium. *Corrosion Science* 49: 402-417.
9. Radojčić, I., Berković, K., & Vorkapić-Furač, J.(2008),. Natural Honey and Black Radish Juice as Tin Corrosion Inhibitors. *Corrosion Science* 50: 1489-1505.
10. Orubite, K.O. & Oforka, N.C. (2004). Inhibition of The Corrosion Of Mild Steel in Hydrochloric Acid Solutions by The Extract of Leaves Of Nypa Fruiticans Wurmb. *Materials Letters* 58: 1768-1772.
11. Hortling, B., Tamminen, T. & Kentta, E. (1997). Determination of Carboxyl and Non-Conjugated Carbonyl Groups in Dissolved and Residual Lignins by IR Spectroscopy. *Holzforschung,* 51: 405–410.
12. Abiola O. K. & Oforka N. C., (2003). Corrosion Inhibition Effect of Cocos Nuciferal Juice on Mild Steel in 5% Hydrochloric Acid Solution. *Scientia Africa.2:* 82
13. Sun, X. F., Xu F., Sun R. C.,Fowder P., & Baird M. S. (2005). Characteristics of Degraded Cellulose Obtained from Steam-Exploded Wheat Straw. *Carbohydrate Resource* 340:97-106.
14. Adapa, P. K., Karunakaran C., Tabil L. G., & Schoenau G. J. (2009). Potential Applications of Infrared and Raman Spectromicroscopy for Agricultural Biomass. *Agricultural Engineering International* 1081: 1-25.
15. Robert Baboian (2005). Corrosion Tests And Standards: Application And Interpretation. *ASTM International*: 295.
16. Sakakibara, I., Katsuhara, T., Ikeya, Y., Hayashi, K. & Mitsuhashi, H. (1991). Cannabisin A, An Arylnaphthalene Lignanamide from fruits of *Cannabis sativa*. *Phytochemistry* 30 (9): 3013-3016.
17. Vanquez, G., Antorrena, G., Gonzalez, J. & Freire, S. (1997). FTIR, H—1 and C-13 NMR Characterization of Acetosolv-Soloubilized Pine and Eucalyptus Lignins. *Holzforschung* 51 (2): 158-166.
18. Sun, Y. L., Zhang, Q., Schwab, J. J., Demerjian, K. L. Chen, W. N., Bae, M.S., Hung, H. M. Hogrefe, O., Frank, B., Rattigan, O. V. &. Lin, Y. C. Characterization Of The Sources And Processes Of Organic And Inorganic Aerosols In New York City With A High-Resolution Time-Of-flight Aerosol Mass Apectrometer. *Atmospheric Chemistry and Physics* 11(4): 1581-1602.
19. Freeman, R. A & Silverman, D. C. (1992). Error Propagation in Coupon Immersion Tests. *Corrosion* 48 (6). 1992: 463.
20. Tebbiji, K., Oudda, H., Hammouti, B., Benkaddour, M., El Kodadi, M., Malek, F., & Ramdani, A. (2005). Inhibitive Action of Two Bipyrazolic Isomers Towards Corrosion of Steel in 1 M HCl Solution. *Applied Surface Science* 241: 326-334.

21. Ashassi-Sorkhabi, H., Majidi, M. R. & Seyyedi K. (2004). Investigation of Inhibition Effect of Some Amino Acids Against Steel Corrosion in HCl Solution. *Applied Surface Science* 225:176-185.
22. O. L. Riggs Jr. (1973), Corrosion Science, Second ed., C. C Nathan, Houston, Texas.

The Malaysian Journal of ANALYTICAL SCIENCES ISSN 1394-2506

# DEVELOPMENT OF SPECTROPHOTOMETRIC METHOD FOR ALLOPURINOL IN URINE BASED ON THE DIAZOTIZATION REACTION

## (Pembangunan Kaedah Spektrofotometrik untuk Penentuan Allopurinol dalam Air Kencing Berdasarkan Reaksi Diazotisasi)

Edy Agustian Yazid[1]*, Ganden Supriyanto[1,2], Tjitjik Srie Tjahjandarie[1]

[1]*Chemistry Department, Faculty of Science and Technology,*
[2]*Institute of Tropical Disease,*
*Airlangga University, Surabaya, Indonesia*

**Corresponding author: estien_y@yahoo.co.id*

**Abstract**

A simple, rapid, low cost, accurate and sensitive spectrophotometric method for the determination of allopurinol (ALP) in urine was developed. This method is based on the reaction of diazotized sulfanilamide with ALP as coupling agent in an alkaline medium. The resulting intense yellow dye has a maximum absorption at 400 nm and stable for more than 1 hour. The Beer's law limits was obeyed over the concentration range of ALP in aqueous medium from 5.0-50 µg/mL. The molar absorptivity and Sandell's sensitivity were obtained $2.5 \times 10^3$ L $mol^{-1}$ $cm^{-1}$ and 0.061 µg $cm^{-2}$ /0,001 absorbance unit, respectively. The optimum reaction conditions and other analytical parameters have also been investigated. The correlation coefficient (r) was obtained 0.999. LOD and LOQ were found 2.2 µg/mL and 7.5 µg/ mL, respectively. The percent recovery and relative standard deviation (RSD) were found 99.18-100.10 % and 0.3-1.3 %, respectively. The proposed method can be applied successfully to assay ALP in urine by standard addition method and can be considered as an alternative method for determination ALP in the urine samples.

**Keywords:** spectrophotometry, allopurinol, sulfanilamide, diazotization reaction, coupling

**Abstrak**

Satu kaedah spektrofotometri mudah, cepat, kos efektif, tepat dan sensitif telah dibangunkan untuk penentuan allopurinol (ALP) dalam air kencing. Kaedah ini dibangunkan berdasarkan tindak balas diazotisasi sulfanilamide dengan ALP sebagai ejen gandingan dalam medium beralkali. Pewarna kuning terang yang terhasil mempunyai penyerapan maksimum pada 400 nm dan stabil selama lebih daripada 1 jam. Had hukum Beer dipatuhi pada julat kepekatan ALP dalam medium akueus 5.0-50 µg/mL. Penyerapan molar dan sensitiviti Sandell's masing-masing diperolehi $2.5 \times 10^3$ L $mol^{-1}$ $cm^{-2}$ dan 0.061 µg $cm^{-2}$ /0,001 unit serapan. Keadaan tindak balas optimum dan parameter analisis lain juga telah dikaji. Pekali korelasi (r) telah didapati 0.999. LOD dan LOQ didapati masing-masing 2.2 µg/mL dan 7.5 µg/mL. Nilai kebolehulangan dan kejituan sisihan piawai relatif (RSD) didapati masing-masing 99.18-100.10% dan 0.3-1.3%. Kaedah yang dicadangkan boleh digunakan dengan jayanya untuk asai ALP dalam air kencing dengan kaedah tambahan piawai dan boleh dianggap sebagai kaedah alternatif untuk penentuan ALP dalam sampel air kencing.

**Kata kunci**: spektrofotometri, allopurinol, sulfanilamide, reaksi diazotisasi, gandingan

## Introduction

Allopurinol (ALP), chemically known as 1H-pyrazolo [3,4-d] pyrimidin-4-ol shown in Figure1, is used for treatment of gout and hyperuricaemia [1]. It is a xanthine oxidase inhibitor [2,3], which prevents the oxidation of hypoxanthine to xanthine and xanthine to uric acid [4]. Thus results in the reduction of urate and uric acid concentrations in plasma and urine [5]. Synthesis of uric acid plays a role in creating oxidative stress through the formation of oxygen radicals [6]. Physical activity in the form of aerobic exercise can increase free radicals and cause oxidative stress [7]. Reactive oxygen species (ROS) is a very dangerous type of free radicals in the body

because it can cause damage to cells, tissues or organs [8, 9] and the underlying pathogenesis of various degenerative diseases such as cancer, hypertension, coronary heart disease, lung disease, diabetes mellitus and premature aging [10].

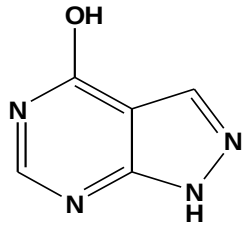



Fig 1: Chemical structure of allopurinol ($C_5H_4N_4O$)

Based on the results of the study showed that administration of allopurinol is able to reduce the production of ROS and can prevent tissue damage caused by aerobic exercise [11]. The provision of high dose allopurinol can reduce oxidative stress in vascular tissue and improve endothelial dysfunction [12]. In addition to treating gout allopurinol is potentially used by athletes as a doping substance because allopurinol supplementation can correct endurance athletes and protect them from injury due to oxidative stress [6].

Several methods have been developed for allopurinol analysis, including conventional volumetric titration method [13], spectrophotometry [14], chromatography techniques [4], capillary electrophoresis [15, 16], flow injection technique [17], and anodic polarographic detection [18]. Volumetric methods need large amounts of chemicals and many steps in preparing standard solutions for analysis before the measurement. In the spectrophotometric method developed by Khayoon *et al*., [14] showed that the application is still limited only for the determination of allopurinol tablet formulation in pharmaceutical preparations. While other methods that have been mentioned quite complicated and requires considerable time and is not always ideal for practical purposes, especially for the analysis of large numbers of samples.

The aim of present work was to develop simple, cheap, rapid, and sensitive spectrophotometric method for determination ALP in biological fluids (urine) based on diazotization coupling reaction with the new reagent sulfanilamide.

## Materials and Methods

### Instruments

Spectral and absorbance measurements were carried out using Shimadzu UV-Visible Recording spectrophotometer UV-1800, with 1 cm matched quartz cells. The pH measurements were performed on pH meter type HANNA HI 96107 pH - Ion meter.

### Reagents and solutions

All reagents and chemicals used were of analytical grade and all solutions were prepared from double distilled water. Allopurinol (ALP) was obtained from Sigma-Aldrich (China), sulfanilamide (Merck), sodium nitrite (Merck), sodium hydroxide (Merck), hydrochloric acid (Merck), trychloroacetic acid (Merck). All solutions were stored in a dark colored bottles.

### Sulfanilamide (0.3%)

The solution was prepared by dissolving 0.3000 g of sulfanilamide in 75 mL of double distilled water and diluted up to 100 mL with double distilled water.

**Sodium nitrite solution (1 %)**
The solution was prepared by dissolving 1.0000 g of sodium nitrite in 100 mL double distilled water in volumetric flask.

**Hydrochloric acid solution (1.0 N)**
The solution was prepared by diluting 8.3 mL of concentrated hydrochloric acid to a 100 mL double distilled water in a volumetric flask.

**Sodium hydroxide solution (2.5 M)**
This solution was prepared by dissolving 10 g of sodium hydroxide in double distilled water and adding the double distilled water to 100 mL in a volumetric flask. Sodium hydroxide solution (0.1 M) was prepared from 2.5 M stock solution.

**Working ALP solution (500 μg/mL)**
ALP solution (500 μg/mL) was prepared by dissolving an accurately amount of ALP in alkaline double distilled water and completed to the mark with double distilled water.

**Preparation of callibration curve**
Sulfanilamide (0.3%, 3 mL) solution was acidified by the addition of 3.0 mL of 1 M hydrochloric acid, followed by the addition of 5.0 mL of 1% nitrite solution. The solutions were agitated and kept for 3 minutes at room temperature to allow the completion of diazotization reaction. The resulting diazotized product was coupled with an aliquot of standard ALP solutions (5.0-50 μg/mL) followed by heating on a boiling-water bath for 5 minutes. The resulting yellow coloured azo dye was diluted to 25 mL with double distilled water and the absorbance was measured at 400 nm against the reagent blank, which gave negligible absorbance at this wavelength.

**Determination of ALP in urine**
Blank urine sample (1 mL) was spiked with ALP at a concentration level of 5.0-50 μg/mL. Then, 1 mL of 10% trichloroacetic acid was added to each sample and vortex for 1 minute and centrifuged for 5 minutes at 4000 rpm. The clear part of this solution was transferred into a test tube for the coupling reaction according to the procedure recommended above.

## Results and Discussion

**Absorption spectra**
In this method, sulfanilamide underwent diazotization reactions after treated with sodium nitrite and hydrochloric acid. The solution was frequently shaken to allow the escape of nitrogen. For the diazotization process, sulfanilamide was readily diazotized in acidic medium and that the diazonium cation would then react with a coupling reagent of ALP in alkaline medium to produce yellow coloured azo product. This yellow colour shows maximum absorbance at 400 nm. This wavelength was then used for all measurements. The corresponding reagent blank has practically negligible absorbance at this wavelength.

**Optimization of Experimental Conditions**
The effect of various parameters on the absorption intensity of the coloured azo dye was investigated, and the reaction conditions were optimized by conducting a series of experiments. The optimum conditions were established by varying one parameter at a time and keeping the others fixed and observing the effect on absorbance of chromogen for the proposed method.

**Effect of the order of addition**
The effect of the order of reagents addition was studied by preparing three solutions with different addition orders (Table 1). Based on the value of absorbance obtained, the order No. I was selected because it gave the highest sensitivity.

Table 1: Effect of order of reagents addition

| Order No. | order of addition | Absorbance |
|---|---|---|
| I | S + H + N + A | 0.561 |
| II | S + N + H + A | 0.499 |
| III | H + N + S + A | 0.423 |

[S = sulfanilamide; H = hydrochloric acid; N = sodium nitrite; A = allopurinol].

**Effect of diazotization time and azo product formation**

The effect of time on both reaction steps of diazotization and coupling reaction for maximum formation of the azo dye was investigated by allowing the reaction to proceed for varying times. The diazotization reaction time was found to be completed within 3 minutes as shown in Figure 2. Slow coupling reaction between the diazotized product and ALP was obseved at room temperature. In order to increase the reaction rate, the mixed reagent solution was heated on a boiling-water bath, and heating time was optimized as shown in Figure 3. The azo dye formation developed rapidly after the solution was heated, attained maximum intensity up to 5 minutes. The absorbance was decreased for a longer heating time. Further analyses were performed on 5 minutes heating on a boiling-water bath.

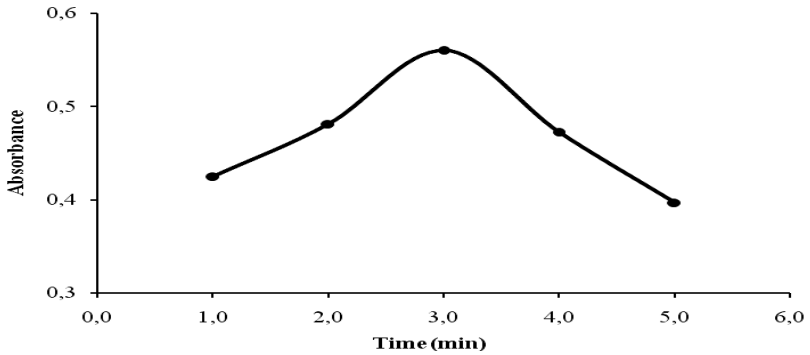



Figure 2: Effect of diazotization time for the formation of maximum azo dye

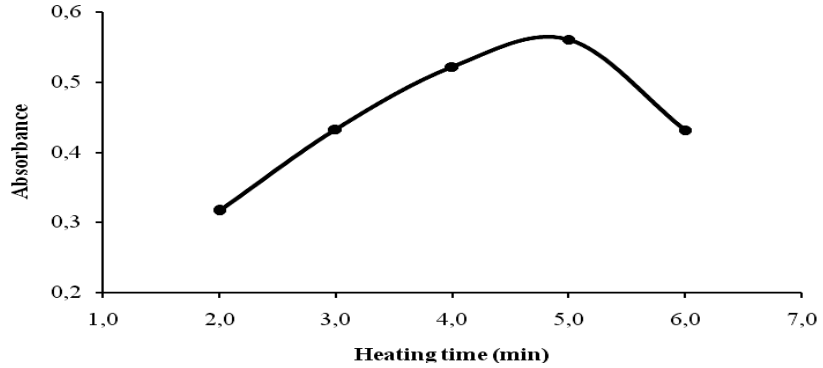



Figure 3: Effect of heating time for the formation of maximum azo dye

**Effect of sulfanilamide**

The effect of different volumes of sulfanilamide on the maximum formation of the azo dye was studied and presented in Figure 4. The results showed that 3.0 ml of 0.3% sulfanilamide is enough to form the diazonium ion and it was used in the subsequent experiments.

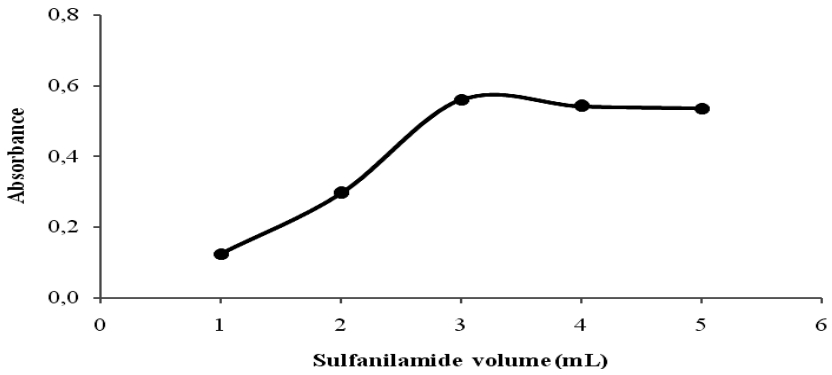



Figure 4: Effect of the volume of 0.3 % sulfanilamide solution for the formation of maximum azo dye

**Effect of hydrochloric acid**

The diazotization reaction occurred in acidic condition. The effect of hydrochloric acid concentration was investigated for maximum diazotization. It was found that the absorbance was increased with increasing acid volume from 1.0-3.0 mL of 1 M hydrochloric acid solution as shown in Figure 5. Above this range, a decrease in absorbance was observed. Thus, 3.0 mL of 1M hydrochloric acid was used in all methods.

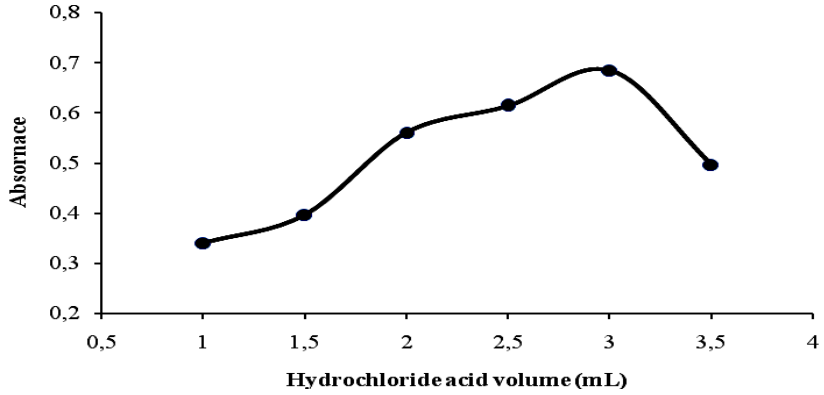



Figure 5: Effect of the volume of 1.0 M hydrochloride acid solution for the formation of maximum azo dye

**Effect of sodium nitrite**

For maximum formation of azo dye, the influence of sodium nitrite concentration was investigated and present in Figure 6. The results demonstrate that there is an increase in absorbance and tend to have a constant value for

sodium nitrite solution with a volume of 5.0 mL. This volume was sufficient for complete diazotization and selected in order to ensure an excess of reagent to guarantee the reaction development.

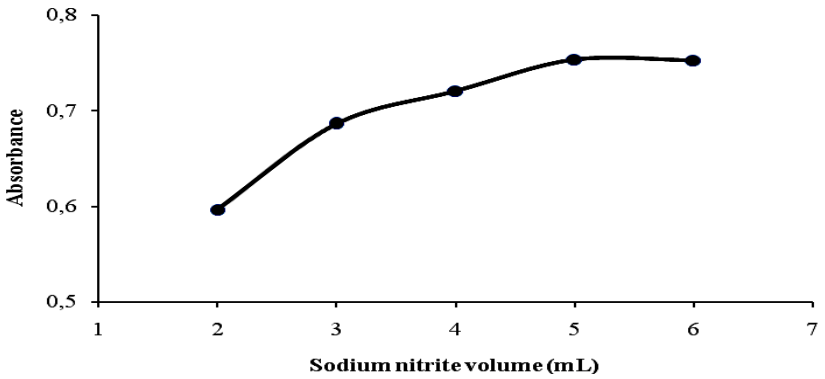



Figure 6: Effect of the volume of 1% sodium nitrite solution for the formation of maximum azo dye

**Stability of the azo dye**

The yellow color of azo dye develops instantaneously after the solution was heated on a boiling-water bath and remains stable for more than 1 hour at room temperature. The absorbance measurements are carried out in the subsequent experiments after dilution to mark up immediately.

Table 2: Optical characteristics of proposed method for spectrofotometric determination of ALP

| **Parameter** | **Values** |
|---|---|
| Type of method | Azo coupling |
| Reagent | sulfanilamide |
| Maximum wavelength, λmax (nm) | 400 |
| Colour of the dye | yellow |
| Beer's law range (µg/ mL) | 5.0-50 |
| Molar absorptivity (L $mol^{-1}$ $cm^{-1}$) | $2.5 \times 10^3$ |
| Sandell's sensitivity (µg $cm^{-2}$ / 0,001 Absorbance unit) | 0.061 |
| **Regression equation (Y = bx + a)** | |
| Slope (b) | 0.0103 |
| Intercept (a) | 0.0986 |
| Correlation coefficient (r) | 0.999 |
| Average recovery (%) | 99.57 |
| Relative standard deviation (%) | 0.89 |
| Limit of detection, LOD (µg/ mL) | 2.246 |
| Limit of quantitation, LOQ (µg/ mL) | 7.488 |

**Analytical performance and calibration curve**

Analytical performance carried out on the proposed method reveal satisfactory results. Recovery studies results are close to 100%, which indicates good accuracy of the method. Calibration curve between the absorbance at the maximum wavelength of 400 nm and the concentration of ALP within Beer´s law limits was found linear over the concentration range 5.0-50 µg/mL. Regression analysis using method of least squares of the calibration data. The correlation coefficient was found from the linear regression equation r = 0.999, which indicated an excellent linearity (Figure 7). The high molar absorptivities of the resulting colored complex indicate the high sensitivity of the method. The low value of relative standard deviation showing the reproducibility of the proposed methods. Table 2 presents the optical characteristic such as maximum absorption, molar absorptivity, Sandell's sensitivity and others.

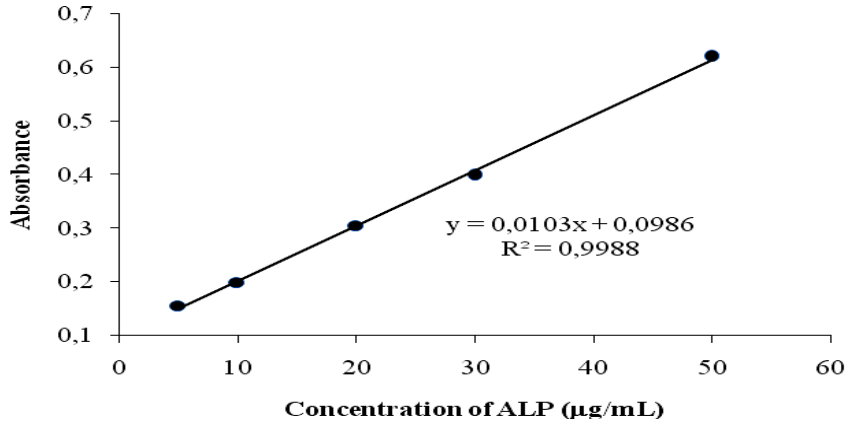



Figure 7: Calibration curve of spectrophotometric determination of ALP at λ 400 nm.

**Accuracy and precision of the method**

To check the accuracy and precision of the proposed analytical method, ALP is determined at three different concentrations with three replications. The results are shown in Table 3, which indicate good accuracy and precision.

Table 3: Accuracy and precision of the proposed method

| ALP given (µg/mL) | ALP obtained (µg/mL) | SD | RSD (%) | Recovery (%) |
|---|---|---|---|---|
| 10 | 9.8 | 0.21 | 2.17 | 98.45 |
| 20 | 20.1 | 0.32 | 1.60 | 100.68 |
| 50 | 50.7 | 0.92 | 1.81 | 101.44 |

**Application of the method**

To test the application of this method, accuracy and precision further ascertained by performing recovery experiments at three different concentrations using the standard addition method and the results are shown in Table 4. Standard addition method was applied to the determination of ALP in urine to prove that the proposed method is not affected by the sample matrices.

Table 4: Accuracy and precision of the proposed method (standard addition method)

| **Amount of ALP added (μg/mL)** | **Amount of ALP found (μg/mL)** | **Recovery (%) (n =3)** | **RSD (%) (n =3)** |
|---|---|---|---|
| 10 | 9.9 | 99.42 | 1.212 |
| 25 | 24.8 | 99.18 | 1.190 |
| 40 | 40.1 | 100.10 | 0.259 |

## Conclusion

A simple, rapid, low cost, accurate and sensitive spectrophotometric method for assay of ALP in urine was developed. Analysis based on the reaction diazotized of sulfanilamide with ALP as the coupling reagent in alkaline medium to form intense yellow coloured product, which having maximum absorption at 400 nm. The proposed method was successfully applied as an alternative method to assay ALP in urine using standard addition method.

## Acknowledgement

The authors are grateful to Analytical laboratory of Chemistry Department of Airlangga University, Surabaya, Indonesia for providing the facilities to carry out this research work.

## References

1. Ruiz, T.P., Lozano, C.M., Tomas, V. & Martin, J., (2003). Determination of allopurinol by micelle-stabilised room temperature phosphorescence in real samples. *Journal of Pharmaceutical and Biomedical Analysis*, 32: 225–231.
2. Amal A. Ammar, A.A., Samy, A.M., Marzouk, M.A., Ahmed, M.K., (2011). Formulation, Characterization And Biopharmaceutical Evaluation Of Allopurinol Tablets, *International Journal of Biopharmaceutics*, 2(2): 63-71.
3. Sreeram, V., Rao, M.V.B., Karumuri, S.R., (2013), A Validated and Stability Indicating Ultra Performance Liquid Chromatographic Method for Allopurinol in Pharmaceutical Preparation, *Paripex-Indian Journal Of Research*, 3: 6–10.
4. Reinders, M.K., Nijdam, L.C.,Van-Roon, E.N., Movig, K.L.L., Jansen, T.L.Th.A., Van De Laar, M.A.F.J., Brouwers, J.R.B.J., (2007). A Simple Method for Quantification of Allopurinol and Oxipurinol in Human Serum by High-Performance Liquid Chromatography with UV-Detection, *Journal of Pharmaceutical and Biomedical Analysis*, 45(2): 312-317.
5. Ali, N.W., Abdelwahab, N.S., EL-fatatry, H.M., and Osman, W.M., (2013). Spectrophotometric Methods for Simultaneous Determination of Two Hypouricemic Drugs in their Combined Dosage Form. *Pharm Anal Acta*, 4(6): 2-8.
6. Purwanto, B., (2012). Supplementation Allopurinol Pre-Exercise For Athletes Safeguard Against Oxidative Stress, *IPTEKOR Journal*, 5 (1) : 1 - 11.
7. Chevion, S., Moran, D.S., & Heled, Y., (2003). Serum Antioxidant Stress and Cell Injury After Severe Physicaal Exercise, *Proceedings of The United State of America*, 100 (9): 5119-5123.
8. Cortina-Puig, M., & Camp, M., (2007). Electrochemical Biosensors as a Tool for Antioxidant Capacity Assessment, *J Sens Actua*, 129: 459-466.
9. Small, D.M., Coombes, J., Bennett, M., Johnson, D.W., and Gobe, G.C., (2012). Oxidative Stress, Anti-Oxidant Therapies and Chronic Kidney Disease, *Asian Pacific Society Of Nephrology* 17(4): 311-321.
10. Halliwell. B., Gutteridge J.M.C., (2007). *Free Radical in Biology and Medicine*, 4th ed, Oxford University Press, New York.
11. Graham, S., Day, R.O., Wong, H., Mclachlan, A.J., Bergendal, L., Miners, J.O., & Birkett, D.J., (1996). Pharmacodynamics of Oxypurinol After Administration of Allopurinol to Healthy Subjects, *Br J Clin Pharmacol*, 41: 299–304.

12. George, J., Carr, E., Davies, J., Belch, J.J., Struthers, A., (2009). High-Dose Allopurinol Improves Endothelial Function by Profoundly Reducing Vascular Oxidative Stress and Not by Lowering Uric Acid, *Circulation*, 114: 2508–2516.
13. Hassib, S.T., Safwat, H.M., and El-Bagry. R.I., (1986). Spectrophotometric Determination of Some Anti-Inflammatory Agents Using ***N***-Bromosuccinimide, *Analyst*, 111: 45-48.
14. Khayoon, W.S., M.Q. Al-Abaichy, M.Q., Jasim, M, and M.A. Al-Hamadany, M.A., (2008). Spectrophotometric Determination of Allopurinol in Tablet Formulation, *Journal. Phys. Sci*., 19(2): 23-30.
15. Ruiz, T.P., Lozano, CM., Tomás, V., and Galera, R., (2003). Development of a Capillary Electrophoresis Method for The Determination of Allopurinol And its Active Metabolite Oxypurinol, *Journal Chromat. B*, 798: 303–308.
16. Sun, X., Cao, W., Bai, X., Yang, X., Wang, E., (2001). Determination of Allopurinol and its Active Metabolite Oxypurinol by Capillary Electrophoresis with End-Column Amperometric Detection, *Analytica Chimica Acta*, 121–128.
17. Zen, J.M., Chen, P.Y., and Kumar, A.S., (2002). Flow Injection Analysis of Allopurinol by Enzymeless Approach at Glassy Carbon Electrodes, *Electroanalysis*, 14 (10): 645-649.
18. Cataldi, T.R.I., Palmisano, F., Zambonin, P.G., (1989). Flow Injection with Anodic Polarographic Detection for The Determination of Allopurinol in Pharmaceutical Formulations, *Analyst*., 114(1989): 1449- 1452.

The Malaysian Journal of ANALYTICAL SCIENCES ISSN 1394-2506

# DIGESTION STUDY OF WATER LEACH PURIFICATION (WLP) RESIDUE FOR POSSIBILITY OF THORIUM EXTRACTION

## (Kajian Penghadaman Residu Pemurnian Larut Resap Air (WLP) Untuk Kebarangkalian Pengekstrakan Torium)

Wadeeah M. AL-Areqi*, Amran Ab. Majid, Sukiman Sarmani

*Nuclear Science Programme, School of Chemical Sciences & Food Technology,*
*Faculty of Science and Technology,*
*Universiti Kebangsaan Malaysia, 43600 UKM Bangi, Selangor, Malaysia*

**Corresponding author: walareqi@yahoo.com*

**Abstract**

Water leach purification (WLP) is the main residue being produced by Lynas Advanced Materials Plant (LAMP). During rare earths elements extraction process, thorium is removed completely to WLP. The objective of this study was to extract thorium from WLP in order to reduce the level of radioactivity and to store Th for future nuclear fuel. Alkali and concentrated acids process was used to recover the Th from WLP. The concentration of Th and U in WLP was determined by Instrumental Neutron Activation Analysis (INAA) and found to be 1952.9 ± 17.6 mg/kg and 17.2 ± 2.4 mg/kg respectively. Digestion process of WLP via sodium hydroxide, concentrated nitric and sulphuric acids using different time and temperature has been tested. The Th concentrations in liquid phrase were determined by Inductively Coupled Plasma-Mass Spectroscopy (ICP-MS). In both processes less than 5% recovery of Th has been achieved. This study showed that very low Th recovery was achieved due to thorium was probably converted into refractory and insoluble form through the calcination stage of LAMP processing. Therefore different techniques should be used to recover the thorium.

**Keywords**: thorium, digestion, WLP, Th recovery

**Abstrak**

Pemurnian Larut Resap Air (WLP) merupakan residu utama yang dihasilkan oleh *Lynas Advanced Materials Plant* (LAMP). Semasa proses pengekstrakan unsur nadir bumi, torium telah dikeluarkan sepenuhnya kepada WLP. Objektif kajian ini adalah untuk mengekstrak torium daripada WLP dalam usaha untuk mengurangkan aras radioaktiviti dan penyimpanan torium untuk bahan api nuklear. Kepekatan Th dan U dalam WLP telah ditentukan melalui Analisis Pengaktifan Neutron (APN) dan didapati kepekatan masing – masing adalah 1952.9 ± 17.6 mg/kg dan17.2 ± 2.4 mg/kg. Proses penghadaman WLP telah diuji menggunakan natrium hidroksida, asid nitrik pekat dan asid sulfurik pekat pada masa dan suhu yang berbeza. Kepekatan Th dalam fasa cecair telah ditentukan menggunakan Induktif Plasma Pasangan– Spektroskopi Jisim (ICP-MS). Dalam kedua- dua proses pemulihan, didapati kurang daripada 5% Th telah ditemui. Kajian ini menunjukkan bahawa penemuan Th adalah sangat rendah kerana torium mungkin telah ditukar kepada bentuk refraktori/ tahan panas dan tidak melalui peringkat pengklasinan dari pemprosesan LAMP. Oleh itu, teknik yang berbeza perlu digunakan untuk mendapatkan torium.

**Kata kunci:** torium, penghadaman, WLP, mendapatkan Th

## Introduction

Thorium- based nuclear fuel has been special interested in nuclear energy recently and in the near decade thorium will be the essential future nuclear fuel [1, 2, 3, 4, 5]. Thorium is the most abundant natural radioactive element, 8 ppm in earth crust and three times abundant in nature compared to uranium. Soil commonly contains thorium in the range of 3.4 –10.5 mg/kg. Th concentration in natural water is extremely low: 1.5 ng/l in sea water and less than 1 ng/l in ground water because its compounds solubility is very low [6]. The highest known world thorium resource is estimated in United States (440,000 tonnes), Australia (300,000 tonnes) then, India (290,000 tonnes) and

Malaysia has 0.4% of thorium world resources (4500 tonnes) [7]. Primary source of thorium is the rare-earth and thorium phosphate mineral- monazite (Ce, La, Nd, Th) $PO_4$ which contains 2.5% of thorium. Thorium occurs in various minerals including thorite ($ThSiO_{4)}$ and thioriate ($ThO_2$), can be associated with several other minerals and also is a by-product in rare-earth production industry [8, 9].

Extraction of thorium from different matrix has been achieved for a century using all types of separation techniques. Typically, thorium is extracted from its minerals with either hot sulphuric acid or hot alkali, converted to thorium nitrate and extracted from impurities with organic solvent using tributyl phosphate TBP in kerosene [10, 11, 12]. Nitrates and chlorides of thorium in acid solutions are widely used to extract thorium into organic solvents.The basis of the separation and purification of thorium depends on the solubility of thorium in water and organic solvents. Due to thorium chemistry such as low solubility, researches on thorium are still being carried out [6]. In general thorium compounds are water insoluble, with the exception of the nitrate, sulfate, chloride, and perchlorate.
Thorium is a by-product of Lynas Advanced Materials Plant (LAMP) which is processing the rare earth ores (lanthanide concentrate) to produce rare earth elements. About 32000 tonnes per year of Water Leach Purification (WLP) is generated by the plant as well as two other types of residue i.e Flue Gas Desulphurisation (FGD) and Neutralisation Underflow (NUF). WLP residue contains thorium and uranium with concentration of 1655 ppm and 22 ppm respectively [13] and it can be estimated that Lynas will produce about 53 tonnes per year of Th in WLP. Sulphuric acid digestion process is used to digest lanthanide concentrate at 650°C for 2.5 hours in a stirred reactor. During the digestion most of Th, rare earth elements and U go into the solution with sulfate and phosphate anions. Because of the chemical similarity between thorium and lanthanides cations in solution selective precipitation is used to separate Th from rare earth elements.

According to Lynas report, over 99% of thorium in the feed lanthanide concentrate is removed to WLP and through the calcination at temperature up to 600$^o$c, Th is converted into refractory and insoluble form and disposal into WLP residue [13, 14]. From fundamental chemistry of Th, solubility of Th is very little when the pH is above 1. During the calcine leaching stage at 650 °C in LAMP process, Th is completely precipitated probably as thorium pyrophosphate ($ThP_2O_7$) when pH of the leach solution was adjusted to 3.5 by addition MgO [13]. Thorium pyrophosphate, iron and a few other heavy metals, with other insoluble matter such as barium sulphate, calcium sulphate and silica are all together constituted WLP residue [14].

In the view of the best matrices storage for Th radioactive waste materials, thorium phosphate compounds is chosen due to their radiation resistance and low solubilises [11] .

The purpose of this research is to find out the possibility of thorium extraction from WLP residue using alkali and acid digestion process and produce thorium nitrate which is the best form for solvent extraction. Research on separation and purification of Th from RE residue can also reduce the level of radioactivity in the residue and obtain high –purity Th for saving future nuclear fuel.

## Materials and Methods

### Determination of Th and U in WLP samples

The WLP residue sample was collected from LAMP and treated to produce fine powder. Instrumental Neutron Activation Analysis (INAA) was employed to determine the concentration of Th and U in WLP. In INAA analysis, Standard reference materials used were IAEA 312N and IAEA 313B. About 0.1 g of WLP sample, 0.2 g of standards were placed in high-purity polyethylene irradiation vials and sealed by heat sealing process. Triplicates were prepared for each sample. Samples, standard reference materials were irradiated for 1 hour in the rotary rack (RR) facility of the TRIGA Mark II reactor at Malaysian Nuclear Agency. The measurements were carried out using a HPGe detector (GC3018) with a relative efficiency of 30 % and resolution of 1.8 keV at 1.33 MeV and the analysis of photo peaks were performed using Genie-2000 software (Canberra Inc). The samples were measured for 1 hour at different cooling times, ranging from 2 days to 4 weeks and counted at 4 cm distances from the detector.

### Chemical processing of WLP

Sodium hydroxide, nitric acid and sulphuric acid were used in the digestion of WLP. The digestion experiments were performed using the glass beakers and a crucible on the stirring hot plate. Various molarities of sodium

hydroxide, concentred nitric and sulphuric acids, different digestion temperatures and digestion times were employed to establish optimum digestion conditions.

In the alkaline processing, about 2 g of fine powder residue was treated with an aqueous solution of sodium hydroxide having a concentration about 73% and 40% by weight under constant stirring (600 rpm) at a temperature about 150°C and under constant digestion time (2 hours). Whereas, the ratio by weight of sodium hydroxide/ WLP residue about 1 was digested in a crucible for 45 min at 130 °C. The produce mass was dissolved in concentrated nitric acid and the filtrate solution was prepared for Th determination via ICP-MS [11, 10, 15]. On the other hand, acid digestion of WLP was carried out using concentrated nitric and sulphuric acid, at different temperatures, time and stirring. The product filtrate solutions were prepared for Th analysis.

**Determination of Th in filtrate samples**

The Th content in the filtrate solutions obtained from alkaline and acid digestion was determined using ICP-MS. The ICP-MS instrument used was an ELAN 9000 (PerkinElmer SCIEX). Prior to ICP-MS analyses, standard solution was prepared using PerkinElmer Pure Plus (multi-element calibration standard 2). Concentration of Th was calculated from the measurement of standard solutions and filtrate after WLP digestion process. The recovery of thorium was calculated from concentration of Th in the initial WLP samples and concentration of Th in filtrate sample. The recovery of thorium will indicate the efficiency of digestion process and dissolution of Th compound existing in the WLP. The scheme for proposed NaOH digestion of WLP and recovery of Thorium shown in Figure 1.

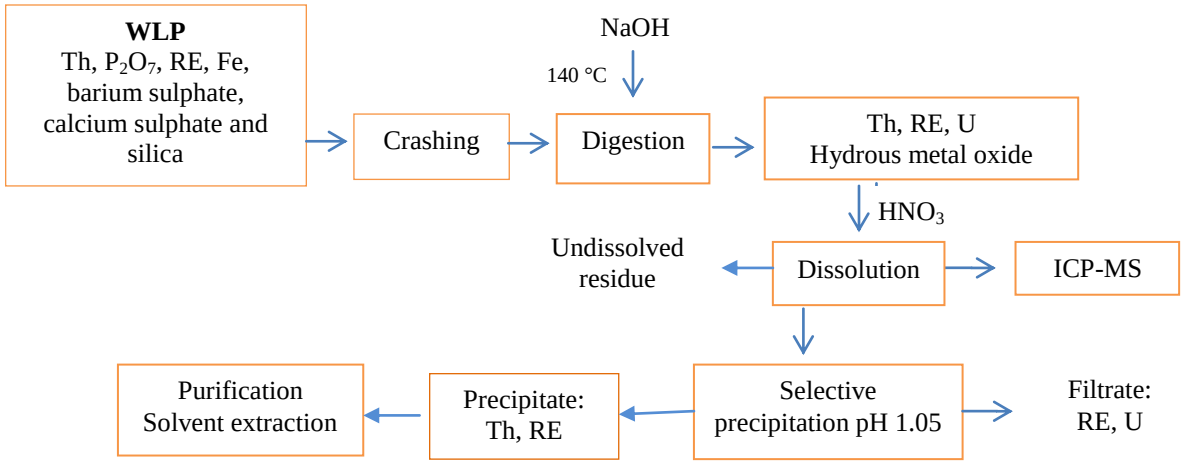



Figure 1: Simplified Scheme for Proposed NaOH Digestion of WLP and Recovery of Thorium

## Results and Discussion

Determination of Th concentration in WLP residue was done before carrying out the alkali and acid digestion. Table 1 shows the concentration of Th and U in WLP residue determined by INAA. Th concentration in residue was 1952.9 ppm (7.98 Bq/g) which was higher than 1 Bq/g therefore; it needs to be considered for regulatory control as the radioactive residue. Rare earth ore reacted with sulphuric acid process according to the following reaction (1) and (2):

$$2REPO_4 + 3H_2SO_4 \rightarrow RE_2(SO_4)_3 + 2H_3PO_4 \text{ and} \quad (1)$$

$$Th_3(PO_4)_4 + 6H_2SO_4 \rightarrow 3Th(SO_4)_2 + 4H_3PO_4 \quad (2)$$

The temperature should be kept below 230 °C otherwise formation of water insoluble thorium pyrophosphate ($ThP_2O_7$) will take place by converting the sulphate of thorium while the rare earth sulphates remain stable in sulphate solution [14,16]. In LAMP process, about 650°C is used to digest the rare earth ore with concentrated sulphuric acid. The reaction product is leached in water followed by reduction of acidity and the filtration produces a rare earth sulphate solution and a filter cake containing thorium pyrophosphate which is the most important content in WLP. This study and experiments based on the fact that chemical form of thorium is pyrophosphate as mentioned by Lynas.

$$ThP_2O_7 + 4NaOH \rightarrow Th(OH)_4 + Na_4P_2O_7 \quad (3)$$

Theoretically, Thorium pyrophosphate reacts with sodium hydroxide as the equation (3), the resulted water insoluble Th hydroxide was dissolved with nitric acid to produce soluble Th nitrate. In practical, WLP was digested with sodium hydroxide which was expected to dissolve thorium pyrophosphate and concentrated nitric and sulphuric acids were also used for digestion of WLP. The concentrations and recovery of Thorium after WLP residue digestion via sodium hydroxide and concentrated acids digestion are presented in Table 2.

It is obvious that by using different digestion approaches either alkali or acids have given less than 5% for Th recovery i.e in the range between 0.17and 4.99 % because of the undissolved chemical form of Th. Digestion using strong NaOH solutions 73% by a weight ratio of sodium hydroxide/ WLP about 7 was relatively recovered Th much compare to NaOH 40% or NaOH (1:1) solid. The best result from digestion was used concentrated nitric acid at 70 °C for 1.5 h and the weight ratio of nitric acid/WLP about 10. Changing type of acids with similar conditions; don't increase the recovery of Th. It is likely that Th is converted to refractory and insoluble form in Lynas process which is difficult and not possible to dissolve by strong alkaline solutions or concentrated acids.

Table 1: Elemental concentration (ppm) of Th and U in Water Leach Purification (WLP) residue of LAMP by INAA

| **Elements** | **WLP** | **RSD %** | **Relative error %** |
|---|---|---|---|
| Th | 1952.9 ± 17.6 | 0.9 | 9.2 |
| U | 17.2 ± 2.4 | 13.6 | 11.8 |

Table 2: Concentrations and recovery of Thorium after WLP residue digestion via sodium hydroxide and concentrated acid digestion

| **Digestion method** | **T (ºC)** | **Time (hours)** | **Weight ratio** | **Stir rpm** | **Concentration ppm (ICP-MS)** | **Recovery %** |
|---|---|---|---|---|---|---|
| NaOH 73% | 140 | 2 | 7 (soda/WLP) | 600 | 25.71 | 1.32 |
| NaOH 40% | 150 | 2 | 4 (soda/WL) | 600 | 14.35 | 0.73 |
| NaOH (s:s) | 130 | 0.75 | 1 (soda/WLP) | | 3.41 | 0.17 |
| HNO3 65% | 70 | 1.5 | 10 (acid/WLP) | 600 | 97.45 | 4.99 |
| HNO3 65% | 130 | 2 | 10 (acid/WLP) | 400 | 28.78 | 1.47 |
| $H_2SO_4$ 98% | 210 | 3 | 18 (acid/WLP) | 450 | 29.99 | 1.54 |

## Conclusion

Proposed digestion process has been tried to extract Th from WLP residue. Different digestion methods were used such as sodium hydroxide, concentrated nitric and sulphuric acids with various temperatures and time to obtain a good recovery of Th. The digestion process has recovered very low Th in the range of 0.17- 4.99 %. The recovery percentage was very less than it was expected. It can be concluded that thorium was probably converted into refractory and insoluble form through the calcination stage of LAMP processing and it was difficult to recover it by strong sodium hydroxide or concentered nitric and sulphuric acids. Perhaps different techniques should be studied to recover thorium. Further researches and investigations on WLP residue and rare earth residue are recommended and possibility of separation Th from RE residue will reduce the level of radioactivity in the residue as well as obtain high –purity Th which will be store for future nuclear fuel usages.

## References

1. AEA. (2005). Thorium fuel cycle- Potential benefits and challenges. IAEA-TECDOC-1450.
2. Mathieu, L., Heuer D., Brissot , R., Garzenne, C., Le Brun, C., Lecarpentier, D., Liatard, E., Loiseaux, J.-M., Me´plan, O., Merle-Lucotte, E., Nuttin , A., Walle, E. & Wilson, J. (2006). The thorium molten salt reactor: Moving on from the MSBR. Progress in Nuclear Energy 48: 664-679.
3. Hania, P.R. & Klaassen, F.C. (2012). Thorium Oxide Fuel. *Comprehensive nuclear material* 3: 87–108.
4. Csom G., Reiss, T., Fehér, S.& Czifrus, S.(2012). Thorium as an alternative fuel for SCWRs. *Annals of Nuclear Energy* 41: 67–78.
5. Björk, K. I., Fhager, V. & Demazière, C. (2011). Comparison of thorium-based fuels with different fissile components in existing boiling water reactors. Progress in Nuclear Energy 53: 618- 625
6. Lehto, J. & Hou, X. (2011). *Chemistry and Analysis of Radionuclides*: Laboratory Techniques and Methodology. Wiley-VCH Verlag & Co. KGaA
7. USGS. (2012). U.S. Geological Survey, Mineral Commodity Summaries, January 2012.
8. Kabata-Pendias, A. and Mukherjee, A. B. (2007). *Trace Elements from Soil to Human*. Berlin : Springer.
9. Cordier, D.J. (2012). U.S. Geological Survey. Mineral Commodity Summaries. (703) 648-7723, dcordier@usgs.gov.
10. Hughes, K.C. & Singh, R. (1980). The isolation of thorium from monazite by solvent extraction. *Hydrometallurgy* 6: 25-33.
11. Wickleder, M. S. Fourest, B. & Dorhout,P. K. (2010). The Chemistry of the Actinide and Transactinide Elements, chapter three: Thorium.
12. Abrao, A., Alves de Freitas, A., & Sequeira de Carvalho, F. M. (2001). Preparation of highly pure thorium nitrate via thorium sulfate and thorium Peroxide. *Journal of Alloys and Compounds* 323–324: 53- 56.
13. RIA (2011). Radiological impact Assessmant of Lynas Advanced Materials Plant 2011: Exective Summary, Rev 4, November (2011).
14. IAEA (2011). Radiation Protection and NORM Residue Management in the Production of Rare Earths from Thorium Containing Minerals, Safety Reports Series No. 68.
15. Ali, A.M.I. El-Nadi, Y.a. Daoud, J.a.& Aly, H.F. (2007). Recovery of thorium (IV) from leached monazite solutions using counter-current extraction. *International Journal of Mineral Processing* 81: 217-223.
16. Cardarelli, F. (2008). *Materials Handbook*: A Concise Desktop Reference, 2nd Edition.

**Malaysian Journal of Analytical Sciences Vol 18 No 2 2014**

Articles 15 - 28 are selected papers from the "Malaysia Polymer International Conference (MPIC 2013), 25-26 September 2013, Hotel Equatorial Bangi-Putrajaya, Selangor, Malaysia."

Guest Editors: Ishak Ahmad and Azlin Mohmad Azman

**Page**

1. FORENSIC ANALYSIS OF BLUE BALLPOINT PEN INKS ON QUESTIONED DOCUMENTS BY HIGH PERFORMANCE THIN LAYER CHROMATOGRAPHY TECHNIQUE (HPTLC) 226
(Analisis Forensik Dakwat Biru Pen Mata Bulat Atas Dokumen Yang Dipertikai Dengan Kromatografi Lapisan Nipis Berprestasi Tinggi (HPTLC))
*Loong Chuen Lee, Sitti Mariam Nunurung, Ab Aziz Ishak*

2. PENGGUNAAN KAEDAH KEMOMETRIK BAGI MENENTUKAN KUALITI MINYAK KELAPA SAWIT, MINYAK JAGUNG DAN MINYAK KELAPA SEGAR DAN TERPAKAI 234
(Utilization of Chemometric Technique to Determine the Quality of Fresh and Used Palm, Corn and Coconut Oil)
*Hamizah Mat Agil, Mohd Zuli Jaafar, M. Suzeren Jamil, Azwan Mat Lazim*

3. POTENTIAL OF PALM OLEIN AS GREEN LUBRICANT SOURCE: LUBRICATION ANALYSIS AND CHEMICAL CHARACTERISATION 245
(Potensi Minyak Sawit Olein Sebagai Sumber Lubrikan Hijau: Analisis Pelinciran dan Pencirian Kimia)
*Darfizzi Derawi and Jumat Salimon*

4. SYNTHESIS, STRUCTURAL AND ANTIBACTERIAL STUDIES OF NEW DITHIOCARBAMATE COMPLEXES OF Sb(III) AND Bi(III) 251
(Sintesis, struktur dan kajian antibakteria kompleks baru ditiokarbamat Sb(III) dan Bi(III))
*Nur Amirah Jamaluddin, Ibrahim Baba, Nazlina Ibrahim*

5. DAUN HIBISCUS ROSA SINENSIS: ANALISIS PROKSIMAT, AKTIVITI ANTIOKSIDAN DAN KANDUNGAN BAHAN INORGANIK 260
(Hibiscus rosa sinensis Leaves: Analysis of Proximate, Antioxidant Activities and Inorganic Compound)
*Saiful Irwan Zubairi & Nurul Shahreda Jaies*

6. REMOVAL OF SELECTED HEAVY METALS FROM GREEN MUSSEL VIA CATALYTIC OXIDATION 271
(Penyigkiran Logam-Logam Tertentu Daripada Kupang Melalui Pengoksidaan Bermangkin)
*Faizuan Abdullah, Abdull Rahim Mohd Yusoff, Wan Azelee Wan Abu Bakar, Razali Ismail, Dwi Priya Hadiyanto*

7. ASSESSMENT OF NATURALLY OCCURING RADIONUCLIDE IN THE SEDIMENT CORE IN SOUTHERN OF KUALA SELANGOR COASTAL AREA 284
(Kajian Radionuklida Tabii di dalam Teras Sedimen di Kawasan Pesisir Pantai Selatan Kuala Selangor)
*Zaini Hamzah, Umi Kalsum Abdul Karim, Ahmad Saat, Sabarina Md Yunus*

8. SINTESIS HIDROGEL BERASASKAN NATA DE COCO DENGAN ASID AKRILIK SEBAGAI KO-MONOMER MENGGUNAKAN KAEDAH PEMPOLIMERAN RADIKAL BEBAS 299
(Synthesis of Hydrogel Based on Nata De Coco and Acrylic Acid as Co-Monomer using Free Radical Polymerization Method)
*Melissa Liew, Rizafizah Othaman, Rozida Khalid, M.C.Iqbal M.Amin, Azwan Mat Lazim*

9. KAJIAN AWALAN TERHADAP PENULENAN DAN PENGENALPASTIAN ASID AMINO AROMATIK L-DOPA DARIPADA KAKI PEREKAT KUPANG HIJAU AIR TAWAR MALAYSIA 306
(Preliminary Study on Purification and Identification of Aromatic Acid Amino L-DOPA from Malaysia Freshwater Green Mussel Byssus)
*Saiful Irwan Zubairi, Wan Rosmaryana Wan Musa, Syed Anuar Faua'ad Syed Mohammad*

10. METHYL ESTER (BIODESEL) PRODUCTION FROM WASTE COOKING VEGETABLE OIL BY MICROWAVE IRRADIATION 321
(Penghasilan Metil Ester (Biodesel) Daripada Sisa Minyak Sayuran oleh Penyinaran Gelombang Mikro)
*M.S.Khatun, M.A. Khatun, M.Z.H. Khan, M. Debnath*

11. DETERMINATION OF MODAFINIL IN TABLET FORMULATION USING THREE NEW VALIDATED SPECTROPHOTOMETRIC METHODS 329
(Penentuan Modafinil Dalam Formulasi Tablet Menggunakan Tiga Kaedah Spektofotometrik Ditentusahkan)
*Pawan Kumar Basniwal & Deepti Jain*

12. PENILAIAN RISIKO KANSER DARI SAMPEL TANIH DI SEKITAR KAWASAN PERINDUSTRIAN GEBENG, PAHANG DAN SAMPEL AMANG DI PERAK 337
(Assessments of Cancer Risk from Soil Samples in Gebeng Industrial Estate, Pahang and Amang Samples in Perak)
*Che Nor Aniza Binti Che Zainul Bahri, Khoo Kok Siong, Amran Ab. Majid, Norafatin binti Khalid*

13. THE EFFECT OF BLEND RATIO ON PROPERTIES OF RECYCLED POLYPROPYLENE/RECYCLED HIGH DENSITY POLYETHYLENE GEO- COMPOSITES 344
(Kesan Nisbah Adunan Ke Atas Sifat-Sifat Geo-Komposit Polipropilena Kitar Semula/Polietilena Ketumpatan Tinggi Kitar Semula)
*A.A.S Mariam Atiqah, H.Salmah, Z. Firuz, D.N.U. Lan*

14. PHYTOCHEMICAL SCREENING, TOTAL PHENOL ESTIMATION, ANTIOXIDANT ACTIVITY OF BLAINVILLEA ACMELLA LEAF AND STEM SUCCESSIVE EXTRACTS 351
(Ujian Penyaringan Fitokimia, Penganggaran Fenol dan Aktiviti Antioksidan Blainvillea Acmella dan Ekstrak Berturutan Daun dan Stem)
*Piush Sharma, Ganesh N. Sharma, B. Shrivastava, Hemant R. Jadhav*

15. RHEOLOGICAL AND THERMAL BEHAVIOR OF POLYPROPYLENE-KAOLIN COMPOSITES 360
(Reologi dan Sifat Thermal Komposit Polipropilena-Kaolin)
*Saw Lip Teng, Nor Azura Abdul Rahim, Du Ngoc Uy Lan*

16. MECHANICAL AND MORPHOLOGY PROPERTIES OF FEATHER FIBER COMPOSITE FOR DENTAL POST APPLICATION 368
(Sifat- Sifat Mekanikal dan Morfologi Komposit Serat Bulu Untuk Aplikasi Pos Pergigian)
*Siti Maizatul Farhain Salehuddin, Mat Uzir Wahit, Mohammed Rafiq Abdul Kadir, Eshamsul Sulaiman, Noor Hayaty Abu Kasim*

17. CARBOXYMETHYL CELLULOSE FROM KENAF REINFORCED COMPOSITE POLYMER 376

ELECTROLYTES BASED 49% POLY(METHYL METHACRYLATE)-GRAFTED NATURAL RUBBER
(Komposit Polimer Elektrolit Berasaskan 49% Poli(metil metakrilat)-cangkukan Getah Asli Diperkuat Karboksimetil Selulosa Daripada Kenaf)
*Serawati Jafirin, Ishak Ahmad, Azizan Ahmad*

18. EFFECT OF FERMENTED CHITIN NANOWHISKERS ON PROPERTIES OF POLYLACTIC ACID BIOCOMPOSITE FILMS 385
(Kesan Kitin Terfermentasi Terhadap Sifat Filem Biokomposit Asid Poli Laktik)
*Syazeven Effatin Azma Mohd Asri, Zainoha Zakaria, Azman Hassan, M. K. Mohamad Haafiz*

19. FLEXURAL PROPERTIES OF ACTIVATED CARBON FILLED EPOXY NANOCOMPOSITES 391
(Sifat Lenturan Nanokomposit Epoksi Berpengisi Karbon Teraktif)
*H.P.S. Abdul Khalil, M. Jawaid, P. Firoozian, Othman Y. Alothman, M. T. Paridah, E.S. Zainudin*

20. GRAFT COPOLYMERIZATION OF METHYL METHACRYLATE ONTO AGAVE CELLULOSE 398
(Pengkopolimeran Cangkukan Metil Metakrilat ke atas Selulosa Agave)
*Noor Afizah Rosli, Ishak Ahmad, Ibrahim Abdullah, Farah Hannan Anuar*

21. EFFECT OF REAGENTS CONCENTRATION AND RATIO ON DEGRADATION OF NATURAL RUBBER LATEX IN ACIDIC MEDIUM 405
(Kesan Kepekatan dan Nisbah Reagen ke Atas Pendegradasian Lateks Getah Asli dalam Media Berasid)
*Suhawati Ibrahim, Asrul Mustafa*

22. SYNTHESIS OF CHITOSAN-GRAFTED-POLY(METHYL METHACRYLATE) WITH FENTON'S REAGENT (Fe2+ - H2O2) AS A REDOX INITIATOR 415
(Sintesis Kitosan-Cangkuk-Poli(Metil Metakrilat) Dengan Reagen Fenton (Fe2 + - H2O2) Sebagai Pemula Redoks)
*Nur Azmyra Abdul Aziz, Aznizam Abu Bakar, Azman Hassan, Nurulhusna Azmi*

23. ROLE OF ANTI-OXIDANTS ON NORMOXIC METHACRYLIC ACID GELATIN (MAG) POLYMER GEL DOSIMETER AT 6-MV PHOTON BEAM USING SINGLE SPIN ECHO MRI 423
(Peranan Anti-Oksida Dalam Normosik Asid Methakrilik Gelatin (MAG) Dosmeter Gel Polimer Pada 6-MV Sinaran Photon Menggunakan Aturan Nada Denyut Tunggal MRI)
*Nik Noor Ashikin Nik Ab Razak, Azhar Abd Rahman, Sivamany Kandaiya, Iskandar Shahrim, Nor Zakiah Yahaya, Noor Faizura Zainal, Eng Kae Yann*

24. MECHANICAL PROPERTIES OF STARCH FILLED POLYPROPYLENE UNDER EXPOSURE OF HYGROTHERMAL CONDITIONS 434
(Sifat-sifat Mekanikal Bagi Komposit Polipropilena Terisi Kanji di Bawah Pendedahan Higroterma)
*Wan Zakaria Wan Nor, Nor Azura Abdul Rahim, Hakimah Osman and Muthmirah Ibrahim*

25. EFFECT OF DIFFERENT HEALING TEMPERATURE ON SOLID STATE SELF-HEALING SYSTEM 444
(Kesan Suhu Pemulihan Yang Berbeza Terhadap Sistem Swa-Pemulihan Dalam Keadaan Pepejal)
*S. M. Makenan, N. N. Muhamad, M. J. Mohd Suzeren, S. Salihan, M.A.S. Mat Lazim*

26. PALM-BASED POLYURETHANE WITH SOYBEAN PHOSPHATE ESTER AS A FIRE RETARDANT 456
(Poliuretana Sawit dengan Ester Fosfat Soya Sebagai Perencat Api)
*Nor Rabbi'atul 'Adawiyah Norzali, Khairiah Haji Badri, Ong Soo Ping, Ishak Ahmad*

27. THERMAL PROPERTIES, STRUCTURE AND MORPHOLOGY OF GRAPHENE REINFORCED POLYETHYLENE TEREPHTHALATE/POLYPROPYLENE NANOCOMPOSITES 466

(Sifat Termal, Struktur dan Morfologi Graphene Bertetulang Polietilena Tereftalat /Polipropilena)
*I. M. Inuwa, A. Hassan, S. A. Shamsudin*

28. TOUGHENING OF EPOXY BY SILANE-TREATED NANOTITANIUM DIOXIDE 478
(Penguatan Epoksi oleh Silana Terawat Nanotitanium Dioksida)
*Phasapan Sanemuang and Jantrawan Pumchusak*

The Malaysian Journal of ANALYTICAL SCIENCES ISSN 1394-2506

# FORENSIC ANALYSIS OF BLUE BALLPOINT PEN INKS ON QUESTIONED DOCUMENTS BY HIGH PERFORMANCE THIN LAYER CHROMATOGRAPHY TECHNIQUE (HPTLC)

## (Analisis Forensik Dakwat Biru Pen Mata Bulat Atas Dokumen Yang Dipertikai Dengan Kromatografi Lapisan Nipis Berprestasi Tinggi (HPTLC))

Loong Chuen Lee*, Sitti Mariam Nunurung, Ab Aziz Ishak

*Forensic Science Programme, Faculty of Health Sciences,*
*Universiti Kebangsaan Malaysia, Jalan Raja Muda Abdul Aziz, 50300 Kuala Lumpur, Malaysia*

**Corresponding author: lc_lee@ukm.edu.my*

**Abstract**

Nowadays, crimes related to forged documents are increasing. Any erasure, addition or modification in the document content always involves the use of writing instrument such as ballpoint pens. Hence, there is an evident need to develop a fast and accurate ink analysis protocol to solve this problem. This study is aimed to determine the discrimination power of high performance thin layer chromatography (HPTLC) technique for analyzing a set of blue ballpoint pen inks. Ink samples deposited on paper were extracted using methanol and separated via a solvent mixture of ethyl acetate, methanol and distilled water (70: 35: 30, v/v/v). In this method, the discrimination power of 89.40% was achieved, which confirm that the proposed method was able to differentiate a significant number of pen-pair samples. In addition, composition of blue pen inks was found to be homogeneous (RSD <2.5%) and the proposed method showed good repeatability and reproducibility (RSD <3.0%). As a conclusion, HPTLC is an effective tool to separate blue ballpoint pen inks.

**Keywords:** forensic science, ink analysis, High Performance Thin Layer Chromatography, discrimination power, ballpoint pen

**Abstrak**

Baru-baru ini, jenayah yang berkaitan dengan dokumen palsu semakin meningkat. Sebarang pemadaman, penambahan atau pengubahsuaian dalam kandungan dokumen sering melibatkan penggunaan alatan tulis seperti pen mata bulat. Oleh itu, ia terdapat satu keperluan yang nyata untuk membangunkan satu protokol analisis dakwat yang cepat dan tepat untuk menyelesaikan masalah ini. Kajian ini bertujuan untuk menentukan kuasa diskriminasi teknik lapisan nipis berprestasi tinggi (HPTLC) menganalisis satu set dakwat biru pen mata bulat. Sampel dakwat yang termendap pada kertas diekstrak mengguna metanol dan dipisahkan dengan campuran pelarut yang mengandungi etil asetat, etanol dan air suling (70:35:30). Dalam kaedah ini, 89.40% kuasa diskriminasi tercapai, ini mengesahkan kaedah yang dicadangkan berupaya membeza bilangan pasangan pen yang signifikan. Sebagai tambahan, komposisi dakwat biru pen mata bulat didapati homogen (RSD < 2.5%) dan kaedah yang dicadangkan menunjukkan kebolehulangan dan keterulangan yang baik (RSD<3.0%). Sebagai kesimpulan, HPTLC adalah satu alatan yang efektif untuk memisahkan dakwat biru pen mata bulat.

**Kata kunci:** sains forensik, analisis dakwat, kromatografi lapisan nipis berprestasi tinggi, kuasa diskriminasi, pen mata bulat

## Introduction

Forensic document examination always involves the analysis of blue ballpoint pen inks. Chemical analysis of inks is therefore an important procedure aimed at detecting any kind of frauds. There are quite a number of articles

reporting the examination of blue ballpoint pen inks using chromatography techniques [1-10]. Each of them reported discrimination power (DP) above 90% for blue ballpoint pen inks.

In 1998, Tsutsumi & Ohga [1] described a preliminary preparation of a standard thin layer chromatography (TLC) library for a total of 35 ballpoint pens composing of black, red and blue inks. Authors found that Merck normal phase plate using ethyl acetate/ethanol/water (14:7:6) [1] gave higher degrees of dye separation if compared to the one using ethyl acetate/methanol/28% aqueous ammonia (5:2:1) and tricholoethylene/1,1,1-trichloroethane/ethyl acetate (10:1:1). On the other hand, Roux et al. [2] stated that TLC was able to discriminate inks between and within brands, models, and batches of blue ballpoint pen inks in Australia with DP of 98%.

Djozan et al [3] proposed a simple and easy method for discrimination of blue ballpoint pen inks on a document. The proposed method includes a new and fast data acquisition by designing new and specific image analysis software for evaluating TLC chromatograms after scanning with ordinary office scanner, without in need of expensive instruments. This method allows one to compare two inks by considering the retention factor (Rf), color range and intensity of the separated ink components. They reported the DP of the proposed method as 92.8% [3].

An improved TLC technique, i.e. high performance thin layer chromatography (HPTLC), was introduced in the early 2010s. Senior et al [4], Neumann and Margot [5-7], Neumann et al [8] demonstrated the possibility of retrieving quantitative data from HPTLC chromatograms. Thus, statistical techniques can be applied on data interpretation and this greatly improves the accuracy of identification and discrimination of pen inks based on HPTLC technique.

To date, there has been no report presenting results of HPTLC analysis of blue ballpoint pen that collected from the market in Malaysia. Thus, taking into account the above-mentioned successful application of TLC and HPTLC techniques to the analysis of blue pen inks, we decided to make an effort to fill in the gap in current analytical methodology of forensic questioned document examination. Therefore, the aim of this paper was to determine the discrimination power of HPTLC technique to analyze blue ballpoint pen inks. Furthermore, homogeneity of inks and reproducibility as well as repeatability of HPTLC technique was also determined.

## Materials and Methods

### Chemical and reagents

The chemicals used throughout the experiments were methanol, ethanol and ethyl acetate produced by Fisher Scientific (UK). Crystal violet (CV) dye was purchased from Acros Organics, USA. Distilled water was used to prepare all solutions. The HPTLC silica gel plate 60 with layer thickness 0.2 mm and 20 X 20 cm aluminum cards (Merck, Germany) and horizontal developing chambers were used at the forensic science laboratory, Universiti Kebangasaan Malaysia, for chromatographic separation of dyes in ink entries.

### Samples

A set of blue ballpoint pen consists of 12 varieties were purchased from stationary shops in Malaysia. All pens were allocated a reference number during this study, as shown in Table 1. Four different individual pens were sampled for each of the pen variety. Experimental work was carried out on inks extracted from ink entries produced on white photocopier paper. All papers used for written were of the same batch to avoid substrate variability.

Table 1. Reference (ID) number of all 12 varieties of pen samples

| Brand | Model | ID number |
|---|---|---|
| Faber Castell | Click Ball 1422 Fine | A1 |
| | Ball Point 1432 Medium | A2 |
| G'soft | R100 Fine | B1 |
| | PDA2 Delta Semi Fine | B2 |
| Faster | Ball Pen CX1006 Super Smooth Semi Fine | C1 |
| | Ball Pen CX444 Super Smooth Fine | C2 |
| Stabilo | Performer Fine | D1 |
| | Performer X-Fine | D2 |
| LINC | Glycer Ball Pen | E1 |
| | Ultra Ball Pen | E2 |
| Paper Mate® | KV2 Medium | F1 |
| | InkJoy 100 RT | F2 |

**Sample Preparation**

Each of the pens was used to write "BMW" on a piece of white paper. After ink deposited on a paper, the absorbed ink was extracted from the ink entry of about 1 cm X 0.5 cm with 200 uL of methanol in a polypropylene micro vial. A blank sample was prepared by treating a blank white paper with methanol. CV was prepared as standard reference dye by dissolving the dye with methanol.

**High Performance Thin Layer Chromatography**

The origins were at 1.5 cm from the base of the plates. HPTLC analyses were performed using ethyl acetate, ethanol and distilled water (7:3:2) as an eluent mixture. Each extracted ink sample was spotted manually using capillary tube manually. CV used as standard dye and a paper blank as well solvent blank was included in each run. To check the role of sampling on analytical results, another extraction with methanol was performed directly from the pen ink reservoir, obtaining indistinguishable data if compared with the samples extracted from the lines of paper. The mobile phase was prepared freshly daily and replaced after every two runs. Before daily operation, the tank was conditioned with mobile phase for at least 20 min. The uniform origin position on the plates, proper loading at the origin, and the solvent saturation in the developing tank were kept constant during all the HPTLC analyses to ensure high reproducibility.

**Discriminating Power (DP)**

The discriminating powers (DP) of the different brands and different models of the same brand were calculated according to Smalldon and Moffat [11], where Equation 1:

$$DP = (\text{Number of discriminated pairs}) / (\text{number of possible pairs}) \quad \text{(Eq. 1)}$$

**Ink homogeneity, repeatability and reproducibility**

Two varieties of pen inks (choose from the 12 studied ink varieties) presented the most versatile HPTLC profile were selected to determine the homogeneity of ink as well as the precision of the HPTLC methods. Relative standard deviation (RSD) was determined for each test.

For determination of ink homogeneity, each of the two selected inks was used to prepare nine different ink entries on white paper. After then, each of the nine extracted inks were spotted once on the plate and were analyzed according to procedures explained above on a single HPTLC plate.

Repeatability of method was determined by preparing one single ink entries from each of the selected pen ink varieties. Later, nine different ink spots were deposited on HPTLC plate from each of the two prepared ink extracts on a single HPTLC plate and analyzed according to procedures explained above. In order to examine the reproducibility of the method, the procedures described for determination of repeatability were repeated at four different HPTLC plates in four different days.

## Results and Discussion

### HPTLC Analysis

HPTLC profiles of the 12 studied blue pen inks were shown in Figure 1. In general, the HPTLC profiles of most inks were very similar. The HPTLC results reflected that CV was the major dye component present in the blue ballpoint pen inks. Based on Figure 1, all the pen inks contained CV as their main coloring agent, except sample pen D1 and D2, i.e. models of Stabilo. Previous literature reports also agreed with our observation that CV is one of the main coloring agents in blue pen inks [12-14].

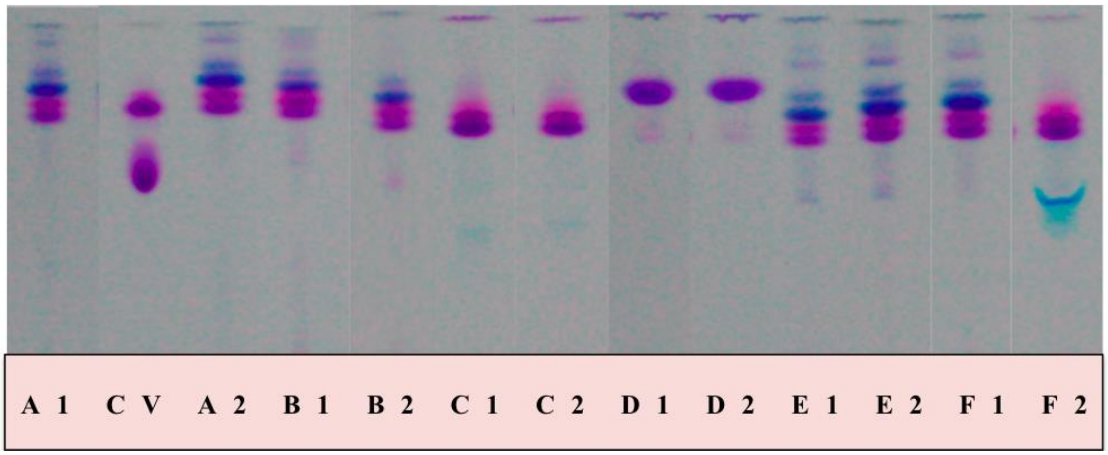



Figure 1. HPTLC plate showing dye profile of 12 blue ballpoint pen inks (A1-F2).

Second track from the left was standard dye CV. The figure was reconstructed from several HPTLC chromatograms for easy comparison between ink spots of different pen varieties. On the other hand, solvent blank and paper blank did not give any observable band under both normal white light and UV light. The retention factor (Rf) values recorded for each bands of each pen variety were the average product of dye profiles separated from four different individual pens of a particular pen variety. Analyzing of four different individual pens for each pen variety aimed to average out and minimize any errors. It was observed that ink profiles as well as the associated Rf values of a single pen ink variety extracted from four different individual pens were highly similar (Figure 2). This means the inks were quite homogeneous across different individual pens that produced within a single batch of production for a selected pen variety.

In addition, this study also conducted a parallel set using inks extracted directly from the reservoir. None of previous studies have done such verification step. Based on this study, differences observed between HPTLC profiles of four different individual pens were not significant for all pen varieties. This indicated extraction via methanol was efficient to extract all the dyes present in the ink entries.

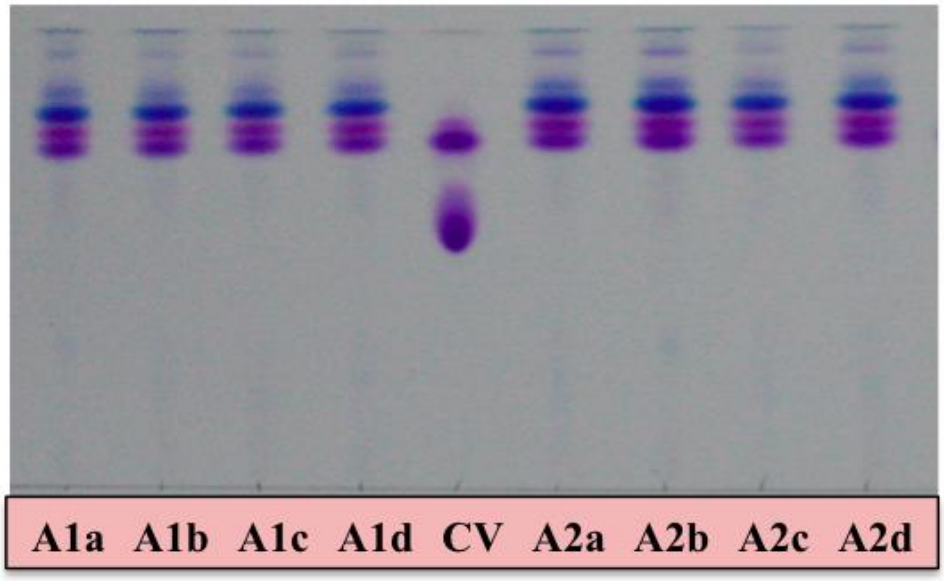



Figure 2. First four tracks (from the left) and the subsequent four tracks were extracted from pen A1 and A2, respectively. Each of the four spots were originated from four different individual pens of pen A1 and A2, respectively

**Classification and differentiation**

Based on Figure 1, the color tones of the bands separated by the normal-phase HPTLC analysis enable the classification of the writing pens into four different groups. Group one (named as G1) consisted of only sample D which did not have CV in its ink composition. Whereas, sample C1-2, i.e. models of Faster pens containing only CV as they major dye were grouped in the second group (named as G2). Sample F2 which contained CV as well as a light blue-colored bands at the lower position relative to the CV, named as G3. The fourth group (named as G4) consisted of the remaining sample A1-2, B1-2, E1-2, and F1 which evidenced the presence of CV and another dye (blue-colored band on the top of the band of CV) in their ink composition.

Within G1, both pen models from Stabilo, i.e., D1 and D2 refer to Performer F and Performer X-F, used dye other than CV as their major coloring agents. The color profiles, i.e. relative intensity of color and shape of the separated bands, of both models of Stabilo were appeared very similar to each other. Stabilo appears to use the same inks for all the models tested that only differed at point size.

On the other hand, both pen models from Faster were grouped in G2. They contained only one major dye, i.e. CV, as their coloring agent. Nonetheless, the appearance of another very light-blue-colored band below the CV's band supported that Faster did add in another minor dye in their formulation. Again, both pen models of Faster were models that only differed at point size, i.e. Ballpen semi fine and Ballpen fine, and thus exhibited very similar dye profiles.

The third group (G3) included only a single pen model, i.e. Inkjoy 100 RT (F2), from PaperMate. The scenario presented here was totally different from both cases mentioned before this. Both models of PaperMate can be differentiated from each other in which F1 did not show an extra light-blue colored band (Fig. 1), indicating both are from different sources. This can be explained by the fact that F2 was produced in India compared to F1 was manufactured in Malaysia.

The last group (G4) included the results obtained for inks of producers other than Stabilo, Faster and F2 of PaperMate, which included FC, G'soft, LINC and F1 of PapaerMate. Their chromatogram profiles were characterized predominantly by two prominent dyes, i.e. CV and another unidentified dye (dark-blue colored bands). HPTLC profiles of all of them looked very similar to each other (Fig. 1). However, detailed examination revealed that both models of G' soft (B1-2) and LINC (E1-2) could be differentiated from the rest by a hardly visible band located at the lowest Rf values for each of them. The color of that minor band of B1-2 and E1-2 exhibited pink and blue color, respectively.

**Discriminating power (DP)**

Figure 3 showed the summary results of differentiation of 12 blue pen inks varieties. In the group of 12 blue ballpoint pen inks, 66 possible pairs of compared samples have been created. It has been found that all samples except seven pairs can be identified based on their HPTLC chromatogram (Fig. 1). Thus the DP has been equal to about 89.40%.

DP= (66-7)/66=59/66=89.40%

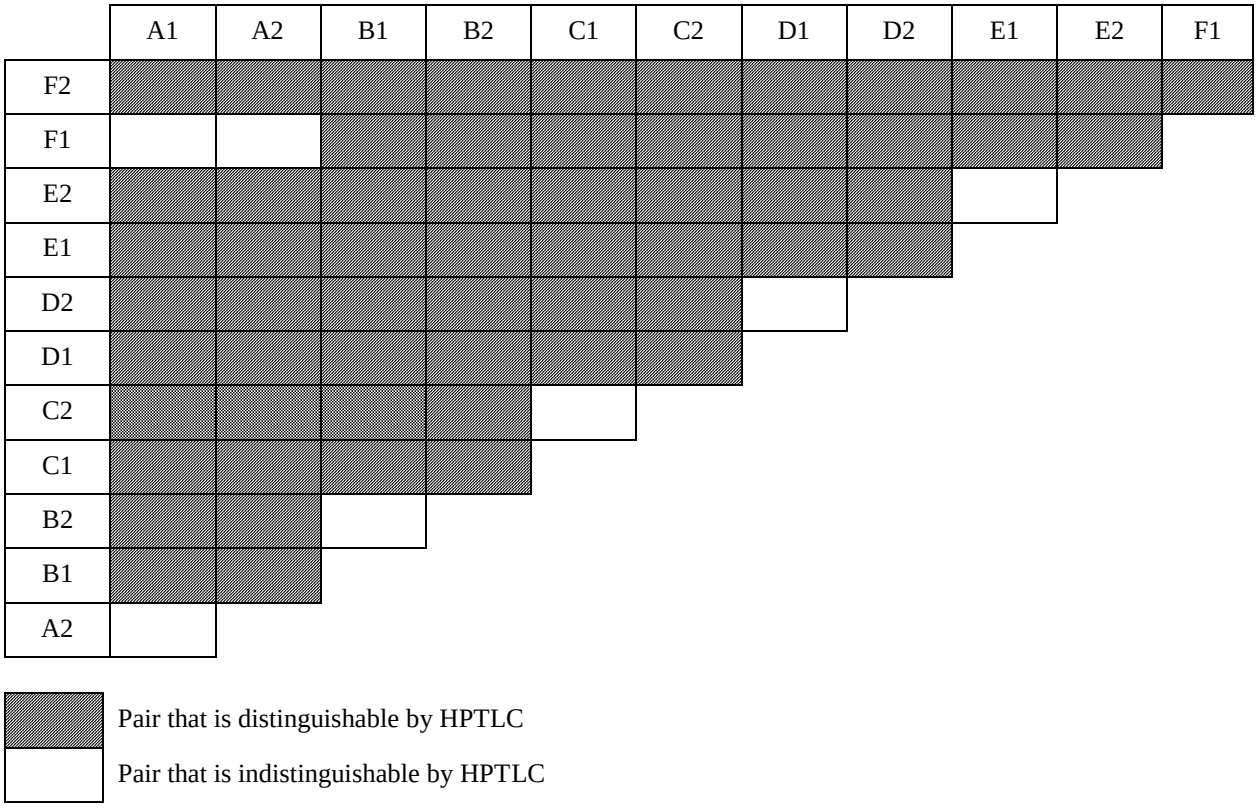



Figure 3. Differentiation of blue ballpoint pen inks based on HPTLC technique

Nonetheless, there was some possibility of distinguishing between the inks extracts of the remaining pen varieties by calculating the relative color intensity of bands. However, this study did not determine the relative color intensity of bands due to unavailable of CAMAG TLC Scanner with WinCats software (CAMAG AG, Switzerland). Alternatively, colorless components, i.e. additives, could be used to discriminate models from a single

manufacturer. The occurrence of the same separation patterns is possibly attributed to the situation that plural products from one manufacturer contain common dyestuff components, and ink compositions depend on the limited raw dyestuffs provided by dyestuff makers, which are smaller in number compared to writing instrument makers [8].

**Ink homogeneity, repeatability and reproducibility**

Verification of the repeatability and reproducibility as well as determination of ink homogeneity was conducted with the use of two selected pen varieties, E2 and F2. They were chosen because both of them presenting the most diversify HPTLC profiles. RSD values were calculated for each test and summarized in Table 2.

Table 2. Ink homogeneity, repeatability and reproducibility of HPTLC technique using pen E2 and F2

| Spot No. | Homogeneity RSD (%) | | Repeatability RSD (%) | | Reproducibility RSD (%) | |
|---|---|---|---|---|---|---|
| | E2 | F2 | E2 | F2 | E2 | F2 |
| 1 | 1.2850 | 2.0528 | 0.7917 | 1.4969 | 1.3597 | 1.9959 |
| 2 | 1.2216 | 1.9388 | 1.3321 | 1.7839 | 2.8193 | 2.0672 |
| 3 | 1.6975 | 0.9374 | 1.2318 | 2.2311 | 1.5162 | 2.1167 |
| 4 | 0.5775 | 1.5680 | 1.4608 | 1.8213 | 2.3096 | 2.5279 |
| 5 | 0.5779 | 1.3280 | 0.8302 | 0.8343 | 1.9646 | 2.4950 |
| 6 | 0.4712 | na | 1.0982 | na | 1.9247 | na |

na= not available

As a test of homogeneity, the highest and lowest RSD were exhibited by the first spot of F2 and spot number sixth of E2, respectively. The errors associated with the measurements were a combination of human error and the heterogeneity inherent in sample. Nonetheless, both pen samples gave very satisfy results (RSD<2%) and their inks were concluded as homogeneous.

The validation study focused on the precision of the method in terms of repeatability and reproducibility of the retention factor (Rf) of bands. By looking at the RSD values of the nine repetitions of a sample (repeatability column of Table 2), the conclusion was that different HPTLC plates did not have a great impact on the precision of the method (in all cases RSD was less than 3%). On the other hand, by referring to the reproducibility of Table 2, the effect of different plates triggered a slightly higher RSD values if compared to the one obtained for repeatability for both pen samples.

## Conclusion

The discrimination power (DP) of HPTLC technique to analyses blue ballpoint pen inks was determined to be around 89.40%. The inks of two selected models were found homogenous within the ink reservoir. The HPTLC technique proved to be simple, reproducible (RSD<3%) and repeatable (RSD <3%). The results showed that it is worthy to expand the study by including more samples. Subsequently, the qualitative data from HPTLC plates could be converted into quantitative data by using certain image analysis software. So that, higher DP could be achieved while multivariate statistical techniques can also be applied on data interpretation.

## Acknowledgement

We would like to express our deep gratitude and appreciation to all the staffs of the Forensic Science Program from UKM.

## References

1. Tsutsumi, K. & Ohga, K. (1998). Analysis of writing ink dyestuffs by TLC and FTIR and its application to forensic science. *Analytical Science* 14: 269-274.

2. Roux, C., Novotny, M., Evans, I., & Lennard, C. (1999). A study to investigate the evidential value of blue and black ballpoint pen inks in Australia. *Forensic Science International* 101: 167-176.
3. Djozan, D., Baheri, T., Karimian, G. & Shahidi, M. (2008). Forensic Discrimination of Blue Ballpoint Pen Inks Based on Thin Layer Chromatography and Image Analysis. *Forensic Science International* 179(2–3): 199-205.
4. Senior, S., Hamed, E., Masoud, M. & Shehata, E. (2012). Characterization and dating of blue ballpoint pen inks using principal component analysis of UV-Vis absorption spectra, IR spectroscopy and HPTLC. *Journal of Forensic Sciences* 57:1087-1093.
5. Neumann, C. & Margot, P. (2009). New perspectives in the use of ink evidence in forensic science: Part I: Development of a quality assurance process for forensic ink analysis by HPTLC. *Forensic Science International* 185: 29-37.
6. Neumann, C. & Margot, P. (2009). New perspectives in the use of ink evidence in forensic science: Part II: Development and testing of mathematical algorithms for the automatic comparison of ink samples analysed by HPTLC. *Forensic Science International* 185: 38-50.
7. Neumann, C. & Margot, P. (2009). New perspectives in the use of ink evidence in forensic science: Part III: Operational applications and evaluation. *Forensic Science International* 192: 29-42.
8. Neumann, C., Ramotowski, R. & Genessay, T. (2011). Forensic Examination of Ink by High-Performance Thin Layer Chromatography—the United States Secret Service Digital Ink Library. *Journal of Chromatography A* 1218(19): 2793-2811.
9. Kher, A., Mulholland, M., Green, E., Reedy, B. (2006). Forensic classification of ballpoint pen inks using high performance liquid chromatography and infrared spectroscopy with principal components analysis and linear discriminant analysis. *Vibrational spectroscopy* 40:270-277.
10. Causin, V., Casamassima, R., Marega, C., Maida, P., Schiavone, S., Marigo, A., Villari, A. (2008). The discrimination potential of UV spectrophotometry, TLC, and FTIR for the forensic analysis of black and blue ballpoint inks, *Journal of Forensic Science* 53(6):1468-1473.
11. Smalldon, K.W., Moffat, A.C. (1973). The calculation of discrimination power for a series of correlated attributes. *Journal of Forensic Science* 13:291-295.
12. Seifar, R.M., Verheul, .M., Aiese, F., Brinkman, U.A. & Gooijer, C. (2001). Applicability of surface-enhanced resonance Raman scattering for the direct discrimination of ballpoint pen inks. *Analyst* 126:1418-1422.
13. Ng, L-K., Lafontaine, P. (2002). Ballpoint pen inks: Characterization by positive and negative ion-electrospray ionization mass spectrometry for the forensic examination of writing inks. J. Forensic Science 47: 1238-1247.
14. Zieba-Palus, J. & Kunicki, M. (2006). Application of the micro-FTIR spectroscopy, Raman spectroscopy and XRF method examination of inks. *Forensic science international* 158:164-172.

The Malaysian Journal of ANALYTICAL SCIENCES ISSN 1394-2506

# PENGGUNAAN KAEDAH KEMOMETRIK BAGI MENENTUKAN KUALITI MINYAK KELAPA SAWIT, MINYAK JAGUNG DAN MINYAK KELAPA SEGAR DAN TERPAKAI

## (Utilization of Chemometric Technique to Determine the Quality of Fresh and Used Palm, Corn and Coconut Oil)

Hamizah Mat Agil[1], Mohd Zuli Jaafar[2], M. Suzeren Jamil[1], Azwan Mat Lazim[1]*

[1]*School of Chemical Sciences and Food Technology,*
*Faculty of Science and Technology*
*Universiti Kebangsaan Malaysia, 43600 Bangi, Selangor, Malaysia*
[2]*Universiti Teknologi MARA Kampus Kuala Pilah, 72002 Kuala Pilah, Negeri Sembilan, Malaysia*

**Corresponding author: azwanlazim@ukm.edu.my*

**Abstrak**

Kajian ini dijalankan untuk mengkaji kemerosotan kualiti minyak sebelum dan selepas digoreng. Sebanyak 12 sampel minyak daripada sumber yang berlainan iaitu daripada minyak kelapa sawit, minyak jagung dan minyak kelapa telah digunakan. Proses pengorengan diulang sebanyak empat kali pada suhu 180 $^{o}$C bertujuan untuk mengecam sebarang perubahan yang berlaku pada suhu yang tinggi. Sebanyak tiga parameter utama dikaji bagi menentukan kualiti minyak iaitu nilai peroksida, nilai iodin dan nilai asid. Kaedah kemometrik yang berdasarkan pencaman corak digunakan sebagai kaedah alternatif untuk penentuan kualiti minyak dalam kajian ini berdasarkan serapan FTIR pada rantau 4000-700 cm$^{-1}$. Analisis data dijalankan dengan menggunakan kaedah PCA dan PLS dalam permodelan Matlab. PCA memberikan pengkelasan data mengikut jenis minyak manakala PLS memberikan penentuan kualiti terhadap tiga parameter yang dikaji. Bagi pengkelasan minyak segar PC1 mempunyai nilai peratus varian 70 % manakala PC2 mempunyai nilai peratus varian 15 %. Bagi minyak goreng pula, PC1 mempunyai nilai peratus varian 57 % dan PC2 mempunyai nilai peratus varian 25 %. Menerusi PLS, model nilai iodin bagi pembolehubah terpilih berdasarkan korelasi, $R^2$CV pada > 0.984 merupakan model yang terbaik untuk minyak segar. Manakala model bagi nilai peroksida bagi pemboleubah terpilih berdasarkan korelasi, $R^2$CV pada > 0.7423 untuk minyak goreng adalah model terbaik.

**Kata kunci:** minyak masak, kemometik, nilai peroksida, nilai iodin dan nilai asid

**Abstract**

This study was conducted to evaluate the quality of natural oil and the deterioration of frying oil. A total of 12 different oil samples from palm oil, corn oil and coconut oil were used. The frying process was repeated four times at 180 $^{o}$C in order to observe the stability of the oil towards oxidation. Three main parameters have been studied to determine oil qualities which were peroxide value, iodine value and acid value. This study emphasized on the usage of FTIR in the range of 4000-700 cm$^{-1}$. Alternatively, the chemometrics method based on pattern recognition has been used to determination the oil quality. Data analysis were conducted by using PCA and PLS method in the Matlab modeling. The PCA provided data classification according to types of oil while PLS predicted the oil quality of the parameters studied. For the classification of pure oil, the variance for PC1 was 70% while PC2 was 15 %. For the fried/used oil, PC1 gave 57 % while PC2 gave 25 %. By using PLS, the iodine the best model for pure oils value model variable based on correlation with $R^2$CV > 0.984. Whereas, the peroxide value model for fried/used oils, was the best obtained $R^2$CV > 0.7423.

**Keywords**: cooking oil, chemometric, peroxide value, iodine value and acid value

## Pengenalan

Kualiti lemak dan minyak ditentukan oleh beberapa parameter fizikal dan kimia, yang mana ia bergantung kepada sumber minyak serta keadaan pemprosesan dan penyimpanan. Kemerosotan kualiti minyak ini berpunca daripada

proses hidrolisis dan pengoksidaan yang berlaku ke atas minyak disebabkan oleh suhu yang tinggi serta penyerapan oksigen dan air [1]. Pendedahan yang maksimum kepada haba, cahaya dan udara akan menyebabkan minyak menjadi tengik. Apabila minyak menjadi tengik, pembentukkan radikal bebas yang terjadi akan mempercepatkan kerosakkan minyak [2].

Terdapat tiga ujian utama yang selalu digunakan bagi menentukan kualiti minyak iaitu nilai peroksida, nilai iodin dan nilai asid. Penentuan terhadap nilai peroksida merupakan satu kaedah umum yang digunakan untuk mengukur pengoksidaan lipid dan pembentukan peroksida pada peringkat awal pengoksidaan [3]. Penentuan nilai iodin adalah bertujuan untuk menentukan jumlah asid lemak tak tepu dalam minyak. Ia juga boleh ditakrifkan sebagai bilangan iodin yang bertindak balas dengan 100 g lemak di bawah ujian kawalan [4]. Nilai asid pula bertujuan untuk mengetahui kandungan asid lemak bebas (FFA). Selain daripada itu, fosfat dan asid amino juga menyumbang kepada nilai asid. Nilai FFA yang tinggi di dalam sampel bermakna nilai keasidan adalah tinggi dan ini menunjukkan kualiti minyak adalah rendah [5].

Nilai parameter yang diperolehi daripada kaedah pentitratan bagi kesemua jenis minyak dibandingkan dengan menggunakan teknik yang baharu iaitu kemometrik. Sebelum perbandingan dibuat, sampel yang telah diuji melalui teknik pentitratan perlu dianalisis dengan menggunakan teknik inframerah transformasi fourier (FTIR). Analisis ini bertujuan untuk mengetahui peratus komposisi unsur yang hadir dalam minyak berdasarkan nombor gelombang dan peratus serapan [6]. FTIR dalam bidang analisis kimia telah mendapat perhatian untuk kegunaan dalam analisis kuantitatif lemak dan minyak. FTIR berpontensi untuk mengesan sebarang pencemaran atau percampuran dalam kandungan minyak [7].

Istilah kemometrik diperkenalkan oleh Svante World pada tahun 1974 [8]. World menyatakan istilah kemometrik diambil sempena dengan penggunaan teknik statistik dan matematik untuk latihan data kimia. Kemometrik juga turut digunakan dalam pelbagai bidang sebagai salah satu kaedah perbandingan, pelaksanaan statistik dan matematik. Bagi penggunaan kaedah ini dalam bidang ekonomi disebut sebagai ekonometrik [9]. Kemometrik menggunakan pendekatan statistik untuk mentafsir corak dalam data multivarian. Kemometrik bukan sahaja dapat memberikan hasil kajian dengan cepat, malah dapat menghasilkan penentuan yang tepat bagi komposisi sampel dari segi sifat-sifat kimia dan fizikal. Teknik kemometrik berpontensi digunakan sebagai kaedah alternatif untuk menggantikan teknik konvensional yang mengambil masa yang lama. Selain itu, teknik ini boleh mengurangkan penggunaan bahan kimia toksik yang berbahaya kepada manusia serta persekitaran [10].

Dalam kajian ini, kaedah konvensional digunakan untuk mendapat data parameter kualiti minyak. Data-data parameter kualiti minyak akan digunakan untuk membuat perbandingan antara kaedah konvensional dengan kaedah kemometrik. Jika perbandingan data antara dua kaedah adalah hampir sama, ini membuktikan bahawa kaedah kemometrik adalah sesuai dan boleh dijadikan alternatif bagi menggantikan kaedah konvensional (eksperimen makmal) dalam penentuan kualiti minyak

## Bahan dan Metodologi

Bagi menentukan kualiti minyak masak bahan-bahan kimia berikut telah digunakan seperti penunjuk kanji, natrium tiosulfat, natrium hidroksida, kalium iodida, larutan wijs (iodin monoklorida) dan larutan dietileter: alkohol, larutan asid asetik – kloroform. Sampel-sampel minyak kelapa sawit, minyak jagung dan minyak kelapa pula telah dibeli dari pasaran.

Bagi menentukan kualiti minyak masak, kaedah piawaian MPOB telah digunakan. Secara umum terdapat tiga penenentuan kualiti minyak yang akan diukur, iaitu nilai iodin, nilai peroksida dan nilai asid.

**Nilai Peroksida**

Sebanyak 5.00 g sampel akan ditimbang ke dalam kelalang kon 250 mL. Seterusnya, sebanyak 30 mL larutan asetil glacial dan 20 mL kloroform dengan nisbah 3:2 ditambah. Larutan kemudiannya digoncang. Diikuti sebanyak 0.5 mL iodida tepu ditambah dan digoncang selama satu minit dan kemudiannya,diikuti dengan penambahan 30 mL air suling yang telah dididih dan disejukkan. Larutan kemudiannya dititrat dengan larutan piawai 0.1 natrium tiosulfat

sambil kelalang kon digoncang. Apabila warna kuning hampir hilang, beberapa titik larutan penunjuk kanji (1 %) ditambah, dimana larutan kemudiannya bertukar menjadi biru. Larutan diteruskan titrat sehingga larutan biru hilang.

**Nilai Iodin (IV)**

Sampel sebanyak 0.15 gram ditimbang tepat kepada 0.0001 dan dimasukkan ke dalam 250 mL kelalang kon berpenutup. Seterusnya, 15 mL karbon tetraklorida ($CCI_4$) ditambahkan untuk melarutkan minyak. Diikuti sebanyak 25 mL larutan Wijs ditambah dengan cepat ke dalam campuran tersebut. Kemudian kelalang kon ditutup lalu digoncangkan dan disimpan pada tempat yang gelap selama satu jam. Setelah satu jam kelalang kon itu akan dikeluarkan. 20 mL larutan kalium iodida akueus 10 % dan 150 mL air suling ditambah ke dalam campuran. Kelalang digoncang untuk mencampur larutkan campuran didalam kon dengan baik. Kemudian campuran dititrat dengan larutan tiosulfat ($Na_2S_2O_3$) 0.1 N sehingga warna kunig hilang. Setelah itu, campuran ditambah dengan 1 hingga 2 mL larutan kanji 1% sebagai penunjuk warna dan warna biru akan terbentuk. Pentitratan akan diteruskan sehingga warna biru hilang setelah di goncang dengan kuat. Kemudian, isipadu titratan iaitu isipadu larutan natrium tiosulfat yang telah digunakan dicatat. Langkah yang sama diulang sebanyak 3 kali bagi setiap sampel di bawah keadaan yang sama. Nilai purata akan di hitung untuk mendapatkan nilai yang lebih jitu.

**Nilai Asid (AV)**

Dalam langkah penentuan nilai asid ini, sebanyak 10 gram sampel menghampiri 0.02 gram ditimbang ke dalam kelalang kon 250 mL. Seterusnya 50 mL pelarut yang telah dineutralkan di masukkan ke dalam kelalang kon dan kemudiannya di letakkkan ke atas plat pemanas dan suhu ditetapkan pada 40$^oC$. Kelalang di goncang dengan perlahan semasa proses pentitratan dengan larutan alkali piawai natrium hidroksida (NaOH). Takat akhir pentitratan ditentukan apabila warna merah jambu muncul dan kekal sekurang-kurangnya 30 saat.

**Analisis FTIR**

Sampel minyak telah dianalisa menggunakan instrumen spektrometer FTIR. Semua spektrum inframerah (4000-400 $cm^{-1}$) telah diambil dengan Perkin Elmer Spektrum 100 spektrometer FTIR (Perkin Elmer Inc. Wellesley, MA). Instrumen ini telah dilengkapi dengan aksesori *Horizontal Attenuated Total Reflectance* (HATR) (Kristal ZnSe) dan pengesan *Deuterated Tri-glycerine Sulphate* (DTGS). Aksesori HATR digunakan untuk mengumpul data spektrum minyak. Resolusi ditetapkan pada 2 $cm^{-1}$ dan bilangan imbasan yang dikumpul untuk setiap spektrum adalah sebanyak 128.

**Analisis Kemometrik**

Dalam kajian ini kaedah PCA dan PLS digunakan dalam model Matlab 7.6.0 (2008)a. Kelebihan Matlab ialah sistemnya yang berorientasikan matrik yang mana mudah digunakan dalam analisis data multivarian. Penggunaan Microsoft Excel juga diperlukan pada awalnya untuk memindahkan data-data yang diperolehi daripada FTIR ke dalam sistem kemometrik. Penggunaan Matlab kebiasaannya melibatkan penggunaan Microsoft Excel dan Matlab secara serentak [11].

**Prapemprosesan Data**

Semua kaedah kemometrik memerlukan pemprosesan data terlebih dahulu. Ini adalah untuk menyediakan maklumat yang diperlukan sebelum algoritma matematik di aplikasikan [11]. Prapemprosesan data merupakan langkah yang perlu diutamakan. Langkah prapemprosesan ini akan menentukan keputusan akhir pembinaan model. Keputusan yang berbeza akan diperolehi apabila menggunakan kaedah prapemprosesan yang berlainan. Urutan langkah prapemprosesan bermula dengan perubahan individual seterusnya penskalaan baris dan terakhir ialah penskalaan lajur [9]. Penskalaan lajur terdiri daripada dua bahagian iaitu nilai purata tertumpu *(mean centering)* dan pempiawaian (*standardization).*

**Analisis Komponen Utama**

PCA adalah salah satu keadah multivarian yang membolehkan untuk meneroka corak dalam data. Multivarian bermaksud lebih daripada satu pengukuran boleh dibuat ke atas sampel tunggal [11]. Contohnya spektoskopi boleh merekod beratus-ratus nilai nombor gelombang dalam sampel tunggal. Rekabentuk matrik merupakan konsep utama bagi kemometrik bertujuan untuk menenerangkan data eksperimen dengan membentuk hubungan matematik

diantara pembolehubah [11]. Dalam kajian ini, sebanyak 12 sampel digunakan dalam baris dan sebanyak 3301 pembolehubah digunakan dalam lajur. Algoritma *Nonlinear Iterative Partial Least Squares*, NIPALS digunakan dalam kajian ini. Matrik data asal akan berkurang kepada matrik data baru sebagai komponen utama (principal component, PC). Skor dan muatan (*loading*) akan dikeluarkan dari data matrik asal. Plot skor PCA akan menerangkan corak data bagi sampel. Manakala, plot *loading* PCA untuk menunjukkan corak bagi pelbagai pembolehubah yang dikaji [9]

## Keputusan dan Perbincangan

### Analisis FTIR

Dalam kajian ini sebanyak 12 jenis sampel yang berlainan dianalisis dengan menggunakan FTIR bagi tujuan kuantitatif. Kajian ini ditumpukan kepada kawasan serapan antara 4000-700 $cm^{-1}$. Dengan menggunakan FTIR, ianya dapat menunjukkan kumpulan berfungsi pada nombor gelombang yang tertentu.

Penggunaan infra merah tengah (MIR) semakin meningkat dalam industri makanan dan lain-lain komoditi kebelakangan ini [12]. Kepentingannya terletak pada keupayaan untuk mencirikan kumpulan berfungsi yang berbeza-beza dengan cepat dan dapat dilakukan secara serentak [13]. Pada kawasan spektrum yang diukur, terdapat serapan kumpulan berfungsi daripada kawasan cap jari yang mencirikan sesuatu sebatian [14]. Data yang diperolehi kemudiannya akan digunakan untuk di aplikasikan dalam teknik kemometrik.

### Analisis FTIR Minyak Segar dan Minyak Goreng

Rajah 1 menunjukkan pertindihan spektrum bagi jenama minyak yang sama antara minyak segar dan minyak goreng. Spektrum berwarna biru adalah bagi minyak goreng dan spektrum berwarna merah adalah bagi minyak segar. Rajah 1 (i dan ii) menunjukkan kelas minyak jagung, (iii dan iv) kelas minyak kelapa dan (v dan vi) kelas minyak kelapa sawit.

Spektum pertindihan minyak jagung bagi jenama Mazola dan Daisy memperlihatkan perbezaan pada semua nombor gelombang. Komposisi minyak jagung yang terdiri daripada 52 % asid linoleik, yang merupakan asid lemak poli tak tepu [15] menyebabkan minyak ini lebih mudah mengalami tindak balas pengoksidaan, hidrolisis dan pempolimeran [16].

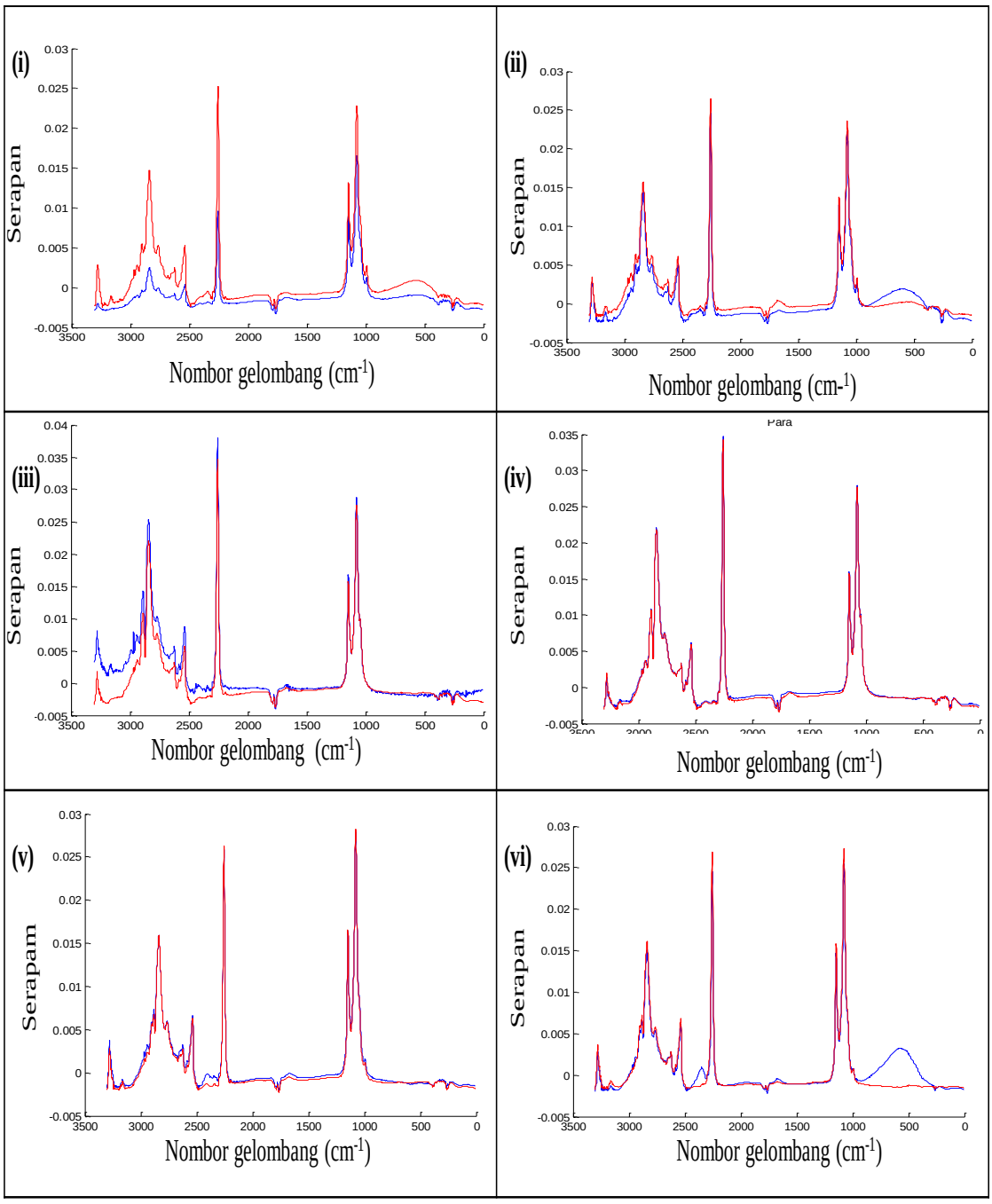
Bagi minyak kelapa, jenama buatan rumah menunjukkan pertindihan spektrum sedikit berlainan berbanding minyak jenama Para. Cara penghasilan minyak ini boleh mengakibatkan sifat-sifat antara kedua jenama minyak adalah sedikit berlainan. Salah satu faktor yang memberi kesan kepada kualiti minyak ialah cara pengendalian, pengilangan, penyimpanan dan penghantaran [17]. Minyak jenama Para menunujukkan pertindihan yang hampir sama. Ini disebabkan minyak kelapa mempunyai komposisi asid lemak tepu yang tinggi iaitu sebanyak 48.2 % asid laurik dan 20.2 % asid miristik [15].

Minyak kelapa sawit memperlihatkan pertindihan spektum yang hampir sama. Ini kerana minyak kepala sawit mengandungi kandungan asid lemak tak tepu dan asid lemak tepu yang seimbang iaitu sebanyak 50 % asid lemak tak tepu, 40 % asid lemak mono tak tepu dan 10 % asid lemak poli tak tepu [18]. Oleh itu, tindakbalas seperti pengoksidaan adalah lebih rendah berbanding minyak lain.

### Kaedah Kemometrik

Dalam penyelidikan ini, analisis data regresi linear yang dijalankan adalah dengan menggunakan kaedah PCA dan PLS dalam permodelan Matlab. Matlab merupakan satu singkatan (Matrix Laboratory) bagi satu perisian yang digunakan untuk menganalisis data dalam jumlah yang besar. Model yang dibina adalah berasaskan skrip dan pengaturcaraan yang direka untuk menganalisis data [11].

Rekabentuk matrik merupakan konsep utama dalam kemometrik. Rekabentuk ini membolehkan ujian dapat dilaksanakan dalam beberapa parameter yang berbeza seperti penentuan nilai peroksida, nilai asid dan nilai iodin.




Rajah 1. Pertindihan spektum FTIR mengikut kelas antara minyak segar dengan minyak goreng. Rajah (i) menunjukkan kelas minyak Daisy, (ii) minyak Mazola, (iii) minyak buatan rumah, (iv) minyak Para, (v) minyak Saji dan (vi) minyak Buruh.

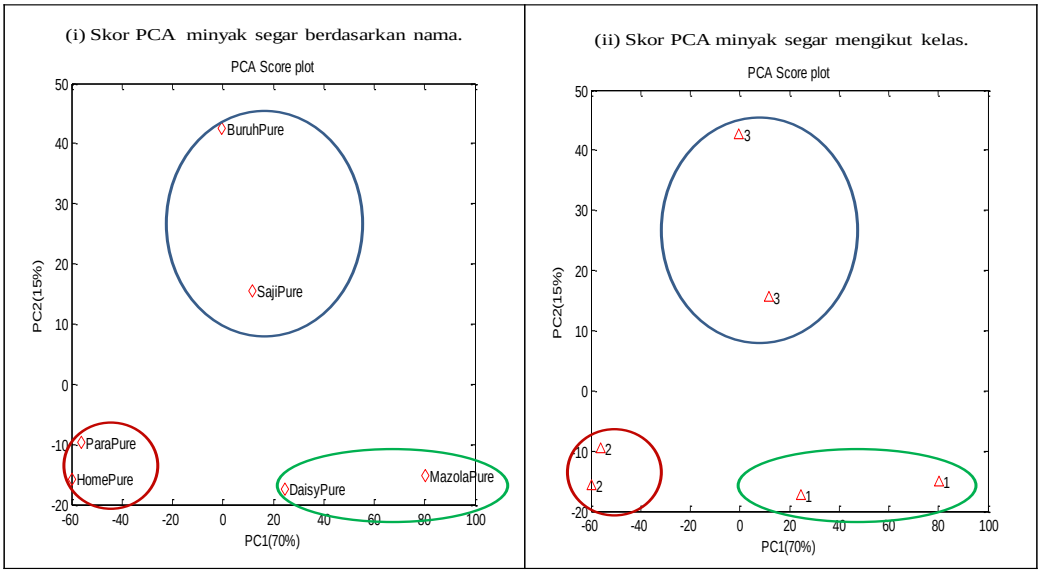
**Analisis Komponen Utama**

PCA merupakan kaedah dalam kemometrik yang membenarkan bilangan pembolehubah untuk dikurangkan tetapi masih mengekalkan kebanyakan maklumat yang menerangkan keseluruhan data [12]. Peratusan varian setiap komponen dalam PCA dikira untuk menentukan pembolehubah yang paling banyak menerangkan keseluruhan data. PCA mengurangkan data set kepada paksi baru yang dikenali sebagai (PC1) dan seterusnya. Skor (*score*) iaitu sampel dan muatan (*loading)* iaitu pembolehubah diplotkan di atas paksi PC1 dan PC2 yang mempunyai peratusan varian yang paling tinggi. Komponen utama (PC1) merangkumi jumlah pemboleh ubah maksimum dalam data dan diikuti PC seterusnya [11].

Kebiasaannya juga, graf PC1 melawan PC2 di plot untuk membezakan dan mengkelaskan sampel yang berlainan jenis. Paparan grafik bagi skor akan menentukan pengkelasan minyak. Pengkelompokan dalam set data bagi sampel yang serupa cenderung untuk berdekatan di antara satu sama lain [11]. PCA digunakan untuk mengenalpasti pola dalam data dengan cara memberi penekanan terhadap persamaan dan perbezaan sifat-sifat serta komposisi sampel. Selain itu, ianya turut digunakan untuk menunjukkan hubungan di antara pembolehubah dalam set data atau menunjukkan hubungan yang mungkin ada di antara sampel [11].

PCA dapat ditentukan berdasarkan plot skor dan muatan (*loading*). Plot skor PCA adalah untuk menunjukkan corak atau taburan bagi jenis-jenis sampel. Manakala plot muatan (*loading*) PCA untuk menunjukkan taburan corak dalam data berdasarkan kesemua pembolehubah [11].

Rajah 2 menunjukkan plot skor bagi sampel minyak segar untuk PC1 melawan PC2. Sebanyak 85 % jumlah PCA berjaya menerangkan keseluruhan maklumat sampel yang dikaji. PC1 mempunyai nilai peratus varian 70 % yang menerangkan sampel sebanyak 70 % data manakala PC2 mempunyai nilai peratus varian sebanyak 15 % yang dapat menerangkan 15 % data. Di dalam analisis komponen skor, komponen utama yang tinggi nilai peratus variannya diambil untuk membayangkan data di dalam PCA [19].

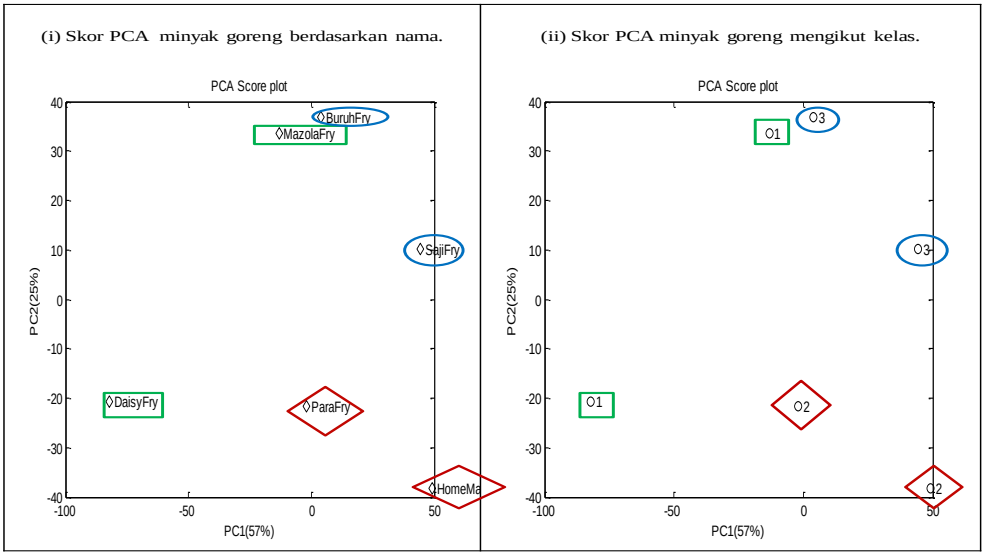



Rajah 2. Skor PCA bagi minyak segar berdasarkan (i) jenama dan (ii) kelas

Secara keseluruhannya, keputusan taburan plot skor bagi setiap sampel boleh membentuk perkumpulan mengikut jenis minyak dari kelas (jenis) yang sama. Sebagai contoh, minyak Mazola dan minyak Daisy cenderung untuk berada berdekatan kerana kedua-dua minyak ini adalah berasal dari jenis kumpulan yang sama iaitu minyak jagung (kelas nombor satu). Minyak jenama Para dan minyak kelapa buatan rumah daripada jenis minyak kelapa juga cenderung membentuk titik yang berdekatan dan membentuk kelas nombor dua. Manakala minyak jenama Buruh dan Saji daripada jenis minyak kelapa sawit membentuk kelas nombor tiga. Titik yang berdekatan menunjukkan minyak itu adalah dari kelas yang sama. Bagi minyak segar sebelum diberi rawatan lain seperti pendedahan kepada suhu yang tinggi atau cahaya, kebanyakkannya mempunyai komposisi asid lemak yang sama dan memberikan nilai parameter seperti nilai iodin, nilai peroksida dan nilai asid yang hampir sama [20].

Rajah 3 menunjukkan plot skor bagi sampel minyak goreng untuk PC1 melawan PC2. PC1 mempunyai nilai peratus varian 57 % yang menerangkan sampel sebanyak 57 % data. Manakala PC2 mempunyai nilai peratus varian 25 % yang menerangkan sebanyak 25 % data. Keseluruhannya, model PCA dengan hanya dua komponen penting (PC1 dan PC2) dapat menerangkan 82 % keseluruhan data. Dari segi taburan skor untuk minyak goreng pula, pembentukkan titik bagi minyak goreng ini menunjukkan dalam pengkelompokan yang berjauhan. Titik-titik ini berjauhan kerana berlakunya tindak balas kimia bagi minyak goreng apabila dipanaskan pada suhu yang tinggi secara berulang kali. Apabila minyak dikenakan pada suhu yang tinggi, ianya boleh menyebabkan berlakunya pengoksidaan, hidrolisis dan pempolimeran [20]. Ini mengakibatkan perubahan terhadap sifat kimia dan fizikal minyak.

Sebagai contohnya, titik bagi minyak Daisy dan Mazola berada berjauhan setelah digoreng (jika dibandingkan dengan plot bagi minyak Daisy dan Mazola sebelum digoreng seperti dalam Rajah 3). Perkumpulan di antara minyak ini dapat memberi gambaran kepada penentuan nilai-nilai parameter sebelum dan selepas minyak digoreng di mana nilai-nilai tersebut akan berubah dan berbeza dari nilai asalnya.




Rajah 3 Skor PCA bagi minyak goreng berdasarkan (i) jenama dan (ii) kelas

**Separa Kuasa Dua Terkecil (PLS)**

Kaedah PLS telah digunakan untuk membina model bagi penentu ukuran. Perkaitan spektum menunjukkan hubungkait di antara serapan pada nombor gelombang tertentu dengan ciri-ciri yang dikehendaki [21]. Perkaitan spektrum ini dikaji untuk mengenal pasti ciri-ciri spektrum yang berhubung kait dengan data-data parameter yang dikaji iaitu nilai asid, nilai peroksida dan nilai iodin.

Model PLS dibina menggunakan keseluruhan pembolehubah tanpa menggunakan kaedah pemisahan sampel telah dibina. Model yang dibina tersebut boleh digunakan untuk meramal nilai tiga parameter minyak masak. Kualiti model ditentusahkan oleh nilai $R^2$CV (Pekali Korelasi Kuasa Dua Ramalan). Nilai ini diperolehi dari model dan boleh diplot bagi menunjukkan hubungan diantasa nilai ramalan terhadap nilai sebenar. Bagi mendapatkan model yang terbaik, dua model dibina bagi setiap parameter iaitu model yang menggunakan keseluruhan pembolehubah dan model yang hanya menggunakan pembolehubah berkaitan dengan parameter yang diinginkan iaitu nilai peroksida, nilai iodin dan nilai asid melalui kaedah pemilihan pembolehubah. Kaedah pemilihan pembolehubah kepada pembolehubah yang hanya berkaitan dengan parameter yang diinginkan di dalam analisis minyak melalui kaedah spektoskopi FTIR terbukti dapat meningkatkan kualiti model melalui peningkatan nilai $R^2$CV [11]. Jadual 1 dan 2 menunjukkan ringkasan bagi pekali korelasi ($R^2$CV) dan komponen PLS yang berkaitan untuk pembinaan model bagi setiap parameter. Nilai pada barisan yang dihitamkan menunjukkan pembinaan model yang terbaik sebagai penentuan parameter kualiti minyak yang dikaji.

Jadual 1. Keputusan regresi PLS bagi minyak segar untuk setiap parameter, nilai iodin, nilai peroksida dan nilai asid

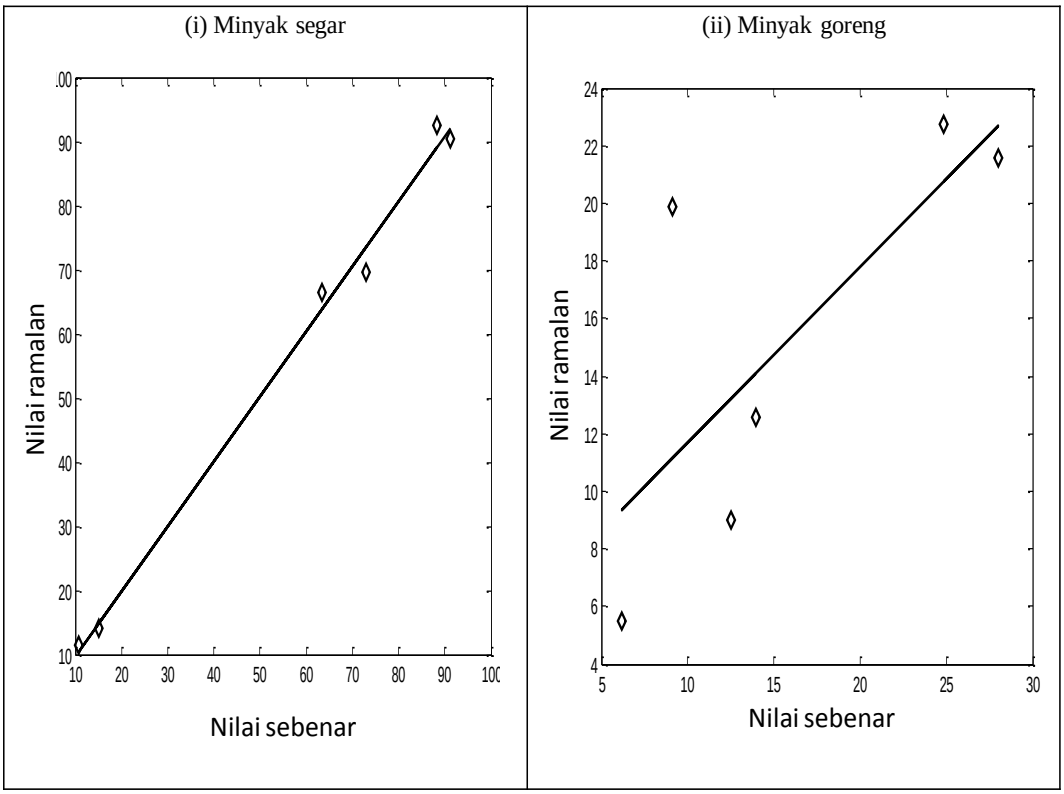
| **Parameter** | **Model (PLS)** | **Hubung kait** | **$R^2$CV** | **Komponen PLS** |
|---|---|---|---|---|
| IV | Pembolehubah terpilih | > 0.9000 | 0.9972 | 1 |
| | Pembolehubah semua | - | 0.9959 | 9 |
| PV | Pembolehubah Terpilih | > 0.7000 | 0.8014 | 1 |
| | Pembolehubah semua | - | 0.0450 | 5 |
| AV | Pembolehubah Terpilih | > 0.6000 | 0.9722 | 9 |
| | Pembolehubah semua | - | 0.0352 | 2 |

Jadual 2. Keputusan regresi PLS bagi minyak goreng untuk setiap parameter, nilai iodin, nilai peroksida dan nilai asid

| **Parameter** | **Model (PLS)** | **Hubung kait** | **$R^2$CV** | **Komponen PLS** |
|---|---|---|---|---|
| IV | Pembolehubah terpilih | > 0.7000 | 0.8239 | 18 |
| | Pembolehubah semua | - | 0.7400 | 1 |
| PV | Pembolehubah Terpilih | > 0.7000 | 0.7423 | 1 |
| | Pembolehubah semua | - | -0.6416 | 15 |
| AV | Pembolehubah Terpilih | > 0.5000 | 0.1509 | 3 |
| | Pembolehubah semua | - | -0.2014 | 14 |

Ujian pengesahan perlu dilakukan bagi memastikan pemilihan sesuatu arkitektur adalah baik. Plot aktiviti sebenar melawan aktiviti ramalan menunjukkan model yang dibangunkan dengan kaedah langkah demi langkah mempunyai taburan secara rawak di sepanjang garisan ideal. Ciri ini menunjukkan tiada sebarang masalah kepada model yang dihasilkan. Menurut Miller (2000), jika kecerunan garis regresi yang diperolehi ialah >1 atau <1, menunjukkan terdapat ralat sistematik dalam salah satu plot kalibrasi yang dibuat. Namun begitu, dengan kecerunan menghampiri satu, ini memberikan keyakinan bahawa keputusan yang diperolehi adalah betul [22].

Kualiti model terbaik bagi meramal nilai iodin mengunakan pembolehubah terpilih berdasarkan korelasi ditunjukkan seperti pada Rajah 4. Pada rajah ini plot aktiviti sebenar melawan aktiviti ramalan nilai iodin bagi minyak segar memberikan nilai $R^2CV$ sebanyak 0.9972, adalah model yang paling baik. Manakala bagi minyak goreng, nilai peroksida bagi pembolehubah terpilih berdasarkan korelasi, $R^2CV$ terhadap parameter nilai peroksida di > 0.7423 adalah yang paling baik. Plot aktiviti sebenar melawan aktiviti ramalan menunjukkan tiada sebatian yang berbeza dengan ketara atau tersasar jauh dari garisan ideal dan boleh meramal nilai parameter minyak.




Rajah 4. Plot aktiviti sebenar melawan aktiviti ramalan. (i) Minyak segar dan (ii) Minyak goreng

## Kesimpulan

Secara keseluruhannya, kajian terhadap penentuan kualiti minyak menggunakan teknik kemometrik berdasarkan pencaman corak berjaya dilakukan. Dalam kajian ini, kaedah PCA mengurangkan bilangan pembolehubah untuk membuat model yang menerangkan maklumat keseluruhan data, di mana model yang mempunyai peratus varian yang tinggi dibina. PCA juga menggambarkan persamaan dan perbezaan di antara jenis minyak dan minyak sebelum dan selepas digoreng melalui taburan skor yang diplotkan. Manakala kaedah PLS dapat menentukan kualiti

minyak bagi ketiga-tiga parameter yang dikaji iaitu nilai iodin, nilai peroksida dan nilai asid. Melalui ujian pengesahan, nilai iodin bagi minyak segar dipilih sebagi model yang terbaik untuk memberi nilai ramalan. Manakala bagi minyak goreng nilai peroksida dipilih sebagai pembinaan model yang terbaik. Kajian seterusnya mungkin boleh mengaplikasikan kaedah kemometrik yang lain seperti untuk pengkelasan di antara minyak segar dan minyak goreng. Kaedah seperi SVM (*Support Vector Machine*) dan LDA (*Linear Discrimination Analysis*) boleh digunakan untuk mengkelaskan minyak kepada kelas masing-masing.

**Penghargaan**

Penulis ingin mengucapkan terima kasih kepada Kementerian Pendidikan Malaysian (Pengajian Tinggi) untuk geran penyelidikan INDUSTRI-2013-022 dan INDUSTRI-2013-052 Universiti Kebangsan Malaysia untuk geran.

**Rujukan**

1. Aderolu, A.Z. & Akinremi, O.A. 2009. Dietary effacts of coconut and peanut oil in improving biochemical characteristic of *Clarias gariepinus* Juvenile. *Turkish Journal of Fisheries and Aquatic Sciences*. 9: 105-110.
2. Arrifin, D. & Fairus, H. 2002. *Introduction to Malaysian Palm Oil Industry*. Palm Oil Familiarization Programme 2002. Kuala Lumpur. POFP 2002: 1-15.
3. Azwani S. 2004. Penggunaan perceptron pelbagai lapisan untuk penentuan kualiti minyak sawit berdasarkan pencaman corak. Thesis Ijazah Sarjana Sains. Bangi: Universiti Kebangsaan Malaysia.
4. Brereton R.G. 2003. *Applied Chemometrics for Scientists*. John Wiley & Sons, Ltd. hlmn 183-315.
5. Brereton R. G. 2009. *Chemometrics for Pattern Recognition*. John Wiley & Sons, Ltd.
6. Bothell. 1996. Chemometrics applications overview. Infometric, Inc. http://www.infometrix.com/apps/14-0296_chromatogao.pdf [8 Mei 2012]
7. Brown S. 2011. http://www.infometrix.com/chemometrics/chemometrics.html [12 November 2011].
8. Che Man, Y.B., Setiowatty, G. & Van De Voort, F.R. 1999. Determination of iodine value of palm oil by fourier transform infrared spectroscopy. Journal *Am. Oil. Chem. Soc. Press* 76(6): 693-699.
9. Che Man, Y.B. 2004. Syarahan Inaugural. *Oils and fats analysis-Recent advances and future prospects*. ISBN 967-960-171-4. Universiti Putra Malaysia.
10. Choo, Y.M. & Yap, S.C. 1992. The role of free radicals in the properties of palm oil; chemical basic atherosclerosis. *PORIM Annual Research Report Project CT 187087*.51.
11. Choo, Y.M. 1994. Palm oil carotenoids. *Food & Nutrition Bulletin* 15: 1-14.
12. Choo, Y.M. 1999. Speciality products: carotenoids. *Advance in Oil Palm Research.* hlm. 34-52. Kuala Lumpur: PORIM.
13. Choe, E. & Min, D.B. 2007. Chemistry of deep-fat frying oils. *Journal of Food Science*. 72(5): 78-85.
14. Elias, C. & Yvonne, T. 2005. Coconut oil Bailey's industrial oil and fat products. *John Wiley & Sons. Inc*. Vol 6
15. Fulop, A., Krar, M. & Hancsok, J. 2008. Application of NIR spectroscopy by determination of quality properties of vegetable oils and their derivatives. *Hungarian Journal of Industrial Chemistry Veszprem* 36: 1-2
16. Gee, P.T. 1995. Iodine value determination by FTIR spectroscopy. *Mal. Oil Sci. Tech*. 4: 182-185.
17. Gunstone, F. D. 2004. *The Chemistry of Oils and Fats*. Source, composition, properties and uses.
18. Ghidurus, M., Turtoi, M., Boskou, G., Niculita, P. & Stan, V. 2010. Nutritional and health aspects related to frying (1). *Romanian Biotechnological Letters* 15, No 6
19. Hong, Y., Joseph, I. & Manish, M.P. 2004. Discrimination analysis of edible oils and fats by FTIR, FT-NIR and FT-Raman spectroscopy. Food Chemistry 93: 25-32.
20. Jing, D., Deguang, W., Linfang, H., Shilin, C. & Minjian, Q. 2011. Application of chemometrics in quality evolution of medicinal plants. *Journal of Medicine Plants Research*. 5(17): 4001-4008.
21. Jumat, S., Said, M., Ramli, S. & Azwani, S. 2006. *Oils and Fats Analysis*. Ed 1. Bangi: Universiti Kebangsaan Malaysia.
22. Kamaliah, M. & Norsaadah, A.R. 1997. Kaedah spektroskopi dalam pengenalpastian sebatian organik. Kuala Lumpur: Penerbit Universiti Malaya.
23. Karoui, K., Downey, G. & Blecker, C. 2010. Mid-infrared spectroscopy coupled with chemometrics: A tool for the analysis of intact food system and the exploration of their molecule structure. *Chem Rev*. 110(10): 6144-6168.
24. Kuntom, A. 1990. Oxidation and palm oil. *PORIM Bulletin* 20: 32-40

25. Lawson, H. 1995. Deep fat frying. Chapter 2: *Food Oil and Fats*: *Technology, Utilization and Nutrition.* New York: Champan & Hall. Page 6-14
26. March, J.G., Simonet, B.M. & Grases, F. 1999. Determination of phytic acid by catalytic fluorimetric. *Analyst* 124: 897-900
27. McMurry, J. 2004. Organic Chemistry. Singapore: Thomson Learning Inc
28. Miller, J.N. & Miller, J.C. 2000. Statistic and chemometrics for analytical chemistry. Ed. Ke-4. England. Pearson Education Limited.
29. Moh, M.H. & Tang, T.S. 1999. A review on the quantitative analysis of fats and oils using FTIR. *PORIM Bulletin*. 41: 30-37
30. Muzik, B., Lendi, B., Molina-Diaz, A. & Ayora-Canada, M.J. 2005. Direct monitoring of lipid oxidation in edible oils by Fourier transform Roman spectroscopy chemistry physics of lipid. 134: 173-182.
31. Rethinam, P. 2003. *Health and Nutritional Aspects of Coconut Oil*. Asian and Pacific Coconut Comunity. Jakarta: 1-7.
32. Rohaya, M. & Ma, A.N. 2001. Effect of temperature on the quality of fresh crude palm oil at different stages of processing. *Palm Oil Bulletin* 43: 31-37.
33. Rohman, A., Ismail, A., Che Man, Y.B. & Hashim, A. 2011. Monitoring the oxidative stability of virgin coconut oils during oven test using chemical indexes and FTIR spectroscopy. *International Food Research Journal.* 18: 303-310.
34. Rohman, A. & Che Man, Y.B. 2011. Quantification and classification of corn and sunflower oils as adulterations in olive oil using chemometrics and FTIR spectra. *Scientific World Journal*. Article ID 250795.
35. Sarfaraz, A. M. 2010. Analytical characterization & quality evaluation of poultry feed commercially available in Sindh with emphasis on poultry feed oil. Thesis Ph.D. Pakistan: University of Sindh, Jamshoro
36. Serjouie, A., Tan, C. P., Mirhosseini, H. & Che Man Y.B. 2010. Effect of vegetable based-oil blends on physicochemical properties of oils during deep-fat frying. *American Journal of Food Technology*. 5: 310-323
37. Sivakesava, S. & Irudayaraj, J. 2001. Detection of Inverted beet sugar adulteration of honey by FTIR spectroscopy. *Journal of the Science of Food and Agriculture*. 81: 683-690.
38. Stavros L. 2009. Advance in Deep-Fat Frying of Foods. Chapter 4: Quality of frying oil. Taylor & Francis Group. Page 59-74.
39. Sunisa, W., Warapong, U., Sunisa, S., Saowaluck, J. & Saowakan W. 2011. Quality changes of chicken frying oil as affected of frying conditions. *International Research Journal* 18: 615-620.
40. Tang, T.S. 1991. Palm kernel and palm kernel oil quality today. *PORIM Bulletin*. Vol 23: 15-31.
41. The Healthy Benefits of Coconut Oil. *Bioriginal Food & Science Corp*. www.bioriginal.com/services/files/healthbenefitsofcoconutoil.pdf [25 December 2011]
42. Van de Voort, F.R., Ismail, A.A., Sedman, J., Dubois, J. & Nicodemo, T. 1994. The determination of peroxide value by FTIR. *Journal Am. Oil Chem. Soc* 71: 921-926
43. Vlachos, N., Skopelitis, Y., Psaroudaki, M., Konstantinidau, V., Chatzilazarou, A. & Tegou, E. 2006. Application of fourier transform-infrared spectroscopy to edible oils. *Analytica Chimica Acta*. Vol 573-574: 459-465
44. Yahya, S.A.D., Al-Ghouti & Nidaa S. 2011. Determination of frying quality of vegetable oils used for preparing falafel using infrared spectroscopy and multivariate calibration. *Journal Food Anal. Methods.* 4: 540-549
45. Yingxu, Z. 2010. Exploring the capabilities of gas chromatography and liquid chromatography single and random mass spectrometry for discriminating and characterizing marine oils by using chemometric tools. Thesis Phd. University of Bergen.
46. Zuli, J. 2011. Chemometric and pattern recognition methods with applications to environmental and quantitative structure activity relationship studies. Thesis Phd. University of Bristol.

The Malaysian Journal of ANALYTICAL SCIENCES ISSN 1394-2506

# POTENTIAL OF PALM OLEIN AS GREEN LUBRICANT SOURCE: LUBRICATION ANALYSIS AND CHEMICAL CHARACTERISATION

## (Potensi Minyak Sawit Olein Sebagai Sumber Lubrikan Hijau: Analisis Pelinciran dan Pencirian Kimia)

Darfizzi Derawi* and Jumat Salimon

*School of Chemical Sciences and Food Technology,*
*Faculty of Science and Technology,*
*Universiti Kebangsaan Malaysia, 43600 Bangi, Selangor, Malaysia*

**Corresponding author: darfizzi@ukm.edu.my*

**Abstract**

Palm olein ($PO_o$) is widely used as edible oil in tropical countries. The lubrication properties and chemical compositions of $PO_o$ being considered to be used as renewable raw material for biolubricant synthesis. $PO_o$ is suitable to be used directly as biolubricant for medium temperature industrial applications. Palm olein has good viscosity index, oxidative stability, flash and fire point as a lubricant source. $PO_o$ contains unsaturated triacylglycerols (TAG): Palmitin-Olein-Olein, POO (33.3 %), Palmitin-Olein-Palmitin, POP (29.6 %), which are very important to produce good lubricant properties. This unsaturated bond is preferable in chemical modification to produce biolubricant. The chemical compositions of $PO_o$ were tested by using high performance liquid chromatography (HPLC) and gas chromatography (GC) techniques.

**Keywords**: Palm olein, Renewable Source, Lubrication Analysis, Biolubricant

**Abstrak**

Minyak sawit olein ($PO_o$) digunakan secara meluas sebagai minyak masak bagi negara-negara beriklim tropika. Sifat-sifat pelinciran dan komposisi kimia $PO_o$ dinilai untuk digunakan sebagai bahan mentah dalam sintesis biolubrikan. $PO_o$ sesuai digunakan secara terus sebagai biolubrikan untuk aplikasi industri bersuhu sederhana. Minyak sawit olein adalah baik sebagai sumber lubrikan berdasarkan indeks kelikatan, kestabilan oksidatif, takat kilat dan api. $PO_o$ mengandungi triasilgliserida tak tepu (TAG): POO (33.3 %), POP (29.6 %) iaitu sangat pnting untuk menghasilkan sifat-sifat lubrikan yang baik. Ikatan tak tepu diperlukan dalam modifikasi kimia untuk menghasilkan biolubrikan. Komposisi kimia $PO_o$ diuji menggunakan teknik kromatografi cecair berprestasi tinggi (HPLC) dan kromatografi gas (GC).

**Kata kunci:** Minyak Sawit Olein, Sumber Boleh Diperbaharui, Analisisi Pelinciran, Biolubrikan

## Introduction

Lubrication industry plays an important role in the national economic sector. This leads to the improvement of research and development in lubrication industries particularly on the synthesis works by using different raw materials. Conventionally, lubrication industries use petroleum based sources as the raw materials. Recently, researchers all over the world talked about the new approaches in chemical synthesis techniques to produce industrial products such as polymers, fuels and lubricants [1]. As a result, some of the environmental friendly sources that can initiate green technology in chemical synthesis were found out. Commonly, these sources had been used traditionally as herbs or food usage for a long time. Because of the lack of scientific researches, the potential of these crops as natural friendly sources on developing the industrial products are not being discovered.

Palm oil is from the fleshy endosperm of oil palm with its scientific name *Elaies guineensis* [2]. Palm oil undergoes some refinery stages such as fractionation distillation, refining, bleaching and deodorization to produce refined,

bleached and deodorized palm oil (RBDPO). A single fractionation converts palm oil to palm olein by 75-80 % yield [3]. Palm olein ($PO_o$) is the most valuable liquid fraction of palm oil (the largest renewable resource in Malaysia). It is used for frying food and salad oils [2].

It mainly consists of mono-unsaturated triacylglycerol (TAG), palmitin-olein-palmitin (POP) (42.8 %) and di-unsaturated TAG, palmitin-olein-olein (POO) (35.7 %). The iodine value of $PO_o$ is about 51.0 – 61.0 [4]. $PO_o$ consists of oleic acid (42.7-43.9 %) and palmitic acid (39.5-40.8 %) [5]. Oleic acid is a mono-unsaturated fatty acid while palmitic acid is a saturated fatty acid attached to the TAG of $PO_o$. Oleic acid is needed to improve the pour point and cloud point value of $PO_o$. While, the palmitic acid is needed to improve the oxidative and thermal stability. Thus, the combination of mono-unsaturated and saturated properties of $PO_o$ makes it preferable as raw materials in biolubricant production. In this paper, we report that the physico-chemical properties and chemical compositions of $PO_o$ have promising potential to be developed as raw materials in biolubricant synthesis.

## Materials and Methods

### Raw materials

Palm Olein (Seri Murni brand, FFM Marketing Sdn. Bhd.) was purchased directly from the market.

### Chemical composition tests

Gas chromatography analysis was studied via GC instrument, 17A Shimadzu model. The capillary column used is non-polar stationery phase (BPX70) with Helium as mobile gas. The initial temperature is 120 $^oC$ and final temperature is 250 $^oC$ with temperature rate 3 $^oC$ per minute. High Performance Liquid Chromatography (HPLC) analysis was performed by HPLC auto sampler instrument, Dionex Ultimate 3000 model with non-polar column (C18, 150 mm x 4.8 mm x 3 µm). The mobile phase used is a mixture of aceton : acetonitrile (60:40 v/v) [6].

### Chemical characterization tests

The iodine value of $PO_o$ sample was determined by Wijs method (British standard BS 684: Section 2.13:1976) [6]. It can be defined as a measure of the unsaturation of fatty acids and is expressed in terms of the number of centigrams of iodine absorbed per gram of sample (% iodine absorbed). The acidity of $PO_o$ was determined by AOCS 5a-40 (1989) [6]. The acid value is the number of milligrams of potassium hydroxide required to neutralize the free fatty acids in 1 g of sample. The cloud point is the temperature at which, under certain test conditions (A.O.C.S. Cc 6-25), a cloud is induced in the sample caused by the first stage of crystallization [6]. The moisture content of $PO_o$ tested by Karl Fischer method (A.O.C.S. Tb 2-64) [7]. This method is to determine the actual water content of oil by titration with Fischer reagent which reacts quantitatively with water. The saponification value (British standards BS 684 2.6:1977) [6] done to calculate the milligrams of potassium hydroxide (KOH) required to saponify 1 g of fat under the conditions specified. It is a measure of the average molecular weight of all the fatty acids present. 10 g of $PO_o$ was used to test the unsaponifiable matter (A.O.C.S. Ca 6a-40) [6]. This method is to test the unsaponifiable matter includes those substances frequently found dissolved in oils which cannot be saponified by the caustic alkalies, but are soluble in the ordinary fat solvents which include higher aliphatic alcohols, sterols, pigments, and hydrocarbons.

### Lubrication analysis

Oxidative stability of $PO_o$ was tested by using Pressurized Differential Scanning Calorimeter (PDSC), Mettler Toledo DSC 822 model with StarE software [8]. A 10 $^oC\ min^{-1}$ heating rate (25 $^oC$ to 300 $^oC$) was used for the test. The oxidation onset (OT, $^oC$) and signal maximum temperatures (SMT, $^oC$) were calculated from a plot of heat flow (W/g) versus temperature. Pour point can be defined as the lowest temperature, expressed as a multiple of 3 $^oC$ at which the oil is observed to flow when cooled and examined under prescribed conditions (ASTM D 97-66) [9]. The fire and flash point test as according to the ASTM D 92-78 [7]. The test cup was filled to a specified level with the sample. The temperature of the sample was increased rapidly at first and then at a slow constant rate as the flash point approaching. At specified intervals a small test flame was passed across the cup. The lowest temperature at which application of the test flame causes vapours above the surface of the liquid to ignite is taken as the flash point. In order to determine the fire point, the test was continued until the application of the test flame causes the oil to ignite and burn for at least 5 seconds. The kinematic viscosity of $PO_o$ was tested by using Anton Paar rheometer

(Physica MCR 301 model) according to ASTM D 445-79 [7]. The viscosity index (ASTM D2270) was calculated by using the kinematic viscosity at 40 $^{o}$C and 100 $^{o}$C [10].

**Determination of ISO Lubricant Grade**

The classification of ISO lubricant grade according to the American Society of Lubrication Engineers (ASLE) and British Standards Institution (BSI) [11].

## Results and Discussion

**Chemical composition**

Based on the GC analysis done, there was three major FFAs of $PO_o$ (Table 1). These FFAs are oleic acid (47.7 %) followed by palmitic acid (36.3 %) and linoleic acid (10.4 %). The others are lauric acid (0.2 %), myristic acid (0.8 %), stearic acid (3.7 %), linolenic acid (0.3 %), and arachidic acid (0.1 %). If compared to the theory, palm olein contains lauric acid (0.1-0.2 %), myristic acid (0.9-1.0 %), palmitic acid (39.5-40.8 %), C16:1 (<0.2 %), stearic (3.9-4.4 %), oleic (42.7-43.9 %), linoleic (10.6-11.4 %), linolenic (<0.4 %) and arachidic acid (0.1-0.3 %) [5]. The FFA compositions of $PO_o$ had been reported before [12]. It contains lauric acid (0.2 %), myristic acid (1.1 %), palmitic acid (35.7 %), stearic (3.5 %), oleic (45.4 %), linoleic (13.1 %) and linolenic (0.3 %). The separation of GC peaks was based on the carbon number and boiling point of each compound. The greater carbon number leads to longer retention time for the peak to be detected. Similar scenario happens to the FFA that had double bond on its structure because the double bond will increase the intermolecular force. By increasing the intermolecular force, the boiling point can be increased, therefore increasing the retention time.

Table 1. The Free Fatty Acid Compositions of $PO_o$

| No. | Free Fatty Acid Type | Retention Time (minutes) | Relative Area (%) |
|---|---|---|---|
| 1 | Lauric acid | 10.829 | 0.2 |
| 2 | Myristic acid | 14.689 | 0.8 |
| 3 | Palmitic acid | 19.518 | 36.3 |
| 4 | Palmitoleic acid | 20.187 | 0.2 |
| 5 | Stearic acid | 24.085 | 3.7 |
| 6 | Oleic acid | 24.895 | 47.7 |
| 7 | N/A | 25.581 | 0.2 |
| 8 | Linoleic acid | 25.986 | 10.4 |
| 9 | N/A | 27.515 | 0.1 |
| 10 | Linolenic acid | 27.773 | 0.3 |
| 11 | Arachidic acid | 28.558 | 0.1 |

Based on the HPLC analysis done, there were two major TAGs found which are POO (33.3 %) and POP (29.6 %) (Table 2). This is because of the major FFA of $PO_o$ are oleic acid followed by palmitic acid. The separation of HPLC peaks was based on the equivalent carbon number (ECN) and the polarity of each TAG. Different ECN produces different based line of the peak. The greater ECN number, leads to shorter retention time. But, for the same baseline of TAGs, the less polar of TAG was firstly detected. The arrangement of TAGs is PLL (2.8 %), OOL (1.4 %), POL (12.4 %), PPL (7.3 %), OOO (3.6 %), POO (33.3 %), POP (29.6 %), SOO (2.6 %) and POS (3.8 %). The theoretical TAG compositions of palm oil are mainly contain of POP (27-31 %) and POO (20-26 %) [2]. Due to the fact that the palm oil had fractionised to produce $PO_o$, thus the TAG produced has higher olein. If compared to the HPLC analysis of $PO_o$ done before, there were OLL (0.7 %), OOL (2.6 %), POL (14.8 %), PPL (10.2 %), OOO (5.5 %), POO (30.6 %), POP (18.0 %), SOO (3.3 %) [12].

Table 2. The Triacylglycerol (TAG) Compositions of $PO_o$

| TAG Type | Equivalent Carbon Number (ECN) | Relative Area (%) |
|---|---|---|
| PLL | 44 | 2.8 |
| OOL | 46 | 1.4 |
| POL | 46 | 12.4 |
| PPL | 46 | 7.3 |
| OOO | 48 | 3.6 |
| POO | 48 | 33.3 |
| POP | 48 | 29.6 |
| SOO | 50 | 2.6 |
| POS | 50 | 3.8 |

**Physico-chemical characterisation**

The physico-chemical of $PO_o$ is shown in Table 3. The iodine value of $PO_o$ is 61.67 whereas the acidity is 3.01 %. This acidity may happen during the storage and delivering time of the sample. The saponification value is 197.18 mgKOH/g and its average molecular weight of $PO_o$ is 854.3 $gmol^{-1}$. $PO_o$ contains 0.17 of unsaponifiable matter. This commercial oil only contains 0.22 % of water. The cloud point is 7 $^oC$ (± 1 $^oC$) and the pour point is 5 $^oC$ (± 2 $^oC$). Both fire and flash point were over 320 $^oC$ (± 5 $^oC$). The oxidative stability by DSC was 179 $^oC$. $PO_o$ has kinematic viscosity about 45.9 cSt (40 $^oC$) and 9.4 cSt (100 $^oC$) with viscosity index of 195. $PO_o$ was categorized as ISO VG 46 of viscosity grade [10]. Theoretically, the iodine value is not less than 55. Then, the cloud point was 7 – 10 $^oC$. The saponification value was 194-202 and the unsaponifiable matter was less than 1.4 [2]. So, most of the characterizations of $PO_o$ observed in this work are almost the same with the theoretical values. By referring to the flash and fire point, kinematic viscosity and viscosity index, it can be proposed that $PO_o$ has the promising lubricant properties. Then, if compared with other ISO 46 commercialised samples which are Priolube 2065 and Priolube 2089 (Table 3) [13], some of the characterisations of $PO_o$ were almost similar especially on the kinematic viscosity (40, 100 $^oC$), viscosity index and flash point. But $PO_o$ is still poor in its cloud and pour point. Priolube 2065 is the standard oleate base fluid for medium temperature application while Priolube 2089 is the medium temperature applications with superior low temperature properties [10].

Table 3. The Physico-chemical Properties of Palm Olein ($PO_o$)

| Physico-chemical Test | Value $_{(exp.)}$ | Priolube 2065 | Priolube 2089 |
|---|---|---|---|
| Iodine value | 61.67 | 84 | 72 |
| Acidity, % | 3.01 | 0.20 | 0.05 |
| Saponification value, mgKOH/g | 197.18 | - | - |
| Average molecular weight, $gmol^{-1}$ | 854.3 | - | - |
| Unsaponifiable matter | 0.17 | - | - |
| Moisture content (Karl Fischer), % | 0.22 | - | - |
| Cloud point, $^oC$ | 7 (± 1) | -21 | -25 |
| Pour point, $^oC$ | 5 (± 2) | -51 | -54 |
| Flash point, $^oC$ | > 320 (± 5) | 320 | 315 |
| Fire point, $^oC$ | > 320 (± 5) | - | - |
| Oxidative stability (DSC), $^oC$ | 179 | - | - |
| Kinematic viscosity (40 $^oC$), cSt | 45.9 | 48 | 44 |
| Kinematic viscosity (100 $^oC$), cSt | 9.4 | 9.8 | 8.7 |
| Viscosity index | 195 | 196 | 181 |
| ISO VG Grade | ISO 46 | ISO 46 | ISO 46 |

By referring to Figure 1, the Stribeck curve has three types of lubricant conditions which are boundary, mixed and hydrodynamic lubricant. In the middle between mixed and hydrodynamic lubricant conditions, there is an elastohydrodynamic lubricant which shows that the friction coefficient decreasing during the increasing of parameter [14]. The comparison of tribological properties of $PO_o$ at 40 $^oC$ and 100 $^oC$ is shown in Figure 2. $PO_o$ exhibits low friction coefficient (min. 0.2 μ) at 40 $^oC$, nonetheless, $PO_o$ has recorded good friction coefficient (min. 1.2 μ) at 100 $^oC$. This shows that $PO_o$ have better lubrication properties even if the temperature is increased.

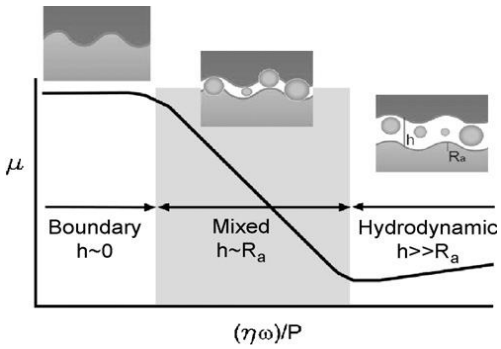



Figure 1. Sketch of a Stribeck curve relating friction coefficient; h: fluid film thickness, $R_a$: average surface roughness

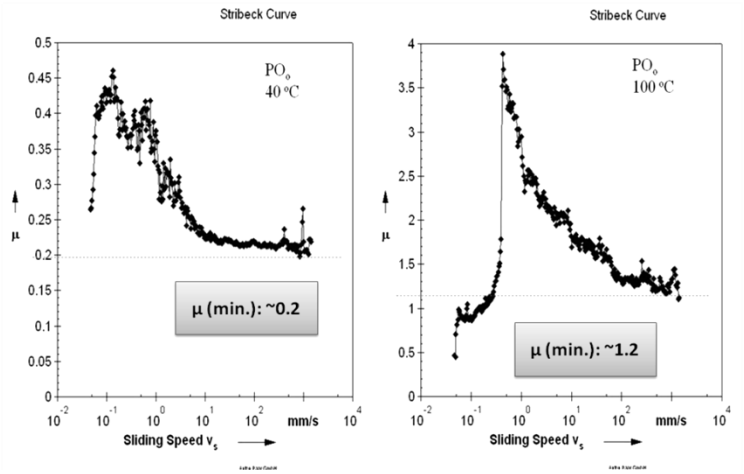



Figure 2. Comparison of Stribeck curves of $PO_o$ at 40 $^oC$ and 100 $^oC$

## Conclusion

Based on the chemical compositions and lubrication analysis of palm olein observed in this research works, it is proven that it has potential to be developed as biolubricant base stock through some chemical modifications. $PO_o$ can also be used directly as lubricant for medium temperature applications. The modifications used might improve some poor lubricating properties of palm olein.

**Acknowledgement**

Authors would like to acknowledge the Universiti Kebangsaan Malaysia for the financial support through research grant no. OUP-2012-139 and research facilities provided. Authors also would like to thank Mr. Hassanudin Salleh for the technical works.

**References**

1. Derawi, D. & Salimon, J. (2010). Optimization on Epoxidation of Palm Olein by Using Performic Acid.*E-Journal of Chemistry*, 7 (4): 1440 – 1448.
2. Gunsotne, F. D. (2004). The Chemistry of Oils and Fats, Sources, Composition, Properties and Uses, Blackwell Publishing Ltd., UK.
3. Gunstone, F. D. & Padley, F. B. (1997). Lipid Technologies and Applications, Marcel Dekker, Inc., New York.
4. O'Brien, R. D. (1998). Fats and Oils: Formulating and Processing for Applications, Technomic Publishing AG., Switzerland.
5. Gunstone, F. D., Harwood, J. L. & Padley, F. B. (1994). The Lipid Handbook, 2nd ed. Chapman & Hall, UK.
6. Salimon, J., Said, M., Ramli, S. & Mat Lazim, M. A. S. (2006). Oils and Fats Analysis, Penerbit UKM, Bangi.
7. Emery (1983). Emery Analytical Testing Procedures, Emery Industries, USA.
8. Salih, N. Salimon, J. Yousif E. & Abdullah, B. M. (2013). Biolubricant basestocks from chemically modified plant oils: ricinoleic acid based-tetraesters, *Chemistry Central Journal*, 7 (128).
9. Salimon, J. Abdullah, B.M. & Salih, N. (2012). Diesters biolubricant base oils: synthesis, optimization, characterization and physicochemical characteristics, International Journal of Chemical Engineering, Article ID 896598.
10. Stachowiak, G. W. & Batchelor, A. W. (2005). Engineering Tribology, 3rd ed. Elsevier Inc., UK.
11. ISO 3448 (1975). International Standard, Industrial Liquid Lubricants, ISO Viscosity Classification. ISO International Standards, US.
12. Ramli, M. R., Siew, W. L. & Cheah, K. Y. (2008). Properties of high-oleic palm oils derived by fractional crystallization. *Journal of Food Science*, 73 (3): 1750 – 3841.
13. Uniqema (2006). Oleochemical Ester Base Fluids for European Eco-label Compliant Lubricant Formulations, Uniqema Inc, USA.
14. Hironaka, S. (1984). Boundary Lubrication and Lubricants, Three Bond Co. Ltd., Japan.

The Malaysian Journal of ANALYTICAL SCIENCES ISSN 1394-2506

# SYNTHESIS, STRUCTURAL AND ANTIBACTERIAL STUDIES OF NEW DITHIOCARBAMATE COMPLEXES OF Sb(III) AND Bi(III)

## (Sintesis, struktur dan kajian antibakteria kompleks baru ditiokarbamat Sb(III) dan Bi(III))

Nur Amirah Jamaluddin[1], Ibrahim Baba[1]*, Nazlina Ibrahim[2]

*[1]School of Chemical Sciences and Food Technology,*
*[2]School of Biosciences and Biotechnology,*
*Faculty of Science and Technology,*
*Universiti Kebangsaan Malaysia, 43600 Bangi, Selangor, Malaysia*

**Corresponding author: aibi2005@gmail.com*

**Abstract**

Six new dithiocarbamate complexes from three different amines, e.g. N-ethylethanol-, N-butylethyl- and N-benzylmethylamine were successfully prepared using *in situ* method. All complexes were characterized by elemental analysis, IR, UV-Vis, $^{13}$C and $^{1}$H NMR. Elemental analysis data (C, H, N and S) showed an agreement with the general formula of $MCl(S_2CNR'R'')_2$, (M = Sb(III), Bi(III); R' = ethyl, butyl and benzyl; R" = ethanol, ethyl and methyl). The complexes had been characterized by infrared spectroscopy that showed a thioureide bands, ν(C═N) in the region of 1427 - 1490 cm$^{-1}$ followed by ν(C═S) bands that can be seen in the region of 935 - 1060 cm$^{-1}$ and ν(M-S) bands existed in the region of 350 - 392 cm$^{-1}$. Maximum wavelength absorption for ultraviolet-visible spectroscopy for N═C═S group was at 254 nm which indicates π→π* transition. Data from $^{13}$C NMR showed a signal in the region of 198.39 – 199.44 ppm that corresponded to the $NCS_2$ group. The crystal structure of bis(*N*,*N*'-butylethyldithiocarbamato)chlorido antimony(III), $SbCl[S_2CN(C_4H_9)(C_2H_5)]_2$ demonstrated a five-coordination geometry, triclinic system, space group P*1* with *a* = 10.0141(8) Å, *b* = 10.1394(7) Å, *c* = 11.8665(9) Å, α = 67.960(2)°, β = 87.616(2)° and γ = 80.172(2)°. Minimum inhibitory concentration (MIC) and minimum bactericidal concentration (MBC) tests were done using five dithiocarbamate complexes which are $BiCl[S_2CN(C_2H_5)(C_2H_4OH)]_2$, $SbCl[S_2CN(C_2H_5)(C_2H_4OH)]_2$, $BiCl[S_2CN(C_4H_9)(C_2H_5)]_2$, $SbCl[S_2CN(C_4H_9)(C_2H_5)]_2$, $BiCl[S_2CN(C_7H_7)(CH_3)]_2$ towards *S. aureus*, *S. epidermidis*, *E. aerogenes* and *E. coli*. It was found that all four complexes were active against *S. aureus* except $SbCl[S_2CN(C_2H_5)(C_2H_4OH)]_2$ while $BiCl[S_2CN(C_7H_7)(CH_3)]_2$ and $BiCl[S_2CN(CH_3)(C_6H_{11})]_2$ complexes were active against *S. epidermidis* with MIC value of 5.0 mg/mL and 2.5 mg/mL respectively and MBC value of 5.0 mg/mL for both compounds. Only $BiCl[S_2CN(C_2H_5)(C_2H_4OH)]_2$ was active against *E. aerogenes* with MIC, 1.25 mg/mL and MBC, 10 mg/mL. All complexes were less active as antibacterial agent against *E. coli* strain.

**Keywords**: Dithiocarbamate, antimony(III), bismuth(III), antibacterial

**Abstrak**

Enam sebatian ditiokarbamat baru daripada tiga jenis amina yang berbeza, iaitu N-etilaminoetanol, N-butiletil, N-benzilmetil telah berjaya disediakan dengan menggunakan kaedah *in situ*. Kesemua sebatian telah dicirikan dengan analisis unsur, IR, UV-Vis, $^{13}$C dan $^{1}$H NMR. Data analisis unsur (C, H, N dan S) bagi kesemua sebatian menepati formula umum $MCl(S_2CNR'R'')_2$ (M = Sb(III), Bi(III); R' = etil, butil dan benzil; R" = etanol, etil dan metil). Kompleks dicirikan menggunakan kaedah spektroskopi inframerah menunjukkan jalur tioreida, ν(C═N) berada dalam julat 1427 - 1490 cm$^{-1}$ diikuti jalur ν(C═S) yang diperhatikan dalam julat 935 - 1060 cm$^{-1}$ dan jalur logam sulfur, ν(M-S) berada dalam julat 350 - 392 cm$^{-1}$. Serapan jarak gelombang maksimum untuk spektroskopi ultralembayung-nampak untuk kumpulan N═C═S ialah pada 254 nm yang menunjukkan peralihan π→π*. Data daripada $^{13}$C NMR menunjukkan isyarat dalam julat 198.39 – 199.44 ppm merujuk kepada kumpulan $NCS_2$. Struktur hablur bis(*N*,*N*'-butiletilditiokarbamato)klorido stibium(III), $SbCl[S_2CN(C_4H_9)(C_2H_5)]_2$ menunjukkan geometri lima koordinatan, sistem *triklinik*, kumpulan ruang P*1* dengan *a* = 10.0141(8) Å, *b* = 10.1394(7) Å, *c* = 11.8665(9) Å, α = 67.960(2)°, β = 87.616(2)° and γ = 80.172(2)°. Ujian kepekatan minimum perencatan (MIC) dan kepekatan minimum bakterisidal (MBC) telah dijalankan menggunakan lima sebatian ditiokarbamat, iaitu $BiCl[S_2CN(C_2H_5)(C_2H_4OH)]_2$, $SbCl[S_2CN(C_2H_5)(C_2H_4OH)]_2$, $BiCl[S_2CN(C_4H_9)(C_2H_5)]_2$, $SbCl[S_2CN(C_4H_9)(C_2H_5)]_2$, $BiCl[S_2CN(C_7H_7)(CH_3)]_2$ terhadap *S. aureus*, *S. epidermidis*, *E. aerogenes* and *E. coli*. Kesemua empat sebatian adalah aktif terhadap *S. aureus* kecuali

$SbCl[S_2CN(C_2H_5)(C_2H_4OH)]_2$ manakala sebatian $BiCl[S_2CN(C_7H_7)(CH_3)]_2$ dan $BiCl[S_2CN(CH_3)(C_6H_{11})]_2$ aktif terhadap *S. epidermidis* dengan nilai MIC masing-masing ialah 5.0 mg/mL dan 2.5 mg/mL manakala nilai MBC 5.0 mg/mL untuk kedua-dua sebatian. Hanya sebatian $BiCl[S_2CN(C_2H_5)(C_2H_4OH)]_2$ yang aktif terhadap *E. aerogenes* dengan nilai MIC, 1.25 mg/mL dan nilai MBC, 10 mg/mL. Kesemua sebatian kurang aktif sebagai agen antibakteria terhadap strain *E. coli*.

**Kata kunci**: Ditiokarbamat, stibium(III), bismuth(III), antibakteria

## Introduction

Dithiocarbamate is a type of ligand with S donor ligand that can act as monodentate or bidentate mode of complexation towards metal. Dithiocarbamate compounds are strong metal chelators, exhibiting interesting chemical characteristics [1]. There are many applications of dithiocarbamate complexes mainly in rubber industry, analytical chemistry, biology, medicine, agriculture and chemical industries [2]. Dithiocarbamates are considered privileged scaffolds in drug discovery with a wide array of biological activities [3]. The use of antimony and bismuth dithiocarbamate compounds were widely reviewed due to their varied applications. Extensive literatures were available on the tris(dithiocarbamato)bismuth(III) and tris(dithiocarbamato)antimony(III) complexes [4] and only a few reports on the closely related bis(dithiocarbamato)chloro bismuth(III) and bis(dithiocarbamato)chloro antimony(III) complexes. The tris(dithiocarbamato)bismuth(III) and tris(dithiocarbamato) antimony(III) complexes generally have the chelated metal atom with a capped octahedral geometry, since the lone pair of electrons was stereochemically active [5, 6]. The sulphur atom has a vacant dπ orbital, and can therefore form multiple π-bonds. The additional π-electrons available between nitrogen and sulphur, via a planar delocalized π-orbital system, result in dithiocarbamates being strong electron donors [7]. The (*N*,*N*-diethyldithiocarbamato-$\kappa^2$S:S′)phenylbismuth(III)-$\mu$-chlorido (Figure 1) is an example of dithiocarbamate complex with one chlorine attached to bismuth and with five-coordinated and the geometry between trigonal bipyramidal and square pyramidal with the slight tendency towards the former [8].

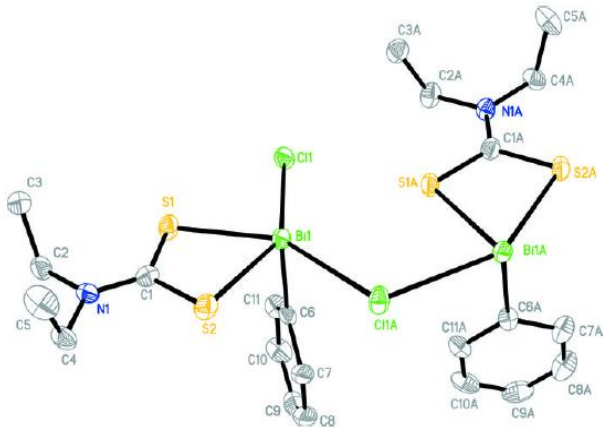



Figure 1. ORTEP plot of (*N*,*N*-diethyldithiocarbamato $\kappa^2$S:S′)phenylbismuth(III)-$\mu$-chlorido at the 50% probability level.

## Materials and Methods

### Materials

All chemicals and solvents that have been used in these experiments e.g. N-ethylaminoethanolamine, N-butylethylamine, N-benzylmethylamine, bismuth(III) trichloride, antimony(III) trichloride, carbon disulphide, chloroform and ethanol (Merck) are pure and used as supplied.

### Instrumentations

Melting point was measured on Electrotherma IA 9100 apparatus. Elemental Analysis data was measured on Fisons EA1108 instrument. The infrared data was recorded on Fourier Transform Infrared (FTIR) Perkin-Elmer Spectrum

GX spectrophotometer. Ultraviolet (UV) spectra were recorded on Cary 100 spectrophotometer. Nuclear Magnetic Resonance (NMR) spectra, $^{1}H$ and $^{13}C\{^{1}H\}$, were recorded on Joel JNM-ECP 400 spectrometer.

**Synthesis of complexes**

All the complexes were prepared using direct reaction by mixing metal and ligand with molar ratio 1:2. The ligand was prepared by addition of carbon disulphide, $CS_2$ to an ethanolic solution of selected amine (N-ethylethanol-, N-butylethyl- or N-benzylmethylamine) in a same molar ratio. The mixture was stirred for one hour at temperature 277 K. After one hour of stirring, the solution was added by dropwise to a solution of antimony(III) trichloride in 20 mL of ethanol. The mixture was stirred again for another one hour. The white precipitate was filtered and washed with cold ethanol and dried in desiccator. The similar steps was used to prepare bismuth(III) dithiocarbamate complexes with yellow colour precipitate. Recrystallization was carried out by using ethanol and chloroform solvents at ratio 1:2.

**Crystallographic studies**

Crystals for compound **3**, bis(*N*,*N*'-butylethyldithiocarbamato)chlorido antimony(III) was obtained by slow evaporation of the mixture of ethanol and chloroform solution with ratio 1:2. Intensity data for the compound **3** was measured at 173 K on a Bruker APEX-II CCD fitted with Mo K$\alpha$ radiation. Data processing (APEX2 and SAINT [9]) and absorption correction (SADABS [10]) were accomplished using routine methods. Details of cell data, X-ray data collection, and structure refinement are given in Table 4. The structures were solved by direct methods [11]. Full-matrix least-squares refinement on $F^2$ with anisotropic displacement parameters for all non-hydrogen atoms was performed [11].

**Antibacterial Tests**

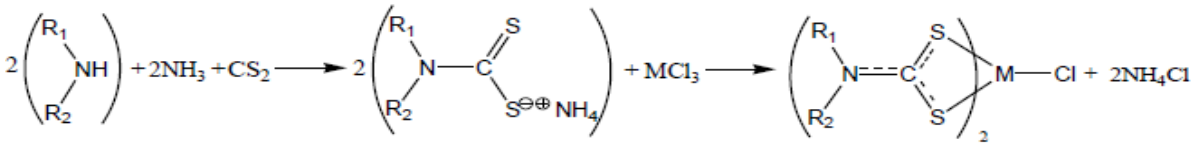
All six dithiocarbamate complexes synthesized were tested for antibacterial activities except for **5**. The test organisms chosen for the antibacterial activity were two gram positive (*Staphylococcus aureus* and *Staphylococcus epidermidis*) and two gram negative (*Escherichia coli* and *Enterobacter aerogenes*). The screening properties were done by minimum inhibitory concentration (MIC) and minimum bacterial concentration (MBC) methods.

## Results and Discussion

Six new antimony(III) and bismuth(III) dithiocarbamate compounds have been prepared by using the insertion technique [5], which involves the reaction between metal(III) trichloride ($SbCl_3$ and $BiCl_3$), amines and carbon disulphide at 277 K in ethanol to give stable compounds. General scheme for the reaction involved in the synthesis is shown in Figure 2. All compounds exhibit as solid powder either white or yellow in colour. Elemental analysis (C, H, N and S) showed that the experimental values are in agreement with theoretical values based on their general formula (Table 1).

A summary of the main peak positions on the IR spectra of the metal complexes is shown in Table 2. All synthesized complexes showed thioureide band $\nu$(C⁼⁼⁼⁼N) in 1450-1550 $cm^{-1}$ range and $\nu$(C⁼⁼⁼⁼S) band in 950-1050 $cm^{-1}$ [12] proving that there were dithiocarbamate groups in the compounds. Compound (**1**) and (**2**) showed broad and intense peak at 3360 and 3294 $cm^{-1}$ respectively which indicated the presence of hydroxyl, (OH) group. These were lower than the stretching of free hydroxyl group which was at 3640 $cm^{-1}$. This proved that there was a possibility of the formation intermolecular hydrogen bonding in the complex [13].

Bidentate nature of the chelation with dithiocarbamate ligands can be seen in the region of 959-1003 $cm^{-1}$ with the existence of non-splitted $\nu$(C⁼⁼⁼⁼S) band and monodentate if splitted [14]. The presence of metal-sulphur, (M-S) bond was observed around 350 – 398 $cm^{-1}$ [15].



(M = Sb or Bi)

Figure 2. General reaction between secondary amine, carbon disulphide and metal(III) trichloride (M = Sb or Bi).

Table 1. Physical and elemental analysis of complexes

| No. | Complex | Percentage yield (%) | Melting point (˚C) | % | | | | |
|---|---|---|---|---|---|---|---|---|
| | | | | C | H | N | S | M |
| **1** | $SbCl[S_2CN(C_2H_5)(C_2H_4OH)]_2$ | 78 | 135-136 | 24.32 | 3.19 | 6.29 | 24.83 | 24.30 |
| | | | | **24.73** | **4.15** | **5.77** | **26.40** | **25.07** |
| **2** | $BiCl[S_2CN(C_2H_5)(C_2H_4OH)]_2$ | 80 | 128-131 | 22.25 | 3.63 | 5.88 | 20.23 | 35.11 |
| | | | | **20.96** | **3.52** | **4.89** | **22.39** | **36.47** |
| **3** | $SbCl[S_2CN(C_4H_9)(C_2H_5)]_2$ | 87 | 95.4-95.1 | 32.49 | 5.17 | 5.50 | 24.52 | 23.05 |
| | | | | **32.98** | **5.54** | **5.49** | **25.16** | **23.88** |
| **4** | $BiCl[S_2CN(C_4H_9)(C_2H_5)]_2$ | 89 | 102-104 | 28.16 | 4.73 | 3.69 | 21.48 | 35.00 |
| | | | | **28.00** | **5.32** | **3.26** | **21.03** | **34.14** |
| **5** | $SbCl[S_2CN(C_7H_7)(CH_3)]_2$ | 88 | 139-140 | 34.09 | 3.41 | 4.01 | 17.60 | 28.20 |
| | | | | **35.00** | **3.56** | **4.30** | **19.67** | **29.55** |
| **6** | $BiCl[S_2CN(C_7H_7)(CH_3)]_2$ | 89 | 131-133 | 40.17 | 3.80 | 5.29 | 22.09 | 25.85 |
| | | | | **39.32** | **3.67** | **5.09** | **23.33** | **26.34** |

bold = theoretical values

Table 2. FT-IR and UV spectral data for all dithiocarbamate complexes

| No. | Complex | Infrared | | | | Ultraviolet-visible |
|---|---|---|---|---|---|---|
| | | Wavenumber ($cm^{-1}$) | | | | Wavelength (nm) |
| | | ν(C ---- N) | ν(C ---- S) | ν(-OH) | ν(M-S) | |
| 1 | $SbCl[S_2CN(C_2H_5)(C_2H_4OH)]_2$ | 1498s | 976s, 994s | 3360b | 351s | 261 |
| 2 | $BiCl[S_2CN(C_2H_5)(C_2H_4OH)]_2$ | 1480s | 955s, 980s | 3294b | 354m | 361, 260 |
| 3 | $SbCl[S_2CN(C_4H_9)(C_2H_5)]_2$ | 1464s | 971s | - | 352s | 255 |
| 4 | $BiCl[S_2CN(C_4H_9)(C_2H_5)]_2$ | 1466s | 957s | - | 352s | 361, 259 |
| 5 | $SbCl[S_2CN(C_7H_7)(CH_3)]_2$ | 1452s | 960s | - | 358s | 355, 255 |
| 6 | $BiCl[S_2CN(C_7H_7)(CH_3)]_2$ | 1452s | 953s | - | 355s | 355, 255 |

s = strong; b = broad; m = medium

Deduced from ultraviolet spectra of antimony complexes, the maximum absorption occurred in the range of 251 - 254 nm for $\pi \rightarrow \pi^*$ transition of N-C-S group due to the intramolecular charge transfer of the ligand [16]. At the vicinity of 287 nm and above, $n \rightarrow \pi^*$ transition of the non-bonding electron on sulfur atoms to the conjugated system in N ---- C ---- S group occured. The analytical data indicated that there was characteristic of double bond character between carbon and nitrogen and between carbon and sulfur [17]. Singh and Kaushik [18] stated that chromophore group of $NCS_2$ in complexation will cause the absorption band shift to lower wavelength.

Table 3. $^{1}$H-NMR spectral data for all dithiocarbamate complexes

| No. | Complex | Chemical shift, δ (ppm) | |
|---|---|---|---|
| | | **-NR' ; R' =, $C_2H_5$ $C_4H_9$, $C_7H_7$** | **-NR" ; R" = $C_2H_4OH$, $C_2H_5$, $CH_3$** |
| 1 | $SbCl[S_2CN(C_2H_5)(C_2H_4OH)]_2$ | 1.36(t), 3.89(q) | 3.93(t), 4.67(s) |
| 2 | $BiCl[S_2CN(C_2H_5)(C_2H_4OH)]_2$ | 1.34(t), 3.91(q) | 3.95(t), 4.39(s) |
| 3 | $SbCl[S_2CN(C_4H_9)(C_2H_5)]_2$ | 0.91(t), 1.31(m), 1.64(q), 3.79(t) | 2.5(t) |
| 4 | $BiCl[S_2CN(C_4H_9)(C_2H_5)]_2$ | 0.95(t), 1.35(s), 1.75(q), 3.69(t) | 3.32(s) |
| 5 | $SbCl[S_2CN(C_7H_7)(CH_3)]_2$ | 3.80(s), 5.07(s), 5.34(s), 7.36(s) | 1.62(s) |
| 6 | $BiCl[S_2CN(C_7H_7)(CH_3)]_2$ | 2.68(s), 3.21(s), 4.37(s), 5.00(s) | 1.81(s) |

q = quartet; t = triplet; s = singlet

Table 4. $^{13}$C-NMR spectral data for all dithiocarbamate complexes

| No. | Complex | Chemical shift, δ (ppm) | | |
|---|---|---|---|---|
| | | **$N^{13}CS_2$** | **-NR' ; R' = $C_2H_5$, $C_4H_9$, $C_7H_7$** | **-NR" ; R" = $C_2H_4OH$, $C_2H_5$, $CH_3$** |
| 1 | $SbCl[S_2CN(C_2H_5)(C_2H_4OH)]_2$ | 196.14 | 11.32, 50.89 | 55.62, 58.63 |
| 2 | $BiCl[S_2CN(C_2H_5)(C_2H_4OH)]_2$ | 201.64 | 11.46, 50.59 | 55.29, 59.02 |
| 3 | $SbCl[S_2CN(C_4H_9)(C_2H_5)]_2$ | 197.59 | 12.18, 42.57 | 50.63, 58.48 |
| 4 | $BiCl[S_2CN(C_4H_9)(C_2H_5)]_2$ | 199.32 | 13.81, 20.12, 28.93, 56.66 | 41.74 |
| 5 | $SbCl[S_2CN(C_7H_7)(CH_3)]_2$ | 198.00 | 48.58, 56.56, 77.31, 134.25 | 11.74 |
| 6 | $BiCl[S_2CN(C_7H_7)(CH_3)]_2$ | 201.50 | 40.94, 128.14 129.18, 134.37 | 31.99 |

The $^{1}$H- and $^{13}$C-NMR spectral data of all complexes were shown in Table 3 and Table 4 respectively. Deuterated $DMSO_{d6}$, $CD_2Cl_2$ and $CDCl_3$ solvents were used for this analysis. The resonance frequencies of the protons of the aromatic rings were observed in complexes **5** and **6**. The higher peaks ascribed to the protons that were ortho to the carbon of the thioureide group. They were more deshielded due to the electronegativity of the nitrogen atom and the proximity to the $CS_2$ group, while the lower resonance frequency was due to the proton on the meta carbon [19]. A

signal in the region of 199.13 – 199.66 ppm was observed due to the $NCS_2$ carbon atoms of dithiocarbamate moieties [20]. Table 4 below discussed the $^{13}C$ NMR spectra data of all six dithiocarbamate compounds (δ, ppm) in details.

**Crystal structure and data of bis(N,N'-butylethyldithiocarbamato)chlorido antimony(III), $SbCl[S_2CN(C_4H_9)(C_2H_5)]_2$**

Compound **4** was successfully crystallized and analyzed by using Bruker APEX-II CCD fitted with Mo Kα radiation. Figure 3 showed ORTEP plot of bis(*N*,*N*' butylethyldithiocarbamato)chlorido antimony(III) in the unit cell which showed that the antimony atom was five-coordinated and geometry between trigonal bipyramidal and square pyramidal with the slight tendency towards the former. The crystallographic data and refinement detail for compound **4** were given in Table 5 including selected bond lengths in Table 6. The Sb-S distances can be described as short bond [Sb-S1 = 2.5456(10) Å], [Sb-S2 = 2.615(2) Å], [Sb-S3 = 2.852(2) Å] and [Sb-S4 = 2.463(2) Å]. Compound 4 had short thioureide C-N distance, 1.299(9) and 1.324(10) Å, suggesting a partial double bond character [21]. The coordination geometry around antimony atom can be desribed as a pyramidal geometry because of the asymmetrically coordinated dithiocarbamate ligands. The S atoms in these complexes lie in the equatorial plane, with S-Sb-S angles distorted significantly from 90˚.

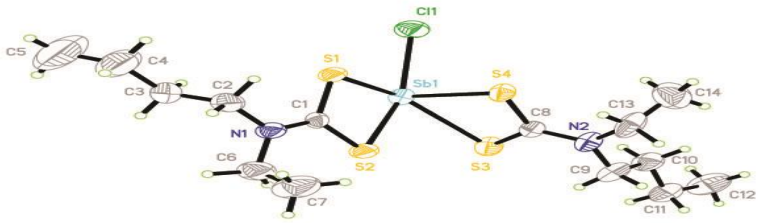



Figure 3. ORTEP plot of bis(N,N'-butylethyldithiocarbamato)chlorido antimony(III) at the 50% probability level.

Table 5. Crystal data for bis(*N*,*N*'-butylethyldithiocarbamato)chlorido antimony(III)

| **Complex** | **$SbCl[S_2CN(C_4H_9)(C_2H_5)]_2$** |
|---|---|
| Emperical formula | $C_{14}H_{28}ClN_2S_4Sb$ |
| Formula weight | 509.82 |
| *T* (K) | 301(2) |
| Crystal system | *Triclinic* |
| Space group | $P\bar{1}$ |
| a (Å) | 10.0141(8) |
| b (Å) | 10.1394(7) |
| c (Å) | 11.8665(9) |
| α (°) | 67.960(2) |
| β (°) | 87.616(2) |
| γ (°) | 80.172(2) |
| V ($Å^3$) | 1100.12(14) |
| Z | 2 |
| Calculated density, $Mg/m^{-3}$ | 1.539 |
| F(000) | 16 |
| θ Range (0°) | 2.7 - 25.5° |
| *R* Indices(final) $F^2 > 2\sigma(F^2)$ | $R_1 = 0.0569$, $wR_2 = 0.1502$ |
| R indices (all data) | $R_1 = 0.0665$, $wR_2 = 0.1727$ |

Table 6. Selected bond lengths (Å) and angles (°) for bis(*N*,*N*'-butylethyldithiocarbamato) chlorido antimony(III) complex

| | | | |
|---|---|---|---|
| Sb(1)-S(1) | 2.5456(19) | S(1)-C(1) | 1.733(7) |
| Sb(1)-S(2) | 2.615(2) | S(2)-C(1) | 1.726(7) |
| Sb(1)-S(3) | 2.852(2) | S(3)-C(8) | 1.703(8) |
| Sb(1)-S(4) | 2.463(2) | S(4)-C(8) | 1.736(8) |
| Sb(1)-Cl(1) | 2.637(2) | N(1)-C(1) | 1.299(9) |
| S(4)-Sb(1)-S(1) | 93.22(7) | N(2)-C(8) | 1.324(10) |
| S(4)-Sb(1)-S(2) | 90.54(7) | S(1)-Sb(1)-S(2) | 69.33(6) |
| S(4)-Sb(1)-Cl(1) | 86.11(8) | S(1)-Sb(1)-Cl(1) | 80.01(7) |
| S(2)-Sb(1)-Cl(1) | 148.92(7) | C(1)-N(1)-C(2) | 121.9(7) |
| C(6)-N(1)-C(2) | 115.9(7) | C(8)-N(2)-C(9) | 120.9(7) |

**Antibacterial studies of synthesized dithiocarbamate complexes**

All six dithiocarbamate complexes synthesized were tested as antibacterial agent using MIC and MBC tests. Compounds were dissolved in 10% DMSO with 20 mg/mL as starting concentration. Two gram positive bacteria which were *Staphylococcus aureus* and *Staphylococcus epidermidis* and two gram negative bacteria, *Escherichia coli* and *Enterobacter aerogenes* were selected. Compounds were dissolved in 10% DMSO with 20 mg/mL as starting concentration. The bacterial single colony were maintained in nutrient agar and were subcultured in Mueller-Hinton broth for tests. There were ten times dilution, duplicated, apart from having positive and negative control as comparison using 96 well plate. Two types of commercial antibacterial agent used i.e. Penicillin for gram positive bacteria and Kanamycin for gram negative species. Results were tabulated in Table 7. Ajibade [22] reported that a value greater than the dilution concentration of 20 mg/mL shows that it was the least active complex that can act as antimicrobial agent. In Table 7, some of the complexes were found to be moderate active against bacteria. Compound **1** was active against *E. aerogenes* while compound 2 was active against *S. aureus*. Compound **6** was active against *S. epidermidis* because of the electron withdrawing group which increases the activity of antibacterial. The velocity of compound to diffuse into membrane cell depends on the density of electron in the compound. The faster the compound diffuse into the membrane cell, the more active antibacterial activity of the compound [23].

Table 7. Results of MIC and MBC tests using dithiocarbamate complexes

| **No.** | **Complex** | ***S. aureus*** | | ***S. epidermidis*** | | ***E. coli*** | | ***E. aerogenes*** | |
|---|---|---|---|---|---|---|---|---|---|
| | | MIC | MBC | MIC | MBC | MIC | MBC | MIC | MBC |
| 1 | $SbCl[S_2CN(C_2H_5)(C_2H_4OH)]_2$ | 10.0 | 10.0 | 20.0 | >20 | 20.0 | 20.0 | 1.25 | 1.25 |
| 2 | $BiCl[S_2CN(C_2H_5)(C_2H_4OH)]_2$ | 1.25 | 1.25 | 20.0 | >20 | >20 | ND | >20 | ND |
| 3 | $SbCl[S_2CN(C_4H_9)(C_2H_5)]_2$ | >20 | ND | >20 | ND | >20 | ND | 5.00 | 10.0 |
| 4 | $BiCl[S_2CN(C_4H_9)(C_2H_5)]_2$ | 10.0 | 20.0 | >20 | ND | >20 | ND | >20 | ND |
| 6 | $BiCl[S_2CN(C_7H_7)(CH_3)]_2$ | >20 | ND | 5.0 | 5.0 | 20.0 | 20.0 | >20 | ND |

*values are in mg/mL, ND = not determined

## Conclusion

Six new dithiocarbamate complexes using antimony(III) and bismuth(III) trichloride were successfully synthesized and characterized. The structure of bis(*N*,*N*'-butylethyldithiocarbamato)chlorido antimony(III), $SbCl[S_2CN(C_4H_9)(C_2H_5)]_2$, demonstrated a five-coordination geometry, *triclinic* system with space group P*1*. MIC and MBC tests done on five complexes showed that dithiocarbamate complexes are good antibacterial agents towards certain bacteria.

## Acknowledgement

The authors gratefully acknowledge Prof Dr Bohari Mohd Yamin for crystal data and financial support from Science Fund (06-01-02-SF0887) and MyMaster Higher Education Ministry of Malaysia scholarship given to Nur Amirah binti Jamaluddin. Highest gratitude towards School of Chemical Science and Food Technology, Science and Technology Faculty, Universiti Kebangsaan Malaysia.

## References

1. Marinovich, M., Viviani, B., Capra, V., Corsini, E., Anselmi, L., D'Agostino, G., Nucci, A. G., Binaglia, M., Tonini, M., Galli, C. L. 2002. Facilitation of acetylcholine signaling by the dithiocarbamate fungicide propineb. *Chemical Research in Toxicology* 15: 26.
2. Hou, X. L., Ge, Z. M., Wang, T. M., Guo, W., Cui, J. R., Cheng, T. M., Lai, C. S., Li, R.T. 2006. Dithiocarbamic acid esters as anticancer agent. Part1: 4- substituted piperazine-1-carbodithioc acid 3-cyano-3,3-diphenyl-propyl esters. *Bioorganic & Medicinal Chemistry Letters* 16: 4214.
3. Duan, Y. C., Zheng, Y. C., Li, X. C., Wang, M. M., Ye. X. W., Guan. Y. Y., Liu, G. Z., Zheng, J. X., Liu. H. M. 2013. Design, synthesis and antiproliferative activity studies of novel 1,2,3-triazoleedithiocarbamateeurea hybrids. *European Journal of Medicinal Chemistry* 64: 99-110.
4. Halimehjani, A. Z., Marjani, K., Ashouri, A., Amani. V. 2011. Synthesis and characterization of transition metal dithiocarbamate derivatives of 1 aminoadamantane: crystal structure of (N-adamantyldithiocarbamato) nickel (II). *Inorganica Chemica Acta* 373: 282.
5. Ibrahim Baba, Karimah Kassim, Yang Farina, Abdul Hamid Othman, Abdul Razak Ibrahim, Awang Usman, Hoong-Kun and Seik Weng Ng. 2002. Tris(N-butyl-N-ethyldithiocarbamato)bismuth(III). *Acta Crystallographica Section E* E58: m756-m757.
6. Kean Yong Low, Ibrahim Baba, Yang Farina, A. Hamid Othman, Abdul Razak Ibrahim, Hoong-Kun Fun and Seik Weng Ng. 2001. Crystal structure of tris(2-hydroxyethylisopropyldithiocarbamato)antimony and Tris(2-hydroxyethylisopropyldithiocarbamato)bismuth hemihydrates. *Main Group Metal Chemistry* 4(7): 451-452.
7. Tiekink, E. R. T. 2003. Molecular architecture and supramolecular association in the zinctriad 1,1-dithiolates. Steric control as a design element in crystal engineering. *Crystal Engineering Communication* 5: 101.
8. Cui, L., Han-dong, Y., Yang, M., Quan, L., Wang, D., 2008. *Catena*-poly[[(*N*,*N*-diethyldithiocarbamato-$\kappa^2$S:S′)phenylbismuth(III)]-$\mu$-chlorido]. *Acta Crystallographica Section E* 64: 1452.
9. APEX-II and SAINT. 2000. Bruker AXS Inc., Madison, Wisconsin, USA.
10. Sheldrick G. M. 2007. SADABS, Bruker AXS Inc., Madison, Wisconsin, USA.
11. Sheldrick, G. M. 2008. A short history of SHELX. *Acta Crystallograhica* A64: 112-122.
12. Onwudiwe, D. C., Arfin, T., Strydom, C.A., Kriek, R. J. 2013. Synthesis, spectroscopic characterization and behavior of AC impedance spectroscopy of Cd(II) bis(N para methylphenyl dithiocarbamate). *Electrochimica Acta* 10: 106.
13. Zhang, R., Sun, J. & Ma, C. 2005. Structural chemistry of mononuclear, tetranuclear and hexanuclear organotin(IV) carboxylates from the reaction of di-*n*-butyltin oxide or diphenyltin oxide with rhodanine-*N*-acetic acid. *Journal of Organometallic Chemistry* 690: 4366-4372.
14. Sovilj, S. P., Vučković, G., Babić, K., Sabo, T. J., Macura, S., Juranić, N. 1997. Mixed ligand complexes of cobalt(III) with dithiocarbamates and a cyclic tetradentate secondary amine. *Journal of Coordination Chemistry* 41: 19.
15. Onwudiwe, D. C. & Ajibade, P. A. 2010. Synthesis and characterization of Zn(II), Cd(II), and Hg(II) alky-aryl dithiocarbamate: X-ray crystal structure of $[(C_6H_5N(et)CS_2)Hg(C_6H_5N(butyl)CS_2)]$. *Synthesis Reactivity in Inorganic Metal Organic Chemistry* 40: 279.
16. Chauhan, H.P.S. & Shaik, N.M. 2005. Synthetic, spectral, thermal and antimicrobial studies on some mixed 1,3-dithia-2-stannacyclopentane derivatives with dialkyldithiocarbamates. *Journal of Inorganic Biochemistry* 99: 538–545.

17. Zheng, H., Sun, X., He, Q., Liang, K., Zhang, P. 2008. Synthesis and trapping properties of N-dithiocarbamate macromolecule heavy-metal flocculants. *Journal of Applied Polymer Science* 110: 2461–2466.
18. Singh, R. & Kaushik, N.K. 2008. Spectral and thermal studies with anti-fungal aspects of some organotin(IV) complexes with nitrogen and sulphur donor ligands derived from 2- phenylethylamine. *Spectrochimica Acta Part A.* 71: 669–675.
19. Shaheen, F., Badshah, A., Gielen, M., Dusek, M., Fejfarova, K., de Vos, D. & Mirza, B. 2007. Synthesis, characterization, antibacterial and cytotoxic activity of new palladium(II) complexes with dithiocarbamate ligands: X-ray structure of bis(dibenzyl-1-S:S0- dithiocarbamato) Pd(II). *Journal of Organometallic Chemistry* 692: 3019–3026.
20. Fuentes-Martinez, P. J., Toledo-Martiez, I., Roman-Bravo, P., Garcia, Y. G. P., Godoy-Alcantar, C., Lopez-Cardoso, M. & Morales-Rojas, H., 2009. Diorganotin(IV) dithiocarbamate complexes as chromogenic sensors of anion binding. *Polyhedron* 28: 3953-3966.
21. Singh, N. & Bhattacharya, S. 2012. Synthesis and characterization of some triorgano, diorgano, monoorganotinand a triorganolead heteroaromatic dithiocarbamate complexes. *Journal of Organometallic Chemistry* 700: 69–77.
22. Ajibade, P. A., Idemudia, O. G., Okoh, A. I. 2013. Synthesis, characteriazation, and antibacterial studies of metal complexes of sulfadiazine with N-alkyl-N phenyldithiocarbamate. *Bulletin of the Chemical Society of Ethiopia* 27(1): 77-84.
23. Hania, M. M. 2009. Synthesis and Antibacterial Activity of Some Transition Metal Complexes of Oxime, Semicarbazone and Phenyldrazone. *E-Journal of Chemistry* 6:508-514.

The Malaysian Journal of ANALYTICAL SCIENCES ISSN 1394-2506

# DAUN *HIBISCUS ROSA SINENSIS*: ANALISIS PROKSIMAT, AKTIVITI ANTIOKSIDAN DAN KANDUNGAN BAHAN INORGANIK

## (*Hibiscus rosa sinensis Leaves*: Analysis of Proximate, Antioxidant Activities and Inorganic Compound)

Saiful Irwan Zubairi* & Nurul Shahreda Jaies

*Pusat Pengajian Sains Kimia & Teknologi Makanan,*
*Fakulti Sains & Teknologi,*
*Universiti Kebangsaan Malaysia, 43600 UKM Bangi, Selangor, Malaysia*

**Corresponding author: saiful-z@ukm.edu.my*

**Abstrak**

Sehingga kini, pelbagai spesies tumbuh-tumbuhan herba banyak digunakan di dalam perubatan tradisional. Kebanyakan tumbuh-tumbuhan ini mempunyai bahan bio-aktif dan kandungan nutrisi yang berpotensi untuk memberikan kesan kesihatan yang positif seperti antioksidan dan antipiretik. Bunga raya atau nama saintifiknya, *Hibiscus rosa sinensis*, dikatakan mempunyai khasiat seperti teh kerana mengandungi bahan antioksidan yang dapat membantu mengawal kolesterol. Di samping itu, lendir yang terdapat di dalam daunnya boleh menurunkan suhu badan melampau ketika demam panas (berpotensi sebagai bahan antipiretik). Oleh yang demikian, kajian awalan terhadap daun *H. rosa sinensis* segar dan kering dijalankan bagi menganalisis dan mengenalpasti kandungan nutrisi penting, aktiviti antioksidan dan kandungan bahan inorganik. Kaedah penentuan kandungan jumlah fenolik (TPC) digunakan bagi sampel daun segar dan kering sebelum aktiviti antioksidan penangkapan radikal bebas DPPH dan kuasa penurunan ion ferik (FRAP) dijalankan bagi tujuan pengesahan komponen antioksidan. Manakala, komposisi logam berat dikaji menggunakan kaedah spektrometri jisim plasma berpeningkatan berganda (ICP-MS). Keputusan analisis proksimat daun segar menunjukkan terdapatnya kandungan lembapan (9.03%), protein (10.44%), lemak (6.43%), serat kasar (11.55%), abu (11.22%) dan karbohidrat (51.33%). Manakala, kandungan bahan inorganik adalah seperti berikut: kadmium (Cd), kromium (Cr), arsenik (As), nikel (Ni), plumbum (Pb), ferum (Fe) dan zink (Zn). Selain daripada itu, analisis antioksidan menunjukkan daun kering *H. rosa sinensis* mempunyai nilai DPPH dan FRAP yang tinggi berbanding daun segar ($p$<0.05) bagi pelarut aseton dan air. Nilai korelasi positif yang tinggi di antara analisis TPC dan dua ujian aktiviti antioksidan FRAP dan DPPH ($p$<0.05) menunjukkan kewujudan komponen penting antioksidan di dalam hasil ekstrak aseton dan air. Secara keseluruhan, kebolehdapatan komponen nutrisi penting, bahan antioksidan yang tinggi dan kepekatan bahan inorganik berbahaya yang rendah di dalam daun *H. rosa sinensis* membolehkan ia berpotensi besar di dalam pembangunan produk perubatan semulajadi bagi merawat demam panas (piretik).

**Kata kunci**: *Hibiscus rosa sinensis*, proksimat, antioksidan, komponen nutrisi penting, bahan inorganik

**Abstract**

A variety of herbal plants species has been used in traditional medicine. Most of these plants contained several potent bio-active ingredients and nutrients that could give potential positive effects to the health such as antioxidant and antipyretic. *Hibiscus rosa sinensis*, commonly known as *Bunga raya*, have similar concoction characteristic to tea which contain antioxidants that help to control cholesterol. In addition, mucilage that was found in the leaves could helps to reduce extreme body heat during fever (which potentially acts as an antipyretic). Therefore, this preliminary study on the fresh and dried *H. rosa sinensis* leaves was carried out to analyze and identify the nutrients content, anti-oxidants and inorganic material. Total phenolic content (TPC) method was used for both fresh and dried leaves prior to the antioxidant activities of DPPH free radicals scavenging and ferric ion reducing antioxidant power (FRAP) as to confirm the existence of antioxidant constituents. Meanwhile, the composition of heavy metals was studied using ***inductively coupled plasma mass spectrometry*** (ICP-MS). The proximate analysis of the fresh leaves showed the presence of moisture content (9.03%), protein (10.44%), fat (6.43%), crude fiber (11.55%), ash (11.22%) and carbohydrate (51.33%). Meanwhile, the inorganic contents are as follows: cadmium (Cd), chromium (Cr), arsenic (As), nickel (Ni), lead (Pb), iron (Fe) and zinc (Zn). Furthermore, the antioxidant activities of FRAP and DPPH showed that dried leaves of *H. rosa sinensis* was higher than the fresh leaves ($p$<0.05) irrespective of any solvent used. The positive

correlation between TPC and two other antioxidant activities of DPPH and FRAP ($p$<0.05) indicates the presence of antioxidant components in the acetone and water extracts. Therefore, the high availability of essential nutritional component, anti-oxidants and low concentration of hazardous inorganic matter in *H. rosa sinensis* leaves enable it to be used as one of the potential natural products to treat high fever (pyretic).

**Keywords**: *Hibiscus rosa sinensis*, proximate, antioxidant, essential nutrient component, inorganic materials

## Pengenalan

Bunga raya atau nama saintifiknya *Hibiscus rosa sinensis* dikenali di antara tumbuhan yang mempunyai pelbagai khasiat dan telah digunakan di dalam perubatan tradisional untuk mengubati pelbagai penyakit di samping ketidakbolehupayaan kesihatan seperti demam panas. Bunga ini juga dikenali dengan pelbagai nama seperti *Japa* dalam bahasa Sanskrit, *Jasum* (Hindi), *Jaba* (Bengali), *Chinese Hibiscus* (English) dan sebagainya [1]. *Hibiscus rosa sinensis* didapati berasal daripada keluarga *Malvaceae* dan ia ditanam secara meluas sebagai tumbuhan hiasan di negara beriklim tropika dan subtropika Asia Timur, serta mempunyai pelbagai bentuk, saiz dan warna dengan sekurang-kurangnya 250 jenis spesis yang berbeza [2]. Tumbuhan hijau berbunga ini bersifat malar dan renek dengan ketinggian sekurang-kurangnya 5-8 kaki [1]. Ia juga merupakan sejenis tumbuhan renek berkayu dan sesuai ditanam atau tumbuh di tanah yang teduh dan bersifat sederhana berasid [3]. Semua bahagian tumbuhan ini seperti akar, daun, batang dan bunga mempunyai khasiat teraputik yang tersendiri [1].

Disebabkan ianya begitu mudah diperolehi, pelbagai kegunaan secara penyediaan tradisional telah dilakukan sejak turun temurun [1]. Sebagai ubatan tradisional, jus daun *H. rosa sinensis* segar kerap digunakan untuk merawat gonorea manakala serbuk akar dan air rendaman kelopak bunganya digunakan untuk merawat *menorrhagia* (haid dengan pendarahan berat) dan minuman penyejuk badan untuk demam panas [4, 5]. Selain daripada itu, hasil ekstrak daun *H. rosa sinensis* mempunyai potensi sebagai pembunuh sel kanser diperingkat awalan pembentukan sesuatu sel tumor [6]. Potensi tersebut diperkukuhkan lagi dengan kewujudan beberapa sebatian biologi aktif (seperti sterol tumbuhan) penting yang bertindak sebagai agen antioksidan, pelindung kardio dan pengawal kepada tekanan darah tinggi (kategori pra-hipertensi dan hipertensi sederhana) [6, 7, 8]. Oleh yang demikian, tumbuhan ini dilihat mampu menjadi salah satu sumber tumbuhan herba semula jadi berpotensi tinggi untuk pembangunan ubat-ubatan baru dan ianya berpotensi menyediakan kesan efektif dalam merawat kanser [6] dan penyakit-penyakit bawaan bakteria [5].

Sebagai tambahan, apa yang lebih menarik berkenaan dengan tumbuhan ini adalah daunnya yang berlendir mempunyai bahan bioaktif yang dapat menurunkan suhu badan ketika demam panas (antipiretik). Beberapa bahan bioaktif utama yang terdapat di dalam lendir dan hasil ekstraknya seperti β-sitosterol (sterol tumbuhan semula jadi dan mempunyai struktur yang hampir sama dengan kolesterol), stigmasterol, asetat taraxeril dan tiga sebatian saiklopropan yang bersifat surfaktan turut memberi kesan yang efektif dalam penurunan suhu badan yang tinggi [9, 10, 11]. Oleh yang demikian, kajian ini dilakukan untuk mengetahui secara terperinci kandungan proksimat (perbandingan dilakukan dengan beberapa tumbuhan (Rajah 1) yang mempunyai ciri-ciri aktiviti biologi antipiretik yang sama), tahap keupayaan aktiviti antioksidan dan komposisi kepekatan bahan inorganik berbahaya yang mungkin wujud di dalam daun *H. rosa sinensis* segar dan kering. Hasil analisis kajian ini dilihat penting dalam memberikan gambaran secara holistik tentang potensi besar kandungan nutrisi dan bahan bioaktif penting yang dilihat boleh dijadikan sebagai perubatan alternatif kepada *paracetamol* di dalam menurunkan suhu akibat demam panas.




Rajah 1. Daun-daun tumbuhan yang mempunyai ciri-ciri aktiviti biologi antipiretik yang sama dengan daun *H. rosa sinensis*. (a) *H. rosa sinensis*, (b) *Hypericum perforatum*, (c) *Moringa oleifera* dan (d) *Verbena officinalis.*

## Bahan dan Kaedah

### Pengumpulan daun

Daun *H. rosa sinensis* segar diperolehi di Hutan Pendidikan Alam (HPA) kampus Universiti Kebangsaan Malaysia (UKM), Bangi, Selangor. Hanya satu lokasi dipilih bagi mengurangkan ralat dalam analisis komponen hasil ekstrak. Penetapan spesis dijalankan dengan menggunakan kaedah visual dan kemudiannya dibandingkan dengan ciri-ciri morfologi daun *H. rosa sinensis* sepertimana yang dilaporkan di dalam kajian Nwachukwu dan Mbagwu (2008) [2].

### Penyediaan sampel

Sebanyak 100 g daun *H. rosa sinensis* segar yang telah dibasuh dimasukkan ke dalam oven untuk pengeringan pada 60 °C selama 6 jam (sampel segar tidak melalui proses pengeringan di dalam oven dan ia dikeringkan menggunakan suhu bilik). Daun yang telah kering dikisar dengan menggunakan pengisar *Waring Commercial Blender* bagi penyediaan dalam bentuk seratan halus. Seratan daun halus kering dan segar seterusnya dimasukkan ke dalam botol universal dan di simpan di dalam bilik sejuk (15 $^{o}$C) sebelum analisis jumlah kandungan fenolik dan aktiviti antioksidan.

### Analisis proksimat

Kaedah piawaian AOAC (1990) [12] digunakan untuk menentukan kandungan nutrisi penting yang terdapat di dalam sampel daun *H. rosa sinensis* segar. Kandungan lembapan (basis basah) bagi daun segar yang dikisar halus ditentukan dengan menggunakan pengeringan ketuhar (*Thermo Scientific Heratherm GP*) pada suhu 105 °C selama 24 jam atau sehingga tiada perubahan berat (mg) berlaku. Kandungan lemak ditentukan dengan menggunakan

pengekstrakan berterusan *soxhlet*. Pelarut organik heksana digunakan di dalam proses pengekstrakan tersebut. Manakala, kandungan abu pula ditentukan dengan memasukkan sampel daun ke dalam relau pada suhu 550 °C dan kandungan serat kasar ditentukan dengan melalui proses penghadaman panas berurutan dengan larutan asid dan alkali yang dicairkan. Kandungan karbohidrat ditentukan secara teori iaitu dengan menggunakan kaedah perbezaan bagi semua jumlah komponen-komponen nutrisi penting seperti di dalam persamaan (1):

$$\text{Kandungan karbohidrat (\%)} = 100 - (\text{Jumlah kandungan protein + lemak + air + abu + serat kasar}) \quad (1)$$

**Proses pengekstrakan**

Sebanyak 1 g seratan halus kering dan segar daun *H. rosa sinensis* ditimbang dan dimasukkan ke dalam botol universal yang mengandungi 10 ml pelarut organik aseton dan air suling sebelum proses pengekstrakan celuran normal (*normal soaking extraction*) dijalankan pada suhu 30 ± 2 $^{o}$C selama 1 jam. Hasil ekstrak yang telah ditapis, diperah, diempar (10 minit masa pengemparan pada kelajuan 1000 rpm) dan disimpan di dalam peti sejuk pada suhu 4 $^{o}$C sebelum analisis kandungan fenolik dan aktiviti antioksidan dijalankan [36].

**Penentuan jumlah kandungan fenolik (TPC)**

Prosedur analisis Musa et al. (2011) [13] digunakan bagi menentukan jumlah kandungan fenolik di dalam sampel sebelum aktiviti antioksidan dijalankan. Penentuan aktiviti antioksidan menggunakan TPC dimulakan dengan penambahan 100 µl sampel hasil ekstrak segar dan kering ke dalam larutan khas yang mengandungi 0.4 ml air suling dan 0.5 ml reagen *Folin-Ciocalteu*. Larutan tersebut dibiarkan selama 5 minit. Kemudian, 1 ml 7.5% sodium karbonat ditambah kepada larutan tersebut disimpan selama 2 jam. Nilai bacaan *absorbance* (abs) diambil dengan menggunakan spektrofotometer sinar tampak (UV-Vis) pada nilai panjang gelombang 765 nm. Pembacaan *absorbance* dilakukan sebanyak 3 kali bagi mendapatkan purata nilai bacaan ± sisihan piawai ($n$ = 3).

**Aktiviti antioksidan**

Aktiviti antioksidan dijalankan dengan menggunakan sampel ekstrak air dan aseton setelah penentuan jumlah kandungan fenolik (TPC) memberikan nilai bacaan fenolik positif. Pelarut aseton digunapakai kerana hasil ekstrak yang menggunakan pelarut tersebut terbukit menghasilkan tahap aktiviti antioksidan tertinggi [34]. Nilai aktiviti antioksidan pelarut aseton dijadikan sebagai *benchmark* kepada hasil ekstrak yang menggunakan pelarut air. Dua ujian antioksidan tersebut adalah pemerangkapan radikal bebas DPPH dan kuasa penurunan ion ferik (FRAP) berdasarkan kepada prosedur Musa et al. (2011) [13]. Prosedur dua ujian aktiviti antioksidan adalah seperti berikut:

**Pemerangkapan radikal bebas DPPH**

Larutan stok disediakan dengan penambahan 40 mg 2,2-diphenyl-1-picrylhydrazyl (DPPH) ke dalam 100 ml metanol dan disimpan pada suhu -20 °C. Sebanyak 350 ml larutan stok ditambah kepada 350 ml metanol untuk memastikan nilai bacaan *absorbance* berada diantara 0.70 ± 0.01 unit pada panjang gelombang 516 nm. Pembacaan *absorbance* dilakukan sebanyak 3 kali bagi mendapatkan purata nilai bacaan ± sisihan piawai ($n$ = 3). Campuran 100 µl sampel dan 1 ml metanolik DPPH disediakan dan disimpan semalaman di dalam ruang gelap. Nilai aktiviti pemerangkapan radikal bebas (%) dikira mengikut formula persamaan 2 berikut:

$$\text{\% Aktiviti pemerangkapan radikal bebas} = \frac{(\text{Daya serapan awal} - \text{Daya serapan sampel})}{\text{Daya serapan awal}} \times 100\% \quad (2)$$

**Kuasa penurunan ion ferik (FRAP)**

Reagen FRAP disediakan dengan penyediaan 300 mM penimbal asetat, pH 3.6 (3.1 g sodium asetat trihidrat) ditambah ke dalam 16 ml asid glasial dengan nisbah pencampuran air suling 1:1) + 10 mM TPTZ (2,4,6-tris-2-pyridyl)-striazine) + 40 mM HCl + 20 mM $FeCl_3 \cdot 6H_2O$ mengikut nisbah 10:1:1. Sebanyak 100 µl hasil ekstrak dicampur bersama 1 ml reagen FRAP dan disimpan selama 30 minit sebelum bacaan *absorbance* (abs) diambil pada panjang gelombang 595 nm. Pembacaan *absorbance* dilakukan sebanyak 3 kali bagi mendapatkan purata nilai bacaan ± sisihan piawai ($n$ = 3).

**Penentuan kandungan bahan inorganik**

Radas kaca yang digunakan dalam penentuan kandungan bahan inorganik direndam semalaman di dalam larutan asid nitrik 5% (v/v) dan dikeringkan di dalam relau. Kaedah piawaian AOAC (1990) [12] digunakan bagi analisis ini. Pengekstrakan daun *H. rosa sinensis* segar dilakukan dengan menggunakan kaedah penghadaman berasid. Sebanyak 2 g sampel yang telah dikeringkan (setelah dibasuh) dimasukkan ke dalam kelalang kon berserta dengan 25 ml larutan 65% (v/v) asid nitrik pekat. Campuran tersebut dipanaskan di atas kukus pasir pada suhu 120 $^{o}$C sehingga wasap perang asid nitrik tersejat. Kemudian, 15 ml larutan 70% (v/v) asid perklorik ditambahkan dan dipanaskan sehingga warna kuning jernih terhasil. Larutan tersebut disejukkan pada suhu bilik dan kemudian dituras dengan kertas turas Whatman No. 6. Hasil turasan tersebut dicairkan dengan air suling sehingga ke paras 50 ml. Akhir sekali, 1 ml hasil turasan yang telah dicairkan digunakan bagi analisis logam berat menggunakan instrumentasi spektrometri jisim plasma berpeningkatan berganda (ICP-MS). Analisis kandungan dilakukan sebanyak 3 kali bagi mendapatkan purata nilai bacaan ± sisihan piawai ($n$ = 3).

**Analisis statistik**

Kesemua data hasil ujikaji dianalisa dengan menggunakan perisian MINITAB versi 16.0. Ujian T-tak bersandar atau '*Student T-test'* dijalankan pada aras kebarangkalian signifikan 95% ($p$<0.05) bagi penentuan perbezaan signifikan di antara sampel.

## Keputusan dan Perbincangan

**Kandungan proksimat**

Kebanyakan tumbuh-tumbuhan herba mempunyai potensi untuk dijadikan sebagai sumber makanan berkhasiat dan juga untuk kegunaan perubatan. Kandungan nutrisi tertentu yang disintesis semasa metabolik primer seperti karbohidrat dan lemak banyak memainkan peranan yang penting dalam penghasilan bahan bioaktif fitokimia yang berkualiti dan berfungsi pada peringkat metabolik sekunder. Oleh yang demikian, bagi menentukan kandungan nutrisi utama sesuatu tumbuhan, analisis kandungan proksimat perlu dilakukan. Bahagian yang dianalisa adalah daun *H. rosa sinensis* segar. Sehingga kini, tiada analisa awalan diperolehi dalam menentukan komposisi nutrisi yang terdapat di dalam daun *H. rosa sinensis*. Kebanyakan analisa kandungan proksimat yang dijalankan bagi tumbuhan ini hanya tertumpu kepada bahagian akar, benih dan kelopak bunganya. Oleh yang demikian, analisis komposisi nutrisi penting yang terdapat di dalam daun *H. rosa sinensis* dijalankan dan perbandingan secara tidak langsung komposisi nutrisi penting di antara tumbuh-tumbuhan lain yang dikatakan mempunyai ciri-ciri antipiretik (secara penyediaan tradisional) yang sama ditunjukkan di dalam Jadual 1.

Jadual 1. Komposisi kandungan nutrisi penting (%) bagi daun segar *H. rosa sinensis*, *Moringa oleifera*, *Hypericum perforatum* dan *Verbena officinalis*.

| **Komposisi kandungan (%)** | ***Hibiscus rosa sinensis*** | ***Moringa oleifera*[a]** | ***Hypericum perforatum*[b]** | ***Verbena officinalis*[c]** |
|---|---|---|---|---|
| Lembapan | 9.00 ± 0.04 | 3.21 ± 0.10 | 8.31 ± 0.06 | 6.82 ± 0.09 |
| Protein | 10.44 ± 0.32 | 17.01 ± 0.10 | 9.54 ± 0.16 | 4.39 ± 0.09 |
| Lemak | 6.43 ± 0.03 | 2.11 ± 0.11 | 5.06 ± 0.08 | 4.14 ± 0.09 |
| Serat kasar | 11.55 ± 0.26 | 7.09 ± 0.11 | 13.0 ± 0.00 | 16.78 ± 0.09 |
| Abu | 11.22 ± 0.26 | 7.93 ± 0.12 | 4.54 ± 0.014 | 17.10 ± 0.08 |
| Karbohidrat | 51.33 ± 0.25 | 63.11 ± 0.09 | 72.2 ± 0.09 | 67.52 ± 0.07 |

a - c: Komposisi kandungan nutrisi tumbuhan yang mempunyai ciri-ciri aktiviti biologi antipiretik [14, 15].

Tumbuhan ini digunakan dalam penyediaan ubatan trandisional. Tiada kajian saintifik diperolehi berkenaan dengan aktiviti antipiretik. Tiada analisis statistik dijalankan kerana nilai yang diperolehi bukan daripada data mentah

kajian. Sebagai permulaan, analisis kandungan kelembapan daun *H. rosa sinensis* menunjukkan tahap kelembapan yang tinggi (9.00 ± 0.04%) berbanding daun *Moringa oleifera*, *Hypericum perforatum* dan *Verbena officinalis*. Perbezaan nilai kelembapan dilihat boleh berpunca dari lokasi pensampelan daun *H. rosa sinensis* di dalam kawasan hutan yang agak lembap. Di samping itu, jenis-jenis tanah (laterit, gambut dan berpasir) dan suhu persekitaran turut mempengaruhi kandungan komposisi nutrisi sesuatu tumbuhan kerana keadaan yang lembap dan suhu yang tinggi menyebabkan banyak air yang diserap oleh tumbuhan. Kelembapan yang berlebihan berpotensi menyebabkan kebolehdapatan kandungan nutrisi penting yang rendah [16].

Seterusnya, kaedah Kjehldal digunakan dalam penentuan kandungan protein yang terdapat di dalam daun *H. rosa sinensis.* Molekul protein terbentuk daripada atom karbon (C), hidrogen (H), oksigen (O), nitrogen (N) dan kemungkinan sulfur (S). Untuk menentukan kandungan protein di dalam sesuatu tumbuhan, nilai nitrogen akan didarabkan dengan faktor penukaran iaitu 6.25. Teknik ini mengandaikan bahawa semua nitrogen berasal daripada sumber protein [14]. Kandungan protein yang terdapat di dalam daun *H. rosa sinensis* adalah lebih tinggi (10.44 ± 0.32%) berbanding daun *Hypericum perforatum* dan *Verbena officinalis* dan rendah berbanding daun *Moringa oleifera*. Perbezaan kandungan protein dalam sesuatu tumbuhan amat dipengaruhi oleh kandungan nutrisi tanah dan air. Penggunaan baja dan lokasi tanah yang kaya dengan sumber nitrogen (N) dan sulfur (S) boleh mempengaruhi kandungan protein tumbuhan [17]. Perkara ini disokong oleh kajian Zhang et al. (2002) [18] di mana variasi alam sekitar seperti lokasi dan perubahan musim secara mendadak boleh mempengaruhi kandungan protein sesuatu tumbuhan.

Kaedah pengekstrakan *soxhlet* digunapakai dalam penentuan kandungan lemak. Di dalam kajian ini, didapati daun *H. rosa sinensis* mempunyai lemak yang tinggi iaitu 6.43 ± 0.03% berbanding daun-daun yang lain. Data analisis lemak adalah di antara data yang terpenting dalam kajian ini. Ia menggambarkan kewujudan secara tidak langsung bahan bioaktif utama iaitu β-sitosterol di dalam sampel daun *H. rosa sinensis.* Bahan bioaktif tersebut dilihat berkait rapat dengan kandungan lemak yang diperolehi dan ianya disifatkan sebagai agen utama aktiviti biologi positif seperti antipiretik, antioksidan dan antikanser. β-sitosterol dikatakan mempunyai persamaan seperti komponen kolesterol yang mana mempunyai ciri-ciri antioksidan pemerangkap radikal bebas dan mampu mengawal pertumbuhan sel-sel kanser. Menurut Awad et al. (2001) [19], fitosterol iaitu β-sitosterol ialah lemak yang banyak terdapat di dalam diet vegetarian di mana ia berupaya meningkatkan sistem isyarat intrasel sel-sel kanser supaya tidak membahagikan sel kanser secara berterusan dan seterusnya mengawal proses pembahagian sel tersebut.

Seterusnya adalah analisis kandungan abu. Abu dikenali sebagai zat tidak organik yang tidak terbakar manakala bahan-bahan organik yang melalui proses pembakaran akan terbebas menjadi gas karbon dioksida dan air [20]. Kandungan abu yang tinggi di dalam sesuatu sampel akan menunjukkan kehadiran jumlah nutrisi tidak organik yang tinggi [21]. Terdapat dua jenis kaedah yang boleh digunakan dalam penentuan abu pada sesuatu sampel makanan iaitu pengabuan kering yang memang dikhaskan untuk analisis proksimat dan pengabuan basah yang digunakan untuk penyediaan dalam penentuan mineral. Dalam kajian ini, pengabuan kering digunakan dan kandungan abu yang terdapat di dalam daun *H. rosa sinensis* adalah 11.22 ± 0.26% lebih tinggi berbanding daun *Moringa oleifera* dan *Hypericum perforatum*. Data ini juga menjelaskan perkaitan penting kandungan keseluruhan bahan inorganik (kandungan abu) dengan keputusan analisis komposisi kandungan bahan inorganik yang terdapat di dalam ekstrak daun *H. rosa sinensis*. Kewujudan beberapa bahan inorganik penting (Jadual 5) di dalam daun *H. rosa sinensis* menggambarkan kebolehupayaan bahan tersebut secara tidak langsung dalam membantu mempertingkat dan meregulasi proses penghasilan produk metabolik sekunder penting antaranya seperti β-sitosterol [35].

Analisis kandungan proksimat terakhir adalah karbohidrat. Ia dikira secara teori berdasarkan kepada persamaan (1) setelah ke semua kandungan komponen nutrisi penting yang lain (kandungan abu, lembapan, protein, lemak dan serat kasar) dikira. Keputusan menunjukkan bahawa kandungan karbohidrat di dalam daun *H. rosa sinensis* dan beberapa tumbuhan yang lain adalah melebihi 50% daripada kandungan keseluruhan nutrisi yang dicerap. Kandungan tersebut menunjukkan keupayaan daun *H. rosa sinensis* dan tumbuhan yang lain dalam menyediakan substrat berkarbon tinggi (hasil metabolisma primer) bagi penghasilan bahan-bahan fitokimia penting yang tinggi untuk proses metabolisma produk sekunder [20].

Secara keseluruhan, walaupun daun *H. rosa sinensis*, *Moringa oleifera*, *Verbena officinalis* dan *Hypericum perforatum* mempunyai karakteristik antipiretik yang sama dan kaya dengan bahan bioaktif antioksidan, analisis proksimat menunjukkan terdapatnya perbezaan yang kecil di antara setiap peratusan komposisi nutrisi yang dinilai. Perkara ini mungkin disebabkan oleh daya penyerapan nutrisi daripada komposisi tanah yang pelbagai (berbaja, kandungan mineral tinggi, tahap pencemaran dan kelembapan tanah) dan kebolehupayaan metabolisma bagi tumbuhan berlainan spesis [15]. Walaubagaimanapun, kesemua tumbuh-tumbuhan tersebut dilihat berpotensi besar dalam industri berasaskan produk herba dan ujikaji lanjutan dilihat perlu dilakukan bagi mendapatkan pula kandungan optimum bahan bioaktif yang kaya dengan sumber antioksidan dan antikanser.

**Jumlah kandungan fenolik (TPC)**

Sebatian fenolik di dalam sesuatu tumbuhan dikenali untuk bertindak sebagai pemerangkapan radikal bebas yang juga berkaitrapat dengan aktiviti antioksidan [22]. Jadual 2 menunjukkan kandungan keseluruhan fenolik yang terdapat di dalam ekstrak daun *H. rosa sinensis*. Analisis TPC mendapati daun bunga raya yang telah dikeringkan mengandungi jumlah kandungan fenolik yang tinggi ($p<0.05$) secara signifikan berbanding daun segar tanpa mengira penggunaan pelarut pengekstrakan aseton atau air suling. Oleh yang demikian, dengan adanya kewujudan bahan fenolik di dalam kedua-dua sampel daun tersebut, maka dua jenis aktiviti antioksidan penting iaitu DPPH dan FRAP boleh dijalankan bagi mengenalpasti keberkesanan hasil ekstrak tersebut.

Jadual 2. Jumlah kandungan fenolik di dalam daun *H. rosa sinensis.*

| Sampel | mg GAE/100 g (aseton)[a] | mg GAE/100 g (air suling)[a] |
|---|---|---|
| Daun segar | 526.15 ± 5.30 | 305.33 ± 8.08 |
| Daun kering | 1307.33 ± 3.06* | 921.67 ± 1.16* |

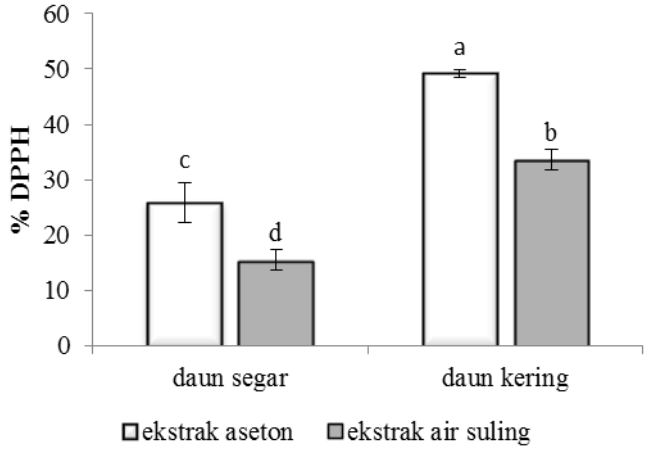
*$p<0.05$: Perbezaan signifikan di antara daun kering dan segar,
[a]Jumlah kandungan fenolik (TP) adalah sebagai mg *Gallic Acid Equivalents* (GAE)/100 g berat sampel.

**Aktiviti antioksidan**

Menurut Stoilova et al. (2007) [23], aktiviti antioksidan terhadap ekstrak tumbuhan yang mengandungi komponen polifenol adalah disebabkan oleh keupayaan mereka untuk menjadi penderma atom hidrogen atau elektron dan untuk menangkap radikal bebas. Radikal bebas adalah hasil sampingan yang sangat reaktif yang terhasil daripada proses kimia yang berlaku dalam badan. Bahan ini boleh memudaratkan serta merosakkan sel dan tisu badan. Oleh yang demikian, kaedah pemerangkapan radikal bebas (DPPH) dan kuasa penurunan ion ferik (FRAP) telah digunakan dalam penentuan aktiviti antioksidan bagi ekstrak daun *H. rosa sinensis*. Merujuk kepada Rajah 2, peratusan DPPH menggunakan ekstrak aseton dilihat lebih tinggi ($p<0.05$) secara signifikan berbanding ekstrak air suling tanpa mengira penggunaan daun segar atau kering. Pengekstrakan dengan menggunakan pelarut yang berbeza polariti dan ketumpatan dilihat mempengaruhi aktiviti penangkapan radikal bebas. Proses pengekstrakan yang menggunakan pelarut aseton menghasilkan kandungan fenolik yang tinggi ($p<0.05$) secara signifikan berbanding air suling (Jadual 2). Ini disebabkan oleh kecenderungan komponen fenolik untuk melarut di dalam pelarut organik yang mempunyai polarisasi yang sederhana (polariti 5.2 aseton) adalah tinggi berbanding pelarut yang mempunyai polariti yang tinggi (melebihi 6 pada skala polariti). Di samping itu, faktor kelikatan dan ketumpatan pelarut organik yang rendah turut membantu dalam memberikan daya resapan yang tinggi di mana pelarut tersebut lebih mudah meresap ke dalam liang-liang tumbuhan untuk mengeluarkan komponen bioaktif [24]. Aseton mempunyai ketumpatan yang rendah berbanding air iaitu 0.791 $gcm^{-3}$ dan ketumpatan air ialah 1 $gcm^{-3}$. Oleh yang demikian, nilai aktiviti antioksidan DPPH daripada proses pengekstrakan menggunakan aseton adalah terbukti lebih tinggi berbanding daripada pengekstrakan air suling.

Selain daripada itu, Jadual 3 menunjukkan penggunaan pelarut aseton bagi daun kering mempunyai aktiviti kuasa penurunan ion ferik yang tinggi secara signifikan ($p<0.05$) berbanding penggunaan air suling. Secara umumnya, kuasa penurunan ion ferik berkaitrapat dengan kehadiran sebatian yang bersifat *reductone* di mana ia berkeupayaan untuk menderma ion hidrogen (Shimada et al. 1992) [25]. Salah satu contoh sebatian tersebut adalah sebatian

fenolik. Kehadiran sebatian *reductone* ini akan menstabilkan radikal bebas dan menamatkan tindak balas rantaian radikal (antioksidan) [26]. Oleh yang demikian, kandungan sebatian fenolik yang terdapat di dalam kedua-dua jenis daun (kering dan basah) membuktikan akan keupayaan bahan tersebut dalam aktiviti antioksidan.




[a-d]: Abjad yang berbeza menunjukkan perbezaan yang signifikan ($p$<0.05) bagi setiap jenis daun.

Rajah 2. Aktiviti pemerangkapan radikal DPPH bagi ekstrak daun *H. rosa sinensis.*

Jadual 3. Kuasa penurunan ferik (FRAP) di dalam daun *H. rosa sinensis.*

| Sampel | mg TE/100 g (aseton)[a] | mg TE/100 g (air suling)[a] |
|---|---|---|
| Daun segar | 646.67 ± 5.0 | 310.56 ± 9.48 |
| Daun kering | 2322.22 ± 7.52* | 1690.01 ± 4.41* |

*$p$<0.05: Perbezaan signifikan di antara daun kering dan segar,
[a]Kapasiti antioksidan diukur melalui asai ORAC (*oxygen radical absorbance capacity*) sebagai mg *Trolox Equivalents* (TE)/100 g berat sampel.

**Korelasi di antara jumlah kandungan fenolik dan aktiviti antioksidan**

Jadual 4 menunjukkan kolerasi antara kandungan jumlah fenolik (TPC) dan dua aktiviti antipengoksida iaitu aktiviti pemerangkapan radikal DPPH dan kuasa penurunan ion ferik (FRAP). Analisis kolerasi menunjukkan jumlah kandungan fenolik mempunyai kolerasi positif yang tinggi secara signifikan dengan kedua-dua aktiviti antioksidan iaitu pemerangkapan radikal DPPH (r = 0.743, $p$<0.05) dan kuasa penurunan ion ferik (r = 0.546, $p$<0.05). Secara keseluruhannya, korelasi ini membuktikan bahawa semakin tinggi nilai TPC, semakin tinggi nilai aktiviti antioksidan bagi ekstrak daun *H. rosa sinensis.*

Jadual 4. Analisis korelasi antara jumlah kandungan fenolik dan aktiviti-aktiviti antioksidan.

| | TPC | DPPH | FRAP |
|---|---|---|---|
| TPC | 1.00 | +0.74 | +0.55 |
| DPPH | +0.74 | 1.00 | +0.71 |
| FRAP | +0.55 | +0.71 | 1.00 |

**Kandungan bahan inorganik**

Jadual 5 menunjukkan komposisi kandungan bahan inorganik yang terdapat di dalam ekstrak daun *H. rosa sinensis* segar dengan menggunakan kaedah spektrometri jisim plasma berpeningkatan berganda (ICP-MS). Menurut Berg (1997) [27], tumbuh-tumbuhan memerlukan sumber bahan inorganik penting seperti Cu, Fe, Mn dan Zn untuk tumbesarannya manakala kehadiran Cd dan Pb amat berpotensi menjadi toksik dan tidak baik untuk pertumbuhan.

Jadual 5. Komposisi kandungan bahan inorganik di dalam daun *H. rosa sinensis.*

| Bahan inorganik | Kandungan (mg/kg) |
|---|---|
| Cd | 0.002 ± 0.001 |
| Cr | 0.15 ± 0.01 |
| Pb | 0.04 ± 0.02 |
| As | 0.06 ± 0.01 |
| Ni | 0.06 ± 0.01 |
| Fe | 9.54 ± 1.29 |
| Zn | 0.85 ± 0.33 |

Kandungan bahan inorganik bertoksik seperti kadmium (Cd) di dalam sampel ekstrak adalah 0.002 ± 0.001 mg/kg iaitu jauh lebih rendah ($p$<0.05) secara signifikan berbanding jumlah kadmium yang dibenarkan oleh WHO/FAO iaitu 0.10 mg/kg. Manakala, kandungan kromium (Cr) pula adalah sebanyak 0.15 ± 0.01 mg/kg iaitu berada ditahap yang selamat mengikut piawaian yang ditetapkan oleh WHO (2007) [28] iaitu 1.30 mg/kg. Seterusnya, kandungan plumbum (Pb) (0.04 ± 0.02 mg/kg) dilihat rendah ($p$<0.05) secara signifikan berbanding had selamat WHO (2007) [28] iaitu 0.3 mg/kg. Bagi ujikaji ini, sampel daun *H. rosa sinensis* yang digunakan diperolehi dari kawasan pinggir hutan yang jauh daripada sumber pencemaran seperti di tapak pelupusan sampah. Pencemaran Pb pada tumbuh-tumbuhan boleh berpunca daripada bateri asid-plumbum yang mengalir masuk ke dalam sistem perparitan. Oleh yang demikian, penggunaan sebarang sampel tumbuh-tumbuhan bagi tujuan kajian perubatan (seperti pengambilan secara *oral*) perlulah terlebih dahulu memastikan persekitaran tumbuhan tersebut tidak terdedah kepada sebarang pencemaran. Bahagian tumbuhan (akar, daun dan batang), buah-buahan dan sayur-sayuran yang telah terdedah kepada pencemaran Pb tidak akan mudah dilhilangkan melalui teknik pembasuhan kerana ianya telah terkumpul dan sebati dalam kepekatan yang tinggi di dalam bahagian tersebut [29]. Seterusnya, kandungan arsenik (As) yang terdapat di dalam daun *H. rosa sinensis* (0.06 ± 0.01 mg/kg) adalah lebih rendah ($p$<0.05) secara signifikan berbanding kandungan piawaian yang ditetapkan oleh WHO (2007) [28] iaitu 1 mg/kg. Arsenik adalah bahan inorganik tidak penting untuk tumbesaran dan toksik kepada tumbuhan. Ia amat mudah terkumpul di bahagian daun dan buah-buahan sekiranya terdapatnya pencemaran arsenik [30]. Oleh yang demikian, kandungan arsenik yang terdapat di dalam daun *H. rosa sinensis* dilihat cukup selamat bagi sebarang penyediaan ubatan tradisional. Zat besi (Fe) merupakan mikronutrien yang diperlukan oleh tumbuhan dalam jumlah yang tinggi berbanding logam lain [31]. Ia merupakan unsur yang mudah larut dan ia cenderung untuk diserap oleh tumbuhan dalam kuantiti yang banyak [32]. Hasil ekstrak daun *H. rosa sinensis* menunjukkan kandungan zat besi yang tinggi (9.54 ± 1.29 mg/kg) ($p$<0.05) secara signifikan berbanding sumber mineral yang lain. Akhir sekali, kandungan zink (Zn) yang terdapat di dalam daun *H. rosa sinensis* adalah (0.85 ± 0.33 mg/kg) jauh di bawah tahap kandungan selamat ($p$<0.05) mengikut piawaian WHO (2007) [28] iaitu 99.4 mg/kg. Zink merupakan sumber mineral penting yang membantu dalam fungsi biologi seperti respon imuniti terhadap penyakit dan stimulan penting bagi enzim. Selain daripada itu, Zn juga dikenali dengan sifat antivirus, antibakteria, antikulat dan antikanser [33]. Oleh yang demikian, kewujudan mineral zink di dalam sampel ekstrak daun *H. rosa sinensis* menunjukkan potensi kebolehupayaan ekstrak tersebut dalam penggunaannya sebagai agen antipiretik, antikanser dan antioksidan.

**Kesimpulan**

Analisis komposisi proksimat di dalam daun *H. rosa sinensis* menunjukkan jumlah nutrisi penting yang tinggi seperti karbohidrat dan lemak. Kandungan komponen produk metabolik primer tersebut secara tidak langsung berkaitrapat dengan penghasilan bahan bio-aktif fitokimia penting (hasil daripada proses metabolik sekunder) yang mempunyai ciri-ciri aktiviti biologi positif seperti antioksidan dan antipiretik. Ini dibuktikan dengan jumlah kandungan fenolik (TPC) yang tinggi di dalam daun *H. rosa sinensis.* Oleh yang demikian, dua ujikaji aktiviti antioksidan DPPH dan FRAP turut dijalankan bagi membuat pembuktian lanjutan dan keputusan analisis menunjukkan aktiviti antipengoksida yang tinggi bagi kedua-dua ujikaji tersebut. Seterusnya, analisis korelasi di antara analisis TPC dan dua ujikaji antioksidan turut memperlihatkan korelasi positif yang tinggi di antara TPC dan FRAP dan DPPH di mana semakin tinggi nilai TPC, semakin tinggi aktiviti antioksidan sesuatu sampel. Di samping itu, komposisi kandungan bahan-bahan inorganik merbahaya seperti Cd, As dan Pb bagi hasil ekstrak daun *H. rosa sinensis* segar menunjukkan ia berada di paras yang selamat berdasarkan kepada piawaian yang ditetapkan oleh *World Health Organisation* (WHO). Oleh yang demikian, hasil ekstrak air daun *H. rosa sinensis* dilihat mempunyai potensi yang besar sebagai salah satu daripada sumber penghasilan produk perubatan tradisional alternatif bagi merawat demam panas sekiranya pengambilan dibuat secara *oral* dalam menurunkan suhu badan melampau dengan pantas. Demam panas dilihat mempunyai perkaitan dengan kesan respon badan terhadap jangkitan virus dan bakteria. Sehubungan dengan itu, kajian lanjut untuk menilai keberkesanan hasil ekstrak daun *H. rosa sinensis* terhadap respon mortaliti mikroorganisma virus/bakteria dan juga tahap penghasilan sel darah putih secara model tiga dimensi (3-D) *in vitro* perlu dilakukan. Ujikaji diperingkat klinikal juga dilihat penting bagi mengesan sebarang kesan sampingan jangka masa panjang (kronik) mahupun singkat (akut) akibat daripada penggunaan produk alternatif yang berasaskan ekstrak daun *H. rosa sinensis*.

**Rujukan**


1. Kumar, L., Chakraborthy, G., Singh, V. & Mazumder, A. (2012). *Hibiscus Rosa-Sinensis*: A review on divine herb. *Journal of Advances in Pharmacy and Healthcare Research* 2(4): 9-18.
2. Nwachukwu, C.U. & Mbagwu F.N. (2008). Anatomical features of the roots and leaves of *Hibiscus rosa sinensis* and abelmoschus esculenta. *Life Science Journal* 5(1): 68-71.
3. Sayed, Z.I.E., Ateya, A.-M.M. & Fekry, M. (2012). Macro- and micromorphological study of the leaf, stem, flower and root of *Hibiscus rosa-sinensis L. Journal of Applied Sciences Research* 8(1): 34-56.
4. Upadhyay, S. & Upadhyay, P. (2011). *Hibiscus rosa-sinensis*: pharmacological review. *International Journal of Research in Pharmaceutical and Biomedical Sciences.* 2(4): 1449-1450.
5. Soni, D. & Gupta, A. (2011). An evaluation of antipyretic and analgesic potentials of aqueous root extract of *Hibiscus rosa sinesis linn*. (malvacae). *International Journal of Research in Phytochemistry & Pharmacology* 1(3): 184-186.
6. Sharma, S. & Sultana, S. (2004). Effect of *Hibiscus rosa sinensis* extract on hyperproliferation and oxidative damage caused by benzoyl peroxide and ultraviolet radiations in mouse skin. *Basic & Clinical Pharmacology & Toxicology* 95(5): 220-225.
7. Ghaffar, F.R.A. & El-Elaimy, I.A. (2012). *In vitro*, antioxidant and scavenging activities of *Hibiscus rosa sinensis* crude extract. *Journal of Applied Pharmaceutical Science* 2(1): 51-58.
8. Diane, L.M., Oliver, C.C-Y., Edward, S. & Jeffrey, B.B. (2010). *Hibiscus Sabdariffa* L. tea (tisane) lowers blood pressure in prehypertensive and mildly hypertensive adults. *J. Nutr.* 140(2): 298-303.
9. Ye, J.C., Chang, W.C., Hsieh, D.J.Y. & Hsiao, M.W. (2010). Extraction and analysis of β-sitosterol in herbal medicines. *Journal of Medicinal Plants Research.* 4(7): 522-527.
10. Divya, K., Tripathi J.S., Tiwari S.K. (2013). Study of antiasthmatic properties and chemical characterization of indigenous ayurvedic compounds (polyherbal formulations). *American Journal of Phytomedicine and Clinical Therapeutics*. 6(1): 457-466.
11. Kumar, A.A.S. (2012). Review on *Hibiscus rosa sinensis. International Journal of Research in Pharmaceutical and Biomedical Sciences*. 3(2): p. 534-53.
12. AOAC (1990). Official Method of Analysis. 15th Edn. Arlington. Official Analytical Chemists.
13. Musa, K.H., Abdullah, A., Jusoh, K. & Subramaniam, V. (2011). Antioxidant activity of pink-flesh guava (*Psidium guajava* L.): effect of extraction techniques and solvents. *Food Analytical Methods* 4(1): 100-107.
14. Ogre, A.O. & John, P.A. (2011). Proximate study, mineral and anti nutrisi composition of*moringa oleifera* leaves harvested from lafia, Nigeria: potential benefits in poultry nutrition and health. *Journal of Microbiology,*

*Biotechnology and Food Sciences* 1(3): 296-308.
15. Hussain, J., Bahader, A., Ullah, F., Rehmen, N. U., Khan, A. L., Ullah, W. & Shinwari, Z. K. (2009). Proximate and nutrient analysis of the locally manufactured herbal medicines and its raw material. *Journal of American Science* 5(6): 1-5.
16. Champolivier, L. & Merrien, A. (1996). Effect of water stress applied at different growth stages to *Brassica napus* L. var Oleifera on yield components and seed quality. *Eur. J. Agron.* 5: 153-160.
17. Malik, A.H., Holm, L. & Johansson, E. (2012). Soil and starter fertilizer and its effect on yield and protein compositon of malting barley. *Journal of Soil Science and Plant Nutrition* 12(4): 835-849.
18. Zhang, G., Chen, J., Wang, J. & Ding, S. (2001). Cultivar and environmental effects on (1→3, 1→4)-β-d-glucan and protein content in malting barley. *J. Cereal Sci.* 34(3): 295-301.
19. Awad, A.B., Fink, C.S., Williams, H. & Kim, U. (2001). In vitro and in vivo (SCID mice) effects of phytosterols on the growth and dissemination of human prostate cancer PC-3 cells. *Eur J Cancer Prev.* 10(6): 507-13.
20. Vickery, M.L. & Vickery, B. (1981). Secondary plant metabolism. Macmillan Press: London.
21. Iqbal, A., Khalil, I. A., Ateeq, N. & Khan, M. S. (2006). Nutritional quality of important food legumes. *Food Chem.* 97: 331–335.
22. Skerget, M., Kotnik, P., Hadolin, M., Hras, A.R., Simonic, M. & Knez, Z. (2005). Phenols, proanthocyanides, flavones and flavonols in some plant materials and their antioxidant activities. *Food Chem*. 89: 191-198.
23. Stoilova, I., Krastanov, A., Stoyanova, A., Denev, P. and Gargova, S. (2007). Antioxidant activity of a ginger extracts (*Zingiber officinale*). *Food Chem.* 102: 764-770.
24. Naczk, M. & Shahidi, F. (2006). Phenolics in cereals, fruits and vegetables: occurrence, extraction and analysis. *J Pharm Biomed Anal* 41: 1523-1542.
25. Shimada K., Fujikawa K., Yahara K. & Nakamura T. (1992). Antioxidative properties of xanthone on the auto oxidation of soybean in cylcodextrin emulsion. *J. Agr. Food Chem.* 40: 945–948.
26. David, C. & Simon, V. (2009). Does high antioxidant capacity indicate low oxidative stress*?Functional Ecology*. 23(3): 506-509.
27. Berg, L.R. (1977). Introductory Botany: Plants, People and the Environment. New York: Saunders College Publishing.
28. WHO (2007). Health Risks of Heavy Metals from Long Range Transboundary Air Pollution. Germany: WHO Regional Office for Europe.
29. Itanna, F. (2002). Metals in leafy vegetables grown in Addis Ababa and toxicological implications. *Ethiop. I. Health Dev* 16(3): 295-302.
30. Garg, N. & Singla, P. (2011). Arsenic toxicity in crop plants: Physiological effects and tolerance mechanisms. *Environ. Chem. Lett.* 9: 303-321.
31. Hopkins, W.G. (1999). Introduction to Plant Physiology. New York: John Wiley & Sons.
32. Johnston, W.R. & Proctor, J. (1997). Metal concentrations in plants and soil from two British serpentine sites. *Plant Soil* 46: 275-286.
33. Moyo, B., Masika, P.J., Hugo, A. & Muchenje, V. (2011). Nutritional characterization of *Moringa* (*Moringa oleifera Lam*.) leaves. *Journal of Biotechnology*. 10(60): 12925-12933.
34. Zhao, H., Dong, J., Lu, J., Chen, J., Li, Y., Shan, L., Lin, Y., Fan, W. & Gu, G. (2006). Effects of extraction solvent mixtures on antioxidant activity evaluation and their extraction capacity and selectivity for free phenolic compounds in barley (*Hordeum vulgare* L.). *Journal of Agricultural and Food Chemistry* 54: 7277-7286.
35. Chunhong, Z., Qianquan, L., Muxin, Z., N, Z. & Minhui, L. (2013). Effects of rare earth elements on growth and metabolism of medicinal plants. *Acta Pharmaceutica Sinica B*. 3(1): 20-24.
36. Zubairi S.I., Suradi H., Mutalib S.A.A., Othman Z.S., Bustaman N. & Wan Musa W.R.M. 2014. Kajian Awalan Terhadap Kinetik Pengekstrakan Pepejal-Cecair dan Analisis Komponen Bio-Aktif Bagi Daun *Hibiscus rosa sinensis*. *The Malaysian Journal of Analytical Sciences.* 18(1): 43-57.

The Malaysian Journal of ANALYTICAL SCIENCES ISSN 1394-2506

# REMOVAL OF SELECTED HEAVY METALS FROM GREEN MUSSEL VIA CATALYTIC OXIDATION

## (Penyigkiran Logam-Logam Tertentu Daripada Kupang Melalui Pengoksidaan Bermangkin)

Faizuan Abdullah, Abdull Rahim Mohd Yusoff, Wan Azelee Wan Abu Bakar*, Razali Ismail, Dwi Priya Hadiyanto

*Department of Chemistry,*
*Faculty of Science,*
*Universiti Teknologi Malaysia,81310 UTM Johor Bahru, Johor Darul Ta'zim, Malaysia.*

**Corresponding author: wazelee@kimia.fs.utm.my*

**Abstract**

*Perna viridis* or green mussel is a potentially an important aquaculture product along the South Coast of Peninsular Malaysia especially Johor Straits. As the coastal population increases at tremendous rate, there was significant effect of land use changes on marine communities especially green mussel, as the heavy metals input to the coastal area also increase because of anthropogenic activities. Heavy metals content in the green mussel exceeded the Malaysian Food Regulations (1985) and EU Food Regulations (EC No: 1881/2006). Sampling was done at Johor Straits from Danga to Pendas coastal area for green mussel samples. This research introduces a catalytic oxidative technique for demetallisation in green mussel using edible oxidants such as peracetic acid (PAA) enhanced with alumina beads supported CuO, $Fe_2O_3$, and ZnO catalysts. The lethal dose of $LD_{50}$ to rats of PAA is 1540 mg $kg^{-1}$ was verified by National Institute of Safety and Health, United State of America. The best calcination temperature for the catalysts was at 1000 ºC as shown in the X-Ray Diffraction (XRD), Nitrogen Adsorption (BET surface area) and Field Emission Scanning Electron Microscopy (FESEM) analyses. The demetallisation process in green mussel was done successfully using only 100 $mgL^{-1}$ PAA and catalyzed with $Fe_2O_3/Al_2O_3$ for up to 90% mercury (Hg) removal. Using PAA with only 1 hour of reaction time, at room temperature (30-35ºC), pH 5-6 and salinity of 25-28 ppt, 90% lead (Pb) was removed from life mussel without catalyst. These findings have a great prospect for developing an efficient and practical method for post-harvesting heavy metals removal in green mussel.

**Keywords:** Green mussel **(***Perna viridis)*, heavy metals, catalytic oxidative demetallisation, peracetic acid

**Abstrak**

*Perna viridis* atau kupang adalah produk akuakultur penting dan berpotensi tinggi di selatan Semenanjung Malaysia terutama di Selat Johor. Akibat kepesatan peningkatan populasi manusia dan aktiviti pembangunan di sekitar selat tersebut, kesan signifikan yang berlaku menyebabkan hidupan marin terutama kupang turut tercemar dengan peningkatan kandungan logam berat. Kandungan logam tersebut telah melebihi had yang dibenarkan Peraturan Makanan Malaysia 1985 dan Peraturan Makanan Kesatuan Eropah (EU) (EC No:1881/2006). Pensampelan telah dilakukan di Selat Johor dari Teluk Danga hingga ke Pendas untuk sampel kupang. Kajian ini memperkenalkan teknik pengoksidaan bermangkin untuk penyingkiran logam dalam kupang menggunakan agen pengoksidaan yang selamat dimakan seperti asid perasetik (PAA) dimangkinkan oleh CuO, $Fe_2O_3$, dan ZnO yang disokong pada permukaan manik alumina ($Al_2O_3$). $LD_{50}$ utk PAA ialah 1540 $mgkg^{-1}$, telah disahkan Institut Keselamatan dan Kesihatan Kebangsaan (NIOSH) Amerika Syarikat. Bagi mangkin yang digunakan, suhu kalsinasi terbaik ialah pada suhu 1000 ºC seperti yang dibuktikan dengan analisa XRD, Analisis Penjerapan Nitrogen (keluasan permukaan BET) dan mikrograf FESEM. Proses penyingkiran logam dari kupang telah dilakukan dengan hanya menggunakan 100 $mgL^{-1}$ PAA dimangkinkan oleh $Fe_2O_3/Al_2O_3$ untuk penyingkiran hampir 90% merkuri (Hg), dan menggunakan PAA tanpa mangkin untuk penyingkiran hampir 90% plumbum (Pb) dengan masa tindakbalas hanya 1 jam, dalam suhu sekitar 30-35 ºC, pH 5-6 dan kemasinan air 25-28 ppt. Penemuan ini memberikan prospek yang sangat baik dalam membangunkan kaedah yang efisyen dan praktikal untuk menyingkirkan logam dari kupang yang masih hidup sebelum dipasarkan.

**Kata kunci:** Kupang (*Perna viridis*), logam berat, penyingkiran logam pengoksidaan bermangkin, asid perasitik

## Introduction

Asia productions of aquaculture give 90% of fisheries output compared with overall places [1]. The small and traditionally coastal aquaculture that has been practiced 500 years ago is being developed to the high commercial scale with intensive technologies and well-managed system especially in Southeast Asia. Among all sites, coastal aquaculture contributes 66-69% of production [2]. Anthropogenic activities such as effluents, marine and coastal developments, dredging, sewage discharge, oil slicks and spill form shipping activities, agricultural land runoff (fertilizers and pesticides), and climate changes are the prime sources of pollutions that affecting direct and indirectly the aquaculture development as the water quality reduce significantly [2-8]. Land use change for development via dredging activities considered as vital sources of water quality change and heavy metals enrichment in the Peninsular Malaysia coastal water, as the sediment with the secondary pollutants dredge up and mixed with the water body up to the surface, and accumulate pollutants such as heavy metals (Cd, Cu, Pb and Zn) to the fish and mollusk species green mussel [9].The spawning for cultural of this species are mainly from southern coast of Johor Strait, and currently being expanded up to Kedah because of mussel seeds transplantations [10].

*Perna viridis* (Linnaeus.) or green mussel are widely distributed in the Indo-Pacific coastal waters and also in the shallow waters along west coast of Peninsular Malaysia [10-13]. The coast comprises about 100,000 hectares contribute significantly the coastal productivity including green mussel. Green mussel is one of the mollusk species that is used around the world as an established bioindicator and biomonitoring agent for heavy metals as it is filter feeder type of organism [14]. It is also a commercially popular seafood species worldwide with easily found, and sampled [15-16]. Green mussel could grow up to 83 mm shell length in a year and its marketable size is 50-60 mm shell length, achievable for only approximately for 6 month. Besides, there are potential factors for reproduction, culture and growth of green mussel outside of its natural habitat [17]. Normally, the main food sources of green mussel are phytoplankton or algae such as Isochrysis galbana, Chaetocerus sp., and Pavlova sp. [18-19].

Studied had shown that lysosomal integrity directly affected by exposure of high concentration of copper [20], mercury [21] polyaromatic hydrocarbons (PAH) [22], low dissolve oxygen (DO) and high total ammoniacal-nitrogen (TAN) [23-24], and sudden temperature change and paraquat exposure[24]. Yap et al., 2002 reported that the concentration of heavy metals especially lead (Pb) in green mussel exceeding the permissible limits stated by Malaysian Food regulations (1985) and EU food regulations [9]. Demetallisation is a possible solution to reduce the excess or unneeded compounds. Table 1 shows maximum permissible limit by several regulations globally.

Table 1. Guidelines of maximum permissible limits of heavy metals (μg/g) in seafood from Different countries (Yap *et al*. 2004) [16]

| Location | Cd | Pb | Zn |
|---|---|---|---|
| Permissible limits by Malaysian Food Regulation (1985) | 1.00 | 2.00 | 100.0 |
| EU Food Regulations (EU) | 1.00 | 0.50 | - |
| International Council for the Exploration of the Sea (ICES, 1988) | | | |
| Maximum permissible levels established by Brazilian Ministry of Health (ABIA, 1991) | 5.00 | 10.0 | 250 |
| Permissible limit set by Ministry of Public Health, Thailand (MPHT, 1986) | - | 6.67 | 667 |
| Food and Drug Administration of the United State (USFDA, 1990) | 3.7 | 1.7 | - |
| Australian Legal Requirement (NHMRC, 1987) | 10.0 | - | 750 |
| Permissible limit set by the Hong Kong Environmental Protection Department (HK EPD, 1997) | 2.00 | 6.00 | - |

## Materials and Methods

### Sampling, Sample Preservations and Preparations

As shown in Figure 1, green mussel samples were collected along Johor Strait started from S1 (Sg. Danga Estuaries) to S11 (Pendas) for heavy metals (Pb and Hg) content analyzing. The present sampling session were conducted three times between January - November in 2011. The green mussel samples were collected and grouped according to size. Before the mussels been shucked, the external shell surface was thoroughly cleaned with a brush and water to remove all the sand and dirt adhering to the shell to prevent the contamination of composite samples. The mussels then thawed and shucked, and the flesh was collected in a clean dish and homogenized by mixing. The green mussels (2g) then were weighed and digested on a wet basis, using a modified reflux system by digesting the samples overnight on a hot plate. The digested samples were filtered and diluted using distilled deionized water (DDW) to ensure the acid in the samples less than 5%. The digestion method used was adopted from the American Public Health Association (APHA) 3030E, which was a nitric acid digestion method. In this study, only the heavy metals content of adult mussels (7 to 9 cm) was analyzed on a dry weight basis. The green mussel samples analyzed for baseline of heavy metals content, and for simulation test in heavy metals removal.

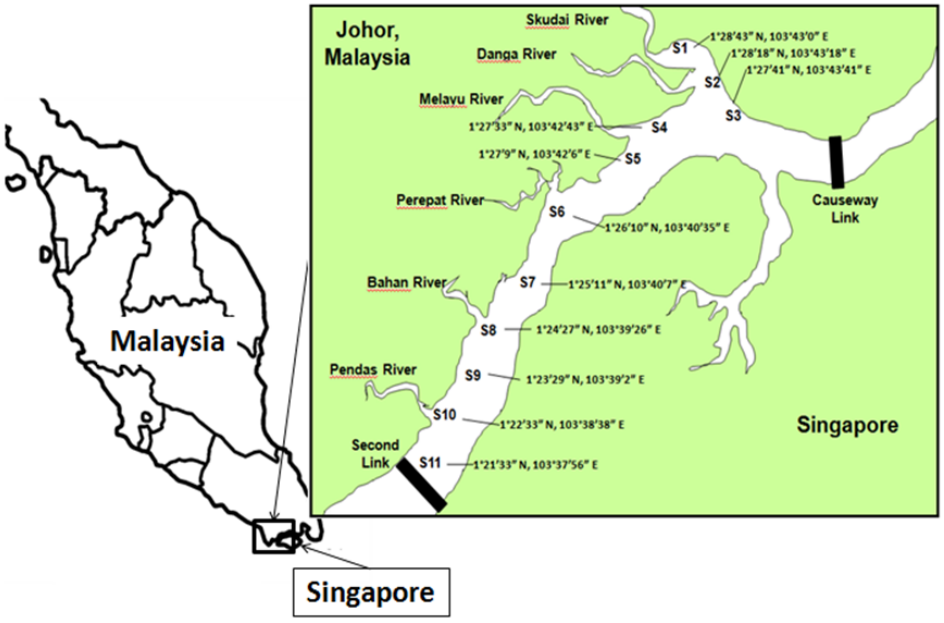



Figure 1. Sampling stations map (Johor Strait)

### Development of oxidants-catalyst combination

For this purpose, several combinations of oxidants and catalyst were studied for heavy metals removal. The oxidant that were used at this time for the simulation test using standards metals solutions and dead mussel flesh was peracetic acid (PAA). The preparation of PAA was via the mixture of acetic acid and hydrogen peroxide with the ratio of 1:1. The catalysts that were used for this stage were alumina supported catalyst (granular) for the single transition metals catalyst consisting 5M of CuO, ZnO and $Fe_2O_3$. These common alumina supported catalysts were prepared by using impregnation method, and calcined for three different temperatures for every metal, which were 900°C, 1000°C, and 1100°C for six hours. The characterization of these catalysts was done by XRD and FESEM.

### Demetallisation of heavy metals in green mussel

Pre-harvesting green mussels were collected at Johor Strait and were sustained for living in an aquarium laboratory scale. Mussels were fed twice for a day with *Chatocaerus sp.*, *Pavlova sp.*, and *Isochrysis sp*. The salinity of the

water in the aquarium was controlled for 25 to 28ppt using ultrapure sodium chloride salt, and the temperature was maintained at ambient scale which was 30 to 35°C, in pH 5-6 with continuously flowing water using water filter. The demetallisation of selected heavy metals that adsorbed in the mussel flesh removal using oxidation technique was done by using PAA with concentration of 100, 200, 300 and 500 mg $L^{-1}$ with and without catalyst. Mussel flesh were treated using this technique and the heavy metals content were analyzed using AAS for untreated samples as control and treated samples for comparison. For both type of mussel, the treatment process also done with five different times of treatment, with one hour interval.

**Instrumentation**

All the samples were analyzed using Perkin Elmer Atomic Absorption Spectrophotometer AAnalyst 400 (Flame) for heavy metals content. X-Ray Diffraction Scaterring system for catalyst diffractogram was done using X-RD Bruker model, nitrogen surface adsorption (BET surface area) using Micromeritics ASAP 2010 and micrographs of the catalyst was analyzed using FESEM-EDX Jeol 7600F model.

## Results and Discussion

**Baseline of Heavy Metals Concentration in Green Mussels**

Figure 2 describes the heavy metals content in green mussel flesh that has been analyzed from January to June 2011. The content of mercury varied from 0.343 to 0.988 mg L-1, 0.033 to 0.082 mg L-1 for arsenic, 0.028 to 0.517 mg L-1 for lead, 0.020 to 0.089 mg L-1for cadmium, and 0.058 to 0.103 mg L-1 for nickel. All the heavy metals concentration in water and green mussel were the preference baseline of the heavy metals removal study using the combinations of specific oxidants and catalysts.

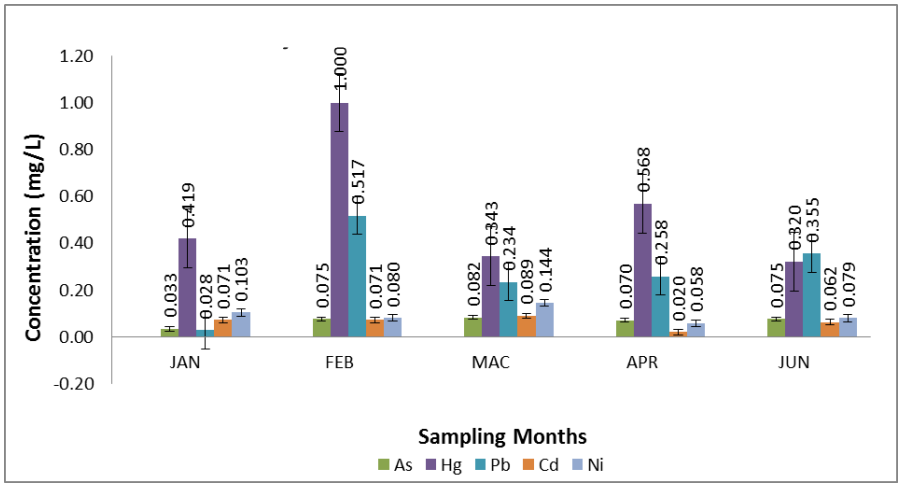



Figure 2. Heavy metals content in green mussel sample from January to June 2011

**Results for XRD Analysis of Alumina Supported Transition Metals Catalysts**

The X-Ray Diffraction (XRD) analysis was performed to all the alumina supported transition metals oxide catalysts in order to identify the crystalinity and particle size of the catalysts. The following diffractograms were used to be compared with the FESEM-EDX micrographs to implement the best calcination temperature for heat treatment in producing the best catalyst with smallest particle size for enhancing the heavy metals removal process. Three types of catalysts from transition metals group, supported with alumina were synthesized for the enhancement of peracetate ions productions, in order to increase the removal percentage of heavy metals from green mussel. These catalysts were prepared in laboratory scale includes copper, iron (III), and zinc using impregnation methods and calcined with three different temperatures which were 900 °C, 1000 °C, and 1100 °C in scientific laboratory furnace. Figures 3 to 5 described the characterization of the catalysts.

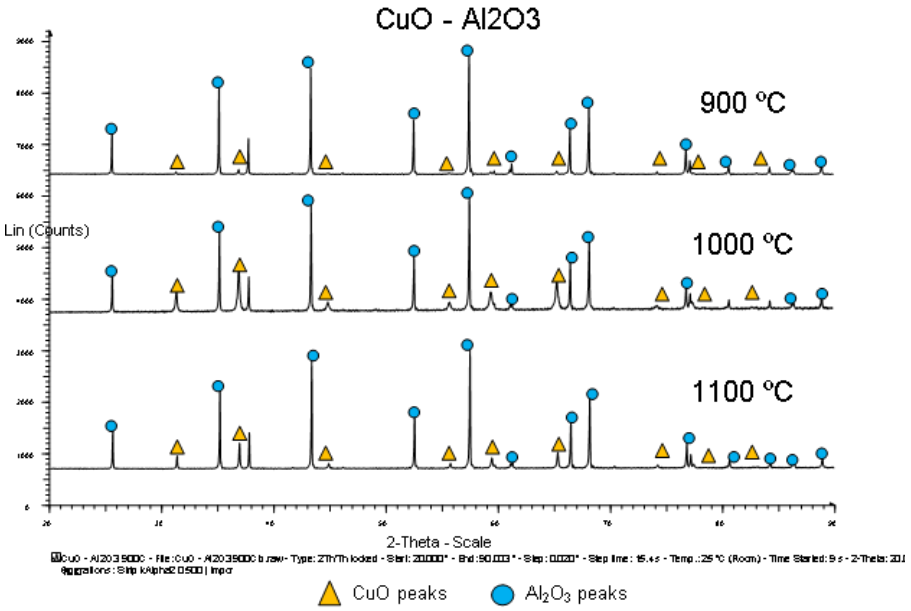



Figure 3. Diffractograms for alumina supported copper oxide catalyst with calcination temperatures of (a) 900 °C, (b) 1000 °C and (c) 1100 °C

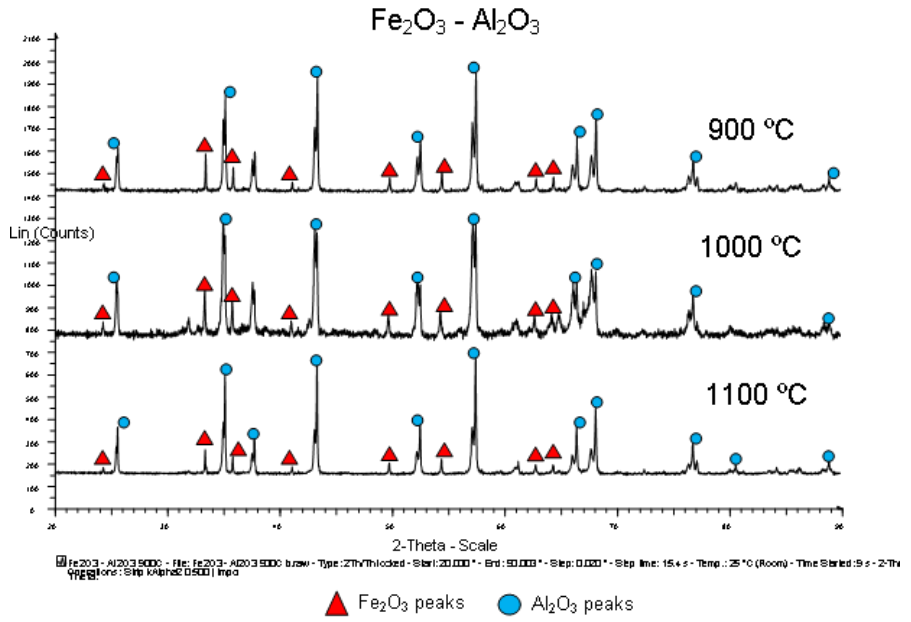



Figure 4. Diffractograms for alumina supported iron (III) oxide ($Fe_2O_3$) catalyst with calcination temperatures of (a) 900 °C, (b) 1000 °C and (c) 1100 °C

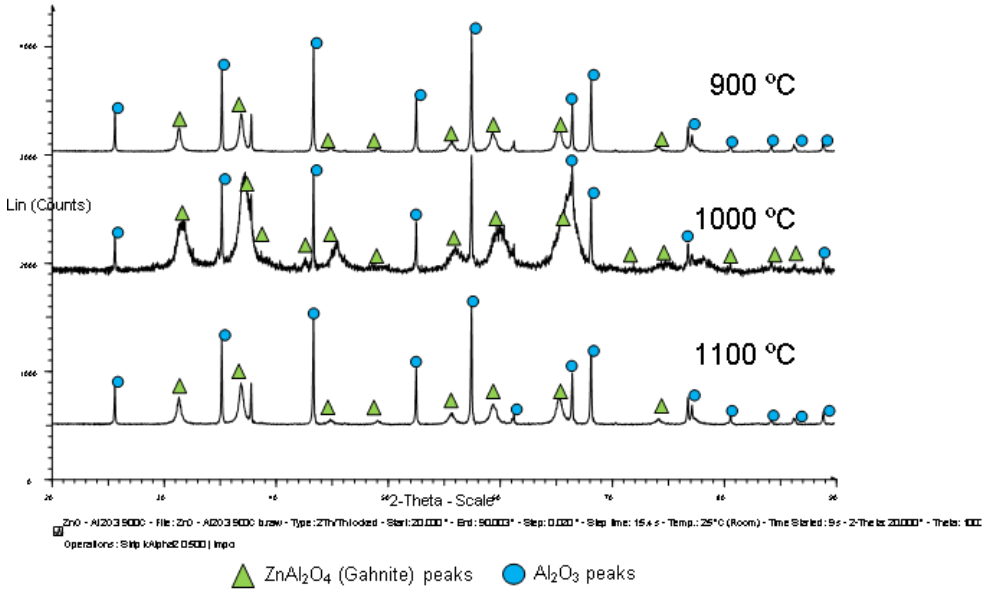



Figure 5. Diffractograms for alumina supported zinc oxide catalyst with calcination temperatures of (a) 900 °C, (b) 1000 °C and (c) 1100 °C

All of the catalysts ($CuO/Al_2O_3$, $Fe_2O_3/Al_2O_3$, and $ZnO/Al_2O_3$) with concentration of 5 Molar were analyzed using XRD for preliminary data of morphology and particle size. From the diffractograms in Figures 3 - 5, all the copper, iron, and zinc oxides catalysts with different calcination temperatures showed the different intensity. However, all the catalyst with heat treatment of 1000 °C showed the diffractograms with broad base width compared to other calcination temperatures, representing the amorphous structure of the catalyst. In amorphous phase, x-ray diffraction was scattered in many directions leading to a large bump distributed in a wide range (2 theta) instead of high intensity narrower peaks. From Figure 5, it was observed that the peaks which represent binary compound $ZnAl_2O_4$ (gahnite phases) were detected with high degree of amorphous could be seen in the diffractogram. The gahnite phase were appeared more in the catalyst structures after calcination at temperature of 1000°C for 5 hours, at 2 theta ( 31.8°, 37.2°, 39.0°, 45.5°, 49.8°, 56.4°, 60.0°, 66.0°, 69.5°, 70.5°, 78.3°, 79.4°, 83.6°, and 86.9°). According to Scherrer equation, the τ value of all diffractograms of 1000 °C heat treatment catalysts gave the smallest value indicated the smallest particle size exist for these catalysts. On the other hand, these catalysts were in highly amorphous in structure, and this temperature of heat treatment gave the rhombohedral phase of metals oxide with more ordered in structure. The FESEM-EDX micrographs had support the evidence in the form of particle size obtained. These behaviors described by Scherrer in Equation 1.

$$\tau = \frac{K\lambda}{\beta cos\theta} \qquad \text{(Eq.1)}$$

where k is defne as constant, λ is the X-rays wavelength. While θ is the value of Bragg diffraction angle of the plane, and β is the full width at half-maximum of diffraction peak.

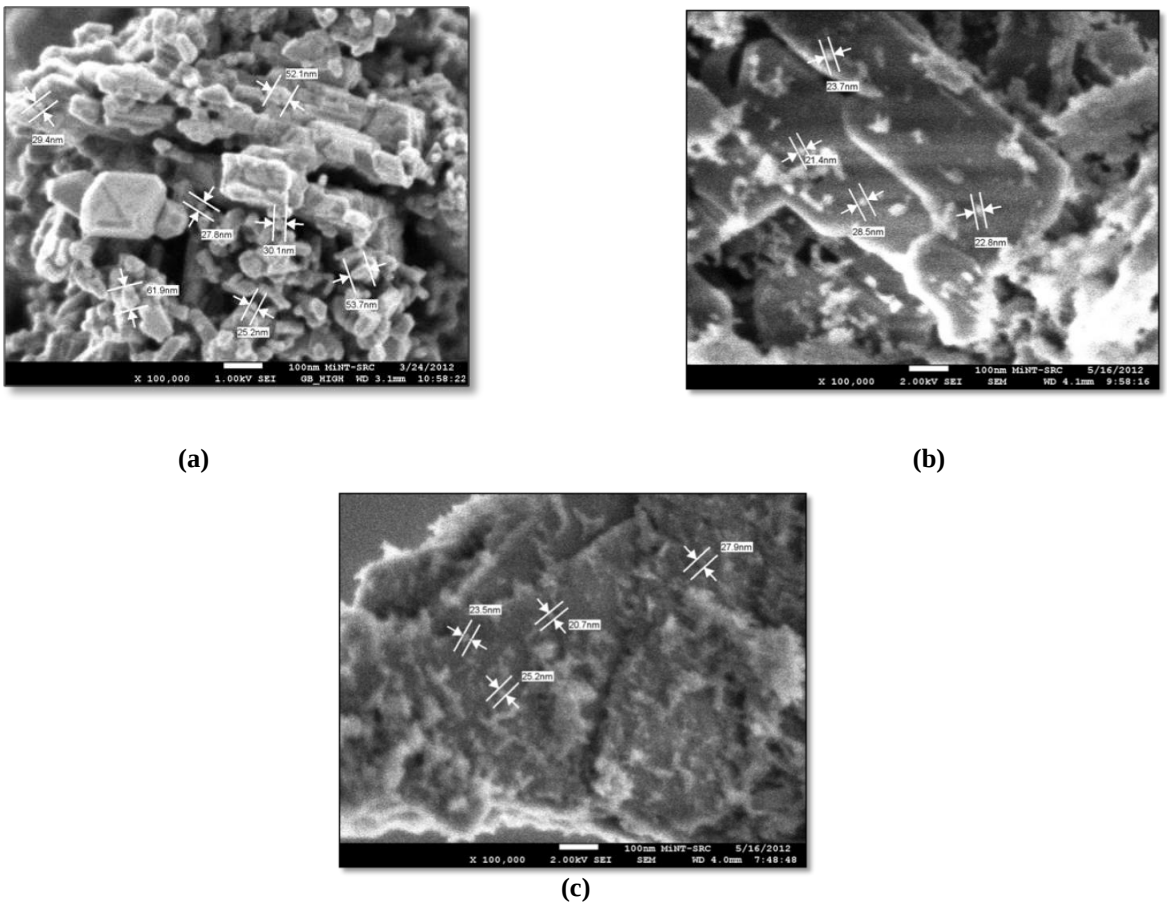
**Nitrogen Adsorption Analysis (BET surface area)**

Micromeritics ASAP 2010 was used for the analysis. About 0.2-0.3 g powder form of catalyst sample was degassed at 120$^o$C using a vacuum pump before the analysis. As an example, the catalyst sample used in this study $ZnO/Al_2O_3$ surface area was then calculated from the adsorption curve according to the Brunauer-Emmett-Teller (BET) Theory. The data as shown in Table 2 shows that the surface area of $ZnO/Al_2O_3$ catalyst is inversely proportional to the calcination temperature. As the calcination temperature was increase, the surface areas

decreased. BET surface area of $ZnO/Al_2O_3$ catalyst (50.93 $m^2/g$) calcined at 1000°C was lower than that calcined at 900°C (77.33 $m^2/g$), in agreement with XRD analysis whereby when the degree of crystallinity of catalyst increases, the surface area decreases. However, calcination at 1100°C temperature gave low surface area (77.33 $m^2/g$) that most probably due to the presence of large aggregation and agglomeration compared to the calcination at 900°C and 1000°C as shown in FESEM analysis in Figure 6. According to the catalytic activity results the catalyst calcined at 1000°C gave the highest heavy metals removal. This finding implies that the surface area property is not the only main factor contributing to the higher catalytic activity.

Table 2. BET surface area of $ZnO/Al_2O_3$ catalyst calcined at 900°C, 1000°C and 1100°C for 5 hours.

| Catalyst | Calcination temperature | Surface Area ($m^2/g$) |
|---|---|---|
| $ZnO/Al_2O_3$ | 900°C | 77.33 |
| | 1000°C | 50.93 |
| | 1100°C | 24.43 |




**(a)** **(b)**

**(c)**

Figure 6. The FESEM micrographs with 100,000 magnifications of (a) $CuO/Al_2O_3$ (b) $Fe_2O_3/Al_2O_3$ and (c) $ZnO/Al_2O_3$ calcined at 1000 °C for 5 hours. Scale bar: 100nm.

**Field Emission Scanning Electron Microscopy (FESEM) for Analysis of Alumina Supported Transition Metals Catalysts**

FESEM analysis was performed to investigate the morphology and particle size of the transition metals oxide catalysts (CuO, $Fe_2O_3$, and ZnO) with different heat treatment temperatures. This characterization will prove the evidences given by XRD analysis with specific micrographs of the surface particles with size scale down to nanometers. Thus, the combination of analysis method will complement each other. The micrographs of FESEM with 100,000 magnifications in Figure 6 indicates the morphology and particle size of a) $CuO/Al_2O_3$, b) $Fe_2O_3/Al_2O_3$, and c) $ZnO/Al_2O_3$ with the nanosize scale. As shown in the micrographs, the metal oxide with heat treatment of 1000 °C gave the smallest particle sizes in nanometer. The transition metal oxides with rhombohedral phase were homogenously distributed on the supporting material alumina ($Al_2O_3$). The size of the particles was below 100 nm, proving that most of the catalysts were in nano size.

**Removal of Heavy Metals in Green Mussel via Oxidation Technique**

Figure 7 shows the percentage of Hg removal using 200, 300, and 500 mg $L^{-1}$ PAA for different time of reactions from 1 hour to 5 hours. The initial concentration of Hg in controlled green mussel was 0.911 mg $L^{-1}$. The removal percentage of Hg using 200 mg $L^{-1}$ of PAA showed a significant increase from 1 to 5 hours of reaction. For the first hour, the removal was 40 %, followed by 50 % for second hour, 60 % for third hour, 70% for fourth hour and 80% for fifth hour. It can be concluded that the removal percentage was increased with time of reaction. For 300 mg $L^{-1}$ and 500 mg $L^{-1}$ of PAA, the removal percentage was not significantly increased with time, the removal percentage for 300 mg $L^{-1}$ of PAA started with 80 % of removal for the first hour, 85 % for second hour, dropped to 81% for third hour and increased again to 86 % for fourth hour and 96 % for fifth hour of reaction. By using 500 mg $L^{-1}$ of PAA the removal was 100 % except for second and fifth hour. These results showed that the study for optimum value for PAA concentration used would be much higher using 600 mg $L^{-1}$ and above to get the comparison of removal percentage with 500 mg $L^{-1}$ of PAA used.

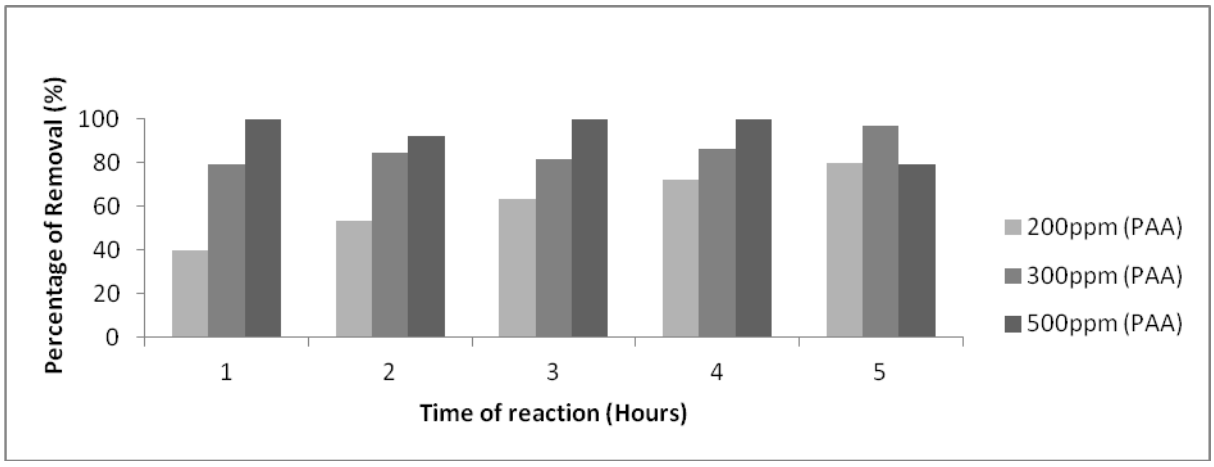



Figure 7**.** Percentage of mercury (Hg) removal of dead mussel flesh after treatment

For removal percentage of lead (Pb) in the dead mussel flesh, Figure 8 shows that the studied of different PAA concentration and reaction showed that only 200 mg $L^{-1}$ of PAA and 1 hour reaction time was enough to remove 100 % of lead content in the green mussel. The initial concentration in the controlled mussel's flesh was 1.275 µg $g^{-1}$.

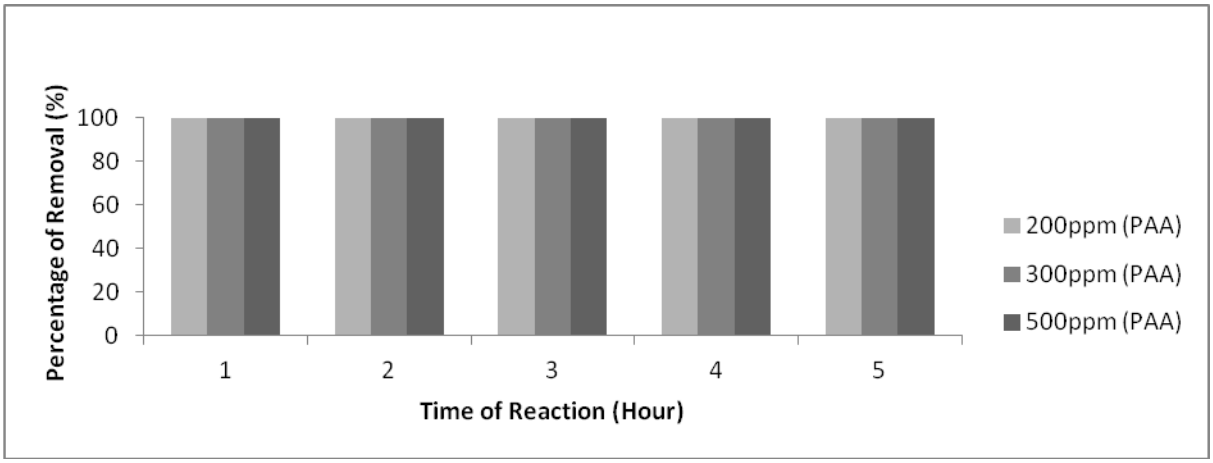



Figure 8. Percentage of lead (Pb) removal from dead mussel flesh after treatment (all concentrations of PAA gave 100 % removal)

**Removal of Heavy Metals in Green Mussel via Oxidation Technique Catalyzed with $CuO/Al_2O_3$, $Fe_2O_3/Al_2O_3$ and $ZnO/Al_2O_3$**

For preliminary result of Hg and Pb removal in dead mussel flesh using PAA with $CuO/Al_2O_3$, $Fe_2O_3/Al_2O_3$, and $ZnO/Al_2O_3$ catalysts, Figures 9 to 14 represent the percentage of Hg and Pb removal using 100, 200, 300, and 500 mg $L^{-1}$ PAA for 5 hours reaction, with 1 hour interval. In Figure 9, the initial concentration of Hg in controlled green mussel was 1.690 mg $L^{-1,}$ and Pb was 2.400 mg $L^{-1}$. The reaction was performed in 1 L of water with constant temperature of 32.5 °C and stirred using IKA HS-7 magnetic stirrer. The removal percentage of Hg using 100, 200, 300, and 500 mg $L^{-1}$ of PAA at first hour showed a significant increase as the PAA concentration increased which was 10 % to 100 % except for first and second hour. For the second hour of reaction using all concentrations of PAA, the removal of mercury was at 100 %. These can be concluded that for the reaction of Hg removal using $CuO/Al_2O_3$ catalyst, only 100 mg $L^{-1}$ of PAA needed to remove mercury with two hours of reaction time.

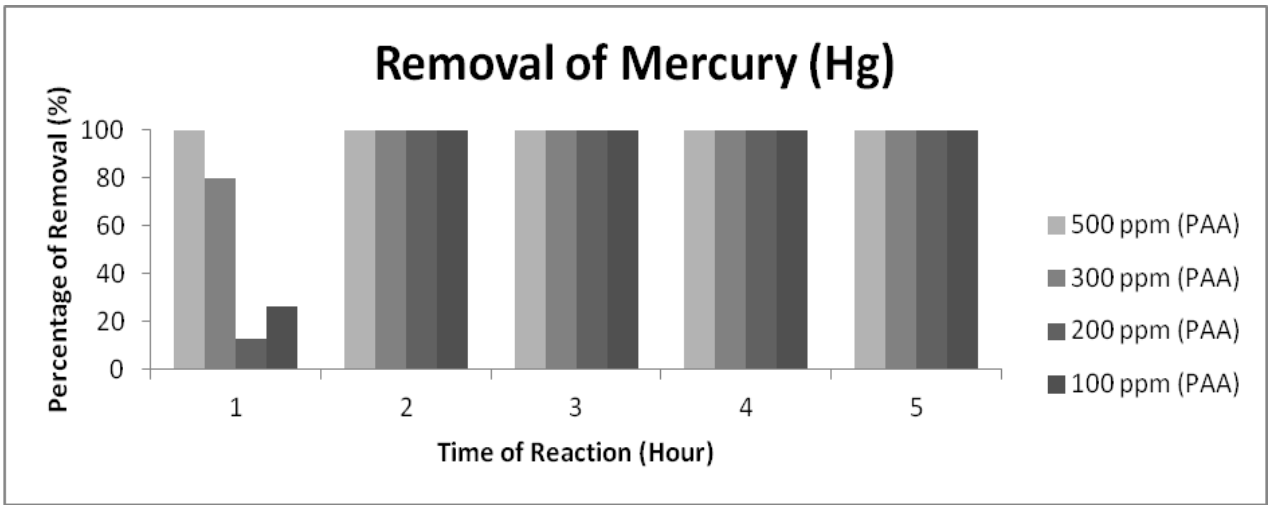



Figure 9. Percentage of mercury (Hg) removal from dead mussel flesh after treatment using PAA catalyzed with $CuO/Al_2O_3$.

For the removal of Pb in Figure 10, most of the PAA concentrations gave 100 % removal at the fifth hour of reaction time. This indicated that a serious uncertainty has been observed for the Pb removal using PAA catalyzed with CuO.

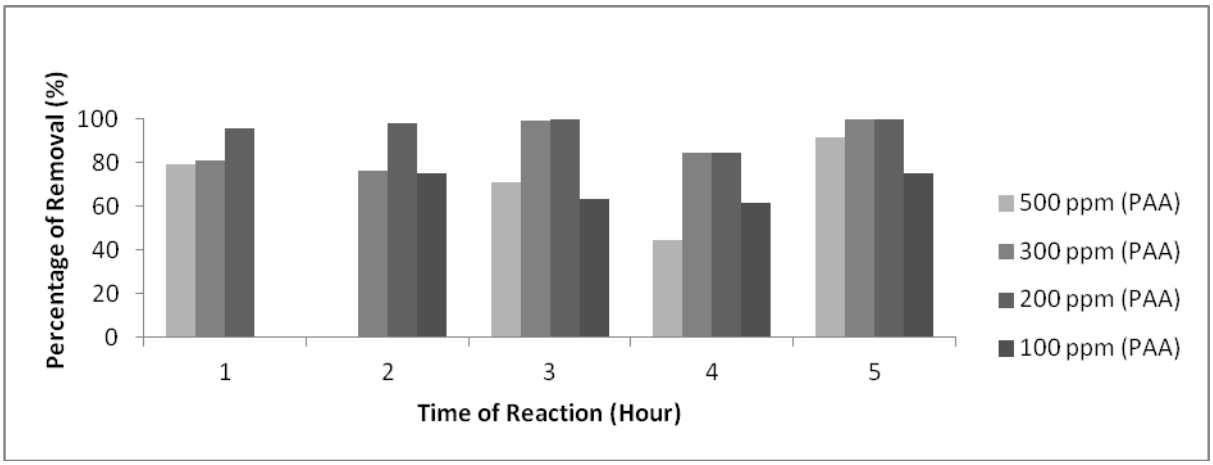



Figure 10. Percentage of lead (Pb) removal from dead mussel flesh after treatment using PAA catalyzed with $CuO/Al_2O_3$.

For removal percentage of mercury (Hg) in the dead mussel flesh using PAA catalyzed with $Fe_2O_3/Al_2O_3$, Figure 11 showed that the studied of different PAA concentration and reaction showed that only 200 mg $L^{-1}$ of PAA and 1 hour reaction time was enough to remove 100 % of mercury content in the green mussel.

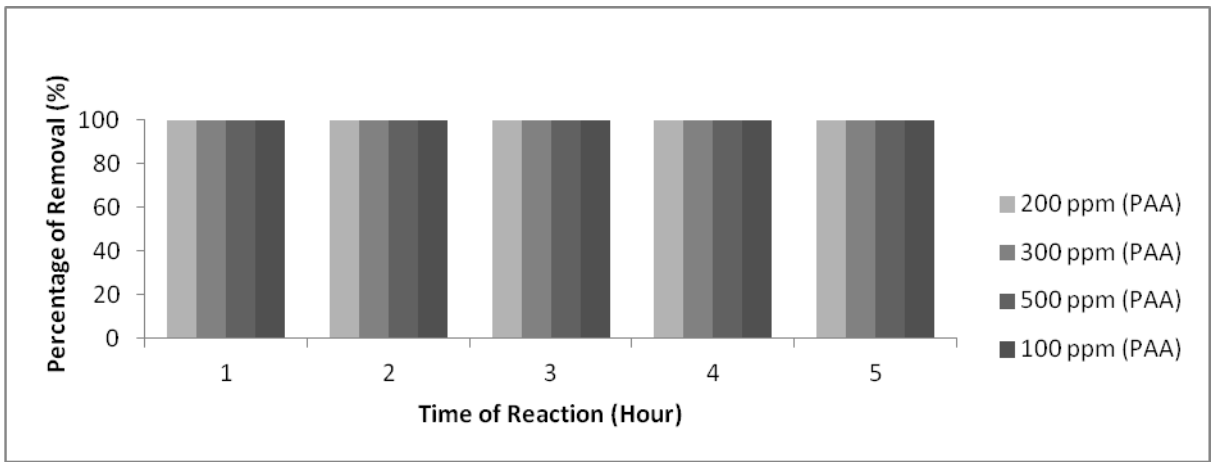



Figure 11. Percentage of mercury (Hg) removal from dead mussel flesh after treatment using PAA catalyzed with $Fe_2O_3/Al_2O_3$.

Figure 12 describes the percentage of Pb removal from dead flesh of green mussel using PAA catalyzed with $Fe_2O_3/Al_2O_3$. As the time of reaction increase, the removal percentage was decrease accordingly among all PAA concentrations used, until the third hour the removal percentage stared to increase again for an hour and decrease again up to fifth hour of reaction time. This pattern of graph indicated that the metal that has been removed by peracetate ions from the mussel's flesh react was absorbed again. $Fe_2O_3/Al_2O_3$ catalyst might not be suitable for the removal of lead from the green mussel's flesh.

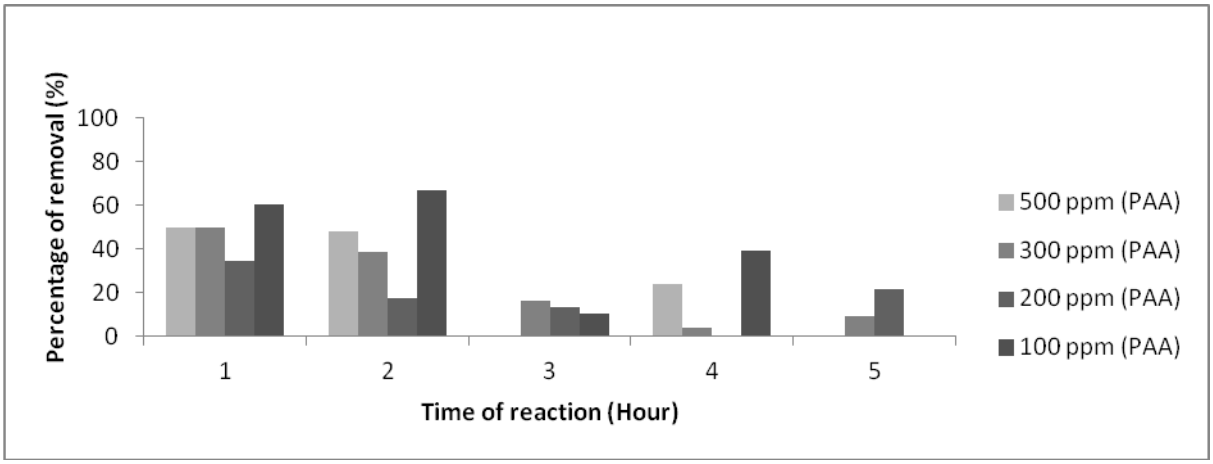



Figure 12. Percentage of lead (Pb) removal from dead mussel flesh after treatment using PAA catalyzed with $Fe_2O_3/Al_2O_3$

For the removal of mercury from dead mussel's flesh using PAA catalyzed with $ZnO/Al_2O_3$ as shown in Figure 13, the Hg content was totally removed from the mussel using all concentrations of PAA at all five hour of reaction time, indicates that the minimum concentration of PAA needed was only 100 mg $L^{-1}$ for only one hour of reaction time. However, for the second hour of 200 and 500 mg $L^{-1}$ PAA, the method was not effective. It was observed that $ZnO/Al_2O_3$ catalyst was efficient for removal of Hg.

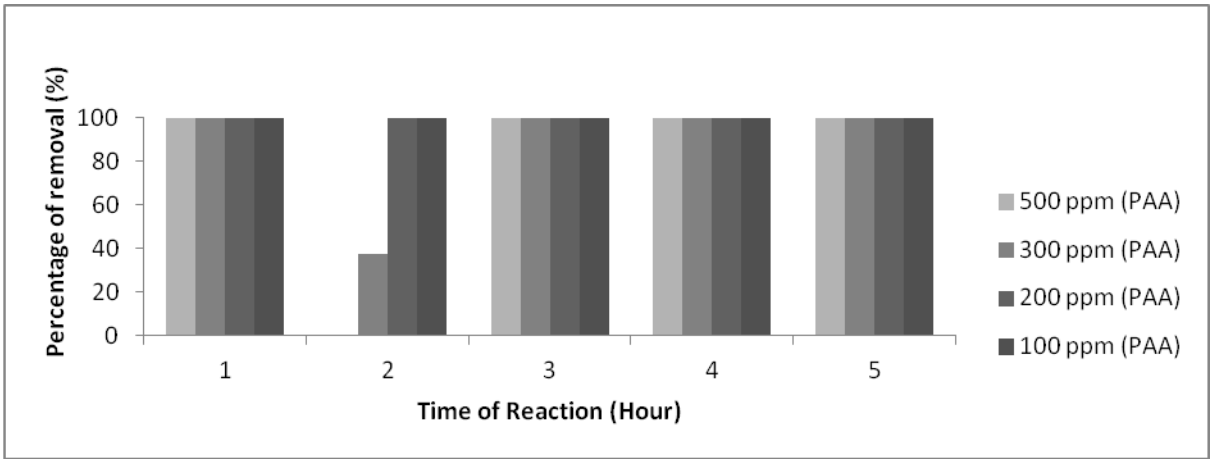



Figure 13. Percentage of mercury (Hg) removal from dead mussel flesh after treatment using PAA catalyzed with $ZnO/Al_2O_3$

The graph in Figure 14 describes on the removal of Pb using PAA catalyzed with $ZnO/Al_2O_3$. From the graph pattern, there were a lot of uncertain especially involving the PAA concentration used in the reaction. Among all concentrations of PAA, only 200 mg $L^{-1}$ gave 100 % of removal at second hour of reaction. There was no significance pattern in the Pb removal percentage as the PAA concentrations and reaction time increase. It can be conclude that the $ZnO/Al_2O_3$ catalyst was not practically reliable to remove Pb from the mussel's flesh.

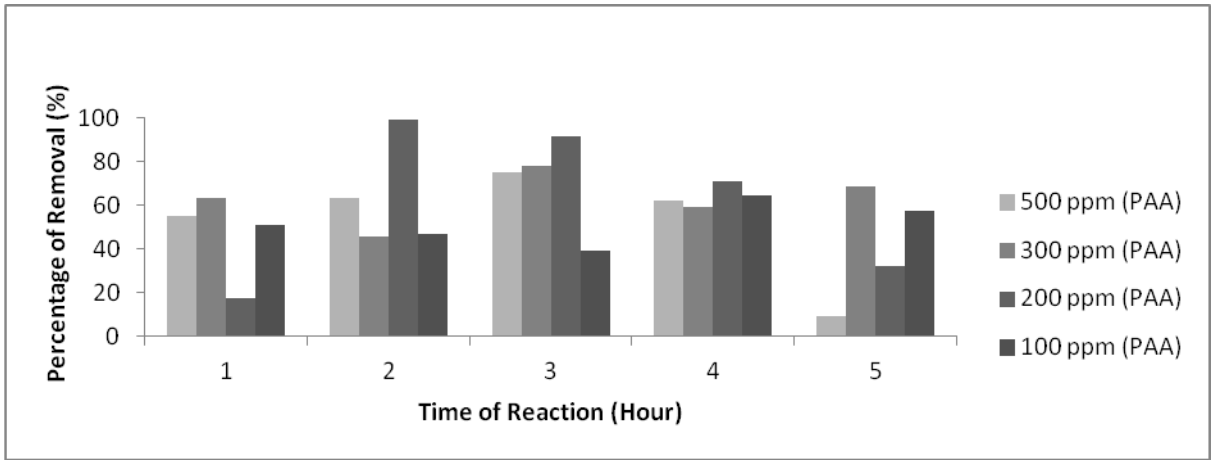



Figure 14. Percentage of lead (Pb) removal from dead mussel flesh after treatment using PAA catalyzed with $ZnO/Al_2O_3$

## Conclusion

The study for heavy metals removal in green mussel, have been done successfully. The best calcination temperature of the catalyst used was 1000 ºC as proven with XRD diffractograms, BET and FESEM micrographs. Thus, the demetallisation process in green mussel was more efficient using only 100 $mgL^{-1}$ of PAA catalyzed with $Fe_2O_3/Al_2O_3$ for Hg removal, and using PAA without catalyst for Pb removal. However, the other catalyst also showed positive results in removal of Hg and Pb especially $ZnO/Al_2O_3$ that give almost 100% removal of Hg in 3 to 5 hours of reaction using only 100 mg $L^{-1}$ of PAA and could remove up to 90% of Pb at 5 hours of reaction.

## Acknowledgement

The authors would like to acknowledge Ministry of Higher Education Malaysia (MOHE) and Research Management Center (RMC) UTM for research fund under Research University Grant, VOT number Q.J13000.7122.00H90 and Q.J130000.2622.06J19 Department of Chemistry, Faculty of Science UTM, and Institute of Environmental and Water Resources Management (IPASA) UTM for research facilities, and also due to the Department of Mollusk, Fisheries Research Institute (FRIM) Department of Fisheries Malaysia, Kuala Muda, Kedah for their collaboration in providing information regarding bivalve mollusk species especially green mussel (*Perna viridis*).

## References

1. Bondad-Reantaso M.G., Subasinghe R.P., Arthur J.R., Ogawa K., Chinabut S., Adlard R., Tan Z., Shariff M. (2005). Desease and Health Management in Asian Aquaculture. *Veterinary Parasitology*, 132: 249 – 272.
2. Chua T.E., Paw J.H., Guarin F.Y. (1989). The Environmental Impact of Aquaculture and the Effects of Pollution on Coastal Aquaculture Development in Southeast Asia. *Mar. Poll. Bull,* 20 (7): 335-343.
3. Hertler H., Boettner A.R., Ramrez-Toro G.I., Minnigh H., (1989). The Environmental Impact of Aquaculture and the Effects of Pollution on Coastal Aquaculture Development in Southeast Asia. *Mar. Poll. Bull,* 20(7): 335-343.

4. Hung C.L.H., Xu Y., Lan J.C.W., Connel D.W., Lam M.H.W., Nicholson S., Richardson B.J., Lam P.K.S., (2006) A preliminary Risk Assessment of Organochlorines Accumulated in Fish to The Indo-Pacific Humpback Dolphin (*Sousa chinensis*) in the Northwestern Waters of Hong Kong. *Environmental Pollution*, 144: 190-196.
5. Waldichuck M. (1974). Coastal Marine Pollution and Fish. *Ocean Management*, 2: 1-60.
6. Monaghan R.M., Wilcock R.J., Smith L.C., Tikkisetty B., Thorrold B.S., Coastall D. (2007). Linkages Between Land Management Activities and Water Quality in an Intensively Farmed Catchment in Southern New Zealand. *Agriculture Ecosystem & Environment*, 118: 211-222.
7. Tuteja N.K., Beale G., Dawes W., Vaze J., Murphy B., Barnett P., Rancic A., Evans R., Geeves G., Rassam D.W., Miller M. (2003). Predicting the Effects of Landuse Change on Water and Salt Balance- A Case Study of A Catchment Affected by Dryland Salinity in NSW, Australia. *Journal of Hydrology*, 283: 67-90.
8. Tal Y., Schreier H.J., Sowers K.R., Stubbefield J.D., Place A.R., Zohar Y. (2009). Environmentally Sustainable Land-based Marine Aquaculture. *Aquaculture*, 286: 28-35.
9. Yap C.K., Ismail A., Tan S.G., Omar H. (2002). Correlations Between Speciation of Cd, Cu, Pb and Zn in Sediment and Their Concentrations in Total Soft Tissue of Green-Lipped Mussel Pernaviridis from The West Coast of Peninsular Malaysia. *Environmental International*, 28: 117-126.
10. Al-Barwani S.M., Arshad A., Nurul Amim S.M., Japar S.B., Siraj S.S., Yap C.K. (2007). Population Dynamics of The Green Mussel *Perna Viridis* from The High Spat-Fall Coastal Water of Malacca, Peninsular Malaysia. *Fisheries Research*, 84: 147-152.
11. Nicholson S., (2003). Lysosomal Membrane Stability, Phagocytosis and Tolerance to Emersion in The Mussel *Perna viridis* (Bivalvia: Mytilidae) followingexposure to acute, sublethal, copper. *Chemoephere*, 52: 1147-1151.
12. Nicholson S. and Lam P.K.S., (2005). Pollution Monitoring in Southeast Asia Using Biomarkers in The Mytilid Mussel *Perna viridis* (Mytilidae: Bivalvia). *Cement Environmental International*, 31: 121-1.
13. Tanabe S., Prudente M.S., Kan-atireklap S., Subramanian A. (2000). Mussel Watch: Marine Pollution Monitoring of Butyltins and Organochlorines in Coastal Waters of Thailand, Philippines and India. *Ocean & Coastal Management*, 43: 819-839.
14. Yap C.K., Ismail A., Tan S.G. (2003). Background Concentrations of Cd, Cu, Pb And Zn In The Green-Lipped Mussel Perna Viridis (Linnaeus) from Peninsular Malaysia. *Mar. Poll. Bull.*, 46: 1035-1048.
15. Monirith I., Ueno D., Takahashi S., Nakata H., Sudaryanto A., Subramanian A., Karuppiah S., Ismail A., Muchtar M., Jinshu Zheng, Richardson B.J., Prudente M., Hue N.D., Tana T.S., Tkalin A.V., Tanabe S. (2003). Asia-Pacific Mussel Watch: Monitoring Contamination of Persistent Organochlorine Compounds in Coastal Waters of Asian Countries. *Mar. Poll. Bull.*, 46: 281-300.
16. Yap C.K., Ismail A., Omar H., Tan S.G. (2004a). Toxicities and Tolerances of Cd, Cu, Pb And Zn In a Primary Producer (*Isochrysis Galbana*) and in a Primary Consumer (Perna viridis). *Environmental International*, 29: 1097-1104.
17. Rajagopal S., Venugopalan V.P., nair K.V.K., Jenner H.A., den Hartog C., (1998). Reproduction, Growth Rate And Culture Potential Of The Green Mussel, *Perna viridis L.*/ In Edaiyur Backwaters, East Coast of India. *Aquaculture*, 162: 187-202.
18. LokmanShamsudin (1992). Lipid and Fatty Acid Composition of Microalgae Used in Malaysian Aquaculture as Live Food for the Early Stage of Penaeid Larvae. *Journal of Applied Physicology*. 4: 371-378.
19. Okay O.S., Donkin P., Peters L.D., Livingstone D.R. (1999). The Role Of Algae (Isochrysisgalbana) Enrichment on The Bioaccumulation of Benzo[*a*]Pyrene and Its Effects on The Blue Mussel Mytilusedulis. *Environ. Poll*, 110: 103-113.
20. Nicholson S., (1999). Cardiac and Lysosomal Responses to Periodic Copper in the Mussel Pernaviridis (Bivalvia: Mytilidae). *Mar. Poll. Bull*, 38(12): 1157-1162.
21. Krishnakumar P.K., Asokan P.K., Pillai V.K., (1990). Physiological And Cellular Responses To Copper And Mercury In The Green Mussel *Perna viridis* (Linnaeus). *Aquatic Toxicology*, 18: 163-174.
22. Fernley P.W., Moore M.N., Lowe D.M., Donkin P., Evans S., (2000). Impact Of The Sea Empress Oil Spill on Lysosomal Stability in Mussel Blood Cells. *Marine Environmental Research*, 50: 451-455.
23. Fang J.K.H., Wu R.S.S., Zheng P.G.J., Lam P.K.S., Shin P.K.S., (2008a). Induction, Adaptation and Recovery of Lysosomal Integrity in Green-lipped Mussel *Perna viridis*. *Mar. Poll. Bull.*, 57, 467-472.
24. Moore M.N., Viarengo A., Donkin P., Hawkins A.J.S., (2007). Autophagic and Lysosomal Reactions to Stress in The Hepatopancreas of Blue Mussels. *Aquatic Toxicology*, 84: 80-91.

The Malaysian Journal of ANALYTICAL SCIENCES ISSN 1394-2506

# ASSESSMENT OF NATURALLY OCCURING RADIONUCLIDE IN THE SEDIMENT CORE IN SOUTHERN OF KUALA SELANGOR COASTAL AREA

## (Kajian Radionuklida Tabii di dalam Teras Sedimen di Kawasan Pesisir Pantai Selatan Kuala Selangor)

Zaini Hamzah, Umi Kalsum Abdul Karim*, Ahmad Saat, Sabarina Md Yunus

*Faculty of Applied Sciences,*
*Universiti Teknologi MARA, 40450, Shah Alam, Selangor, Malaysia*

**Corresponding author: ikacome@yahoo.com*

**Abstract**

This study is to determine naturally occurring radionuclide activity concentrations of $^{226}$Ra, $^{228}$Ra and $^{40}$K in sediment core using gamma-ray spectrometry with a high-purity germanium (HPGe) detector. Sediment core was taken from 14 locations in two areas in Kuala Selangor which are Pantai Remis and Pantai Jeram. Samples were taken during Northeast Monsoon in January and March 2011. $^{40}$K was measured via its 1460 keV energy peak, $^{226}$Ra (of the $^{238}$U) and $^{228}$Ra (of the $^{232}$Th) through their γ-ray lines 609.3 keV ($^{214}$Bi) and 911.1 keV ($^{228}$Ac). The mean activity concentration of $^{226}$Ra in Pantai Remis is 37.49±1.38 Bq/kg and ranged between 19.44-55.74 Bq/kg. For $^{228}$Ra the activity concentration ranged between 40.75-82.23 Bq/kg with a mean value of 58.64±2.60 Bq/kg; and that of $^{40}$K from 206.53-398.30Bq/kg with a mean of 316.95 ± 10.88 Bq/kg. Meanwhile the mean activity concentration of $^{226}$Ra in Pantai Jeram is 32.35±1.27 Bq/kg and ranged between 21.28-38.67 Bq/kg. For $^{228}$Ra the activity concentration ranged between 34.25-106.72 Bq/kg with a mean value of 57.96±2.55Bq/kg; and that of $^{40}$K from 246.12-394.53 Bq/kg with a mean of 325.14±10.87 Bq/kg. Different vertical profile of $^{226}$Ra, $^{228}$Ra and $^{40}$K activity concentration observed between sampling locations might due to the sediment mineralogy, source of radioactivity, geochemistry of the area and oceanic process. Plus, smaller $^{228}$Ra/$^{226}$Ra activity ratio range suggests that interaction on these two series with the surrounding were very similar. Value of study radionuclides in present study were almost comparable with study done in other part in Malaysia. Moreover, world mean value of $^{226}$Ra, $^{228}$Ra and $^{40}$K provided by UNSCEAR (1993) fall within the value range of radionuclides in present study.

**Keywords**: Natural radionuclides, activity concentration, sediment core, coastal area, gamma spectrometer

**Abstrak**

Kajian ini adalah untuk menentukan aras radionuklid tabii ($^{226}$Ra, $^{228}$Ra dan $^{40}$K) di dalam teras sedimen menggunakan spektrometer gama yang dilengkapkan dengan pengesan germanium lampau tulen (HPGe). Teras sedimen telah di ambil daripada 14 lokasi di dua kawasan di Kuala Selangor iaitu Pantai Remis dan Pantai Jeram. Sampel telah di ambil semasa monsun timur laut pada Januari dan Mac 2011. Radionuklid $^{40}$K diukur melalui puncak tenaga 1460 keV. Untuk $^{226}$Ra (daripada $^{238}$U) dan $^{228}$Ra (daripada $^{232}$Th) garisan sinar gama 609.3 keV ($^{214}$Bi) dan 911.1 keV ($^{228}$Ac) digunakan. Purata kepekatan aktiviti $^{226}$Ra di Pantai Remis ialah 37.49±1.38 Bq/kg dan julat di antara 19.44-55.74 Bq/kg. Untuk $^{228}$Ra, kepekatan aktiviti julat diantara 40.75-82.23Bq/kg dengan purata 58.64±2.60 Bq/kg; dan bagi $^{40}$K julat di antara 206.53-398.30Bq/kg dengan purata 316.95 ± 10.88 Bq/kg. Sementara itu purata kepekatan aktiviti $^{226}$Ra di Pantai Jeram ialah is 32.35±1.27 Bq/kg dan julat diantara 21.28-38.67 Bq/kg. Untuk $^{228}$Ra kepekatan aktiviti berjulat diantara 34.25-106.72 Bq/kg dengan purata bernilai 57.96±2.55Bq/kg; dan bagi $^{40}$K julat diantara 246.12-394.53 Bq/kg dengan purata 325.14±10.87 Bq/kg. Terdapat perbezaan profil mencangcang bagi kepekatan aktiviti untuk $^{226}$Ra, $^{228}$Ra and $^{40}$K, yang mugkin disebabkan oleh mineralogi sedimen, punca radioaktif, geokimia kawasan tersebut serta proses lautan. Tambahan pula, nilai lingkungan kecil bagi nisbah activiti untuk $^{228}$Ra/$^{226}$Ra mengcadangkan bahawa interaksi di antara dua siri ini dengan persekitaran adalah sama. Nilai radionuklida yang dikaji di dalam kajian ini adalah sebanding dengan kajian yang dijalankan di kawasan lain di Malaysia. Nilai purata dunia bagi $^{226}$Ra, $^{228}$Ra and $^{40}$K yang dinyatakan oleh UNSCEAR (1993) jatuh di dalam lingkungan nilai radionuklida di dalam kawasan kajian ini.

**Kata kunci:** Radionuklid tabii, kepekatan aktiviti, teras sedimen, kawasan pesisir pantai, spektrometer gama

## Introduction

Kuala Selangor is located in the Sungai Selangor estuary in the west coast of Peninsular Malaysia. Its coastal zone is characterized by semi diurnal, micro tidal regime with the mean spring tidal range of about 4.0 m [1]. Pantai Remis and Pantai Jeram coastal area which are located in the southern part of Kuala Selangor is enriched with mangrove forest which play an important role in coastal protection and sustaining local fisheries. Land in the area is used primarily for forestry; fishing and harvesting of mangrove products; housing estates, industry and agriculture including mixed cropping, coconut and palm plantations in adjacent areas.

A wide range of radionuclides has been released into the oceans. Their distribution in space and time can be quite complex, but is always related to four general processes: the input function/source, radioactive decay, biogeochemistry, and oceanic processes [2]. Meanwhile, coastal area acts as deposition areas for washed-out materials due to human activities occurring around the catchment area. Those materials include radionuclide contaminants due to naturally occurring radioactive materials (NORM) and/or technologically enhanced NORM (TENORM) [3]. Examples of NORM and/or TENORM are $^{226}$Ra, $^{228}$Ra and $^{40}$K. The movement of these radionuclides into the coastal area is affected by geographical characteristic, tidal forces and physical characteristics of the sediment particles itself. Sediment which is one of the components in marine environment is vital in determining the concentration and dispersion of radionuclide as its offers large surface areas for adsorption [4].

Hence, the objective of this study is to determine the activity concentration of $^{226}$Ra, $^{228}$Ra and $^{40}$K in the sediment core in southern of Kuala Selangor coastal area specifically at 'Pantai Remis' and 'Pantai Jeram' area.

## Materials and Methods

### Sampling location

Sediment core samples were taken from 14 locations in southern part of Kuala Selangor coastal area where 7 locations are from Pantai Remis and another 7 locations are from Pantai Jeram, Kuala Selangor as shown in Figure 1.

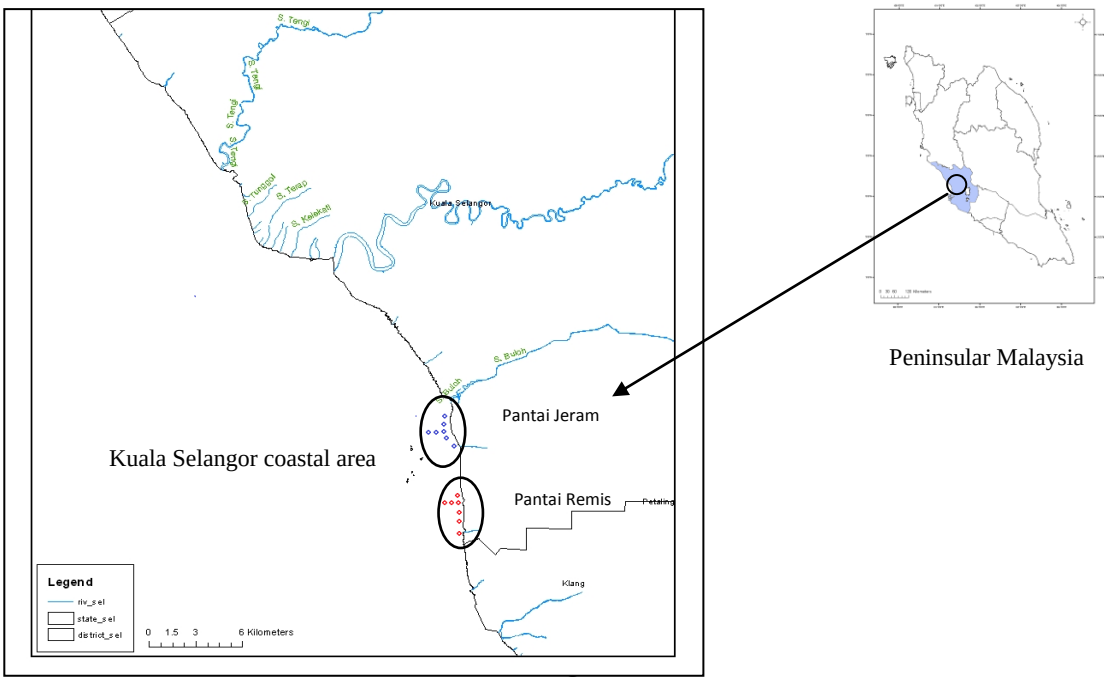



Figure 1. Map of sampling location

The samples were taken in the intertidal zone which is along the coastal area and 200 to 300 m away from land (toward the sea) as shown in Figure 2a and Figure 2b.




Figure 2a. Sampling point in Pantai Remis




Figure 2b. Sampling point in Pantai Jeram

Distance between each consecutive point is about 100 meters to 300 meters. The position of sampling points was determined using Global Positioning System (GPS). Table 1 shows the GPS coordinate and sampling location of the study area.

Table 1. Coordinates and sampling locations for collecting sediment in the study area

| Area | Sample code | GPS Coordinate | | Location |
|---|---|---|---|---|
| | | Longitude | Latitude | |
| Pantai Remis | PR1 | 101°18.422´ | 03°12.074´ | Along the coastal |
| | PR2A | 101°18.419´ | 03°11.994´ | Along the coastal |
| | PR2B | 101°18.397´ | 03°11.995´ | Toward the sea |
| | PR2C | 101°18.255´ | 03°11.999´ | Toward the sea |
| | PR3 | 101°18.347´ | 03°11.850´ | Along the coastal |
| | PR4 | 101°18.335´ | 03°11.701´ | Along the coastal |
| | PR5 | 101°18.379´ | 03°11.565´ | Along the coastal |
| Pantai Jeram | PJ1 | 101°18.364´ | 03°13.261´ | Along the coastal |
| | PJ2 | 101°18.285´ | 03°13.542´ | Along the coastal |
| | PJ3A | 101°18.265´ | 03°13.599´ | Along the coastal |
| | PJ3B | 101°18.247´ | 03°13.680´ | Toward the sea |
| | PJ3C | 101°18.226´ | 03°13.711´ | Toward the sea |
| | PJ4 | 101°18.238´ | 03°13.762´ | Along the coastal |
| | PJ5 | 101°18.074´ | 03°30.905´ | Along the coastal |

**Sample collection**

Sediment core samples were taken manually using 42 cm length PVC pipe. Each sediment core was sliced into 4 cm and dried in the oven at 60$^{o}$C until constant weight. The dried sample was then grounded into fine particle and pass through 250 mesh sieve. About 100 - 150 g of surface sediment was packed into polyethylene container and were carefully sealed using cellophane tape to avoid the escape of gaseous radon and thoron from the sample [5]. Then, it is allowed to achieve equilibrium for at least 3 weeks.

**Sample analysis**

The activity concentration $^{226}$Ra, $^{228}$Ra, and $^{40}$K in the sediment core samples were counted for 14400 seconds using gamma spectrometry system with ORTEC p-type HPGe coaxial detector coupled to a spectrum processing system. The HPGe has a resolution of 1.85 keV and 25 % relative efficiency at 1332 keV $^{60}$Co gamma-ray. The background radiation was also measured to carry out the necessary correction. Efficiency calibration of the spectrometer was carried out by using analytical grade $UO_3$ ore in KCl matrix prepared in the laboratory using identical container geometry as the samples. The spectrum processing and analysis were done using ORTEC Gamma Vision$^{TM}$ Version 6.07 [6].

$^{226}$Ra activities were determined by measuring the photo peaks of its daughter nuclides; $^{214}$Bi at 609.3 keV. The $^{228}$Ra activities in the samples were determined by measuring the intensity of $^{228}$Ac at 911.1 keV. Meanwhile, the activity concentration of $^{40}$K was determined directly via its 1460 keV energy peak [7].

## Results and Discussion

**Sediment dry bulk density**

Dry bulk density in sediment is the mass of dry sediment in a given bulk volume of sediment [8]. Dry bulk density in the sediment core along the coastal and toward the sea in Pantai Remis and Pantai Jeram were shown in Figures 3a - 4b respectively.

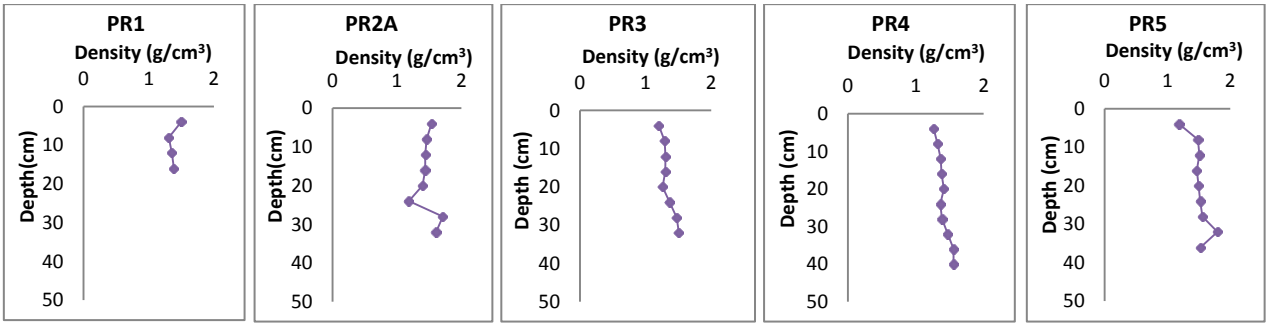



Figure 3a. Density in the sediment core along coastal area in Pantai Remis

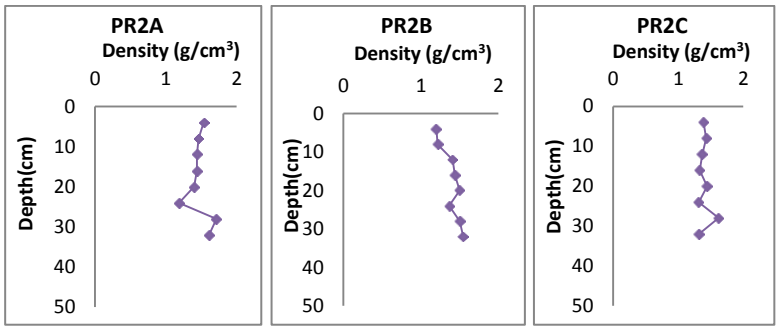



Figure 3b. Density in the sediment core toward the sea in Pantai Remis

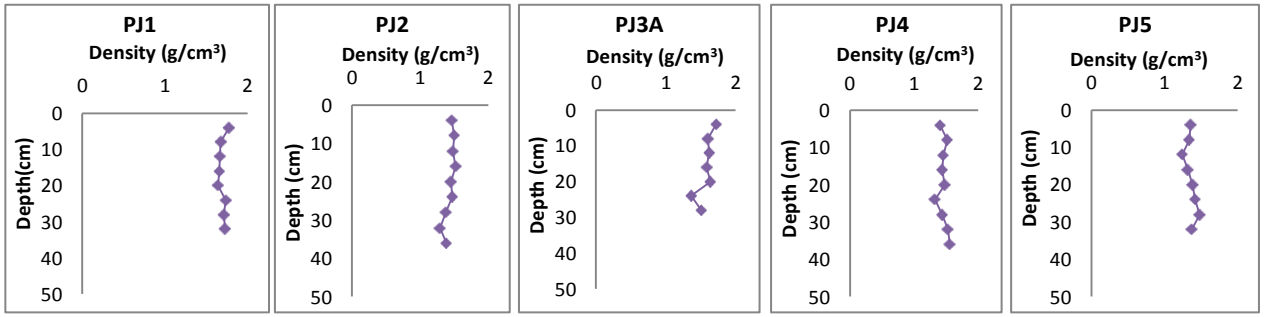



Figure 4a. Density in the sediment core along the coastal area in Pantai Jeram

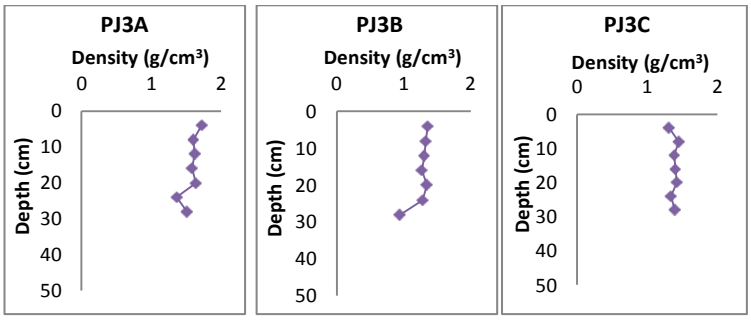



Figure 4b. Density in the sediment core toward the sea Pantai Jeram

The depth distribution of density the sediment core along coastal area and toward the sea in Pantai Remis was characterized by generally increase down the core. However, a spike was observed at 24 cm and 28 cm depth in PR2A sample as well as at 32 cm depth in PR5 sample. Meanwhile, densities of the sediment core along the coastal and toward the sea in Pantai Jeram were also increasing from the top layer to the bottom layer except in PJ3A and PJ3B samples. Pantai Remis and Pantai Jeram area can be classified as mudflat area located in the intertidal zone. Sediment mineralogy in the mudflat area may largely consist of silt and clay. Meanwhile, sand was also presence in the top layer of the core for location located along the coastal area. Some sea shells were also observed attach to the sediment in some location in Pantai Remis and Pantai Jeram. According to [9], dry bulk density is related, directly or indirectly to the softness (or hardness) of the sediment, its vulnerability to erosion, re-suspension and other mechanical properties. Hence, sediment mineralogy and sediment characterization as well as interaction with the coastal ecosystem may affect the dry bulk density of the sediment. Furthermore, removal of sediment cores from in situ conditions results in changes in porosity and saturated bulk in particular, not only as a result of disturbance during the penetration of the gravity corer in the sediment but also because the cores are removed from in situ temperature conditions to surface conditions [10].

**Vertical profile of natural radioactivity in sediment core**

Vertical profile of $^{226}$Ra, $^{228}$Ra and $^{40}$K in sediment core were discussed in two parts which is "along the coastal" and "towards the sea" for both Pantai Remis and Pantai Jeram respectively.

**Along the coastal area in Pantai Remis**

Vertical profiles of $^{226}$Ra and $^{228}$Ra along the coastal area in Pantai Remis were shown in Figures 5a. Generally, the activity concentration of $^{226}$Ra and $^{228}$Ra in all samples shows almost similar trend. However, activity concentration of $^{228}$Ra is higher than $^{226}$Ra in all samples.$^{228}$Ra is a daughter product of $^{232}$Th which comes from Thorium (Th) decay series meanwhile $^{226}$Ra is a daughter product of $230^{Th}$ which comes from Uranium (U) decay series. According to [11], concentration of Th is higher than U in sedimentary rock. Hence, activity concentration of $^{228}$Ra is higher than $^{226}$Ra because their activity concentration is in accordance with their respective parent nuclides.

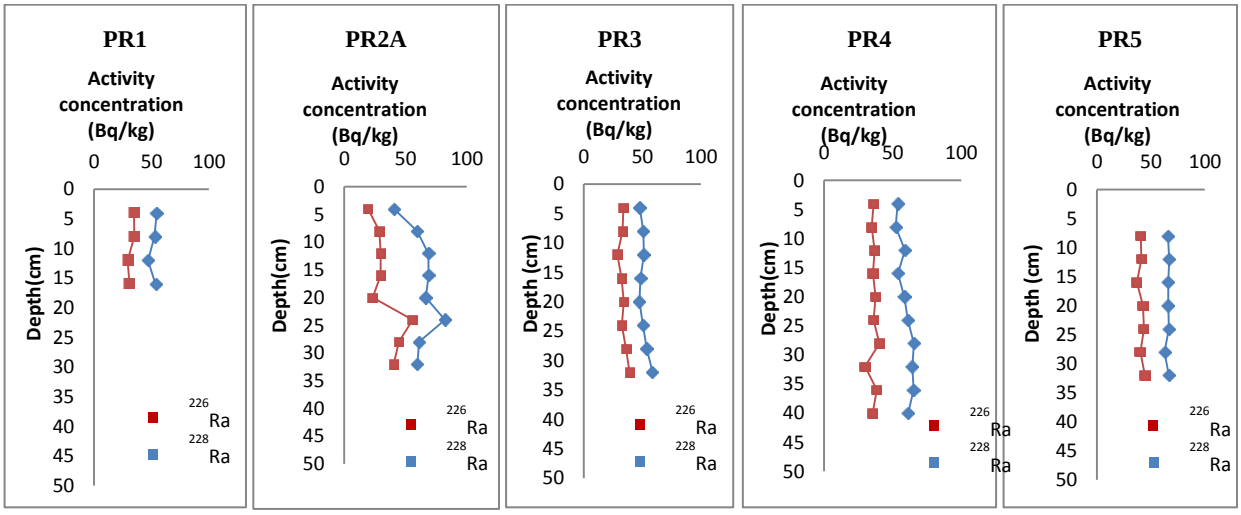



Figure 5a. Vertical profile of $^{226}$Ra and $^{228}$Ra activity concentration along coastal area in Pantai Remis

In PR1 sample, the vertical distribution of study radionuclides is up to 16 cm depth because the sampling point is characterized as a rocky shores area. The sediment core mainly dominated by *barnacles species* that inhabit on the rock surface. Hence, the sediment core which taken manually using PVC pipe experience difficulty to penetrate into deeper level. The activity concentration for $^{226}$Ra and $^{228}$Ra were ranged from 29.29-35.16 Bq/kg (mean = 32.51±1.30 Bq/kg) and 47.01-54.42 Bq/kg (mean = 51.89±2.47 Bq/kg) respectively. Activity concentration of the

study radionuclides show inconsistent pattern which might because of bioturbation. The bioturbation normally affects only the top few cm of the core. The assumption that biological and physical mixing was restricted to the surface mixed layer (SML) [12].

However, PR2A sample shows an increasing trend of $^{226}$Ra activity concentration until 24 cm depth and decreasing back until 32 cm, similar trends were also observed in activity concentration of $^{228}$Ra. A spike at 24 cm is probably related to its density as at 24 cm the density is lower, and density is closely related to the mineralogy composition of the sediment. According to villagers in the area, our sampling location used to be a village but because of the coastal erosion, the coastal area had moved inward. Thus, probably the presence of building materials and other materials embedded in the old sediment increase the amount of radioactivity due to the human activities in that area long time ago.

PR3 sample shows generally consistent trend throughout the core ranging from 28.60 - 39.01 Bq/kg (mean = 33.66 ± 1.35 Bq/kg) for $^{226}$Ra and 47.39-58.59 Bq/kg (mean = 51.01±2.50 Bq/kg) for $^{228}$Ra. In PR4, $^{226}$Ra and $^{228}$Ra activity concentration show the trend of decreasing after 30 cm depth. Constant variation of vertical profile in PR5 sample was observed. The activity concentration of $^{226}$Ra ranging from 37.02 - 44.69 Bq/kg (mean = 41.00±1.39) and activity concentration of $^{228}$Ra ranging from 56.34 - 67.02 Bq/kg (mean = 64.82 ± 2.65). Deeper levels in a core correspond to earlier times, so that radioactive decay is manifested as decreasing concentration with depth [13]. Besides, the constant value of radionuclides activity concentration in the bottom sediment can act as a natural background level as proposed by [14, 15]. Natural background may be non-homogenous in the analyzed area because several factors determine the distribution pattern of minerals and elements in an estuary (e.g. the sediment grain size and the physical-chemical conditions of waters and hydrology). For that reason, an accurate determination of the natural background levels could be achieved by taking deep sediment distributed across the estuary as a reference.

Vertical profile of $^{40}$K along coastal area in Pantai Remis was shown in Figure 5b. The vertical profile of $^{40}$K is variable in PR1 indicating that the core up to 16 cm depth is in the mixing layer. PR2, PR3 and PR4 samples generally show a decreasing pattern of activity concentration of $^{40}$K with a near surface enrichment. Meanwhile, PR5 sample shows an increase in activity concentration of $^{40}$K from surface until 12 cm depth with a value of 350.92 Bq/kg. Then, it decrease and reach a constant value at the deeper part of the core. The higher values in PR5 samples may be attributed to the presence small water irrigation into the area. The point source of the water irrigation is from the terrestrial area that passed through the oil palm plantation. Hence, the water irrigation might carry fertilize agricultural soil which may increase the concentration of $^{40}$K in the area.

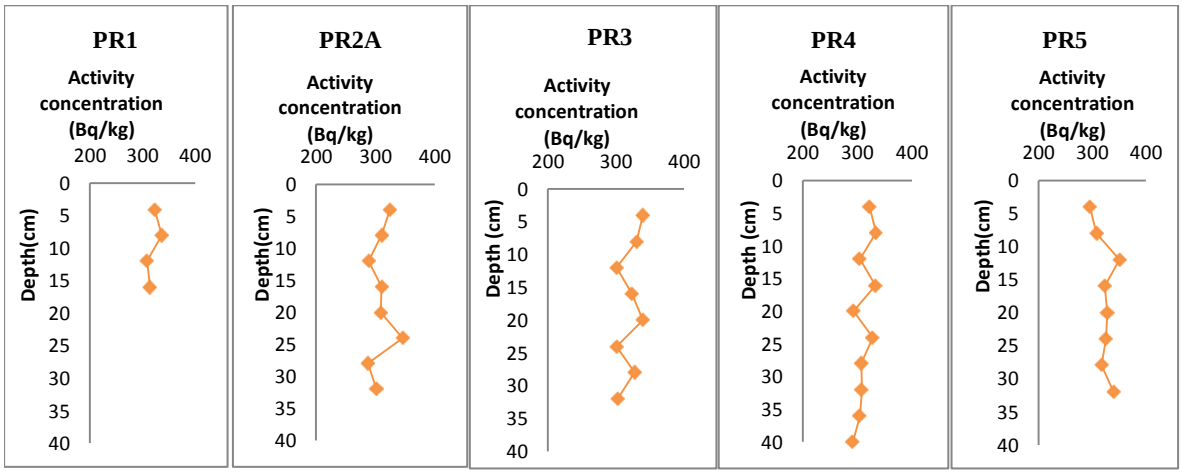



Figure 5b. Vertical profile of $^{40}$K activity concentration along coastal area in Pantai Remis

**Toward the coastal area in Pantai Remis**

The vertical profile of $^{226}$Ra and $^{228}$Ra towards the sea in Pantai Remis were shown in Figure 6a. Almost similar trend of $^{226}$Ra and $^{228}$Ra vertical profile in PR2B and PR2C samples were observed. The activity concentrations initially decrease from the surface to 8 cm depth. The activity concentrations were then generally constant throughout the core until 28 cm depth and fluctuate at 32 cm depth. This trend may due to the effect of water current during high tide and sediment mineral composition in the area. Figure 6b. shows the vertical profile of $^{40}$K towards the sea in Pantai Remis.

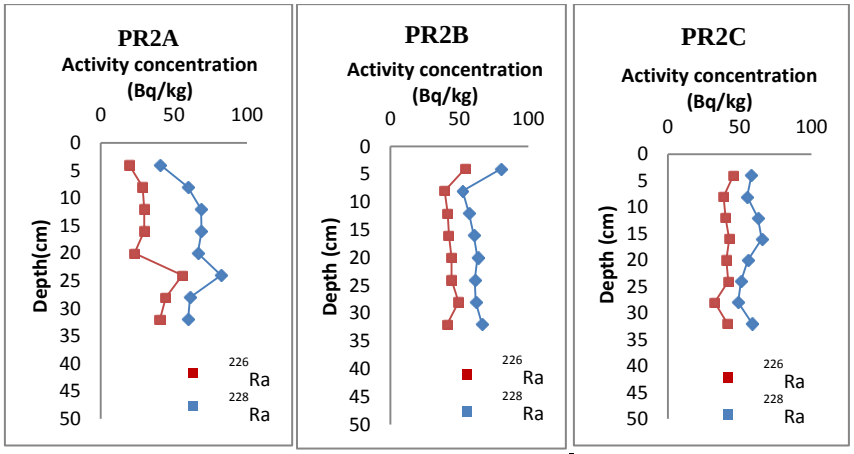



Figure 6a. Vertical profile of $^{226}$Ra and $^{228}$Ra activity concentrations towards the sea in Pantai Remis

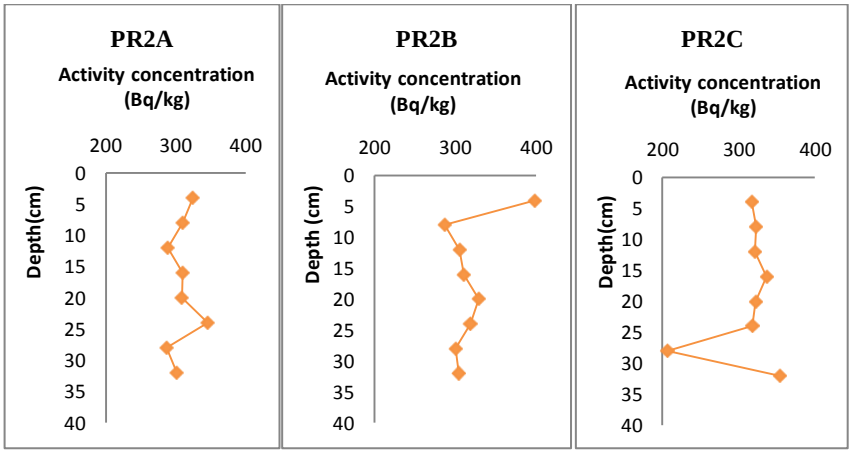



Figure 6b. Vertical profile of $^{40}$K activity concentration towards the sea in Pantai Remis

Vertical profile of $^{40}$K for PR2A and PR2B is varied but with generally decreasing down the core. Conversely, PR2C samples show roughly constant trend throughout the core but with a spike observed at 28 cm depth. The spike with a value of 206.53 ± 8.22 Bq/kg may indicate different particle size observed in the core [16].

**Along the coastal area in Pantai Jeram**

Vertical profiles of $^{226}$Ra and $^{228}$Ra activity concentrations along coastal Pantai Jeram were shown in Figure 7a. The activity concentration of $^{226}$Ra in the sediment core show generally uniform trend from the surface up to the deeper level.

Meanwhile, vertical profile of $^{228}$Ra activity concentration in PJ1, PJ2, PJ3A, PJ4 and PJ5 show almost similar trend as it is increasing from top layer to the bottom layer. Owing to its soluble and mobile nature, $^{228}$Ra is supplied to the ocean mainly by released from coastal sediment near to the land ocean interface where its produces [17]. There are two small rivers channel into the Pantai Jeram area which is "Sungai Buloh" and "Sungai Jeram". The interaction between the rivers and tidal effect may reduce the $^{228}$Ra activity in the surface sediment by active release of $^{228}$Ra from coastal sediment in the surface layer to the seawater.

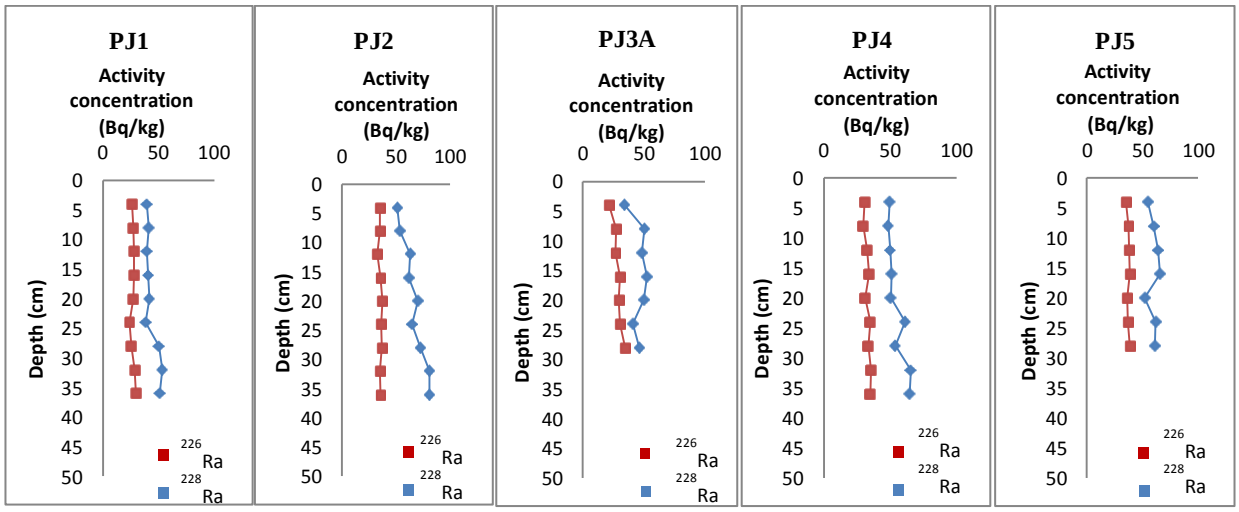



Figure 7a. Vertical profile of $^{226}$Ra and $^{228}$Ra activity concentrations along coastal area in Pantai Jeram

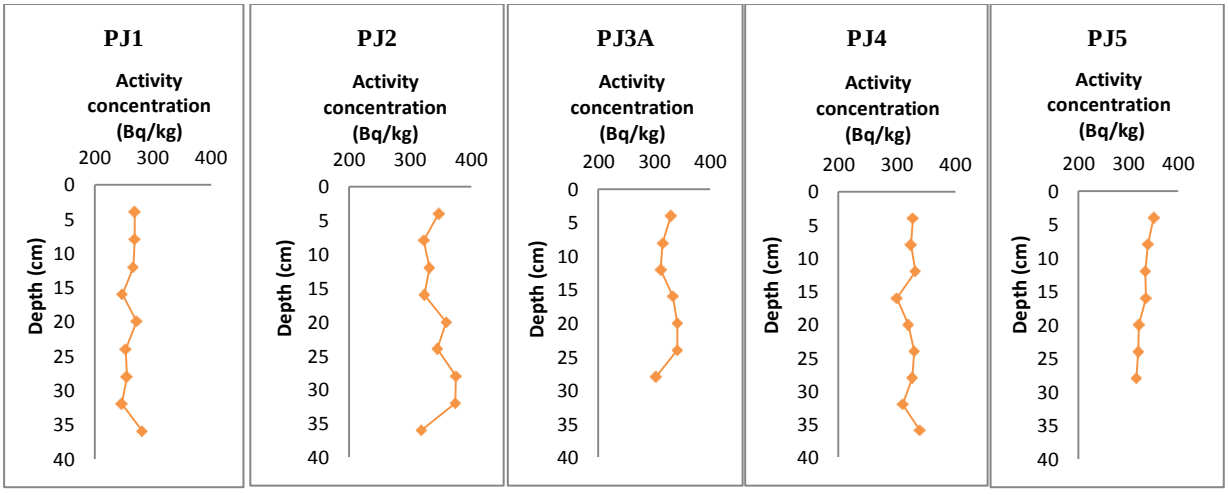



Figure 7b. Vertical profile of $^{40}$K activity concentration along coastal area in Pantai Jeram

Vertical profiles of $^{40}$K along coastal area in Pantai Jeram were shown in Figure 7b. Vertical profiles of $^{40}$K in PJ1 and PJ4 samples show almost similar trend. However, activity concentration of $^{40}$K in PJ4 is higher than PJ1 which ranging from 299.89 - 339.15 Bq/kg (mean= 323.07 ± 10.82) for PJ4 and 246.12 - 281.60 Bq/kg (mean = 261.84 ± 9.04 Bq/kg) for PJ1 respectively. PJ1 has the lowest activity of $^{40}$K down the core, this probably due to its location that far from 'Sungai Selangor' as the river that flows into the area might carry fertilized agricultural soil. On the other hand PJ2 and PJ3A samples show a mixing pattern in the upper layer and the activity of $^{40}$K start to decrease at depth of 36 cm and 28 cm respectively. However, PJ5 sample shows no discernible mixing pattern in the upper layer suggesting that minimal sediment reworking exist by decreasing the water dynamic energy and providing enough time for fine grain size to sink and deposit [18].

**Towards the sea in Pantai Jeram**

Vertical profile of $^{226}$Ra, $^{228}$Ra and 40K activity concentrations towards the sea in Pantai Jeram were shown in Figure 8a and 8b respectively.

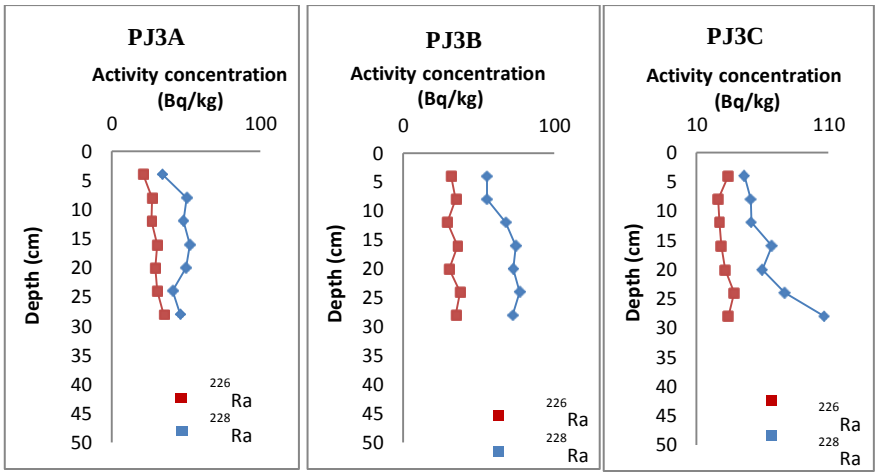



Figure 8a. Vertical profile of $^{226}$Ra and $^{228}$Ra activity concentrations towards the sea in Pantai Jeram

Vertical profiles of $^{226}$Ra towards the sea in Pantai Jeram were not changing very much with depth. Meanwhile, vertical profile of $^{228}$Ra in PJ3A, PJ3B and PJ3C shows a trend of increasing from top to the bottom layer. Lower activity concentration of $^{228}$Ra in the top section of the core samples might due to the nature of the coring method compaction [19].

Vertical profile of $^{40}$K activity concentrations towards the sea in Pantai Jeram show variable pattern mainly in PJ3C samples. PJ3C is located farthest away from the land. Input of $^{40}$K in the area might come from adjacent land and sea as well.

The activity concentration of study radionuclides in all locations and $^{228}$Ra/$^{226}$Ra activity ratio were tabulated in Table 2 and Table 3. $^{228}$Ra/$^{226}$Ra activity ratio was calculated based on the mean value of $^{226}$Ra and $^{228}$Ra activity concentration respectively.

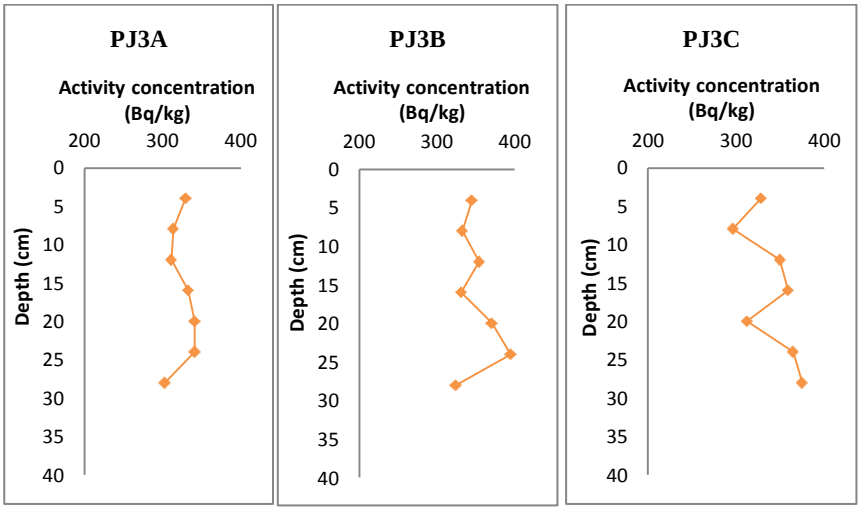



Figure 8b. Vertical profile of $^{40}$K activity concentrations towards the sea in Pantai Jeram

Table 2. $^{226}$Ra, $^{228}$Ra and $^{40}$K activity concentrations in sediment core at Pantai Remis in Bq/kg

| Sample code | Activity concentration (Bq/kg) | | | | | | $^{228}$Ra/$^{226}$Ra activity ratio |
|---|---|---|---|---|---|---|---|
| | $^{226}$Ra | | $^{228}$Ra | | $^{40}$K | | |
| | Range | Mean | Range | Mean | Range | Mean | |
| PR1 | 29.29-35.16 | 32.51±1.30 | 47.01-54.42 | 51.89±2.47 | 308.76-335.87 | 320.43±11.08 | 1.60 |
| PR2A | 19.44-55.74 | 33.90±1.28 | 40.75-82.23 | 63.40±2.66 | 287.00-345.69 | 309.44±10.60 | 1.87 |
| PR2B | 39.39-54.19 | 44.60±1.52 | 52.32-80.48 | 62.87±2.72 | 286.99-398.30 | 319.24±11.04 | 1.41 |
| PR2C | 32.63-45.60 | 40.54±1.44 | 49.00-65.33 | 56.99±2.58 | 206.53-354.18 | 312.23±10.87 | 1.41 |
| PR3 | 28.60-39.01 | 33.66±1.35 | 47.39-58.59 | 51.01±2.50 | 300.99-339.72 | 320.69±11.30 | 1.52 |
| PR4 | 29.98-40.37 | 36.18±1.36 | 52.32-65.22 | 59.50±2.63 | 291.37-334.08 | 312.84±10.87 | 1.64 |
| PR5 | 37.02-44.69 | 41.00±1.39 | 56.34-67.02 | 64.82±2.65 | 295.78-350.92 | 323.81±10.41 | 1.58 |
| Average | 19.44-55.74 | 37.49±1.38 | 40.75-82.23 | 58.64±2.60 | 206.53-398.30 | 316.95±10.88 | 1.56 |

Table 3. $^{226}$Ra, $^{228}$Ra and $^{40}$K Activity concentrations in sediment core at Pantai Jeram in Bq/kg

| Sample code | Activity concentration (Bq/kg) | | | | | | $^{228}$Ra/$^{226}$Ra activity ratio |
|---|---|---|---|---|---|---|---|
| | $^{226}$Ra | | $^{228}$Ra | | $^{40}$K | | |
| | Range | Mean | Range | Mean | Range | Mean | |
| PJ1 | 23.76-29.54 | 27.07±1.07 | 38.20-53.30 | 43.93±2.05 | 246.12-281.60 | 261.84±9.04 | 1.62 |
| PJ2 | 32.82-37.24 | 35.60±1.34 | 50.96-81.20 | 66.64±2.75 | 318.50-374.92 | 343.75±11.27 | 1.87 |
| PJ3A | 21.28-34.92 | 28.71±1.14 | 34.25-52.51 | 46.13±2.18 | 303.46-341.41 | 324.88±10.35 | 1.61 |
| PJ3B | 29.50-38.01 | 33.67±1.39 | 55.52-74.78 | 68.09±2.98 | 324.36-394.53 | 350.34±12.16 | 2.02 |
| PJ3C | 26.25-38.67 | 31.55±1.28 | 46.19-106.72 | 65.65±2.75 | 296.54-374.99 | 340.84±11.11 | 2.08 |
| PJ4 | 29.74-35.67 | 33.09±1.28 | 48.85-65.44 | 55.03±2.48 | 299.89-339.15 | 323.07±10.82 | 1.66 |
| PJ5 | 33.41-38.63 | 36.75±1.39 | 51.99-65.82 | 60.23±2.68 | 316.39-351.89 | 331.26±11.35 | 1.64 |
| Average | 21.28-38.67 | 32.35±1.27 | 34.25-106.72 | 57.96±2.55 | 246.12-394.53 | 325.14±10.87 | 1.79 |

The mean activity concentration of $^{226}$Ra, $^{228}$Ra and $^{40}$K activity concentrations in sediment core at Pantai Remis and Pantai Jeram are almost similar. Thus, the radioactivity in the area might have similar biogeochemistry and oceanic process. However, the sources that contribute to the activity concentration of radionuclide in the area are different. As reported in [20], Kapar coal power plant that located near to Pantai Remis area may release some natural radioactivity due to the combustion of coal through atmosphere and consequently being absorbed into the sediment. Pantai Jeram is near to Sungai Selangor which is about, thus radioactivity in Pantai Jeram may largely due to human activities and plantation and development along Sungai Selangor.

The mean value of $^{228}$Ra/$^{226}$Ra activity ratio was 1.56 and 1.79 in Pantai Remis and Pantai Jeram respectively. $^{238}$U and $^{232}$Th commonly occur together in nature. This frequently leads to a relatively constant $^{238}$U/$^{232}$Th or $^{228}$Ra/$^{226}$Ra ratio in many natural systems. This ratio may vary from the original value if the sample was subjected to physical or chemical interaction that may affect one series more or less than the other one. Smaller ratio range suggests that interaction on these two series with the surrounding were very similar [21].

**Comparison to other studies**

Normally, in coastal areas and on the continental shelf which are not very far from the land-based pollutants, it is reasonable to assume that the sediments have a range of concentration of natural radionuclides similar to that of terrestrial rocks, and the radioactive equilibrium is maintained [21]. For that reason, activity concentration of $^{226}$Ra, $^{228}$Ra and $^{40}$K in sediment core at Pantai Remis and Pantai Jeram were compared with the study done by [22] which determines the activity concentration of naturally occurring radionuclide in Selangor soil. Based on the study, the average activity concentration of $^{226}$Ra, $^{228}$Ra and $^{40}$K in Selangor soil is 66 ± 16 Bq/kg, 95 ± 32 Bq/kg and 204 ± 90 Bq/kg respectively. The activity concentration of $^{226}$Ra, $^{228}$Ra and $^{40}$K in Selangor soil are higher than the average activity concentration of $^{226}$Ra, $^{228}$Ra and $^{40}$K in the sediment core in Pantai Remis and Pantai Jeram. Possible reason is that the radionuclides determined in Selangor soil are near to the catchment area. Besides, radionuclides determined in the Selangor soil may enriched with igneous rock as compared to radionuclides determined in the present study which are enriched with shales and /or sedimentary rock. According to [23], igeneous rock contained higher concentration of uranium and thorium (parent of $^{226}$Ra and $^{228}$Ra respectively) than in shales and sedimentary

rock. The activity concentrations of $^{226}$Ra, $^{228}$Ra and $^{40}$K in study area were compared with other study and world mean value as shown in Table 4.

Table 4. Comparison of activity concentrations of $^{226}$Ra, $^{228}$Ra and $^{40}$K in study area with study in other region and world mean value

| Study area | Activity concentration (Bq/kg) | | | Reference |
|---|---|---|---|---|
| | $^{226}$Ra | $^{228}$Ra | $^{40}$K | |
| Pantai Remis | 19.44-55.74 | 40.75-82.23 | 206.53-398.30 | Present study |
| Pantai Jeram | 21.28-38.67 | 34.25-106.72 | 246.12-394.53 | Present study |
| EEZ Peninsular Malaysia | 16-46 | 28-87 | 171-690 | [21] |
| West Coast Peninsular Malaysia | 14.25–38.90 | 16.91–97.18 | - | [24] |
| Coastal sediment in Malacca Strait | 16.4 – 81.8 | 23.8 – 113.1 | - | [25] |
| Coastal of Sabah | 16 -30 | 23–45 | 402–842 | [26] |
| Coastal of Sarawak | 23–41 | 27–45 | 142–680 | [26] |
| Xinghua Bay mouth, Fujian, China | 22.4–27.9 | 54.4–71.9 | 684–795 | [27] |
| World mean value | 25 | 25 | 373 | [28] |

Mainly, value of study radionuclides in present study were almost comparable with study done in EEZ Peninsular Malaysia, West Coast Peninsular Malaysia, coastal sediment in Malacca Strait, coastal of Sabah and Sarawak as well as Xinghua Bay mouth, Fujian China. Moreover, world mean value of $^{226}$Ra, $^{228}$Ra and $^{40}$K provided by UNSCEAR (1993) fall within the value range of radionuclides in present study.

## Conclusion

The mean activity concentration of $^{226}$Ra in Pantai Remis is 37.49±1.38 Bq/kg and ranged between 19.44-55.74 Bq/kg. For $^{228}$Ra the activity concentration ranged between 40.75-82.23Bq/kg with a mean value of 58.64±2.60 Bq/kg; and that of $^{40}$K from 206.53-398.30 Bq/kg with a mean of 316.95 ± 10.88 Bq/kg. Meanwhile the mean activity concentration of $^{226}$Ra in Pantai Jeram is 32.35 ± 1.27 Bq/kg and ranged between 21.28-38.67 Bq/kg. For $^{228}$Ra the activity concentration ranged between 34.25-106.72 Bq/kg with a mean value of 57.96 ± 2.55Bq/kg; and that of $^{40}$K from 246.12-394.53 Bq/kg with a mean of 325.14±10.87 Bq/kg. Different vertical profile of $^{226}$Ra, $^{228}$Ra and $^{40}$K activity concentration observed between sampling locations might due to the sediment mineralogy, source of radioactivity, geochemistry of the area and oceanic process. Plus, smaller $^{228}$Ra/$^{226}$Ra activity ratio range suggests that interaction on these two series with the surrounding were very similar. Value of study radionuclides in present study were almost comparable with study done in other part in Malaysia. Moreover, world mean value of $^{226}$Ra, $^{228}$Ra and $^{40}$K provided by UNSCEAR (1993) fall within the value range of radionuclides in present study.

## Acknowledgement

The authors thank to Faculty of Applied Science UiTM Shah Alam for gamma spectrometry system facilties. The author also thank to Research Management Institute (RMI) UiTM Shah Alam for grant provided with project code 600-RMI/DANA 5/3/RIF(3/2012).

## References

1. Theng, T.L. & Mohamed, C. A. R. (2005). Activities of $^{210}$Po and $^{210}$Pb in the water column at Kuala Selangor, Malaysia. *Journal of Environmental Radioactivity*, 80: 273-286.
2. IAEA-TECDOC-1429. January (2005). Radionuclide levels in oceans and seas. *Worldwide marine radioactivity studies (WOMARS)*. Final report of a coordinated research project .
3. IAEA. 19–22 March (2007). Naturally occurring radioactive material NORM V. In: Proceedings of an International Symposium, Seville, Spain.
4. John R. C., Ranjeet, K. R. & Sokhi, S. (2003). Radioactive Releases in the Environment: Impact and Assessment. *John Wiley & Sons, Ltd*. (1), England

5. Alatise, O.O., Babalola, I. A. & Olowofela, J. A. (2008). Distribution of some natural gamma-emitting radionuclides in the soils of the coastal areas of Nigeria. *Journal of Environmental Radioactivity*, 99: 1746-1749.
6. Saat, A., Hamzah, Z., Yusop. M. F. & Zainal, M. A. (2010). Experimental Determination of the HPGe Spectrometer Efficiency Calibration Curves for Various Sample Geometry for Gamma Energy from50 keV to 2000 keV. *Progress of Physic Research in Malaysia, American Institute of Physic*, 5: 39 – 42.
7. Hamzah, Z., Saat, A., Mashuri, N. H. & Redzuan, S. D. (2008). Surface Radiation Dose and Radionuclide Measurement in Ex-Tin Mining Area, Kg Gajah Perak. *The Malaysian Journal of Analytical Science*, 12: 419-431.
8. Brady, N.C. (1984). The Nature and Properties of Soils, 9. *Macmillan Publishing Co., New York*, 750.
9. Avnimelec. Y, Ritvo. G, Meijer. L. E, & Kochba. M. (2001). Water content, organic carbon and dry bulk density in flooded sediments. *Aquacultural Engineering* 25: 25–33.
10. Opreanu. G. (2003). Porosity, density and other physical properties of deep sea sediment from the black sea. National Institute of Marine Geology and Geo-ecology Modern and Ancient Fluvial, Deltaic and Marine Environments and Processes Proceedings of Euro-EcoGeoCentre-Romania: GEO-ECO-MARINA 9-10/2003-2004.
11. Molinari & Snodgrass. (1990). The chemistry and radiochemistry of radium and the other elements of the uranium and thorium and natural decay series. *The environmental Behaviour of Radium, 1*. Technical Report Series No.310 IAEA.
12. Choy, C. C., Zaharuddin. A. & Mohamed, C. A. R. (2007). Vertical profile of $^{210}$Pb in the sediment core in Kuala Selangor Malaysia. *The Malaysian Journal of Analytical Science*, 11: 274-279.
13. Jetter, H. H. (2000). Determining the Ages of Recent Sediments Using Measurements of Trace Radioactivity. *Terra et Aqua*, 78 : 21 – 28.
14. Lauria, D. C., Almeida, R. M. R., Godoy, J. M. O. & Sracek, O. (2002). On the high radium concentrations and low pH values in ground waters of a Brazilian coastal region. Radioactivity in the Environment (Proc. Conf. Monaco).
15. Godoy, J.M., Lauria, D.C., Godoy, M.L.D.P. & Cunha, R.P. (1994). Development of a sequential method for the determination of $^{238}$U, $^{234}$U, $^{232}$Th, $^{230}$Th, $^{228}$Th, $^{228}$Ra, $^{226}$Ra, and $^{210}$Pb in environmental samples. *J. Radioanalyt. Nucl. Chem: Articles*, 182 (1)165–169.
16. Sanders, L. M., Sanders, C. J., Luiz-Silva, W., Machado, W. E., Silva-Filho, V. & Patchineelam. S. R. (2010). Anthropogenic source assessment of $^{226}$Ra and $^{210}$Pb in a sediment core from the Cubatao River estuary (SE Brazil), *Journal of Radioanalytical and Nuclear Chemistry*, 287:729 – 732.
17. Chung, Y. C & Chen, C. T. A. (2007). Natural and Anthropogenics Radionuclides. *Encyclopedia of Life Support Systems (EOLSS)*, Eolss Publishers, Oxford, UK, ISBN: 978-1-905839-62-9 e-Book, 1 : 359-388.
18. Tavakoly Sany, S. B., Salleh, A., Sulaiman, A. B., Sasekumar, A., Tehrani, G. M. & Rezayi, M. (2012). Distribution, characteristic and ecological risk of heavy metals in surface sediments of West Port, Malaysia. *Environment Protection Engineering*, 38(4): 139 – 155.
19. Saat, A., Hamzah, Z., Abu Bakar, Z., Ahmad, Z. &Wood, A. B. (14 – 15 March 2009). Applicability of Pb-210 method for ages and sedimentation study of a recent freshwater ex-minig lake. *Conferences on Scientific & Social Research (CSSR)*, paper number: 5281121.
20. Hamzah, Z., Abdul Karim, U. K. & Saat, A. (2012). Measurement of natural radioactivity level in surface sediment in southern Kuala Selangor coastal area. *Malaysian Journal of Fundamental and Applied Sciences*, 8:266 – 270.
21. Yii, M.W., Wan Mahmood, Z., , Ahmad, Z, Md. Jaffary, N. A. I. & Ishak, K. (2011). NORM activity concentration in sediment cores from the Peninsular Malaysia East Coast Exclusive Economic Zone. *Journal of Radioanalytical and Nuclear Chemistry*, 289: 653-661.
22. Omar M., Ibrahim M.Y., Hassan A., Mahmood C.S & Sharifuddin M. A. (1991). Aras Sinaran dan Keradioaktifan Alam Sekitar di Malaysia, Seminar Kebangsaan IRPA sektor strategik.
23. Turekian, K. K.; Wedepohl, K. H. (1961). Distribution of the elements in some major units of the earth's crust. *Geol. Soc. Am. Bull*., 72 : 175 – 192.
24. Ismail, A. K., Ahmad, Z., Mohamed, N. & Yii, M. W. (23–27 April 2007). Proceeding International Conference on Environmental Radioactivity, International Atomic Energy Agency, Vienna, 255.

25. Ahmad, Z., Ishak, A. K. & Yii M. W. (2007). Marine Environment Related Activities in Malaysia Using Nuclear Technologies. *Country Report Malaysia*. Industrial Technology Division, Malaysian Institute for Nuclear Technology Research (MINT).
26. Yii, M. W., Ahmad, Z. & Ishak, A. K. (2009). Distribution of natural occurring radionuclides activity concentration in East Malaysia marine sediment. *Applied Radiation and Isotopes*, 67: 630-635.
27. Li, D. M., Xu, M. Q., Liu, G. S. & Li, C. (2007). Distribution of radioisotopes in sediment cores from nearshore off Xinghua Baymouth, Fujian, China. *Journal of Radioanalytical and Nuclear Chemistry*, 273: 151-155.
28. UNSCEAR (1993). Sources and effects of ionizing radiation. Report of the United Nations Scientific Committee on the Effects of Atomic Radiation to the General Assembly, with Scientific Annexes, United Nations, New York, USA.

The Malaysian Journal of ANALYTICAL SCIENCES ISSN 1394-2506

# SINTESIS HIDROGEL BERASASKAN *NATA DE COCO* DENGAN ASID AKRILIK SEBAGAI KO-MONOMER MENGGUNAKAN KAEDAH PEMPOLIMERAN RADIKAL BEBAS

## (Synthesis of Hydrogel Based on *Nata De Coco* and Acrylic Acid as Co-Monomer using Free Radical Polymerization Method)

Melissa Liew, Rizafizah Othaman, Rozida Khalid, M.C.Iqbal M.Amin, Azwan Mat Lazim*

*Pusat Pengajian Sains Kimia dan Teknologi Makanan*
*Fakulti Sains dan Teknologi*
*Universiti Kebangsaan Malaysia, 43600 UKM Bangi, Selangor, Malaysia*

**Corresponding author: azwanlazim@ukm.edu.my*

**Abstrak**

Nata de coco merupakan sejenis selulosa bakteria yang dihasilkan oleh bakteria dari spesis Acetobacter xylinum. Sifatnya yang lebih stabil secara fizikal berbanding selulosa daripada tumbuhan memberikan kelebihan yang luar biasa untuk dibangunkan sebagai hidrogel yang sensitif terhadap persekitaran. Hidrogel selulosa bakteria-ko-asid akrilik disintesis berdasarkan kaedah pempolimeran radikal bebas. Agen pemula , ammonium persulfat (APS)telah digunakan untuk memulakan tindak balas. Manakala agen taut silang, N,N'-metilena bisakrilamida telah digunakan supaya tindak balas pempolimeran menghasilkan jaringan yang lebih baik dan efektif. Ujian pembengkakan ke atas hidrogel dijalankan pada larutan yang mempunyai pH yang berbeza untuk mengenalpasti kebolehan hidrogel bertindak balas terhadap pH persekitaran. Analisis ATR-FTIR dijalankan untuk memastikan wujudnya interaksi molekul antara selulosa bakteria dan asid akrilik. Selain itu, penentuan nilai peralihan kaca ($T_g$) menggunakan kaedah DSC dijalankan ke atas hidrogel yang berjaya disintesis.

**Kata kunci:** Nata de Coco, hidrogel, kaedah pempolimeran radikal bebas, asid Akrilik

**Abstract**

Nata de Coco or known as bacterial cellulose is produced by Acetobacter xylinum where it is more stable than plant cellulose. Moreover, it also provides outstanding advantages to be developed as an environmental responsive hydrogels. In this study the bacterial cellulose-g-acrylic acid hydrogel was synthesized by using a free radical polymerization method. Ammonium persulfate (APS) was used to initiate the reaction, while N,N'-methylene bisacrylamide has been used as the crosslinking agent. In order to test the hydrogel respond, swelling tests were made at different pH. Furthermore, ATR-FTIR analysis was used to determine the interactions between bacterial cellulose and acrylic acid. Finally, the determination of glass transition (Tg) was made by using DSC.

**Keywords**: Nata de Coco, hydrogel, free radical polymerization, acrylic acid

## Pengenalan

Hidrogel merupakan satu rangkaian polimer hidrofilik yang boleh menyerap air dan memegang kuantiti air yang banyak. Pada masa yang sama, hidrogel masih lagi dapat mengekalkan strukturnya [1]. Selain daripada itu ia juga stabil secara kimia dan boleh terbiodegradasi [2]. Hidrogel juga merupakan polimer hidrofilik tiga dimensi yang linear atau bercabang dengan kebolehan menyerap air garam atau larutan fisiologikal yang banyak [3]. Kebolehan hidrogel menyerap air adalah disebabkan oleh kehadiran kumpulan hidrofilik seperti -OH, -CONH, $-CONH_2$, $NH_2$, -COOH dan $-SO_3H$ [4]. Kandungan air hidrogel mempunyai kesan yang kuat ke atas ketelapan, sifat mekanikal, sifat permukaan dan bio-keserasian. Hidrogel mempunyai sifat fizikal yang hampir sama dengan tisu hidupan. Hal Ini disebabkan keserasian dari segi kandungan air yang tinggi, konsistensi yang lembut dan bergetah dan ketegangan antara muka yang rendah dengan air atau cecair biologikal [5].

Sifat pengembangan hidrogel bergantung kepada persekitaran luaran yang dikenakan ke atasnya. Terdapat beberapa faktor yang boleh mengawal pengembangan hidrogel yang responsif secara fisiologikal adalah pH, kekuatan ionik, suhu dan radiasi elektromagnetik [6]. Contohnya, aplikasi dalam bidang bioperubatan, hidrogel yang sensitif terhadap persekitaran adalah paling sesuai untuk dibangunkan sebagai sistem penghantaran ubat [1] kerana sifatnya yang menyerupai tisu hidupan semulajadi berbanding bahan bio-sintetik yang lain. Kandungan air yang tinggi dalam bahan tersebut menyumbang kepada kebioserasiannya. Selain itu, hidrogel boleh digunakan sebagai kanta sentuh, membran untuk biosensor dan peranti untuk penghantaran ubat [7].

Penggunaan selulosa sebagai ko-monomer dalam penghasilan hidrogel semakin pesat dibangunkan. Ini kerana selulosa merupakan sumber yang boleh diperbaharui dan berpotensi menjadi sumber bahan kimia yang utama pada masa hadapan [8]. Pelbagai bahan berfungsi baru yang dihasilkan daripada selulosa yang masih dibangunkan untuk aplikasi yang luas kerana permintaan yang meningkat untuk produk yang mesra alam [9]. Selulosa (β-1,4-glukan) merupakan salah satu polimer paling banyak yang boleh didapati secara semulajadi. Selulosa ini merupakan komponen yang sering terikat dengan polimer lain (pektin, lignin, arabinan dan lain-lain) di dalam dinding sel tumbuhan, alga, sesetengah haiwan peringkat rendah (Tunicata) dan sesetengah genus bakteria (*Rhizobium, Agrobacterium* dan *Alcaligenes*). Bakteria seperti *Acetobacter xylinum* menghasilkan jaringan selulosa sebagai gentian secara ekstrasel[10]. Selulosa dari sumber bakteria dan tumbuhan adalah sama dari segi kimia tetapi mempunyai struktur makromolekul dan sifat fizikal yang berbeza [11].

Selulosa bakteria adalah tulen sepenuhnya manakala selulosa tumbuhan biasanya dikaitkan dengan sebatian biogenik yang lain seperti lignin dan pektin. Ia mempunyai sifat mekanikal yang tinggi termasuklah kekuatan tegangan, kemampuan memegang air yang tinggi, kehabluran tinggi dan bio-keserasian yang tinggi. Hidrogel berasaskan selulosa bakteria mempunyai aplikasi yang luas dalam bidang kejuruteraan tisu kerana ia mempunyai asas dengan ketulenan yang tinggi dan sifat fizikokimia yang luar biasa [12].

Kajian yang telah dijalankan oleh Nadia dan rakan penyelidik (2012) membuktikan bahawa hidrogel berasaskan *Nata de Coco* dan asid akrilik berjaya dihasilkan dengan menggunakan kaedah sinaran elektron. Hidrogel yang berjaya dihasilkan ini berupaya memberi respon terhadap perubahan pH. Hidrogel ini sesuai digunakan sebagai sistem penghantaran ubat dalam badan manusia.

Namun begitu, kaedah yang bersesuaian, ekonomik dan praktikal membolehkan hidrogel ini mampu dihasilkan dengan skala yang lebih besar dan boleh digunakan kelak. Sehubungan itu, kajian ini dijalankan bertujuan untuk menggunakan kaedah pempolimeran radikal bebas bagi mensintesis hidrogel dan dapat memberikan keputusan yang baik.

## Bahan dan kaedah

Asid akrilik 99% (AA dari Sigma-Aldrich), selulosa bakteria yang disediakan daripada *Nata de Coco* yang telah ditulenkan, diliofilisasikan dan dikisar, ammonium persulfat (APS), *N,N'*-metilena bisakrilamida 99% (BIS dari Sigma-Aldrich), larutan penimbal dan air suling.

Selulosa bakteria daripada *Nata de Coco* digunakan sebagai monomer manakala asid akrilik digunakan sebagai ko-monomer. Ammonium persulfat (APS) digunakan sebagai agen pemula anionik, *N,N'*-metilena bisakrilamida (BIS) berfungsi sebagai agen taut silang dan air suling digunakan untuk menyediakan larutan akueus.
Mantel pemanas, kelalang berleher-3, pengacau bermagnet, termometer, kondenser dengan pam elektronik CC1, kaki retort, gas nitrogen, bikar, pengukur pH, Jumlah Pantulan Teratenuat-Spektroskopi Fourier Transform Inframerah (ATR-FTIR) dan Kalorimetri Pengimbasan Perbezaan (DSC) model 822$^e$ syarikat Mettler-Toledo (M) Sdn. Bhd.

### Penyediaan Hidrogel

Hidrogel yang disintesis menggunakan kaedah pempolimeran radikal bebas seperti yang telah dilaporkan oleh Zhou et al. pada tahun 2011. Serbuk *Nata de Coco* disebarkan di dalam air suling dan diletakkan ke dalam kelalang berleher-3 bersama dengan pengacau bermagnet. Pengacau bermagnet digunakan untuk kacauan secara berterusan. Serbuk APS dilarutkan dengan air suling di dalam bikar dan ditambah ke dalam kelalang tersebut. Campuran larutan dipanaskan di atas mantel pemanas kepada 70°C. Gas nitrogen dialirkan untuk mengeluarkan

gas oksigen yang terdapat di dalam kelalang. Setelah larutan mencapai suhu 70°C, serbuk BIS yang dilarutkan dalam air suling dimasukkan ke dalam campuran tersebut. Larutan dikacau sehingga likat dan dituang ke dalam piring petri dan kemudian diletakkan ke dalam ketuhar bersuhu 40°C.

**Ujian pembengkakan pada larutan pH yang berbeza**

Ujian pembengkakan hidrogel dalam larutan pH yang berbeza adalah untuk mengetahui kesan pH terhadap hidrogel. Hidrogel direndam di dalam larutan pada suhu bilik dan beratnya akan ditimbang setiap lima minit selama 2 jam. Perubahan yang berlaku diperhatikan. Nisbah pembengkakan hidrogel dikira dengan menggunakan persamaan 1 berikut:

$$S = (M_t - M_o) / M_o \times 100 \quad (1)$$

di mana $M_o$ (g) merupakan jisim asal hidrogel dan $M_t$ (g) ialah jisim hidrogel yang mengalami pembengkakan pada masa t (min).

**Analisis menggunakan spektroskopi ATR-FTIR**

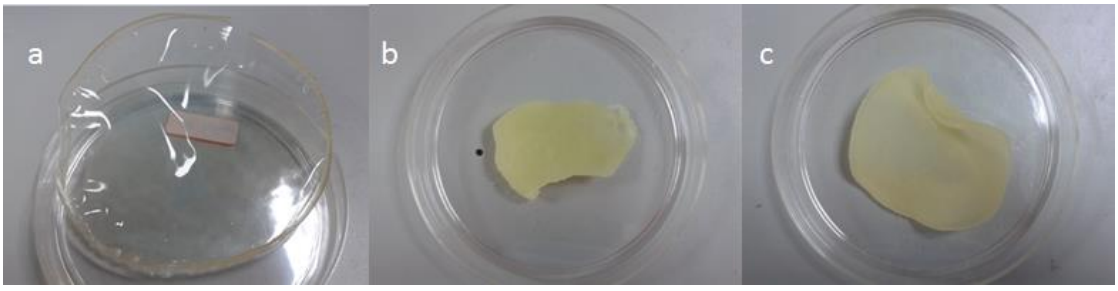
Spektrogram inframerah hidrogel diukur dengan menggunakan ATR-FTIR. Sampel hidrogel disediakan dengan memotong sampel ke bentuk segi empat tepat berukuran 0.5 cm x 0.5 cm.

**Analisis menggunakan kalorimetri pengimbasan perbezaan (DSC)**

Perbezaan suhu antara sampel dan rujukan adalah kesan primer daripada kejadian terma di dalam sampel. Kalorimetri Pengimbasan Perbezaan merupakan kaedah yang cepat untuk penentuan sifat terma bahan polimerik [15]. Sampel dianalisis dengan menggunakan peralatan DSC model Perkin Elmer ModeL DSC-7, USA.

## Keputusan dan Perbincangan

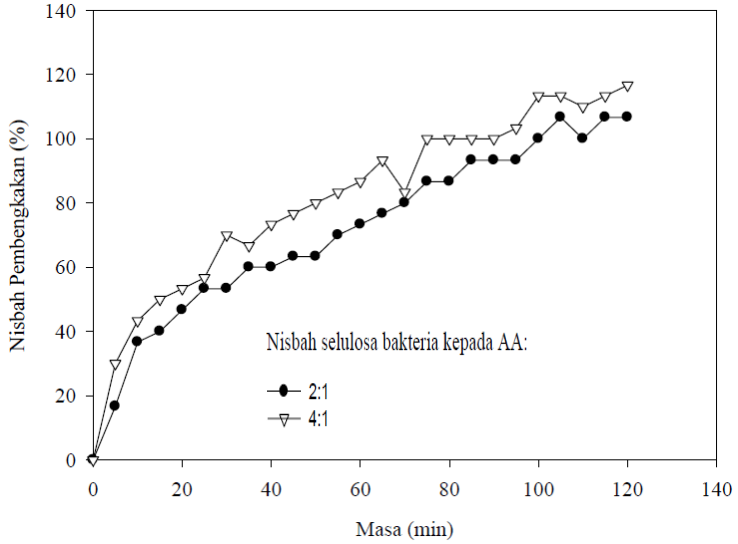
Hidrogel (selulosa bakteria-ko-asid akrilik) telah berjaya disintesis dengan menggunakan nisbah selulosa bakteria kepada asid akrilik yang berlainan. Nisbah isipadu selulosa:asid akrilik yang telah digunakan adalah 2:1 dan 4:1. Hidrogel asid akrilik disintesis sebagai kawalan seperti yang ditunjukkan dalam Rajah 1a, di mana hidrogel yang telah disintesis mempunyai tekstur yang lembut dan elastik seakan-akan plastic dan mempunyai sifat lut cahaya. Namun begitu didapati hidrogel selulosa bakteria-ko-asid akrilik dengan nisbah 2:1 dan 4:1 adalah tidak lut cahaya (Rajah 1b dan 1c).




Rajah 1. Hidrogel yang telah disintesis di mana a) hydrogel brasaskan asid akrilik yang dijadikan sampel kawalan b) hydrogel dengan nisbah 2:1 dan c) hydrogel dengan nisbah 4:1

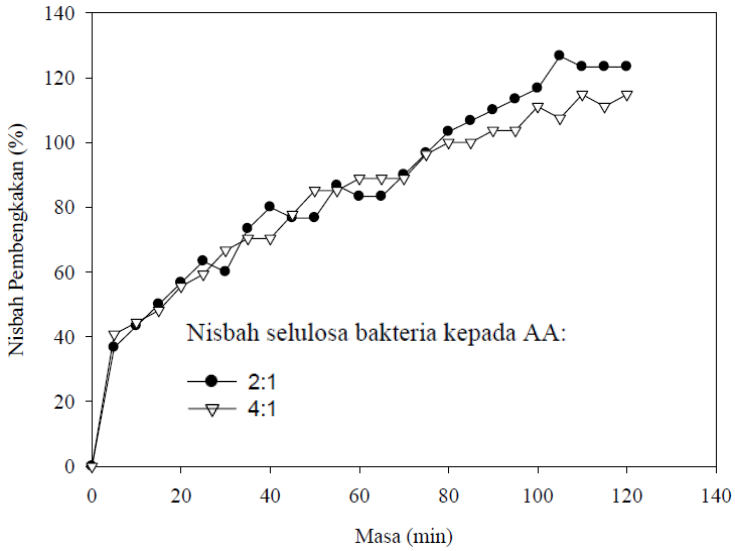
**Keputusan ujian pebengkakan pada larutan pH yang berbeza**

Bagi menentukan kebolehan menyerap air, hidrogel yang dihasilkan telah diuji dengan memasukkannya ke dalam larutan penimbal yang mempunyai nilai pH yang berbeza. Rajah 2 menunjukkan keputusan dalam larutan penimbal pH 1, nilai peratusan nisbah pembengkakan bagi hidrogel 4:1 yang tertinggi ialah 116.67% manakala bagi hidrogel 2:1 ialah 106.67%. Hidrogel 4:1 mempunyai nisbah pembengkakan yang lebih tinggi daripada hidrogel 2:1.




Rajah 2. Graf nisbah pembengkakan (%) lawan masa (min) bagi hidrogel yang berbeza nisbah selulosa bakteriakepada asid akrilik (AA) di dalam larutan penimbal pH 1.

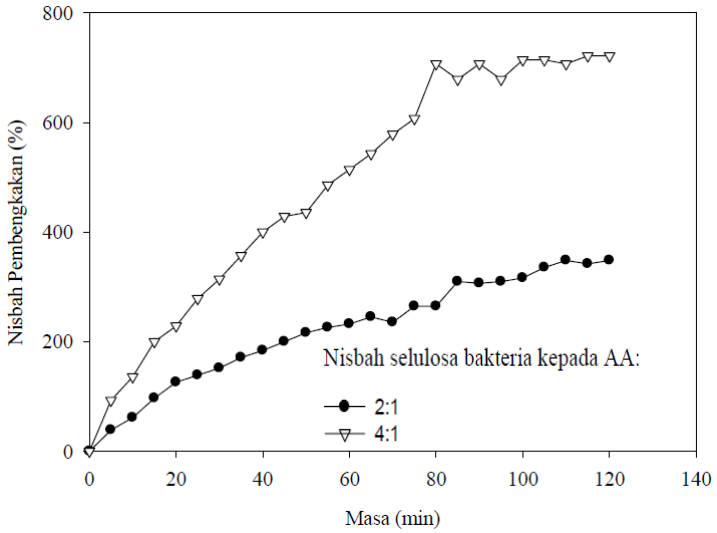
Pada larutan pH 7 (Rajah 3) dapat diperhatikan bahawa peratusan nisbah pembengkakan kedua-dua hidrogel tidak mempunyai perbezaan yang ketara pada awal ujian. Pada akhir ujian, nilai peratusan nisbah pembengkakan hidrogel 2:1 dalam larutan penimbal pH 7 adalah lebih tinggi daripada hidrogel 4:1 dengan nilai masing-masing 126.67% dan 114.81%.




Rajah 3. Graf nisbah pembengkakan (%) lawan masa (min) bagi hidrogel yang berbeza nisbah selulosa bakteria kepada asid akrilik (AA) di dalam larutan penimbal pH 7.

Nilai peratusan nisbah pembengkakan mempunyai perbezaan yang sangat ketara di dalam larutan penimbal pH 13 (Rajah 4). Nilai tertinggi yang dicatat oleh hidrogel 4:1 ialah 721.43% manakala hidrogel 2:1 mempunyai nilai tertinggi 348.39%. Nilai tertinggi hidrogel 4:1 adalah lebih dua kali ganda daripada nilai tertinggi hidrogel

2:1. Pada pH 1 dan 13, hidrogel dengan nisbah 4:1 mempunyai nisbah pembengkakan yang lebih tinggi daripada hidrogel dengan nisbah 2:1 sepanjang masa ujian dijalankan.




Rajah 4. Graf nisbah pembengkakan (%) lawan masa (min) bagi hidrogel yang berbeza nisbah selulosa bakteria kepada asid akrilik (AA) di dalam larutan penimbal pH 13.

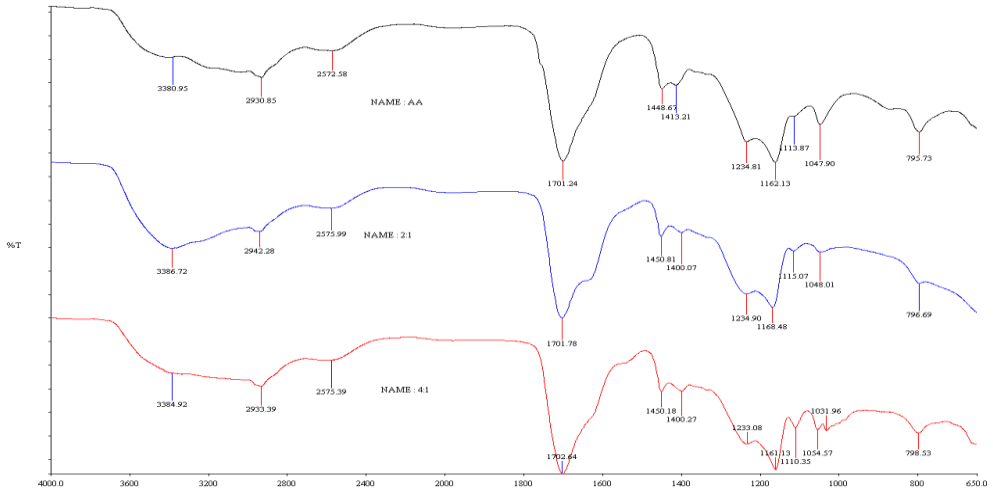
Berdasarkan ketiga-tiga graf (Rajah 2 - 4) hidrogel 4:1 yang mempunyai kandungan selulosa bakteria yang lebih tinggi adalah lebih sensitif dalam larutan penimbal pH 1 dan 13 berbanding hidrogel 2:1 yang mempunyai kandungan selulosa bakteria yang lebih rendah. Hidrogel 4:1 adalah paling sensitif di dalam larutan pH 13 di mana ia memberi kesan pembengkakan yang sangat tinggi. Ini bermaksud hidrogel 4:1 mempunyai kebolehan penyerapan yang paling baik di dalam larutan pH 13. Ini adalah kerana jaringan hidrogel yang disintesis mempunyai cas-cas negatif dan larutan pH 13 bersifat bes yang mana mempunyai banyak cas-cas negatif. Oleh itu, sekiranya hidrogel ini di masukkan ke dalam larutan pH 13, cas-cas negatif dalam jaringan hidrogel dan larutan akan saling menolak antara satu sama lain seterusnya akan menyebabkan hidrogel itu membengkak [13].

**Keputusan analisis menggunakan spektroskopi ATR-FTIR**

Spektrum inframerah (Rajah 5) untuk kedua-dua hidrogel 2:1 dan 4:1 masing-masing menunjukkan puncak penyerapan pada sekitar 3386 $cm^{-1}$ dan 3384 $cm^{-1}$ yang mewakili kumpulan –OH selulosa yang mempunyai ikatan hidrogen. Selain itu, kedua-dua spektrum tersebut mempunyai puncak sekitar 2900 $cm^{-1}$ (2942.28 $cm^{-1}$ untuk hidrogel 2:1 dan 2933.39 $cm^{-1}$ untuk hidrogel 4:1) yang merupakan kesan daripada peregangan $–CH_2$ tidak simetri kumpulan $–CH_2OH$ di dalam selulosa bakteria [14].

Kewujudan puncak 1702.64 $cm^{-1}$ pada hidrogel 2:1 dan 1701.72 $cm^{-1}$ pada hidrogel 4:1 adalah kerana getaran peregangan C=O kumpulan –COOH daripada asid akrilik. Puncak pada sekitar 1400 $cm^{-1}$ berkaitan dengan regangan simetri kumpulan –COO- [17]. Puncak-puncak pada julat 1710-1569 $cm^{-1}$ dan 1411 $cm^{-1}$ membuktikan kumpulan karboksil wujud di dalam hidrogel selepas proses pempolimeran antara kedua-dua monomer. Peregangan C-O-C ikatan eter selulosa dapat dilihat pada 1168 $cm^{-1}$ pada hidrogel 2:1 dan 1161 $cm^{-1}$ pada hidrogel 4:1 [18].

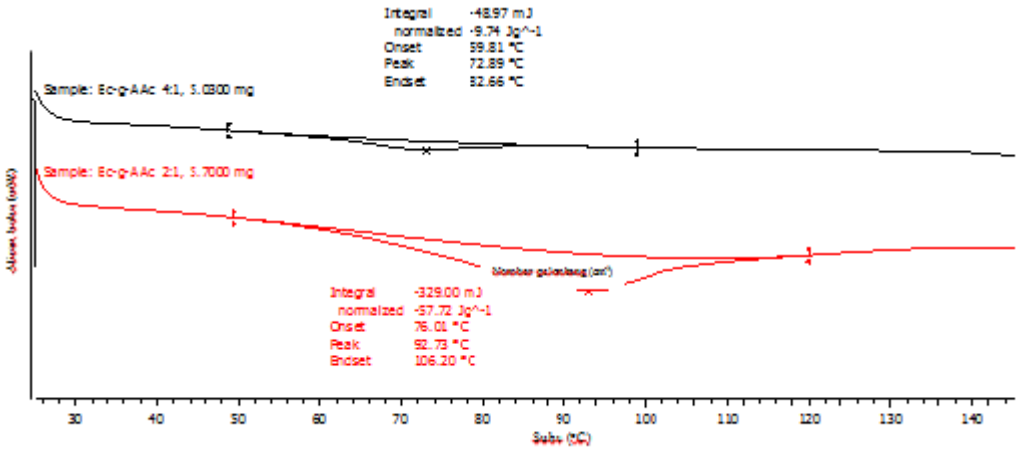
Dalam Rajah 5, spektrum hidrogel asid akrilik menunjukkan puncak yang tajam pada 1701.24 kerana kehadiran ikatan C=O. Puncak yang luas dapat diperhatikan pada julat 3400-2400 $cm^{-1}$ kerana kehadiran ikatan O-H [19].




Rajah 5. Spektogram Perbandingan spektrum inframerah untuk ketiga-tiga hidrogel

**Keputusan analisis menggunakan kalorimetri pengimbasan perbezaan (DSC)**

Seperti yang ditunjukkan dalam Rajah 6 nilai peralihan gelas ($T_g$) bagi hidrogel 2:1 ialah 76.01 °C manakala nilai peralihan kaca ($T_g$) bagi hidrogel 4:1 ialah 59.81 °C. Hidrogel 2:1 mempunyai nilai $T_g$ yang lebih tinggi berbanding hidrogel 4:1. Hal ini menunjukkan bahawa hidrogel 2:1 mempunyai kestabilan terma yang lebih baik berbanding hidrogel 4:1. Hal ini disebabkan oleh perbezaan kandungan selulosa bakteria di dalam hidrogel. Menurut Amin dan rakan penyelidik(2012) [18], kandungan selulosa bakteria yang lebih tinggi dalam hidrogel akan menyebabkan nilai $T_g$ lebih rendah. Molekul air yang terikat pada selulosa bertindak sebagai pemplastik (*plasticizer*) akan menyebabkan penurunan nilai $T_g$ [18].




Rajah 6. Termogram perbandingan nilai peralihan gelas hidrogel 2:1 dan hidrogel 4:1

## Kesimpulan

Berdasarkan kajian ini, hidrogel (selulosa bakteria-ko-asid akrilik) berjaya disintesis dengan menggunakan kaedah pempolimeran radikal bebas. Hidrogel yang telah disintesis dicirikan dengan ujian pembengkakan, Spektroskopi Jumlah Pantulan Teratenuat-Fourier Transform Inframerah dan Kalorimetri Pengimbasan Perbezaan. Ujian pembengkakan menunjukkan hidrogel 4:1 yang mengandungi kandungan selulosa bakteria yang lebih tinggi mempunyai peratusan nisbah pembengkakan yang lebih tinggi berbanding hidrogel 2:1 dalam larutan penimbal pH 1 dan 13. Dalam larutan penimbal pH 7 pula, hidrogel 2:1 mempunyai peratusan nisbah

pembengkakan yang tinggi sedikit berbanding hidrogel 4:1. Bagi spektroskopi Jumlah Pantulan Teratenuat-Fourier Transform Inframerah pula, kedua-dua hidrogel 2:1 dan 4:1 menunjukkan puncak-puncak yang lebih kurang sama tetapi pada keamatan yang berbeza. Kaedah pencirian ini turut membuktikan bahawa terdapat interaksi ikatan antara selulosa bakteria dan asid akrilik di dalam hidrogel. Nilai peralihan gelas ($T_g$) pula ditentukan dengan menggunakan kaedah Kalorimetri Pengimbasan Perbezaan. Nilai $T_g$ bagi hidrogel 2:1 adalah lebih tinggi daripada hidrogel 4:1. Hal ini menunjukkan bahawa hidrogel 2:1 mempunyai kestabilan terma yang lebih baik berbanding hidrogel 4:1. Berdasarkan keputusan yang diperoleh, hidrogel berasaskankan nata de coco ini berpotensi untuk digunakan sebagai bahan penyerap sisa seperti pewarna dan logam berat dalam proses pembersihan alam sekitar. Selain itu ia juga boleh diaplikasikan dalam bidang bioperubatan seperti perawat luka (wound dressing) disebabkan sifatnya yang bioserasi dan tidak toksik.

**Penghargaan**

Penulis ingin merakamkan ucapan terima kasih kepada UKM dan juga geran penyelidikan INDUSTRI-2013-022.

**Rujukan**

1. Qiu, Y. & Park, K. 2001. Environment-sensitive hydrogels for drug delivery. *Advanced Drug Delivery Reviews* 53: 321-339.
2. Hoffman, A.S. 2002. Hydrogels for biomedical applications. *Advanced Drug Delivery Reviews* 43: 3-12.
3. Chang, C., Duan, B., Cai, J. & Zhang, L. 2010. Superadsorbent hydrogels based on cellulose for smart swelling and controllable delivery. *European Polymer Journal* 46: 92-100.
4. Kost, J. 1996. Controlled drug delivery systems. *Polymeric Materials Encyclopedia* 1: 1509-1515.
5. Blanco, M.D., Garcia, O., Trigo, R.M., Teijon, J.M. & Katime, I. 1996. 5-Fluorouracil release from copolymeric hydrogels of itaconic acid monoester. *Biomaterials* 17: 1061-1067.
6. Peppas, N.A. 1991. Physiologically responsive gels. *Bioactive and Compatible Polymers* 6 (3): 241-246.
7. Peppas, N.A., Bures, P., Leobandung, W. & Ichikawa, H. 2000. Hydrogels in pharmaceutical formulations. *European Journal of Pharmaceutics and Biopharmaceutics* 50: 27-46.
8. Eichhorn, S.J., Young, R.J. & Davies, G.R. 2005. Modeling crystal and molecular deformation in regenerated cellulose fibres. *Biomacromolecules* 6: 507.
9. Klemm, D., Heublein, B., Fink, H. & Bohn, A. 2005. Cellulose: fascinating biopolymer and sustainable raw material. *Angewandate Chemie International Edition* 44: 3358.
10. Vandamme, E.J., De Baets, S., Vanbaelen, A., Joris, K. & De Wulf, P. 1998. Improved production of bacterial cellulose and its application potential. *Polymer Degradation and Stability* 59: 93-99.
11. Sannino, A., Demitri, C. & Madaghiele, M. 2009. Biodegradable cellulose-based hydrogels: design and applications. *Materials* 2: 353-373.
12. Kakugo, A., Gong, J. & Osada, Y. 2007. Bacterial cellulose based hydrogel for articular soft tissue. *Cellulose Communication* 14: 50.
13. Nadia Halib, Mohd. Cairul Iqbal Mohd. Amin & Ishak Ahmad. 2012. Physiochemical properties and characterisation of nata de coco from local food industries as a source of cellulose. *Sains Malaysiana* 41(2): 205-211.
14. Zhou, Y., Fu, S., Liu, H., Yang, S. & Zhan, H. 2011. Removal of methylene blue dyes from wastewater using cellulose-based super-adsorbent hydrogels. *Polymer Engineering and Science* 51(2): 2417-2424.
15. Pielichowski, K. & Njuguna, J. 2005. Thermal degradation of polymeric materials. United Kingdom: Rapra Technology Limited.
16. Majumdar, S., Dey, J. & Adhikari, B. 2006. Taste sensing with polyacrylic acid grafted cellulose membrane. *Talanta* 69: 131-139.
17. Mohd. Cairul Iqbal Mohd. Amin, Naveed Ahmad, Nadia Halib & Ishak Ahmad. 2012. Synthesis and characterisation of thermo- and pH-responsive bacterial cellulose/acrylic acid hydrogels for drug delivery. *Carbohydrate Polymers* 88: 465-473.
18. Pavia, D.L., Lampman, G.M., Kriz, G.S. & Vyvyan, J.R. 2009. Introduction to spectroscopy. United States of America: Brooks/Cole Cengage Learning.

The Malaysian Journal of ANALYTICAL SCIENCES ISSN 1394-2506

# KAJIAN AWALAN TERHADAP PENULENAN DAN PENGENALPASTIAN ASID AMINO AROMATIK L-DOPA DARIPADA KAKI PEREKAT KUPANG HIJAU AIR TAWAR MALAYSIA

## (Preliminary Study on Purification and Identification of Aromatic Acid Amino L-DOPA from Malaysia Freshwater Green Mussel Byssus)

Saiful Irwan Zubairi[1]*, Wan Rosmaryana Wan Musa[1], Syed Anuar Faua'ad Syed Mohammad[2]

*[1]Pusat Pengajian Sains Kimia & Teknologi Makanan,*
*Fakulti Sains & Teknologi,*
*Universiti Kebangsaan Malaysia, 43600 UKM Bangi, Selangor Darul Ehsan, Malaysia*
*[2]Jabatan Kejuruteraan Bioproses,*
*Fakulti Kejuruteraan Kimia & Kejuruteraan Sumber Asli,*
*Universiti Teknologi Malaysia, 81310 UTM Skudai, Johor Darul Takzim, Malaysia*

**Corresponding author: saiful-z@ukm.edu.my*

**Abstrak**

L-DOPA (L-3,4-dihidroksifenilalanin) adalah sejenis asid amino aromatik yang dapat dikesan melalui kaedah pengekstrakan larutan berasid dan penulenan daripada perekat kaki kupang hijau. Oleh yang demikian, objektif utama kajian ini adalah untuk membuat pencirian dan penulenan asid amino L-DOPA dengan menggunakan kaedah kromatografi penurasan gel Sefadak G-200 melalui penggunaan dua jenis larutan fasa bergerak gel berasid dan beralkali. Penghancuran atau penghomogenan sampel perekat kaki kupang dilakukan dengan menggunakan mortar dan alu beserta penambahan cecair nitrogen bagi memecahkan struktur protein perekat kaki kupang hijau. Sampel yang dihancurkan dicampurkan dengan asid perklorik 0.7%, 1.0%, dan 1.5% (v/v) (pra-rawatan sampel) sebelum proses proses pengekstrakan dijalankan. Seterusnya, proses pengekstrakan dilakukan dengan mengempar sampel pada 11,000 rpm selama 10 min pada suhu 10 $^{o}$C. Supernatan S1 diambil dan ditambah dengan aseton dan asid sulfurik pekat, kemudiannya diempar untuk kali kedua untuk pengambilan pellet dan dilarutkan menggunakan larutan fasa bergerak sebelum proses penulenan dijalankan. Proses penulenan dijalankan menggunakan dua jenis fasa bergerak iaitu asid asetik 5% (v/v) dan NaOH 1M. Bacaan nilai penyerapan (abs) untuk fraksi sampel ekstrak berprotein ditulen dianalisa pada jarak gelombang di antara 214 nm ke 400 nm menggunakan UV-spektrofotometer. Bacaan penyerapan (abs) tertinggi akan dipilih bagi proses pengesanan dan pembuktian kewujudan asid amino L-DOPA di dalam fraksi tertulen. Proses verifikasi dilakukan dengan menggunakan kromatografi cecair berprestasi tinggi (HPLC) dan kromatografi lapisan nipis (TLC). Keputusan ujikaji menunjukkan penggunaan asid perklorik 0.7% dan asid asetik 5% bagi proses pra-rawatan dan cecair fasa bergerak proses penulenan masing-masing menghasilkan profil abs efluan yang tertinggi (menghampiri nilai 1.0) pada jarak gelombang 260 nm. Analisis TLC membuktikan kewujudan beberapa asid amino penting selain L-DOPA iaitu tirosin dan fenilalanin pada masa (jam) penggumpulan efluan ke-78. Manakala, analisis HPLC menunjukkan kepekatan L-DOPA adalah yang tertinggi (2.94 ± 0.12 mg/l) secara signifikan ($p$<0.05) berbanding pada masa penggumpulan efluan yang lain.

**Kata kunci**: L-3,4-dihidroksifenilalanin (L-DOPA), perekat kaki, kupang hijau, gel Sefadak G-200, TLC, HPLC

**Abstract**

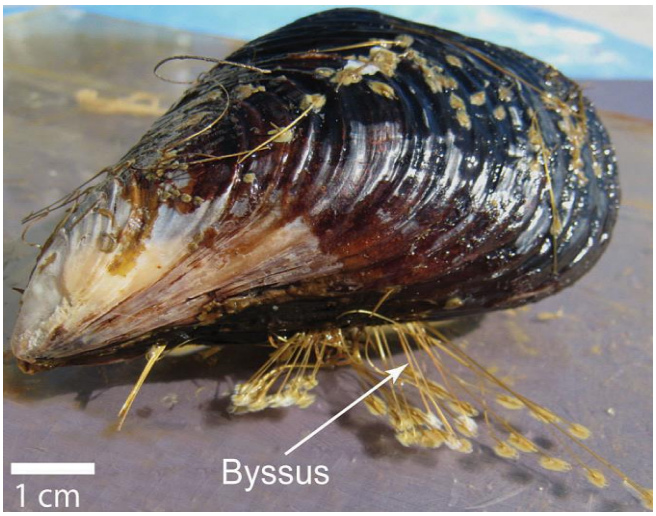
L-DOPA (L-3, 4-dihydroxyphenylalanine) is a type of aromatic amino acid which can be detected by using acidic extraction and purification method involving adhesive byssus green mussel protein. The main objective of this study is to identify and purify the aromatic amino acid L-DOPA via the utilization of gel Sephadex G-200 filtration chromatrography based on two types of acidic and basic mobile phase solution. The crushing and homogenizing for adhesive byssus green mussel were conducted using a mortar and a pestle with the aid of liquid nitrogen. The samples that had been crushed were then mixed and dissolved in perchloric acid 0.7%, 1.0% and 1.5% (v/v) (pre-treatment) prior to the extraction process. The extraction was carried out by centrifuging the extracts at 11,000 rpm for about 10 mins and at a temperature of 10 $^{0}$C to obtain supernatant S1. The supernatant was mixed with acetone and sulphuric acid and centrifuged for the second time to produce a pellet and then it was dissolved in

the respective mobile phase solutions prior to purification process. Purification was later performed using two mobile phase solutions which were acetic acid 5% (v/v) and NaOH 1M. The absorbance (abs) value of each purified protein extract fractions was collected and analysed at 214 nm to 400 nm with the help of UV-spectrophotometer. The highest abs value was selected for identification and verification of amino acid L-DOPA in the purified solution. Verification was carried out by utilizing high performance liquid chromatography (HPLC) and thin layer chromatrography (TLC). The results showed that the use of 0.7% (v/v) perchloric acid and 5% (v/v) acetic acid for pre-treatment process and mobile phase solution of purification process respectively, yielded the highest effluent abs profile at a wavelength of 260 nm. TLC analysis proved the existence of several important amino acids besides L-DOPA which were tyrosine and phenylalanine after 78 hrs of collection of effluents. Meanwhile, the analysis of HPLC revealed the highest concentration of amino acid L-DOPA ($p$<0.05) as compared to the other collected effluents.

**Keywords**: L-3,4-dihydroxyphenylalanine (L-DOPA), adhesive byssus, green mussel, gel Sephadex G-200, TLC, HPLC

## Pengenalan

Kupang hijau atau nama saintifiknya adalah *Perna viridis* adalah sejenis haiwan maritim yang diklasifikasikan dalam kumpulan invertebrata yang hidup di dalam air masin. Kupang hijau merupakan haiwan dwikutub yang mempunyai cengkerang yang keras, organ dalaman yang lembut dan kaki yang berotot untuk membantu pergerakkannya. Bahagian dalaman lembut terdiri daripada organ respirator, pencernaan dan pembiakan. Pembiakan kupang hijau yang kondusif memerlukan persekitaran air laut yang bersuhu 26 - 32 $^{o}$C, pH 7.1 - 8.5, kemasinan air 27 - 35%, oksigen terlarut 4 - 6 mg/l dan kedalaman air surut terendah pada ketinggian 3 - 4 meter [1]. Kupang hijau ini mempunyai ciri-ciri unik untuk hidup iaitu merembeskan bebenang daripada kelenjar fenol yang terdapat pada bahagian kakinya bagi tujuan membantu melekatkan dirinya kepada bahan lain seperti kayu, batu, logam dan plastik yang terdapat di dasar muara sungai [2]. Bebenang yang dihasilkan oleh kupang ini dikenali sebagai 'byssus' yang terbina daripada protein perekat (Rajah 1) [3]. 'Byssus' ini mempunyai kelebihan yang luar biasa di mana ia mempunyai kekuatan elastik yang tinggi sehingga boleh bertahan sehingga 200 MPa. Bebenang ini terhasil setiap 5 min per benang dan bebenang asalnya tidak akan mudah rosak dalam jangka masa satu atau dua tahun.




Rajah 1. Perekat (*byssus*) kupang hijau yang mengandungi asid amino penting L-DOPA [4].

Oleh yang demikian, protein yang terdapat di dalam perekat kaki kupang ini dilihat mempunyai potensi yang besar bagi industri komersial bahan pelekat dan juga bidang perubatan. Protein adalah polimer yang mengandungi beberapa jenis ikatan monomer asid amino yang dihubungkan oleh ikatan kovelan yang disebut ikatan peptida. Protein perekat kaki perekat (*byssus*) kupang hijau terbina daripada tiga asid amino aromatik utama iaitu L-3,4-dihidroksifenilalanin (L-DOPA), ditirosin dan tirosin [5]. L-DOPA adalah sebahagian daripada kelas pengantaraan kimia yang dikenali sebagai 'catecholamines' di mana ia adalah hasil daripada proses hidrolisis asid amino tirosin.

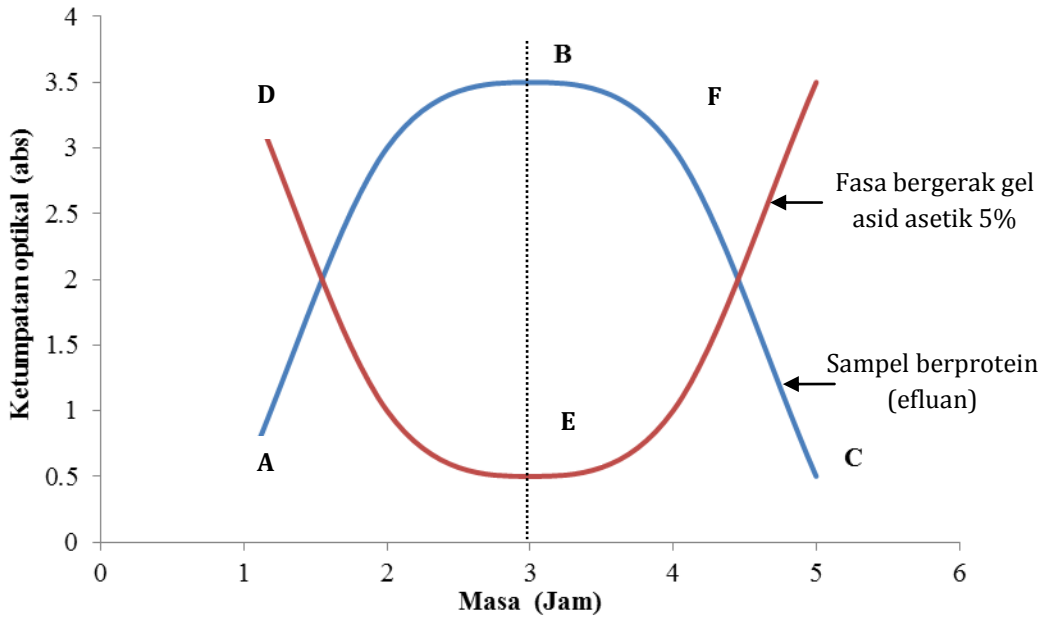
Kajian terhadap protein perekat bermula semenjak tahun 1980 apabila Jabatan Laut Amerika Syarikat mengadakan program mengenalpasti molekul protein perekat daripada hidupan invertabrata marin seperti kupang, tiram dan teritip [5, 6]. Kajian yang dilakukan dikhususkan kepada kupang biru dan hasil daripada kajian tersebut mendapati bahawa terdapatnya kewujudan asid amino L-DOPA pada perekat kupang tersebut dan ianya enam kali lebih besar berbanding kolagen tendon manusia dan keupayaan mekanikalnya setanding dengan *kevlar* dan serat karbon [7]. Asid amino L-DOPA yang wujud di dalam ekstrak protein perekat kaki kupang merupakan asid amino terpenting yang boleh memberi manfaat yang besar dalam bidang perubatan dan industri pembuatan. Dalam bidang perubatan, ia dapat mampu mengubati penyakit Parkinson's iaitu sejenis penyakit yang disebabkan oleh pengurangan pembentukan sel saraf di dalam otak [8]. Protein perekat ini juga berkeupayaan memberikan signal biologi untuk pelekatan sel sihat dan sel tumor di dalam kajian pengkulturan sel mamalia secara dua/tiga dimensi (3-D) tanpa menghasilkan toksin dan kesan [9]. Selain daripada itu, sifat protein perekat ini juga mempunyai keupayaan melekat pada pelbagai jenis permukaan seperti kaca, plastik, asetal, lapisan kayu nipis dan teflon di samping mampu melekat pada tulang dan gigi. Protein ini boleh dikomersilkan menjadi agen pelekat yang baik dan berpotensi untuk digunakan di dalam industri bahan pembuatan dan penggunaan domestik.

Disebabkan oleh potensi kepelbagaian penggunaan ekstrak protein kaki perekat kupang hijau di dalam bidang perubatan dan industri bahan pembuatan, keperluan untuk mengenalpasti dan membuat pengesahan komposisi asid amino yang terkandung di dalam ekstrak protein tersebut adalah penting. Oleh yang demikian, penggunaan teknik kromatografi adalah teknik yang terbaik dalam penghasilan/pengasingan fraksi tulen asid amino samada melalui polariti/cas molekul, pengasingan saiz molekul dan affiniti ikatan kovalen di antara molekul yang dibawa oleh fasa bergerak dan fasa pegun. Di dalam kajian ini, kaedah penurasan kromatografi gel Sefadak G-200 (penjerapan saiz molekul protein 5 - 500 kDa) digunakan bagi mendapatkan protein tulen yang mengandungi asid amino L-DOPA dengan cara pengasingan saiz molekul protein. Kromatografi gel merupakan satu teknik pemisahan komponen dalam sesuatu sebatian yang mana prinsip asas penggunaannya adalah sama dengan penurasan atau penapisan gel [10]. Kromatografi penapisan gel merupakan kaedah yang penting bagi menulenkan sebarang sampel berprotein bagi membuang sebarang bendasing yang tidak dikehendaki [11]. Ia terdiri daripada butiran manik-manik yang disediakan dengan merantaisilang molekul dekstran dengan epiklohirin (*Pharmacia*) dan mempunyai perbezaan daripada segi darjah kebolehanrantaian silang serta darjah pengembangan dan julat penceraian [12]. Rajah 2 menunjukkan teori ringkas proses penulenan menggunakan kaedah penurasan kromatografi gel Sefadak G-200. Profil perjalanan efluan bagi proses penulenan adalah seperti berikut:

1) Titik A ke B: Bacaan abs mula meningkat apabila sampel mulai turun daripada gel. Larutan fasa bergerak (contoh: asid asetik 5%) mulai berkurangan secara langsung (Titik D ke E).
2) Titik puncak B: Titik di mana bacaan abs sampel adalah maksimum atau lapisan terakhir larutan sampel yang akan ditulenkan berada lapisan terakhir gel sebelum larutan fasa bergerak baru dituangkan (Titik E).
3) Titik B ke C: Bacaan abs sampel mulai menurun disebabkan oleh pertambahan kembali larutan fasa bergerak gel ke dalam buret yang mengandungi gel (pencairan efluan berlaku) (Titik E ke F).

Selain daripada itu, gel Sefadak terbukti sangat stabil daripada segi kimia dan tidak larut dalam semua pelarut. Walaubagaimanapun, ikatan glikosidiknya merupakan satu kelemahan utama, di mana ia mudah terhidrolisis sekiranya terdedah kepada larutan yang berasid. Gel Sefadak adalah lebih stabil di dalam larutan beralkali dan pendedahan yang lama pada agen pengoksidaan akan menyebabkan penambahan kandungan kumpulan karboksil yang kesannya akan merosakkan sifat-sifat Sefadak tersebut [13].

Secara keseluruhan, kajian awalan terhadap protein perekat kaki kupang hijau yang mengandungi asid amino penting L-DOPA mempunyai potensi yang sangat besar dalam bidang bioteknologi dan bio-perubatan. Ia juga mampu dikomersilkan untuk diaplikasikan dalam sektor pembuatan komersial sebagai bahan perekat semulajadi yang mesra alam. Sehubungan dengan itu, pencirian bagi parameter pemprosesan pengekstrakan dan penulenan protein tersebut akan dapat memberikan gambaran awal penggunaan parameter yang terbaik bagi meningkatkan keberhasilan protein tersebut pada skala yang lebih besar (loji pandu).




Rajah 2. Profil efluan dan fasa bergerak bagi proses penulenan menggunakan kaedah penurasan kromatografi gel Sefadak G-200.

## Bahan dan Kaedah

**Pennyediaan sampel**

Sebanyak 150 ekor sampel kupang hijau diambil dari Sungai Danga, Johor Bahru, Malaysia. Kupang hijau diceraikan daripada tali sarangnya bersama-sama dengan kakinya. Kaki kupang bersama plak perekat kaki kupang dikikiskan dengan menggunakan pisau cukur dan diletakkan di dalam botol. Setiap ekor kupang yang diambil diikat kembali dengan menggunakan gelang getah dan disisipkan kepada tali tangsi yang telah diikat kepada cermin-cermin kaca segi empat. Cermin-cermin kaca tersebut diletakkan di dalam raga besar dan ditenggelamkan ke dalam air selama beberapa hari bergantung kepada cuaca dan air pasang surut sebelum kitaran seterusnya dilakukan.

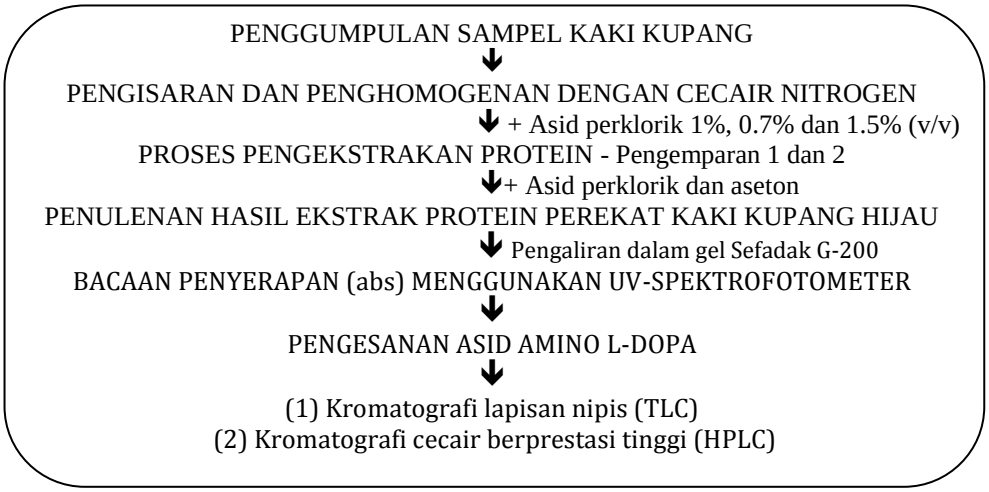
**Proses penghomogenan atau penghancuran kaki kupang**

Sampel perekat kaki kupang hijau yang telah dibersihkan dikeluarkan dari penyejuk beku (-10 $^{o}$C) dan dibiarkan seketika pada suhu bilik. Sampel kemudiannya dikeringkan dengan menggunakan kertas turas dan ditimbang. Seterusnya, mortar dan alu digunakan bagi menghancurkan kaki kupang kepada serbuk halus dengan menuangkan cecair nitrogen secara kerap. Serbuk halus kaki perekat kupang diletakkan di dalam bekas kaca kedap udara sebelum proses pengesktrakan protein dijalankan.

**Proses pengekstrakan sampel protein**

Proses pengekstrakan protein daripada perekat kaki kupang hijau adalah berdasarkan kepada protokol Taylor et al. (1994) [14]. Kaki kupang yang telah dihancurkan dicampur dengan 25 ml 0.7%, 1.0% dan 1.5% (v/v) asid perklorik (AP) dan dimasukkan ke dalam 50 ml tiub apendof. Ia kemudiannya diemparkan pada kadar kelajuan 11,000 rpm untuk jangka masa 10 min pada suhu 10 $^{o}$C. Supernatan (S1) bagi setiap tiub apendorf dikumpulkan dan disukat kuantitinya. Sebanyak 450 µl asid sulfurik dimasukkan ke dalam larutan supernatan S1 dan digoncang dengan kuat. Kemudian aseton ditambah dengan isipadu dua kali ganda isipadu S1. Campuran larutan tersebut dikacau menggunakan pengaduk magnetik di dalam bilik bersuhu 4 $^{o}$C selama 20 min sebelum dimasukkan semula ke dalam tiub apendorf. Kesemua tiub diemparkan sekali lagi pada kadar 11,000 rpm untuk 10 min pada suhu 10 $^{o}$C. Pellet yang tehasil ditimbang sebelum dilarutkan dengan asid asetik. Asid asetik ditambahkan kepada pellet yang terhasil berdasarkan nisbah 1:6 daripada berat pellet yang diperolehi. Pellet terlarut ini kemudiannya dimasukkan ke dalam

peti sejuk sebelum memulakan proses penulenan. Hasil ekstrak protein kaki perekat kupang hijau akan ditulenkan dengan kaedah penurasan kromatografi gel Sefadak G-200 sebelum proses pengesanan asid amino utama L-DOPA dijalankan dengan menggunakan kromatografi lapisan nipis (TLC) dan kromatografi cecair berprestasi tinggi (HPLC). Carta alir lengkap proses pengekstrakan protein kaki perekat kupang hijau dan analisis kewujudan asid amino L-DOPA ditunjukkan pada Rajah 3.

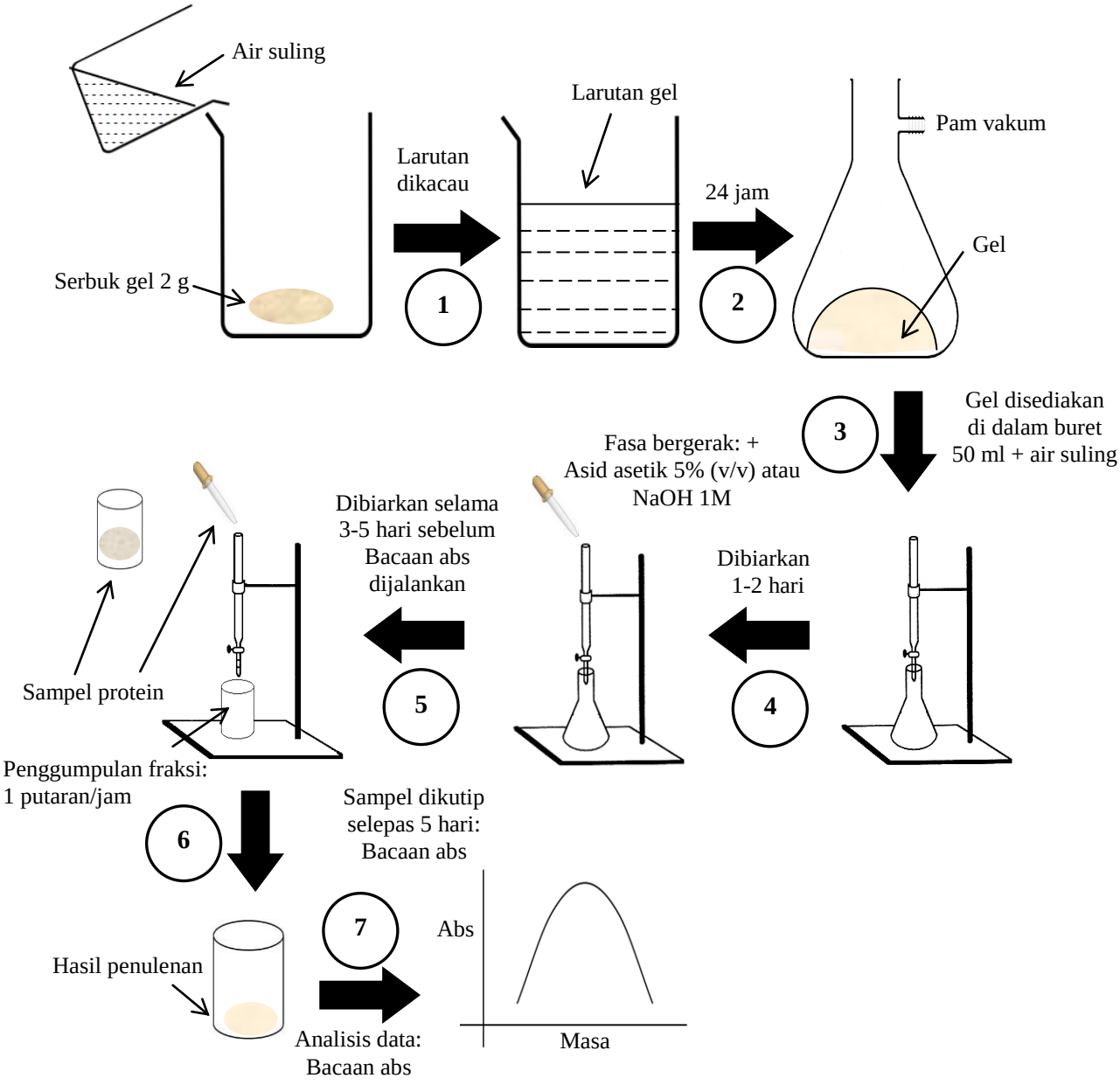



Rajah 3. Carta alir proses pengekstrakan dan pengesanan asid amino L-DOPA daripada ekstrak protein perekat kaki kupang hijau.

**Penyediaan turus penurasan kromatografi gel Sefadak G-200**

Dalam proses penulenan yang dijalankan, aspek penting yang perlu dititikberatkan adalah faktor-faktor yang mempengaruhi keadaan penyediaan gel tersebut. 1) Kewujudan bendasing dalam gel serta gelembung udara banyak memberi kesan dalam proses penulenan sampel berprotein. Gel yang disediakan perlulah bebas daripada sebarang gelembung udara sebelum dan semasa pemindahan gel kedalam turus kromatografi. Gelembung udara yang wujud mungkin disebabkan oleh pengadukan serbuk gel dengan air suling yang tidak sekata dan penuangan larutan gel terlalu pantas boleh menyebabkan kewujudan gelembung-gelembung udara tersebut [15]. Oleh yang demikian, penggunaan pam vakum amat penting dalam penyediaan larutan gel yang bebas daripada gelembung udara. Di samping itu, kadar pengadukan serbuk gel dan air suling hendaklah sekata dan mengikut arah lawan jam atau arah jam secara bertukar ganti. Proses penuangan air suling pada serbuk gel juga perlu dilakukan secara perlahan-lahan agar larutan gel yang terbentuk bebas gelembung udara serta ketulan tidak larut. 2) Suhu persekitaran bagi penyediaan gel kromatografi 15 $^{o}$C. Keadaan ini diperlukan agar tiada perubahan suhu yang besar di antara sampel ekstrak dan gel semasa proses penulenan berjalan agar protein yang ditulen tidak mengalami sebarang denaturasi [16].

Penyediaan turus kromatografi dimulakan dengan pencampuran gel dan air suling dengan kadar pencampuran yang perlahan-lahan bagi mengelakkan daripada ketidaklarutan atau penggumpalan gel berlaku. Ia dibiarkan selama 24 jam di dalam kelalang kon. Kemudian, gel tesebut divakumkan dengan menggunakan pam vakum bagi memastikan tiada gelembung-gelembung udara yang terperangkap dan dituangkan ke dalam buret 50 ml (60 cm panjang). Gel dibiarkan selama sehari bagi memastikan gel adalah padat sebelum proses penulenan dijalankan [13]. Kadar alir bagi fasa ini ditentukan untuk mengetahui selang masa bagi proses pemungutan larutan fasa bergerak yang dituruskan melalui gel ini. Kadar alir yang dikira adalah 1.5 ml/jam.




Rajah 4. Kaedah penulenan hasil ekstrak protein perekat kupang hijau menggunakan kaedah penurasan kromatografi gel Sefadak G-200.

**Faktor-faktor yang mempengaruhi proses penulenan sampel protein dan bacaan abs**

Hasil ekstrak protein yang dituangkan ke dalam turus kromatografi perlu berada pada julat suhu 4 - 10$^{0}$C bagi mengelakkan sebarang denaturasi protein sepanjang proses penulenan. Selain daripada itu, proses pembacaan abs perlu berada dalam persekitaran sejuk (15 $^{o}$C) agar tiada ralat di dalam bacaan data akibat denaturasi protein. Penggunaan kuvet kaca adalah di antara kriteria terpenting kerana bacaan abs bagi sampel berprotein yang

mempunyai jisim molekul yang tinggi memerlukan kadar penembusan dan campahan gelombang UV yang tetap dan bebas ralat walaupun replikasi pembacaan dilakukan.

**Penulenan hasil ekstrak protein kupang hijau**

Sebelum proses penulenan hasil ekstrak protein kupang hijau dijalankan, fasa bergerak dialirkan terlebih dahulu bagi mengeluarkan sebarang bahan-bahan asing yang masih terkandung di dalam gel Sefadak termampat dan memastikan bacaan abs asas kekal stabil (pemeriksaan efluan dilakukan bagi melihat tiada kewujudan sebarang puncak). Proses penulenan yang dijalankan adalah secara berasingan bagi setiap fasa bergerak yang berlainan (Jadual 1) dan fasa bergerak dibiarkan mengalir selama 3 hingga 5 hari. Sampel hasil ekstrak protein dituangkan ke dalam buret penulenan dengan kadar alir tetap penggumpulan fraksi ditulen iaitu 1.5 ml/jam sebelum analisis dijalankan. Bacaan abs bagi jarak gelombang $\lambda_{260nm}$ dan $\lambda_{280nm}$ diambil dengan menggunakan UV-spektrofotometer bagi efluan asas (fasa bergerak sahaja) dan hasil penulenan cecair ekstrak protein. Carta alir lengkap proses penulenan hasil ekstrak protein kupang hijau bagi mengesan asid amino L-DOPA ditunjukkan pada Rajah 4.

Jadual 1. Penggunaan pelbagai cecair penampan pada gel Sefadak G-200.

| Kepekatan asid perklorik | Fasa bergerak gel Sefadak G-200 | Polariti |
|---|---|---|
| 0.7% (v/v) | Asid asetik 5% (v/v) | 6.2 |
| 1.0% (v/v) | Asid asetik 5% (v/v) | 6.2 |
| 1.5% (v/v) | NaOH 1M | Garam alkali |

**Analisis kromatografi lapisan nipis (TLC) atau kromatografi cecair berprestasi tinggi (HPLC)**

Analisis pengesanan asid amino L-DOPA secara kualitatif bagi hasil penulenan ekstrak protein perekat kaki kupang dijalankan dengan menggunakan instrumen separa automatik TLC (CAMAG Linomat 5). Parameter analisis bagi CAMAG Linomat 5 adalah seperti berikut: Saiz plat (TLC lapisan nipis aluminium yang mengandungi silika; 10 cm × 10 cm), lebar tompokan: 4 mm, paksi *x* dan *y*: 11 mm and 10 mm masing-masing, jarak ujikaji penompokan: 10.0 mm dan isipadu semburan: 4.0 µl. Plat yang telah disembur dimasukkan di dalam tabung pembangunan bagi proses pemisahan asid amino yang terdapat di dalam hasil ekstrak protein tulen dengan menggunakan fasa bergerak berkomposisi 0.05M asid sitrik, sodium EDTA 50 µM, sodium oktilsulphonat 0.4 nM pada pH 2.9 dan 8% metanol (v/v). Penanda bagi setiap asid amino yang tercerap pada plat diperlihat, ditanda dan direkod menggunakan lampu UV pada jarak gelombang (λ) 260 nm dan 360 nm. Faktor terencat, $R_f$ bagi setiap cerapan asid amino piawai dan sampel ekstrak protein tulen dikira dan ditunjukkan pada Jadual 3. Lima replikasi dilakukan bagi setiap sampel dan asid amino piawai ($n$ = 5).

Parameter analisis HPLC bagi pengenalpastian keberhasilan asid amino L-DOPA hasil penulenan ekstrak protein perekat kaki kupang adalah seperti berikut: (1) Fasa bergerak disediakan dengan komposisi yang terdiri daripada 0.05M asid sitrik, sodium EDTA 50 µM, sodium octilsulphonat 0.4 nM pada nilai pH 2.9 and 8% (v/v) metanol. (2) Kadar alir fasa bergerak adalah 1 ml/min pada suhu kolum 25 °C. (3) Kolum Chromolith RP-18 (Inertsil 7 ODS-3 4.6 mm ID, 250 mm, Merck®) digunakan mengikut prosedur Cannazza et al. (2010) [17]. (4) Jarak gelombang pengesan cahaya UV ditetapkan pada 220 nm [14]. Fasa bergerak dibiarkan mengalir di dalam kolum selama 30 min sehingga garisan asas yang stabil diperolehi. Sebanyak 20 µl sampel disuntikkan dan bacaan kromatografi dijalankan sehingga semua puncak terhasil pada masa operasi yang ditetapkan (45 min).

**Analisis statistik**

Kesemua data hasil ujikaji dianalisa dengan menggunakan perisian SPSS (IBM) versi 17.0. Ujian-t sampel tidak bersandar atau '*Student t-test'* dijalankan untuk pada aras kebarangkalian signifikan 95% ($p$<0.05) bagi penentuan perbezaan signifikan di antara sampel.

## Hasil dan Perbincangan

### Pengekstrakan protein perekat kaki kupang hijau

Nilai bacaan abs bagi julat jarak gelombang di antara 200 nm hingga 400 nm bagi hasil ekstrak protein yang diekstrak menggunakan tiga kepekatan asid perklorik (AP) berbeza ditunjukkan pada Jadual 2. Pencirian and pemeriksaan jarak gelombang yang paling stabil dan sesuai bagi sampel ekstrak protein (tanpa pencairan) dijalankan dengan menggunakan instrumen analisis UV-spektrofotometer agar nilai bacaan yang terhampir dengan 1.0 dapat diperolehi (bacaan maksimum abs) diletakkan pada nilai 1.0 = 100%). Pada jarak gelombang 214 nm, ketiga-tiga kepekatan larutan AP menunjukkan nilai bacaan yang tinggi iaitu melebihi 2.0. Bacaan abs yang tinggi menunjukkan hasil ekstrak tersebut mempunyai kepekatan protein yang tinggi. Manakala pada jarak gelombang cahaya UV tampak (400 nm), bacaan abs adalah sangat rendah iaitu dibawah 0.3. Oleh yang demikian, jarak gelombang yang sesuai bagi cerapan kepekatan hasil ekstrak protein adalah pada jarak gelombang di antara 260 dan 280 nm. Pemilihan dibuat berdasarkan kepada dua daripada tiga kepekatan AP yang digunakan (iaitu 0.7% dan 1.0%) menghasilkan nilai abs yang menghampiri nilai 1.0 (100%). Penetapan nilai abs 1.0 dilakukan agar proses normalisasi kepada 100% tidak dilakukan.

Jadual 2. Bacaan abs pada julat jarak gelombang (λ) 200 nm - 400 nm bagi hasil ekstrak protein melalui penggunaan tiga kepekatan asid perklorik berbeza (0.7% (v/v), 1.0% (v/v) dan 1.5% (v/v)).

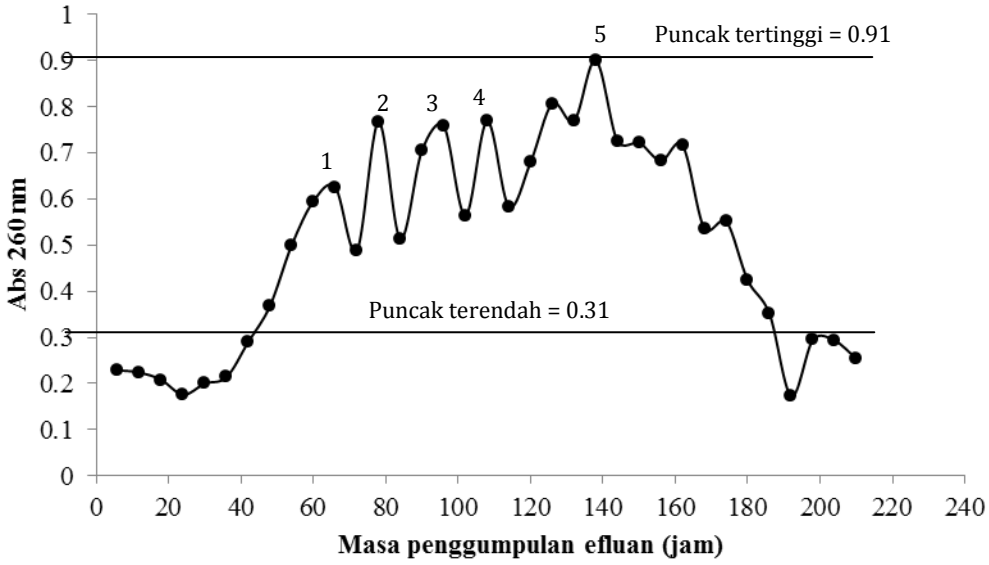
| λ (nm) | 0.7% AP | 1.0% AP | 1.5% AP |
|---|---|---|---|
| 214 | 2.00 ± 0.15 | 2.13 ± 0.11 | 2.34 ± 0.16* |
| 230 | 1.77 ± 0.12 | 1.25 ± 0.15 | 1.18 ± 0.08 |
| 260 | 0.97 ± 0.02 | 0.98 ± 0.01 | 1.70 ± 0.10* |
| 280 | 0.90 ± 0.05 | 0.81 ± 0.09 | 1.38 ± 0.15 |
| 360 | 0.08 ± 0.01 | 0.11 ± 0.01 | 0.33 ± 0.10 |
| 400 | 0.10 ± 0.01 | 0.11 ± 0.04 | 0.27 ± 0.07 |

### Penulenan hasil ekstrak melalui penggunaan fasa bergerak berlainan

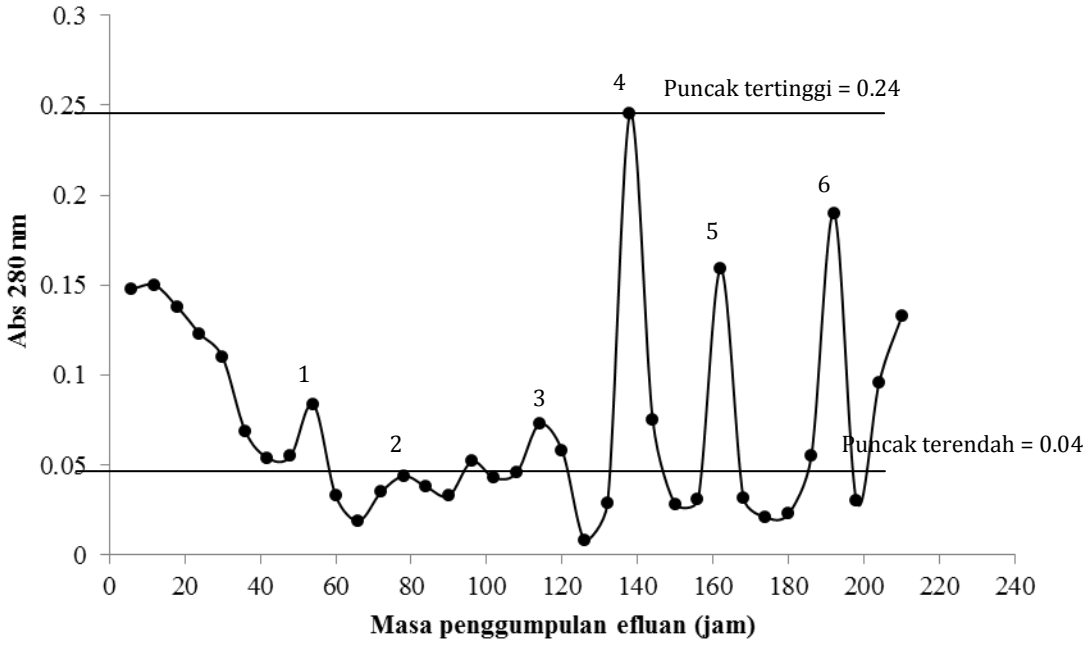
Keputusan analisa sampel penulenan bagi hasil ekstrak protein 0.7%, 1.0% dan 1.5% (v/v) asid perklorik ditunjukkan pada Jadual 2. Suhu persekitaran bagi proses penulenan ketiga-tiga set penurasan kromatografi gel adalah pada suhu 15 $^{o}$C dan set tersebut dibiarkan dengan menggunakan alat pengumpul sampel automatik dan disetkan pada masa maksimum 1 jam. Fraksi yang dikumpulkan dianalisa dan graf abs melawan masa penggumpulan fraksi diplotkan bagi mengenalpasti parameter-parameter pomprosesan (kepekatan AP, jarak gelombang dan fasa bergerak) yang terbaik sebelum analisis kualititatif dan kuantitatif komponen penting protein seperti asid amino L-DOPA dijalankan. Secara teori, konsep utama proses penulenan protein melalui gel kromatografi adalah pengasingan saiz molekul (kDa) iaitu molekul protein yang bersaiz besar akan keluar daripada turus kromatografi lebih awal berbanding molekul protein bersaiz kecil. Molekul protein bersaiz kecil atau molekul protein yang terhidrolisis menjadi komponen asid amino oleh fasa bergerak bersifat asid/alkali akan mudah masuk ke dalam liang-liang halus gel dan terjerap di permukaan gel. Manakala, saiz molekul yang besar akan terus diefluan disebabkan oleh ketidakupayaan saiz molekul tersebut masuk ke liang-liang halus gel Sefadak [18].

Rajah 4 menunjukkan profil abs efluan hasil ekstrak protein yang terbaik pada jarak gelombang 260 nm dengan penggunaan 0.7% (v/v) asid perklorik (larutan pengekstrakan berasid) dan 0.7% (v/v) asid asetik sebagai fasa bergerak kromatografi. Julat abs yang tinggi (0.31 - 0.91) dengan kewujudan 5 puncak nyata jerapan molekul-molekul protein diperolehi berbanding nilai julat yang dihasilkan bagi profil efluan yang lain (Rajah 5, 6, 7, 8 dan 9). Walaubagaimanapun, profil puncak efluan dilihat lebih baik bagi Rajah 5, 6, 7, 8 dan 9 di mana jarak pemisahan di antara komponen adalah lebih besar dan lengkung kitarannya menghampiri ke garisan asas berbanding pada Rajah 4. Penggunaan turus buret yang lebih panjang atau sistem kawalan kadar alir fasa bergerak dilihat perlu agar jarak puncak pemisahan efluan bagi Rajah 4 menjadi lebih besar. Selain daripada itu, komposisi molekul-molekul protein dan bendasing yang mempunyai polariti yang tinggi dan bersaiz kecil dilihat terjerap lebih awal di

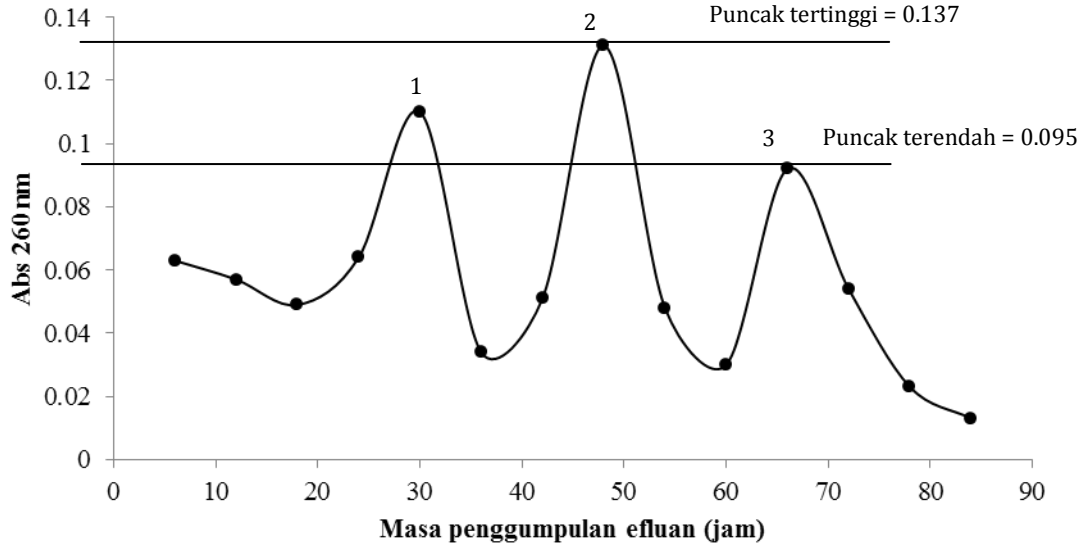
permukaan liang-liang halus gel Sefadak G-200 bagi penggunaan fasa bergerak asid asetik yang berkepekatan tinggi dan NaOH (alkali kuat) berbanding penggunaan kepekatan asid asetik yang rendah. Fenomena ini dilihat berpunca daripada sifat kimia larutan alkali kuat NaOH dan asid asetik berkepekatan tinggi yang turut membantu memecahkan lebih banyak ikatan peptida di dalam ekstrak protein kepada beberapa molekul-molekul protein yang bersaiz lebih kecil. Akan tetapi, kewujudan molekul-molekul protein yang sedikit bagi kondisi di atas (Rajah 6, 7, 8 dan 9) memperlihatkan ia amat bergantung kepada kesuaian kepekatan asid perklorik yang digunakan semasa proses pengesktrakan. Walaupun penggunaan kepekatan AP yang tinggi (1.5%) menghasilkan bacaan abs hasil ekstrak protein yang tinggi, hanya beberapa puncak penahanan sahaja yang muncul dengan bacaan abs yang rendah apabila proses penulenan dijalankan. Secara teori, kepekatan sesuatu larutan yang tinggi tidak semestinya mengandungi berat molekul yang tinggi (MW). Ini dapat dijelaskan dengan kewujudan fenomena indeks polidispersiti yang tinggi iaitu kewujudan kepelbagaian saiz molekul protein di dalam hasil ekstrak tersebut (kewujudan saiz molekul yang lebih besar berbanding saiz kecil). Oleh yang demikian, nilai abs yang besar berkemungkinan berlakunya pemecahan ikatan peptida kepada molekul-molekul yang lebih kecil (banyak penjerapan berlaku di dalam liang-liang halus gel Sefadak G-200) berbanding nilai abs yang rendah tetapi berkemungkinan mengandungi saiz molekul protein yang amat besar. Lima fraksi efluan abs yang tinggi pada Rajah 4 (puncak 1 - 5) digunakan untuk pencirian kandungan asid amino penting L-DOPA dengan menjalani analisis kualitatif TLC dan kuantitatif HPLC.



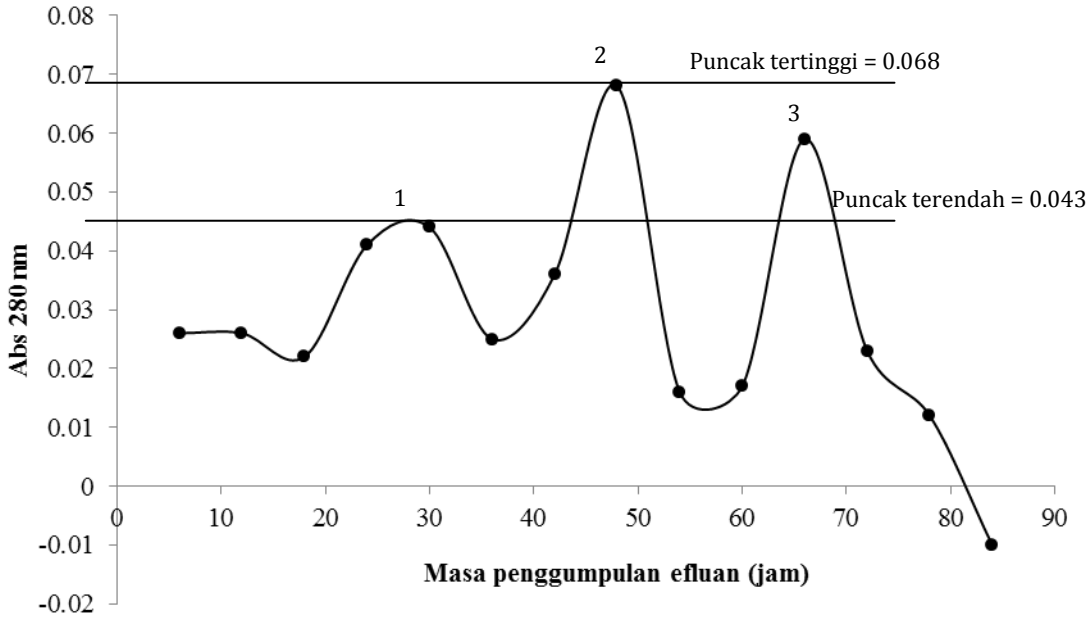

Rajah 4. Profil abs efluan hasil ekstrak protein bagi sampel 0.7% (v/v) asid perklorik dengan fasa bergerak asid asetik 5% (v/v) pada suhu 15 $^{0}$C dan jarak gelombang $\lambda_{260nm.}$ Nombor puncak 1- 5: Hanya lengkung kitaran lengkap sahaja diambil untuk analisis asid amino L-DOPA.



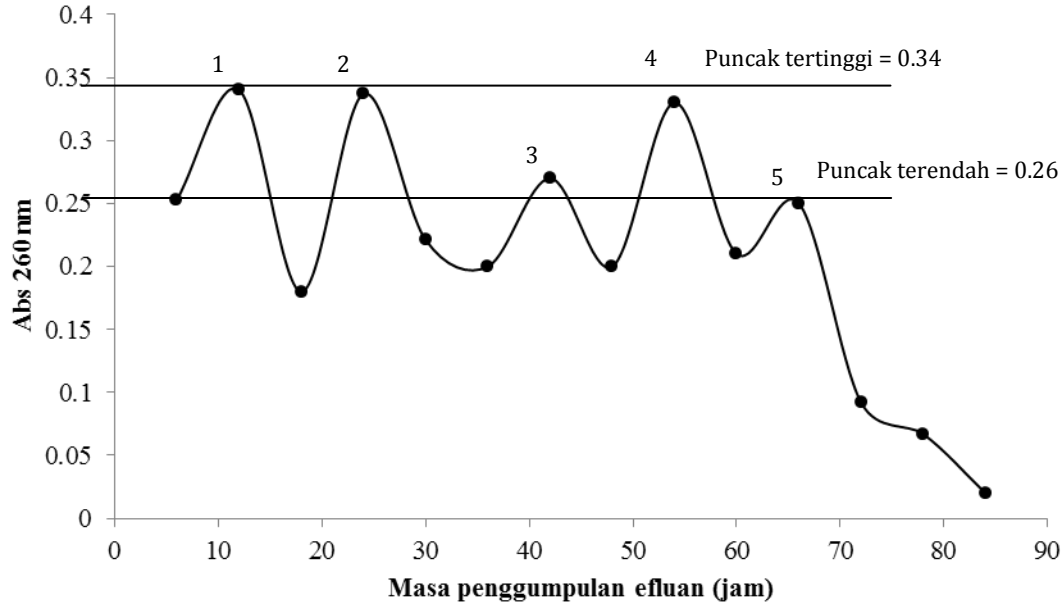

Rajah 5. Profil abs efluan hasil ekstrak protein bagi sampel 0.7% (v/v) asid perklorik dengan fasa bergerak asid asetik 5% (v/v) pada suhu 15 $^{o}$C dan jarak gelombang $\lambda_{280nm.}$ Nombor puncak 1- 6: Lengkung kitaran lengkap.



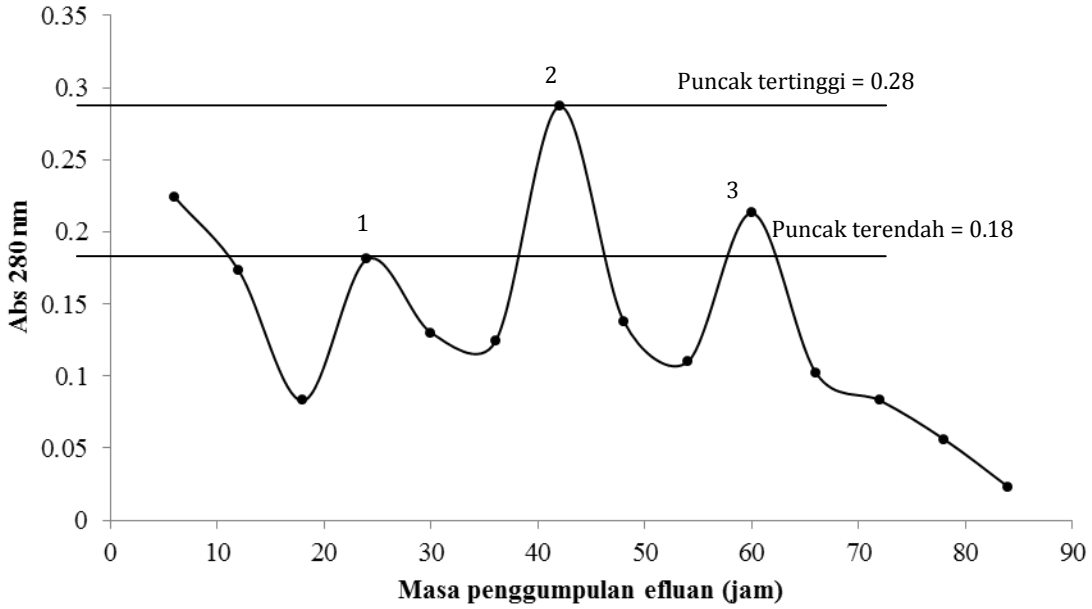

Rajah 6. Profil abs efluan hasil ekstrak protein bagi sampel 1.0% (v/v) asid perklorik dengan fasa bergerak asid asetik 5% (v/v) pada suhu 15 $^{o}$C dan jarak gelombang $\lambda_{260nm}$. Nombor puncak 1- 3: Lengkung kitaran lengkap.




Rajah 7. Profil abs efluan hasil ekstrak protein bagi sampel 1.0% (v/v) asid perklorik dengan fasa bergerak asid asetik 5% (v/v) pada suhu 15 $^{o}$C dan jarak gelombang $\lambda_{280nm}$. Nombor puncak 1- 3: Lengkung kitaran lengkap.




Rajah 8. Profil abs efluan hasil ekstrak protein bagi sampel 1.5% (v/v) asid perklorik dengan fasa bergerak NaOH 1M pada suhu 15 $^{o}$C dan jarak gelombang $\lambda_{260nm}$. Nombor puncak 1- 5: Lengkung kitaran lengkap.




Rajah 9. Profil abs efluan hasil ekstrak protein bagi sampel 1.5% (v/v) asid perklorik dengan fasa bergerak NaOH 1M pada suhu 15 $^{o}$C dan jarak gelombang $\lambda_{280nm}$. Nombor puncak 1- 3: Lengkung kitaran lengkap.

**Analisis kromatografi lapisan nipis (TLC)**

Jadual 3 menunjukkan bacaan jarak jaluran $R_f$ bagi 3 jenis asid amino (L-DOPA, L-fenilalanin dan L-tirosin) penting yang terdapat di dalam hasil ekstrak protein perekat kaki kupang menggunakan 0.7% (v/v) asid perklorik (proses pengesktrakan) dan 5% (v/v) asid asetik (fasa bergerak proses penulenan) . Keputusan bagi penggumpulan fraksi tulen pada jam ke-78 memberikan petanda positif yang terbaik dengan kewujudan ketiga-tiga komponen asid amino penting tersebut dengan nilai $R_f$ yang sama dengan nilai piawaian asid amino. Walaubagaimanapun, kesemua efluan terkumpul dilihat mempunyai petanda positif asid amino L-DOPA penting. Oleh yang demikian, semua sampel efluan dari jam ke-69 sehingga ke-138 dipilih bagi mengetahui kepekatan (mg/l) asid amino penting L-DOPA yang terkandung di dalam hasil penulenan ekstrak protein tersebut menggunakan analisis HPLC.

Jadual 3. Nilai $R_f$ asid amino piawai L-DOPA, L-fenilalanin dan L-tirosin dan sampel ekstrak protein ditulen pada 4 puncak efluan bagi masa penggumpulan pada jam ke-78, 90, 108 dan 138 (0.7% (v/v) asid perklorik dengan fasa bergerak asid asetik 5% (v/v)).

| **Komponen** | **Nilai $R_f$** | | |
|---|---|---|---|
| **Asid amino piawai** | | | |
| L-DOPA | 0.68 ± 0.01 | | |
| L-fenilalanin | 0.70 ± 0.05 | | |
| L-tirosin | 0.80 ± 0.02 | | |
| **Sampel ekstrak protein ditulen*** | | | |
| **Efluan hasil tulen** | **L-DOPA** | **L-fenilalanin** | **L-tirosin** |
| 0.7% (v/v) Asid perklorik (69 jam) | 0.66 ± 0.01 | ND | ND |
| 0.7% (v/v) Asid perklorik (78 jam) | 0.67 ± 0.01 | 0.69 ± 0.02 | 0.77 ± 0.02 |
| 0.7% (v/v) Asid perklorik (90 jam) | 0.66 ± 0.02 | ND | 0.76 ± 0.03 |
| 0.7% (v/v) Asid perklorik (108 jam) | 0.67 ± 0.01 | ND | ND |
| 0.7% (v/v) Asid perklorik (138 jam) | ND | 0.68 ± 0.03 | 0.75 ± 0.01 |

*$p$>0.05: Tiada perbezaan signifikan di antara nilai R$f$ sampel ekstrak protein efluan dan asid amino piawai ($n$ = 5).
ND: *Not detected* - Tiada kewujudan plot warna asid amino dikesan di atas plat TLC.

**Analisis kromatografi cecair berprestasi tinggi (HPLC)**

Jadual 4 menunjukkan komposisi kepekatan (mg/l) bagi 4 efluan penggumpulan hasil penulenan ekstrak protein kaki perekat kupang hijau. Daripada keputusan yang diperolehi, pada masa penggumpulan jam ke-78, kepekatan asid amino L-DOPA adalah yang tertinggi secara signifikan berbanding dengan masa penggumpulan efluan yang lain ($p$<0.05).

Jadual 4. Analisis HPLC bagi 4 puncak efluan penurasan kromatografi gel Sefadak G-200 bagi sampel ekstrak protein 0.7% (v/v) asid perklorik dengan fasa bergerak asid asetik 5% (v/v).

| Masa penggumpulan (jam) | Kepekatan L-DOPA (mg/l) |
|---|---|
| 69 | 0.33 ± 0.05 |
| 78 | 2.94 ± 0.21* |
| 90 | 0.82 ± 0.13 |
| 108 | 0.46 ± 0.18 |
| 138 | ND |

*$p$<0.05: Perbezaan signifikan di antara masa penggumpulan puncak efluan gel Sefadak G-200 (jam) t = 90 dan 108 ($n$ = 3).
ND: *Not detected* - Tiada kewujudan asid amino L-DOPA.

Oleh yang demikian, parameter pemprosesan dan analisis yang terbaik bagi mendapat kepekatan asid amino penting L-DOPA yang tinggi di dalam hasil penulenan ekstrak protein kaki kupang adalah seperti di Jadual 5.

Jadual 5. Parameter pemprosesan dan analisis terbaik dalam memberikan nilai bacaan kepekatan (mg/l) asid amino L-DOPA yang tinggi.

| **Proses pengekstrakan berasid** | |
|---|---|
| Kepekatan larutan berasid | 0.7% (v/v) asid perklorik |
| **Proses penulenan gel Sefadak G-200** | |
| Kepekatan fasa bergerak | 5% (v/v) asid asetik |
| Jarak gelombang[a] | 260 nm |
| Masa penggumpulan (jam) | 78 |

[a]Bacaan abs bagi penggunaan instrumen UV-spektrofotometer.

## Kesimpulan

Penulenan hasil ekstrak protein kaki perekat kupang hijau yang mengandungi asid amino aromatik penting L-DOPA dilihat banyak dipengaruhi oleh pelbagai faktor penggunaan parameter pemprosesan dan analisis pencirian komponen. Di antaranya adalah pemilihan jenis fasa bergerak gel kromatografi, keadaan penyediaan gel dan sampel ekstrak berprotein tersebut. Fasa bergerak larutan berasid seperti asid asetik 5% memberikan kehadiran beberapa puncak efluan nyata dan pemisahan di antara komponen-komponen ditulen tersebut yang ketara kecuali bagi hasil ekstrak 0.7% asid perklorik. Akan tetapi, bacaan abs adalah rendah walaupun puncak pemisahan yang ketara berlaku. Manakala bagi fasa bergerak beralkali seperti NaOH 1M pula memberikan kehadiran puncak efluan dan pemisahan yang ketara tetapi mempunyai nilai abs yang agak rendah sama dengan beberapa set fasa bergerak larutan berasid pada dua jarak gelombang yang berbeza (260 nm dan 280 nm). Kadar pergerakan sampel di dalam fasa bergerak bergantung kepada jenis pelarut yang digunakan. Pemilihan pelarut yang sesuai penting untuk menghasilkan pemisahan yang baik antara komponen di dalam sampel. Setiap pelarut mempunyai kuasa pemisahan yang berbeza. Oleh yang demikian, larutan asid asetik berkepekatan 5% (v/v) dilihat sesuai bagi mendapatkan lebih banyak pemisahan komponen-komponen penting di dalam ekstrak berprotein perekat kaki kupang hijau. Di samping itu, faktor penyediaan gel juga turut mempengaruhi proses penulenan yang dijalankan. Kewujudan gelembung udara boleh menyebabkan hasil penulenan ekstrak berprotein terperangkap di dalam gelembung yang terbentuk dan memberi kesan yang besar terhadap nilai bacaan abs. Penggunaan pam vakum serta pengaliran air suling beberapa

kali sebelum pengaliran larutan fasa bergerak gel sangat penting dalam mengelakkan ralat dalam pembacaan abs. Sampel yang disediakan juga perlulah dalam keadaan yang sentiasa sejuk lebih kurang pada suhu 15 $^0$C dan keadaan gel yang disediakan juga perlu kekal pada suhu tersebut. Ia bertujuan untuk memastikan sampel ekstrak berprotein tidak mengalami sebarang denaturasi. Denaturasi protein boleh berlaku sekiranya berlakunya perubahan suhu bilik yang ketara di mana jenis protein yang berlainan mempunyai sensitiviti terhadap suhu yang berlainan. Selain daripada itu, dalam memberikan bacaan abs yang tepat dan kurang ralat, pemilihan jarak gelombang bagi instrument UV-spektrofotometer turut memainkan peranan yang penting dalam pengenalpastian parameter pemprosesan yang terbaik. Dalam kajian ini, julat jarak gelombang daripada 214 nm sehingga 400 nm (cahaya tampak UV) digunakan bagi mendapatkan nilai bacaan yang menghampiri bacaan 1.0. Bacaan abs <1.0 pada jarak gelombang 260 dan 280 nm dipilih agar tiada normalisasi dilakukan. Secara kesimpulan, daripada kajian keseluruhan yang dijalankan, dapat dibuktikan bahawa hasil penulenan sampel ekstrak berprotein perekat kaki kupang hijau yang mengandungi asid amino penting L-DOPA banyak terkandung di dalam hasil ekstrak yang menggunakan larutan 0.7% (v/v) asid perklorik (proses pengekstrakan) dengan penggunaan larutan fasa bergerak asid asetik 5% (v/v) pada suhu bilik sejuk 15$^0$C bagi proses penulenan penurasan kromatografi gel Sefadak G-200.

**Rujukan**


1. Nishida, A., Ohkawa, K., Ueda, I. & Yamamoto, H. (2003). Green mussel *Perna viridis L.:* attachment behaviour and preparation of antifouling surfaces. *Biomolecular Engineering*. 20(4-6): 381-387.
2. Troncoso, O.P., Torres F.G. & Grande, C.J. (2008). Characterization of the mechanical properties of tough biopolymer fibres from the mussel byssus of Aulacomya ater. *Acta biomaterialia*, 2008. 4(4):1114-7.
3. Marin, C., Bonastre, M., Mengod, G., Cortes, R., Giralt, A. Obeso, J.A. & Schapira, A.H. (2014). Early L-dopa, but not pramipexole, restores basal ganglia activity in partially 6-OHDA-lesioned rats. *Neurobiology of disease*. 64: 36-47.
4. Greenfieldboyce, N. (2010). Mighty Mussels Have Industrial Strength. *NPR Research News.* Washington DC.
5. Waite, J.H. & Tanzer, M.L. (1980). The Bioadhesive of mytilus byssus: A protein containing L-DOPA.*Biochemical and Biophysical Research Communication*. 96: 1554-1561.
6. DeMoor, S., Waite, J.H., Jangoux, M. & Flammang, P. (2003). Characterization of the adhesive from cuvierian tubules of the sea cucumber *Holothuria forskali (Echinodermata, Holothuroidea). Marine biotechnology*. 5(1): 45-57.
7. Suhre, M.H. & Scheibel, T. (2014). Structural diversity of a collagen-binding matrix protein from the byssus of blue mussels upon refolding. Journal of structural biology. 186(1): 75 – 85
8. Kwak, Y., Bohnen, N.I., Muller, M.L., Dayalu, P., Burke, D.T. & Seidler, R.D. (2013). Task-dependent interactions between dopamine D2 receptor polymorphisms and L-DOPA in patients with Parkinson's disease. *Behavioural brain research*. 245: 128-36.
9. Xiaoixia, Q. & Herbert, W.J. (1995). Exotic collagen gradients in the byssus of the mussel *Mytilus edulis. The Journal of Experimental Biology*. 198: 633-644.
10. Morris, C.J.O.R. (1964). Thin-layer chromatography of proteins on sephadex G-100 and G-200. *Journal of Chromatography*. 1964: 167-176.
11. Chen, L.-G. & Wang, C.-C. (2009). Preparative separation of oligostilbenes from *Vitis thunbergii var. taiwaniana* by centrifugal partition chromatography followed by Sephadex LH-20 column chromatography. *Separation and Purification Technology*. 66(1): 65-70.
12. Buyel, J.F., Bautista, J.A., Fischer, R. & Yusibov, V.M. (2012). Extraction, purification and characterization of the plant-produced HPV16 subunit vaccine candidate E7 GGG. *Journal of chromatography. B, Analytical technologies in the biomedical and life sciences*. 880(1): 19-26.
13. Joustra, M., Soderqvist, B. & L. Fisher (1967). Gel filtration in organic solvents. *Journal of Chromatography.* 28(1967): 21-25.
14. Taylor, S.W., Waite, J.H., Ross, M.M., Shabanowitz, J.H. & Donald F. (1994). Trans-2,3-cis-3,4-Dihydroxyproline, a new naturally occurring amino acid, is the sixth residue in the tandemly repeated consensus decapeptides of an adhesive protein from *Mytilus edulis*. *Journal of the American Chemical Society*. 116(23): 10803-10804.
15. Hine, P.T. & Bursill, D.B. (1983). Gel permeation chromatography of humic acid Problems associated with sephadex gel. *Journal of Water Resources*. 18(1983): 1561-1465.

16. Tantanasarit, C., Babel, S., Englande, A.J. & Meksumpun, S. (2013). Influence of size and density on filtration rate modeling and nutrient uptake by green mussel (*Perna viridis). Marine pollution bulletin*. 68(1-2): 38-45.
17. Cannazza, G., Di Stefano, A., Mosciatti, B., Braghiroli, D., Baraldi, M., Pinnen, F., Sozio, P., Benatti, C. & Parenti, C. (2005). Detection of levodopa, dopamine and its metabolites in rat striatum dialysates following peripheral administration of L-DOPA prodrugs by mean of HPLC-EC. *J Pharm Biomed Anal*. 36(5): 1079-84.
18. Rosenberg, I.M. (2004). Protein Analysis and Purification: Benchtop Techniques. 2 edn., Munich Birkhäuser.

The Malaysian Journal of ANALYTICAL SCIENCES ISSN 1394-2506

# METHYL ESTER (BIODESEL) PRODUCTION FROM WASTE COOKING VEGETABLE OIL BY MICROWAVE IRRADIATION

## (Penghasilan Metil Ester (Biodesel) Daripada Sisa Minyak Sayuran oleh Penyinaran Gelombang Mikro)

M.S.Khatun*, M.A. Khatun, M.Z.H. Khan, M. Debnath

*Department of Chemical Engineering,*
*Jessore University of Science & Technology, Jessore- 7408, Bangladesh.*

**Corresponding author:* sheauly.jstu@gmail.com

**Abstract**

In this study we tried to develop, test and optimize a batch microwave system using waste cooking vegetable oil (WCVO) that was used as biodiesel feedstock. Two catalysts, sodium hydroxide (NaOH) and potassium hydroxide (KOH) were tested in this study. Transesterification reactions between oil and methanol were carried out in presence of microwaves. It was observed that by using of microwaves, the reaction times were drastically reduced. As high as 99.5% conversions could be achieved for 0.5% KOH concentration. Moreover, quality analysis of biodiesels according to international standards was performed and the samples were found to meet the necessary specifications.

**Keywords:** methyl ester biodiesel; waste cooking vegetable oil; microwave irradiation; biofuel

**Abstrak**

Dalam kajian ini penulis cuba membangunkan, menguji dan mengoptimumkan suatu sistem penghasilan bahan mental biodesel secara gelombang mikro menggunakan sisa minyak sayuran memasak sisa (WCVO). Dua pemangkin, natrium hidroksida (NaOH) dan kalium hidroksida (KOH) telah diuji dalam kajian ini. Tindakbalas transesterifikasi antara minyak dan metanol telah dijalankan mengunakan gelombang mikro. Kajian mendapati bahawa dengan menggunakan gelombang mikro, masa tindakbalas berkurangan secara drastik. Penukaran boleh dicapai sehingga 95% bagi kepekatan KOH 0.5%. Selain itu, analisis kualiti biodiesel mengikut piawaian antarabangsa telah dilakukan dan sampel didapati memenuhi spesifikasi yang diperlukan.

**Kata kunci**: biodiesel metil ester; sisa minyak masak sayuran; penyinaran gelombang mikro; biofuel

## Introduction

There is increasing interest in developing alternative energy resources. An immediately applicable option is replacement of diesel fuel by biodiesel, which consists of the simple alkyl esters of fatty acid [1, 2]. Vegetable oil has been considered for a long time as an alternative energy source to produce biodiesel. The conversion of vegetable oils into biodiesel is a potential solution to the increasing demand for energy and environmental concerns [3]. But, using refined vegetable oil to produce biodiesel will reduce the edible oil. Thus, the use of waste vegetable oil instead of refined vegetable oil to produce biodiesel is an effective way to reduce the raw material cost and reduce food shortages. Additionally, using waste vegetable oil could also help solve the problem of waste oil disposal [4, 5].

The development of biodiesel is being driven by the need to reduce emissions from diesel engines without modifying them. Biodiesel can be produced from animal fats or vegetable oils with methanol or ethanol as the catalyst via a transesterification reaction. Biodiesel used as alternative fuel can reduce emissions of hydrocarbons, CO, SO, PAHs, and polychlorinated dibenzo-p-dioxin/ 2 dibenzofurans [6-12]. However, the major obstacle to biodiesel commercialization is its high cost, which is approximately 1.5 times higher than that of petroleum diesel fuel [13, 14]. Therefore, we need to increase biodiesel yield and reduce biodiesel cost. One of the best ways to

reduce the cost of biodiesel is to decrease reaction time of transesterification and to increase biodiesel yields. Reaction temperature, reaction time, catalyst amount, and the alcohol-to-oil ratio are important parameters in biodiesel production. Catalytic reactions can use alkali catalysts, acid catalysts, or enzymatic transesterification to achieve the best results.

Biodiesel can be produced at a lower temperature and shorter reaction time with an alkali catalyst compared to those required for an acid catalyst [15-18]. The conventional heating of a sample has a few significant drawbacks, such as heterogenic heating of the surface, limitations dependent on the thermal conductivity of materials, specific heat, and density when compared to microwave irradiation [19,20], and thus many research groups have recently focused on the latter approach. In recent years, microwave irradiation has been used for the production of biodiesel [21] used single-step, base catalyst transesterification for the production of biodiesel from waste cooking oil. However, this method used an unmodified household microwave oven.

In this work, a feasibility study has therefore been carried out to produce biodiesel from waste cooking vegetable oil using a modified household microwave oven in presence of different catalysts. Another aim of this study was to determine the optimum conditions of fatty acid methyl ester (FAME) production from waste cooking vegetable oil.

## Materials and Methods

### Materials

Laboratory grade methanol (99.8%), sodium hydroxide (NaOH), potassium hydroxide (KOH), silica gel were used as purchased without any further purification. In this experiment, waste cooking vegetable oil (WCVO) was collected from restaurants, residences, hotels, etc. Residual food in the waste vegetable oil used in this study was removed by filtering.

### Instrument

The used modified microwave was SHARP FTR-219, which could offer microwave power from 0-800W. The microwave oven consisted of a single neck glass reactor of 500 ml capacity with two neck adapter, one neck for condenser and other inlet for the reactants, to the set up.

### Experimental procedure

In this experimental procedure, the WCVO was first filtered through silica-gel 60 mesh (10.00 g) to eliminate free fatty acids and water. The WCVO had an acid value of 0.40 mg KOH and 0.02% water content prior to base-catalyzed transesterification [22]. The transesterification reaction performed at different molar ratio of oil to methanol, varying from 1:3, 1:4, 1:5, 1:6 and 1:7 at different power level. The reaction time was varying 2-10 minutes for all experiments. Two types of catalysts have been used NaOH and KOH at a range 0.5% wt. of oil. After transesterification reaction the biodiesel was separated from glycerol using separating funnel and finally washed with 5% water followed by magnesium sulfate anhydrous to remove the water. Several basic variables, namely, catalyst type, methanol to oil ratio and reaction time of transesterification were investigated as they play a significant difference in biodiesel produced [23]. Reaction conditions are given in Table 1.

Table1. Reaction conditions

| Use of the catalyst (wt%) | Time (min) | Oil: methanol molar ratio |
|---|---|---|
| NaOH | 2 | 1:3 |
| KOH | 4 | 1:4 |
| - | 6 | 1:5 |
| - | 8 | 1:6 |
| - | 10 | 1:7 |

## Results and Discussion

**Analysis of the result from the characterization of the Biodiesel produced**.

The characterization of the produced biodiesel was carried out and the physical properties were presented in Table 2. The result is placed with the corresponding limit set for biodiesel standard [24]. One of the most important characteristics of any fuel is its flash point; this is defined as the lowest temperature at which it can vaporize to form an ignitable mixture in air. The biodiesel has a higher flash point of 100 ℃ as compared to that of the petro diesel (flash point of 80 ℃ ). This makes the biodiesel sample safe for use and storage. Also, fuels with lower flash point tend to ignite at lower temperature making it highly dangerous if it is not stored and use properly. The viscosity of a fuel is important because it affects the atomization of the fuel being injected into the engine combustion chamber. A small fuel drop is desired so that complete combustion can occur. A high viscosity fuel will produce a larger drop of fuel in an engine combustion chamber which may not burn as clean as a fuel that produces a smaller drop. Unburned oxidized fuel will build up in the engine around valves, injector tips and on piston side walls and rings. The higher the viscosity the greater the tendency of the fuels to cause problems such as clogging of engine components. The specific gravity of a fuel is another important factor for good engine performance; the higher the specific gravity, the more difficult it becomes to pump the fuel.

Table2. Physical properties of waste cooking vegetable oil fuel and a comparison with diesel fuel

| Physical properties | Produced biodiesel value | Biodiesel standard [24] | Diesel standard [25] |
|---|---|---|---|
| Specific gravity at 25 $^0$C | 0.85 | 0.88 at 15.5 ℃ | 0.88 at 15.5 ℃ |
| Kinematic viscosity (mm$^2$/s @ 40 $^o$C) | 4.96 | 1.9-6 | 1.3-4.1 |
| Water content max. (wt%) | 0.05 | 0.05max. | 0.161 |
| Cloud point | 4 | -3 to 12 | -15 to 5 |
| Pour point $^0$C | 0 | -15 to 10 | -35 to -15 |
| Flash point min $^0$C | 100 | 100 - 170 | 80 to 60 |

**Effect of microwave power level**

The transesterification reaction has been investigated at the same molar ratio of oil: methanol at the various powers of microwave irradiation and the different reaction times. The results are shown in Figure 1.The yield increases with the increase of power level. This may be due to the fact that the increase of power level increases the heating rate. In this case more molecules absorb microwave energy to interact with each other and this absorption rate enhances the ionic compound present in reaction through ionic conductance, the better results are obtained as microwave irradiation intensity increases. We have not been able to isolate the compound of biodiesel from glycerine when power levels are 800W. Probably the compound was decomposed at this level. As indicated, the temperature increased with power level. Since microwave heating significantly increases the reaction temperature [26], it is possible that microwave reaction temperature can exceed the temperature (activation energy) required for a new reaction that is not possible for a lower temperature. If this is the case, different products can be obtained in the microwave reactions. However, in these instances, the amount of the desired product should be small or decomposed. This observation confirmed that power level 400W showed the highest yield, that is, 99.5%. Therefore, it can be recommended that for transesterification of waste cooking oil with methanol to biodiesel production suitable power level is 400W.

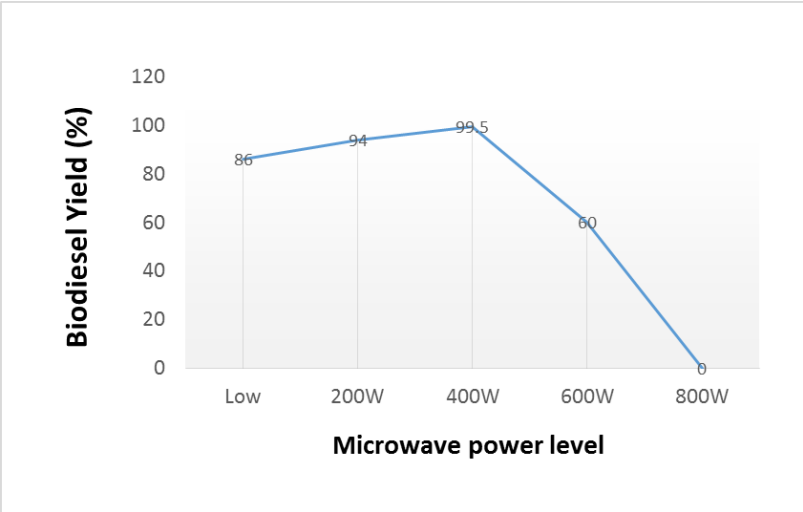



Figure 1. Effect of microwave power level on biodiesel production rate

**Effect of oil/ methanol molar ratio**

The oil to alcohol molar ratio is one of the important factors affecting the conversion of transesterification reaction of waste cooking vegetable oil to biodiesel. Methanolysis of WCVO was carried out with catalyst concentration 0.5 wt% of oil at microwave power level with different oil/ methanol molar ratio e.g. 1:3, 1:4, 1:5, 1:6, and 1:7 and the results exhibit that highest biodiesel yield is nearly 99.5% at 1:6 oil/methanol (Figure 2). From the Figure 2, it can be noticed that biodiesel yield continuously increases with the raise of molar ratio 1:3 to 1:6 but suddenly decreases for the molar ratio 1:7. Biodiesel yield observed in this study was higher than published data [27].

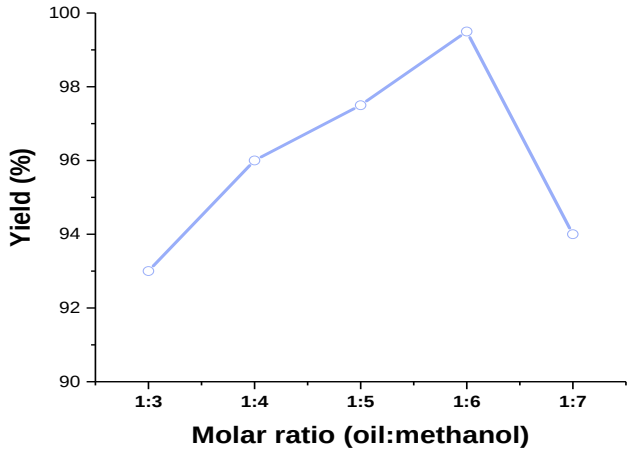



Figure 2. Effects of molar ratio on biodiesel conversion

**Effect of different catalysts on biodiesel yield.**

The further study, for example, impact of catalyst was performed using oil: methanol (1:6) has attained the most elevated rate. Past study demonstrates that production of biodiesel from waste cooking vegetable oil used catalyst sodium hydroxide with the reaction carried out at ambient pressure and temperature, the transformation rate of 98.4% were accomplished [28]. From Figure 3, it could be seen that highest biodiesel yield (99.5 %) has been

achieved using KOH. Incomprehensibly throughout separating, washing of biodiesel the emulsification phenomena have been watched. In spite of the fact that the basic catalysts are the most well-known as the methodology using them is speedier and the reaction conditions are moderate these catalysts have some drawbacks[29]: they must be neutralized giving rise to waste waters and can't be reutilized, they make troubles to differentiate the methyl esters (biodiesel) by formation of stable emulsions, the by-product glycerol is gotten as a watery result of relatively low purity and the reaction gets to be extremely delicate to the vicinity of water and free fatty acids [30]. In this study it has been watched that this emulsification might be lightened lessening shaking power throughout washing and partition of biodiesel from glycerol. Notwithstanding higher yield, using NaOH causes more emulsion than KOH and makes muddled to separate biodiesel from glycerin.

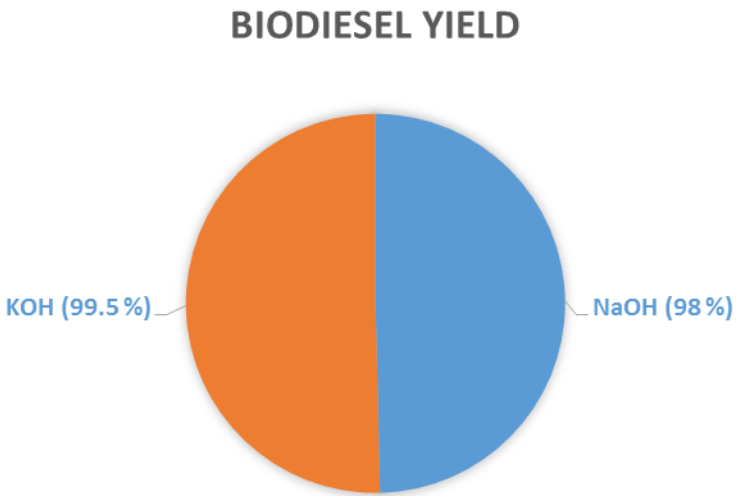



Figure 3. Different catalysts vs conversion rate

**Effect of reaction time.**

Figure 4 shows effects of the reaction time for the conversion rate. In order to ameliorate the mixing level between alcohol and oil, alkali catalysts were added to the reacting mixture. Results showed that after 4 minutes, the biodiesel conversion rate was more than 90%. The conversion rate reached to a noticeable value of 99.5% when the reaction time was 6 minutes. According to the normative standards of biodiesel, the required conversion rate must be 96.4%. In this work, microwave assists the catalyzing process of biodiesel production and the total reaction time required was 6 min. The total reaction time was less than previous studies [9, 15, 18, 19] which also trans-esterification of high FFA content oils with alcohol to biodiesel catalyzed by $H_2SO_4$ and NaOH.

The biodiesel samples produced under optimum condition of 1:6 oil-to-methanol molar ratio, 0.5% KOH catalyst and 6 minutes reaction time at 400W microwave power were analysed concerning some significant specifications as fuel in diesel engine.

There are two mechanisms by which microwave energy can interact with a sample. If a molecule possesses a dipole moment, then, when it is exposed to microwave irradiation, the dipole tries to align with the applied electric field. Because the electric field is oscillating, the dipoles constantly try to realign to follow this. At 2.45 GHz, molecules have time to align with the electric field but not to follow the oscillating field exactly. This continual reorientation of the molecules results in friction and thus heat. If a molecule is charged, then the electric field component of the microwave irradiation moves the ions back and forth through the sample while also colliding them into each other. This movement again generates heat. Because the mixture of vegetable oil, methanol, sodium hydroxide and

potassium hydroxide contains both polar and ionic components, rapid heating is observed upon microwave irradiation, and because the energy interacts with the sample on a molecular level, very efficient heating can be obtained. In addition, because the energy is interacting with the molecules at a very fast rate, the molecules do not have time to relax and the heat generated can be, for short times, much greater than the overall recorded temperature of the bulk reaction mixture. In essence, there will be instantaneous localized superheating [31]. Thus, the bulk temperature may not be an accurate measure of the temperature at which the actual reaction is taking place. Microwave heating compares very favourably over conventional methods, where heating can be relatively slow and inefficient because transferring energy into a sample depends upon convection currents and the thermal conductivity of the reaction mixture.

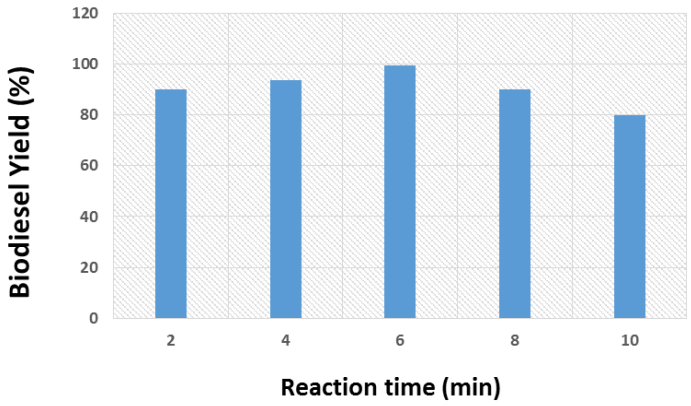



Figure 4: Effect of KOH reaction time on biodiesel yield.

## Conclusion

The biodiesel from waste cooking vegetable oil was produced with microwave assistance by operating at various powers. The properties of oil, diesel, and biodiesel for waste cooking oil such as acid value, flash and fire point etc., were determined and compared. The properties of the biodiesel produced met all the required specifications as per standard limit. The most important observation was the reaction was completed within six minutes duration as compared to one hour reaction time with the conventional heating. Biodiesel from used cooking vegetable oils could be used as a diesel fuel which considered as renewable energy and environmental recycling process from waste oil after frying.

## References

1. Knoth, G., Gerpen, J. V., Krahl, J. (2005). The Biodisel Handbook. *American oil chemists' society,* Urbana IL.
2. Koonin, S.E. (2006). Properties on biofuel and biomaterials. *Science*, 311: 435.
3. Lopez, D.E.,Goodwin, J. G., Bruce, D. A. and Lotero, E. (2005). Transesterification of triacetin with Alcohol on solid Acid and Base Catalysts. Applied Catalysis A: General, 295(2) : 97-105.
4. Zhang, Y., Dube, D. A., McLean, D. D. and Kates, M. (2003). Biodiesel Production from Waste Cooking Oil: Proc-ess Design and Technological Assessment. *Bioresource Technology*, 89 (1): 1-16.
5. Marchetti, J. M., Miguel, V. U. and Errazu, A. F. (2007). Hetero-geneous Esterification of Oil with High Amount of Free Fatty Acids. *Fuel*, 86(5): 906-910.
6. Dorado, M.P., Ballesteros, E., López, F. J. and Mittelbach, M. (2004). Optimization of alkali-catalyzed transesterification of *Brassica carinata* oil for biodiesel production. *Energ. Fuel*, 18(1): 77-83.
7. Lin, Y.C., Lee, W. J. and Hou, H.C. (2006). PAH emissions and energy efficiency of palm-biodiesel blends fueled on diesel generator. *Atmos. Environ*., V 40(21): 3930-3940.

8. Lin, Y.C., Lee, W. J., Wu,T.S. and Wang, C. T. (2006). Comparison of PAH and regulated harmful matter emissions from biodiesel blends and paraffinic fuel blends on engine accumulated mileage test. *Fuel*, 85(17-18): 2516-2523.
9. Lin, Y.C., Lee, W. J., Chao, H. R., Wang, S. L., Tsou, T. C., Chang-Chien, G.P. and Tsai, P. J. (2008). Approach for energy saving and pollution reducing by fueling diesel engines with emulsified biosolution/ biodiesel/diesel blends. *Environ. Sci. Technol.*, 42(10): 3849-3855.
10. Lin, Y.C., Tsai, C. H., Yang, C. R., Wu, C. H., Wuand, T. Y. and Chang-Chien, G. P. (2008). Effects on aerosol size distribution of polycyclic aromatic hydrocarbons from the heavy-duty diesel generator fueled with feedstock palm-biodiesel blends. *Atmos. Environ.*, 42(27): 6679-6688.
11. Lin, Y.C., Liu, S.H., Chen, Y. M. and Wu, T.Y. (2011). A new alternative paraffinic-palmbiodiesel fuel for reducing polychlorinated dibenzo-p-dioxin/ dibenzofuran emissions from heavy-duty diesel engines. *J. Hazard. Mater*, 185(1): 1-7.
12. Lin, Y.C., Hsu, K.H. and Chen, C.B. (2011). Experimental investigation of the performance and emissions of a heavy-duty diesel engine fueled with waste cooking oil biodiesel/ultra-low sulfur diesel blends. *Energy*, 36(1): 241-248.
13. Zhang, Y., Dube, M. A., McLean, D. D. and Kates, M. (2003). Biodiesel production from waste cooking oil: 2. Economic assessment and sensitivity analysis. *Bioresource Technol.*, 90(3): 229-240.
14. Haas, M.J., McAloon, A. J., Yee, W.C. and Foglia, T. A. (2006). A process model to estimate biodiesel production costs. *Bioresource Technol.*, 97(4): 671-678.
15. Fukuda, H., Kondo, A. and Noda, H. (2001). Biodiesel fuel production by transesterification of oils. *J. Biosci. Bioeng.*, 92(5): 405-416.
16. Dmytryshyn, S.L., Dalai, A. K., Chaudhari, S.T., Mishra, H. K. and Reaney, M. J. (2004). Synthesis and characterization of vegetable oil derived esters: Evaluation for their diesel additive properties. *Bioresource Technol*., 92(1): 55-64.
17. Saifuddin, N. and Chua, K.H. (2004). Production of ethyl ester (biodiesel) from used frying oil: Optimization of transesterification process using microwave irradiation. *Malaysian J. Chem*., 6(1): 77-82.
18. Vicente, G., Martinez, M. and Aracil, J. (2004). Integrated biodiesel production: A comparison of different homogeneous catalysts systems. *Bioresource Technol*., 92(3): 297-305.
19. Carslaw, H.S. and Jaeger, J.C. (1959). Conduction of Heat in Solids. *Oxford University Press*, Oxford, UK.
20. Metaxas, A.C. (1996). Foundations of Electro-heat. *Wiley*, New York.
21. Leadbeater, N. E. and Stencel, L.M. (2006). Fast, easy preparation of biodiesel using microwave heating. *Energ. Fuel.*, 20(5): 2281-2283.
22. Sandro, L. B., Savio, E. O. M., Stanlei, I. K., Gabriela, R. H., Adriano, C. M. B. and Miguel, J. D. (2013). Microwave irradiation aiding ethanolysis of waste cooking oil. *European International Journal of Science and Technology*., 2(2): 211 – 222.
23. Ma, F. and Hanna, M.A. (1999). Biodiesel production. A Review. *Bioresour. Technol.*, 70 : 1-15.
24. Morshed, M., Ferdous, K., Khan, M. and Mazumder, R. (2011). Rubber seed oil as a potential source for biodiesel production in Bangladesh. *Fuel*, 90 : 2981-2986.
25. Joshi, R.M., Pegg, M. J. (2007). Flow properties of biodiesel fuel blends at low temperatures. *Fuel*, 86: 143-151.
26. Gedye, R.N., Rank, W. and Westaway, K.C. (1991). The rapid synthesis of organic compounds in microwave ovens. *Canadian Journal of Chemistry*, 69(4): 706–711.
27. Azcan, N. and Yilmaz, O. F. (2013). Microwave assisted transesterification of waste frying oil and concentrate methyl ester content of biodiesel by molecular distillation. *Fuel*, 104: 614–619.
28. Hossain, A.B. and Boyce, A.N. (2009). Biodiesel production from waste sunflower cooking oil as an environmental recycling process and renewable energy. *Bulgarian journal of agricultural science*, 15(4): 312-317.
29. Freedman, B., Prude, E. H. and Mounts, T. L. (1984). Variables affecting the yields of fatty esters from transesterified vegetable oils. *J. Am Oil Chem. Soc*., 61(10): 1638-1643.
30. Arzamendia G., Campoa, I., Arguinarenaa, E., Sanchezb, M., Montesb, M. and Gandia, L. M. (2007). Synthesis of biodiesel with heterogeneous NaOH/alumina catalysts: Comparison with Homogeneous NaOH. *Chemical Engineering Journal*, 134: 123-130.

31. Stuerga, D. (2006). For an introduction to the physical chemistry concepts of microwave heating. In Microwaves Organic Chemistry, *Wiley-VCH*: Weinheim, Germany.

The Malaysian Journal of ANALYTICAL SCIENCES ISSN 1394-2506

# DETERMINATION OF MODAFINIL IN TABLET FORMULATION USING THREE NEW VALIDATED SPECTROPHOTOMETRIC METHODS

## (Penentuan Modafinil Dalam Formulasi Tablet Menggunakan Tiga Kaedah Spektofotometrik Ditentusahkan)

Pawan Kumar Basniwal[1,2]* and Deepti Jain[1]

[1]*School of Pharmaceutical Sciences,*
*Rajiv Gandhi Technological University, Bhopal – 462033, Madhya Pradesh, India*
[2] *LBS College of Pharmacy, Jaipur – 302004, Rajasthan, India*

**Corresponding author: pawanbasniwal@gmail.com*

**Abstract**

In this study, three new UV spectrophotometric methods viz. linear regression equation (LRE), standard absorptivity (SA) and first order derivative (FOD) method were developed and validated for determination of modafinil in tablet form. The Beer-Lambert's law was obeyed as linear in the range of 10-50 µg/mL and all the methods were validated for linearity, accuracy, precision and robustness. These methods were successfully applied for assay of modafinil drug content in tablets in the range of 100.20-100.42%, 100.11-100.58% and 100.25-100.34%, respectively with acceptable standard deviation (less than two) for all the methods. The validated spectrophotometric methods may be successfully applied for assay, dissolution studies, bio-equivalence studies as well as routine analysis in pharmaceutical industries.

**Keywords**: Modafinil, linear regression equation, standard absorptivity, first order derivative, tablets

**Abstrak**

Dalam kajian ini, tiga kaedah spektrofotometri UV baru iaitu persamaan regresi linear (LRE), daya penyerapan piawai (SA) dan terbitan tertib pertama (FOD) kaedah telah dibangunkan dan distentusahkan terhadap penentuan modafinil di dalam bentuk tablet. Hukum Beer-Lambert telah dipatuhi sebagai linear dalam julat kepekatan 10-50 µg/mL dan semua kaedah telah ditentusahkan tehadap kelinearan, ketepatan, kejituan dan keteguhan. Kaedah-kaedah ini telah berjaya diaplikasi bagi ujikaji kandungan dadah modafinil di dalam bentuk tablet iaitu masing – masing pada julat 100.20 – 100.42%, 100.11 – 100.58% dan 100.25-100.34%, dengan sisihan piawai yang boleh diterima (kurang dari dua) untuk semua kaedah. Kaedah spektrofotometri disahkan berjaya digunapakai terhadap ujikaji pelatutan, kajian bio-kesetaraan serta analisis rutin di dalam industri farmaseutikal.

**Kata kunci:** Modafinil, persamaan regresi linear, keberserapan standard, perintah pertama terbitan, tablet

## Introduction

Chemically, modafinil (AMD) is 2-(benzhydryl sulfinyl)acetamide (Figure 1) and its R-enantiomer is known as armodafinil. It is a non-amphetamine, wakefulness-promoting agent which is indicated for use in patients with excessive sleepiness associated with narcolepsy, obstructive sleep apnoea/hypopnoea syndrome or shift work sleep disorder [1]. It is active metabolite of adrafinil [2-(benzhydrylsulfinyl)-N-hydroxyacetamide] (Figure 1), which is one of the psychostimulants causing behavioral activating effects. Adrafinil is also metabolized into modafinil acid.

The pharmacokinetics of adrafinil was investigated by liquid chromatography/tandem mass spectrometric (LC–MS/MS) method along with determination of its metabolite [2]. Very few analytical chromatographic methods were reported for determination of armodafinil in human plasma [3] and in plasma and urine [4]. Armodafinil also was determined by HPLC along with its synthetic intermediates [5-6] and enantiomeric determination was reported by capillary electrophoresis with sulfobutyl ether-β-cyclodextrin as chiral selector [7]. Spectrophotometric methods may be suitable for routine analysis as these are economic, rapid, simple, maintenance-free, and show comparable

accuracy and precision with chromatographic methods [8-9]. Hitherto, as per knowledge of authors, there is no UV spectrophotometric method reported in literature for the determination of modafinil. Thus, the aim of present work was to develop spectrophotometric assay methods for determination of modafinil in the bulk drug and pharmaceutical dosage forms.

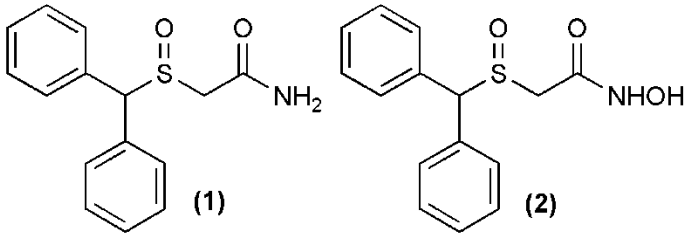



Figure 1. Structure of modafinil (1) and adrafinil (2).

## Materials and Methods

### Instruments, reagents and chemicals

Ultraviolet spectrophotometer (1700 series and 1800 series Shimadzu) with 1 cm matched quartz cells were used for the measurement of absorbance of samples. Shimadzu-Ax-200 electronic balance was used for weighing. Modafinil WS (working standard) was procured from APL Research Centre (A Division of Aurobindo Pharma Limited) Hyderabad, India, as a gift sample. Analytical grade of methanol was procured from Merck Specialities, Private Limited, India and Distilled water was prepared in-house by distillation assembly. Modafinil (AMD) tablets (Armod-50, Emcure Pharmaceutical Ltd., Jammu, India) were purchased from local market.

### Linear regression equation (LRE) method

About 10 mg of modafinil (AMD) was accurately weighed and dissolved in 1 mL of methanol and volume was made upto 10 mL by distilled water (1000 µg/mL, Stock P). The aliquot of stock P was diluted by 10% aqueous methanol to get stock Q of 100 µg/mL. Aliquots of stock Q were further diluted to get concentration of 10, 20, 30, 40, and 50 µg/mL of AMD and these dilutions were scanned in the range of 400-200 nm against 10% aqueous methanol as blank. The absorbances of the dilutions were measured at its absorbance maxima 252 nm and linear regression equation was calculated.

### Standard absorptivity (SA) method

As per LRE method, five standard dilutions were prepared in triplicates and their absorbances were measured against 10% aqueous methanol as blank. These observations of the absorbance were used to determine standard absorptivity A (1%, 1cm) and molar extinction coefficient ε; which would be used to determine the AMD content of dosage forms.

### First order derivative (FOD) method

As per LRE method, five standard dilutions were prepared and their absorbance was measured in first order derivative mode of Gaussian spectra against 10% aqueous methanol as blank. The absorbances were measured at 234 nm and linear regression equation for the FOD method was calculated.

### Validation of methods

As per ICH guidelines, [10-11] the developed all three methods were validated. Five standard serial dilutions were prepared in triplicate linearity and repeatability (within day). The accuracy of the methods was assured by recovery method (standard addition to pre-analysed samples); intermediate precision was determined by three variables viz. days, analyst and instrument variation; methanol variation in solvent system was studied for the robustness (9, 10 and 11 %).

**Dosage formulation analysis**

Twenty AMD tablets (Armod-50, Emcure Pharmaceutical Ltd., Jammu, India) were weighed and finely powdered; a quantity equivalent to 50 mg of AMD was sonicated to dissolve in 10 mL of methanol. The solution was filtered through Whatman filter paper No. 41 and volume was made upto 100 mL by distilled water to give Stock I. Aliquots of stock I were diluted to obtain sample concentrations (20, 30 and 40 μg/mL) in the range of linearity. The absorbance values of these sample solutions were observed in Gaussian and derivative mode of spectra. The absorbances were used to determine drug content by the respective validated method.

## Results and Discussion

**Linear regression equation (LRE) method**

AMD drug is soluble in methanol and acetone and insoluble in water. Different percentages of methanol as solvent for spectrophotometric analysis were tried to make the method more eco-friendly and cost-effective for routine analysis. The minimum concentration of methanol was 10%; in which drug was soluble and give characteristic Gaussian spectra (Figure 2). Acetone was not preferred due to its cut-off wavelength is higher than methanol. The drug AMD was found to be stable in the aqueous solution as there was no deviation from Gaussian spectrum after one week storage of the stock solutions. The six replicates of all dilutions were processed for the linear regression method and the linear regression equation was found to be $Y = 0.003 x + 0.002$ with correlation coefficient $R^2 = 0.999$ as shown in Figure 3.

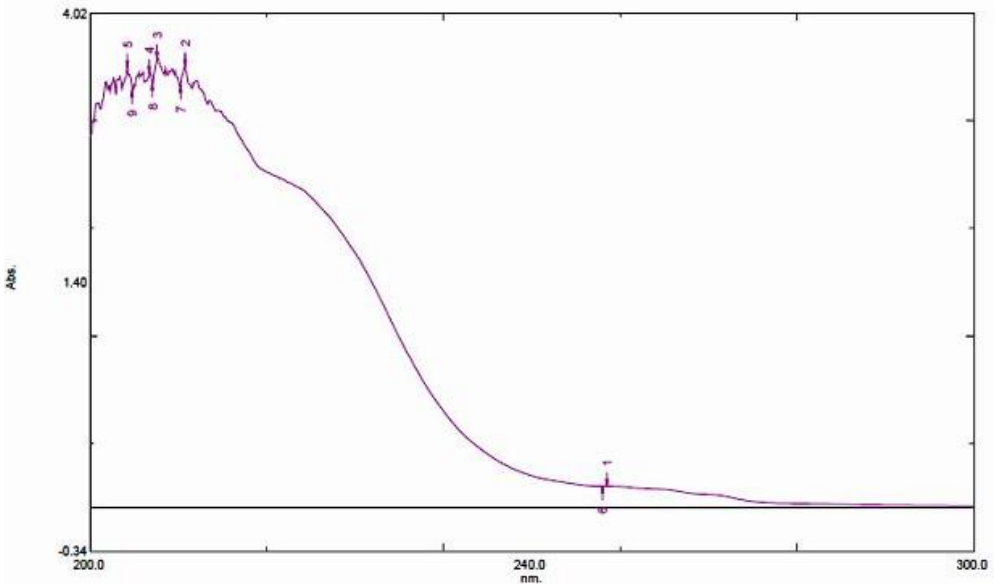



Figure 2. Gaussian spectrum of AMD in 10% methanol.

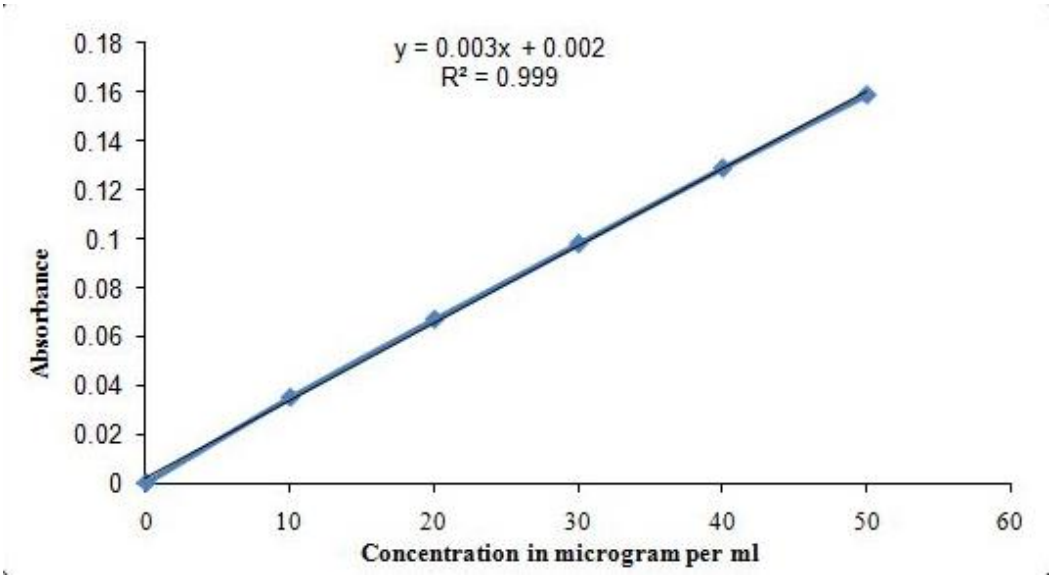



Figure 3. Linear regression line for LRE method.

**Standard absorptivity (SA) method**

The standard absorptivity A (1%, 1cm) and molar extinction coefficient (ε) were determined from absorbances of serial dilutions (10, 20, 30, 40 and 50 µg/mL) in three replicates, which were found to be 41.017 dl/g/cm and 1121.191 $Mol^{-1}$ $cm^{-1}$, respectively (Table 1). This standard absorptivity A (1%, 1cm) of AMD may be used for direct determination of drug content in tablet formulation in single step using single UV observation of drug sample.

Table 1. Standard absorptivity A (1%, 1cm) and molar extinction coefficient (ε)

| Conc. (µg/mL) | Absorbance at 252 nm | | | Standard Absorptivity [A (1%, 1cm) = A/bc] | | |
|---|---|---|---|---|---|---|
| | I | II | III | I | II | III |
| 10 | 0.035 | 0.048 | 0.045 | 35.0 | 48.0 | 45.0 |
| 20 | 0.067 | 0.091 | 0.090 | 33.5 | 45.5 | 45.0 |
| 30 | 0.098 | 0.135 | 0.136 | 32.7 | 45.0 | 45.3 |
| 40 | 0.129 | 0.175 | 0.177 | 32.3 | 43.8 | 44.3 |
| 50 | 0.159 | 0.222 | 0.219 | 31.8 | 44.4 | 43.8 |

*Mean of 15 above standard absorptivities determination;

**Molar extinction coefficient ε = A (1%, 1cm) x Molecular weight/10

**First order derivative (FOD) method**

The first order derivative mode of Gaussian spectra was used to nullify the effect of other analytes in determination of AMD (Figure 4). FOD technique is very useful in spectrophotometry, which is additional tool and resolve various analytical problems where chances of interference in absorbance by other analyte. The absorbances in derivative mode of six replicates of all standard serial dilutions were processed for the linear regression method and the linear regression equation was found to be Y = 0.03 x - 0.000 with correlation coefficient $R^2$ = 0.999 (Figure 5).

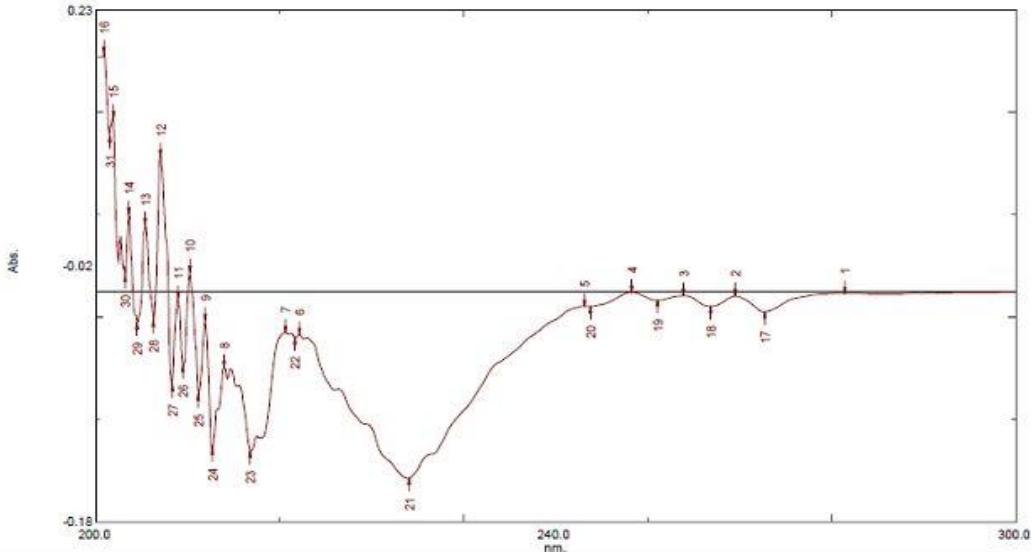



Figure 4. First order derivative of Gaussian spectrum of AMD in 10% methanol.

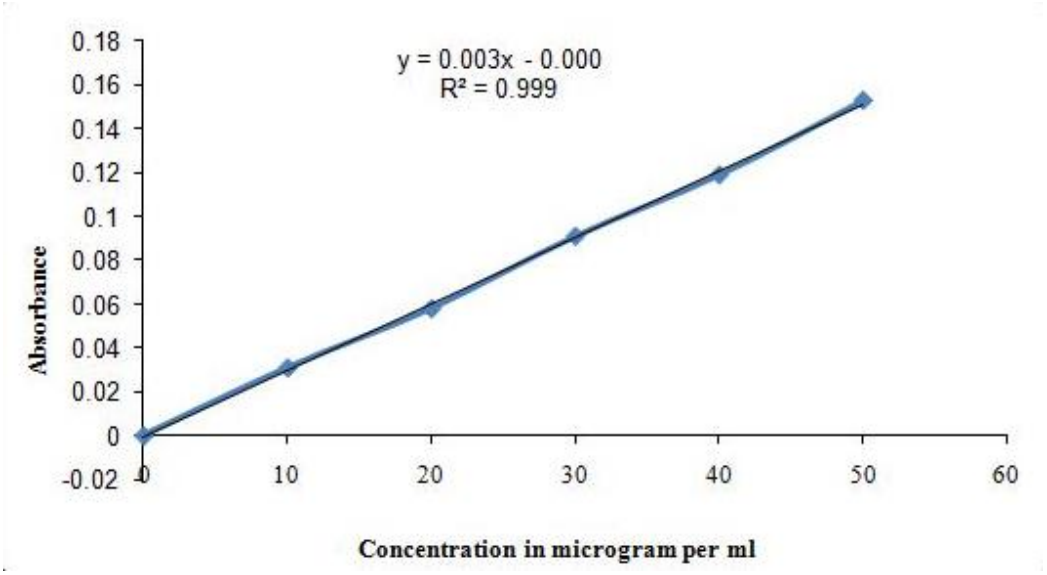



Figure 5. Linear regression line for FOD method.

**Validation of the methods**

All three methods were validated as per ICH guidelines to assure the reliability and applicability of the methods. Results of validation parameters for all three methods were summarized in Table 2.

Table 2. Results of validation parameters for all three methods

| Validation parameter | % Result Obtained (mean)* ± SD | | |
|---|---|---|---|
| | LRE method | SA method | FOD method |
| Linearity | 99.89 ± 0.081 | 100.93 ± 0.087 | 100.12 ± 0.057 |
| Accuracy | 100.63 ± 0.092 | 100.83 ± 0.092 | 100.12 ± 0.082 |
| Precision | | | |
| I. Repeatability | 99.79 ± 0.086 | 101.06 ± 0.063 | 99.85 ± 0.043 |
| II. Intermediate precision | | | |
| a. Days | 100.94 ± 0.031 | 99.98 ± 0.073 | 100.04 ± 0.059 |
| b. Analysts | 99.98 ± 0.099 | 100.45 ± 0.089 | 100.86 ± 0.042 |
| c. Instruments | 100.75 ± 0.071 | 99.79 ± 0.062 | 99.96 ± 0.084 |
| Robustness | | | |
| 35° C | 100.42 ± 0.059 | 100.05 ± 0.079 | 101.01 ± 0.076 |
| 30° C | 100.08 ± 0.094 | 99.79 ± 0.083 | 99.86 ± 0.065 |
| 25° C | 99.88 ± 0.069 | 100.32 ± 0.049 | 99.93 ± 0.082 |

* mean of six dilutions in three replicates. SD = standard deviation.

The Beer-Lambart's law was obeyed at the concentration of 10-50 µg/mL and the linearity for the all the methods (LRE, SA and FOD method) were determined as 99.89 %, 100.93% and 100.12% respectively (Table 2), which were acceptable as standard deviation was within limit (0.057-0.087). Recovery method was adopted to assure the accuracy of the methods which was found to be in between 100.12-100.83% by all the methods with far less than one unit of standard deviation. The repeatability and intermediate precision were studied to assure the precision of the methods. The repeatability of the methods was found in between 99.79-101.06%. The intermediate precision was studied for variation in day of analysis, analyst-to-analyst and instrument-to-instrument. The results for all variations were within 99.79-100.94% limit for all methods. Robustness study was performed to assure the reliability of the methods over the temperature variation (25-35° C) during analysis of the drug and the variation results were in between 99.86-101.01% with low standard deviation. Therefore, results of the validation parameters were proved that all methods may be equally applicable.

**Dosage formulation analysis**

The AMD drug was freely soluble in methanol; the drug powder of tablets was sonicated in methanol to extract the drug content (AMD) from the tablet powder and finally the stock was prepared in 10% aqueous methanol. All the three methods were applied to determine the drug content in tablet formulation which was found to be in the range of 99.36-101.28%, 99.48-101.09% and 99.78-101.05%, respectively (Table 3). The standard deviation was found in the range of 0.42-0.69, which was acceptability of the all method.

At 95% confidence interval, P value less than 0.05 is considered significant. Results showed P value for tablet analysis using validated methods at all concentration levels was found to be, non-significant as: 0.904, 0.647 and 0.428 respectively. Even different concentration levels (20, 30 and 40 µg/mL) in individual method was also not significant with P value 0.774, 0.282 and 0.949 (Table 3).

Table 3. Analysis of AMD tablets.

| **Batch ↓** | **AMD % found in modafinil tablets** | | | | | | | | |
|---|---|---|---|---|---|---|---|---|---|
| | **LRE method** | | | **SA method** | | | **FOD method** | | |
| Conc. (µg/mL) → | 20 | 30 | 40 | 20 | 30 | 40 | 20 | 30 | 40 |
| I | 100.76 | 99.85 | 100.34 | 100.63 | 101.09 | 100.84 | 99.96 | 100.93 | 100.01 |
| II | 99.92 | 100.67 | 101.12 | 100.92 | 100.02 | 100.06 | 101.05 | 99.87 | 99.93 |
| III | 101.28 | 99.79 | 99.75 | 99.92 | 100.13 | 99.79 | 99.78 | 100.16 | 101.02 |
| IV | 100.39 | 100.73 | 99.68 | 100.06 | 99.48 | 101.07 | 100.76 | 100.73 | 99.97 |
| V | 100.82 | 100.75 | 100.29 | 100.26 | 100.16 | 101.01 | 100.47 | 99.85 | 100.06 |
| VI | 99.36 | 100.47 | 100.02 | 99.89 | 99.78 | 100.73 | 99.99 | 99.93 | 100.81 |
| Mean | 100.42 | 100.38 | 100.20 | 100.28 | 100.11 | 100.58 | 100.34 | 100.25 | 100.30 |
| SD | 0.69 | 0.44 | 0.53 | 0.42 | 0.54 | 0.53 | 0.51 | 0.47 | 0.48 |
| P value* | 0.774 | | | 0.282 | | | 0.949 | | |
| Conc. (µg/mL) → | 20 | | | 30 | | | 40 | | |
| P value** | 0.904 | | | 0.647 | | | 0.428 | | |

* P value (P trend) of all three concentration levels for the method.
** P value (Pearson Chi Square) of all three methods for the concentration

## Conclusion

Three new spectrophotometric methods were developed and validated as per ICH guidelines and these were successfully applied for determination of modafinil in tablet formulation. All the methods were equally applicable for the assay of AMD and these may be applied for assay, dissolution studies, bio-equivalence studies as well as routine analysis in pharmaceutical industries.

## Acknowledgement

One of the authors, Pawan Kumar Basniwal is earnestly indebted to Science and Engineering Research Board (SERB), DST, New Delhi, for the financial support for this research work under Fast Track Scheme for Young Scientists. Authors are highly thankful to Head, School of Pharmaceutical Sciences, RGPV, Bhopal and Principal, LBS College of Pharmacy, Jaipur for providing the experimental facilities for this research work.

## References

1. Keating, G.M., Raffin, M.J. (2005) Modafinil: a review of its use in excessive sleepiness associated with obstructive sleep apnoea/hypopnoea syndrome and shift work sleep disorder. *CNS Drugs,* 19(9): 785-803.
2. Rao, N.R., Shinde, D.D., Talluri, M.V.N., Agawane, S.B., (2008). LC–ESI-MS determination and pharmacokinetics of adrafinil in rats. *Journal of Chromatography B*, 873: 119–123.

3. Devadiga, M. P., Anandan, P., Mukhopadhyay, A. (2011). Development of a rapid and sensitive method for estimation of armodafinil in human plasma by *LCMS/MS. International Journal of Applied Biology and Pharmaceutical Technology*, 2(1): 323-327.
4. Schwertnera, H. A., Kong, S. B. (2005). Determination of modafinil in plasma and urine by reversed phase high-performance liquid-chromatography. *Journal of Pharmaceutical and Biomedical Analysis*, 2005; 37, 475–479.
5. Rao, N. R., Shinde, D.D., Kumar T.M.V. (2008). Enantioselective HPLC resolution of synthetic intermediates of armodafinil and related substances. *Journal of Separation Science*, 31(6-7): 981-989.
6. Rao, N. R., Shinde, D.D., Ramesh, V., Srinivas, R. (2009). LC-MS of novel narcoepileptics and related substances. *Journal of Separation Science*, 32: 1312–1322.
7. Wang, W., Xiang, S., Zhou, X., Ji, Y., Xiang, B. (2012). Enantiomeric separation and determination of the enantiomeric impurity of armodafinil by capillary electrophoresis with sulfobutyl ether-β-cyclodextrin as chiral selector. *Molecules*, 17: 303-314.
8. Basniwal, P. K., Kumar, V., Shrivastava, P.K., Jain, D. (2010). Spectrophotometric determination of cilostazol in tablet dosage form. *Tropical Journal of Pharmaceutical Research*, 9(5): 499-503.
9. Jain, D., Basniwal, P. K. (2013). Spectrophotometric determination of olopatadine hydrochloride in eye drops and tablets *Journal of Pharmaceutical Research*,12(2): 48-52.
10. Text on Validation of Analytical Procedures. International conference on harmonization of technical requirements for registration of pharmaceutical for human use; Geneva; 2000.
11. Validation of Analytical Procedure: Methodology; International conference on harmonization of technical requirements for registration of pharmaceutical for human Use; Geneva; 2000.

The Malaysian Journal of ANALYTICAL SCIENCES ISSN 1394-2506

# PENILAIAN RISIKO KANSER DARI SAMPEL TANIH DI SEKITAR KAWASAN PERINDUSTRIAN GEBENG, PAHANG DAN SAMPEL AMANG DI PERAK

## (Assessments of Cancer Risk from Soil Samples in Gebeng Industrial Estate, Pahang and Amang Samples in Perak)

Che Nor Aniza Binti Che Zainul Bahri*, Khoo Kok Siong, Amran Ab. Majid, Norafatin binti Khalid

*Program Sains Nuklear, Jabatan Fizik Gunaan*
*Fakulti Sains dan Teknologi,*
*Universiti Kebangsaan Malaysia, 43600 UKM Bangi, Selangor, Malaysia*

**Corresponding author: anizazainul@gmail.com*

**Abstrak**

Aktiviti perindustrian seperti industri amang dan industri pemprosesan nadir bumi menyumbang kepada risiko radiologi terhadap kesihatan manusia dan alam sekitar. Aktiviti- aktiviti ini boleh meningkatkan keradioaktifan tabii (NORM) yang signifikan dalam persekitaran. Tujuan kajian ini dijalankan adalah untuk menentukan kepekatan aktiviti Torium-232 ($^{232}$Th), Uranium-238 ($^{238}$U) dan Kalium-40 ($^{40}$K) dalam sampel tanih di sekitar Kawasan Perindustrian Gebeng, Pahang dan sampel ilmenit dan monazit dari tiga buah kilang pemprosesan amang di Perak dengan menggunakan spektrometri sinar gama. Seterusnya kadar dos terserap sinar gama, dos tahunan dan risiko kanser ditentukan. Kepekatan aktiviti $^{232}$Th, $^{238}$U dan $^{40}$K dalam sampel tanih di Gebeng masing - masing telah ditemui dalam julat 14.3 – 102.4, 23.8 – 81.3 dan 73.3 - 451 Bq kg$^{-1}$. Manakala julat kepekatan aktiviti $^{232}$Th, $^{238}$U dan $^{40}$K bagi sampel ilmenit dan monazit adalah masing - masing 259 - 166500, 194 - 28750 dan 26.4 - 11991 Bq kg$^{-1}$. Julat kadar dos terserap sinar gama di Kawasan Perindustrian Gebeng adalah 22 - 108 nGy j$^{-1}$ dan di kawasan pemprosesan amang adalah 390 - 6650 nGy j$^{-1}$. Dos tahunan di Kawasan Perindustrian Gebeng dan kawasan pemprosesan amang masing - masing adalah 0.02 – 0.15 dan 0.47 - 68 mSv tahun$^{-1}$. Kajian menunjukan risiko kanser di Kawasan Perindustrian Gebeng adalah 4 per sejuta orang dan 3702 per sejuta orang di kawasan pemprosesan amang. Kepekatan aktiviti dalam tanih di Kawasan Perindustrian Gebeng berada dalam julat yang dilaporkan oleh UNSCEAR 2000 di Malaysia. Kepekatan aktiviti, kadar dos terserap sinar gama, dos tahunan dan risiko kanser di Kawasan Perindustrian Gebeng lebih rendah daripada kawasan pemprosesan amang kerana kawasan pemprosesan amang mempunyai aktiviti yang tinggi di sekitar kawasannya disebabkan kehadiran monazit yang tinggi dengan torium. Kajian ini mencadangkan pemantauan dos sekitaran perlu dilakukan secara berterusan untuk menjamin kelestarian manusia dan alam sekitar.

**Kata kunci:** kepekatan aktiviti, risiko kanser, amang, keradioaktifan tabii

**Abstract**

Industrial activities such as the tin tailings and rare earth processing contribute to radiological risk to human health and environment. Those activities can accumulate the naturally occurring radioactive materials (NORM) with significant concentration in the environment. The aims of this study was to determine the activities concentration of Thorium -232 ( $^{232}$Th ), Uranium -238 ( $^{238}$U ) and Potassium - 40 ( $^{40}$K ) in soil samples around the Gebeng Industrial Estate, Pahang and in samples of ilmenite and monazite from three tin tailings processing plants in Perak using gamma ray spectrometry. The terrestrial gamma dose rate, the annual dose and cancer risk were also determined. The activities concentration of $^{232}$Th, $^{238}$U and $^{40}$K in the Gebeng soil samples were found in the range of 14.3 - 102.4, 23.8 - 81.3 and 73.3 - 451 Bq kg$^{-1}$, respectively. While the activities concentration of $^{232}$Th, $^{238}$U and $^{40}$K for ilmenite and monazite samples were in the range of 259 - 166500, 194 - 28750 and 26.4 - 11991 Bq kg$^{-1}$, respectively. The range terrestrial gamma dose rate at the Gebeng Industrial Estate was 22 - 108 nGy h$^{-1}$ and the tin tailings processing plants was 390 – 6650 nGy h$^{-1}$. Whereas the annual dose at the Gebeng Industrial Estate and tin tailings processing plants were 0.02 – 0.15 and 0.47 - 68 mSv y$^{-1}$, respectively. The study showed that the cancer risk in the Gebeng industrial area were 4 peoples per million and 3702 peoples per million in the tin tailings processing plants. The activity concentration of soil from industrial area reported by UNSCEAR 2000 was in range of the Malaysia soil background. The

activity concentration, the terrestrial gamma dose rate, the annual dose and the cancer risk were lower in the industrial area compared to tin tailings processing plants due to the high activity among the tin tailings processing area due to the high content of thorium in monazite. This study is recommended to monitor the environmental dose continuously in order to ensure the sustainability of human and environment.to ensure the sustainability of human and environment.

**Keywords:** activity concentration, cancer risk, amang, natural radionuclide

## Pengenalan

Setiap manusia tidak terlepas daripada menerima dedahan dos sinaran dari pelbagai sumber sama ada semulajadi ataupun buatan manusia. Kadar dos sinaran yang berpunca daripada sumber semulajadi menyumbang kira-kira 2.4 mSv tahun$^{-1}$[1]. Kehadiran bahan radioaktif semulajadi iaitu NORM (*Naturally Occuring Radioactive Material*) dalam tanih telah menyumbang sekurang-kurangnya 85% daripada sinaran latar belakang [2]. Selain daripada sumber semula jadi, aktiviti penyelidikan dan teknologi juga menyumbang kepada aras sinaran latar belakang. Industri minyak dan gas, pemprosesan unsur nadir bumi dan pemprosesan sisa timah boleh menyebabkan pengumpulan NORM yang tinggi dalam hasil sampingan dan sisa aliran.

Kawasan Perindustrian Gebeng yang terletak di Kuantan, Pahang merupakan zon aktiviti perindustrian yang menempatkan pelbagai industri termasuk industri minyak dan gas serta industri pemprosesan nadir bumi. Pemprosesan nadir bumi melibatkan proses pengekstrakan, pengasingan dan penapisan di mana menggunakan sejumlah besar bahan kimia yang menyebabkan terhasilnya sisa buangan dalam bentuk gas, pepejal dan cecair. Bahan cemar yang dilepaskan dalam bentuk cecair mengandungi unsur radioaktif seperti uranium, torium, kalium-40 dan sisa sampingannya. Sebahagian besar NORM yang hadir dalam tanih adalah tergolong sebagai hasil akhir daripada aktiviti perindustrian [3]. Uranium, torium dan kalium-40 merupakan penyumbang utama kepekatan aktiviti daratan di Semenanjung Malaysia [4]. Secara umumnya, peningkatan aktiviti radionuklid dalam tanih dengan ketara boleh meningkatkan kadar dos terserap sinar gama.

Perak merupakan negeri yang aktif dalam aktiviti perlombongan dan pemprosesan bijih timah. Di negeri ini terdapat beberapa kilang pemprosesan sisa timah iaitu amang atau tahi timah yang dapat meningkatkan bacaan dos sinaran persekitaran dan penyumbang kepada peningkatan sinaran latar belakang. Pemprosesan amang yang dijalankan adalah untuk mengekstrak pelbagai mineral berharga seperti monazit, xenotim, ilmenit dan zirkon. Mineral tersebut mengandungi unsur radioaktif atau NORM dengan kepekatan aktiviti yang tinggi terutama torium dalam monazit. Dalam industri ini terdapat kemungkinan pendedahan sinaran kepada pekerja, orang awam dan alam sekitar kesan daripada penguraian bahan radioaktif tersebut dan ianya bergantung kepada kepekatan aktiviti radionuklid dan kadar dos sinaran. Justeru itu, langkah keselamatan perlu diambil bagi mengelakkan berlakunya dedahan sinaran yang melampau kepada pekerja, orang awam dan alam sekitar.

Dos sinaran berpotensi mendatangkan kesan kesihatan terhadap penduduk setempat [5]. Oleh kerana aktiviti perindustrian tersebut mempunyai kepentingan, pemantauan yang teliti terhadap sinaran latar belakang adalah perlu dilakukan kerana peningkatan aras dos sinaran berpotensi menimbulkan kesan terhadap kesihatan dan kemungkinan menyumbang kepada risiko kanser. Oleh itu, matlamat kajian ini dijalankan adalah untuk menentukan kepekatan aktiviti tanih di Kawasan Perindustrian Gebeng, Pahang dan dalam sampel amang di Perak, penentuan kadar dos terserap sinar gama, dos tahunan dan anggaran risiko kanser penduduk di kawasan kajian.

## Bahan dan Kaedah

### Kawasan kajian

Sampel tanih diambil di sekitar Kawasan Perindustrian Gebeng, Pahang iaitu di lima stesen terpilih dengan keluasan 100 hektar bagi mewakili kawasan tersebut. Koordinat latitud dan longitud kawasan persampelan adalah seperti dalam Jadual 1 di bawah. Bacaan koordinat ditentukan menggunakan *Global Positioning System* (GPS). Rajah 1 menunjukkan peta 5 stesen kajian. Manakala sampel monazit dan ilmenit pula diambil dari tiga kilang pemprosesan amang yang terletak di Kampar, Perak.

Jadual 1.Koordinat stesen pensampelan

| Stesen | Koordinat GPS | |
|---|---|---|
| | Utara | Selatan |
| 1 | N: 4˚0.505’ | E: 103˚22.971’ |
| 2 | N: 4˚0.445’ | E: 103˚22.708’ |
| 3 | N: 4˚0.397’ | E: 103˚22.562’ |
| 4 | N: 3˚59.901’ | E: 103˚22.438’ |
| 5 | N: 4˚0.127’ | E:103˚22.974’ |




Rajah 1. Peta kawasan kajian

**Penyediaan sampel tanih**

Dua kilogram sampel tanih di setiap stesen diambil pada kedalaman 10 - 15 cm dengan menggunakan gerudi tanih. Kedalaman 10- 15 cm dipilih kerana bahan cemar tidak larut air seperti dioksin dan PCB berada pada kedalaman 10- 15 dari permukaan tanih [6]. Sampel dimasukkan ke dalam beg plastik, diikat dan dilabelkan mengikut stesen pengambilan sampel. Sampel di bawa pulang dan proses perawatan sampel dilakukan di Makmal Sains Nuklear, Universiti Kebangsaan Malaysia. Sampel tanih dibersihkan dari pelbagai bendasing dan dikeringkan dalam ketuhar pada suhu 80 - 90 ºC selama 48 jam sehingga mencapai berat tetap [7]. Kemudian, sampel dilerai dan dihancurkan sebelum diayak menggunakan pengayak bersaiz 0.8 mm bagi memastikan ia berada dalam keadaan homogen. Hasil ayakan diisi ke dalam bekas polietelina mengikut ketinggian piawai iaitu setinggi 4 cm, dikedapkan dengan pita pelekat dan disimpan selama 30 hari untuk mencapai keseimbangan sekular antara nuklid induk ($^{238}$U dan $^{232}$Th) dan progeninya. Dalam keseimbangan sekular, aktiviti kedua- dua nuklid induk dan progeni adalah sama. Piawai IAEA tanih-375 digunakan sebagai piawai bagi kaedah bandingan.

**Penyediaan sampel amang**

Sampel monazit dan ilmenit diperolehi secara terus daripada pihak pengurusan kilang. Sampel dibersihkan dan dikeringkan dalam ketuhar pada suhu 80 - 90 ºC selama 48 jam sehingga mencapai berat tetap. Kemudian, sampel dimasukkan ke dalam bekas polietilena berpenutup dan dikedapkan dengan pita pelekat. Seterusnya, sampel disimpan selama 30 hari bagi mencapai keseimbangan sekular antara nuklid induk ($^{238}$U dan $^{232}$Th) dan progeninya. Piawai kaedah bandingan yang digunakan dalam kajian ini ialah Piawai IAEA tanih-375.

**Pengukuran aktiviti radionuklid**

Sampel dibilang selama 12 jam menggunakan sistem pembilang sinar gama (spektrometeri sinar gama) HPGe untuk menentukan kepekatan aktiviti $^{232}$Th, $^{238}$U dan $^{40}$K dalam semua sampel. Pengesan HPGe yang digunakan adalah dari model Canbera 747 dan kecekapan relatifnya 30% dengan leraian 1.80 keV pada puncak tenaga 1332.5 keV. Kepekatan aktiviti $^{232}$Th, $^{238}$U dan $^{40}$K masing - masing ditentukan melalui puncak tenaga 2.614 MeV ($^{208}$Tl), 1.764 MeV ($^{214}$Bi) dan 1.46 MeV ($^{40}$K ) [8].

**Penentuan kepekatan aktiviti**

Kepekatan aktiviti$^{232}$Th, $^{238}$U dan $^{40}$K dalam sampel tanih, monazit dan ilmenit dikira berdasarkan rumus di bawah [7].

$$W_s = \frac{M_p \times A_s}{M_s \times A_p} \times W_p \quad (1)$$

di mana,$W_s$ adalah kepekatan aktiviti sampel (Bq kg$^{-1}$), $W_p$ adalah kepekatan aktiviti piawai (Bq kg$^{-1}$), $M_s$ adalah jisim sampel (g), $M_p$ adalah jisim piawai (g), $A_s$ adalah aktiviti sampel (cps) dan $A_p$ adalah aktiviti piawai (cps).

**Kadar dos terserap sinar gama**

Hasil daripada kepekatan aktiviti $^{232}$Th, $^{238}$U dan $^{40}$K dalam sampel tanih dan amang (monazit dan ilmenit), kadar dos terserap sinar gama dikira menggunakan faktor penukaran yang diterbitkan dalam [9] seperti di bawah:

$$ADRE = (6.62\ C_{Th} + 4.27\ C_U + 0.43\ C_K)\ \text{nGy/jam} \quad (2)$$

di mana $C_{Th}$ adalah kepekatan aktiviti torium (Bq kg$^{-1}$), $C_U$ adalah kepekatan aktiviti uranium (Bq kg$^{-1}$) dan $C_K$ adalah kepekatan aktiviti kalium-40 (Bq kg$^{-1}$).

**Dos tahunan**

Hasil daripada pengiraan kadar dos terserap sinar gama, dos tahunan dapat dikira menggunakan rumus yang diterbitkan oleh UNSCEAR 2000 [1]. Di sini, sampel tanih mewakili dos tahunan di Kawasan Perindustrian Gebeng, Pahang. Manakala sampel amang mewakili dos tahunan di Perak.

$$AEDE = ADRA \times DCF \times OF \times T \quad (3)$$

di mana *AEDE* adalah had dos tahunan (μSv tahun$^{-1}$), *ADRA* kadar dos terserap sinar gama (nGy j$^{-1}$), *DC* adalah faktor penukaran dos (0.7 Sv/Gy), *OF* adalah faktor penghunian (faktor penghunian luaran ialah 0.2), *T* adalah masa (8760 jam/tahun).

**Penentuan risiko kanser**

Akhir sekali, risiko kanser yang diterima oleh penduduk per sejuta orang dikira menggunakan persamaan berikut [10]:

$$\text{Risiko Kanser} = \frac{AEDE \times RF \times 10^{6}}{10^{-3}} \quad (4)$$

di mana *AEDE* adalah dos tahunan (mSv tahun$^{-1}$) dan *RF* adalah faktor risiko (Sv$^{-1}$). Bagi kesan stokastik, faktor risiko kanser yang dicadangkan oleh ICRP 2007 [10] adalah 5.5 x 10$^{-2}$ Sv$^{-1}$ untuk orang awam.

## Hasil dan Perbicangan

**Kepekatan aktiviti**

Julat kepekatan aktiviti bagi $^{232}$Th, $^{238}$U dan $^{40}$K dalam sampel tanih, monazit dan ilmenit ditunjukkan dalam Jadual 2. Hasil kajian menunjukkan kepekatan aktiviti $^{232}$Th dan $^{238}$U adalah tinggi dalam sampel monazit diikuti dengan ilmenit dan tanih. Julat kepekatan aktiviti $^{232}$Th dalam sampel monazit, ilmenit dan tanih masing – masing adalah 30,758 - 166,500 Bq kg$^{-1}$, 259 - 1,182 Bq kg$^{-1}$dan 14.3 – 102.4 Bq kg$^{-1}$. Keadaan ini memang dijangkakan kerana mineral monazit mengandungi kandungan torium yang tinggi secara semulajadi [11]. Manakala kandungan torium dalam ilmenit adalah dalam julat 200 - 2000 Bq kg$^{-1}$ [12]. Julat kepekatan aktiviti $^{238}$U bagi sampel monazit, ilmenit dan tanih masing-masing 13,321 - 28750 Bq kg$^{-1}$, 194 - 4,662 Bq kg$^{-1}$ dan 23.8 - 81.3 Bq kg$^{-1}$. Sampel monazit juga menunjukkan kepekatan aktiviti $^{40}$K yang tinggi iaitu 3,104 - 11,991 Bq kg$^{-1}$ berbanding ilmenit dan tanih. Seterusnya, kepekatan aktiviti $^{40}$K dalam tanih dengan julat 73.3 - 451.8Bq kg$^{-1}$dan diikuti oleh ilmenit dengan julat 26.4 - 86.49Bq kg$^{-1}$. Kehadiran $^{40}$K yang tinggi dalam tanih adalah normal kerana ianya wujud secara semulajadi dan terdapat dalam jumlah yang besar dalam kerak bumi. Kandungan $^{40}$K yang tinggi dalam tanih menunjukkan tanih yang subur kerana ia merupakan nutrien penting yang diperlukan oleh tumbuhan [13].

Jadual 2. Julat kepekatan aktiviti $^{232}$Th, $^{238}$U dan $^{40}$K dalam sampel tanih, ilmenit dan monazite

| Jenis sampel | Bilangan sampel | Kepekatan aktiviti (Bq kg$^{-1}$) $^{232}$Th | $^{238}$U | $^{40}$K |
|---|---|---|---|---|
| Tanih | 25 | 14.3 - 102.4 | 23.8 - 81.3 | 73.3 - 451.8 |
| Ilmenit | 15 | 259 - 1182 | 194 - 4662 | 26.4 - 86.49 |
| Monazit | 15 | 30758 – 166500 | 13321 - 28750 | 3104 - 11991 |

**Kadar dos terserap sinar gama**

Hasil daripada penentuan kepekatan aktiviti $^{232}$Th, $^{238}$U dan $^{40}$K, kadar dos terserap sinar gama dapat dikira dan hasilnya ditunjukkan dalam Jadual 3. Julat kadar dos di Kawasan Perindustrian Gebeng dan kawasan pemprosesan amang masing - masing menunjukkan 22 – 108 nGy j$^{-1}$ dan 390 – 6650 nGy j$^{-1}$. Kadar dos sinar gama di kawasan pemprosesan amang menunjukkan bacaan yang tinggi melebihi nilai purata kadar dos sinar gama di dunia iaitu 57 nGy j$^{-1}$ dengan julat antara 18 - 93 nGyj$^{-1}$ seperti dilaporkan oleh UNSCEAR (2000) [1]. Walau bagaimanapun, kajian yang dijalankan oleh Mohanty et al. 2004 [14], di Chhatrapur India juga menunjukkan bacaan kadar dos sinar gama yang tinggi di kawasan monazit iaitu pada julat 375 – 5000 nGyj$^{-1}$. Peningkatan kadar dos sinar gama di kawasan perindustrian amang adalah disebabkan kehadiran torium dan uranium dalam kedua-dua sampel monazit dan ilmenit pada kepekatan yang tinggi. Di beberapa kawasan termasuk di Guarapari di Brazil, Yangiang di China, dan Tamilnadu di India, kawasan tersebut juga menunjukkan bacaan kadar dos sinar gama yang tinggi disebabkan kehadiran monazit yang mempunyai kandungan torium yang tinggi [15]. Ini menunjukkan tahap kadar dos sinar gama secara langsung dapat dikaitkan dengan kepekatan aktiviti $^{232}$Th dan$^{238}$U [16].

**Dos tahunan**

Kesan kesihatan dari dedahan sinaran mengion dalam persekitaran telah ditentukan dengan pengiraan dos sinaran berkesan biologi dan risiko kanser yang disebabkan oleh dedahan sinaran latar belakang [17]. Had dos tahunan dan risiko kanser telah dikira menggunakan persamaan (3) dan (4) dan hasilnya ditunjukkan dalam Jadual 3. Julat had dos tahunan bagi Kawasan Perindustrian Gebeng dan kawasan pemprosesan amang masing - masing 0.02 – 0.15 mSv tahun$^{-1}$ dan 0.47 - 68 mSv tahun$^{-1}$. Nilai had dos tahunan yang ditetapkan untuk orang awam ialah 1 mSv tahun$^{-1}$dan pekerja sinaran 20 mSv tahun$^{-1}$. Walau bagaimanapun, nilai yang dilaporkan tidak melebihi had dos maksimum tahunan dalam tempoh lima tahun iaitu 50 mSv tahun$^{-1}$. Sebagai langkah keselamatan, beberapa tindakan perlu diambil untuk mengelakkan penerimaan dos yang tinggi kepada pekerja. Antaranya ialah mengurangkan masa bekerja dan menggunakan topeng keselamatan untuk mengelakkan diri dari menyedut udara yang mengandungi unsur radioaktif iaitu radon ($^{222}$Rn) [18].

**Risiko kanser**

Penerimaan dos dedahan yang rendah dalam jangka masa yang lama dan berterusan boleh menyebabkan kesan stokastik iaitu kanser. Walaupun punca sebenar berlakunya kanser tidak diketahui, namun dedahan kepada sinaran mengion merupakan salah satu risiko kepada beberapa jenis kanser antaranya tiroid dan paru - paru. Pengiraan risiko kanser di Kawasan Perindustrian Gebeng dan kawasan pemprosesan amang menunjukkan perbezaan yang signifikan iaitu masing - masing 4 dan 3702 orang per sejuta. Penilaian risiko kanser merupakan kebarangkalian mendapat kanser yang akan diterima oleh penduduk sekitar per sejuta akibat dedahan kepada sinaran atau bahan toksik yang ditanggung sepanjang hayat [19]. Kajian yang dijalankan di Nigeria menunjukkan bacaan risiko kanser yang rendah iaitu 1.37 orang per sejuta menerima kanser daripada dedahan sinaran latar belakang [20].

Jadual 3. Perbandingan kadar dos, dos tahunan dan risiko kanser di Kawasan Perindustrian Gebeng, kawasan pemprosesan amang, Perak dan Mazandar, Iran.

| | Kawasan Perindustrian Gebeng, Pahang | Kawasan pemprosesan amang | Mazandar, Iran [15] |
|---|---|---|---|
| Kadar dos (nGy j$^{-1}$) | 22 - 108 | 390 - 6650 | 26 - 27255 |
| Dos tahunan (mSv tahun$^{-1}$) | 0.02 – 0.15 | 0.47 - 68 | 75 (purata) |
| Risiko kanser (per sejuta orang) | 4 | 3702 | - |

## Kesimpulan

Hasil kajian mendapati kepekatan aktiviti $^{232}$Th, $^{238}$U dan $^{40}$K adalah tinggi dalam sampel amang berbanding tanih. Manakala kadar dos terserap sinar gama, dos tahunan dan risiko kanser di kawasan pemprosesan amang, Kampar, Perak menunjukkan bacaan yang tinggiberbanding di Kawasan Perindustrian Gebeng, Kuantan, Pahang. Ini menunjukkan kepekatan aktiviti sinaran latar belakang akibat pemprosesan amang mempengaruhi kadar dos terserap sinar gama, dos tahunan dan boleh meningkatkan risiko kanser kepada penduduk setempat. Oleh yang demikian, aktiviti pemantauan sinaran latar belakang yang berterusan adalah perlu dilakukan bagi memastikan alam sekitar tidak terdedah kepada sinaran latar belakang yang tinggi kesan daripada aktiviti perindustrian. Kajian penentuan sinaran latar belakang merupakan isu utama dalam pemantauan alam sekitar yang telah dilakukan di seluruh dunia untuk menentukan kepekatan aktiviti tanih serta menilai impak radiologi dan risiko kesihatan terhadap manusia

.

## Penghargaan

Setinggi-tinggi penghargaan dan terima kasih kepada Kementerian Pengajian Tinggi di atas geran penyelidikan yang diberikan iaitu FRGS/ 1/ 2013/ ST01/UKM/01/2 untuk projek ini dan ketiga-tiga kilang pemprosesan amang di Perak yang telah membekalkan pelbagai sampel amang.

## Rujukan

1. UNSCEAR (2000). Exposures from natural radiation sources. United Nations Scientific Committee on the

Effects of Atomic Radiation.*Report to General Assembly, With Annexes.New York: United Nations*.
2. International Atomic Energy Agency (IAEA). 1987. IAEA handbook on nuclear activation data. *Technical series report No. 273*.
3. Krmar, M., J.Sliviska, E. Varga, I. Bikit and M. Veskovic.(2009). Correlations of natural radionuclides in sediment from Danube. Journal of Geochemical Exploration., 100(1): 20-24.
4. Ramli, A. T. (2007). Kajian Radiologi ke Atas Kesan Amang di Negeri Perak.Laporan akhir Projek Penyelidikan Vot 68878.Universiti Teknologi Malaysia dan Lembaga Perlesenan Tenaga Atom.
5. Willson, M.J. (1993). Anthropogenic and naturally occurring radioactive materials detected on radiological survey of properties in Monticello, Utah. *EnvironmentalHealth Physics ; 26th midyear topical meeting, 24-28 Januari* : 564. Idaho : Coeur d'Alene.
6. IAEA. (2004). *Soil Sampling for Environmental Contaminants*. *IAEA- TECDOC-* 1415: 20- 26. Vienna: International Atomic Energy Agency.
7. Yasir, M.S., Majid, A. Ab., Ibrahim, F., Tap, M.S.Q & Abidin, M.R.Z. (2006). Analisis $^{238}$U, $^{232}$Th, $^{226}$Ra dan $^{40}$K dalam sampel amang, tanah dan air di Dengkil, Selangor menggunakan spektrometri sinar gama .*Malaysia Journal of Analytical Sciences.*10 (1) : 35- 40.
8. Selvaskarapandian, S., Sivakumar, R., Manikandan, N.M., Meenakshisundaram, V., Raghunanth, V.M. & Gajendran,V. (2000). Natural Radionuclide Distribution in Soil of Gudalore India. *Applied Radiation and Isotopes* 52 : 299- 306.
9. UNSCEAR. (1987). Ionizing radiation. Sources, effects and risk of ionizing radiation.United Nations Scientific Committee on the Effects of Atomic Radiation. *Report to the General Assembly*. United Nation, New York.
10. International Commission Radiation Protection (ICRP) (2007). Recommendations of the ICRP: Annals of the ICRP volume 37/2-4.
11. Nasirian, M., Bahari, I. & Abdullah, P. (2008). Assessment of Natural Radioactivity in water and sediment from amang (Tin Tailing) processing Ponds. *Malaysian Journal of Analytical Sciences* 12 (1): 150 - 159.
12. Australian Radiation Protection and Nuclear Safety Agency (ARPANSA). (2005). Naturally Occurring Radioactive Materials (NORM) in Australian Industries – Review of Current inventories and Future Generation. EnviroRad Services Pty. Ltd.
13. Robert Mikkelson. (2008). Managing Potassium for Organic Production. Vol. 92. No. 2. Page 26 – 29. Better Corporation
14. Mohanty, A. K., Sangupta, D., Das, S. K., Saha, S. K., Van, K.V, (2004). Natural radioactivity and radiation exposure in high background area at Chhatraputra beach placer deposit of Orissa India. *Journal of Environmental Radioactive* 75(1):15-33.
15. Abbaspour, M., Moattar, F., Okhovatian, A. & Kharrat, M.S. (2010). Relationship of soil terrestrial radionuclide concentrations and the excess life time cancer risk in Newstern Mazandran Province, Iran. *Radiation Protection Dosimetry* 142: 265 - 272.
16. Taskin, H., M. Karavus P. Ay, A. Topuzoglu, S. Hindiroglu and G. Karahan.(2009). Radionuclides concentration in soil and lifetime cancer risk due to the gamma radioactivity in Kirklareli, Turkey. *Journal of Environmental Radioactivity* 70: 223-235.
17. Kapdan, E., Varinlioglu, A., and Karahan, G. (2011).Radioactive Levels and Health Risk due to Radionuclides in the Soil of Yolova, Northwestern Turkey *International Journal Environment*. 5 (4): 837-846.
18. IAEA (2009). *Radiation Workers Handbook: Radiation Control in the Mining & Mineral Processing Industry*. Vienna: International Atomic Energy Agency.
19. International Commission Radiation Protection (ICRP). 1990. Recommendations of the ICRP: ICRP Publication 60. Pergamon Press. New York.
20. Jibiri. N. N. (2001). Assessment of Heaith Risk Levels Associated with terrestrial gamma radiation dose rates in Nigeria. *Environment International* 27 (2001): 21- 26.

The Malaysian Journal of ANALYTICAL SCIENCES ISSN 1394-2506

# THE EFFECT OF BLEND RATIO ON PROPERTIES OF RECYCLED POLYPROPYLENE/RECYCLED HIGH DENSITY POLYETHYLENE GEO- COMPOSITES

## (Kesan Nisbah Adunan Ke Atas Sifat-Sifat Geo-Komposit Polipropilena Kitar Semula/Polietilena Ketumpatan Tinggi Kitar Semula)

A.A.S Mariam Atiqah, H.Salmah*, Z. Firuz, D.N.U. Lan

*School of Materials Engineering,*
*Universiti Malaysia Perlis,Taman Muhibah, Jejawi, 02600 Arau, Perlis,Malaysia*

**Corresponding author: irsalmah@unimap.edu.my*

**Abstract**

The effect of blends ratio of Recycled Polypropylene (rPP) and Recycled High Density Polyethylene (rHDPE) on tensile properties of rPP/rHDPE geo-composites were studied. The increasing of rHDPE ratios has decreased the tensile strength and elongation at break of rPP/rHDPE geo-composites, but the modulus of elasticity increased. The effects of rPP ratios have enhance the tensile strength and modulus of elasticity of geo-composites. The elongation of break of rPP/rHDPE was decreased with increasing the rPP content. At similar blends ratio, the rPP/rHDPE geo-composites higher tensile strength and modulus of elasticity compared to rHDPE/rPP geo-composites. The MFI value of rPP/rHDPE higher than rHDPE/rPP blends. The SEM micrograph showed that rPP/rHDPE has smooth failure surface.

**Keywords:** recycled polypropylene, recycled high density polyethylene, tensile properties, blends, geo-composites.

**Abstrak**

Kesan nisbah adunan ke atas sifat- sifat tegangan geo komposit polipropilena kitar semula (rPP)/ polietilena ketumpatan tinggi kitar semula (rHDPE) telah dikaji. Peningkatan nisbah rHDPE telah mengurangkan kekuatan tegangan dan rPP/rHDPE tetapi meningkatkan ketegangan modulus. Kesan nisbah rPP telah meningkatkan kekuatan tegangan dan pemanjangan geo- komposit. Pemanjagan rPP/rHDPE telah menurun dengan peningkatan kandungan rPP. Pada campuran nisbah yang sama, rPP/rHDPE geo-komposit kekuatan tegangan modulus tinggi berbanding rHDPE/rPP geo-komposit. Nilai MFI adunan rPP/rHDPE lebih tinggi berbanding adunan rHDPE/rPP. Mikrograf SEM menunjukkan rPP/rHDPE mempunyai permukaan yang licin.

**Kata kunci:** polipropilena kitar semula, polietilena ketumpatan tinggi kitar semula, sifat-sifat tegangan, adunan, geo-komposit

## Introduction

For the past ten years, total consumption of plastics and the range of their practical application had demonstrated significant increase [1]. This development is caused by the properties of the plastic materials, also with their adaptability and lower manufacturing cost [2]. Once plastics become waste at the end of their functional usage, they could lead to a serious environmental problem [3]. These plastic wastes are almost non-degraded in the natural environment even after being exposed to extreme weather [4]. Hence, recycling of plastics has become an alternative method in reducing the plastic wastes [4].

Recycled high density polyethylene (rHDPE) and recycled polypropelene (rPP) were used in this study to accomplish solid waste reduction and to achieve advance development of sustainable materials [5]. High Density Polyethylene (HDPE) and PP are nearly not degraded in the natural environment although had been in a long period of exposure [6]. The slow degradation properties of these plastics give off worthful properties as construction material [6, 7]. In today's construction, the presence of weak layers consists of soft soil has led to applications of various types of ground improvement techniques [8]. Common types of geosynthetics used for soft soil

reinforcement are geotextiles (particularly woven geotextiles), geogrids and geocells [8-9]. The main aim of developing construction geo-composites from recycled plastic are to reduce resource consumption, direct or indirect harmful emissions and to produce environmentally-friendly product that meet functional criteria as the conventional product [7]. The development of construction materials from recycled plastics is important to both construction and plastic recycling industries.

This study is aim to investigate effect of blend composition of Recycled Polyproylene (rPP) and Recycled High density polyethylene (rHDPE) blends geo-composite on tensile properties.

## Materials and Methods

### Materials

The recycled HDPE and recycled PP were obtained from SLT. Plastic Sdn. Bhd., Penang, Malaysia. The density of rHDPE and rPP were 0.92 g/cm3 and 0.9 g/cm3. Melt flow index (MFI) of rHDPE and rPP were 0.93 g/10min and 4.03 g/10min at 230°C, respectively.

### Preparations of rHDPE/rPP blends

The rHDPE/rPP blends were prepared using co-rotating twin screw extruder. The temperatures in all three zones of the extruder and die exit were set to $180^0$C, and the speed was set at 180 rpm. The extrudates were fed directly into the pelletizer. The samples were compress with compression molding. The compression procedure involve preheat at 3 minutes, compress at 2 minutes and followed by cooling at 4 minutes. Table 1 shows the formulation of rPP/rHDPE blends.

Table 1. Formulation of rPP/rHDPE blend

| Materials | Blends 1 | Blends 2 |
|---|---|---|
| rPP (php) | 100, 80, 70, 60, 50 | 0, 20, 30, 40, 50 |
| rHDPE (php) | 0, 20, 30, 40, 50 | 100, 80, 70, 60, 50 |

*php= part per hundred polymer

### Tensile testing

Tensile test was done according to ASTM D638. Testing was done at room temperature by using a crosshead speed of 20 mm/min. The mean value of five specimens of each sample was taken. The value of tensile strength, elongation at break and modulus of elasticity were calculated from software.

### Melt flow index

Melt flow index measurement was carried out according to ASTM 1238 using GoTech MFI machine. The die diameter and length were 8 mm and 2095 mm, respectively. The entry angle was 180°. The testing temperature was set at 230°C with load 2.16 kg. Melt flow index (MFI) values of the blends were measured and recorded.

### Morphology

The morphology of tensile fracture surfaces of blends were examined with scanning electron microscope (SEM) model JEOL 6460 LA. The fracture surfaces of the samples were sputter coated with thin layer of palladium before analyzed to avoid electrostatic charging during examination.

## Results and Discussion

Figure 1 show the results from tensile strength of rPP/rHDPE and rHDPE/rPP with different blend ratios. The tensile strength of rPP/rHDPE blends decreased with increasing rHDPE content. The reduced value of tensile strength of blend was due to the addition of rHDPE that influenced the strength of the blends. The tensile strength of rHDPE/rPP blends increased with rPP content increase. This is due to the increasing content of rPP that has a rigid

short methyl group attached to every second carbon atom of the polymer chain. The restriction of the chain rotation produce a stronger but less flexible material compared to rHDPE. The tensile strength for pure HDPE is 24 MPa and theoretically as recycled plastics rHDPE tensile strength is in the range of 20.9 - 34.2 MPa [4, 10]. In this study, the tensile strength of rHDPE is 21.5 MPa. However, the tensile strength of rPP is almost the same as virgin PP which is 30.2 -35.0 MPa [4, 11].

Figure 2 shows the value of elongation at break of rPP/rHDPE blend increased with increasing rHDPE content. This due to the elongation at break of virgin rHDPE is higher than virgin rPP. Hence, the addition of rHDPE gives significant increment to the elongation at break of rPP/rHDPE blends. . At different blend ratios of the rHDPE/rPP, the elongation at break decreased. This is due to the presence of additives in the rPP that give rigid behavior to the recycled thermoplastic. It was found that the rPP/rHDPE blends show lower elongation at break compared to rHDPE/rPP.

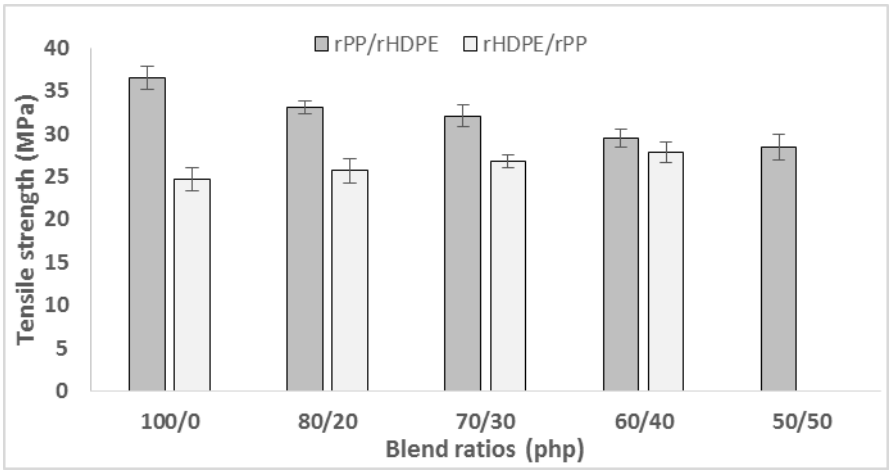



Figure 1. Effect of different blend ratios on tensile strength of rPP/rHDPE and rHDPE/rPP

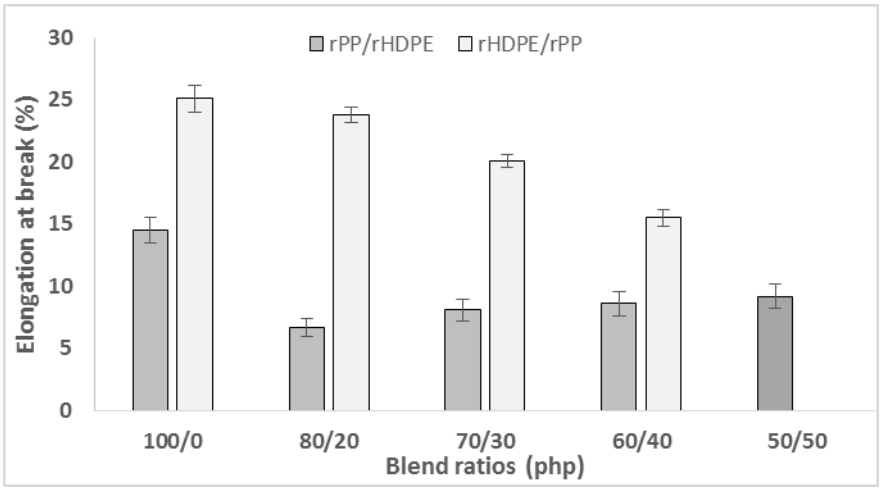



Figure 2. Effect of different blend ratios on elongation at break of rPP/rHDPE and rHDPE/rPP.

As the rHDPE content increased, there was signifcant reduction in tensile strength and modulus of elasticity. This result clearly indicates that the addition of rHDPE can influenced the tensile properties. The modulus of elasticity rPP/rHDPE and rHDPE/rPP blends is shown in Figure 3. The results show that increasing of rHDPE content in rPP/rHDPE blends has decreased the modulus of elasticity of the blends. The lower value of modulus of elasticity of rPP/rHDPE blends attributed to the addition of rHDPE that reduced the stiffness of the blends. Modulus of elasticity of virgin rHDPE is lower than modulus of elasticity of virgin rPP which shows that virgin rHDPE has lower stiffness than rPP. At similar blend ratios the modulus of elasticity of rHDPE/rPP blend increased with blend ratios.

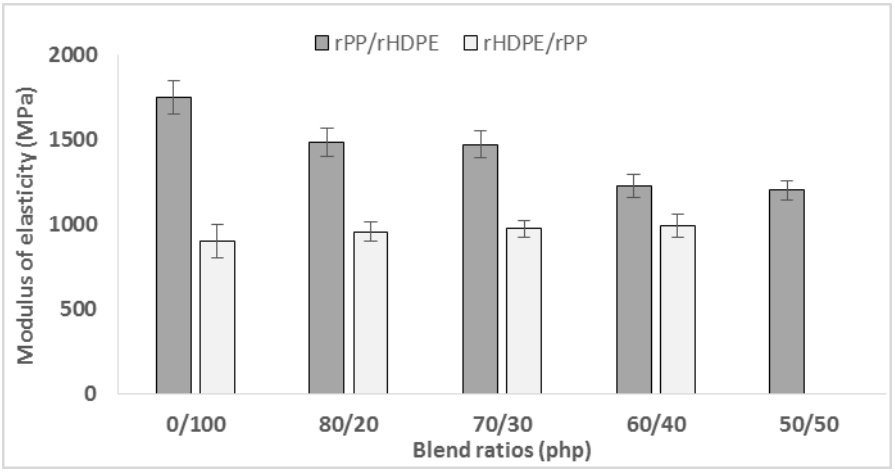



Figure 3. Effect of different blend ratios on modulus of elasticity of rPP/rHDPE and rHDPE/rPP.

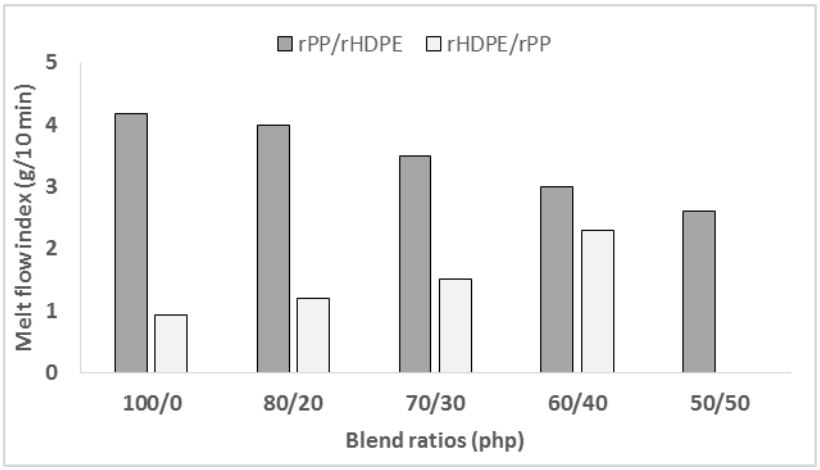



Figure 4. Effect of different blend ratios on melt flow index of rPP/rHDPE and rHDPE/rPP blends.

Melt flow index is described as weight of polymer in grams flowing in 10 minutes through a capillary of specific diameter and length by a pressure applied by prescribed alternative gravimetric weight under prescribed temperature [12-13]. Figure 4 shows the MFI value of the of rPP/rHDPE and rHDPE/rPP blends. From Figure 4, it shows that the increasing of rPP content from 20 to 50 php had change the melt behavior of the blends. The MFI values of

rPP/rHDPE blends decreased with increasing rHDPE content. This is due to the rHDPE structure that consist of little branching which restrict the mobility of the short part of the chain or side groups of the blends and lead to small changes of the melt flow. At different blend ratios, the MFI values of rHDPE/rPP blends increased with rPP content increases. This is due to the incorporation of rPP that have high melt flow index compared to rHDPE and ease the flowability of blends.

Figures 5 - 8 showed the scanning electron micrograph of tensile fractured surfaces of the rPP/rHDPE and rHDPE/rPP blends at different blend ratios, respectively. Figure 5 and 6 present the homogenous surface of rPP and rHDPE which exhibit rHDPE showed ductile tearing mode and rPP showed rough tearing. SEM micrograph of rPP/rHDPE at 80/20 blend ratio exhibit the smooth fracture surface as shown in Figure 7, meanwhile the SEM morphology of rHDPE/rPP at 80/20 blend ratio indicated the rough surface as shown in Figure 8.

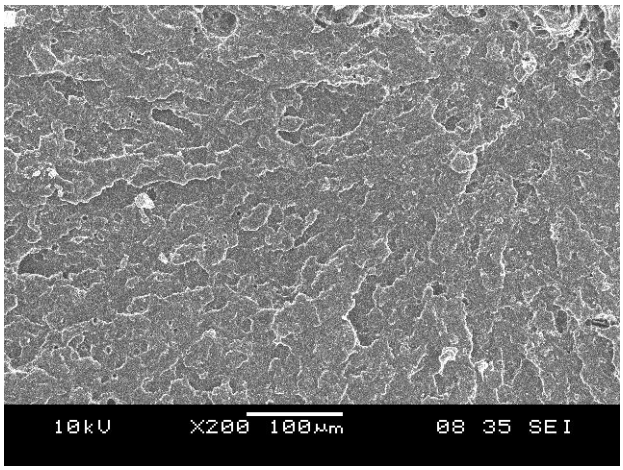



Figure 5. Scanning electron micrograph of tensile fracture surface of rPP.

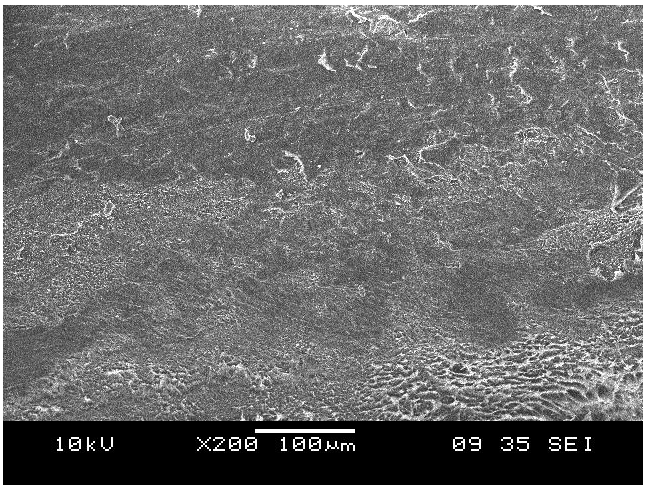



Figure 6. Scanning electron micrograph of tensile fracture surface of rHDPE.

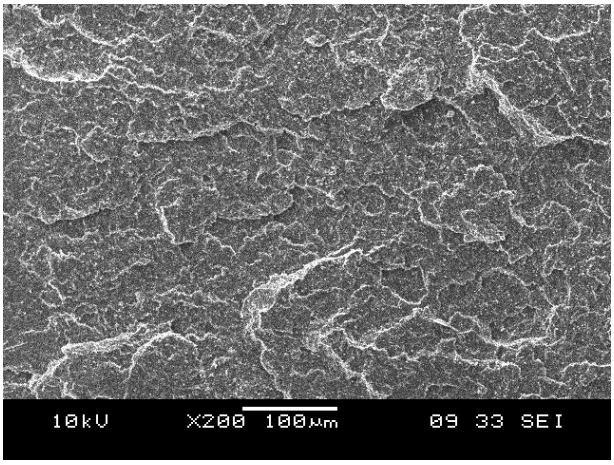



Figure 7. Scanning electron micrograph of tensile fracture surface of rPP/rHDPE blends at 80/20 composition.

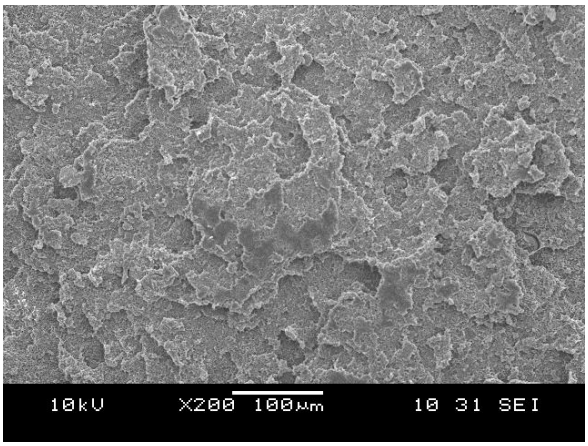



Figure 8. Scanning electron micrograph of tensile fracture surface of rHDPE/rPP blends at 80/20 composition.

## Conclusion

The effect of rPP content has increase the tensile strength and the modulus of elasticity but reduced elongation at break. The addition of rHDPE has decreased the tensile strength and also modulus of elasticity but increased the elongation at break. The MFI values of rPP/rHDPE blends decreased with increasing rHDPE content. The presence of rPP in the blends of rHDPE/rPP blends had increased the flowability of the blends. The SEM study proved that the morphology of rPP/rHDPE blends showed the smooth failure surface, whereas rHDPE/rPP has rough failure surface.

## Acknowledgement

This research was supported by Ministry of Higher Education (MOHE) for providing MTUN CEO Grant No. 9016-00001.

**References**


1. Rahman M.M., Islam M.A., Ahmed M. (2012). Recycling of Waste Polymeric Materials as a Partial Replacement for Aggregate in Concrete. International Conference on Chemical, Environmental and Biological Sciences (ICCEBS'2012), Penang, Malaysia.
2. Sukunya C. A study of compatibilization and properties of recycled high densitypolyethylene/polyethylene teraphthalate blends. Institute of Engineering, Polymer Engineering, Suranaree University of Technology, (2007) MSc Thesis.
3. Albano L. & Sanchez G. (1999). Study of the Mechanical, Thermal and Thermodegradative Properties of Virgin PP with Recycled and Non Recycled HDPE. PolymerEngineering and Science. 39(8): 1456-1462.
4. La Mantia F. (2002). Handbook of Plastic Recycling. Rapra Technology Ltd., Shropshire,UK, London. pg.132-167
5. Oza S.,Wang R., Lu N. (2011). Thermal and Mechanical Properties of Recycled High Density Polyethylene/hemp Fiber Composites. International *Journal of Applied Science and Technology*,1 (5), 31-36.
6. Batayney M., Marie I., Asi I. (2007). Use of selected waste materials in concrete mixes. Faculty of Engineering, Civil Engineering Department, The Hashemite Univeristy, Jordan. *Waste Management*, 27: 1870-1876.
7. Siddique R., Khatib J., Kaur I. (2008). Use of Recycled plastic in concrete: A review. *Waste Management*, 28: 1835-1852.
8. Fasanella E.L., Jackson E.K., Kellas S. (2007). Soft Soil Impact testing and Simulation of Aerospace Structures. NASA langley Research Center, Hampton, Virginia, US.
9. Palmeira E.M., Tatsuoka F., Bathurst R.J., Stevenson P.E., Zornberg J.G. (2008). Advances in Geosynthesis Materials and Applications for Soil Reinforcement and Environmental Protection Works. *Electronic Journal of Geothecnical Engineering*: 1 - 38.
10. Vijay C., John S.K.,Thomas J., George J.N. (2010). World's First Thermoplastic Bridges. Parsons Brinckerhoff Inc. New York.
11. Pan B., Ning N., Liu J.,Bai L., Fu Q. (2009). Mechanical Properties of SMC Whisker Reinforced High Density Polyethylene Composites. *Chinese Journal of Polymer Science*, 27 (2), 267 – 274.
12. Lei Y.,Wu Q.,Yao F.,Xu Y. (2007). Preparation and Properties of recycled HDPE/natural fiber composites. *Composites: Part A*, 38, 1664-1674.
13. Shenoy A.V., Saini D.R., Nadkarni V.M. (1984). Melt rheology of polymer blends from melt flow index. *International Journal of Polymeric Materials and Polymeric Biomaterials*, 10,231-235.
14. Utracki L.A. (1983). Melt flow of polymer blends. *Polymer Engineering and Sciences: Polymer Blends*. 23(11), 602-609.

The Malaysian Journal of ANALYTICAL SCIENCES ISSN 1394-2506

# PHYTOCHEMICAL SCREENING, TOTAL PHENOL ESTIMATION, ANTIOXIDANT ACTIVITY OF *BLAINVILLEA ACMELLA* LEAF AND STEM SUCCESSIVE EXTRACTS

## (Ujian Penyaringan Fitokimia, Penganggaran Fenol dan Aktiviti Antioksidan *Blainvillea Acmella* dan Ekstrak Berturutan Daun dan Stem)

Piush Sharma[1]*, Ganesh N. Sharma[2], B. Shrivastava[2], Hemant R. Jadhav[3]

[1]*Maharishi Arvind College of Pharmacy, Ambabari, Jaipur (Raj). India-302023*
[2]*School of Pharmaceutical Sciences, Jaipur National University, Jaipur (Raj) India-302025*
[3]*Department of Pharmacy, Birla Institute of Technology & Science, Pilani, Rajasthan, India-333031*

**Corresponding author: joshipiush@gmail.com*

**Abstract**

The aim of present work was to investigate antioxidant potential of different extracts of *Blainvillea acmella* leaf and stem. The successive extraction of individual plant part was carried out using solvents of different polarity viz. n-hexane, ethyl acetate, methanol and water. Preliminary phytochemical screening of all the extracts was done. The present total phenolic contents were estimated by Folin-Ciocalteu reagent method and expressed as µg/mg of gallic acid equivalent. The antioxidant potential and reducing power of all the prepared extracts were measured against DPPH, as compared to standard ascorbic acid, and BHA respectively. The result data indicate that the phenolic contents were higher in methanolic extracts of leaf (73.67±0.38mg/g) followed by ethyl acetate (29.08±0.38mg/g), aqueous (21.50±0.28 mg/g), and n-Hexane (9.29±0.38 mg/g); gallic acid equivalent. The similar pattern in stem part was also observed i.e. methanolic extracts (41.90±0.45mg/g), ethyl acetate (21.92±0.28 mg/g), aqueous (15.13±0.18mg/g), and n-Hexane (3.69±0.28 mg/g). The antioxidant capacity of methanolic extract of both the part i.e leaf and stem was found to be maximum, as IC50 values were 226.49±0.16, 402.05±1.10 respectively. The reducing power was also highest in methanol extract of both parts. The result data conclude that the higher antioxidant as well as reducing power may be due to present phenolic contents.

**Keywords***: Blainvillea acmella*, Antioxidant, Reducing Power, DPPH, IC50

**Abstrak**

Kajian ini bertujuan meneliti potensi bahan antioksidan dari ekstrak daun dan batang Blainvillea acmella yang berbeza. Pengekstrakan berturutan pada bahagian tertentu tumbuhan telah dijalankan dengan menggunakan pelarut berkutub berbeza seperti n-heksana, etil asetat, metanol dan air. Saringan awal fitokimia terhadap semua sampel ekstrak telah dilakukan. Jumlah kandungan fenolik telah dianggar dengan mengunapakai kaedah reagen Folin-Ciocalteu dan dinyatakan sebagai kesetaraan µg/ mg asid Gallic. Potensi antioksidan dan kuasa penurun bahan sampel terekstrak diukur melawan DPPH, sebagai perbandingan masing – masing terhadap asid askorbik piawai dan BHA. Data kajian menunjukkan bahawa kandungan fenolik adalah lebih tinggi di dalam daun mengunakan pengekstrak metanol (73.67 ± 0.38mg /g) diikuti etil asetat (29.08 ± 0.38mg /g), air (21.50 ± 0.28 mg /g) dan n-heksana (9.29 ± 0.38 mg/g) kesetaraan asid Gallic. Corak yang sama di bahagian batang juga diperhatikan iaitu ekstrak metanol (41.90 ± 0.45mg /g), etil asetat (21.92 ± 0.28 mg/g), air (15.13 ± 0.18mg/ g), dan n-Heksana (3.69 ± 0.28 mg/g). Kapasiti antioksidan mengunakan pengekstrak metanol daripada kedua-dua bahagian iaitu daun dan batang didapati maksimum, dengan nilai IC50 masing – masing adalah 226.49 ± 0.16 dan 402.05 ± 1.10. Kuasa pengurnagn juga paling tinggi di dalam ekstrak metanol bagi kedua-dua bahagian. Kesimpulan bahawa kehadiran kandungan fenolik menyebabkan nilai antioksidan dan kuasa pengurangan menjadi lebih tinggi.

**Kata kunci***: Blainvillea acmella*, Antioksidan, Kuasa penurun, DPPH, IC50

## Introduction

The free radicals are involved in a number of biochemical processes and also represent an essential part of aerobic life and metabolism. These radicals are continuously produced in body's normal utilization of oxygen such as respiration and some cell-mediated immune functions, and may also be generated through environmental pollutants, automobile exhaust fumes, pesticides, cigarette smoke, radiation, air pollutants etc.[1]**,** which become part and parcel of our daily inhaling/ingesting life, and appears no escape from them [2].

The antioxidants are fighter against these free radicals and terminate the chain reaction before vital molecules are damaged. Antioxidants prevent cellular damages, and the pathway of a variety of diseases [3]**.** A wide range of antioxidants, both natural and synthetic are being utilized in treatment of various diseases, mediated by free radicals [4, 5]. The synthetic compounds have their own adverse effects, so an attempt is being made regularly with use of natural resources.

The *Blainvillea acmella (Family: Asteraceae)* is one of the important annual herb**,** which is native of America and found throughout India. Also found in Indonesia, Malaysia, Myanmar, Nepal, Philippines, Thailand, Vietnam; Africa and Australia [6]. The various parts of the plant have been reported for the presence of number of phytoconstituents [7], although we tried to confirm the presence of these phytoconstituents in extracts of solvents with different polarity. The *Blainvillea acmella* has also been used traditionally for various purposes [8]. The plant have been found effective as ovicidal, larvicidal and pupicidal [9], diuretic [10], anti fungal [11], antipyretic [12.], anti-inflammatory [13], and few others. Main objective of this study was to estimate phenolic content, free radical scavenging activity and reducing power of the leaf and stem of *Blainvillea acmella* extracted successively with n-Hexane, Ethyl Acetate, Methanol and Water.

## Materials and Methods

### Reagents and chemicals

All the chemicals used in the study were of analytical grade. The reagents used in the preliminary phytochemical study were freshly prepared. Folin Ciocalteu reagent (Qualigens), Gallic acid (Fluka), DPPH (Sigma), Ascorbic acid, Iron chloride, Butylated hydroxy anisole (BHA), Trichloroacetic acid (Merck), Potassium ferricyanide (Thomas Baker) were incorporated in study.

### Collection and authentification of plant parts

The leaves and stem of *Blainvillea acmella* was collected from *tehsil* Aamer, Jaipur (Raj.) India, in the month of September to November (most suited period as the phytoconstituents and secondary metabolite are abundant in plant part) and was authenticated by Joint Director, Botanical survey of India, Jodhpur. Specimen samples are stored at herbarium of Maharishi Arvind college of Pharmacy, Ambabari, Jaipur.

### Preparation of plant part extracts

The leaf and stem part was cleaned and shade dried. The samples were broken into small pieces with cutter mill, powdered and passed through sieve no. 44. The leaf and stem samples separately; were extracted successively using soxhlet apparatus with n-hexane, ethyl acetate and methanol. Finally remaining marc was extracted with water. The collected extracts were vacuum dried and were labeled as indicated in Table 1.

Table 1. Labels of successive extracts of leaf and stem of *Blainvillea acmella*

| Plant Part | n-Hexane | Ethyl Acetate | Methanol | Water |
|---|---|---|---|---|
| Leaf | BALH | BALEA | BALM | BALW |
| Stem | BASH | BASEA | BASM | BASW |

**Preliminary phytochemical screening of extracts**

The collected extracts were subjected to preliminary phytochemical screening for qualitative determination of phytoconstituents [14, 15].

**Estimation of total phenolic content**

The total polyphenolic content of all extracts were measured by Folin- Ciocalteu reagent method, and are expressed as µg/mg of gallic acid equivalent. The absorbance was measured at 760 nm using UV spectrophotometer (Jasco V530 – UV/VIS/NIR) [16].

**Estimation of free radical scavenging activity by DPPH method**

Scavenging free radical potential of collected extracts was evaluated against a methanolic solution of 1, 1- diphenyl-2- picryl hydrazyl (DPPH) as method describe by Cengiz 2008[17]. The 200µM methanolic solution of DPPH was prepared. 1ml of different concentration (10µg to 4 mg/ml) of extract solution and standard Ascorbic acid solution (10- 60 µg/ml) were taken in different vials. To this 1 ml of methanolic solution of DPPH was added, shaken well and mixture was allowed to stand at room temperature for 20 min. A blank was also prepared in the similar way and the absorbance was measured at 517nm. Scavenging activity was expressed as the percentage inhibition calculated using the Equation 1.

$$\% \text{ Anti-radical activity} = \frac{\text{Control Abs - Sample Abs}}{\text{Control Abs}} \times 100 \qquad \text{(Eq. 1)}$$

**Reducing power assay**

The reducing capability was measured by the transformation of $Fe^{3+}$- $Fe^{2+}$ in presence of different extracts. Different concentrations of extracts (250-2500 µg) in 1ml of water were mixed with 2.5 ml of phosphate buffer (pH 6.6) and 2.5 ml of 1% potassium ferrocyanide. The mixture was incubated at $50^0$C for 20 min. 2.5 ml (10%) of trichloroacetic acid was added to the mixture, and was centrifuged at 3000 RPM for 10 min. 2.5 ml of upper layer solution was mixed with 2.5 ml distilled water and 0.5 ml of 0.1% Fecl3 solution and the absorbance was measured at 700 nm. Increased absorbance of reaction mixture indicated increased reducing power [18, 19]. BHA solution (1000 µg/ml) prepared in phosphate buffer was used as standard.

## Results and Discussion

**Percentage yield of extracts (%)**

*Blainvillea acmella* extract yield was minimum for methanol and hexane extract, for leaf 1.36% and for stem 0.62% respectively, while extractive value was maximum for ethyl acetate (Leaf 4.93%) and aqueous (3.34%). The result data are given in Table 2.

Table 2. Percentage yield of extracts by successive extraction

| Plant Part | Extract (% w/w) | | | |
|---|---|---|---|---|
| | n-Hexane | Ethyl Acetate | Methanol | Water |
| Leaf | 2.02 | 4.93 | 1.36 | 3.83 |
| Stem | 0.62 | 2.20 | 1.23 | 3.34 |

**Preliminary phytochemical screening results**

The phytochemical screening result data are shown in Table 3, which implies that the carbohydrates, flavanoids and phenolic compounds are present in methanolic extracts of leaf and stem.

Table 3. Preliminary phytochemical screening of *Blainvillea acmella*

| Constituents | Test | ***Blainvillea acmella*** | | | | | | | |
|---|---|---|---|---|---|---|---|---|---|
| | | **Leaf** | | | | **Stem** | | | |
| | | **n-Hexane** | **Ethyl Acetate** | **Methanol** | **Water** | **n-Hexane** | **Ethyl Acetate** | **Methanol** | **Water** |
| Alkaloids | Dragendroff's test | - | - | + | - | - | - | - | - |
| | Mayer's test | - | - | + | - | - | - | - | - |
| | Hager's test | - | - | + | - | - | - | - | - |
| | Wagner's test | - | - | + | - | - | - | - | - |
| Carbohydrates | Molish test | - | - | - | + | - | - | + | - |
| | Fehling's test | - | - | - | + | - | - | + | - |
| | Barfoed's test | - | - | - | + | - | - | + | - |
| Glycosides | Kellar-Killani test | - | - | - | - | - | - | + | - |
| | Borntrager's test | - | - | - | - | | - | - | - |
| | Legal's test | - | + | + | + | - | + | + | - |
| Flavonoids | Shinoda test | - | - | + | - | - | + | + | - |
| Saponin | Foam test | - | - | - | - | - | - | - | - |
| | Haemolytic test | - | - | - | - | - | - | - | - |
| Sterols/ Steroids | Salkowaski reaction | + | - | - | - | - | - | - | - |
| Tannins and Phenolic compounds | 5% Ferric chloride solution | + | + | + | + | - | + | + | + |
| | Lead acetate solution | + | + | + | + | - | + | + | + |
| | Dil. Potassium permanganate solution | + | + | + | + | - | + | + | + |
| | Bromine water | + | + | + | + | - | + | + | + |
| Amino acids | Ninhydrin test | - | - | - | - | - | - | - | - |
| Proteins | Biuret test | - | - | - | - | - | - | - | - |

**Total polyphenolic content determination**

*Blainvillea acmella* methanolic extract was found to contain maximum phenolic content (73.67mg/g from leaves, 41.90mg/g from stem), while its hexane extract shows 9.29mg/g from leaves, 3.69mg/g from stem. The present phenolic contents were found as given in Table 4.

Table 4. Total polyphenolic content in *Blainvillea acmella* extracts

| Plant Part | Total Phenolic Content mg/g equivalent to Gallic Acid | | | |
|---|---|---|---|---|
| | n-Hexane | Ethyl Acetate | Methanol | Water |
| Leaf | 9.29±0.38 | 29.08±0.38 | 73.67±0.38 | 21.50±0.28 |
| Stem | 3.69±0.28 | 21.92±0.28 | 41.90±0.45 | 15.13±0.18 |

**Antioxidant assay of extracts**

***Results for DPPH free radical scavenging activity***

Scavenging activity of various extracts and ascorbic acid was studied against DPPH radicals. All the samples were analysed in triplicate. The DPPH assay of BALH extract found to produce no response (% inhibition) even at concentration 4000µg/ml. The BALEA, BALM and BPLW extract at the level of 300µg/ml, 250µg/ml and 350µg/ml showed > 50% inhibition respectively, along with concentration dependent response. The methanolic extract of *Blainvillea acmella* leaves exhibited a maximum DPPH scavenging activity. IC50 value (Figure 1) was 226.49±0.16 µg/ml followed by ethyl acetate and water extract whose scavenging activities (IC50) were 283.35±0.56 and 337±0.44 µg/ml, respectively. The IC50 value of ascorbic acid was also 36.14±0.26, while n-hexane extract did not produced any response.

BASH extract also produced similar results up to concentration 4000µg/ml as of BPLH extract i.e. no response was generated. The BASEA, BASM, BASW extract, at the concentration level of 500µg/ml, 400µg/ml and 600µg/ml was found to exhibit > 50% inhibition, which was a concentration dependant response. The IC50 value (the concentration with scavenging activity of 50%) of methanolic extract of stem part was, 402.05±1.10, followed by ethyl acetate and water extract, whose IC50 values were 498.56±0.87, and 579.85±1-34 µg/ml respectively (Figure 2). Again no response was generated with hexane extract of stem part also.

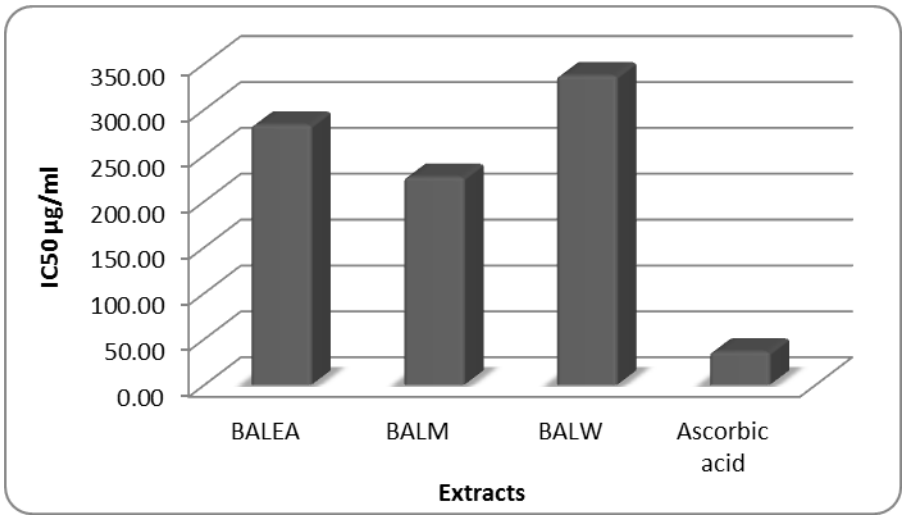



Figure 1. IC 50 of *Blainvillea acmella* leaves extracts

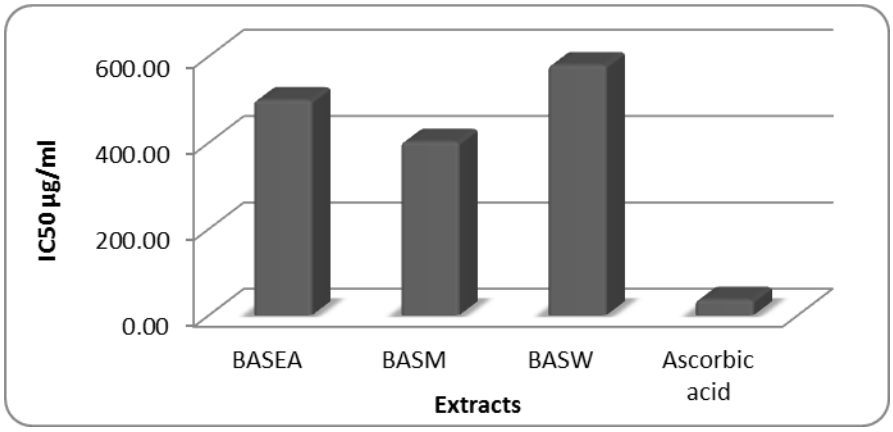



Figure 2. IC 50 of *Blainvillea acmella* stem extracts

***Results for reducing power activity***

The reducing power of different extracts of leaf and stem of *Blainvillea acmella* was assayed and compared with butylated hydroxy anisole (BHA) (Figure 3 and 4). Maximum reducing capacity was recorded with methanolic extract of leaf (BALM), although the response generated with BALEA and BALW were also significant as compared to standard, and was lowest with BALH. The similar finding was also observed with different extracts of *Blainvillea acmella* stem. The result data were found as in Table 5 and 6.

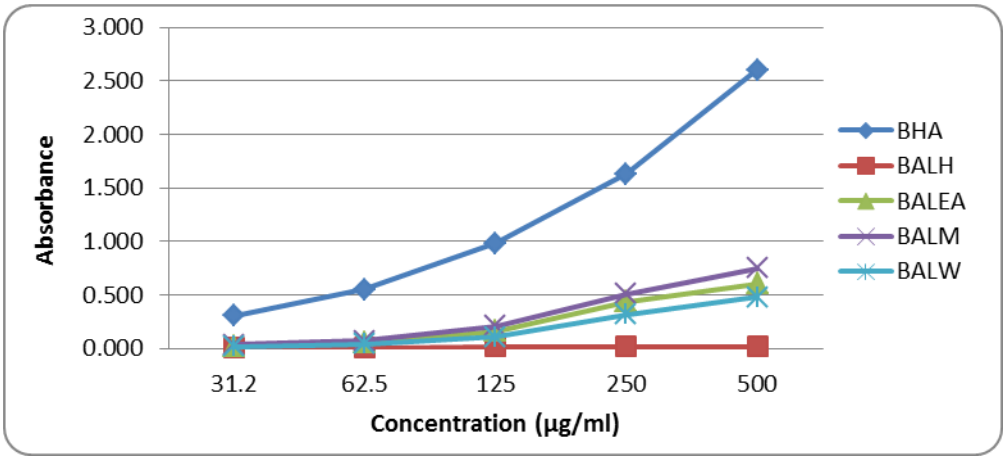



Figure 3. Reductive potential of different concentrations of *Blainvillea acmella* leaves extracts

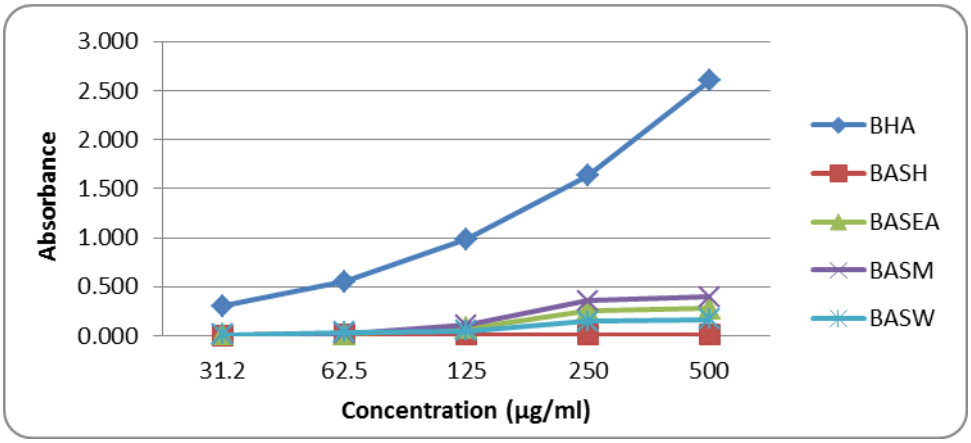



Figure 4. Reductive potential of different concentrations of *Blainvillea acmella* stem extract

Table 5. Reducing power of *Blainvillea acmella* leaves extracts

| Sequence No. | Conc (µg/ml) | BHA | BALH | BALEA | BALM | BALW |
|---|---|---|---|---|---|---|
| 1 | 31.2 | 0.306±0.001 | 0.006±0.001 | 0.024±0.001 | 0.034±0.001 | 0.017±0.001 |
| 2 | 62.5 | 0.551±0.002 | 0.009±0.002 | 0.053±0.002 | 0.071±0.002 | 0.041±0.002 |
| 3 | 125 | 0.985±0.001 | 0.018±0.001 | 0.164±0.002 | 0.208±0.001 | 0.107±0.002 |
| 4 | 250 | 1.631±0.001 | 0.021±0.001 | 0.438±0.002 | 0.513±0.002 | 0.319±0.002 |
| 5 | 500 | 2.603±0.002 | 0.021±0.001 | 0.605±0.002 | 0.749±0.003 | 0.483±0.002 |

n=3, Data are given as mean ± S.D

Table 6. Reducing power of *Blainvillea acmella stem* extracts

| Sequence No. | Conc (µg/ml) | BHA | BASH | BASEA | BASM | BASW |
|---|---|---|---|---|---|---|
| 1 | 31.2 | 0.306±0.001 | 0.004±0.001 | 0.010±0.001 | 0.012±0.001 | 0.010±0.001 |
| 2 | 62.5 | 0.551±0.002 | 0.006±0.002 | 0.015±0.001 | 0.022±0.002 | 0.036±0.002 |
| 3 | 125 | 0.985±0.001 | 0.008±0.001 | 0.076±0.002 | 0.105±0.002 | 0.050±0.002 |
| 4 | 250 | 1.631±0.001 | 0.009±0.001 | 0.260±0.002 | 0.357±0.002 | 0.149±0.002 |
| 5 | 500 | 2.603±0.002 | 0.009±0.001 | 0.280±0.002 | 0.392±0.002 | 0.167±0.002 |

n=3, Data are given as mean ± S.D

## Conclusion

An attempt has been made here to establish the antioxidant measures of the *Blainvillea acmella*, which might be helpful in establishing its therapeutic values. The leaf and stem part of the plant were extracted successively using

solvents of different polarity. The extracts were subjected to phtyochemical screening to confirm presence of phytoconstituents and secondary metabolites. The results data regarding presence of total phenolic contents implies that the methanolic extract of both the part was most abundant, as compared to other extracts. From this we can conclude that the phenolic compounds can be better isolated with solvents of higher polarity range. The antioxidant potential as well as reducing power of the extracts was determined and was found better in methanolic extract. Still it was higher with leaf extract as compared to stem extract.

At the same time the results also demonstrate that the IC50 values of different extracts may be co-related with present phenolic content as it was in proportion to that of concentration of the extract and present phenolic moieties. The results confirm the superiority of the different leaf extracts than the stem part extracts. In this study, it seemed that, the higher total phenolic content of plants extracts resulted in higher antioxidant activity.

**Acknowledgement**

Authors are thankful to School of Pharmaceutical Sciences, Jaipur National University, Jaipur (Raj.) for providing necessary support and facility to carry out this research work.

**References**

1. Tiwari, A. K. (2001). Imbalance in antioxidant defence and human disease, multiple approach of natural antioxidants therapy. *Current Science,* 81(9):1179-1187.
2. Tiwari, A. K. (2004). Antioxidants, new-generation therapeutic base for treatment of polygenic disorders. *Current Science*, 86(8): 1092-1102.
3. Balz, F. (1994). Molecular biological mechanisms of antioxidant action. *The FASEB Journal*, 13(9): 963-964.
4. Byungpal, P. Y. (1994). Cellular defenses against damage from reactive oxygen species. *Physiological Reviews*, 74(1): 139-162.
5. Halliwell, B., Gutteridge, J. M. & Cross, C. E. (1992). Free radicals, antioxidants, and human disease: where are we now? *The Journal of Labarotary and Clinical Medicine,* 119(6): 598-620.
6. Wei, B. N. (2011). Blainvillea acmella (Linnaeus) Philipson, *Flora of China*, 20-21: 868.
7. Singh, P., Sharma, A. K., Joshi, K. C., Jakupovic, J. & Bohlmann, F. (1985). Acanthospermolides and other constituents from *Blainvillea acmella*. *Phytochemistry*, 24(9): 2023-2028.
8. Kshirsagar, R. D. & Singh, N. P. (2001). Some less known ethnomedicinal uses from Mysore and Coorg, districts, Karnataka, Southern India. *Ancient Science of Life*, 20(3):20-25.
9. Saraf, D. K. & Dixit, V. K. (2002). Spilanthes acmella Murr. : Study on Its Extract Spilanthol as Larvicidal Compound. *Asian Journal of Experimental Sciences,* 16(1-2): 9-19.
10. Ratnasooriya, W. D., Pieris, K. P., Samaratunga, U. & Jayakody, J. R. (2004). Diuretic activity of Spilanthes acmella flowers in rats. *Journal of Ethnopharmacology*, 91(2-3): 317-320.
11. Rani, S. A. & Murty, S. U. (2006). Antifungal potential of flower head extract of Spilanthes acmella Linn. *African Journal of Biomedical Research*, 9: 67-69.
12. Chakraborty, A., Devi, B. R., Sanjebam, R., Khumbong, S. & Thokchom, I. S. (2010). Preliminary studies on local anesthetic and antipyretic activities of Spilanthes acmella Murr. in experimental animal models. *Indian Journal of Pharmacology*, 42(5): 277-279
13. Chakraborty, A., Devi, R. K. B., Rita, S., Sharatchandra, K. H. & Singh, T. I. (2004). Preliminary studies on antiinflammatory and analgesic activities of Spilanthes acmella in experimental animal models. *Indian Journal of Pharmacology*, 36(3):148-150.
14. Khandelwal, K. R. (2010). Practical Pharmacognosy. *Nirali Prakashan*, Pune, India. 25.1-25.9.
15. Harborne, J. B. (1998) Phytochemical methods. *Chapman and Hall*, London. 90-203.
16. Maurya, S. & Singh D. (2010). Quantitative analysis of total phenolic content in *Adhatoda vasica* Nees extracts. *International Journal of Pharmtech Research*, 2(4):2403-2406.
17. Cengiz, S., Bektas, T., Dimitra, D., Moschos, P. & Mansur, H. (2008). Studies on the antioxidant activity of the essential oil and methanol extract of *Marrubium globosum* subsp. *Globosum lamiaceae* by three different chemical assays. *Bioresource Technology*, 99(10):4239-4246.
18. Ilkay, O., Murat, K., Mahmoud, A. A., Sezer, S. F., Gulderen, Y. & Bilge, S. (2009). Free radical scavenging properties and phenolic characterization of some edible plants. *Food Chemistry*, 114(1): 276–281.

19. Jeng, L. M., Hsiu, C. L., Chin, C. C. (2002). Antioxidant properties of several medicinal mushrooms. *Journal of Agriculture and Food Chemistry*, 50(21):6072-6077.

The Malaysian Journal of ANALYTICAL SCIENCES ISSN 1394-2506

# RHEOLOGICAL AND THERMAL BEHAVIOR OF POLYPROPYLENE-KAOLIN COMPOSITES

## (Reologi dan Sifat Thermal Komposit Polipropilena-Kaolin)

Saw Lip Teng, Nor Azura Abdul Rahim, Du Ngoc Uy Lan*

*School of Materials Engineering,*
*Universiti Malaysia Perlis (UniMAP), Kompleks Pengajian Jejawi, Jejawi 2, 02600 Arau, Perlis, Malaysia*

**Corresponding author: uylan@unimap.edu.my*

**Abstract**

Kaolin's effect on rheological behaviour of polypropylene-kaolin composites was investigated. The research found that not only the kaolin content influence the rheological behaviour but also the compounding using internal mixer and twin screw extruder. In details, viscosity and shear stress increased with addition of kaolin content. These characteristics also exhibited higher in polypropylene-kaolin composite suspensions compounded using twin screw extruder than using internal mixer. Chain scission was assumed to occur and affect the melt properties. Further justification characterized by Differential Scanning Calorimeter (DSC) showed that the effect of kaolin and loading content were more evident on the onset melting temperature and crystallinity. Besides, due to the different cooling operation in both processes, the effect of compounding on melting characteristic was conspicuous.

**Keywords**: Polypropylene-kaolin composite, twin screw extruder, brabender internal mixer, melt rheology, capillary rheometer, and MFI.

**Abstrak**

Kesanan kaolin terhadap tingkahlaku rheologi komposit polipropilena-kaolin telah dikaji. Kajian ini mendapati bahawa bukan sahaja kandungan kaolin yang mempengaruhi tingkahlaku reologi tetapi juga pengkompaunan yang menggunakan mesin pencampur dalaman dan skru extruder berkembar. Secara terperinci, kelikatan dan tegasan ricih telah meningkat dengan penambahan kandungan kaolin. Ciri-ciri ini juga menunjukkan suspensi polipropilena-kaolin komposit yang dikompaunkan oleh skru extruder berkembar adalah lebih tinggi daripada menggunakan mesin pencampur dalaman. Kepisahan rantaian diandaikan terlaku dan menjejaskan sifat-sifat leburan. Justifikasi selanjutnya dicirikan oleh kalorimetri pengimbas pembezaan (DSC) menunjukkan bahawa kesan kaolin dan kandungan terbukti pada peleburan suhu awal dan penghabluran. Selain itu, akibat daripada operasi penyejukan yang berbeza dalam kedua-dua proses, kesan pengkompaunan pada sifat keleburan adalah senang dilihat.

**Kata kunci**: Komposit Polipropilena-Kaolin, Skru Extruder Berkembar, Mesin Pencampur Brabender, Rheologi Keleburan, Kapilari Reometer, dan MFI.

## Introduction

The use of kaolin in polymer composites has attracted industrial interest due to low contamination of toxic element. As other commercial inorganic fillers, kaolin enables to improve thermal endurance, fire resistance, mechanical properties and dimensional stability of a product. Kaolin consist of 1:1 layer lattices (silica-alumina), platy particle shape and particle size down to 0.2 µm. Due to its unique structure, many researcher believes kaolin has specified functionality in polymer composites such as improve process-ability, product's physical and mechanical performances. Like other general filler, presence of kaolin increases the composite viscosity. Research done by Rahim et al. [1] reported viscosity of polypropylene increased with increasing in kaolin loading since kaolin hindered the polymer suspensions movement. High content of kaolin loading not only result in high viscosity but also caused lower mechanical properties. This is due to filler agglomeration. This circumstance was surmounted by the addition of compatibilizer but still unsatisfactory at high kaolin loading contents [1-3].

Compounding process has an important role to control composite's properties. During compounding, the equipment generates heat and shear which significantly gives an effect on polymer molecular weight and structure. Other than matrix condition, compounding process affected distribution and dispersion of fillers which also give major influences to the composite's properties [4-5]. Focus in this article is to comprehend the effect of filler loading and compounding process on rheological properties of PP/Kaolin composite. The most common melt blending of twin screw extruder and internal mixer were selected to study the effect of compounding. The evaluation was based on rheological properties of composite measured by using melt flow index (MFI) and capillary rheometer. Melting transition characteristic was studied by using differential scanning calorimeter.

## Materials and Methods

### Materials and Sample Preparation

Polypropylene co-polymer grade TitanPro SM340 with melt flow index 4g/10min at 230°C (ASTM D1238) supplied by Titan polypropylene Polymer (M) Sdn. Bhd. Kaolin was provided by Sigma-Aldrich with catalog K7375 and linear formula of $\sim Al_2Si_2O_5(OH)_4$. Polypropylene grafted Maleic Anhydride (PPgMA) was supplied by Uniroyal Chemical.

PP/Kaolin composites were prepared via internal mixer (Brabender) and twin screw extruder (Lab Tech), and the recipe was shown in Table 1. Compounding in internal mixer was carried out at 190°C and 50min$^{-1}$ rotor speed for 6 minutes. Polypropylene was preheated for 2 minutes, further by the addition of kaolin. The compounds were taken out and cooled in ambient atmosphere. After that, compounds were crashed into small pieces before rheological test. Same processing temperature was used on twin screw extruder with screw speed 50rpm. Extrudates were cooled by water bath and pelletized right afterward. Twin screw extruder model LTE 16-40 has 16 mm screw diameter and 40 L/D screw ratio with inter-mesh co-rotational design.

Table 1. PP/Kaolin composite formulation

| Sample nomination | | Polypropylene (wt%) | Kaolin loading (wt%) | PPgMA Content (phr) |
|---|---|---|---|---|
| Internal mixer | Twin screw extruder | | | |
| IM0 | TSE0 | 100 | 0 | 0 |
| IM5 | TSE5 | 95 | 5 | 2 |
| IM10 | TSE10 | 90 | 10 | 2 |
| IM15 | TSE15 | 85 | 15 | 2 |
| IM20 | TSE20 | 80 | 20 | 2 |

### Capillary Rheological Test

Rheological behavior of PP/Kaolin composites was studied by using Dynicso LCR-7001 capillary rheometer according ASTM D 3835 testing standard. Viscosity and shear stress versus shear rate were reported based on the built-in software. Testing temperature was carried out at 190°C and preheats 6 minutes. Input shear rate was varies from 50s$^{-1}$ till 5000s$^{-1}$ [3].

### Melt Flow Index (MFI)

MFI test was done according to ASTM D 1238. Testing temperature was carried at 190°C with 2.16kg load and preheated for 6 minutes. MFI values were calculated using formulation (equation 1) below:

$$MFI = 600W / t \quad (1)$$

where W is weight of extrudate, and t is interval time (in seconds) to collect the extrudates. Units for MFI is g/10min [3].

**Differential Scanning Calorimeter (DSC)**

Melting characteristic and crystallinity of PP/Kaolin composites were measured by using a TA Instrument Q-10 DSC. The samples were heated from room temperature up to 190°C with a 10°C/min of heating rate in nitrogen gas atmosphere. First DSC scan results were reported in order to reflect thermal history from different compounding equipments. Heat changes obtained from thermograms were calculated to crystalline percentage by using heat changes reference of polypropylene, $\Delta h^0_f = 207.1$ J/g with equation (2) below:

$$Crystallinity = \frac{\Delta h_f}{\Delta h_f^0} x100\% \quad (2)$$

where, $\Delta h_f$ is the enthalpy of melt transition in polypropylene [6].

## Results and Discussion

**Rheological Properties of PP/Kaolin Composites**

Figure 1 illustrates MFI values of PP/Kaolin composites with different kaolin contents from both compounding processes. It was found that, MFI values dropped gradually with increase in kaolin content. The effect of kaolin particles was as expected by causing a relative increase in the polymer's melt viscosity and reduction the output. This is in agreement with Rahim et al. (2011) founding. The main reason is that kaolin particles hindered the fluency of polypropylene flow [3]. The more the loading of kaolin, the high the obstruction are the lower MFI results. In comparison between two compounding processes, sample from twin screw extruder displayed slightly lower MFI values than those from internal mixer. The difference was in a range of 0.1 ± 0.05 g/10min. However, the distinction became smaller after 10 wt% of kaolin loading. It could be assumed that the effect of different compounding process was insignificant and covered by the high kaolin content effect. It is noted that MFI is only reflecting the rheological properties of PP/Kaolin composites at low shear rate. The rheological behaviour at high stress rate was examined from capillary rheometer testing.

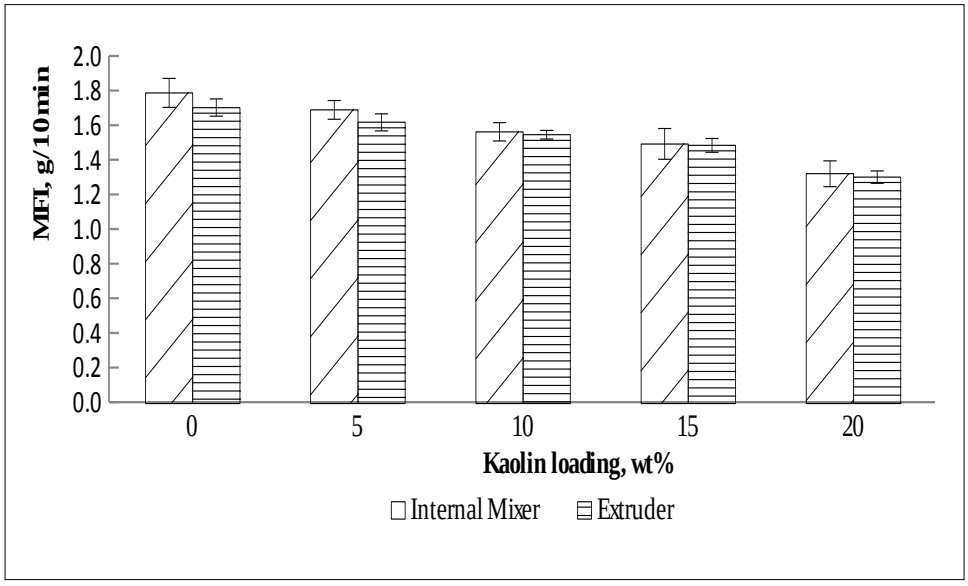



Figure 1. MFI values of PP/Kaolin composites

As inferred, PP/Kaolin composites exhibit non-Newtonian pseudo-plastic behavior (Figure 2). It could be said that kaolin does not interfere or cause any significant change in pseudo-plastic behaviour of PP/Kaolin composites from polypropylene control. As an un-interactive filler to polypropylene, the incorporation of kaolin only leaded the PP

composite suspension in relatively higher viscosity at all shear rates. Similar effect also can be found in titanium-oxide and nano-$CaCO_3$ [7-8]. Due to the polymer structure, polypropylene is considered as a kind of low intermolecular forces. Increase in shear rate confers and exalts chain mobility of polypropylene so that the polymer chains align along the stress direction. Directionally induced polypropylene chain exhibits low frictional force between the wall-melt interfaces causing increase in melt's velocity hence decrease in viscosity [2].

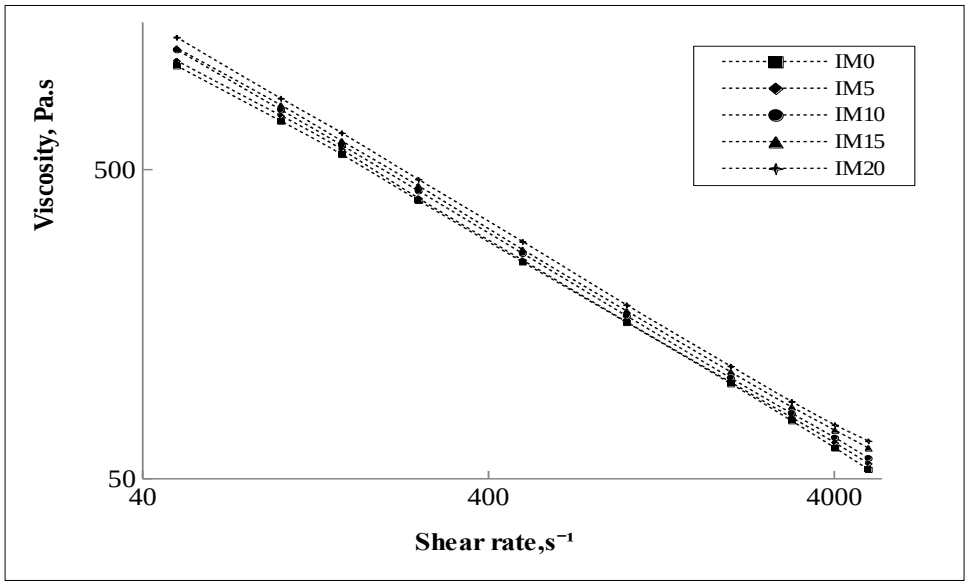



Figure 2. Viscosity against shear rate of PP/Kaolin composites compound via internal mixer

Similar effect of kaolin on PP/Kaolin composite's shear stress was observed. Figure 3 shows that higher shear stress obtained for polypropylene composite suspension with increase in kaolin weight percentage. Such factors as immobility of kaolin, shelf-attraction of kaolin molecular, low interaction between kaolin and polypropylene caused difficulties for polypropylene chain to carry and move along [3]. This particular difference turned to be more obviously with increase in shear rate due to higher mobility of polypropylene polymer chains.

In order to compare the effect of compounding process, rheological behaviour of polypropylene control and polypropylene composite with 15wt% kaolin from two process were plotted and showed in Figure 4 (representing viscosity) and Figure 5 (shear stress) respectively. Samples from internal mixer have lower viscosity compared to twin screw extruder, for both polypropylene control and its composite. In fact, polypropylene was compounded for 6 minutes in internal mixer, while about 1 minute in twin screw extruder at same temperature, hence, higher heat generation at internal mixer is expected. It could be inferred that thermal degradation occurred in internal mixer, which imparted chain scission of polypropylene chains [5]. Shorter polymer chain will had easier alignment and therefore if exhibited lower viscosity. Another possibility is the chain scission happened during sample preparation for capillary rheometer characterization. Samples from internal mixer were crushed and trimmed into small pieces compared to palletizing of twin screw extruder.

Differences of viscosity between IM0 and TSE0 became insignificant at high shear rate. It could be said the scission in internal mixer was quite minor and acceptance for PP control. Moreover, due to the uni-direction alignment of PP chain; the flow mechanism and flow-ability are almost alike causing by high speed of testing piston in capillary rheometer. On the other hand, presence of kaolin intensified the effect of processing and the difference was still present obviously on PP/Kaolin composite's viscosity even at high shear rate (zoom in part in Figure 4). The

possible explanation is kaolin was generated and amplified PP chain scission in internal mixer. Kaolin was added into melt polymer after 2 minutes. It required a higher torque to disperse the cool kaolin, hence inducing a high shear in melt suspension polypropylene in internal mixer chamber, which could accelerate the chain scission phenomenon (for 4 minutes after addition of kaolin). In contrast, kaolin and polypropylene were mixed in advanced, the rotation and conveyance of twin screw within 1 minute could minimize the chain scission. Therefore, TSE15 exhibited higher viscosity compared to IM15 for all share rates.

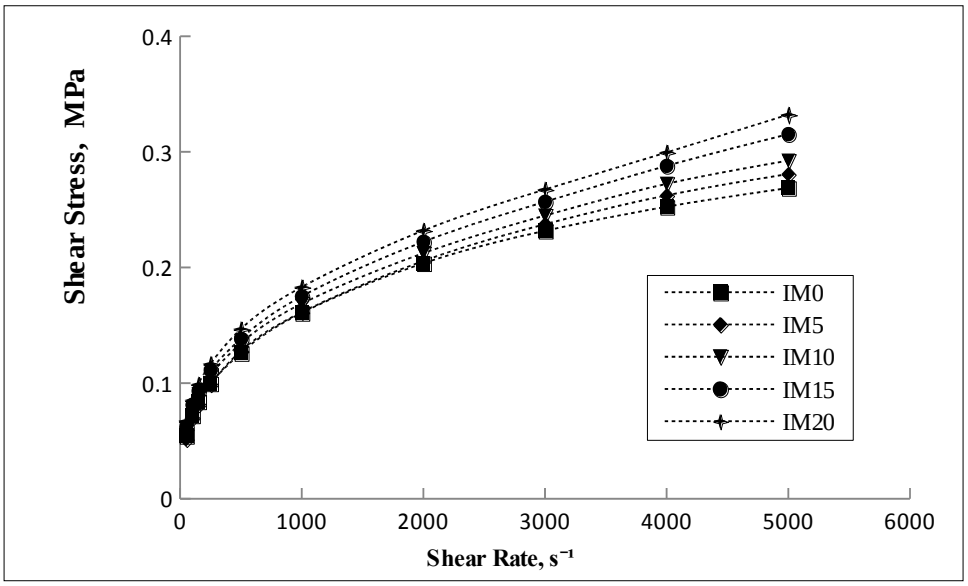



Figure 3. Shear stress against shear rate of PP/Kaolin composites compound via internal mixer

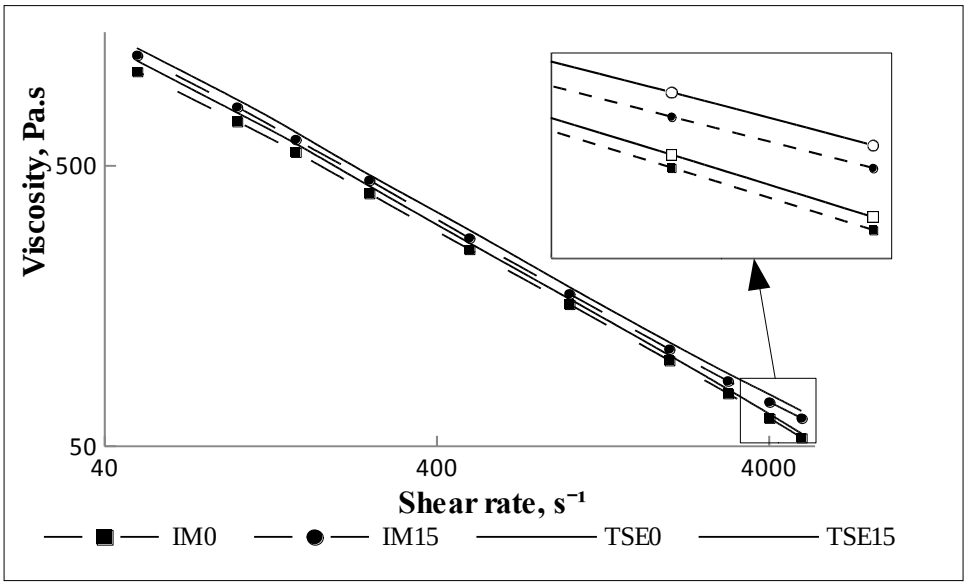



Figure 4. Effect of processing on PP/Kaolin composite's viscosity

Similar influence of compounding processes without and with kaolin was also reflected by shear stress as shown in Figure 5. Furthermore, the compounding effect was more detected on shear stress compare to viscosity, especially in high shear rate. These features are other evidences of chain scission taking place in internal mixture more than twin screw extruder. In additional, the results of capillary rheometer expressed more profound rheological behaviour compared to MFI results. It provided more details of the different effect of compounding PP/Kaolin composites using internal mixer and twin extruder.

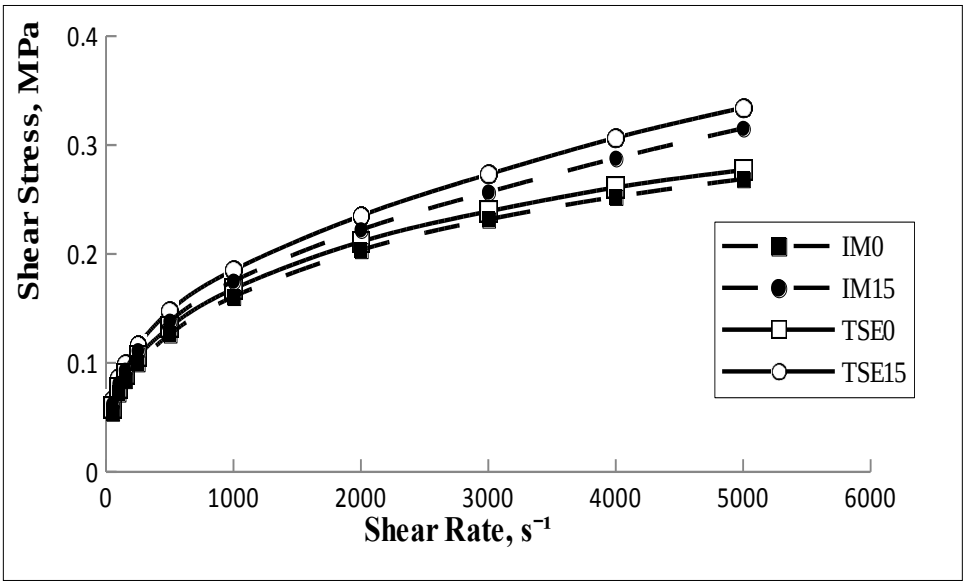



Figure 5. Effect of processing on PP/Kaolin composite's shear stress

**Melt transition of PP/Kaolin composites**

Table 2 reported the onset temperature, melting points and crystallinity percentage of PP/Kaolin composites. It was found that melt temperature of PP dropped 1.4 ± 0.6ºC with addition of kaolin, but kept similar values with higher kaolin loading. The influences of kaolin content and compounding processes were only more evident for the onset temperature – as the start of melting transition and crystallinity, which will be discussed later. The decrease in melting point of PP/Kaolin composites is a common trend. Liang and Li [9] reported the presence of inorganic phase within polymer matrix enhances heat transfer between intermolecular chains which also impart fasten melting of polymer [9]. Moreover, different crystallization leaded by kaolin filler resulted in defectiveness crystal, which caused the decrease in the enthalpy needed to melt the matrix [10].

Table 2. Onset temperature, Melting point, and Crystallinity of PP/Kaolin Composites

| Kaolin Loading, wt% | Onset temperature,°C | | Melting Point, °C | | Crystallinity, % | |
|---|---|---|---|---|---|---|
| | IM | TSE | IM | TSE | IM | TSE |
| 0 | 157.2 | 157.9 | 166.3 | 165.7 | 63.8 | 57.5 |
| 5 | 156.3 | 156.7 | 164.8 | 164.9 | 64.5 | 59.6 |
| 10 | 156.4 | 157.1 | 164.4 | 164.3 | 67.9 | 62.4 |
| 15 | 154.9 | 155.7 | 164.5 | 164.3 | 60.1 | 55.5 |
| 20 | 154.5 | 155.2 | 164.4 | 164.9 | 56.4 | 48.4 |

IM= Internal Mixer, TSE= Twin Screw Extruder

To comprehend the effect of kaolin and compounding processes on PP/Kaolin composite's melt transition, the onset temperature and crystallinity was plotted in Figure 6. The onset temperature showed a slight reduction with kaolin content as well as in internal mixer compared to twin screw extruder. These results were well agreement with rheological behaviour, and chain scission of PP into lower molecular weight due to kaolin and compounding processes were responsible for these [11].

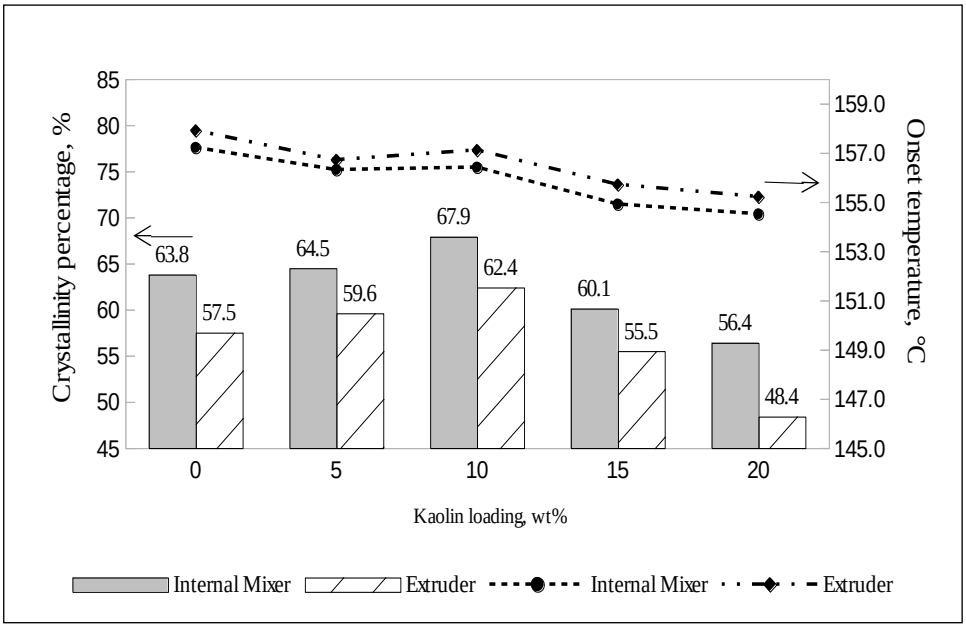



Figure 6. Crystallinity percentage and melt onset temperature of PP/Kaolin composites

Nucleating effect of kaolin on PP was only found at 5 wt% and 10 wt% of kaolin loading, in which kaolin particles act as nuclei within PP matrix during cooling, and initiate the crystallization. The nucleating effect of kaolin could be originated from its high thermal conductivity, which accelerated exothermal crystallization process. In contrast, higher kaolin loading induce excess nuclei and impeded with each other during crystal growth therefore causing lower crystallinity [12-13]. In addition, crystallinity is proportional to crystallization activation energy of the composites which was reported by Ariffin et al. [14]. By using Kissinger method, 10wt% kaolin loaded PP/Kaolin composite was found having the lowest crystallization activation energy, therefore it has highest crystallinity. In comparison, PP/Kaolin composites prepared by internal mixer possessed higher crystallinity than those prepared by twin screw extruder. The differences were around 3~7%. The most appreciable origination came from the distinct cooling processes. The cooling process of internal mixer was carried out in ambient while extrudates were cooling down in water bath for twin screw extruder process.

## Conclusion

Kaolin increased viscosity and shear stress of PP/Kaolin composite. This effect turned to be significant at high kaolin loading, and especially at high testing shear rate. For melting characteristic, the optimum kaolin content in polypropylene was 10% in weight, where kaolin could act as nucleating agent. The further addition of kaolin would reduce polymer's crystallinity. Besides, the addition of kaolin caused the composite's melting point decrease but maintain at higher kaolin loading. In comparison, twin screw extruder showed better compounding result compare to internal mixer. The drawbacks in internal mixer were claimed to chain scission of polypropylene, which became more obviously with the incorporation of kaolin.

**Acknowledgement**

This work is supported under Fundamental Research Grant Scheme (FRGS: 9003-00328) provided by the Higher Ministry of Education Malaysia.

**References**

1. Rahim, N. A., Ariff, Z., Ariffin, A., & Jikan, S.S. (2011) Study on effect of filler loading on the flow and swelling behaviors of polypropylene-kaolin composites using single-screw extruder. *Journal of Appllied Polymer Science 119*(1): 73-83.
2. Snabre, P., & Mills, P. (1999). Rheology of concentrated suspensions of viscoelastic particles. *Colloids and Surfaces A: Physicochemical and Engineering Aspects 152*(1): 79-88.
3. Ariff, Z., Ariffin, A., Jikan, S.S., and Rahim, N.A. (2012). Rheological Behaviour of Polypropylene Through Extrusion and Capillary Rheometry. In Dr. Fatih Dogan (Eds.), *Polypropylene.* InTech.
4. Pukánszky, B., Belina, K., Rockenbauer, A., & Maurer, F. (1994). Effect of nucleation, filler anisotropy and orientation on the properties of PP composites. *Composites 25*(3): 205-214.
5. Tochacek, J., & Jancar, J. (2012). Processing degradation index (PDI) – A quantitative measure of processing stability of polypropylene, *Polymer Testing 31*(8): 1115-1120.
6. Chen, H. L., & Hwang, J. C. (1995). Some comments on the degree of crystallinity defined by the enthalpy of melting, *Polymer 36*(22): 4355-4357.
7. Dangtungee, R., & Supaphol, P. (2008). Melt rheology and extrudate swell of titanium (IV) oxide nanoparticle-filled isotactic polypropylene: Effects of content and surface characteristics. *Polymer Testing 27*(8): 951-956.
8. Karamipour, S., Ebadi-Dehaghani, H., Ashouri, D., & Mousavian, S. (2011). Effect of nano-CaCO3 on rheological and dynamic mechanical properties of polypropylene: Experiments and models, *Polymer Testing 30*(1): 110-117.
9. Liang, J., & Li, F. (2007). Heat transfer in polymer composites filled with inorganic hollow micro-spheres: A theoretical model, *Polymer Testing 26*(8): 1025-1030.
10. Wunderlich, B. (1964). The melting of defect polymer crystals, *Polymer 5*: 611-624.
11. Guessoum, M., Nekkaa, S., Fenouillot-Rimlinger, F., & Haddaoui, N. (2012). Effects of Kaolin Surface Treatments on the Thermomechanical Properties and on the Degradation of Polypropylene. *International Journal of Polymer Science* (1): 1-9.
12. Holger S., Robert M. W., Curtis W. F. (2003). Nucleation and crystallization of low-crystallinity polypropylene followed in situ by hot stage atomic force microscopy. *Macromolecules* 36(7): 2412-2418.
13. Jikan, S.S., Ariff, Z.M., & Ariffin, A. (2010). Influnce of filler content and procesing parameter on the crystallization behaviour of PP/kaolin composites. *Journal of Thermal Analysis of Calorimetry* 102: 1011-1017
14. Ariffin, A., Ariff, Z. M., & Jikan, S.S. (2011). Evaluation on nonisothermal crystallization kinetics of polypropylene/kaolin composites by employing Dobreva and Kissinger methods. *Journal of Thermal Analysis of Calorimetry 103*(1):171-177.

The Malaysian Journal of ANALYTICAL SCIENCES ISSN 1394-2506

# MECHANICAL AND MORPHOLOGY PROPERTIES OF FEATHER FIBER COMPOSITE FOR DENTAL POST APPLICATION

## (Sifat- Sifat Mekanikal dan Morfologi Komposit Serat Bulu Untuk Aplikasi Pos Pergigian)

Siti Maizatul Farhain Salehuddin[1], Mat Uzir Wahit[2]*, Mohammed Rafiq Abdul Kadir[3], Eshamsul Sulaiman[4], Noor Hayaty Abu Kasim[4]

*[1]Department of Polymer Engineering, Faculty of Chemical Engineering,*
*[2]Center of Composite, Faculty of Mechanical Engineering,*
*[3]Medical Implant Technology Group, Faculty of Biosciences & Medical Engineering,*
*Universiti Teknologi Malaysia, 81310 UTM Skudai, Johor Bahru, Malaysia*
*[4]Department of Restorative Dentistry, Faculty of Dentistry Building,*
*Universiti Malaya, Kuala Lumpur, Malaysia*

**Corresponding author: mat.uzir@cheme.utm.my*

**Abstract**

Feather/plastic composite material was fabricated from polymethyl methacrylate (PMMA), feather fiber (FF) and montmorillonite (MMT) using brabender internal mixer. PMMA based composites were produced with 1, 3, 5, 7 and 10 phr composite of mass feather fiber with and without 4 % of montmorillonite (MMT). Alkali treatment was used to improve the interfacial adhesion among the feather fiber (FF) and the PMMA. Flexural properties of FF/PMMA and FF/PMMA/MMT composites were investigated. Composites were analyzed by Scanning Electron (SEM) and Fourier Transform Infra Red (FTIR) spectroscopy techniques. The result showed that, the addition of FF significantly increased the flexural strength of the composites. The hydrophobic nature of feather fiber displayed an excellent compatibility among fibers and PMMA matrix.

**Keywords:** PMMA, Feather Fiber, alkali treatment

**Abstrak**

Dalam kajian ini, bulu / bahan komposit plastik telah diperbuat daripada polimetil metakrilat (PMMA), serat bulu (FF) montmorilonit (MMT) menggunakan brabender percampuran dalaman. PMMA komposit dihasilkan berasaskan dengan 1, 3, 5, 7 dan 10 phr komposit berat serat bulu dengan dan tanpa 4% daripada MMT. Kaedah rawatan alkali telah digunakan untuk meningkatkan lekatan antara muka antara serat bulu dan PMMA. Sifat mekanik FF/PMMA dan FF /PMMA/ MMT komposit kekuatan lenturan itu telah disiasat. Spesimen yang diperolehi dianalisis dengan mikroskop imbasan elektron (SEM) dan teknik spektroskopi FTIR. Keputusan menunjukkan bahawa penambahan FF meningkatkan kekuatan lenturan bahan komposit ini. Sifat hidrofobik serat menunjukkan satu keserasian yang baik antara gentian dan matrik PMMA.

**Kata kunci**: PMMA, serat bulu, rawatan alkali

## Introduction

An endodontically treated tooth often requires an endodontic post as an additional retention element for buildup with crown restoration. Dental post which will act as an anchor for the placement of crown is used to reinforce the remaining tooth structure when the amount of coronal tooth structure remaining is small. The current existing posts which are metal based post and zirconia based posts have drawbacks. Metal post has high rigidity and corrosive while ceramic post made from zirconium oxide has risk in the occurrence stress peaks. Thus, fiber reinforced composite (FRC) posts have recently become the center of interest for dentists and scientist. The reason this occurs is because the dentin-like modulus of elasticity of the FRC post allows better distribution of forces along the length of the root.

The goose feather is made up of keratin which contains ordered α-helix or β-sheet structure and some disordered structure and approximately 91 % protein (acid amino), 1 % lipids and 8 % water [1]. Feather is a special protein. It has a high content of cysteine, which may vary between 2 to 18 wt % in the acid amino sequence and cystine has –SH groups cause the sulfur-sulfur (disulfide) chemical bonds which link adjacent keratin protein network as shown in Figure 1. These strong covalent bonds stabilized the three-dimensional protein structure and are very difficult to break [2].

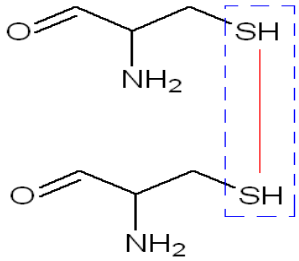



Figure 1. Two cysteines connect to each other by disulfide bonds [2].

The use of feather fiber as reinforcement materials for polymer matrix has drawn considerable interest from the engineering industry in recent years. A few studies have investigated feather fibers for biocomposite material applications, and it was found that materials which derived from feathers can be used advantageously as reinforcing materials in polymer matrix composites [3]. This is due to the considerations of developing an environmental friendly material and partly replacing currently used glass or carbon fibers in fiber reinforced composites. Some of the advantages of the FF are high specific strength and modulus materials, low priced and recyclable [4]. FF inclusion in a composite would potentially lower the overall density, compared with the density in a composite of synthetic reinforcement.

Nondegradable polymers as polymethyl methacrylate (PMMA) were widely used in various biomedical applications from the beginning of biometric development and have been an essential material in medicine and dentistry [5]. The popularity of PMMA is associated with its favorable working characteristics, processing ease, accurate fit, stability in the oral environment, superior esthetics, and the ability to be used with inexpensive equipment [6]. In this study, an exploration will be made on the use of feather fiber (FF) filled polymethyl methacrylate (PMMA) composite in the development of bio composite dental posts.

## Materials and Methods

### Materials

Commercial Goose Feather Fiber (FF) was purchased from the Shuttlecock (Malaysia). Polymethyl methacrylate (PMMA) pellets were supplied by Chi Mei Corporation (Taiwan) and trade name is PMMA Acryrex CM-205. MMT was obtained from Nanocor Inc., Arlington Heights, IL, USA (Nanomer 1.30 P) organically modified with octadecylamine with mean dry particle size of 16 – 22 µm. PMMA/FF based composites were produced in range 1 to 10 phr of FF fiber loading with and without 4 wt % of MMT.

### Alkali Treatment Method

The feathers were cleaned using a constant pH of water, then treated by immersion in a 0.5 M sodium hydroxide (NaOH) aqueous solution for two hours at 25 ºC followed by washing with distilled water. The feathers were then, dried in a vacuum oven at 60 ˚C for 12 hours. The treated feather was crushed using a laboratory mixer, National Blender MX-491N. Only particles that pass through a sieve of mesh 20 (841 µm) were used in this study.

### Fabrication of Composites

The mixing of each composite was prepared via Brabender plastograph EC (C. Melchers GmbH & Co Malaysia) set at a temperature of 180 °C which is an intermediary temperature between matrix and fiber and the mixing speed of

50 rpm is used to homogenize the composition. The mixing time for each composite formulation is 10 minutes for PMMA to melt. The hot melt composites were allowed to cool at room temperature. Each of the composites was compressed via Motor Hydrolic Lab Press (Gutrie Malaysia) to produce the composites in film form. The hot press machine was set at 180 ˚C for both top and bottom platens. The composites were put into the mold, preheated partially for 8 minutes, followed by full compression for 4 minutes at the same temperature and subsequently cooled under pressure for 4 minutes. This results in film approximately 1 mm and 2 mm in size. The composite in film form was used to prepare test specimens for testing analysis according to standard.

**Characterization: Flexural Testing**

The three point bending flexural test was performed on a Tensile Tester EZ 20 kN Lloyd at a crosshead speed of 1 mm $min^{-1}$ and span length of 40 mm under an ambient condition according to ISO 14125: 1998 specifications.

**Morphological Analysis**

The morphology of the SEM fractured surface of composites was observed by a scanning electron microscope (JEOL JSM-6390LV). The sample was mounted on an aluminium stub and sputtered coating with thin layers of gold about 12 µm thickness by using a JEOL JFC-1600 Auto-Fine coater in order to prevent any electrical discharge during testing.

**Characterization Analysis**

The nature of bonding of the fiber was characterized using a Perkin Elmer spectrum 2000 Fourier Transform Infrared spectroscopy (FTIR) at a spectral resolution of 4 $cm^{-1}$ over the spectral range of 4000-650 $cm^{-1}$.

## Results and Discussion

**Flexural Properties**

Figure 2 and Figure 3 shows the flexural strength and modulus of FF/PMMA composites with and without MMT. Both types of composite showed increase in flexural strength and modulus with addition of FF. The flexural strength of the FF/PMMA/MMT composites is greater than FF/PMMA composites. The flexural strength values of FF/PMMA composites increased slowly from 57.08 MPa to 72.31 MPa while the flexural strength values of FF/PMMA/MMT composites increased linearly from 58.53 MPa to 78.82 MPa as shown in Figure 2. From Figure 3, it can be seen that flexural modulus also showed a similar trend as flexural strength, where increasing FF contents will increase the flexural modulus of the composites.

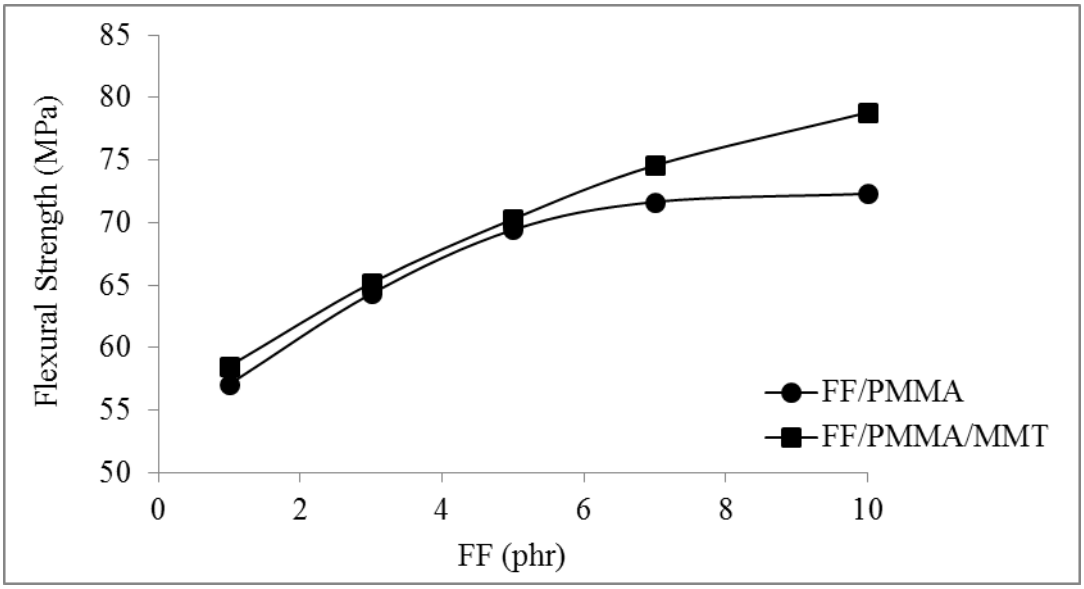



Figure 2. Flexural Strength of FF/PMMA and FF/PMMA/MMT composites.

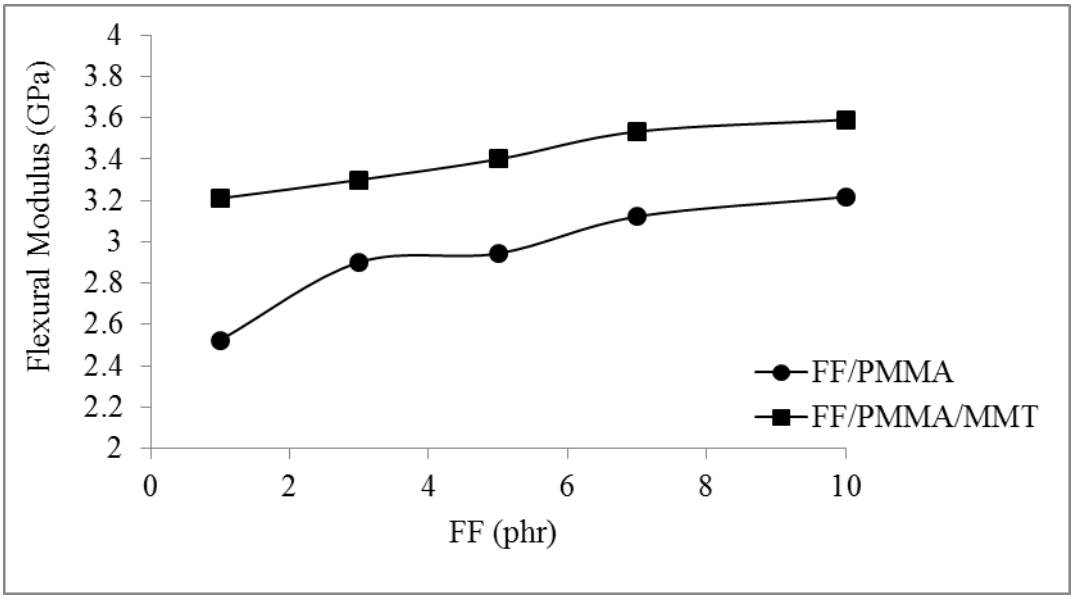



Figure 3. Flexural Modulus of FF/PMMA and FF/PMMA/MMT composites.

Overall, it was observed that the flexural strength and flexural modulus of the composite improved with increasing FF contents into the FF/PMMA and FF/PMMA/MMT composites. The significant improvement in strength of the composites is possibly due to the role of NaOH treatment played as fiber surface modifier as shown in Figure 4 which enhance the bonding between the FF surface and PMMA matrix. The fiber is expected to act as a bridge to prolong the fracture process of composites. The presence of FF also restricts the mobility and deformability of the matrix, thus increased the modulus of FF/PMMA and FF/PMMA/MMT composites. Ramaniah et al. studied the effect of fiber loading on the mechanical properties of Borassus seed shoot fiber reinforced polyester composite [7]. They reported that by increasing the fiber content in the polyester matrix, the tensile strength and flexural properties also increased. They attributed this to the fact that the polyester resin transmitted and distributed the applied stress to Borassus fiber resulting in higher strength.

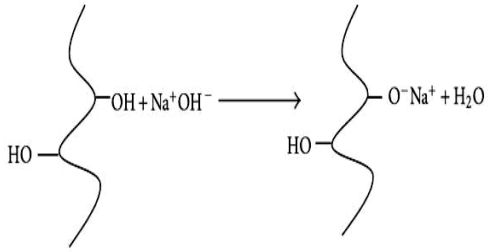



Figure 4. Alkali Treatment Reaction of Fiber with NaOH.

Besides, the incorporation of MMT led to substantial improvement in strength and exhibited the desirable reinforcement effect in modulus. This is probably due to the nanoscale structure, large aspect ratio and the corresponding strong interaction between polymer molecule chains and silicate surface. The formation of supramolecular assemblies obtained by the presence of dispersed anisotropic laminated nanoparticles.

**Fourier Transform Infra Red Spectroscopy (FTIR) Analysis**

The FTIR spectra of feather fiber (FF) and the FTIR spectra of FF/PMMA-10 and FF/PMMA/MMT-10 are shown in Figure 5 and Figure 6 respectively. Examining the three spectra in Figure 5 and Figure 6, a number of change can be distinguishable peaks.

Figure 5 shows infrared spectroscopy spectrum of the FF. The peak at 3280.63 $cm^{-1}$ was due to N–H (amine) group from an amino acid from FF. The peak at 2923.89 $cm^{-1}$ shows the C–H stretch. The characteristic peak of nitrile C–N stretch at 2360.26 $cm^{-1}$ and the peak at 1647.36 $cm^{-1}$ shows the C=C stretch. The peak at 1537.46 $cm^{-1}$ shows the C=C bending. On the other hand, the peak at 1235.37 $cm^{-1}$ related to C-O (carboxylic acid) originating mainly from amino acid of the feather fiber. Mishra et al. studied bio-waste reinforced epoxy composites [8] and found that, when the feather was treated with an alkali solution before mixing with resin, the chemical reaction between the matrix and reinforcement takes place which give rise to the formation of ester and amine.

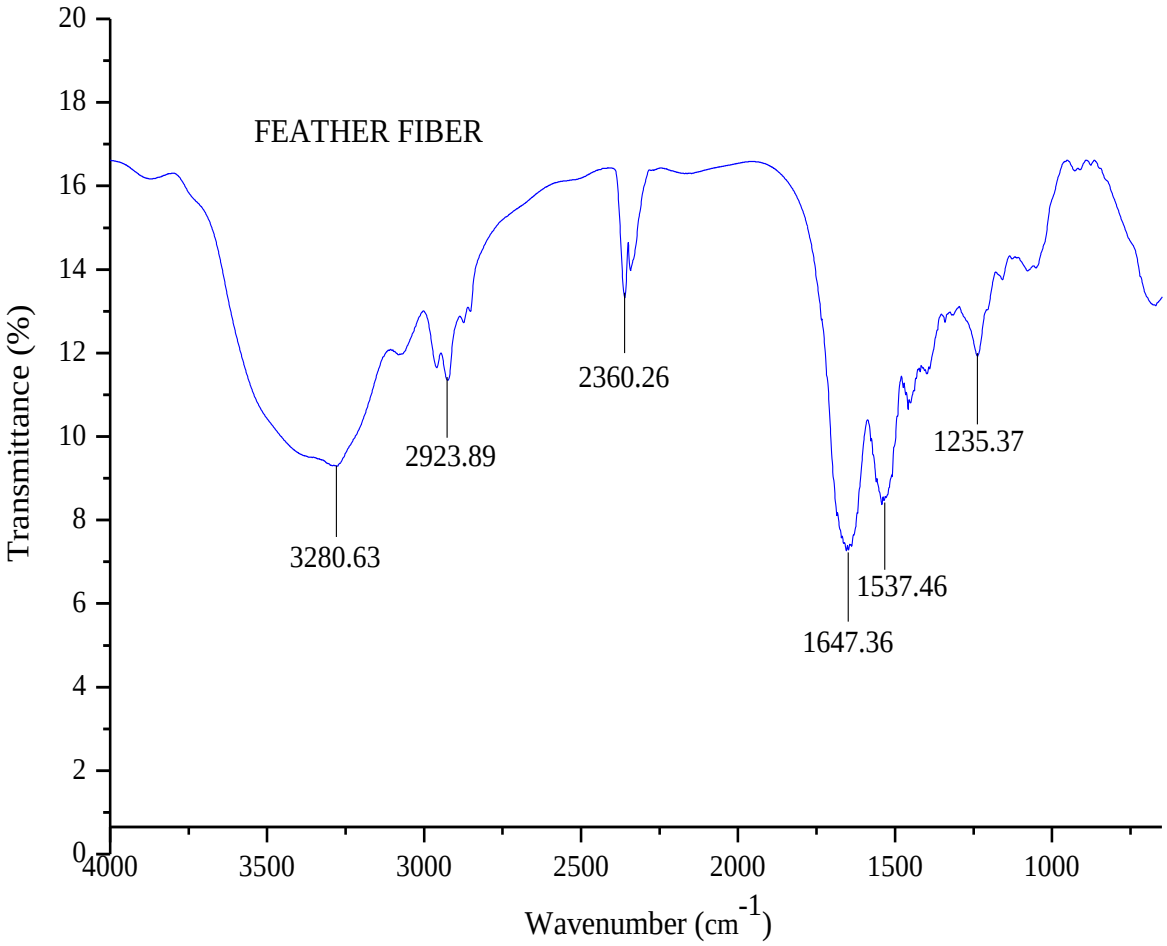



Figure 5. FTIR spectrograph of the feather fiber (FF).

Figure 6 shows the FTIR spectra of FF/PMMA-10 and FF/PMMA/MMT-10 composites with fiber loading of 10 phr. Both spectra show similar characteristic peak patterns indicate OH groups from water of the feather fiber, sodium hydroxide solution and MMT at a frequency around 2947.55 $cm^{-1}$. The characteristic peaks of a C=O stretch are at 1724.06 $cm^{-1}$ and have been observed in both spectrums of FF/PMMA-10 and FF/PMMA/MMT-10 composites. The peaks which appeared around 1434.89 $cm^{-1}$ region in both spectra show C–H bending formation occurs. The peak at 1238.55 $cm^{-1}$ related to C-O (carboxylic acid) originating mainly from amino acid of the feather fiber respectively. The peak at 1142.49 $cm^{-1}$ indicated that nitrile C–N stretch in both composites. A previous study by Madejova (2003) revealed that the band appeared near 3620 $cm^{-1}$ is due to the stretching vibrations of structural O-H groups and a broad band near 3440 $cm^{-1}$ on the other hand is due to the O-H stretching vibrations of $H_2O$ present in the clay [9].

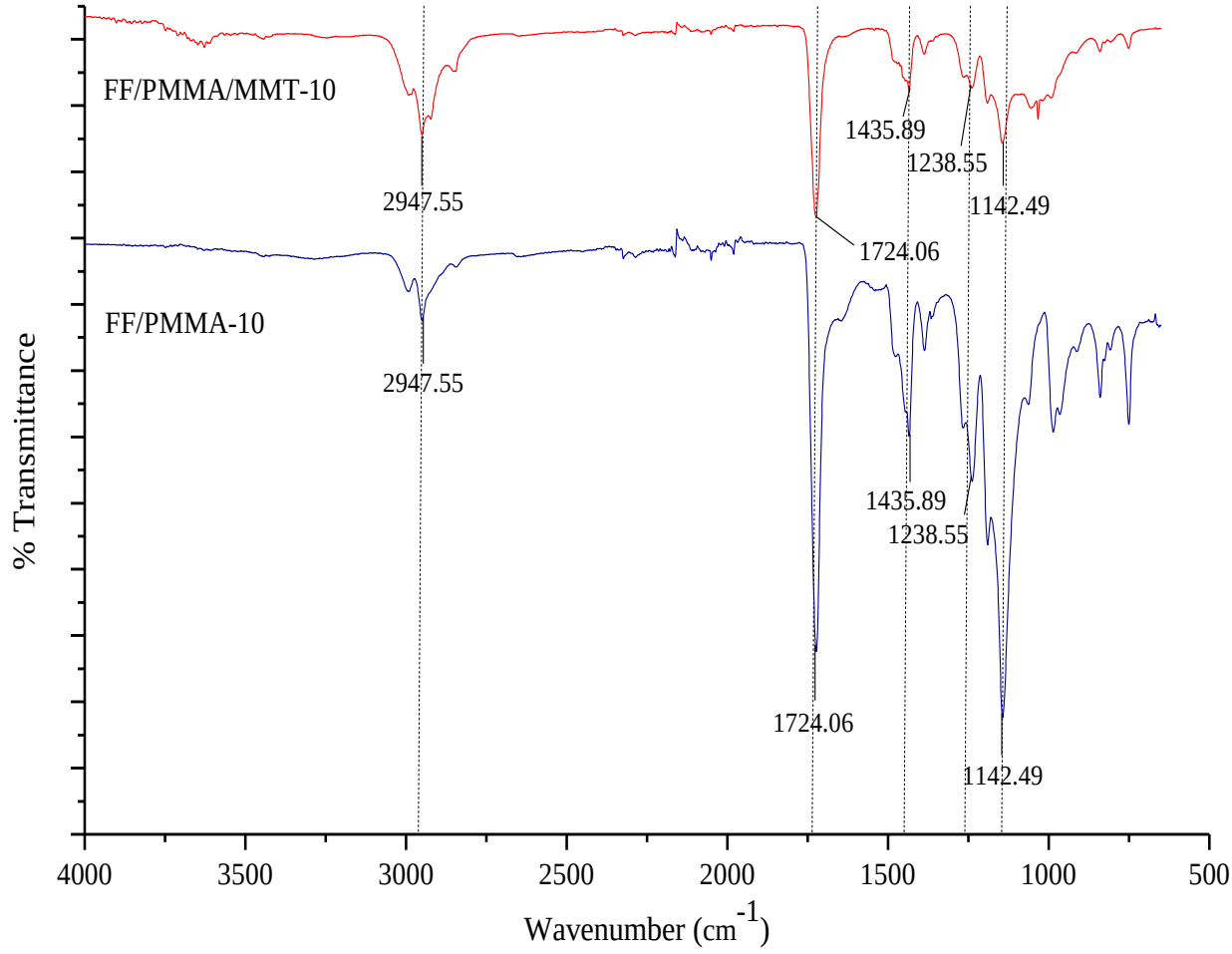



Figure 6. FTIR spectrograph of FF/PMMA-10 and FF/PMMA/MMT-10 composites.

**Scanning Electron Microscopy (SEM) Analysis**

Morphological information of a composite after a mechanically induced break of composite with different composition was studied using SEM micrographs. Feather fiber (FF) and Polymethyl methacrylate (PMMA) are two kinds of materials with different physical properties and microstructures. The micrographs of fractured surfaces of FF containing 1, 5 and 10 phr FF composition are shown in Figure 7 (a - c) respectively. It can be observed that

the FF distribution is uniform throughout the PMMA matrix. Better dispersion of FF results in strength enhancements, which allow stress to be fairly distributed. The FF particles were found embedded in a PMMA matrix with possibly through a certain degree of mechanical bonding between two phases and it is believed that only mechanical bonding exists between the FF and PMMA matrix. The presence of void on the matrix surface is believed as a result from deboned FF fiber and was bended during mechanical testing.

The keratin feather fiber should be compatible with hydrophobic polymers to some degree [10]. The amino acid sequence of feather keratin shows that the protein has 40 % hydrophilic and 60 % hydrophobic groups [11]. Castano et al. found that the FF keratin biofibers allows an even distribution within and adherence to polymers due to their hydrophobic nature [12]. Martínez-Hernández et al. studied the mechanical properties evaluation of new composites with protein biofibers reinforcing poly (methyl methacrylate)[13]. They reported the possibility of observing the keratin fiber-PMMA composites because of the good compatibility between these materials.

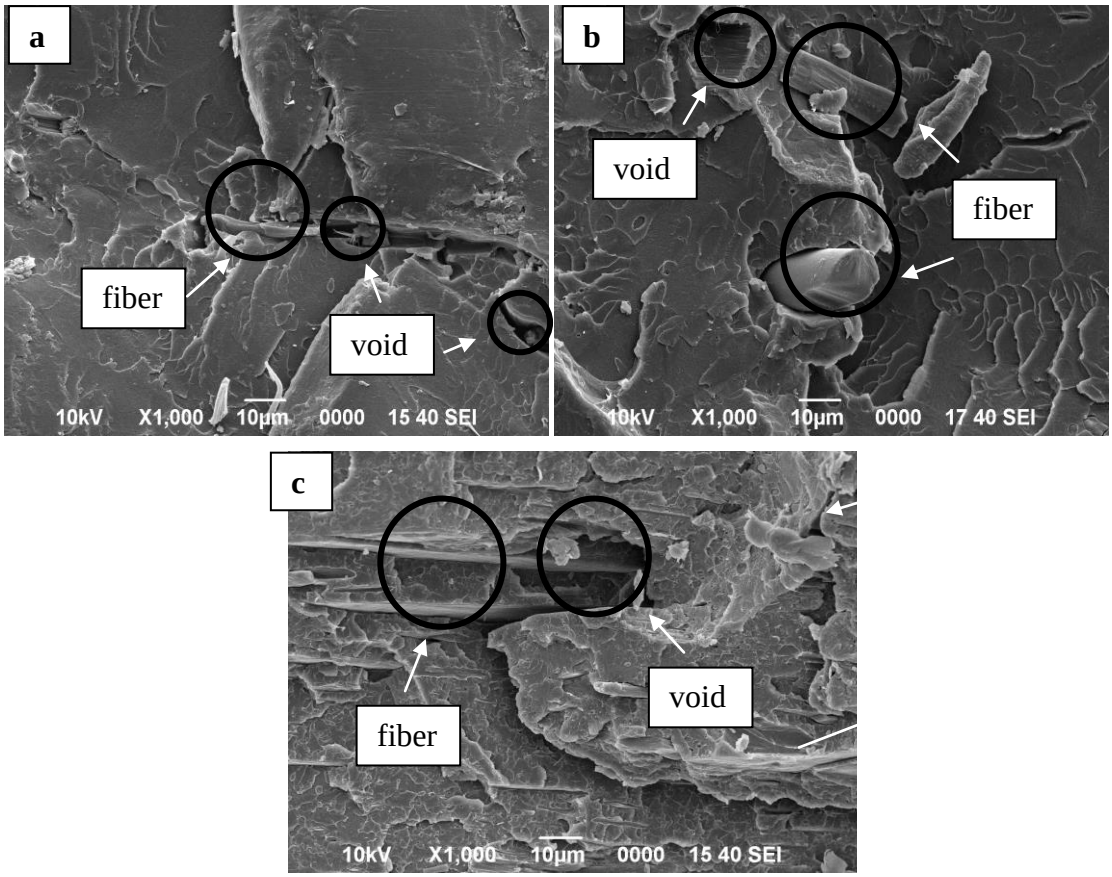



Figure 7. Morphology SEM micrographs fractured surfaces of FF containing 1, 5, and 10 phr composition. (a) FF/PMMA-1 (b) FF/PMMA-5 and (c) FF/PMMA-10 composites at 1000 X magnification.

## Conclusion

The effect of FF loadings on the morphological and mechanical properties of FF/PMMA and FF/PMMA/MMT composites on were studied. The improvement in strength indicated an improvement in mechanical bonding between FF and PMMA matrix due to the homogenous distribution of FF in the polymer matrix. Incorporation of FF restricting the mobility and deformability of the matrix, thus increased the modulus. A substantial improvement

observed in strength and modulus of FF/PMMA/MMT composites with the inclusion of MMT. SEM results revealed that only mechanical bonding between exist between FF and PMMA. The morphological characterization composites showed a relatively uniform distribution of the fiber in the polymer matrix.

**Acknowledgement**

This project was supported financially by the Ministry of Science, Technology & Innovation Malaysia, and the Ministry of Higher Education Malaysia (Vote No: 4L021). We would like to express our gratitude and deepest thanks to the Research Management Centre, Universiti Teknologi Malaysia (UTM), for managing the project.

**References**

1. Kock J. W. (2006). *Physical and Mechanical Properties of Chicken Feather Materials.* Master School of Civil and Environmental Engineering, Georgia Institute of Technology.
2. Alberts, B., Bray, D., Lewis, J., Raff, M., Robert, K., & Watson, J. D. (1994). Molecular Biology of the Cell. 3 rd edition. Garland Press. New York.
3. Jeffrey, W. K. (2006). Physical and Mechanical Properties of Chicken Feather Material. Master of Science. Georgia Institute of Technology.
4. Ananda R.V., Alok, S., & Mirsha, S. C. (2007). Polymer Composites Reinforced with Short Fibers Obtained from Poultry Feathers. Proceedings of International and INCCOM-6 Conference.
5. Unemori, M., Matsuya, Y., Matsuya, S., Akashi, A., & Akamine, A. (2003). Water Absorption of Poly(methyl methacrylate) Containing 4-methacryloxyethyl Trimellitic Anhydride. *Biomaterials.* 24(8): 1381-1387.
6. Nidal, W. E. (2006). Mechanical and Enviroment Properties of Denture Base Poly(methylmethacrylate) Filled by Brium Titanate. Master of Science. Universiti Sains Malaysia (USM).
7. Ramanaiah. K, Ratna Prasad. A. V., & Hema Chandra Reddy, K. (2012). Effect of Fiber Loading on Mechanical Properties of Borassus Seed Shoot Fiber Reinforced Polyester Composites. *Journal of Material Environment Science.* 3(3): 374-378.
8. Mishra, S. C., Nayak, N. B., & Satapathy, A. (2010). Investigation on Bio-waste Reinforced Epoxy Composites. *Journal of Reinforced Plastics and Composites.* 29(19): 3016-3020.
9. Madejova, J. (2003). FTIR Techniques in clay Mineral studies. *Vibrational Spectroscopy* 31: 1-10.
10. Barone, J. R., & Schmidt, W. F. (2005). Polyethylene Reinforced with Keratin Fibers Obtained from Chicken Feathers. *Composites Science and Technology.* 65(2): 173-181.
11. Murayama-Arai K., Takahashi R., Yokote Y., Akahane K. (1983). Amino acid sequence of feather keratin from fowl. *European Journal of Biochemistry.* 132: 501 - 507.
12. Castano V.M., Martinez-Harnandez A. L., Velasco-Santos C., & De-Icaza M. (2007). Dynamical- mechanical and thermal analysis of polymeric composites reinforced with keratin biofibers from chicken feathers, *Composites B.* 38(3): 405-410.
13. Martínez-Hernández, A. L., Velasco-Santos, C., Icaza, M. d., & Castaño, V. M. (2005). Mechanical Properties Evaluation of New Composites with Protein Biofibers Reinforcing Poly(methyl methacrylate). *Polymer.* 46(19): 8233-8238.

The Malaysian Journal of ANALYTICAL SCIENCES ISSN 1394-2506

# CARBOXYMETHYL CELLULOSE FROM KENAF REINFORCED COMPOSITE POLYMER ELECTROLYTES BASED 49% POLY(METHYL METHACRYLATE)-GRAFTED NATURAL RUBBER

## (Komposit Polimer Elektrolit Berasaskan 49% Poli(metil metakrilat)-cangkukan Getah Asli Diperkuat Karboksimetil Selulosa Daripada Kenaf)

Serawati Jafirin[1], Ishak Ahmad[1,2]*, Azizan Ahmad[1,2]

[1]*School of Chemical Sciences and Food Technology,*
[2]*Polymer Research Centre (PORCE),*
*Faculty of Science and Technology*
*Universiti Kebangsaan Malaysia, 43600, Bangi, Selangor Darul Ehsan, Malaysia*

**Corresponding author: gading@ukm.edu.my*

**Abstract**

Composite polymer electrolytes based 49% poly(methyl methacrylate)-grafted natural rubber (MG49) incorporating lithium triflate ($LiCF_3SO_3$) were prepared. The study mainly focuses on the ionic conductivity performances and mechanical properties. Prior to that, carboxymethyl cellulose was synthesized from kenaf fiber. The films were characterized by electrochemical impedance (EIS) spectroscopy, linear sweep voltammetry (LSV), universal testing machine and scanning electron microscopy (SEM). The conductivity was found to increase with carboxymethyl cellulose loading. The highest conductivity value achieved was $6.5 \times 10^{-6}$ $Scm^{-1}$ upon addition of 6 wt% carboxymethyl cellulose. LSV graph shows the stability of this film was extended to 2.7 V at room temperature. The composition with 6 wt% carboxymethyl cellulose composition showed the highest tensile strength value of 7.9 MPa and 273 MPa of Young's modulus. The morphology of the electrolytes showed a smooth surface of films after addition of salt and filler indicating amorphous phase in electrolytes system. Excellent mechanical properties and good ionic conductivity are obtained, enlightening that the film is suitable for future applications as thin solid polymer electrolytes in lithium batteries.

**Keywords**: carboxymethyl cellulose, ionic conductivity, mechanical properties, polymer electrolytes

**Abstrak**

Komposit polimer elekrolit berasaskan 49% poli(metil metakrilat)-cangkukan getah asli (MG49) dengan penambahan garam triflat ($LiCF_3SO_3$) telah disediakan. Kajian ini lebih menumpukan kepada ciri-ciri kekonduksian ion dan kekuaan sifat mekanik sistem elektolit yang dihasilkan. Sebelum itu, karboksimetil selulosa daripada kenaf disediakan terlebih dahulu. Filem yang dihasilkan dicirikan menggunakan spekroskopi impedans (EIS), voltametri sapuan linear (LSV), mesin pengujian universal dan mikroskopi imbasan elektron (SEM). Nilai kekonduksian ion didapati meningkat dengan penambahan karboksimetil selulosa. Kekonduksian ion tertinggi diperolehi dengan nilai $6 \times 10^{-6}$ $Scm^{-1}$ pada penambahan 6 bt% karboksimetil selulosa. Graf LSV menunjukkan kestabilan filem yang dihasilkan mencapai sehingga 2.7 V pada suhu bilik. 6 bt.% karboksimetil selulosa menunjukkan 7.9 MPa kekuatan regangan dan 273 MPa modulus young. Morpologi permukaan elektrolit mempamerkan permukaan lebih licin selepas penambahan garam dan pengisi yang menunjukkan kawasan amorfus pada sistem elektrolit. Kekuatan regangan dan kekonduksian ion memberansangkan yang diperolehi menunjukkan filem yang dihasilkan sesuai digunakan sebagai filem pepejal elektrolit polimer dalam bateri litium.

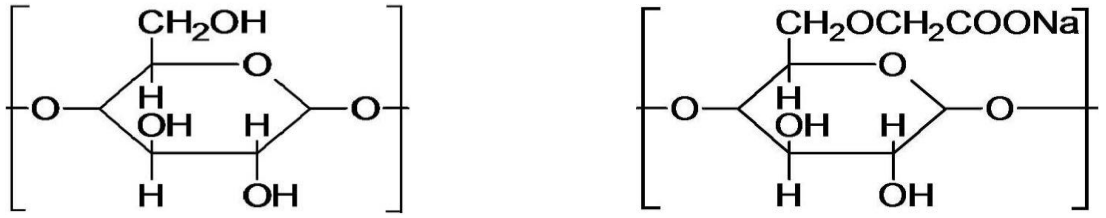
**Kata kunci:** karboksimetil selulosa, kekonduksian ion, sifat mekanik, polimer elektrolit

## Introduction

Nowadays, composite polymer electrolytes have attracted much attention due to potential applications in electrochemical devices especially in lithium batteries. Polymer electrolytes have the potential to be used as rechargeable batteries, fuel cells, and light-emitting fuels, and in many other applications in electrochemistry [1].

Many studies have focused on the enhancement of ionic conductivity at ambient temperature, excellent mechanical properties, and stable performances of polymer electrolytes since various finding about practical applications as electrolytes in high energy density, thin, and lightweight secondary Li-ion batteries [2].

Moreover, the need of low cost, ecologically friendly, and safe becomes fundamental for the sustainable mass production of the next generation energy storage systems. The introduction of carboxymethyl cellulose from kenaf in polymer electrolytes as an alternative to traditional glass fibres such as $Al_2O_3$ and $TiO_2$ in commercial composite materials has drawn much attention [3]. The impressive mechanical properties and reinforcing capability, abundance, low weight, and biodegradability of cellulose make them ideal candidates for the processing of polymer composites [2]. Futhermore, the preparation process is easy, low cost and does not involve chemical reactions. Various sources of cellulose such as cavendish banana pseudo stem [4], chitosan [5], sago starch [6], etc have been used to synthesize carboxymethyl cellulose by different method depend on its application.




a) b)

Figure 1. Structure of a) cellulose and b) carboxymethyl cellulose

In this work, polymer electrolyte from 49% poly(methyl methacrylate)-grafted natural rubber and cellulose or cellulose derivative which is carboxymethyl cellulose was chosen due to the naturally occurring polysaccharide and the most abundant organic sub- stance on the earth. Carboxymethyl cellulose was synthesized from extracted cellulose and using as fillers in polymer electrolytes system. The incorporation of carboxymethyl cellulose as filler in MG49 composite polymer doped with lithium triflate was prepared via solution casting. Polymer electrolytes films were characterized by using electrochemical impedances spectroscopy (EIS) and electrochemical stability window (ESW) by linear sweep voltametry (LSV). The evaluation of the mechanical performances of the films was obtained via tensile strength and Young's modulus.

## Materials and Methods

### Materials

Kenaf fibres were supplied by Kenaf Fibres Industry Sdn. Bhd. (Malaysia). Chemical used during this study were sulphuric acid (98%), sodium chlorite, sodium hydroxide (99%) and acetic acid glacial 99.5%, isopropanol, ethanol, methanol, sodium chloroacetate (SCA) were purchased from SYSTERM-chemAR (Malaysia) and Sigma-Aldrich (Germany). Tetrahydrofuran (THF) was purchased from JT Baker. MG49 rubber was commercially obtained from Green HPSP (M) Sdn. Bhd. Lithium triflate ($LiCF_3SO_3$) salt was supplied by Fluka. All chemicals were used without further purification.

### Synthesis of Carboxymethyl Cellulose

Prior to that, cellulose powder from kenaf was extracted according to [7]. Preparation of cellulose consisting two steps, alkali treatment and bleaching process. The carboxymethylation reaction consist two steps, alkalization and etherification of cellulose under heterogeneous condition [8]. For alkalization, 5% cellulose was suspended in isopropyl alcohol, and 20% NaOH was added to the mixture under mechanical stirring at room temperature for 1 hour to yield alkali cellulose. Etherification reaction was continued by the addition of SCA to the mixture for 30 min. It was left to stir and heated up to reaction temperature of 50°C for 4 hours. The mixture was terminated by adding alcohol. Carboxymethyl cellulose was then recovered by filtration and washed three times with methanol. Finally, the product was dried at 50°C in cabinet drier.

**Preparation of Film**

Composite polymer electrolytes were prepared by dissolving MG49 in conical flasks containing THF for 24 hours. The solution was then stirred with efficient magnetic stirring for the next 24 hours until complete dissolution of MG49. Salt solution with 25% $LiCF_3SO_3$ salt was stirred in THF solution and added to the MG49 solutions for the next 24 hours with continuous stirring. THF suspension of carboyxmethyl cellulose was added to the MG49/salt in conical flask with continuous stirring for 24 hours to obtain a homogeneous solution. The electrolyte solutions were cast onto a glass petri dish and the solvent was allowed to slowly evaporate at room temperature for 24 hours. Resulting films were dried under vacuum oven for 24 hours at 40$^{o}$C to remove remaining solvents. The films were then kept in desiccators for further use.

**Sample Characterization**

Ac impedance measurement was carried out using a high frequency resonance analyzer (HFRA): Solartron model 1260 with applied frequencies from 1 MHz to 0.1 Hz at a perturbation voltage of 1000 mV. The samples were placed between two stainless-steel blocking electrodes. The bulk impedance ($R_b$) value was obtained from the plot of negative imaginary impedance ($Zi$) versus real part ($Zr$) of impedance. The conductivity of electrolytes was calculated from the equation 1,

$$\sigma = \frac{l}{R_b A} \tag{1}$$

where; $A$ = Area of film-electrode contact and $l$ = thickness of the film (in cm) [1]. Electrochemical stability window also carried out to complete the electrochemical testing. It was evaluated by linear sweep voltametry. Mechanical performance of the films was evaluated tensile strength and Young's modulus with universal testing machine (Instron model 5566, USA) at room temperature according to ASTM D882. A crosshead speed of 50 mm/min, initial grip distance of 40 mm and load cell of 50 N were used to perform this test. The samples were cut into a dumbbell shape and average value of 5 replicates for each sample was taken. Morphological characterization of the samples was performed by Zeiss Supra 55VP scanning electron microscope (SEM).

## Results and Discussion

**Ionic Conductivity Study**

Table 1 shows the variation of conductivity values of polymer electrolytes at room temperature. The conductivity of the carboxymethyl cellulose polymer electrolytes systems at room temperature is illustrated in Fig. 2. The conductivity of polymer electrolytes is expected to increase after addition of carboxymethyl cellulose. This is due to the modification of cellulose will enhance the amorphous phase of systems. Thus, polymeric chains in the amorphous phase become more flexible which results in the enhancement of segmental motion of the polymer [5].

It can be seen in Fig. 2 that ionic conductivity increases with the amount of carboxymethyl cellulose up to a maximum of $6.5 \times 10^{-6}$ $Scm^{-1}$ for the sample containing 6 wt% of carboxymethyl cellulose. The increase in ionic conductivity is strongly ascribed to the effective interaction between oxygen atoms and lithium ions in the electrolytes [1]. Mobarak et al. [5] reported that the amount of oxygen was increase after modification of cellulose with sodium chloroacetate. By increasing the amount of oxygen, the conductivity value of samples also will increase accordingly. The ionic conductivity value is comparable with the previous studies that using synthetic filler. Low et al. [9] produced nanocomposite polymer electrolyte with the titanium dioxide ($TiO_2$) as inert ceramic filler and the highest conductivity achieved was $1.4 \times 10^{-5}$ $Scm^{-1}$with 6 wt.% filler. It is found that ionic conductivity achieved maximum value ($1.0 \times 10^{-7}$ $Scm^{-1}$) at 12 wt.% $Al_2O_3$ as reported by [10].

However the addition of carboxymethyl cellulose higher than 6 wt% shows the reduction of the ionic conductivity. The conductivity rapidly reduced with high percentage of carboxymethyl cellulose loading due to fibre agglomeration, which reduced the $Li^+$ ion mobility and thus the bulk conductivity [11].

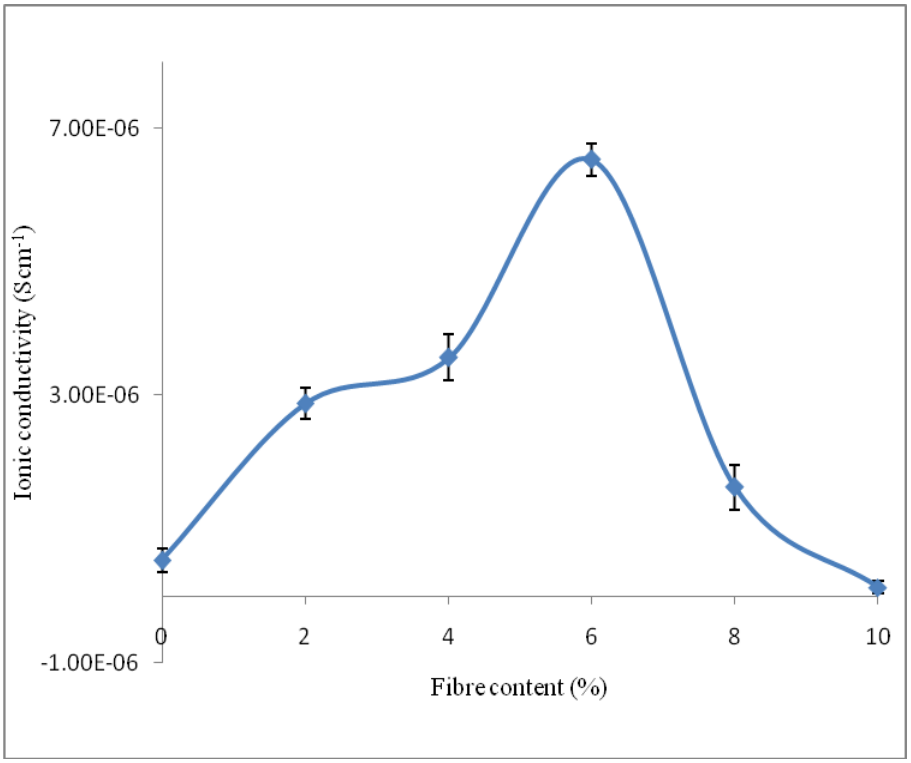



Figure 2. Ionic conductivity of composite polymer electrolytes at the variation of fibre content

Table 1. The ionic conductivity of composite polymer electrolyte MG49-$LiCF_3SO_3$-Carboxymethyl cellulose

| **Carboxymethyl Cellulose content, wt%** | **Conductivity, σ [$Scm^{-1}$]** |
|---|---|
| 0 | $5.3 \times 10^{-7}$ |
| 2 | $2.9 \times 10^{-6}$ |
| 4 | $3.6 \times 10^{-6}$ |
| 6 | $6.5 \times 10^{-6}$ |
| 8 | $1.6 \times 10^{-6}$ |
| 10 | $1.3 \times 10^{-7}$ |

**Linear Sweep Voltammetry**

Electrochemical stability window was carried out by choosing the sample at the highest ionic conductivity which is 6 wt% of carboxymethyl cellulose. For lithium battery, the anodic reaction occurs in the vicinity of 0 V (vs. Li), while the cathode potentials can be approached as high as 4.5 V (vs. Li) [12]. MG49/carboxymethyl cellulose/$LiCF_3SO_3$ film shows an appreciably high anode breakdown voltage which makes it suitable in battery application. From the current-voltage obtained in the voltage range 0 and 5.0 V (vs. Li) at room temperature by linear sweep voltametry can be seen in Figure 3. The plateau is flat and straight with wide ESW which no electrochemical reactions occurs at positive potentials ranging from the lithium plating to above 2.7 V (vs. Li) at 25°C. Composite polymer electrolytes system is sensitive to oxygen, water and other impurities [13]. Therefore, this system can be categorized as pure system because it gives very low residual current level prior to breakdown

voltages, which no peaks at the lower voltage ranges. The increase of current during anodic scan was taken in correspondence to the onset of a low current peak at ~2.7 V related the decomposition of the electrolytes [2].

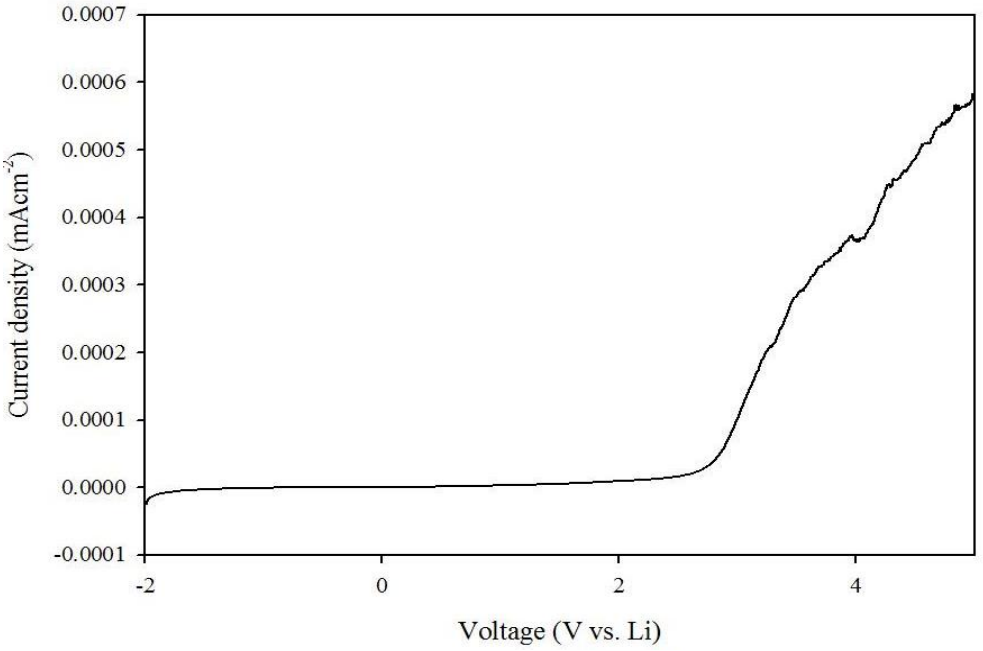



Figure 3. Current vs voltage curves in the anodic voltage range

**Mechanical Properties**

Figure 4 shows the effect of the carboxymethyl cellulose loading on the tensile strength and Young's modulus of the composite polymer electrolytes. The result showed the increase of tensile strength with filler loading. It is noted that 2 wt% of carboxymethyl cellulose show the lowest tensile strength value at 4.9 MPa. The optimum value for the composite polymer electrolytes films is 7.9 MPa obtained at 6 wt% carboxymethyl cellulose loading. The increase is due to effective interaction between carboxymethyl cellulose and MG49 or salt. This is explained by the increase of uniformity that contributes to the increase in strength. The formation of a rigid percolating cellulose fiber network also assumed to be formed through strong hydrogen bonds interactions in carboyxmethyl cellulose fiber [11].

Moreover, Young's Modulus also can be considered high for small amount fiber upon addition of $LiCF_3SO_3$. Polymer electrolytes films with 6 wt% carboxymethyl cellulose showed the optimum value of the modulus which is 273 MPa. This due to a stabilizing effect of the salt which may lead to better dispersion cellulose on the polymer matrix [14].

However, when the percentage of fibre further increased up to 8-10 wt% the tensile strength and Young's Modulus was decreased. The reduction is due to non-uniform distribution of carboxymethyl cellulose in the matrix. The increasing of the cellulose concentration cause the rigidity of network is increase and agglomeration occurred. So, the mechanical behaviour of polymer electrolytes will decrease for 8-10 wt% of fibres. These results reveal that the incorporation of carboxymethyl cellulose into MG49 matrix is quite effective reinforcement.

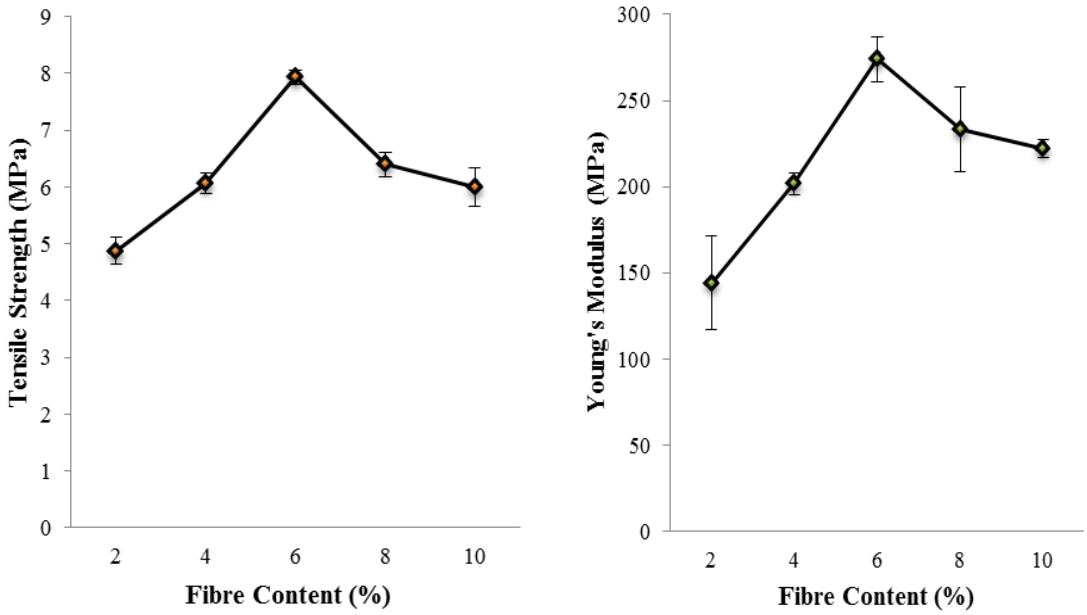



Figure 4. Graph of the a) tensile strength, b) Young's Modulus of composite polymer electrolytes

**Morphological Investigation**

The morphology of the films was characterized by SEM analysis. SEM micrographs were obtained from cross-section on the polymer electrolytes based MG49, carboxymethyl cellulose and $LiCF_3SO_3$ salt. SEM micrographs for (a) pure MG49, (b) 0 wt% carboxymethyl cellulose, (c) 6 wt% carboxymethyl cellulose and (d) 10 wt% carboxymethyl cellulose are shown in Figure 5. It can be seen from that a pure MG49 film shows a rough morphology with some rumples. Differences in the phase structure can be observed due to the existence of dark and bright areas on the surface that represent the crystalline and the amorphous phase fraction, respectively. From Fig. 5b, the white dots can be interpreted as carboxymethyl cellulose fibres in MG49 composite polymer electrolytes with no apparent aggregates [3]. A homogeneous distribution of white dots was observed due to the good dispersion of carboxymethyl cellulose in MG49.

The blending of MG49 with salt and carboxymethyl cellulose, improved surface morphology to be smoother compared to the pure MG49. The addition of 6 wt% of carboxymethyl cellulose seems to be optimum percentage of fibre as shows in Fig. 5c with smoother surface compare to 10 wt% carboxymethyl cellulose. Therefore, the highest conductivity obtained with the addition of 6 wt% carboxymethyl cellulose is represented by overall mobility of ion in polymer matrix which leads to the increase in ionic and segmental mobility. The smoother surface morphology may associate with a reduction in the degree of crystallinity of the polymer matrix after the addition of salt and fibres. This was due to the formation of coordinate bonds of lone pair electrons of oxygen atoms from MMA with $Li^+$ ions from the salt to form polymer complexes [1].

From Figure 5 (e), we can see some agglomeration occurred for the sample with higher amount of carboxymethyl cellulose which resulted in the reduction of mechanical properties of SPEs. These observation support the conductivity result that shows the ionic conductivity of polymer electrolytes decreased after addition more than 6 wt% of carboxymethyl cellulose.

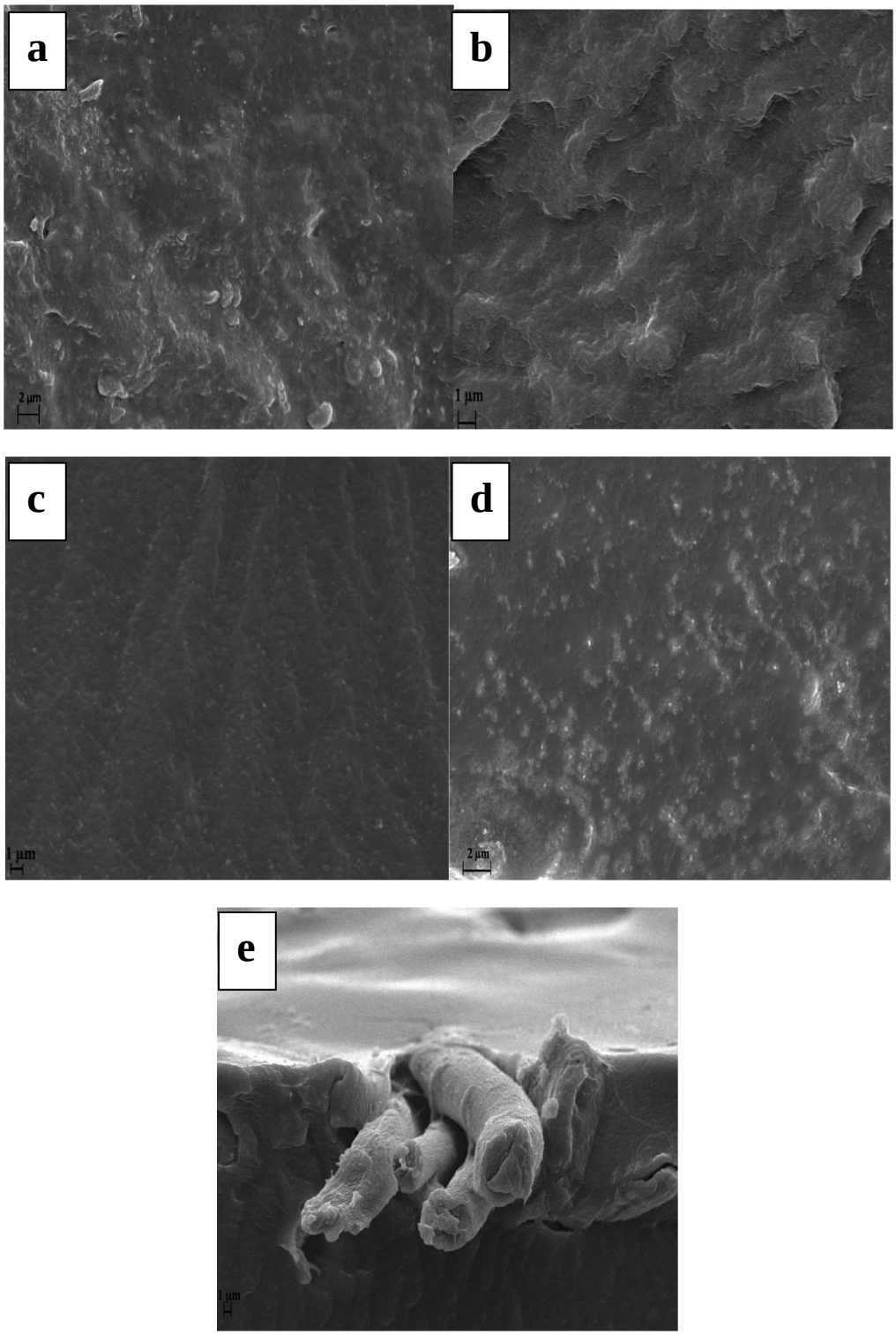



Figure 5. SEM micrographs of composite polymer electrolytes a) pure MG49; b) 0 wt% c) 6 wt%; d) 10 wt% of carboxymethyl cellulose with 1.0 Kx magnification; e) 10 wt% of carboxymethyl cellulose with 2.5 kx magnification

## Conclusion

The development of modified natural rubber incorporating carboxymethyl cellulose has potential in composite polymer electrolytes system. The highest conductivity achieved was $6.5 \times 10^{-6}$ $Scm^{-1}$. The electrochemical stability window (~2.7 V (vs.Li)) evidenced a wide window and interesting performed in real battery application. The incorporation of carboxymethyl cellulose in lithium polymer electrolytes leads to high-performance composite electrolytes with 6 wt% carboxymethyl cellulose loading showed the optimum tensile strength and Young's modulus with the of values of 7.9 MPa and 273 MPa respectively. From these results, we summarized that the promising reinforced with natural fibre polymer electrolytes could be used in various electrochemical energy sources which demonstrate both high ionic conductivities and good mechanical characteristics.

## Acknowledgement

The authors would like to thank Universiti Kebangsaan Malaysia for the permission for this research to be carried out within the university premises. Financial support was received from the Ministry of Higher Education under research grant numbers ERGS/1/2012/STG01/UKM/02/4 and UKM-DLP-2012-02.

## References

1. Su'ait, M. S., Ahmad, A. & Rahman, M. Y. A. (2009). Ionic Conductivity Studies of 49% poly(methyl methacrylate)-grafted Natural Rubber-based Solid Polymer Electrolytes.*Ionics*, 15 (4): 497 - 500.
2. Chiappone, A., Nair, J. R., Gerbaldi, C., Jabbour, L., Bongiovanni, R., Zeno, E., Beneventi, D. & Penazzi, N. (2011). Microfibrillated Cellulose as Reinforcement for Li-ion Battery Polymer Electrolytes with Excellent Mechanical Stability.*Journal of Power Sources*, 196: 10280 - 10288.
3. Alloin, F., D'Apreaa, A., Kissi, N. E., Dufresne, A. & Bossard, F. (2010). Nanocomposite Polymer Electrolyte Based on Whisker or Microfibrils Polyoxyethylene Nanocomposites.*Electrochimica Acta*, 55 (18): 5186 – 5194.
4. Adinugraha, M. P., Marseno, D. W. & Haryadi. (2005). Synthesis and Characterization of Sodium Carboxymethylcellulose from Cavendish Banana Pseudo Stem (*Musa cavendishii* LAMBERT).*Carbohydrate Polymers*, 62 (2): 164 - 169.
5. Mobarak, N. N., Ahmad, A., Abdullah, M. P., Ramli, N. & Rahman, M. Y. A. (2013). Conductivity Enhancement via Chemical Modification of Chitosan Based Green Polymer Electrolyte. *Electrochimica Acta*, 92: 161 - 167.
6. Yaacob, B., Mohd Amin, M. C. I., Hashim, K. & Abu Bakar, B. (2011). Optimization of Reaction Condition for Carboxymethylated Sago Starch.*Iranian Polymer Journal*, 20 (3): 195 - 204.
7. Kargarzadeh, H., Ahmad, I., Abdullah, I., Dufresne, A., Zainudin, S. Y. & Sheltami, R. M. (2012). Effects of Hydrolysis Conditions on the Morphology, Crystallinity, and Thermal Stability of Cellulose Nanocrystals Extracted from Kenaf Bast Fibers.*Cellulose*, 19 (13): 855 - 866.
8. Bono, A., Ying, P. H., Yan, F. Y., Muei, C. L., Sarbatly, R. & Krishnaiah, D. (2009). Synthesis and Characterization of Carboxymethyl Cellulose from Palm Kernel Cake.*Advances in Natural & Applied Sciences*, 3 (11): 5 - 11.
9. Low, S. P., Ahmad, A., Hamzah, H. & Rahman, M. Y. A. (2011). Nanocomposite Solid Polymeric electrolytes of 49% poly(methyl methacrylate)-grafted Natural Rubber-titanium Dioxide-lithium Tetrafluoroborate (MG49-$TiO_2$-$LiBF_4$).*Journal of Solid State Electrochemistry*, 15 (11-12): 2611 - 2618.
10. Chang H. P, Kim, D. W., Prakash, J. & Sun, Y. K. (2003). Electrochemical Stability and Conductivity Enhancement of Composite Polymer Electrolytes. *Solid State Ionics*, 159 (1-2): 111 - 119.
11. Azizi Samir, M. A. S., Mateos, A. M., Alloin, F., Sanchez, J. Y., and Dufresne, A. (2004). Plasticized Nanocomposite Polymer Blectrolytes based on Poly(oxyethylene) and Cellulose Whiskers.*Electrochimica Acta*, 49 (26): 4667 - 4677.
12. Nair, J. R., Chiapponea, A., Gerbaldia, C., Ijeri, V. S., Zenod, E., Bongiovannia, R., Bodoardoa, S. & Penazzia, N. (2011). Novel Cellulose Reinforcement for Polymer Electrolyte Membranes with Outstanding Mechanical Properties.*Electrochimica Acta*, 57: 104 - 111.

13. Nair, J. R., Gerbaldi, C., Chiappone, A., Zeno, E., Bongiovanni, R., Bodoardo, S. & Penazzi, N. (2009). UV-cured Polymer Electrolyte Membranes for Li-cells: Improved Mechanical Properties by a Novel Cellulose Reinforcement.*Electrochemistry Communications*, 11 (9): 1796 - 1798.
14. Schroers, M., Kokil, A., & Weder, C. (2004). Solid Polymer Electrolytes based on Nanocomposites of Ethylene oxide-epichlorohydrin Copolymers and Cellulose Whiskers.*Journal of Applied Polymer Science*, 93 (6): 2883 - 2888.

The Malaysian Journal of ANALYTICAL SCIENCES ISSN 1394-2506

# EFFECT OF FERMENTED CHITIN NANOWHISKERS ON PROPERTIES OF POLYLACTIC ACID BIOCOMPOSITE FILMS

## (Kesan Kitin Terfermentasi Terhadap Sifat Filem Biokomposit Asid Poli Laktik)

Syazeven Effatin Azma Mohd Asri[1], Zainoha Zakaria[1]*, Azman Hassan[2], M. K. Mohamad Haafiz[2,3]

[1]*Department of Chemistry, Faculty of Science,*
[2]*Department of Polymer Engineering, Faculty of Chemical Engineering,*
*Universiti Teknologi Malaysia 81310 Skudai, Johor, Malaysia*
[3]*School of Industrial Technology,*
*Universiti Sains Malaysia, 11800 USM Penang, Malaysia*

**Corresponding author: zainoha@kimia.fs.utm.my*

**Abstract**

The fermented chitin nanowhiskers (FCNW) filled polylactic acid (PLA) biocomposite films were successfully produced using solution casting method. The biocomposite films were characterized in terms of tensile properties. The Young's modulus increased with increasing FCNW content while the tensile strength increased and reached the maximum value at 4 phr FCNW loading. Therefore it can be concluded that the optimum loading of FCNW is at 4 phr and further addition of FCNW may lead to agglomeration resulting in a decrease in tensile strength. The elongation at break of the biocomposite films decreased rapidly upon addition of FCNW into PLA. From the Atomic Force Microscopy, the surface morphology of the PLA changed upon addition of FCNW and tendency for agglomeration of FCNW at high loading was observed.

**Keywords:** chitin, nanowhiskers, polylactic acid, film, solution casting

**Abstrak**

Kitin nanowisker daripada kitin terfermentasi (FCNW) yang memenuhi filem biokomposit asid poli laktik (PLA) telah berjaya dihasilkan melalui kaedah tuangan larutan. Filem biokomposit itu kemudiannya dicirikan berdasarkan sifat kekuatan tensilnya. Modulus Young meningkat seiring dengan peningkatan kandungan FCNW manakala kekuatan tensil meningkat dan mencapai nilai maksimum pada 4 phr. Oleh yang demikian, boleh disimpulkan bahawa pengisian optimum FCNW adalah pada 4 phr dan penambahan berterusan FCNW mungkin akan membawa kepada penggumpalan yang mengakibatkan penurunan dalam kekuatan tensil. Ciri pemanjangan takat putus filem biokomposit menurun secara mendadak dengan penambahan FCNW ke dalam PLA. Daripada mikroskop daya atom, morfologi permukaan PLA berubah setelah ditambah dengan FCNW dan potensi kepada penggumpalan pada pengisian tinggi FCNW telah diperhatikan.

**Kata kunci:** kitin, nanowisker, asid polilaktik, filem, tuangan larutan

## Introduction

Nowadays, the market share of biodegradable polymers from renewable sources has grown rapidly in the plastic industry. This is due to two major factor; i) environmental concerns and ii) consciousness that petroleum resources are limited. Generally, polymers from renewable resources can be classified into three groups; i) natural polymers including starch, protein and cellulose, ii) synthetic polymers from natural monomers such as polylactic acid (PLA) and iii) polymers from microbial fermentation including polyhydroxybutyrate (PHB). Through blending and composite formation, properties of these polymers from renewable resources can be enhanced [1].

The concept of biodegradable plastics is of a considerable interest with respect to solid waste accumulation. Bigger efforts have been made to replace petroleum-based traditional plastics by developing degradable biological materials without any environmental pollution. PLA being an aliphatic polyester and a biocompatible thermoplastic is currently considered as the 'green' eco friendly material for the future. PLA fulfill many requirements as a

packaging thermoplastic and is suitable for general packaging applications such as loose-fill packaging, compost bags, food packaging and disposable tableware [2]. However, PLA has several disadvantages including high cost production, brittleness, hydrophobic and poor thermal resistance [2]. PLA can be combined with other suitable natural sources such as the abundantly available chitin which acts as additive to enhanced its properties [3].

Chitin is one of the most abundant natural polymers after cellulose that exist in nature but its functionality and limited solubility have restricted its applications. Chitin is a polysaccharide and is found in many crustacean sources such as crabs, shrimp shells and lobsters in the α-crystalline form while β-chitin is found in squid pens. Chitin, a linear polymer of *N*-acetyl-D-glucosamine linked by α (1,4) glycosidic bond [4,5] can be obtained from seafood industrial waste such as prawn waste. Both chitin and its derivatives chitosan, possess huge range of useful properties; such as biocompatibility, antibacterial and environmentally friendly polyelectrolyte [6]. In contrast, its derivatives chitosan has been commercialized for a variety of applications such as waste water treatment, textile and paper industry, cosmetic, medicine and agriculture [7]. However, interest in chitin has been recently revived because chitin is found to have desirable mechanical property due to their natural stacks of chitin nanocrystals which have a Young's modulus as high as 41 GPa measured by X-ray diffraction [8].

However, their industrial applications are scarce largely due to high prices. Chitin is usually obtained through chemical treatments which discard large amount of chemical wastes. In the last decade, a biotechnological approach using lactic acid fermentation to purify chitin from crustacean waste is gaining its popularity due to its environmentally clean approach and cheaper production cost. Previous research [9] has successfully extracted a rich protein liquor and a partially purified chitin from tiger prawn waste through solid state bacterial fermentation process. If chitin can be converted into potential new material such as forming polylactide-chitin composite, it would be a very great advantage to the prawn processing industries which discarded nearly 50% of the whole processed prawn.

## Materials and Methods

### Materials

Polylactic acid (NatureWork$^{TM}$ PLA 300ID) in pellet form was obtained from NatureWork® LLC, Minnetonka, MN USA. The density of PLA is 1.25 g/cm$^3$, melting temperature of 145-155°C, glass transition temperature of 55-58°C, cystallinity of up to 37% and it has average molecular weight of $M_w$: 220 kDa and $M_n$: 101 kDa. Fermented chitin nanowhiskers (L=50 nm, D=10 nm) was produced from chitin obtained from prawn waste fermentation through acid hydrolysis [10]. The reagent used was hydrochloric acid and chloroform from Merck, Malaysia.

### Preparation of PLA and PLA/FCNW biocomposites

A 10 wt% solution of PLA pellets in chloroform was prepared by stirring the solution in water bath at 60ºC until the pellets were fully dissolved. The PLA solution was immediately cast on clean glass plates and left for the solvent to evaporate at ambient temperature for 48 hours. The cast solution noted as pure PLA.

For the preparation of PLA/FCNW biocomposites, 10 wt% solution of PLA was mixed with different amount of FCNW (2, 4 and 6 phr) and the mixture was kept at 60ºC with strong agitation until the PLA pellets were fully dissolved. The suspension was then sonicated for 5 min and was immediately cast on a clean glass plate to remove the solvent. The composites were designated as PLA/FCNW2, PLA/FCNW4 and PLA/FCNW6.

### Characterization

Mechanical test was done using the Instron 4400 Universal Tester to measure the tensile strength. Tensile tests were carried out at room temperature, according to the ASTM D882. A fixed crosshead rate was utilized in all cases and the results were taken as an average of eleven tests.

The morphology of samples was observed using atomic force microscopy (AFM). AFM observation was performed using SPA-300HV atomic force microscope with a SPI 3800 controller, the pure PLA and biocomposite samples with dimension of 0.1 mm x 0.1 mm were analyzed directly.

## Results and Discussion

### Atomic Force Microscopy (AFM) analysis

Surfaces of PLA and PLA/FCNW biocomposites were observed using AFM to further explore the nature of interactions between PLA and FCNW. The surface morphology of PLA and PLA/FCNW biocomposite with various contents of FCNW are shown in Figure 1.

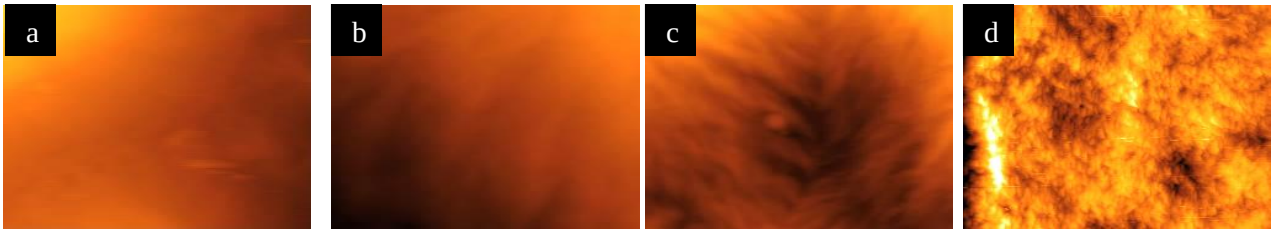



Figure 1. AFM images of a) PLA composite and PLA/FCNW composite with different FCNW loading (b) 2 phr, (c) 4 phr and (d) 6 phr

From Figure 1(a), smooth surface of neat PLA was observed while the inclusions of FCNW into the PLA matrix change the surface topography of the pure PLA (Figure 1 (b)-(d)). It interesting to note that at lower FCNW content (2 phr), the filler was well dispersed inside the PLA with no sign of agglomeration. However at higher FCNW contents (4 and 6 phr) the FCNW has started to agglomerate. The presence of these FCNW agglomerations provides evidence of the poor filler dispersion in matrix which affect the tensile properties of PLA biocomposite as discussed in detail in the next section. Similar observation was also reported [11] when using microcrystalline cellulose as filler in PLA.

### Tensile properties

The tensile properties of PLA/FCNW were investigated in order to determine the effect of FCNW loading on PLA. The tensile strength, Young's modulus and elongation at break of PLA/FCNW biocomposite at different FCNW loading are shown in Figure 2, 3 and 4 respectively and the results are summarized in Table 1.

Table 1. Mechanical properties of PLA/FCNW biocomposite film

| Material Code | Tensile Strength (MPa) | Elongation at Break (%) | Young's Modulus (GPa) |
|---|---|---|---|
| PLA | 11.2 ± 0.7 | 90.0 ± 14.7 | 1.36 ± 0.6 |
| PLA/FCNW2 | 11.3 ± 0.8 | 20.1 ± 1.1 | 2.22± 0.5 |
| PLA/FCNW4 | 12.4 ± 0.6 | 22.8 ± 1.8 | 2.997 ± 0.3 |
| PLA/FCNW6 | 8.8 ± 0.7 | 7.2 ± 1.2 | 3.73 ± 0.6 |

Figure 2 shows the tensile strength of PLA/FCNW biocomposites. Tensile strength of PLA/FCNW showed improvement when incooperating with FCNW loading up to 4 phr before decrease with further addition of FCNW. The reduction in tensile strength for the PLA/FCNW at higher FCNW loading may be attributed to aggregation of FCNW due to Van der Waal's forces. The results seem support the microscopy analysis discussed in previous section. On the other hand at the low filler content, the reinforcing effect of FCNW is dominant but as the filler content increased, the filler-filler interaction become dominant compared to filler-matrix interaction which lead to poor interfacial adhesion between FCNW and PLA. This may likely to be the explanation for the decrease recorded in the tensile strength.

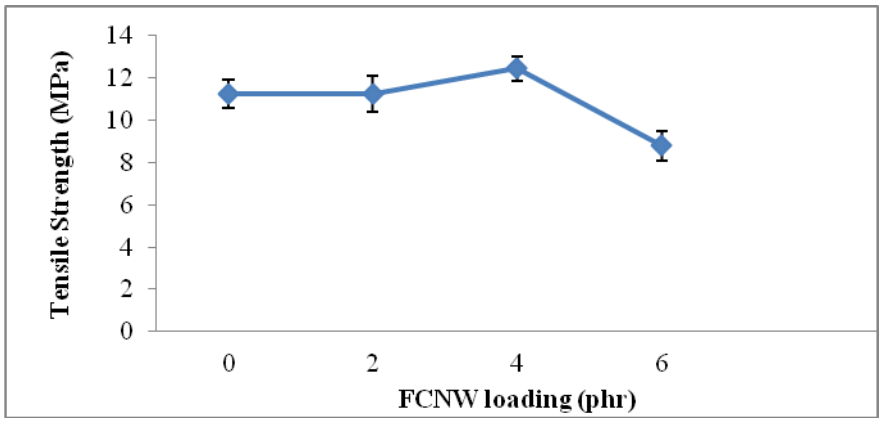



Figure 2. Tensile strength of PLA/FCNW biocomposite film

The Young's modulus of PLA/FCNW biocomposite was increased with increasing of FCNW loading as shown in Figure 3. This behaviour is attributed to stiffening effect of filler which decrease the polymer chains mobility and consequently enhanced the modulus of biocomposite. The increase in modulus with increasing filler loading can be explained by increased in hydrogen bonding, stiffening effect and high crystallinity index of the filler which is a typical characteristics of filler/polymer composite [12].

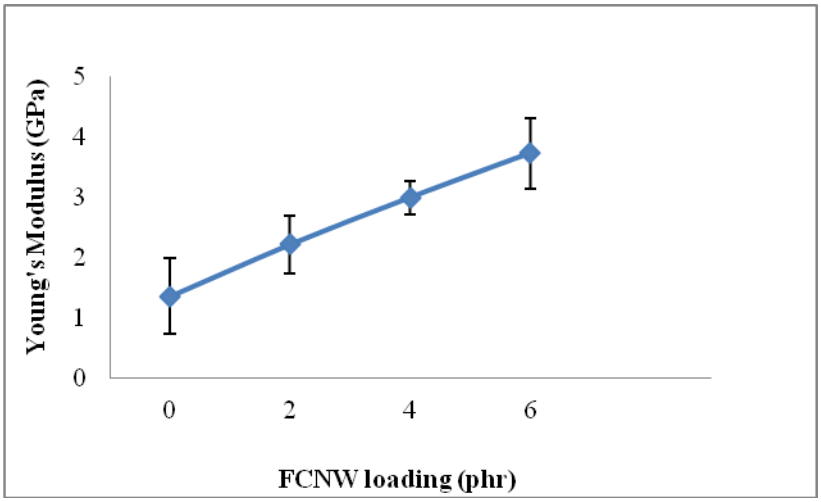



Figure 3. Young's modulus of PLA/FCNW biocomposite film

It also revealed that the addition of FCNW in the PLA matrix give the negative impact to the elongation at break for biocomposites. The elongation at break of PLA/FCNW decrease dramatically as compared to the PLA as shown in Figure 4. It can be clearly seen that the elongation at break decreased gradually as the concentration of filler increased for all formulations of PLA becomes more brittle. These observations may be attributed to the stiffening action of the filler by restricting the segmental chain movement of PLA during tensile testing. Similar result has been reported by Bulota et al. [13] in study of mechanical behaviour of PLA reinforced TEMPO-Oxidized cellulose and by Wang et al. [14] in cooperating cellulose whisker with soy protein thermoplastic.

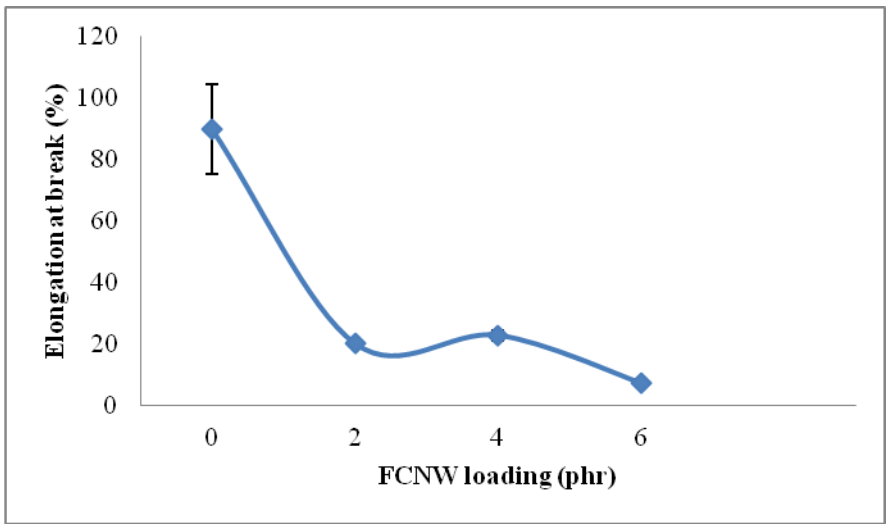



Figure 4. Elongation at break of PLA/FCNW biocomposite film

## Conclusion

PLA/FCNW biocomposite film was successfully produced using solution casting method. AFM showed that at 2 phr FCNW content, the filler was well dispersed with no evidence of agglomeration. Agglomeration of FCNW started to be observed at 4 phr. which indicates poor filler dispersion in matrix. Young's modulus increased with increasing of FCNW content while tensile strength increased up to a maximum value at 4 phr FCNW loading. Elongation at break of the PLA/FCNW biocomposite film decreased sharply with addition of FCNW.

## Acknowledgement

The authors would like to thank Ministry of Higher Education for supporting this work through ERGS Grant 4L099 and GUP 05J88.

## References

1. Yu, L. et al. (2006). Polymer Blends and Composites from Renewable resources. *Progress in Polymer Science*, 31: 576-602.
2. Nampoothiri, K. M, Nair, N. R., & John, R. P. (2010). An overview of the recent developments in polylactide (PLA) research. *Bioresource Technology*, 101**:** 8493-850.
3. Rizvi, R., Cochrane, B., Naguib, H & Lee, P.C. (2011). Fabrication and characterization of polylactide-chitin composites and their foams. *Journal of Cellular Plastics* 47: 283-300.
4. Chaussard, G. & Domard, A. (2004). New Aspects of the Extraction of Chitin from Squid Pens. *Biomacromolecules*. 5, 559-564.
5. Chandumpaia, A., Singhpibulpornb, N., Faroongsarngc, D. & Sornprasita, P. (2004). Preparation and physico-chemical characterization of chitin and chitosan from the pens of squid species. *Loligo lessoniana* and *Loligo formosana*, *Carbohydrate Polymers*. 58: 467-474.
6. Struszczyk, M.H. (2006). Global Requirements for Medical Applications of Chitin and its Derivatives. *Polish Chitin Society, Monograph* XI, 95-102.
7. Rinaudo, M. (2006). Chitin and chitosan: Properties and applications. *Progress in Polymer Science*. 31: 603-632.
8. Nishino, T., Matsui, R. & Nakamae, K., (1999). Elastic Modulus of the crystalline regions of chitin and chitosan. *J. Polymer Science Part B*. 37: 1191-1196.

9. Nor, N.M., Zakaria, Z., Manaf, M.S.A. & Salleh, M.,M. (2011). The Effect of Partial Replacement of Dietary Fishmeal with Fermented Prawn Waste Liquor on Juvenile Sea Bass Growth. *Journal of Applied Aquaculture* 23: 51-57.
10. Nair G.K., & Dufresne A. (2003). Crab Shell chitin whisker reinforced natural rubber nanocomposites. 1. Processing and Swelling Behavior *Biomacromolecules*, 4: 657-665.
11. Haafiz, M.K.M., Hassan, A., Zakaria, Z., Inuwa, I.M., Islam, M.S. & Jawaid, M. (2013). Properties of polylactic acid composites reinforced with oil palm biomass microcrystalline cellulose. *Carbohydrate Polymer* 98:139-145.
12. Cheng, Q., Wang, S., & Rials, T.G. (2009). Poly (vinyl alcohol) nanocomposites reinforced with cellulose fibrils isolated by high intensity ultrasonication. *Composites: Part A*, 40*:* 218-224.
13. Bulota, M., Vesterinen, A.H., Hughes, & Seppälä, J. (2013). Mechanical Behavior, Structure, and Reinforcement Processes of TEMPO-Oxidized Cellulose Reinforced Poly(lactic) Acid. *Polymer Composites.* 34:173-179.
14. Wang, Y., Cao, X. & Zhang, L. (2006). Effects of Cellulose Whiskers on Properties of Soy Protein Thermoplastics. *Macromolecule Biosciences.* 6: 524-531.

The Malaysian Journal of ANALYTICAL SCIENCES ISSN 1394-2506

# FLEXURAL PROPERTIES OF ACTIVATED CARBON FILLED EPOXY NANOCOMPOSITES

## (Sifat Lenturan Nanokomposit Epoksi Berpengisi Karbon Teraktif)

H.P.S. Abdul Khalil[1,2], M. Jawaid[2,3]*, P. Firoozian[1], Othman Y. Alothman[3], M. T. Paridah[2], E.S. Zainudin[2]

[1]*School of Industrial Technology,*
*Universiti Sains Malaysia, 11800 USM Penang, Malaysia*
[2]*Department of Biocomposite Technology, Institute of Tropical Forestry and Forest Products (INTROP),*
*Universiti Putra Malaysia, 43400 Serdang, Malaysia*
[3]*Department of Chemical Engineering, College of Engineering*
*King Saud University, Riyadh 11451, Saudi Arabia*

**Corresponding author: jawaid_md@yahoo.co.in*

**Abstract**

Activated carbon (AC) filled epoxy nanocomposites obtained by mixing the desired amount of nano AC viz., bamboo stem, oil palm empty fruit bunch, and coconut shell from agricultural biomass with the epoxy resin. Flexural properties of activated carbons filled epoxy nanocomposites with 1%, and 5% filler loading were measured. In terms of flexural strength and modulus, a significant increment was observed with addition of 1% vol and 5% vol nano-activated carbon as compared to neat epoxy. The effect of activated carbon treated by two chemical agents (potassium hydroxide and phosphoric acid) on the flexural properties of epoxy nanocomposites were also investigated. Flexural strength of activated carbon-bamboo stem, activated carbon-oil palm, and activated carbon-coconut shell reinforced epoxy nanocomposites showed almost same value in case of 5% potassium hydroxide activated carbón. Flexural strength of potassium hydroxide activated carbon-based epoxy nanocomposites was higher than phosphoric acid activated carbon. The flexural toughness of both the potassium hydroxide and phosphoric acid activated carbon reinforced composites range between 0.79 – 0.92 J. It attributed that developed activated carbon filled epoxy nanocomposites can be used in different applications.

**Keywords**: epoxy matrix; activated carbon; nanocomposites; flexural properties

**Abstrak**

Nanokomposit epoksi berpengisi karbon teraktif diperoleh dengan mencampurkan sejumlah nano karbon teraktif iaitu buluh, kelapa sawit tandan buah kosong, dan tempurung kelapa yang dikehendaki daripada biomas pertanian dengan resin epoksi. Sifat lenturan nanokomposit epoksi berpengisi karbon teraktif dengan 1% dan 5% muatan pengisi telah diukur. Dari segi kekuatan lenturan dan modulus, peningkatan ketara diperhatikan dengan jumlah penambahan 1% dan 5% nano-karbon teraktif berbanding epoksi tanpa pengisi. Kesan karbon teraktif menggunakan dua bahan kimia (kalium hidroksida dan asid fosforik) terhadap sifat lenturan terawat juga dikaji. Kekuatan lenturan karbon teraktif-batang buluh, karbon teraktif-kelapa sawit, dan karbon teraktif-tempurung kelapa diperkukuh nanokomposit epoksi menunjukkan nilai yang hampir sama seperti 5% kalium hidroksida karbon teraktif. Kekuatan lenturan kalium hidroksida karbon teraktif berasaskan nanokomposit epoksi adalah lebih tinggi daripada asid fosforik karbon teraktif. Ketahanan lenturan bagi kedua-dua kalium hidroksida dan asid fosforik karbon teraktif diperkukuh komposit epoksi adalah di antara 0.79 – 0.92 J. Ia menyifatkan bahawa pembangunan nanokomposit epoksi berpengisi karbon teraktif boleh digunakan dalam aplikasi yang berbeza.

**Kata kunci:** matrik epoksi; karbon teraktif; nanokomposit; sifat lenturan

## Introduction

Epoxy resin possess long service time, good physical properties, favorable cost–performance ratio in comparison to other thermosets. Epoxy resins have wide range of applications in electronics, transportation in composite structural and furnishing elements. In Malaysia, huge amount of agricultural biomass available which can be converted to useful, value-added products to solve agricultural waste disposal problems. Agricultural biomass such as oil palm

empty fruit bunch fibres, bamboo stem and coconut shells are available in Malaysia. However, there are limited studies reported on the utilization of oil palm empty fruit bunch (EFB) fibres, bamboo stem and coconut shells, especially on conversion of EFB into activated carbon (AC)[1-2]. ACs with high specific surface area and pore volumes can be prepared from a variety of carbonaceous materials such as coconut shell [3-4], agricultural wastes [5-7], or industrial wastes [8-9].

AC can be introduced into polymeric materials such as epoxy to modify their properties and to develop composites materials with improved thermal and mechanical properties. AC filled polymer composites are lightweight materials, readily availability in different structural forms and are known to enhance the thermal, mechanical and electrical properties and the ease of fabrication of these composite through compression molding. A combination of epoxy matrix with various types of nano-filler reinforcement materials lead to the development of epoxy nanocomposites which can be used in wide range of potential applications. Several researchers reported on preparation and characterization of nano-filler based epoxy composites [10-12].

This research is extension of previous work deals with preparation and characterization of activated carbon filled epoxy nanocomposites by using activated carbon treated with two chemical reagents, phosphoric acid ($H_3PO_4$) and potassium hydroxide (KOH) [13-16]. The focus of this study to develop high performance composites materials from biomass (agricultural wastes) materials with aimed to reduce the overall cost of the material preparation by using of inexpensive inorganic fillers. Present study reported flexural properties of chemical reagents ($H_3PO_4$ or KOH)-treated ACs filled epoxy nanocomposites and compared measured flexural strength, modulus and toughness of chemical reagents ($H_3PO_4$ or KOH)-treated AC epoxy nanocomposites.

## Materials and Methods

### Materials

Waste biomass oil palm EFB fibre obtained from Ecofuture Berhad, Malaysia, Bamboo stem supplied by Forest Research Institute Malaysia (FRIM), and coconut shell procured from Anjung Juara Sdn, Bhd, used without further treatments. Potassium hydroxides (KOH) (~85% alkali) and phosphoric acid ($H_3PO_4$) obtained from R&M Chemical Essex, UK. All chemicals used in this investigation were of analytical grade. Morphological, chemical, and thermal properties of raw materials (oil palm EFB, bamboo stem, and coconut shells) reported in our previous work [15].

### Preparation of epoxy nanocomposites

Epoxy nanocomposites filled with activated carbon derived from oil palm empty fibre bunch (AC-EFB), bamboo stem (AC-BS), and coconut shells (AC-CNS) were obtained by mixing the required amount of AC with epoxy resin as reported in our previous work [13].

### Characterization

The flexural properties were measured using a three-point bending test method on Instron Universal Testing Machine (Model 5582). The tests were carried out at room temperature at a crosshead speed of 1.15 mm/min as per ASTM D790-02. Rectangular shaped composite samples of 120 mm × 20 mm × 3 mm were tested using a span of 40 mm. An average of at least five tests per sample was performed to report flexural strength and flexural modulus.

## Results and Discussion

### Abbreviations of Activated Carbons

The chemically activated carbon samples obtained from EFB, BS, and CNS were named AC-EFB, AC-BS, and AC-CNS, respectively. Carbon samples activated by phosphoric acid (H) were named AC-EFB H, AC-BS H, and AC-CNS H and those activated by potassium hydroxide (K) were named AC-EFB K, AC-BS K, and AC-CNS K, respectively.

### Flexural Properties

Flexural properties normally will be enhanced with incorporation of fillers, this is in agreement with many researchers [17-20]. Fig. 1 showed flexural strength and modulus of the cured epoxy (0% AC) and nano-activated carbon based epoxy composites with different volume percentage (1, 5, 10% vol) of AC-CNS. In terms of flexural

strength and modulus, a significant increment was observed with addition of 1% vol and 5% vol nano-activated carbon as compared to neat epoxy. The value of flexural strength of neat epoxy, 1% vol AC-CNS, and 5% vol AC-CNS nano-epoxy composites were 113 MPa, 123 MPa, and 133 MPa, respectively (Figure 1). The increase in flexural strength of epoxy nanocomposites could be attributed to greater physical interaction in the activated carbon filled epoxy composites. Smaller aggregate size increased the activated carbon surface area interacting with epoxy matrix, which resulted in enhanced flexural properties.

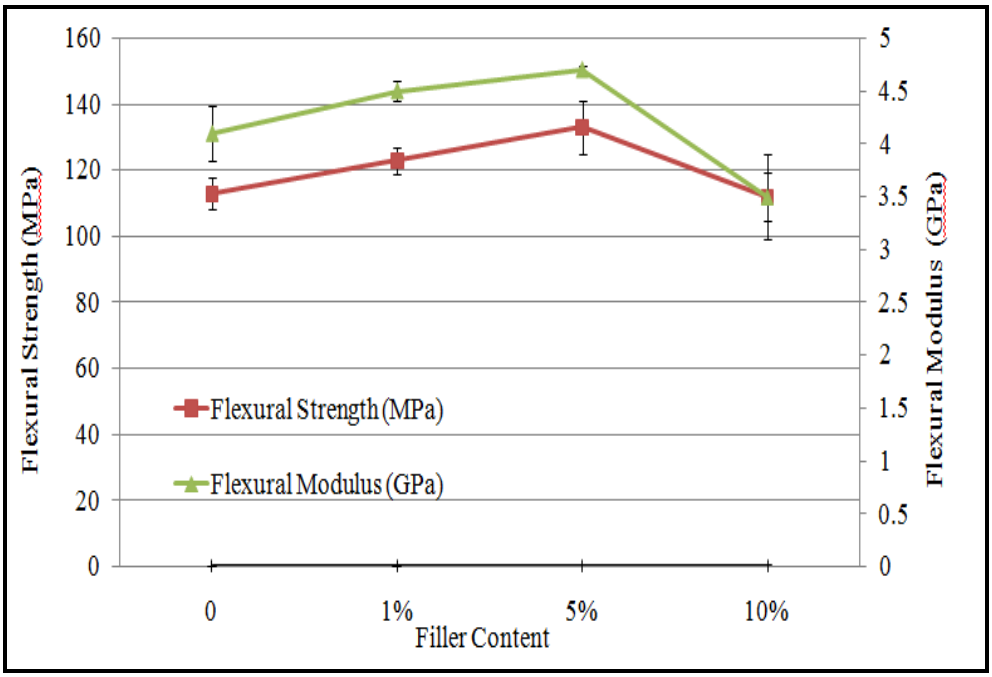



Figure 1. Flexural strength and modulus of AC-CNS K epoxy nanocomposites at 0%, 1%, 5% and 10% loading.

The flexural strength and modulus of nano AC-CNS epoxy composite decreased with increase in AC-CNS content. Earlier reports have shown that at higher filler loading, filler agglomeration and formation of micro void might cause decrease in stress transfer between the matrix and the reinforcing filler [21]. Also, a decrease in the effective cross-section area due to agglomeration of several nano-activated carbon have been reported by other workers [22]. The flexural modulus of the AC-CNS epoxy nanocomposites increased until 5% addition of nano AC-CNS and after that it started to decrease. These results suggest that optimum flexural modulus can be achieved with 5% filler loading above which a sharp deceased was recorded. It was observed that the flexural modulus decreased at 10% AC-CNS which was slightly higher than neat epoxy matrix. Similar study was reported on polyhedral oligomer silsesquioxanes (POSS)/ epoxy composites, it showed decreasing trend of flexural strength and modulus at higher volume of reinforcing materials [23]. The flexural strength of microparticle filled composites reduced with increasing filler content [24], especially in the case where load transfer between matrix and filler was insufficient and interface was weak. The adhesion between resin and nano AC-CNS become weaker as the filler content increases. Consequently, the flexural property of the composite decreased as the nano AC-CNS content increases. Small-size nano AC-CNS possessed more surface area than longer filler particles [25].

It is obvious from above that 1% and 5% AC-CNS reinforced epoxy nanocomposites gave improved and better flexural strength and modulus. These results suggest that optimum flexural strength and modulus were obtained

with 5% AC-CNS reinforced epoxy nanocomposites. On this basis, further study mainly concentrates on 1% and 5% AC-BS, AC-EFB, and AC-CNS for both activating agents. Fig. 2 showed flexural strength of AC-BS, AC-EFB, and AC-CNS based epoxy nanocomposites at 1%, and 5% AC by using $H_3PO_4$ (H), and KOH (K) activating agents. Flexural strength of AC-BS, AC-EFB, and AC-CNS epoxy nanocomposites showed almost same value in case of 5% KOH activated carbon while flexural strength of KOH activated carbon based epoxy nanocomposites was higher than $H_3PO_4$ activated carbon. It may be due to better quality of interface in KOH activated carbon than in $H_3PO_4$ activated carbon. It is clear from previous work that that activated carbon obtained by using KOH has the high surface area and uniform surface structure as compared to $H_3PO_4$ ([16]. Due to that AC obtained by using KOH show improved flexural strength. The adhesion strength and the interfacial stiffness usually play a very important role in the materials capability to transfer stresses and elastic deformation from matrix to fillers [26]. Another important aspect was the significant role of dispersion of nano-particle within matrix. 5% nano-activated carbón-CNS filled epoxy composite gave good dispersion of nano-particle as compared to 10% filler loading [14]. Allaoui et al. [27] advised that it not be helpful to use high filler concentrations to improve the mechanical properties of composites if they are in random distribution and homogeneity of the composite is a critical point for mechanical behavior of the nanocomposites.

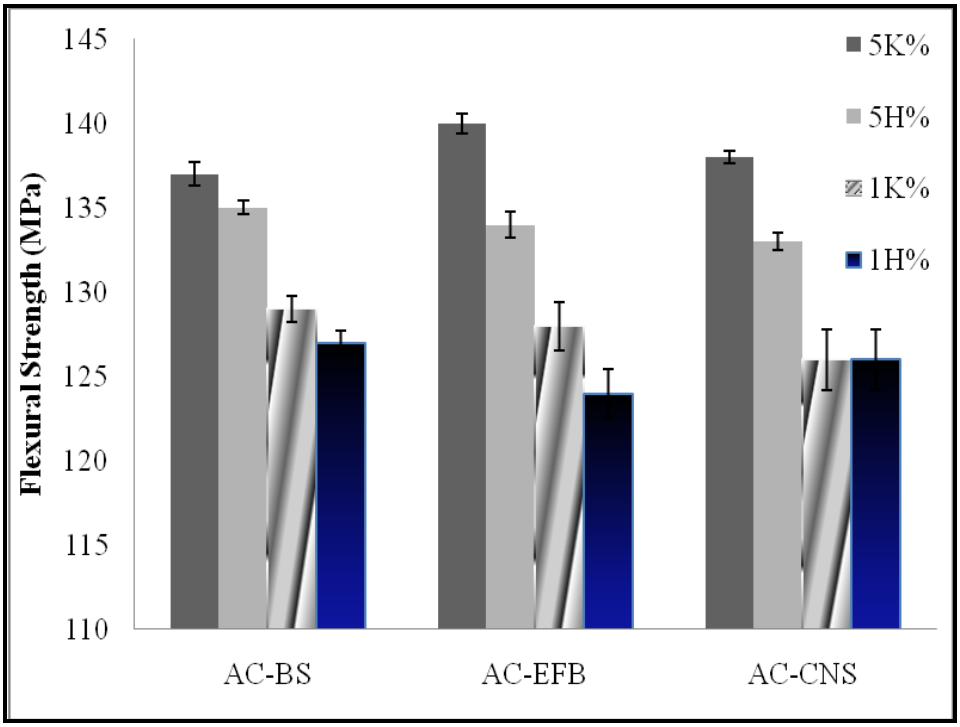



Figure 2. Flexural strength of AC-BS, AC-EFB, and AC-CNS based epoxy nanocomposites at 1% and 5% by using $H_3PO_4$ (H) and KOH (K) activating agent.

Flexural strength increased in epoxy composites reinforced by AC K possibly due to the presence of the activated carbons at the higher surface area, which may improve the interfacial properties between the matrix and the activated carbon [15-16]. It may also possible to conclude that the compressive strength of the epoxy matrix is improved by the presence of the nano-activated carbon and which ultimately increases the bending strength of the corresponding epoxy nanocomposites. At higher filler loading (10%) in epoxy matrix which may causes agglomeration in the epoxy matrix and propagating crack could encounter a stress concentration locally and then easily causes initiation of failure [28]. Table 1 represents the flexural toughness of various 5% AC filled epoxy composite. The flexural toughness of both the $H_3PO_4$ and KOH activated carbon reinforced composites range

between 0.79–0.92 J. These values are higher than the value obtained for un-reinforced epoxy composite which recorded the value of 0.78 J. Comparison of AC K samples indicate that AC-CNS K gave the highest value of 0.92 J whereas AC-EFB K gives the lowest toughness value of 0.83 J. Similarly for AC H samples, AC-CNS H shows the highest value of 0.84 and AC-EFB H gives 0.79 as the lowest value.

Table 1. Comparison of Fracture Toughness (J) of 5% AC filled epoxy composite.

| Composite | Fracture Toughness (J) | STD |
|---|---|---|
| Neat Epoxy | 0.78 | 0.04 |
| 5%AC-CNS K | 0.92 | 0.06 |
| 5%AC-BS K | 0.88 | 0.01 |
| 5% AC-EFB K | 0.83 | 0.03 |
| 5%AC- CNS H | 0.84 | 0.03 |
| 5%AC-BS H | 0.82 | 0.01 |
| 5% AC-EFB H | 0.79 | 0.05 |

The gradient of variation of fracture toughness is not high and the difference between the minimum and maximum values is only 0.5 J as against 0.9 J in case of AC K. Overall, AC-EFB H gives the lowest fracture toughness value while AC-CNS K recorded the highest value of 0.92 J. The value of 0.79 J obtained for AC-EFB H is slightly higher than neat epoxy matrix (0.78 J). The higher values obtained by the addition of 5% of filler suggests increased flexural strength of the composite. The fracture toughness results follow the same trend as quoted by Kim et al. who used carbon black filled epoxy composite[29].

## Conclusion

Epoxy nanocomposites developed by reinforcement of AC-EFB, AC-BS, and AC-CNS by hand lay-up technique. Obtained results indicated that 5% AC-CNS display higher flexural strength and modulus compared to 1% and 10% nano filler loading. Flexural strength of AC-BS, AC-EFB, and AC-CNS epoxy nanocomposites showed almost same value in case of 5% KOH activated carbon while flexural strength of KOH activated carbon based epoxy nanocomposites was higher than $H_3PO_4$ activated carbon. Flexural toughness of both the $H_3PO_4$ and KOH activated carbon reinforced composites range between 0.79–0.92 J and obtained values are higher than neat epoxy matrix (0.78 J). Overall, AC-EFB by $H_3PO_4$ gives the lowest fracture toughness value while AC-CNS by KOH recorded the highest value of 0.92 J.

## Acknowledgement

M. Jawaid and Othman Y. Alothman extend their appreciation to the Deanship of Scientific Research at King Saud University for funding this work through research group no RGP-VPP-133.

## References

1. Rahman, S. H. A., Choudhury, J. P., Ahmad, A. L. & kamaruddin, A. H. (2007). Optimization studies on acid hydrolysis of oil palm empty fruit bunch fiber for production of xylose. *Bioresource Technology*, 98(3): 554-559.
2. Umikalsom, M. S., Ariff, A. B., Zulkifli, H. S., Tong, C. C., Hassan, M. A. & Karim, M. I. A. (1997). The treatment of oil palm empty fruit bunch fibre for subsequent use as substrate for cellulase production by Chaetomium globosum Kunze. *Bioresource Technology*, 62(1-2): 1-9.
3. Qiao, W., Korai, Y., Mochida, I., Hori, Y. & Maeda, T. (2002). Preparation of an activated carbon artifact: oxidative modification of coconut shell-based carbon to improve the strength. *Carbon*, 40(3): 351-358.
4. Sekar, M., Sakthi, V. & Rengaraj, S. (2004). Kinetics and equilibrium adsorption study of lead(II) onto activated carbon prepared from coconut shell. *Journal Colloid Interface Science*, 279(2): 307-313.
5. Youssef, A. M., Radwan, N. R. E., Abdel-Gawad, I. & Singer, G. A. A. (2005). Textural properties of activated carbons from apricot stones. *Colloid Surface A: Physicochem Engineering Aspects*, 252(2-3)**:** 143-151.

6. Zhang, T., Walawender, W. P., Fan, I. T., Fan, M., Daugaard, D. & Brown, R. C. (2004). Preparation of activated carbon from forest and agricultural residues through CO2 activation. *Chemical Engineering Journal*, 105(1-2): 53-59.
7. Guo, J., Xu, W. S., Chen, Y. L. & Lua, A. C. (2004). Adsorption of NH3 onto activated carbon prepared from palm shells impregnated with H2SO4. *J ournal Colloid Interface Science*, 281(2): 285-290.
8. Ko, D. C. K., Mui, E. L. K., Lau, K. S. T. & Mckay, G. (2004). Production of activated carbons from waste tire-process design and economical analysis. *Waste Management*, 24(9): 875-888.
9. Hayashi, J., Yamamoto, N., Horikawa, T., Muroyama, K. & Gomes, V. G. (2005). Preparation and characterization of high specific surface area activated carbons from K2CO3 treated waste polyurethane. *J. Colloid Interface Sci*, 281(2): 437-443.
10. Mirmohseni, A. & Zavareh, S. (2010). Preparation and characterization of an epoxy nanocomposite toughened by a combination of thermoplastic, layered and particulate nano-fillers. *Materials & Design*, 31(6): 2699-2706.
11. Bakar, M., Kostrzewa, M., Hausnerova, B. & Sar, K. (2010). Preparation and property evaluation of nanocomposites based on polyurethane-modified epoxy/montmorillonite systems. *Advances in Polymer Technology*, 29(4): 237-248.
12. Palencia, C., Mazo, M. A., Nistal, A., Rubio, F., Rubio, J. & Oteo, J. L. (2011). Processing and properties of carbon nanofibers reinforced epoxy powder composites. *Journal of Nanoparticle Research*, 13(11), 6021-6034.
13. Abdul Khalil, H.P..S., Firoozian, P., Jawaid, M., Akil, H.M., Hassan, A. (2013a). Preparation of activated carbon filled epoxy nanocomposites: Morphological and thermal properties. *Journal of Thermal Analysis and Calorimetry*, 113(2): 623-631.
14. Abdul Khalil, H.P.S., Jawaid, M., Firoozian, P., Zainudin, E.S., Paridah, M.T. (2013b). Dynamic Mechanical Properties of Activated Carbon–Filled Epoxy Nanocomposites. *International Journal of Polymer Analysis and Characterization*, 18(4): 247-256.
15. Abdul Khalil, H.P..S., Firoozian, P., Bakare, I.O., Akil, H.M., Noor, A. M. (2010). Exploring biomass based carbon black as filler in epoxy composites: flexural and thermal properties. *Material & Design*, 31(7): 3419-3425.
16. Firoozian, P., Bhat, I.U.H., Abdul Kahlil, H.P.S., Noor, A.M., Akil, H.M., Bhat, A.H. (2011). High surface area activated carbon prepared from agricultural biomass: empty fruit bunch (EFB), bamboo stem and coconut shells by chemical activation with H3PO4. *Material Technology*, 26: 222-228.
17. Teh, P. L., Mariatti, M., Akil, H. M., Seetharamu, K. N., Wagiman, A. N. R. & Beh, K. S. (2008). Effect of Ethanol as Diluent on the Properties of Mineral Silica Filled Epoxy Composites. *Journal of Composite Materials*, 42(2): 129-142.
18. Selvin, T. P., Kuruvilla, J. & Sabu, T. (2004). Mechanical properties of titanium dioxide-filled polystyrene microcomposites. *Materials Letters*, 58(3-4): 281-289.
19. Debnath, S., Ranade, R., Wunder, S. L., Mccool, J., Boberick, K. & Baran, G. (2004). Interface effects on mechanical properties of particle-reinforced composites. *Dental Materials*, 20(7): 677-686.
20. Teh, P. L., Mariatti, M., Akil, H. M., Yeoh, C. K., Seetharamu, K. N., Wagiman, A. N. R. & Beh, K. S. 2007. The properties of epoxy resin coated silica fillers composites. *Materials Letters*, 61(11-12): 2156-2158.
21. Moodley, V. K. (2007). *The Synthesis, Structure And Properties Of Polypropylene Nanocomposites.* MSc., Durban university of technology.
22. Rothon, R. N. (2003). Particulate-Filled Polymer Composites. *In:* ROTHON, R. N. (ed.) *R.N. Rothon.* Second Edition ed. Shawbury, Shrewsbury, Shropshire, SY4 4NR, United Kingdom: Rapra Technology Limited.
23. Rashid, E. S. A., Ariffin, K.., Kooi, C. C. & Akil, H. M. (2009). Preparation and properties of POSS/epoxy composites for electronic packaging applications. *Materials & Design*, 30(1): 1-8.
24. Lee, J. H., Jang, Y. K., Hong, C. E., Kim, N. H., Li, P. & Lee, H. K. (2009). Effect of carbon fillers on properties of polymer composite bipolar plates of fuel cells. *Journal of Power Sources*, 193(2): 523-529.
25. Kuan, H.-C., Ma, C.-C. M., Chen, K. H. & Chen, S.-M. (2004). Preparation, electrical, mechanical and thermal properties of composite bipolar plate for a fuel cell. *Journal of Power Sources*, 134(1): 7-17.
26. Zhang, M., Zeng, H., Zhang, L., Lin, G. & Li, R. K. Y. (1993). Fracture characteristics of discontinuous carbon fibre-reinforced PPS and PES-C composites. *Polymers and Polymer Composites*, 1: 357-365.
27. Allaoui, A., Bai, S., Cheng, H. M. & Bai, J. B. (2002). Mechanical and electrical properties of a MWNT/epoxy composite. *Composites Science and Technology*, 62(15): 1993-1998.

28. Gojny, F. H. & Schulte, K. (2004). Functionalisation effect on the thermo-mechanical behaviour of multi-wall carbon nanotube/epoxy-composites. *Composites Science and Technology,* 64**:** 2303-2308.
29. Kim, B. C., Park, S. W. & Lee, D. G. (2008). Fracture toughness of the nano-particle reinforced epoxy composite. *Composite Structures,* 86(1-3): 69-77.

The Malaysian Journal of ANALYTICAL SCIENCES ISSN 1394-2506

# GRAFT COPOLYMERIZATION OF METHYL METHACRYLATE ONTO AGAVE CELLULOSE

## (Pengkopolimeran Cangkukan Metil Metakrilat ke atas Selulosa Agave)

Noor Afizah Rosli, Ishak Ahmad*, Ibrahim Abdullah, Farah Hannan Anuar

*School of Chemical Science and Food Technology, Faculty of Science and Technology*
*Universiti Kebangsaan Malaysia, 43600 Bangi, elangor, Malaysia*

**Corresponding author: gading@ukm.edu.my*

**Abstract**

The grafting polymerization of methyl methacrylate (MMA) and Agave cellulose was prepared and the grafting reaction conditions were optimized by varying the reaction time and temperature, and ratio of monomer to cellulose. The resulting graft copolymers were characterized by Fourier transform infrared, X-ray diffraction analysis, thermogravimetric analysis, and scanning electron microscopy (SEM). The experimental results showed that the optimal conditions were at a temperature of 45 ºC for 90 min with ratio monomer to cellulose at 1:1 (g/g). An additional peak at 1738 $cm^{-1}$ which was attributed to the C=O of ester stretching vibration of poly(methyl methacrylate), appeared in the spectrum of grafted Agave cellulose. A slight decrease of crystallinity index upon grafting was found from 0.74 to 0.68 for cellulose and grafted cellulose, respectively. Grafting of MMA onto cellulose enhanced its thermal stability and SEM observation further furnished evidence of grafting MMA onto Agave cellulose with increasing cellulose diameter and surface roughness.

**Keywords**: agave, cellulose, Graft copolymerization, methyl methacrylate

**Abstrak**

Pempolimeran cangkukan metil metakrilat (MMA) dan selulosa Agave telah disediakan dan keadaan tindak balas cangkukan dioptimumkan dengan mempelbagaikan masa dan suhu tindak balas, dan nisbah monomer kepada selulosa. Kopolimer cangkukan yang terhasil dicirikan oleh spektroskopi jelmaan Fourier inframerah (FTIR), belauan sinar-x (XRD), analisis termogravimetri, dan mikroskopi elektron pengimbasan (SEM). Keputusan eksperimen menunjukkan bahawa keadaan optimum adalah pada suhu 45°C selama 90 minit dengan nisbah monomer kepada selulosa pada 1:1 (g/g). Satu puncak tambahan pada 1738 $cm^{-1}$ yang menunjukkan kepada getaran regangan C=O daripada poli(metil metakrilat) muncul pada spektrum selulosa cangkukan. Indeks penghabluran menurun sedikit melalui cangkukan dari 0.74 ke 0.68, masing-masing bagi selulosa dan selulosa cangkukan. Cangkukan MMA ke atas selulosa meningkatkan kestabilan terma dan pemerhatian SEM melengkapkan lagi bukti cangkukan MMA ke atas selulosa dengan peningkatan diameter dan permukaan kasar selulosa.

**Kata kunci:** agave, selulosa, Pengkopolimeran cangkukan, metil metakrilat

## Introduction

Cellulose is a unique polymeric material which is the most abundant on earth. It possesses several good properties such as a fine cross-section, high durability and thermal stability, good biocompatibility, and good mechanical properties. Cellulose is a semicrystalline polysaccharide with a large number of hydroxyl groups. It is generated from repeating β-D-anhydroglucopyranose units that are covalently joined together through acetal functions between the equatorial group of the C4 and C1 carbon atom [1]. The sensitivity of the β-1,4-glycosidic linkages between the glucose repeating units towards hydrolytic attack determined the chemical stability of the cellulose molecule [1]. Agave angustifolia is a promising reinforcement element for polymer composites because of its high cellulose content (67%) [2]. However, there are some limitations in cellulose applications due to its poor solubility in common solvent, poor dimensional stability, lack of thermoplasticity, and high hydrophilicity [3]. To overcome these major drawbacks, physical and chemical modification such as graft copolymerization of the cellulose structure is necessary.

Graft copolymerization permits one to combine the best properties of two or more polymers by taking advantages of synergy effects of the graft copolymer. It can be classified into three major groups: (i) free radical polymerization, (ii) ionic and ring opening polymerization, and (iii) living radical polymerization. Among these three methods, free radical polymerization has received greatest amount attention due to its many characteristics, such as mild reaction conditions, wide temperature range, simple to implement and inexpensive [3]. The grafting of MMA onto natural polymers like *Saccharum spontaneum L.* fiber [4], wood fiber [5], etc. with different redox systems has been reported. However, no work has been directed towards grafting of MMA monomer onto cellulose isolated from Agave angustifolia.

Keeping the view to promote an ecologic through value added application, cellulose was isolated from the Agave angustifolia fibre followed by grafting of MMA onto cellulose to develop a commercially viable product. The work of graft copolymerization of MMA onto cellulose was investigated in the presence of ceric ammonium nitrate as redox initiator with a view that grafted cellulose may find better applications than native cellulose.

## Materials and Methods

### Materials

Agave leaves used in this study were harvested in Kajang, Selangor (Malaysia). The chemical reagents used were sodium chlorite ($NaClO_2$), and nitric acid from Sigma-Aldrich, acetic acid glacial (99%), acetone, methanol, and sodium hydroxide (NaOH) purchased from Systerm and ceric ammonium nitrate (CAN) from E. Merck. All of these chemical reagents were used without further purification. Methyl methacrylate (MMA) (stabilised) for synthesis was purchased from E. Merck. The MMA was passed through a column of basic alumina oxide ($Al_2O_3$) to remove the stabilizer.

### Extraction of cellulose

The ground Agave fibres were treated with 4% NaOH at 70 to 80 ºC for two hours, after which bleaching treatment was carried out using 1.7 w/v% $NaClO_2$ at 70 to 80 ºC for four hours. The ratio of the fibres to liquor was 1:25 (g/mL). Each fibre treatment was done twice and the fibres were washed with distilled water after each treatment.

### Graft copolymerization

The grafting reaction was carried out under nitrogen atmosphere in 250 ml three-necked flask equipped with a reflux condenser, dropping funnel and a gas inlet system immersed in a water bath. 1 g of cellulose was dispersed in a 50 ml of water with constant stirring and bubbling of nitrogen for one hour at 45 ºC. Then, a freshly prepared 10 ml solution of CAN ($0.91 \times 10^{-3}$ mol) in nitric acid 0.3 N was added and stirred for 15 min. MMA monomer was added gradually over a period of 30 min and the mixture was stirred for a further 90 min. The ratio of cellulose to monomer was kept constant to 1:1 (g/g). After the reaction, the grafted cellulose was washed with 750 ml of distilled water followed by 250 ml of methanol and dried to a constant weight in an oven at 40 ºC. The dried product was extracted with acetone in a Soxhlet apparatus to remove the homopolymer. The suspension was filtered and the filtrate was washed with acetone and dried to a constant weight. The grafting reaction conditions were optimized by varying the reaction time, temperature, and monomer to cellulose ratios.

The grafting efficiency is defined as the ratio between the amounts of grafted monomer and the total polymerized monomer [6].

### Infrared (IR) spectral analysis

The Fourier transform infrared (FTIR) spectra of the cellulose and grafted cellulose were recorded on a Perkin-Elmer spectrometer (SpectrumGX) in the range of 500-4000 $cm^{-1}$ with a scanning resolution of 1 $cm^{-1}$. The cellulose and grafted cellulose were ground into powder, mixed with KBr, and pressed into an ultra-thin pellet.

### X-ray diffraction study

X-ray diffraction (XRD) analyses were performed with a Bruker AXS D8 Advance diffractometer at 40 kV, 40 mA with Cu-Kα radiation ( $\lambda$=0.1541 nm). The data were acquired in a 2θ range from 10 to 60º. The percent crystallinity was calculated using the following equation 1 [7].

$$\% \text{ Cr} = \frac{I_{002}}{I_{002} + I_{am}} \quad (1)$$

where $I_{002}$ is the maximum intensity of diffraction of the (002) lattice peak between 22º to 23º, and $I_{am}$ the intensity of diffraction of the amorphous material between 18º to 19º where the intensity is minimum.

**Thermogravimetric analysis**

A Mettler Toledo model TGA/SDTA851e thermogravimetric analyzer was used to characterize the thermal stability of the cellulose and grafted cellulose. Approximately 2 to 12 mg of each sample was heated from 30 ºC to 600 ºC at a heating rate of 10 ºC/min. All the measurement was performed under nitrogen atmosphere.

**Scanning electron microscopy**

The scanning electron microscopy (SEM) micrographs of the cellulose and grafted cellulose were recorded on a Leo 1450VP microscope at a voltage of 15 kV. The samples were coated with gold to avoid charging.

## Results and Discussion

**Effects of reaction time**

Figure 1 shows the results of grafting MMA onto cellulose as a function of time. It can be seen that the percent grafting efficiency (%GE) increases with increase reaction time up to 90 min. Increase in the %GE with time is due to more contact time of the monomer molecules with the cellulose macroradical sites. Depletion of monomer concentration with the progress of reaction explained in the decrement of %GE after 90 min.

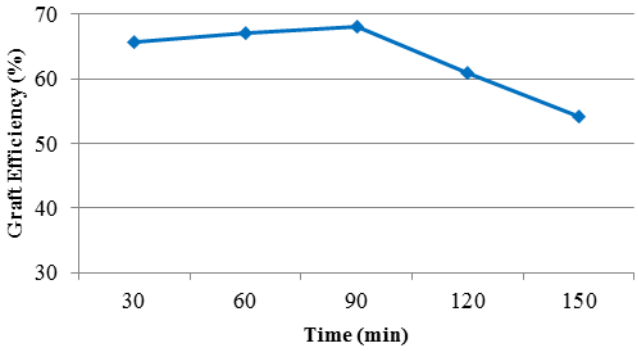



Figure 1. The effect of time on the percentage of graft efficiency of the grafting polymerization of 1:1 (MMA:cellulose) at 45 °C

**Effects of temperature**

Figure 2 shows the results of graft copolymerization of MMA onto cellulose as a function of temperature. The %GE increases with the initial increased in temperature, reaches the optimum at 45ºC, and then decreases with further increased in temperature. As the kinetic energy of the molecules increases with temperature, more radicals drifted at faster rate onto the cellulose backbone, hence, increase in the %GE. Further increase in temperature leads to termination processes and thermally initiate the monomer resulted in the formation of a homopolymer, thereby decreasing the %GE.

**Effects of monomer to cellulose ratios**

Figure 3 shows the effect of monomer:cellulose ratios on the %GE. The %GE decrease with increase monomer to cellulose ratios. The %GE decrease with increasing the MMA to cellulose ratios is due to the formation of homopolymer over the cellulose macroradicals [8]. The formation of homopolymer at high MMA to cellulose ratios is due to formation of a three-component complex which comprise of a substrate, monomer, and water. These three-

component complex rearranges to provide a requisite free radical site with liberation of atomic hydrogen and thus initiates the homopolymerisation.

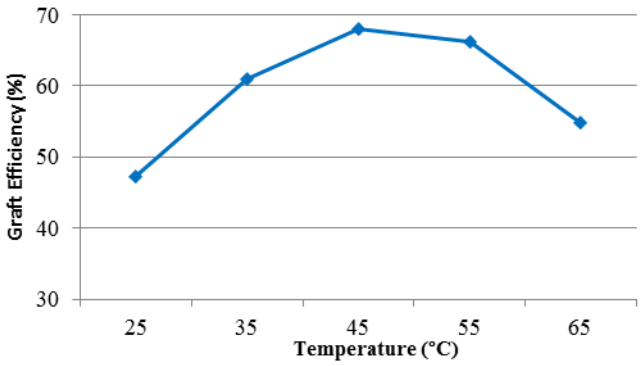



Figure 2. The effect of temperature on the percentage of graft efficiency of the grafting polymerization of 1:1 (MMA:cellulose) for 90 min

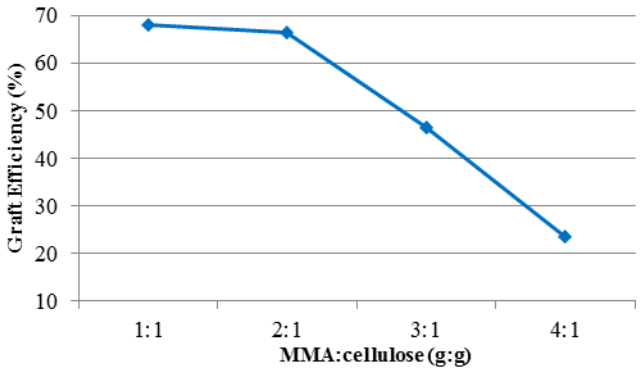



Figure 3. The effect of MMA:cellulose ratios on the percentage of graft efficiency of the grafting polymerization at 45 °C for 90 min

**Infrared spectroscopy analysis**

The FTIR spectroscopy analysis of the cellulose and grafted cellulose are shown in Figure 4. It reveals that compositional changes occurred upon grafting. Both of the spectra exhibited a broad band in the region 3400-3300 $cm^{-1}$ which indicates the free O-H stretching vibration of the OH group. Moreover, the vibration peak detected at 2910 $cm^{-1}$ in both samples is related to stretching vibration of C-H. In addition, both of the spectra showed the characteristic of C-H and C-O bending vibration bond in the polysaccharide aromatic rings around 1360-1375 $cm^{-1}$. An additional peak at 1732 $cm^{-1}$ was observed in the grafted cellulose spectra. This peak is attributed to the stretching vibrations of C=O of the PMMA chains. Furthermore, there is another one characteristic peaks of PMMA in the grafted cellulose spectra which appeared at 843 $cm^{-1}$. This peak is attributed to the C-O-C bending vibration of PMMA. Note that the absorbance peak at 1640 $cm^{-1}$ was slightly decreased for the grafted cellulose spectra. This peak is attributed to the O-H bending of the absorbed water [9]. Improved of hydrophobicity with grafting leads to reduce the amount of absorbed water.

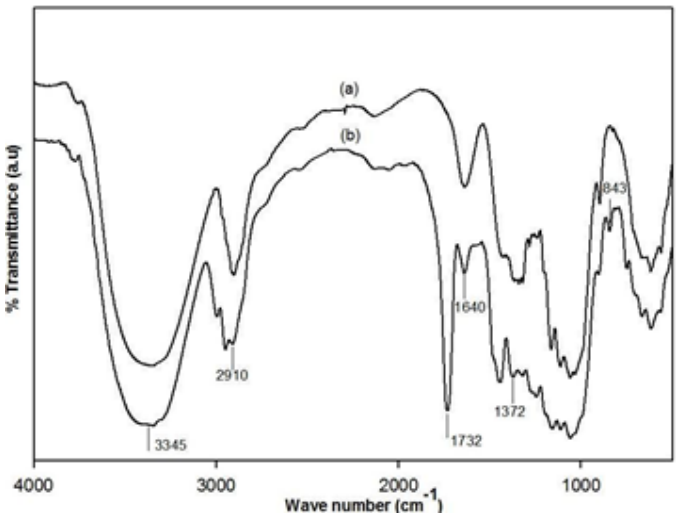



Figure 4. FTIR spectra of (a) cellulose, and (b) cellulose-g-PMMA

**X-ray diffraction study**

Figure 5 shows X-ray diffraction patterns of cellulose and grafted cellulose. The crystallinity of Agave cellulose and grafted cellulose were determined to see the changes in the fine structure of cellulose as a results of grafting MMA onto the cellulose backbone. The result in Table 1 clearly showed that the percent crystallinity slightly decreased upon grafting from 80.14% to 75.48% for cellulose and grafted cellulose, respectively. Crystallinity decrease with grafting, indicates that the grafted chain occurred in the ordered and amorphous region of cellulose [10].

Table 1. Percent crystallinity of cellulose and cell-g-PMMA

| Sample | % Crystallinity |
|---|---|
| Cellulose | 80.14 |
| Cellulose-g-PMMA | 75.48 |

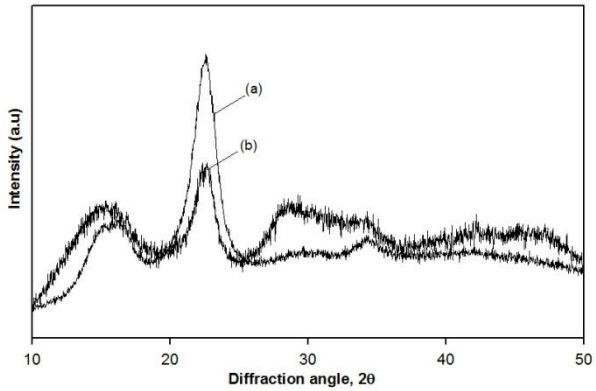



Figure 5. X-ray diffraction patterns for (a) cellulose, and (b) cellulose-g-PMMA

**Thermogravimetric analysis**

Figure 6 shows the thermal behaviour of cellulose and grafted cellulose as a function of % weight loss with temperature. Cellulose samples shows two degradation steps related to: (i) moisture evaporation, and (ii) cellulose degradation while grafted cellulose only shows one degradation step which related to cellulose degradation. The absence of the first step in grafted cellulose is due to the improved hydrophobicity on the grafted cellulose. The second step decomposition of the cellulose (260 to 370 °C) shifts to higher temperature in comparison with the grafted cellulose (289 to 416 °C). The shift can be explained by assuming that the presence of PMMA improved the thermal stability. At the end of the test at 600°C, the residue of 13, and 8 wt% of the original mass remains for the cellulose, and grafted cellulose, respectively.

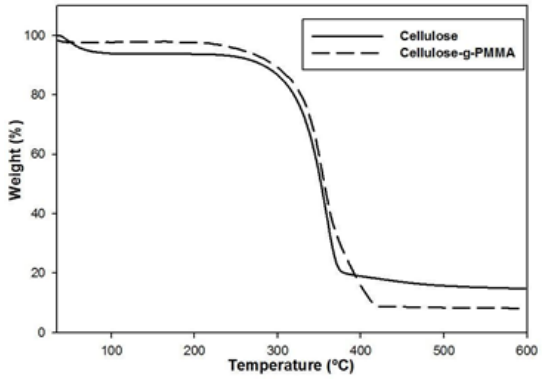



Figure 6. TGA thermograms of cellulose, and cellulose-g-PMMA

**Morphological analysis**

The evidence of grafting on the surface morphology was examined with SEM. Microscopic examinations on the cellulose and grafted cellulose were depicted in Figures 7(a) and 7(b), respectively. The cellulose appears completely fibrous. The cellulose surface was very smooth and covered with the thin PMMA layer as seen in grafted cellulose micrograph. The diameter also increased from 5.8 ± 1.2 µm to 8.9 ± 0.6 µm for cellulose and grafted cellulose, respectively.

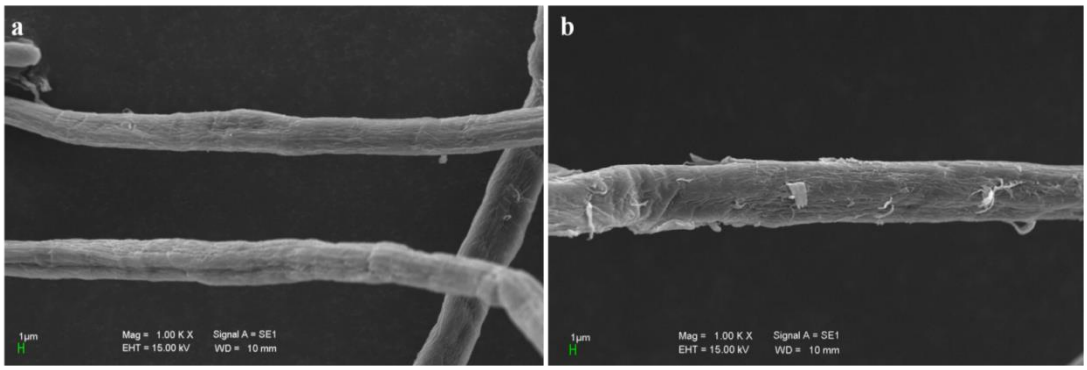



Figure 7. SEM micrographs of (a) cellulose, and (b) cellulose-g-PMMA

## Conclusion

The graft copolymerization of PMMA onto Agave cellulose was successfully carried out using CAN as redox initiator. The optimized conditions for grafting obtained are as follows: MMA:cellulose ratio, 1:1 (g/g); reaction time, 90 min; temperature of 45 ºC. The characterization of the grafted cellulose by means of FTIR , and SEM elucidated the structure changes in comparison with the ungrafted cellulose. Although the crystallinity and crystallinity index decreased, the incorporation of PMMA chains onto the cellulose backbone slightly improved the thermal stability of grafted cellulose.

## Acknowledgement

This work was supported by research grants from the Ministry of Higher Education (MOHE) and Universiti Kebangsaan Malaysia under research grant ERGS/1/2012/STG01/UKM/02/4. The authors would also like to thank Dr. Md. Akhir Hamid from Malaysian Agriculture Research & Development Institute (MARDI) for the processing of raw Agave fibres.

## References

1. Krassig, H.A. Cellulose and Its Derivatives: Chemistry, Biochemistry and Applications. Kennedy, J. pg 3 – 25.
2. Rosli, N. A., Ahmad, I., & Abdullah, I. (2013). Isolation and characterization of cellulose nanocrystals from Agave angustifolia fibre. *Bioresources*, 8 (2): 1893–1908.
3. Roy, D., Semsarilar, M., Guthrie, J.T., & Perrier, S. (2009). Cellulose Modification by Polymer Grafting: A Review. *Chemical Society Reviews*, 38: 2046-2064.
4. Kaith, B.S., Jindal, R., & Maiti, M. (2009). Induction of Chemical and Moisture Resistance in Saccharum spontaneum L Fiber through Graft Copolymerization with Methyl Methacrylate and Study of Morphological Changes. *Journal of Applied Polymer Science*, 113 (3): 1781-1791.
5. Román-Aguirre, M., Márquez-Lucero, A., & Zaragoza-Contreras, A. (2004). Elucidating the graft copolymerization of methyl methacrylate onto wood-fiber. *Carbohydrate Polymers* 55 (2): 201-210.
6. Princi, E., Vicini, S., Pedemonte, E., Mulas, A., Franceschi, E., Luciano, G., & Trefiletti, V. (2005). Thermal Analysis and Characterisation of Cellulose Grafted with Acrylic Monomers. *Thermochimica Act*, 42 (1-2): 173-179.
7. Mwaikambo, L.Y., & Ansell, M.P. (2002). Chemical Modification of Hemp, Sisal, Jute, and Kapok Fibres by Alkalization. *Journal of Applied Polymer Science*, 84 (12): 2222–2234.
8. Kumar, V., Naithani, S., & Pandey, D. (2011). Optimization of Reaction Conditions for Grafting of α-Cellulose Isolated from Lantana camara with Acrylamide. *Carbohydrate Polymers*, 8 (2): 760–768.
9. Troedec, M., Sedan, D., Peyratout, C., Bonnet, J., Smith, A., & Guinebretiere, R. (2008). Influence of Various Chemical Treatments on The Composition and Structure of Hemp Fibres. *Composites Part A-Applied Science and Manufacturing*, 39 (3): 514-522.
10. Jain, V., Xiao, H., & Ni, Y. (2007). Grafting of Poly(methyl acrylate) onto Sulfite Pulp Fibers and Its Effect on Water Absorbance. *Journal of Applied Polymer Science* 105 (6): 3195-3203.

The Malaysian Journal of ANALYTICAL SCIENCES ISSN 1394-2506

# EFFECT OF REAGENTS CONCENTRATION AND RATIO ON DEGRADATION OF NATURAL RUBBER LATEX IN ACIDIC MEDIUM

## (Kesan Kepekatan dan Nisbah Reagen ke Atas Pendegradasian Lateks Getah Asli dalam Media Berasid)

Suhawati Ibrahim*, Asrul Mustafa

*Fine Chemicals and Biomaterials Programme,*
*Bahagian Teknologi dan Kejuruteraan,*
*Lembaga Getah Malaysia, 47000 Sungai Buloh, Selangor, Malaysia*

**Corresponding author: suhawati@lgm.gov.my*

**Abstract**

The molecular weight of natural rubber (NR) was reduced via degradation to liquid natural rubber (LNR) using hydrogen peroxide and sodium nitrite as reagents in latex solution. In this study, the reaction was carried out in an acidic medium at 70$^{o}$C at various ratio and concentration of reagents. Results showed that the properties of degraded product i.e. LNR depends on the concentration and ratio of the reagents added into reaction mixtures. Increasing the concentration of hydrogen peroxide and sodium nitrite as reagents at 1 to 1 ratio efficiently reduced the molecular weight of LNR, but the gel content increased when reagents were added more than 0.2 mol. Hydrogen peroxide was found to have greater effect on degradation reaction compared to sodium nitrite when excessive amount of hydrogen peroxide showed further reduction in molecular weight of LNR. The degradation reaction also resulted in the formation of certain functional groups such as hydroxyl and carbonyl as shown from spectroscopy microstructure analysis.

**Keywords:** Liquid natural rubber (LNR), OH radical, redox reaction

**Abstrak**

Berat molekul getah asli (NR) telah diturunkan secara pendegradasian kepada getah asli cecair (LNR) menggunakan hidrogen peroksida dan natrium nitrit sebagai reagen-reagen dalam lateks. Dalam kajian ini, tindak balas dilakukan dalam media berasid pada suhu 70$^{o}$C pada nisbah dan kepekatan reagen yang berbeza. Keputusan menunjukkan bahawa sifat hasil pendegradasian iaitu LNR bergantung kepada kepekatan dan nisbah reagen yang digunakan semasa tindak balas. Penambahan kepekatan reagen pada nisbah 1:1 menurunkan berat molekul LNR dengan berkesan, tetapi kandungan gel meningkat bila kepekatan reagen lebih dari 0.2 mol digunakan. Hidrogen peroksida didapati memberikan pengaruh yang lebih besar ke atas tindak balas pendegradasian berbanding natrium nitrit bila berat molekul LNR terus menunjukkan penurunan bila jumlah berlebihan digunakan. Tindak balas pendegradasian juga menghasilkan kumpulan berfungsi yang tertentu seperti hidroksi dan karbonil seperti ditunjukkan dari analisa spektroskopi.

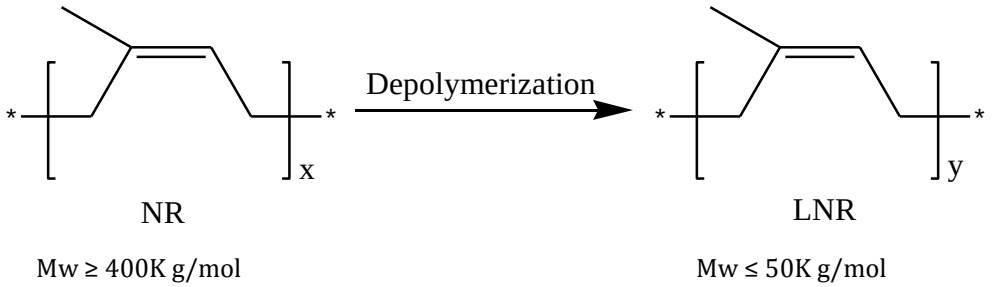
**Kata kunci:** Getah asli cecair (LNR), radikal OH, tindak balas redoks

## Introduction

Degraded natural rubber (NR) in the form of liquid namely liquid natural rubber (LNR) can be considered as a type of oligomer (Scheme 1). Functionalized oligomer having certain functional groups are attracting interests as they can be used in various applications such as surface coating [1], adhesives [2, 3], compatibilizer [4-7] and precursor to synthesize advanced materials [8-13].

In NR degradation, the rubber chains are cleaved and the chain length is reduced, hence leaving different end groups depending on the methods used. This end groups mostly are reactive groups such as carbonyl [14], hydroxyl [15], phenylhydrazone [16] etc. Ravindran [15] reported a novel route in preparing hydroxyl telechelic liquid natural

rubber (HTLNR) using photochemical degradation process. This toluene-based reaction later was used by some workers in their works to produce LNR as soft segment in polyurethane [17-19].




Scheme 1. Degradation of NR to LNR.

LNR can be obtained from various methods of degradation of NR either using mechanical, chemical or photodegradation. The degradation reaction is feasible in solution such as toluene [14], yielding degraded rubber with low molecular weight (MW) and narrow molecular weight distribution (MWD). Due to environmental concern, degradation of NR in latex state has been explored and developed. The degradations of NR latex were successfully carried out using chemicals such as phenylhydrazine/ferrous chloride [20] phenylhydrazine/oxygen [16], peroxide/metal nitrite or chlorite [21], periodic acid [22], kalium persulfat/propanal [23], ammonium persulfate/propanal and ozone/hydrogen peroxide [24].

In our recent work, it is found that LNR with hydroxyl and carbonyl functionalities can be prepared via degradation reaction using hydrogen peroxide and sodium nitrite in an acidic medium [25]. Determination of LNR structure and possible routes of reactions in NR degradation is important in order to have a better control on the product properties and also for further modifications of the LNR produced. This paper discusses the effect of concentration and ratio of the reagents on the chemical structure of LNR.

## Materials and Methods

### Materials

Latex used in this study was low ammonia NR latex (LATZ) (Mn 657 kDa, MWD 7.8) supplied by Lee Rubber. The ammonia of latex was removed by stirring the latex at room temperature for at least 3 hours. Hydrogen peroxide (30%), sodium nitrite, methanol, sodium dodecyl sulfate (emulsifier), tetrahydroforun (THF), $CDCl_3$ and formic acid were purchased from Merck, USA and used as received.

### Degradation of NR latex

Firstly, dilution with emulsifier and water at judicious amount was carried to prepare NR latex with 20% of dry rubber content (DRC). The NR latex was then stirred continuously until a homogeneous mixture is obtained. The NR latex mixture was further acidified with formic acid to achieve the required pH for reaction. The solution was poured into a five necked reaction flask equipped with an overhead stirrer, condenser and thermometer. Hydrogen peroxide and sodium nitrite were added simultaneously into the solution at temperature of 70$^{o}$C. The reaction was then allowed to occur for 8 hours. The degraded natural rubber or LNR obtained was coagulated and washed with methanol, then dried in a vacuum oven at 60$^{o}$C. Further purification by dissolving LNR in toluene and re-precipitated in methanol followed by drying until a constant weight was achieved.

### Characterizations

Fourier Transform Infrared (FTIR) spectrum was recorded on Thermo Nicolet 6700 spectrometer using attenuated total reflection (ATR) accessory at a wave number range of 4000 to 500 $cm^{-1}$. The $^{1}H$ NMR was measured using Bruker 500 Hz using deuterated chloroform as solvent. Tetramethyl silane (TMS) was used as the internal standard for zero axis calibration. Number average molecular weight of the LNR was determined using Viscotex multi-

detector Gel Permeation Chromatography (GPC) using THF as a solvent and also as an eluent. The molecular weight was determined from an internal standardized molecular weights curve which was prior obtained using polyisoprene molecular weights standard.

## Results and Discussion

It is known that the concentration of chemicals involved in a reaction is one of main factors affecting the final result or reaction yield. In a degradation reaction, the concentration of reagents used will determine the degree of reaction to a certain extend. In this work, hydrogen peroxide and sodium nitrite were used to degrade the NR chain. Both reagents were varied in their concentration ranging from 0.1 mol to 0.4 mol at different ratios. The LNR samples obtained were examined for their molecular weight and chemical structure.

The molecular weight of the LNR samples prepared is tabulated in Table 1. Degradation of NR was observed where the molecular weight of the NR was reduced from 657 $\times 10^3$ g/mol to less than $10^4$ g/mol. At the ratio of 1:1 hydrogen peroxide to sodium nitrite, greater degradation was found to occur at higher reagents concentration where Mn was reduced from 64.64 $\times 10^3$ g/mol to 24.13$\times 10^3$ g/mol when the concentrations of reagents increased from 0.1 mol to 0.4 mol. However, polydispersity of all samples were not markedly changed or influenced by the increasing of concentrations of reagents. The gel content of LNR samples prepared at the concentration 0.1 and 0.2 mol reagents were found to be very low and slightly increased when the concentration of reagents increased. This suggested that the presence of side reaction or crosslink is most possible to occur at higher reagent concentrations.

When the concentration of hydrogen peroxide was fixed at 0.2 mol, the LNR sampels prepared with varying concentrations of sodium nitrite revealed that the lowest Mn was obtained when 0.2 and 0.3 mol of the sodium nitrite was used, but 0.3 mol exhibited higher polydispersity. The result suggested that both reagents are required in an equal concentration to perform the degradation reaction effectively. Excessive amount of sodium nitrite slightly increased the Mn and polydispersity of LNR, probably due to an interference of reagent during chain breaking reaction.

Alternatively, when sodium nitrite was fixed at 0.2 mol, increasing the concentrations of the hydrogen peroxide slightly reduced the Mn of LNRs obtained.

Table 1. Mn, Mw and polydispersity of LNRs

| **Reagents concentration (mol)** | | **Mn $\times 10^3$ (g/mol)** | **Mw $\times 10^3$ (g/mol)** | **Polydispersity** | **Gel content (%)** |
|---|---|---|---|---|---|
| **$H_2O_2$** | **$NaNO_2$** | | | | |
| NR latex (Control) | | 657.00 | 5120 | 7.800 | 11.73 |
| 0.1 | 0.1 | 64.64 | 168.00 | 2.606 | 0.05 |
| 0.2 | 0.2 | 36.77 | 81.45 | 2.215 | 0.01 |
| 0.3 | 0.3 | 34.31 | 89.27 | 2.602 | 0.79 |
| 0.4 | 0.4 | 24.13 | 57.35 | 2.376 | 3.75 |
| 0.2 | 0.1 | 56.41 | 160.00 | 2.836 | - |
| 0.2 | 0.3 | 35.43 | 112.67 | 3.180 | - |
| 0.2 | 0.4 | 44.56 | 139.50 | 2.933 | - |
| 0.1 | 0.2 | 62.12 | 166.10 | 2.674 | - |
| 0.3 | 0.2 | 35.90 | 101.85 | 2.837 | - |
| 0.4 | 0.2 | 30.62 | 74.13 | 2.422 | - |

Figure 1 shows the $^{1}$H-NMR spectra of LNRs prepared at 1:1 ratio of hydrogen peroxide and sodium nitrite with the concentrations ranging from 0.1 to 0.4 mol. The spectra obtained showed similar pattern to that of NR spectrum except a small peak appeared at $\delta$=3.75 ppm. This peak corresponds to the proton of α carbon and was used as an indication of the presence of hydroxyl groups on LNR chains [11, 26, 27]. However, no proton peak for the hydroxyl group itself was observed. This may due to highly variable chemical shift of the protons of the hydroxyl group as they rapidly exchanges and their position depends largely on concentration, solvent and temperature [28]. The intensity of this peak increased as the concentration of hydrogen peroxide and sodium nitrite increased from 0.1 to 0.3 mol reflected the increase in the amount of hydroxyl group produced in the reaction. However, a reduction in peak intensity was observed for further increment of hydrogen peroxide and sodium nitrite at 0.4 mol.

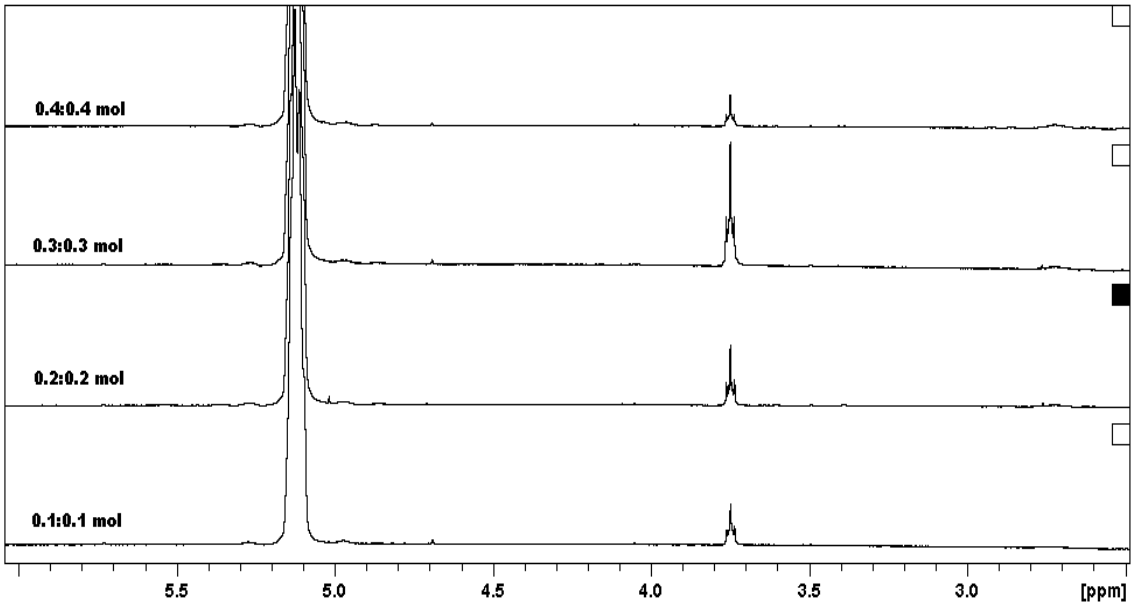



Figure 1. $^{1}$H-NMR spectra of LNRs prepared at same ratio of hydrogen peroxide and sodium nitrite

Figure 2 illustrates $^{1}$H NMR spectra of LNRs prepared at 0.1, 0.2, 0.3 and 0.4 mol of sodium nitrite to a fixed 0.2 mol of hydrogen peroxide. It is noticed that methylene proton of adjacent carbon of hydroxyl group appeared at chemical shift $\delta$=3.75 ppm for all LNR samples. The $^{1}$H NMR spectra for LNR samples prepared at various concentrations of hydrogen peroxide with a fixed concentration of sodium nitrite of 0.2 mol are shown in Figure 3. Very weak peak at 3.75 ppm was observed when hydrogen peroxide concentration exceeded 0.2 mol and was not observable when the level reached 0.4 mol. Any presence of aldehyde peak at 9-10 ppm was not observed. This may due to very low amount or the carbonyl groups observed in the FTIR spectrum are attributed to ketone.

The presence of OH groups on the LNR chain was confirmed by $^{13}$C NMR spectrum as shown in Figure 4. There are two small peaks located at chemical shifts 69.79 ppm and 74.98 ppm corresponded to the methylene and methine carbons of hydroxyl groups respectively.

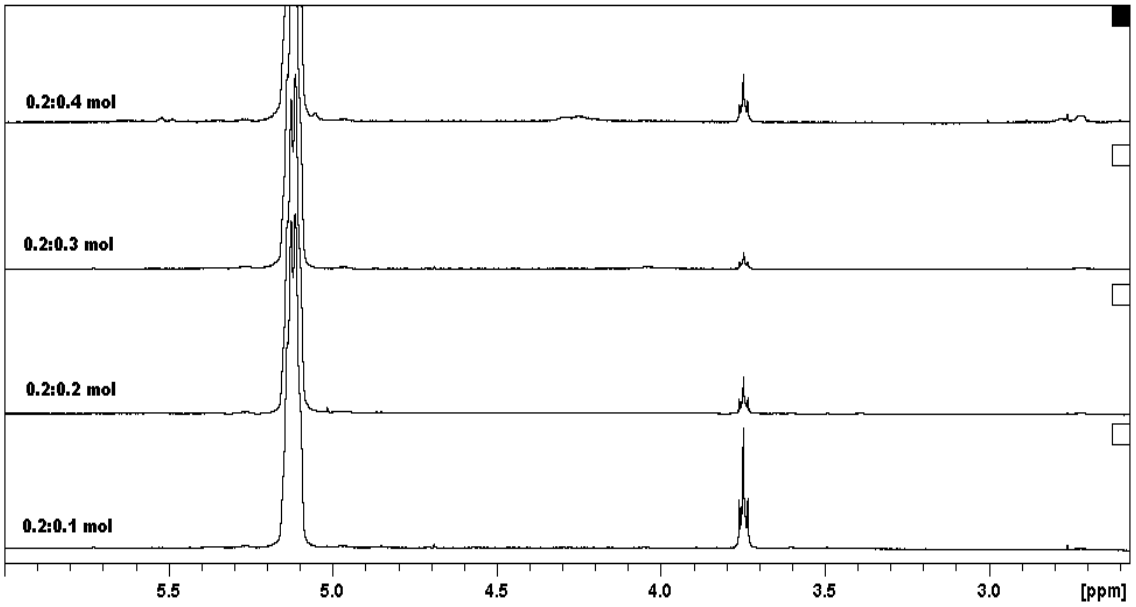



Figure 2. $^{1}$H NMR spectra of LNRs prepared at 0.2 mol of hydrogen peroxide and various concentration of sodium nitrite

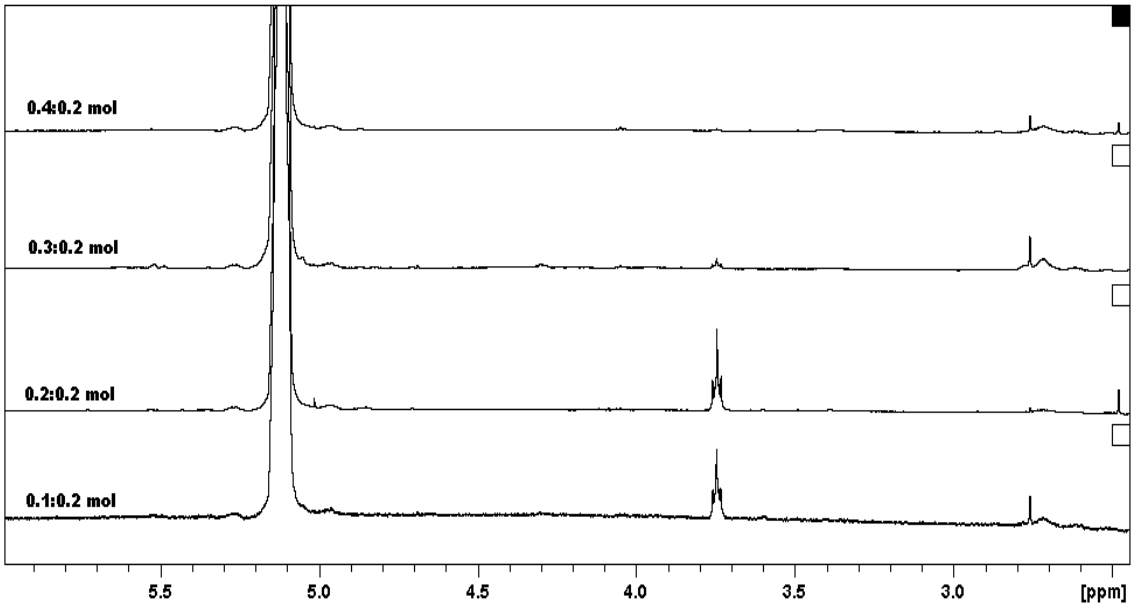



Figure 3. $^{1}$H NMR spectra of LNRs prepared at various concentration of hydrogen peroxide and 0.2 mol of sodium nitrite

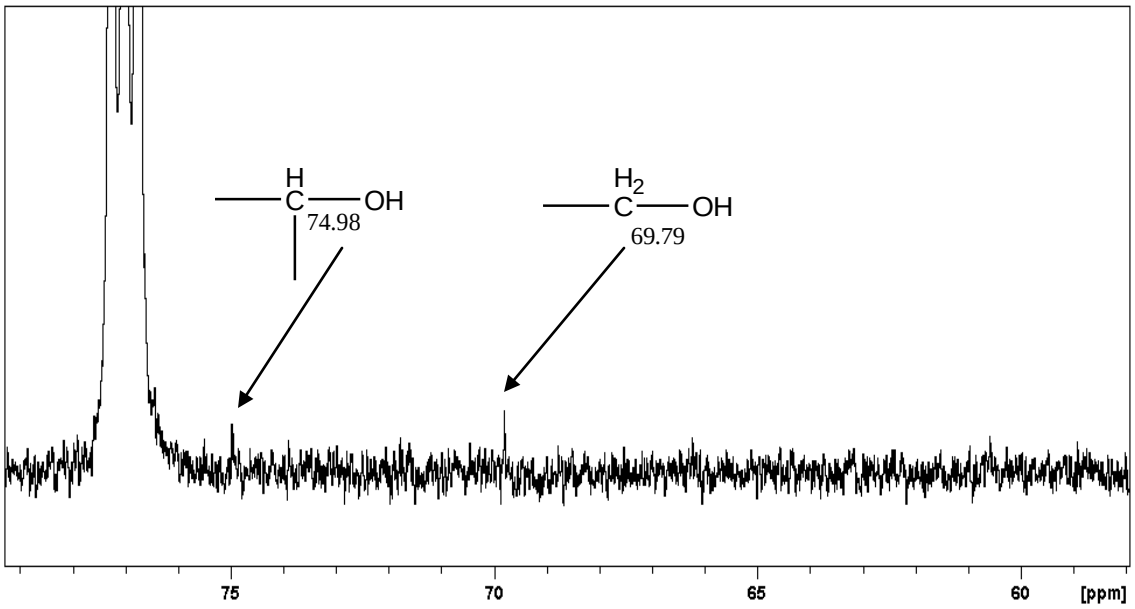



Figure 4. $^{13}$C NMR spectrum of LNR prepared with 0.2:0.2 mol reagents

The microstructure of LNR samples obtained was determined using FTIR. The spectra of LNR samples showed similar pattern to that of NR spectrum, but with few different peaks and intensity (Figure 5). The absorption peaks of C=C bond, C-C bond and =C-H at 1667, 1446 and 835cm$^{-1}$ respectively were found to decrease when NR was degraded to LNR. The presence of other groups on the LNR chains can be attributed to the appearance of carbonyl peak at 1720 cm$^{-1}$ and a broad peak at 3400 cm$^{-1}$ for O-H groups. Similar observation was seen in the NMR analysis as mentioned in the earlier section.

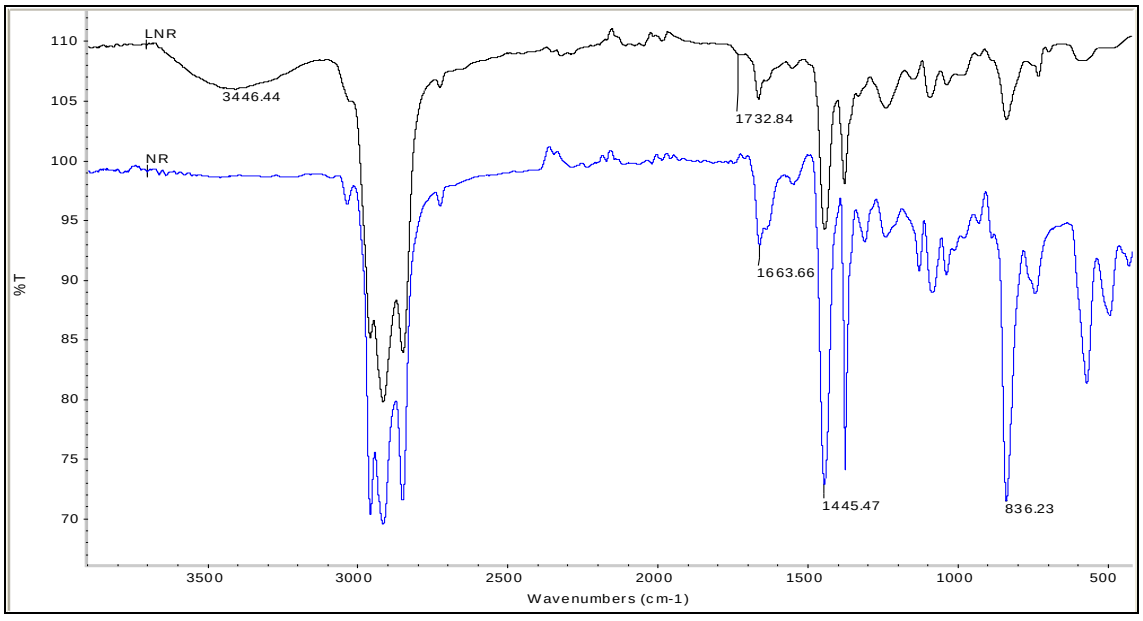



Figure 5. IR spectra of NR and LNR

Figure 6 shows the spectra of LNR samples prepared at reagents ratio of 1:1. The intensity of the broad peak at 3400 $cm^{-1}$ was the highest when reagents concentration used was at 0.2 mol. The peak intensity then decreased with increasing reagents concentrations. The decrease of the peak intensity is compromised by an increase in carbonyl peak at 1720 $cm^{-1}$.

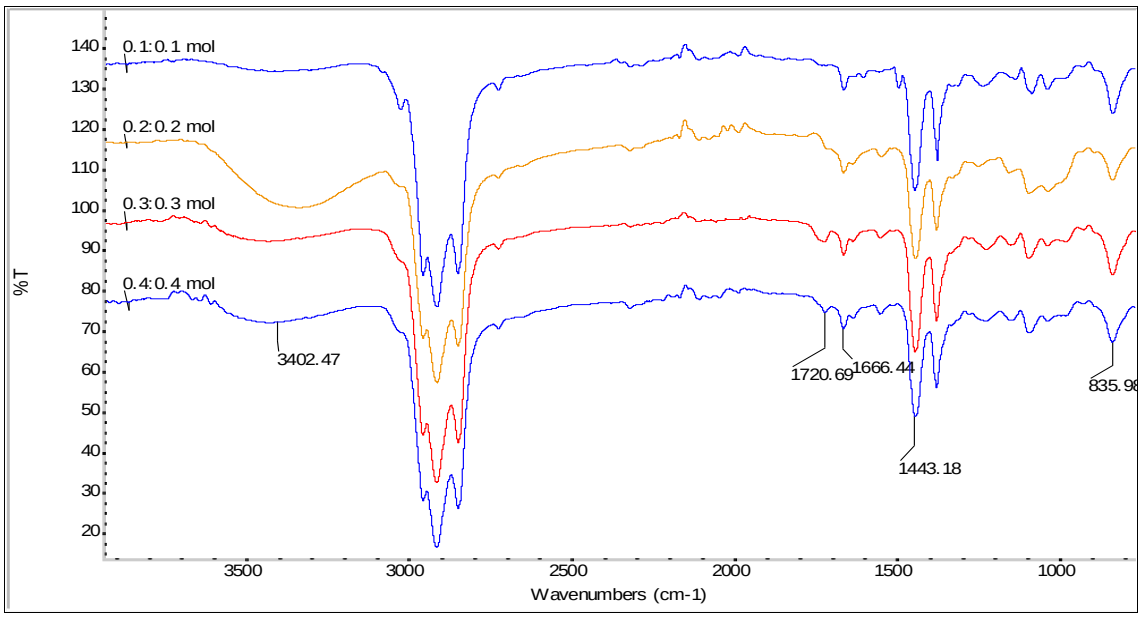



Figure 6. IR spectra of LNRs prepared at same ratio of hydrogen peroxide and sodium nitrite

IR spectra of LNR samples prepared at various concentrations of sodium nitrite to a fixed amount of 0.2 mol hydrogen peroxide are shown in Figure 7. When sodium nitrite concentration was less than hydrogen peroxide (0.1 mol of sodium nitrite to 0.2 mol of hydrogen peroxide), the intensity of 3400 $cm^{-1}$ broad peak that indicates hydroxyl group is negligible, but increased considerably when both the reagents were of same concentration (0.2 mol of sodium nitrite to 0.2 mol of hydrogen peroxide). This peak remained when the concentration of sodium nitrite was further increased to 0.3 and 0.4 mol. At the same time, no significant change was observed for carbonyl groups as the intensity of peak at 1715 $cm^{-1}$ remains unchanged.

The LNR samples prepared at various concentrations of hydrogen peroxide with a fixed amount of 0.2 mol sodium nitrite is shown in Figure 8. It was found that the intensity of peak at 1715 $cm^{-1}$ that corresponded to carbonyl groups, which increased when the concentration of hydrogen peroxide was higher than sodium nitrite.

Radical initiated reaction in NR modification causes by radical species leading to chain rupture can be contributed by unbalanced structure and weakened $CH_2$-$CH_2$ bond, [15]. This is also induced by the steric hindrance occurring at *cis* position of NR chain. The C=C in the chain is a nucleophilic site which becomes favorable for cleavage by redox reaction. Thus, the reduction of C=C and C-C bonds as shown in FTIR spectrum of LNR indicated that the degradation of NR had occurred at both C=C and C-C bonds and suggested the possibility that more than one cleavage sites occurred concurrently in the degradation reaction.

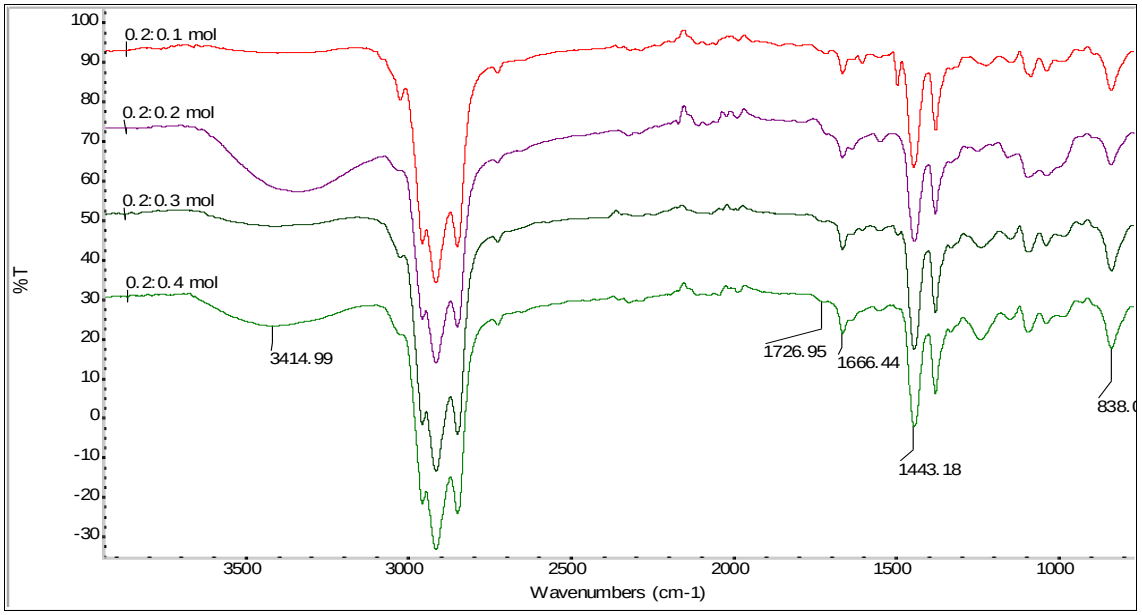



Figure 7. IR spectra of LNRs prepared at various concentration of sodium nitrite and 0.2 mol hydrogen peroxide

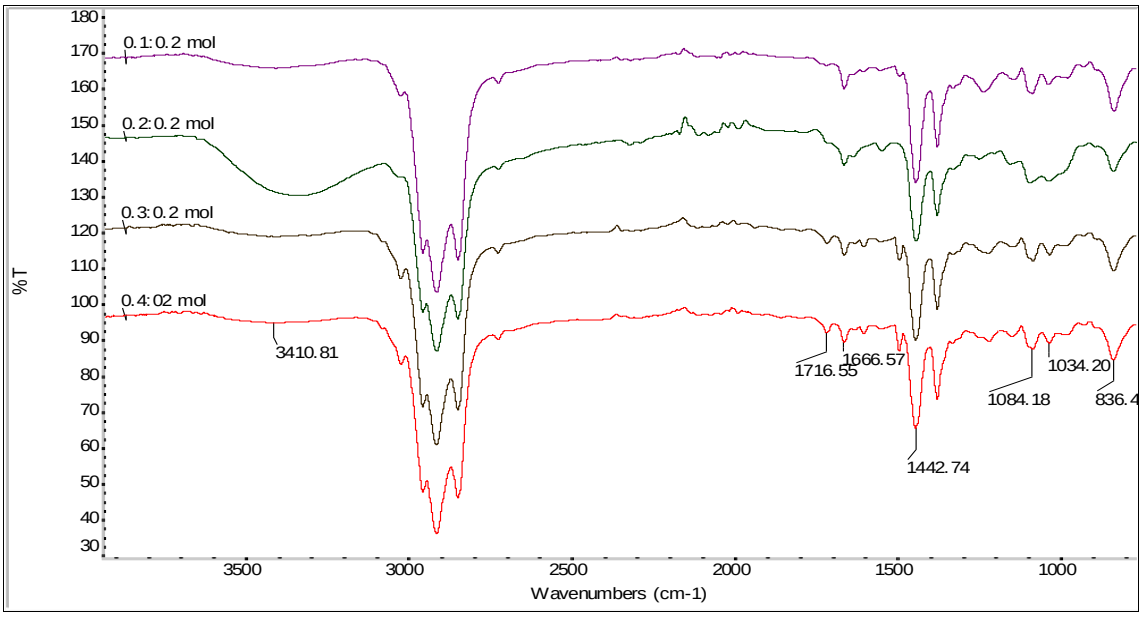



Figure 8. IR spectra of LNRs prepared at various concentration of hydrogen peroxide and 0.2 mol sodium nitrite

The C=C bond was cleaved by the redox reaction induced by hydrogen peroxide and sodium nitrite, whilst C-C bond cleavage as a result of hydroxyl radical activity. Hydrogen peroxide and sodium nitrite are known to react chemically in acidic medium to produce peroxynitrite acid, which then can undergo homolytic decay to release

hydroxyl radical [29]. This hydroxyl radical is highly reactive species that can break the C-C bond of NR chain [15].

Carbonyl and OH groups were present in the LNR chain as indicated by both FTIR and NMR spectra. The formation of these groups came from cleavage of C=C by redox reaction that leave carbonyl as terminal groups, while C-C bond that broken by hydroxyl radical would produce LNR with hydroxyl end chain [25, 30].

Highest amount of hydroxyl group was observed when the LNR prepared with 0.2 mol of hydrogen peroxide to sodium nitrite at a ratio of 1:1. This suggested that the degradation reaction was predominantly affected by OH radical in the bond cleavage when the ratio of reagents used was 0.2 mol. On the other hand, redox reaction predominated if the concentration of reagents used was higher than 0.2 mol as indicated by the increasing of carbonyl group.

The reactions conducted with excessive amount of sodium nitrite compared to hydrogen peroxide showed the presence of higher hydroxyl groups on LNR chain, whilst the reactions added with excessive amount of hydrogen peroxide showed the presence of higher carbonyl group. This suggested that the primary reaction either by redox or hydroxyl radical is strongly influenced by the concentrations and ratios of reagents.

## Conclusion

Degradation of NR latex by using sodium nitrite and hydrogen peroxide was successfully conducted and yielding LNR having Mn of less than 50 x $10^3$ g/mol. One to one ratio of 0.2:0.2 mol of hydrogen peroxide and sodium nitrite reagents concentrations was found to be the best ratio to produce LNR that having low Mn, gel content and polydispersity. It is found that increasing the concentrations of sodium nitrite resulted in the increase of Mn and the chains attached with OH groups. Meanwhile, excessive concentrations of hydrogen peroxide reduced the Mn and increased the number of carbonyl groups attached on the chains, while the hydroxyl groups was almost negligible.The degradation reaction is suggested to occur at both C=C and C-C bonds by redox reaction and hydroxyl radical respectively.

## Acknowledgement

The authors would like to extend gratitude to Malaysian Rubber Board for approval of funding for this research under grant no. SN12NM0408.

## References

1. Mathew V. S, Sinturel C, George S. C, & Thomas S (2010). Epoxy resin/liquid natural rubber system: Secondary phase separation and its impact on mechanical properties. *J Mater Sci* 45: 1769-1781.
2. Wayakron Phetphaisit C, Bumee R, Namahoot J, Ruamcharoen J, & Ruamcharoen P (2012). Polyurethane polyester elastomer: Innovative environmental friendly wood adhesive from modified PETs and hydroxyl liquid natural rubber polyols. *Int J Adhes Adhes* 41: 127-131.
3. Dileep U, & Avirah S. A (2003). Studies on carboxy-terminated natural rubber in filled NR and NR latex vulcanizates. *Iranian Polymer Journal (English Edition)* 12: 441-448.
4. Abdullah I. (1992). Liquid natural rubber as a compatibilizer in the blending of natural rubber with polypropylene. *Mater Forum* 16: 353-357.
5. Ahmad S, Abdullah I, Sulaiman C. S, Kohjiya S, & Yoon J. R (1994). Natural rubber -HDPE blends with liquid natural rubber as a compatibilizer. I. Thermal and mechanical properties. *J Appl Polym Sci* 51: 1357-1363.
6. Srilathakutty R, Noushad V, Joseph R, & George K. E (1996). Studies on the properties of microcellular soles based on NBR/PVC blends. *Polymer - Plastics Technology and Engineering* 35: 97-119.
7. Dahlan H. M, Zaman M..D..K, & Ibrahim A. (2002). Liquid natural rubber (LNR) as a compatibiliser in NR/LLDPE blends - II: The effects of electron-beam (EB) irradiation. *Radiat Phys Chem* 64: 429-436.
8. Paul C. J, Gopinathan Nair M. R, Neelakantan N. R, Koshy P, Idage B. B, & Bhelhekar A. A (1998). Segmented block copolymers of natural rubber and 1, 3-butanediol-toluene diisocyanate oligomers. *Polymer* 39: 6861-6874.
9. Gopakumar S, & Gopinathan Nair M. R (2006). Natural rubber-polyurethane block copolymers: Nonlinear structural variations with NCO/OH ratio. *Polym Eng Sci* 46: 1812-1821.

10. Nair M. N. R, Sukumar P., Jayashree V, & Nair M. R. G (2010). Mechanical properties and fractography of block copolymers based on NR and MDI-based polyurethanes. *Polymer Bulletin* 65: 83-96.
11. Kébir N, Campistron I, Laguerre A, Pilard J, & Bunel C. (2011). New crosslinked polyurethane elastomers with various physical properties from natural rubber derivatives. *J Appl Polym Sci* 122: 1677-1687.
12. Saetung A, Kaenhin L, Klinpituksa P, Rungvichaniwat A, Tulyapitak T, Munleh S, Campistron I, & Pilard J (2012). Synthesis, characteristic, and properties of waterborne polyurethane based on natural rubber. *J Appl Polym Sci* 124: 2742-2752.
13. Kaenhin L, Klinpituksa P, Rungvichaniwat A, & Pilard J. F (2012). Waterborne polyurethane: Effect of functional groups in aromatic isocyanate and the chain length of hydroxyl terminated natural rubber. *Advanced Materials Research* 415-417: 2032-2035
14. Saetung A, Rungvichaniwat A, Campistron I, Klinpituksa P, Laguerre A, Phinyocheep P, & Pilard J. F (2010) Controlled degradation of natural rubber and modification of the obtained telechelic oligoisoprenes: Preliminary study of their potentiality as polyurethane foam precursors. *J Appl Polym Sci* 117: 1279-1289.
15. Ravindran T, Nayar M..R..G, & Francis D. J (1988). Production of hydroxyl-terminated liquid natural rubber mechanism of photochemical depolymerization and hydroxylation. *J Appl Polym Sci* 35: 1227-1239.
16. Lemoine A. J (1988) Production of Liquid Natural Rubber on a Pilot Scale. Proceedings of International Rubber Technology Conference Kuala Lumpur
17. Gopakumar S, Paul C. J, & Gopinathan Nair M. R (2005) Segmented block copolymers of natural rubber and 1,4-butanediol-toluene diisocyanate oligomers. *Materials Science- Poland* 23: 227-245.
18. Maier G, Knopfova V, Voit B, Ly P. H, Dung B. T, & Thanh D. B (2004). Synthesis and characterization of segmented block copolymers based on hydroxyl-terminated liquid natural rubber and α,ω-diisocyanato telechelics. *Macromolecular Materials and Engineering* 289: 927-932.
19. Paul C. J, Nair M. R. G, Koshy P, & Idage B. B (1999). Segmented block copolymers of natural rubber and bisphenol A-toluene diisocyanate oligomers. *J Appl Polym Sci* 74: 706-721.
20. Ha T. H, Nguyen T. N, Le Q. H, & Chu N. S (1996). Depolymerization of Natural Rubber Latex using Phenylhydrazine-$FeCl_2$ System. *Pure Applied Chemistry*: 1923-1930.
21. Gazeley K. F, & Mente P. G (1990). Method for reducing the molecular weight of rubber latex. Malaysian Patent 1,00304-A
22. Phinyocheep P, Phetphaisit C. W, Derouet D, Campistron I, & Brosse J. C (2005) Chemical degradation of epoxidized natural rubber using periodic acid: Preparation of epoxidized liquid natural rubber. *J Appl Polym Sci* 95: 6-15.
23. Phetphaisit C. W, & Phinyocheep P (2003). Kinetics and Parameters Affecting Degradation of Purified Natural Rubber. *J Appl Polym Sci* 90: 3546-3555
24. Kodama S, Nishi K, & Furukawa M (2003). Preparation of low molecular weight natural rubber by ozonolysis of high ammonia latex. *Journal of Rubber Research* 6: 153-163
25. Suhawati I (2012). Preparation of Liquid natural rubber via chemical degradation of natural rubber latex and preparation of LNR-based polyurethane. MSc Thesis
26. Kébir N, Campistron I, Laguerre A, Pilard J, Bunel C, Couvercelle J-, & Gondard C (2005). Use of hydroxytelechelic cis-1,4-polyisoprene (HTPI) in the synthesis of polyurethanes (PUs). Part 1. Influence of molecular weight and chemical modification of HTPI on the mechanical and thermal properties of PUs. *Polymer* 46: 6869-6877
27. Sakdapipanich J. T, Suksawad P, Insom K, Kawahara S (2005). Preparation of functionalized low molecular weight natural rubber latex using solid nanometric TiO2 film as a photocatalyst. *Rubber Chemistry and Technology* 78: 597-605.
28. Pavia D. L, Lampman G. M, Kriz G. S, & Vyvyan J. A (2009) Introduction to Spectroscopy, 4th edn. Cengage Learning, Brooks/Cole
29. Halfpenny E, & Robinson P. L (1952) Pernitrous acid. The reaction between hydrogen peroxide and nitrous acid, and the properties of an intermediate product. *Journal of the Chemical Society* (Resumed): 928-938
30. Solanky S. S, & Singh R (2003) Functional and group determination in photo-degraded liquid rubbers. . *Journal of Rubber Research* 6: 1-11.

The Malaysian Journal of ANALYTICAL SCIENCES ISSN 1394-2506

# SYNTHESIS OF CHITOSAN-GRAFTED-POLY(METHYL METHACRYLATE) WITH FENTON'S REAGENT ($Fe^{2+}$ - $H_2O_2$) AS A REDOX INITIATOR

## (Sintesis Kitosan-Cangkuk-Poli(Metil Metakrilat) Dengan Reagen Fenton ($Fe^{2+}$ - $H_2O_2$) Sebagai Pemula Redoks)

Nur Azmyra Abdul Aziz*, Aznizam Abu Bakar, Azman Hassan, Nurulhusna Azmi

*Enhanced Polymer Research Group (ENPRO),*
*Department of Polymer Engineering, Faculty of Chemical Engineering,*
*Universiti Teknologi Malaysia, 81310 UTM Skudai, Johor, Malaysia.*

**Corresponding author: azmyra_aziz@yahoo.com*

**Abstract**

Graft copolymerization of poly(methyl methacrylate)(PMMA) onto chitosan fiber has been successfully carried out using Fenton's Reagent which is consisted of hydrogen peroxide($H_2O_2$) as initiator and ferrous ammonium sulphate(FAS) as co-catalyst under inert atmosphere in an aqueous medium. The PMMA homopolymer formed during the reaction was removed from the grafted copolymer by Soxhlet extraction using acetone as the solvent. The grafting percentage and efficiency obtained were 449.16% and 85.94%, respectively. The maximum grafting percentage and efficiency were achieved when 0.3 g chitosan copolymerized with 3 mL monomer at 70°C for 120 minutes with [FAS] = 6 x $10^{-5}$ M, [$H_2O_2$] = 6 x $10^{-3}$ M and 8 mL water. The grafted copolymers were characterized by using FTIR, DSC, TGA and SEM analysis. The presence of absorbance band at 1724 $cm^{-1}$ provided strong evidence of grafting.

**Keywords:** graft copolymers, chitosan, monomers, radical polymerization

**Abstrak**

Pengkopolimeran cangkuk poli(metil metakrilat)(PMMA) terhadap gentian kitosan telah berjaya dilakukan dengan menggunakan Reagen Fenton yang terdiri daripada hidrogen peroksida ($H_2O_2$) sebagai pemula dan ferus ammonium sulfat (FAS) sebagai ko-mangkin pada persekitaran atmosfera lengai dalam medium berair. Homopolimer PMMA terbentuk semasa tindakbalas telah disingkirkan daripada kopolimer cangkuk melalui kaedah pengekstrakan Soxhlet dengan menggunakan aseton sebagai pelarut. Peratusan pencangkukan dan peratusan kecekapan pencangkukan yang diperolehi masing-masing ialah 449.16% dan 85.94%. Peratusan maksima pencangkukan dan kecekapan pencangkukan diperolehi apabila 0.3 g kitosan dikopolimer dengan 3 mL monomer pada 70°C selama 120 minit dengan mengunakan [FAS] = 6 x $10^{-5}$ M, [$H_2O_2$] = 6 x $10^{-3}$ M dan 8 ml air. Kopolimer tercangkuk telah dicirikan dengan menggunakan analisis FTIR, DSC, TGA dan SEM. Kehadiran kumpulan penyerapan pada 1724 $cm^{-1}$ menunjukkan bukti kukuh berlakunya pencangkukan.

**Kata kunci:** kopolimer cangkuk, kitosan, monomer, radikal pempolimeran

## Introduction

With growing worldwide ecological awareness, there has been a trend to produce low cost, biodegradable materials with improved properties. Lately, there has been a great interest to produce thermoplastic composites reinforced with natural products. Chitosan is a deacetylated derivative of chitin which is a polymer second abundance polysaccharide natural polymer on earth after cellulose [1], biodegradable, non-toxic and biocompatible [2]. It is a unique basic polysaccharide with high molecular weight [3]. In particular, chitosan are becoming popular because it has lower cost, lower density and exhibit better processing ability. Nowadays, chitosan is no longer a waste by-product from the seafood processing industry because currently this material is being used by biomedical and pharmaceutical industry.

Graft copolymerization is a well-established technique for modification of the chemical and physical characteristic of polymer. Grafting various vinyl monomers onto an existing polymer backbone is a promising method for the preparation of new materials. This is because the potential and multiple applications of this versatile material can be increased and its chemical and physical properties can be improved greatly [1]. Grafting technique is used to enhance the compatibility of lignocellulosic fibres with thermoplastic material [4]. This is because the thermoplastics are hydrophobic, and thus they are incompatible with lignocellulosic fibres. The modification of chitosan via grafting of vinyl monomers is one of the most effective methods to incorporate desirable properties into chitosan without sacrificing its biodegradable nature [5]. In addition, graft copolymers had been used as stabilizers between grafted and ungrafted polymer. The properties of cellulose obtained by blending synthetic polymers do not last long due to the separation of blended synthetic polymers, whereas cellulose obtained by grafting of monomer gives rise to everlasting properties [6].

There are a few reports on grafting of poly(methyl methacrylate)(PMMA) onto chitosan. Lagos and Reyes [7], studied on the graft copolymerization of methyl methacrylate onto chitosan with Fenton's reagent as a redox initiator in the presence of atmospheric oxygen. Harish Prashanth [8] studied the graft copolymerization of chitosan with poly(methyl methacrylate)(PMMA) and polyacrylonitrile(PAN) using potassium persulfate as an initiator. They found that, the percentage grafting of chitosan-*g*-PMMA was higher than chitosan-*g*-PAN because of bulky methyl groups of PMMA. Harish Prashanth [9] also studied on the biodegradation of chitosan-graft-polymethyl methacrylate film.

According to Liu et al. [1] chitosan-*g*-polymethyl acrylate (PMA) may improve the compatibility of two phases of chitosan and PVC. With this in mind, the grafting technique was used to modify the chitosan for being used as filler in polymer composites. In this study, chitosan fiber was grafted with methyl methacrylate (MMA) to improve the compatibility of hydrophilic chitosan fiber with a hydrophobic polymer matrix, particularly for PVC composites application.

Therefore, the aims of this work are to synthesize graft copolymer of chitosan onto methyl methacrylate using $H_2O_2/Fe^{2+}$ as a redox initiator in aqueous medium and under nitrogen atmosphere. The resulting chitosan grafted methyl methacrylate was characterized by using Fourier-Transform Infrared Spectroscopy, Differential Scanning Calorimeter, Thermogravimetry Analysis and Scanning Electron Microscopy.

## Materials and Methods

### Materials

Chitosan from shrimp shell with medium molecular weight and degree deacetylation (75%- 85%) in a powder form and yellow in colour were purchased from Sigma Aldrich (Malaysia). The methyl methacrylate (MMA) monomer used is manufactured by Merck Schuhardt (Hohenburnn, Germany) was used for grafting onto chitosan. The MMA was chosen because it is widely used in the grafting of synthetic polymers and cellulosic fibers [10]. Analytical-grade hydrogen peroxide ($H_2O_2$) was purchased from QRec (Malaysia) as an initiator, while ammonium ferrous sulfate, obtained from BDH Sigma Aldrich Chemie Gmbh (Steinheim, Germany) was used as catalyst. All solvents and other analytical-grade chemicals were used as received from the manufacturers without further purification.

### Removal of the inhibitor from the monomer

MMA was purified by passing through a column packed with an activated alumina to remove its inhibitor (hydroquinone). The reagent bottle was immersed in an ice bath. A burette was filled with glass wool and followed by activated alumina. The burette was attached to the retort stand. MMA was poured into burette through a conical funnel and allow to flow through the burette. The activated alumina changed in colour from white to pink when the inhibitor was trapped. Finally, the purified MMA was collected in a reagent bottle, sealed in a refrigerator below $10^oC$.

### Preparation of Chitosan -*grafted*- poly (methyl methacrylate)

To prepare the chitosan/PMMA copolymer, 0.3 g chitosan was placed in 250 mL three-necked flasks equipped with a magnetic stirrer. A 250 mL three necked flask was properly arranged and immersed in a thermostated water bath.

0.3 g of chitosan and 8 mL of distilled water was transferred into the flask. After that, the flask was placed into a water bath at a desired temperature. Nitrogen was purged into the flask for 30 minutes to remove the presence of oxygen during the reaction. Then, followed by adding the required volume of hydrogen peroxide and required amount of ammonium ferrous sulphate. The reaction mixture was mixed for 5 min and then the required amounts of monomer (MMA) were added into the mixture. The reaction mixture was stirred under nitrogen at the chosen temperature and reaction period. Immediately, after the reaction period was over, the reaction flask was exposed to the ambient atmosphere and the product was filtered. The crude product was washed thoroughly with distilled water and kept in an oven at 60$^{o}$C for 24 hours until a constant weight was achieved. The grafted product was further treated with the Soxhlet extraction techniques to removed PMMA homopolymer that was formed during the reaction.

**Removal of homopolymer and determination of graft level**

Initially, the three necked- flask was filled with acetone. A thimble used for the extraction process was preheated in an oven before its application in the Soxhlet extractor. The preheated thimble was then kept in a desiccator to remove moisture. Firstly, the initial weight of the empty thimble was determined. The grafting product was took out from the oven and allowed to cool down to room temperature. Later, this grafting product was added into thimble and the weight of thimble with grafting product (including homopolymer of PMMA) was taken. The thimble is then was inserted into Soxhlet extractor and the extraction was ran for 24 hours to remove homopolymer of PMMA. Afterwards, the thimble was dried in an oven at 60$^{o}$C for another 24 hours until constant weight was achieved. The thimble was removed from the oven and immediately transferred to desiccators to avoid thimble from absorbing the moisture. The thimble was allowed to cool down to room temperature. Finally, the weight of thimble and grafting product without homopolymer of PMMA was determined. The grafting percentage, *%G* and grafting efficiency, *%E* was determined using Equations 1 and 2, respectively.

$$\% G = [(w_3 - w_1)/ (w_1)] \text{ x } 100\% \quad (1)$$

$$\% E = [(w_3 - w_1) / (w_2 - w_1)] \text{ x } 100\% \quad (2)$$

*% G* is the grafting percentage, *% E* is the efficiency percentage, $w_1$ is the weight of the original chitosan, $w_2$ is the weight of the grafted product after copolymerization, and $w_3$ is the weight of the grafted product after copolymerization and purification (extraction) [10].

**FTIR spectroscopy**

Infrared (IR) spectra of the chitosan, PMMA and chitosan-*g*-PMMA were recorded on a Fourier transform – IR spectrometer (Pelkin Elmer Spectrum 2000) using a KBr disk pellet to identify the functional groups present in the chitosan, PMMA and chitosan-*g*-PMMA.

**Differential scanning calorimeter (DSC)**

A DSC study was carried out with a Perkin-Elmer DSC2 according to ASTM D 3418-2 at heating rate of 10$^{o}$C/min from 30$^{o}$C to 450$^{o}$C. Liquid nitrogen was used at a steady state of 50 ml/min. a sample was placed in a sealed aluminium pan, and an empty pas was used as the reference. This analysis is used to obtain the melting temperature of chitosan and chitosan-*g*-PMMA.

**Thermogravimetry analysis (TGA)**

Thermogravimetry experiments were carried out using a Perkin-Elmer Thermal Analyzer. This analysis was carried out in nitrogen atmosphere from 35$^{o}$C to 1000$^{o}$C at heating rate 10$^{o}$Cmin$^{-1}$ with nitrogen flow rate of 50ml min$^{-1}$. Thermograms were obtained by plotting percentage residual weight against temperature. This study is used to identify the degradation temperature of chitosan and chitosan-*g*-PMMA.

**Scanning electron microscopy (SEM)**

Studies on the surface morphologies of grafted chitosan and original chitosan were performed with a Philips ZL 40 scanning electron microscopy. Samples were mounted on the stub and sputter-coated with a thin layer of gold to avoid electrostatic charging during examination.

## Results and Discussion

### Graft copolymerization reaction analysis

The parameters of the grafting reaction used to produce chitosan-*g*-PMMA were obtained from Lagos and Reyes [7] with some modification on the grafting method. The grafting method used was based on our previous study [10]. In this study, the grafting percentage and grafting efficiency were found to be about 449.16% and 85.94% respectively. Based on previous study [7] the grafting percentage was 332% with 3 mL monomer at 70$^{o}$C for 120 minutes with [FAS] = 6 x $10^{-5}$ M, [$H_2O_2$] = 6 x $10^{-3}$ M and 8 mL water in the presence of atmospheric oxygen. In contrast, in this work chitosan-grafted-poly(methyl methacrylate) were done under nitrogen. The grafting percentage and efficiency showed that MMA monomer was grafted successfully onto the chitosan surface. The postulated mechanism is shown in Figure 1.

### FTIR spectroscopy

Infrared spectroscopy is the best tool to confirm the grafting reaction. The FTIR spectra of pure PMMA,grafted and ungrafted chitosan in the frequency range 4000 – 370 $cm^{-1}$ are shown in Figure 2. All spectra show a characteristic absorption band of hydroxyl group around 3500-3100 $cm^{-1}$. This is attributed to OH stretching vibrations of cellulose and absorbed water of chitosan. The absorption band within this range changed with the amount of grafting [11]. The FTIR spectrum of chitosan shows some characteristic extension vibration of N-H and intermolecular hydrogen bonds of polysaccharides at 1645 $cm^{-1}$ due to N-H bending vibrations indicating the presence of $NH_2$ groups on C2 of the glucosamine unit and at 1066 $cm^{-1}$ corresponding to stretching vibrations of –C –O –C bond. The amide I and amide II absorptions were seen around 1645 and 1584 $cm^{-1}$, and with increase in percent grafting a progressive weakening of amide II band was observed [8].

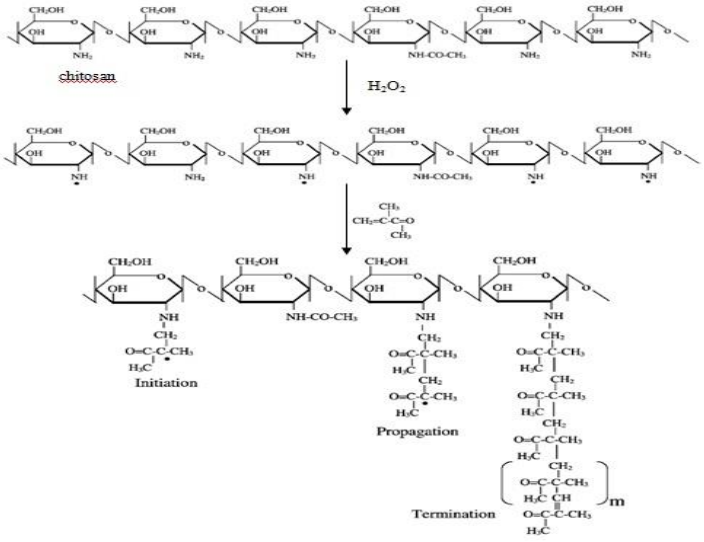



Figure 1. Schematic representation of graft-copolymerization of chitosan

The appearance in chitosan-*g*-PMMA at absorption 1723 $cm^{-1}$ is due to –C = O (carbonyl) absorption and methyl and methylene asymmetric stretching vibrations at 2991 and 2946 $cm^{-1}$ respectively. With increase in percent grafting, the intensity of these grafting also increase [5]. A broad peak around 3363 $cm^{-1}$ due to stretching vibration of N-H and O-H bonds and a peak around 1649 $cm^{-1}$ (N-H bending vibration) are observedindicating the existence of chitosan in the grafted copolymers. The vibrations peak corresponding to the out-of plane C-H bending, rocking C-$H_2$ and the stretching vibration of C-N are observed at 752, 842 and 986 $cm^{-1}$, respectively in the chitosan-*g*-PMMA. The presence of the characteristic peaks clearly proves that PMMA has been successfully grafted onto the chitosan surface.

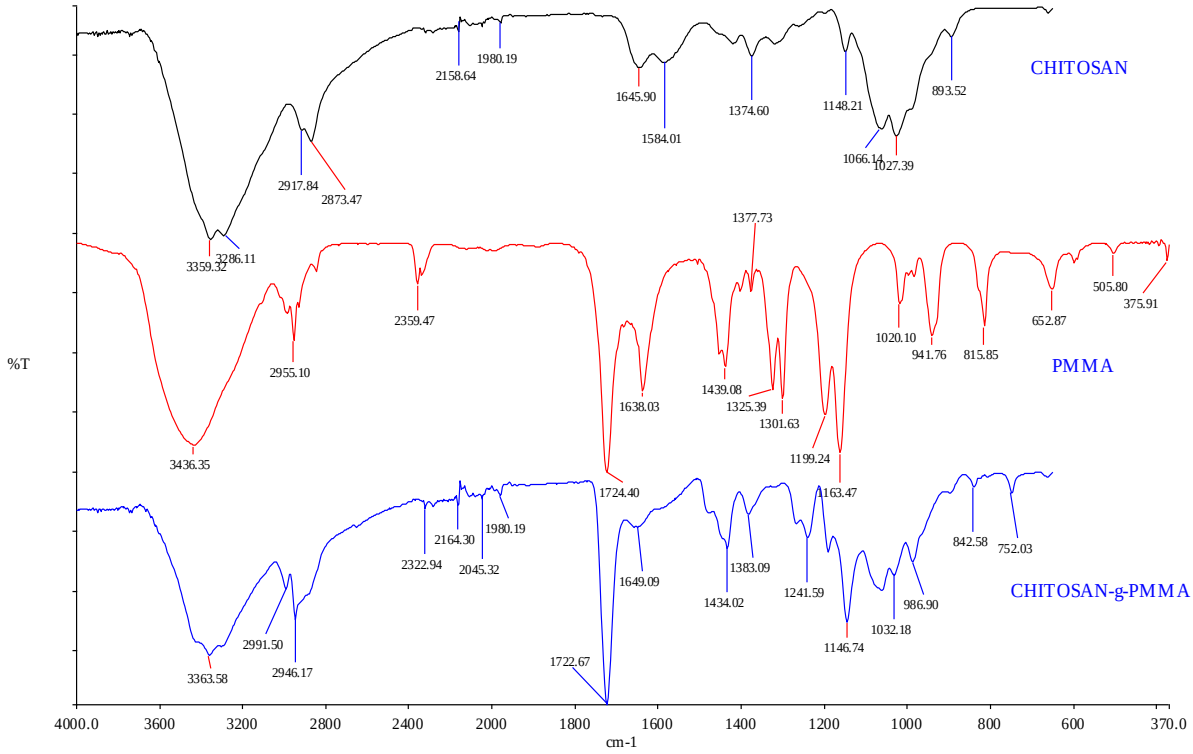



Figure 2. FTIR spectra of (a) chitosan (b) PMMA (c) chitosan-*g*-PMMA

**DSC analysis**

Figure 3 and Table 1 show the DSC results of pure chitosan and chitosan-grafted-PMMA. The chitosan shows melting temperature at around 300$^{o}$C while the grafted chitosan exhibits melting temperature at 402$^{o}$C, is similar to those reported by [8]. The increase in melting temperature is probably caused by the restricted mobility of the PMMA grafted to the cellulose. DSC analysis also shows that the PMMA was successfully grafted onto chitosan surface.

Table 1. Melting temperature of pure chitosan and chitosan-g-PMMA

| **Material** | **Melting Temperature($T_m$)** |
|---|---|
| Chitosan | 300.00$^{o}$C |
| Chitosan-g-PMMA | 402.00$^{o}$C |

**Thermogravimetric analysis**

TGA is the simplest accurate method for analysing the thermal stability of polymers. TGA thermogram of pure chitosan and the grafted chitosan is shown in Figure 4. The TGA of pure chitosan shows a two stages weight loss. The first stage occurs in the temperature range of 30$^{o}$C - 231$^{o}$C with a weight loss of 4.25%. This may be attributed to the loss of adsorbed and bound water. The second stage of weight loss starts at 401$^{o}$C and continues up to 571$^{o}$C during which there is 88.41% of weight loss due to the degradation of chitosan.

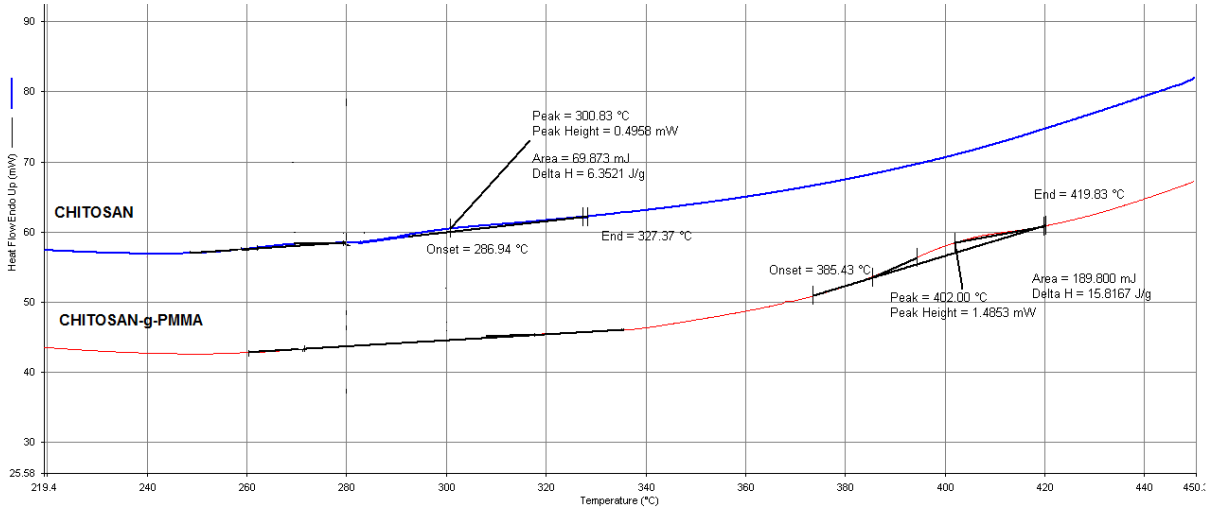



Figure 3. DSC thermograms of chitosan and chitosan-g-PMMA

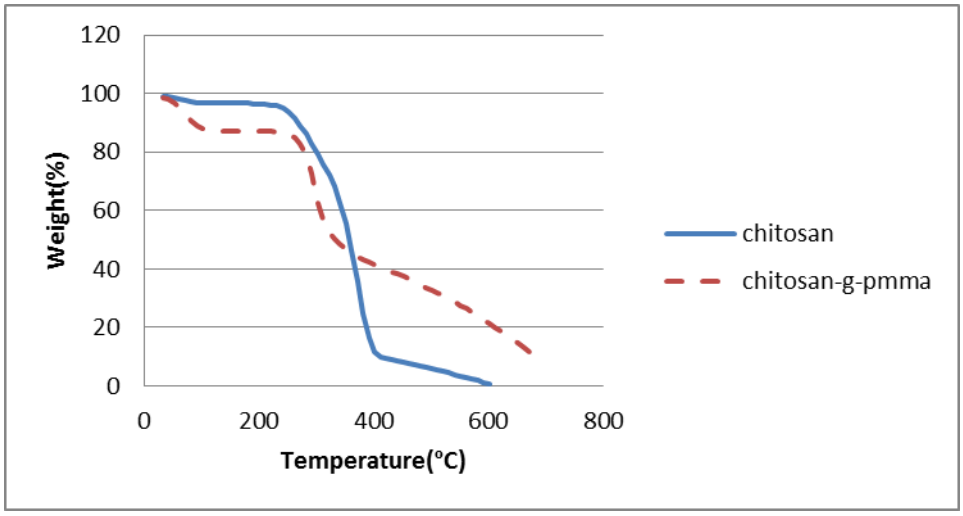



Figure 4. TG curves of chitosan and chitosan-grafted-PMMA (grafting percentage = 449.16%)

The TGA curve of chitosan-grafted-PMMA (Figure 4) also shows two stages of degradation. The first stage occurs in the temperature range of 31°C- 111°C with a weight loss of 12.38%.This may be due to the devolatilization of moisture. The second stage weight loss starts at 231°C to 361°C with weight loss of 54.51%.

Table 2 compares the degradation temperature at 20% and 65% weight loss for the grafted and ungrafted chitosan. The thermal stability at 65% weight loss of chitosan-grafted-PMMA increases drastically compared to pure chitosan. The increase in thermal stability at 611°C in chitosan-grafted-PMMA may be due to the PMMA enveloping the chitosan surface, thus increasing the overall thermal stability of the grafted chitosan. In addition, the grafted polymers entangle and form a physical crosslinked type of network, which when heated forms an insulative carbonaceous char barrier on the surface, thus inhibiting degradation [11]. Thus, the grafting chitosan onto PMMA enhances the stability of pure chitosan at elevated temperature.

Table 2. Thermal degradation analysis at 20% and 65% weight loss

| Material | $T_{20}$ | $T_{65}$ | Char Residue |
|---|---|---|---|
| Chitosan | 301°C | 381°C | 0.755% |
| Chitosan-g-PMMA | 281°C | 611°C | 21.46% |

**Scanning Electron Microscopy**

Graft copolymerization considerably modifies chitosan morphology. It also alters the chemical, physical and biodegradable characteristics, which varies with respect to the nature of the synthetic side chains incorporated [8]. Figure 5 shows the SEM micrographs of ungrafted chitosan and grafted chitosan respectively. The difference can be observed on the surface of ungrafted and grafted chitosan. On Figure 5 (B) and (D) the surface of the grafted chitosan was almost covered by PMMA after the grafting process. It is believed that the PMMA is strongly attached onto the chitosan surface.

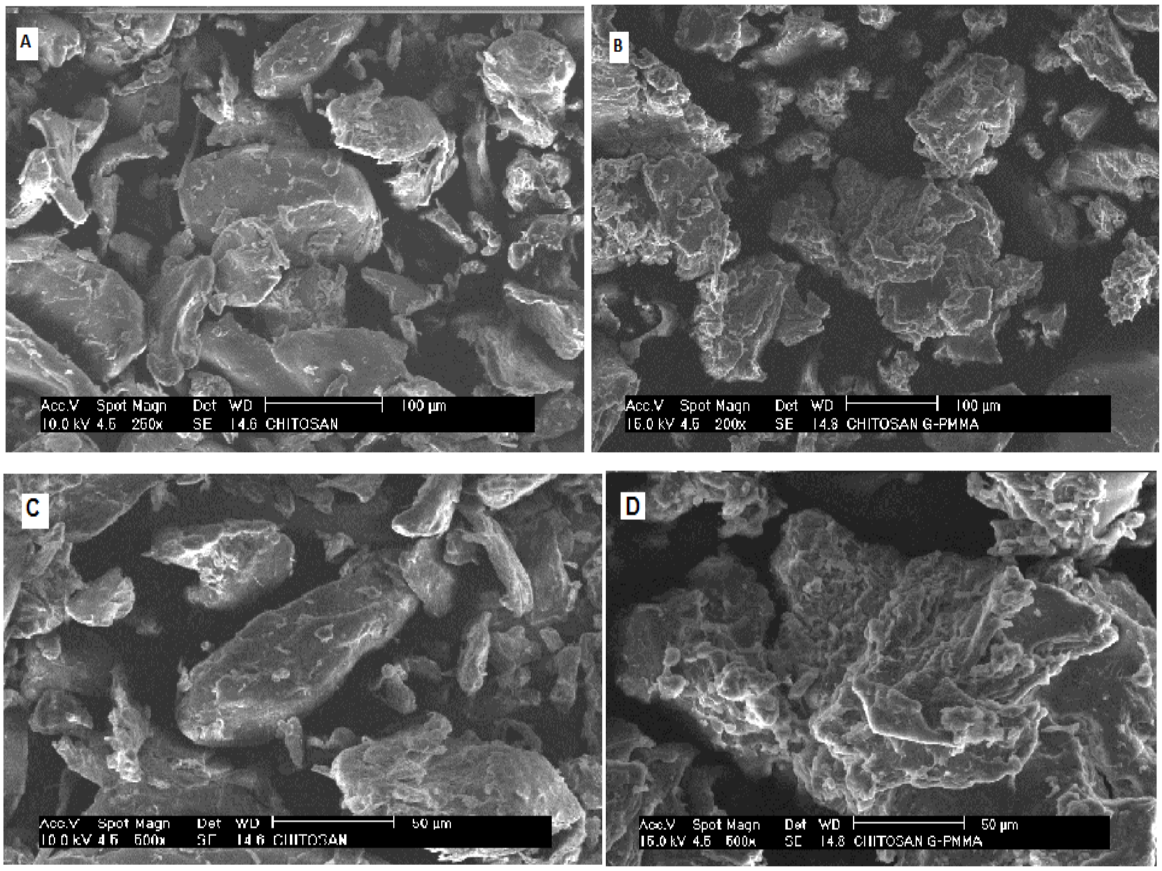



Figure 5. SEM photographs (A) chitosan (x 250), (B) chitosan-*g*-PMMA(x 200), (C) chitosan (x500), D) chitosan-*g*-PMMA(x 500)

## Conclusion

The graft coplymerization of hydrophobic monomer (MMA) onto chitosan was successfully carried out by free radicals using hydrogen peroxide and ferrous ion as initiator/co-catalyst system. The parameters used for the grafting process were 0.3 g chitosan copolymerized with 3 mL monomer at 70$^{o}$C for 120 minutes with [FAS] = 6 x $10^{-5}$ M, [$H_2O_2$] = 6 x $10^{-3}$ M and 8 mL water. These parameters produced 449.16% and 85.94% of grafting percentage and efficiency respectively. The presence of PMMA on the chitosan surface was confirmed by FTIR spectra, TGA, DSC and SEM analysis. The chitosan-grafted-PMMA exhibited better thermal resistance than pure chitosan.

## Acknowledgement

The authors gratefully acknowledged the Ministry of Higher Education (MOHE), Malaysia under the Exploratory Research Grant Scheme (ERGS Project No. 4L028) for financial support, and the Polymer Processing Laboratory, Faculty of Chemical Engineering, Universiti Teknologi Malaysia for technical assistance.

## References

1. Liu, Z., Wu, G. & Liu, Y. (2006). Graft copolymerization of methyl acrylate onto chitosan initiated by potassium diperiodatoargentate (III). *Journal of Applied Polymer Science*. 101 (1): 799-804.
2. Flores-Ramirez, N., Luna-Barcenas, G., Vasquez-Garcia, S., Munoz-Saldana, J., Elizalde-Pena, E., Gupta, R., Sanchez, I., Gonzalez-Hernandez, J., Garcia-Gaitan, B. & Villasenor-Ortega, F. (2008). Hybrid natural-synthetic chitosan resin: thermal and mechanical behavior. *Journal of Biomaterials Science, Polymer Edition*. 19 (2): 259-273.
3. Radhakumary, C., Nair, P. D., Mathew, S. & Nair, C. P. R. (2005). Biopolymer composite of chitosan and methyl methacrylate for medical applications. *Trends Biomater. Artif. Organs*. 18 (2): 117-124.
4. Bledzki, A. K., Reihmane, S. & Gassan, J. (1996). Properties and modification methods for vegetable fibers for natural fiber composites. *Journal of Applied Polymer Science*. 59 (8): 1329-1336.
5. Prashanth, K. V. H. & Tharanathan, R. N. (2003). Studies on graft copolymerization of chitosan with synthetic monomers. *Carbohydrate Polymers*. 54 (3): 343-351.
6. Gupta, K., Sahoo, S. & Khandekar, K. (2002). Graft copolymerization of ethyl acrylate onto cellulose using ceric ammonium nitrate as initiator in aqueous medium. *Biomacromolecules*. 3 (5): 1087-1094.
7. Lagos, A. & Reyes, J. (1988). Grafting onto chitosan. I. Graft copolymerization of methyl methacrylate onto chitosan with Fenton's reagent ($Fe^{2+}$–$H_2O_2$) as a redox initiator. *Journal of Polymer Science Part A: Polymer Chemistry*. 26 (4): 985-991.
8. Prashanth, K. & Tharanathan, R. (2003). Studies on graft copolymerization of chitosan with synthetic monomers. *Carbohydrate Polymers*. 54 (3): 343-351.
9. Harish Prashanth, K., Lakshman, K., Shamala, T. & Tharanathan, R. (2005). Biodegradation of chitosan-graft-polymethylmethacrylate films. *International Biodeterioration & Biodegradation*. 56 (2): 115-120.
10. Abu Bakar, A., Nik Mat, N. S. & Isnin, M. K. (2008). Optimized conditions for the grafting reaction of poly (methyl methacrylate) onto oil-palm empty fruit bunch fibers. *Journal of Applied Polymer Science*. 110 (2): 847-855.
11. Das, R. K., Basu, D. & Banerjee, A. (1999). Study of methyl-methacrylate-viscose fiber graft copolymerization and the effect of grafting on thermal properties. *Journal of Applied Polymer Science*. 72 (1): 135-140.

The Malaysian Journal of ANALYTICAL SCIENCES ISSN 1394-2506

# ROLE OF ANTI-OXIDANTS ON NORMOXIC METHACRYLIC ACID GELATIN (MAG) POLYMER GEL DOSIMETER AT 6-MV PHOTON BEAM USING SINGLE SPIN ECHO MRI

## (Peranan Anti-Oksida Dalam Normosik Asid Methakrilik Gelatin (MAG) Dosmeter Gel Polimer Pada 6-MV Sinaran Photon Menggunakan Aturan Nada Denyut Tunggal MRI)

Nik Noor Ashikin Nik Ab Razak[1]*, Azhar Abd Rahman[1], Sivamany Kandaiya[1], Iskandar Shahrim[1], Nor Zakiah Yahaya[1], Noor Faizura Zainal[2], Eng Kae Yann[3]

[1]*School of Physics,*
*Universiti Sains Malaysia, 11800 Minden, Penang, Malaysia*
[2]*Imaging Department, Institut Perubatan dan Pergigian Termaju (Advanced Medical & Dental Institute),*
*Universiti Sains Malaysia, 13200 Kepala Batas, Penang, Malaysia*
[3]*Radiotherapy and Oncology Department,*
*Pantai Mutiara Hospital, 11900 Penang, Malaysia*

**Corresponding author: ohm_poisse@yahoo.com*

**Abstract**

The primary goal of radiation therapy is to deliver a sufficient radiation dose to a target volume while minimizing the dose to surrounding healthy tissue. In this study the dose response of methacrylic acid-gelatin (MAG) polymer gel dosimeter using different type of anti-oxidants; ascorbic acid (AscA) and tetrakis-hydroxy-methyl-phosphonium chloride (THPC) is determined by using single spin echo sequence magnetic resonance imaging (MRI). The concentrations of methacrylic acid (MAA) were varied and using MRI, the optimal formulation that gives the maximum R2-dose response of the polymer gel upon irradiation was determined. The polymer gel was irradiated using a 6 MV photon from a linear accelerator (LINAC) for a dose range varying from 0 to 20 Gy. The transverse relaxation rates (R2) of the irradiated gels from MRI were read. A linear relationship between dose and R2 was obtained for a dose range of 0 to 20 Gy for MAG gel composed of ascorbic acid (MAGAS) and linear response from 0 to 10 Gy for MAG gel composed of THPC (MAGAT). The sensitivity of MAGAS showed lower sensitivity compared to MAGAT. The optimum concentrations for the MAGAS and MAGAT polymer gel were 6% MAA and 5% gelatin as it gave the highest sensitivity of 0.0989 $s^{-1}Gy^{-1}$ and 1.1180 $s^{-1}Gy^{-1}$ respectively. The results are compared to Multiple Spin Echo Sequence MRI.

**Keywords**: MAGAS polymer gel, MAGAT polymer gel, dose sensitivity, ascorbic acid, THPC, single spin echo sequence

**Abstrak**

Tujuan utama radioterapi adalah untuk memberi dos sinaran yang mencukupi kepada isipadu sasaran sementara meminimumkan jumlah dos di sekitar tisu yang sihat. Dalam kajian ini tindak balas dos oleh asid metakrilik-gelatin (MAG) dosmeter gel polimer menggunakan anti-oksida yang berlainan iaitu asid askorbik (AscA) dan tetrakis-hydroxy-methyl-phosphonium chloride (THPC) telah di kaji menggunakan aturan nada denyut tunggal MRI. Kepekatan methacrylic acid (MAA) di ubah dan dengan menggunakan MRI, komposisi yang optimum di perolehi daripada tindak balas dos yang maksimum pada gel selepas di iridiasi. Gel polimer diiridiasi oleh 6-MV sinaran photon dari pemecut linear (LINAC) untuk linkungan dos dari 0 sehingga 20 Gy. Kadar relaksasi melintang (R2) bagi gel yang telah di iridiasi di ukur oleh MRI. Satu hubungan berkadar lurus di antara dos dengan R2 di perolehi pada julat dos 0 sehingga 20 Gy bagi gel MAG yang mengandungi asid askorbik (MAGAS) dan hubungan berkadar lurus dari 0 sehingga 10 Gy untuk gel MAG yang mengandungi THPC (MAGAT). Kepekatan optimum bagi MAGAS dan MAGAT gel polimer diperolehi daripada 6% MAA dan 5% gelatin yang menghasilkan nilai sensitif yang paling tinggi iaitu masing-masing 0.0989 $s^{-1}Gy^{-1}$ dan 1.1180 $s^{-1}Gy^{-1}$. Hasil kajian akan di bandingkan dengan urutan nada denyut berganda.

**Kata kunci:** Polimer gel MAGAS, polimer gel MAGAT, sensitiviti dos, asid askorbik, tetrakis-hydroxy-methyl-phosphonium chloride (THPC)

## Introduction

Radiotherapy gel dosimeter is a chemical dosimeter fabricated from radiation sensitive chemicals in an aqueous gelatin network. Upon irradiation, free radicals from radiolysis process were formed in the gel induce polymerization where amount of polymerization increase and related to absorbed dose [1]. The use of radiation sensitive gel for radiation dosimetry was first suggested in the 1950s by Day where radiation induced color changes in dyes were related to radiation dose [2, 3]. Polymer gel dosimetry is one of the gel dosimetry techniques that can be used to verify the spatial dose distribution in complex radiotherapy. The change in dose distribution can be recorded in 3-D by various techniques such as magnetic resonance imaging (MRI) [1], optical scanning [4, 5], x-ray computed tomography [6] or FT Raman spectroscopy [7].

To date, MRI is frequently used modality for measuring 3D dose information in a polymer gel [7]. MRI is a tomographic imaging technique that is based on nuclear magnetic resonance (NMR) signals to produces images [1]. The absorbed dose is quantified using the spin-spin relaxation rate (R2=1/T2). The T2 relaxation time is a biological parameter that is used in MRI to distinguish between tissue types. From R2 images of polymer gel dosimeters, the dose maps can be reconstructed through the calibration curve obtained from a series of samples irradiated to a range of doses. For an extensive details on MR imaging, see the review by Baldock [7] and Doran [8].

A few types of imaging sequences can be applied to acquire quantitative R2 maps. These imaging sequences may differ in performance in terms of accuracy, precision and speed. Two main imaging sequences have often been used. First is *single spin echo sequence* method where each acquisition collects only a single echo, but can be repeated with different echo times [9]. The advantages of the single spin echo sequence is that it is readily available on all scanners and it is easy to understand and measure the R2 relaxation rate data with good signal-noise-ratio (SNR). The gel manufacturer (MGS Research Inc., Guilford, CT) recommends the use of a two echo sequence in order to reduce the data required for each echo (TE1 and TE2) which then reduces the radio frequency power [9]. Consequently the gel temperature will be more stable and it is an important factor for MRI imaging. If one has only access to a single spin–echo sequence, a two-point(s) (two different echo times) method is preferred [10]. The other sequence is *multiple spin echo (MSE) sequence* which applies a train of equally spaced spin-echoes, each corresponding to a different echo time [11, 12].

Despite the advantages of gel dosimetry for 3D dose verifications, the system is not yet establish as a standard clinical tool. Polymer gel dosimetry systems have a major limitation where oxygen during manufacturing procedure known as hypoxic or anoxic gel dosimeters, inhibits the polymerization process in polymer gel as it scavenges free radical initiators (such as OH and H) produced during water radiolysis [1, 13, 14]. In the first generation of polymer gel dosimeters, during the gel fabrication the oxygen was removed by bubbling the gel solution with inert gasses such as nitrogen and argon for several hours [1, 13, 15, 16]. In addition, the gel had to be poured in the containers with low oxygen permeability and solubility.

In modern polymer gel dosimeters, the problem with oxygen is solved by adding an antioxidant in the gel solution that binds to the oxygen and consequently prevents free radical scavenging [17]. As a result the polymer gels can be fabricated under normal atmospheric conditions and are therefore called 'normoxic'. In 2001, Fong et al introduced a new gel composition known as MAGIC (methacrylic and ascorbic acid in gelatin initiated by copper). These gels show a positive responds to absorbed dose when manufactured under normal atmospheric conditions [17]. Moreover, these gels offered several practical and convenient improvements over the early version, such as handling and storage. Since the introduction of the MAGIC normoxic polymer gel dosimeter, a number of other formulations have been investigated for their potential use as normoxic polymer gel dosimeters. This study investigates the dose response and dose sensitivity of MAG gel dosimeter system composed of two different anti-oxidants to find the best anti-oxidant that provide the greatest effect on the dose response. The R2-dose response is examined at various concentrations MAA and a formulation that gave the greatest dynamic range in the R2-dose response was investigated.

## Materials and Methods

### Fabrication of gel dosimeter

The gel formulation consisted of methacrylic acid (Acros, Organics), gelatin (250 bloom, Bovine) (Sigma Aldrich), de-ionised water, ascorbic acid (Sigma Aldrich) and THPC (Sigma Aldrich). The MAG polymer gels were manufactured under normal atmospheric conditions. The gelatine was mixed with de-ionised water in a mixing vessel and was continuously stirred at approximately 48˚C until the gel was completely dissolved and a clear solution was obtained. The solution was cooled to 40˚C then the methacrylic acid monomer was added and continuously stirred until the monomer was completely dissolved. For manufacturing the normoxic polymer gel, an anti-oxidant was finally added to minimise the oxygen exposed to the solution [18]. The fabrication procedures of gel solution are shown as Figure 1. The MAG gels were then poured into 4 ml tissue equivalent polystyrene cuvettes of inner dimensions 1 cm x 1 cm x 4.5 cm ( width x length x height ) with the top sealed by a parafilm tape. Finally they were wrapped in aluminium foils to avoid any preliminary polymerisation from the ambient light. The sample vials were stored at 3˚C before irradiation. In this study, both MAGAS and MAGAT polymer gel used the concentration of gelatin 5% (w/w), ascorbic acid 10 mM and at 10 mM THPC. These concentrations were obtained from our previous study where optimisation of gelatin, ascorbic acid and THPC has been done and the optimised values of the compositions are shown in the Table 1. The concentrations of methacrylic acid had varied from 4 %( w/w) to 9 %( w/w) to obtain the optimum dose response with respect to the MRI signal. After the optimum concentrations were obtained, the MAGAT gel had varied the concentration of THPC to investigate the effect of THPC variation towards the dose response as shown in Table 2.

Table 1. MAGAS and MAGAT gel compositions according to their concentration

| Composition | MAGAS | MAGAT |
|---|---|---|
| Gelatin | 5% (w/w) | 5% (w/w) |
| Methacrylic Acid | 4 - 9% (w/w) | 4 - 9% (w/w) |
| Ascorbic Acid | 10 mM | - |
| THPC | - | 10 mM |
| De-ionised water | 86 – 91% (w/w) | 86 – 91%(w/w) |
| Dose range | 0-20 Gy | 0-20 Gy |

Table 2. MAGAT gel composition with variation of THPC concentrations

| Composition | MAGAT concentration |
|---|---|
| Gelatin | 5% (w/w) |
| Methacrylic Acid | 6% (w/w) |
| THPC | 1 mM, 5 mM, 10 mM, 20 mM, 100mM |
| De-ionised water | 89% (w/w) |
| Dose range | 0-10 Gy |

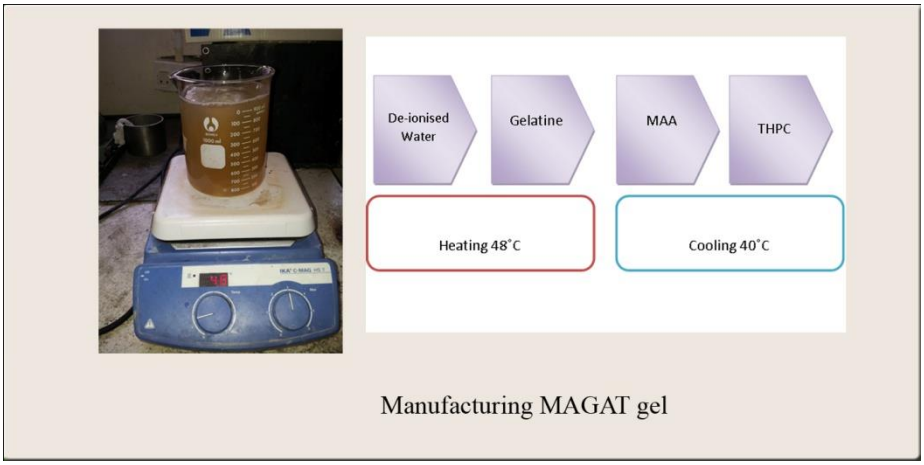



Figure 1. The fabrication of normoxic MAG dosimeter

**Irradiation of gel dosimeter**

Irradiations were performed using a 6 MV photon beam by a linear accelerator (Primus LINAC, Siemens), with a field size of 10 cm x 10 cm at the isocentre and at 100 cm source axis distance (SAD). The dose rate was 3 Gy $min^{-1}$. The samples were irradiated from 0 to 20 Gy by parallel opposed beams so that the gels received a uniform dose at 5 cm depth. One sample of each batch is left unirradiated for background measurement. Solid water phantom slabs were placed above and below the Perspex cuvette holder and the samples were placed at the midregion of the phantom as shown in Figure 2. For THPC concentrations study, the gels were irradiated from 0 to 10 Gy.

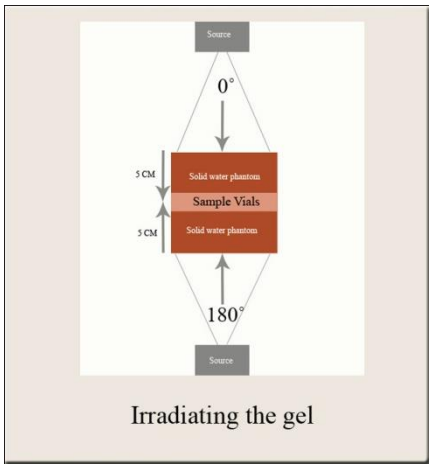



Figure 2. The irradiation of normoxic MAG gel by parallel opposed dual beam technique.

**MRI Imaging technique**

All the sample vials were inserted in a dedicated styrofoam holder and placed in a MRI Signa HDxt 1.5 T whole body scanner using a head coil as shown in Figure 3. The imaging sequence was a *single spin-echo sequence* with time echoes of TE1=20 ms and TE2= 300 ms and a relaxation time (TR) of 3500 ms. The other scanning parameters used such as NEX = 3, slice thickness = 5 mm, slice spacing = 0 mm, FOV = 22 mm, flip angle = 90˚ and matrix size 512 x 256. TE1 and TE2 gave a SNR of 125 % and 128% respectively. Coronal images through the centre of the entire set of calibration vials were acquired and recorded. The T2 dicom images were transferred to a personal computer and analyzed using MATLAB 7.1 (Math Works, Inc.) software. From the time series of T2-weighted images (TE=20 ms, and TE=300 ms), R2-maps were calculated from these images for each sequence pixel by pixel basis using pixel signal intensities and applying the two-point method [11].

$$R2 = \frac{\ln S1 - \ln S2}{TE2 - TE1} \quad \text{(Eq. 1)}$$

The two-point method; where $S_1$, $S_2$ is the measured MR signal intensity at a given echo time, TE and R2 is the transverse relaxation rate.

R2 maps can be converted to dose maps using a linear dose response equation that has been reported by several independent investigators [15, 19, 20].

$$\mathbf{R2 = \alpha D + Ro} \quad \text{(Eq.2)}$$

Linear dose response equation: where $\alpha$ is the slope of the dose–R2 curve, $R_o$ is R2 background and R2 is R2 value of the irradiated gel.



Figure 3. The scanning of the gel samples by 1.5T MRI

## Results and Discussion

### MAGAS and MAGAT polymer gel dose-response with varying MAA compositions

Figure 4 and Figure 5 illustrate the transverse relaxation rate (R2) as a function of the absorbed dose (D) for MAGAS and MAGAT dosimeter at different concentrations of MAA. The absorbed doses selected were from 0 to 20 Gy. For MAGAS gel, the transverse relaxation rates (R2) were linearly proportional to the dose up to 20 Gy (Figure 4). R2 is obtained from the nuclear magnetic resonance (NMR) signal which is dose dependent. In polymer gel dosimeter, R2 value is rely on amount of polymer formed within the gel dosimeter after irradiated. As the dose increased, the formation of polymer increased therefore R2 increased. This linear dose response was maintained even though the MAA concentrations were increased. While for MAGAT gel, R2 were linearly proportional to the dose up to 10 Gy only (Figure 5). This linear dose response was maintained even though the MAA concentrations were increased. However between 10 to 20 Gy dose ranges, the response was change in slope due to the saturation of the gel at high dose range. As obtained from T2 weighted image of our study (Figure 6 and Figure 7), as the dose increased from 0 to 20 Gy, the pixel value decreased. This is due to the rapid attenuation of signal intensity at high energy of photon (high dose) after irradiation, caused an increased in polymer formation in gel dosimeter thus drop the pixel value (T2-weighted image become darker due to high formation of polymer in gel dosimeter). At high dose (15 to 20 Gy), maximum polymerization occurs which causes a small change in the pixel intensity and later results in the signal being saturated.

The linear and the non-linear ranges depend on the type of polymer gel dosimeter. The R2-dose response of the MAGAT polymer gel dosimeter was found to be higher than that of MAGAS gel dosimeter, which is prepared with AscA in place of THPC. The results showed that anti-oxidant plays an important role that will affect the dose response of the gel.

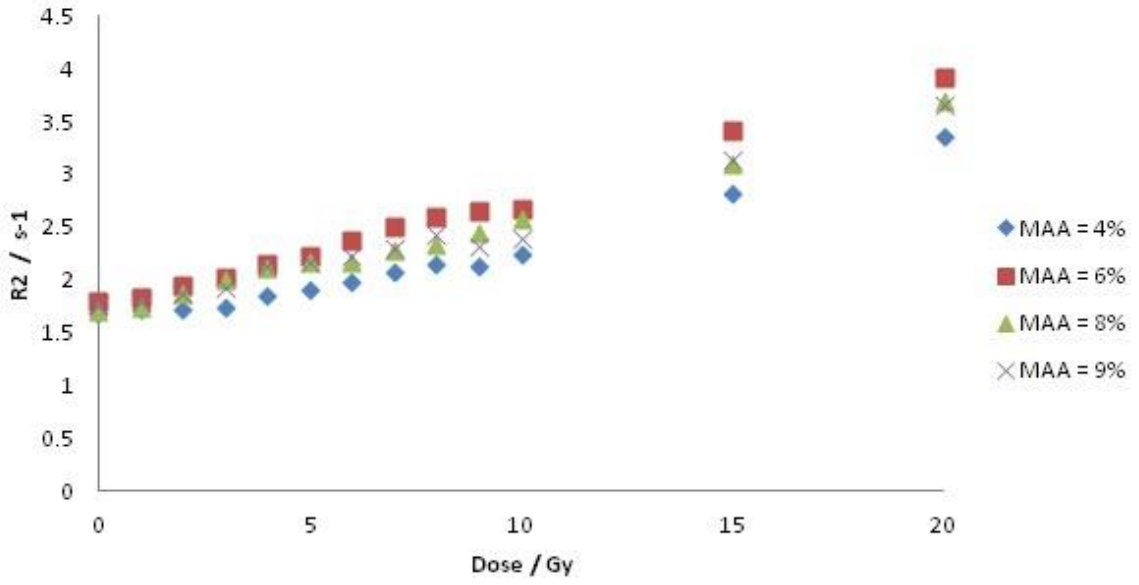



Figure 4. Transverse relaxation rate (R2) as a function of absorbed dose (D) for MAGAS gel dosimeter of 5% gelatin for varying concentrations of MAA irradiated from 0 to 20 Gy

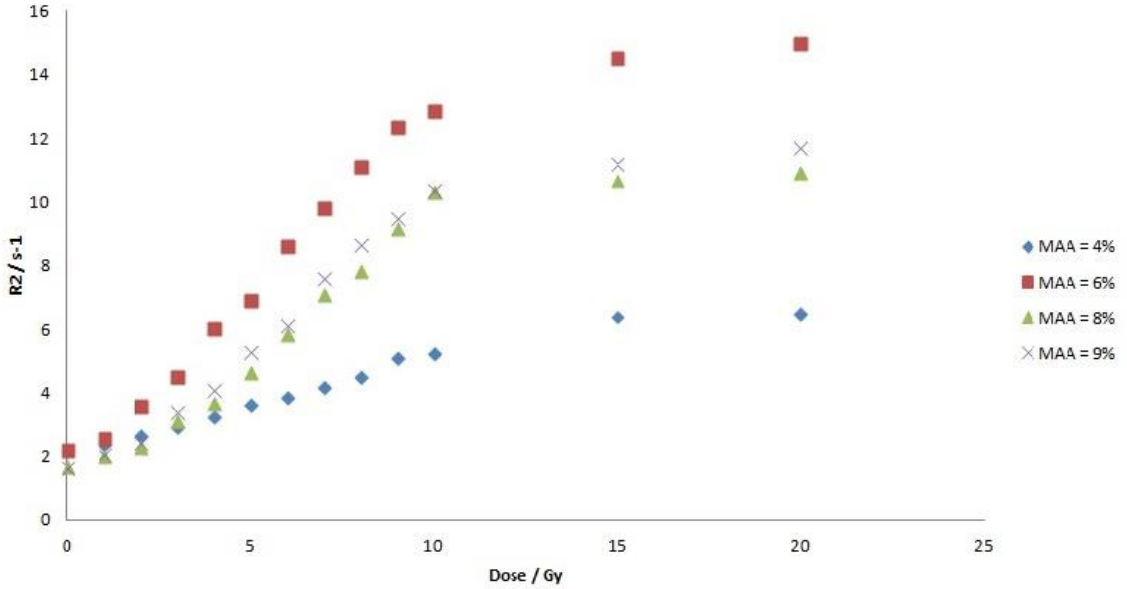



Figure 5. Transverse relaxation rate (R2) as a function of absorbed dose (D) for MAGAT gel dosimeter of 5% gelatin for varying concentrations of MAA irradiated from 0 to 20 Gy

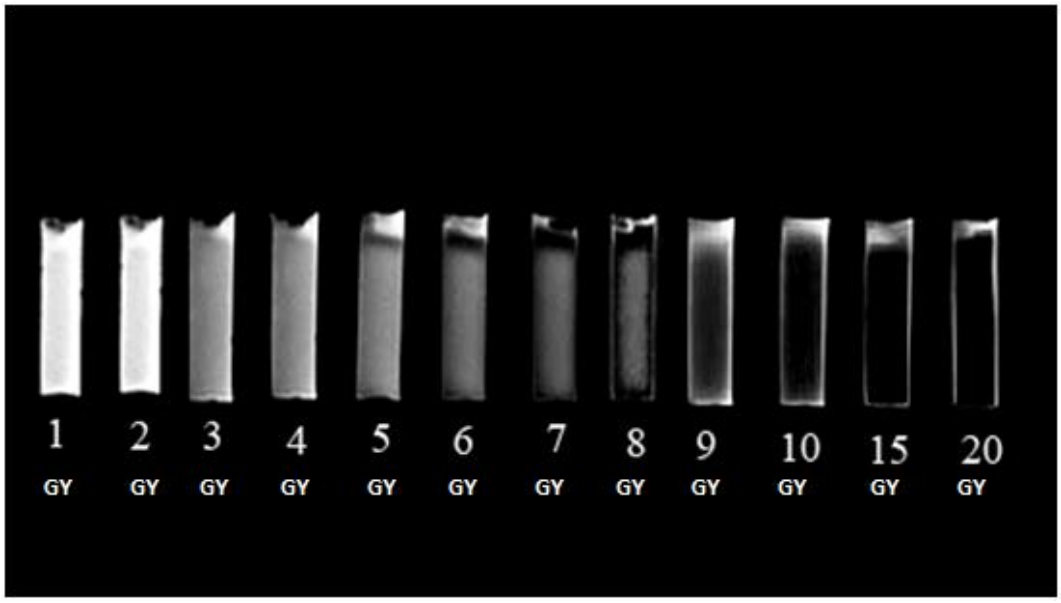



Figure 6. The T2-weighted image of MAGAT gel dosimeter irradiated at 0 to 20 Gy. (The white colour of image (1 to 7 Gy) has high pixel value as formation of polymer is small while dark colour of image (8 to 20 Gy) has small pixel value as formation of polymer is large).

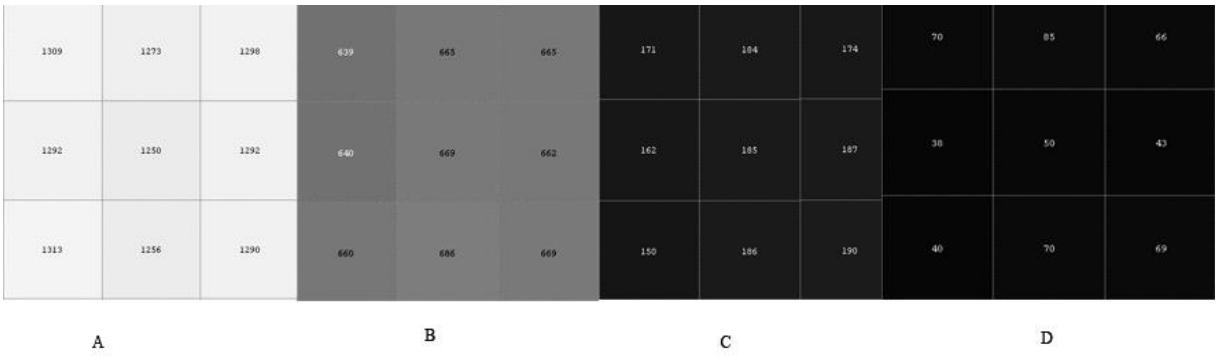



Figure7. The pixel value of T2-weighted image according to Fig. 6 at different dose. (A) 1 Gy, (B) 5 Gy, (C) 10 Gy, (D) 15 Gy.

The dose sensitivity is defined as the slope of the dose response curve ($[\frac{dR2}{dD}]$). The linear fit $(R2 = \alpha D + R_0)$ between R2 and the dose region of 0 to 10 Gy, provided the values of dose sensitivity ($\alpha$) and the offset ($R_0$). For the MAGAS and MAGAT polymer gel dosimeter used in this study, it was found that the optimal concentration of MAA that produced the highest changes in R2-dose response was 6% (w/w) MAA and 5% (w/w) gelatin as shown in Table 3. From the study using S*ingle spin echo sequence***,** the MAGAT gel has a sensitivity of 1.1180 $s^{-1}Gy^{-1}$ with a linear regression of 0.9957. However studies from *Multiple spin echo sequence* showed MAGAT gel has a sensitivity of 3.42 $s^{-1}Gy^{-1}$ [21] and 3.2 $s^{-1}Gy^{-1}$ [22]. On the other hand, from *Single spin echo sequence* study MAGAS gel exhibits 10 times lower dose sensitivity of 0.0989 $s^{-1}Gy^{-1}$ with a linear regression of 0.9856 whereas study from *Multiple spin echo sequence* showed MAGAS gel has a sensitivity of 0.50 $s^{-1}Gy^{-1}$ [23]. Although the sensitivity of MAGAS gel is low compared to MAGAT gel dosimeter but the presence of an AscA is sufficient to prevent oxygen from inhibiting the polymerization of the polymer gel dosimeter. Hence MAGAT gel is considered as the most standard gel dosimeter with superior sensitivity and dose resolution [22, 24, 25]. From this study, the sensitivity of *Single spin echo sequence* is much lower than *Multiple spin echo sequence* study, but its sensitivity is much higher than the other type of gel [22].

The sensitivity of MAGAT gel increment depends on the MAA concentrations. An increase in MAA concentrations from 4% to 6% lead to an increase in R2-dose response. After the maximum polymerization occurred at 6% of MAA, the R2 dose response starts to decrease with the increasing of MAA from 8% to 9%. Higher concentrations of MAA associate with more acrylic monomers available for the polymerization reaction. The rate of polymerization within a certain polymer gel dosimeter is determined by temperature, monomers concentration, gelatin concentration and other elements in gel dosimeter recipe. Thus, different concentrations of MAA will produce different rates of polymerization, hence it may vary the R2-dose response and sensitivity of the polymer gel dosimeter.

Table 3. The dose sensitivity and the linear regression of MAGAS and MAGAT gel at various concentration of MAA at doses 0 – 10 Gy.

| | MAGAS | | MAGAT | |
|---|---|---|---|---|
| MAA concentration | Sensitivity/$s^{-1}$ $Gy^{-1}$ | R2 | Sensitivity/$s^{-1}$ $Gy^{-1}$ | R2 |
| 4% | 0.0594 | 0.9692 | 0.3156 | 0.9917 |
| 6% | 0.0989 | 0.9856 | 1.1180 | 0.9957 |
| 8% | 0.0841 | 0.9805 | 0.8961 | 0.9888 |
| 9% | 0.0701 | 0.9368 | 0.9336 | 0.9937 |

**Effect of varying THPC concentrations on dose response**

MAGAT polymer gel dosimeters with THPC concentrations between 5 to 10 mM produced the greatest R2 sensitivity as shown in Figure 8. A threshold concentration of 1mM THPC was found to be required for an adequate R2-dose response to avoid inhibition of polymerization. A small decrease in the dose sensitivity was observed after increasing the concentrations of THPC from 20 mM to 100 mM THPC thus 10mM of THPC gave the best sensitivity. This indicated that THPC may also act as a promoter of the polymerization reaction [11].

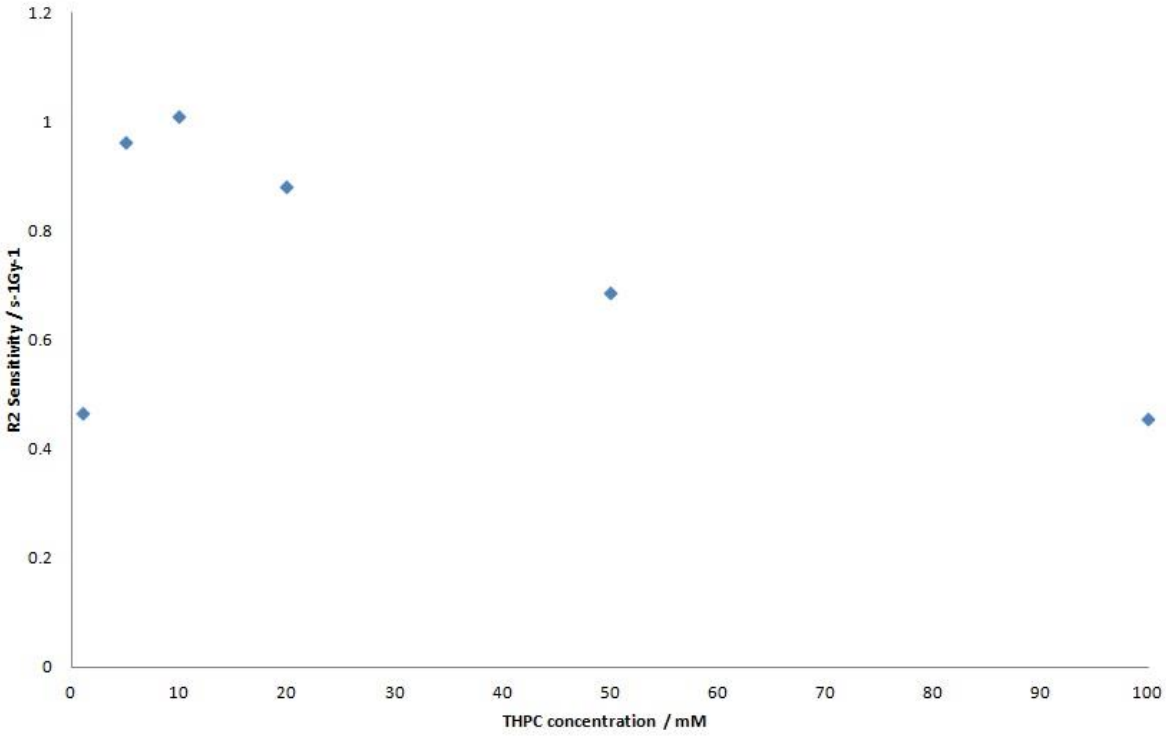



Figure 8. The dose sensitivity of MAGAT gel at different concentrations of THPC

## Conclusion

We have investigated role of antioxidant in a MAG gel dosimeter system composed of MAA, gelatin and two different anti-oxidants using single spin echo sequence MRI. The formulation that provided the greatest change of R2 is from MAGAT gel composed of 10mM THPC, 6% MAA and 5% gelatin with the sensitivity 1.1180 (s-1 Gy-1). Whilst MAGAS gel shows 10 times lower in dose sensitivity compared to MAGAT gel. The sensitivity of MAGAT and MAGAT gel obtained from single spin echo sequence study is much lower than multiple spin echo sequence study.

## Acknowledgement

We are indebted to Universiti Sains Malaysia for providing us a short term grant. We would like to thank to Pantai Mutiara Hospital, Penang for giving us the opportunity to use the linear accelerator unit and Institut Perubatan dan Pergigian Termaju (Advanced Medical & Dental Institute), Penang for the use of the Magnetic Resonance Imaging unit.

**References**


1. Maryanski, M.J., Gore, J.C., Kennan, R.P. & Schulz, R.J. (1993 ). NMR relaxation enhancement in gels polymerized and cross-linked by ionizing radiation: a new approach to 3D dosimetry. *MRI Magn. Reson. Imaging*, 11: 253–258.
2. Day, M.J., Andrews, H.L., Murphy, R.E. & Lebrun, E.J. (1957). Gel dosimeter for depth dose measurements. *Review of Scientific Instruments*, 28: 329–332.
3. Day, M.J. and G. Stein. (1950). Chemical effects of ionising radiation in some gels. *Nature*, 166: 146–147.
4. Doran, S.J., K.K. Koerkamp, M.A. Bero, P. Jenneson, E.J. Morton, and W.B. Gilboy. (2001). A CCD-based optical CT scanner for high-resolution 3D imaging of radiation dose distributions: equipment specifications, optical simulations and preliminary results. *Phys. Med. Biol*., 46: 3191–3213.
5. Doran, S.J. (2013). How to perform an optical CT scan: an illustrated guide. *Journal of Physics: Conference Series*, 444 (1): 012004.
6. Jirasek, A. (2010). Alternative imaging modalities for polymer gel dosimetry. *Journal of Physics: Conference Series*, 250: 012070.
7. Baldock, C., Y. De Deene, S. Doran, G. Ibbott, A. Jirasek, M. Lepage, K.B. McAuley, M. Oldham, and L.J. Schreiner. (2010). Polymer gel dosimetry. *Phys. Med. Biol.*, 55 p. R1–R63
8. Doran, S.J. (2010). Imaging and 3-D dosimetry: top tips for MRI and optical CT. *Journal of Physics: Conference Series,* 250(1): 012086.
9. Low, D.A., J. Markman, J.F Dempsey, S. Mutic, M. Oldham, R. Venkatesan, E.M. Haacke, and J.A. Purdy. (2000.). Noise in polymer gel measurements using MRI. *Med. Phys*., 27: 1814-1817.
10. De Deene, Y., R. Van de Walle, E. Achten, and C. De Wagter. (1998). Mathematical analysis and experimental investigation of noise in quantitative magnetic resonace imaging applied in polymer gel dosimetry. *Sig Proc.*, 70:. 85-101.
11. De Deene, Y. and C. Baldock. (2002).Optimization of multiple spin-echo sequences for 3D polymer gel dosimetry. *Phys. Med.Biol.*, 47: 3117-3141.
12. Baldock, C., M. Lepage, S. Back, P. Murry, P. Jayasekera, D. porter, and T. Kron. (2001). Dose resolution in radiotherapy polymer gel dosimetry: effect of echo spacing in MRI pulse sequence. *Phys. Med. Biol.*, 46: 449-460.
13. Maryanski, M.J., R.J. Schulz, G.S. Ibbotq, J.C. Gatenby, J. Xiell, D. Hortonq, and J.C. Gore. (1994). Magnetic resonance imaging of radiation dose distributions using a polymer-gel dosimeter. *Phys. Med. Biol.*, 39: 1437-1455.
14. Hepworth, S.J., M.O. Leach, and S. Dorran. (1999). Dynamics of polymerisation in polyacrylamide gel (PAG) dosimeters: (II) modelling oxygen diffusion. *Phys. Med. Biol.*, 440: 3105 -3113.
15. Maryanski, M.J., G.S. Ibbott, P. Eastman, R.J. Schulz, and J.C. Gore. (1996). Radiation therapy dosimetry using resonance imaging of polymer gels. *Med. Phys*., 23: 699–705.
16. Baldock, C., R.P. Burford, N. Billingham, G.S. Wagner, S. Patval, R.D. Badawi, and S.F. Keevil. (1998). Experimental procedure for the manufacture and calibration of polyacrylamide gel (PAG) for magnetic resonance imaging (MRI) radiation dosimetry. *Phys. Med.Biol.*, 43: 695-702.
17. Fong, P.M., D.C. Keil, M.D. Does, and J.C. Gore. (2001). Polymer gels for magnetic resonance imaging of radiation dose distributions at normal room atmosphere. *Phys. Med. Biol*., 46: 3105–3113.
18. De Deene, Y., C. Hurley, A. Venning, K. Vergote, M. Mather, B..J Healy, and C. Baldock. (2002). A basic study of some normoxic polymer gel dosimeters. *Phys. Med. Biol.*, 47 p. 3441–3463.
19. Ibbott, G.S., M.J. Maryanski, P. Eastman, S.D. Holcomb, Y.S. Zhang, R.G. Avison, M. Sanders, and J.C. Gore. (1997). 3D visualization and measurement of conformal dose-distributions using MRI of BANG-gel dosimeters. *Int.J. Radiat. Oncol. Biol. Phys.*, 38: 1097–1103.
20. Oldham, M., I.B. Baustert, C. Lord, T.A.R. Smith, M. McJury, M. Leach, A.P. Warrington, and S. Webb. (1998). An investigation into the dosimetry of a 9 field tomotherapy irradiation using BANG-gel dosimetry. *Phys. Med. Biol.*, 43: 1113–1132.
21. Jason J.S. Lee, Chia-Jung Tsai, Man-Kuok Lo, Yung-Hui Huang , Chien-Chuan Chen, Jay Wu, Yeu-Sheng Tyan, and Tung-Hsin Wud. (2008). Investigation of dose characteristics in three-dimensional MAGAT-type

polymer gel dosimetry with MSE MR imaging. *Nuclear Instruments and Methods in Physics Research B,* 266: 2199–2202.

22. Jirasek, A. (2006). Experimental investigations of polymer gel dosimeters. *J.Physics: Conference Series,* 56: 23–34.
23. Venning, A., B. Healy, K. Nitschk, and C Baldock. (2005). Investigation of the MAGAS normoxic polymer gel dosimeter with Pyrex glass walls for clinical radiotherapy dosimetry. *Nuclear Instruments and Methods in Physics Research A*, 555: 396–402.
24. Shin-ichiro, H., Y. Munenori, U. Shuji, H. Kiyofumi, K. Takahiro, k.B. McAuley, and T. Takahiro. (2010). A study on the role of gelatin in methacrylic-acid-based gel dosimeters. *Radiation Physics ans Chemistry*, 79: 803–808
25. Yoshioka, M., S. Hayashi, S. Usui, K. Haneda, H. Numasaki, T. Teshima, and T. Tominaga. (2009). A new polymer gel dosimeter composed of methacrylic acid,agarose gel and THPC with gelatin. *J.Physics: Conference Series*, 164: 012013.

The Malaysian Journal of ANALYTICAL SCIENCES ISSN 1394-2506

# MECHANICAL PROPERTIES OF STARCH FILLED POLYPROPYLENE UNDER EXPOSURE OF HYGROTHERMAL CONDITIONS

## (Sifat-sifat Mekanikal Bagi Komposit Polipropilena Terisi Kanji di Bawah Pendedahan Higroterma)

Wan Zakaria Wan Nor*, Nor Azura Abdul Rahim, Hakimah Osman and Muthmirah Ibrahim

[1]*School of Materials Engineering,*
*Universiti Malaysia Perlis, Kompleks Pengajian Jejawi, Jejawi 2, 02600 Arau, Perlis, Malaysia.*

**Corresponding author: wanzakariawannor@gmail.com*

**Abstract**

The hygrothermal properties of starch filled polypropylene (PP) composites with different types of starches; sago, tapioca, and corn content at 20 wt% were studied. The PP composites were compounded using Brabender Plasticoder machine and the composites samples were prepared through by compression molding technique. The hygrothermal absorption test was conducted out to investigate the moisture absorption at different temperatures (i.e. room temperature, 40°C and 70°C). Thus, the flexural test was carried out to study the effect of hygrothermal conditions on mechanical properties and scanning electron microscopy (SEM) used to verify the obtained results through morphological study. The results revealed that the mechanical properties of PP composites deteriorate after a period of immersion time and the hygrothermal aging of composites was accelerated as the temperature increased.

**Keywords:** polypropylene composites, starch filled polypropylene, hygrothermal absorption, mechanical properties

**Abstrak**

Sifat-sifat higroterma bagi komposit polipropilena (PP) terisi kanji; sagu, ubi kayu, dan jagung yang terkandung 20% berat telah dikaji. Komposit-komposit PP telah disebatikan menggunakan mesin Brabender Plasticoder dan sampel-sampel komposit disediakan menggunakan teknik pengacuanan mampatan. Ujian penyerapan higroterma telah dijalankan untuk menyiasat kadar serapan lembapan pada beberapa suhu yang berbeza (suhu bilik, 40°C, dan 70°C). Seterusnya, ujian lenturan telah dijalankan untuk menkaji kesan keadaan higroterma ke atas sifat-sifat mekanikal dan mikroskopi pengimbasan electron (SEM) digunakan untuk mengesahkan keputusan yang diperolehi melalui kajian morfologi. Keputusan menunjukkan bahawa sifat-sifat mekanikal bagi komposit-komposit PP merosot selepas direndam untuk suatu tempoh masa dan kadar penuaan higroterma bagi komposit-komposit telah dipercepatkan apabila suhu meningkat.

**Kata kunci:** komposit polipropilena, polipropilena terisi kanji, serapan higroterma, sifat-sifat mekanikal

## Introduction

Polyolefin is not degraded by microorganisms in the environment, which contribute to large volume of plastic waste [1]. For this reason, there is a growing interest in the development of composite materials since the starch is cheap, biodegradable, renewable, and majorly form of stored carbohydrate which can be found in plants such as corn, wheat, rice, sago, tapioca, and potatoes [2]. The compounding of the biodegradable materials, such as starch with inert polymers, such polyethylene (PE), polypropylene (PP), low density poly ethylene (LDPE), have been receives considerable attention among the researcher.

Thus, natural fillers have been receiving considerable attention as substitutes for synthetic fiber reinforcements such as glass in plastics due to their low density, acceptable specific strength, good thermal insulation properties, reduced tool wear, reduced thermal and respiratory irritation as well as renewable resources and the end product would be biodegradable and cheap [3, 4]. Generally, starch is a semicrystalline polymer composed of two polymers with

repeating α-D-glucopyranosyl units. These substances are amylose and amylopectin, a linear and a highly branched polysaccharide, respectively. The repeating units in amylose are linked by α (1–4) linkage. The amylopectin has an α(1–4) linked backbond and about 5% α(1–6) linked branches [5, 6].

In previous research, a lot of studies have been carried out, for examples Liu et al. [7], Zullo and Iannace [8] and Guimarães et al. [9] in optimizing the processing conditions of the starch. Besides that, many have dedicated in modifying or induce cross-linking of the starch. Garg and Jana [10], Kim and Lee [11], Kuniak and Marchessault [12], and Delval et al. [13] were among those who had studied the interfacial properties using the cross-linked or modified starch. In engineering practice, moisture absorption test was done for quality control purposes and to measure the degradation of the quality for the composite materials [14]. The study on the moisture absorption and hygrothermal aging properties also has captured an interest of a scientist in the polymer field [15-19].

The chemical and physical changes can be determined through the aging process. Natural aging tests are very representative to reproduce identical conditions of exposure that is biodegradation, but they require longer time which will take several years [20]. To accelerate the aging process, the hygrothermal testing condition is applied. However, study on the aging behaviors of the starch filled polypropylene exposed in hygrothermal environment is rarely reported. In this paper, we focuses on study of hygrothermal effect on the mechanical properties of starch filled polypropylene composites that exposed under hygrothermal conditions at different temperatures.

## Materials and Methods

### Materials

The grade of PP used is Titanpro SM340, produced by Titan Petchem (M) Sdn. Bhd. This type PP resin provided their density at 0.9 g/cm$^3$ and a melt flow index value (MFI) at 4.0 g/10 min (2.16 kg at 230 °C). The starch (i.e. corn (C), sago (S), and tapioca (T) starch) was supplied by Zarm Scientific Sdn. Bhd., Malaysia.

### Preparation of samples

Compounding process of PP composites was carried out using the Brabender Plasticoder machine at the temperature of 170 °C and a rotary speed of 50 rpm. The PP/starch composites were compounded according to Table 1. First, PP was added in the mixing chamber for 4 minutes until completely melted. Then, starch was added and mixing was continued for another 4 minutes. Compounded samples were prepared by using compression molding machine (GoTech GT7014-A30C, Taiwan). Samples were pressed into flexural shaped mould at 180 °C using pressure of 15 MPa for 6 minutes and cooled under pressure for 2 minutes.

Table 1. Formulation of PP/starch composite

| Designation | Part (wt%) |
|---|---|
| PP | 100 |
| PP/20C | 80/20 |
| PP/20S | 80/20 |
| PP/20T | 80/20 |

### Melt flow index (MFI)

MFI measurements of PP/starch composites were conducted by using Melt Flow Indexer at temperature of 180 °C and load 2.16 kg. Extruded samples were cut every one minute and five samples of each composition were taken to be analyzed.

**Mechanical properties**

The flexural tests were conducted using Instron 5569 universal testing machine according ASTM D790. The crosshead speed 5 mm $min^{-1}$ was used with a support span of 50 mm. Five samples of each composition were selected for this testing method and the mechanical test was carried out under ambient temperature.

**Moisture absorption**

The composite samples were dried inside the oven at 70 °C for 24 h and then, the moisture absorption test was carried out by the immersion of the samples in distilled water that was placed in the water bath (Memmert, Germany) at room temperature (RT), 40 °C, and 70 °C. The moisture uptake was determined through periodically recorded the composite sample weight using Sartorius M-pact Analytical Balance AX224. The percentage of moisture absorbed, $M_t$, at any time t was calculated using equation (1):

$$M_t\ (\%) = (W_w - W_d) / W_d \times 100 \quad (1)$$

where $W_d$ denote, weight of the initial specimens and $W_w$ is the weight of the specimens after exposure to the moisture respectively.

In the previous report, several models had been introduced to analyze the diffusion molecules in the polymeric materials [18, 19, 21, 22]. Fick's law is the popular method that usually used to describe one dimensional moisture absorption process with dependence of time [23]. The weight gained from the moisture absorption can be measured through equation (2):

$$\frac{M_t}{M_\infty} = 1 - \frac{8}{\pi^2}\, exp\left[-\left(\frac{Dt}{h^2}\right)\pi^2\right] \quad (2)$$

where $M_\infty$ representing the percentage of equilibrium content of sample, h is the thickness of the test sample, while D is diffusion coefficient or diffusivity which is related to rate of diffusion into the sample and it can be calculated from the slope of the absorption curve.

## Results and Discussion

**Melt flow index (MFI)**

Table 2 shows the MFI value of PP and PP/starch composites. The results reveal that the MFI values of PP/starch composites were decreased with the presence of 20 wt% of starch content (i.e. corn, sago, and tapioca starch) compared to neat PP. Since the MFI could be indirectly method to measure the viscosity, the starch must act as rigid filler since the main effect of rigid fillers is to increase the elastic modulus of a composite or the viscosity of a fluid suspension [24].

Table 2. MFI values of neat PP and PP/starch composites

| Designation | MFI value (g/10 min) |
|---|---|
| PP | 1.3952 |
| PP/20C | 1.3302 |
| PP/20S | 1.3596 |
| PP/20T | 1.1656 |

**Moisture absorption**

The relations of percentages of moisture uptake, $M_t$ under exposure of different hygrothermal conditions with respect to exposure square root of time, $t^{½}$ are shown in Fig. 1, 2, 3 and 4. It can be seen that the moisture absorption

rate for all samples were significantly change after being exposed to hygrothermal conditions at RT, 40 °C, and 70 °C for several days. In all exposure conditions, the $M_t$ values increase linearly with $t^{½}$ until it reached its equilibrium state.

Refer to the absorption curves of PP and PP/starch composites in figures below, it can be seen that the rate of $M_t$ has a small effect on tested samples after exposed at RT and 40 °C. However, at higher temperature of 70 °C, the rate of $M_t$ rapidly increased in PP/starch composites with respect to neat PP. These proved that the degradability of the PP/starch composites were accelerated at high temperature of 70 °C compared to RT and 40 °C. Besides that, the $M_t$ values in the composites can attributed to the hydrophilic nature of the starch (corn, sago, and tapioca) by presence of a hydroxyl groups which are available for interaction with of water molecules. Preechawong et al. [25] stated that starch was absorbed the water due to its hygroscopic nature. It was acted as a natural plasticizer in starch which provided the flexibility in starch as compared to hard and rigid filler in it while in dry state.

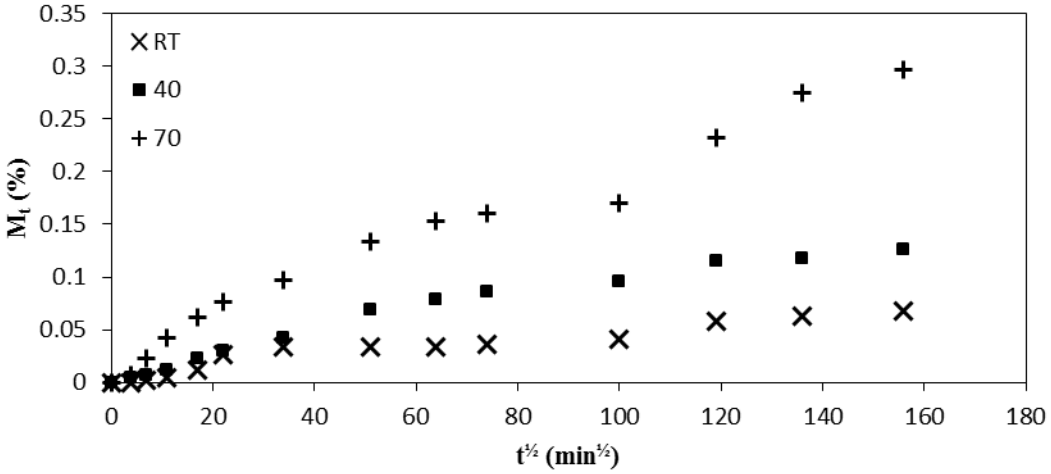



Figure 1. The effect of hygrothermal condition on PP sample at different temperatures

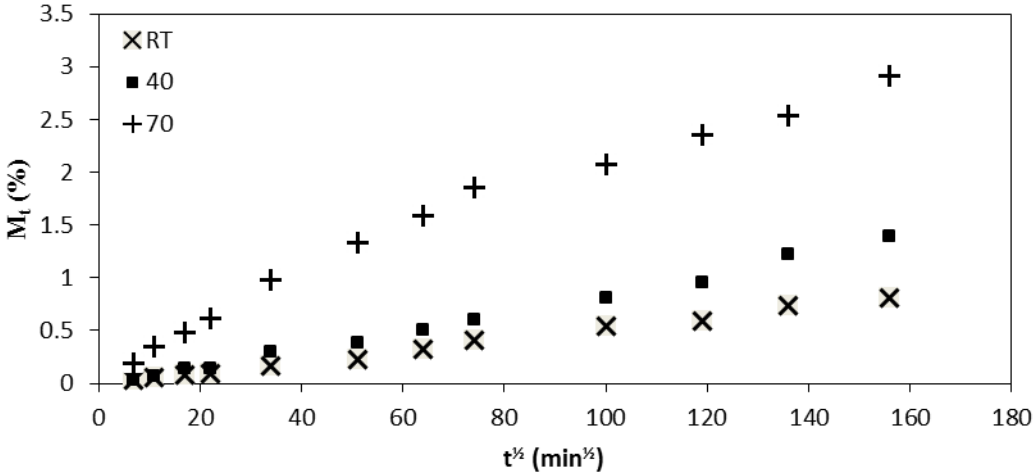



Figure 2. The effect of hygrothermal condition on PP/20C composite at different temperatures

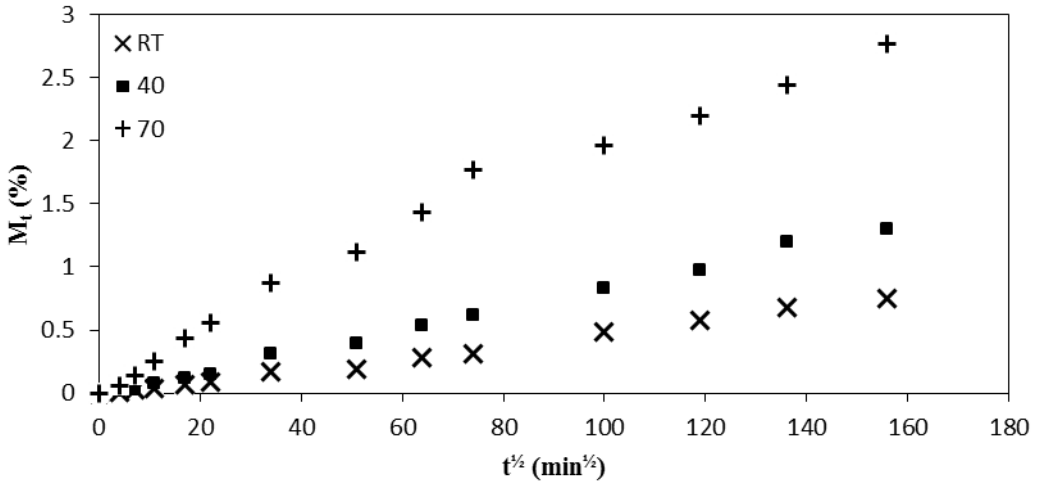



Figure 3. The effect of hygrothermal condition on PP/20S composite at different temperatures

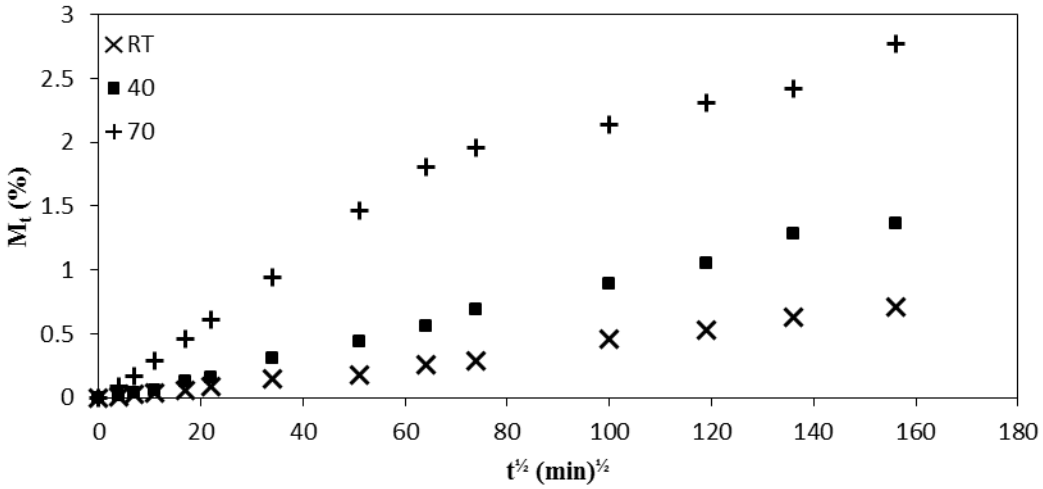



Figure 4. The effect of hygrothermal condition on PP/20T composite at different temperatures

**Mechanical properties**

Table 3 shows the mechanical properties of the PP/starch composites. The mechanical properties decreased slowly when water aging approach with time and temperatures. Before being exposed in a hygrothermal conditions, most of the samples have lower flexural strength compared to the neat PP. As expected the flexural strength of the composites were reduced after exposed at difference hygrothermal conditions for two weeks. In this particular test, at higher testing temperature (i.e. 70 °C) the samples tend to deteriorate which significantly reduce their mechanical properties. Meanwhile, the flexural strength of the neat PP showed a slower reduction rate even at temperature of 40 °C or 70 °C.

Table 3. The flexural properties of neat PP and PP/starch composites before and after exposed under hygrothermal conditions.

| Compound | Mechanical Properties | Controlled | Test Temperature (°C) | | |
|---|---|---|---|---|---|
| | | | RT | 40 | 70 |
| PP | FS (MPa) | 31.25 | 31.02 | 30.9 | 30.65 |
| | FM (MPa) | 691.55 | 690.66 | 687.61 | 665.15 |
| PP/20C | FS (MPa) | 26.81 | 24.55 | 24.36 | 23.41 |
| | FM (MPa) | 825.28 | 798.61 | 774.34 | 683.92 |
| PP/20S | FS (MPa) | 26.30 | 26.02 | 24.96 | 23.20 |
| | FM (MPa) | 817.56 | 811.50 | 746.27 | 649.82 |
| PP/20T | FS (MPa) | 27.19 | 26.89 | 26.48 | 26.25 |
| | FM (MPa) | 830.24 | 798.61 | 781.35 | 727.98 |

Note: FS = Flexural Strength, FM = Flexural Modulus

Thakore et al. [26] have demonstrated that the mechanical properties of composites reduced as increasing of the biodegradable component or starch were incorporated. Whereas, Wang et al. [27] founded, the moisture content has absolute effect on the interfacial bonding between starch and plastic. The starch granules that embedded in the plastic were observed to be swollen, thus resulting poor mechanical strength. They had also reported that the mechanical properties will drop as the moisture content increased. It is attributed to the hydrophilic characteristic of the components. Since this composite involved starch which is hydrophilic in nature hence, the homogeneity and adhesion between starch (C, S, and T) and the hydrophobic PP has substantially reduce.

As can be seen in Table 3, the modulus of all the PP/starch composites were slightly higher than neat PP. 690.66 MPa of flexural modulus value was recorded for controlled or unexposed sample of PP, while there are no significant changes of PP samples although they were exposed in hygrothermal condition at RT and 40 °C. In comparison with controlled PP, a different result was recorded for PP sample which was exposed at 70 °C. The decrement of modulus property almost dropped until 3.8 %. It may be due to the moisture content inside the composites is not in an equilibrium state within the test time. Although, the modulus between those three types of the starch used has not significantly affected but there is an obvious reduction after the immersion at 70 °C compared to the controlled samples. Ke et al. [28] suggested that the increasing modulus in the starch blends can be explained by the crystallinity, hydrogen bonding and stiffening effect of the starch granules.

However, the reduction of the mechanical properties also indicates the presence of a weak adhesion between the starch and matrix. Some of the researchers have discussed about the microcavities phenomena inside the composites which effected by the moisture inside the material and cause the disruption of the filler-matrix bonds. Athijayamani et al. [29], Mohd Ishak et al. [30], & Vlasveld et al. [31] conclude, these microcavities will act as crack concentrators which initiate the internal cracking and subsequently reduce the stiffness and strength of the composites. Duanmu et al. [22] studied the hygro-mechanical properties of the thermoplastic starch reported that the moisture uptake significantly reduces the strength and stiffness of the samples. The presences of moisture also cause the plasticization effect on the composites. The water that filled inside the microcavities will act as a plasticizer and to reduce the stiffness [32].

**Morphological studies**

SEM micrographs taken from the fractured surface of controlled PP highlight the hygrothermal effects on the morphology of the sample at 70 °C states are shown in Figs. 5(a) and (b). There are some evidences of plastic deformation in the form of matrix drawing or yielding. A contrasting view is observed for neat PP after it was exposed to hygrothermal condition of 70 °C, where the fracture surfaces of exposed sample are flatter and less yielding compare to controlled sample.

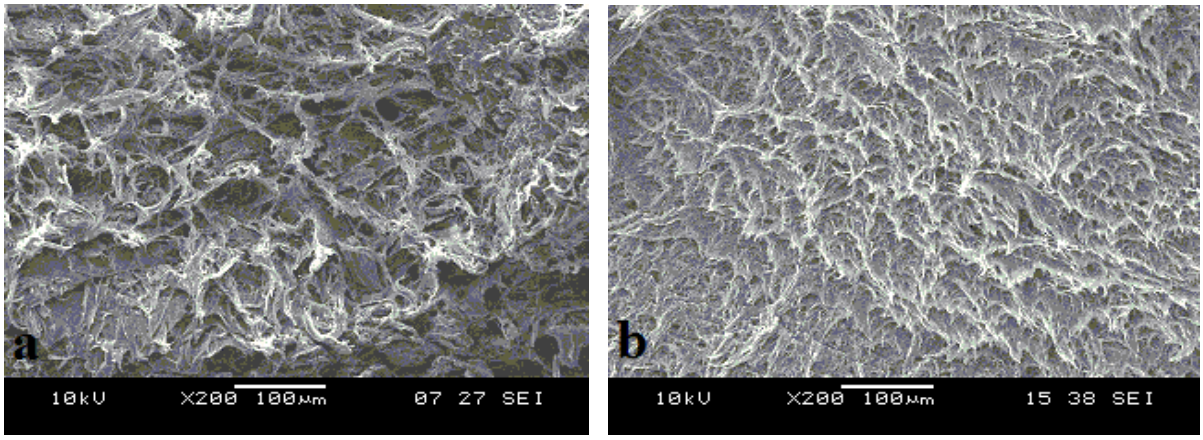



Figure 5. SEM micrographs taken from the fracture surface of (a) controlled PP and (b) neat PP after exposed in hygrothermal condition of 70 °C.

The surface appearence of starch filled PP composites shown by the SEM micrographs in Fig. 6(a-b) and 7(a-b) clearly provide good evidences to prove the effect of the hygrothermal environment on the composites properties. As it can be seen from the figure, the fracture surfaces of the hygrothermally exposed PP/20S and PP/20T shows flatter than unexposed samples. Normally, the fracture surfaces are flat with no evidence of plastic deformation. This explains the hygrothermal conditions are totally effect which cause the brittle behavior of composite samples during the flexural test.

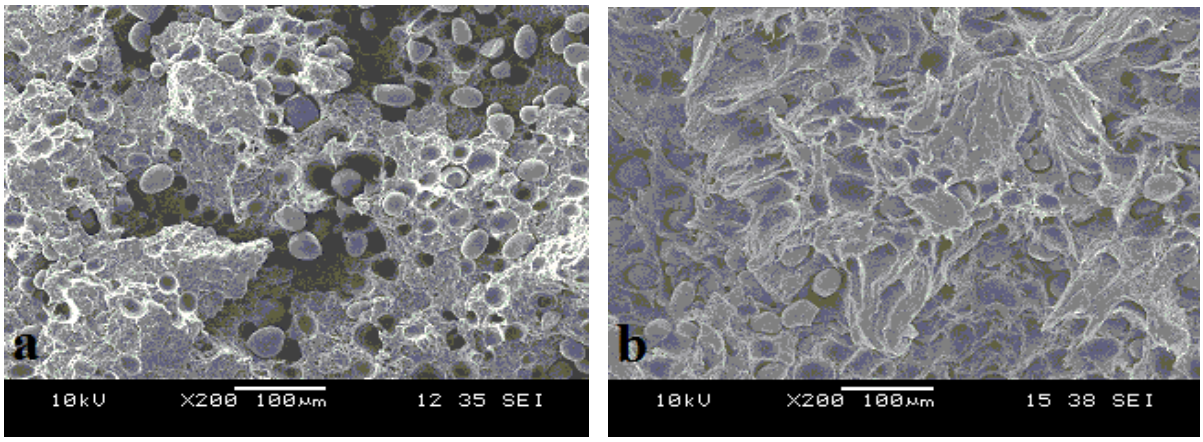



Figure 6. SEM micrographs taken from the fracture surface of (a) PP/20S and (b) PP/20S after exposed in hygrothermal condition of 70 °C.

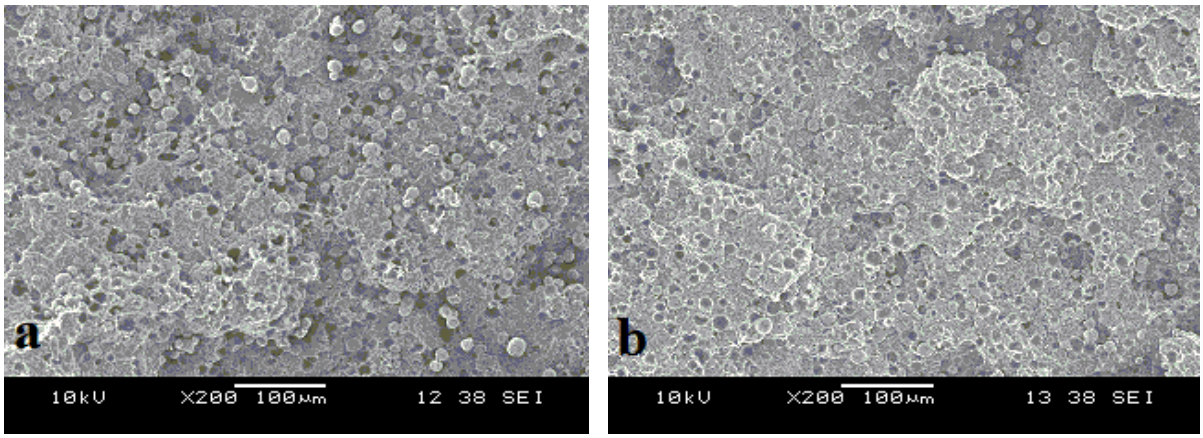



Figure 7 . SEM micrographs taken from the fracture surface of (a) PP/20T and (b) PP/20T after exposed in hygrothermal condition of 70 °C.

In addition, these micrographs strongly evidence to relate the dropped of mechanical properties of PP/20S than PP/20T samples. The bigger size of granule can cause the voids or cavities formation after it was exposed to hygrothermal environments. These formations will act as stress concentration point and further decrease the mechanical properties of the PP/starch composites. The fine particle size of T granule causing the filler well dispersed throughout the composites and well coated by PP matrix thus, reducing the voids and cavities formation. This is agreed with the observed embritllement of the composites and explains the dramatic drop of mechanical properties of the composites after they were exposed in hygrothermal environments.

## Conclusion

In the present study, the mechanical properties of the PP/starch blends were reduced after being exposed under hygrothermal conditions. The mechanical properties of PP/starch composites decreased drastically upon exposure at 70 °C of hygrothermal condition. The results also show that PP/20T composite was found to be more stable in hygrothermal conditions due to better flexural properties compared to PP/20C and PP/20S composites that proven by morphology analysis.

## Acknowledgment

This work is supported under Fundamental Research Grant Scheme (FRGS: 9003-00328) provided by the Ministry of Education Malaysia (MOE).

## References

1. Potts, J., R. Clendinning, W. Ackart, and W. Niegisch. (1973), The Biodegradability of Synthetic Polymers. Springer. 61-79. US.
2. Gaffney, S. (2008). Corn Refiners Association 1. *Journal of Agricultural & Food Information*, 9 (2): 94-100.
3. Pedroso, A.G. and D.d.S. Rosa. (2005). Mechanical, thermal and morphological characterization of recycled LDPE/corn starch blends. *Carbohydrate Polymers*, 59 (1): 1-9.
4. Haque, M.M., M. Hasan, M.S. Islam, and M.E. Ali. (2009). Physico-mechanical properties of chemically treated palm and coir fiber reinforced polypropylene composites. *Bioresource technology*, 100 (20): 4903-4906.
5. Ramkumar, D., U. Vaidya, M. Bhattacharya, M. Hakkarainen, A.-C. Albertsson, and S. Karlsson. (1996). Properties of injection moulded starch/synthetic polymer blends—I. Effect of processing parameters on physical properties. *European polymer journal*, 32 (8): 999-1010.
6. Svensson, E. and A.-C. Eliasson. (1995). Crystalline changes in native wheat and potato starches at intermediate water levels during gelatinization. *Carbohydrate Polymers*, 26 (3): 171-176.
7. Liu, H., F. Xie, L. Yu, L. Chen, and L. Li. (2009). Thermal processing of starch-based polymers. *Progress in Polymer Science*, 34 (12): 1348-1368.

8. Zullo, R. and S. Iannace. (2009). The effects of different starch sources and plasticizers on film blowing of thermoplastic starch: Correlation among process, elongational properties and macromolecular structure. *Carbohydrate Polymers*, 77 (2): 376-383.
9. Guimarães, J., F. Wypych, C. Saul, L. Ramos, and K. Satyanarayana. (2010). Studies of the processing and characterization of corn starch and its composites with banana and sugarcane fibers from Brazil. *Carbohydrate Polymers*, 80 (1): 130-138.
10. Garg, S. and A.K. Jana. (2007). Studies on the properties and characteristics of starch–LDPE blend films using cross-linked, glycerol modified, cross-linked and glycerol modified starch. *European polymer journal*, 43 (9): 3976-3987.
11. Kim, M. and S.-J. Lee. (2002). Characteristics of crosslinked potato starch and starch-filled linear low-density polyethylene films. *Carbohydrate Polymers*, 50 (4): 331-337.
12. Kuniak, L. and R. Marchessault. (1972). Study of the crosslinking reaction between epichlorohydrin and starch. *Starch-Stärke*, 24 (4): 110-116.
13. Delval, F., G. Crini, S. Bertini, C. Filiatre, and G. Torri. (2005). Preparation, characterization and sorption properties of crosslinked starch-based exchangers. *Carbohydrate Polymers*, 60 (1): 67-75.
14. Leman, Z., S. Sapuan, A. Saifol, M. Maleque, and M. Ahmad. (2008). Moisture absorption behavior of sugar palm fiber reinforced epoxy composites. *Materials & Design*, 29 (8): 1666-1670.
15. Berthé, V., L. Ferry, J. Bénézet, and A. Bergeret. (2010). Ageing of different biodegradable polyesters blends mechanical and hygrothermal behavior. *Polymer Degradation and Stability*, 95 (3): 262-269.
16. Haghighi-Yazdi, M., J.K. Tang, and P. Lee-Sullivan. (2011). Moisture uptake of a polycarbonate blend exposed to hygrothermal aging. *Polymer Degradation and Stability*, 96 (10): 1858-1865.
17. Mohd Ishak, Z. and J. Berry. (1994). Effect of moisture absorption on the dynamic mechanical properties of short carbon fiber reinforced nylon 6, 6. *Polymer composites*, 15 (3): 223-230.
18. Hu, R.-H., M.-y. Sun, and J.-K. Lim. (2010). Moisture absorption, tensile strength and microstructure evolution of short jute fiber/polylactide composite in hygrothermal environment. *Materials & Design*, 31 (7): 3167-3173.
19. Phua, Y., W. Chow, and Z. Mohd Ishak. (2011). The hydrolytic effect of moisture and hygrothermal aging on poly (butylene succinate)/organo-montmorillonite nanocomposites. *Polymer Degradation and Stability*, 96 (7): 1194-1203.
20. Boubakri, A., K. Elleuch, N. Guermazi, and H. Ayedi. (2009). Investigations on hygrothermal aging of thermoplastic polyurethane material. *Materials & Design*, 30 (10): 3958-3965.
21. Mohd Ishak, Z., U. Ishiaku, and J. Karger-Kocsis. (2000). Hygrothermal aging and fracture behavior of short-glass-fiber-reinforced rubber-toughened poly (butylene terephthalate) composites. *Composites Science and technology*, 60 (6): 803-815.
22. Duanmu, J., E.K. Gamstedt, and A. Rosling. (2007). Hygromechanical properties of composites of crosslinked allylglycidyl-ether modified starch reinforced by wood fibres. *Composites Science and technology*, 67 (15): 3090-3097.
23. Yew, G., A. Mohd Yusof, Z. Mohd Ishak, and U. Ishiaku. (2005). Water absorption and enzymatic degradation of poly (lactic acid)/rice starch composites. *Polymer Degradation and Stability*, 90 (3): 488-500.
24. Nielsen, L.E. (1974), Mechanical properties of polymers and composites. Vol. 2. Dekker New York
25. Preechawong, D., M. Peesan, P. Supaphol, and R. Rujiravanit. (2004). Characterization of starch/poly (ε-caprolactone) hybrid foams. *Polymer testing*, 23 (6): 651-657.
26. Thakore, I., S. Desai, B. Sarawade, and S. Devi. (2001). Studies on biodegradability, morphology and thermo-mechanical properties of LDPE/modified starch blends. *European polymer journal*, 37 (1): 151-160.
27. Wang, W., M. Sain, and P. Cooper. (2006). Study of moisture absorption in natural fiber plastic composites. *Composites Science and technology*, 66 (3): 379-386.
28. Ke, T., S.X. Sun, and P. Seib. (2003). Blending of poly (lactic acid) and starches containing varying amylose content. *Journal of applied polymer science*, 89 (13): 3639-3646.
29. Athijayamani, A., M. Thiruchitrambalam, U. Natarajan, and B. Pazhanivel. (2009). Effect of moisture absorption on the mechanical properties of randomly oriented natural fibers/polyester hybrid composite. *Materials Science and Engineering: A*, 517 (1): 344-353.
30. Mohd Ishak, Z., A. Ariffin, and R. Senawi. (2001). Effects of hygrothermal aging and a silane coupling agent on the tensile properties of injection molded short glass fiber reinforced poly (butylene terephthalate) composites. *European polymer journal*, 37 (8): 1635-1647.

31. Vlasveld, D., J. Groenewold, H. Bersee, and S. Picken. (2005). Moisture absorption in polyamide-6 silicate nanocomposites and its influence on the mechanical properties. *Polymer*, 46 (26): 12567-12576.
32. Huang, G. and H. Sun. (2007). Effect of water absorption on the mechanical properties of glass/polyester composites. *Materials & Design*, 28 (5): 1647-1650.

The Malaysian Journal of ANALYTICAL SCIENCES ISSN 1394-2506

# EFFECT OF DIFFERENT HEALING TEMPERATURE ON SOLID STATE SELF-HEALING SYSTEM

## (Kesan Suhu Pemulihan Yang Berbeza Terhadap Sistem Swa-Pemulihan Dalam Keadaan Pepejal)

S. M. Makenan, N. N. Muhamad, M. J. Mohd Suzeren*, S. Salihan, M.A.S. Mat Lazim

*School of Chemical Sciences and Food Technology,*
*Faculty of Science and Technology*
*Universiti Kebangsaan Malaysia, 43600 UKM Bangi, Selangor, Malaysia*

**Corresponding author: suzeren@ukm.edu.my*

**Abstract**

The aim of this study is to identify the effect of using various healing temperatures ranging from 120$^{o}$C to 180$^{o}$C with temperature interval of 10$^{0}$C on self-healing resin system containing diglycidyl ether of bisphenol-A (DGEBA), the hardener nadic methyl anhydride (NMA), the catalyst benzylmethylamine (BDMA) and poly(bisphenol-A-co-epichlorohydrin) (PDGEBA) as healing agent. The effects of different healing temperatures on the resin systems were investigated by means of Fourier-transform Infrared Spectrometer (FTIR), Dynamic Mechanical Thermal Analysis (DMTA), and izod test. Optical image of the sample morphology was observed using optical microscope. Healing efficiencies ($H_E$) were evaluated using izod test and the optimum healing temperature of 160$^{o}$C was obtained within the third healing cycles with $H_E$ 37%. The results indicate that the healing temperature affected the physical aging and the chemical reaction between the secondary hydroxyl group and carboxyl group occurred at high temperature of ≥180$^{o}$C.

**Keywords:** Self-healing; healing temperature; epoxy resin

**Abstrak**

Tujuan kajian ini adalah untuk mengenalpasti kesan menggunakan suhu pemulihan yang berbeza iaitu 120$^{o}$C, 140$^{o}$C, 150$^{o}$C, 160$^{o}$C, 170$^{o}$C dan 180$^{o}$C terhadap sistem swa-pemulihan resin yang mengandungi diglisidil eter bisfenol-A (DGEBA), pengeras nadik metil anhidrida (NMA), pemangkin benzilmetilamina (BDMA) dan poli(bisfenol-A-ko-epiklorohidrin) (PDGEBA) sebagai agen pemulihan. Kesan penggunaan suhu pemulihan yang berbeza terhadap sistem resin dikaji menggunakan Spektrometer Infra Merah Fourier-transform (FTIR), Analisis Terma Mekanikal Analisis (DMTA), ujian izod dan mikroskop optik. Keberkesanan pemulihan ($H_E$) diukur menggunakan ujian izod dan suhu pemulihan terbaik pada 160$^{o}$C didapati di kitaran pemulihan yang ketiga dengan nilai $H_E$ sebanyak 37% . Keputusan ini menunjukkan bahawa suhu pemulihan menyebabkan berlaku penuaan fizikal dan tindak balas kimia antara kumpulan hidroksil sekunder dan kumpulan karboksil berlaku pada suhu yang tinggi sekitar ≥180$^{o}$C.

**Kata kunci:** Swa-pemulihan; suhu pemulihan; resin epoksi

## Introduction

Throughout their lifetime, polymeric materials are susceptible to mechanical damages such as matrix cracking and delamination. These damages reduce the mechanical properties of these materials [1-4]. To overcome these limitations, a rapidly emerging field of research has resulted in the material itself is capable of repairing the crack and restoring the functionality of the material, thus expanding the lifetime of the material, which is referred as self-healing material. The self-healing system can be divided into two types, namely, extrinsic; without any external intervention (autonomously) [5, 6] and intrinsic; required external stimulus [7, 8].

Solid-state healable system; one of the types of intrinsic self-healing system, is the thermoplastic-thermosetting semi-interpenetrating network. This employs a thermosetting resin, in to which a thermoplastic is dissolved. In miscible mixing, Hayes and colleagues (co-workers) [9, 10] studied the incorporation of a soluble linear polymer; poly(bisphenol-A-co-epichlorohydrin) (PDGEBA), which is highly compatible with the thermosetting resin; diglycidyl bisphenol A. Upon curing, the thermoplastic material remains dissolved in the thermosetting matrix. Although requiring additional external activation, this system is repeatable over a number of healing events.

The recovery occurs by heating the systems above the minimum healing temperature (glass transition temperatures, $T_g$). At this temperature, the linear polymer of healing agent would mobilize and diffuse through the thermosetting matrix, to the cracked surfaces with some chains bridging to close the cracks and thereby facilitating healing. After healing the damage PDGEBA will return to its immobilize state [9, 11]. Wool [12] elaborated a microscopic theory on the basic of the "Reptation model", that originally proposed by de Gennes [13], that described the diffusion and randomization in polymer-polymer crack interphase for strength recovery. These crack healing systems are time and temperature dependent; and occur via void closure of "free volume", surface interaction, and molecular entanglement between the damage faces [14, 15].

Ideally, solid state system exhibits the ability to undergo multiple healing cycles. However, Hayes et al. [10] reported a reduction in the percentage of healing efficiency within the second and third healing cycles. The diffusion through reptation of healing agent is related to the free volume within the thermosetting resin which can be affected by physical aging which has been well documented [16-18]. The objective of this study is to examine the effect of healing efficiency when using different healing temperatures which are 120$^o$C, 140$^o$C, 150$^o$C, 160$^o$C, 170$^o$C and 180$^o$C.

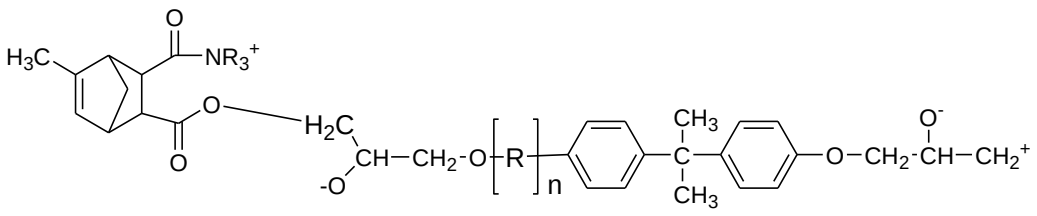
## Materials and Methods

### Materials

The materials used to produce epoxy resin were diglycidyl ether of bisphenol-A (DGEBA) with Mw of 384.36g/mol, the hardener nadic methyl anhydride (NMA) (MW of 178.18g/mol) and the catalyst benzylmethylamine (BDMA) (MW of 135.21g/mol) and all were purchased from Sigma–Aldrich. Unreactive Poly(bisphenol-A-co-epichlorohydrin) or PDGEBA with average Mw of 4400 g/mol obtained from Sigma -Aldrich, was used as healing agent.

The control (or non-healable) resin was prepared by heating the DGEBA at 90$^o$C for 5 minutes under the mechanical stirrer. NMA hardener was added and stirred for 1 minute until it was completely dissolved and was followed by BDMA with further stiring for 30 seconds. The ratios by weight of 100.0, 81.2 and 2.0 for the epoxy-hardener-catalyst mixture were used [9]. The resin mixture was degassed in the vacuum oven at 90$^o$C to eliminate any gas bubbles generated during the mixing process. After degassing, the mixture was poured into the silicon mould. Then the mould was placed into the air convection oven at 90$^o$C to cure for 4 hours followed by 1 hour post-cure at 140$^0$C, to ensure the resin was fully cured.

For the self-healing (or healable) resin, the healing agent; PDGEBA was dissolved in DGEBA under mechanical stirring at 120$^o$C for approximately 24 hours to form a homogenous solution [9]. After this point, the method for sample preparation was following the same procedures as in the control resin with the addition of NMA and BDMA for curing (Figure 1).



whereas :

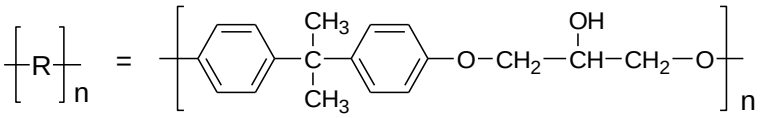



Figure 1. The chemical structure of repeating unit of resin produced from the curing of the anhydride (NMA) and the epoxy (DGEBA) under catalyst (tertiary amine)

**Assessment of Healing**

The impact machine was using a manual clamping of a manual clamping vice with a specimen adapter according to ASTM D256 (Standard Test for Izod Pendulum Impact Resistance of Plastics) The dimension of the specimen was 64 mm x 13 mm x 4 mm with 3 mm notch (Figure 2a). The sample was correctly positioned in the vice with a centering device adapted for notched specimens. Izod impact tests were performed at room temperature with on notched specimens cut by motorized notching cutter (Ray-Ran) using a Ray-Ran Test Equipment RR/IMT (RR/MT/100)

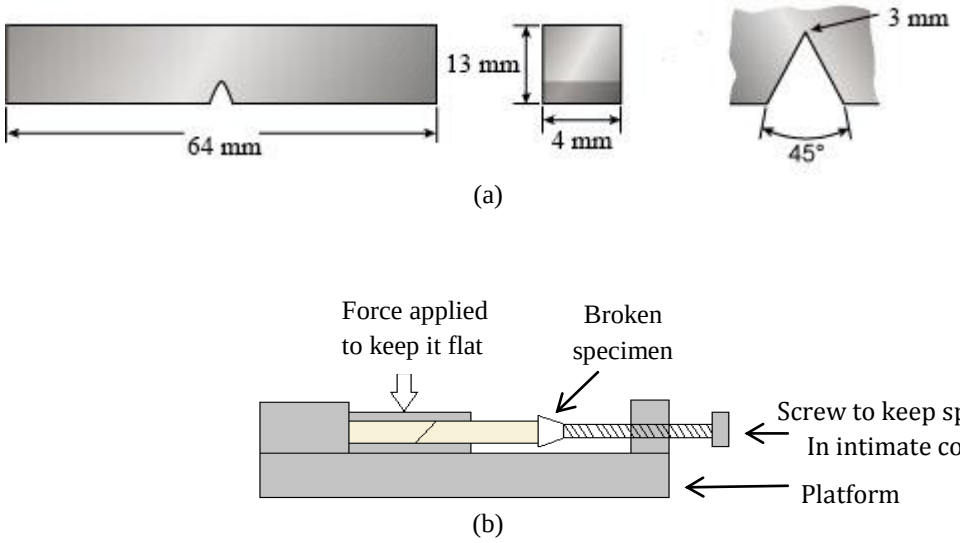



Figure 2. a) Dimension of the izod test specimen (in mm) and b) the alignment machine for healing process [10]

At least five specimens were tested for each set of data. By following the initial fracture, all samples including control resin and healable resin, were immediately healed using the alignment machine (Figure 2b) at different healing temperatures (120°C, 140°C, 150°C, 160°C, 170°C and 180°C) for 6 hrs before cooling back to 25°C at 2°C/min in each healing cycle. The percentage of recovery efficiency ($R_E$) was be calculated by using Equation 1;

$$R_E = \frac{100 \times E_{healed}}{E_{initial}} \quad (1)$$

where $E_{healed}$ and $E_{initial}$ are the impact energy after healing and the impact energy at initial crack respectively [19].

**Fourier-Transform Infrared Spectrometer (FTIR)**

FTIR observation was made with a Perkin Elmer Spectrum (BX200) to determine the functional group in resin system. 1-2 mg of the solid sample was mixed with potassium bromide and grounded into fine powder before being

pressed into thin discs for FTIR measurement. All spectra are recorded at room temperature with the infrared spectra range of 4000 - 400 $cm^{-1}$.

**Dynamic Mechanical Thermal Analyzer (DMTA)**

DMTA was performed on a TA Instruments Thermal Analysis (DMA 2980) operating in the single cantilever-bending mode at an oscillation frequency of 1Hz. Data were collected from room temperature to 180 $^{o}C$ at a scanning rate of 2$^{o}C$/min. The sample specimens were made in the form of rectangular bars of a nominal 35 mm x 15 mm x 5 mm.

**Optical Microscopy**

Optical images of the morphology of the crack surface of samples from izod test specimens were taken using an Axiolab A450909 Image Analyzer with camera lens model Zeiss.

## Results and Discussion

Solid state self-healing system involves the process of diffusion of linear polymer within the epoxy resin when heat is applied. Matrix resin was prepared based on DGEBA matrix.

**Preparation of Matrix DGEBA Epoxy Resin**

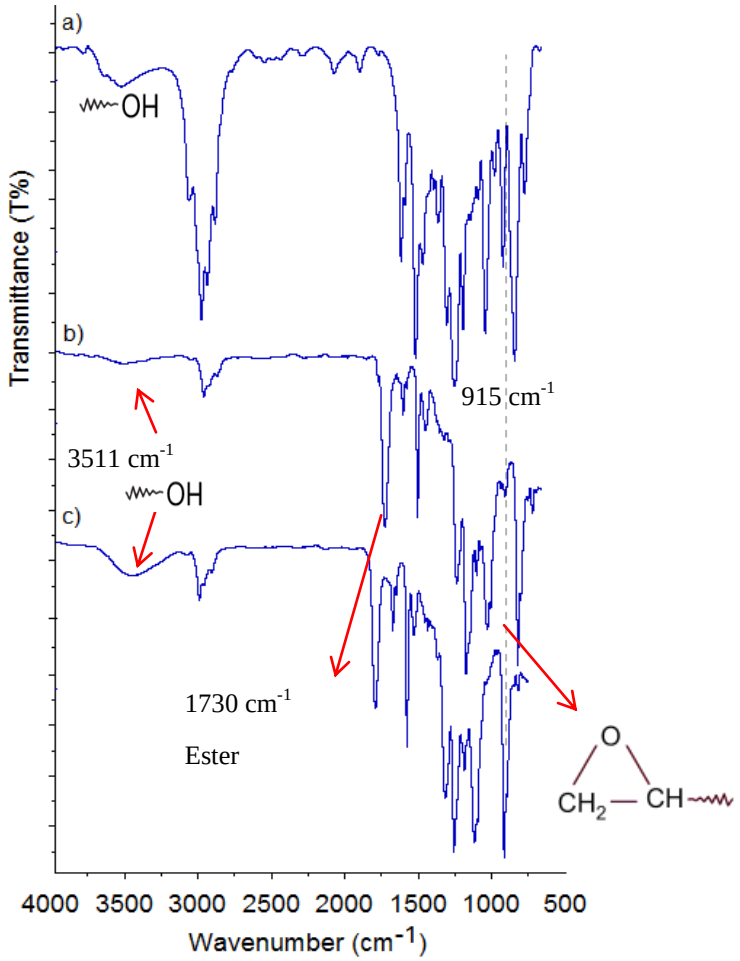



Figure 3. FTIR spectra recorded at room temperature of a) DGEBA b) healable resin and c) control resin

The curing reaction in epoxy resin was observed by infrared spectrum through the determination of interactions between the functional groups. An epoxy group intensity was monitored at a wavelength of 915 $cm^{-1}$ (Figure 3). FTIR spectra of healable and control resin possessed O-H peaks in the region of 3300-3600 $cm^{-1}$ (Figures 3b and 3c) that can be attributed to the self-associated hydroxyl. The formation of that covalent bonding was seen at the appearance of a new peak at 1730$cm^{-1}$ (Figures 3b and 3c) that can be attributed to the formation of an ester. It is possible that this peak resulted/originated from anhydride-epoxy reaction. The reduction of epoxy peak intensities of control resin compared to the healable resin (Figure 3) indicates that more epoxy rings (915$cm^{-1}$) have been opened during curing process.

Meanwhile, the dynamic mechanical thermal analysis was used to determine the minimum healing temperature ($T_g$) of epoxy resin. At this point, the linear polymer starts to mobilize and diffuse to the crack plane [22]. Glass transition temperature ($T_g$) is defined as the maximum in tan δ. Tan δ versus temperature data for control and healable resin are shown in Figure 4.

Clearly, only single peak around 140$^{o}$C existed in both epoxy systems, indicating a homogenous phase structure [20]. There was no significant change in $T_g$ with the addition of healing agent into control resin system.

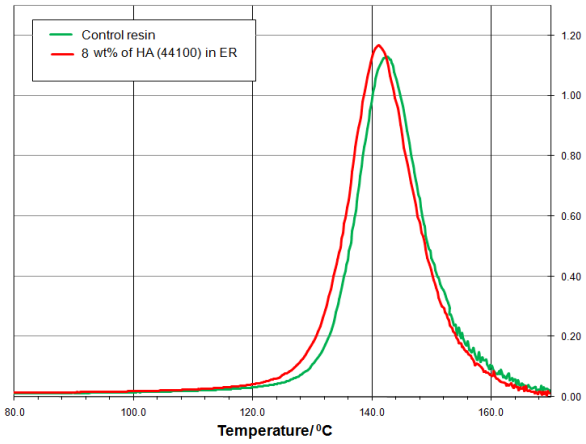



Figure 4. Dynamic mechanical thermal analysis curves for the control resin and healable resin between the temperature ranges from 80$^{0}$C to 180$^{o}$C

**Healing Efficiency at Different Healing Temperature**

In this study, the samples of control and healable resin were subjected to repeating impact/heal cycles. Each sample was subjected to a 2.706 J impact energy followed by a healing cycle of 6 hrs at various healing temperatures. This procedure was repeated for a total of three impact/heal cycles. Impact energy values, the change of energy per area unit from notch (kJ/$m^2$) were obtained from the Fracta$^{TM}$ software. It is clearly indicated that the healing effects of healable resin specimens are much greater than that of control resin (Figure 5).

The control resin can be thermally healed to a limited extent after 6 hrs at 160˚C (Figure 5). The healing effect on the control resin can be explained by two possibilities; dangling chains (or chain slippage) at healing temperature above $T_g$ and through interaction of excess epoxy group in the epoxy resin [12]. The recovery effeciency ($R_E$) was calculated (Equation 1) from the average of impact energy obtained from the izod test. The actual "Healing effeciency" (Equation 2) ; to compensate for the residual healing effect in the control resin system, was obtained by correcting for healing in the control system from Equation 1.

$$H_E = R_E - R_E^o \quad (2)$$

where $R_E$ is the percentage recovery efficiency and $R_E^0$ is recovery effeciency of control resin [19]. Whereas, the healing effect on healable resin was reasoned by the diffusion of PDGEBA to the crack surface when the heat was introduced to the system (above $T_g$ temperature) [7]. The polymer matrix is actually healed by bringing two pieces of identical samples into contact due to molecular diffusion along the polymer/polymer interface [15]. Figure 6 shows the mechanism of the solid state healing resin in order to understand the phenomena of self-healing, proposed by Wool and O'Connor [12] which involving five steps of surface rearrangement.

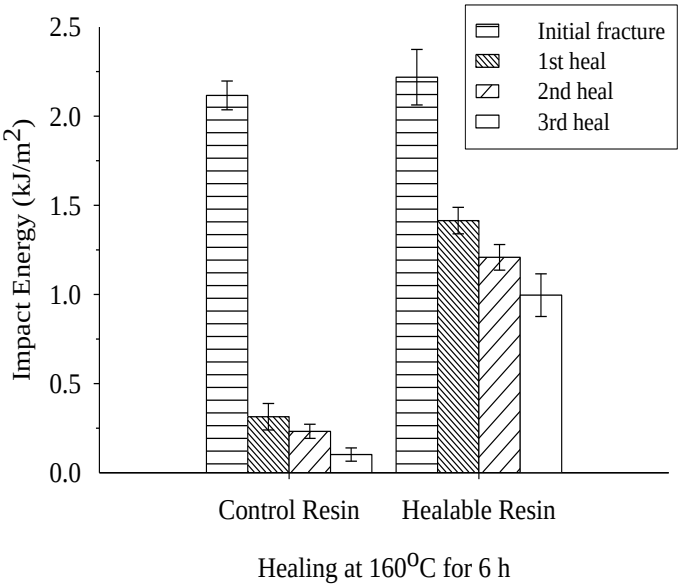
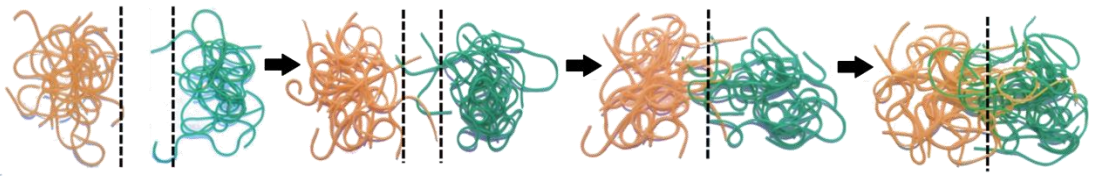



Figure 5. Impact energies (kJ/m$^2$) of control and healable resin (with 8% of healing agent) on healing temperature 160˚C for 6 hrs with three healing cycle



a) surface rearrangement
b) surface approach
c) wetting
d) diffusion
e) randomization

Figure 6. Schematic of self-healing mechanism of the solid state healing resin [15]

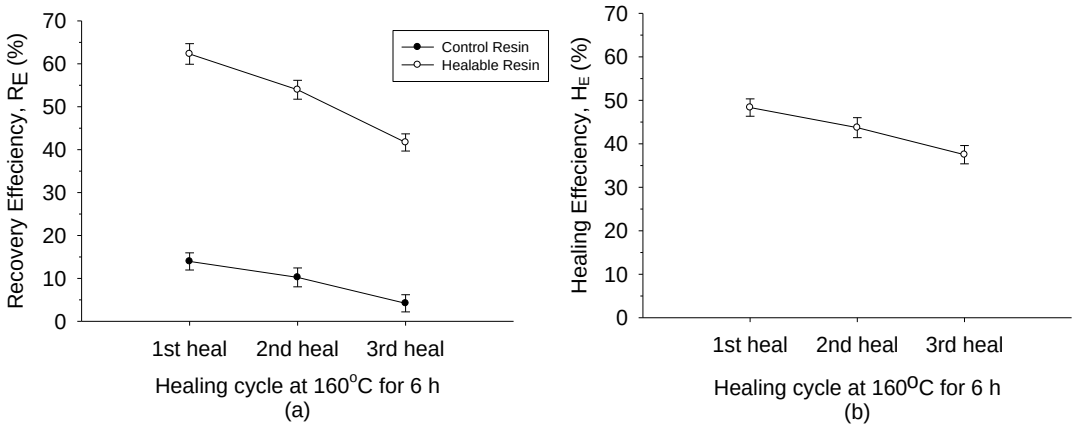



Figure 7. Graph showing a) the recovery effeciency ($R_E$) and b) healing effeciency ($H_E$) percentage of the control and healable resin vs healing cycle for healing resin at healing temperature 160°C

Based on the concept of diffusion of healing agent, different healing temperature has been studied. Figure 7(a) and Figure 7(b) show the recovery effeciency, $R_E$ (Equation 1) and healing effeciency, $H_E$ (Equation 2) respectively for the healing cycle of healable resin (healing temperature of 160°C). The percentage of healing effeciency, $H_E$ in the range 48% to 37% were achieved for three healing cycles (Figure 7b).

By using $T_g$ value (minimum healing temperature for resin epoxy) from DMTA results (Figure 4) as a reference, various healing temperature which were from 120°C (below $T_g$ value) to 180°C have been used. The comparison of healing efficiency, $H_E$ of resin epoxy usingdifferent healing temperatures showed that the healable resin with healing temperature of 120°C has the lowest healing efficiency (Figure 7). This resulted from less movement of healing agent within the matrix resin at the healing temperature below the $T_g$ ($T_g$ = 140°C) [9].

On the contrary, samples with healing temperature range from 140-180˚C showed high percentages of healing efficiencies. This resulted from the heat stimulus that cause the diffusion process and the movement of molecular chain of healing agent into the matrix resin [7, 21]. Healing efficiencies are higher with higher healing temperature and these values are in agreement with the literature [22].

On average, it has been demonstrated from figure 8a that there was a drop in the percentage of healing efficiency, $H_E$ at the second and the third healing cycle of resin under all conditions (from 120-180˚C). This is possibly due to physical aging effect. Physical aging of resin epoxy can be explained by the molecular relaxation in which the epoxy network loses the mobility and the free volume during its approach towards the equilibrium glassy state [16, 23]. This behaviour was reported previously by other authors [10, 11]. The full detailed study on the healing cycle and the physical aging will be explored in the future.

The highest degree of healing effeciencies at about 48%, 43% and 37% from the first, second and third healing cycles wereachieved at 160°C of healing temperature. However, the obvious reduction of $H_E$ percentage value can be seen at the healing temperature of 180˚C (Figures 8a and 8b) at the second healing cycles. The reaction between the secondary hydroxyl and carboxyl group can occur at high temperature will restrict the movement of healing agent due to the chemical reaction between matrix resin and healing polymer. It can be concluded that high healing temperature (>180˚C) would decrease the percentage oh healing effeciency of the resin.

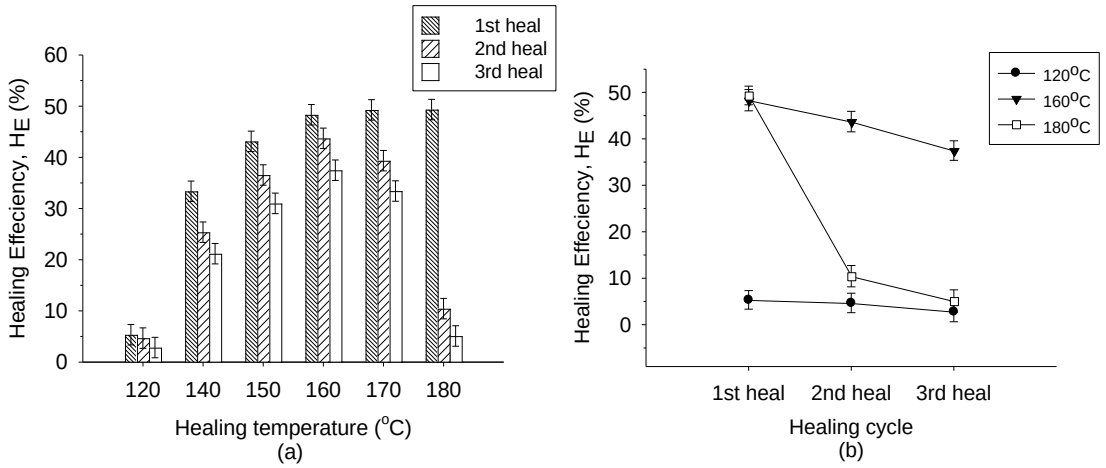



Figure 8. Graph showing the results for healing efficiency, $H_E$ of; a) healable resin at different healing temperature as a function of healing event and b) the healing cycle as a function of healing temperature

**Reaction of Secondary Hydroxyl**

To monitor changes in the functional group of epoxy resin, further heating at temperature of 160°C for up to 3 healing events (18 hrs) has been done. FTIR was used to compare the intensity of epoxide and hydroxyl functional groups. The comparison of FTIR spectra of healable resin and 3rd healing cycle healable resin at healing temperature 160°C (Figure 9) shows there was no significant change between the peaks. It was considered that there was no change in chemical structure in the system. However, the comparison of spectra of healable resin at low (160°C) and high healing temperature (180°C) (Figure 10) showed that the peak for O-H group (3700-3100 $cm^{-1}$) for high healing temperature resin has been shifted to the lower wavenumber (shifted to the right) compared to low healing temperature resin.

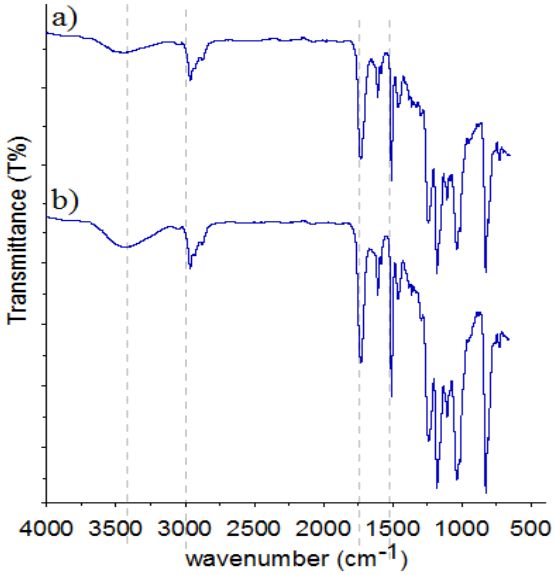



Figure 9. FTIR spectra in region 4000-500$cm^{-1}$ recorded at room temperature of a) healable resin and b) 3rd healing cycle of healable resin

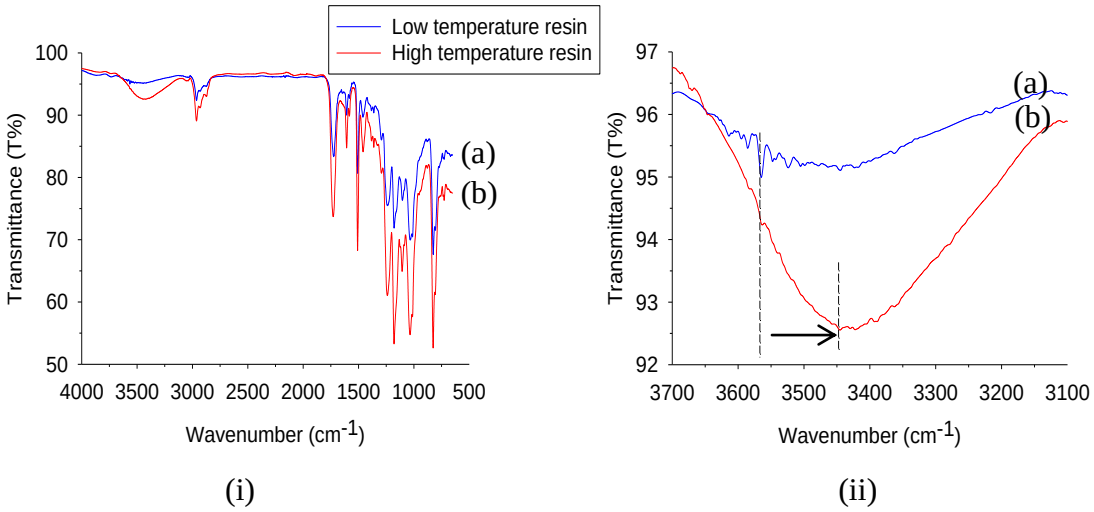



Figure 10. FTIR spectra in region 4000-500cm$^{-1}$ for healable resin with healing process at a) low and b) high temperature. (ii) : A magnification of FTIR spectra in range from 3700 to 3100cm$^{-1}$

This result suggests that healing at low temperature (below 160$^{o}$C) occurs via physical processes (diffusion of polymer) rather than chemical reactions [9]. On the other hand, healing at high temperature (180$^{o}$C) causes chemical interaction between the functional group in the system. Painter et al. [24] showed that absorption bands of OH-$\pi$ bonds at ~3516cm$^{-1}$ and self-associated OH groups at ~3400cm$^{-1}$. It is more likely that this transition in hydroxyl group peak might be due to the chemical interaction of the carboxyl group and secondary hydroxyl group (Figure 11) [24].

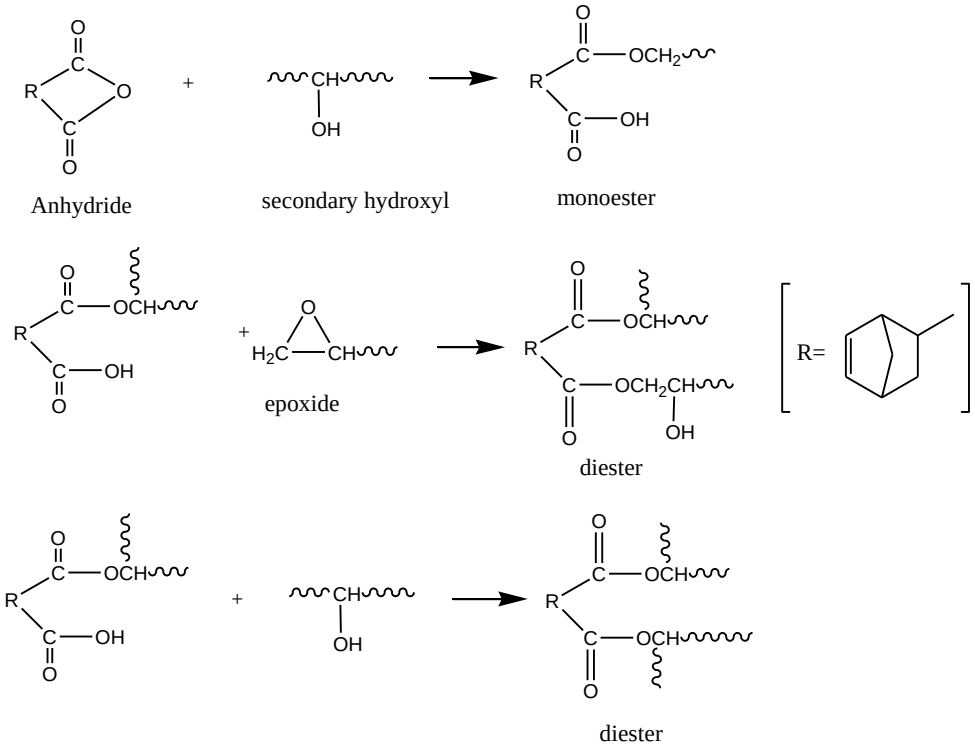



Figure 11. Curing reaction mechanism of the anhydride (NMA) and epoxy resin (DGEBA) in the present of a catalyst [28]

In healing process, post-reaction between curing agent and hydroxyl group in epoxy resin can occur until the limited stage as shown in Figure 11. There are two possible reactions to open the epoxy ring; reaction between anhydride group and secondary hydroxyl group and reaction between epoxide group and carboxyl group. Whereas, the third reaction is between carboxyl group and secondary hydroxyl group that can occur at high temperature (≥180$^{o}$C). Two different products are formed in the ring opening reaction of the epoxy group with a carboxyl group; i) the ester of the primary hydroxyl group and ii) the ester of the secondary hydroxyl group (if the temperatures > 180 $^{0}$C) (Figure 11). The reaction between the secondary hydroxyl and carboxyl at high healing temperature will restrict the movement of healing agent in system and resulted in low healing efficiency.

To further explore the impact of healing temperature upon the epoxy network, dynamic mechanical thermal analysis was performed on healable resin at various healing temperatures for up to 3 healing events (18 hrs). Comparison of $T_g$ values (maximum in the tan δ) with healing temperature of 120˚C (at 140.2˚C), 140˚C (at 141.6˚C), 160˚C (at 145.8˚C) and 180˚C (at 153.4˚C) was shown in Figure 12.

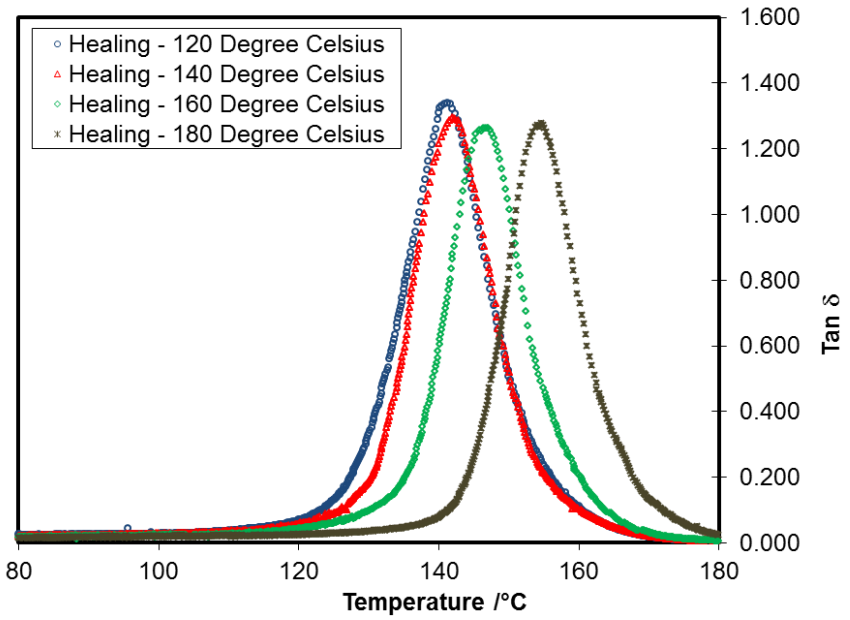



Figure 12. DMTA scan of tan δ for healable resin (with 8 wt% of HA) that subjected to different healing temperature

There was a slightly increase of $T_g$ value at healing temperature 140˚C and 160˚C compared to 120˚C. These differences suggest that further curing process of epoxy at varied degrees occured in the systems [25]. However, the increasing of $T_g$ value at 180˚C was more significant. As discussed elsewhere [26, 27], $T_g$ increases with increased cross-linking due to the restriction on molecular mobility. In relation to this, the increasing of $T_g$ could be due to futher curing of epoxy and also chemical interaction of the carboxyl group and secondary hydroxyl group, thus more highly crosslinked polymers have been found.

**Microscopy Analysis**

Optical microscope was used to investigate the surface morphology of the healable resin. A typical healing process of a damage resin as viewed through optical microscope as shown in Figures 13b and 13c. By comparing the two images of epoxy resins, the crack can be seen clearly in resin epoxy that was introducing crack (Figure 13b) and heating for 6 hrs causes the crack to virtually disappear (Figure 13c).

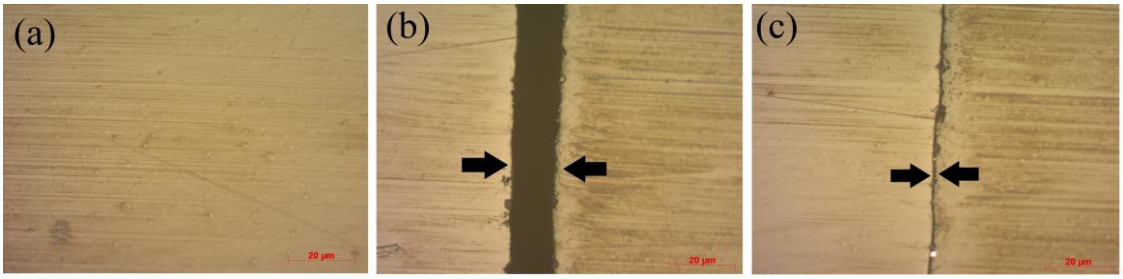



Figure 13. Optical micrograph of a test specimen izod test cross-section from the resin containing 8.0 wt% of healing agent with the magnification of 10x ; a) before introducing crack, b) after introducing crack and c) after healing process

Further, the surface morphology also demonstrated that the healable resin washomogenous without signs of phase separation. These results are accordance with DMTA analysis as discussed above.

## Conclusion

A solid state self-healing system can be prepared by mixing the thermoset polymer; DGEBA and the thermoplastic polymer; PDGEBA and the effects of using various healing temperatures; from 120$^{o}$C to 180$^{o}$C have been studied. The resin systems used in this study was able to self-healing at healing temperature above the minimum healing temperature (>$T_g$). Healing efficiencies ($H_E$) were evaluated using izod test and the optimum healing temperature at 160$^{o}$C within the third healing cycles with $H_E$ 37% was achieved. The healing process at low healing temperature (140$^{o}$C to 160$^{o}$C) occurred by diffusion of healing agent (physically process). Meanwhile, the healing process at high temperature (180$^{o}$C) occurred by the physically and the chemically processess. It is demonstrated that there was a reduction in the percentage of healing efficiency, $H_E$ at the second and the third healing cycles of resin under all conditions. The results indicate that the healing temperature affected the physical aging and the chemical reaction between the secondary hydroxyl group and carboxyl group occurred at high temperature (≥180$^{o}$C).

## Acknowledgement

The authors acknowledge the financial support of this study by Government of Malaysia through FRGS/1/2012/SE07/UKM/03/1, GGPM-2012-014 and ERGS/1/2012/TK04/UKM/03/3 grants. The authors also wish to thank the School of Chemical Sciences and Food Technology of the National University of Malaysia for the continuous support of this project.

## References

1. Dry, C. (1996). Procedures developed for self-repair of polymer matrix composite materials. *Composite Structures*, 35(3): 263-269.
2. Kim, V. T. & Nele, D. B. (2013). Self-Healing in Cementitious Materials—A Review *Materials*, 6: 2182-2217.
3. Colquhoun, H. & Klumperman, B. (2013). Self-healing polymers. *Polymer Chemistry*, 4(18): 4832-4833.
4. Tyagi, P., Deratani, A., & Quemener, D. (2013). Self-Healing Dynamic Polymeric Systems. *Israel Journal of Chemistry*, 53(1-2): 53-60.
5. Billiet, S., Van Camp, W., Hillewaere, X. K. D., Rahier, H., & Du Prez, F. E. (2012). Development of optimized autonomous self-healing systems for epoxy materials based on maleimide chemistry. *Polymer*, 53(12): 2320-2326.
6. White, S. R., Sottos, N. R., Geubelle, P. H., J.S.Moore, Kessler, M. R., Sriram, S. R., Brown, E. N., & Viswanathan, S. (2001). Autonomic healing of polymer composites. *Nature*, 409: 794-797.

7. Blaiszik, B. J., Kramer, S. L. B., Olugebefola, S. C., Moore, J. S., Sottos, N. R., & White, S. R. (2010). Self-Healing Polymers and Composites. *Annual Review of Materials Research,* 40(1): 179-211.
8. Williams, K. A., Dreyer, D. R., & Bielawski, C. W. (2008). The Underlying Chemistry of Self-Healing Materials. *MRS Bulletin*, 33: 759-765.
9. Hayes, S. A., Jones, F. R., Marshiya, K., & zhang, W. (2007). A self-healing thermosetting composite material. *Composites Part A: Applied Science and Manufacturing*, 38(4): 1116-1120.
10. Hayes, S. A., Zhang, W., Branthwaite, M., & Jones, F. R. (2007b). Self-healing of damage in fibre-reinforced polymer-matrix composites. *Journal of The Royal Society Interface*, 4(13): 381-387.
11. Peterson, A. M., Kotthapalli, H., Rahmathullah, M. A. M., & Palmese, G. R. (2012). Investigation of interpenetrating polymer networks for self-healing applications. *Composites Science and Technology*, 72(2): 330-336.
12. Wool, R. P. & O'Connor, K. M. (1981). A theory crack healing in polymers. *Journal of Applied Physics*, 52(10): 5953-5963.
13. de Gennes, P. G., *Scaling Concepts in Polymer Physics*. 1979, Ithaca, New York: Cornell Univ. Press.
14. Jud, K. & Kausch, H. H. (1979). Load transfer through chain molecules after interpenetration at interfaces. *Polymer Bulletin*, 1: 697-707.
15. Diana, D., philipp, M., & Wolfgang, B., eds. *Principles of Self-Healing Polymers, In: Self Healing Polymers : From Principles to Applications Self-Healing Polymers*. 2013, Wiley-VCH Verlag GmbH & Co. KGaA.: USA. 5-60.
16. Kong, E.,(1986). *Physical aging in epoxy matrices and composites Epoxy Resins and Composites IV*, Dušek, K., Editor, Springer Berlin / Heidelberg. p. 125-171.
17. Lévêque, D., Schieffer, A., Mavel, A., & Maire, J.-F. (2005). Analysis of how thermal aging affects the long-term mechanical behavior and strength of polymer–matrix composites. *Composites Science and Technology*, 65(3–4): 395-401.
18. Hu, H. & Sun, C. T. (2000). The characterization of physical aging in polymeric composites. *Composites Science and Technology*, 60(14): 2693-2698.
19. Brown, E. N., White, S. R., & Sottos, N. R. (2005). Retardation and repair of fatigue cracks in a microcapsule toughened epoxy composite – Part I: Manual infiltration. *Composites Science and Technology*, 65(15–16): 2466-2473.
20. Fox, T. G. & Flory, P. J. (1950). Second-order transition temperatures and related properties of polystyrene. I. Influence of molecular weight. *Journal of Applied Physics*, 21(6): 581.
21. Jones, F. R., Zhang, W., & Hayes, S. A. ( 2007). Thermally induced self healing of thermosetting resins and matrices in smart composites. *Self Healing Materials*, 100: 69-93.
22. Rahmathullah, M. A. M. & Giuseppe, R. P. (2009). Crack-healing behavior of epoxy-amine thermosets. *Applied Polymer Science*, 113(4): 2191-2201.
23. Hutchinson, J. M. (1995). Physical aging of polymers. *Progress in Polymer Science*, 20(4): 703-760.
24. Miura, K. (1998). A new method to estimate hydrogen bondings in coal by utilizing FTIR and DSC. *Fuel and Energy Abstracts*, 39(3): 167-167.
25. Kausch, H. H. & Tirrell, M. (1989). Polymer interdiffusion. *Annual Review of Materials Science*, 19(1): 341-77.
26. Cook, W., Mehrabi, M., & Edward, G. (1999). Ageing and yielding in model epoxy thermosets. *Polymer*, 40(5): 1209-1218.
27. Barral, L., Cano, J., Lopez, J., Lopez-Bueno, I., Nogueira, P., Abad, M. J., & Ramirez, C. (1999). Physical aging of an epoxy/cycloaliphatic amine resin. *European Polymer Journal*, 35(3): 403-411.
28. Thomas, R., Durix, S., Sinturel, C., Omonov, T., Goossens, S., Groeninckx, G., Moldenaers, P., & Thomas, S. (2007). Cure kinetics, morphology and miscibility of modified DGEBA-based epoxy resin – Effects of a liquid rubber inclusion. *Polymer*, 48(6): 1695-1710.

The Malaysian Journal of ANALYTICAL SCIENCES ISSN 1394-2506

# PALM-BASED POLYURETHANE WITH SOYBEAN PHOSPHATE ESTER AS A FIRE RETARDANT

## (Poliuretana Sawit dengan Ester Fosfat Soya Sebagai Perencat Api)

Nor Rabbi'atul 'Adawiyah Norzali[1], Khairiah Haji Badri[1,2]*, Ong Soo Ping[1], Ishak Ahmad[1,2]

[1]*School of Chemical Sciences and Food Technology*
[2]*Polymer Research Center*
*Faculty of Science and Technology*
*Universiti Kebangsaan Malaysia, 43600 UKM Bangi, Selangor, Malaysia*

**Corresponding author: kaybadri@ukm.edu.my*

**Abstract**

Palm-based polyurethane (PU) with soybean oil phosphate ester (PE) as a fire retardant was prepared. The effect of PE to the mechanical and burning properties of the PU was investigated. The PE was synthesized via ring-opening hydrolysis between *o*-phosphoric acid (*o*-$H_3PO_4$) and epoxidized soybean oil. The synthesis was conducted at 60-70 °C. The concentration of *o*-$H_3PO_4$ was varied at 2.5, 5.0 and 7.5 wt%. PE with 2.5 wt% $H_3PO_4$ showed the lowest acid value (2.8 $mg \cdot g^{-1}$) but high hydroxyl value (351.6 $mg \cdot g^{-1}$). PU containing PE (PU-PE) has higher density (60-61 $kg \cdot m^{-3}$) compared to control PU (49.7 $kg \cdot m^{-3}$). Burning rate decreased from $2.16 \times 10^{-3}$ $m \cdot s^{-1}$ for control PU to $1.26 \times 10^{-3}$ $m \cdot s^{-1}$, 1.06 $10^{-3}$ $m \cdot s^{-1}$ and $0.6 \times 10^{-3} m \cdot s^{-1}$ for PU-PE at 5, 10 and 15 wt% PE respectively. However, the addition of PE into the PU system gradually decreased the compression stress and modulus of the PU-PE.

**Keywords:** Epoxidized soybean oil, fire retardant, palm-based polyurethane, phosphate ester

**Abstrak**

Poliuretana sawit (PU) mengandungi ester fosfat minyak soya (PE) sebagai perencat api telah berjaya dihasilkan. Kesan PE terhadap sifat mekanik dan kebakaran PU telah dikaji. PE disintesis melalui tindak balas hidrolisis pembukaan gelang antara asid fosforik (o-$H_3PO_4$) dan minyak soya terepoksida. Sintesis dijalankan pada 60-70 °C. Kepekatan o-$H_3PO_4$ divariasikan pada 2.5, 5.0 dan 7.5 bt%. PE dengan 2.5 bt% o-$H_3PO_4$ menunjukkan nilai asid yang rendah (2.8 $mg \cdot g^{-1}$) tetapi tinggi nilai hidroksil 351.6 $mg \cdot g^{-1}$). PU yang mengandungi PE(PU-PE) mempunyai ketumpatan yang tinggi (60-61 $kg \cdot m^{-3}$) berbanding PU kawalan (49.7 $kg \cdot m^{-3}$). Kadar kebakaran menurun dari $216 \times 10^{-3}$ $m \cdot s^{-1}$ untuk PU kawalan kepada $1.26 \times 10^{-3}$ $m \cdot s^{-1}$, 1.06 $10^{-3}$ $m \cdot s^{-1}$ and $0.6 \times 10^{-3} m \cdot s^{-1}$ masing-masing untuk PU dengan 5, 10 and 15 bt% PE. Walau bagaimanapun, penambahan PE ke dalam sistem PU menyebabkan kekuatan dan modulus mampatan menurun secara berperingkat.

**Kata kunc**i: Minyak soya terepoksida, perencat api, poliuretana sawit, ester fosfat

## Introduction

Palm-based polyurethane (PU) exists in various forms such as foams (in rigid and flexible form), coating, elastomers, sealant and adhesive [1]. It consists of polyol and polyisocyanate in the structural chain to form urethane linkage (NHC(O)O). Polyols are industrially produced from petroleum derivatives. Higher demand and consumption of petroleum and its derivatives has led to depletion and escalation in petroleum prices [2]. Furthermore, petroleum is a nonrenewable material. Sustainable technologies were developed to produce PU by using renewable resources such as vegetable oil as an alternative to petroleum [3]. Soybean oil, sunflower oil, safflower oil, and palm kernel oil has been used in many researches to produce eco-friendly PU [2,4-9]. Triacylglycerol (TAG), the main component in vegetable oils can be converted into high value polymers with some modifications in their chains [2]. Eco-PU is comparable to synthetic PU in term of strength.

PU is flammable when in direct contact with heat or fire [10]. Flame retardants (FR) are introduced to the PU system to overcome this problem. Although they improve the fire resistivity of the polymer, their presence deteriorate the mechanical properties. This is due to the interphase separation that occurred between FR and the polymer. FR with high degree of compatibility with the polymer was synthesized in order to improve the flammability as well as the mechanical properties of the PU. Liquid FRs i.e. commercial halogenated FR tris(1-chloro-2-propyl) phosphate (TCPP) or tris (mono-chloro-propyl) phosphate (TMCP) are manufactured as an alternative to improve the mechanical properties [11]. However, these liquid FRs are mostly halogenated compounds. They are potentially toxic and create environmental problem during storage, transportation and combustion [12-13]. Phosphorus-containing compound has been considered as an alternative to replace the halogenated FRs.

Soybean oil-based phosphate ester (PE) was produced via acid hydrolysis of soybean oil in the presence of phosphoric acid. Phosphoric acid was used in the preparation of PE from epoxidized soybean oil for coatings, elastomers and rigid polyurethane foams [4,14-17]. In this reaction, phosphoric acid not only initiates the reaction but also chemically becomes part of the product which is the PE [4]. This paper reported the effect of PE loading on the mechanical and burning properties of palm-based PU.

## Materials and Methods

### Materials

***For epoxidation:***

Soybean oil (SO) (iodine value, IV of 124.4 $I_2 \cdot 100\ g^{-1}$) was purchased from Mewah Oleoindustries, Malaysia while hydrogen peroxide ($H_2O_2$ with concentration of 30–32 wt%) was distributed by Friendemann Schmidt Chemicals, German. Glacial acetic acid ($CH_3COOH$ with concentration of 99.8 wt%) and sulphuric acid ($H_2SO_4$ with concentration of 98 wt%) were purchased from Merck, Malaysia. For esterification: *o-p*hosphoric acid, $H_3PO_4$ (85 wt%) was purchased from Merck, Malaysia and *tert*-butyl alcohol was produced by BDH Limited Poole, England.

***For polyurethane preparation:***

Palm-based polyester polyol (PKO-p) was supplied by UKM Technology Sdn Bhd, Pekan Bangi Lama, Malaysia. Silicone surfactant (Niax L5440) was supplied by Witco Ltd, Singapore. Glycerol ($C_4H_8O_3$) was supplied by BHD Laboratory Supplies, Poole England, while tetramethyl hexanediamine (TMHDA) and pentamethyl dietilenetriamine (PMDETA) were distributed by Cosmopolyurethane (M) Sdn Bhd, Port Klang, Malaysia. Crude isocyanate of type 2, 4-methylene diphenyldiisocyanate (MDI) was supplied by Cosmopolyurethane (M) Sdn Bhd, Port Klang, Malaysia.

### Epoxidation of SO

About 300 g soybean oil and 44.0 g glacial acetic acid were placed in a 500 ml three-necked reactor equipped with a thermometer, mechanical stirrer and a condenser. A sufficient amount of $H_2O_2$ and 3.85 ml of $H_2SO_4$ was dropped into the mixture at 40 °C. After the final dropping, the temperature was raised to the reaction temperature of 50–60 °C and allowed to react for 6 h. The stirring speed was fixed at 400 rpm. Upon completion of reaction, the bilayer mixture was separated using a separation funnel and neutralized with saturated sodium chloride and distilled water until it reached pH 7. The top part was then retrieved for acid hydrolysis.

### Hydrolysis and Esterification of Epoxidized SO

Ring-opening hydrolysis of epoxidized soybean oil (eSO) was conducted based on the study by Guo et al.[4]. In a glass reactor equipped with a thermometer, dropping funnel, water cooled condenser and mechanical stirrer, an amount of *o*-$H_3PO_4$, a portion of 50 wt% *tert*-butyl alcohol and 10 wt% distilled water were charged. The mixture was heated to 30 °C at a slow heating rate under mechanical stirring at 400–500 rpm for 30 min. The eSO was dissolved in a portion of *tert*-butyl alcohol and added drop wise into the mixture over the period of 45 min. After the final dropping of the eSO, the temperature was increased to 80–90 °C for 6 h or until the oxirane oxygen content (OOC) content reached below 0.2%. Upon completion of the reaction, the mixture was separated using a separation funnel. The yellow oily phase (PE) was retrieved. The amount of *o*-$H_3PO_4$ was varied at 0, 2.5, 5.0 and 7.5 wt% of the eSO.

**Preparation of palm-based polyurethane containing PE**

The resin was prepared prior to polymerization by mixing 90 wt% of PKO-p with 10 wt% glycerol, 2 wt% Niax L5440, 0.45 wt% TMHDA, 0.40 wt% PMDETA and 4.00 wt% of water. The polyurethane containing PE (PU-PE) was prepared by mixing the resin with PE at varying amount of PE at 0, 5, 10 and 15 wt% before the reaction with MDI. The mass ratio of the resin to MDI was 1:1. The mixture was mechanically stirred at 1000 rpm for 10 s. The mixture was then poured into a mold and demolded after 15 min. The molded PU foam was then conditioned for 16 h according to BS 4370 Part 1: 1988: Method 3 (*Method of Test for Rigid Cellular Material: Compression*) standard before characterization.

**Characterization of SO, eSO, PE and PU-PE: Fourier Transform Infrared Spectroscopy Analysis**

The functional groups in SO, eSO, PE and PU-PE were determined using Fourier transform infrared (FTIR) Spectroscopy analysis. This test was conducted using Perkin Elmer spectrometer model Spectrum BX with sodium chloride (NaCl) method for SO, eESO and PE samples and potassium bromide (KBr) pellet method was used for PU-PE samples. Samples were analyzed at a wavenumber ranging from 700 to 4000 $cm^{-1}$.

**Compression Test**

The compression test was conducted according to BS 4370: Part 1: 1988 *(Method of Test for Rigid Cellular Material):* Method 3 *(Compression)* standard. Samples were cut into dimension of 50 mm × 50 mm × 50 mm. The test was carried out using Instron Universal Test Machine model 5566 at cross-head speed of 50 $mm \cdot min^{-1}$ until the thickness was reduced to 90% of its original thickness. The compression stress and modulus were recorded as an average of five readings.

**Burning Test**

The burning test was carried out to determine the fire resistivity of the PU according to ASTM D 5048-09 Procedure B method 2 (*Standard Test Method for Measuring the Comparative Burning Characteristics and Resistance to Burn-Through of Solid Plastics Using 125-mm Flame*) standard. The PU foam was cut into samples of dimension 125 mm × 30 mm × 10 mm (length×width×thickness). The test sample was then clamped at one end so that its position was at 30°. A Bunsen burner with blue flame was positioned within the range of 25–30 mm from the test samples for 5 s and was then removed. The burning rate was determined using equation (1):

$$\text{Burning rate, m/s} = \frac{(\text{final length of specimen} - \text{initial length of specimen}), \text{m}}{\text{Total burning time, s}} \quad (1)$$

**Bomb Calorimetry Analysis**

Bomb Calorimetry analysis was conducted using oxygen bomb calorimeter model Parr 6100 coupled to a built-in printer with star SP700 software that automatically calculate the enthalpy of combustion ($\Delta H_c$) of the PUs. This test was in accordance to ASTM D240-09 (*Standard Test Method for Heat of Combustion of Liquid Hydrocarbon Fuels by Bomb Calorimeter*) standard.

## Results and Discussion

**FTIR Spectroscopy Analysis**

Figure 1 shows the FTIR spectra for SO, eSO and PE respectively. The SO spectrum (Figure 1(a)) showed stretching vibration peak for C=C at 3009 $cm^{-1}$ and HC=CH bonding peak at 1652 $cm^{-1}$ [18]. Upon completion of epoxidation, these peaks disappeared and a new peak was observed at 824 $cm^{-1}$ indicated the formation of epoxide ring [19]. It verified the ring-opening of the alkene group. The peak at 1746 $cm^{-1}$ belongs to the carbonyl group (C=O) in the fatty acid. After epoxidation, the peak shifted to the right (1744 $cm^{-1}$) to the carbonyl group of the ester. The disappearance of epoxide group in the PE as shown in Figure 1(c) indicated that the epoxide group has undergone hydrolysis. The presence of P-O-C of the PE was detected at 1025 $cm^{-1}$ upon completion of the hydrolysis reaction of the eSO. On the other hand, the presence of the hydroxyl (-OH) group in the PE was observed

at 3394 $cm^{-1}$ as a strong and intense peak [4]. The FTIR spectrum of the PU comprised of 0, 5, 10 and 15 wt% PE are as shown in Figure 2 and further summarized in Table 1. The inclusion of PE showed insignificant difference in the spectrum of the PU containing PE (PU-PE). The presence of PE did not affect the polymerization reaction and the formation of the urethane linkages.

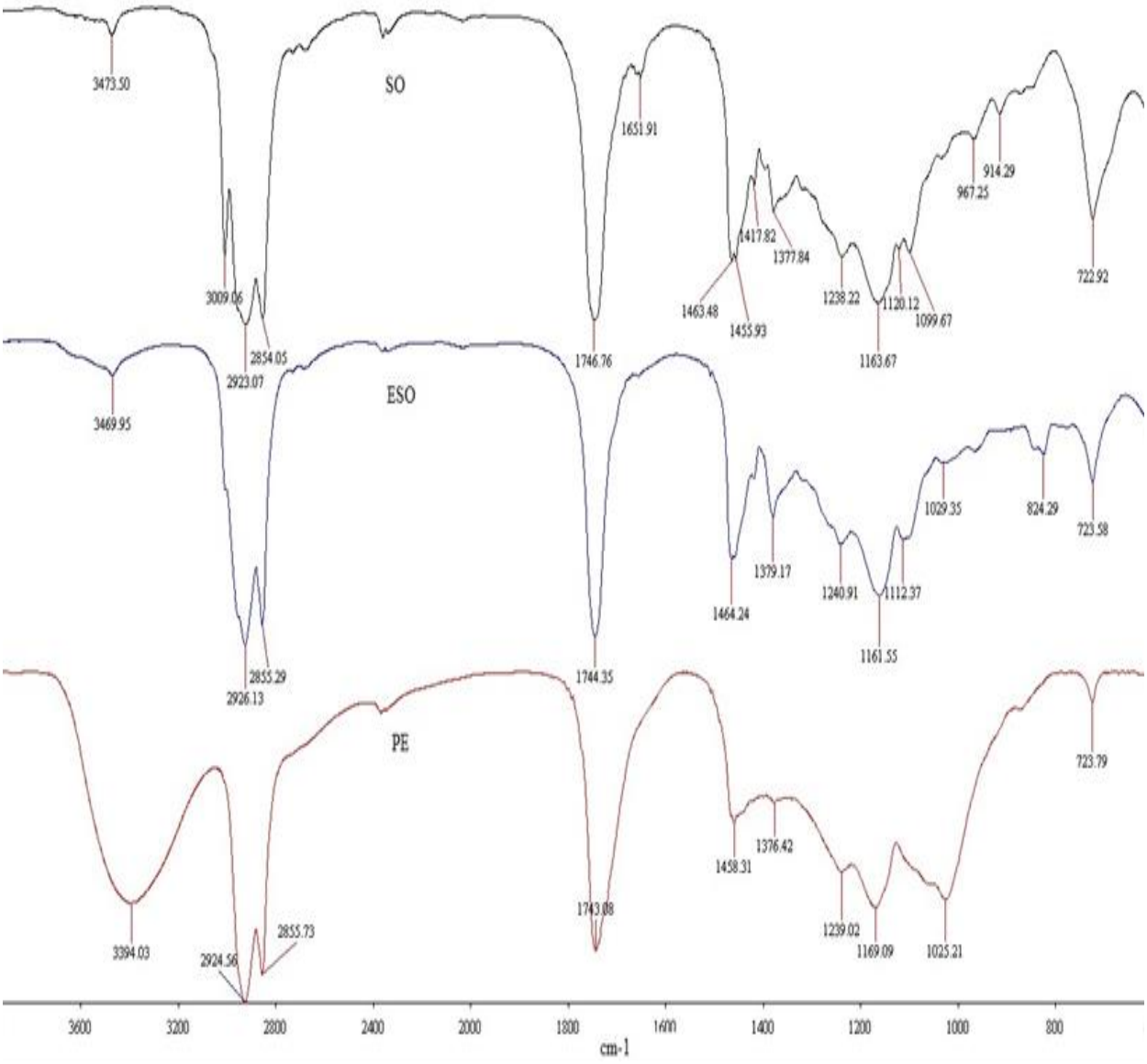



Figure 1. FTIR spectra of SO, eSO and PE

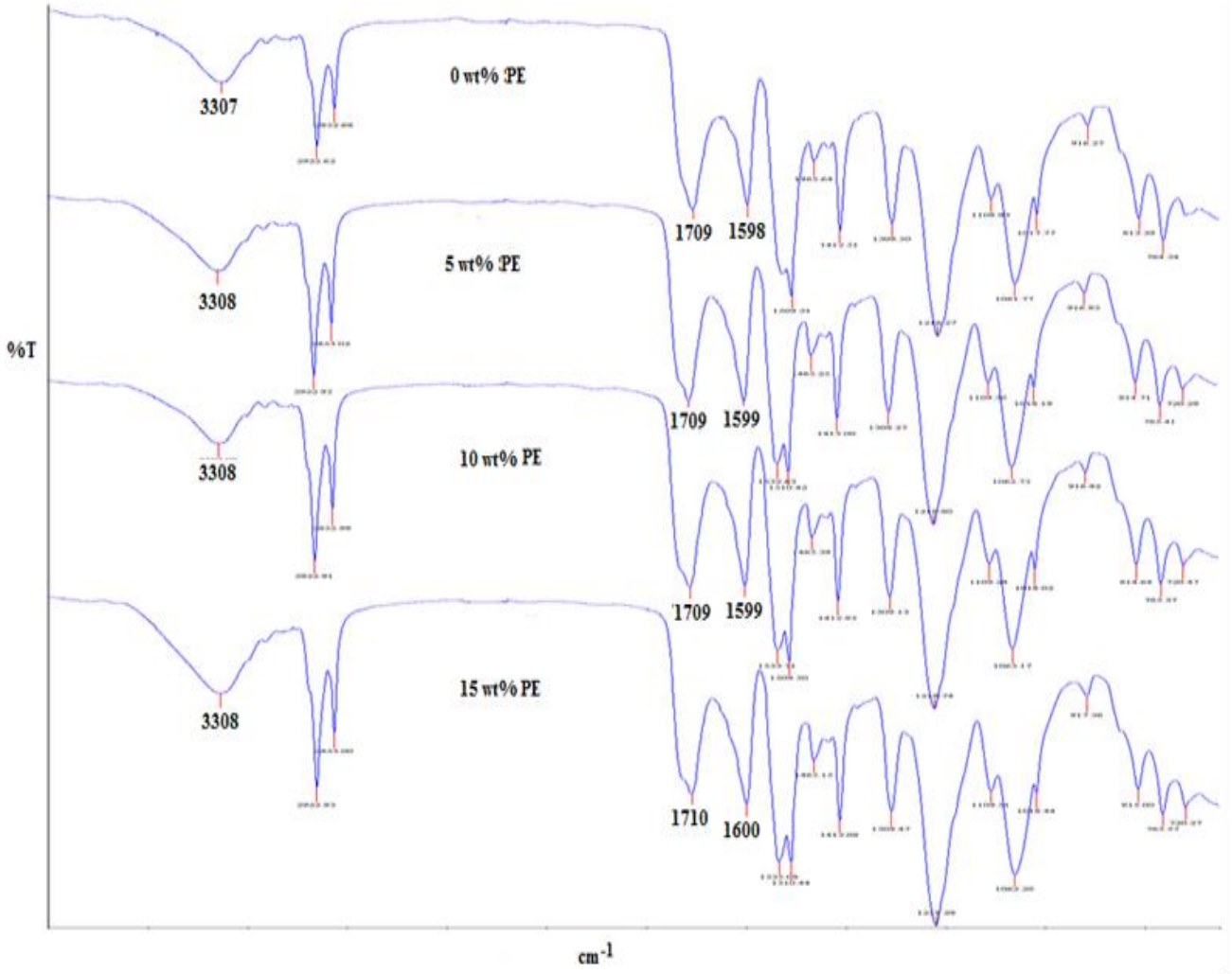



Figure 2. FTIR spectra of PU comprised of 0, 5, 10 and 15 wt% PE

Table 1. Summarised data from the FTIR spectrum of PU and PU-PE

| **Stretching or vibration peaks** | **Wavenumber, $cm^{-1}$** | | | |
|---|---|---|---|---|
| | **0 wt% PE** | **5 wt% PE** | **10 wt% PE** | **15 wt% PE** |
| Amine (N-H) | 3307 | 3308 | 3308 | 3308 |
| Isocyanate (-NCO) | - | - | - | - |
| Carbonyl (-C=O) | 1709 | 1709 | 1709 | 1710 |
| Carbamate (-C-N) | 1598 | 1599 | 1599 | 1600 |

**Mechanical Properties**

Figure 3 shows the effect of PE loading on the compression stress and modulus of the PU foam. Addition of PE to PU has decreased the compression stress and modulus. Compression stress and modulus for pristine PU was at 225 ± 43 kPa and 804 ± 203 kPa respectively. Further addition of PE at 5 to 15 wt% decreased the compression stress dramatically to 105 ± 11 kPa (15 wt% PE). Addition of 10 wt% PE has slightly increased the compression modulus to 130 ± 19 kPa from 122 ± 23 kPa (5 wt% PE). According to Fan et al. [16], compression stress and modulus are depending on density and degree of cross-linking of the polymer network. Higher density and degree of cross-linking give higher compression stress and modulus. The PE has secondary hydroxyl in the middle chain of the TAG. The bulky chain in the PE when reacted with isocyanate produced dangling chain. This dangling chain created plasticizing effect in the PU. When stress was loaded onto the PU, the plasticizing effect weaken the networks by limiting the movement of the PU molecules and thus decreased the mechanical properties [20].

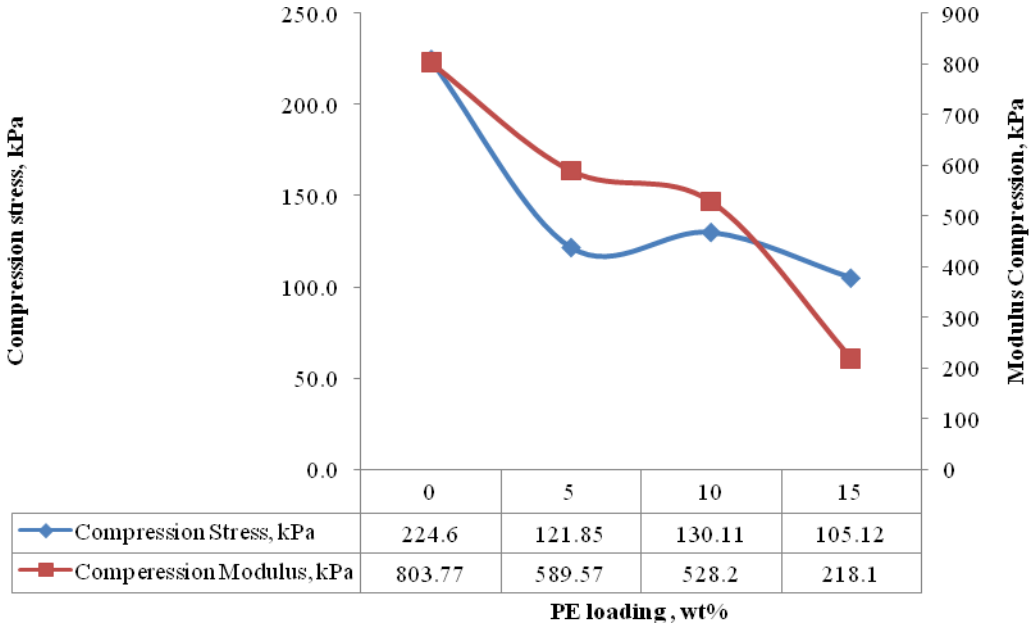



Figure 3. Compression stress and modulus of PU containing PE at 0, 5, 10 and 15 wt%

**Burning Properties**

Figure 4 showed that control PU has showed higher burning rate at $2.16 \times 10^3$ $m \cdot s^{-1}$. Addition of PE to the PU has decreased the burning rate (Figure 4). The flammability of PU was contributed by the soft segment in the PU structure (Figure 5). The soft segment in PU tends to degrade at lower temperature than the hard segments. It starts to dissociate and produces alcohol. During degradation, the combustible compound evaporates and mixes with air and thus forms flammable air. When this mixture is saturated, and the temperature reached flammability limits, PU starts to burn [21]. Phosphorus in PE (Figure 6) decomposes to produce phosphoric acid. Further decomposition of phosphoric acid leads to dehydration of PU and produces phosphorus-rich layer. This phosphorus-rich layer prevents PU surface from heat and oxygen [22]. The carbon layer forms on the surface of PU acts as a barrier and prevents combustible gases and oxygen from diffusing to the inner layer of the PU [23]. It protects the underneath layer of PU from any contact with heat [24].

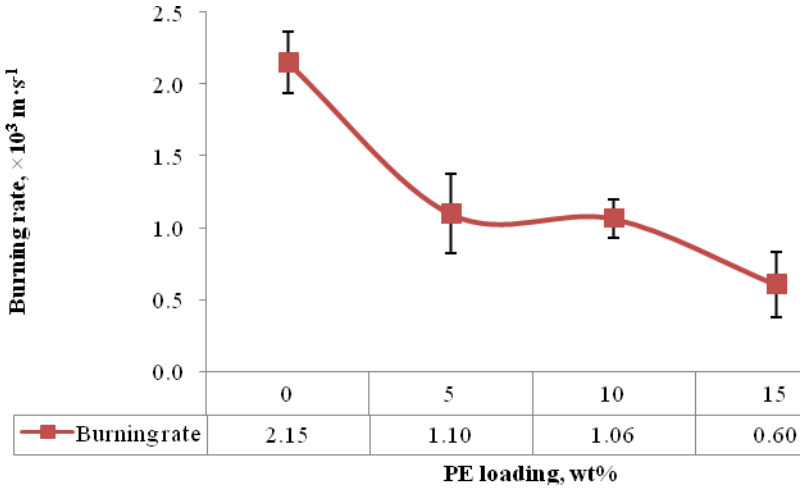



Figure 4. Burning rate of PU-PE at varying loading percentage of PE

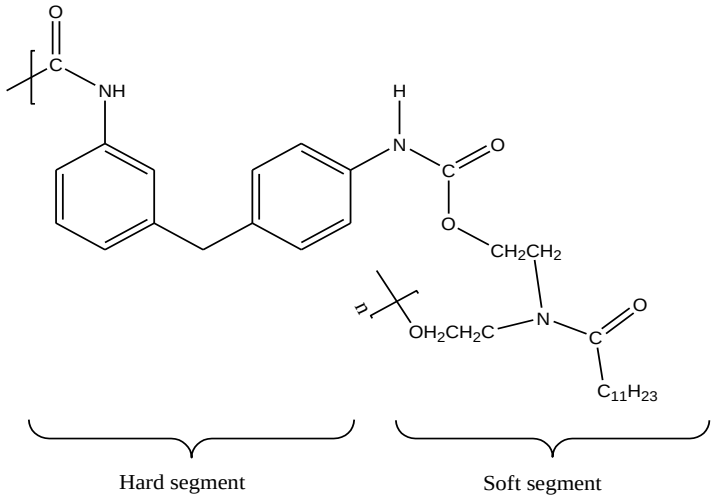



Figure 5. The hard and soft segments in the polyurethane structure

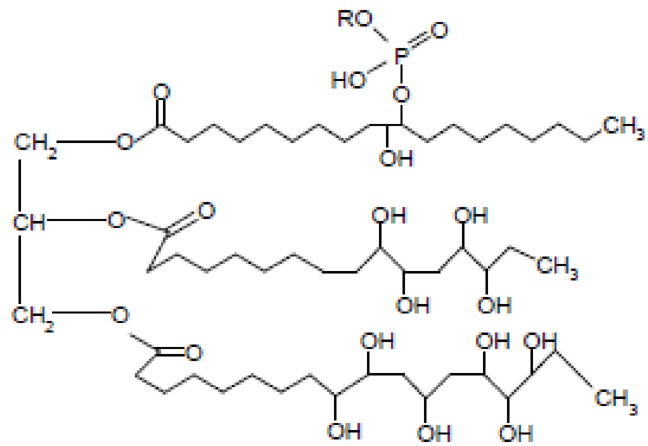



Figure 6. Structure of soybean oil-based phosphate ester (PE)

**Bomb Calorimetry**

Bomb calorimetry was conducted to support the fire characteristic by determine the enthalpy of combustion for PU and PU-PE. Figure 7 showed the enthalpy of combustion of the PU and PU-PE. Enthalpy of combustion for PU was $2.66\times10^{4}$ $kJ\cdot kg^{-1}$. The enthalpy of combustion decreased for PU-PE compared to PU. Further addition of PE at 10 and 15 wt% into the PU system exhibited insignificant difference. Lower heat of combustion indicated that there was a small interaction between PE and PKO-p with MDI. Phosphorus in the PE thermally decomposed to phosphoric acid during the pyrolyzing process [25]. Kuryla [26] stated that further thermal decomposition of phosphoric acid leads to the formation of polyphosphoric acid. Polyphosphoric acid dehydrates the pyrolyzing polymer and at the end of the process, char was formed on the polymer (PU). Char formation occurs through cross-linking reaction. It reduces the production of combustible and volatile materials. The char layer restricted the flow of heat to below surface of the PU and it obstructs permeation of combustible gases from the pyrolyzing polymer [27].

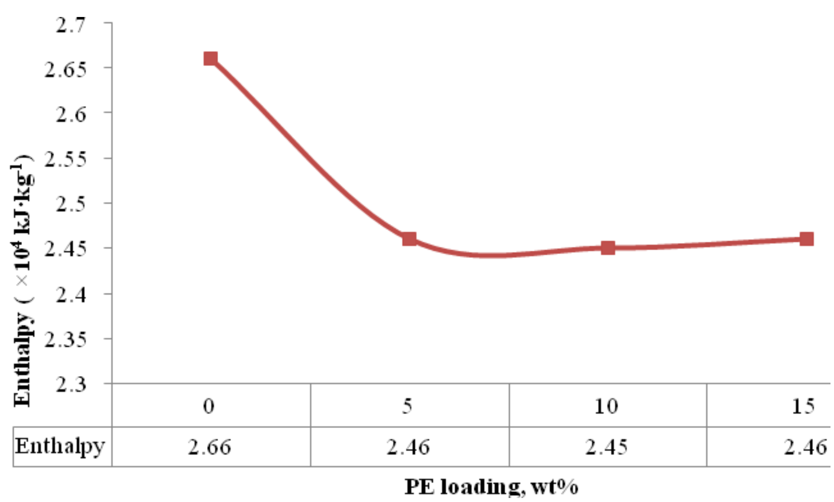



Figure 7. Combustion enthalpy of PU-PE at varying loading percentage of PE

## Conclusion

PE has proved to increase the fire resistivity of the palm-based polyurethane. Optimum loading of the PE was detected at 5 wt% based on the mechanical properties where higher compression stress and modulus were observed. However, higher loading of PE to PU system decreased the compression stress and modulus. Lower heat of combustion indicated that there was an interaction between PE with PKO-p and MDI.

## Acknowledgement

The authors would like to thank Polymer Research Center and School of Chemical Sciences and Food Technology, Faculty of Science and Technology, Universiti Kebangsaan Malaysia for the laboratory facilities and working space; Ministry of Science, Technology and Innovation (MOSTI) for funding of this research via Sciencefund Project No. 03-01-02-SF0949 and Ministry of Higher Education for the financial support via MyPhd grant for the graduate research assistant.

## References

1. Ferrer, M.C.C., Babb, D. & Ryan, A.J. (2008). Characterisation of polyurethane networks based on vegetable derived polyol. *Polym*. 49: 3279-3287.
2. Badri, K.H. (2012). Biobased Polyurethane from Palm Kernel Oil-Based Polyol. Polyurethane. InTech.
3. Beltran, A. A. & Boyaca, L.A. (2011). Preparation of Oleochemical Polyols Derived from Soybean Oil. *Lat. Am. Applied Research*. 41: 69-74.
4. Guo, Y., Hardesty, J.H., Mannari, V.M. & Jr, J.L.M. (2007). Hydrolysis of Epoxidized Soybean Oil in the Presence of Phosphoric Acid. *J. Am. Oil Chem. Soc*. 84: 929-935.
5. Jia, L.K., Gong, L.X., Ji, W.J. & Kan, C.Y. (2011). Synthesis of vegetable oil based polyol with cottonseed oil and sorbitol derived from natural source. *Chinese Chem. Let*. 22 (11): 1289-1292.
6. Montero de Espinosa, L. & Meier, M.A.R. (2011). Plant oils: The perfect renewable resource for polymer science *European Polym. J*. 47 (5): 837-852.
7. Pfister, D.P., Xia, Y. & Larock, R.C. (2011). Recent Advances in Vegetable Oil-Based Polyurethanes. *ChemSusChem*. 4 (6): 703-717.
8. Norzali, N.R.A., Badri, K.H. & Nuawi, M.Z. (2011). Effect of Aluminum Hydroxide Loading on the Compression Stress and Modulus, Thermal Conductivity and Acoustic Properties of Palm-Based Polyurethane Hybrid Composite. *Sains Malaysiana*. 40 (4): 379-384.
9. Badri, K.H., Othman, Z.B. & Razali, I.M. (2005). Mechanical properties of poyurethane composites from oil palm resources. *Iranian Polym. J*. 14 (5): 441-448.
10. Chung, Y.-j., Kim, Y. & Kim, S. (2009). Flame retardant properties of polyurethane produced by the addition of phosphorous containing polyurethane oligomers (II). *J. Ind. Eng. Chem*. 15 (6): 888-893.
11. Ashida, K., (2007). Polyurethane and Related Foams: Chemistry and Technology. Taylor & Francis: New York.
12. Liang, S., Neisius, M., Mispreuve, H., Naescher, R. & Gaan, S. (2012). Flame retardancy and thermal decomposition of flexible polyurethane foams: Structural influence of organophosphorus compounds. *Polym. Deg. Stab*. 97 (11): 2428-2440.
13. Van der Veen, I. & De Boer, J. (2012). Phosphorus flame retardants: Properties, production, environmental occurrence, toxicity and analysis. *Chemosphere*. 88 (10): 1119-1153.
14. Guo, Y., Mannari, V., Patel, P. & Massingill, J. (2006). Self-emulsifiable soybean oil phosphate ester polyols for low-VOC corrosion resistant coatings. *J. Coatings Tech. and Research*. 3 (4): 327-331.
15. Firdaus, F.E. (2011). Relationship od ReactionTemperature on Phosphate Oligomers Reactivity to Properties of Soy-Poyurethane. *World Academy of Science, Engineering and Technology*. 76: 230-234.
16. Fan, H., Tekeei, A., Suppes, G.J. & Hsieh, F.-H. (2012). Physical Properties of Soy-Phosphate Polyol-Based Rigid Polyurethane Foams. *Int. J. Polym. Sci*. 2012: 1-8.
17. Latere Dwan'Isa, J.-P., Mohanty, A.K., Misra, M., Drzal, L.T. & Kazemizadeh, M. (2003). Novel Biobased Polyurethanes Synthesized from Soybean Phosphate Ester Polyols: Thermomechanical Properties Evaluations. *J. Polym. and the Environment*. 11 (4): 161-168.

18. Derawi, D. & Salimon, J. (2010). Optimization on Epoxidation of Palm Olein by Using Performic Acid. *e-Journal of Chemistry*. 7 (4): 1440-1448.
19. Pavia, D.L., Lampman, G.M. & Kriz, G.S., (2001). Introduction to Spectroscopy. Brooks/Cole: California.
20. Narine, S.S., Kong, X., Bouzidi, L. & Sporns, P. (2007). Physical Properties of Polyurethanes Produced from Polyols from Seed Oils: II. Foams. *J. Am. Oil Chem. Soc*. 84: 66-72.
21. Badri, K.H. & Redwan, A.M. (2010). Effect of Phosphite Loading on the Mechanical and Fire Properties of Palm-Based Polyurethane. *Sains Malaysiana*. 39 (5): 769-774.
22. Zhang, L., Zhang, M., Hu, L. and Zhou, Y. 2014. Synthesis of Rigid Polyurethane Foams with Castor Oil-based Flame Retardant Polyols. *Industrial Crops and Products*. 52: 380-388.
23. Pan, L.L., Li, G.Y., Su, Y.C. and Lian, J.S. 2012. Fire retardant mechanism analysis between ammonium polyphosphate and triphenyl phosphate in unsaturated polyester resin. *Polym Deg Stab*. 97 (9): 1801-1806.
24. Chattopadhyay, D.K. and Webster, D.C. 2009. Thermal stability and flame retardancy of polyurethanes. *Prog. Polym. Sci*. 34 (10): 1068-1133.
25. Hörold, S. 1999. Phosphorus flame retardants in thermoset resins. *Polym. Deg. Stab*. 64 (3): 427-431.
26. Kuryla, W.C. and Papa, A.J. 1978. Flame Retardancy of Polymeric Materials. Vol. 4. Marcel Dekker, Inc: New York
27. Shih, Y.-F., Wang, Y.-T., Jeng, R.-J. and Wei, K.-M. 2004. Expandable graphite systems for phosphorus-containing unsaturated polyesters. I. Enhanced thermal properties and flame retardancy. *Polym. Deg. Stab*. 86 (2): 339-348.

The Malaysian Journal of ANALYTICAL SCIENCES ISSN 1394-2506

# THERMAL PROPERTIES, STRUCTURE AND MORPHOLOGY OF GRAPHENE REINFORCED POLYETHYLENE TEREPHTHALATE/POLYPROPYLENE NANOCOMPOSITES

## (Sifat Termal, Struktur dan Morfologi Graphene Bertetulang Polietilena Tereftalat /Polipropilena)

I. M. Inuwa, A. Hassan*, S. A. Shamsudin

*Department of Polymer Engineering,*
*Faculty of Chemical and Natural Resources Engineering,*
*Universiti Teknologi Malaysia, UTM 81310, Skudai, Johor Darul Takzim, Malaysia*

**Corresponding author: azmanh@cheme.utm.my*

**Abstract**

In this work the thermal properties, structure and morphology of a blend of polyethylene terephthalate (PET) and polypropylene (PP) reinforced with graphene nanoplatelets (GNP) were investigated. A blend of PET/PP (70/30 weight percent) compatibilized with styrene-ethylene-butylene-styrene grafted maleic anhydride triblock copolymer (10 phr) were fabricated by melt extrusion process in a twin screw extruder. The effective thermal conductivity of the nanocomposites increased as a function of the GNP concentration. More than 80% increase in effective thermal conductivity was observed for the 7 phr reinforced sample compared to the neat blend. This observation was attributed to the development interconnected GNP sheets which formed heat conductive bridges that are suitable for maximum heat transfer. However, in the case of thermal stability which is a function of dispersibility of GNP in polymer matrix, the maximum increase was observed at 3 phr GNP loading which could be attributed to the uniform dispersion of GNPs in the matrix... It is explained that the GNP nanofillers migrated to the surface of matrix forming an effective oxygen barrier due to char formation. Morphological studies revealed uniform dispersion graphene in the polymer matrix at 3 phr GNP loading along with isolated instances of exfoliation of the graphene layers.

**Keywords**: Thermal conductivity, thermal stability, polyethylene terephthalate, polypropylene, graphene nanoplatelets

**Abstrak**

Dalam kajian ini, sifat haba, struktur dan morfologi adunan polietilena tereftalat (PET) dan polipropilena (PP) diperkukuhkan dengan nanoplatlet grafit berkelupasan (GNP) telah dikaji. Adunan PET / PP (70/30 peratus berat) diserasikan dengan kopolimer triblok maleat anhidrida tercangkuk stirena-etilena-butilena-stirena (10 phr) telah dipalsukan oleh proses penyemperitan mencairkan dalam ekstruder skru berkembar. Keberaliran haba berkesan daripada nanokomposit meningkat sebagai fungsi kepekatan GNP. Peningkatan lebih daripada 80% dalam kekonduksian terma berkesan diperhatikan untuk sampel diperkukuhkan 7 phr berbanding dengan gabungan kemas. Pemerhatian ini disebabkan oleh pembangunan saling kunci GNP yang membentuk jambatan haba konduktif yang sesuai untuk pemindahan haba maksimum. Walau bagaimanapun, dalam kes kestabilan terma yang merupakan fungsi penyerakan GNP dalam matriks polimer, peningkatan maksimum diperhatikan pada kandungan 3 phr GNP yang boleh dikaitkan dengan penyebaran seragam GNPs dalam matriks. Ia menjelaskan bahawa yang pengisi nano GNP berhijrah ke permukaan matriks membentuk halangan oksigen yang berkesan kerana pembentukan char. Kajian morfologi mendedahkan penyebaran seragam graphene dalam matriks polimer pada kandungan 3 phr GNP bersama-sama dengan kes terpencil pengelupasan lapisan graphene.

**Kata kunci**: kekonduksian terma, kestabilan terma, polietilena tereftalat, polipropilena, nanoplatlet graphene

## Introduction

Engineering thermoplastics such as polyamides, or polycarbonates, possess superior mechanical and thermal properties, and hence are finding widespread use as structural materials in such areas as the automobile, aircraft or electrical/electronic industries. Consequently, growing demand has led to a hike in prizes of these thermoplastics. It

is predicted that the global revenue for engineering thermoplastics will hit 77 billion dollars by the year 2017 [1]. However, the increasing cost of engineering thermoplastics has motivated researchers both in academia and industry into focusing attention towards finding cheaper alternatives. Commodity thermoplastics such as polyethylene terephthalate (PET) or polypropylene (PP) are relatively inexpensive but have lower performance mechanical and thermal properties when compared to engineering thermoplastics. PET is a semicrystalline commodity thermoplastic with good mechanical properties, low melt viscosity, and spinnability. PET has been used in several fields such as food packaging, film technology, automotive, electrical, beverages containers and textile fibers [2]. Although PET is widely used in the fibers and packaging industries, its use in areas where high thermal stability and thermal conductivity are required is severely limited due its poor thermal stability and conductivity. Such areas include but not limited to heat dissipation in electrical/electronic components. Blending PET and PP would offer an opportunity to combine the excellent properties of the two polymers due to synergistic effect and to overcome their individual shortcomings. Since PET and PP are thermodynamically incompatible due to differences in chemical structure and polarity, the use of suitable compatibilizers is then necessary in order to produce a material with desired properties. Elastomeric compatibilizers such as styrene-ethylene-butylene-styrene-g-maleic anhydride (SEBS-g-MAH) has led to remarkable enhancement of impact properties of PET/PP blends but has also deteriorated other properties such as stiffness and strength [3]. Thermally conductive polymer nanocomposites, offer new possibilities for replacing metal parts in several applications including power electronics, electric motors, generators and heat exchangers due to their light weight, low cost and ease of production.

Recently there has been increasing interest in the use of exfoliated graphite nanoplatelets (GNP) as a multifunctional reinforcement phase in polymer nanocomposites. These graphitic nanoplatelets, derived from graphite, combine the low-cost and layered structures of nanoclays with a unique plethora of properties usually exhibited by carbon nanotubes including electrical conductivity, superior mechanical, physical, thermal and flame retardants properties. Presently, research activities into the properties and structure of graphene has moved from curiosity-oriented to application-oriented [4,5]. Graphene is a monolayer carbon nano particle that consists of $sp^2$ hybridized carbon atoms arranged in hexagonal planar structures. Properties that have endeared this unique material to diverse applications are its exceptional mechanical strength (Young's modulus of 1 TPa, tensile strength of 20 GPa) [6, 7], excellent electrical (5000 S/m) [8] thermal conductivities and stability (~3000 W/m.K) [9]. Therefore, it is logical to assume that incorporating graphene and its derivatives (e.g. GNP) into polymeric matrices will impart significantly on thermal stability and thermal conductivity of the host polymers. Consequently, several studies have been reported on the development of multifunctional polymer nanocomposites (PNC) [10-15] using GNP as the reinforcement phase.

Several studies have been conducted to assess the thermal conductivity of graphene reinforced polymer nanocomposites [16-19]. Min et al [20] observed 157% increases in thermal conductivity of graphite nanoplatelets/epoxy composites over that of pure epoxy . Teng et al [17] studied the effect of non-covalent functionalized graphene on epoxy composites and observed remarkable improvement in thermal conductivity much higher than epoxy reinforced with multi wall carbon nanotubes. Steady state thermal analysis is a method of measurement of thermal conductivity of polymer composites and nanocomposites. This method is useful for specimens having thermal resistance in the range of 10 to 400 x $10^{-4}$ $m^2$.K/W. which can be obtained from materials of thermal conductivity in the approximate range from 0.1 to 30 W/(m.K) [21]. Although GNPs have been used to improve thermal stability and thermal conductivity in polymer nanocomposites with promising results, its use to improve the thermal conductivity of widely used commodity thermoplastics such as PET and PP or their blends is still lacking.

In this study, thermal conductivity, thermal stability, thermal behavior, morphological features and structure of GNP reinforced polyethylene terephthalate/polypropylene blends were investigated as a function of concentration of GNPs. SEBS-g-MAH is expected to serve a dual function, to compatibilize PET/PP blends and to aid the dispersion of GNPs in the polymer matrix. Conventional melt extrusion process is used to prepare PET/ PP/GNP nanocomposites because it is more economical, compatible with industrial processes (extrusion and compression molding) and free of environmentally harmful or dangerous solvents as might be encountered with other methods. To the best of our knowledge no similar report for same polymer system is published in the open literature.

## Materials and Methods

### Materials

Exfoliated graphite nanoplatelets, GNP-M-5 grade (99.5% carbon) of average diameter 5 µm and average thickness of less than 10 nm were purchased as dry powder from XG Sciences, Inc. (East Lansing, MI, USA) and used as received. Polyethylene terephthalate (grade M100) was obtained from Espet Extrusion Sdn Bhd (Malaysia) with intrinsic viscosity of 0.82 g/dl. PP, a copolymer grade (SM240) with density of 0.96 g/cm$^3$ and melt flow index of 35 g/10 min (230$^o$C and 2.16 kg load) was supplied by Titan chemicals (Malaysia). Styrene-ethylene-butylene-styrene triblock copolymer grafted with 1.84 wt % of maleic anhydride (SEBS-g-MAH) was supplied by Shell Chemical Company under the trade name of Kraton FG 1901X with ratio of styrene to ethylene/butylene in the triblock copolymer is 30/70 wt %. Melt flow index (MFI) = 20g/10 min (270$^o$C, 5kg), molecular weight of styrene block is 7000g/mol. and ethylene/butylene block is 37500g/mol.

### Blends and Nanocomposites fabrication

PET was pre-dried in vacuum oven at 120 °C for 48 hours, PP was dried at 80 °C for 24 hours and SEBS-g-MAH was dried for 8 hours at 60 °C. PET, PP, SEBS-g-MAH and GNP with various ratios were melt blended using a counter-rotating twin screw extruder (Brabender Plasticoder, P 2000). All materials were compounded in a single step with various amounts of GNPs according to sample formulation Table shown in Table 1. The temperature setting from the hopper to the die were 265/275/280/285 °C and the screw speed was 60 rpm. The composites were pelletized and then dried at 100 °C for 12 hours before pressing into sheets of 3mm thickness using a hydraulic press set at a temperature of 250$^o$C for both lower and upper plates and 100 psi pressure.

Table 1. Sample Formulations (70 wt% PET, 30 wt % PP, and 10 wt% SEBS-g-MAH) with GNP variation.

| Sample name | GNP (phr) |
|---|---|
| GNP0 | 0 |
| GNP1 | 1 |
| GNP2 | 2 |
| GNP3 | 3 |
| GNP4 | 4 |
| GNP5 | 5 |
| GNP6 | 6 |
| GNP7 | 7 |

### Nanocomposites characterization

Cussons thermal conductivity analyser was used to measure the thermal conductivity of various materials, which include polymers, glasses, ceramics, rubbers composites, few metals and other materials with medium to low thermal conductivity by steady state method. In the present work, this instrument is used to measure the room temperature effective thermal conductivity of the composites specimens. This test is conducted in accordance with ASTM E1530 standards. The material was held under uniform compressive load between two polished surfaces, each controlled at a different temperature. The lower surface is part of a calibrated heat flow transducer. The heat flows from the upper surface through the sample to the lower surface establishing an axial temperature gradient in the stack. After reaching thermal equilibrium (steady state), the temperature difference across the sample was measured along with the output from the heat flow transducer. The temperature difference and the sample thickness were then used to calculate the effective thermal conductivity using equation 1. The temperature drop through the

sample was measured with temperature sensors in the highly conductive metal surface layers on either side of the sample. By definition thermal conductivity is the exchange of energy between adjacent molecules and electrons in a conducting medium, it is material property that describes heat flow within a body for a given temperature difference per unit area.

The thermal conductivity of nanocomposites was calculated according to equation 1.

$$k = \sum \frac{q \cdot L}{T_1 - T_2} \quad (1)$$

k = thermal conductivity (W/mK),
q = heat flow ($W/m^2$)
L = specimen thickness (m),
$T_1$ = temperature of one surface of the specimen ($^oC$ ),
$T_2$ = temperature of the other surface of the specimen ($^oC$).

**Thermal Stability**

In order to examine the thermal degradation behavior of samples, thermogravimetric analysis (TGA) was performed on Perkin Elmer TGA 7 instrument at a rate of $10^oC$/min under nitrogen atmosphere in the temperature range 30 – $600^oC$.

**Differential Scanning Calorimetry**

The melting and crystallization behavior of PET/PP and PET/PP/GNP composites were characterized through differential scanning calorimetry (DSC) (Perkin Elmer DSC-6), using 5-10 mg samples sealed in aluminum pans. The temperature was raise from 30 to 300 $^oC$ at a heating rate of $10^oC$/min, and after a period of 1 min, it was swept back at the rate of $10^oC$/min. The fusion enthalpies, ΔHf(PET) and ΔHf(PP) were measured and the degree of crystallinity, $X_{c(PET)}$ and $X_{c(PP)}$ were calculated using the following equations 2 and 3 :

$$\%X_c(PET) = \frac{\Delta H_{f(PET)}}{\Delta H^0_{f(PET)}} \times \frac{1}{W(PET)} \times 100 \quad (2)$$

$$\%X_c(PP) = \frac{\Delta H_{f(PP)}}{\Delta H^0_{f(PP)}} \times \frac{1}{W(PP)} \times 100 \quad (3)$$

$\Delta H^0_{f(PET)}$ = 140 J/g and $\Delta H^0_{f(PP)}$ = 209J/g [22]. Where $w_{PET}$ and $w_{PP}$ are the weight fractions of PET and PP, respectively

**Morphological characterization**

Dispersion of the graphite nanoplatelets was observed using field emission scanning electron microscopy (FESEM) and transition electron microscopy (TEM). FESEM micrographs of fractured surfaces of the unreinforced blend and nanocomposites were obtained using a Hitachi S-4800. The blend control and the nanocomposites were gold coated using a Balzers Union MED 010 coater. For TEM analysis, a thin section (thickness of 70 nm) was used for transmission imaging. Samples were microtomed using Reichert Jung Ultracut E microtome. Transmission micrographs were collected using a JEOL JEM-2100 microscope, with an operating voltage of 200 kV.

**X-ray diffraction analysis**

X-ray diffraction patterns were collected using X'Pert, X-ray diffractometer (Siemens XRD D5000) and Ni-filtered Cu Kα radiation at an angular incidence of 0° to 70°(2θ angle range). XRD scans of the GNP powder along with the composites samples were collected at 40 kV and 50 mA with an exposure time of 120s. Diffraction patterns were obtained using equation 4 to evaluate the dispersion of GNPs in the matrix.

$$n\lambda = 2\theta \sin \theta_p \quad (4)$$

where $\theta_p$ = diffraction angle of the primary diffraction peak and λ = X-ray wave length, n = 1.

## Results and Discussion

### Thermal Conductivity

The effect of GNP loading on effective thermal conductivity of PET/PP/GNP nanocomposites is shown in Fig. 1 below. The effective thermal conductivity of PET/PP/GNP nanocomposites was increased with increase in GNP concentration. However, sharp rise in the effective thermal conductivity can be seen at 3 phr GNP loading which corresponds to the establishment thermal percolation threshold. Chu *et al* [23] in their recent work, "Thermal conductivity of composites with hybrid carbon nanotubes and graphene nanoplatelets", have elaborated on the concept of thermal percolation threshold of graphite nanoplatelets.

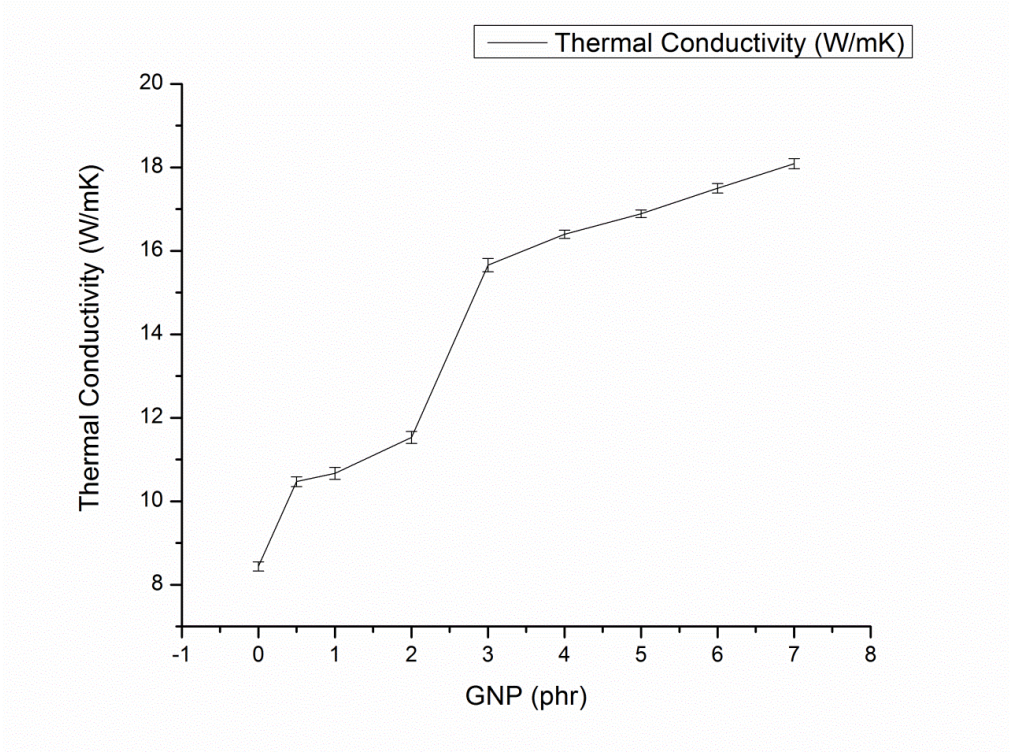



Figure 1. Effect of GNP loading on effective thermal conductivity of PET/PP/GNP nanocomposites

The thermal conductivity of 7 phr reinforced PET/PP/GNP nanocomposites was 18.709 W/mK, more than two times improvement compared that of the neat PET/PP blends. It can be seen that the relative increase in the effective thermal conductivity is higher with increase in GNP loading beyond the established percolation threshold at 3 phr. This observation is presumed to correspond to the development of effective interconnected GNP network that is most suitable for heat transfer. Prior to this filler concentration, the GNPs are thought to be randomly distributed in the polymer matrix standing isolated without contact to each other as depicted in the illustrated scheme in Fig. 2 which led to low efficiency for thermal conductivity [21]. This resulted in lower improvement in the values of the effective thermal conductivity. At higher concentration the GNP platelets are aligned and overlapped with each other leading to development of effective interconnected network that sharply enhanced thermal conductivity at 3 phr GNP loading.

Recently, it was found that fillers with high aspect ratio, such as whiskers and platelets, can form more continuous thermally conductive network in the polymer matrix and thus more effective in enhancing thermal transfer [19].

This factor combined with the high intrinsic thermal conductivity of GNPs offered reasonable explanations for the larger increments of thermal conductivity of PET/PP/GNP with increasing filler content. Due to Van der Waals' attraction a homogenous GNP network could be achieved under relatively high filler content. This evidence can be corroborated by the TEM micrographs of the PET/PP/GNP nanocomposites (3 phr filler level). The formation GNP interconnected network would also ensure the decrease in scattering of phonon transfer and promote the diffusion of phonons in the overall nanocomposites. Similar observation has been made in the polymeric systems filled with hybrid GNP/carbon nanotubes [24].

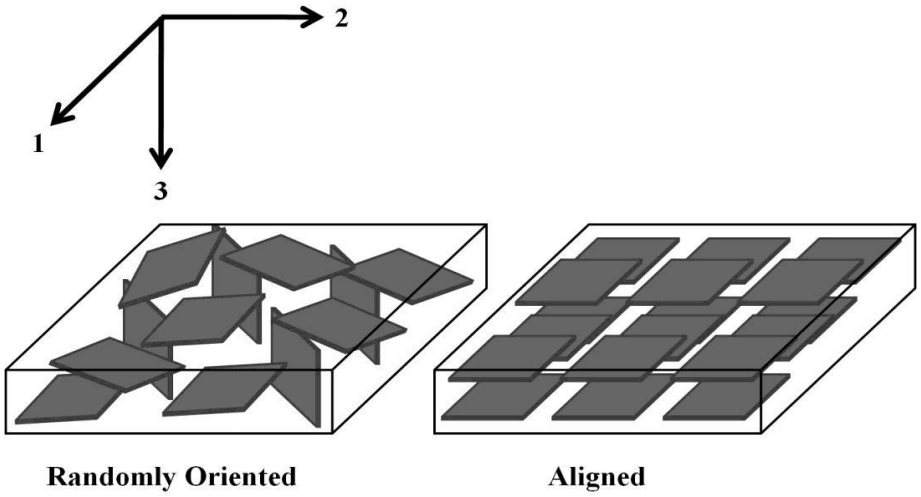



Figure 2. Distribution of GNPs in PET/PP; random orientation (low GNP concentration) and aligned orientation (higher GNP concentration at 3phr and above)

**FESEM Analysis**

Studies of the surface morphology and compositions of polymer nanocomposites by FESEM have been used extensively to characterize the dispersion of nanofillers in polymeric matrices [25,26]. Fig.3 is a typical FESEM of PET/PP blends and PET/PP/GNP nanocomposites. Fig. 3a shows the FESEM micrograph of unreinforced PET/PP blend. It is interesting to note that addition of SEBS-g-MAH has compatibilized the immiscible PET/PP blend (shown by arrow) by reducing the particle size of the dispersed PP phase and eliminating the voids. This resulted in the improved adhesion of the different phases and reduced interfacial tension. Similar finding was reported by Heino et al [27]. FESEM image of the impact fractured surface of PET/PP/GNP nanocomposites taken in the transverse direction is depicted in Fig.3b. The GNPs appear to be embedded and uniformly dispersed in the nanocomposites with the edges of the graphene sheets projecting out of the fractured surface. The uniform dispersion of GNPs in the polymer matrix is responsible for the observed increase in the properties. This observation is consistent with that of Ramanathan et al. [28]. Fig.3c shows the interaction of the GNP particles with the SEBS-g-MAH particles as shown by arrow. The compatibilizer can be seen attached to the surface of GNP sheets. This indicates that the compatibilizer functions by aiding the dispersion of GNPs in the polymer matrix through encapsulation of GNPs by the rubber particles in addition to improving the adhesion between PET and PP particles. Similar findings were reported by Zhang and Deng [29]

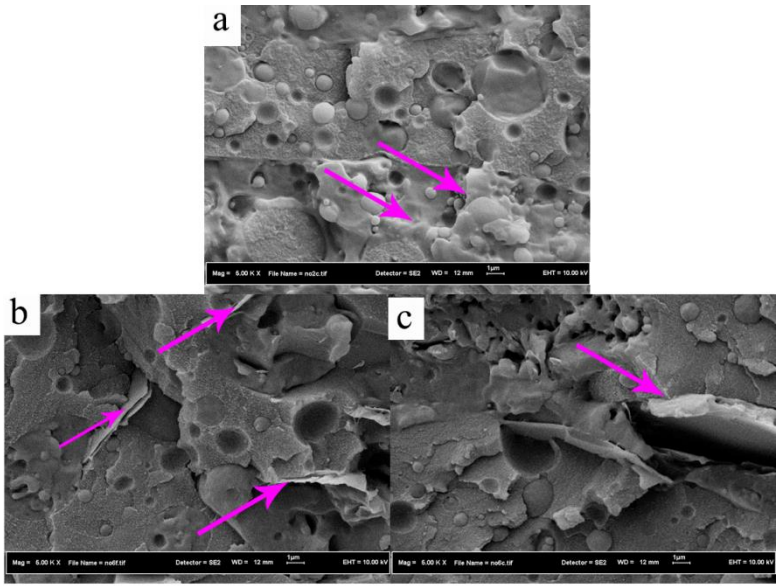



Figure 3. FESEM images of PET/PP/GNP nanocomposites at 3 phr showing a) pure PET formation of b) PET/PP blend c) uniform dispersion of GNP d) attachment of GNP particles on the compatibilizer surface

**TEM Analysis**

TEM analysis is a proven and reliable technique for investigating the dispersion of nanofillers in polymer matrix. Fig.4 is the image analysis of GNP3. In Fig. 4a, the interconnected GNP sheets can be seen within the matrix with maximum of three sheets overlapping on each other. Interconnected morphology is the most suitable for improvement of transport properties such as thermal conductivity. This confirms that the number of sheets was reduced from 5 to 3 sheets originally supplied by the manufacturer which can be attributed to shear mixing in the extruder equipment. Close examination of Fig. 4b can reveal the interaction of GNP with the polymer matrix possibly SEBS-g-MAH. Folded graphene sheet off-plane, can be seen surrounded by matrix which is represented by the blurred grey background with improved adhesion by the compatibilizer elastomer particle or absorption by the PET/PP chains [32]. The shear mixing also involve wrinkling (Fig. 4c) and crumpling (Fig. 4d) of exfoliated single layers due to the thin thickness of the graphene particles. It has been reported that the presence of the wrinkled and crumpled exfoliated graphene sheets may actually lead to nanoscale surface roughness which would likely produce an enhanced mechanical interlocking and adhesion with the polymer chains [30]. It is reported that SEBS-g-MAH improved the dispersion of fillers in the polymeric matrices thereby improving the toughness and wear resistance of the matrix due to interaction with fillers [29, 31]. Overall it is evident that good dispersion of GNP sheets has been achieved with isolated instances of exfoliation.

**Thermogravimetric analysis**

Thermal stability of the neat blend and composites were investigated under nitrogen gas atmosphere as described section 2.3.2. The results of the measurements are shown in Fig. 5a, and 5b respectively and the corresponding data is shown in Table 2. The thermal decomposition temperature of the blends and composites show a single step decomposition process indicating effective compatibilization of the blends. The results also show the effect of GNPs on the thermal stability of the neat PET/PP blends. From Table 2, the $T_{10}$ and $T_{50}$ as well as maximum decomposition temperatures $T_{max}$ are characteristically high for all the composites compared with the neat blend. In particular, the 3 phr GNP concentration yielded highest thermal stability.

The enhanced thermal stability of the composites was attributed to the high aspect ratio of GNPs which serve as a barrier and prevented the emission of gaseous molecules during thermal degradation. The dramatic improvement at

3.0 phr is attributed to the homogenous dispersion of the GNPs in the matrix at this filler level. Homogeneously dispersed GNP disrupted the oxygen supply by forming charred layers on the surfaces of the composites thereby enhancing thermal stability [32]. However the weight residue shows that highest amount of ash was obtained with the 5.0 phr GNP loading. This logically means that as the quantity of the GNP increased the residue was also increased due to very high thermal stability of the graphene platelets. These observations are consistent with those made by Tantis et al. [33].

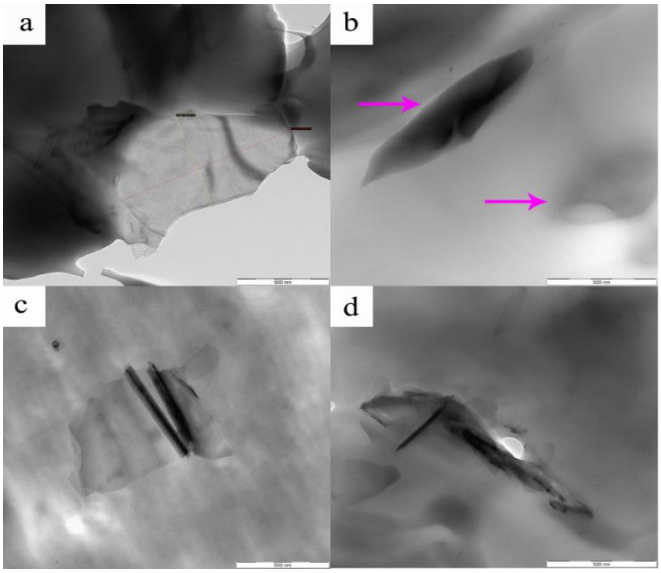



Figure 4. a) Interconnected GNP sheets at 3 phr loading, b) adhesion of GNP to polymer matrix promoted by SEBS-g-MAH, c) wrinkled GNP sheets and d) crumpled GNP sheets.

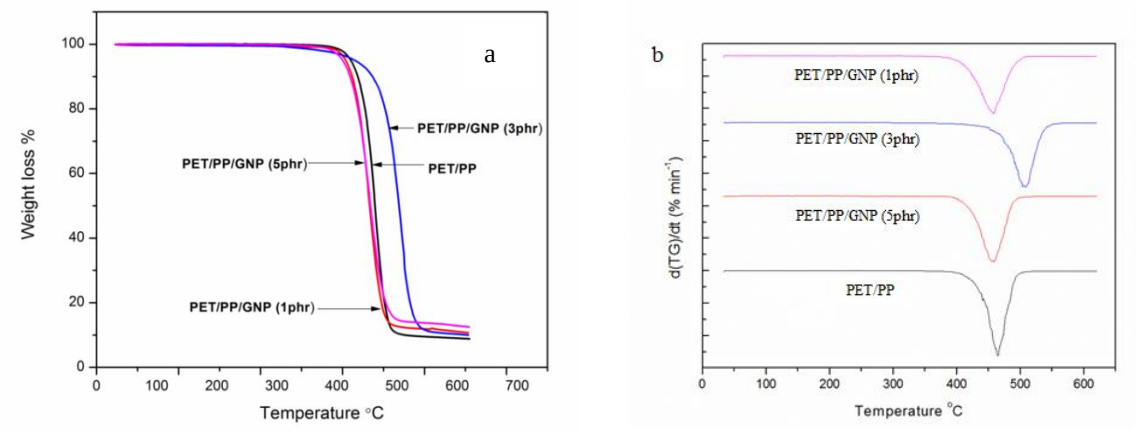



Figure 5. a) TGA and b) DTG curves of neat PET/PP and PET/PP/GNP nanocomposites

Table 2. TGA and DTG data

| Sample | Degradation Temp (°C) | | DTG Peak Temp | Residual Weight (%) at 600°C |
|---|---|---|---|---|
| | $T_{10}$ | $T_{50}$ | $T_{max}$ | |
| Neat Blend | 424°C | 454°C | 466°C | 8.774 |
| GNP 1.0phr | 426°C | 457°C | 457°C | 10.068 |
| GNP 3.0 phr | 458 °C | 502 °C | 505°C | 11.808 |
| GNP 5.0 phr | 421°C | 456°C | 455°C | 12.867 |

**Differential Scanning Calorimetry**

Fig. 6a and b show the heating and cooling scans of DSC traces for blends and nanocomposites. The corresponding thermal data is provided in Table 3. From the Table it is clear that the $T_c$ values of all nanocomposites are higher than those of the unreinforced PET/PP blend and increase with increasing GNP content. This phenomenon can be explained by the heterogeneous nucleation effect of the GNPs on the chain segments, which leads to the crystallization of PET at higher temperatures. Similar explanation can be made for the $T_{cPP}$. This is consistent with previous studies [34].

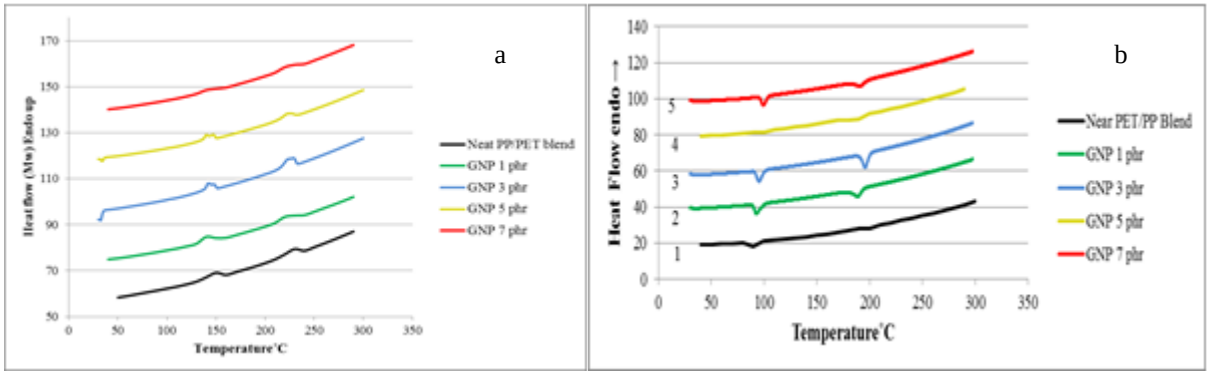



Figure 6. DSC plots a) Heating scans and b) cooling scans of PET/PP, PET/PP/GNP nanocomposites

However, the crystallinity of PET and PP in PET/PP/GNP nanocomposites decreased with the addition of GNP. It can be thought that the presence of GNP has restricted the mobility of PET and PP chains during the crystallization process. The high surface area of the GNP sheets enables them to act as vast heterogeneous nucleation points which increased crystallization rates. Subsequently less crystalline regions are formed due to shorter time available. Additionally, due to the nanosized dimension of GNP particles; they can present in both PET and PP phases resulting in the increased $T_c$ for both PET and PP. The $T_m$ of both PET and PP however, remain essentially unaffected. Karevan and Kalaitzidou [35] observed that the decrease in the degree of crystallinity of PA12 with GNP content may be due to the decrease in the free volume and constrains of the polymer chains imposed by the rigid GNP that do not allow them to rearrange and form crystals.

Table 3. DSC data of PET, PET/PP and PET/PP/GNP nanocomposites

| Designation | Crystallization Temperature $^{o}$C | | Melting Temperature $^{o}$C | | Crystallinity (%) | |
|---|---|---|---|---|---|---|
| | PET | PP | PET | PP | PET | PP |
| GNP0 | 178.1 | 89.3 | 230.1 | 150.4 | 24.1 | 19.8 |
| GNP1 | 189.7 | 93.3 | 230.0 | 140.6 | 21.6 | 17.6 |
| GNP3 | 196.3 | 97.4 | 229.8 | 148.4 | 20.2 | 15.3 |
| GNP5 | 186.5 | 99.5 | 228.7 | 148.3 | 19.5 | 13.4 |
| GNP7 | 190.2 | 100.0 | 230.1 | 150.5 | 19.0 | 12.1 |

**X-Ray Diffraction**

The XRD patterns of the pristine GNP, neat PET/PP blend and PET/PP/GNP composites are shown in Fig. 7 The characteristic peaks of diffraction pattern for the graphene nanoplatelets shows the graphene-2H characteristic peaks at 26.6$^{o}$ (d=3.35 A °) and 54.7$^{o}$ (d=1.68 A°) 2θ. The absence of the characteristic graphene peaks in the nanocomposites along with the observations by TEM and FESEM suggest a uniform dispersion of GNP sheets in the matrix. It may be concluded that GNPs in the composites may not have been substantially exfoliated but homogenously distributed in the matrix thereby improving the properties. Bandla et al. [36] have reported similar observations.

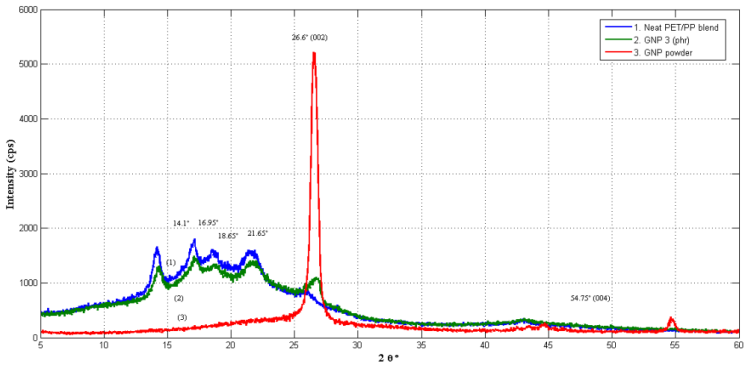



Figure 7. X-ray diffraction features of the neat PET/PP blends GNP powder and PET/PP/GNP nanocomposites

**Conclusion**

Nanocomposites based on blends of PET/PP compatibilized with SEBS-g-MAH and GNPs have been successfully prepared by melt extrusion technique. Thermal conductivity, thermal behavior, morphological features and structure of the resulting nanocomposites were investigated. Thermal conductivity exhibited linear relationship with increased GNP loading with percolation established at 3 phr loading. This was attributed to the development of effective heat conduction bridges of interconnected GNPs that increased the efficiency for thermal conductivity. Morphological features show uniform dispersion and the development of interconnected GNP sheets at 3 phr loading with isolated instances of exfoliated GNP sheets. Addition of GNPs also led to decrease in the degree of crystallinity of PET/PP/GNP nanocomposites and the melting temperature remained almost the same. This study has showed the potential of using GNPs to develop a thermally conductive polymer nanocomposites based on

blends of PET/PP blends for applications in electrical/electronics industry where heat dissipation in electrical components are essential.

**Acknowledgement**

The authors would like to thanks Ministry of Higher Education of Malaysia (MOHE) and Universiti Teknologi Malaysia (UTM) for Research Universiti Grant vote number 02H26 and sub code Q.J130000.7113.02H26.

**References**

1. Emory, K. (2013). The eco-friendly car is driving engineering plastics market to $76 billion by 2017. Retrieved 12 January, 2014, from http://www.tgdaily.com/general-sciences-features/78573-the-eco-friendly-car-is-driving-engineering-plastics-market-to-76-bi#VRkDTSm6J5LpjbcK.99
2. Bartolome, L., Imran, M. and Cho,B.G. (2012). Recent Developments in the Chemical Recycling of PET in Material Recycling – Trends and Perspectives. ed. Achilias. D. S. 65-84.
3. Abdul Razak, N. C., Inuwa, I. M., Hassan, A. & Samsudin, S. A. (2013). Effects of compatibilizers on mechanical properties of PET/PP blend. *Compos. Interfaces*, 20 (7): 507-515.
4. Liu, X.G. (2013). How will carbon material lead to a Low Carbon Society – A review of Carbon 2012. *Carbon*, 51: 438.
5. Hussain, F. H., Mehdi O., Masami Gorga, & Russell E. (2006). Review article: Polymer-matrix Nanocomposites, Processing, Manufacturing, and Application: An Overview. *J. Compos. Mater.*, 40 (17): 1511-1575.
6. Geim, A. K., & Novoselov, K. S. (2007). The rise of graphene. *Nat Mater*, 6 (3): 183-191.
7. Lee, C. W., Xiaoding K., Jeffrey W. & Hone, J. (2008). Measurement of the Elastic Properties and Intrinsic Strength of Monolayer Graphene. *Science*, 321 (5887): 385-388.
8. Zhang, Y. A., Dervishi, S. F., Xu, E., Li, Y., Casciano, Z. & Biris, D. A. S. (2010). Cytotoxicity effects of graphene and single-wall carbon nanotubes in neural phaeochromocytoma-derived PC12 cells. *ACS Nano*, 4: 3181.
9. Balandin, A. A., Ghosh, S.B., Wenzhong, C., Teweldebrhan, I., Miao, D., Lau, F. & Ning, C. (2008). Superior Thermal Conductivity of Single-Layer Graphene. *Nano Lett.*, 8 (3): 902-907.
10. Kuila, T. B., Saswata, K., Partha, K., Nam, H. R., Kyong, Y. L., & Joong, H. (2011). Characterization and properties of in situ emulsion polymerized poly(methyl methacrylate)/graphene nanocomposites. *Composites Part A*, 42 (11): 1856-1861.
11. Kuila, T. B., Saswata, K., Partha, K., Nam, H. R., Kyong, Y. L., & Joong, H. (2012). Effect of functionalized graphene on the physical properties of linear low density polyethylene nanocomposites. *Polym. Test.*, 31 (1): 31-38.
12. Zhao, X. Z., Qinghua, C. & Dajun, L. (2010). Enhanced Mechanical Properties of Graphene-Based Poly(vinyl alcohol) Composites. *Macromolecules*, 43 (5): 2357-2363.
13. Rafiee, M. A., Rafiee, J., Wang, Z., Song, H., Yu, Z. Z. & Koratkar, N. (2009). Enhanced mechanical properties of nanocomposites at low graphene content. *ACS Nano*, 3: 3884.
14. Haafiz, M. K., Hassan, A., Zakaria, Z. & Inuwa, I. M. (2014). Isolation and characterization of cellulose nanowhiskers from oil palm biomass microcrystalline cellulose. *Carbohydr. Polym.*, 103: 119-125.
15. Bandla, S. & Hanan, J. C. Manufacturing tough amorphous thermoplastic-graphene nanocomposites. in Nanotechnology 2012: Advanced Materials, CNTs, Particles, Films and Composites - 2012 NSTI Nanotechnology Conference and Expo, NSTI-Nanotech 2012. 2012. Santa Clara, CA.
16. Prusty, G. S. & Sarat K. (2013). Dispersion of expanded graphite as nanoplatelets in a copolymer matrix and its effect on thermal stability, electrical conductivity and permeability. *Carbon*, 51: 436.
17. Teng, C. C. M., Chen-Chi, M. L., Chu-Hua, Y., Shin-Yi, L., Shie-Heng, H., Min-Chien, Y., Ming-Yu, C., Kuo-Chan, L. & Tzong, M. (2011). Thermal conductivity and structure of non-covalent functionalized graphene/epoxy composites. *Carbon*, 49 (15): 5107-5116.
18. Jiang, X. D. & Lawrence, T. (2012). Exploring the potential of exfoliated graphene nanoplatelets as the conductive filler in polymeric nanocomposites for bipolar plates. *J. Power Sources*, 218: 297-306.
19. Yu, S., Jeong, S.G., Chung, O. & Kim, S. (2014). Bio-based PCM/carbon nanomaterials composites with enhanced thermal conductivity. *Sol. Energy Mater. Sol. Cells*, 120, Part B: 549-554.

20. Min, C. Y., Demei, C., Jingyu, W. & Lihua, G.F. (2013). A graphite nanoplatelet/epoxy composite with high dielectric constant and high thermal conductivity. *Carbon*, 55: 116-125.
21. Han, Z. & Alberto, F. (2011). Thermal conductivity of carbon nanotubes and their polymer nanocomposites: A review. *Prog. Polym. Sci*., 36 (7): 914-944.
22. Li, W., Schlarb, A. K. & Evstatiev, M. (2009). Study of PET/PP/TiO2 microfibrillar-structured composites, part 1: Preparation, morphology, and Dynamic mechanical analysis of fibrillized blends. *J. Appl. Polym. Sci.*, 113 (3): 1471-1479.
23. Chu, K., Li., W.S., Jia, C. C. & Tang, F. L. (2012). Thermal conductivity of composites with hybrid carbon nanotubes and graphene nanoplatelets. *Appl. Phys. Lett*., 101 (21).
24. Huang, X., Zhi, C. & Jiang, P. (2012). Toward effective synergetic effects from graphene nanoplatelets and carbon nanotubes on thermal conductivity of ultrahigh volume fraction nanocarbon epoxy composites. *J. Phys. Chem. C*, 116 (44): 23812-23820.
25. Verdejo, R., Bernal, M., Mar, R., Laura, J., Manchado, L. & Miguel A. (2011). Graphene filled polymer nanocomposites. *J. Mater. Chem*., 21 (10): 3301-3310.
26. Wakabayashi, K., Brunner, P. J., Masuda, J., H., Sheldon A., & Torkelson, J. M. (2010). Polypropylene-graphite nanocomposites made by solid-state shear pulverization: Effects of significantly exfoliated, unmodified graphite content on physical, mechanical and electrical properties. *Polymer*, 51 (23): 5525-5531.
27. Heino, M., Kirjava, J., Hietaoja, P. & Seppala, J. (1997). Compatibilization of polyethylene terephthalate/polypropylene blends with styrene-ethylene/butylene-styrene (SEBS) block copolymers. *J. Appl. Polym. Sci.*, 65 (2): 241-249.
28. Ramanathan T., Stankovich S., Dikin D. A., Liu, H. Shen, H. Nguyen S. T., Brinson, L. C. (2007). Graphitic nanofillers in PMMA nanocomposites—An investigation of particle size and dispersion and their influence on nanocomposite properties. *J. Polym. Sci., Part B: Polym. Phys.*, 45 (15): 2097-2112.
29. Zhang, J. G. & Deng J. (2011). Effect Of SEBS- g -MA on wear friction of PA6-CNT composite. *Polym-Plast Technol*, 50: 1533–1536.
30. Ramanathan, T. Abdala, A. A. Stankovich, S. Dikin, D. A. Herrera-Alonso, M. Piner, R. D. Adamson, D. H. Schniepp, H. C. Chen, X. Ruoff, R. S. Nguyen, S. T. Aksay, I. A. nPrud'homme, R. K. & Brinson, L. C. (2008). Functionalized graphene sheets for polymer nanocomposites. *Nat. Nanotechnol*., 3 (6): 327-331.
31. Lim, S. R. & Chow, W. S. (2012). Impact, thermal, and morphological properties of functionalized rubber toughened-poly(ethylene terephthalate) nanocomposites. *J. Appl. Polym. Sci*., 123 (5): 3173-3181.
32. Li, M., & Jeong, Y. G. (2011). Poly(ethylene terephthalate)/exfoliated graphite nanocomposites with improved thermal stability, mechanical and electrical properties. *Composites Part A*, 42 (5): 560-566.
33. Tantis, I., Psarras, G. C. & Tasis. D. (2012). Functionalized graphene – poly(vinyl alcohol) nanocomposites: Physical and dielectric properties. *Express Polym Lett*, 6 (4): 283 -292.
34. Akbari, M. Zadhoush, A. Haghighat, M. (2007). PET/PP blending by using PP-g-MA synthesized by solid phase. *J. Appl. Polym. Sci*., 104 (6): 3986-3993.
35. Karevan, M., Eshraghi, S., Gerhardt, R., Das, S., & Kalaitzidou, K. (2013). Effect of processing method on the properties of multifunctional exfoliated graphite nanoplatelets/polyamide 12 composites. *Carbon*, 64: 122-131.
36. Bandla, S. & Hanan, J. (2012). Microstructure and elastic tensile behavior of polyethylene terephthalate-exfoliated graphene nanocomposites. *J. Mater. Sci.*, 47 (2): 876-882.

The Malaysian Journal of ANALYTICAL SCIENCES ISSN 1394-2506

# TOUGHENING OF EPOXY BY SILANE-TREATED NANOTITANIUM DIOXIDE

## (Penguatan Epoksi oleh Silana Terawat Nanotitanium Dioksida)

Phasapan Sanemuang and Jantrawan Pumchusak*

*Department of Industrial Chemistry,*
*Faculty of Science,*
*Chiang Mai University, 50200 Chiang Mai, Thailand*

**Corresponding author: jantrawan@gmail.com*

**Abstract**

In this research, treated titanium dioxide in the contents of 0.1-0.5 wt % was applied into epoxy resin in order to toughen it. Vibracell ultrasonic with various electric power and times was used to disperse the particles successfully. It was found that the epoxy nanocomposites with 0.1 wt % of silane-treated nano titanium dioxide provided the highest impact strength and fracture toughness ($K_{IC}$) of 69.4 J/m. and 2.18 MPa.m$^{1/2}$, respectively, while, those properties of the neat epoxy were 41.3 J/m. and 1.16 MPa.m$^{1/2}$. However, the impact strength and fracture toughness of nanocomposites decreased by about 50 % and 8 %, respectively by further increasing amount of treated Nano titanium dioxide particles 0.2 to 0.5 wt %.

**Keywords:** epoxy, treated nanotitanium dioxide, nanocomposite, toughening

**Abstrak**

Dalam kajian ini, sebanyak 0.1 - 0.5wt % titanium dioksida terawat telah dimasukkan ke dalam resin epoksi sebagai penguat. Alat vibracell ultrasonic telah digunakan untuk melarutkan titanium dioksida terawat ke dalam larutan etanol/air dengan memvariasikan masa(*t*) dan unit kuasa eletrik(*watt*) yang digunakan. Didapati bahawa nanokomposit epoksi dengan 0.1wt % silane terawat nano titanium dioksida menunjukkan kekuatan impak dan kekuatan patahan ($K_{IC}$) yang paling tinggi iaitu 69.4 J/m dan 2.18 MPa.m$^{1/2}$. Epoksi tulen pula adalah masing-masing 41.3 J/m dan 1.16 MPa.m$^{1/2}$. Namun, kekuatan impak dan kekuatan patahan nanokomposit tersebut menurun sebanyak 50 % dan 8 %, dengan penambahan kandungan partikel nano titanium dioksida terawat daripada 0.2 hingga 0.5 bt %.

**Kata kunci:** epoksi, nanotitanium dioksida terawat, nanokomposit, penguat

## Introduction

Epoxy resins are being extensively used as matrix materials in high performance composites especially in aerospace industry, shipbuilding or electronics devices automobiles, fusion reactors and structural applications [1,2,3]. It is widely used for adhesive, and coating because of when of its less shrinkage [4,5]. However, the brittleness is the weakness of this material. There were several attempts aimed to improve its weak point including the modifying the molecular architecture and structure [6]. However, the easier way to improve the toughness of epoxy is the addition of fillers. Several research studies have found that nanocomposite can improve the mechanical properties of the epoxy. For example, the influence of the insertion of 10% $TiO_2$-nanoparticles into the epoxy resin on the mechanical performance was examined using three-point bending, Charpy impact and fracture toughness tests. It was demonstrated that the application of $TiO_2$ nanoparticles lead to a simultaneous improvement of all mentioned properties [7]. Moreover, it was found that the addition of 1 wt % of nano-$TiO_2$/$SiO_2$ significantly improved the corrosion resistance of epoxy [4]. Wetzel et al. reported that the addition of 1-2 wt% of $Al_2O_3$ could increase the wear resistance, stiffness, flexural modulus, flexural strength and impact energy of epoxy [8]. Moreover, the addition of nano-$Fe_2O_3$ into epoxy matrix was found to improve the thermal stability and viscoelastic properties considerably higher [9]. This research has selected the titanium dioxide nanoparticles to toughen the epoxy for the

glass coating application. In this paper, the fracture toughness and impact strength of nanocomposites were investigated.

## Materials and Methods

The epoxy resin (NPEL 128) and hardener (H-3839) were kindly supplied by SB United Co., Ltd. The nanoparticle of $TiO_2$ with diameter of 21 nm was supplied by Sigma Aldrich. 3-aminopropyl triethoxysilane (APTES) was purchased from Sigma Aldrich.

Prior to using, $TiO_2$nanopowder was dispersed in 400 ml of the media of ethanol/water (19:1 v/v) and 2 vol. % of 3-APTES by ultrasonication for 15 min. Then, the mixture was stirred for 4 h at 70 $^oC$. After that, the mixture was filtered and washed with acetone and deionized water. The modified particles were dried in an oven at 80 $^oC$ for 24 h.

For the composite preparation, the treated $TiO_2$ was dispersed in epoxy using vibracell ultrasonic with the electric power of 150, 350 and 750 watts for 1, 3 and 5 min. Ethanol was used as diluent in order to reduce the epoxy viscosity to facilitate the particle dispersion. The sample was cured at 80 $^oC$ for 2 h and at 100 $^oC$ for another 2 h.

The Surface morphology of the materials was observed using a scanning electron microscope (SEM) type JSM-5910LV. The specimen surfaces for the SEM were sputter coated with gold to avoid charging. The impact strength was measured using Cometech Instruments QC-639K testing machine according to ASTM D256 with the single-edge notched bar specimen of 75×12×6 mm. The impact tests were carried out at room temperature and impact energy was reported in J/m. Fracture toughness tests were performed according to ASTM D5045 with single-edge notched bending (SENB) bar specimen of 75×12×6 mm. Cracks were introduced at the bottom of 2 mm deep side notches by scrolling a chilled razor blade. The fracture toughness tests were performed using a Lloyd Instruments (LRX model) with 52 mm of gauge length and the cross-head speed was 50 mm/min.

## Results and Discussion

### Effect of Dispersion Condition by Vibracell Ultrasonic on Mechanical Properties of Composites

The composites were prepared by mixing the epoxy resin with 0.1 wt% of $TiO_2$ by vibracell ultrasonic. The effects of electrical power which are 150, 350 and 750 watts on the mechanical properties of the epoxy composites are shown in Figure 1and 2. The results showed that the $K_{IC}$ decreased as the electrical power increased with value of 2.38, 1.95 and 1.61 MPa-$m^{1/2}$for the 150, 350 and 750 watts, respectively. Moreover, the impact strength of the composites increased with increase of electrical power.

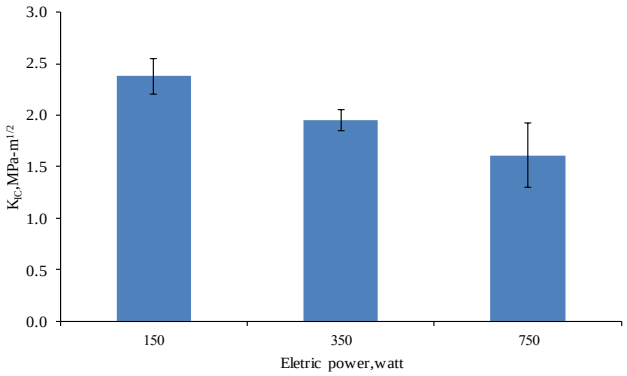



Figure 1. The effect of electrical power on $K_{IC}$ of $TiO_2$-toughend epoxy.

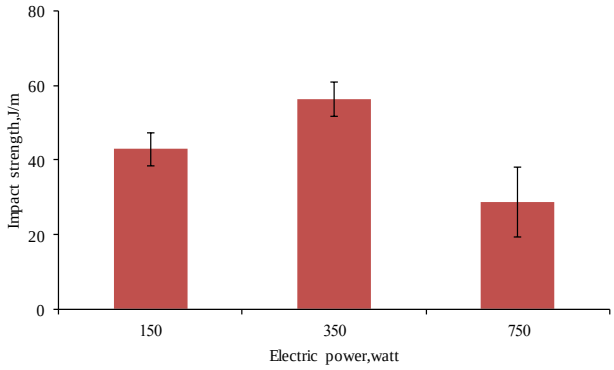



Figure 2. The effect of electrical power on impact strength of $TiO_2$-toughend epoxy.

The composite which was used the electrical power of 350 watts showed the highest impact strength of 56.4 J/m. However, the impact strength substantially decreased when the electrical power of 750 watts was applied. Thismight causefromthe lower nano-$TiO_2$ particles dispersion in the epoxy matrix due to the higher viscosity of the mixture. This was the result of the solvent evaporation of the system during dispersion process by vibracell ultrasonic at high power. The high power ultrasonication produced high amount of heat. Thus, the mechanical properties ofcomposites extensively decreased.

Therefore, the electrical power of 350 watts was selected to apply for the suitable dispersion time in the composite preparation process. The effect of dispersion time, which were 1, 3 and 5 min, on the mechanical properties of the epoxy composites are shown in Figure 3 and 4. The results showed that the $K_{IC}$ of the composites which were applied the dispersion time of 1, 3 and 5 min were 1.93, 2.12 and 2.33 MPa-$m^{1/2}$, respectively and the impact strength of the composites were 47.3, 59.8 and 36.4 J/m, respectively.

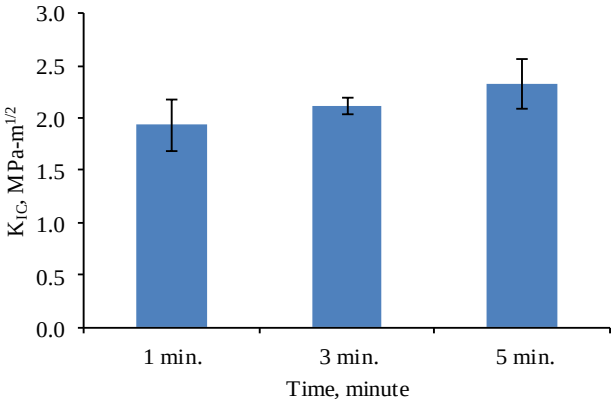



Figure 3. The effect of dispersion time on $K_{IC}$ of $TiO_2$-toughend epoxy.

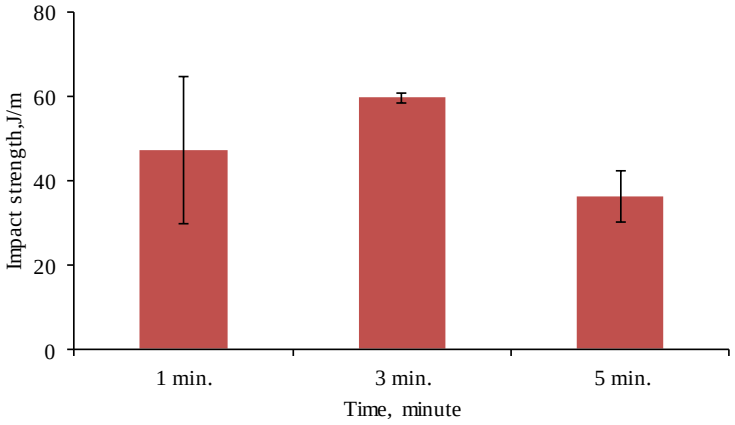



Figure 4. The effect of dispersion time on impact strength of $TiO_2$-toughend epoxy.

The composites which were applied the dispersion timeof 3 min showed the highest impact strength. However, due to the apparatus limitation, the dispersion process was carried out in the opened system. Therefore, the selected condition for the nanoparticle dispersion is based on this opened system. The electrical power of 350 watt and the dispersion time of 3 min were selected to prepare the epoxy composites with different content of treated $TiO_2$.

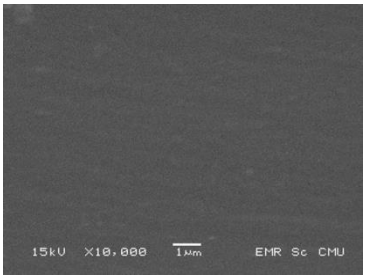



Figure 5. SEM micrograph of neat epoxy

**Morphology**

The fracture surface of epoxy composites were observed by SEM. The fracture surface of neat epoxy was shown in Figure 5. From the micrograph, it shown that the fracture surface of neat epoxy were smooth which represented the brittleness of epoxy. The fracture surface of epoxy composites with 0.1 wt% of $TiO_2$ was shown in Figure 6. It was seen that the fracture surface of epoxy composites with $TiO_2$ was much rougher than neat epoxy and there were a ladder features on the fracture surface (circle area). To create such surface texture, energy is needed, so this is one of the toughening mechanisms for this composite. Figure 7 and 8 show the fracture surfaces of the 0.3 and 0.5 wt % of $TiO_2$ composites, respectively. It was seen that $TiO_2$ nanoparticles were agglomerated.

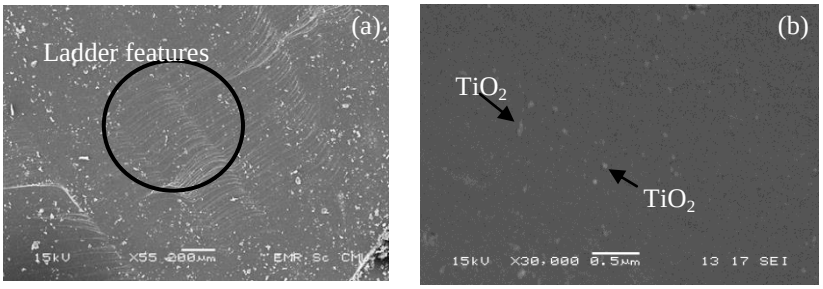



Figure 6. SEM micrographs of 0.1 wt % treated $TiO_2$nanocomposite. a) circle area show much rougher and there were a ladder features on the fracture surface, b) show dispersion of $TiO_2$ nanoparticle into matrix

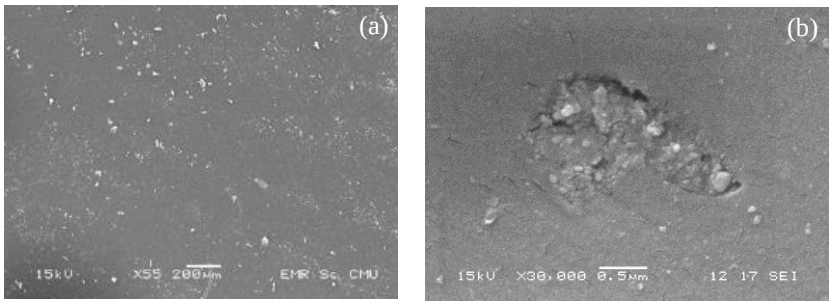



Figure 7. SEM micrographs of 0.3 wt% treated $TiO_2$nanocomposite.

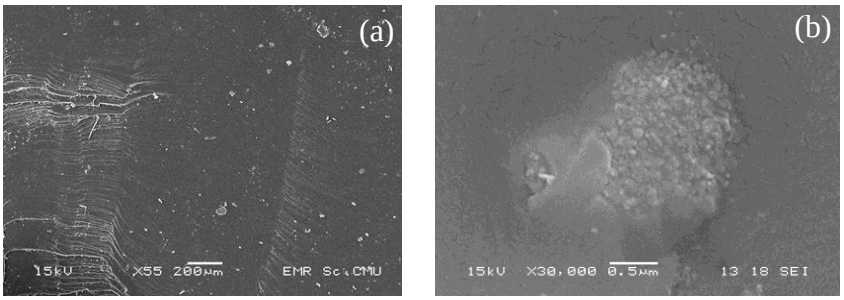



Figure 8. SEM micrographs of 0.5 wt% treated $TiO_2$nanocomposite.

**Mechanical Properties of Untreated and Treated TiO2 Particles by 3-Aminopropyltriethoxysilane**

The $K_{IC}$ and impact strength of the epoxy composites with 0.1 wt% untreated $TiO_2$ and 0.1 – 0.5 wt% treated $TiO_2$ are shown in Figure 9 and 10. The results show that the $K_{IC}$ of epoxy composites with 0.1 wt% of untreated $TiO_2$ were improved by 80 % when compared to the $K_{IC}$ of neat epoxy; however, the impact strength of composites decreased by 32 %.

Comparing the use of 0.1 wt% of untreated and treated $TiO_2$, it was found that the treating of $TiO_2$ with silane did not affect the $K_{IC}$. However, the addition of 0.1 wt% of treated $TiO_2$ improved the impact strength of the composites. The impact strength of the 0.1 wt% of treated $TiO_2$ epoxy composites were improved by 60 % when

compared to that of 0.1 wt% of untreated $TiO_2$ epoxy composites. It is known that $TiO_2$ and silane coupling agent are chemically bonded after the surface modification [9]. In addition, the silane-treated $TiO_2$ strongly bonded to the epoxy matrix, so the impact strength of the epoxy could be improved.

By using the different content of $TiO_2$ in the composites, it was indicated that all $TiO_2$ content did not make a significant difference in the $K_{IC}$ of epoxy composites, but all composites showed the tough character with $K_{IC}$ of about 2MPa-$m^{1/2}$. However, the impact strength considerably declined, when the $TiO_2$ content increased due to the agglomeration of $TiO_2$ particles at the high contents which can be seen in Figure 4 and 5.

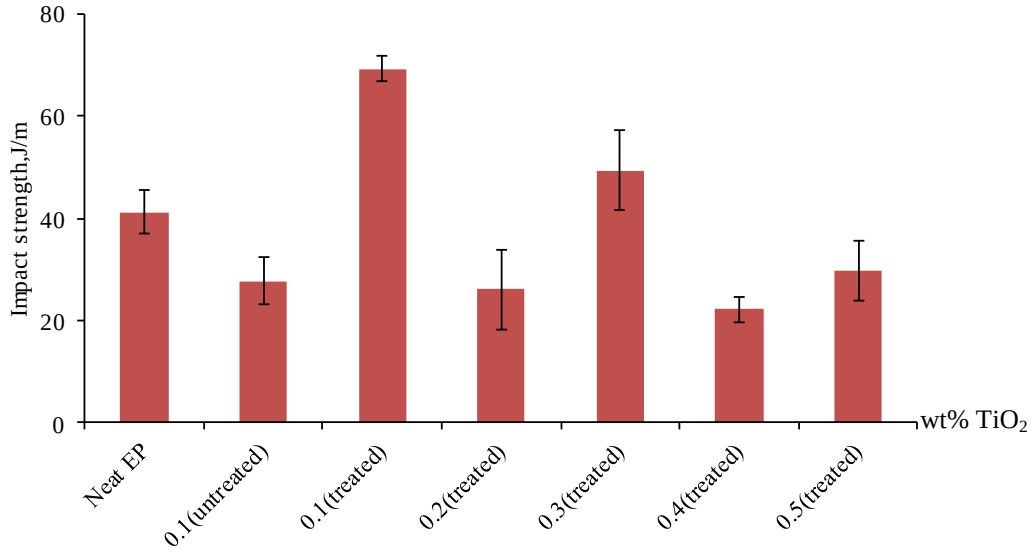



Figure 9. The effect of different weight fraction of $TiO_2$ on impact strength of $TiO_2$-toughend epoxy.

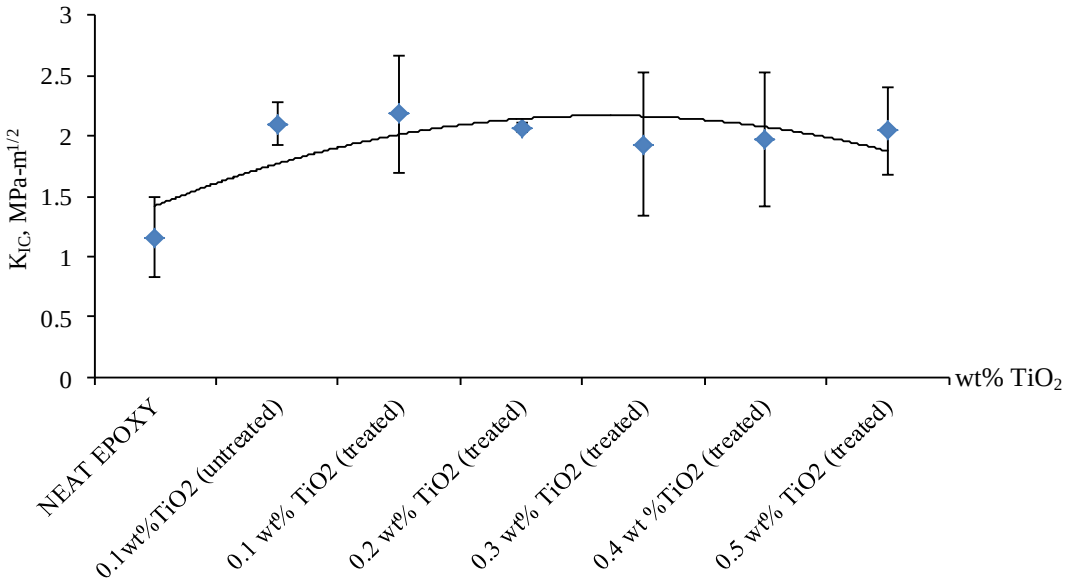



Figure 10. The effect of different weight fraction of$TiO_2$on $K_{IC}$ of $TiO_2$-toughend epoxy.

## Conclusion

This research studied the utilization of vibracell ultrasonic to disperse $TiO_2$ nanoparticles in the epoxy matrix and found that it influenced the dispersion and also the mechanical properties of composites. The used of 350 watt 3 min was found to be a good condition for the preparation. The epoxy composites with 0.1 wt% of treated $TiO_2$ gave the highest $K_{IC}$ and impact strength of 2.18 MPa-$m^{1/2}$ and 69.4 J/m, respectively. When the electric power of 750 watt was applied, the agglomeration of nano-$TiO_2$ was found. Therefore, the high fluctuation of results was obtained.

## Acknowledgement

This research was financially supported by National Research University (NRU) and the Graduated School, Chiang Mai University.

## References

1. Hussain, M., Nakahira, A., Nishijima S. & Niihara, K. (1996). Fracture behavior and fracture toughness of particulate filled epoxy composites. *Material Letter*, 27:21–25.
2. Wetzel, B., Rosso, P., Haupert, F. & Friedrich, K. (2006). Epoxy nanocomposites-fracture and toughening mechanisms. *Engineering Fracture Mechanics*, 73:2375–2398.
3. Omrani, A., Simon C.L. &Rostami A.A. (2008). Influences of cellulose nanofiber on the epoxy network formation. *Materials Science and Engineering A*, 490:131–137.
4. Shi, H., Liu F., Yang, L. & Han, E. (2008). Characterization of protective performance of epoxy reinforced with nanometer-sized $TiO_2$ and $SiO_2$. *Progress in Organic Coating*, 62:359–368.
5. Chatterjee, A. & Islam, M.S. (2008). Fabrication and characterization of $TiO_2$-epoxy nanocomposite. *Materials Science and Engineering A*,487:574–585.
6. Sue, H.J., Puckett, P.M., Bertram, J.L. & Walker, L.L. (2000). The Network Structure of Epoxy Systems and Its Relationship to Toughness and Toughen ability. *ACS Symposium Series*, 759.
7. Bittmann, B., Haupert F., &Schlarb, A.K. (2011). Preparation of $TiO_2$/epoxy nanocomposite by ultrasonic dispersion and their structure property relationship.*UltrasonicsSonochemistry*, 18: 120 – 126.
8. Wetzel, B., Rosso, P., Haupert, F. &Zhang, M.Q. (2003). Epoxy nanocomposites with high mechanical andtribological performance. *Composites Science and Technology*, 63 :2055–2067.
9. Zabihi, O., Hooshafza, A., Moztarzadeh, F., Payravand, H., Afshar, A.&Alizadeh, R. (2012).Isothermal curing behavior and thermo-physical properties of epoxy-based thermoset nanocomposites reinforced with $Fe_2O_3$ nanoparticles.*ThermochimicaActa*, 527:190 – 198.
10. Zhao, J., Milanova, M., Warmoeskerken, M.M.C.G. &Dutschk, V. (2012). Surface modification of $TiO_2$ nanoparticles with silane coupling agents. *Colloids and Surfaces A: Physicochem. Eng.Aspects*, 413:273–279.

**Malaysian Journal of Analytical Sciences Vol 18 No 3 2014**

Articles 23 - 32 are selected papers from the "International Conference on Global Sustainability and Chemical Engineering, 20 - 22 August 2014, Cititel Midvalley Kuala Lumpur; organised by Faculty of Chemical Engineering, Universiti Teknologi MARA, 40450 Shah Alam, Selangor, Malaysia."

Guest Editors: Yoshihito Shirai, Ku Halim Ku Hamid, Miradatul Najwa Mohd Rodhi

**Page**

1. THE CHARACTERIZATION STUDY OF FERRITES (MAGNESIUM AND MANGANESE) USING SOL GEL METHOD (Kajian Pencirian untuk Ferit (Magnesium dan Mangan) Menggunakan Kaedah Sol Gel) 485
*Rita Sundari, Tang Ing Hua, Madzlan Aziz, Umar Kalmar Nizar*

2. FOUR SPECTROPHOTOMETRIC METHODS FOR SIMULTANEOUS DETERMINATION OF CARBAMAZEPINE AND LAMOTRIGINE IN BINARY MIXTURES AND URINE SAMPLES (Penentuan Serentak Karbamazapin dan Lamotrigin Di Dalam Campuran Perduaan Dan Sampel Urin Melalui Empat Kaedah Spektrofotometrik) 491
*Fadhil M. Najib, Muhammad S. Mustafa*

3. SCHIFF BASES DERIVED FROM ISATIN AS MILD STEEL CORROSION INHIBITORS IN 1 M HCl (Bes Schiff Yang Terhasil Daripada Isatin Sebagai Perencat Kakisan Keluli Lembut Dalam 1 M Asid Hidroklorik) 507
*Aliyin Abdul Ghani, Hadariah Bahron, Mohamad Kamal Harun, Karimah Kassim*

4. CADMIUM, CHROMIUM, COPPER, LEAD, FERUM AND ZINC LEVELS IN THE COCKLES (Anadara granosa) FROM KUALA SELANGOR, MALAYSIA (Tahap Kadmium, Kromium, Kuprum, Plumbum, Ferum dan Zink di dalam Kerang (Anadara granosa) dari Kuala Selangor, Malaysia) 514
*Sabarina Md Yunus, Zaini Hamzah, Nik Azlin Nik Ariffin, Mohd Busairi Muslim*

5. SYNTHESIS OF NANOCRYSTALLINE OLIVINE $LiNiPO_4$ POWDER PREPARED BY SOL-GEL METHOD: THERMAL ANALYSIS AND XRD STUDIES (Penyediaan Serbuk Nanokristal $LiNiPO_4$ dengan Struktur Olivin Melalui Kaedah Sol-Gel: Analisis Terma dan Kajian XRD) 522
*Azlin Sanusi, Shanti Navaratnam, Wan Jeffrey Basirun*

6. DETERMINATION OF ENZYME KINETIC PARAMETERS ON SAGO STARCH HYDROLYSIS BY LINEARIZED GRAPHICAL METHODS (Penentuan Enzim Parameter Kinetik pada Hidrolisis Kanji Sagu dengan Kaedah Grafik Lelurus) 527
*Long Wee Lai, Chee Loong Teo, Suzana Wahidin, Mohamad Suffian Mohamad Annuar*

7. SEPARATION OF N-NITROSAMINES BY MICELLAR ELECTROKINETIC CHROMATOGRAPHY (Pemisahan N-Nitrosamina Menggunakan Kromatografi Elektrokinetik Misel) 534
*Nur Amira Md Ali, Mohd Marsin Sanagi, Wan Aini Wan Ibrahim*

8. DESIGN, DEVELOPMENT AND EVALUATION OF A SIMPLE SEMI-AUTOMATED SYSTEM FOR [18F]-FLUOROCHOLINE SYNTHESIS (Reka bentuk, pembangunan dan penilaian sistem pensintesis [18F]-Fluorocholine separa automatik) 544

*Faizal Mohamed, Mohd Fadli Mohammad Noh, Irman Abd. Rahman, Nur Ratasha Alia Md. Rosli, Cheong Kai Heng, Zulkifli Mohamed Hashim, Mohamad Arif Hamzah, Fadil Ismail*

9. EFFECT OF GAMMA RADIATION ON AMINO ACID BASED VESICLE CARRYING RADIOSENSITIZER 555
(Kesan Sinaran Gama ke atas Vesikel berasaskan Asid Amino yang membawa Pemeka Sinaran)
*Nur Ratasha Alia Md. Rosli, Faizal Mohamed, Muhammad Amir Syafiq Md. Sah, Irman Abdul Rahman*

10. SYNTHESIS AND CHARACTERIZATION OF 5,5,7,12,12,14-HEXAMETHYL-1,4,8,11-TETRAAZACYCLOTETRADECA-7,14-DIENIUM DIPERCHLORATE COPPER(II) COMPLEX 562
(Sintesis dan Pencirian Kompleks Di(Perklorat) 5,5,7,12,12,14-Heksametil-1,4,8,11-Tetraazasiklotetradeka-7,14-Dienium Kuprum(II))
*Nur Hasyareeda Hassan, Noorhanani M Ali, Bohari M Yamin, Nurul Huda Abd Karim, Noor Azlina Abd Ghani*

11. THE INFLUENCE OF MODIFIED SODIUM MONTMORILLONITE AS FILLER ON THE PERFORMANCE OF GLASS POLYALKENOATE CEMENT 572
(Kesan Natrium Montmorilonit Terubahsuai Sebagai Bahan Pengisi Dalam Meningkatkan Prestasi Simen Kaca Polialkenoat)
*Nur'Izzah Md Nasir, Norhazlin Zainuddin, Wan Md Zin Wan Yunus, and Khamirul Amin Matori*

12. PREPARATION OF EPOXIDIZED PALM OLEIN AS RENEWABLE MATERIAL BY USING PEROXY ACIDS 584
(Penyediaan Minyak Sawit Olein Terepoksida Sebagai Bahan Keterbaharuan Menggunakan Asid Peroksi)
*Darfizzi Derawi, Jumat Salimon, Waled Abdo Ahmed*

13. REMOVAL OF METHYL RED FROM AQUEOUS SOLUTION BY ADSORPTION ON TREATED BANANA PSEUDOSTEM FIBERS USING RESPONSE SURFACE METHOD (RSM) 592
(Penyingkiran Metil Merah daripada Larutan Akues oleh Serapan Fiber Batang Pisang Yang Telah Dirawat Mengunakan Kaedah Permukaan Sahutan (RSM))
*Zaida Rahayu Yet and Mohd Zulkhairi Abdul Rahim*

14. IMPROVING FILLER DISPERSION AND PHYSICAL PROPERTIES OF EPOXIDISED NATURAL RUBBER/SILICA COMPOUND BY USING DUAL FILLERS AND COUPLING AGENT IN MIXING PROCESS 604
(Meningkatkan Penyerakan Pengisi dan Sifat Sifat Fizikal Sebatian Getah Asli Terepoksida/Silika dengan Menggunakan Dual Pengisi dan Ejen Gandingan di dalam Proses Pencampuran)
*Teku Zakwan Zaeimoedin, Ahmad Kifli Che Aziz, Mazlina Mustafa Kamal*

15. PREPARATION AND CHARACTERIZATION OF TAPIOCA STARCH FILLED POLYCAPROLACTONE COMPOSITE FILMS 612
(Penyediaan dan Pencirian Filem Komposit Polikaprolakton Terisi Kanji Ubi Kayu)
*Nurulhusna Azmi, Aznizam Abu Bakar, Sani Amril Samsudin, Nur Azmyra Abdul Aziz*

16. CONSTRUCTION OF RADON CHAMBER FOR DETERMINATION OF RADON EMANATION USING CONTINUOUS RADON MONITOR 618
(Pembinaan Kebuk Radon untuk Penentuan Emanasi Radon Menggunakan Alat Permonitoran Radon)
*Norafatin Khalid, Amran Ab Majid, Redzuwan Yahaya, Muhammad Samudi Yasir, Faizal Mohamed*

17. THE EFFECTIVENESS OF POLYDIMETHYLSILOXANE (PDMS) AND HEXAMETHYLDISILOXANE 629

(HMDSO) AS COMPATIBILIZER ON THE PREPARATION OF BETEL NUT FIBER (BNF) AND POLYPROPYLENE (PP) /POLYSTYRENE (PS) WOOD COMPOSITES
(Keberkesanan Polidimetilsiloksana (PDMS) dan Heksametildisiloksana (HMDSO) Sebagai Pengserasi Dalam Penyediaan Komposit Kayu Berasaskan Serabut Pinang dan Polipropilena (PP)/Polistirena (PS))
*Nurul Izzaty Khalid, Azizah Baharum, Siti Sarah Ramli, Siti Norhana Mohd Nor*

18. CHARACTERIZATION OF POLYLACTIC ACID/MICROCRYSTALLINE CELLULOSE/MONTMORILLONITE HYBRID COMPOSITES 642
(Pencirian Komposit Polilaktik asid/Selulosa Mikrohablur/ Hibrid Montmorilonit)
*Reza Arjmandi, Azman Hassan, M.K. Mohamad Haafiz, Zainoha Zakaria, I. M. Inuwa*

19. EFFECT OF REINFORCED HYBRID PALM SHELLS ON MECHANICAL PROPERTIES OF POLYURETHANE-JUTE WOVEN/VINYL ESTER SANDWICH BOARD 651
(Kesan Tenunan Hibrid Biji Kering Kelapa Sawit Terhadap Sifat-sifat Mekanikal Poliuretana-Jute Wooven/Ester Vinil Papan Sandwic)
*Teo Siew Cheng, Nurul Ain binti Nanyan, Du Ngoc Uy Lan, Teh Pei Leng*

20. EFFECTS OF USING DIFFERENT HEALING AGENTS ON HEALING EFFICIENCY IN SOLID STATE SELF-HEALING SYSTEM 660
(Kesan menggunakan Agen Pemulihan Berbeza ke atas Keberkesanan Pemulihan Sistem Swa-Pemulihan Keadaan Pepejal)
*N. N Muhamad, S. M. Makenan, M. J. Mohd Suzeren, S. Abdullah, M.A.S Mat Lazim*

21. IMPROVEMENT OF MECHANICAL PROPERTIES OF POLY(LACTIC ACID) BY ELASTOMER 669
(Penambahbaikkan Sifat Mekanikal Poli (Asid Laktik) Oleh Elastomer)
*Penwarat Sennan and Jantrawan Pumchusak*

22. BENZOFURAN GLYCOSIDES FROM STYRAX BENZOIN 676
(Glikosida bezofuran daripada Styrax benzoin)
*Hasliza Yusof, Laily B. Din, Wan A. Yaacob*

23. FTIR ANALYSIS OF PHENOLIC COMPOUND AS PANCREATIC LIPASE INHIBITOR FROM INOCULATED AQUILARIA MALACCENSIS 683
(Analisis Sebatian Fenolik daripada Aquilaria malaccensis yang di Inokulasi sebagai Perencat kepada Enzim Lipase Pankreas Menggunakan FTIR)
*Nur Fahana Jamahseri, Miradatul Najwa Mohd Rodhi, Nur Hidayah Zulkarnain, Nursyuhada Che Husain, Ahmad Fakhri Syahmi Masruddin*

24. EFFECT OF ULTRASONIC-ASSISTED EXTRACTION ON PHENOLIC CONTENT OF AVOCADO 690
(Kesan Pengekstrakan Bantuan Ultrasonik ke Atas Kandungan Komponen Phenolik Dalam Buah Avokado)
*Rafidah Husen, Yoshito Andou, Amin Ismail, Yoshihito Shirai*

25. HYDROTHERMAL OXIDATIVE DEGRADATION OF ORGANIC COMPOUNDS DERIVED FROM PRODUCED WATER 695
(Penguraian Secara Pengoksidaan Hidrotermal Bahan Organik daripada Air Hasilan)
*Ahmad Rafizan Mohamad Daud, Mohd Zahid Marzuki, Mohd Muslim Abu Hassan*

26. PRODUCTION OF BIOCHAR WITH HIGH MINERAL CONTENT FROM OIL PALM BIOMASS 700
(Pengeluaran Biochar dengan Kandungan Mineral yang Tinggi dari Biomas Kelapa Sawit)
*Juferi Idris, Yoshihito Shirai, Yoshito Ando, Ahmad Amiruddin Mohd Ali, Mohd Ridzuan Othman, Izzudin Ibrahim, Mohd Ali Hassan*

27. THERMOGRAVIMETRIC ANALYSIS OF RICE HUSK AND COCONUT PULP FOR POTENTIAL BIOFUEL PRODUCTION BY FLASH PYROLYSIS 705
(Analisa Thermogravimetrik Sekam Padi dan Pulpa Kelapa Untuk Mengkaji Potensi Penghasilan Minyak Bio Melalui Pirolisis Pantas)
*Noorhaza Alias, Norazana Ibrahim, Mohd. Kamaruddin Abd. Hamid, Hasrinah Hasbullah, Roshafima Rasit Ali, Aziatul Niza Sadikin, Umi Aisah Asli*

28. THERMAL CHARACTERIZATION OF MODIFIED TACCA LEONTOPETALOIDES STARCH AND NATURAL RUBBER BASED THERMOPLASTIC ELASTOMER 711
(Pencirian Termal antara Modifikasi Kanji Tacca leontopetaloides dan Getah Semulajadi berasaskan Termoplastik Elastomer)
*Ainatul Mardhiah Mohd Amin, Nur Shahidah Ab Aziz, Nurul Shuhada Mohd Makhtar, Miradatul Najwa Mohd Rodhi, Suhaila Mohd Sauid*

29. STUDY ON THE STRUCTURE, TEXTURE AND THERMAL STABILITY OF CeZrYO2 NANOPARTICLES SYNTHESIZED VIA MICROEMULSION METHOD 718
(Kajian Terhadap Struktur, Tekstur dan Kestabilan Termal CeZrYO2 Nanopartikel Disintesis Melalui Kaedah Microemulsi)
*Abdul Hadi, M. Nazri Abu Shah, Noraakinah Hassan, S. Azurah Suliman, S. Hanim Md Nor, Mahidin, Kamariah Noor Ismail*

30. PHYSICO-CHEMICAL CHARACTERIZATIONS OF SAWDUST-DERIVED BIOCHAR AS POTENTIAL SOLID FUELS 724
(Pencirian Fizikal-Kimia bagi Biochar Diperoleh daripada Debu Kayu Sebagai Potensi Bahan Bakar Pepejal)
*Wan Azlina Wan Ab Karim Ghani, Gabriel da Silva, Azil Bahari Alias*

31. THERMOGRAVIMETRIC ANALYSIS (TGA) PROFILE OF MODIFIED SBA-15 AT DIFFERENT AMOUNT OF ALKOXYSILANE GROUP 730
(Profil Thermografimetrik Analisis SBA-15 Berfungsi Pada Jumlah Kumpulan Alkoxysilane Yang Berlainan)
*Norhasyimi Rahmat, Nur Fathilah Mohd Yusof, Ezani Hafiza*

32. EFFECT OF MECHANICAL GRINDING AND IONIC LIQUID PRE-TREATMENT ON OIL PALM FROND 737
(Kesan Pra-rawatan Pengisaran Mekanikal dan Cecair Ionik ke atas Pelepah Kelapa Sawit)
*Siti Norsyarahah Che Kamarludin, Nor Sharliza Mohd Safaai, Amizon Azizan , Hazimah Madzaki, Mimi Suhada Mamat, Niswah Hashina Zulkifli, Mohd Firdaus Zainuddin*

The Malaysian Journal of ANALYTICAL SCIENCES ISSN 1394-2506

# THE CHARACTERIZATION STUDY OF FERRITES (MAGNESIUM AND MANGANESE) USING SOL GEL METHOD

## (Kajian Pencirian untuk Ferit (Magnesium dan Mangan) Menggunakan Kaedah Sol Gel)

Rita Sundari*, Tang Ing Hua, Madzlan Aziz, Umar Kalmar Nizar

*Department of Chemistry, Faculty of Science,*
*Universiti of Technologi Malaysia, 81310 Skudai, Johor, Malaysia*

**Corresponding author: ritsun2003@yahoo.com*

**Abstract**

A sol gel method with citric acid as an anionic surfactant was used to fabricate nano magnesium ferrites ($MgFe_2O_4$) and manganese ferrites ($MnFeO_3$) under different calcination temperatures (300°C, 600°C and 800°C) for 2h, respectively. The Fourier Transformation Infrared (FTIR) spectra of magnesium ferrites showed the formation of tetrahedral and octahedral peaks of the metal oxides, which are getting remarkable after calcination at 300°C because of the volatile matters removal ($H_2O$, $CO_2$, $NO_2$, etc.). The results of the single point Brunauer, Emmett and Teller (BET) method showed a substantial decrease of surface area for both the magnesium and manganese ferrites as the calcinated temperatures getting increased from 300°C to 800°C. The SEM micrograph of the magnesium ferrite showed flake structures at 800°C, and that of manganese ferrite showed granule structures at the same temperature. The results of X-Ray Diffraction (XRD) analysis of magnesium ferrite obtained a range of crystalline sizes from 11 nm to 60 nm, and those of manganese ferrite from 27 nm to 38 nm as the temperatures of both ferrites (magnesium and manganese) increased from 300°C to 800°C. The results of this study are useful for further applications, such as semiconductors, heterogeneous and photo catalysts, magnetic materials and sensors.

**Keywords:** magnesium and manganese ferrites; calcinations; characterizations

**Abstrak**

Kaedah sol gel dengan asid sitrik sebagai anionik surfaktan telah digunakan untuk menghasilkan nano ferit magnesium ($MgFe_2O_4$) dan ferit mangan ($MnFeO_3$), di bawah suhu pengkalsinan yang berbeza (300°C, 600°C dan 800°C) untuk 2 jam. Inframerah Transformasi Fourier (FTIR) spektrum bagi ferit magnesium menunjukkan pembentukan puncak tetrahedral dan oktahedral oksida logam yang semakin menonjol selepas proses pengkalsinan pada 300°C, disebabkan penyingkiran jirim mudah meruap ($H_2O$, $CO_2$, $NO_2$, dll). Keputusan kaedah titik tunggal Brunauer, Emmett dan Teller (BET) menunjukkan apabila suhu pengkalsinan semakin meningkat daripada 300°C ke 800°C, luas permukaan turun dengan ketara untuk kedua- dua ferit magnesium dan mangan. Mikrograf SEM ferit magnesium pada 800°C menunjukkan struktur serpihan, dan pada suhu yang sama ferit mangan menunjukkan struktur granul. Keputusan analisis pembelauan X-Ray (XRD) bagi ferit magnesium menunjukkan julat saiz kristal daripada 11 nm hingga 60 nm, dan ferit mangan daripada 27 nm hingga 38 nm, apabila suhu bagi kedua-dua ferit (magnesium dan mangan) meningkat dari 300°C ke 800°C. Keputusan kajian ini amat berguna untuk aplikasi lanjut, seperti semikonduktor, pemangkin heterogen dan foto, bahan magnet dan sensor.

**Kata kunci:** Magnesium dan mangan ferit, pengkalsinan, pencirian

## Introduction

Magnesium ferrites ($MgFe_2O_4$) are classified as spinel ferrites, which the $Mg^{2+}$ and $Fe^{3+}$ ions can occupy either the tetrahedral or octahedral interstitial sites, and the oxygen atoms form the close-packed face-centered cubics. Manganese ferrites ($MnFeO_3$) have perovskite structure, which is capable of forming 12-fold coordination with oxygen atoms and therefore, it is suitable for octahedral coordination [1]. Many perovskite ferrites have cubic or nearly cubic structures, and they are likely to have more transitional phases at low temperatures [2].

Previous publications reported that ferrites were used for many applications, such as composites, catalysts, magnetic materials, sensors and conductors [3]. The fabrication of nano ferrites has attracted much greater interest because of their large surface-to-volume ratio yielding remarkable material properties. A number of methods have been developed to fabricate ferrites including electrospinning [3,4], coprecipitation [1,5], high energy ball milling [6], solid state reaction [7], and oxidative thermal decomposition [8]. Among the various methods, the sol–gel method yields more promising results in the fabrication of ferrites particularly at a fairly low temperature [9]. The sol gel method for preparing ferrites has many advantages with respect to good stoichiometric control and particle size distribution at a lower temperature [5].

The study of characterizations on ferrites would provide a meaningful correlation of their structures and effective changes in the environs of ions related to different calcination temperatures. To our knowledge, only a few published reports about the comparative study of metal ferrites with respect to characterizations exist in the current literatures. Therefore, a comparative study of magnesium and manganese ferrites by a sol gel method using a solution of citric acid as an anionic surfactant, which was stirred and heated up to 100°C for 24 h was investigated. Different calcination temperatures (300°C, 600°C and 800°C) were carried out in a furnace for respective 2h after heating the gel at 100°C. The effects of calcination temperature on morphology, structure, and properties of the fabricated ferrites were the subject to be studied.

## Materials and Methods

The fabrication of magnesium and manganese ferrites by a sol gel method using a solution of citric acid as an anionic surfactant included several steps: (i) a solution of ferric nitrate, magnesium nitrate or manganese (IV) oxide, and citric acid was mixed; (ii) the mixture was constantly stirred and heated up to 100 °C for 24h to form the gel; (iii) the brown, fluffy gel was calcinated at different temperatures (300°C, 600°C and 800°C) for respective 2h; (iv) the calcination products were examined by BET (Brunauer, Emmett and Teller), UVDR (Ultra Violet Diffuse Reflectance), FTIR (Fourier Transformation Infrared), XRD (X-Ray Diffraction) and SEM-EDX (Scanning Electron Microcope-Energy Dispersive X-ray) for characterizations.

A micrometrics PulseChemiSorb 2705 using 30% N2: 70% O2 was used to run the analysis of BET. A Lambda 90 Diffused Reflectance Spectrometer was used to perform the UV-Vis spectra. The FTIR analysis was carried out by a Perkin Elmer instrument using a KBr pelletizer with a scanning region of 400 cm-1 to 4000 cm-1, and the XRD analysis was conducted by a Siemens Diffractometer D5000 using CuKα radiation at 30 mA and 40 kV to examine the structure of ferrites. Furthermore, the SEM mappings of the fabricated ferrites accomplished by the Energy Dispersive X-ray (EDX) spectra were investigated by a Philips XL instrument using 25.0 kV.

## Results and Discussion

The results of BET analysis showed the reductions of the surface area of magnesium and manganese ferrites of 106 to 4 $m^2/g$ and 35 to 7 $m^2/g$, respectively, which was related to the calcination temperatures from 300°C to 800°C. The reduction in surface area of the ferrites was caused by particles' agglomeration; thus, optimization is important to produce better quality. The difference of the surface area reduction with respect to magnesium and manganese ferrites is that manganese element has several oxidation numbers and could be able to form more various crystalline structures. The UV-Vis spectra (not shown here) of magnesium ferrite showed a broadband absorption to 400 nm. One of the requirements for a promising photocatalyst is a catalyst that can be used for a photocatalytic reaction in visible region that has lower energy.

The absorption peaks of the FTIR spectra at 3393 $cm^{-1}$, 1624 $cm^{-1}$ and 1384 $cm^{-1}$ of the fabricated magnesium ferrites were disappeared as the calcinations increased from 300°C to 800°C indicated the removal of the -OH, -CO and -NO groups from the material of interest, which is shown in Fig. 1. The absorption peak of the FTIR spectra (400 $cm^{-1}$ to 800 $cm^{-1}$) was more obviously shown as the calcination temperatures getting increased (from 300°C to 800°C) that indicated the formation of tetrahedral – octahedral structures of the metals oxide after octahedral structures of metal complexes at 561 $cm^{-1}$ and 437 $cm^{-1}$ of the FTIR spectra of magnesium ferrite that attributed to the shorter bond length of tetrahedral complex producing more stable structure. At the same time, the FTIR spectra (400 – 800 $cm^{-1}$) of manganese ferrite did not show remarkable peaks as that in magnesium ferrite since manganese

ferrite possesses its transition metal properties and more valence oxidation numbers that performs more flexible structure.

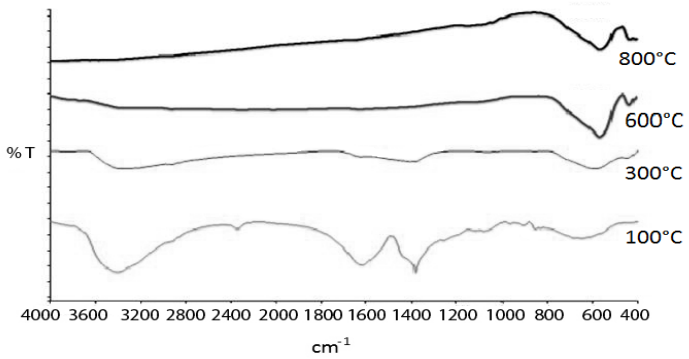



Figure 1. The FTIR spectra of magnesium ferrites at 100°C, 300°C, 600°C and 800°C. (Sol gel method using citric acid).

Fig.2 showed the XRD spectra of manganese ferrites and other compound from 100°C to 800°C. The XRD spectra indicated the alteration of amorphous phase to crystalline structure as the calcination temperature increased. At the 300°C calcination, despite the formation of manganese ferrite ($MnFeO_3$), the $Fe_3O_4$ was produced in minority corresponding to planes (3 1 1) and (4 4 0). However, the only manganese ferrite ($MnFeO_3$) was produced corresponding to planes (2 1 1), (2 2 2), (4 4 0), and (6 2 2) at 600°C and 800°C, because the $Fe_3O_4$ was not detected in the XRD spectra attributed to planes (2 2 0), (3 1 1), (5 1 1) and (4 4 0). Furthermore, the plane (4 4 0) of manganese ferrite was sited $2\theta = 55°$, while the plane (4 4 0) of Fe3O4 was sited at different position ($2\theta = 63°$). Therefore, the formation of manganese ferrites ($MnFeO_3$) in this conditions (600°C and 800°C) were more possible. The particle sizes at different calcinations (300°C, 600°C, and 800°C) were found to be 16.8 nm, 36.9 nm, and 44.8 nm, using the Debye–Scherrer's equation based on the full width at half maximum (FWHM). The results of XRD were in good agreement with that of BET. Based on the particle sizes, there is an indication that the present method can be able to produce nano ferrites. Naseri et al. [10] reported the average particle sizes of manganese ferrite of 12 nm to 22 nm at calcination temperatures of 450 °C to 600°C using a polyvinyl pyrrolidone (PVP) as a capping agent to control the agglomeration process. It was apparent that PVP prevented the formation of larger particle size.

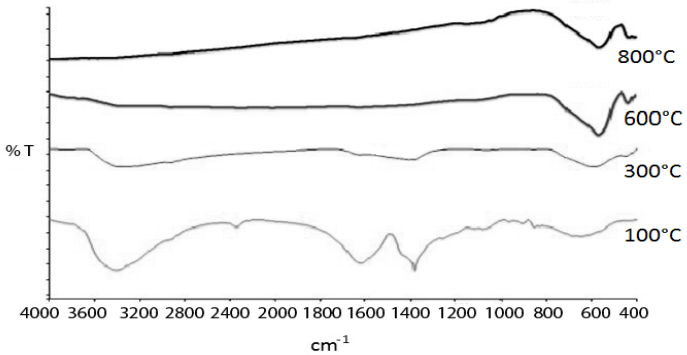
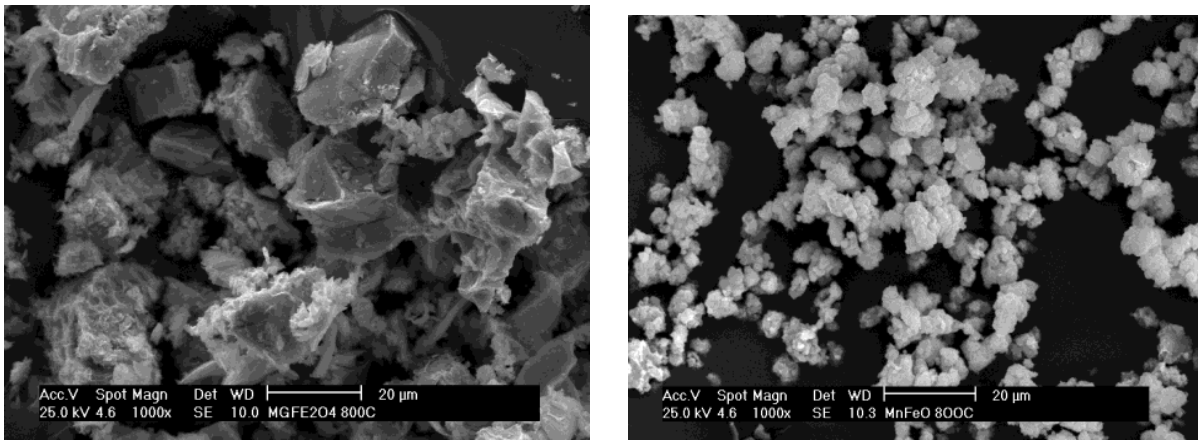



Figure 2. The XRD spectra of manganese ferrites at 100°C, 300°C, 600°C and 800°C. (Sol gel method using citric acid).

Figure 3 showed the SEM micrographs of both magnesium and manganese ferrites at 800°C. The micrograph of magnesium ferrite at 800°C showed flake particles (Fig. 3a), and the manganese ferrite showed granulated particles (Fig. 3b) at the same temperature. The different in particle shape of both ferrites (magnesium and manganese) at 800°C is because both elements have different crystalline characterizations associated to the relationship between oxidation state and electronic configuration of the atomic element. Flake particles were shown by the SEM image of magnesium ferrite prepared by the sol gel method at 600°C calcinations using citric acid, but granulated forms were produced using the co-precipitation method [4]. Furthermore, granulated particles were shown by the SEM image of magnesium ferrite fabricated by co-precipitation and sintered methods using polyvinyl alcohol (PVA) binder [11]. It was suggested that the co-precipitation method induced the formation of granulated particles. Granulated particles were shown by the SEM micrograph of manganese ferrites fabrication using co-precipitation and thermal methods at 1000°C [12].




**(a)** **(b)**

Figure 3. The SEM micrographs of (a) magnesium ferrite and (b) manganese ferrite, both at 600°C. (Sol gel method using citric acid); (1000 x magnificaion).

The SEM mappings of magnesium ferrite at 600°C are shown in Fig. 4 in relation to the distribution of magnesium (Fig. 4a), iron (Fig. 4b) and oxygen (Fig. 4c). The EDX analysis of magnesium ferrites at 600°C showed the element distribution of magnesium (≈ 6%), iron (≈ 50%,) and oxygen (≈ 17%), while the EDX spectra is shown in Fig. 4d. Similar EDX analysis was shown by the fabricated magnesium ferrite using co- precipitation and thermal methods at 900°C with PVA binder [11]. The EDX analysis showed that the NaOH used in the co-precipitation method did not take part in the reaction [11]. This study reported that the XRD analysis of magnesium ferrites ($MgFe_2O_4$) showed the formation of $Fe_2O_3$ besides the magnesium ferrite at 600°C. The higher concentration of iron as shown in the SEM mapping of iron and EDX analysis (≈ 50%) was caused by the formation of $MgFe_2O_4$ and $Fe_2O_3$ at 600°C. Besides, this study used a mol ratio of 2:1 of $Fe(NO_3)_3$ and $Mg(NO_3)_2$ as precursors. According to Naseri et al. (2011), there is a possibility of the transfer of $Fe^{3+}$ ions from B site to A site in the spinel structure of $MgFe_2O_4$ at calcinations of 600°C.

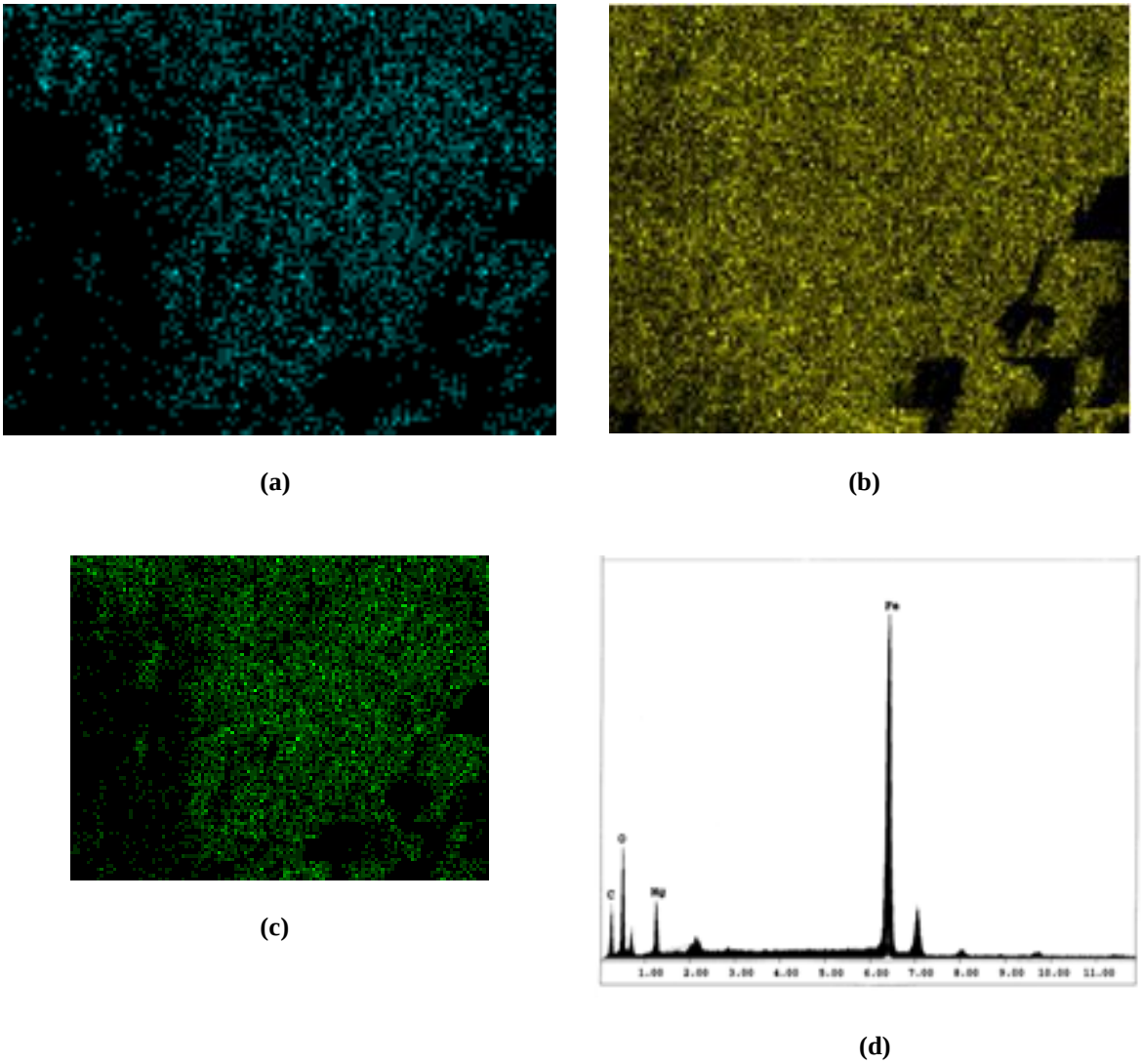



Figure 4. The SEM mappings of magnesium ferrite at 600°C for the distribution of (a) magnesium, (b) iron, (c) oxygen, and (d) the associated EDX spectra. (Sol gel method using citric acid).

The present study in relation to the effects of calcinations on the structures and properties of ferrites (magnesium and manganese) is useful for future applications particularly focused on the fabrication of ferrites for the purpose of catalyst and semiconductors.

## Conclusion

The present study shows that the crystal structure and morphology of the fabricated ferrites were influenced by the calcination temperatures. The FTIR spectra of magnesium ferrite showed the remarkable peak (400 $cm^{-1}$ – 600 $cm^{-1}$) both at the 600°C and 800°C, because the tetrahedral and octahedral structures were obviously formed after all volatile matters removed at both the temperatures of interest. The XRD spectra of manganese ferrite

showed the formation of pure manganese ferrites at 600°C and 800°C in the crystalline structure compared to the semi-amorphous structure of the related ferrite at 300°C. The SEM micrograph of magnesium ferrite showed a flake-form structure and that of manganese ferrite showed a granule structure, which they were calcinated at 800°C. This study provides meaningful correlation of the effects of calcination temperature on the crystalline structure of the ferrites of interest.

**Acknowledgement**

This research was financially supported by a Research University Grant of Universiti Teknologi Malaysia (Vote No 77545, Sub Project No 77263D046 and Vote No 02J02, Sub Project No 712602J02), which is gratefully acknowledged.

**References**

1. Siemons, M., Weirich, Th., Mayer, J. & Simon, U. (2004). Preparation of nanosized perovskite-type oxide via polyol method. *Journal of Inorganic & General Chemistry* 630(12): 2083-2089.
2. Wolfram, T. & Elliatioglu, S. (2006). Electronic and Optical Properties of D-Band Perovskites. United Kingdom, University Press, Cambridge. 1-24.
3. Maensiri, S., Sangmanee, M. & Wiengmoon, A. (2008). Magnesium ferrite ($MgFe_2O_4$) nanostructure fabricated by electrospinning. *Nanoscale Research Letters*, 4(3): 221-228.
4. Liu, C.P., Li, M.W., Zhong, C., Huang, J.R., Tian, Y.L., Tong, L. & Mi, W.B. (2007). Comparative study of magnesium ferrite nanocrystallites prepared by sol-gel and co-precipitation methods. *Journal of Material Science*, 42: 6133-6138.
5. Pradeep, A. & Chandrasekaran, G. (2005). FTIR study of Ni, Cu and Zn substituted nano-particles of $MgFe_2O_4$. *Material Letters*, 60(3): 371-374.
6. Pradhan, S.K., Bidb, S., Gateshki, M. & Petkov, V. (2005). Microstructure characterization and cation distribution of nanocrystalline magnesium ferrite prepared by ball milling. *Journal of Material Chemistry & Physics*, 93(1): 224-230.
7. Mishra, S., Kundu, T.K., Barick, K.C., Bahadur, D. & Chakravorty, D. (2006). Preparation of nanocrystalline $MnFe_2O_4$ by doping with $Ti^{4+}$ ions using solid state reaction route. *Journal of Magnetism & Magnetic Materials*, 307(2): 222-226.
8. Lick, L.D. & Soria, D.B. (2009). The synthesis of $MnFeO_3$ from the oxidative thermal decomposition of $Mn[Fe(CN)_5NO].2H_2O$. *Journal of Argentine Chemical Society*, 97(1): 102-108.
9. Pradeep, A., Priyadharsini, P. & Chandrasekaran, G. (2008). Sol gel route of synthesis of nanoparticles of $MgFe_2O_4$ and XRD, FTIR and VSM study. *Journal of Magnetism & Magnetic Materials*, 320(21): 2774-2779.
10. Naseri, M.G., Saion, E.B., Ahangar, H.A., Hashim, M. & Shaari, A.H. (2011). Synthesis and characterization ofmanganese ferrite nanoparticles by thermal treatment method. *Journal of Magnetism & Magnetic Materials*, 323(13): 1745-1749.
11. Hankare, P.P., Vader, V.T., Patil, N.M., Jadhav, S.D., Sankpal, U.B., Kadama, M.R., Chouguleb, B.K. & Gajbhiye, N.S. (2009). Synthesis, characterization and studies on magnetic and electrical properties of Mg ferrite with Cr substitution. *Journal of Material Chemistry & Physics*, 113(1): 233-238.
12. Rashad, M.M. (2006). Synthesis and magnetic properties of manganese ferrite from low grade manganese ore. *Material Science & Engineering B*, 127(2-3): 123-129.

The Malaysian Journal of ANALYTICAL SCIENCES ISSN 1394-2506

# FOUR SPECTROPHOTOMETRIC METHODS FOR SIMULTANEOUS DETERMINATION OF CARBAMAZEPINE AND LAMOTRIGINE IN BINARY MIXTURES AND URINE SAMPLES

## (Penentuan Serentak Karbamazapin dan Lamotrigin Di Dalam Campuran Perduaan Dan Sampel Urin Melalui Empat Kaedah Spektrofotometrik)

Fadhil M. Najib*, Muhammad S. Mustafa

*Chemistry Department,*
*Faculty of Science and Science Education,*
*Sulaimani University, Kurdistan Region, Iraq*

**Corresponding author: fadhil.najib@yahoo.com*

**Abstract**

In this work four different UV-spectrophotometric methods are described for simultaneous determination of antiepileptic drugs; carbamazepine (CBZ) and lamotrigine (LMT) in binary synthetic mixtures and urine samples without separation. First method was by solving the two simultaneous equations (SEQ) based on total absorbance according to Beer's law. Second was Dual wavelength (DWSP) method; Absorbance difference between 304 and 313 nm was measureable for CBZ but was zero for LMT. Likewise the absorbance difference between 282 and 290 nm was significant for LMT, and zero for CBZ. Third involved the use of zero- crossing first derivative method (ZCDSP) using the amplitudes at 308.9 and 286.6 nm for CBZ and LMT respectively. Ratio Derivative Spectrophotometry (RDSP) was the last. Here, the absorbance at different concentrations of CBZ or LMT, was divided, wavelength by wavelength, by the absorbance of a divisor, which was LMT standard for the analyte CBZ, and vice versa for LMT, (Divisor=2.0µg.mL$^{-1}$) in both cases. The amplitude of the derivative ratio spectra at 290 nm with wavelength interval ($\Delta\lambda$=6.0nm) and 328 nm ($\Delta\lambda$=4.0 nm) were selected for the determination of CBZ and LMT respectively. CBZ and LMT were simultaneously determined in synthetic mixtures and urine samples by the four methods giving good linearity, $r^2$ ranged between 0.9990 - 0.9997. Detection Limit (D.L) was mostly less than 0.4µg.mL$^{-1}$,while in case of ZCDSP and RDSP were between 0.01-0.2 µg.mL$^{-1}$ with wider linearity range (1-50 for CBZ and 1 - 80µg.mL$^{-1}$ for LMT). A slightly lower sensitivity was observed when suppressing solution for urine analysis was used to remove interferences. The recoveries of CBZ and LMT in samples of urine of a healthy person spiked with the drugs and using urine of a healthy person as a blank were, in most cases, around (101.0% - 103.33%) and (98.33% - 102.16%) with RSD $\leq$ 3.61 and 3.63% for CBZ and LMT respectively. The recoveries using suppressing solution were (101.66% - 105.41%) and (94.56% - 101.0%) with RSD $\leq$ 2.43 and 3.62% for CBZ and LMT respectively. Statistical comparison of the results with the mixture of standard solutions using F, and t-tests showed no significant differences between each of the four methods at 95% C.L. The proposed methods were successfully applied for the determination of CBZ and LMT in binary mixtures and urine samples.

**Keywords**: dual wave length, zero crossing derivative, ratio derivative spectrophotometry, tegretol and lamotigine determination

**Abstrak**

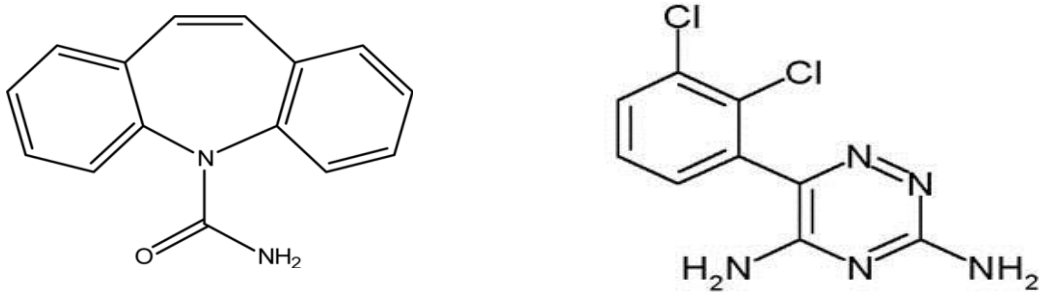
Dalam kajian ini empat kaedah spektrofotometri UV yang berbeza dijelaskan terhadap penentuan serentak dadah antiepilepsi; karbamazepin (CBZ) dan lamotrigin (LMT) dalam campuran sintetik perduaan dan sampel urin tanpa pemisahan. Kaedah pertama adalah dengan menyelesaikan dua persamaan serentak (SEQ) berdasarkan jumlah serapan menurut hukum Beer. Kedua adalah kaedah panjang gelombang dual (DWSP); Perbezaan serapan diukur antara 304 dan 313 nm terhadap CBZ manakala sifar bagi LMT. Begitu juga perbezaan serapan antara 282 dan 290 nm adalah penting untuk LMT dan set sifar untuk CBZ. Kaedah ketiga melibatkan penggunaan kaedah lintasan sifar terbitan pertama (ZCDSP) pada amplitud masing – masing 308.9 dan 286.6 nm untuk CBZ dan LMT. Kaedah spektrofotometri nisbah terbitan (RDSP) adalah yang terakhir. Serapan pada kepekatan yang berbeza CBZ atau LMT mengikut panjang gelombang, oleh serapan pembahagi, dimana larutan LMT adalah piawai untuk analit CBZ analit, dan sebaliknya. (Kepekatan Pembahagi = 2.0µg.mL$^{-1}$) dalam kedua-dua kes. Amplitud nisbah spektrum terbitan pada 290 nm dengan selang jarak gelombang ($\Delta\lambda$ = 6.0nm) dan 328 nm ($\Delta\lambda$ = 4.0 nm) masing – masing telah dipilih untuk

penentuan CBZ dan LMT. CBZ dan LMT telah ditentukan secara serentak di dalam campuran sintetik perduaan dan sampel urin oleh kesemua kaedah memberi kelinearan baik, r2 adalah antara 0.9990 - 0.9997. Had pengesanan adalah kurang daripada 0.4μg.mL$^{-1}$, manakala bagi kaedah lintasan sifar terbitan pertama dan spektrofotometri nisbah terbitan adalah di antara 0.01 – 0.2 μg.mL$^{-1}$ dengan julat kelinearan lebih besar (1-50 bagi CBZ dan 1 - 80μg.mL$^{-1}$ untuk LMT). Nilai sensitiviti diperhatikan lebih rendah apabila larutan tekanan digunakan terhadap analisis sampel urin untuk menghilangkan gangguan. Perolehan semula di dalam sampel urin bagi orang yang sihat yang dipaku bersama dadah CBZ dan LMT dan larutan pengosong dalam kebanyakan kes didapati pada julat (101.0% - 103.33%) dan (98.33% - 102.16%) dengan RSD 3.61 dan 3.63% masing – masing terhadap CBZ dan LMT. Perolehan semula menggunakan larutan tekanan adalah (101.66% - 105.41%) dan (94,56% - 101.0%) dengan RSD 2.43 dan 3.62% masing – masing terhadap CBZ dan LMT. Perbandingan statistik hasil kajian menggunakan ujian F dan ujian-t terhadap larutan piawai menunjukkan tidak ada perbezaan yang signifikan antara setiap satu daripada empat kaedah pada 95%. Kaedah yang dicadangkan telah berjaya diggunakan terhadap penentuan campuran perduaan CBZ dan LMT dan sampel urin.

**Kata kunci**: panjang gelombang dual, kaedah lintasan sifar terbitan pertama, kaedah spektrofotometri nisbah terbitan, penentuan tegretol dan lamotigine

## Introduction

Carbamazepine (CBZ) or Tegretol and Lamotrigine (LMT) or Lamictal, Fig.(1) are two important antiepileptic drugs[1-4]. The CBZ is chemically known as 5H-dibenzo [b,f] azepine-5-carboxamide, is a highly lipophilic neutral tricyclic compound with a white to off white color almost odorless crystalline powder and has acid equilibrium constant (pKa of 13.9).It is slightly soluble in water but soluble in alcohol and acetonitrile[5,6]. In 1970, CBZ was approved in the United States for the management of seizure disorder in adults and in 1979 for children older than 6 years and remains widely used today[7,8]. LMT is chemically known as[6-(2,3-dichlorophenyl)-1,2,4-triazine-3,5-diamine], has a broad-spectrum of the phenyltriazine class, chemically unrelated to other anticonvulsants[2-4]. It is a white to pale cream-colored powder and has a pKa of 5.7, slightly soluble in water but soluble in 0.1M $H_2SO_4$ [9], methanol and acetone[10].LMT is used as a monotherapy and as an adjunct with other antiepileptic drugs for treatment of partial and generalized tonic-clonic seizures. It is also used as tranquilizer and has also been studied in the treatment of neurological lesions[9].




(a) Tegretol (CBZ) (b) Lamotrigine (LMT)

Figure 1. The chemical structure of a. CBZ and b.LMT

Various analytical techniques have been reported in the literature to estimate CBZ and LMT in dosage forms and biological fluids including**:** Enzyme immunoassay methods [7, 8] for the estimation of CBZ and radioimmunoassay for the determination of LMT in human plasma were reported [11]. Most and a large number of methods for both CBZ and LMT analysis alone or together with other antiepileptic drugs or with their metabolites utilize, mainly HPLC techniques, and other chromatographic methods. Because of that,only those references appeared after 2010 are cited here[12-20]. Electroanalytical methods [1, 21-29] mostly voltammetric and few Ion- selective electrode methods, particularly for CBZ and rather few for LMT have been reported. Only few spectrophotometric methods,

both absorption and emission, were found reported for the determination of CBZ[30-35] and LMT[3,9,10,36-42] in pure forms or in pharmaceutical preparations. In a previous paper, Najib and Aziz [34] have developed two absorption methods for the determination of CBZ. In the present work four methods were tested for the determination of CBZ and LMT, in synthetic mixtures and human urine. For the best of the authors' knowledge, none of the published spectrophotometric methods have attempted the determination of these drugs together in a mixture and not by any of the developed methods in the present work. The methods studied in this work were; Calculation, dual wave length, zero crossing derivative and ratio derivative methods.

## Materials and Methods

### Apparatus and software

All spectra and absorbance measurements were recorded with (CECIL, CE9500, super aquarius) and (Perkin Elmer, Lambda 25 UV/VIS) double beam Scanning Spectrophotometers with 1.0cm matched quartz cells. Epson Printer LQ-2180, Grapher software (7.1.2005) Patch.msp, Microsoft office Excel 2007, Micropipettes from Gilson, France (variable and fixed).

### Chemicals, Reagents and Drugs

All chemicals used were of analytical reagent grade, distilled water (D.W) was used throughout all the experiments. The organic solvents chloroform (Thomas Baker 99%), carbon tetrachloride (FISONS 95%), diethyl ether (Gainland Chemical Company 99.5%), acetone (Gainland Chemical Company 99.97%), n-hexane (Riedel de-Haen 97 %), cyclohexane (Merck 99.5%), methanol (Alpha chemika 99.9%) and ethanol (Scharlau 99.9%) without further purification. Pure and standard powder of lamotrigine was obtained from the (Hikma company, Jordan). Standard carbamazepine as a pure compound was obtained from (Samarra drug-company-Iraq). Tablets of the drugs from different origins were purchased from local market.

Stock standard solutions:100 μg/mL of each of CBZ and LMT were prepared by dissolving accurately weighed 0.01g of each drug in ethanol: water mixture (2:1) in 100 mL volumetric flasks. Different solutions of the compounds needed were prepared in the usual way.

Deproteinization of urine samples were performed [43] by taking 2.0 mL of spiked urine in a beaker. A portion of 1.2 mL from 0.15 M $Ba(OH)_2$ were followed by 1.2mL of 2.5% w/v $ZnSO_4.7H_2O$ and mixed well. Then filtered through a filter paper, no.41 (pore size, 20-25μm, particle retention) from Whatman. The filtrate was diluted to 50 mL by D.W in a volumetric flask. Unless otherwise stated, the blank was always ethanol: water mixture (2:1).

## Results and Discussion

### Choice of the organic solvent and the absorption spectra

The organic solvents chloroform, carbon tetrachloride, diethyl ether, acetone, n-hexane, cyclohexane methanol and ethanol were studied for their suitability, as shown in Table 1.

Volumes of 0.6 mL of CBZ and 1.0 mL of LMT, completed with each solvent to 10 mL were tested by recording their overlaid absorption spectra over the range 200-400 nm using corresponding solvent as a blank. The only suitable solvent among them, regarding both solubility and smooth output spectra, was ethanol. Among different ratios of this solvent with water, the mixture of ethanol: water (2:1) was chosen as the most suitable solvent, Fig. 2. This figure shows that ($\lambda_{max}$) were 286 and 308 nm for CBZ and LMT, respectively. The figure also shows partial spectral overlaps which did not allow their direct individual spectrophotometric analysis when present together in a mixture.

Table 1. Choosing best solvents for dissolving CBZ and LMT

| Solvents | Carbamazepine | Lamotrigine | Results |
|---|---|---|---|
| Chloroform | Soluble | Soluble | Not suitable; both CBZ and LMT gave noisy absorption spectra |
| n-Hexane | Slightly Soluble | Insoluble | Not suitable |
| Diethyl ether | Soluble | Soluble | Not suitable; for CBZ due to noisy absorption spectrum. |
| Acetone | Soluble | Soluble | Not suitable for both CBZ and LMT. Noisy absorption spectra were obtained |
| $CCl_4$ | Insoluble | Insoluble | Not suitable |
| Cyclohexane | Slightly Soluble | Slightly Soluble | Not suitable |
| Ethanol | Soluble | Soluble | Suitable |
| Methanol | Soluble | Soluble | Suitable |

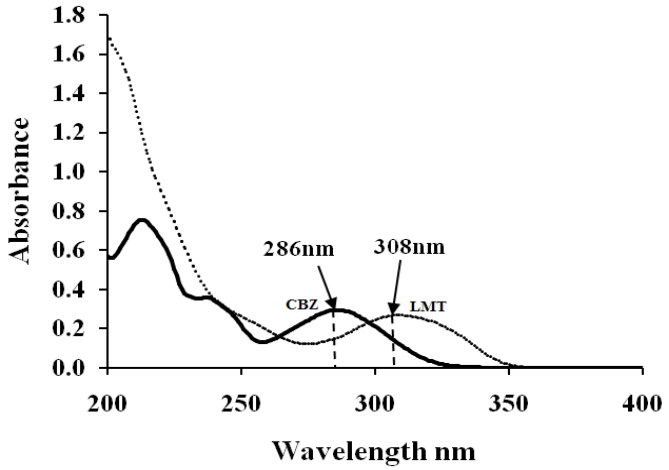



Figure 2. Zero-order absorption spectra of 6.0 µg/mL CBZ (——) and 10 µg/mL LMT ( ·····) using mixture of ethanol: water (2:1) as a solvent and blank.

**The determination of CBZ and LMT in binary mixtures without separation**

***The calculation method (SEQ)***

Although this method might be considered as a straight forward attempt, but it has not been tried before for these drugs and perhaps for others; it has been used for the determination of binary mixtures of textile dye[44]. The concentration C of each component of the sample will be calculated from the additive absorbance *A* in Beer's Law at $\lambda_{max}$ of each of (a)and (b) following simultaneous equations, assuming CBZ = a and LMT = b.

$$A_{\lambda a\max} = \varepsilon_{\lambda a\max} C_a + \varepsilon'_{\lambda a\max} C_b \quad (1)$$

$$A_{\lambda b\max} = \varepsilon_{\lambda b\max} C_a + \varepsilon'_{\lambda b\max} C_b \quad (2)$$

The four molar absorptivity **ε** values were calculated from individual standards of (a) and (b) using Beer's law. The concentrations of (a) and (b) will then be calculated from equations3 and 4.

$$C_a = \frac{A_{\lambda a\max}\varepsilon'_{\lambda b\max} - A_{\lambda b\max}\varepsilon'_{\lambda a\max}}{\varepsilon'_{\lambda b\max}\varepsilon_{\lambda a\max} - \varepsilon'_{\lambda a\max}\varepsilon_{\lambda b\max}} \quad (3)$$

$$C_b = \frac{A_{\lambda b\max}\varepsilon_{\lambda a\max} - A_{\lambda a\max}\varepsilon_{\lambda b\max}}{\varepsilon'_{\lambda b\max}\varepsilon_{\lambda a\max} - \varepsilon'_{\lambda a\max}\varepsilon_{\lambda b\max}} \quad (4)$$

***Dual wavelength method (DWSP)***

This method is based on the principle that absorbance difference between two points of the wavelength spectra of the mixture is directly proportional to concentration of the component of interest, while the unwanted compound gives a ΔA=zero[45,46]. In an easy way, the selective determination of both drugs CBZ and LMT in a binary mixture will become possible.

***Selection of suitable wavelengths***

Selection of suitable wavelengths plays an important role in dual wavelength method; to do this different wavelengths from Fig.(3) were tried for CBZ and LMT as shown in table (2). Using the absorbance values at 304 and 313nm for CBZ (where LMT has ΔA= zero) and the absorbance values at 282 and 290nm for LMT (where CBZ has ΔA= zero) were chosen for determination of CBZ and LMT respectively. It can be deduced from the table that, the wavelengths mentioned above gave best linear range and average recovery percent in the binary mixtures and urine samples.

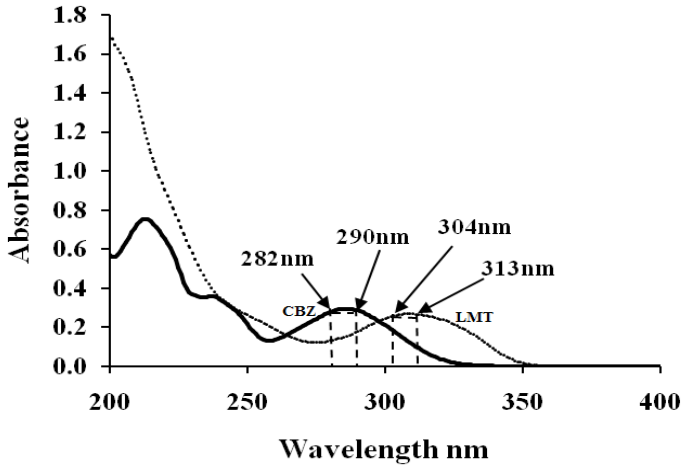



Figure 3. Zero-order absorption spectra of 6.0 µg/mL CBZ ( ——) and 10 µg/mL LMT ( ·····) using mixture of ethanol: water (2:1) as a solvent and a blank.

***Zero-crossing first derivative spectrophotometric method (ZCDSP)***

Zero-crossing derivative spectrophotometry involves measurement of the amplitude of the analyte at a wavelength at which absorbance of the unwanted species is nearly zero for different concentrations while the other component (the analyte) has appreciable absorbance (amplitude) [ 47,48].

Figure 4 shows first derivative UV- spectra of the same solutions of Figure (2). Derivatization of the zero-order spectra leads to an improvement of the spectral details and the resulting first derivative presents spectral features which can be used for simultaneous determination of CBZ and LMT. The figure shows that the signals of the first derivative of LMT are crossing zero at 309.8 nm and 275.6 nm and calibration curves for CBZ were linearly proportional to its concentration. The chosen wavelength, however, was found better to be at 309.8 nm. The same figure also shows the zero-crossing wavelength of CBZ at 286.6 nm, while at this wave length the derivative amplitude was found to be proportional to LMT concentration.

Table 2. Optimization of wavelength for simultaneous determination of CBZ and LMT by dual wavelength method

| Compound | Wavelength nm | Linear range µg/mL | Slope | Intercept | Correlation coefficient |
|---|---|---|---|---|---|
| CBZ | 255 and 297 | 3.0-15 | 0.0159 | 0.0014 | 0.9995 |
| | 300 and 319 | 6.0-17 | 0.0287 | - 0.0049 | 0.9992 |
| | 250 and 306 | 3.0-16 | 0.0115 | - 0.0029 | 0.9996 |
| | 304 and 313 | 3.0-21 | 0.0155 | - 0.0017 | 0.9996 |
| LMT | 276 and 296 | 4.0-26 | 0.0101 | - 0.0017 | 0.9993 |
| | 245 and 285 | 3.0-19 | 0.0155 | - 0.0020 | 0.9994 |
| | 282 and 290 | 3.0-32 | 0.0041 | -0.0005 | 0.9994 |

***Selection of optimum instrumental conditions***

The main instrumental parameters that affect the shape of the derivative spectra are the wavelength scanning speed and the smoothing of the resulting derivatives. Different scanning rates were tested and it was found that 25 nm/sec was a suitable scanning speed with band width of 2.0 nm. Several values of smoothing orders between (2-9 nm) were tested and the order 3.0 nm was selected due to its optimum signal, linearity range and recovery for synthetic mixtures of CBZ and LMT.

***Effect of each of the two drugs on the peak height of the other***

Two sets of standard solutions, the first was containing different concentrations of LMT (6.0-14 µg/mL) with constant concentration (3.0 µg/mL) of CBZ. The second contained between (3-5.0 µg/mL) of CBZ with (3.0 µg/mL) of LMT.

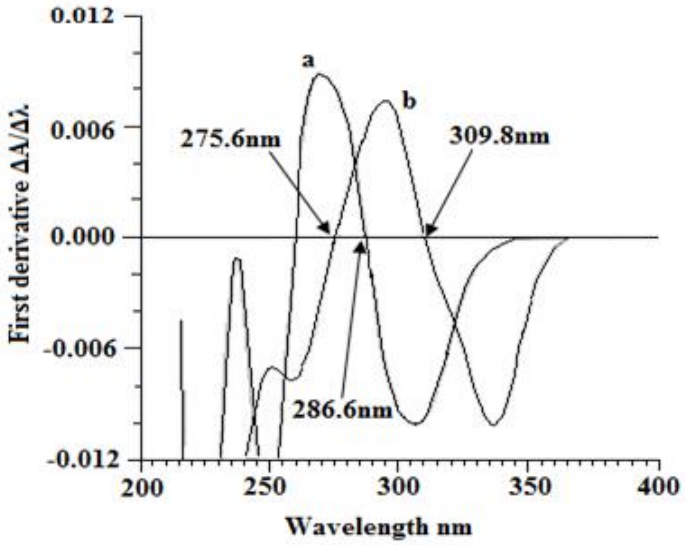



Figure 4. First derivative spectra of (a) 6.0 µg/mL CBZ and (b) 10 µg/mL LMT.

Their first derivative spectra, show that the heights at 309.8 and 286.6 nm were not affected by the presence of CBZ and LMT over the range of concentrations studied. According to previous optimizations, calibration curves for the determination of CBZ and LMT by measuring amplitude of the derivative spectra at 309.8 (Fig.5a) and 286.6 nm (Fig.5b) for both CBZ and LMT respectively, using (Grapher software (7.1.2005) Patch.msp),were found to be linear in the range of (1.0-50.0 and 1.0-80.0) µg/mL with ($r^2$=0.9995 ) and ($r^2$=0.9997) for both CBZ and LMT respectively. At lower concentrations, the first derivative amplitude could not be measured while at higher concentrations the first derivative amplitude was out of scale in both cases.

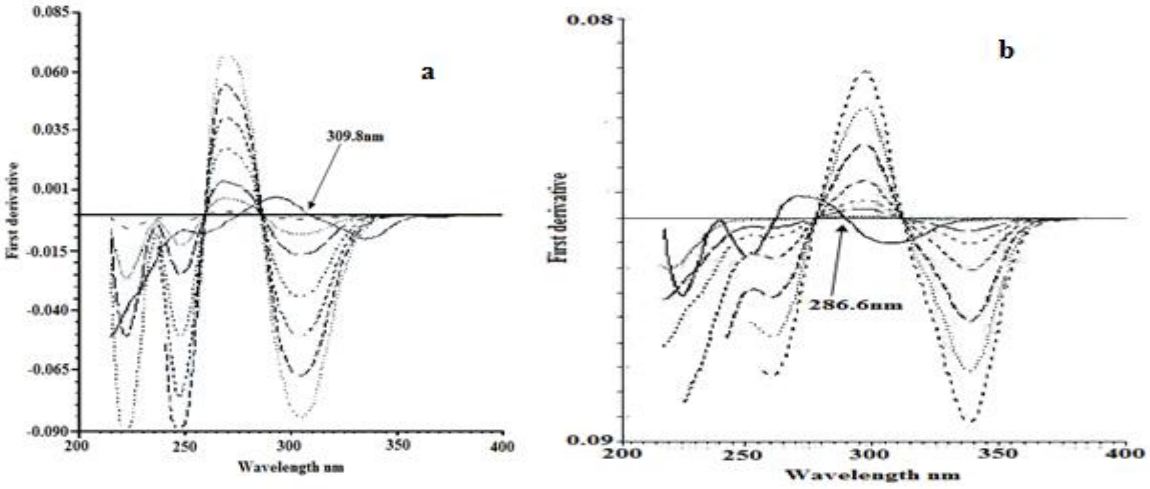



Figure 5. (a) First derivative absorption spectra of 10 µg/mL of LMT ( ——— ) and (1.0-50.0) µg/mL of CBZ (····· ), (b) 6.0 µg/mL of CBZ ( ——— ) and (1.0-80.0) µg/mL of LMT ( ····· ) using ethanol: water (2:1) as a blank (smoothing = 3.0 nm).

***Ratio derivative spectrophotometric method (RDSP)***

This is a modification of derivative spectrophotometric method based on the derivation of the ratio-spectra for resolving binary mixtures. The main advantage is the chance of performing easy measurements in correspondence of peaks; so that it permits choosing a wavelength at which the analytical signals of highest value (whether a maximum or minimum). Moreover, the presence of many maxima and minima will give the analyst more than one option to choose the most suitable wavelengths for the determination of one of the component in presence of the other which possibly interfere with the assay.

In this method, the absorption spectra of the mixture at each wavelength are divided by the absorption of a standard solution of one of the components, which is named a divisor. The first derivative of this ratio spectrum is obtained. The concentration of the other component is then determined from a calibration graph [49-50]. To apply this method for the determination of CBZ and LMT, it was necessary to optimize wavelength scanning speed, the concentration of the standard solution used as a divisor and the wavelength increment ($\Delta\lambda$) over which the derivative is obtained.

The effect of wavelength scanning speed was first studied. It was found that at high speed, noisy spectra were obtained while at low scanning speed, longer time was needed for measurements. Therefore medium scanning speed, 240 nm/min with spectral band width 2.0 nm were chosen for measurements. Different concentrations of CBZ and LMT standards were examined as divisors for each other. Several tests were carried out to study both the divisors concentrations and ($\Delta\lambda$). Increasing or decreasing the concentration of any one as the divisor, has made the resulting derivative values (hence, the slope of calibration graphs) proportionately decreased or increased, with potential variation of both sensitivity and linear range. Accordingly, best results for the divisors with minimal differences were found to be2.0-10 μg/mL in both cases. Outside these concentration ranges, the noise has greatly increased; with distortion and variation of the shape of curves and location of the peaks. For all subsequent measurements, a standard divisor 2.0 μg/mL for both CBZ and LMT were selected.

In Figure 6a and 7a, there are two series of ratio spectra of CBZ (from 1.0-50 μg/mL) and LMT (1.0-80 μg/mL) respectively. While Figs. (6b,7b), show the corresponding calculated first derivative ratio spectra of Figs, (6a,7a) using excel program. For the determination of CBZ by measuring amplitude at 266 and 290 nm, good linearity was observed but analytical signal and recovery percent were better at 290nm. For the determination of LMT, however, measuring amplitude at 328 nm, gave good linearity and recovery with low concentration of the divisor which was an important factor.

The $\Delta\lambda$ values of 6.0 nm for CBZ and 4.0 nm for LMT were selected as suitable wavelength intervals. Since in both cases the signals of the analytes (CBZ or LMT) that remain constant were not affected when the concentration of the variable analytes were increased up to 8.0 and 10 nm for CBZ and LMTrespectively. According to above optimizations, calibration curves were drawn for the determination of CBZ and LMT by measuring amplitude of the ratio derivative spectra at 290 and 328 nm against concentrations for both CBZ and LMT respectively. The calibration curves were linear in the range of 1.0-50.0 and 1.0-80.0 μg/mL, ($r^2$=0.9998) for both CBZ and LMT respectively.

***Analysis of Synthetic Mixtures of CBZ and LMT by the Proposed Methods***

Analyzing synthetic mixtures, other parameters not mentioned with the individual studies are given here. In order to demonstrate the validity and applicability of the proposed methods, recovery studies were performed. Results of table (3) which represent different composition ratios of CBZ and LMT, gave reasonable accuracies for the four methods, without any questionable data. Other data studied include, sensitivity, selectivity, accuracy and precision. Sensitivity represented by detection limit (D.L. μg/mL) according to equation,

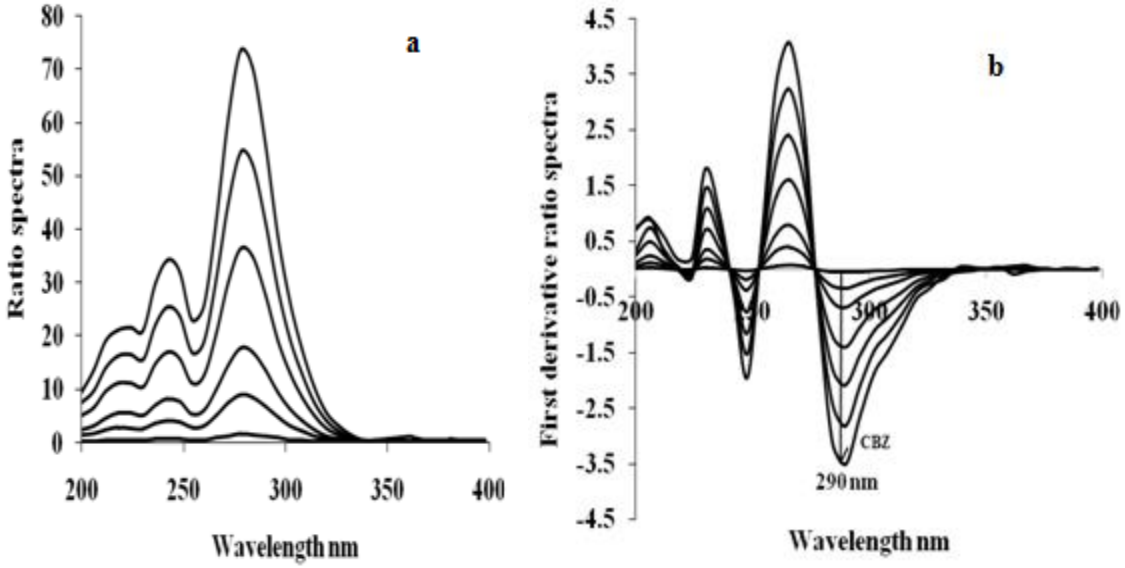



Figure 6. (a) Ratio spectra for 1.0, 5.0, 10, 20, 30, 40, 50 µg/mL solution of CBZ in ethanol: water (2:1) when 2.0 µg/mL LMT used as a divisor (Δλ= 6.0 nm).(b) is its first derivative.

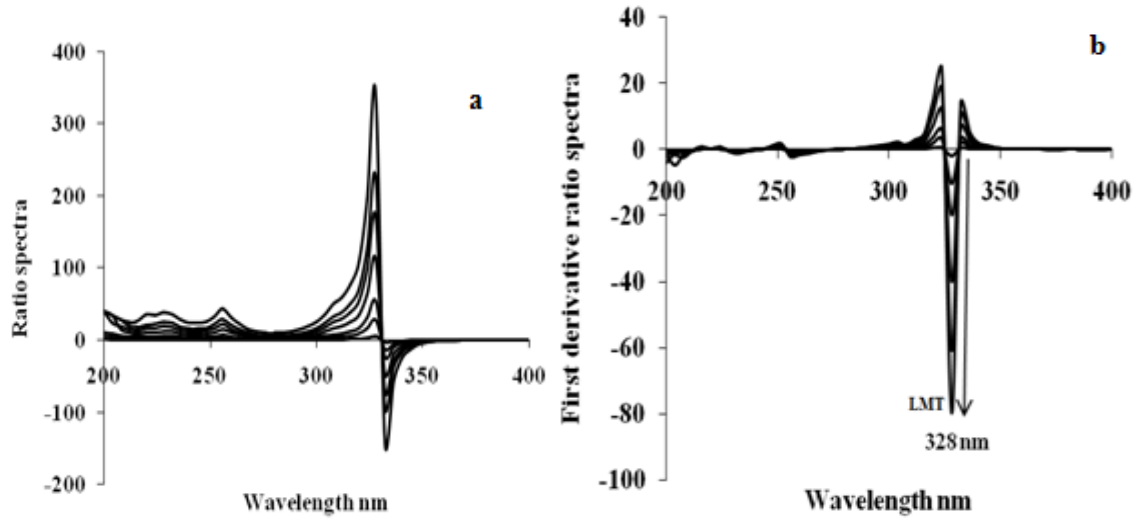



Figure 7. (a) Ratio spectra for 1.0, 5.0, 10, 20, 30, 40, 60, 80 µg/mL solution of LMT in ethanol: water (2:1) when 2.0 µg/mL CBZ used as a divisor (Δλ= 4.0 nm). (b) Its First derivative.

D.L =3.3σ/S, [σ = standard deviation of Blank signal and **S** = slope of the calibration curve] [51] for the methods, (SEQ, DWSP, ZCDSP and RDSP) were (0.12, 0.26), (0.11, 0.20), (0.09, 0.10) and (0.08, 0.03) for CBZ and LMT respectively. The precision of CBZ and LMT determination by the proposed methods was found by taking two samples of known concentration and their analytical signals were measured 10 times for the same sample, showing mainly, the precision of the instrumental measurements. The precision was also found on 10 times repeating the whole operation on the same sample; which confirms the precision of the whole procedure. The results, generally, indicate good precision, while the results of derivative methods show better precision than the other two methods.

The %Recovery and %Error for the determination of known concentrations of CBZ and LMT in mixtures made from their standard solutions were quite reasonable. The difference between the mean ( $\overline{X}$ ) and the true value (μ) was tested for the existence of a systematic error in the results. The results were obtained by comparing the actual difference between ( $\overline{X}$ ) and (μ); ( $\overline{X}$ - μ) and the term (t.S/$\sqrt{N}$ ) at 95% confidence limit DOF = 2. From the results of t-test for the four methods, it can be concluded that the difference between ( $\overline{X}$ - μ) and (t.S/$\sqrt{N}$ ) was not significant at 95% C.L, indicating the existence of too small or no significant systematic error.

Table 3. Analysis of synthetic mixtures of CBZ and LMT using the proposed methods.

| Sample number | CBZ taken (μg/mL) | LMT taken (μg/mL) | SEQ %Recovery | | DWSP %Recovery | | ZCDSP %Recovery | | RDSP %Recovery | |
|---|---|---|---|---|---|---|---|---|---|---|
| | | | CBZ | LMT | CBZ | LMT | CBZ | LMT | CBZ | LMT |
| 1 | 8.0 | 3.0 | 96.50 | 95.30 | 95.00 | 95.20 | 96.89 | 96.50 | 97.04 | 97.15 |
| 2 | 7.0 | 3.0 | 100.20 | 96.62 | 97.60 | 100.30 | 97.02 | 101.20 | 97.42 | 99.37 |
| 3 | 6.0 | 3.0 | 97.09 | 96.80 | 96.70 | 98.10 | 98.06 | 100.80 | 96.63 | 97.83 |
| 4 | 5.0 | 3.0 | 96.00 | 96.70 | 96.60 | 95.90 | 97.65 | 98.80 | 98.66 | 101.65 |
| 5 | 4.0 | 3.0 | 98.70 | 97.50 | 98.80 | 99.10 | 102.80 | 103.20 | 97.51 | 101.60 |
| 6 | 3.0 | 3.0 | 99.00 | 98.30 | 98.70 | 101.40 | 99.93 | 97.02 | 98.50 | 99.11 |
| 7 | 3.0 | 4.0 | 97.40 | 98.50 | 97.50 | 99.60 | 98.52 | 99.72 | 100.60 | 98.90 |
| 8 | 3.0 | 5.0 | 97.34 | 98.65 | 103.30 | 97.80 | 99.30 | 97.04 | 101.77 | 100.15 |
| 9 | 3.0 | 6.0 | 98.96 | 101.80 | 101.00 | 97.30 | 99.79 | 98.89 | 100.90 | 101.20 |
| 10 | 3.0 | 7.0 | 98.45 | 103.30 | 102.30 | 98.40 | 99.40 | 100.40 | 103.70 | 102.30 |
| 11 | 3.0 | 8.0 | 99.71 | 104.00 | 104.20 | 98.60 | 101.30 | 100.20 | 99.34 | 99.54 |
| 12 | 3.0 | 9.0 | 99.06 | 103.70 | 103.70 | 99.00 | 100.30 | 100.80 | 101.90 | 100.30 |
| 13 | 3.0 | 10.0 | 102.30 | 97.60 | 103.00 | 97.50 | 103.60 | 101.13 | 101.20 | 101.90 |

***Selectivity of the Methods***

The interfering effects of most of the ions and compounds that expected to be present in urine and of other antiepileptic drugs such as phenobarbital (PHE) were examined and are shown in table (4 and 5). It can be seen from table (4) that phenobarbital, carbamazepine and lamotrigine least interfere with each other in case of ratio derivative but interfere more with dual wavelength method, and the effect was more severe in the presence of CBZ. In general the results are still quite acceptable. The interfering effects of the most possible ions present in urine on simultaneous determination of CBZ and LMT are shown in table (5). The study has aimed to find maximum quantity of the interference on a synthetic mixture of 3.0 μg/mL of CBZ and 6.0 μg/mL of LMT, which can cause

not more than ±5% error (tolerance level, T.L). The cations chosen were ($Na^+$, $K^+$, $Ca^{2+}$ and $Mg^{2+}$) in the forms of ($Cl^-$, $HPO_4^{2-}$ and $NO_3^-$). It was found that the effect was mostly due to creatinine, and uric acid which were present in urine at a high level in addition to some cations and anions. The effect of the cation interferences was confirmed by examination of the cations [$Na^+$, $K^+$ and $Mg^{2+}$] all in chloride form showing high T.L. The cations [$Na^+$, $K^+$] were not effective when they were in the form of $HPO_4^{2-}$ while [$Na^+$, $K^+$, $Mg^{2+}$and $Ca^{2+}$] were more effective when they were in the form of ($NO_3^-$). This indicated that the effect of $NO_3^-$ was much severe than chloride and phosphate ions. Table (5) also shows very small interferences of [urea, glucose, fructose, and sucrose] present in urine.

***Removing of Interferences Using Suppressing Solution (S.S)***

The basic principle of this idea is that those interferences which are expected to be present in urine sample are added to the sample and to the blank solutions. The net result is subtraction of their effect from the sample. This solution is added only when the urine sample is analyzed [34]. The suppressing solution was prepared by dissolving 0.2069 g (800 ppm K), 0.015 g Uric acid(150 ppm) and 0.025 g Creatinine (250 ppm) in 100 mL D.W. After several tests, it was found that a portion of 0.10 mL of this solution (S.S) was optimum for 3.0 µg/mL CBZ and LMT, to obtain correct analytical signal.

***Simultaneous determination of CBZ and LMT in a synthetic and Urine Samples***

The proposed methods were applied for simultaneous quantification of CBZ and LMT in synthetic and urine samples. To decrease the effect of interferences present in urine samples taken from healthy volunteers not taking any drugs, a 2.0 mL portion of fresh urine was spiked with a known amount of standard solutions of CBZ and LMT. After deproteinization, the dilution of the urine sample was necessary. Correct result was obtained when the filtrate of urine sample was diluted to 50 mL (25 folds dilution).

Table 4. The tolerance levels (T.L) of interferences from other antiepileptic drugs on synthetic mixtures of CBZ**:** LMT = (1.0**:**2.0) and effect of each of them on the individual concentration of 3.0 µg/mL CBZ and 6.0 µg/mL LMT, which causes not more than ±5% error.[T.L] = [Interference] / [Analyte]

| **Drugs name, as Analyte in the Mixture** | **T.L (folds) SEQ** | | **T.L (folds) DWSP** | | **T.L (folds) ZCDSP** | | **T.L (folds) RDSP** | |
|---|---|---|---|---|---|---|---|---|
| | CBZ | LMT | CBZ | LMT | CBZ | LMT | CBZ | LMT |
| CBZ | ..... | +5 | ..... | +5 | ..... | +6 | ..... | +6 |
| LMT | -3 | ..... | -2.5 | ..... | -3 | ..... | -3 | ..... |
| PHE | +10 | -7 | +12 | -5 | +14 | -8 | +16 | -8 |

The analytes were determined by the present methods, with and without using (S.S) and %Recovery of the two methods was calculated from the calibration curves. The results obtained were statistically compared with those obtained with corresponding mixture of standard solutions of CBZ and LMT. Statistical analysis of the results, using variance ratio F-test and t-test, revealed no significant difference between the performance of the proposed methods and the result of mixtures of standard solution of CBZ and LMT since the calculated F-values and t-values at 95 % confidence level were less than the tabulated values.

Test for the presence of differences between the means of the four proposed methods with and without using (S.S) in this work ($urine_{(1)}$ and $urine_{(2)}$) has been performed. This was done by comparing the difference between the values ($\overline{X}_1 - \overline{X}_2$), with $t.S_{pooled} \times \sqrt{(N1+N2)/N1N2}$ at 95% DOF = 4. The results showed that:

$$(\overline{X}_1 - \overline{X}_2) < t.S_{pooled} \times \sqrt{(N1+N2)/N1N2}$$

meaning no significant difference between the performance of the proposed methods (with and without S.S).

Table 5. The tolerance levels of interferences on a synthetic mixture of 3.0 µg/mL of CBZ and 6.0 µg/mL of LMT, which causes not more than ± 5% error; [T.L] = [Int.] / [Analyte] folds

| **Cations** | **Salts of cations** | **T.L (folds) LMT** | **T.L (folds) CBZ** |
|---|---|---|---|
| $Na^+$ | NaCl | 850 | 2200 |
| $K^+$ | KCl | 860 | 2400 |
| $Mg^{2+}$ | $MgCl_2.6H_2O$ | 180 | 990 |
| $Na^+$ | $Na_2HPO_4$ | >1300 | >2600 |
| $K^+$ | $K_2HPO_4$ | >1300 | >2600 |
| $K^+$ | $KNO_3$ | 6.0 | 8.0 |
| $Ca^{2+}$ | $Ca(NO_3)_2.4H_2O$ | 35 | 19 |
| $Mg^{2+}$ | $Mg(NO_3)_2.6H_2O$ | 27 | 18 |
| Creatinine | $C_4H_7N_3O$ | 21 | 15 |
| Glucose | $C_6H_{12}O_6$ | 280 | 1300 |
| Urea | $(NH_2)_2CO$ | 410 | 800 |
| Fructose | $C_6H_{12}O_6$ | 230 | 780 |
| Sucrose | $C_{12}H_{22}O_{11}$ | 320 | 950 |
| Uric acid | $C_5H_4N_4O_3$ | 3.0 | 2.0 |

**Precision and Accuracy of the Methods:**

To evaluate the precision and accuracy of the proposed methods, a known amount of the standard CBZ and LMT concentrations were spiked into the urine samples simultaneously determined by the four proposed methods. The accuracy as (%Recovery), is presented in table (6) showing generally good to reasonable results. The precision as percent relative standard deviation (%RSD), was determined by analyzing two series of ten urine samples having spiked with mixtures of CBZ and LMT (5.0:3.0) µg/mL and (3.0:6.0) µg/mL each. The low values of the %RSD, ranged between (0.63 -3.63) indicated high precision.

The accuracy of the derivative methods was better than the other two methods which may be due to the effect feature of the derivative methods. Non spiked urine was used as a blank while in the second method the effects of interferences were minimized by using the suppressing solution. The %Error in case of CBZ and LMT (5.0:3.0) µg/mL each, of dual wavelength method was slightly more than 5% only in one case for CBZ and another for LMT. The reason of this error may be due to the quantity of 0.1mL S.S which was thought not to be sufficient to minimize the effect of interferences. But the error has not increased to such an extent needing further treatment, and has not been repeated again during the whole process. The difference between the mean ( $\overline{X}$ ) and the true value (µ) was performed to test for existence of a systematic error in the results as shown in table (6). The results were obtained by comparing the actual difference between ( $\overline{X}$ ) and (µ); ( $\overline{X}$ - µ) and the term (t.S/$\sqrt{N}$ ) at 95% confidence level DOF = 9.

The difference between ( $\overline{X}$ - µ) and (t.S/$\sqrt{N}$ ) was significant at 95% C.L in both methods, indicating the existence of a small systematic error. This was mainly due to the coexistences of the drugs and the effect of (S.S), which may affect one method more than another or has different effects on CBZ compared to LMT; but in general the error values were still satisfactory.

The test for the presence of differences between the means of any two pairs of the proposed methods in the mixture CBZ and LMT ratio (5.0:3.0) and (3.0:6.0) were determined by comparing the difference between the values ( $\overline{X}_1$- $\overline{X}_2$), with the term $t.S_{pooled} \times \sqrt{(N1+N2)/N1N2}$ at 95% C.L DOF = 18.

The results showed no significant difference between the performance of the two proposed methods (with and without using S.S) for simultaneous determination of CBZ and LMT in urine samples.

Table 6. Application of the present methods on a synthetic and urine samples for CBZ and LMT mixtures, with and without using the Suppressing Solution (S.S).

| **Sample Type** | **CBZ:LMT Mixing Ratio** | **% Recovery** | | | | | | | |
|---|---|---|---|---|---|---|---|---|---|
| | | **SEQ** | | **DWSP** | | **ZCDSP** | | **RDSP** | |
| | | **CBZ** | **LMT** | **CBZ** | **LMT** | **CBZ** | **LMT** | **CBZ** | **LMT** |
| Synthetic | 5:3 | 98.00 | 96.33 | 96.10 | 101.60 | 98.40 | 98.13 | 98.66 | 101.20 |
| | 3:3 | 101.00 | 101.33 | 98.66 | 103.30 | 101.20 | 101.60 | 98.50 | 99.11 |
| | 3:6 | 97.00 | 97.33 | 98.66 | 100.30 | 101.90 | 97.85 | 100.90 | 99.80 |
| Urine 1 No S.S | 5:3 | 98.80 | 98.00 | 104.10 | 101.60 | 101.00 | 98.83 | 104.40 | 97.00 |
| | 3:3 | 102.60 | 105.00 | 100.40 | 98.33 | 101.00 | 101.50 | 97.33 | 101.00 |
| | 3:6 | 104.00 | 102.00 | 102,60 | 103.60 | 102.80 | 102.70 | 102.70 | 98.16 |
| Urine 1 With S.S | 5:3 | 103.80 | 96.00 | 106.00 | 94.74 | 103.00 | 97.00 | 103.40 | 96.70 |
| | 3:3 | 100.60 | 95.33 | 102.20 | 103.50 | 100.30 | 97.66 | 102.30 | 98.57 |
| | 3:6 | 101.60 | 101.60 | 102.20 | 95.66 | 104.70 | 99.66 | 100.50 | 101.40 |
| Urine 2 No S.S | 5:3 | 102.00 | 95.33 | 100.20 | 101.60 | 103.80 | 100.30 | 96.60 | 100.30 |
| | 3:3 | 104.60 | 104.36 | 102.60 | 103.30 | 102.00 | 102.60 | 96.00 | 103.70 |
| | 3:6 | 101.30 | 104.30 | 100.30 | 99.66 | 100.60 | 101.00 | 102.00 | 97.50 |
| Urine 2 With S.S | 5:3 | 101.00 | 95.00 | 97.76 | 96.49 | 100.80 | 96.33 | 99.60 | 95.66 |
| | 3:3 | 103.00 | 95.60 | 102.20 | 100.90 | 103.60 | 101.30 | 101.30 | 96.66 |
| | 3:6 | 101.30 | 98.83 | 104.10 | 96.50 | 104.90 | 98.16 | 103.00 | 100.30 |

## Conclusion

Four sensitive and simple UV-Spectrophotometric methods were developed for simultaneous determination of antiepileptic drugs, carbamazepine (CBZ) and lamotrigine (LMT), in binary mixtures and urine without separation from each other. Interferences expected to be present in the urine samples were removed by addition of a suppressing solution to both samples and blank solutions or by using urine of a normal person not taking the drugs as a blank. The proposed methods were also selective for simultaneous determination of the two drugs in the presence of other co-administered antiepileptic drugs, such as phenobarbital. The suppressing solution was prepared from the salts of most interfering ions.

For validation, the determinations of CBZ and LMT in mixtures by the proposed methods were performed using their standards. Statistical analysis showed no significant difference between them at 95% C.L. Visible spectrophotometric methods published in the literature are only applicable for the determination of CBZ and LMT in tablets. In the UV region literature methods are only applicable for simultaneous detection of CBZ and LMT in biological fluid after extraction or separation with aid of other complicated techniques like HPLC. While this work has succeeded to determine the mixture of the two drugs in urine samples without separation.

**Acknowledgement**

The authors would like to thank the Chemistry Department, Faculty of Science and Science education and the Presidency of Sulaimani University for their kind support to perform this study.

**References**

1. Kalanur S. S., Seetharamappa J.( 2010). Elechtrochemical oxidation of bioxidative carbamazepine and its interaction with DNA. *Analytical Letters.* 43: 618–630.
2. Greiner-sosanko E., Lower D.R., Virji M.A., Kraswski M.D. ( 2007). Simultaneous determination of lamotrigine, zonisamide, and carbamazepine in human plasma by high-performance liquid chromatography. *Biomed. Chromatogrphy.* 2: 225–228.
3. El-Enany N.M., El-Sherbiny D.T., Abdelal A.A., Belal F.F.( 2010). Validated spectrophotometric method for determination of lamotrigine in tablets and human plasma through derivatization with o-phthalaldehyde. *J. Fluorescence.* 20: 463–472.
4. Mishra B., Ary N., Tiwari S. (2010). Investigation of formulation variables affecting the properties of lamotrigine nanosuspension using fractional factorial design. *J. Daru.* 18: 1-8.
5. Shucho Wu, Wei Xu, Qamar S., Bingcheng Y., Deying C., Yan Z., Lanjuan L. (2012).Ion chromatography combined with online electrochemical derivatization and fluorescence detection for the determination of carbamazepine in human plasma. *Talanta.* 101: 541-545.
6. Rao S. K., Belorkar N.(2010). Development and validation of a specific indicating liquid chromatographic method for carbamazepine in bulk and pharmaceutical dosage forms. *Journal of Advanced Pharmaceutical Research*. 1: 36-47.
7. Mcillin A. G., Juenke M. J., Tso G., Dasgupta A.(2010). Estimation of carbamazepine and carbamazepine-10,11-epoxide concentrations in plasma using mathematical equations generated with two carbamazepine immunoassays. *American J. for Clinical Pathology*. 133: 728-736.
8. Mcillin A. G., Juenke J. M., Johnson M. J., Dasgupta A. (2011). Discordant carbamazepine values between two immunoassays: carbamazepine values determined by ADVIA centaur correlate better with those determined by LC-MS/MS than PETINIA assay. *Journal of Clinical Laboratory Analysis;* 25: 212-216.
9. Rajendraprasad N., Basavaiah K., Vinay K.B. (2010). Micro and nanogram determination of lamotrigine in pharmaceuticals by visible spectrophotometry using bromophenol blue. *Indian J. of Chemical Technology* 17: 220–228.
10. Youssef N.F., Taha E.A. (2007). Development and validation of spectrophotometric, TLC and HPLC methods for the determination of lamotrigine in presence of its impurity. *J. Chemical and Pharmaceutical Bulletin;* 55: 541–545.
11. Biddlecombe R.A., Dean K.L., Smith C.D.Jeal S.C.(1990). Validation of a radiommunoassay for the determination of human plasma concentrations of lamotrigine. *J. Pharmaceutical and Biomedical Analysis.;* 8: 691– 694.
12. Patel A., Kataria M.( 2012). RP-HPLC method development and validation of lamotrigine in tablet dosage form. *International Journal of Advanced Research in Pharmaceutical and Bio Sciences;* 1: 95-102.
13. Al-Hadithi N., Saad B., Grote M.(2011). A solid bar microextraction method for the liquid chromatographic determination of trace diclofenac, ibuprofen and carbamazepine in river water. *J. Microchim Acta.*172: 31-37.
14. Bhaskara Reddy T. V., Ramu G., Babu A.B., Rambabu C.(2013). Development and validation of HPLC method for the estimation of lamotrigine in bulk and pharmaceutical formulations. *J. of Chemistry*: 1-4.
15. Rivas N., Zarzuelo A., Lopez F.G.(2010). Optimisation of high-efficiency liquid chromatography technique for measuring lamotrigine in human plasma. *Farmacia Hospitalaria.* 34: 85-89.
16. Fortuna A., Sousa J., Alves G., Falcao A., Soares-da-Silva P.(2010). Development and validation of an HPLC-UV method for the simultaneous quantification of carbamazepine, oxcarbazepine, eslicarbazepine acetate and their main metabolites in human plasma. *Ana. Bioanal. Chem.* 397: 1605-1615.
17. Mashayekhi H.A., Abroomand-Azar P., Saber-Tehrani M., Husain S.W.(2010). Rapid determination of carbamazepine in human urine, plasma samples and water using DLLME followed by RP_LC. *Chromatographia.* 71: 517-521.
18. Rani S.,Malik A.K., Singh B. (2012). Novel micro-extraction by packed sorbent procedure for the liquid chromatographic analysis of antiepileptic drugs in human plasma and urine. *J. Sep. Sci.* 35: 359-366.

19. Sharma M.C., Sharma S. (2011). Validated densitometric method for the quantification of lamotrigine in dosage form. *International Journal of Pharm. Tech.* Research 3: 1174-1178.
20. Paw B., Matysiak J., Kowalczuk D. (2011). Development and validation of a capillary electrophoresis method for the determination of lamotrigine in pharmaceutical dosage form. *Annales.* 24: 9-14.
21. Burgoa Clavo M. E., Renedo, O. M., Arcos Martinez .M. J.(2005). Optimization of the experimental parameters in the determination of lamotrigine by adsorptive stripping voltammetry. *J. Analytical Chimica Acta* 549: 74-80.
22. Dominguez-Renedo O., Burgoa Calvo M.E., Arcos Martinez M. (2008). Determination of lamotrigine in pharmaceutical preparations by adsorptive stripping voltammerty using screen printed electrodes. *J. Sensors.* 8: 4201– 4212.
23. Garcia-Garcia M.A., Dominguez-Renedo O., Alonso-Lomillo A., Arcos-Martinez M.J.(2009). Electrochemical methods of carbamazepine determination. *Sensor Letters.* 7: 586-591.
24. Atkins S., Sevilla J.M., Blazquez M., Pineda T., Gonalez-Rodriguez J. (2010). Electrochemical Behaviour of carbamazepine and dimethylformamide using glassy carbon electrodes and microelectrodes. *Electroanalysis.* 22: 2961-2966.
25. Veiga A., Drdio A., Carvallo Palac A.J., Teixeira D. M., Teixeira J. G.(2010). Uitra-sensitive voltammetric sensor for trace analysis of carbamazepine. *J. Analytical Chimica.* 674: 182–189.
26. Khim Chng E. L., Pumera M.(2011). Nanographitic impurities are responsible for electrocatalytic activity of carbon nanaotubes towards oxidation of carbamazepine. *J. Electrochemistry Communications* 13: 781-784.
27. Kalanur S.S., Jaldappagari S., Balakrishnan S. (2011). Enhanced electrochemical response of carbamazepine at a nano-structured sensing film of fullerene-$C_{60}$ and its analytical applications. *Electrochimica Acta.* 56: 5295-5301.
28. Liu Li-Hong, Duan Cheng-qian, Gao Zuo-Ning.(2012). Electrochemical behavior and electrochemical determination of carbamazepine at an ionic liquid modified carbon paste electrode in the presence of sodium dodecyl sulfate. *Journal of Serbian Chemical Society.* 77: 483-496.
29. Gupta V.K., Singh A.k., Gupta B.(2007). Development of membrane electrodes for selective determination of some antiepileptic drugs in pharmaceuticals, plasma and urine. *Analytical and Bioanalytical Chemistry*. 389: 2019-2028.
30. Ulu Tatar S.(2006). Determination of carbamazepine in pharmaceutical preparations using high-performance liquid chromatography and derivative spectrophotometry. *Turkish Journal Pharmaceutical Sciences.* 3: 123-139.
31. Abdulrahman S.A.M., Basavaiah K., Revanasiddappa H.D., Vinay K.B.(2010). Use of eco-friendly brominating agent for the spectrophotometric determination of carbamazepine in pharmaceutical formulations. *Malay J. Pharm. Sci.* 8: 1-17.
32. Frag E.A.Z., Zayed M.A., Omar M.M., Elashery S.E.A.,Mohamed G.G.(2012). Spectrophotometric Determination of Carbamazepine in Pure and Pharmaceutical Preparations; *Arabian Journal of Chemistry* 5: 375-382.
33. Lee H. Sang, Li Ming, Suh K. J.(2003). Determination of carbamazepine by chemiluminescence detection using chemically prepared Tris(2,2′-bipyridine)-ruthenium (III) as oxidant. Japan, *Analytical Sciences.* 19: 903–910.
34. Najib F.M., Aziz K.H.H. (2013). Spectrophotometric determination of lamotrigine in pharamaceutical preparations and urine samples using bromothymol blue and bromrophenol blue. *Malysian Journal of Analytical Sciences* 17: 310-325.
35. Escandar G.M., Gomez D.G., Mansilla A.E., De la Pena A.M., Goicoechea H.C.(2004). Determination of carbamazepine in serum and pharmaceutical preparations using immobilization on a nylon support and fluorescence detection. *Anal. Chim. Acta,* 506: 161-170.
36. Revanasiddappa H.D., Feepakumari H.N., Mallegowda S.M. (2011). Development and validation of indirect spectrophotmetric methods for lamotrigine in pure and the tablet dosage forms. *Analele Universitatii din Bucuresti-Chimie (serienoua).* 20: 49-55.
37. Alizadeh N., Khakinahad R., Jabbari A. (2008). Spectrophotometric determination of lamotrigine in pharmaceutical preparations and urine by charge-transfer complexation. *Pharmazie.* 63: 791–795.

38. Vinay K.B., Revanasiddappa H.D., Rajendraprasad N. (2009). Development and validation of spectrophotometric methods for the sensitive and selective determination of lamotrigine in pharmaceuticals using bromocresol purple. *J. of Food and Drug Analysis.* 17: 424–433..
39. Rajendraprasad N., Basavaiah K., Vinay K.B.(2010). Sensitive spectrophotometric determination of lamotrigine in bulk drug and pharmaceutical formulations using bromocresol green. Ecl. *Quim., Säo paulo.* 35: 55–66.
40. Ulu T. S.(2011). Sensitive and simple spectrophotometric method for the determination of lamotrigine in pure and pharmaceutical preparations of charge-transfer complex. *Rev. Chim.* 62: 261-264.
41. Vinay K.B., Revanasiddappa H.D., Rajendraprasad N., Basavaiah K.. (2011). Sensitive, selective and extraction-free spectrophotometric determination of lamotrigine in pharmaceuticals using two sulphonthalein dyes. *Thai. J. Pharm.* 35: 65-76.
42. Chandan R.S., Gurupadayya, Indupriya M., (2013). Quantitative Determination of lamotrigine by gas chromatography using ethyl chloroformate as a derivatizing reagent in pure and pharmaceutical preparation; *Indo American Journal of Pharmaceutial Research.* 3: 8284-8289.
43. Abolfathi Z., Belanger P.M., Gilbert M., Rouleau JR.(1992). Improved high-performance liquid chromatographic assasy for the stereoselective determination of mexiletine in plasma. *J. Chromatography.* 2: 579: 366.
44. Ekrami E., Okazi M. (2010). Analysis of dye concentrations in binary dye solutions using derivative spectrophotometric techniques. *World Applied Sciences Journal* 11: 1025-1034.
45. Amin G., Chapla B., Pandya A., Kakadiya Dr. J., Baria D.(2010). Development and validation of dual wavelength uv spectrophotometric method for simultaneous estimation of tadalafil and dapoxetine hydrochloride in their combined tablet dosage form. *International Journal of Pharmaceutical Research and Bio-scince* 2: 247-255.
46. Dashrath H.P., Dipti B.P., Patel Shree S.k. (2012). Development and validation of dual wavelength spectrophotometric method for simultaneous estimation of cefixime trihydrate and sulbactam sodium in combined dosage form. *International Journal of Universal of pharmacy and Life Science*. 2: 62-71.
47. Al-Shaalan N. H.(2010). Determination of phenylephrine hydrochloride and chlorpheniramine maleate in binary mixture using chemometric-assisted spectrophotometric and high-performance liquid chromatographic-UV methods. *Journal of Saudi Chemical Society.* 14: 15-21.
48. Relan G.R., Dubey A.N., Vaidyanathan S. (1995). A ratio derivative spectrophotometric method for the simultaneous determination of uranium and plutonium. *Journal of Radioanalytical and Nuclear Chemistry*. 204: 15-22.
49. Farouk M., Abd El-Aziz L., El-Gindy A.E., Shokry E.(2011). Validated methods for determination of yohimbine hydrochloride in the presence of its degradation products. *Bulletin of Faculty of Pharmacy*, Cairo University. 49: 67-79.
50. Darwish H.W., Hassan S.A., Salem M.Y., El-Zeiny B.A.(2011). Three different spectrophotometric methods manipulating ratio spectra for determination of binary mixture of amlodipine and atorvastatin. *Spectrochimica Acta Part A*. 83: 140-148.
51. Patel S. A., Patel N. J. (2011). Development and validation of dual wavelength spectrophotometric method for simultaneous estimation of cefixime trihydrate and ofloxacin in tablet dosage form. *International Research Journal of Pharmacy*. 2: 145-148.

The Malaysian Journal of ANALYTICAL SCIENCES ISSN 1394-2506

# SCHIFF BASES DERIVED FROM ISATIN AS MILD STEEL CORROSION INHIBITORS IN 1 M HCl

## (Bes Schiff Yang Terhasil Daripada Isatin Sebagai Perencat Kakisan Keluli Lembut Dalam 1 M Asid Hidroklorik)

Aliyin Abdul Ghani[1]*, Hadariah Bahron[1], Mohamad Kamal Harun[1], Karimah Kassim[2]

[1]*Faculty of Applied Sciences,*
[2]*Institute of Science,*
*Universiti Teknologi MARA (UiTM), 40450 Shah Alam, Selangor, Malaysia*

**Corresponding author: aliyinabdulghani@gmail.com*

**Abstract**

Two Schiff bases namely, 3-(phenylimino)indolin-2-one (PII) and 3,3- (1,4-phenylenebis (azan-1-yl-1-ylidene))diindolin-2-one (PDI) were successfully synthesized from the condensation reaction giving yields of 72% and 84%, respectively. The ligands were characterized *via* physical and spectroscopic techniques namely melting point, Elemental Analysis (C, H, N), $^{1}$H and $^{13}$C Nuclear Magnetic Resonance (NMR) and Fourier Transform Infrared (FTIR) Spectroscopy. The corrosion inhibiting property of the Schiff bases on mild steel in 1 M HCl solution were investigated by the weight loss measurements, electrochemical impedance spectroscopy (EIS) and linear polarization resistance (LPR). The concentrations of the Schiff bases were varied from 1 x $10^{-3}$ M to 1 x $10^{-5}$ M. The inhibition efficiencies obtained from all the methods employed were in good agreement where the percentage of inhibition efficiencies increased with concentration. Results showed that PDI was the better inhibitor with inhibition efficiency of 84% at 1 x $10^{-3}$ M additive concentration. This is likely due to the effect of its bigger molecular size, higher number of heteroatoms and bigger π-electron cloud of the conjugated double bond system.

**Keywords:** Schiff base, Isatin, Corrosion inhibitor, Mild steel, Hydrochloric acid

**Abstrak**

Dua bes Schiff, 3-(phenylimino)indolin-2-one (PII) dan 3,3- (1,4-phenylenebis (azan-1-yl-1-ylidene))diindolin-2-one (PDI) telah disintesis dengan jaya dari reaksi kondensasi memberikan hasil 72% dan 84%. Ligan-ligan telah dicirikan oleh pelbagai teknik kimia-fizikal seperti menentu takat lebur, analisis unsur, $^{1}$H and $^{13}$C spektroskopi resonans magnet nuklear, dan spektroskopi inframerah. Ciri-ciri perencat kakisan bagi Bes Schiff di atas keluli lembut dalam 1 M asid hidroklorik telah dikaji melalui kaedah penghilangan jisim, spektroskopi impedans elektrokimia dan rintangan polarisasi linear. Kepekatan Bes Schiff disediakan dari 1 x $10^{-3}$ M to 1 x $10^{-5}$ M. Kecekapan perencat dari semua kaedah telah menunjukkan keserasian di mana peratus kecekapan perencat meningkat apabila jumlah kepekatan ligan bertambah. Keputusan menunjukkan PDI adalah perencat yang lebih baik dengan kecekapan perencat sebanyak 84% pada kepekatan 1 x $10^{-3}$ M. Ini adalah kerana efek molekul yang lebih besar, jumlah heteroatom yang tinggi dan π-elektron yang lebih besar dari konjukasi system ikatan kembar.

**Kata kunci:** Bes Schiff, Isatin, Perencat kakisan, Keluli lembut, Asid Hidroklorik

## Introduction

The investigation of corrosion inhibition of mild steel in hydrochloric acid is a subject of practical interest as it is commonly used in many engineering applications [1,2]. The use of organic inhibitors to reduce the corrosion rate of mild steel in acidic medium can be considered to be among the first line of defense against corrosion in the industries [3]. Compounds containing π bonds and lone electron pairs generally exhibit good inhibitive properties as they can facilitate effective adsorption through their interaction with the vacant *d*-orbitals of metal atoms [4,5]. Several studies reported that the inhibition efficiency of a Schiff base was much greater than its precursor molecules due to the presence of -C=N- group(s) in the molecule. Their effectiveness is also related to the chemical composition, molecular structure and their affinities for the metal surface [6,7].

The aim of the present work was to synthesize and characterize two Schiff bases, 3-(phenylimino)indolin-2-one (PII) and 3,3- (1,4-phenylenebis (azan-1-yl-1-ylidene))diindolin-2-one (PDI), to study the corrosion behaviour of mild steel in 1 M HCl using weight loss measurements, linear polarization resistance and electrochemical impedance spectroscopy. Several isotherms were tested for their relevance to describe the adsorption behavior. The differences in inhibitive behavior for the two compounds are explained from their structural properties.

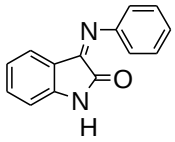
## Materials and Methods

### Synthesis and characterization of 3-(phenylimino)indolin-2-one, PII

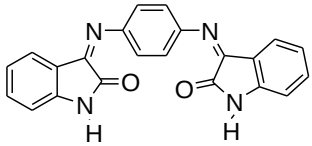
A mixture of 10 mmol of isatin and 10 mmol of aniline in absolute ethanol was refluxed for 6 hours. The precipitate formed was filtered off and washed thoroughly with cold ethanol. The product (Fig. 1) was dried in vacuum pump. Yield = 0.799 g (72%), m.p. 223.7 °C; Found %: C, 74.97; H, 4.54; N, 12.59. Calculated % for $C_{14}H_{10}N_2O$: C, 75.66; H, 4.54; N, 12.60; $\nu_{max}$ (KBr): C=N, 1651.8 $cm^{-1}$; C=C, 1614.57 $cm^{-1}$; $^1$H NMR ($CDCl_3$,300MHz) δ/ppm: 6.65-7.44 (9 H, m, Ph), 9.70 (1 H, s, NH), $^{13}$C NMR ($CDCl_3$, 75MHz) δ/ppm: 116.1-134.4 (CH Ar), 145.6-150.2 (CN), 154.7 (C=O), 165.4 (C=N).

### Synthesis and characterization of 3,3-(1,4-phenylenebis(azan-1-yl-1-ylidene))diindolin-2-one, PDI

A mixture of 10 mmol of isatin and 5 mmol of para-phenylenediamine was synthesized the same manner as PII giving the product as in Fig 1. Yield = 1.53 g, (84%), m.p 328 °C, Found %: C, 72.88; H, 4.14; N, 15.30. Calculated % for $C_{22}H_{14}N_4O_2$ C, 72.12; H, 3.85; N, 15.29 %); $\nu_{max}$ (KBr): C=N $cm^{-1}$, 1649.16; C=C, 1614. 16 $cm^{-1}$; $^1$H NMR (DMSO, 300MHz) δ/ppm: 6.67-7.30 (6 H, m, Ph), 2.48 (1 H, s, NH), $^{13}$C NMR (DMSO, 75MHz) δ/ppm: 116.2-135.0 (CH Ar), 147.4-147.8 (CN), 155.5 (C=O), 163.9 (C=N).




3-(phenylimino)indolin-2-one (PII)




3,3'-(1,4-phenylenebis(azan-1-yl-1-ylidene)) diindolin-2-one (PDI)

Fig. 1. Molecular structure of the investigated compounds, PII and PDI

### Weight loss measurements

Mild steel with the dimension of 1 cm x 1 cm were polished to a mirror finish using 120, 320, 600, 800 and 1200 grit emery paper, immersed in ethanol, washed with deionized water and dried before being weighed. The specimens were immersed for 24 hours in 50 mL 1 M HCl solution containing various concentrations of the inhibitors. The masses before and after immersion were determined using analytical balance. The measurements were done in triplicate, where the average values were used to calculate the inhibition efficiencies.

### Electrochemical analysis

Electrochemical experiments were carried out by using a conventional three-electrode cell consisting of a mild steel working electrode, a Ag/AgCl electrode as reference and platinum rod as counter electrode. The working electrode was prepared by embedding the mild steel in epoxy resin and exposing a flat surface of approximately 0.049 $cm^2$ to the electrolyte. Prior to each measurement, the electrode surface was mechanically abraded with a series of grit emery paper (120, 320, 600, 800, 1200) rinsed with deionized water and dried. The concentrations of the Schiff bases in 1 M HCl were varied from 1 x $10^{-3}$ M to 1 x $10^{-5}$ M. In order to obtain a steady state open circuit potential, the working electrode was immersed into the test solution for 15 minutes before the measurements. All experiments were done in triplicate.

## Results and Discussion

### Synthesis and characterization of PII and PDI

The elemental analysis, $^{1}H$ NMR and $^{13}C$ NMR indicated that the desired Schiff bases have been obtained. This was reinforced by the appearance of the characteristic ν(C=N) infrared peaks and the disappearance of ν(C=O) and ν(N-H).

### Weight loss measurements

Table 1. Inhibition efficiencies for various concentrations of PII and PDI for corrosion of mild steel in 1 MHCl from weight loss measurements

| Inhibitor | Concentration (M) | Weight loss (g) | Inhibition efficiency, $\eta_w$ (%) |
|---|---|---|---|
| Blank | - | 0.0240 | - |
| PII | $1 \times 10^{-5}$ | 0.0211 | 11.9 |
| | $1 \times 10^{-4}$ | 0.0133 | 44.3 |
| | $1 \times 10^{-3}$ | 0.0065 | 72.6 |
| PDI | $1 \times 10^{-5}$ | 0.0095 | 60.4 |
| | $1 \times 10^{-4}$ | 0.0067 | 71.8 |
| | $1 \times 10^{-3}$ | 0.0036 | 85.0 |

The values of inhibition efficiency obtained from the weight loss method at different concentrations of inhibitors are summarized in Table 1. It is apparent that the inhibition efficiencies increased with inhibitor's concentration. At $1 \times 10^{-3}$ M concentration for PII and PDI, the inhibition efficiency values obtained are 72% and 85%, respectively. From the measurement, PDI was found to be the more effective inhibitor for mild steel in 1 M HCl.

### Impedance measurements

The Nyquist plots of mild steel in 1 M HCl in the presence and absence of PII and PDI are given in Fig. 2 (a) and (b). The impedance parameters are given in Table 2.

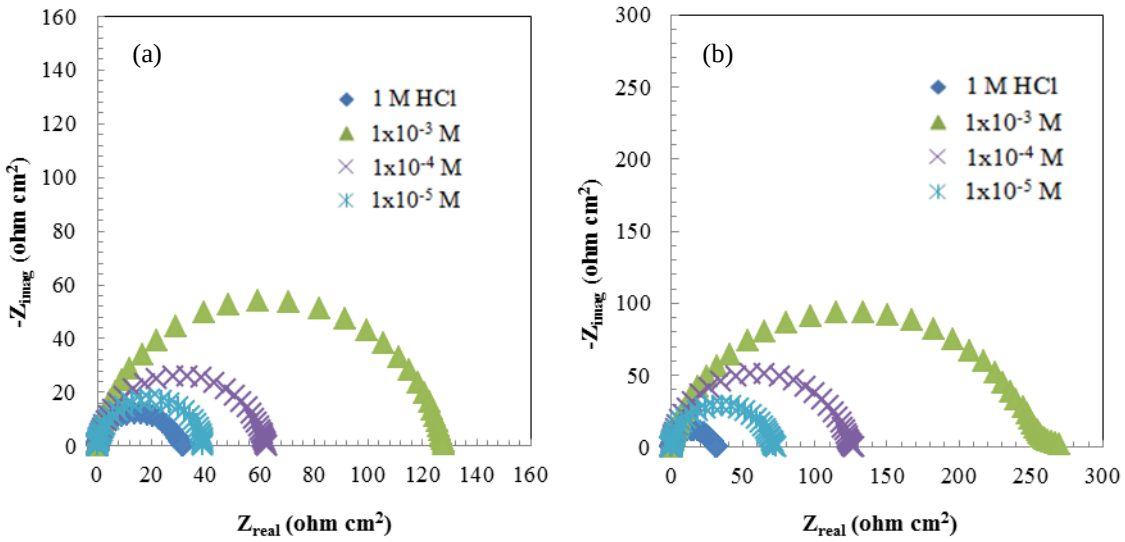



Fig. 2. Nyquist plot for mild steel in 1 M HCl in the presence and absence of different concentrations of (a) PII and (b) PDI.

The impedance response changed with the addition of organic additives. The presence of the two inhibitors enhanced the polarization resistance, $R_p$, in acidic solution and the effect was more pronounced with PDI that gave a maximum inhibition efficiency of 87.3%. The increase in polarization resistance by increase in inhibitor's concentration indicated the adsorption of inhibitor on metal surface to block the active sites and inhibits corrosion.

**Polarization measurements**

The Tafel plots of mild steel in 1 M HCl at various concentrations are shown in Fig. 3 (a) and (b), whereas the electrochemical parameters are summarized in Table 3.

From the plots, it can be interpreted that the addition of PII and PDI into the acidic media changed the anodic and cathodic slopes. The changes were more prominent in the anodic domain for PII making it an anodic type inhibitor. This result indicates that the compound was adsorbed on the anodic sites, hence inhibition occurred.

As for PDI, the addition of additive decreased both anodic and cathodic current densities and produced a small shift in the corrosion potential to more noble values. Thus these prominent changes suggested that it is a mixed type inhibitor.

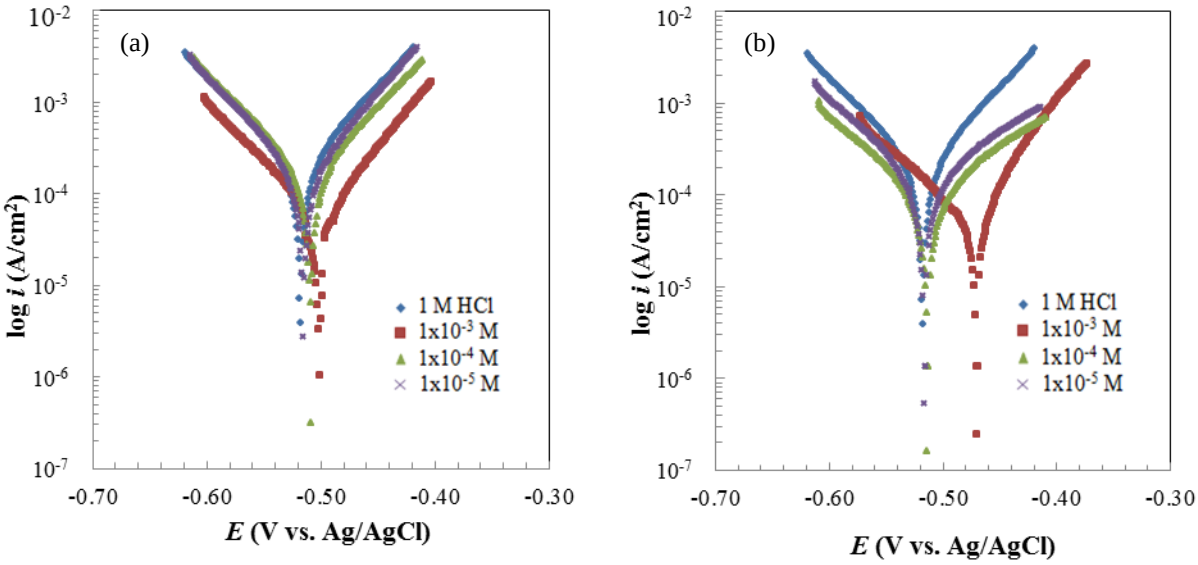



Fig. 3. Tafel plot for mild steel in 1 M HCl in the presence and absence of different concentrations of (a) PII and (b) PDI.

Table 2. Impedance parameters for mild steel electrode in 1 M HCl in the presence of different concentrations of PII and PDI

| Compound | Concentration,C (M) | Solution resistance, $R_s$ ($\Omega$ $cm^2$) | Polarization resistance, $R_p$ ($\Omega$ $cm^2$) | Inhibition efficiency (%) |
|---|---|---|---|---|
| PII | Blank 1 M HCl | 0.13 | 31.90 | - |
| | 1 x $10^{-5}$ M | 0.16 | 38.95 | 17.9 |
| | 1 x $10^{-4}$ M | 0.15 | 61.98 | 48.4 |
| | 1 x $10^{-3}$ M | 0.18 | 126.90 | 74.8 |
| PDI | Blank 1 M HCl | 0.13 | 31.90 | - |
| | 1 x $10^{-5}$ M | 0.19 | 72.60 | 56.1 |
| | 1 x $10^{-4}$ M | 0.17 | 125.70 | 74.6 |
| | 1 x $10^{-3}$M | 0.24 | 250.90 | 87.3 |

Table 3. Polarization parameters for mild steel electrode in 1 M HCl in the presence of different concentrations of PII and PDI

| Compound | Concentration (M) | $\beta_a$ (mV/dec) | ß$_c$ (mV/dec) | -$E_{corr}$ (mV) | $i_{corr}$ ($\mu A/cm^2$) | Polarization resistance, $R_p$ ($\Omega$ $cm^2$) | Inhibition efficiency (%) | Surface coverage (θ) |
|---|---|---|---|---|---|---|---|---|
| PII | Blank 1 M HCl | 83.0 | 91.1 | 518.0 | 235.0 | 47.9 | - | - |
| | 1 x $10^{-5}$ M | 78.5 | 85.5 | 520.0 | 191.0 | 59.3 | 19.2 | 0.23 |
| | 1 x $10^{-4}$ M | 65.3 | 70.3 | 509.0 | 143.0 | 82.5 | 41.9 | 0.37 |
| | 1 x $10^{-3}$ M | 73.3 | 86.0 | 501.0 | 68.6 | 215.2 | 77.7 | 0.69 |
| PDI | Blank 1 M HCl | 83.0 | 91.1 | 518.0 | 235.0 | 47.9 | - | - |
| | 1 x $10^{-5}$ M | 52.8 | 45.4 | 516.0 | 51.0 | 131.1 | 63.5 | 0.62 |
| | 1 x $10^{-4}$ M | 59.8 | 52.5 | 514.0 | 45.4 | 188.3 | 74.5 | 0.75 |
| | 1 x $10^{-3}$ M | 25.6 | 38.2 | 471.0 | 21.7 | 238.9 | 80.0 | 0.93 |

**Adsorption isotherm**

Adsorption isotherm can describe the adsorptive behavior of a corrosion inhibitor where it provides important information on the nature of the metal-inhibitor interaction. Several adsorption isotherms were tested for the description of adsorption behavior of studied compounds and it was found to obey the Langmuir adsorption isotherm. The surface coverage, θ, for various concentrations of the inhibitor was been calculated and the plot of C/θ vs. C yields straight lines as shown in Fig 4. Experimental results are in good agreement with Langmuir adsorption isotherm shown in Equation 1:

$$\frac{C_{inh}}{\theta} = \frac{1}{K_{ads}} + C_{inh} \quad (1)$$

where $C_{inh}$ is the inhibitor concentration and $K_{ads}$ is the adsorption equilibrium constant.

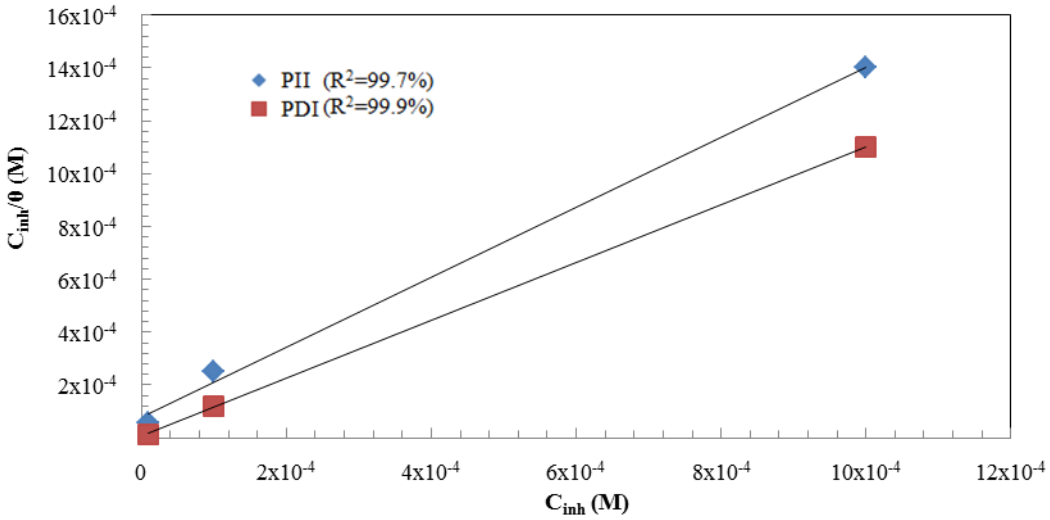



Fig. 4. Langmuir plots for PII and PDI on mild steel in 1 M HCl

The value of $K_{ads}$ is found as 12.5 x $10^3$ and 166.7 x $10^3$ $M^{-1}$for PII and PDI, respectively. The increasing value of $K_{ads}$ shows increasing adsorption capability of PDI on metal surface [7] due to its structure. The $K_{ads}$ is also related to the standard free energy of adsorption ($\Delta G_{ads}$) according to Equation 2:

$$K_{ads} = \frac{1}{55.5} \exp\left(\frac{-\Delta G_{ads}}{RT}\right) \quad (2)$$

where R is the universal gas constant (J $mol^{-1}$ $K^{-1}$), T the absolute temperature (K) and 55.5 the value for molar concentration of water in solution (mol $L^{-1}$).

The values obtained were -33.3 kJ/mol and -39.7 kJ/mol for PII and PDI, respectively. The decreasing value of $\Delta G_{ads}$ indicates the increasing adsorption capability and the negative values show spontaneous adsorption of inhibitor molecule on metal surface [4].

The differences in inhibition efficiencies between both compounds are caused by the different sizes of the organic compounds. It is apparent that PDI is larger due to the presence of two of heterocyclic isatin moieties. The introduction of the second π-electron system in PDI gives higher inhibition efficiency value. The inhibition of active dissolution of metal in acidic media is due to the adsorption of inhibitor on metal surface forming protective layers through electron transfer from adsorbed species to vacant orbitals of low energy in metal to form coordinate type link [4]. The more efficient adsorption of PDI compared to PII is attributed to the increase in electron density from the presence of N and O atoms, azomethine groups, heterocyclic and aromatic ring that form effective adsorption on the metal surface.

## Conclusion

Both Schiff bases, PII and PDI were successfully synthesized and characterized. Corrosion inhibition investigations showed that both compounds display inhibitor properties. However PDI promoted higher inhibition efficiency because it has a larger size that affected more surface coverage on mild steel and higher electron density that promoted efficient adsorption of the inhibitor on mild steel. The adsorption process obeys the Langmuir adsorption isotherm.

**Acknowledgement**

Gratitude is extended to the Research Management Institute for the Excellence Fund Scheme (600-RMI/ST/DANA 5/3/Dst 493/2011) and to the Faculty of Applied Sciences, UiTM for providing research facilities.

**References**

1. Ahamad, I., Prasad, R., Quraishi, M.A., (2010). Adsorption and inhibitive properties of some new Mannich bases of Isatin derivatives on corrosion of mild steel in acidic media. *Corrosion science*, 52: 1472-1481.
2. Mallaiya, K., Subramaniam, R., Srikandan, S. S., Gowri, S., Rajasekaran, N., Selvaraj, A., (2011). Electrochemical characterization of the protective film formed by the unsymmetrical Schiff's base on the mild steel surface in acid media. *Electrochimica Acta*, 56: 3857-3863
3. Emregul, K. C., Duzgun, E., Atakol, O., (2006). The application of some polydentate Schiff base compounds containing aminic nitrogens as corrosion inhibitors for mild steel in acidic media. *Corrosion Science*, 48: 3243-3260.
4. Kustu, C., Emregul, K. C., Atakol, O., (2007). Schiff bases of increasing complexity as mild steel corrosion inhibitors in 2 M HCl. *Corrosion Science*, 49: 2800-2814.
5. Qu, Q., Hao, Z., Li, L., Bai, W., Liu, Y. and Ding, Z., (2009). Synthesis and evaluation of Tris-hydroxymethyl-(2-hydroxybenzylidenamino)-methane as a corrosion inhibitor for cold rolled steel in hydrochloric acid. *Corrosion Science*, 51: 569-574.
6. Hosseini, M.G., Ehteshamzadeh, M. and Shahrabi, T., (2007). Protection of mild steel corrosion with Schiff bases in 0.5 M $H_2SO_4$ solution. *Electrochimica Acta*, 52: 3680-3685.
7. Lece, H., D., Emregul, K., C., Atakol, O., (2008). Difference in inhibitive effect of some Schiff base compounds containing oxygen, nitrogen and sulfur donors. *Corrosion Science*, 50: 1460-1468.

The Malaysian Journal of ANALYTICAL SCIENCES ISSN 1394-2506

# CADMIUM, CHROMIUM, COPPER, LEAD, FERUM AND ZINC LEVELS IN THE COCKLES (*Anadara granosa*) FROM KUALA SELANGOR, MALAYSIA

## (Tahap Kadmium, Kromium, Kuprum, Plumbum, Ferum dan Zink di dalam Kerang (*Anadara granosa*) dari Kuala Selangor, Malaysia)

Sabarina Md Yunus*, Zaini Hamzah, Nik Azlin Nik Ariffin, Mohd Busairi Muslim

*Faculty of Applied Sciences,*
*Universiti Teknologi MARA, 40450 Shah Alam, Selangor, Malaysia*

**Corresponding author: sabarina2020@salam.uitm.edu.my*

**Abstract**

The aim of this study is to provide information on the concentration of metals in cockles (*Anadara granosa*) from Kuala Selangor, Malaysia. Cockles in this study area were taken by local people as part of their diet, therefore necessary to determine metal concentrations in the cockles. Sample collection activity was conducted at Kuala Selangor (03°20'N - 101°15'E) between the month of March, and April 2012. About two kilograms of samples were purchased from local fish market at Kuala Selangor. The concentration of Cd, Cr, Cu, Pb, Fe and Zn in the samples were analysed using Inductively Coupled Plasma Optical Emission (ICP-OES). The observed mean concentration of Cd, Cr, Cu, Pb, Fe and Zn is 1.48 ± 0.33, 1.43 ± 0.91, 15.78 ± 5.28, 1.11 ± 0.46, 875.55 ± 343.43 and 94.17 ± 7.91 mg/kg respectively. From the public health point of view, these metal concentrations were below the maximum permissible levels set by the Malaysian Food Act (1983) and Regulations (1985). Therefore, cockles from Kuala Selangor are safe for human consumption.

**Keywords**: Kuala Selangor, Heavy Metals, *Anadara granosa*, ICP-OES

**Abstrak**

Tujuan kajian ini dijalankan, adalah untuk memberi maklumat terhadap kepekatan logam berat di dalam kerang di Kuala Selangor, Malaysia. Kerang di kawasan ini telah digunakan oleh penduduk setempat sebagai sebahagian daripada makanan mereka. Oleh itu, adalah perlu untuk menentukan kepekatan logam berat di dalam kerang. Aktiviti persampelan dijalankan di Kuala Selangor diantara bulan Mac dan April 2012.Sebanyak dua kilogram sampel telah dibeli daripada penjual di pasar tempatan di Kuala Selangor. Kepekatan Cd, Cr, Cu, Pb, Fe dan Zn di dalam sampel telah dianalisis dengan menggunakan kaedah Spektrometer Plasma Gandingan Aruhan Pancaran Optik (ICP-OES). Purata kepekatan yang didapati bagi Cd, Cr, Cu, Pb, Fe dan Zn adalah1.48 ± 0.33, 1.43 ± 0.91, 15.78 ± 5.28, 1.11 ± 0.46, 875.55 ± 343.43 dan 94.17 ± 7.91 mg/kg masing-masing. Dari pandangan sudut kesihatan untuk orang awam, kepekatan logam berat adalah di bawah tahap bahaya yang telah ditentukan oleh Akta Makanan Malaysia (1983) dan Peraturan (1985). Oleh itu, kerang dari Kuala Selangor adalah selamat untuk di makan.

**Kata kunci**: Kuala Selangor, Logam Berat, *Anadaragranosa*, ICP-OES

## Introduction

*Anadara granosa* is a major cockle species and important protein source in Southeast Asia that is commercially cultured in the tidal mudflats along the western coast of Peninsular Malaysia. This cockle is a good revenue source for the local population [1]. An investigation of global contaminant patterns in this oceanic organism is required, especially for this region of Malaysia. Kuala Selangor is a coastal town about 70 km away from Kuala Lumpur, perched next to a large river mouth that feeds into the sea. Hence, its name means 'Confluence of the Selangor River'. Once Kuala Selangor was the centre for a tin mining industry that helped defines the early history of Malaysia. For this reason, Kuala Selangor was chosen as a study area. The location is shown in Figure 1 below.

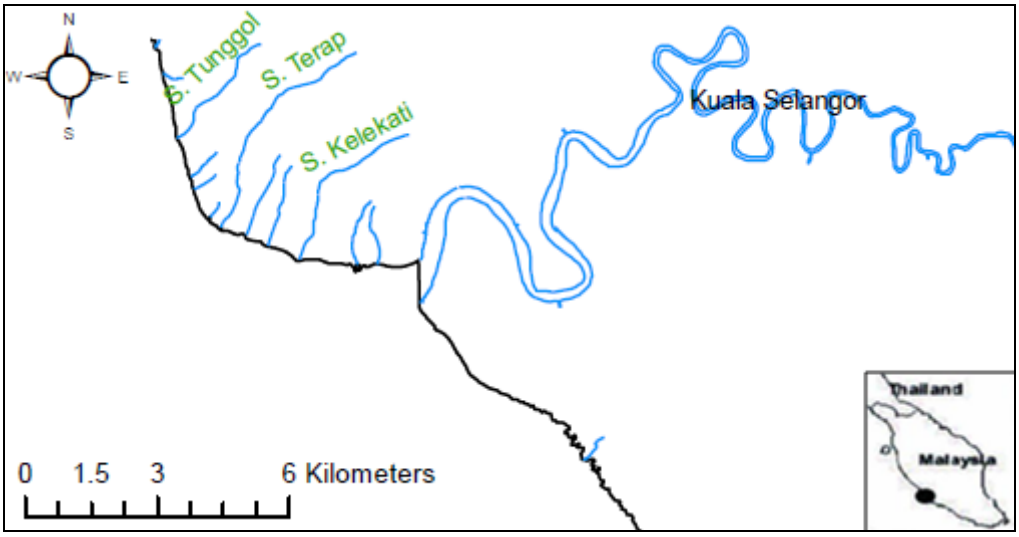



Figure 1. Location of study area

Heavy metal is defined as metallic chemical element that has a relatively high density and is toxic even at low concentrations. The common heavy metals that can be found in the cockles are Pb and Cd [2]. The presence of these heavy metals in the environment, especially aquatic ecosystems, could lead to health problems if being consumed by living organisms such cockles over a long period of time. The metals in the aquatic biota such as cockles are in constant interaction with the metals in the surface water, suspended matter, sediment and the interstitial water [3]. The data from this study will be used as a reference for future research on determination of source of heavy metals in cockle from Kuala Selangor (03°20'N - 101°15'E).

## Materials and Methods

### Sample Collection

Sample collection was conducted at Kuala Selangor between the months of March - April 2012. Two kilograms of samples were purchased from local fisherman, and were kept in a refrigerator at temperature below 4$^{o}$C to reduce all the activities and metabolism of the organism in the water.

### Sample Preparation

The cockles were grouped into four ranges of sizes (A, B, C and D). Sample A with size range below 25 mm, sample B with size range from 25 to 30 mm, sample C with size 30 to 40 mm and sample D for size greater than 40 mm. Total of 20 similar size samples were separated from all cockles samples. Prior to analysis, cockle samples were cleaned with running tap water to remove the sand particles. Cockles' tissues were separated from the shell and washed with deionised water [4]. All the samples were made in triplicate and kept in oven at 60 $^{o}$C until a constant weight was obtained [5].

### Sample analysis

A constant weight of 0.5 g dried tissue was weighed and transferred to the beaker for acid digestion process. Blanks was digested in beakers containing 8 mL of concentrated $HNO_3$ (65 % A.R. Grade) overnight digestion. After digestion was complete, the solution was cooled at room temperature then the solution was filtered using cellulose filter paper (0.45 µm). Deionised water was added until it reached 100 mL mark of volumetric flask. This solution was stored in plastic bottles at temperature 4°C until analysis was performed to determine the contents of heavy metals (Cu, Fe, Zn, Cd, Cr, and Pb) in the sample. The working standard solutions are from 0.05 to 5 ppm. Then, the heavy metal concentrations in cockles were determined by using ICP-OES.

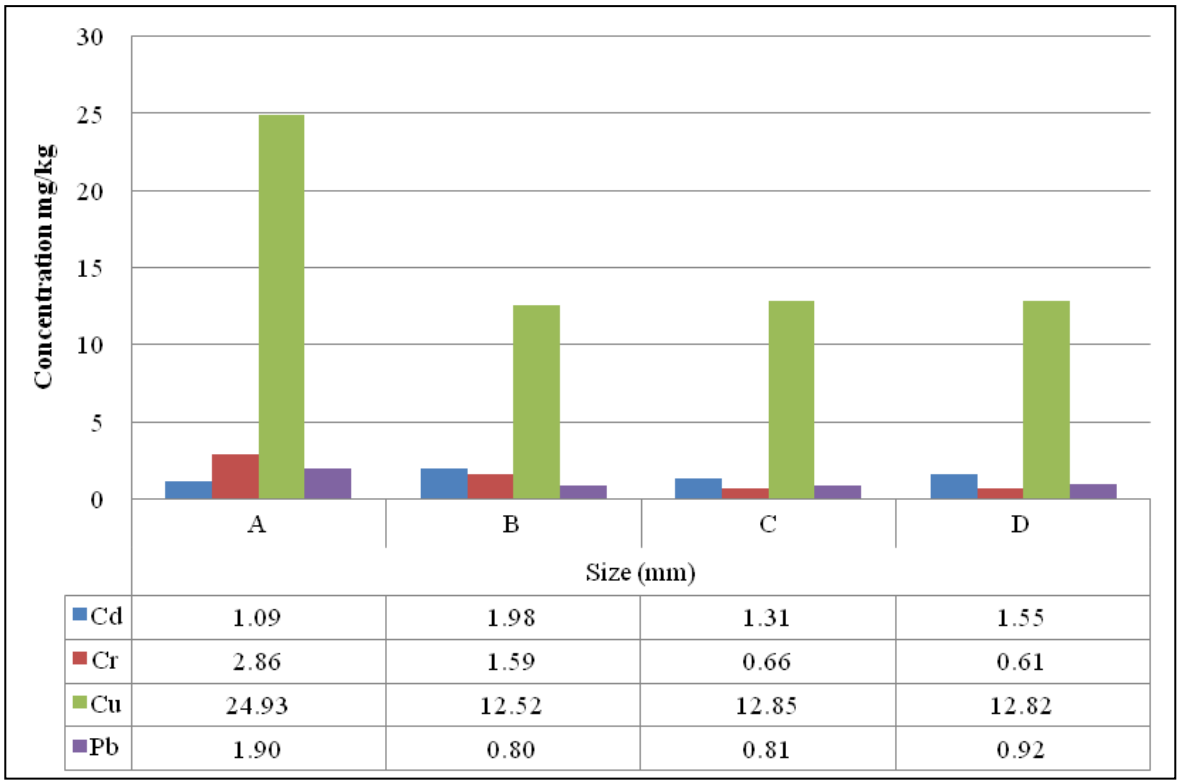
## Results and Discussion

### Heavy metals contents

Sizes of 4 samples that were analysed in this study are shown in Table 1. The concentration of metals in the cockles is summarized in Figure 1. Knowledge on the living habitats is very important as it may represent the basis for the accumulation of heavy metals and other trace metals in bivalves.

Table 1. List of samples blood cockle (*Anadara granosa*) with narrow range of weight and length

| Sample | Length (mm) | Width (mm) |
|---|---|---|
| A | 21.1 - 24.6 | 15.0 – 18.3 |
| B | 23.1 – 27.9 | 18.2 – 20.8 |
| C | 34.0 – 38.5 | 21.5 – 28.9 |
| D | 33.0 – 39.5 | 25.0 – 31.0 |
| E | 40.0 – 49.0 | 29.0 – 38.0 |




| | A | B | C | D |
|---|---|---|---|---|
| Cd | 1.09 | 1.98 | 1.31 | 1.55 |
| Cr | 2.86 | 1.59 | 0.66 | 0.61 |
| Cu | 24.93 | 12.52 | 12.85 | 12.82 |
| Pb | 1.90 | 0.80 | 0.81 | 0.92 |

Figure 2. Concentration of Cd, Cr, Cu and Zn in cockles

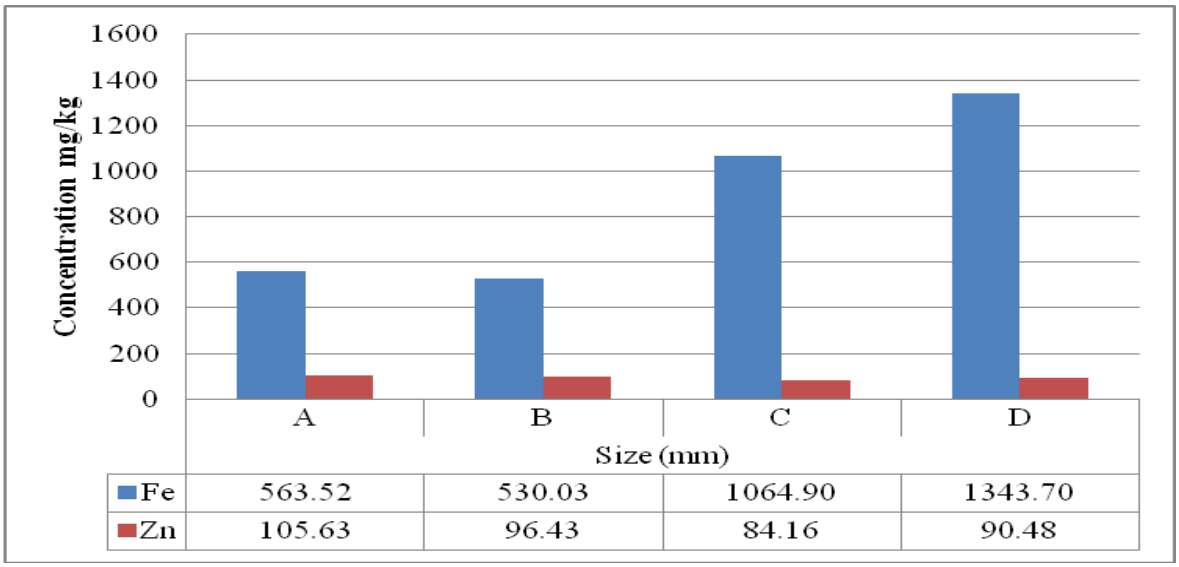



Figure 3. Concentration of Fe and Zn in cockles

**Cadmium**

Concentrations of Cd in this study are 1.09, 1.98, 1.31 and 1.55 mg/kg for samples A, B, C and D, respectively. The average concentration of Cd in all samples is 1.48 ± 0.38 mg/kg. The highest concentration of Cd was found in sample size between 25 to 30 mm with concentration of 1.98 mg/kg. The lowest concentration of Cd in this study is in sample size less than 25 mm or sample A, with concentration 1.09 ± 0.19 mg/kg. All samples were exceeding the permissible level set by Malaysian Food Act 1983and Regulation 1985 and FAO/ WHO 2004. The limit for Cd set by Malaysian Food Act 1983 and Regulation 1985 is 1.00 mg/kg and for WHO/FAO is 0.05 mg/kg.

Table 3 shows the comparison concentration of heavy metals in blood cockles from previous study. The concentration of Cd from previous study was range from 0.20 to 6.90 mg/kg [4, 6, 7, 8]. The highest reported concentration of heavy metal in blood cockles in the range of 8.25 - 12.20 mg/kg was reported by [4 and 9]. In this study the concentration of Cd in blood cockle is almost the same with others researcher [2, 6, 7, 8].

Figure 2 shows distribution of Cd in cockles' sample. The concentration of Cd is the highest due to the ability of Cd that can accumulate in shellfish in the form of Cd binding peptides [9]. Human activities may contribute to the higher level of Cd in the cockles. Cockles' aquaculture area is located near estuaries which receive sewage and waste deposits from the mainland [4]. Cd is present in rock and soil along with other metals.

**Chromium**

The concentration of Cr in sample A, B C and D is 2.86, 1.59, 0.66 and 0.61 mg/kg respectively. The average concentration of Cr in blood cockle is 1.43± 1.05 mg/kg. The highest concentration of Cr in this study is in sample A or sample length below 25 mm, the concentration is 2.86 mg/kg. The lowest concentration of Cr in blood cockles in sample D or sample size 30 to 40 mm, with concentration of Cr is 0.61 mg/kg. The concentration of Cr is decreasing with an increasing of blood cockle size. Malaysian Food Act 1983 and Regulation 1985 and WHO/FAO 2004 did not set any limit for Cr in bivalves. However, IAEA – 407 was reported that a permitted level for Cr in the marine organism is 0.73 mg/kg base on this permitted limit level all the samples were higher from the permissible level. Even though Cr level is slightly higher from limit set by IAEA-407, it still safe to consume.

Concentration found in this study is lower from other reported research [2,4 and 8]. The range of Cr in previous study is 0.18 to 9.80 mg/kg [2, 4, and 8]. The highest of Cr was found is 4.25 to 9.80 mg/kg. The highest

concentration of Cr in Kuala Selangor might come from fertilizer from agriculture industry, emission from motor vehicle, steam generation power plant and from basic steel work foundries. All these industries are located near to Kuala Selangor region.

**Copper**

The concentration of Cu in cockles is 24.93, 12.52, 12.85 and 12.82 mg/kg for sample A, B, C and D respectively. The average concentrations of Cu in all blood cockle samples are 15.78 $\pm$ 6.10 mg/kg. The highest concentration of Cu in blood cockles in sample with length below 25 mm or sample A with concentration 24.93 mg/kg. While the lowest concentration of Cu in blood cockles is in sample size 25 to 30 mm or sample B with concentration 12.52 mg/kg. The entire sample is below the permitted level set by Malaysian Food Act 1983 and Regulation 1985 and WHO/FAO. The Cu concentration limit set by Malaysian Food Act 1983 and Regulation 1985 and WHO/FAO is 10 and 30 mg/kg respectively.

In this study the concentration of Cu is in the range of 8.48 - 24.93 mg/kg. The concentration of Cu in this study is higher compared to the others reported results [7, 8, 10-12]. Most of the researchers reported the range of Cu is 2.44 – 16.28 mg/kg [7, 8, 10-12]. The higher concentrations of Cu in Kuala Selangor samples might probably due to existing activities such as loading and offloading of fishes, cleaning and maintenance of boats, antifouling paint applications, and fuelling the crafts. Figure 1 shows distribution of Cu in cockle soft tissue.

**Lead**

The concentrations of Pb in cockles are 1.90, 0.80, 0.81 and 0.92 mg/kg for sample A, B, C and D respectively. The average concentrations of Pb in all cockles sample are 1.11 $\pm$ 0.53 mg/kg. The highest concentration of Pb is in sample A or shell length less than 25 mm, with concentration 1.90 mg/kg, while the lowest concentration of Pb in blood cockle is in sample B or shell length between 25 to 30 m, with concentration 0.80 mg/kg. The permitted concentration of Pb set in the Malaysian Food Act (1983) and Regulation (1985) is 2 mg/kg while WHO/FAO (2004) is 1.5 mg/kg. Only sample A exceed the permitted level set by WHO/FAO 2004, others sample is within the limit set by the WHO/FAO 2004. The results of this study show all sample have concentration of Pb below the concentration limit set by the Malaysian Food Act 1985. All samples are safely to consume because the range of Pb concentration in the cockles below the permitted limit set by Malaysian government.

The concentration of Pb in this study is in the range of 0.80 - 1.90 mg/kg. Most of the researchers found the concentration of Pb in cockles' soft tissue were ranged from 9 to 18.55 mg/kg [7, 8, 10-12]. Although blood cockle tissues have relatively low Pb contents, their Pb compositions reflect mixing of natural Pb with modern anthropogenic Pb emission sources (high Pb level in sediment). These emission sources include unleaded automotive gasoline, diesel fuel and leaded aviation gasoline [13]. Figure 3 shows the distribution of Pb in blood cockle soft tissue.

**Ferum**

Fe is the highest concentration that contain in cockles. The concentration of Fe in cockles' soft tissue in sample A, B, C and D are 563.52, 530.03, 1064.90 and 1343.70 mg/kg respectively. The average concentration of Fe in all samples is 875.55 $\pm$ 396.55 mg/kg. The highest concentration of Fe in blood cockles is 1343.70 mg/kg in sample D or sample size greater than 40 mm. The lowest concentration of Fe is 530.03 mg/kg in sample B or sample size 25 – 30 mm. Figure 2 shows the distribution of Fe concentration in cockles' samples vary with length shell size. The trends accumulation of Fe in blood cockles vary with shell length. From this graph, the trend of the Fe accumulation is higher at sample with length greater than 40 mm. the trend shows the increasing of Fe concentration with increasing of blood cockles sample length. The highest concentrations of Fe in cockles' were found at Kuala Selangor also may be related to human activities. Other factors that may contribute heavy metals into the Sungai Selangor including mining activities in the downstream rivers, oil palm and some residential areas located along the river [14].

**Zinc**

In this study the concentration of Zn in soft tissue of cockles' are 105.63, 96.43, 84.16 and 90.48 mg/kg for sample A, B, C and D respectively. The average concentrations of Zn in all cockles' samples are 94.17 + 9.13 mg/kg. The

highest concentration of Zn is in sample size below than 25 mm or sample A with concentration 105.63 mg/kg. The lowest concentration of Zn in the sample of blood cockles is in sample size 30 to 40 mm or sample C is 84.16 mg/kg.

From this study, the concentration of Zn in all cockles' samples was below the permitted level set by Malaysian Food Act (1983) and Regulation (1985) and WHO/FAO2004. The allowable limit for Zn is 100 mg/kg for Malaysian Food Act1983 and Regulation 1985 and WHO/FAO 2004. All samples are safe to consume by consumer because the level of Zn is below the allowable limits. Figure 5 shows the distribution of Zn concentration in the blood cockle samples.

The concentration of Zn in blood cockles is only having slightly different from one to another researcher. Most of the researcher found that Zn concentration in blood cockles is over the limit set by the Malaysian Food Act (1985) and WHO/FAO, (2004) [10, 4, 8]. From this study shows that *Anadara granosa* was also well documented that organisms tend to accumulate light metals such as Zn, Cu and Fe in higher concentration in their tissue than the heavy metals such as Pb, Cd and Hg due to their significant role as a precursors in various enzymatic reactions. Similar results were reflected in this study where the bioaccumulation of Zn and Cu was multifold higher in the sample tissue than Pb accumulation [10].

**Size-metal relationships**

The highest concentrations of heavy metals were found in the cockles' with less shell length. Relationships between shell length of the two bivalve species and the concentration of heavy meals can be noticed that, all metals have negative correlations with shell-length. These inverse relationships can be attributed to different reasons: a) variation in the uptake and excretion rates of metals between small and large animals, b) small animals have ability to eat more than the large one which Pb accumulate pollutant in its body, c) dilution of the pollutant in the tissues of the large animals. Heavy metal levels considerably vary among individuals of the same species. The lower age of same species accumulated more heavy metal. Higher concentration of heavy metals were found in younger blood cockle and this reflects the short residence time of these metals within the blood cockle, combined with the higher rate of metabolism compared to older organism [14]. Accumulation of heavy metal levels in soft tissue of *Anadara granosa* from Kuala Selangor in this following order of abundance Fe> Zn> Cu> Cr>Pb> Cd. Figure 2 show the distribution of heavy metal in all samples of cockles.

**Safe Rate Intake**

The ingestion rate of cockle based on the mean value for Malay, Chinese and Indian ethnicities in Peninsular Malaysia are 5.36, 3.10 and 3.61 g/day, respectively [15]. Average Daily Intake (EDI) for an adult of 70kg (µg/kg body weight) of all metals in this studied is shown in Table 2. The entire sample in this study is safe to consume by all major races in Malaysia.

Table 2. The Estimated Daily Intake (EDI) for Cockles

| Elements | PTDI[a] | Malay | Chinese | India |
|---|---|---|---|---|
| **Cd** | 70 | 7.94 | 4.59 | 5.35 |
| **Cr** | - | 7.67 | 4.43 | 5.16 |
| **Cu** | 35 000 | 84.57 | 48.91 | 56.96 |
| **Pb** | 250 | 5.94 | 3.44 | 4.00 |
| **Fe** | 56 000 | 4692.3 | 2714.19 | 3160.72 |
| **Zn** | 70 000 | 339.97 | 291.94 | 339.97 |

PTDI[a] : Permissible tolerable daily intake (ug/daily/70 kg body weight)

Table 3. Concentration range of Heavy Metals in Cockles

| Studies | Concentration Range | | | | | | |
|---|---|---|---|---|---|---|---|
| | **Locations** | **Cd** | **Cr** | **Cu** | **Fe** | **Pb** | **Zn** |
| **Present Study** | Kuala Selangor | 1.09-1.98 | 0.61-2.86 | 12.52 24.93 | 530.03-1343.70 | 0.80 - 1.90 | 84.16 - 105.63 |
| **Alina et al ., 2012** | Straits of Malacca | 0.25-0.47 | - | - | - | 0.19-0.28 | - |
| **Zahir et al., 2011** | Kuah | - | - | 9.75 - 14.95 | - | 1.23-2.23 | 99.75-121.75 |
| | Kuala Triang | - | - | 5.22 - 8.22 | - | 0.02-0.01 | 46.81-77.51 |
| | Pantai Kok | - | - | 7.42 - 9.70 | - | 0.03 - 0.05 | 71.88 - 88.12 |
| **Koh et al.,2008** | Kuala Juru | 3.60 -8.25 | 5.50 - 8.97 | 10.19 - 16.28 | 641.5 -1350 | 6.1 - 18.55 | 103.60 - 201.70 |
| | Kuala Sepetang | 1.25 -5.50 | 4.25 - 9.80 | 3.97 - 13.6 | 421.0 - 822.5 | 13.55 - 20.75 | 72.15 - 89.40 |
| | Kuala Selangor | 9.95 -12.20 | 6.74 - 9.08 | 2.44 - 6.59 | 686.50 - 878.50 | 4.1 -8.15 | 110.95 - 139.65 |
| **Yap et al.,2008** | Jeram, Kuala Juru and Kuala Kurau | 1.3 -9.44 | - | 5.41 – 7.39 | 455.91 - 1125.50 | - | 91.90 - 23.50 |
| **Mat & Maah, 2004** | Kuala Selangor | 4.66 -9.20 | | 2.20 - 4.60 | | 7.20 - 9.60 | 35.00 - 93.00 |
| | Batu Kawan | 1.40-2.80 | | 3.7 0-5.30 | | 2.10 - 3.70 | 50.20 - 61.80 |
| **Noordin Ibrahim, 1995** | Kuala Juru | - | 2.20 - 7.20 | - | 1426 -2075 | - | 185 -236 |
| **David & Kosol, 1985** | Thailand | 1.33 -6.47 | 0.18 - 0.56 | 4.89 - 8.75 | - | 0.37 - 1.41 | 65 -117.6 |

## Conclusion

From this study, the results showed different sizes of soft tissues of *Anadara granosa* accumulated different levels of metals. The results of the shells showed the following order of abundance Fe> Zn> Cu> Cr > Pb > Cd. All the results were below the limits for blood cockle proposed by Malaysian Food Act 1983 and Regulation 1985. In this study shows that blood cockles with less shell length has more concentration of heavy metal compare from blood cockle has longer shell length. According from this results, blood cockle were within the limit for human consumption. Mean metal concentration were found to be higher in blood cockle have smaller shell length than those in blood cockle that have longer shell length. In this study also proved the limited ability of *Anadara granosa* in accumulating various heavy metals from its habitat in different rates. Nevertheless, high concentration of metals in surrounding sediment might partially from anthropogenic activities which would reflect in metal levels in aquatic

organisms especially bivalves. Although level of heavy metal is not high, potential dangers emerge in future depending on the industrial wastewaters and domestic activities in this region.

**Acknowledgement**

This study has been funded by Research Intensive Faculty Grants 600-RMI/DANA 5/3RIF (3/2012). Authors are also thankful to Faculty of Applied Sciences, UiTM and local people at Kuala Selangor for valuable assistance during sampling and analysis.

**References**

1. Sofia, (2005). Metal contamination in commercially important fish and shrimp species collected from Aceh (Indonesia), Penang and Perak (Malaysia). (Unpublished Master's thesis), University Sains Malaysia
2. Noorddin Ibrahim (1994). Trace element content of Malaysian cockles (Anadara granosa). *Food Chemistry*, 54; 133 - 135.
3. Yap, C.K., Hatta, Y., Edward, F.B. and Tan, S.G. (2008). Comparison of heavy metal concentrations (Cd, Cu, Fe, Ni and Zn) in the shells and different soft tissues of Anadara granosa collected from Jeram, Kuala Juru and Kuala Kurau, Peninsular Malaysia. *Pertanika Journal of Tropical Agricultural Science*, 31(2); 205-215.
4. Koh, S. M., Koh P. K., Sim. K. T., Lee, Y. H., and Surif, S. (2011). Proximate Analysis and Heavy Metal Concentrations of Tissues of Cockles (Anadara granosa) from Several Cockle Farms in Peninsular Malaysia. *Sains Malaysiana* 40(2); 139–146.
5. Kamaruzzaman, B.Y., Ong, M.C. and Khali, A.H., (2007). Mercury Concentration of four Dominant Species in Bebar peat swampy forest river Malaysia. Pakistan. *Journal of Biological Science*, 10, 1103-1107.
6. Alina, M., Azrina, A., Mohd Yunus, A.S., Mohd Zakiuddin, S., Mohd Izuan Effendi, H. and Muhammad Rizal, R., (2012). Heavy Metals (mercury, arsenic, cadmium, plumbum) in selected marine fish and shellfish along the Straits of Malacca. *International Food Research*, 19(1), 135-140.
7. Mat, I. and Maah, M.J., (1994). An assessment of trace metal pollution in the mud flats of Kuala Selangor and Batu Kawan, Malaysia. *Marine Pollution Bulletin*, 28(8); 512-514.
8. David, J.H., P and Kosol, M., (1985). Trace metals in bivalve mollusks from Thailand. *Marine Environmental Research*, 15(3); 215-234.
9. Kerdthep, P., Tongyonk, L., and Rojanapantip, L., (2009). Concentrations of Cadmium and Arsenic in Seafood from Muang District, Rayong Province. *Journal Health Research*, 23(4); 179-184.
10. Zahir, M. S. M., Kamaruzzaman, B. Y., John, B. A., Shahbudin, S., and Goddard, J. S., (2011). Bioaccumulation of Selected Metals in the Blood Cockle (Anadara granosa ) from Langkawi Island , Malaysia. *Oriental Journal of Chemistry*, 27 (3); 979-984.
11. Koh, S. M., Koh P. K., Sim. K. T., Lee, Y. H., and Surif, S. (2010). Proximate Analysis and Heavy Metal Concentrations of Tissues of Cockles (Anadara granosa) from Several Cockle Farms in Peninsular Malaysia. *Sains Malaysiana* 40(2); 139–146.
12. Abdullah, M.H., Sidi, J. and Aris, A.Z. (2007). Heavy metals (Cd, Cu, Cr, Pb and Zn) in Meretrix, meretrix Roding, water & sediments from estuaries in Sabah, North Borneo. *International Journal of Environmental and Science Education*, 2; 69-74
13. Sharifah N.R., (2006). Penilaian pencemaran logam berat dalam kerang, Anadara granosa L. dari pantai barat Semenajung Malaysia. (Unpublished master's thesis). Universiti Kebangsaan Malaysia.
14. Zhang, Z., He, L., Li, J., and Wu, Z.-bin. (2007). Analysis of Heavy Metals of Muscle and Intestine Tissue in Fish in Banan Section of Chongqing from Three Gorges Reservoir. China. *Polish Journal of Environment study*, 16(6); 949-958.
15. Ministry of Health Malaysia, (2003). Food consumption statistics of Malaysia 2003 for adult population aged 18 to 59 years. In: Research Report No. KKM/2000/2006 of Family Health Development Division and Food Safety and Quality Division, Putrajaya, Malaysia

The Malaysian Journal of ANALYTICAL SCIENCES ISSN 1394-2506

# SYNTHESIS OF NANOCRYSTALLINE OLIVINE $LiNiPO_4$ POWDER PREPARED BY SOL-GEL METHOD: THERMAL ANALYSIS AND XRD STUDIES

## (Penyediaan Serbuk Nanokristal $LiNiPO_4$ dengan Struktur Olivin Melalui Kaedah Sol-Gel: Analisis Terma dan Kajian XRD)

Azlin Sanusi[1,2,3]*, Shanti Navaratnam[2,3], Wan Jeffrey Basirun[4]

[1]*INTEC Education College,*
*Jalan Senangin Satu 17/2A, Seksyen 17, 40200 Shah Alam, Selangor, Malaysia*
[2]*Faculty of Applied Sciences,*
[3]*Institue of Science,*
*Universiti Teknologi Mara,40450 Shah Alam , Selangor Malaysia*
[4]*Chemistry Department, Faculty of Science,*
*University of Malaya,50732 Kuala Lumpur, Malaysia*

**Corresponding author: azlin457@salam.uitm.edu.my*

**Abstract**

$LiMPO_4$ have attracted much attention as potential cathode material as it does not liberate oxygen on decomposition unlike lithium transition metal oxides (LMO). In this work, $LiNiPO_4$ powder was prepared by sol gel method using LiOH, $Ni(CH_3COO)_2$, $NH_4H_2(PO_4)$ and tartaric acid as chelating agent .The precursor powders were studied by thermogravimetric analysis (TGA). Based on the TGA results, the sample was calcined at $1000^oC$ in air. The TGA/DTGA studies have been employed to analyse the reaction of raw materials during the formation of $LiNiPO_4$ .The formation mechanism for the synthesis of $LiNiPO_4$ and the overall decomposition equation for the precursor were proposed from the TGA/DTGA analysis. The calculated total weight loss from the overall proposed decomposition process which is 66.4% shows agreement with the percentage weight loss from the TGA curves which is 68%. The X-ray diffraction analysis was carried out to confirm the formation of $LiNiPO_4$. The precursors and the calcined powders were characterized by X-ray diffraction (XRD). Analysis of the synthesized $LiNiPO_4$ using XRD demonstrated the formation of a pure $LiNiPO_4$ phase powder.

**Keywords**: lithium nickel phosphate, sol-gel, mechanism

**Abstrak**

$LiMPO_4$ telah menarik banyak minat terhadap potensinya sebagai bahah katod untuk bateri litium. kerana tidak seperti litium oksida logam peralihan (LMO) bahan ini tidak melepaskan oksigen ketika proses penguraian. Didalam kajian ini $LiNiPO_4$ telah disintisis dengan mencampurkan LiOH, $Ni(CH_3COO)_2$, $NH_4H_2(PO_4)$ dan asid tartarik dengan menggunakan kaedah sol-gel. Analisis TGA telah dilakukan keatas prapenanda $LiNiPO_4$ untuk menetukan suhu pembakaran dan didapati suhu yang sesuai adalah $1000^0C$. Unjuran persamaan bagi penguraian prapenanda $LiNiPO_4$ telah diperolehi dengan menggunakan lekok TGA/DTGA. Pengiraan peratus penurunan berat menggunakan persamaan unjuran (66.4%) dan lekok TGA (68%) adalah hampir sama. Spektrum belauan sinar –X (XRD) menunjukkan bahan sampel $LiNiPO_4$ adalah tulin.

**Kata kunci**: litium nikel fosfat, kaedah sol-gel, mekanisme

## Introduction

In recent years, lithium metal phosphate ($LiMPO_4$) with the olivine structure has received a lot of attention to be a potential candidate for cathode materials in lithium ion batteries [1-4]. Unlike lithium transition metal oxides (LMO), $LiMPO_4$ does not liberate oxygen on decomposition. In addition, $LiMPO_4$ is cheaper, benign, and environmentally friendly and has greater stability than LMO. Various methods have been used to synthesize $LiMPO_4$ cathode material such as solid-state [1], sol-gel [2-4], hydrothermal [5-7] and aqueous precipitation [8].

Many of the sol-gel method reported used citric acid as chelating agent and argon or nitrogen ambient during calcinations of precursor powders.

This paper reports the synthesis and characterization of $LiNiPO_4$ (lithium nickel phosphate) which belongs to the olivine structure. In this work, $LiNiPO_4$ was prepared by the sol-gel method with tartaric acid and calcined in air. Sol-gel has considerable advantages of good mixing of the starting materials and good chemical homogeneity of the product. To the best of our knowledge, reports on $LiMnPO_4$ nanocrystalline structured powders prepared by tartaric acid and calcined in air are rare.

The resulting $LiNiPO_4$ powders obtained were then characterized by thermogravimetric analysis (TGA),) and X-ray diffraction (XRD). The formation mechanism for the synthesis of $LiNiPO_4$ are also discussed in this paper.

## Materials and Methods

### Sample preparation

Stoichiometric amounts of lithium hydroxide ($LiOH.H_2O$, Ajax), nickel acetate ($Ni(CH_3COO)_2 .4H_2O$, Ajax) and ammonium dihydrogen phosphate $NH_4H_2PO_4$(AR grade) were weighed and dissolved in distilled and deionised water separately with 1:1:1 mole ratio. The aqueous solutions were mixed together and stirred constantly. A 1.0 M tartaric acid solution was slowly added to the mixture as the chelating agent. Ammonium hydroxide was added carefully into the mixture until a pH value of 5-7 was achieved. The mixtures were mixed and stirred thoroughly until a greenish gel was obtained. The gels were left for drying in an oven at $60^0$C for 3 days.

### Characterization of sample synthesized

Thermogravimetric analysis (TGA) and differential thernogravimetric analysis (DTGA) analysis of the $LiNiPO_4$ powders were performed in order to examine the thermal decomposition behaviour of the gel precursor. The heating rate was $10^0$C $min^{-1}$and the precursor was heated at $30^0$C-$1000^0$C in nitrogen atmosphere.

The structure and phase of the product was identified by X-ray powder diffraction (XRD) analysis. The measurements were made with Siemens D5000 X-ray diffractometer with CuKα radiation at room temperature.

## Results and Discussion

The TGA/DTGA analysis of the greenish gel obtained in this work is shown in Fig 1. The TGA thermogram of the precursors revealed that there are four significant weight loss regions as shown in Figure 1. A weight loss about 1.1 % ocurred slowly as the temperature was increased to about 150 $^o$C, due to the evaporation of residual water which are still present in the sample. Rapid weight loss occurred around the temperature range between 150 $^o$C -275 $^o$C and is associated with a 34.1 % weight loss. The decomposition process is attributed to the decomposition of unreacted ammonium dihydrogen phosphate as it was one of the reactant materials in the sample. The removal of tartaric acid is also assigned to this region. The weight loss is also due to the decomposition of the Li-Ni acetate gel formed in the experiment. The decomposition process of the precursor is also accompanied by a sharp peak at about 237 $^o$C as seen on the DTGA thermogram in Figure 1. The peak is probably due to the decomposition of ammonium dihydrogen phosphate which is an endothermic process.

The third weight loss occurred at the temperature range from 275 to 325 $^o$C. This decomposition was associated with a weight loss of 8.8 % and can be attributed to the burning out of organic residues which resulted from the Li-Ni acetate complex decomposition. The final decomposition step which is associated with 23.9 % weight loss occurred in the temperature range from 325 $^o$C to 725 $^o$C. The weight loss is attributed to the decomposition of nickel acetate and lithium hydroxide. Nickel acetate steadily decomposed in the temperature range from 272 $^o$C to 400 $^o$C .

The DTGA thermogram reveals a sharp peak at 354 $^o$C indicating the rapid decomposition of nickel acetate. The weight is constant after 725 $^o$C indicating that no heat is used for evaporation or decomposition processes and that $LiNiPO_4$ can be obtained by firing the precursor at temperatures above 750 $^o$C. The tartaric acid is likely to act as a fuel in the pyrolysis and expedite the process of decomposition of acetate ions .The corresponding weight loss, temperature ranges and their assignment are summarized in Table 1.

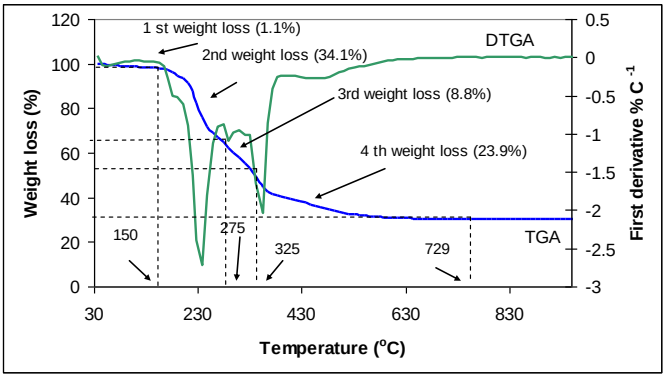



Figure 1. TG-DTGA curves of the precursor

Table 1. TG/DTGA results of the $LiNiPO_4$ precursor

| **Sample** | **Temperature range** | **Weight loss(%)** | **Assignment** |
|---|---|---|---|
| $LiNiPO_4$ from LiOH, $Ni(CH_3COO)_2$ and $(NH_4)H_2PO_4$ with tartaric acid. | 30-150 | 1.1 | Evaporation of absorbed water. |
| | 150-275 | 34.1 | Decomposition of $(NH_4)H_2PO_4$ and evaporation of tartaric acid. Li-Ni acetate gel(precursor) decomposition |
| | 275-325 | 8.8 | Burning out organic residues resulted from the complex decomposition |
| | 325-725 | 23.9 | Decomposition of $Ni(CH_3COO)_2$. and LiOH. Structural OH bond broken |
| | 725-900 | - | Formation of $LiNiPO_4$ |
| Total weight loss | | 67.9 | |

The reaction mechanism for the synthesis of $LiNiPO_4$ has been proposed as shown below. When tartaric acid ($C_4H_6O_6$) was added to the mixture, it reacted with $(NH_4)H_2PO_4$ and LiOH according to the following equations:

$$2(NH_4)H_2PO_4 + C_4H_6O_6 \rightarrow H_3PO_4 + H_2PO_4^- + ((NH_4)_2C_4H_5O_6)^+ \quad (1)$$

$$LiOH + C_4H_6O_6 \rightarrow Li(C_4H_5O_6) + H_2O \quad (2)$$

LiOH also reacted with $H_3PO_4$ produced in equation (1) according to the following,

$$LiOH + H_3PO_4 \rightarrow LiH_2PO_4 + H_2O \quad (3)$$

On heating,

$$2(Ni(CH_3COO)_2) + 2\,C_4H_6O_6 + 8O_2 \rightarrow 2(Ni\,C_4H_4O_6) + 8CO_2 + 8H_2O \quad (4)$$

and

$$H_2PO_4^- + ((NH_4)_2C_4H_5O_6)^+ + C_4H_6O_6 + {}^5/_2\,O_2 \rightarrow \quad (5)$$

$$((H_2PO_4)(NH_4)_2C_4H_5O_6) + 4CO_2 + 3H_2O$$

Therefore overall reaction is given as,

$$2(NH_4)\,H_2PO_4 + 2LiOH + (Ni(CH_3COO)_2) + 5C_4H_6O_6 + {}^{21}/_2\,O_2 \rightarrow \quad (6)$$

$$LiH_2PO_4 + Li(C_4H_5O_6) + ((H_2PO_4)(NH_4)_2C_4H_5O_6) + 2(NiC_4H_4O_6) + 12CO_2 + 13H_2O$$

Equation (6) suggests that the dried gel precursor is composed of $Li((H_2PO_4)_2(NH_4)_2C_4H_5O_6)\,LiC_4H_5O_6 . (NiC_4H_4O_6)_2$

Therefore the overall proposed decomposition equation for the precursor in air atmosphere i.e. during firing is,

$$Li((H_2PO_4)_2(NH_4)_2C_4H_5O_6)\,Li\,C_4H_5O_6 . (Ni\,C_4H_4O_6)_2 + 10O_2 \rightarrow \quad (7)$$

$$2LiNiPO_4 + 16CO_2 + 12H_2O + 2NH_3$$

Based on equation (7), the percentage weight loss is 66.4 %.The total weight loss of the decomposition process from the TGA curves as shown in Table 1 is 67.9 % which agrees closely with the calculated values based on Equation (7). The discrepancy could be due to the absorbed water from the ambient.

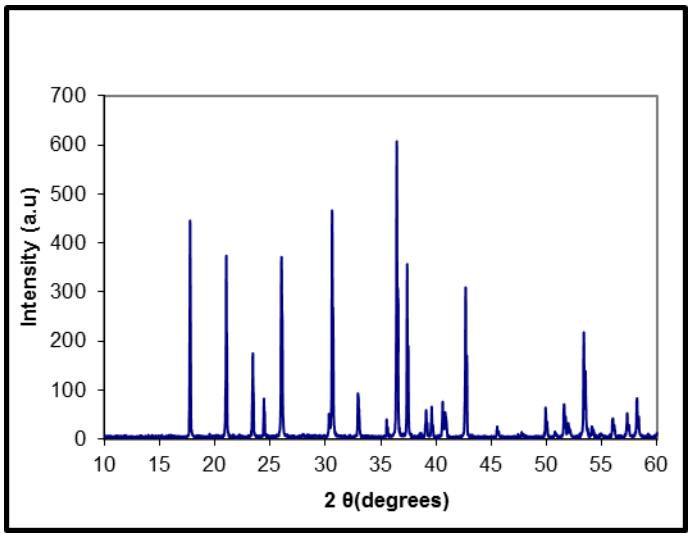



Figure 2. XRD Patterns of the $LiNiPO_4$ sample

The XRD pattern of the sample fired at 1000 $^{o}$C for 24 hours exhibits the characteristic diffraction lines of $LiNiPO_4$ without any impurities and matches the orthorhombic structure listed in JCPDS pattern number 32-0578. The XRD of this sample also agrees with the results of Ruffo and co-workers (2005). The above observations confirmed that a pure compound of $LiNiPO_4$ was successfully synthesized in the present work.

The crystallite size (L) was estimated using the conventional Scherrer equation below.

$$L = \frac{0.94\lambda}{B_r cos\theta} \quad (8)$$

Here λ is the X-ray wavelength 1.5406 Å and $B_r$ is the FWHM of the peak representing the (111) plane. The full width at half maximum (FWHM) of the (111) reflection plane was determined since the peak at $2\theta = 25.9^{0}$ has the highest intensity. The average crystallite size of the prepared pure $LiNiPO_4$ is 66 nm**.**

## Conclusion

The olivine $LiNiPO_4$ powders were successfully synthesized by the sol-gel method with tartaric acid as the chelating agent. TGA/DTGA results showed that the $LiNiPO_4$ powders can be obtained by calcining the precursor at temperature above 750$^{o}$C. The sample prepared at 1000$^{o}$C showed that the position of peaks and the variation in intensity matches the pattern shown in the standard JCPDS data. The weight loss obtained from the thermogram supports the mechanism of reactions proposed. The percentage weight loss is 66.4 % while the total weight loss of the decomposition process from the TGA curves is 67.9 % which agrees closely with the calculated values based on the proposed equation. By using information obtained from the FWHM, the crystallite size of the $LiNiPO_4$ is ~ 66 nm.

## References

1. Liu, H., Li C., Zhang, H. P., Fu, L. Wu, Y. P., and H.Q. Wu (2006). Kinetic study on $LiFePO_4$/C nanocomposites synthesized by solid state technique, *Journal Power Sources* 159: 717-720.
2. Kuei-Feng H., Sun-Yuan T. and Bing-Joe H., (2005). Physical and electrochemical properties of LiFePO4/carbon composite synthesized at various pyrolysis periods, *Journal Power Sources* 146: 529-533.
3. Piana, M., Cushing, B. L., Goodenough, J. B. and Penazzi, N. (2004). A new promising sol–gel synthesis of phospho-olivines as environmentally friendly cathode materials for Li-ion cells, *Solid State Ion.* 175: 233-237.
4. Jingsi Y. and Jun John X, (2004). Nonaqueous Sol-Gel Synthesis of High-Performance $LiFePO_4$. Electrochem. *Solid-State Lett.* 7: 515-A518.
5. Jaewon L., and Amy S. T. (2006). Synthesis of $LiFePO_4$ Micro and Nanoparticles in Supercritical Water, *Mater Lett*, 60: 2105-109.
6. Jiajun C. and M Stanley W. (2006). Hydrothermal synthesis of lithium iron phosphate, *Electrochemistry Communications* 8: 855-858.
7. Shigehisa T., Yosuke I., Kazuyoshi U., Kenji T., Mineo S. (2004) Enhanced electrochemical performance of $LiFePO_4$ prepared by hydrothermal reaction, *Solid State Ion*. 175: 287-290.
8. Arnold, G. Garche, J., Hemmer, R., Strobe, S., Volgler, C., and Wohlfart-Mehrens M. (2003). Fine-particle lithium iron phosphate $LiFePO_4$ synthesized by a new low-cost aqueous precipitation technique, *Journal Power Sources* 119-121:247-251.

The Malaysian Journal of ANALYTICAL SCIENCES ISSN 1394-2506

# DETERMINATION OF ENZYME KINETIC PARAMETERS ON SAGO STARCH HYDROLYSIS BY LINEARIZED GRAPHICAL METHODS

## (Penentuan Enzim Parameter Kinetik pada Hidrolisis Kanji Sagu dengan Kaedah Grafik Lelurus)

Long Wee Lai[1]*, CheeLoong Teo[2], Suzana Wahidin[3], Mohamad Suffian Mohamad Annuar[4]

[1]*Faculty of Science and Biotechnology,*
*Universiti Selangor, Bestari Jaya 45600, Malaysia*
[2]*Faculty of Chemical Engineering,*
*Universiti Teknologi Malaysia, 81310 UTM Sekudai, Johor Bahru, Malaysia*
[3]*Institute of Chemical and Bioengineering Technology,*
*Universiti Kuala Lumpur Malaysia, 78000 Alor Gajah, Melaka, Malaysia*
[4]*Institute of Biological Sciences,*
*University of Malaya, 50603 Kuala Lumpur, Malaysia*

**Corresponding author: zki@unisel.edu.my*

**Abstract**

Amyloglucosidase (E.C. 3.2.1.3) from *Aspergillus niger* was used to hydrolyze the sago (*Metroxylon sagu*) starch into reducing sugars. The experiment was conducted at constant temperature, 55 °C; pH, 4.5 and enzyme amount, 0.2 U/ml, respectively. In this investigation, the substrate concentration was varied ranging from 1.0 – 7.0 g/L. The obtained data were then fixed into linearized plots namely Lineweaver-Burk and Langmuir models to calculate enzyme kinetic parameters, $K_m$ and $V_{max}$. Both of the $K_m$ and $V_{max}$ (mM, mol/min) values from each plot were: Lineweaver-Burk (26.53, 3.31) and Langmuir (13.52, 2.35). Among the linearized models, $K_m$ and $V_{max}$ values acquired from Langmuir plot was chosen.

**Keywords:** enzyme kinetic parameters, $K_m$ and $V_{max}$, Langmuir, Lineweaver-Burk, sago starch hydrolysis

**Abstrak**

Enzim amyloglucosidase (EC 3.2.1.3) dari *Apergillus niger* digunakan untuk menghidrolisis kanji sagu (*Metroxylon sagu*) kepada gula penurun. Eksperimen ini dijalankan pada suhu 55°C; pH, 4.5 dan enzim 0.2U/ml. Kepekatan substrak yang diuji dalam kes ini adalah dalam lingkungan 1.0 – 7.0 g/L. Data yang diperolehi akan digunapakai terus ke dalam linear plot iaitu Lineweaver-Burk serta Langmuir bagi tujuan mengira enzim parameter kinetic: $K_m$ dan $V_{max}$. Kedua-dua nilai $K_m$ dan $V_{max}$ (mM, mol/min) dari Lineweaver-Burk and Langmuir masing – masing adalah 26.53, 3.31; 13.52, 2.35. Nilai $K_m$ and $V_{max}$ dari Langmuir model dipilih dalam kajian ini.

**Kata kunci:** enzim parameter kinetik, $K_m$ dan $V_{max}$, Langmuir, Lineweaver-Burk, hidrolisis kanji sagu

## Introduction

Enzyme kinetic is the branch of enzymology that deals with the factors affecting the rate of enzyme-catalyzed reactions. In general, the most important factors are those of enzyme concentration, ligand concentrations (substrates, products, inhibitors and activators), pH, ionic strength and temperature. When all these factors are analyzed properly, it is possible to learn a great deal about the nature of the enzyme-catalyzed reaction. In addition, a kinetic analysis can lead to a model for an enzyme-catalyzed reaction and conversely, the principles of enzyme kinetic can be used to write the velocity equation for a model which can then be tested experimentally [1]. In general, the Michaelis and Menten [2] framework has proven to be simple yet powerful approach to describe the kinetic of most enzyme reactions (Eq. 1.0):

$$v = \frac{V_{max}[S]}{K_m + [S]} \quad \text{(Eq. 1.0)}$$

where $v$ is the initial reaction velocity, $[S]$ is the concentration of reactant, $V_{max}$ is the maximum rate of reaction at infinite reactant concentration, $K_m$ is the Michaelis constant for reactant. Typical unit for $V_{max}$ and $K_m$ is kg.mol/m$^3$.s and kg.mol/m$^3$, respectively. According to Segel [3], Equation (1.0) is valid only if $v$ is measured over short enough time, so that $[S]$ remains essentially constant. This requires that no more than 5% of substrate to be utilized over the assay period.

In examining the relationship between $v$ and $[S]$ in Equation (1.0), when $[S] < 0.01\ K_m$, the $[S]$ in the denominator can be ignored and the equation reduced to:

$$v = \frac{V_{max}}{K_m}[S] \quad \text{(Eq. 1.1)}$$

This is called first order kinetic. As stated by Segel [1], the zero order kinetic is obtained when $[S] > 100\ K_m$. The $K_m$ in the denominator of Equation (1.0) may be ignored and equation simplifies as shown as below:

$$v = \frac{V_{max}[S]}{K_m + [S]} \rightarrow = \frac{V_{max}[S]}{[S]}$$

$$\rightarrow v = V_{max} \quad \text{(Eq. 1.2)}$$

In general, the Michaelis-Menten equation leads the plot of $v$ versus $[S]$ in the form of a rectangular hyperbolic curve through origin, with asymptotes $v = V_{max}$ and $[S] = -K_m$. Since the $v$ versus $[S]$ gives a hyperbolic curve and thus it is rather difficult to determine $V_{max}$ and the $[S]$ that yields ½ $V_{max}$ (i.e. $K_m$) [3]. In addition, the physical necessity restrict measurement of $v$ to finite positive values of $[S]$ and this consequently make the measurement of $K_m$ and $V_{max}$ become less accurate and precise from such plot. According to Eisenthal & Cornish-Bowden [4], it happened due to asymptotes cannot be approached closely enough. Therefore, the determination of $K_m$ and $V_{max}$ are usually performed by plotting several well-known linear graphs. By using these transformation linear methods, it is easier to estimate the values of kinetic constants. Table 1 depicts the model, equation, slope and intercept of these linearized plots.

Table 1. Common linear transformation methods to evaluate enzyme kinetic parameters [5, 6]

| Model | Equation | Slope and Intercept |
|---|---|---|
| Lineweaver-Burk | $1/v = K_m/V_{max} + 1/V_{max}$ | Slope: $K_m/V_{max}$ |
| | | Intercept: $1/V_{max}$ |
| Langmuir | $[S]/v = K_m/V_{max} + s/V_{max}$ | Slope: $1/V_{max}$ |
| | | Intercept: $K_m/V_{max}$ |

The basic idea of this research is to estimate the kinetic parameters, $K_m$ and *Vmax* on sago starch hydrolysis by using amyloglucosidase (E.C. 3.2.1.3) derived from *Aspergillus niger*. This paper was aimed to demonstrate the determination of $K_m$ and $V_{max}$ values using simple linearized graphical methods particularly Lineweaver-Burk and Langmuir plot.

## Materials and Methods

### Chemicals

All chemical used in the experiment such as acetic acid, $CH_3COOH$; 3, 5–dinitrosalicylic acid, $C_7H_4N_2O_7$; phenol, $C_6H_5OH$; potassium sodium tartrate tetrahydrate, $C_4H_4KNaO_6.4H_2O$; sodium acetate anhydrous, $CH_3COONa$; sodium hydroxide, NaOH and sodium sulfite anhydrous, $Na_2SO_3$ were of analytical grade with highest purity.They were purchased from Merck (M) Sdn. Bhd.

### Substrate

The sago starch (*Metroxylon sagu*) was purchased from local commercial producer, Wah Chang International, Malaysia. The chemical composition of sago starch (dry weight basis, %) is as follows: amylose 28; amylopectin 72; fat 0.18; protein 0.11; ash 0.12 and fiber 0.21 [7].This milky-white starch powder was dried at 60 °C to a constant weight prior to use [8].

The sago starch solution was prepared accordingly to response surface methodology (RSM) design as described by Wee *et al*. [9] i.e. in % (w/v) of 0.0, 0.1, 0.2, 0.3, 0.4, 0.5, 0.6 and 0.7 in 0.05 M acetate buffer solution. (All the substrate concentration in % (w/v) will be expressed in g/L where 0.1 % (w/v) is equivalent to 1.0 g/L and so forth). The sago starch solution was preheated using stirring hotplate while carefully kept from boiling. This procedure was aimed to enhance the solubility of sago starch in buffer solution [10].

### Enzyme

The commercial lyophilized amyloglucosidase (E.C. 3.2.1.3) from *Aspergillusniger*was purchased from Sigma-Aldrich (M) Sdn. Bhd. This enzyme has specific activity at 31.2 U/mg. One unit of enzyme could be defined as liberation of 1.0 mg glucose from starch in 3 min under standard assay conditions i.e. at pH 4.5 and temperature 55 °C. Enzyme solution was prepared by dilute enzyme powder in 0.05 M sodium acetate buffer. After preparation, it was kept at -20 °C before used [11]. The amyloglucosidase enzyme has also been claimed possess wide industrial applications particularly for large scale saccharification of malto-oligosaccharide into β-D-glucose units [12]. Hence it was selected as a biocatalyst to hydrolyze the sago starch in this study. A hydrolysis on starch by amyloglucosidase as followed (Equation 2.0):

$$\text{Starch} + H_2O \xrightarrow{\text{Amyloglucosidase}} \text{D} - \text{Glucose} \qquad \text{(Eq. 2.0)}$$

### Enzyme hydrolysis reaction

In this investigation, the substrate concentrations ranging from 1.0 – 7.0 g/L were verified and tested in order to determine the enzyme kinetic parameters ($K_m$ and $V_{max}$). Meanwhile, the pH (4.5), temperature (55 °C) and enzyme loading (0.2 U/ml) in sago starch hydrolysis were preset at its optimal conditions as described in previous study [9].

The 1.0 ml of amyloglucosidase enzyme (0.2 U/ml) was pipetted and then discharged into test tube which contained 1.0 ml of sago starch solution. Once the enzyme was discharged into test tube, time was recorded accordingly. All trials were performed in triplicate and errors were within ± 5 %. The amount of product formed i.e. reducing sugars (glucose), were determined using the dinitrosalicylic (DNS) acid method [13]. The enzyme hydrolysis reaction was ceased by adding DNS reagent into test tubes and followed by immediately brought to 100 °C in water bath for at least 15 min. The test tubes were then added with 40 % (w/v) Rochelle salt and vortex before left it to cool down to room temperature. The cooled samples were further measured using UV-visible spectrophotometer (Thermo, Genesys 20, USA) at 575 nm to determine the concentration of reducing sugars formed. The absorbance (Abs) was converted to concentration using a calibration curve as shown in Figure 1 and the reading was fitted the following equation (Eq. 3.0):

$$C_{rs} = 769 Abs_{575} \qquad \text{(Eq. 3.0)}$$

where $C_{rs}$ the concentration of the reducing sugars in µg/ml, $Abs_{575}$ the absorbance of the solution at 575 nm.

Equation (3.0) had a regression coefficient of 0.9818 and applied over a concentration range from 0 to 700 μg/ml glucose standard solution. A control blank containing an initial concentration of un-reacted starch and heat-deactivated amyloglucosidase was prepared to correct for the baseline reading in the sample measurement.

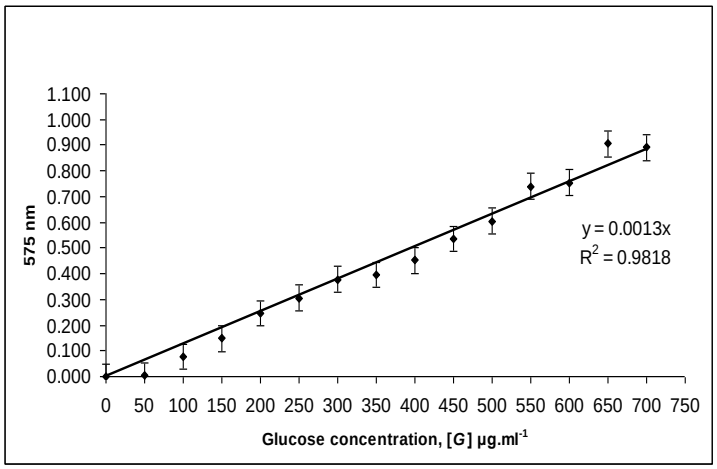



Figure 1. Glucose standard calibration plot

**Calculation of initial reaction velocity, *v***

The initial reaction velocity, *v* can be determined by drawing a straight line on hydrolysis curve as shown in Figure 2. The tangent of the curve is calculated and value of *v* is recorded. The tangent was obtained based on the differentiation of polynomial equation as a function of the time course appearance of product data (reducing sugars). A suitable value of the independent variable i.e. time was then substituted into the differentiated polynomial to obtain the estimate of the tangent. Microsoft Excel® 2003 was used to perform the polynomial fitting. The rate of sago starch hydrolysis, *v* versus substrate concentration, [*S*] is plotted in Figure 3.

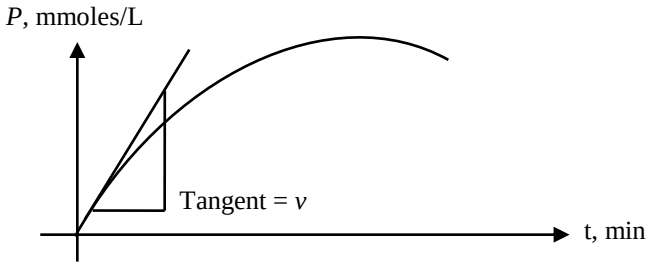



Figure 2. Determination of initial reaction velocity, *v* by drawing a straight line and tangent on hydrolysis curve

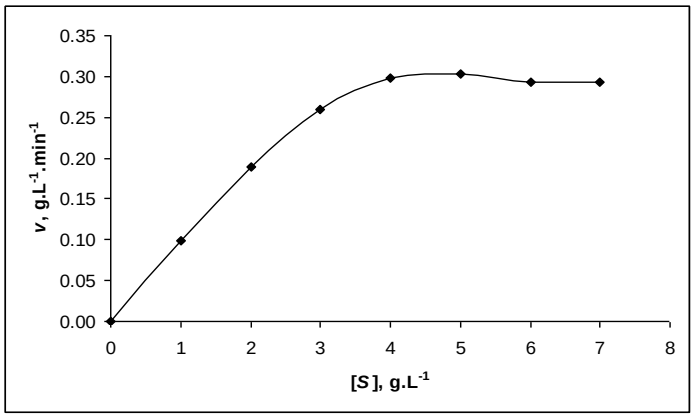



Figure 3. Michaelis-Menten plot

**Results and Discussion**

In order to understand the kinetic aspect of the reaction, an explicit understanding of its kinetic behavior is important. This can be done by determining the enzyme kinetic parameters using mathematical model. Hence, the linearization graphical methods such as Lineweaver-Burk and Langmuir plots were used to estimate the Michaelis constant, $K_m$ and maximum reaction velocity (maximum reaction rate), $V_{max}$. The linearization methods used in this study were Lineweaver-Burk and Langmuir plot, respectively. Both methods provided the regression coefficient, $R^2$ = 0.9687 and 0.9260 as shown in Figures 4 and 5, respectively.

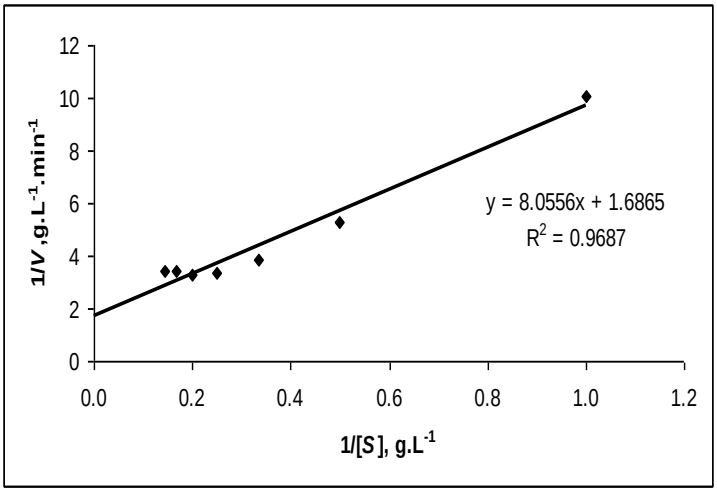



Figure 4. Lineweaver-Burk plot

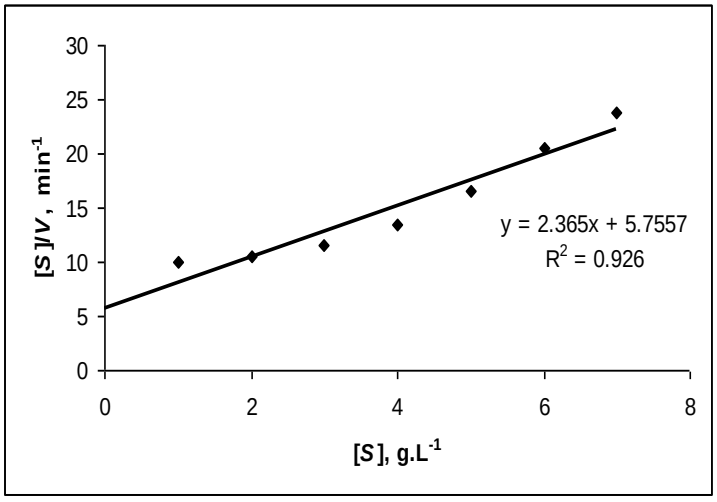



Figure 5. Langmuir plot

Both of $K_m$ and $V_{max}$ values were calculated based on linear equations with y = 8.0556x + 1.6865 (Lineweaver-Burk) and y = 2.365x + 5.7557 (Langmuir). The calculated values of $K_m$ and $V_{max}$ for Lineweaver-Burk and Langmuir models were 4.7762 and 2.4335 g/L; 0.5959 and 0.4228 g/L.min, respectively.

Table 2 shows the $K_m$ and $V_{max}$ values from Langmuir and Lineweaver-Burk plots. In general, the Langmuir plot appears to be more accurate than Lineweaver-Burk. This is because Lineweaver-Burk model was found to distort the experimental error in $v$ and this error is amplified at low substrate concentration. Eventually it will give inaccurate results. Therefore this model is not recommended to evaluate both $K_m$ and $V_{max}$ even though the regression coefficient of Lineweaver-Bulk ($R^2$ = 0.9687) is higher than Langmuir ($R^2$ = 0.9260) [4]. This is also supported by Ranaldi and co-workers [14], i.e. they claimed that since the errors on $v$ are most likely to be significant at low values of $v$, these measurements affect the slope of the plot in decisive manner.

Table 2. Enzyme kinetic values for $K_m$and$V_{max}$ by using linearized model

| **Kinetic parameters** | **Langmuir** | **Lineweaver-Burk** |
|---|---|---|
| $K_m$, g/L | 2.43 | 4.78 |
| $V_{max}$, g/L.min | 0.43 | 0.60 |
| Regression coefficient, $R^2$ | 0.9260 | 0.9687 |
| <u>Conversion of unit</u> | | |
| $K_m$, mM | 13.52 | 26.53 |
| $V_{max}$, mmoles/L.min | 2.35 | 3.31 |

Moser has proposed that the Langmuir model plot is able to minimize distortions in experimental error and therefore it is recommended that Langmuir model should apply in evaluating both values of $K_m$ and $V_{max}$ [15]. The above

statement was also in close agreement with Wilkinson who stated that in the Langmuir plot, the points corresponding to low *v* values cluster on the left side and this only affects the slope of the plot in a very small degree [16]. Apart from that, Doran has also suggested that the Langmuir model is more suitable in the evaluation of $K_m$ and $V_{max}$ for linearization method [6].

Hence, based on these view points, the values of enzyme kinetic parameter determined from Langmuir model were selected. Both $K_m$ and $V_{max}$ values were determined at 13.52 mM and 2.35 mmoles/L.min, respectively. The regression coefficient, $R^2$ at 0.926 was also indicated that less than 7.4 % error was not explained by Langmuir model for the sago starch-amyloglucosidase hydrolysis.

## Conclusion

The sago starch hydrolysis was successfully performed. The enzyme kinetic parameters for both $K_m$ and $V_{max}$ were determined at fix temperature, pH and enzyme amount with varied of substrate concentration. The obtained data were plotted in two difference linearization models to acquire $K_m$ and $V_{max}$. In this case, kinetic parameters values obtained from Langmuir plot ($K_m$ = 13.52 mM and $V_{max}$ = 2.35 mmoles/L.min) were chosen as the best determined values.

## Acknowledgement

The author would like to thank Faculty of Science and Biotechnology, Universiti Selangor for the facilities in order to perform this research.

## References

1. Segel, I.H. (1975). Enzyme kinetics: Behavior and analysis of rapid equilibrium and steady state enzyme systems. USA: John Wiley & Sons.
2. Michaelis, L. &Menten, M.L. (1913). Die kinetikder invertinwirkung. Biochem. Z. 49. 336-369. In: Li, O., Tyler, L.H., Carrie, M. W. & Chester, B. (2014). Standardization of α-L-iduronidase enzyme assay with Michaelis-Menten kinetics.*Mol. Genet. Metab*.,111:113-115.
3. Segel, I.H. (1976). Biochemical calculations: how to solve mathematic problem in general biochemistry, 2nd edn. USA: John Wiley & Sons.
4. Eisenthal, R. & Cornish-Bowden, A. (1974).The direct linear: a new graphical procedure for estimating enzyme kinetic parameters. *Biochem. J.*,139(3):721-730.
5. Emmanuel. M, Papamichael, & Leonidas, G.T. (2006).Enzyme kinetics and modeling of enzymatic system. In: Ashok, P., Colin, W., Carlos, R.S. &Christian, L. (ed), Enzyme technology. India: Springer.
6. Doran, P.M. (1995). Bioprocess Engineering Principles. London: Academic Press Ltd.
7. Elham, F. & Abdorreza, M.N. (2014). Effects of acid-hydrolysis and hydroxypropylation on functional properties of sago starch. *Int. J. Biol. Macromol.*,68: 251-257.
8. Wee, L.L., Annuar, M.S. M. & Ibrahim, S. (2011).Short Communication: Energetics of glucoamylase-catalyzed hydrolysis of commercial sago starch.*AsPac. J. Mol. Biol. Biotechnol.*, 19(4): 117-120.
9. Wee, L.L., Annuar, M.S. M., Ibrahim, S. &Chisti, Y. (2011) Enzyme-mediated production of sugars from sago starch: Statistical process optimization. *Chem. Eng. Comm.*, 198 (11): 1339-1353.
10. Sigma-Alrich. (1995). Product information protocol: enzymatic assay of amyloglucosidase (E.C. 3.2.1.3).
11. Lai, L.W. (2009). Optimization of enzyme mediated sago starch hydrolysis using response surface methodology. *Master dissertation*,Universiti Malaya.
12. Reni, G. & Sankaran, S. (2014). Kinetic and thermodynamic parameters of immobilized glucoamylase different mesoporous silica for starch hydrolysis: A comparative study. *J. Mol. Catal. B-Enzym.*, 106: 81-89.
13. Miller, G.L. (1959). Use of DNS reagent for determination of reducing sugars.*Anal. Chem.*, 31:426-428.
14. Ranaldi, F., Vanni, P. & Giachetti, E. (1999). What students must know about the determination of enzyme kinetic parameters.*Biochem. Educ.*, 27:87-91.
15. Moser, A. (1985). Rate equation of enzyme kinetics. In: Doran, P.M. (1995). Bioprocess Engineering Principles. London: Academic Press).
16. Wilkinson, G.N. (1961). Statistical estimations in enzyme kinetics.*Biochem. J.*, 80:324-332.

The Malaysian Journal of ANALYTICAL SCIENCES ISSN 1394-2506

# SEPARATION OF *N*-NITROSAMINES BY MICELLAR ELECTROKINETIC CHROMATOGRAPHY

## (Pemisahan *N*-Nitrosamina Menggunakan Kromatografi Elektrokinetik Misel)

Nur Amira Md Ali[1], Mohd Marsin Sanagi[1,2]*, Wan Aini Wan Ibrahim[1]

[1]*Department of Chemistry, Faculty of Science,*
[2]*Ibnu Sina Institute for Fundamental Science Studies, Nanotechnology Research Alliance,*
*Universiti Teknologi Malaysia, 81310 UTM Johor Bahru, Johor, Malaysia*

**Corresponding author: marsin@kimia.fs.utm.my*

**Abstract**

A simple and rapid micellar electrokinetic chromatography (MEKC) method was developed for separation of three selected *N*-Nitrosamines namely *N*-nitrosodipropylamine (NDPA), *N*-nitrosodibutylamine (NDBA) and *N*-nitrosodiphenylamine (NDPhA). The effects of composition of the buffer and its pH, concentration of surfactants on the separation and migration times of nitrosamines were investigated. The instrumental variables affecting sensitivity and resolution such as power supply and injection mode were carefully optimized. The best separation was achieved using 40 mM sodium dodecyl sulfate (SDS) as a surfactant in 10 mM phosphate buffer (pH 8.0) at a temperature of 25 ºC, applied voltage of 29 kV, wavelength of 230 nm and electrokinetic injection of 9 s at 5 kV within 10 min analysis time. Excellent linearity was obtained in the concentration range of 2 to 100 µg/mL with coefficients of determination, $r^2 \geq 0.979$. This method showed good reproducibility with relative standard deviation (RSDs) value ranging from 2.46% to 6.61%. The limits of detection (LOD) and limits of quantification (LOQ) ranged from 0.16 to 0.43 µg/mL and 0.54 to 1.44 µg/mL respectively.

**Keywords:** Nitrosamines, surfactants, capillary electrophoresis, micellar electrokinetic chromatography

**Abstrak**

Satu kaedah kromatografi elektrokinetik misel yang mudah dan cepat telah dibangunkan bagi pemisahan tiga sebatian *N*-Nitrosamina yang dipilih iaitu *N*-nitrosodipropilamina (NDPA), *N*-nitrosodibutilamina (NDBA) dan *N*-nitrosodifenilamina (NDPhA). Kesan komposisi penimbal dan pH, kepekatan surfaktan terhadap pemisahan dan masa peralihan nirosamina telah dikaji. Pembolehubah alat yang mempengaruhi kepekaan dan resolusi seperti bekalan kuasa dan mod suntikan telah dioptimumkan dengan berhati-hati. Pemisahan yang terbaik dicapai menggunakan 40 mM SDS sebagai surfaktan di dalam 10 mM penimbal fosfat (pH 8.0) pada suhu 25 ºC, voltan gunakan 29 kV, panjang gelombang 230 nm dan suntikan elektrokinetik 9 saat pada 5 kV dengan masa analisis selama 10 minit. Kelinearan yang baik telah diperolehi dalam julat kepekatan 2 - 100 µg/mL dengan koefisien penentuan, $r^2 \geq 0.979$. Kaedah ini menunjukkan kebolehulangan yang baik dengan nilai sisihan piawai relatif dalam julat 2.46% - 6.61%. Had pengesanan dan had penentuan adalah 0.16 - 0.43 µg/mL dan 0.54 - 1.44 µg/mL, masing-masingnya.

**Kata kunci:** Nitrosamina, surfaktan, elektroforesis kapilari, kromatografi elektrokinetik misel

## Introduction

Nitrosamines are a family compounds discovered 100 years ago and received worldwide attention. These compounds were discovered carcinogen in experimental animals. Nitrosamines have been tested positive as mutagenic (chemicals that can change DNA) and carcinogens which target organs such as live, kidney, lungs, skin and eyes. Nitrosamines are compounds that consist of NNO group and commonly existing in the environment and food. They have been found in many food products [1-2], tobacco smoke [3], rubber [4], water from chlorinated swimming pools [5], wastewater, treated wastewater, groundwater and drinking water [6-9]. Nitrosamines were produced by reaction of amines or their derivatives with nitrosating agents such as nitrous acid, nitrites, or nitrogen oxides. These compounds are relatively stable and difficult to destroy once formed. Nitrosamines have been

detected at ppb levels in a wide variety of matrices. The maximum allowable concentrations levels for nitrosamines in water are generally set at low ng/L. The State of California from California Department of Public Health had issued an action level of 10 ng/L for certain nitrosamines in response to the discovery of N-nitrosodimethylamine (NDMA) in some of its drinking water supplies. Therefore, sensitive analytical methods with the lowest possible detection limits become a demand for their determination at trace level amounts.

Various analytical methods have been studied for determination of these compounds. The most common analytical tools used are gas chromatography (GC) [10-12] and liquid chromatography (LC) [13,14] with highly selective and sensitive detector such as mass spectrometry (MS). However, the choice of such detector for the analysis of nitrosamines is often highly costly and not available in most laboratories. In addition, LC system requires relatively large amounts of samples and eluents containing organic solvents and a long time to treat a separation column.

This has encouraged the development a simpler and less expensive methods for nitrosamines determination. Recently, capillary electrophoresis (CE) emerged as a popular separation technique in many applications such as analysis of proteins [15,16], pharmaceuticals [17,18] and environmental pollutants. CE is relatively new when compared to the more seasoned techniques, HPLC and GC. Each technique comes with its own particular strengths and limitations. GC-MS based techniques have been commonly used for regulatory analysis of this compound. But CE has some very attractive features which make it both competitive and a good alternative. In particular, CE is generally applicable to a broad range of analytes (neutral, charged, organic, inorganic) and offers excellent resolving power.

There are a several modes in CE that can be developed for a wide variety of analytes. As nitrosamines are hydrophilic, neutral and polar compounds, a specialized CE technique is required for their separation. CE methods have been developed previously for determination other group of nitrosamines such as tobacco specific nitrosamines using capillary zone electrophoresis (CZE) mode [19-20]. Micellar electrokinetic chromatography (MEKC) is a mode of CE that enables the separation of electrically neutral analytes by electrophoresis in a manner which is analogous to the principles of chromatography. The aim of this work was to develop a methodology for the separation, identification and quantification of selected nitrosamines using CE. *N*-nitrosodipropylamine (NDPA), *N*-nitrosodibutylamine (NDBA) and *N*-nitrosodiphenylamine (NDPhA) were selected as model compounds (Figure 1). The developed methodology was applied to the determination of these analytes in an aqueous sample.

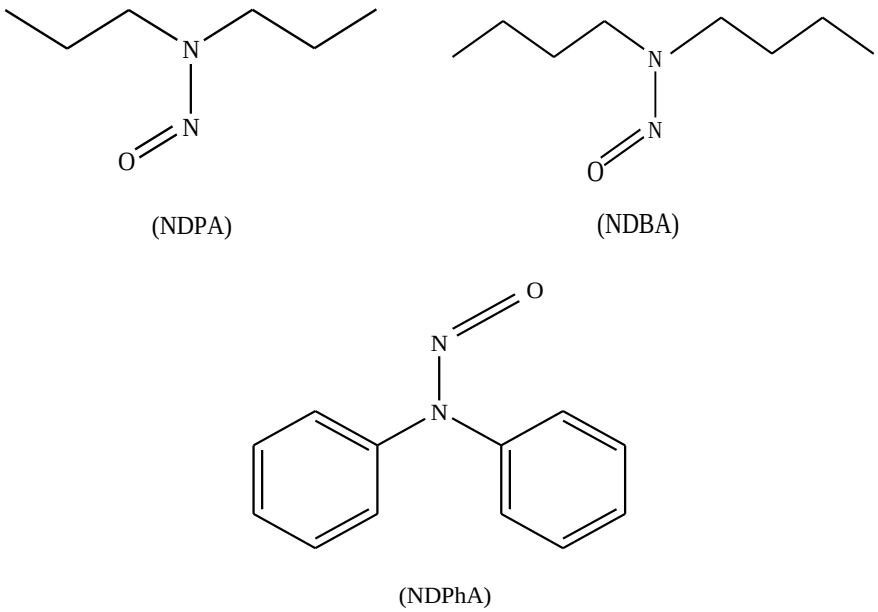



Figure 1. Structures of the NDPA, NDBA and NDPhA used in the development of the CE method.

## Materials and Methods

### Reagents

Disodium hydrogen phosphate 12-hydrate, sodium dodecyl sulfate (SDS) and sodium deoxycholate (SDC) were purchased from Sigma-Aldrich (St. Louis, MO). Sodium cholate (SC) was obtained from Wako Pure Chemical Industries, Ltd. (Osaka, Japan) whereas sodium hydroxide was purchased from Riedel-de Haen (Seelze, Germany). NDPA, NDBA and NDPhA were obtained from Sigma-Aldrich (St. Louis, MO, USA). All other chemicals and solvents were common brands of analytical-reagent grade. The water used for dilutions or as buffer preparation was produced from a Water Purification System from Millipore (Molsheim, France).

### Instrumental

All CE separations were conducted on an Agilent Technologies CE (Waldbronn, Germany) equipped with a photodiode array detection system. The MEKC was performed using a 64.5 cm × 50 µm i.d. uncoated fused-silica capillary with an effective length of 56 cm obtained from Polymicro Technologies (Phoenix, AZ). Samples were injected by using electrokinetic injection (EKI) and detection wavelength used was 230 nm. The CE system was controlled by a PC workstation using Chemstation software.

### Electrophoresis conditions

Prior to the first use, a new capillary was conditioned by passing 1 N NaOH solution for 30 min followed by washing with deionized water for 30 min and finally equilibrating with an appropriate running buffer for 30 min. Between runs, the capillary was washed with 0.1 N NaOH, water and run buffer for 10 min each.

### Preparation of running electrolytes

Running electrolytes were prepared by dissolving surfactants at an adequate concentration in phosphate buffer where phosphoric acid was used to adjust the desired pH.

### Standard solution preparation

A 2000 µg/mL stock standard solution of each analyte was prepared in methanol and stored in the refrigerator in the dark. A working standard solution was made daily by diluting stock with water. The sample to be injected was at a typical concentration of 200 µg/mL. All the separation solutions were filtered through 0.20 µm nylon syringe filter obtained from Whatman (Clifton, NJ, USA).

## Results and Discussion

### Optimization of electrophoretic conditions

The running electrolyte conditions, such as type and concentration of the surfactant also buffer composition significantly affect the electrophoretic separation. Therefore, before selecting the conditions for optimization, a number of preliminary trials were conducted with different type of surfactants and buffer composition at various pH to check the migration time, area, shape and resolution. The electrophoretic parameters were initially evaluated using a 50 mM SC surfactant and 50 mM borate buffer (pH 7.0). The use of this buffer did not give adequate separations (Figure 2). The compounds migrated very close to the electroosmotic flow (EOF) and the peaks overlapped. Then, in another attempt the use of buffer consisting of 50 Mm SDS and 50 mM phosphate buffer (pH 7.0) as a running electrolyte was evaluated. The background electrolyte (BGE) of SDS and phosphate buffer in this ratio was found to be more appropriate since all the desired peaks were obtained. Hence, this BGE was chosen for further optimization. The peaks for each analyte were identified by analysis of individual analytes at typical concentrations of 200 µg/mL.

### Effect of pH, Buffer and Surfactant Concentration

The initial CE separations were carried out at pH 7.0. At this condition, separations of the three nitrosamines peak were achieved within 12 min. Various buffer pHs in the range of 6.0-8.0 was studied by adding phosphoric acid into the solution. A small change of pH can have a dramatic effect on migration time and peak area of analytes. At pH 6.0, long migration times were achieved at 24 min. The change in the buffer pH especially in the lower pH region caused a significant change in the velocity of EOF. Therefore, the electroosmotic mobility was reduced in the acid range and this led to long migration time [21]. Meanwhile, at pH 8.0, high peak areas (>288 mAu) were obtained

as compared to those at pH 7.0 (< 123 mAu). As nitrosamines studied were in ionized form and has the same charge as the micelle, they were incorporated into the micelle to a smaller degree than their neutral forms. Therefore, more analyte distribution occurs at the anionic SDS at pH 8.0. Hence, pH 8.0 was selected as the best pH for the further optimization. Figure 3 shows a comparison of the peak areas of the analytes at different pHs.

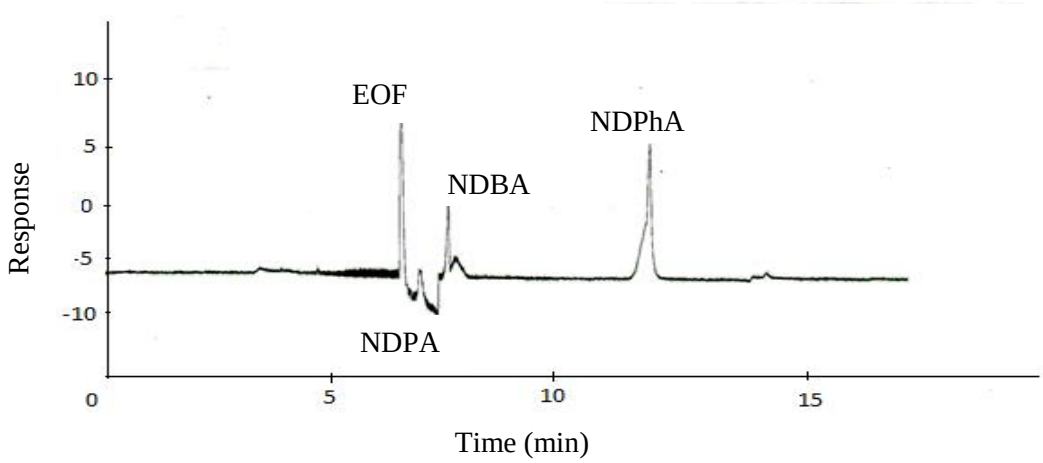



Figure 2. Electropherogram of a nitrosamine standard mixture at 200 µg/mL, before the optimization steps. Separation conditions: 50 mM sodium cholate in 50 mM borate buffer (pH 7); capillary 64.5 cm × 50 µm I.D (effective length, 56 cm); applied voltage, 20 kV; temperature, 25 °C; Injection electrokinetic, 5 kV/5 sec.

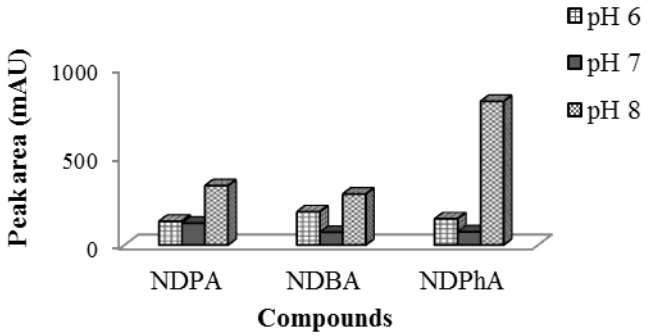



Figure 3. Study effect of pH on the MEKC of nitrosamines at 200 µg/mL. Separation conditions: 50 mM SDS in 10 mM phosphate buffer; capillary 64.5 cm × 50 µm I.D (effective length, 56 cm); applied voltage, 20 kV; temperature, 25 ºC; Injection electrokinetic, 5 kV/5 sec.

To analyze the effect of SDS concentration, it was varied from 30-60 mM. Optimization SDS played a key role in achieving efficient separation in MEKC because it worked as a pseudostationary phase where neutral nitrosamines species partition themselves between the micelles and buffer solution. The optimized concentration of SDS was 40 mM as it gave a good peak area (Figure 5). Further increase the SDS concentration to 60 mM tend to peak become broad due to long migration times. From the Figure 4, it shows that migration time was further increased when concentration SDS was increased. The increased in SDS concentration caused a significant interaction between the analytes with a micelles. Viscosity of solution will also increase, lead to an increase in their migration times.

Different phosphate buffer concentrations in the range of 5-15 mM were investigated. The ionic strength of buffer varies as the concentration was changed. Increased buffer concentration in BGE caused an ionic strength that modulated the EOF and electrophoretic mobility of the analyte. Thus, the migration times of nitrosamines became longer as concentration of phosphate buffer was increased. Further increase in buffer concentration led to peak broadening that is probably due to Joule Heating effect [22]. Therefore, 10 mM was chosen as the optimum buffer concentration as it gave faster migration times than that for 15 mM and better resolution as compared to that for 5 mM.

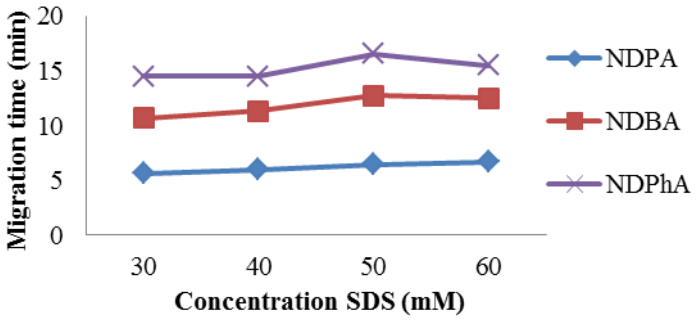



Figure 4. Effects of SDS concentration on the migration time of nitrosamines at 200 µg/mL. Separation conditions: 10 mM phosphate buffer (pH 8.0); capillary 64.5 cm × 50 µm I.D (effective length, 56 cm); applied voltage, 20 kV; temperature, 25 ºC; Injection electrokinetic, 5 kV/5 sec.

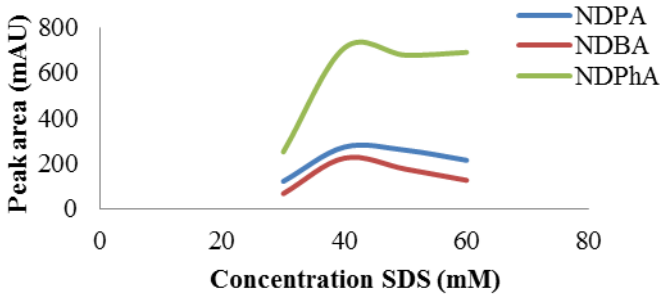



Figure 5. Effects of SDS concentration on the area of nitrosamines at 200 µg/mL. Separation conditions: 10 mM phosphate buffer (pH 8.0); capillary 64.5 cm × 50 µm I.D (effective length, 56 cm); applied voltage, 20 kV; temperature, 25 ºC; Injection electrokinetic, 5 kV/5 sec.

**Effect Injection Time, Applied Voltage and Temperature**

After optimizing the buffer conditions, instrumental variables namely applied voltage, temperature, injection mode and injection were also studied and optimized. Effect of different applied voltages (20, 23, 26 and 29 kV), injection times (3, 5, 7 and 9 sec) and temperatures (15, 20 and 25 ºC) on the separation of nitrosamines was investigated. Varying the applied voltage and temperature gave a significantly changing migration times. Analysis time was decreased with increase in applied voltage. In this study, 29 kV was the maximum voltage that can be reached by the system; higher applied voltage of > 29 kV will cause instrumental current increase. Meanwhile, the optimum temperature obtained was 25 °C which is the maximum temperature that can be reached when 29 kV voltages was applied.

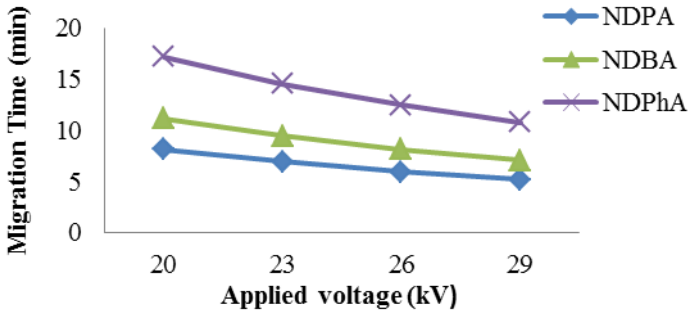



Figure 6. Study effect of applied voltage on the migration of nitrosamines at 200 µg/mL. Separation conditions: 40 mM SDS, 10 mM phosphate buffer (pH 8.0); capillary 64.5 cm × 50 µm I.D (effective length, 56 cm); temperature, 25 ºC; Injection electrokinetic, 5 kV/5 sec.

In this study, electrokinetic injection was used. No separation was observed when hydrodynamic injection was used. Electrokinetic injections at 5 kV and 9 sec was found to be the best conditions achieved as all peak were resolved and high peak areas obtained.

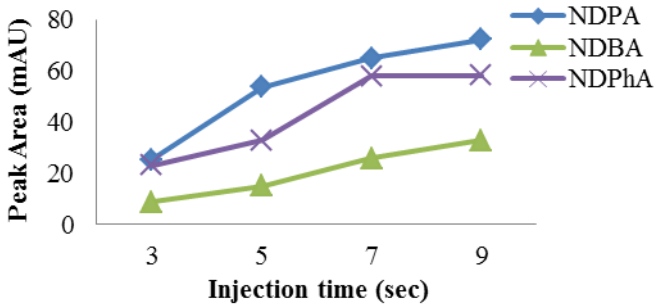



Figure 7. Study effect of injection time the area of nitrosamines at 200 µg/mL. Separation conditions: 40 mM SDS, 10 mM phosphate buffer (pH 8.0); capillary 64.5 cm × 50 µm I.D (effective length, 56 cm); applied voltage, 29 kV; temperature, 25 ºC; Injection electrokinetic, 5 kV.

An electropherogram after the optimization of all these variables is showed in Figure 8 and the optimum conditions are summarized in Table 1. Electrophoretic method was characterized by constructing a calibration graph without any preconcentration of sample in the concentration range of 2-100 µg/mL. The calibration curves with peak area versus concentration were plotted and the curves obtained were linear for three analytes in the mentioned concentration ranges with coefficient of determination, $r^2 \geq 0.979$. The limit of detection (LOD) was calculated using 3-times the standard deviation of the intercept divided by the slope, whereas the limit of quantification (LOQ) was calculated by using 10 times the standard deviation of the intercept divided by the slope. LOD were found to be in the range 0.16 to 0.43 µg/mL and LOQ in the range 0.54 to 1.44 µg/mL. This method was found to be reproducible with relative standard deviation (RSD) for intra day precision less than 6.61%. The analytical performances of MEKC method for the determination of nitrosmines are summarized in Table 2.

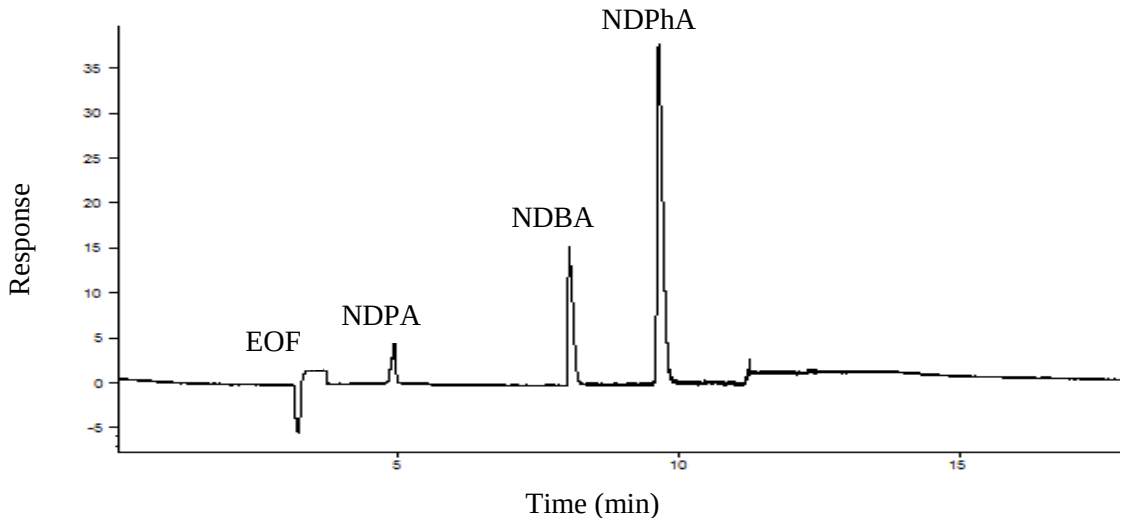



Figure 8. Electropherogram of a nitrosamine standard mixture at 200 µg/mL, after the optimization steps Separation conditions: 40 mM SDS in 10 mM phosphate buffer (pH 8); capillary 64.5 cm × 50 µm I.D (effective length, 56 cm); applied voltage 29 kV; temperature, 25 °C; Injection electrokinetic, 5 kV/9 sec.

Table 1. Optimization parameters and optimized conditions for the development of MEKC method

| **Parameters** | **Studied** | **Optimized** |
|---|---|---|
| Surfactants | SC<br>SDS<br>SDC | SDS |
| Concentration SDS | 30-60 mM | 40 mM |
| Buffer | Borate<br>Phosphate | Phosphate |
| Concentration phosphate | 5-15 mM | 10 mM |
| pH | 6-8 | 8 |
| Injection mode | Hydrodynamic<br>Electrokinetic | Electrokinetic |
| Injection time | 3-9 sec | 9 sec |
| Applied voltage | 20-29 kV | 29 kV |
| Temperature | 15-25 ºC | 25 ºC |

Table 2. Analytical Performance of MEKC method

| Analyte | Equation | $r^2$ | Linear range (µg/mL) | LOD (µg/mL) | LOQ (µg/mL) | % RSD peak area ( n=3) |
|---|---|---|---|---|---|---|
| NDPA | y = 0.2343x + 0.6127 | 0.998 | 2-100 | 0.43 | 1.44 | 2.46 |
| NDBA | y = 0.7955x - 1.3367 | 0.999 | 2-100 | 0.36 | 1.19 | 5.30 |
| NDPhA | y = 2.5679x - 15.006 | 0.979 | 2-100 | 0.16 | 0.54 | 6.61 |

y = peak area, x = concentration (µg/mL)

The developed method was then applied for determination of these three selected compounds in aqueous sample. Dispersive micro-solid phase extraction (D-µ-SPE) technique using multiwall carbon nanotubes (MWCNTs) has been carried out for the extraction of these three selected nitrosamines. The standards solution was spiked in distilled water and undergoes D-µ-SPE. Triplicate analysis was performed on 5, 10 and 15 µg/mL for the precision study. Percent of recovery was calculated by comparing the area before and after the extraction of the aqueous sample. The recoveries obtained for representative nitrosamines was summarize in the Table 3. High recovery obtained only for NDPA and NDBA (between 80.3 % and 97.2 %). However, low recovery obtained for NDPhA may due to the strong π-π interaction of analyte with the MWCNTs used in extraction. The developed method was simple as the separation by CE equipment just required a low cost of capillary and less volume consumption for BGE. In addition, this method also led to significant environmental benefits due to solvent-free consumption in BGE. In the present study, it was a first time separation of these three selected nitrosamines by using MEKC method. Therefore, the analysis time within 10 min was considered rapid and good for separation of neutral, polar compound nitrosamines by MEKC.

Table 3. Analysis of aqueous samples by the proposed method (concentration in µg/mL)

| Analyte | Amount added (µg/mL) | Amount founded (µg/mL) | Recovery (%) |
|---|---|---|---|
| NDPA | 5 | 4.86 | 97.2 |
| | 10 | 8.88 | 88.8 |
| | 15 | 13.26 | 88.4 |
| NDBA | 5 | 4.40 | 88.0 |
| | 10 | 8.22 | 82.2 |
| | 15 | 12.05 | 80.3 |
| NDPhA | 5 | 2.63 | 52.6 |
| | 10 | 4.81 | 48.1 |
| | 15 | 7.81 | 52.1 |

## Conclusion

In the present study, MEKC method was carried out to determine the best optimized conditions for separation of three selected nitrosamines. It can be concluded that this method is simple and rapid using commercial CE equipment. The results obtained were acceptable and suitable for separation and determination of nitrosamines in aqueous sample at µg/mL concentration.

**Acknowledgement**

The authors would like to thank Universiti Teknologi Malaysia and Ministry of Education Malaysia for financial supports through research grant No. R.J130000.7809.4F177 and studentship for Nur Amira Md Ali.

**References**

1. Yurchenko, S. and Mölder, U. (2007). The occurrence of volatile *N*-nitrosamines in Estonian meat products. *Food Chem*., 100 (4): 1713-1721.
2. Huang, M.-C., Chen, H.-C., Fu, S.-C. and Ding, W.-H. (2013). Determination of volatile *N*-nitrosamines in meat products by microwave-assisted extraction coupled with dispersive micro solid-phase extraction and gas chromatography – Chemical ionisation mass spectrometry. *Food Chem.*,138 (1): 227-233.
3. Andra, S. S. and Makris, K. C. (2011). Tobacco-specific nitrosamines in water: An unexplored environmental health risk. *Environ. Int*., 37 (2): 412-417.
4. Incavo, J. A. and Schafer, M. A. (2006). Simplified method for the determination of *N*-nitrosamines in rubber vulcanizates. *Anal. Chim. Act*a, 557 (1–2): 256-261.
5. Chowdhury, S., Alhooshani, K. and Karanfil, T. (2014). Disinfection byproducts in swimming pool: Occurrences, implications and future needs. *Water Res*. 53 (0): 68-109.
6. Krauss, M., Longrée, P., Dorusch, F., Ort, C. and Hollender, J. (2009). Occurrence and removal of *N*-nitrosamines in wastewater treatment plants. *Water Res*., 43 (17): 4381-4391.
7. Nawrocki, J. and Andrzejewski, P. (2011). Nitrosamines and water. *J. Hazard. Mater*., 189 (1–2): 1-18.
8. Rodil, R., Quintana, J. B., Concha-Graña, E., López-Mahía, P., Muniategui-Lorenzo, S. and Prada-Rodríguez, D. (2012). Emerging pollutants in sewage, surface and drinking water in Galicia (NW Spain). *Chemosphere*, 86 (10): 1040-1049.
9. Wang, W., Ren, S., Zhang, H., Yu, J., An, W., Hu, J. and Yang, M. (2011). Occurrence of nine nitrosamines and secondary amines in source water and drinking water: Potential of secondary amines as nitrosamine precursors. *Water Res*., 45 (16): 4930-4938.
10. Byun, M., H, -W., -J, Ahn., Kim-H, J., Lee, J., H, -W., Yook, -S., Han, S. and -B. (2004). Determination of volatile *N*-nitrosamines in irradiated fermented sausage by gas chromatography coupled to a thermal energy analyzer. *J. Chromatogr. A*, 1054 (1–2): 403-407.
11. Jurado-Sánchez, B., Ballesteros, E., and Gallego, M. (2007). Comparison of the sensitivities of seven *N*-nitrosamines in pre-screened waters using an automated preconcentration system and gas chromatography with different detectors. *J. Chromatogr. A*, 1154 (1–2): 66-73.
12. Ozel, M.Z., Gogus, F., Yagci, S., Hamilton, J. F. and Lewis, A.C. (2010). Determination of volatile nitrosamines in various meat products using comprehensive gas chromatography- nitrogen chemiluminiscence detection. *Food Chem. Toxicol.*, 48 (11): 3268-3273.
13. Lee, M., Lee, Y., Soltermann, F. and Von Gunten, U. (2013). Analysis of N-nitrosamines and other nitro(so) compounds in water by high-performance liquid chromatography with post-column UV photolysis/Griess reaction. *Water Res*., 47 (14): 4893-4903.
14. Ripollés, C., Pitarch, E., Sancho, J.V., López, F.J. and Hernández. F. (2011). Determination of eight nitrosamines in water at the ng $L^{-1}$ levels by liquid chromatography coupled to atmospheric pressure chemical ionization tandem mass spectrometry., *Anal.Chim. Acta*, 702 (1): 62-71.
15. Taichrib, A., Pelzing, M., Pellegrino, C., Rossi, M. and Neususs, C. (2011). High resolution TOF MS coupled to CE for the analysis of isotopically resolved intact proteins. *J. Proteomics*, 74 (7): 958-966.
16. Timerbaev, A. R., Pawlak, K., Aleksenko, S. S., Foteeva, L.S., Matczuk, M. and Jarosz, M. (2012). Advances of CE-ICP-MS in speciation analysis related to metalloproteomics of anticancer drugs. *Talanta*, 102 (0): 164-170.
17. Altria, K. D. (2003). Enhanced pharmaceutical analysis by CE using dynamic surface coating system. *J. Pharm. Biomed. Anal.*, 31 (3): 447-453.
18. Aturki, Z., Rocco, A., Rocchi, S. and Fanali, S., (in press). Current applications of miniaturized chromatographic and electrophoretic techniques in drug analysis. *J. Pharm. Biomed. Anal.* (2014), http://dx.doi.org/10.1016/j.jpba.2014.03.041 (0).

19. Liao, J., Pan, Y., Li, C., Wen, D. and Liu, H. (2011). Fast screening for tobacco specific N-nitrosamines by CZE using dynamically coated capillaries. *Chromatographia.*, 74: 415-19.
20. Li, C., Chen, Z., Wen, D., Zhang, J., Cong, W., Yu, B., Liao, Y. and Liu, H. (2006). Determination of tobacco-specific N-nitrosamines in rabbit serum by capillary zone electrophoresis and capillary electrophoresis-electrospray ionization mass spectrometry with solid-phase extraction. *Electrophoresis.*, 27: 2152-2163.
21. Hiroyuki, N. and Terabe, S. (1996). Micellar electrokinetic chromatography Perspectives in drug analysis. *J. Chromatogr. A, 735* (1–2): 3-27.
22. Rathore, A. S. (2004). Joule heating and determination of temperature in capillary electrophoresis and capillary electrochromatography columns. *J. Chromatogr. A, 1037* (1–2): 431-443.

The Malaysian Journal of ANALYTICAL SCIENCES ISSN 1394-2506

# DESIGN, DEVELOPMENT AND EVALUATION OF A SIMPLE SEMI-AUTOMATED SYSTEM FOR [$^{18}$F]-FLUOROCHOLINE SYNTHESIS

## (Reka bentuk, pembangunan dan penilaian sistem pensintesis [$^{18}$F]-Fluorocholine separa automatik)

Faizal Mohamed[1]*, Mohd Fadli Mohammad Noh[1], Irman Abd. Rahman[1], Nur Ratasha Alia Md. Rosli[1], Cheong Kai Heng[1], Zulkifli Mohamed Hashim[2], Mohamad Arif Hamzah[3], Fadil Ismail[3]

*[1]School of Applied Physics, Faculty of Science and Technology*
*Universiti Kebangsaan Malaysia, 43600 Bangi, Selangor, Malaysia*
*[2]Nuclear Medicine Division,*
*[3]Prototype and Plant Development Centre,*
*Malaysian Nuclear Agency, Bangi, 43000 Kajang, Selangor, Malaysia*

**Corresponding author: faizalm@ukm.edu.my*

**Abstract**

Positron Emission Tomography (PET) scanning are usually conducted with [$^{18}$F]-fluoro-2-deoxyglucose (FDG) as tracer. The [$^{18}$F]FDG exhibits several weakness in detecting certain type of tumours such as brain tumour and prostate metastasis. In this study, [$^{18}$F]-fluorocholine (FCH) has been identified as an alternative to [$^{18}$F]FDG. The absence of specific synthesizer for FCH production hampers the application of this tracer in PET studies at local premises. This study focuses on the development of the [$^{18}$F]FCH synthesizer prototype and the [$^{18}$F]FCH synthesis. The design would emphasize on its simplicity, relatively low cost, semi-automated synthesis and purification, as well as good reliability and safety. The [$^{18}$F]FCH was synthesized in two steps approach; reacting [$^{18}$F]-fluoride with dibromomethane into [$^{18}$F]-fluorobromethane before purification using Sep-Pak silica cartridges and finally converted into [$^{18}$F]FCH by reacting with N,N-dimethylaminoethanol. The synthesizer are successfully developed and able to achieve decay-corrected radiochemical yield of 10.131 % in under 110 minutes. Optimization of the radiochemical yield is still underway.

**Keywords**: [18F]-fluorocholine, remotely operated synthesizer, positron emission tomography, radiopharmaceutical

**Abstrak**

[$^{18}$F]-fluoro-2-deoxyglucose (FDG) secara amnya digunakan sebagai penyurih dalam imbasan menggunakan tomografi pancaran positron (PET). Penyurih ini mempunyai beberapa kelemahan dalam mengesan jenis kanser seperti tumor otak dan tumor prostat. Disebabkan oleh faktor ini, [$^{18}$F]-fluorokolina (FCH) telah dikenal pasti sebagai penyurih alternatif. Namun disebabkan tiada pensintesis FCH yang khusus, ia tidak dapat diaplikasikan sebagai penyurih PET di hospital tempatan. Kajian ini dijalankan bertujuan untuk menghasilkan prototaip pensintesis [$^{18}$F] FCH dan mensintesis [$^{18}$F] FCH. Reka bentuk prototaip ini tertumpu pada keringkasan, kos yang rendah, sintesis dan penulenan secara separa automatik, serta faktor keselamatan.[$^{18}$F]FCH telah di sintesis menerusi dua peringkat; [$^{18}$F]-fluorida di tindakbalas dengan dibromomethana menghasilkan [$^{18}$F]-fluorobromethana sebelum penulenan menggunakan kartrij silica Sep-Pak. Kemudiannya [$^{18}$F]-fluorobromethana di tindakbalas dengan N,N-dimethylaminoethanol menghasilkan [$^{18}$F]FCH. Pensintesis [$^{18}$F]FCH telah berjaya dihasilkan dan [$^{18}$F]FCH dapat dihasilkan pada kadar 10.131 % dalam 110 minit. Penghasilan FCH secara optima masih dalam kajian.

**Kata kunci:** [18F]-fluorokolina, pensintesis kawalan jauh, tomografi pancaran positron, radiofarmaseutikal

## Introduction

Cancer has becomes an increasing health problem in Malaysia. It is estimated that one out of four people in Malaysia will develop cancer at certain age of one's life [1, 2]. In order to provide improved quality of life for the cancer patient and ultimately to reduce the mortality, emphasis has been given to detect and delivers effective treatment at early stage of cancer development. In recent years, positron emission tomography (PET) has gained

considerable interest as a mean of cancer imaging tool in Malaysia. PET studies can provide functional information using radio-labelled tracer, especially using [$^{18}$F]-fluoro-2-deoxyglucose ([$^{18}$F]FDG) [3].

It is undeniable that [$^{18}$F]FDG alone is insufficient in solving all diagnostic oncological problems faced by mankind. There are other PET radiopharmaceuticals with large potential that can be used as a tool to explore various metabolic pathways [4, 5] such as [$^{18}$F]-Fluorocholine ([$^{18}$F]FCH). According to Hara [6], the radiopharmaceutical has been proven to be of usefulness, if not beyond doubt, but because there is no specific synthesizer to produce [$^{18}$F]FCH available in local hospitals and institutes, the production of the pharmaceutical in Malaysia has been hampered.

Even though it has been proven that [$^{18}$F]FDG is quite competent to be used as PET tracer, it still has several weaknesses. Reports such as by Price et al., Picchio et al., and Reske et al. [7-9] have shown that [$^{18}$F]-Fluorocholine or [$^{18}$F]FCH is more capable than [$^{18}$F]FDG to detect both primary and metastatic prostate cancer. Other reports also suggested the clinical usefulness of [$^{18}$F]FCH compared to [$^{18}$F]FDG, especially in brain metastases [10].

The [$^{18}$F]FCH was first successfully synthesized by DeGrado et al. [11] by reacting N, N-dimethylaminoethanol with 1-[$^{18}$F]fluoro-2-bromomethane ([$^{18}$F]]FBM). To the best of our knowledge, there are two methods of [$^{18}$F]FCH synthesis reported so far. The first method [11, 12] involves the reaction between [$^{18}$F]-fluoride with dibromomethane, at temperature 100 °C to produce [$^{18}$F]FBM. The precursor is then purified by Gas Chromatography (GC) before it is allowed to react with 2-dimethyl aminoethanol (DMAE), thus producing [$^{18}$F]FCH. The radiochemical yield was reported to be 20 -40 % (not decay-corrected) under 40 min.

The second method employs the use of [$^{18}$F]-fluoromethyl triflate. Iwata et al. [13] has reported a method to purified [$^{18}$F]FBM simply by just using disposable Solid Phase Extraction (SPE) cartridges before the [$^{18}$F]FBM is conveniently converted to more reactive [$^{18}$F]fluoromethyl triflate, in order to synthesize [$^{18}$F]FCH. The [$^{18}$F]FBM is converted to [$^{18}$F]fluoromethyl triflate by passing the freshly purified [$^{18}$F]FBM through a preheated (200 °C) column impregnated with silver triflate (AgOTf). The radiochemical yield at the end of synthesis is within 54-67 %. The time of synthesis is less than 30 minute.

Other choline-analogues such as [$^{18}$F]fluoroethylcholine ([$^{18}$F]FEC) and [$^{18}$F]propylcholine have been synthesized by using ethyl bromide and propyl bromide respectively [12]. Another method involves the use of ethyl tosylate as precursor has been used to synthesize [$^{18}$F]FEC [14-16]. However, [$^{18}$F]FEC has so far seemed holds no significant clinical advantages over [$^{18}$F]FCH [12, 14]. DeGrado et al. reported that the uptake of FCH and choline in cultured prostate cancer cells were comparable, whereas uptake of FEC was approximately one fifth of FCH. Therefore, [$^{18}$F]FCH has potential to be used in PET technique.

Currently, cyclotron-PET facilities in Malaysia have only produce [$^{18}$F]FDG for their routine clinical use. In order to address this deficiency there is effort to synthesis other tracer such as 3, 4-dihydroxy-6-$^{18}$F-fluoro-L-phenylalanine ([$^{18}$F]FDOPA) by Hospital Putrajaya. From the practical points of view, it is hoped that with a home-made synthesizer that is competitively simple and low cost, that the best solution for the problem could be paved.

## Materials and Methods

### Components of the Synthesizer

The [$^{18}$F]FCH synthesizer module consists of two separate plant; namely processing plant and reagent plant. The processing plant is installed inside the hot-cell, where all the process that involves contact with radioactive material are being done, while the reagent plant is use to introduce non-radioactive chemicals into the processing plant. The reagent plant is connected to the processing plant via tygon silicon tubing through special ports at the side of the hot-cell.

Two-way (PN: EW-98302-12) and three-way (PN: EW-98302-12) solenoid operated pinch valves, tygon silicone tubing (PN: EW-95702-01), as well as needles with non-coring deflected tips (PN: EW-25701-32) were purchased from Cole-Palmer. Stainless steel straight barbed connectors (PN: EW-31208-00), y barbed connectors (PN: EW-

31209-55) and tee barbed connectors (PN: EW-31208-31) from Cole-Palmer are used to connect between tubing wherever tolerance to chemical and high temperature are required. We use stainless steel female luer lock with hose barb (PN: EW-31507-29) and male luer lock with hose barb (PN: EW-31507-26) from Cole Palmer to connect Sep-Pak cartridge and needle to tubing. In the same manner, polypropylene straight barbed connectors (PN: P-06365-11), y barbed connectors (PN: EW-30726-41) and male luer lock with hose barb (PN: P-45503-00) are used in less demanding area.

The electrical parts of the synthesizer consist of toggle switches (PN: 320-922), control panel (PN: 580-411), junction box (PN: 580-398), LED indicator (PN: 250-106); all purchased from RS Component, and DC power supply (PN: RS-75-24) from Mean Well. The air process heaters (PN: 200-2496), digital temperature controllers (PN: 461-206) and thermocouple type J (PN: 455-4270) were purchased from RS Component to form the heating system for the synthesizer. The pinch valves were connected to the power supply, toggle switches, LED indicators and manually operated by opening the switches. By applying pressure and vacuum through the tubing, and opening the desired valves, the movement of the fluid is controlled inside the synthesizer from one point to another.

**Reagents for Synthesis**

Anhydrous acetonitrile, dibromomethane, N,N-dimethylaminoethanol, potassium carbonate, ethanol, 0.85% saline solution, Kryptofix 2.2.2, and ethanol were purchased from Sigma-Aldrich. All chemical were used without any further purification. Sep-Pak plus tC18, Sep-Pak plus Silica, Sep-Pak plus Accell plus CM, and Sep-Pak light QMA Carbonate cartridges were obtained from Waters. The Sep-Pak Accell plus CM cartridge was conditioned with 5 mL HCl 0.5N and were rinsed with 10 mL ethanol prior to synthesis. The Sep-Pak Silica and QMA Carbonate were used without preconditioning.

.

**[$^{18}$F]-Fluoride Production**

The no carrier added [$^{18}$F]-fluoride was produced by using a PETtrace cyclotron (GE, Uppsala) at Hospital Putrajaya. A beam of 16.5 MeV proton was allowed to bombard the target material, [$^{18}$O]-water; thus producing the [$^{18}$F]-fluoride via $^{18}$O(p,n)$^{18}$F nuclear reaction. The [$^{18}$F]-fluoride was then delivered into the GE TRACERlab MX FDG synthesizer and collected into a 10 mL sealed vial, readily put inside a lead pot. The lead pot was then placed inside a transport box before transported to Malaysian Nuclear Agency. Upon arrival (transit time ~ 30 min), the radioactivity of [$^{18}$F]-fluoride will be determined using radioisotope calibrator (Capintec CRC-712MH) before being transferred into the hot-cell prior to synthesis.

## Results and Discussion

**Development of the Synthesizer**

The [$^{18}$F]FCH synthesizer are based from several criteria as following: a) relatively easy to develop, b) user friendly, c) high radiochemical yield and purity, d) relatively low cost, as well as e) safe and reliable.

The basic functions of the synthesizer are: a) introduction of [$^{18}$O]-water into the system, b) separation of [$^{18}$F]-fluoride from [$^{18}$O]-water; the most commonly method to do it is by using an anion exchanger resin, c) elimination of water traces by using azeotropic distillation, d) nucleophilic substitution between [$^{18}$F]-fluoride and precursor forming radiolabeled intermediate, e) intermediate purification using silica cartridges, f) methylation process of N,N-dimethylaminoethanol (DMAE) with intermediate, g) product purification by using cation-exchange resin, and g) purification of final product.

Based on the literature review, several models of the synthesizer specific for the [$^{18}$F]FCH would be designed and considered. From these models, a final model would be carefully selected and further modified. Materials needed for the development of the synthesizer were identified and purchased and materialization of the synthesizer was based on the final design.

The synthesizer is consists of two major parts. The first part is the processing plant, where all processes that involved radioactivity were done in a hot cell (Figure 1). The other part is the reagent plant (Figure 2), where all the chemicals, stored in conical vials were transferred into the hot cell via tygon silicon tubing through special ports at the side of the hot-cell. This design has some advantages over single, non separated design especially during

synthesis. It allows reagents to be freshly prepared or changed even when the synthesis process has started. It also contributes to smaller dimension, allowing it to fit into smaller hot cell, since almost all the reagents were located outside of the hot cell.

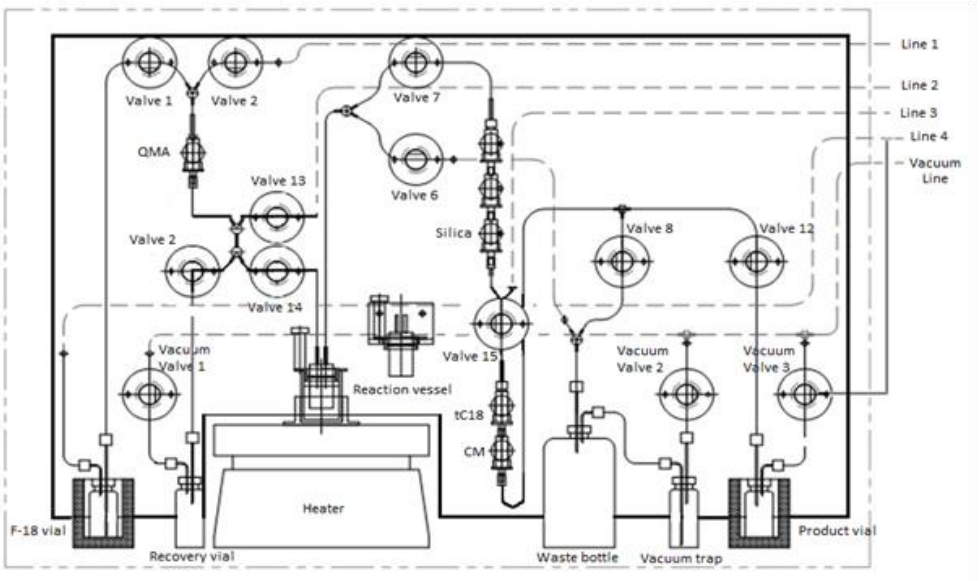



Figure 1. The processing plant of the synthesizer for [$^{18}$F]-FCH. The synthesizer is remotely operated by opening certain valves allowing the pressurized carrier gas to transfer the fluid from reagent plant into certain part of synthesizer for the desired process to happen

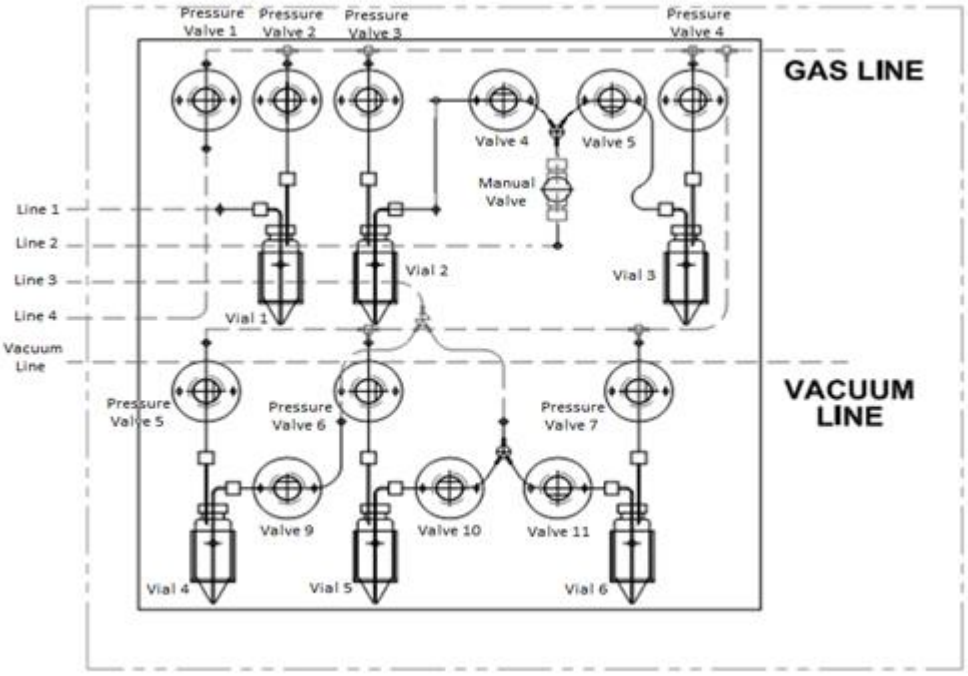



Figure 2. The reagent plant acts as a loading station for the [$^{18}$F]-FCH synthesizer where all the chemicals except for *N*,*N*-dimethylaminoethanol are loaded into their respective vials.

All seven reagents except DMAE were put into disposable 20 mL glass vials and sealed using butyl rubber septa and aluminium crimps. In order to optimize extraction from the flat bottom vials, they are later modified into conical vials with the assistance of the glassblower team. B1 vial contains $K_2CO_3$ solution, B2 contains acetonitrile, B3 contains primary precursor, B4 contains ethanol, B5 contains purified water, and B6 contains saline solution. Each vial was punctured with a pair of needles prior to synthesis, which one of the needle will penetrate until it reach the bottom of the vial and the other will penetrate just deep enough for the gas to flow.

The fluids are transferred into the processing plant through tygon tubes (internal diameter 1/16 inch) by blowing carrier gas (in our case, oxygen-free nitrogen) and under suction of vacuum, created using a mini venturi pump, connected to L5 line. When VP1 valve is opened, the nitrogen gas will flow through the tubing and creating positive pressure at [$^{18}$F]-fluoride vial. By opening V1, V2, VC1 valves, the positive pressure inside the vial and the negative pressure created by vacuum would force [$^{18}$F]-fluoride into tubing. The [$^{18}$F]-fluoride would be trapped at Sep-Pak QMA cartridge (anion exchange resin) while [$^{18}$O]-water would passed through the cartridge and finally collected in the water recovery vial. In the same manner, by controlling which valves to be opened, the direction of the fluid flow can be precisely manipulated for any desired process.

Simulations were run using sterile water to verify that the synthesizer; a) have proper tubing connections and ensure no leakage occurred as well as b) showed intended flow direction. Correction actions were taken to rectify the problems founds. The finished prototype is shown in Figure 1. The dimension of the synthesizer is 0.46m (length) x 0.5m (height) x 0.14m (wide) for the reagent plant and 0.74m (length) x 0.50m (height) x 0.5m (wide). The cost of the synthesizer is estimated around RM 30, 000.

**Calibration of the Heating System**

One of the critical components of the synthesizer is the heating system. In the [$^{18}$F]FCH synthesizer, there are at least two occasions where heating are required. The first heating event happened during the azeotropic distillation, where the mixture of [$^{18}$F]-fluoride, solution of 33 mM $K_2CO_3$ and acetonitrile are heated. The second heating are required for reaction between anhydrous [$^{18}$F]-fluoride with dibromomethane. Therefore, the heating system must be able to achieve accurate and consistent required temperature in order for the synthesizer to function as it should be.

There is a wide range of suggested temperature for the first heating process (evaporation process) from 110 ºC [13], 100 ºC [14], 95 ºC [17] and 90 ºC [18]. The second heating process did not have specific temperature, as the reaction temperature is the manipulated variable for the synthesis. Based from Kryza et al. report, we set the temperature range to be within 70-90 ºC.

It is worth mentioning that since both heating process were not done simultaneously and both processes were done at the same vessel, normally only one heating system is required to do both jobs. Among the heating methods use for synthesis PET fluoro-compound are oil bath for example use by Iwata et al. [13], stream of heated air such as showed by Cheung and Ho [19] and heating tape for example use by Ahmed et al. [20].

We have tested oil bath method using 20 mL silicone oil as heating medium in a custom-made glass cup. The temperature controller was connected to a hotplate and the controller would receive input from a thermocouple soaked in the medium, where once the targeted temperature has been achieved, the controller would cut off power supply to the hotplate. Unfortunately, reliable temperature could not be achieved by using this configuration since temperature fluctuations were high (data not shown). Thus the air process heater is used as an alternative, as it was proven as a success in previous studies.

The new heating system using the air process heater worked principally the same as the hotplate system, instead of using hotplate, air process heater was used where hot air passed through a custom-made inner glass tube (open at the top) surrounded by a glass jacket. The heated air is circulated within the jacket and the heat is transfer from the glass tube to the silicone oil (Figure 3). Once this heating concept has been proved successfully, the glass tube and the jacket were replaced with stainless steel tube and jacket.

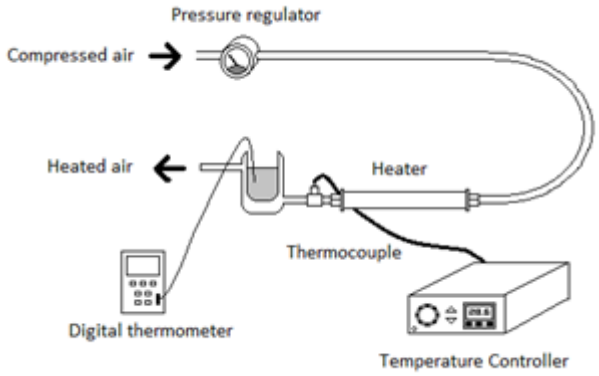



Figure 3. Simplified diagram of the air process heater for the synthesizer. The compressed air is passed through the heater and the temperature of the air is measured with thermocouple probe, which is connected to the temperature controller. The actual temperature of heating medium is measured using digital thermometer.

The heating system was tested and calibrated using a digital thermometer. The heating system showed good accuracy, consistent performance and stable temperature. However, it is found later that the heater required about 30 minute to achieve designated temperatures from ambient temperature (Figure 4), thus two set of heaters are used, one is for evaporation process (Heater A) and the other is for the fluorination process (Heater B). Nevertheless the results showed that the temperature has to be set higher than the required temperature, as a result of heat loss. Therefore, through a series of try and errors, a balance of temperature set and actual temperature of the heating medium is obtained (Figure 5). The calibration curve is then tested and the results are showed in Table 1.

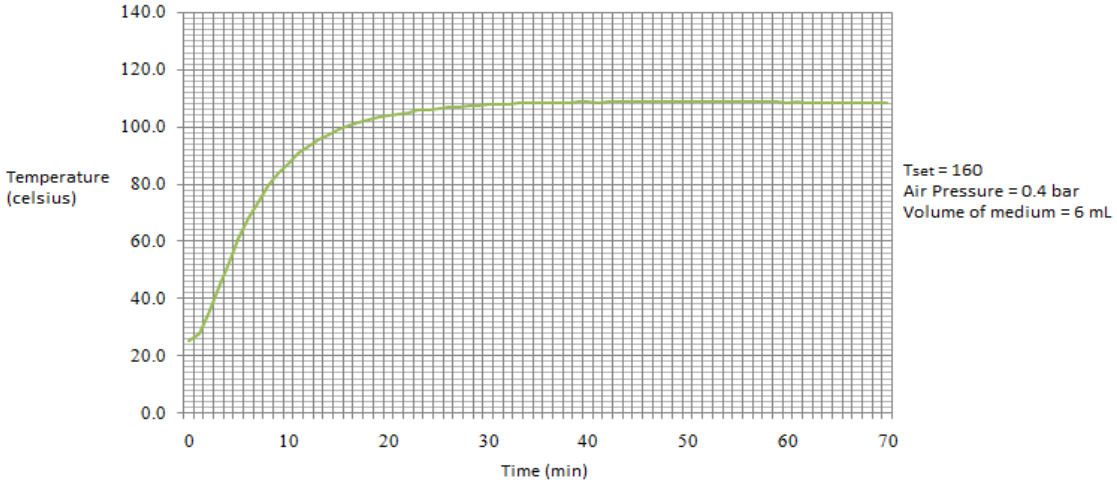



Figure 4. Temperature profile of heating system of the synthesizer. Note that the heating system required about 30 min before it reached equilibrium, thus making double heater system a necessity in order to achieve consistent heating for both the azeotropic distillation and fluorination process.

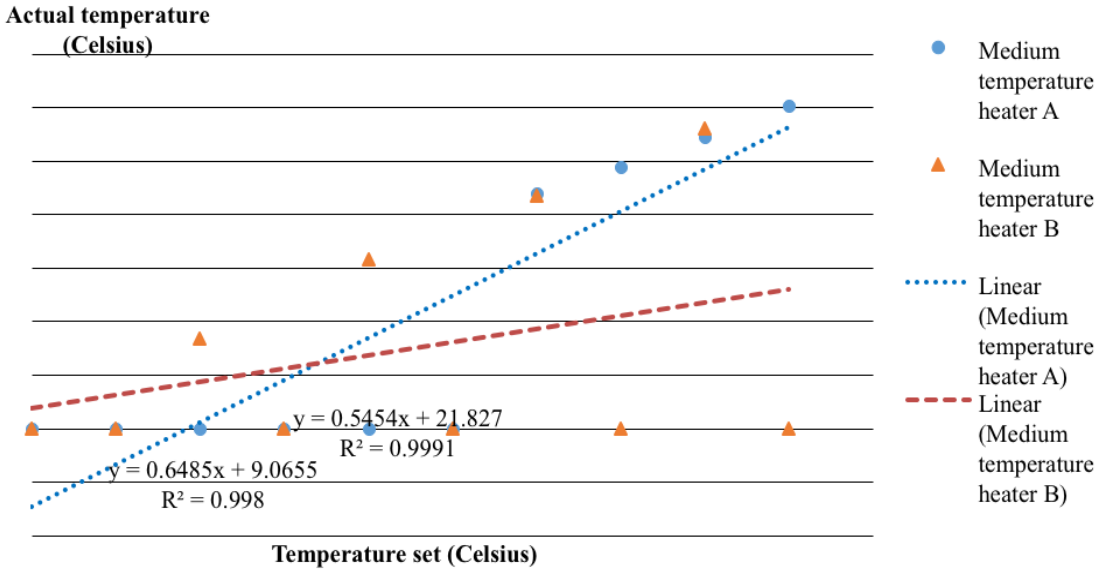



Figure 5. Calibration of the heating system of the synthesizer. The required temperature of the heating medium is achieved by increasing the temperature set at the temperature controller.

Table 1. Validation of the heating system based on value calculated from calibration curve of the heating system.

| $T_{require}$ | $T_{set}$ (°C) | $T_{measure}$ (°C)[b] |
|---|---|---|
| **110** | 161[a] | 111.342 ± 0.149 |
| **90** | 125 | 90.630 ± 0.333 |
| **80** | 109 | 80.822 ± 0.263 |
| **70** | 94 | 72.498 ± 0.272 |

a – Data obtained from heater A. The rest are performed on heater B,
b – Measurements were made from 30$^{th}$ to 90$^{th}$ min after the heater is on.

**Synthesis of [$^{18}$F]FCH**

The trapped [$^{18}$F]-fluoride was eluted from the cartridge by using 1 mL $K_2CO_3$ solution (33 mM) at B1 vial into the reaction vessel. Then 1 mL acetonitrile was added inside the vessel and the mixture was heated at 80-90 °C until dried. The process is repeated three times to ensure no residual water was left for the next process. Primary precursor ($CH_2Br_2$) was added to reaction vessel and allowed to react for 6 minute at temperature of 80-90 °C (based from Kryza et al.). The labelled intermediate was then transferred to triple Sep-Pak silica cartridges for separation of labelled and unlabelled compounds. The labelled compound were directed to tC18 cartridge containing 400 µL DMAE and the product is trapped at Sep-Pak CM cartridge by 10 mL ethanol elution. The cartridges were rinsed with 15 mL purified water. Final step is involving the elution of the product into the product vial by 3 mL 0.85% saline solutions. Data of the synthesis is shown in Table 2.

The resulted radiochemical was lower than originally anticipated. The highest yield achieved is only 1.446 %. In contrast to Kryza et al. [17], they reported non-corrected yield of 15-25 %. Since manipulating the amount of

precursor and solvent, reaction temperature and time, as well as evaporation temperature and time did not give significant increase in radiochemical yield, we suspect the problem lie in QMA carbonate cartridge that we used, compare to ordinary QMA cartridge used by other groups. However, further study proved that was not the case as more than 80% of the activities were collected at the reaction vessel and less than 0.2 % was trapped at the cartridge after elution (Table 3). Another study showed that there is still a significant activity left at the reaction vessel, 78.923 % after a complete synthesis was done (Table 4). The result suggested that the low yield was probably contributed by incomplete reaction between [$^{18}$F]-fluoride and the precursor.

Table 2. Effect of quantity of precursor, reaction temperature, evaporation time on radiochemical yield of [$^{18}$F]FCH

| **Quantity of $CH_2Br_2$ (µL)** | **Reaction Temperature (°C)** | **Evaporation Temperature (°C)** | **Evaporation time (min)** | **Corrected Yield (%)** |
|---|---|---|---|---|
| **300** | 80 | 90 | 10x3 (+ 15 mg $K_{222}$) | 0.089 |
| **700** | 80 | 90 | 10x3 (+ 15 mg $K_{222}$) | 0.193 |
| **700** | 80 | 90 | 15x3 (+ 15 mg $K_{222}$) | 0.100 |
| **700** | 80 | 80 | 15x3 (+ 15 mg $K_{222}$) | 0.291 |
| **700** | 90 | 80 | 15x3 (+ 15 mg $K_{222}$) | 0.334 |
| **100/1 mL asetonitrile** | 90 | 80 | 15x3 (+ 15 mg $K_{222}$) | 0.024 |
| **200/0.5 mL asetonitrile** | 90 | 80 | 15x3 (+ 15 mg $K_{222}$) | 0.206 |
| **1000** | 90 | 80 | 15x3 (+ 15 mg $K_{222}$) | 1.446 |

Table 3. Activity distribution of [$^{18}$F]F vial, Sep-Pak light QMA Carbonate cartridge, collection vial and reaction vessel after elution

| **Component** | **Radioactivity (decay corrected), mCi** | | |
|---|---|---|---|
| | **Sample 1** | **Sample 2** | **Sample 3** |
| **[$^{18}$F]F vial before elution** | 7.610 | 5.550 | 7.080 |
| **[$^{18}$F]F vial after elution** | 0.154 | 0.030 | 0.076 |
| **Cartridge after elution** | 0.008 | 0.004 | 0.007 |
| **Collection vial** | 0.033 | 0.023 | 0.025 |
| **Reaction vessel** | 6.750 | 5.000 | 5.890 |

Table 4. Activity distribution of components of the synthesizer after a complete synthesis run. Note that majority of the remaining activity is concentrated at reaction vessel

| Component | Measured radioactivity (mCi) | Corrected radioactivity, A (mCi) | A/initial activity x 100% |
|---|---|---|---|
| **[$^{18}$F]F$^-$ vial** | 2.110 | 5.893 | 8.007 |
| **QMA cartridge** | 0.042 | 0.132 | 0.179 |
| **Reaction vessel** | 19.900 | 58.087 | 78.923 |
| **Silica cartridges** | 0.459 | 1.491 | 2.026 |
| **tC18 cartridge** | 0.004 | 0.012 | 0.016 |
| **Accell CM cartridge** | 0.001 | 0.003 | 0.004 |
| **Product vial** | 0.069 | 0.188 | 0.255 |

Table 5. Effect of reaction temperature and flow rate of carrier gas on radiochemical yield of [$^{18}$F]FCH

| Quantity of $CH_2Br_2$ (µL) | Reaction Temperature (°C) | Evaporation Temperature (°C) | Flow rate (mL/min) | Corrected Yield (%) |
|---|---|---|---|---|
| **600** | 80 | 90 | 140 | 1.636 |
| **600** | 90 | 90 | 140 | 2.427 |
| **600** | 80 | 90 | 30 | 7.719 |
| **600** | 90 | 90 | 30 | 8.113 |
| **600** | 100 | 90 | 30 | 10.131 |

The results listed in Table 2 were obtained when the radiopharmaceutical was produced under high flow rate setting (>100 mL/min of carrier gas). When the flow rate decreases to 25mL/min during elution process from the triple Sep-Pak silica cartridges, it was observed that there was a significant increase of radiochemical yield (Table 5). These results suggest that low flow rate allows more time for the radiolabelled intermediate to react with DMAE, thus increasing the yield. However, all our attempts to further increase the yield were unsuccessful.

The product was analyzed using HPLC system (column C18 4.6 x 150 mm$^2$, acetonitrile: ammonium formiate 0.1 mol/L at 79:21). From the radiochromatograph, it is clear that the radiochemical purity of the [$^{18}$F]-fluorocholine produced by using our synthesizer is high; >99% (Figure 6). No other peaks were found. Retention time is 4.32 min. When we injected a pure [$^{18}$F]-fluoride into the HPLC system, we find a good separation between [$^{18}$F]-fluoride and [$^{18}$F]-fluorocholine, with retention time = 1.56 min.

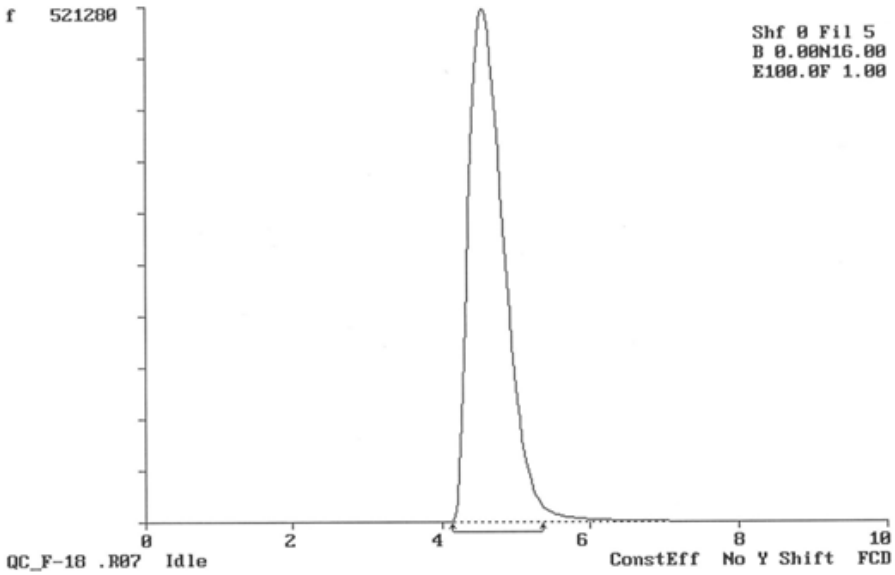



Figure 6. Radiochromatogram of the [$^{18}$F]FCH synthesized

## Conclusion

We have managed to develop a remotely controlled lab-scale [$^{18}$F]FCH synthesizer that is relatively low cost and simple to operate. The synthesizer is divided into two major parts, namely the processing plant where all the processes of synthesis are done and the other part is the reagent plant that serves to introduce the chemicals into the processing plant. Two set of air process heaters are used for the synthesizer and the heating system provides good accuracy, consistent performance and stable temperature. Synthesis of [$^{18}$F]FCH were done with two steps approach, by adding dried [$^{18}$F]-fluoride with dibromomethane to produce [$^{18}$F]-fluorobromethane before converted the radiolabeled compound into [$^{18}$F]FCH by reacting with N,N-dimethylaminoethanol. We were able to achieve decay-corrected radiochemical yield of 10.131% under 110 min and the radiochemical purity achieved is high; >99%. The low radiochemical yield warrants further analyses and optimization is still underway.

## Acknowledgement

We wish to thank the team from Department of Nuclear Malaysia, Hospital Putrajaya for the cooperation and Nuclear Medicine Division, Malaysian Nuclear Agency for their continuous laboratory assistance. We also would like to express gratitude to Ministry of Science, Technology and Innovation for funding this research (02-01-02-SF0675).

## References

1. Lim, C.C., Yahaya, H. and Lim. (2003). First Report of the National Cancer Registry: Cancer Incidence in Malaysia 2002. Kuala Lumpur: National Cancer Registry.
2. Lim, C.C. and Yahaya, H. (2004). Second Report of the National Cancer Registry: Cancer Incidence in Malaysia 2003. Kuala Lumpur: National Cancer Registry.
3. Fass, L. (2008). Imaging and cancer: A review. *Journal of Molecular Oncology* 2: 115-152.
4. Bombadieri, E., Alessi, A., Villano, C., Gerali, A., and Crippa, F. (2008). The relevance of PET in diagnosis oncology. In Biersack, Hans-Jurgen and Freeman, L.M. (editor). *Clinical Nuclear Medicine*, pg. 360-391. Berlin: Springer.
5. Pantaleo, M.A., Nannini, M., Maleddu, A., Fanti, S., Ambrosini, V., Nanni, C., Boschi, S., and Biasco, G. (2008). Conventional and novel PET tracers for imaging in oncology in the era of molecular therapy. *Cancer Treatment Reviews* 34: 103-121.

6. Hara, T. (2001). 18F-Fluorocholine: A new oncologic PET tracer. *Journal of Nuclear Medicine* 42(12): 1815-17.
7. Price, D.T., Coleman, R.E., Liao, R.P., Robertson, C.N., Polascik, T.J., and DeGrado, T.R. (2002). Comparison of [$^{18}$F]fluorocholine and [$^{18}$F]fluorodeoxyglucose for positron emission tomography of androgen dependent and androgen independent prostate cancer. *Journal of Urology* 168: 273-280.
8. Picchio, M.,Messa, C., Gianolli, L., Sironi, S., Brioschi, M., Matarrese, M., Matei, V., De Cobelli, F., Del Mashio, A., Rocco, F., Rigatti, P., and Fazio, F. (2003). Value of [11C]choline-positron emission tomography for re-staging prostate cancer: A comparison with [$^{18}$F]fluorodeoxyglucose-positron smission tomography. *Journal of Urology* 169: 1337-40
9. Reske, S.V., Blumstein, N.M., Neumaier, B., Gottfried, H.W., Finsterbusch, F., Kocot, D., Moller, P., Glatting, G., and Perner, S. (2006). Imaging prostate cancer with 11C-choline PET/CT. *Journal of Nuclear Medicine* 47(8): 1249-54.
10. Pieterman, R.M., Tjin, H.Q., Elsinga, P.H., Pruim, J. van Putten J.W.G., Willemsen, A.T.M., Vaalburg, W., and Groen, H.J.M. (2002). Comparison of $^{11}$C-choline and 18F-FDG PET in primary diagnosis and staging of patients with thoracic cancer. *Journal of Nuclear Medicine* 43: 167-172.
11. DeGrado, T.R., Baldwin, S.W., Wang, S., Orr, M.D., Liao, R.P., Friedman, H.S., Reiman, R., and Price, D.T. (2000). Synthesis and evaluation of $^{18}$F-labeled choline as an oncologic tracer for positron emission tomography: Initial findings in prostate cancer. *Journal of Cancer Research* 61: 110-117.
12. DeGrado, T.R., Baldwin, S.W., Wang, S., Orr, M.D., Liao, R.P., Friedman, H.S., Reiman, R., Price, D.T., and Coleman, R.E. (2001). Synthesis and evaluation of $^{18}$F-labeled choline as an oncologic PET tracers. *Journal of Nuclear Medicine* 42: 1805-14.
13. Iwata, R., Pascali, C., Bogni, A., Furumoto, S., Terasaki, K., and Yana, K. (2002). [18F]fluoromethyl triflate, a novel and reactive [$^{18}$F]fluoromethylating agent; preparation and application to the on-column preparation of [$^{18}$F]fluorocholine. *Applied Radiation and Isotopes* 57: 347-352.
14. Hara, T., Noboru, K. and Hiroichi, K. (2002). development of $^{18}$F-fluoroethylcholine for cancer imaging with PET: Synthesis, biochemistry, and prostate cancer imaging. *Journal of Nuclear Medicine* 43: 187-199.
15. Bauman, A., Piel, M., Schirmacher, R., and Rosch, F. (2003). Efficient alkali iodide promoted fluoroehtylations with 2-[$^{18}$F]fluoroethyl tosylate and 1-bromo-2-[18F]fluoroethane. *Tetrahedron Letters* 44: 9165-67.
16. Piel, M., Bauman, A., Baum, R.P., Hohnemann, S., Klette, I., Wortman, R. and Rosch, F. (2007). Improved automated synthesis of [18F]fluoroethylcholine as a radiotracer for cancer imaging. *Bioorganic and Medicinal Chemistry* 15: 3171-75.
17. Kryza, D., Tadino, V., Filannino, M.A., Villeret, G., and Lemoucheux, L. (2008). Fully automated [$^{18}$F]fluorocholine synthesis in the TracerLab MXFDG Coincidence synthesizer. *Nuclear Medicine and Biology* 35: 255-260.
18. Zuhayra, M., Alfteimi, A., Papp, L., Lutzen, U., Lutzen, A., Von Forstner, C., Meller, B. and Henze, E. (2008). Simplified fast and high yielding automated synthesis of [18F]fluorethylcholine for prostate cancer imaging. *Bioorg Med Chem*. 16(20):9121-9126.
19. Cheung, M.K. and Ho, C.L. (2009). A simple, versatile, low-cost and remotely operated apparatus for [$^{11}$C]acetate, [$^{11}$C]choline, [$^{11}$C]methionine and [$^{11}$C]PIB synthesis. *Applied Radiation and Isotopes* 67: 581–589.
20. Ahmed, N., Langlois, R., Rodrigue, S., Bernard, F., van Lier, J. E. (2007). Automated synthesis of 11B-methoxy-4,16a-[16a-18F]difluoroestradiol (4F-M[$^{18}$F]FES) for estrogen receptor imaging by positron emission tomography. *Nuclear Medicine and Biology* 34: 459–464.

The Malaysian Journal of ANALYTICAL SCIENCES ISSN 1394-2506

# EFFECT OF GAMMA RADIATION ON AMINO ACID BASED VESICLE CARRYING RADIOSENSITIZER

## (Kesan Sinaran Gama ke atas Vesikel berasaskan Asid Amino yang membawa Pemeka Sinaran)

Nur Ratasha Alia Md. Rosli, Faizal Mohamed*, Muhammad Amir Syafiq Md. Sah, Irman Abdul Rahman

*School of Applied Physics, Faculty of Science and Technology*
*Universiti Kebangsaan Malaysia, 43600 UKM Bangi, Selangor, Malaysia*

**Corresponding author: faizalm@ukm.edu.my*

**Abstract**

Vesicles has been developed and studied to be used as a medium to transport radiosensitizer in treating cancer cells by increasing its sensitivity effectively towards the radiation given during radiotherapy. This study was conducted to investigate the effect of gamma radiation on amino acid-based vesicle carrying radiosensitizer. Amino acid based vesicles carrying radiosensitizer were synthesized using sonication method with sodium N-lauroylsarcosinate hydrate and decanol being the primary surfactant, while hydrogen peroxide and sodium hyaluronate as the encapsulated radiosensitizer. The synthesized vesicle was then irradiated at radiation doses equilvalent to those given during radiotherapy. Irradiated vesicle carrying radiosensitizer were then characterized using Transmission Electron Microscopy (TEM), Fourier Transform Infrared Spectroscopy (FTIR) and Polarized Light Microscope. Results obtained shows that there were no significant changes in morphology and molecular conformation of the synthesized vesicle after irradiation. Even at higher radiation dose of 100 Gray and 200 Gray , the results remained unchanged. This indicates that the synthesized vesicle carrying radiosensitizer is morphologically and spectroscopically stable even at high radiation doses.

**Keywords**: Amino acid based Vesicle, Radiosensitizer, Radiation, Radiotherapy, Cancer

**Abstrak**

Vesikel telah dihasilkan dan dikaji sebagai medium untuk membawa pemeka sinaran dalam merawat kanser secara berkesan dengan meningkatkan kesensitifan sel kanser terhadap sinaran yang diberi ketika rawatan radioterapi. Kajian ini dijalankan untuk mengkaji kesan sinaran gama ke atas vesikel berasaskan asid amino yang membawa pemeka sinaran. Vesikel berasaskan asid amino yang membawa pemeka sinaran telah disintesis menggunakan kaedah sonikasi dengan natrium N-lauroylsarcosinat hidrat dan dekanol sebagai sufaktan utama, manakala hidrogen peroksida dan natrium hialuronat sebagai pemeka radio yang dikapsulkan. Vesikel yang disintesis telah disinarkan dengan dos sinaran yang setara dengan dos yang diberi ketika rawatan radioterapi. Pencirian telah dilakukan ke atas vesikel membawa pemeka sinaran yang disinarkan menggunakan Mikroskopi Elektron Transmisi (TEM), Spektroskopi Inframerah Transformasi Fourier (FTIR) dan Mikroskop Cahaya Polarisasi. Hasil kajian menunjukkan bahawa tiada perubahan yang signifikan dari segi morfologi dan konformasi molekul vesikel membawa pemeka sinaran setelah disinar. Walaupun disinarkan pada dos sinaran 100 Gray dan 200 Gray, hasilnya tetap sama. Ini menunjukkan bahawa vesikel membawa pemeka sinaran yang disintesis adalah stabil dari segi morfologi dan spektroskopi terhadap sinaran walaupun dos sinaran yang tinggi telah diberikan.

**Kata kunci:** Vesikel berasaskan Asid Amino, Pemeka Sinaran, Sinaran, Radioterapi, Kanser

## Introduction

Non ionic surfactant vesicle, also known as niosomes, are closed bilayer structures formed from the self-assembly of non ionic amphiphiles in aqueous medium [1]. Through its bilayer structure, vesicles has the ability to encapsulate hydrophilic drugs in its aqueous core and hydrophobic drugs in its membrane [2, 3]. Niosomes possess several advantages in the form of chemical stability, lower cost and availability of material in comparison with conventional liposome vesicles [4]. Thus there has been an increase of interest in studying and developing niosomes

as a tool for drug delivery [5]. Recently, a biodegradable and biocompatible niosome was developed from an amino acid based biosurfactant Sodium N-lauroylsarcosinate Hydrate [6]. The vesicle was proven to have good characteristics and potential as a drug deliverer or carrier [6]. Due to this, studies on the ability of this niosome to encapsulate radiosensitizer was conducted.

Radiosensitizer are chemotherapeutic agents that have been developed to increase the therapeutic effect of radiation treatment by increasing the sensitivity of cancer cells towards radiation [7-10]. In 2011, a combination of radiosensitizers, Hydrogen Peroxide and Sodium Hyaluronate, has been developed and proven clinically to give promising results in treating cancer patients who undergoes radiotherapy. These radiosensitizer not only inactivates anti-oxidative enzymes but also produces oxygen from the degradation mechanism of hydrogen peroxide, resulting hypoxic tumor being reoxygenated [11-12]. Thus cancer cells becomes more sensitive towards radiation. But because of the rapid degradation of Hydrogen Peroxide, the delivery of the radiosensitizers via intratumoral injection causes patient to experience local pain at the injection site [11-12] and may also cause complications such as pulmonary embolism [11]. Thus, studies on the ability of amino acid based vesicle loaded with these radiosensitizers was conducted so that the drug therapeutic index could be increased while reducing the toxicity of the drug. In line with this study, the effect of gamma radiation on amino acid based vesicle carrying radiosensitizers was also studied

## Materials and Methods

### Materials

Sodium N-lauroylsarcosinate Hydrate and Sodium Hyaluronate with 95% purity were purchased from Acros Organics (New Jersey, United States of America), 1-decanol with 97% purity was purchased from Fluka-Chemical (Switzerland) and Hydrogen Peroxide with 30% purity was purchased from Friendemann Schmidt Chemical (Germany). Deionised water was used to prepare all of the samples.

### Synthesis of Radiosensitizer

The radiosensitizing agent used in this study was synthesized according to the method previously reported by Ogawa and Tokuhiro [11-12] with several modifications. Stock solutions of 1% w/v Sodium Hyaluronate and 3% w/v Hydrogen Peroxide were prepared with deionised water. The radiosensitizing agent was synthesized by mixing 3% w/v Hydrogen Peroxide solution with 1% w/v Sodium Hyaluronate at a mixing ratio of 1:5. The mixed agent was then vortex for 3 minutes to achieve homogeneity. Hydrogen Peroxide was added just before in use in order to avoid the degradation of Sodium Hyaluronate by the oxidative effect of Hydrogen Peroxide [11].

### Synthesis of Amino Acid based Vesicles

Amino acid based vesicles (AABV) were prepared according to the sonication method as previously reported by Akter [6] with several modifications. Sodium N-lauorylsarcosinate Hydrate and 1-decanol was added in a test tube at a molar ratio of 1:2. Then 92 wt% of deionised water was added in the test tube and the resulting suspension was sonicated at 60°C for 10 minutes using a bath sonicator. The mixture was then vortex for 5 minutes to obtain microemulsion. The mixture is centrifuged for 4000 rpm for 10 minutes to obtain phase separation.

### Preparation of Amino Acid based Vesicles carrying Radiosensitizer

Amino acid based vesicles carrying radiosensitizers (AABVRS) were prepared in the same protocol as in the control vesicles. However, prior to the additon of sodium n-lauroylsarcosinate hydrate and 1-decanol in the test tube, the prepared radiosensitizers was mixed with 1-decanol at a ratio of 1:1 and vortex for 3 minutes. This allows the radiosensitizer to form a complex with 1-decanol and thus physically be encapsulated in the vesicle.

### Irradiation of Amino Acid based Vesicles carrying Radiosensitizer

The synthesized amino acid based vesicle carrying radiosensitizer samples were then irradiated using a GammaCell 220 Excel (MDS Nordion). Radiation doses of 4 Gy, 8 Gy, 12 Gy, 16 Gy and 20 Gy, equivalent to those given during fractionated radiotherapy , were exposed to samples individually.

### Characterization

The formation of vesicles were characterized using polarised light microscope (PLM, Leica DM100), while

Transmission Electron Microscopy (TEM, FEI Tecnai G2 Spirit BioTwin) was used to characterize the size distribution and morphology of the control and irradiated vesicles. The infrared spectra of the samples were recorded for wavenumbers ranging from 400-4000 $cm^{-1}$ using a Perkin Elmer Spectrometer 400 FT-IR & Spotlight 400 Imaging System.

**Results and Discussion**

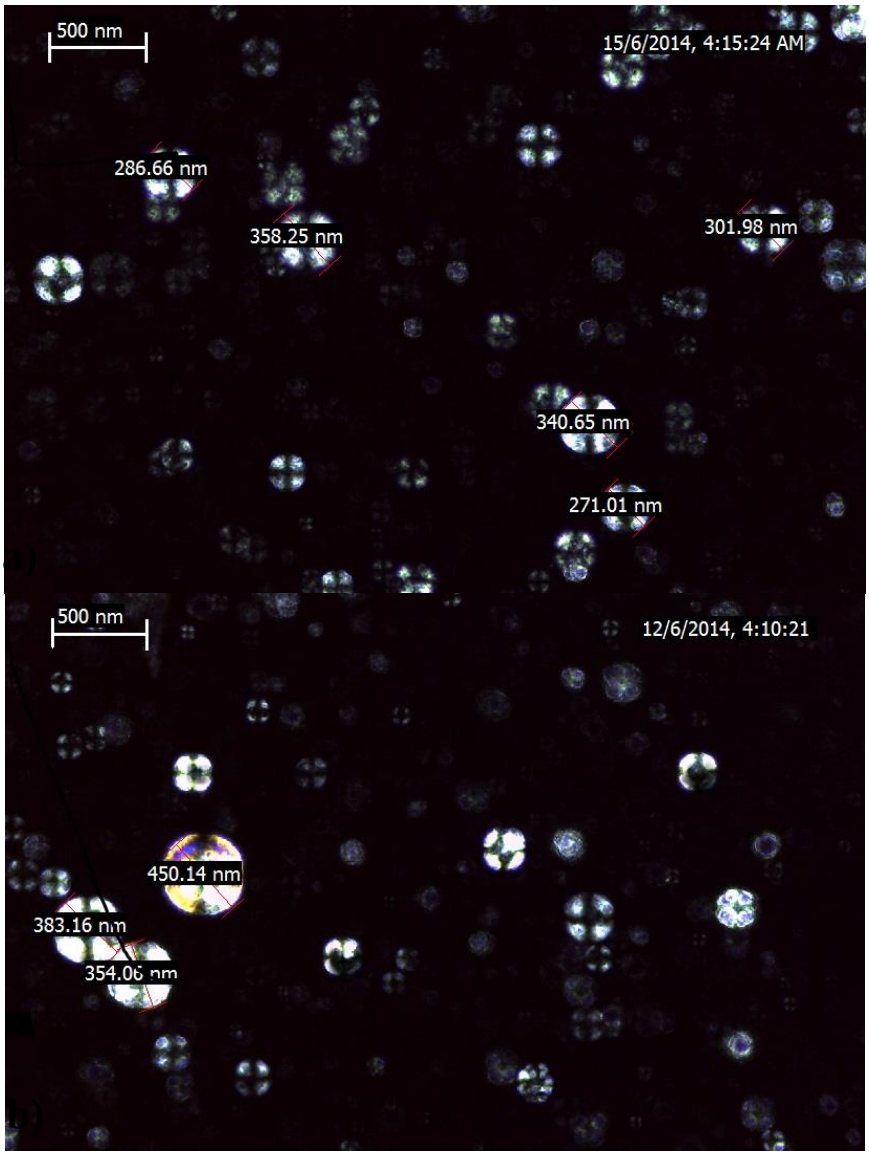



Figure 1. Polarized light microscope images of a) Amino Acid based Vesicles (AABV) and b) Amino Acid based Vesicles carrying Radiosensitizer (AABVRS) indicating vesicle formation through X cross formation

Formation of bilayer vesicle from the self-assembly of non ionic surfactants is characterized by an X cross formation under light polarization microscopy [14]. Based on Figure 1, X cross formation corresponding to the bilayer of the vesicle could be observed for both AABV and AABVRS, confirming the formation of vesicles. Through the use of LAS EZ polarized light microscopy software, AABV has a range of size from 250-360 nm,

while AABVRS has a range of size from 350-450 nm. The slight increase of size for AABVRS is attributed by the entrapment of radiosensitizing agent. The physico chemical properties of encapsulated drug influences the charge and rigidity of the niosome bilayer. The drug interacts with surfactant head group and develop the charge that creates mutual repulsion between surfactant bilayers and hence increase the vesicle size. Entrapment of drug in niosomes increases vesicle size due to interaction of drug with surfactant head group, increasing the charge of the surfactant bilayers, thereby increasing the vesicle size [15]. Thus this confirms that the radiosensitizers are entrapped in the vesicles. Due to the fact the radiosensitizers are hydrophilic [16], thus it is presumed that the drug are encapsulated in the aqueous core of the vesicles [2, 3].

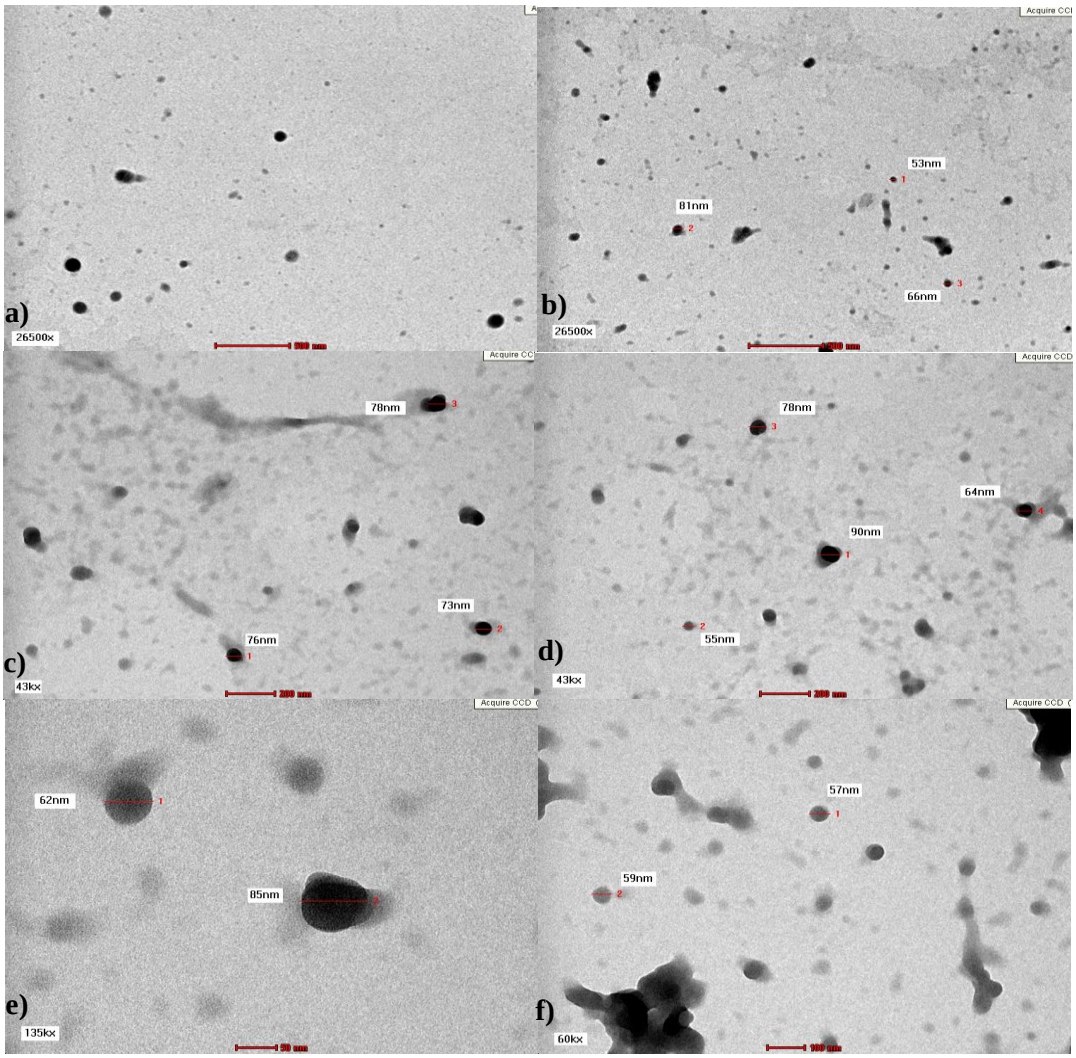



Figure 2. TEM images of Amino Acid based Vesicles carrying Radiosensitizer (AABVRS) irradiated at a) 0 Gy, b) 4 Gy, c) 8 Gy, d) 12 Gy, e) 16 Gy and f) 20 Gy.

The morphology of control and irradiated AABVRS could be observed in the TEM images in Figure 2. It could be seen that the vesicle has a spherical morphology which is represented by a bright border surrounding an internal cavity [6]. Even though the AABVRS were irradiated up to 20 Gy, the morphology of the vesicle remained

unchanged with no deformation observed. IMAGE J software was used to estimate the average size of control and irradiated AABVRS based on the TEM images. Based on Figure 3, the average size of control and irradiated AABVRS is in the range of 73.05-77.30 nm. The average size of AABVRS viewed by TEM is different with the size of those viewed under PLM. This is due to the fact that PLM has a resolution of 200 nm, whereas TEM with a higher resolution approximately 0.2 nm [17] has the ability to visualize smaller constructs [18] and surpasses vesicles which are larger in size. Through Figure 3, based on the average size of irradiated vesicle with the control, it could be deducted that there is no significant changes in the vesicle size after irradiation.

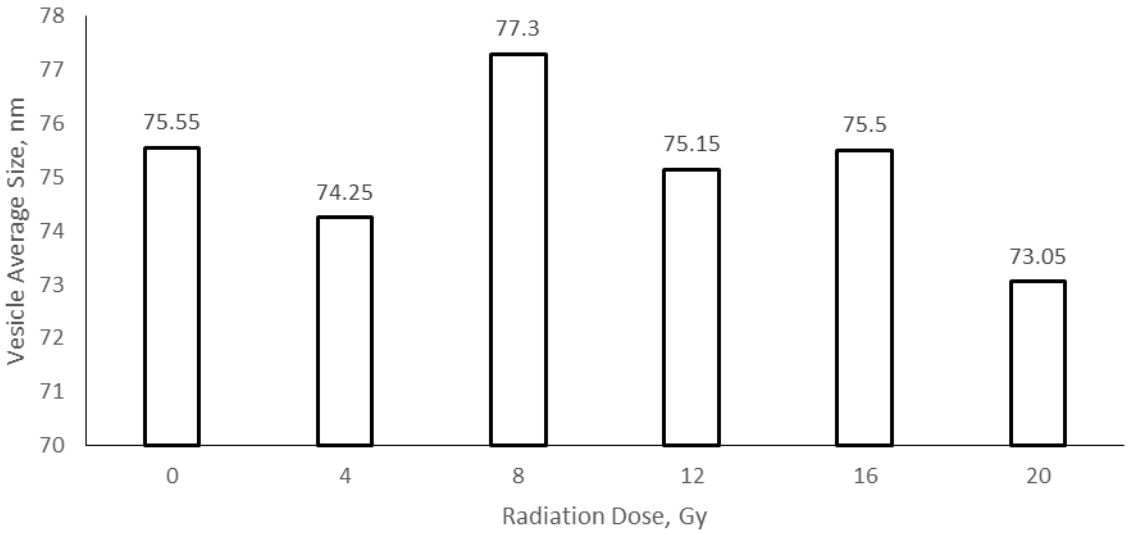



Figure 3. The average size of Amino Acid based Vesicles carrying Radiosensitizer (AABVRS) after being irradiated at 0 Gy, 4 Gy, 8 Gy, 12 Gy, 16 Gy and 20 Gy.

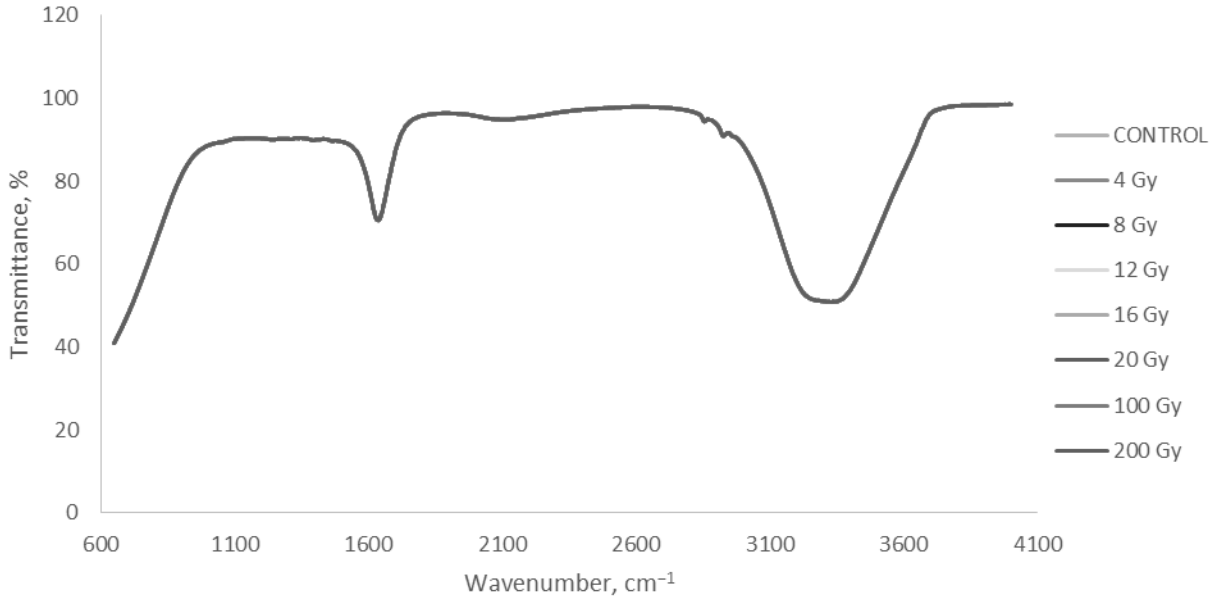



Figure 4. FTIR spectra of Amino Acid based Vesicles carrying Radiosensitizer (AABVRS) after being irradiated at 0 Gy, 4 Gy, 8 Gy, 12 Gy, 16 Gy, 20 Gy, 100 Gy and 200 Gy.

Figure 4 shows the FTIR spectra of the vesicle in deionised water. Maxima were found at 1656cm$^{-1}$ which is shifted from a split peak in the surfactant originally at 1640cm$^{-1}$ and 1648 cm$^{-1}$ [6]. The shift is attributed by the hydrogen bonding between C=O at the amide group and the alcoholic hydroxyl group. Bound water also contributed to this bonding. This is due to the reduction of hydration due to the addition of decanol [6]. Theoretically, the chemical changes that occur when polymer were irradiated includes cross linking where inter or intra molecular bond is formed, bond scission, formation of carbon carbon double bonds or formation of hydrogen and methane [19]. However based on Figure 4, it could be seen that there is no significant changes on the chemical conformation of the vesicle encapsulating radiosensitizer. Even at higher radiation dose of 100 Gray and 200 Gray, no spectroscopic changes were observed. This suggest that radiation does not affect the chemical property of amino acid based vesicle carrying radiosensitizer.

## Conclusion

Through this study, it could be concluded that gamma radiation does not affect the morphology, size and molecular conformation of amino acid based vesicle carrying radiosensitizer. This demonstrates that the vesicle is physically and chemically stable towards ionizing radiation. With this property, the vesicle could be potentially used to encapsulate radiosensitizing drugs delivered during radiation therapy.

## Acknowledgement

The authors would like to acknowledge the financial support from UKM in this study, through grant FRGS/1/SG02/UKM/02/1.

## References

1. Manosroi, A., Chutoprapat, R., Abe, M. & Manosroi J. (2008). Characteristics of niosomes prepared by supercritical carbon dioxide (scCO2) fluid. *Int J Pharm*, 352 (2):248-255.
2. Chu, C., Tong, S.S., Xu, Y., Wang, L., Fu, M., Ge, Y.R., Yu, J.N. & Xu, X.M. (2011). Proliposomes for delivery of dehydrosilymarin: preparation and evaluarion in vitro and in vivo. *Acta Pharmacol.Sin.* 32(7):973-980.
3. Yang, T., Cui, F.D, Choi, M.K., Cho, J.W., Chung, S.J., Shim, C.K. & Kim D.D. (2007). Enhanced solubility and stability of PEGylated liposomal paclitaxel: in vitro and in vivo evaluation. *Int. J. Pharm.* 338(1-2):317-326.
4. Carafa, M., Santucci, E. & Lucania, G. (2002). Lidocaine loaded non ionic surfactant vesicles: characterization and in vitro permeation studies. *Int. J. Pharm.* 231(1):21-32.
5. Nasir, A., Harikumar, S.L. & Amanpreet, K. (2012). Niosome: an excellent tool for drug delivery. *International Journal of Research in Pharmacy and Chemistry*. 2(2) 479-487.
6. Akter, N., Radiman, S., Mohamed, F., Rahman, I.A. & Reza, M.I.H. (2011). Ternary phase behaviour and vesicle formation of a sodium N-lauroylsarcosinate hydrate/1-decanol/water system. *Sci. Rep.* 1:71
7. Wardman, P. (2007). Chemical Radiosensitizers for Use in Radiotherapy. J Clin Oncol. 19(6), 397-417.
8. Lawrence, T.S., Blackstock, A.W. & McGinn, C. 2003. The mechanism of action of radiosensitizer of conventionalchemotherapeutic agents. *Semin Radiat Oncol,* 13(1):13-21.
9. Bohm, L., Roos, W.P. & Serafin, A.M. (2003). Inhibition of DNA repair by pentoxifylline and related methylxanthine derivatives. J Toxicol. 193(1-2):153-160.
10. Milas, L. (2001). Cyclooxygenase-2 (COX-2) enzyme inhibitors as potential enhancers of tumour radio response. *Semin Radiat Oncol.* 11(4): 290-299.
11. Ogawa, Y., Kubota, K., Ue, H., Kataoka, Y., Tadokoro, M., Miyatake, K., Tsuzuki, T., Yamanishi, T., Itoh, S., Hitomi, J., Hamada, N., Kariya, S., Fukumoto, M., Nishioka, A. & Inomata, T. (2009). Phase I study of a new radiosensitizer containing hydrogen peroxide and sodium hyaluronate for topical tumour injection: A new enzyme-targeting radiosensitization treatment, Kochi Oxydol Radiation Therapy for Unresectable Carcinomas Type II (KORTUC II), *Int J Oncol.* 34(3), 609-618.
12. Tokuhiro, S., Ogawa, Y., Tsuzuki, K., Akima, R., Ue, H., Kariya, S. & Nishioka, A. (2010). Development of a Novel Enzyme-targeting Radiosensitizer (KORTUC) Containing Hydrogen Peroxide for Intratumoral Injection for Patients with Low Linear Energy Transfer-radioresistant Neoplasms, *Oncol Lett.* 1(6):1025-1028.
13. Pollack, A. & Ahmed, M. (2011). Hypofractionation: Scientific Concepts and Clinical Experiences. 1st. Ellicot City: LimiText Publishing.

14. Manosroi, A., Wongtrakul, P., Manosroi, J., Sakai, H., Sugawara, F., Yuasa, M. & Abe, M. (2003). Characterisation of vesicles prepared with various non ionic surfactants mixed with cholesterol. *Colloids Surf B.* 30(1-2):129-135.
15. Biswal, S., Murthy, P.N., Sahu, J., Sahoo, P., Amir, F. Vesicles of non ionic surfactants (niosomes) and Drug Delivery Potential. *Int J Pharm Sci Nanotech*. 1:1-8.
16. Necas, J., Bartosikova, L. Brauner, P. & Kolar, J. (2008). Hyaluronic acid (Hyaluronan): a review. *Veterinarni Medicina*. 8: 397-411.
17. Kane J. & Steinheim, M. (1978). Physics. John Wiley and Sons: New York.
18. Bibi, S., Kaur, R., Lacey, M.H., McNeil, S.E., Wilkhu, J., Lattaman, E., Christensen, D., Mohammed, A.R. & Perrie, Y. (2011). Microscopy imaging liposomes: From coverslips to environmental SEM. *Int. J. Pharm.* 417:138-150.
19. Utracki, L.A. (2002). Polymer Blends Handbook. Kluwer Academic Publishers: The Netherlands.

The Malaysian Journal of ANALYTICAL SCIENCES ISSN 1394-2506

# SYNTHESIS AND CHARACTERIZATION OF 5,5,7,12,12,14-HEXAMETHYL-1,4,8,11-TETRAAZACYCLOTETRADECA-7,14-DIENIUM DIPERCHLORATE COPPER(II) COMPLEX

## (Sintesis dan Pencirian Kompleks Di(Perklorat) 5,5,7,12,12,14-Heksametil-1,4,8,11-Tetraazasiklotetradeka-7,14-Dienium Kuprum(II))

Nur Hasyareeda Hassan*, Noorhanani M Ali, Bohari M Yamin, Nurul Huda Abd Karim, Noor Azlina Abd Ghani

*School of Chemical Sciences and Food Technology,*
*Faculty of Science and Technology,*
*Universiti Kebangsaan Malaysia, 43600 UKM Bangi, Selangor Darul Ehsan, Malaysia*

**Corresponding author: syareeda@ukm.edu.my*

**Abstract**

In this study, 5,5,7,12,12,14-hexamethyl-1,4,8,11-tetraazacyclotetradeca-7,14-dienium diperchlorate copper(II) complex was successfully synthesized by reacting macrocyclic tetraaza perchlorate with copper(II) acetate monohydrate in 1:1 ratio. The metal complex was characterized by variety of physicochemical techniques such as melting point, CHN elemental analysis, metal content, ultraviolet-visible spectroscopy, infrared spectroscopy, single crystal X-ray diffraction, thermogravimetric analysis, mass spectrometry and magnetic susceptibility. The infrared spectrum of complex showed four main peaks for *ν*(N-H), ν(C-H), *ν*(C=N) and ν(C-N) bands that appeared in the region of 3432, 2975, 1670 and 1088 $cm^{-1}$ respectively. X-ray single crystal structure showed a four-coordination geometry around the copper atom adopting a *monoclinic* system with a space group P/2c, unit cell dimension with *a* = 26.8271(17) Å, *b* = 7.8778(5) Å and *c* = 17.9908(12) Å; α = 90º, β = 99.05º and γ = 90º. The value of $\mu_{eff}$ (B.M) for copper (II) complex in the range of 1.23-2.21 B revealed that the complex was square planar geometry.

**Keywords**: one-pot synthesis, tetraaza macrocycles, copper (II) complex

**Abstrak**

Dalam kajian ini, kompleks 5,5,7,12,12,14-heksametil-1,4,8,11-tetraazasiklotetradeka-7,14-dienium diperklorat kuprum(II) telah berjaya disintesis hasil tindak balas makrosiklik tetraaza perklorat dengan kuprum(II) asetat monohidrat dengan nisbah 1:1. Kompleks yang terhasil dicirikan dengan pelbagai teknik fizikokimia seperti takat lebur, analisis unsur CHN, kandungan logam, spektroskopi ultra lembayung boleh nampak, spektroskopi inframerah, kristalografi sinar-X, analisis termogravimetri, spektrometri jisim dan penetapan kerentanan magnet. Spektrum inframerah kompleks menunjukkan terdapat empat jalur ν(N-H), ν(C=N), ν(C-H) dan ν(C-N) yang masing-masing wujud pada julat 3483-3151, 1668-1648, 2984-2917 dan 1292-1025 $cm^{-1}$. Struktur hablur tunggal sinar-X menunjukkan atom pusat kuprum berkoordinat empat dan hablur mempunyai sistem *monoklinik* dengan kumpulan ruang *P/2c*, dengan dimensi *a* = 26.8271(17) Å, *b* = 7.8778(5) Å dan *c* = 17.9908(12) Å; α = 90º, β = 99.05º dan γ = 90º. Nilai $\mu_{eff}$ (B) untuk kompleks kuprum(II) berada pada julat 1.7-2.2 B.M menunjukkan bahawa kompleks ini mempunyai geometri satah persegi empat.

**Kata kunci**: sintesis satu bikar, makrosiklik tetraaza, kompleks kuprum (II)

## Introduction

Synthesis of tetraaza macrocyclic ligands developed by Curtis in the 1960s opened a field with great possibilities in preparative chemistry [1]. There is a great interest in the area of synthesis and characterization of transition metal complexes with tetraaza macrocyclic ligands in recent years. However, metal template reactions have been employed in the preparation of various tetraaza macrocyclic complexes where the transition metal ion was used as a templating agent to yield the metal complexes directly [2,3]. In this study, we aimed to synthesize the 5,5,7,12,12,14-hexamethyl-1,4,8,11-tetraazacyclotetradeca-7,14-dienium salt as ligand before its conversion to

transition metal complex. The success of finding a new method for synthesizing the ligand provide an opportunity to apply the same reaction using a variety of different metal ions and could yield a higher yield compared to the metal template reaction. Cu (II) is the most studied metal ion among all the transition metal ions [4,5]. Therefore, we decided to synthesis copper(II) complex from 5,5,7,12,12,14-hexamethyl-1,4,8,11-tetraazacyclotetradeca-7,14-dienium diperchlorate salt as ligand in 1:1 ratio. The reaction is simple, cheap and also high yielding. In this paper, we report the synthesis, characterization and properties of 5,5,7,12,12,14-hexamethyl-1,4,8,11-tetraazacyclotetradeca-7,14-dienium diperchlorate ligand and 5,5,7,12,12,14-hexamethyl-1,4,8,11-tetraazacyclo-tetradeca-7,14-dienium diperchlorate copper(II) complex. The structure of ligand and its complex have been characterized by elemental analysis (CHN), Fourier transform infrared (FTIR), ultraviolet-visible spectroscopy, thermogravimetric analysis, single crystal X-ray diffraction, mass spectrometry, melting point and room temperature magnetic moment.

## Materials and Methods

### Chemicals

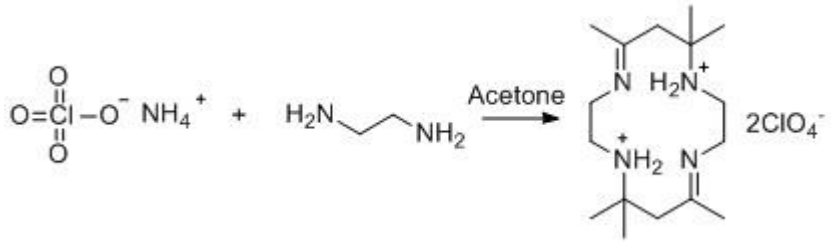
Ammonium perchlorate, ethylenediamine, copper (II) acetate monohydrate and all other reagents were purchased from Sigma-Aldrich and Friendemann Schmidt. All chemicals were of the analytical reagent grade (AR) and used without purification.

### Physical measurement

Microelemental analyses were conducted using Thermo-Finnigan Flash EA 1112 Elemental Analyzer. IR spectra were recorded on KBr discs using FTIR Perkin-Elmer GX model in the spectral range of 4000-400 $cm^{-1}$. The metal content of the copper (II) complex was determined by atomic absorption technique using Perkin-Elmer AAnalyst 800 AA spectrometer. Magnetic susceptibility was measured using Sherwood Magnetic Susceptibility Balance (Auto) at room temperature. Melting point was measured by using Barnsted Electrothermal Melting Point IA9100 series. A single-crystal X-ray diffraction investigation was performed on Bruker D8 QUEST ECO with CMOS detector. The electronic spectrum of the complex in water was recorded on Shimadzu UV-2450 and mass spectrometry was carried out using Bruker MicroTof Q Mass Spectrometer. Thermogram was obtained by using a Matter Toledo TGA/SDTA 851 instrument under $N_2$ atmosphere with a flow rate of 20 mL $min^{-1}$, in the temperature range of 0 to 600 ºC, at the heating rate of 10 ºC $min^{-1}$.

### Synthesis of macrocyclic tetraaza perchlorate, $C_{16}H_{34}N_4(ClO_4)_2$

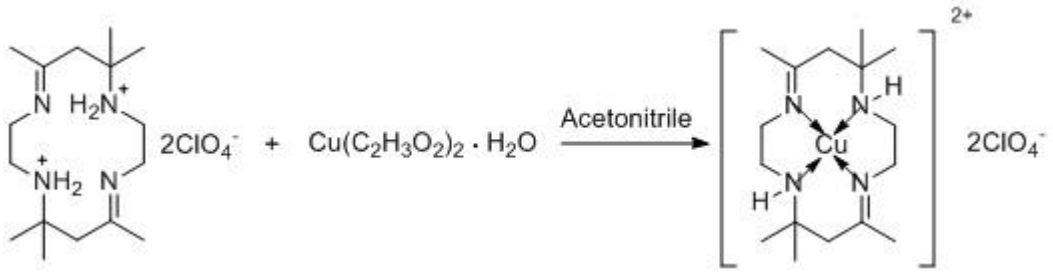
Ethylenediamine (0.01 mol) was added drop wise to a stirring acetone solution (40 mL) of ammonium perchlorate (0.01 mol). The solution mixture was stirred for 20 minutes. The solution was allowed to slowly evaporate at room temperature, upon which a precipitate was obtained. The resulting precipitate was collected by filtration, washed several times with acetone and dried overnight in a desiccator. Schematic representation of the reaction for synthesis of macrocyclic ligand, $C_{16}H_{32}N_4(ClO_4)_2$ is shown in scheme 1.




Scheme 1. Synthetic route of macrocyclic ligand

**Synthesis of 5,5,7,12,12,14-hexamethyl-1,4,8,11-tetraazacyclotetradeca-7,14-dienium diperchlorate copper(II) complex, $C_{16}H_{32}N_4OCu(ClO_4)_2$**

The ligand, (0.001 mol, 0.48 g) was dissolved in acetonitrile (10 mL). Copper (II) acetate monohydrate (0.001 mol, 0.20 g) was dissolved separately in acetonitrile (10 mL) and was then added into the beaker containing the ligand solution. The mixture was stirred for 30 minutes at 45 ºC and filtered. The solution was allowed to slowly evaporate at room temperature, upon which a precipitate was obtained. The solid product was filtered off, washed several times with ethanol and dried overnight in a desiccator. Schematic representation of the reaction for synthesis of copper (II) complex, $C_{16}H_{34}N_4OCu(ClO_4)_2$ is shown in Scheme 2.




Scheme 2. Synthetic route of copper(II) complex

## Results and Discussion

**Physical and Elemental Analysis (C, H, N)**

The ligand was obtained as white solid in 77.60% yield while the complex was synthesized in the form of a purple solid in 71.02% yield and is soluble in water and most of organic solvents. Micro elemental analysis of carbon, hydrogen and nitrogen were carried out in order to determine the elemental content of the synthesized compounds. Based on Table 1, the difference in percentage value of each element's content in the complex obtained with the theoretical value is within ±2 percent. These small differences proved that the complex is pure. The result of this analysis also proved that the stoichiometric ratio of metal to ligand for the complex is 1:1. The melting point of ligand was below 200 °C while for the complex was above 200 °C. This suggested that the compound were stable in air and moisture.

Table 1. Analytical data and physical properties of macrocyclic ligand and its complex

| Compound | Colour | Yield (%) | Melting Point (ºC) | Elemental Analysis | | | |
|---|---|---|---|---|---|---|---|
| | | | | C | H | N | Cu |
| $C_{16}H_{34}N_4(ClO_4)_2$ | White | 77.60 | 165.9-166.4 | 39.84 | 8.23 | 13.42 | - |
| | | | | **39.92** | **7.07** | **11.64** | |
| $C_{16}H_{32}N_4OCu(ClO_4)_2$ | Purple | 71.02 | 290.2-290.4 | 33.82 | 8.49 | 9.95 | 12.46 |
| | | | | **34.26** | **6.83** | **9.99** | **11.34** |

**Mass Spectrometry**

The Electrospray ionization mass spectrometry (ESI-MS) was carried out in order to confirm the composition and the purity of the complex under investigation. Besides that, ESI-MS can provide important information concerning the structure, stoichiometry, and metal oxidation state of dissolved metal complexes which are otherwise hardly obtained by electrochemical or spectroscopic techniques [6]. Figure 1 shows representative mass spectra of a

solution containing copper (II) complex measured by ESI-MS. In the ESI mass spectrum, two groups of peaks corresponding to $[CuL - 2H + ClO_4]^+$ and $[CuL - 2H]^+$ fragments are observed at m/z 442.14 and 342.18, respectively. These assignments are based on $^{63}Cu$.

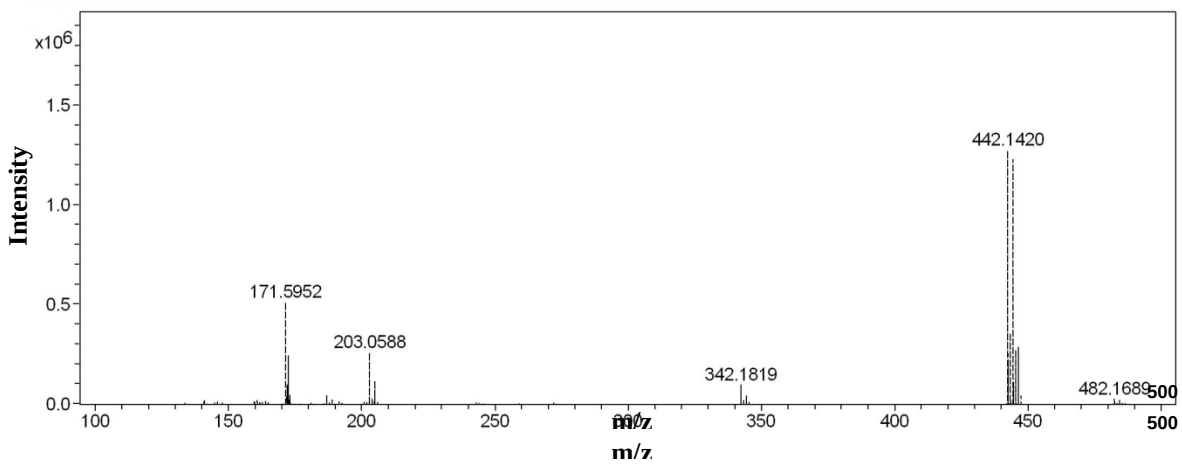



Figure 1. ESI mass spectrum of copper (II) complex

**Infrared Spectroscopy**

Infrared spectroanalysis was carried out in order to determine the functional group of the synthesized compounds. Figure 2 shows FTIR spectra of macrocyclic ligand and its complex. IR spectra of macrocyclic ligand and its complex exhibited absorption bands due to stretching vibrations of some functional groups such as amine, N-H; alkanes, C-H; azomethine, C=N and imine, C-N. The IR spectra of macrocyclic ligand and its copper (II) complex confirmed the expected C=N band at 1667 $cm^{-1}$ and 1670 $cm^{-1}$ respectively. The expected frequency of ν(C-H) and ν(C-N) were observed at 2981-2975 $cm^{-1}$ and 1088-1079 $cm^{-1}$, respectively. There was also the presence of perchlorate ion peak, $ClO_4^-$ for both spectra at 624-623 $cm^{-1}$. The free ligand spectrum exhibit a characteristic splitted band in the 3466-3407 $cm^{-1}$ range which is assigned to ν($NH_2$). The appearance of a single band at a lower frequency, 3432 $cm^{-1}$ in the copper (II) complex spectrum indicated the complexation of the macrocyclic ligand. Futhermore, the formation of copper (II) complex can be confirmed by the presence of new band in the low frequency at 446 $cm^{-1}$ which assignable to ν(Cu-N) band [7]. The comparison infrared spectroscopy data for the macrocyclic ligand and its complex is shown in Table 2.

Table 2. IR absorption peaks of macrocyclic ligand and copper(II) complex

| Compound | FTIR - wavenumbers ($cm^{-1}$) | | | | | |
|---|---|---|---|---|---|---|
| | ν (N-H) | ν (C-H) | ν (C=N) | ν (C-N) | ν ($ClO_4^-$) | ν (Cu-N) |
| $C_{16}H_{34}N_4(ClO_4)_2$ | 3466-3407 | 2981 | 1667 | 1079 | 623 | - |
| $C_{16}H_{32}N_4OCu(ClO_4)_2$ | 3432 | 2975 | 1670 | 1088 | 624 | 446 |

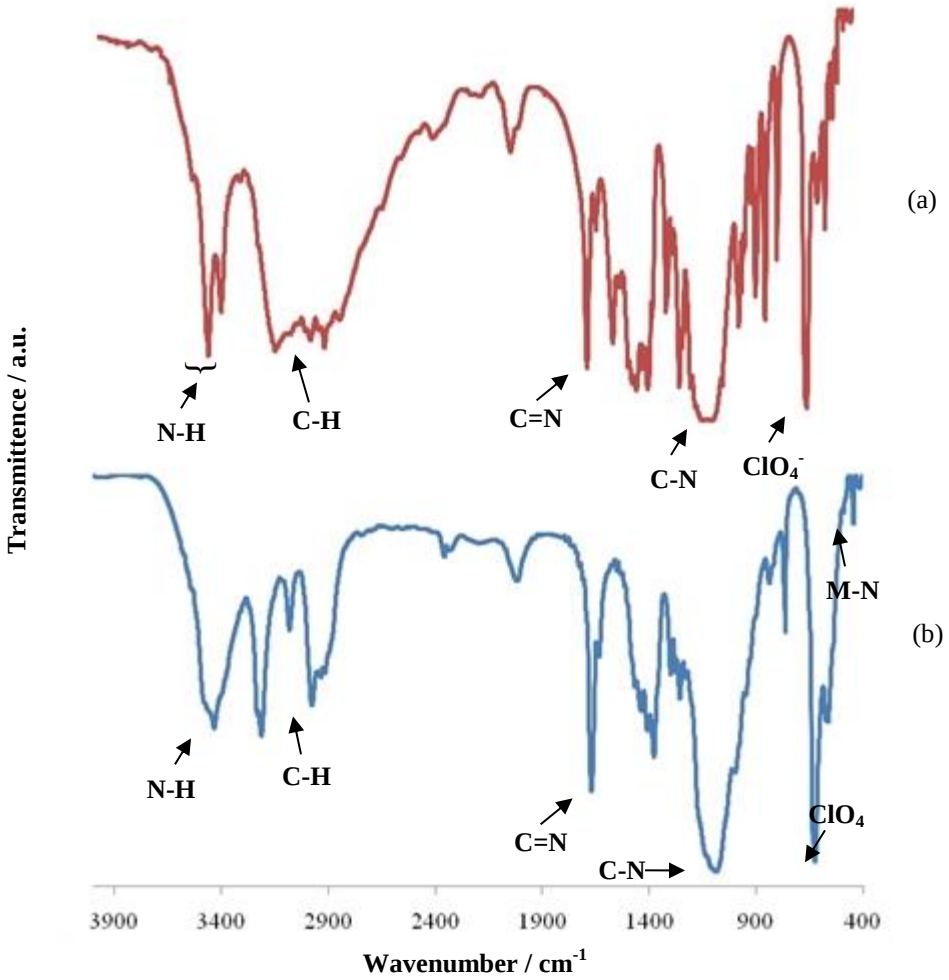



Figure 2. The FTIR spectra of (a) macrocyclic ligand and (b) copper(II) complex

**Electronic Spectral Anaysis**

The UV-Vis spectra of macrocyclic ligand and its complex are depicted in Figure 3 and 4. The characteristic absorption peak of macrocyclic ligand occurred at 241.5 nm (Fig. 3) is associated with high energy $\pi \rightarrow \pi^*$ transition of the ligand [8]. The UV-Vis for the copper II) complex was repeated at higher concentration because of a great difference in molar absorptivity. Therefore, the copper (II) complex showed a broad and very strong band in the visible region at 505 nm (Fig. 4) corresponding to a d–d transition. This band may be assigned to $^2B_{1g} \rightarrow {}^2B_{2g}$ transition which indicated the square planar geometry around the Cu (II) ion [9]. Spectroscopic data for macrocyclic ligand and copper (II) complex is shown in Table 3.

Table 3. Spectroscopic data for macrocyclic ligand and copper (II) complex

| Compound | Concentration ($mol.L^{-1}$) | $\lambda_{max}$ (nm) | Wavenumber ($cm^{-1}$) | ε |
|---|---|---|---|---|
| $C_{16}H_{34}N_4(ClO_4)_2$ | 0.001 | 241.5 | $4.14x10^4$ | 1068.0 |
| $C_{16}H_{32}N_4OCu(ClO_4)_2$ | 0.010 | 505.0 | $1.98x10^4$ | 117.9 |

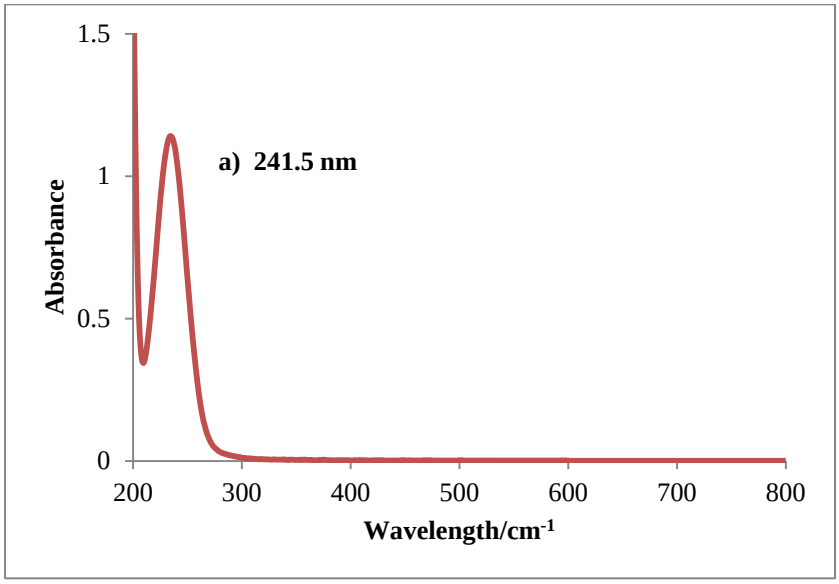



Figure 3. Absorption spectra of macrocyclic ligand at 0.001 mol.L$^{-1}$

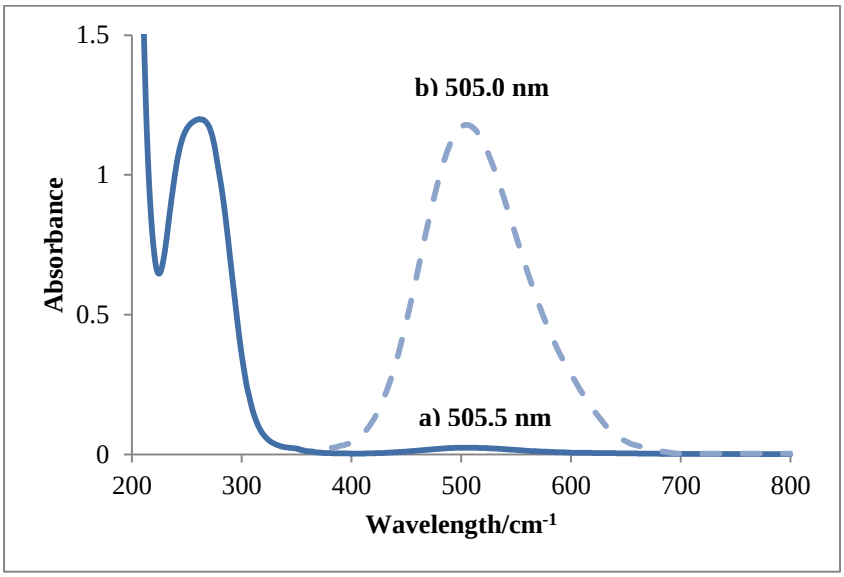



Figure 4. Absorption spectra of copper (II) complex (a) at 0.001 mol.L$^{-1}$, (b) at 0.01 mol.L$^{-1}$

**Magnetic Susceptibility Determination**

The magnetic moment data has been found to be helpful for identifying the number of unpaired electron and determining the geometry of the complexes. The effective magnetic moment is calculated from the molar susceptibility, $\chi_m$ since the magnetic moment cannot be measured directly. The molar susceptibility of copper (II) complex is measured in order to determine the spin properties of the complex [10].

The magnetic moment of the copper (II) complex was found to be in the range of 1.23-2.21 B.M, which is 1.92 B.M and it's corresponded to the one unpaired electron [11]. The complex is paramagnetic, as expected for complex of metal ion with a $d^9$ configuration and agrees with the square planar geometry around the copper (II) ion.

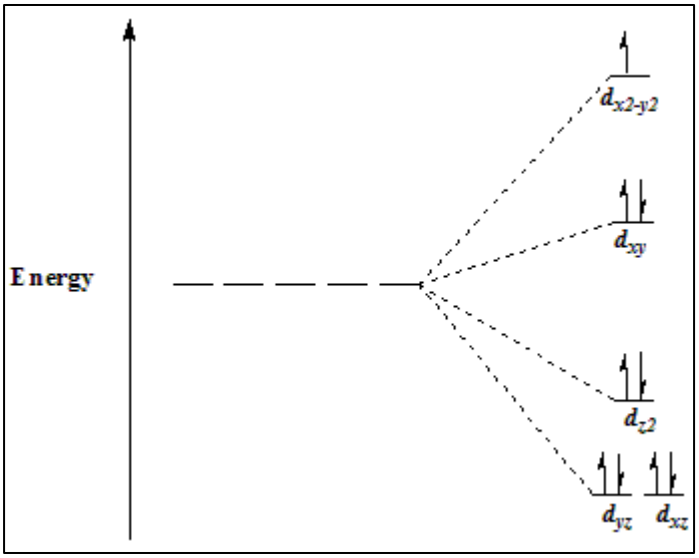



Figure 5. Crystal field diagram of square planar copper (II) complex

**Thermal Analysis**

The thermogravimetric analysis of the macrocyclic ligand and copper (II) complex were recorded under nitrogen atmosphere at the heating rate of 10 °C/min. Figure 6 shows thermograms for both compounds. Both macrocyclic ligand and the copper (II) complex decomposed in a single step but in a different way. The macrocyclic ligand was stable up to 150 °C and showed a slow weight loss up to 240 °C. A major step of decomposition occurred from 245 °C to 255 °C. On the other hand, the thermogram of copper (II) complex suggested that the metal complex was more stable than the macrocyclic ligand since it started to decompose at 290 °C. It showed only a single major decomposition curve in the region 280 °C to 300 °C corresponding to the loss of organic moiety. In term of stability, both compounds are stable for analytical test done at room temperature since their decomposition occurs at a temperature around 150 °C to 550 °C. Thermogravimetric analysis data of macrocyclic ligand and copper (II) complex are given in Table 4.

Table 4. Thermogravimetric analysis data of macrocyclic ligand and copper (II) complex

| Compound | Temperature (°C) | Final residue (%) |
|---|---|---|
| $C_{16}H_{34}N_4(ClO_4)_2$ | 150-245, 245-255 | 10.0 |
| $C_{16}H_{32}N_4OCu(ClO_4)_2$ | 280-300 | 5.8 |

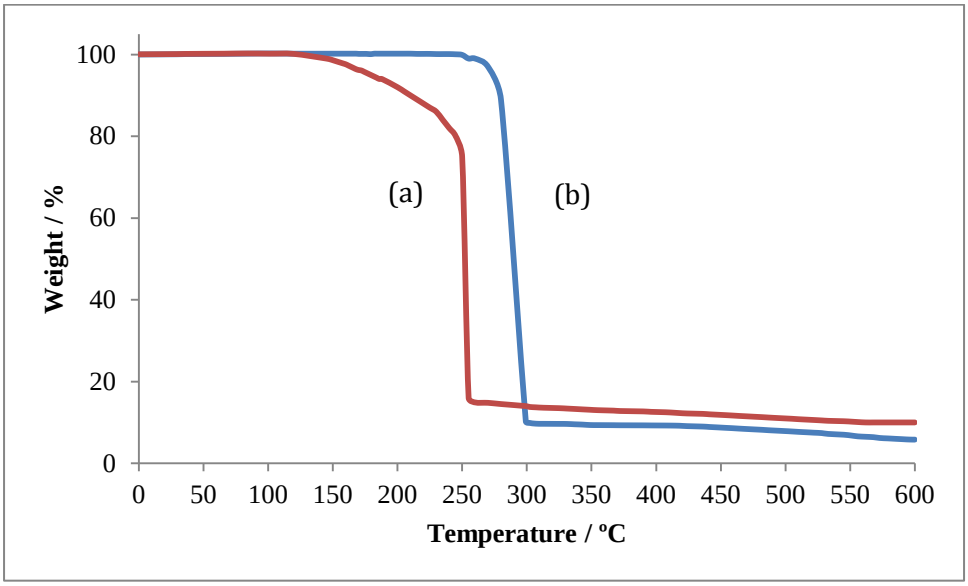



Figure 6. TGA curve for (a) macrocyclic ligand and (b) copper (II) complex

**X-ray Crystallography**

Crystal structure of copper (II) complex, $C_{16}H_{32}N_4OCu(ClO_4)$ (Fig. 7) agreed with the data obtained from elemental analysis, infrared spectroscopy, ultraviolet spectroscopy, magnetic susceptibility and thermogravimetric analysis. The structure of copper (II) complex was determined in a single crystal X-ray diffraction study. Copper atom formed a tetradentate coordination with macrocyclic $C_{16}H_{34}N_4(ClO_4)_2$ through four nitrogen atoms. This dicationic complex is offset by two perchlorate anions. X-ray single crystal structure showed a square planar geometry and *monoclinic* system with a space group P/2c, unit cell dimension with $a$ = 26.8271(17) Å, $b$ = 7.8778(5) Å and $c$ = 17.9908(12) Å; α = 90º, β = 99.05º and γ = 90º. The crystallographic data and some features of the structure refinements are listed in Table 5.

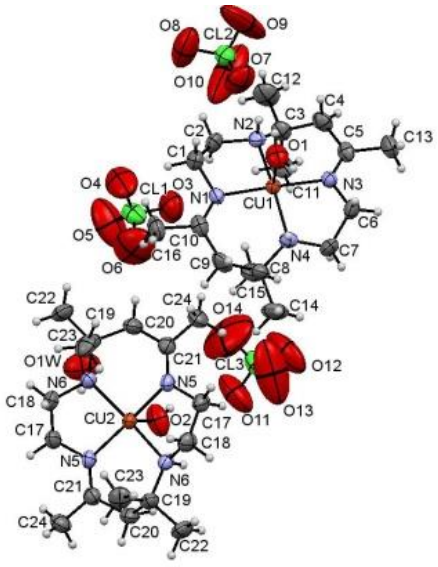



Figure 7. ORTEP plot of $C_{16}H_{32}N_4OCu(ClO_4)_2$

Table 5. Details of crystallographic data collection and structure refinement parameters

| **State** | **Data** |
|---|---|
| Empirical formula | C16 H32 Cl2 Cu N4 O9 |
| Formula weight | 1145.84 |
| Temperature | 296(2) K |
| Wavelength | 0.71073 Å |
| Crystal system, space group | Monoclinic |
| Unit cell dimensions | a = 26.8271(17) Å α = 90º |
| | b = 7.8778 (5) Å β = 99.049(2)º |
| | c = 17.9908(12) Å γ = 90º |
| Volume | 3754.8(4) $Å^3$ |
| Z, calculated density | 3, 1.520 $Mg/m^3$ |
| Absorption coefficient | 1.140 $mm^{-1}$ |
| F(000) | 1798 |
| Crystal size | 0.20 x 0.20 x 0.06 $mm^3$ |
| Theta range for data collection | 3.008 to 25.500º |
| Limiting indices | -32<=h<=32, -9<=k<=9, -21<=l<=21 |
| Reflections collected / unique | 111547 / 6974 [R(int) = 0.2366] |
| Completeness to theta = 25.242 | 99.8% |
| Refinement method | Full-matrix least-squares on $F^2$ |
| Data / restraints / parameters | 6974 / 10 / 489 |
| Goodness-of-fit on F^2 | 1.061 |
| Final R indices [I>2sigma(I)] | R1 = 0.0689, wR2 = 0.1547 |
| R indices (all data) | R1 = 0.1325, wR2 = 0.1914 |
| Largest diff. peak and hole | 0.968 and -0.609 e.$Å^{-3}$ |

## Conclusion

To conclude, we have successfully synthesized and fully characterized copper (II) complex containing macrocyclic tetraaza, $C_{16}H_{34}N_4(ClO_4)_2$. Mass spectrum under ESI-condition was in agreement with the elemental analysis, confirming the composition and purity of the Cu (II) complex. Based on the magnetic moment and electronic spectral studies, we assumed that the copper (II) complex exhibits a square planar geometry. X-ray crystallography showed macrocyclic ligand behaves as a bidentate chelating ligand which binds with the metal ion through azomethine and imine nitrogen.

## Acknowledgement

The authors would like to thank Faculty of Science and Technology, Universiti Kebangsaan Malaysia for the provision of laboratory facilities and lab assistance are equally helpful in making this work. The authors also gratefully acknowledge the research grant from GGPM2013-038 and ETP2013-027.

**References**

1. Curtis, N. F., House, D. A. (1961). *Chemistry and Industry*, 1708.
2. Farha, F., Kaneez, F., Mohammad, A., Shahper, N. K., Asad, U. K., Mohammad, S. (2009). Template synthesis and physico-chemical characterization of 14-membered tetraimmine macrocyclic complexes, $[MLX_2][M=Co(II), Ni(II), Cu(II)$ and $Zn(II)]$. DNA binding study on $[CoLCl_2]$ complex. *Spectrochimica Acta*, 72(3), 591-596.
3. Mohammad, S., Hamida, T. N. C., Poonam, C. (2006). Metal ion-directed synthesis of 16-membered tetraazamacrocyclic complexes and their physico-chemical studies. *Spectrochimica Acta*, 64, 512-517.
4. Ajibade P.A., Zulu N.H. (2011). Metal complexes of diisopropylthiourea : Synthesis, characterization and antibacterial studies. *Int. J. Mol. Sci*, 12, 7186-7198.
5. Reddy P.M., Prasad A.V.S.S., Ravinder V. (2007). Synthesis, spectral characterization, catalytic and antibacterial activity of macrocyclic CuII compounds. Transit. Met. Chem, 32, 507–513.
6. Atsushi M., Takao F., Hiroshi A., Hitoshi W. (1999). Electrospray ionization mass spectrometry of metal complexes. Gas phase formation of a binuclear copper (II)–5-Br-PADAP complex. *Analytical Chimica Acta*, 390(1-3), 193-199.
7. Abdalla M. K., Hadi M.M. (2012). Synthesis, spectral, thermal analyses and molecular modeling of bioactive Cu(II)-complexes with 1,3,4-thiadiazole Schiff base derivatives. Their catalytic effect on the cathodic reduction of oxygen. *International Journal of Electrochemical Science,* 7, 10074 – 10093.
8. Raziyeh A.A., Farshideh H., Giuseppe B., Hadi A.R. and Saeid A. (2013). Synthesis, spectroscopy, and magnetic characterization of copper (II) and cobalt(II) complexes with 2-Amino-5-bromopyridine as ligand. *ISRN Inorganic Chemistry*.
9. Reddy P.M., Rohini R., Krishna E.R., Hu A. and Ravinder V. (2012). Synthesis, spectral and antibacterial studies of copper (II) tetraaza macrocyclic complexes. *Int. J. Mol. Sci*, 13(4), 4982–4992.
10. Manan M.F., Kassim K. and Manan A.F. (2012). Synthesis, characterization and conductivity studies of Schiff base ligand derived from isatin and O-Phenylenediamine with cobalt (II) metal complex and lithium-Schiff base compound. *The Malaysian Journal of Analytical Sciences,* 16(3), 318 – 324.
11. Halim N.I., Kassim K., Fadzil A.H., Yamin B. (2012). Synthesis, characterization and antibacterial studies of Cu (II) complexes hiourea. *The Malaysian Journal of Analytical Sciences*, 16(1), 56-61.

The Malaysian Journal of ANALYTICAL SCIENCES ISSN 1394-2506

# THE INFLUENCE OF MODIFIED SODIUM MONTMORILLONITE AS FILLER ON THE PERFORMANCE OF GLASS POLYALKENOATE CEMENT

## (Kesan Natrium Montmorilonit Terubahsuai Sebagai Bahan Pengisi Dalam Meningkatkan Prestasi Simen Kaca Polialkenoat)

Nur'Izzah Md Nasir[1], Norhazlin Zainuddin[1]*, Wan Md Zin Wan Yunus[2], and Khamirul Amin Matori[3]

[1]*Department of Chemistry, Faculty of Science,*
*Universiti Putra Malaysia, 43300 Serdang, Selangor, Malaysia*
[2]*Department of Chemistry, Centre for Defense Foundation Studies,*
*National Defence Universiti Malaysia, Sungai Besi Camp, Kuala Lumpur, Malaysia*
[3]*Department of Physics, Faculty of Science,*
*Universiti Putra Malaysia, 43300 Serdang, Selangor, Malaysia.*

**Corresponding author: norhazlin@upm.edu.my*

**Abstract**

Modification of sodium montmorillonite (Na-MMT) to aluminium montmorillonite (Al-MMT) and octadecylamine montmorillonite (ODA-MMT) was done by ion exchange process. These MMTs were added as filler to glass polyalkenoate cement(GPC) formulation. The compressive strength and setting reaction of the GPCs were studied. Aluminosilicate glass powder with polyacrylic acid, water and MMT were mixed together with weight ratio of 5:1:1:(1.5wt% powder). The setting reaction was studied from FTIR by monitoring the conversion of COOH in polyacrylic acid to crosslink with metal ions from the glass to form $COO^-M^+$ at different aging time. The addition of Al-MMT slightly sped up the setting reaction of GPCs as early as 3 minutes and recorded significant increment in compressive strength at early aging time. While GPC+ODA-MMT only showed increment in compressive strength at early aging time. However, GPC+Na-MMT had shown the slowest performance in GPCs setting reaction and lowest value of the compressive strength. Although the compressive strength for these GPCs was different at early aging time, all cements recorded almost similar compressive strength at day 28. The study highlighted the potential of modified Na-MMT as filler to enhance the performance of GPCs as posterior filling material.

**Keywords**: sodium montmorillonite, montmorillonite, glass polyalkenoate cement, aluminosilicate glass, compressive strength

**Abstrak**

Pengubahsuaian terhadap natrium montmorilonit Na-MMT kepada aluminium montmorilonit (Al-MMT) dan oktadesilamin montmorilonit (ODA-MMT) dilakukan melalui proses pertukaran ion. MMT ini ditambahkan sebagai pengisi kepada formulasi simen kaca polialkenoat (GPC). Kekuatan mampatan dan tindak balas pengesetan bagi GPC dikaji. Serbuk kaca aluminosilikat dengan asid poliakrilik, air dan MMT dicampur dengan nisbah berat 5:1:1:(1.5 wt% serbuk). Tindak balas pengesetan dikaji melalui FTIR dengan memerhatikan penukaran COOH dalam asid poliakrilik untuk rangkai silang dengan ion logam daripada kaca untuk menghasilkan COO-M+ pada masa penuaan yang berbeza. Penambahan Al-MMT meningkatkan sedikit tindak balas pengesetan GPCs seawal 3 minit dan merekodkan peningkatan yang ketara dalam kekuatan mampatan pada awal masa penuaan. Manakala GPC+ODA-MMT hanya menunjukkan kesan pada ujian kekuatan mampatan di mana ia juga menunjukan peningkatan yang ketara pada awal masa penuaan. Walau bagaimanapun, GPC+Na-MMT telah menunjukkan prestasi paling perlahan dalam tindak balas pengesetan GPCs dan kekuatan mampatan. Walaupun kekuatan mampatan bagi semua jenis GPC sedikit berbeza pada awal masa penuaan, semua simen merekodkan kekuatan mampatan yang hampir sama pada hari ke 28. Kajian ini menumpukan kepada potensi Na-MMT terubahsuai sebagai pengisi untuk meningkatkan prestasi GPC sebagai bahan penampal gigi.

**Kata kunci**: natrium montmorilonit, montmorilonit, simen kaca polialkenoat, kaca aluminosilikat, kekuatan mampatan

## Introduction

Glass polyalkenoate cement, GPC is water based cement, which is formed by the acid base reaction between aqueous polyacid and fluroaluminosilicate glass. The reaction releasing ion such as $Al^{3+}$, $F^{-}$, $Ca^{2+}$ for polyacid linking with the surface of the aluminosilicate glass[1]. Hydrolysis reaction takes place on the surface of glass, where the polyacid in the presence of water attacks the glass network, which causes the leaching of metal cations such as $Al^{3+}$, $Ca^{2+}$ and $F^{-}$ from the glass. These metal cations then ionically cross link with polyacid chain to form polysalt matrix resulting hard ceramic-like cement. While, the surface of the glass developed into silica gel layer, $Si(OH)_4$.

GPC is a great candidate to replace the function of amalgam as it has ability to chemically bond to the tooth structure, biocompatible, low shrinkage and can release fluoride to protect the tooth from secondary caries. Although amalgam is successfully material as a universal tooth filling for over century, controversy still exists mainly because of the presence of mercury in amalgam. Other than that, amalgam also able to tarnish the tooth applied and can form micro-leakage on the tooth.

Various fillers have been applied to conventional glass polyalkenoate restoratives to improve their mechanical properties and enable posterior use clinically, including alumina-silicate[2], fused fibre[3], hydroxyapatite[4], zirconia[5] and montmorillonite clay, MMT[6]. MMT is trilayer smectice clay consisting of stacked platelets constructed of an alumina octahedral layer sandwiched between two silica tetrahedral layers. MMT clay is easy to obtain and modified. MMT can be modified by ion-exchanging organic cationic surfactants (intercalants). The presence of Al, Si, H, and O ions in the MMT structure made it favorable to be used as filler in dental cement. MMT is a special material which has been applied widely such as filler in polymer, nylon 6[7] and acrylic [6], treatment in waste water [8], and absorbent of benzene derivative [9-11].

The modifications on the GPC in order to improve the mechanical properties were widely done previously. However, no one had repeated or improved the work done by Dowling and his co-worker [6, 12]. Dowling [6, 12] had used organo MMT as filler in GPC application and the study only focus on the compressive strength, working characteristic, volumetric wear and wear depth. Up to date, there is no study had been published on the setting reaction of the GPC with addition of modified MMT. In addition, Dowling et al. [6,12] used commercial glass, which might make the study on the setting reaction of the GPC hardly to explain. Therefore, in this study, the glass that we used was experimentally synthesized in our laboratory. Furthermore, we applied larger interlayer spacing of MMT called d spacing compared to the modified MMT used by Dowling et al. [6] to study the effect of MMT's d spacing on the mechanical properties of GPC. The hypothesis proposed in this study was that the addition of MMT would improve the compressive strength and influence the setting reaction of the GPCs. Therefore, in this study, the compressive strength of the GPC with addition of modified Na-MMT would be determined and the setting reaction of GPC with addition of MMT would be understood using FTIR spectroscopy.

## Materials and Methods

### Preparation of Aluminosilicate Glass

Aluminosilicate glass was produced using high temperature melting technique with composition of $4.5SiO_2$. $3CaO$. $3Al_2O_3$. $2CaF_2$. $1.5P_2O_5$. . The reagents were melted in alumina crucible at 1450°C for 3 hours. Then, the resulting melts were rapidly poured into water to prevent phase separation and crystallization. The frit was collected and dried overnight in an oven at 60°C. The glass frit produced was ground by using ball grinding mill and sieved to a fine particle size of less than 45 μm for preparation of GPCs.

### Modification of sodium montmorillonite, Na-MMT.

Na-MMT was used as a starting material. Aluminium montmorillonite (Al-MMT) and octadecylamine montmorillonite (ODA-MMT) were prepared by ion exchange process where $Na^{+}$ in the MMT was exchanged with $Al^{3+}$ in $AlCl_3$ or alkyl ammonium ion in octadecylamine, ODA aqueous solution.

For Al-MMT, ~20 g of the Na-MMT was mixed with 800 mL of water and stirred for two days. After decantation, 200 mL of 0.1 M $AlCl_3$ solution was added. The suspension was stirred for two days and then washed several times with distilled water until negative result for chlorides (using $Ag^{+}$ ions) was achieved.

For ODA-MMT, ~20 g of Na-MMT was stirred vigorously in 600 mL of hot distilled water at approximately 80 °C for 1 hour to form a clay suspension. Subsequently, 13.5 g of surfactant (octadecylamine, ODA) which had been dissolved in 400 mL of hot water and 4.81 mL of concentrated hydrochloric acid (HCl) was added into the clay suspension of (ODA). After stirred vigorously for 1 hour at 80 °C, the ODA-MMT suspension was filtered and washed with distilled water until no chloride was detected with 1.0 M silver nitrate solution. It was then dried at 60°C for 48 hours. The dried Al-MMT and ODA-MMT were ground and sieved with particle size less than 45 μm.

**Preparation of glass polyalkenoate cement**

GPCs were prepared by thoroughly mixing the glass powder with polyacrylic acid, PAA (Mw~30,000) and water at weight ratio of 5:1:1 was chosen according to Griffin and Hill [13] which is suitable for restorative cements. While the weight ratio for addition of MMTs in GPC were 5:1:1:(0.5 to 2.0 wt%). Three types of GPCs with addition of MMT were prepared: GPC added with Na-MMT (GPC+Na-MMT), GPC added with Al-MMT (GPC+Al-MMT) and GPC added with ODA-MMT (GPC+ODA-MMT). The specimens that less than 1 hour aging time were quenched with liquid nitrogen to terminate the reaction and dehydrated using ethanol. For aging time greater than 1 hour, the specimens were placed in oven at 37 °C and were immersed and stored in deionized water prior to termination of the reaction by the above method. The immersion was done to prevent the dehydration for samples up to 28 days.

**X-ray diffraction**

X-ray diffraction analysis for Na-MMT, Al-MMT and ODA-MMT was done to determine the interlayer spacing from the position of the $d_{001}$ peak in the XRD pattern using Bragg's law. XRD analysis was conducted using Shimadzu XRD 6000 diffractometer with Cu-K α radiation (λ = 0, 15406 nm). The diffractogram was scanned in the range of 2θ angle from 2 to 10° at a scan rate of 2° $min^{-1}$.

**Fourier Transform Infrared (FT-IR) analysis**

The functional group, bond formation, and setting reaction of samples were analyzed using Perkin Elmer Spectrum 1000 series FT-IR spectrophotometer equipped with attenuated total reflectance (ATR). The infrared spectra were recorded at wave number 1000 – 4000 $cm^{-1}$.

**Compressive strength test**

GPCs prepared were shaped in cylindrical mould with dimension of 4 mm × 6 mm following the ISO7489:1986 specifications [14–15]. Identical cylindrical standard specimens were produced using the PTFE split-mould. The specimens were test under INSTRON tensile machine at a cross head speed 1 mm/min and maximum load 5 kN.

## Results and Discussion

**XRD analysis**

The XRD patterns for the Na-MMT and modified Na-MMT are given in Figure 1. The peaks at 2θ appeared at 7.52, 5.54 and 2.98 for Na-MMT, Al-MMT, and ODA-MMT, respectively. The basal spacing was calculated and listed in Table 1.

Table 1. The interlayer spacing calculated using Bragg's law for unmodified Na-MMT, cationic clay Al-MMT, and organically modified treated ODA-MMT

| **Montmorillonite, MMT** | **Wavelength, λ** | **Angle, 2Θ** | **Interlayer spacing, $d_{001}$ (nm)** | **Expansion of interlayer spacing (nm)** |
|---|---|---|---|---|
| Na-MMT | 1.59 | 7.52 | 1.21 | - |
| Al-MMT | 1.59 | 5.54 | 1.64 | 0.43 |
| ODA-MMT | 1.54 | 2.98 | 2.96 | 1.75 |

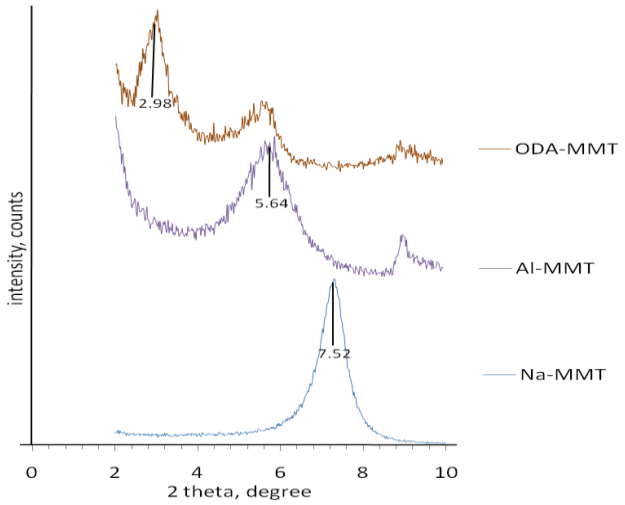



Figure 1. XRD patterns of Na-MMT and modified Na-MMTs (Al-MMT, and ODA-MMT)

Na-MMT gave the lowest spacing with 1.21 nm, followed by Al-MMT with 1.64 nm, and ODA-MMT with 2.96 nm. The expansion of interlayer spacing of 0.43 nm and 1.75 nm for Al -MMT and ODA -MMT, respectively, suggested that modification was successfully done. The d-spacing of Al-MMT was smaller compared to the ODA-MMT. This is due to the structure of ODA is bigger and the molecular weight is higher compares to Al, which gives a greater distance layer. The increase in the interlayer d-spacings ($d_{001}$) for ODA-MMT and Al-MMT clays demonstrated that the modified MMT clays have expanded layers, which may increase the opportunity for the polyacrylic acid chains of the GPC restorative to diffuse into the MMT galleries during manipulation. This finding is supported by Dowling et al. [6].

**Compressive strength**

***Optimization of amount of MMTs in GPC***

The optimum amount of MMT in the GPCs was determined in order to get the highest compressive strength of GPC. Figure 2 shows the compressive strength for GPCs with addition of Na-MMT, ODA-MMT, and Al-MMT from 0.5 – 2.0 wt% at 1 day aging time.

The addition of 0.5 – 2.0 wt% of MMT in GPC was investigated by the author in order to determine the optimum amount of MMT as filler in GPC. It was found that more than 2.0 wt% of MMT, namely 2.5 and 3.0 wt%, resulted in difficulty to mix and easily rupture cement. Therefore, the authors exclude these wt% from the study. From Figure 2, as we increased the amount of clay from 0.5 to 1.5wt%, the compressive strength was also increased. This may be due to high amount of MMTs can react with PAA in the cement to form crosslinkages. However, above 1.5wt%, a reduction in compressive strength for all types of GPCs was observed. Dowling et al. [6] suggested that excess MMT in GPC causes the clays agglomerate into disorganised structures of stacked clay platelets, which decreases the overall surface area available for reaction thereby minimising any potential reinforcing effect. Therefore, 1.5 wt% of MMTs was chosen as optimum amount of MMT in this study.

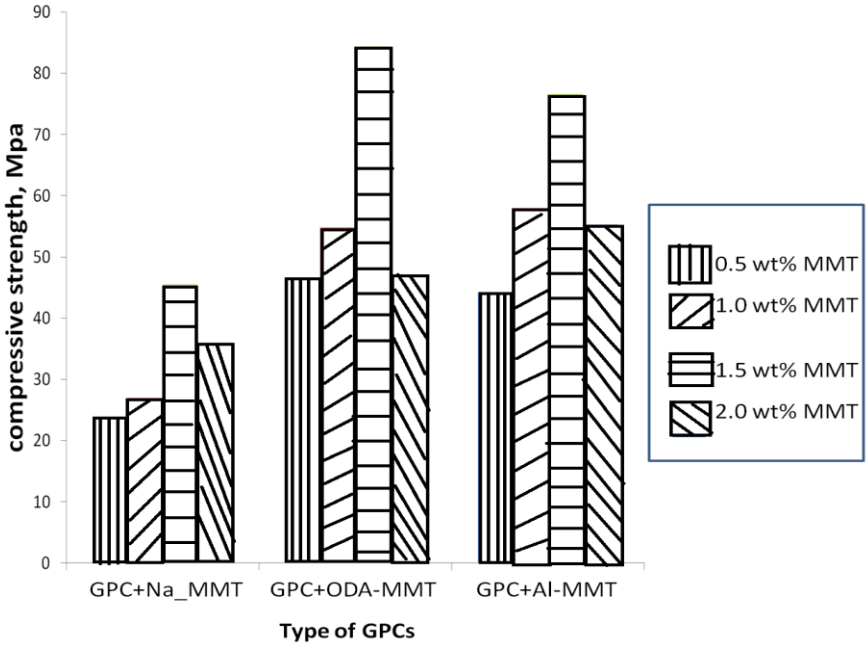



Figure 2. Compressive strength of GPC+Na-MMT, GPC+Al_MMT and GPC+ODA-MMT with 0-2 wt% of MMT at 1 day aging time

***FTIR analysis for GPC***

Figure 3 shows the FTIR spectra of GPCs from 3 minutes to 28 days aging time. The FTIR spectra of PAA and glass were also included as comparison. The IR spectra absorption peaks of GPC without MMT are listed in Table 2.

Table 2: FTIR absorption for GPC without MMT

| **Wave number ($cm^{-1}$)** | **Assignment and Remarks** |
|---|---|
| 1695 | COOH bending |
| 1544 | $COO^-M^+$ (cross linking) |
| 1454 | $-CH_2$ bending |
| 1425 | CH-C=O bending |
| 1070 | Si-O-Si bridging |
| 920 | Si-OH stretching (NBO) |

The major peaks observed in this GPC were bridging Si-O-Si (cement) at 1070 $cm^{-1}$ and shoulder peak at 920 $cm^{-1}$ (Si-OH deformation vibration) , scissor and bending vibrations of $-CH_2$ and CH-C=O at 1410-1450 $cm^{-1}$, COOH bend at 1695 $cm^{-1}$ and lastly new peak at 1544 $cm^{-1}$ due to $COO^-M^+$ (crosslinking).

As early as 3 minutes aging time, the cross linking peak at 1544 $cm^{-1}$ was already clearly observed and COOH peak at 1695 $cm^{-1}$ had become a shoulder peak. After 10 minutes aging time, the intensity of COOH peak decreased and

hardly to be observed. Other peak at 970 $cm^{-1}$ in the alumina silicate glass was assigned Si–O–Si stretching with non bridging oxygen. While in the GPCs, there were two new peaks appeared as early as 3 minutes aging time, which corresponded to Si–O–H (920 $cm^{-1}$) and Si – O – Si in the cement (1070 $cm^{-1}$), respectively. The Si–O–Si stretching peak slightly shifted from low to high wave number due to the hardening reaction. This finding is in good agreement with previous studies done by Matsuya et al.[16] and De Maeyer et al.[17]. Matsuya et al.[16] suggested that the shifting of wave number shows the degree of polymerization in the silicate network kept increasing during hardening of the cement.

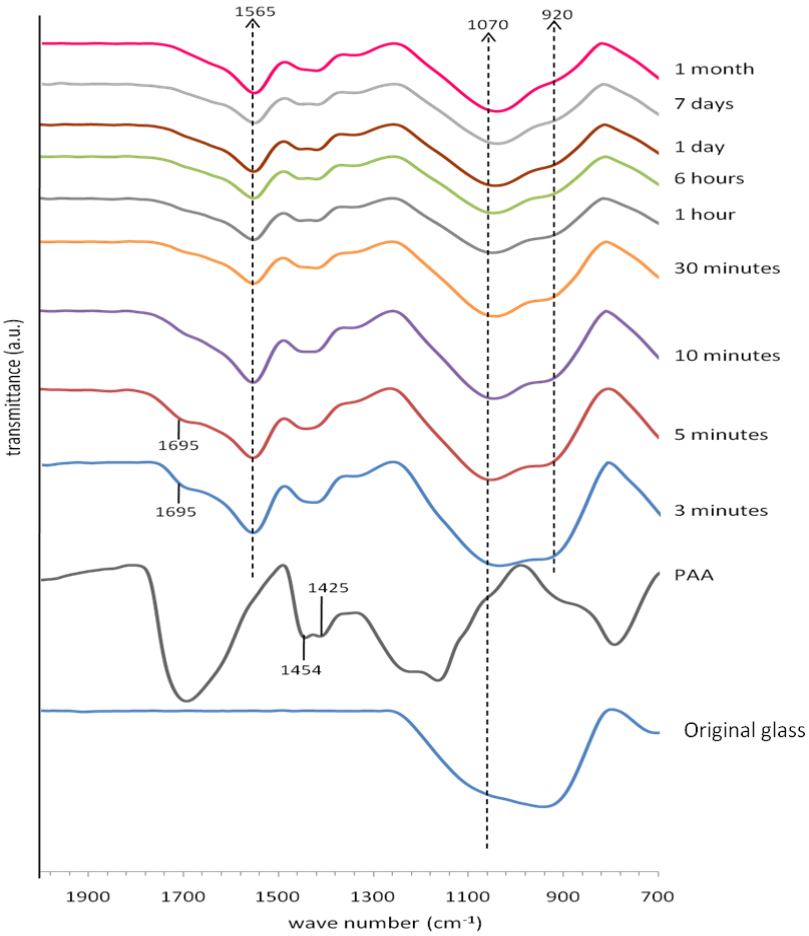



Figure 3. FTIR spectra of GPC without MMTs at wave number 700 $cm^{-1}$ – 2000 $cm^{-1}$ from 3 minutes to 28 days aging time, PAA, and original glass.

The FTIR result also indicated the change in structure of the silicate network of the cement during the setting reaction. The intensity of the shoulder peak, Si-O-H at 920 $cm^{-1}$ decreased with the aging time. It may be due to the condensation reaction by the elimination of water to form Si-O-Si. Matsuya et al.[16] reconstructed the silicate network in the glass starting with the breakage of the Si-O-Al bond by proton attack with releasing $Al^{3+}$ ion. Then, Si-O-H, formed by the hardening reaction were condensed by the elimination of water.

Figure 4 shows interesting peaks of the FTIR spectra cut from Figure 3 for GPCs. There were two weak peaks associated with scissor and bending vibrations of $-CH_2$ and CH-C=O groups appeared at 1440 and 1415 $cm^{-1}$, respectively for PAA backbone.

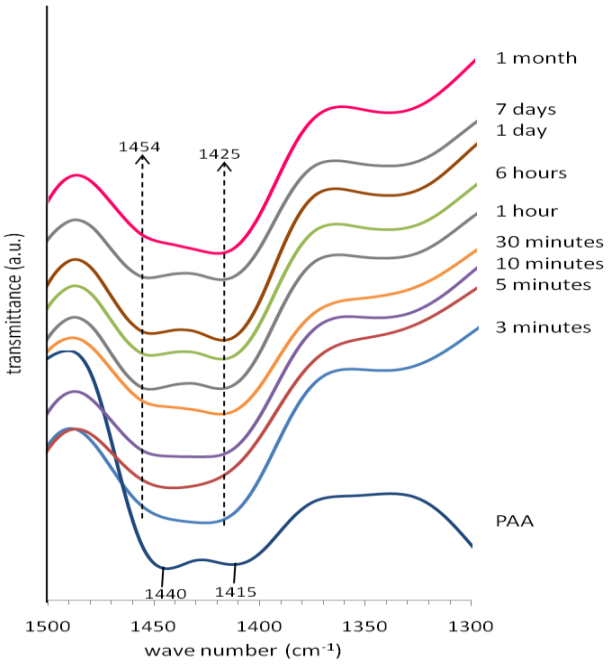



Figure 4. FTIR spectra of GPCs at 1300 – 1500 $cm^{-1}$ for scissor and bending vibrations of $-CH_2$ and CH-C=O groups at 3 minutes to 28 days aging time compared with PAA

During the setting reaction of GPCs, both peaks slightly shifted to the high wave number. This may be due to the cross linking reaction where the angle of C-C=O bond was disturbed to allow $Al^{3+}/Ca^{2+}$ cross link with the polyacid at the surface of glass as shown in Figure 5.

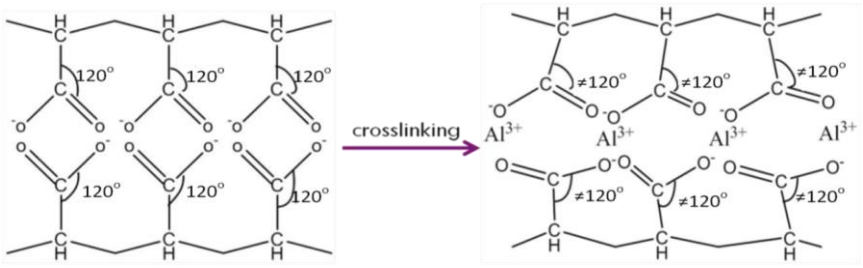



Figure 5. Cross linking reaction at the surface of the glass network

This causes the $-CH_2$ bond near the CH-C=O vibrates and thus disturbs the position of $-CH_2$ bending. Both peaks shifted slightly to a higher wave number in cements, which may be due to higher energy needed to vibrate these two

bonds. The wave number for -$CH_2$ bending shifted from 1440 to 1454 $cm^{-1}$ while CH-C=O shifted from 1415 to 1425 $cm^{-1}$.

Figure 6, 7, and 8 show the FTIR spectra of GPCs with Na-MMT, GPC+ODA-MMT, and GPC+Al-MMT, respectively at wave number from 700 – 2000 $cm^{-1}$. Similar observation for the cross linking formation with the appearance of $COO^-M^+$ (1565 $cm^{-1}$) peak and reduction in the intensity of COOH peak (1695 $cm^{-1}$). There were also hardening reaction with the formation of Si-O-H (920 $cm^{-1}$) and Si-O-Si (1070 $cm^{-1}$) in cement, and shifting of -$CH_2$ and CH-C=O bending peaks (1440 and 1415 $cm^{-1}$). The peaks were similar to GPCs without MMTs but only different on the intensity of the transmittance at different aging time.

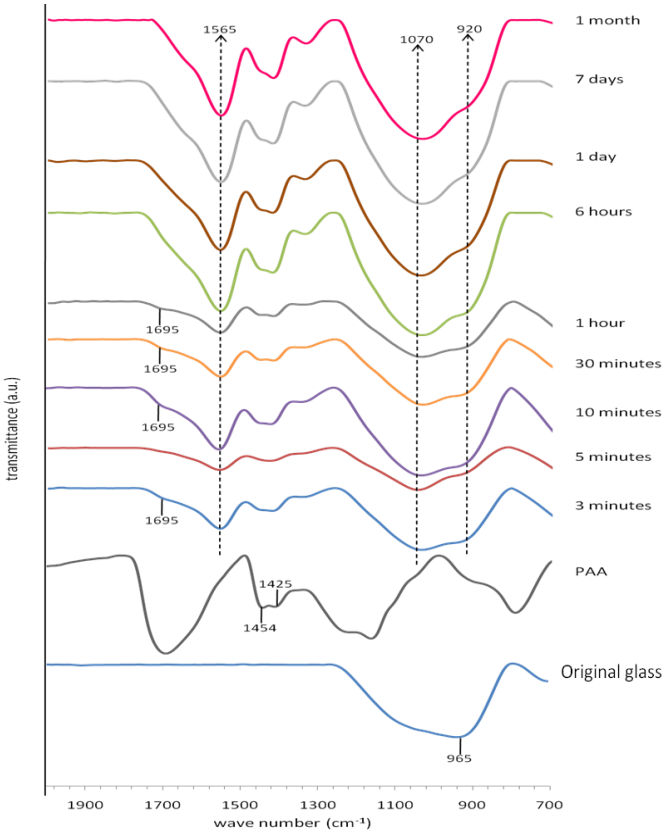



Figure 6. FTIR spectra of GPC+Na-MMT at wave number 700 $cm^{-1}$ – 2000 $cm^{-1}$ from 3 minutes to 28 days aging time, PAA, and original glass

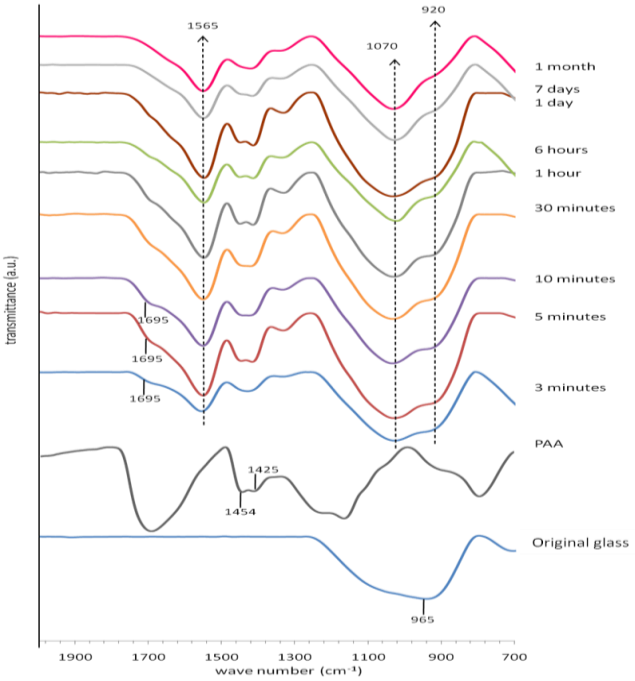



Figure 7. FTIR spectra of GPC+ODA-MMT at wave number 700 $cm^{-1}$ – 2000 $cm^{-1}$ from 3 minutes to 28 days aging time, PAA, and original glass

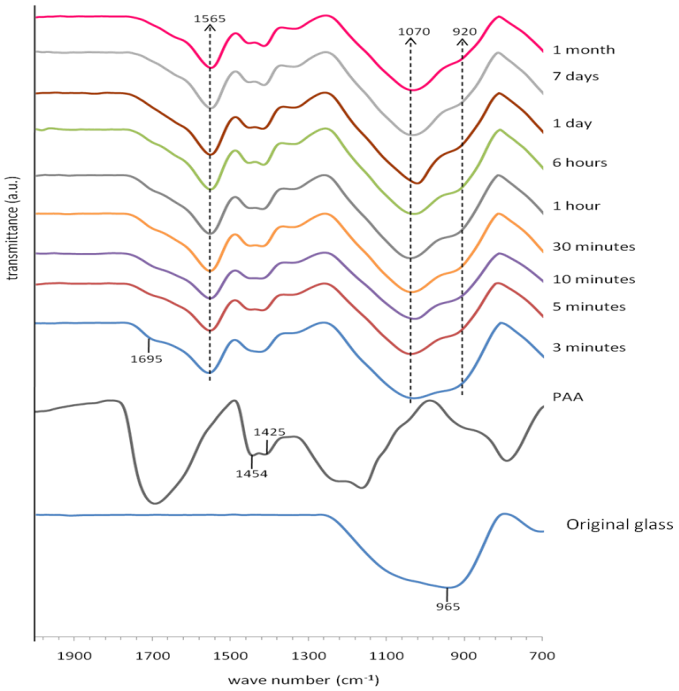



Figure 8. FTIR spectra of GPC+Al-MMT at wave number 700 $cm^{-1}$ – 2000 $cm^{-1}$ from 3 minutes to 28 days aging time, PAA, and original glass

The FTIR spectra of GPC were compared with FTIR spectra of GPC+Na-MMT, GPC+ODA-MMT and GPC+Al-MMT. Similar trend was observed where COOH peak converted to $COO^- M^+$ as crosslinking proceed with aging time, and changes in silicate network as the hardening reaction took place simultaneously. The addition of Na-MMT in GPC (Figure 6) showed that the conversion of COOH to $COO^-M^+$ is not constant up to 1 day aging time. The intensity of $COO^-M^+$ peak appeared as early as 3 minutes aging time but after 10 minutes the COOH peak reappeared and then the intensity of both peaks became constant after 1 hour aging time. De Barra and Hill[18] explained that the presence of sodium ions prevent the COOH in PAA to take part in the crosslinking reaction by forming sodium polyacrylate salt. In our study, Na ions in Na-MMT can form Na-PAA salt at the early aging time and thus delayed the formation of crosslink in the cement. However, at longer aging time, this Na ions from Na-PAA salt were released to water and $COO^-$ became available for crosslinking with metal ions from the glass.

For GPC+ODA-MMT (Figure 7), the peak of $-NH_2$ group from ODA-MMT was not detected from FTIR spectroscopy because very small amount of ODA-MMT has been used in this study (1.5 % of total weight powder). In addition, the peak for $-NH_2$ might be overlapped with the $COO^-M^+$ peak at 1529 $cm^{-1}$. Both GPC and GPC+ODA-MMT showed similar trend on the crosslinking, where the disappearance of COOH peak was found at 10 minutes aging time. It is suggested that the presence of ODA-MMT in the cement did not change the crosslinking reaction of the cement. The presence of amine group is believed to form hydrogen bond with the PAA and thus can only contribute in increasing the compressive strength of GPCs but not the setting reaction.

For GPC+Al-MMT, the IR (Figure 8) spectra showed that the intensity of COOH and $COO^-M^+$ peaks became constant after 5 minutes aging time, which is the fastest, compared to other cements in this study. This might be due to the presence of free aluminium in Al-MMT that can contribute in cross linking reaction and thus speed up the setting reaction of the GPC+Al-MMT. $Al^{3+}$ in the modified MMT is assumed to move freely at ion exchangeable site in MMTs galleries layer. This free ion is believed to diffuse out easily and join the cross linking reaction together with the metal ions that leach out from the glass and speed up the setting reaction of the GPCs.

***Compressive strength for GPC, GPC+ Na-MMT, and GPC+modified Na-MMT (GPC+Al-MMT/ GPC+ODA-MMT)***

The compressive strength for GPC, GPC+Na-MMT, GPC+Al-MMT, and GPC+ODA-MMT were measured at 1, 7, 14, 21, and 28 days (Table 3).

Table 3. Mean compressive strength (MPa) of GPC, GPC+Al-MMT, GPC+ODA-MMT, and GPC+Na-MMT at different aging time

| | **Compressive strength, MPa (SD)** | | | |
|---|---|---|---|---|
| **Day** | **GPC** | **GPC+Na-MMT** | **GPC+Al-MMT** | **GPC+ODA-MMT** |
| **1** | 61.7(3.5) | 45.5(4.1) | 84.4(4.7) | 76.6(8.9) |
| **7** | 78.1(5.3) | 62.2(5.7) | 84.4(1.6) | 90.4(3.6) |
| **14** | 88.7(8.5) | 72.5(8.2) | 91.4(7.5) | 89.4(9.2) |
| **21** | 90.7(5.6) | 74.5(3.8) | 86.3(8.8) | 86.5(1.7) |
| **28** | 93.4(4.6) | 80.4(10.5) | 92.5(8.8) | 86.4(4.7) |

SD = standard deviation

At 1 day aging time, GPCs with addition of modified Na-MMT (ODA-MMT and Al-MMT) gave highest compressive strength compared with GPC without MMT and GPC+Na-MMT. The compressive strength value for GPC+ODA-MMT and GPC+Al-MMT were 76.6 and 84.4 MPa, respectively. While for GPC and GPC+Na-MMT, the compressive strengths were 61.7 and 45.5 MPa, respectively. The compressive strength for all GPCs increased with aging time and reached similar value in the range of 80 to 95 MPa after 28 days aging time.

The high value of compressive strength for GPCs with modified Na-MMT at the early aging time suggested that the addition of modified Na-MMT may contribute to the cross linking reaction during the formation of GPCs. The presence of octadecylamine in montmorillonite brings about the formation of intercalated compound with bilayers of organic molecules in the interlayer spaces. Intercalation is accompanied with water desorption and partial protonisation of NH groups [19]. Thus, there is possibility to form hydrogen bonding between the carboxylic acid groups of PAA and the polar amine groups, $NH^{3+}$ of the ODA-MMT [6]. The formation of hydrogen bond may contribute in increasing the compressive strength of the GPCs.

For GPC+Al-MMT, the modification of Na-MMT to Al-MMT caused excess of free $Al^{3+}$ in the MMT structure. The $Al^{3+}$ was assumed to be moved freely in the layer of MMTs and because $Al^{3+}$ was easily to diffuse out, it contributed in the cross linking reaction by forming $COO^{-}Al^{+}$, hence sped up the setting reaction of GPCs. Thus, gave higher compressive strength at 1 day aging time compared to GPC without MMT and GPC+ Na-MMT.

The addition of modified Na-MMT in GPC network had slightly increase the mechanical properties in early aging time as shown in the table, however, different situation happen to GPC+Na-MMT. The addition of Na-MMT had decreases the compressive strength of the GPC at 1 day aging time. The presence of Na in the MMT may delay the cross linking reaction by forming Na-polyacrylate salt. Thus, prevent the COOH from PAA from taking part in the cross linking reaction. This situation causes the poor compressive strength result at early stage of reaction.

The d spacing of the MMT itself may affect the strength of the GPC at the early aging time. Na-MMT has the smallest d spacing compared with Al-MMT and ODA-MMT with only 1.21 nm. The size of d spacing for Al-MMT and ODA-MMT were 1.64 and 2.96 nm, respectively. Dowling et al. [6] suggested that the increase in interlayer spacing may allow the movement of polyacid chains between the layered montmorillonite platelets and possibly the formation of hydrogen bonds between the carboxylic acid groups of polyacid and the amine groups of the ODA-MMT.

All types of GPCs except GPC + Na-MMT started to reach constant value of compressive strength at 14 to 28 days aging time. The compressive strength of all types of GPCs regardless the addition of MMT increased time.

For GPC+Na-MMT, the compressive strength increased with aging time from 45.5 MPa at 1 day and reached 80.4 MPa at 28 days aging time. Although the compressive strength of GPC+Na-MMT was the lowest at 1 day aging time, it increased and reached almost similar value as in GPC, GPC+Al-MMT and GPC+ODA-MMT at 28 days aging time. As discussed above, the presence of Na ions interrupt the cross linking reaction at the beginning of setting reaction. However, as the aging time increased, the sodium ions from sodium polyacrylate released to water and thus the carboxyl group from PAA became available again for cross linking. This finding is in good agreement with previous study done by Francis et al.[20]. In addition, although the compressive strength of these GPCs was different at 1 day aging time, it reached to a similar value after 28 days aging time regardless the type of MMT added to the GPCs. The reason for the similarity may be due to the same amount of PAA used in all types of the GPCs as well as the same glass composition was used throughout this study. PAA in the GPCs contributed in the cross linking reaction and therefore same amount of cross linking could be formed in the GPCs of all types of MMTs.

## Conclusion

The expansion in d-spacing for Al-MMT and ODA-MMT may enhance the opportunity for the polyacrylic acid chains of the GPC to diffuse into the MMT galleries. Hence, it increased the compressive strength of the GPCs at early aging time. The existence of Al ions in Al-MMT may involve in the crosslinking reaction of GPC. While for ODA-MMT, there was possibility to form hydrogen bond between COOH from PAA and $NH_2$ group from ODA. However, the presence of Na-MMT gave low compressive strength at early aging time and delayed the setting reaction because of the formation of sodium polyacrylate. This study suggested that both modified Na-MMT (Al-MMT and ODA-MMT) increased the compressive strength of GPCs at early aging time.

## Acknowledgement

The authors would like to thank Universiti Putra Malaysia for providing research grant under RUGS (No:9199846).

**References**


1. Nicholson, J. W. (1998). Chemistry of Glass-Ionomer Cements: a review. *Biomaterials*, 19: 485–494.
2. Kobayashi, M., Kon, M., Miyai, K. & Asaoka, K. (2000). Strengthening of Glass-Ionomer Cement by compounding Short Fibres with $CaO$-$P_2O_5$-$SiO_2$-$Al_2O_3$ Glass. *Biomaterials*, 21: 2051–2058.
3. Ruddell, D.E., Maloney, M.M., & Thompson, J.Y. (2002). Effect of Novel Filler Particles on the Mechanical and Wear Properties of Dental Composites. *Dental Materials* , 18: 72–80.
4. Lucas, M.E., Arita, K. & Nishino, M. (2003). Toughness, Bonding and Fluoride-Release Properties of Hydroxyapatite-added Glass Ionomer Cement. *Biomaterials* , 24: 3787–3794.
5. Gu, Y.W., Yap, A.U.J., Cheang, P., Koh, Y.L. & Khor, K.A. (2005). Development of Zirconia-Glass Ionomer Cement Composites. J*ournal of Non Crystalline Solids* , 351: 508–514.
6. Dowling, A.H., Stamboulis, A. & Fleming, G.J.P. (2006). The Influence of Montmorillonite Clay Reinforcement on the Performance of a Glass Ionomer Restorative. *Journal of Dentistry* , 34: 802–810.
7. Fornes, T.D. & Paul, D.R. (2003). Formation and Properties of Nylon 6 Nanocomposite. *Polimeros*, 13:212-217. Available from: http://www.redalyc.org/pdf/470/47013403.pdf [Accessed 21 February 2010]
8. Zhu, J., Wang, T., Zhu, R., Ge, F., Wei, J., Yuan, P. & He, H.P. (2011). Novel Polymer/Surfactant Modified Montmorillonite Hybrids and the Implications for the Treatment of Hydrophobic Organic Compounds in Wastewaters. *Applied Clay Science*, 51: 317–322.
9. Zhou, Q., He, H.P., Ray, L.F. & Yunfei, (2007). Adsorption of p-Nitrophenol on Mono-, Di-, and Trialkyl Surfactant-Intercalated Organoclays: A Comparative Study. *Journal Physical Chemistry*, 111: 7487–7493.
10. Zaghouane-Boudiaf, H. & Boutahala, M. (2011). Preparation and Characterization of Organo-Montmorillonites. Application in Adsorption of the 2,4,5-Trichlorophenol from Aqueous Solution. *Advanced Powder Technology*, 22: 735–740.
11. Moaaz, K.S., Komarneni, S., Cho, Y., Lim, T., Shahien, M.G., Khalil, A.A. & Abd El-Gaid, I.M. (2011). Organosilicas and Organo-Clay Minerals as Sorbents for Toluene. *Applied Clay Science, 52*: 184–189.
12. Dowling, A.H. & Fleming, G.J.P. (2007). The Impact of Montmorillonite Clay Addition on the In Vitro Wear Resistance of a Glass-Ionomer Restorative. *Journal of Dentistry*, 35: 309–317.
13. Griffin, S.G. & Hill, R.G. (2000). Influence of glass composition on the Properties of Glass Polyalkenoate Cements. Part II: Influence of Phosphate Content. *Biomaterials* , 21: 400.
14. Genebra, (1986). International Organization for Standardization. ISO7489. *Dental glass polyalkenoate cements.*
15. Mallmann, A., Ataíde, J.C.O., Amoedo, R., Rocha, P.V. & Jacques, L.B. (2007). Compressive Strength of Glass Ionomer Cements using Different Specimen Dimensions. *Brazillian Oral Restorative*, 21: 204-208. Available from: http://dx.doi.org/10.1590/S1806-83242007000300003, [Accessed 18 july 2014]
16. Matsuya, S., Maeda, T. & Ohta, M. (1996). IR and NMR Analyses of Hardening and Maturation of Glass-ionomer Cement. *Journal of Dentistry Restorative, 75*(12): 1920–1927.
17. De Maeyer, E.A.P., Verbeeck, R.M.H. & Vercruysse, C.W.J. (1998). Reactivity of Fluoride-containing Calcium Aluminosilicate Glasses used in Dental Glass-ionomer Cements. *Journal of Dentistry Restorative, 77* (12): 2005–2011.
18. De Barra, E. & Hill, R.G. (1998). Influence of Alkali Metal Ions on the Fracture Properties of Glass Polyalkenoate (Ionomer) Cements. *Biomaterials* , 19: 495–502.
19. Bujdák, J. and Slosiariková, H. (1992). The Reaction of Montmorillonite with Octadecylamine in Solid and Melted State. *Applied Clay Science* , 7: 263–269.
20. Francis Thoo, V. W., Zainuddin, N., Matori, K. A. & Abdullah, S. A. (2013). Studies on the Potential of Waste Soda Lime Silica Glass in Glass Ionomer Cement Production. *Advances in Materials Science and Engineering*, 2013: 1-6.

The Malaysian Journal of ANALYTICAL SCIENCES ISSN 1394-2506

# PREPARATION OF EPOXIDIZED PALM OLEIN AS RENEWABLE MATERIAL BY USING PEROXY ACIDS

## (Penyediaan Minyak Sawit Olein Terepoksida Sebagai Bahan Keterbaharuan Menggunakan Asid Peroksi)

Darfizzi Derawi*, Jumat Salimon, Waled Abdo Ahmed

*Oleochemistry Research Laboratory, School of Chemical Sciences and Food Technology,*
*Faculty of Science and Technology,*
*Universiti Kebangsaan Malaysia, 43600 UKM Bangi, Selangor Darul Ehsan, Malaysia*

**Corresponding author: darfizzi@ukm.edu.my*

**Abstract**

Epoxidized palm olein ($EPO_o$) was prepared through generated *in situ* of performic acid (HCOOOH), and peracetic acid ($CH_3COOOH$) as epoxidation agent with the presence of sulphuric acid ($H_2SO_4$) 3 % v/wt as catalyst. Formic acid (HCOOH) or acetic acid ($CH_3COOH$) as oxygen carrier and hydrogen peroxide ($H_2O_2$) as oxygen donor in the reaction system. Highly conversion (95.5 %) of oxirane ringwas obtained by usingperformicacid as epoxidation agent at 150 minutes of reaction time. The reaction yield was 90 % by weight. $EPO_o$ has showed good physicochemical properties as renewable material for industrial applications. Carbon ($^{13}$C-NMR) and proton ($^{1}$H-NMR) spectra showed the present of epoxy profile at 54 ppm and 2.9 ppm. Epoxy group was detected on 844 $cm^{-1}$ byfourier transformation infra-red (FTIR) spectra.

**Keywords**: epoxidation, palm olein, *in-situ*, peroxy acid, renewable material

**Abstrak**

Minyak sawit olein terepoksida ($EPO_o$) disediakan melalui proses pengepoksidaan secara *in situ* menggunakan asid performik (HCOOOH), asid perasetik ($CH_3COOOH$) sebagai agen pengepoksidaan dengan kehadiran mangkin asid sulfurik ($H_2SO_4$) 3 % v/wt. Asid formik (HCOOH) atau asid asetik ($CH_3COOH$) sebagai pembawa oksigen dan hydrogen peroksida ($H_2O_2$) sebagai penderma oksigen dalam sistem tindak balas. Peratus penukaran gelang oksirana yang tinggi (95.5 %) diperolehi dengan menggunakan asid performik pada 150 minit tindak balas. Peratus hasil tindak balas adalah sebanyak 90 % berdasarkan berat. $EPO_o$ telah menunjukan sifat fiziko kimia yang baik sebagai bahan keterbaharuan untuk aplikasi industri. Spektrum karbon ($^{13}$C-NMR) dan proton ($^{1}$H-NMR) menunjukan kehadiran profil epoksi pada 54 ppm dan 2.9 ppm. Kumpulan epoksi dikesan pada nombor gelombang 844 $cm^{-1}$ dengan merujuk spektrum transformasi fourier inframerah (FTIR).

**Kata kunci:** pengepoksidaan, minyak sawit olein, *in-situ*, asid peroksi, bahan keterbaharuan

## Introduction

Over the last decade, world concern about utilizing of renewable sources in product synthesis. Fats and oils are renewable resources that can be chemically or enzymatically treated to produce materials that can often act as a replacement for materials derived from petroleum [1]. Among of chemical modifications of polyolefins, epoxidation is a simple and efficient method for introducing a new reactive group and useful properties and wide use in a variety of applications [2]. Epoxidized oils have a high commercial importance and are widely utilized in plastics manufacture, lubricants, detergents, and as intermediates in chemical reactions [1 - 6]. Epoxidized oil has been used widely as stabilizer and plasticizer in polyvinylchloride (PVC). Epoxidized ester can be used as solvent to replace the volatile organic solvent in paints. It also has been studied actively for lubricant production through the reaction of the epoxy group with linear or branching chain [7]. Epoxidized oil with higher oxirane oxygen value and lower iodine value is considered to be of better quality [8, 9]. There are four known technologies to produce epoxides from olefinic type of molecules[1]: (a) epoxidation with per carboxylic acids [10], the most widely used in industry,

can be catalyzed by acids or by enzymes [11,12]; (b) epoxidation with organic and inorganic peroxides which includes alkaline and nitrile hydrogen peroxides epoxidation as well as transition metal catalysedepoxidation [13]; (c) epoxidation with halohydrins using hypochalous acids (HOX) and their salts as reagents for the epoxidation of olefins with electron deficient double bonds [10]; and (d) epoxidation with molecular oxygen [10]. Epoxidation methods vary from case to case depending on the nature of reactants and catalyst used for epoxidation[14].

Palm olein ($PO_o$) is a vegetable oil and liquid fraction of palm oil (the largest renewable resources in Malaysia), consists of mainly mono-unsaturated triacylglycerol (TAG), POP (42.8 %) and di-unsaturated TAG, POO (35.7 %). The iodine value of $PO_o$ is about 51.0 – 61.0 [15]. The present of 40.0 % oleic acid in the $PO_o$ [16] is widely open for further reaction such as epoxidation process. Despite the development of many new oxidation procedures, the use of peroxy acids still constitutes a useful synthetic procedure for the epoxidation of alkenes on a laboratory scale. In the laboratory, epoxides are prepared by treatment of an alkene with a peroxy acid ($RCO_3H$). Commonly epoxidation reactions are carried out using a peroxy acid such as performic and peracetic, either preformed or formed *in situ*, by reacting a carboxylic acid as oxygen carrier with concentrated hydrogen peroxide ($H_2O_2$) as oxygen donor. Formic acid is preferred than acetic acid as oxygen carrier since, owing to its high reactivity, no catalyst is required in the formation of performic acid, but the production costs increase because formic acid's price is frequently higher than acetic acid's price [17].

Comparison between performic and peracetic acid as epoxidation agent on $PO_o$ are not yet been studied. Kinetic study on the epoxidation and oxirane cleavage of methyl ester palm olein (MEPO) by using performic acid generated *in situ* as catalyst has been reported [5]. Performic acid has been used in the epoxidation process on fatty acid methyl ester (FAME) of soybean [18]. High epoxidation yield was obtained at 40 $^oC$ with using high concentration of hydrogen peroxide (60 wt. %). A study on partial and fully epoxidation of plant oils with perhydrolysis lipase as catalyst has been reported [19]. Epoxidation of unsaturated plant oils conducted in industrial process by Prileshajev-epoxidation using short chain peroxy acid generated *in situ*. Novozym ® 435 and hydrogen peroxide have been used to epoxidize the unsaturated plant oils and over than 90 % of conversion was obtained [19].

In this paper, we discuss the preparation of epoxidized palm olein ($EPO_o$) by using three different approaches and the physicochemical properties of the product.

## Materials and Methods

### Raw Materials

Palm olein (Seri Murni brand, FFM Marketing Sdn. Bhd.) was used as raw material. Formic acid (HCOOH) (99 %) and glacial acetic acid ($CH_3COOH$) (100 %)were purchased from Univar and Bendosen. While, hydrogen peroxide ($H_2O_2$) (30 %) from J. T. Baker.

### Production of Epoxidized Palm Olein

Epoxidized Palm Olein ($EPO_o$) was produced by using generated *in situ* peroxy acid with a constant molar ratioof $PO_o$:$HCOOH/CH_3COOH$:$H_2O_2$ (1:5:4 mole/mole) under continuous magnetic stirring at constant temperature (45 $^oC$) [20].The reaction was carried out in a three necked glass (250 ml capacity) flask equipped with thermometer and reflux condenser. Generated *in* situ peroxy acid is produced by mixing formic acid (HCOOH) or acetic acid ($CH_3COOH$) with $H_2O_2$ simultaneously. Hydrogen peroxide was slowly added drop wise into the acidic media. Fast introduction to this reagent will cause an excessive development of oxygen due to the decomposition of $H_2O_2$ at high temperature and is not recommended [2]. After the reaction finished, samples of reaction mixture were taken out and thoroughly washed with sodium bicarbonate (5 wt%), distilled water and sodium chloride (5 wt%) to separate the organic layer from the mixture. The sample was then analyzed for oxirane oxygen content (OOC) value and the percentage of oxirane conversion was calculated.

### Determination of oxirane oxygen content

Oxirane oxygen content (OOC) value was determined by direct method using hydrobromic acid solution in glacialaceic acid (AOCS Cd 9-57) [21,22]. The percentage of conversion can be calculated based on the theoretical

OOC value of $PO_o$ [1,16]. From the oxirane content values, the relative percentage conversion to oxirane was calculated using the Equation 1:

$$\text{Relative percentage conversion to oxirane} = (OOC_{exp} / OOC_{the}) \times 100 \quad \text{(Eq .1)}$$

where $OOC_{exp}$ (g/100 g sample) is the experimentally obtained oxirane oxygen and $OO_{the}$ is the theoretically obtainable maximum oxirane oxygen, which was determined from the Eq. 2:

$$OO_t = \{(IV_0/A_i) / [100 + (IV_0/2A_i)\, A0]\} \times A_0 \times 100 \quad \text{(Eq. 2)}$$

where $A_i$ (126.9) and $A_o$ (16.0) are the atomic weights of iodineand oxygen respectively and $IV_0$ is the initial iodine value of oil sample.

**Detection tests**

FTIR spectrometer (GX model) was used to detect the present of epoxide group by using the NaCl salt window method. Epoxide group can be detected at wavenumber 750 - 880 $cm^{-1}$ and 815 - 950 $cm^{-1}$ [23]. Proton and carbon analysis was performed by using FT-NMR spectrometer 600 MHz Cryo-Probe (Advance 111 600MHz model). Sample was prepared by using chloroform ($CDCl_3$) as a solvent [11].

**Characterisation tests**

Physicochemical tests were carried out to analyze the iodine value, oxidative stability [4], flash and fire point, pour point (ASTM D 97-66) [15], kinematic viscosity at 40 $^oC$ and 100 $^oC$ (ASTM D 445- 79) [15] and viscosity index (ASTM D2270) [13].

## Results and Discussion

Epoxidation of palm olein ($PO_o$) was carried out by using generated *in situ* performic acid (HCOOOH) and a peracetic acid ($CH_3COOOH$). They prepared by mixing of formic acid (HCOOH) and acetic acid as oxygen carrier and hydrogen peroxide ($H_2O_2$) as oxygen donor [24]. Generation reaction of peracid are given in Figure 1.

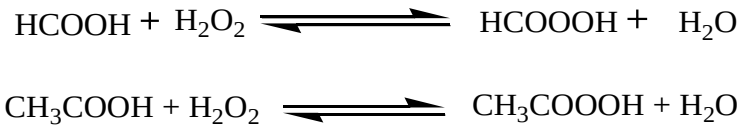



Figure 1. Generation reaction of performic acid (HCOOOH) and a peracetic acid ($CH_3COOOH$)

Preparation HCOOOH and $CH_3COOOH$ as epoxidation agents were carried out as *in situ* since the reaction condition is highly exothermic and not stable. The epoxidation process involved of electrophilic addition mechanism as Figure 2. Unsaturated bond at triacylglycerol (TAG) $PO_o$ was converted to oxirane ring to produce epoxidized palm olein ($EPO_o$) [24]. Peroxy-acids are commonly used epoxidizing agents. They have an extra oxygen atom between the carbonyl group and their acidic hydrogen, and are electrophilic at oxygen. Attack at this position by a nucleophile displaces carboxylate, which is a good leaving group. An example of one such reaction is shown below involving ethylene and peroxyformic acid. The mechanism is essentially an electrophilic attack, with a proton being transferred from the epoxide oxygen to the carboxylic acid by-product. Firstly the nucleophilic π bond donates its electrons to the oxygen, breaking the O-O bond to form the new carbonyl bond. The electrons from the old O-H bond make up the second new C-O bond, and the original carbonyl group uses its electrons to pick up the proton. The transition state for the reaction makes the bond-forming and bond-breaking processes much clearer.

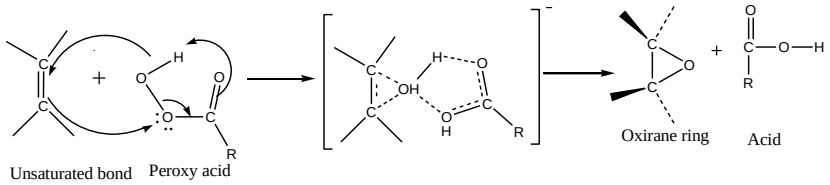



Figure 2. Mechanism for oxirane formation

Based on Figure 3, by introducing acid catalyst in the epoxidation system, it seems to give a high OOC value in a short period (30 minutes) but at the same time, the oxirane cleavage rapidly occur, then, the OOC value will decrease along with the reaction time. The epoxidation process was exothermic and high concentration of peroxy acid must be avoided [7]. Besides, the epoxidation process by using peracetic acid just only gave OOC value below 1.00 %. $CH_3COOOH$ is not an effective epoxidation agent compared to the HCOOOH. HCOOH is better than $CH_3COOH$ for this work because, when reacted with $H_2O_2$, HCOOOH forms at a much faster rate than $CH_3COOOH$ [25,26,4]. The optimum oxirane oxygen content (OOC) value obtained was 3.57 % (± 2.8) compared to the theoretical OOC value was 3.74 % [13]. The optimum oxirane conversion was 95.5 % with 90.0 % yield. Table 1 shows the physicochemical properties of $EPO_o$. It has good properties on oxidative stability (193.9 $^oC$), flash and fire points (> 320 $^oC$), and kinematic viscosity.

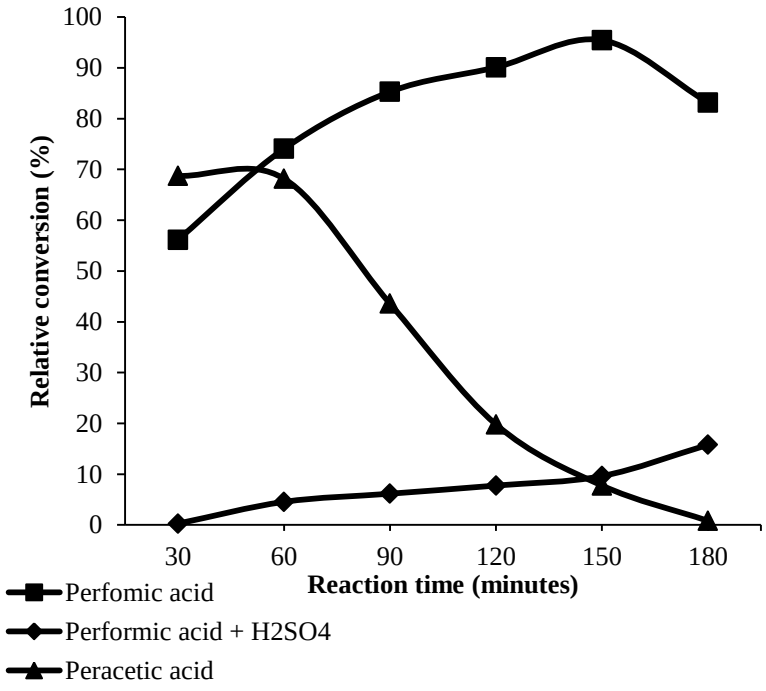



Figure 3. Relative conversion of $EPO_o$

Table 1. Physicochemical properties of $EPO_o$

| **Characterization** | **Unit** | **$EPO_o$** |
|---|---|---|
| Oxidative stability | $^oC$ | 193.9 |
| Flash point | $^oC$ | > 320 |
| Fire point | $^oC$ | > 320 |
| Pour point | $^oC$ | 16 |
| Kinematic viscosity, 40 $^oC$ | cSt | 158.6 |
| Kinematic viscosity, 100 $^oC$ | cSt | 19.8 |
| Viscosity index | - | 144 |
| Physical state (Room temperature) | - | Semi solid |
| Percentage of conversion | % | 95.5 |
| Yield | % | 90 |

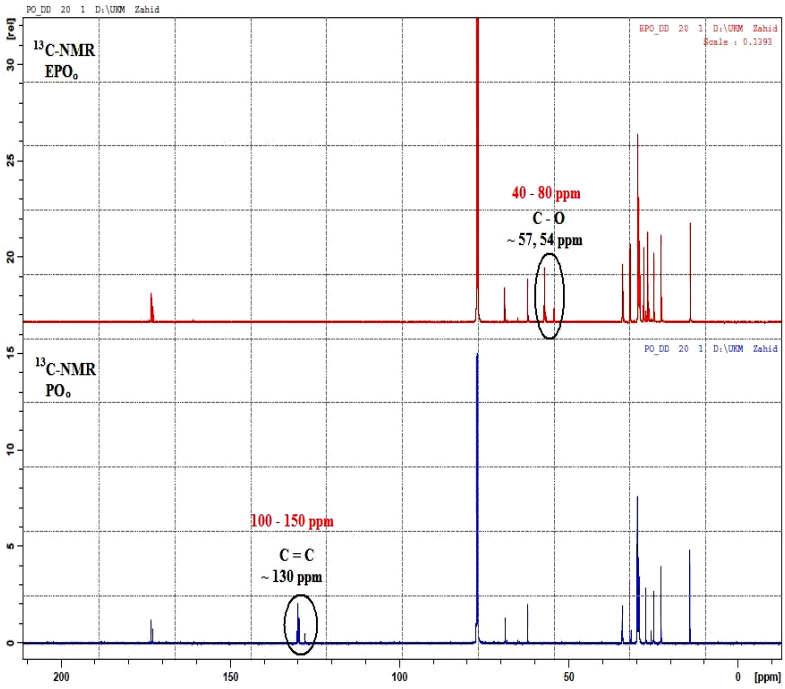



Figure 4. Comparison $^{13}C$-NMR spectra between $PO_o$ and $EPO_o$

The present of oxirane ring of $EPO_o$ proved by $^{13}C$-NMR and $^1H$-NMR spectra. Based on Figures 4 and 5, the presents of oxirane ring can be confirmed with the theoretical $^{13}C$ and $^1H$ chemical shift ranges (ppm). $^{13}C$ chemical shift ranges for unsaturated bond was 100 - 150 ppm while for C - O was 40 - 80 ppm. $^1H$ chemical shift ranges for vinyl hydrogen (C=C–H) was 4.5 - 6.5 ppm and for allyic hydrogen (C=C–C–H) was 1.6 - 2.6 ppm while for epoxide ring appeared in the range 2.5 - 3.5 ppm [23]. Based on comparison between $PO_o$ and $EPO_o$ FTIR (Figure 6), the spectrum of $PO_o$ showed an overtone streching vibration peak of C=O for ester at wavenumber 3473 $cm^{-1}$, streching vibration peak of =CH (3003 $cm^{-1}$) and unsaturation peak of HC=CH (cis) at wavenumber 1651 $cm^{-1}$. While, for the FTIR spectrum of $EPO_o$, the unsaturation peak and streching vibration peak of =CH for $PO_o$ have been disappeared. But the presents of oxirane ring peak was detected at wavenumber 844 $cm^{-1}$. Theoretical [27]

explained that oxirane ring can be detected at wavenumber 750 – 880 $cm^{-1}$ and 815 – 950 $cm^{-1}$, while overtone streching vibration peak of C=O for ester at wavenumber ~3450 $cm^{-1}$, streching vibration peak of =CH can be detected at wavenumber 3050 – 3000 $cm^{-1}$ and bonding peak of HC=CH (cis) at wavenumber 1650 – 1600 $cm^{-1}$. Based on Figure6, FTIR spectrum of $PO_o$ showed an overtone streching vibration peak of C=O for ester at wavenumber 3473 $cm^{-1}$, streching vibration peak of =CH (3003 $cm^{-1}$) and unsaturation peak of HC=CH (cis) at wavenumber 1651 $cm^{-1}$. While, for the FTIR spectrum of $EPO_o$, the unsaturation peak and streching vibration peak of =CH for $PO_o$ have been disappeared. But the presents of oxirane ring peak was detected at wavenumber 844 $cm^{-1}$.

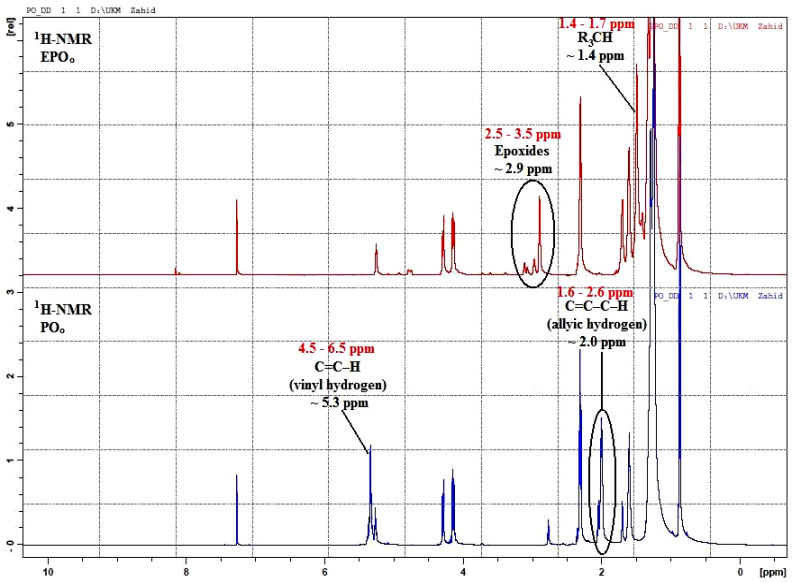



Figure 5. Comparison $^1$H-NMR spectra between $PO_o$ and $EPO_o$

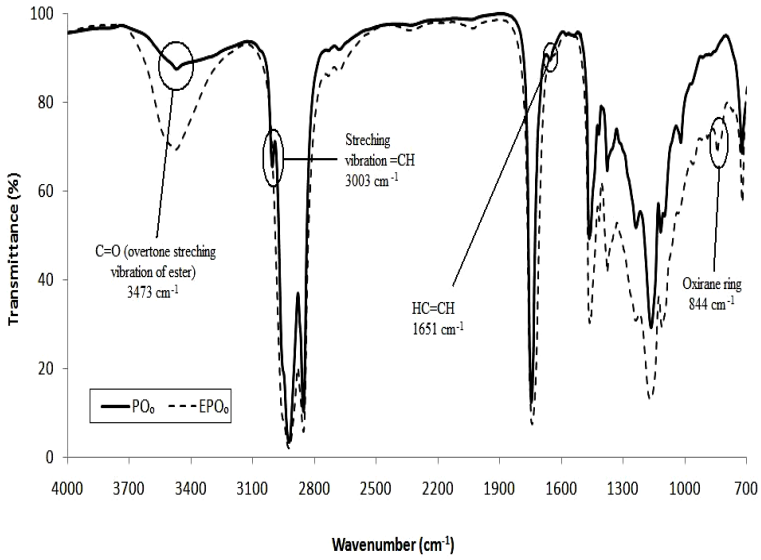



Figure 6. Comparison FTIR spectra between $PO_o$ and $EPO_o$

## Conclusion

Epoxidized palm olein is successfully produced by using peroxy acids. Performic acid is the best epoxidation agent for epoxidation process on palm olein. The presence of epoxide was proved by $^{13}C$, $^{1}H$-NMR and FTIR spectra. $EPO_o$ is potentially to be used as renewable material in synthesis process, coating, biolubricant, plasticizer and polymer industry.

## Acknowledgement

Authors would like to acknowledge Mr. Mohd Zahid Md. Yusoff (UKM's Science Officer) and Mr. Hasanudin Salleh for technical supports in this project. Thanks to the Universiti Kebangsaan Malaysia for the financial support through research grant no. GGPM-2014-033, DPP-2014-058 dan FRGS/2/2014/ST01/UKM/02/2.

## References

1. Goud, V. V., Patwardhan, A. V., & Pradhan, N. C. (2006). Studies on the epoxidation of mahua oil by hydrogen peroxide. *Bioresource technology*, 97 (12), 1365 – 1371.
2. Wang, X., Zhang, H., Wang, Z., & Jiang, B. (1997). *In* situ epoxidation of ethylene propylene diene rubber by performic acid. *Polyme*r, 38 (21), 5407 – 5410.
3. Rangarajan, B., Havey, A., Grulke, E. A., & Culnan, P. D. (1995). Kinetic parameters of a two-phase model for *in situ* epoxidation of soybean oil. *J. Am. Oil. Chem. Soc.,* 72 (10), 1161 – 1169.
4. Scala, J. L. and Wool, R. P. (2002). Effect of FA composition on epoxidation kinetic of TAG. *J. Am. Oil. Chem. Soc*., 79 (4), 373 – 378.
5. Gan, L. H., Goh, S. H. & Ooi, K. S. (1992). Kinetic studies of epoxidation and oxirane cleavage of palm olein methyl esters. *J. Am. Oil. Chem. Soc*., 69 (4), 347 – 351.
6. Goud, V. V., Pradhan, N. C., & Patwardhan, A. V. (2006). Epoxidation of karanja (Pongamiaglabra) oil by $H_2O_2$. *J. Am. Oil. Chem. Soc.*, 83 (7), 635 – 640.
7. Gunstone, F. D. (2004). "*The Chemistry of Oils and Fats: Sources, Composition, Properties and Uses"* Blackwell Publishing Ltd., UK.
8. Carlson, K. D. & Chang, S. P. (1985). Epoxidation of a Natural Unsaturated Epoxy Seed Oil from *Vernoniagalamensis* and a Look at Epoxy Oil Markets, *J. Am. Oil. Chem. Soc*., 62, 934 – 939.
9. Hang, X., & Yang, H. (1999). Model for a cascade continuous epoxidation process. *J. Am. Oil. Chem. Soc.,* 76 (1), 89 – 92.
10. Guenter, S., Rieth, R., Rowbottom, K. T. (2003). "*Ullmann's Encyclopedia of Industrial Chemistry*" Wiley-VCH, 6th Edition.
11. Rios, L. A., Weckes, P., Schuster, H.. & Hoelderich, W. F. (2005). Mesoporous and amorphous Ti–silicas on the epoxidation of vegetable oils J. Catal., 232, 19 – 26.
12. Warwel, S. & Klaas, M. R. (1995). Chemo-enzymatic epoxidation of unsaturated carboxylic acids. *J. Mol. Cat. B: Enzym*, 1, 29 – 35.
13. Sharpless, K. B., Woodard, S. S. & Finn, M. G. (1983). On the mechanism of titanium-tartrate catalyzed asymmetric epoxidation. *Pure Applied Chemistry*. 55 (4), 1823 – 1836.
14. Dinda, S., Patwardhan, A. V, Goud, V. V. & Pradhan, N.C. (2008). Epoxidation of cottonseed oil by aqueous hydrogen peroxide catalysed by liquid inorganic acids. *Bioresource Technology*, 99, 3737 – 3744.
15. O'Brien, R. D. (1998). "*Fats and Oils; Formulating and Processing for Applications",* Technomic Publishing AG, Switzerland.
16. Scrimgeour, C. (2005). *"Chemistry of Fatty Acids"* John Wiley & Sons Inc., Scotland, 6th Edition.
17. Campanella, A., Fontanini, C. & Baltanás, M. A. (2005). *Catalysis Today,* 107-108, 208-214.
18. Campanella, A., Fontanini, C. & Baltanás, M. A., (2008), High yield epoxidation of fatty acid methyl esters with performic acid generated *in-situ, Chemical EngineeringJournal*, 144, 466 – 475.
19. Klaas, M. R. & Warwel, S. (1999). Complete and partial epoxidation of plant oil by lipase-catalysed perhydrolysis. *Ind. Crops Prod.,* 9 (2), 125 – 132.
20. Derawi, D. & Salimon, J. (2010). Optimization on epoxidation of palm olein by using performic acid. *E-Journal of Chemistry*, 7 (4), 1440 – 1448.
21. A.O.C.S. (1998). *Official Metthods and Recommended Practices of AOCS,* AOCS, Illionis.

22. Paquot, C. (1979). "*Standards Methods for the Analysis of Oils, Fats and Derivatives Part-1"* Pergamon Press, Germany, 5th Edition
23. Pavia, D. L. (2001). "*Introduction to Spectroscopy" Thomson Learning*, Inc., United States
24. Derawi, D. & Salimon, J. (2013). Palm olein based biolubricant basestocks: synthesis, characterisation, tribological and rheological analysis. *Malaysian Journal of Analytical Sciences,* 17 (1), 153 – 163.
25. Findley, T. W., Swern, D. & Scanlan, J. T. (1945). Epoxidation of unsaturated fatty materials with peracetic acid in glacial acetic acid solution. *J. Am. Oil. Chem. Soc.,* 67(3), 412 – 414.
26. Greenspan, F. P. (1946). The convenient preparation of per-acids. *J. Am. Oil. Chem. Soc.*, 68(5), 907 – 907.
27. Socrates, G. (2001). *"Infrared and Raman Characteristic Group Frequencies"* John Wiley & Sons Ltd., England, 3rd Edition.

The Malaysian Journal of ANALYTICAL SCIENCES ISSN 1394-2506

# REMOVAL OF METHYL RED FROM AQUEOUS SOLUTION BY ADSORPTION ON TREATED BANANA PSEUDOSTEM FIBERS USING RESPONSE SURFACE METHOD (RSM)

## (Penyingkiran Metil Merah daripada Larutan Akues oleh Serapan Fiber Batang Pisang Yang Telah Dirawat Mengunakan Kaedah Permukaan Sahutan (RSM))

Zaida Rahayu Yet and Mohd Zulkhairi Abdul Rahim

*Department of Chemical Engineering Technology,*
*Universiti Kuala Lumpur (Malaysian Institute of Chemical and Bioengineering Technology), Melaka, Malaysia*

**Corresponding author: zaida@unikl.edu.my*

**Abstract**

The effect of adsorbent dose, pH and contact times on the removal of Methyl Red (MR) from aqueous solution by using agriculture waste (NaOH treated banana pseudostem fibers) were studied. The influence of these parameters on the removal of Methyl Red was examined by using a response surface method (RSM). The experiment was conducted by combining three parameters: adsorbent dose (500-1500 mg/L), pH (2-8) dan contact time (5-75 minutes ). The Box-Behnken Design (BBD) in Response Surface Methodology (RSM) by Design Expert Version 8.0.4 (Stat Ease, USA) was used for designing the experiments. Results showed that the optimum conditions for removal of Methyl Red from an aqueous solution (100 mg/L) were as follows: adsorbent dose (1417.70 mg/L), pH (2.08) and contact time (42.94 minutes) with the value of a coefficient of determination, $R^2$ is 98.98 %. Meanwhile, the second-order polynomial equation indicates that pH and contact times mostly affect the removal of Methyl Red.

**Keywords**: response surface method (RSM), adsorption, methyl red

**Abstrak**

Dalam penyelidikan ini, kesan dos penyerap, pH larutan dan masa untuk membuang Methyl Merah dari larutan media menggunakan sisa buangan pertanian iaitu serat batang pisang yang telah dirawat dengan larutan Sodium Hydroxide (NaOH) telah dikaji. Kesan tiga faktor dalam pengurangan Methyl Merah telah dikaji menggunakan Kaedah Permukaan Sambutan (RSM). Eksperimen dijalankan dengan menggabungkan ketiga – tiga pemboleh ubah iaitu dos penyerap (500-1500 mg/L), pH larutan (2-8) dan masa tindakan (5-75 minit). Reka bentuk Box-Behnken (BBD) di dalam Kaedah Permukaan Sambutan (RSM) menerusi "Design Expert" versi 8.0.4 (Stat Ease, USA) telah digunakan untuk mereka bentuk eksperimen. Keadaan terbaik untuk membuang 100 mg/L Methyl Merah dari larutan media adalah seperti berikut: dos penjerapan (1417.70 mg/L), pH larutan (2.08) dan masa tindakan (42.94 minit) dengan nilai pekali penentu, $R^2$ sebanyak 98.98 %. Persamaan polinomial peringkat kedua diperolehi didapati pH larutan dan masa rawatan adalah paling memberi kesan terhadap pembuangan Methyl Merah dengan menggunakan fiber batang pisang yang telah dirawat.

**Keywords**: kaedah permukaan sambutan, serapan, metil merah

## Introduction

In Malaysia, 97 % of the effluent discharged is mainly from three industrial categories, which are food industry, chemical industry and textiles industry [1]. Some of the industries used dyes in their daily processes such as textile, plastic, cosmetic, paper. Among of these various industries, textile ranks first in the usage of dyes for coloration of fiber [2]. Currently, it was estimated about 10,000 of different commercial dyes and pigments exist and over 7 x $10^5$ tons are produced annually worldwide [3].

Organic dyes are an integral part of many industrial effluents and require a suitable method for disposal.The discharge of colored wastewater from the industries may present an eco-toxic hazard and introduce the potential danger of bioaccumulation, which may eventually affect human through the food chain [4]. However, these dyes, are not normally removed by conventional wastewater treatment systems. Hence, it becomes crucial to find out an alternative approach to removing colourant from the effluents before it can discharge into the water mainstream.

In recent years, adsorption has gained favor due to proven efficiency in the removal of pollutants from the effluents. Activated carbon has excellent adsorption efficiency for the organic compound and because of that; it is widely used [5]. But, it is getting expensive and many studies have been done to find low cost and effective of adsorbent to replace the activated carbon such as tea waste [6], coal ash [7], oil palm trunk fibre [8], sugar cane bagasse as well as rice husk, coconut shell and orange peel [9]. Meanwhile, in Malaysia, plant fibres from an agriculture sector often seen as a waste and not fully utilize. Data show; there are abundant sources of raw material in Malaysia that can be transformed into profitable, useable products [10]. Therefore, full utilization of natural plant for suitable application has become an attractive approach instead of letting them creating pollution problems.

In Malaysia, banana is the second most widely cultivated fruit. It is covering about 26,000 ha, with a total production of 530,000 metric tones [11], which mean much banana waste such as banana trunk fibers were obtained. This waste can be used to something much more valuable but has not received much attention. Scientifically, banana tree is called *Musa accuminata* that comes from *Musa* family. It was reported that the banana pseudostem fibers can be used as an enzyme immobilization matrix [12]. Therefore, it could be possible to utilize it as well in a different way of application such as for removal of azo dyes. Sodium hydroxide treatment has been identified to be able to improve the sorption capacity. The sorption capacity improvement occurred mainly by the dissociation of hydrogen ions bonded to the hydroxyl, carboxyl and other groups, which concomitantly offered a negatively charged surface [13].

The most classic and popular way to achieved highest removal efficiency is by the used of one variable at a time approach, but it involves a huge number of independent run and time consuming. Optimization also can be done by using Response Surface Methodology (RSM). RSM is a collection of mathematical and statistical techniques useful for modeling and analysis of problems in which the response of interest is influenced by several variables, and the objective is to optimize this response [14]. RSM proved very effective and time saving model for studying the influence of process parameters on the response (RSM) factor by significantly reducing the number of experiments and hence facilitating the optimum conditions [15].

In this research, the ability of banana trunk fiber as an alternative low-cost fiber for the removal of methyl red from the aqueous solution was investigated. The main objectives of this study are to obtain the optimum conditions for removal of azo dyes (Methyl Red) by using Response Surface Methodology approach. The sodium hydroxide treated banana pseudostem fibers were used as an adsorbent for this purpose.

## Materials and Methods

### Experimental Design

The Response surface method via Box-Behnken was employed to identify the relationship between a set of controllable experimental factors and observed results. This optimization process involves three major steps; performing the statistically designed experiments, estimating the coefficients in a mathematical model and predicting the response and checking the adequacy of the model [16]. Table 1 shows the experimental range for each factor used and defined in three level (low, basal and high) coded as (-1, 0, +1).

Box-Behnken statistical designed with 3 factors, 3-level and 15 runs as shown in Table 2 and was used for the optimization procedure. This design consists of replicated center points and the set of points lying at the midpoint of each edge of the multidimensional cube that defines the region of interest. The three independent variables were coded according to the following equation (1):

$$x_i = \frac{X_i - X_0}{\Delta X_i} \qquad x_i = 1,2,3 \qquad (1)$$

where $x_i$ is dimensionless value of an independent variable, $X_i$ the actual value of an independent variable i, $X_0$ the actual value of the independent variable i at the center point and $\Delta X_i$ is the step change of $X_i$ corresponding to a unit variation of the dimensionless value.

Table 1. Experimental values and coded levels of the independent variables

| | **Levels** | | |
|---|---|---|---|
| **Independent variables** | **-1** | **0** | **+1** |
| Adsorbent Dose, $X_1$ | 500 | 1000 | 1500 |
| pH, $X_2$ | 2 | 5 | 8 |
| Contact Time, $X_3$ | 5 | 40 | 75 |

Table 2. Box-Behnken experimental design matrix

| | **Coded values of the variables** | | | **Actual values of the variables** | | |
|---|---|---|---|---|---|---|
| **Run** | **Adsorbent dose (mg/L)** | **pH** | **Contact Time (min)** | **Adsorbent dose (mg/L)** | **pH** | **Contact Time (min)** |
| | $X_1$ | $X_2$ | $X_3$ | $X_1$ | $X_2$ | $X_3$ |
| 1 | 0 | +1 | -1 | 1000 | 8 | 5 |
| 2 | +1 | 0 | -1 | 1500 | 5 | 5 |
| 3 | 0 | 0 | 0 | 1000 | 5 | 40 |
| 4 | 0 | 0 | 0 | 1000 | 5 | 40 |
| 5 | 0 | -1 | +1 | 1000 | 2 | 75 |
| 6 | -1 | -1 | 0 | 500 | 2 | 40 |
| 7 | +1 | 0 | +1 | 1500 | 5 | 75 |
| 8 | +1 | +1 | 0 | 1500 | 8 | 40 |
| 9 | -1 | 0 | +1 | 500 | 5 | 75 |
| 10 | 0 | 0 | 0 | 1000 | 5 | 40 |
| 11 | 0 | +1 | +1 | 1000 | 8 | 75 |
| 12 | -1 | 0 | -1 | 500 | 5 | 5 |
| 13 | -1 | +1 | 0 | 500 | 8 | 40 |
| 14 | 0 | -1 | -1 | 1000 | 2 | 5 |
| 15 | +1 | -1 | 0 | 1500 | 2 | 40 |

The mathematical relationship of the responses (% Removal) and the independent variables were modeled by a second order polynomial function as follows:

$$Y = \beta_0 + \beta_1 X_1 + \beta_2 X_2 + \beta_3 X_3 + \beta_{12} X_1 X_2 + \beta_{13} X_1 X_3 + \beta_{23} X_2 X_3 + \beta_{11} X_1^2 + \beta_{22} X_2^2 + \beta_{33} X_3^2 \quad (2)$$

where Y is the predicted response, $\beta_0$, intercept, $\beta_1, \beta_2$ and $\beta_3$, linear coefficients, $\beta_{11}, \beta_{22}$ and $\beta_{33}$, squared coefficients and $\beta_{12}, \beta_{13}$ and $\beta_{23}$, the interactions coefficients of the equation and $X_1, X_2$ and $X_3$ are the independent variables.

The statistical analysis of the data was done by using Design-Expert 8.0.4 in order to determine the best model for the removal of Methyl Red (MR) from aqueous solution. An analysis of variance (ANOVA) by calculating F- value was employed. ANOVA was used to recognize the relationship between the response (% Removal) and the independent variables. The p-value was used as an indicator to verify the significance of each term. If the p-value was less than 0.05 indicates that the factor influences the experiment. The indicator for the fitness of the second order polynomial model was evaluated by coefficient of determination ($R^2$). In order to show the relationship and interaction between variables and the response graphically, the three dimensional surface plot or contour plots were employed.

**Preparation of adsorbent and adsorbate**

Banana pseudostem fibers from the family of *Musa acuminate balbisiana cultivars (BBBc)* or locally called as 'Pisang Nipah' were obtained from local farm at Taboh Naning, Alor Gajah, Melaka. The banana pseudostem fibers were cut into small pieces then washed using distilled water to remove any dirt before it was dried in drying oven at 65 °C for 24 hours. After that, it was ground using a grinder and sieved by using Endecotts Octagon Digital Sieve Shaker. The particles size obtained was in ranged of 63 – 500 micron. Then, 10g of pseudostem sample were stirred with 100 ml of 0.1M Sodium Hydroxide, NaOH solution for 1 hour at room temperature then filtered. The sample then washed using distilled water to neutral pH and dried in the oven at 55 °C for 24 hours. The resulting adsorbent was abbreviated as treated banana pseudostem fibers.

Methyl Red (MR), 2-[4-(dimethylamino)phenylazo] benzoic acid was used as an adsorbate for this study. Methyl Red is red in aqueous solution of pH under 4.4, yellow in pH over 6.2 and orange in between [17]. A stock solution of Methyl Red (100 $mgL^{-1}$) was prepared by dissolving 0.100 g of the dye in 1 L of distilled water. Different concentrations ranges between 20-100 $mgL^{-1}$ were prepared from the stock solution. Distilled water was used for preparing all the solutions and reagents. The initial pH was adjusted with 0.1M HCl or 0.1M NaOH.

**Batch Adsorption Studies**

The effects of adsorbent dosage, pH and contact times were studied. The initial concentration was 100mg/L for all the samples. For the purpose of optimizing, the amount of the adsorbent was performed by adding different weight of pseudostem fiber in the range of 500 – 1500 mg/L into 50 ml of the Methyl Red solution. For each 50 ml of 100 mg/L, the pH was adjusted by using 0.1M HCl or 0.1M NaOH. The experiment was conducted at pH value range of 2-8. Then, the effect of treatment time was studied by varying the contact time in between 5 – 75 minutes at a constant speed of the stirrer. All the adsorption experiments were carried out at room temperature (27±2°C). All samples were analyzed using UV-VIS Spectrophotometer (Perkin Elmer UV/VIS Lambda EZ210) at $\lambda_{max}$ of 463nm, to determine the final concentration of the solution. The percentage removal (Y) of Methyl Red dye by treated banana pseudostem fibers at time, t was calculated as:

$$Y = \frac{100(C_o - C_t)}{C_o} \quad (3)$$

where, $C_o$ is the initial adsorbate concentration (mg/l), $C_t$ is the adsorbant concentration (mg/l) at time t.

**Analytical measurements**

A series of standards solution with concentration ranging from 20 ppm to 100 ppm were prepared from Methyl Red (MR) stock solutions in 50 ml volumetric flask. Then the highest concentration (100 ppm) was used in wavelength scan application. The purpose of wavelength scan is to determine wavelength at maximum absorbance ($\lambda_{max}$ ) of methyl red. Then, the obtained $\lambda_{max}$ was used in photometric scan. The prepared serial of dilutions above (known standards) were scan one by one and the absorbance readings were recorded. The standard calibration graph of methyl red standard was then constructed using a linear least square fit method. Photometric scan also were used to determine the absorbance of residual sample after treatment with banana fiber. The residual concentration after treatment; $C_t$ can be calculated based on working 'standard curve' from a series of known standards (known concentration).

## Results and Discussion

**Statistical analysis**

In order to study the combined effect of three factors, 15 experiments were performed in different combinations of the parameters (Table 3). Table 3 shows the predicted, and an experimental data related to percentage removals of Methyl Red obtained.

**Model Fitting using RSM**

Using the experimental results from Table 3, the full quadratic second order polynomial equation was fitted to the data appropriately and the equation was presented as follows:

$$Y = 33.97 + 1.65X_1 - 33.29X_2 - 4.36X_3 - 3.62X_1X_2 + 3.42X_1X_3 - 4.89X_2X_3 - 3.36X_1^2 + 29.397X_2^2 - 9.48X_3^2 \quad (4)$$

The analysis of variance for the response has been summarized in Table 4. The large value of F indicates that most of the variation in the response can be explained by the regression equation. The p-value is used to estimate whether F is large enough to indicate statistical significance. If p values lower than 0.05 indicates that the model is statistically significant [18].

To decide about the adequacy of model to represent percentage of removal of methyl red, the adequacy of the model test were carried out and the results are given in Table 4. The p-value for the quadratic model was lower than 0.05 and the $R^2$ for the quadratic model was highest as compared with other model. Therefore, the quadratic model was chosen to illustrate the relationship between independent variable and the amount of methyl red removal.

Data obtained were also analyzed to check the normality of the residuals. The normal probability plot or dot diagram of the residuals is plotted as shown in Figure 1. From the plot, the data points lie reasonably close to the straight line, this shown that the developed model is adequate.

Table 5 shows the F-values and p value of the model for percentage removal of methyl red. The F value of the model is 54.10 and the p-value is <0.05, which showed that the model terms are significant. As shown in Table 5, the coefficient of determination ($R^2$) and adjusted $R^2$ of this model were 0.9898 and 0.9715, respectively. The coefficient of determination ($R^2$) is 0.9898 suggesting that 98.98% of the variability in percentage removal can be explained by this model. Regression also provides a way to evaluate the nature and the degree of correlation between dependent and independent variables. The closer the $R^2$ value is to 1.00, the stronger the model and the better the response predictions. The differences between values of $R^2$ (0.9898) and adj. $R^2$ (0.9715) are small; therefore, the similarity between $R^2$ and adjusted $R^2$ shows the adequacy of the model to predict the response.

The lack of fit F-value of 3.09 with p>0.05 implied that the lack of fit was not significant relative to the pure error. A non-significant lack of fit was considered good and was desired for the model to fit. Thus, a well-fitted model was obtained for the equation of percentage removal.

Table 3. Experimental and the predicted values yields for removing Methyl Red

| Run | Adsorbent dose (mg/L) (A) | pH (B) | Contact time (min) (C) | Y Experiment (% Removal) | Y Predicted (% Removal) |
|---|---|---|---|---|---|
| 1 | 0 | +1 | =1 | 24.78 | 29.85 |
| 2 | +1 | 0 | -1 | 25.14 | 23.72 |
| 3 | 0 | 0 | 0 | 31.51 | 33.97 |
| 4 | 0 | 0 | 0 | 37.91 | 33.97 |
| 5 | 0 | -1 | +1 | 92.77 | 87.70 |
| 6 | -1 | -1 | 0 | 84.38 | 88.02 |
| 7 | +1 | 0 | +1 | 19.28 | 21.84 |
| 8 | +1 | +1 | 0 | 28.39 | 24.75 |
| 9 | -1 | 0 | +1 | 10.27 | 11.35 |
| 10 | 0 | 0 | 0 | 32.5 | 33.97 |
| 11 | 0 | +1 | +1 | 10.27 | 11.7 |
| 12 | -1 | 0 | -1 | 29.82 | 27.26 |
| 13 | -1 | +1 | 0 | 31.2 | 28.69 |
| 14 | 0 | -1 | -1 | 87.73 | 86.65 |
| 15 | 0 | -1 | -1 | 5.00 | 3.65 |

Table 4. Adequacy of the model tested

| Source | Sum of Squares | Df | Mean Square | F Value | Prob > F | |
|---|---|---|---|---|---|---|
| Mean | 27478.46 | 1 | 27478.46 | | | |
| Linear | 9038.32 | 3 | 3012.77 | 8.05 | 0.0041 | |
| 2FI | 194.89 | 3 | 64.96 | 0.13 | 0.9380 | |
| Quadratic | 3788.64 | 3 | 1262.88 | 47.22 | 0.0004 | Suggested |
| Cubic | 109.98 | 3 | 36.66 | 3.09 | 0.2541 | Aliased |
| Residual | 23.74 | 2 | 11.87 | | | |
| Total | 40634.03 | 15 | 2708.94 | | | |

| Source | Std. Dev. | R-Squared | Adjusted R-Squared | Predicted R-Squared | PRESS | |
|---|---|---|---|---|---|---|
| Linear | 19.35 | 0.6869 | 0.6017 | 0.3492 | 8561.58 | |
| 2FI | 22.14 | 0.7018 | 0.4782 | -0.5060 | 19812.60 | |
| Quadratic | 5.17 | 0.9898 | 0.9715 | 0.8622 | 1813.12 | Suggested |
| Cubic | 3.45 | 0.9982 | 0.9874 | | | Aliased |

As shows in Table 5, the ANOVA analysis shows that the quadratic effects of pH ($X_2$) and contact time ($X_3$) were significant ($p<0.05$), while linear effect only pH was significant ($p<0.05$). The adsorbent dose does not give an effect to remove the Methyl Red. It may be because of the amount between high and low limit of the dose used is in small range. The pH give high significant to the removal of Methyl Red. This high significant may affected the low order interaction which is the adsorbent dose [18]. The removal of dyes by treated banana pseudostem fibers was found to be a maximum in the acidic medium.

The pH value of the dye solution plays an important role in the whole adsorption process and particularly on the adsorption capacity. As the pH of the adsorption solution was lowered, the positive charges on the surface increased. This would attract the negatively charged functional groups located on the reactive dyes [19]. Contact times also give an effect to the removal of Methyl Red where contact time increased, the percentage removal also increased.

Figure 2 shows the relationship between the actual and predicted values for adsorption of Methyl Red in aqueous solution by using the treated banana pseudostem fibers. The parity plot (Figure 2) shows the satisfactory correlation between the values of experimental and predictive values, wherein, the points cluster around the diagonal line which indicates the good fit of model.

Table 5. ANOVA of the second-order polynomial equation

| Source | Sum of squares | df | Mean Square | F Value | Prob > F | Remark |
|---|---|---|---|---|---|---|
| Model | 13021.85 | 9 | 1446.87 | 54.10 | 0.0002 | significant |
| A-Adsorbent Dose(mg/L) | 21.78 | 1 | 21.78 | 0.81 | 0.4082 | |
| B-pH | 8864.46 | 1 | 8864.46 | 331.46 | < 0.0001 | |
| C-Contact Time (min) | 152.08 | 1 | 152.08 | 5.69 | 0.0628 | |
| AB | 52.49 | 1 | 52.49 | 1.96 | 0.2201 | |
| AC | 46.85 | 1 | 46.85 | 1.75 | 0.2429 | |
| BC | 95.55 | 1 | 95.55 | 3.57 | 0.1173 | |
| $A^2$ | 41.76 | 1 | 41.76 | 1.56 | 0.2668 | |
| $B^2$ | 3190.85 | 1 | 3190.85 | 119.31 | 0.0001 | |
| $C^2$ | 332.03 | 1 | 332.03 | 12.42 | 0.0169 | |
| Residual | 133.72 | 5 | 26.74 | | | |
| Lack of Fit | 109.98 | 3 | 36.66 | 3.09 | 0.2541 | not significant |
| Pure Error | 23.74 | 2 | 11.87 | | | |

$R^2$ = 0.9898
Adjusted R-Squared = 0.9715

**Effect of various parameters on Methyl Red dye removal efficiency**

To evaluate the relationships and interactions of parameters, surface plots give good prescriptions (Figure 1 and 2). The behavior of the production conversion under the process conditions are presented in Figures 3 to 5. To study the effect of adsorbent dose and pH on Methyl Red removal, experiments were carried out by varying adsorbent dose from 500 to 1500 mg/L and pH from 2 to 8. The maximum adsorption of Methyl Red dye (Y) was 96.39% at low of pH (2.08) and higher of adsorbent dose (1417.70 mg/L) as shown in Figure 3. Therefore, there is an interaction

between pH and adsorbent dose.The results also indicates that methyl red adsorption with treated banana pseudostem fibers mainly take place in acidic medium.

Figure 4 shows the effect of adsorbent dose and contact time on the removal of methyl red. In the studied range, time showed smallest effect with the maximum removal efficiency obtained was at 42.94 minutes. At 75 minutes, the percentage removal is lower due to an aggregation of dye molecules with the increase in contact time makes it almost impossible to diffuse deeper into the adsorbent structure at highest energy sites. As the mesopores get filled up and start offering resistance to diffusion of aggregated dye molecules in the adsorbents, that aggregation negates the influence of contact time [18].

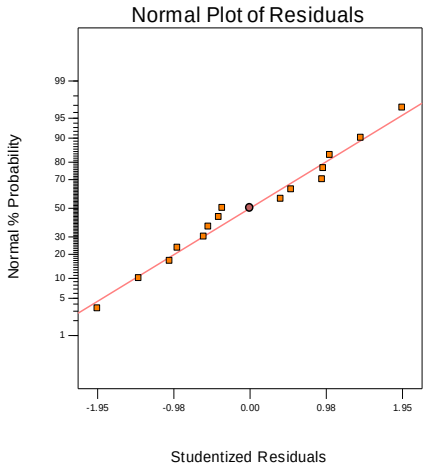



Figure 1. Normal % probability versus residual error of methyl red removal

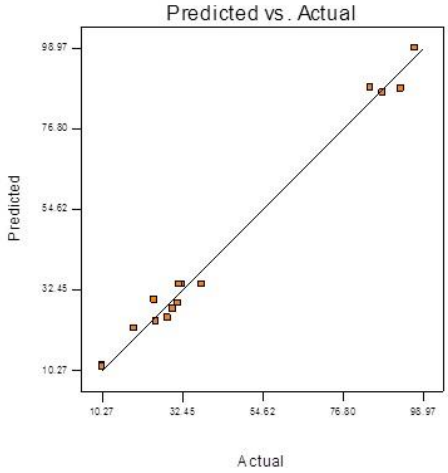



Figure 2. Scatter diagram of predicted response versus actual response of methyl red removal

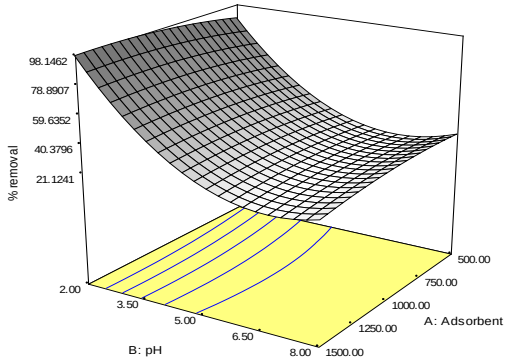



Figure 3. 3D response surface graph for dye removal versus adsorbent dose (mg/L) and pH for Methyl Red dye adsorption system

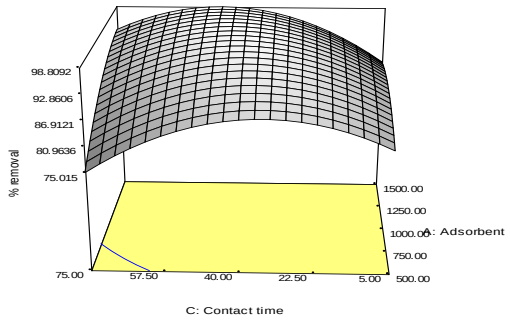



Figure 4. 3D response surface graph for dye removal versus adsorbent dose (mg/L) and contact time (min) for Methyl Red dye adsorption system

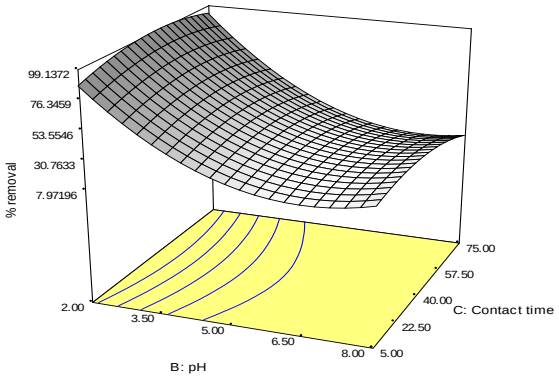



Figure 5. 3D response surface graph for dye removal versus pH and contact time (min) for Methyl Red dye adsorption system

**Validation of the model**

The maximum predicted adsorption capacity for optimum conditions in order to remove Methyl Red in aqueous solution was obtained through point prediction method and surface response plots is given in Table 6. The optimal level for adsorbent dose is 1417.70 mg/L at pH 2.08 and contact time 42.94 minutes with the maximum percentage removal is 96.39 %. The experiment was then performed at the optimal levels of the process parameters and the results shown in Table 7. The results are further analyzed using MINITAB 15 software package. One sample T-test was used to run the confirmation experiment's results. The P-value is 0.056 which is more than 0.05 (Table 8). This proven that, the results confirmed the validity of the model. Where the experimental data obtained was well represented by the Eq. (4).

Table 6. Optimum and confirmative values of process parameters for maximum removal efficiency

| | **Factor** | | |
|---|---|---|---|
| | **Adsorbent Dose (mg/L)** | **pH** | **Contact time (min)** |
| Optimal levels | 1417.70 | 2.08 | 42.94 |

Table 7. Data of confirmation run

| **Run** | **Adsorbance Dose (mg/L)** | **pH** | **Contact time (min)** | **Y (% Removal)** |
|---|---|---|---|---|
| 1 | 1417.7 | 2.08 | 42.94 | 94.31 |
| 2 | 1417.7 | 2.08 | 42.94 | 93.10 |
| 3 | 1417.7 | 2.08 | 42.94 | 91.10 |
| 4 | 1417.7 | 2.08 | 42.94 | 95.55 |

Table 8. Result for validation

| **Variable** | **N** | **Mean** | **St Dev** | **SE Mean** | **T** | **P** |
|---|---|---|---|---|---|---|
| Y (% removal) | 3 | 93.515 | 1.895 | 0.948 | -3.03 | 0.056 |

## Conclusion

The optimum conditions for removal of methyl red from an aqueous solution by using banana fibers were successfully identified. RSM proved is a useful technique for studying the effect of several factors on responses by varying them simultaneously and carrying out a limited number of experiments. It was shown that a second-order polynomial regression model could properly interpret in the experimental data with a coefficient of determination ($R^2$) value of 98.98 %. Results also showed that the optimum conditions for removal of Methyl Red from an aqueous solution (100 mg/L) were as follows: adsorbent dose (1417.70 mg/L), pH (2.08) and contact time (42.94 minutes) with the value of maximum adsorption is 96.39%. Meanwhile, the equilibrium between the adsorbate in

the solution and on the adsorbent surface was practically achieved in 42.94 minutes. A high similarity was observed between the predicted and experimental results, which reflected the accuracy and applicability of the model. Furthermore, this study shows that the Box-Behnken model is suitable to optimize the removal of methyl red. The treated banana pseudostem fiber has a good potential as an adsorbent for the removal of dyestuffs from aqueous solution.

**References**


1. Azira, S., Wong, T. N., Robiah, Y. and Chuah, T. G. (2004) Adsorption of methylene blue onto palm kernel shell activated carbon. E Proceeding. Regionalm Conference For Young Chemists 2004. Universiti Sains Malaysia, Penang, Malaysia.
2. Saiful Azhar S., Ghaniey Liew , Suhardy D., Farizul Hafiz K. , Irfan Hatim M.D (2005). Dye Removal from Aqueous Solution by using Adsorption on Treated Sugarcane Bagasse, *American Journal of Applied Sciences* 2 (11): 1499-1503, 2005.
3. Grag, V.K, M. Anita, R. Kumar and R. Gupta, 2004. Removal from simulated wastewater by adsorption using Indian Rosewood sawdust: A timber industry waste. *Dyes & Pigments*, 63: 243-250.
4. Atef S. Alzaydien (2009). Adsorption of Methylene Blue from Aqueous Solution onto a Low-Cost Natural Jordanian Tripoli. Science Publications. *American Journal of Environmental Sciences* 5 (3): 197-208.
5. Helen K.M., Iyyaswami R., Magesh G.P., and Lima R.M. (2009) Modelling, analysis and optimization of adsorpation parameter for $H_3PO_4$ activated rubber wood sawdust using response surface methodology (RSM). *Journal of Colloids and Surfaces B: Biointerfaces* 70: 35-45.
6. Amarasinghe B.M.W.P.K. and Williams R.A. (2007). Tea waste as a low cost adsorbent for the removal of Cu and Pb from wastewater, *Chemical Engineering Journal* 132: 299.
7. Hawari A.H. and Mulligan C.N. (2006) Biosorption of lead(II), cadmium(II), copper(II) and nickel(II) by anaerobic granular biomass, *Bioresource Technology* 97: 692.
8. Hameed B.H., El-Khaiary M.I. (2008) Batch removal of malachite green from aqueous solutions by adsorption on oil palm trunk fibre: Equilibrium isotherms and kinetic studies, *Journal of Hazardous Materials* 154 : 237–244
9. Dhiraj S., Garima M., Kaur M.P. (2008) Agricultural waste material as potential adsorbent for sequestering heavy metal ions from aqueous solutions – A review *Bioresource Technology* 99: 6017–6027.
10. Goh C.S., Tan K. T., Lee K. T., Bhatia S. (2010) Bio-ethanol from lignocellulose: Status, perspectives and challenges in Malaysia, *Bioresource Technology* 101: 4834–4841.
11. Mak Chai. Ho Y W., Liew K.W. and Asif J.M (2004). Biotechnology and in vitro mutagenesis for banana improvement. © 2004 Science Publications.
12. Rahim MZA (2009), Preliminary Study on Selected Malaysian Plant Based Material as New Immobilize Matrix, 2nd National Symposium on Fermentation Technology (NSFT 2009), Malacca International Trade Centre (MiTC), Ayer Keroh, Melaka, 14-15 .
13. Abdullah A.Z., Salamatinia B. and Kamaruddin A.H. (2009). Application of response surface methodology for the optimization of NaOH treatment on oil palm frond towards improvement in the sorption of heavy metals. *Desalination* 244 :227–238.
14. Montgomery, Douglas C. (2005). Design and Analysis of Experiments: Response surface method and designs. New Jersey: John Wiley and Sons, Inc.
15. Garg U.K., Kaur M.P., Sud D. and Garg V.K. (2009) Removal of hexavalent chromium from aqueous solution by adsorption on treated surgane bagase using response surface methodological approach. *Desalination* 249 : 475-479.
16. Annadurai G., Babu S.R., Nagarajan G. and Ragu K. (2000) Use of Box-Behnken design of experiments in the production of manganese peroxidase by Phanerochaete chrysosporium (MTCC 767) and decolorization of crystal violet. *Bioprocess engineering* 23: 715-719.
17. Mas Rosemal H. Mas Haris and Kathiresan Sathasivam (2009). The Removal of Methyl Red from Aqueous Solutions Using Banana Pseudostem Fibers. © 2009 Science Publications.

18. Paritosh Tripathi, Vimal Chandra Srivastava and Arvind Kumar (2009). Optimization of an azo dye batch adsorption parameters using Box–Behnken design. *Desalination* 249: 1273–1279.
19. Santhy K. and Selvapathy P. (2006). Removal of reactive dyes from wastewater by adsorption on coir pith activated carbon. *Bioresource Technology* 97 : 1329–1336.

The Malaysian Journal of ANALYTICAL SCIENCES ISSN 1394-2506

# IMPROVING FILLER DISPERSION AND PHYSICAL PROPERTIES OF EPOXIDISED NATURAL RUBBER/SILICA COMPOUND BY USING DUAL FILLERS AND COUPLING AGENT IN MIXING PROCESS

## (Meningkatkan Penyerakan Pengisi dan Sifat Sifat Fizikal Sebatian Getah Asli Terepoksida/Silika dengan Menggunakan Dual Pengisi dan Ejen Gandingan di dalam Proses Pencampuran)

Teku Zakwan Zaeimoedin*, Ahmad Kifli Che Aziz, Mazlina Mustafa Kamal

*Malaysian Rubber Board,*
*RRIM Research Station, 47000 Sungai Buloh, Selangor, Malaysia*

**Corresponding author: zakwan@lgm.gov.my*

**Abstract**

Since the introduction of Green Tyre concept, in the early 90ies, the use of silica as reinforcing fillers has spread and grown worldwide. The general advantages of silica as reinforcing filler over carbon black filler are better rolling resistance by achieving at least equal wet traction while tread wear should not be adversely affected. In general, high filler loading in ENR attributes poor dispersion and lack of adhesion to the rubber matrix which in turn affect the processability and physical properties of the rubber compounds. In this work, effect of dual fillers (silica and carbon black) and coupling agent in ENR/silica compound was studied respectively. The mixing was done in a Banbury® BR 1600 internal mixer and the filler dispersion and physical properties were analysed. The carbon black filler was varied from 5 phr to 20 phr, where the total filler was fixed at 60 phr for truck tyre tread compound. The coupling agent was mixed in the mixing at two different stages which is first stage and finalizing stage of mixing. The rheological properties test was conducted by using Mooney Viscometer. The hardness, abrasion and tensile strength for physical properties evaluation were also conducted in this study. In addition, the filler dispersion property was determined by using disperGrader™. The results showed that some of ENR/silica compound properties such as tensile, hardness, filler dispersion and abrasion resistance were slightly improved as compared to control compound.

**Keywords:** ENR, Silica, carbon black, coupling agent, filler dispersion, physical properties

**Abstrak**

Sejak pengenalan konsep Tayar Hijau, dalam awal 90an, penggunaan silika sebagai pengisi pengukuh telah merebak dan berkembang di seluruh dunia. Kelebihan umum silika sebagai pengisi pengukuh terhadap pengisi karbon hitam ialah rintangan gulingan yang lebih baik dengan mencapai sekurang-kurangnya cengkaman basah yang sama manakala kehausan telapak tayar tidak akan terjejas. Secara umum, muatan pengisi yang tinggi dalam ENR menyebabkan sifat penyelerakan yang lemah dan kurangnya lekatan terhadap matriks getah yang seterusnya memberi kesan kepada sifat pemprosesan dan sifat fizikal sebatian getah. Dalam karya ini, kesan dual pengisi (silika dan karbon hitam) dan ejen gandingan dalam sebatian ENR/silika masing-masing dikaji. Pencampuran dilakukan dalam pencampur dalaman Banbury® BR 1600 dan penyerakan pengisi dan sifat sifat fizikal dianalisis. Pengisi karbon hitam telah dilpelbagaikan dari 5 hingga 20 phr, di mana jumlah semua pengisi ditetapkan pada 60phr untuk sebatian telapak tayar trak. Ejen gandingan dicampurkan di dalam pencampuran di dua peringkat yang berbeza iaitu peringkat pertama dan peringkat akhir pencampuran. Ujian sifat-sifat reologi telah dijalankan dengan menggunakan Mooney viscometer. Kekerasan, lelasan dan kekuatan tegangan untuk penilaian sifat sifat fizikal juga dijalankan dalam kajian ini. Di samping itu, penyerakan pengisi telah ditentukan dengan menggunakan disperGrader™. Hasil kajian menunjukkan bahawa beberapa sifat sebatian ENR / silika seperti tegangan, kekerasan, serakan pengisi dan rintangan lelasan telah meningkat sedikit berbanding dengan sebatian kawalan.

**Kata kunci:** ENR, Silika, karbon hitam, ejen gandingan, serakan pengisi, sifat sifat fizikal

## Introduction

The general advantages of silica as reinforcing filler over carbon black filler are reduced rolling resistance with at least equal wet traction while tear and wear should not be adversely affected. ENR-25 which is a polar rubber interacts strongly with silica (silanol group) hence therefore could eliminate or reduce the use of coupling agent. In contrast to carbon black, the surface of precipitated silica is highly polar and hydrophilic due to the presence of numerous silanol groups. The strong intermolecular hydrogen bonds between hydroxyl groups and relative high surface area, agglomeration and flocculation tend to occur during storage and vulcanization process. The processing becomes more crucial under the tropical climate with its high relative humidity and moisture prevalent. Under such ambient conditions, silica filler would easily pick up additional moisture which would have detrimental effects on processing and mixed compound properties. In order to improve the compatibility of silica in rubber and ensure its good coupling to the polymer matrix, the addition of coupling agents are necessary [1]. The use of silanes coupling agent allow modification of the polar silica surface, which makes the silica more compatible with the rubber matrix [2].

Meanwhile the addition of carbon black filler in rubber matrix as a reinforcement is to modify the mechanical properties of the finished product and also to control the viscoelastic behavior of the compound properties. To date, scarce information can be obtained on filler blend particularly in ENR compound. In this work, study on the filler blend dispersion, rheological and physical properties will be discussed. The filler dispersion and rheological properties of a polymer are very important in processing but are complicated by a number of factors such as flow rate, pressure and temperature [3-4].

## Materials and Methods

### Material

In this experiment, the ENR/silica compounds were prepared in Banbury 1600 (Tangential Rotor) internal mixer based on truck tyre tread formulation. The formulations and materials used in this study are given in Table 1 and Table 2**.** For dual fillers study, the carbon black filler pphr was varied from 5 pphr to 20 pphr while the total fillers used were fixed at 60pphr. The addition of Si69 coupling agent was mixed in the mixing at two different conditions which is first stage and finalizing stage of mixing in internal mixer. The effect of dual fillers (silica and carbon black) and addition of coupling agent on the rheological, dispersion and physical properties of ENR/silica compound were investigated.

Table 1. Formulations of filled ENR-25 compound with dual fillers

| **Ingredients** | **Truck Truck Tyre Tread (pphr)** | | | |
|---|---|---|---|---|
| | **Mix 1** | **Mix 2** | **Mix 3** | **Mix 4** |
| ENR-25 | 100 | 100 | 100 | 100 |
| Silica Zeosil 1165MP | 55 | 50 | 45 | 40 |
| C.Black | 5 | 10 | 15 | 20 |
| Process oil | 5 | 5 | 5 | 5 |
| Zinc oxide | 3 | 3 | 3 | 3 |
| Stearic acid | 3 | 3 | 3 | 3 |
| Calcium stearate | 2 | 2 | 2 | 2 |
| Antioxidants | 2 | 2 | 2 | 2 |
| Sulphur | 1.25 | 1.25 | 1.25 | 1.25 |
| Accelerators | 1.5 | 1.5 | 1.5 | 1.5 |

Table 2. Formulations of filled ENR-25 compound with Si69 coupling agent

| **Ingredients** | **Truck Tyre Tread (pphr)** | | |
|---|---|---|---|
| | **Control** | **Mix 1 (Final stage)** | **Mix 2 (First stage)** |
| ENR-25 | 100 | 100 | 100 |
| Silica Zeosil 1165MP | 55 | 55 | 55 |
| C.Black | 5 | 5 | 5 |
| Process oil | 5 | 5 | 5 |
| Zinc oxide | 3 | 3 | 3 |
| Stearic acid | 3 | 3 | 3 |
| Calcium stearate | 2 | 2 | 2 |
| Antioxidants | 2 | 2 | 2 |
| Silane Si69 | - | 1 | 1 |
| Sulphur | 1.25 | 1.25 | 1.25 |
| Accelerators | 1.5 | 1.5 | 1.5 |

**Mixing**

In this work, the mixing of the compound was carried out in three stages. The silica, carbon black and oil were pre-blended prior weighing into the different portions. The silica was kept in air- conditioned room in order to avoid moisture absorption. In the first stage mixing, 0.7 fill factor, 100 rpm of rotor speed, with starting temperature of 50$^{o}$Cwas employed. The dumping temperature was set at (150 to 160$^{o}$C) with a maximum mixing time 7 minutes. Later the master batches were sheet out on warm two-roll mill with minimal passes. In the second stage, the mixing was done in within 3 minutes with a rotor speed of 110 rpm at a temperature of 70$^{o}$C. Finally, the mixing was completed in 2 minutes when the curatives agents were added in the mixer with a temperature and rotor speed of 40$^{o}$C and 50 rpm.

**Mooney Viscosity Determination**

Mooney viscosity measurements were carried out using the MV2000 Viscometer (large rotor) at 100$^{O}$C. The sample weights were in the range of 25-30g. The testing was conducted based on ISO 289-1[5].

**Cure Characteristic**

The cure characteristics were performed on 5 grams of compound at 150$^{O}$C and 30 minutes with oscillation amplitude of 0.5$^{O}$ using a Monsanto MDR 2000P based on ISO 6502 standard.

**Filler Dispersion**

Filler dispersion study was conducted by using DisperGrader$^{TM}$ based on ISO 11345 on cured compounds. Sample preparation involved cutting of hardness test piece sample to generate a‘fresh face’ for analysis and observed using DisperGrader$^{TM}$ optical light microscope.

**Physical Properties**

The physical properties test was conducted according to Standard Methods as tabulated in Table 3.

Table 3. Standard method of physical properties test

| **Physical Properties Test** | **Standard Method** |
|---|---|
| Tensile Strength Hardness | MS ISO 37:1998 |
| IRHD MS | ISO 48:2002 |
| Abrasion Resistant Index | ISO 4649:2002 |

## Results and Discussion

### Mooney Viscosity

The Mooney viscosity of masterbatches and compounds of ENR/silica mixes with different loading level of carbon black (vary from 5 phr to 20 phr) and addition of Si69 coupling agent at two different conditions which is first stage and finalizing stage are shown in Table 4 and Table 5 respectively . For dual fillers mixes, it was found that compound containing 15 phr of carbon black gave the highest value of Mooney viscosity while, compound containing 5 phr of carbon black showed the least value as compared to the other compounds. As for ENR compounds with addition of coupling agent, there is no significant difference between adding coupling agent in first stage mixing and final stage mixing was found but however both viscosity values are slightly higher as compared to control. In general, a lower Mooney viscosity is an indirect indication of good process ability and flow properties due to lower elastic property of rubber mix.

Table 4. Mooney viscosity of master batch and compound of ENR mixes with dual fillers

| | **Internal Mixer BR1600** | | | |
|---|---|---|---|---|
| **Mooney Viscosity** | **Mix 1** (5 phr C.Black) | **Mix 2** (10 phr C.Black) | **Mix 3** (15 phr C.Black) | **Mix 4** (20 phr C.Black) |
| Masterbatch viscosity | 83.7 | 83.8 | 89.4 | 86.9 |
| Compound viscosity | 72.2 | 74.0 | 78.7 | 74.7 |

Table 5. Mooney viscosity of masterbatch and compound of ENR mixes with coupling agent

| | **Internal Mixer BR1600** | | |
|---|---|---|---|
| **Mooney Viscosity** | **Control** | **Mix 1 (Final stage)** | **Mix 2 (First stage)** |
| Masterbatch viscosity | 114.3 | 130.1 | 125.0 |
| Compound viscosity | 77.6 | 84.9 | 83.9 |

**Filler Dispersion**

Usually dispersion involves reduction of the size of filler aggregates to their ultimate size [6]. In general good dispersion and distribution of filler aggregates is important for the full reinforcing potential of fillers to be reached. In this study, the filler dispersion was determined by disperGrader™. Results of ENR compounds with dual fillers showed that dispersion increased with carbon black loading and gradually decreased after reaching 10 pphr (Mix 2) as shown in Table 6 and Figure 1. Indeed, smallest average aggregates size was observed with Mix 2 as compared to other mixes. Hence result indicates that the optimum dispersion can be obtained with 10pphr of carbon black loading. For ENR/silica compounds with coupling agent as shown in Table 7 and Figure 2, the results showed that there is no significant differences between Mix 1 and Mix 2 with both compounds dispersion are slightly higher than control mix. However, all the vulcanizates still did not achieved desirable filler dispersion up to 95 percent.

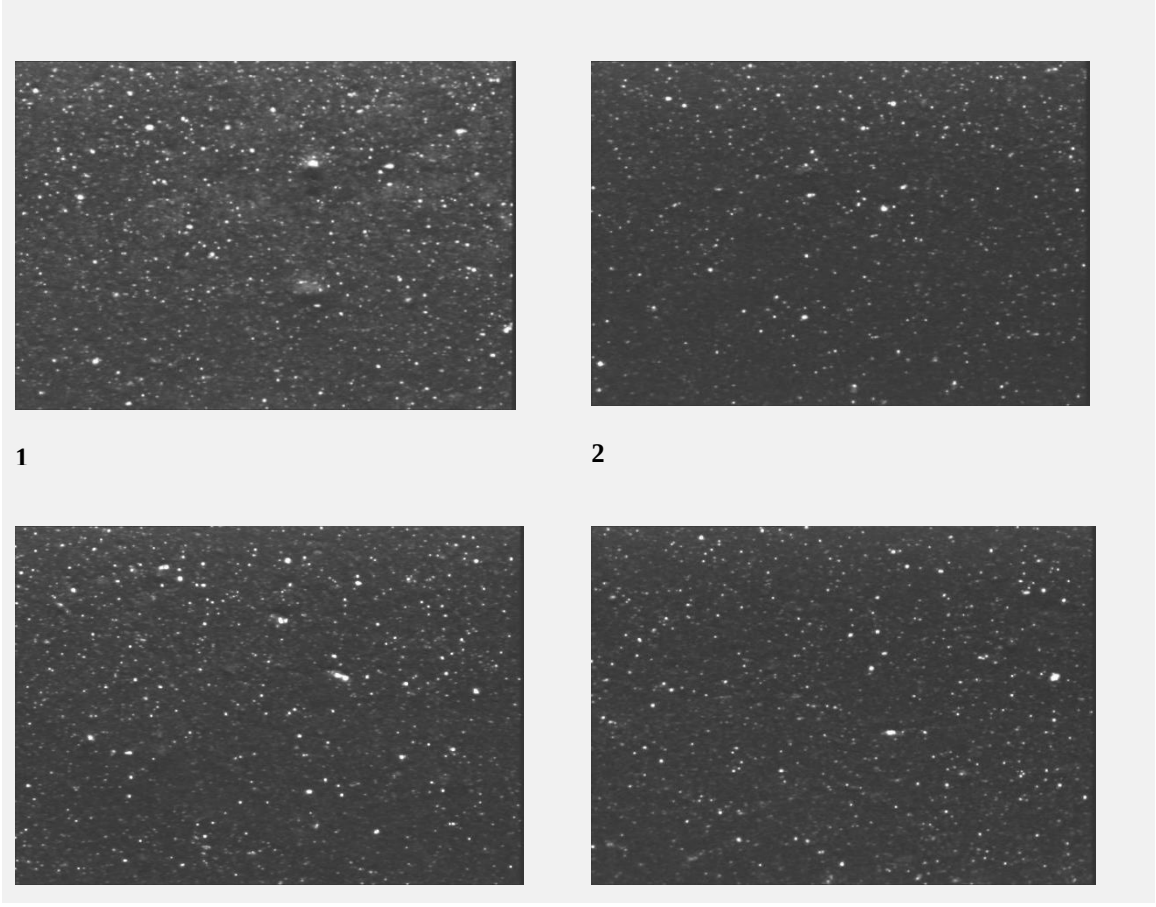



Figure 1. Filler dispersion image of filled ENR vulcanizates with dual fillers

Table 6. Filler dispersion properties of filled ENR compounds with dual fillers

| Parameter | Vulcanizates | | | |
|---|---|---|---|---|
| | 1 (5phr) | 2 (10phr) | 3 (15phr) | 4 (20phr) |
| Avg. Ag. Size, micron | 14.0 ± 0.3 | 13.0 ± 0.3 | 13.9 ± 0.2 | 13.7 ± 0.2 |
| Dispersion, % | 78.1 ± 1.4 | 85.0 ± 3.4 | 74.3 ± 3.0 | 70.6 ± 0.9 |

Table 7: Filler dispersion properties of ENR/Silica compounds with coupling agent

| Parameter | Vulcanizates | | |
|---|---|---|---|
| | Control | Mix 1 (Final stage) | Mix 2 (First stage) |
| Avg. Ag. Size, micron | 13.0 ± 0.3 | 13.5 ± 0.5 | 13.1 ± 0.4 |
| Dispersion, % | 83.3 ± 0.5 | 84.3 ± 1.7 | 85.8 ± 2.6 |

**Physical Properties**

The physical properties of filled ENR vulcanizates with dual fillers and ENR vulcanizates with coupling agent are shown Table 8 and Table 9 respectively. The results of ENR vulcanizates with dual fillers indicate that the properties are affected by the carbon black filler loading. In general, the tensile strength, hardness and abrasion resistance increased and improved with black loading [7]. Hence greater rubber filler interaction was possible responsible for this phenomenon as silica and carbon black posses different type of surface activity. The extremely high dispersive component in carbon black means that carbon black exhibit stronger interaction with non polar or low polar segment in ENR backbone. On the other hand, the very high specific surface energy for silica indicates there will be a strong interaction with polar segments of ENR [8]. Hence a mixed filler system is possible to enhance the rubber filler interaction and adhesion. As for ENR compounds with Si69 coupling agent, the results showed that tensile strength, hardness and abrasion resistance slightly improved with addition of coupling agent with Mix 1 which the mixing of Si69 was done in final stage of mixing gave the best physical properties as compared to control mix (without coupling agent). This silane coupling agent leads to a reduction of the silica-silica network during mixing and hence improved process ability and filler dispersion which could be the reason of this better physical properties result.

Table 8. Physical properties of filled ENR compounds with dual fillers

| Properties | Vulcanizates | | | |
|---|---|---|---|---|
| | 1 (5phr) | 2 (10phr) | 3 (15phr) | 4 (20phr) |
| Tensile Strength, MPa | 21.5 ± 2.0 | 22.8 ± 1.7 | 23.8 ± 2.1 | 25.8 ± 1.0 |
| Hardness (IRHD) | 62.0 ± 0.8 | 63.0± 0.9 | 66.0± 0.4 | 67.0 ± 0.4 |
| Abrasion Resistant Index , % | 86.7 | 91.8 | 91.7 | 90.8 |

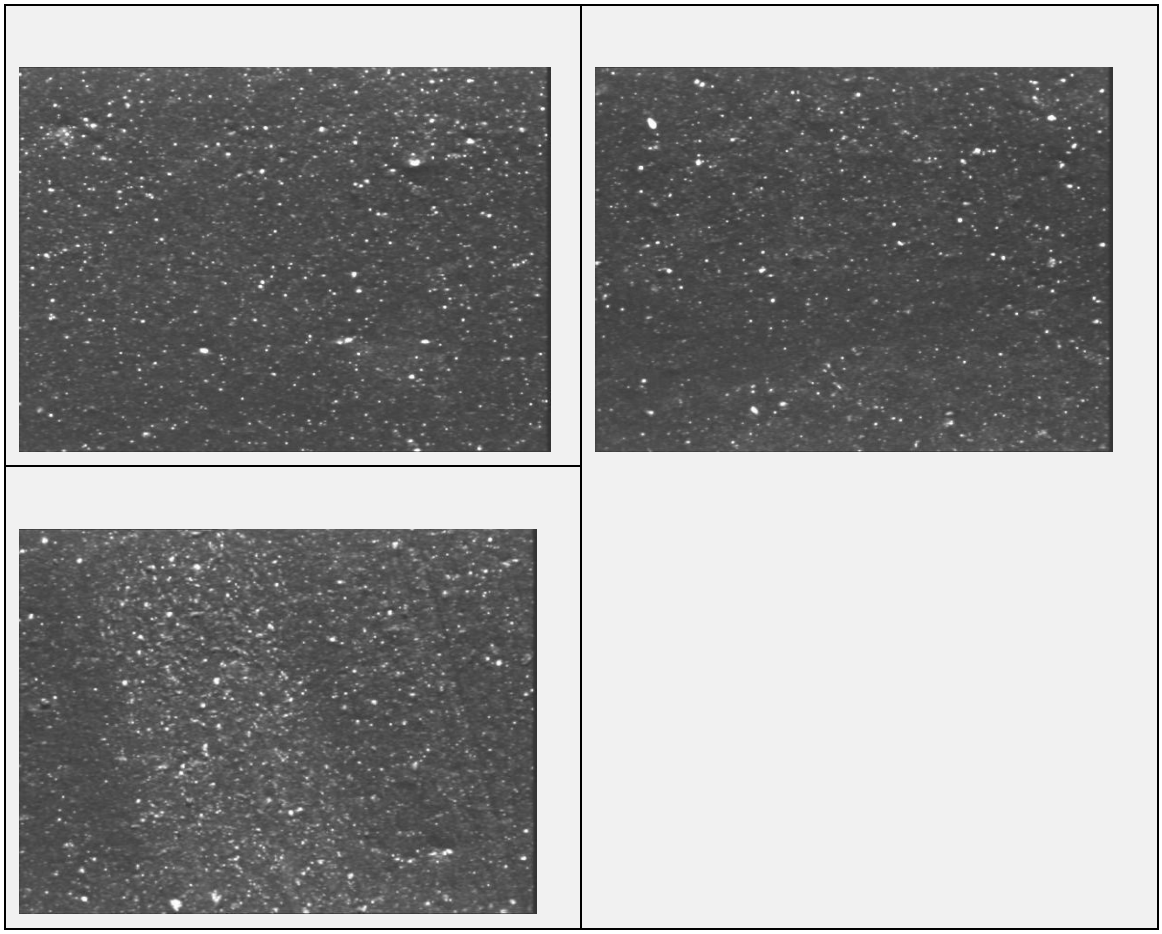


Figure 2. Filler dispersion image of ENR/silica vulcanizates with coupling agen

Table 9. Physical properties of filled ENR/silica compounds with coupling agent

| **Properties** | **Vulcanizates** | | |
|---|---|---|---|
| | **Control** | **Mix 1(Final stage)** | **Mix 2 (First stage)** |
| Tensile Strength, MPa | 20.3 ± 2.5 | 22.7 ± 1.7 | 18.5 ± 0.7 |
| Hardness (IRHD) | 62.0 ± 0.8 | 65.0 ± 0.7 | 68.0 ± 0.8 |
| DIN Abrasion Resistant Index , % | 79.3 | 104.6 | 104.9 |

## Conclusion

From the observations and results obtained in this study, it can be deduced that the tensile strength, hardness and Mooney viscosity of ENR compound with dual fillers improved with increasing carbon black filler loading. However the abrasion and filler dispersion properties, an optimum value was found at 10phr of carbon black loading. For ENR/silica compound with addition of Si69 coupling agent, the tensile strength, hardness and

Mooney viscosity was slightly improved and mixing coupling agent in the final stage gave the best physical properties as compared to control mix.

**Acknowledgement**

The author would like to thank the management of the Malaysian Rubber Board (MRB) for the permission to carry out this study. The assistance from Advanced Rubber Technology Unit officers and staff are gratefully acknowledged.

**References**

1. Gerster, M, Fagouri, C. and Peregi, E. (2010). Novel Coupling Agents For Silica-filled Rubbers with Superior Processing Safety and Improved Hysteresis of the Vulcanizates. *Tire Science and Technology* 38(1): 80-98.
2. Ou Y.-C., Yu Z.-Z., Vidal A., Donnet J.B., (1994). Effect of Alkylation of Silica Filler and Rubber Reinforcement. *Rubber Chem. Technol.* 67: 834 – 844.
3. Brydson, J. A. (1981). Flow Properties of Polymer Melts, 2nd Ed., London: George Godwin.
4. Wood, A. K., Read, A. G. G. and Lovegrove, J. G. A. (1989). Effect of Rheometer Design on the Measurement of the Flow Properties of Polymer Melts. *Rubber Process Appl* 12(1): 15-20.
5. ISO 289-1.(2005). Determinations Using a Shearing Disc Viscometer-Part 1: Determination of Mooney Viscosity, International Organisation for Standardisation.
6. Azemi Samsuri. (2009) An Introduction to Polymer Science and Technology, UPENA UiTM.:166-169.
7. Meng-Jiao W., Phing Z. and Khalid M. (2000). Carbon-Silica Dual Phase Filler, A New Generation Reinforcing Agent for Rubber Part IX, Application to Truck Tire Tread Compound. Rubber Division, ACS, Dallas, Texas; April 4 – 6.
8. Chanvoot K. and White J. L. (2000). Comparison of Intermeshing Rotor and Traditional Rotors of Internal Mixers in Dispersing Silica and Other Fillers. *Journal of Applied Polymer Science*.78: 1551–1554

The Malaysian Journal of ANALYTICAL SCIENCES ISSN 1394-2506

# PREPARATION AND CHARACTERIZATION OF TAPIOCA STARCH FILLED POLYCAPROLACTONE COMPOSITE FILMS

## (Penyediaan dan Pencirian Filem Komposit Polikaprolakton Terisi Kanji Ubi Kayu)

Nurulhusna Azmi*, Aznizam Abu Bakar, Sani Amril Samsudin, Nur Azmyra Abdul Aziz

*Enhance Polymer Research Group (EnPRO), Faculty of Chemical Engineering, Universiti Teknologi Malaysia, 81310 UTM Skudai, Johor, Malaysia*

**Corresponding author: husna.azmi89@gmail.com*

**Abstract**

This research was conducted to develop a new biodegradable polymeric packaging material to replace the current polymer packaging without changing the requirements properties. Polycaprolactone (PCL) was chosen as the matrix because of its biodegradability characteristics. Tapioca starch was used as filler from 10 to 40 wt% loading contents. The composite films were prepared using solvent casting technique and chloroform was used as solvent to dissolve the PCL pellets. The PCL matrix showed result of higher tensile strength which was 65.9 N/mm$^2$ with elongation at break at approximately 731%. The addition of starch in the PCL composite films increased the tensile modulus of the films. The tensile strength of the composite films decreased with increasing starch contents. Similar trends were also observed for elongation at break of the films.

**Keywords**: polycaprolactone (PCL), tapioca starch, casting films, biodegradable, polymer packaging

**Abstrak**

Kajian ini telah dijalankan bagi menghasilkan produk baru untuk menggantikan pembungkus plastik yang sedia ada dengan plastik mesra alam tanpa mengubah kriteria dan ciri-ciri yang diperlukan. Polikaprolakton (PCL) dipilih sebagai matrik kerana cirinya yang boleh terurai secara semulajadi. Kanji digunakan sebagai pengisi didalam komposit filem dari 10 hingga 40 wt%. Komposit ini telah disediakan dengan menggunakan teknik tuangan ke dalam acuan dan klorofom digunakan sebagai bahan pelarut untuk melarutkanpelet PCL. Matrik PCL menunjukkan kekuatan tegangan yang tinggi iaitu 65.9 N/mm$^2$ dengan pemanjangan pada ketika putus lebih kurang 731%. Penambahan kanji didalam PCL meningkatkan modulus tegangan komposit filem. Didapati kekuatan tegangan komposit filem semakin menurun dengan penambahan kanji. Corak yang sama juga dapat dilihat pada pemanjangan filem pada ketika putus.

**Keywords**: polycaprolactone (PCL), kanji ubi kayu, filem casting, biodegradasi, pembungkusan polimer

## Introduction

Conventional plastics have been used in packaging applications for many years. Most of these plastics are non-biodegradable and are almost always discarded after a short period of usage. The use of these materials would induce a serious environmental problem if not controlled. Increase in environmental concern worldwide has highlighted the necessity to reduce and restructure the use of plastics, not only because their degradability characteristic but their production also requires large amount of petroleum supply which is very limited and non-renewable resources. Such awareness has drawn much attention in the development of biodegradable or environmentally sustainable packaging materials [1].

A biodegradable polymer is defined as one that breaks down into smaller fragments due to the action of bacteria and other microorganisms, leading to changes in its physical properties [2]. PCL is known to be a commercially biodegradable polymer with a rather low melting point about 60 $^{o}$C. It is biodegradable, hydrophobic and partially crystalline types of polyester with good mechanical properties [3-6] suitable for packaging application. A strong water-resistance PCL films can be produced when molar mass of the polymer is higher than 40,000 g/mol [7].

However, due to the expensive price of PCL compared to others type of polymer, the use of PCL is limited in packaging applications. To reduce the cost of the matrix, PCL is often reinforced or blended with natural fiber or low cost polymer such as cellulose and starch. This will not only overcome the limitation of polymer in the industry but can also enhance the mechanical and physical properties of the composite itself [8].

Pure starch is white, odorless and tasteless powder that is insoluble in alcohol and water. It is a partially crystalline polymer composed of amylose and amylopectin [9,10]. In developing a product that have short period of usage, starch has been chosen as one of the potential material [11].Furthermore, starch can be easily obtained from renewable resources at low cost and offers several natural advantages. Therefore, starch is widely used to be blended with synthetic thermoplastics polymers in producing many types of products [4,11,12]. Besides that, starch is completely biodegradable in soil and water and as such is environmental friendly material.

Previously in preparing the PCL/starch composite films, the common methods used by the researchers are blown films and extrusion [3-5,7]. The used of solvent casting technique in preparing the composite films is very rare. The aim of this work is to study the effects of starch in the PCL composite films by using solvent casting technique.

## Materials and Methods

### Materials and Sample Preparation

Polycaprolactone (PCL) pellets were purchased from Sigma Aldrich SdnBhd with average $M_n$ 70,000 – 90,000. The solvent used in the experiment was chloroform purchased from Merck Sdn Bhd. Tapioca starch powder manufactured by Spion Product Sdn Bhd Malaysia. Chloroform was used as the solvent to prepare the PCL film by using solvent casting technique. Briefly, 10% (w/v) PCL solution were prepared. The PCL pellets were dissolved in the chloroform and continuously stirred until all of the PCL pellets dissolved completely. Then, the solution was cast onto the 20 cm square glass mold and it was then placed in the fume hood for slow rate of evaporation. The dried film was collected and dried for 48 hours. In preparing the PCL composite films, 10, 20, 30,40wt % of starch were added slowly into the dissolved PCL solution and continuously stirred for 1-2 hours before casting onto the mold. Composite films sample with approximately 1 mm in thickness were formed. The films prepared were then cut according to the standard dimension of specimen test and analyzed.

### Attenuated Total Reflection Fourier Transform Infrared Spectroscopy (ATR-FTIR)

To characterize the composite films, the specimens in the dimension of 2 cm x 2 cm films were scanned directly by using Perkin Elmer 2000 Infrared Spectrometer. The spectra were obtained by accumulating 16 scans in the range of 600-4000 $cm^{-1}$ with a resolution of 4 $cm^{-1}$.

### Tensile Test

Tensile properties of the films were investigated using tensile machine Llyod LRX materials testing machine ( Llyod Instruments Ltd, Fareham, UK) according to ASTM D882-10. The load and the constant crosshead speed were 2.5 kN and 10 mm/min respectively and the testing was carried out at room temperature. Five values of measurements were taken to evaluate the tensile strength, tensile modulus and elongation at break from the strain-stress curve.

## Results and Discussion

### FTIR Analysis

Figure 1 represents the spectra of PCL, starch and PCL composite films. All the characteristic peaks that are consistent with PCL structure were also present in the composite spectra. The broad peak at 3200 – 3600 $cm^{-1}$ in the starch spectrum corresponds to the strong OH bonding in the chain. However, the spectra for all the PCL composite films showed no such peak although the amount of starch added increased in every formulation. This is probably due to poor interaction between starch and PCL matrix.

From the analysis, it can be concluded that the starch and PCL had different polarity, hydrophilic (starch) and hydrophobic (PCL). The same results were also reported by other researchers where they found that PCL and starch seemed too incompatible with each other due to the limited interaction [13,14].

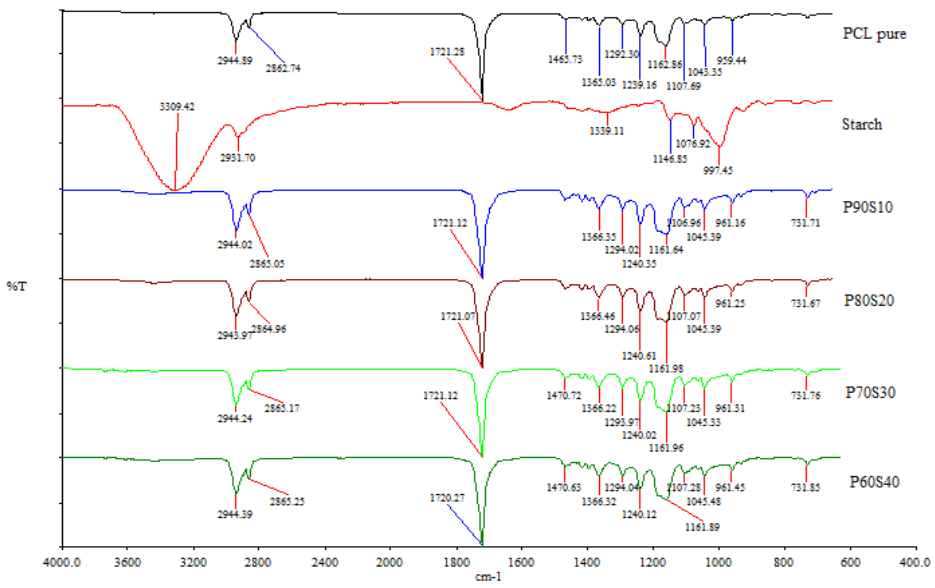



Figure 1. ATR-FTIR spectrum of PCL, starch and PCL composite films

**Tensile Properties**

Figures 2, 3 and 4 represent the tensile strength, elongation at break and the Young's Modulus of PCL and PCL composite films. From Figure 2, it can be seen that the tensile strength of pure PCL was initially high with the value of approximately 66 N/mm$^2$. However, this value dropped drastically to 27.5 N/mm$^2$ when starch was added and continue to decrease with increasing amount of starch. When the starch was added up to 40 wt%, the measured value dropped to 12.8 N/mm$^2$. Nonetheless, tensile strength value of the PCL/starch composite films up to 30 wt % of starch were quite high compared to tensile strength value of low density polyethylene (LDPE) which reported to be in the range of 9.7-17.2 N/mm$^2$ [15], suggesting that these films have great potential to replace LDPE as packaging material.

Similar research has been reported previously by using different methods. From the previous study [4], the tensile strength of the pure PCL prepared using blown films are reported to be 29 N/mm$^2$ but when the starch was added up to 40 wt%, the value obtained was 18.4 N/mm$^2$ which is higher than the value obtained in this research. There are several factors that cause the different in the measured value. As it was prepared using solvent-cast, the interaction of the starch filled in the composite films might be poor compared to blown films as the matrix and the starch was extruded together before blown.

The same trends seemed to appear in Figure 3. The elongation at break of pure PCL was quite higher before starch was added and dropped rapidly from 730% to 184% when 40 wt % of starch was added. When starch was added from 10 to 30 wt%, the values of the elongation at breaks was in the range of 498-419%. The different in the measured values was small.

From the tensile analysis, the well-known ductile polymer, PCL, was able to undergo large deformations. However the addition of starch in the composite films reduced the properties. From the FTIR analysis it was shown that there are poor interaction between the starch and PCL matrix. As such, the tensile strength and elongation at breaks of the films was decreased rapidly when the starch was added. Similar results were also reported [3-5] when natural biopolymer was blended together with polymer matrix. Besides that, good dispersion of starch in the composite films can also affect the results in the tensile analysis. According to Kim *et. al*. [5], they claim that, although starch and PCL are immiscible with each other, to obtain good mechanical properties, it is essential for starch domain to be well dispersed within the PCL composite films.

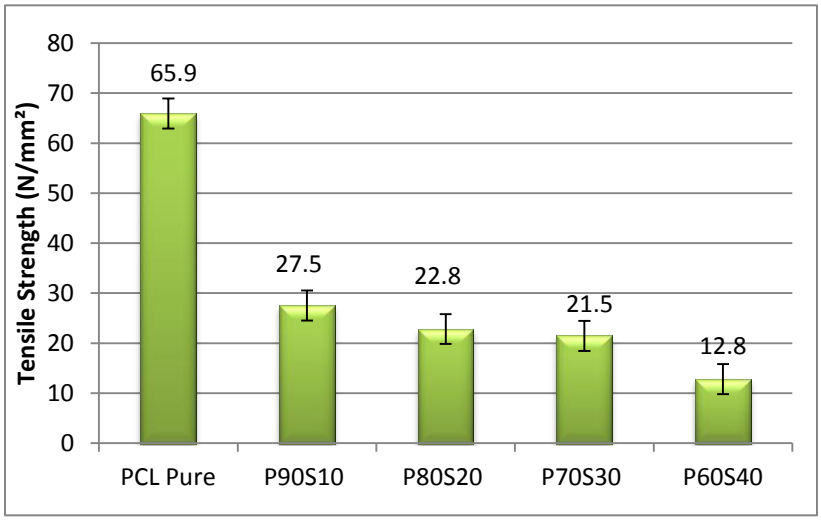



Figure 2. Tensile strength of PCL and PCL composite films

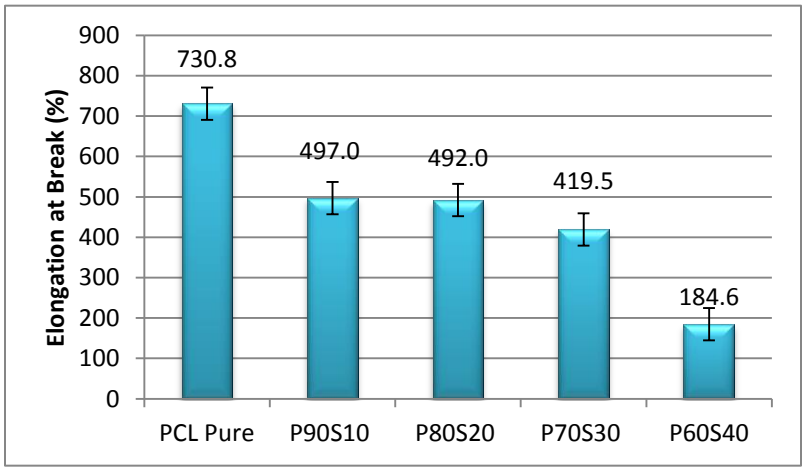



Figure 3. Elongation at break PCL and PCL composite films

The result in Figure 4 indicates that the Young's modulus of the pure PCL increased when the starch was added into the composite films. This is because starch has a high modulus compared to PCL [11]. Thus, the presence of starch in the mechanical blends can contribute to improve in modulus of the composite films. Increasing in the Young's modulus means increased in the stiffness of the composite films and affected the strength of the composite films. This is proven by previous researchers [3], when the starch added in the compositions all the mechanical properties of composite decreased.

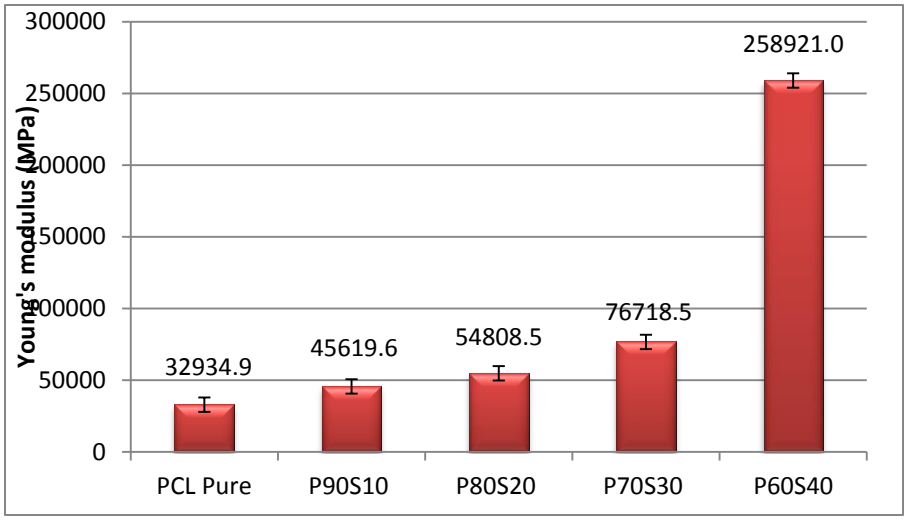



Figure 4. Young's Modulus of PCL and PCL composite films

## Conclusion

The addition of starch as a filler in the composite films show improvement in the stiffness of the films. Although the tensile strength of the films decreased with increasing of the starch contents, the value are still acceptable for packaging application as the good tensile strength for starch contents up to 30 wt% was higher than LDPE strength value. The representative evidence for the presence of starch and PCL in the composite films was confirmed by ATR-FTIR.

## Acknowledgement

The authors would like to express their appreciation to the Polymer Engineering Department, Universiti Teknologi Malaysia (UTM), Ministry of Education Malaysia (MOHE) and Research University Grant 4L028 for financial support.

## References

1. Albertsson, A. C. and Karlsson, S. (1995). Degradable Polymer for the Future.*Acta Polymer*.46:114 – 123.
2. Alire, R. R. (2009). Biodegradable Plastic Packaging Materials.*Free-Flow Packaging International, Inc.*
3. Avella, M., Errico, M. E., Laurienzo, P., Martuscelli, E., Raimo, M. and Rimedio, R. (2000). Preparation and Characterization of CompatibisedPolycaprolactone/Starch Composites.*Polymer Communication.*41:3857 – 3881.
4. Matzinos, P., Tserki, V., Kontoyiannis, A. and Panayiotou, C. (2002). Processing and Characterization of Starch/PolycaprolactoneProducts.*Polymer Degradation and Stability.*77:17 – 24.
5. Kim, E. G., Kim, B.S. and Kim, D.S. (2006). Physical properties and Morphology of Polycaprolactone/Starch/Pine-Leaf Composites.*Journal of Applied Polymer Science.*103:928 – 934.
6. Khatiwala, V. K., Shekhar, N., Aggarwal, S. and Mandal, U. K. (2008). Biodegradation of Poly (ε-caprolactone) (PCL) Film by AlcaligenesFaecalis. *Journal Polymer Environment.*16:61 – 67.
7. Myllymaki, O., Myllarinen, P., Forssell, P., Suortti, T., Lahteenkorva, K., Ahvenainen, R. and Poutanen, K. (1998). Mechanical and Permeability Porperties of Biodegradable Extruded Starch/Polycaprolactone Films. *Packaging Technology and Science*.11:265 – 274.
8. Franco, C. R. D., Cyras, V. P., Busalmen, J. P., Ruseckaite, R. A. and Vazquez, A. (2004). Degradation of Polycaprolactone/Starch Blends and Composites with Sisal Fibre.*Polymer Degradation and Stability*.86:95 – 103.

9. Glenn, G. M., Klamczynski, A. P., Shey, J., Chiou, B. S., Holtman, K. M., Wood, D. F., Ludvik, C., Hoffman, G. D., Orts, W. J. and Imam, S. (2007). Controlled Release of 2-Heptanone Using Starch Gel and Polycaprolactone Matrices and Polymeric Films. *Polymer Advanced Technologies*. 18:636 – 642.
10. Namazi, H and Mosadegh, M. (2011). Preparation and Properties of Starch/Nanosilicate Layer/PolycaprolactoneComposites.*Journal Polymer Environment*.19:980 – 987.
11. Yavuz, H. and Babac, C. (2003). Preparation and Biodegradation of Strach/Polycaprolactone Films.*Journal of Polymer and the Environment*. 11(3): 107 – 113.
12. Choi, E. J., Kim, C. H. and Park, J. K. (1999). Synthesis and Characterization of Strach-g-Polycaprolactone Polymer.*Macromolecules*.32:7402 – 7408.
13. Kweon, D. K., Kawasaki, N., Nakayama, A. and Aiba, S. (2004). Preparation and Characterization of Starch/PolycaprolactoneBlend.*Journal of Applied Polymer Science* 92:1716 – 1723.
14. Sugih, A. K., Drijfhout, J. P., Picchioni, F., Janssen, L. P. B. M. and Heeres, H. J. (2009). Synthesis and Properties of Reactive Interfacial Agents for Polycaprolactone – Starch Blends.*Journal of Applied Polymer Science*.114:2315 – 2326.
15. Koenig, M. F. and Huang, S. J. (1995). Biodegradable Blends and Composites of Polycaprolactone and Starch Derivatives.*Polymer*. 36(9):1877 – 1882.

The Malaysian Journal of ANALYTICAL SCIENCES ISSN 1394-2506

# CONSTRUCTION OF RADON CHAMBER FOR DETERMINATION OF RADON EMANATION USING CONTINUOUS RADON MONITOR

## (Pembinaan Kebuk Radon untuk Penentuan Emanasi Radon Menggunakan Alat Permonitoran Radon)

Norafatin Khalid*, Amran Ab Majid, Redzuwan Yahaya, Muhammad Samudi Yasir, Faizal Mohamed

*School of Applied Physics, Faculty of Science and Technology,*
*Universiti Kebangsaan Malaysia, 43600 Bangi, Selangor, Malaysia*

**Corresponding author: nora.fatin@ymail.com*

**Abstract**

An airtight chamber was designed and constructed in order to determine the emanation and the activity concentration of radon and to optimize measurement of radon emanation in terms of temperature, pressure and humidity. In this study, an airtight chamber in size of 0.50 m (width) x 0.40 m (depth) x 0.35 m (height) with total chamber volume of about 0.07 $m^3$ was built by using a perspex material with 6 x $10^{-3}$ m of thicknesses. A Continuous Radon Monitor (CRM) Sun Nuclear model 1029 was used to measure the emanation of radon in the chamber. This homemade chamber has a rectangular opening with two key systems to insert and remove samples and continuous radon monitor to prevent any of disturbances to the flow of air in the chamber.An efficiency and leakage tests were carried out before radon activity was measured. Xenotime mineral was inserted into the chamber as a source of radon ($^{222}$Rn). Radon measurements were done for each hour over 96 hours counting time. The results indicated that the background of radon concentration in an empty chamber was 21.0 ± 4.8 Bq $m^{-3}$. The usage of 0.15 kg, 0.25 kg and 0.50 kg of xenotime mineral recorded 249.6 ± 119.1 Bq $m^{-3}$, 400.0 ± 187.6 Bq $m^{-3}$, 2236.6 ± 213.8 Bq $m^{-3}$ of radon activities respectively.The effect of volume of the homemade radon chamber, the mass of xenotime, temperature, pressure and humidity to the radon emanation will be discussed in this paper.

**Keywords:** radon, radon monitor, radon chamber, xenotime

**Abstrak**

Kebuk kedap udara telah direka dan dibina bagi menentukan emanasi dan kepekatan aktiviti radon dan mengoptimumkan pengukuran emanasi radon dari sudut suhu, tekanan dan kelembapan. Dalam kajian ini, kebuk kedap udara bersaiz 0.5 m (lebar) x 0.4 m (panjang) x 0.35 m (tinggi) dengan jumlah isipadu kebuk 0.07 $m^3$ telah dibina menggunakan bahan perspek dengan ketebalan 6 x $10^{-3}$ m. Alat permonitoran radon secara berterusan (CRM) model Sun Nuklear 1029 digunakan untuk mengukur emanasi gas radon di dalam kebuk. Kebuk yang direka bina ini mempunyai pembukaan bersaiz segi empat tepat dengan dua system kekunci untuk memasukkan dan mengeluarkan sampel dan juga alat permonitoran radon bagi menghalang berlaku gangguan terhadap aliran udara di dalam kebuk tersebut. Ujian ketahanan dan kebocoran kebuk dilakukan sebelum pengukuran radon dijalankan. Mineral xenotim dimasukkan ke dalam kebuk sebagai sumber radon, ($^{222}$Rn). Pengukuran radon telah dilakukan bagi setiap jam untuk selama 96 jam masa pembilangan. Hasil kajian menunjukkan kepekatan radon latar belakang dalam kebuk kosong adalah 21.0 ± 4.8 Bq $m^{-3}$. Penggunaan sumber radon xenotim dengan jisim 0.15 kg, 0.25 kg, 0.5 kg masing-masing mencatatkan bacaan kepekatan radon iaitu 249.6 ± 119.1 Bq $m^{-3}$, 400.0 ± 187.6 Bq $m^{-3}$, 2236.6 ± 213.8 Bq $m^{-3}$. Perubahan kadar emanasi radon terhadap isipadu kebuk radon, jisim xenotim, suhu, tekanan dan kelembapan menggunakan kebuk buatan sendiri ini dibincangkan dalam kertas ini.

**Kata kunci:** radon, permonitoran radon, kebuk radon, xenotim

## Introduction

It has been known for longer years that radon, a radioactive gas, is present naturally. Radon is an inert radioactive gas hence it does not react chemically with other elements. Since radon is an inert gas, when it is inhaled, the gas is mostly exhaled then the radon will decay to other radioactive decay products, such as polonium-212, bismuth and

lead. These are solid fine radioactive particles that can be inhaled and subsequently reside in the lung. In recent years, the measurement of radon in air continues become an interest subject because radon can potentially contribute for lung cancer caused by the combination effects of radon gas, air pollution and smoking [1]. Radon has been classified as carcinogenic to humans [2] and studies of the activity concentration of radon and its progenies are performed worldwide either at work places (e.g. mines) or at home.

The environmental radon concentration is a function of time and climate conditions. To monitor radon, both active and passive techniques have been developed. Active methods are usually used for short-term measurements of radon while passive methods are more suitable for the assessment long term radon exposure. The active method usually used an advanced radon monitor to determine the emanation of radon. For passive method, practically used for examples activated charcoal to collect the radon gas and the concentration need to process to get the actual radon contration. The parameters involve during the radon measurement are temperature, humidity, pressure and aerosol distribution.

Most radon emanation measurements are based on the accumulation technique. The sample material is placed in a closed container; some days after sealing, e.g. about 4 days by Moore et al. [3], 2 weeks for Moore et al. [4], and 1 month for Greeman et al. [5], a sample of a gas is drawn into an evacuated scintillation cell to measures radon activity. Radon chamber technique also have been developed to produce consistent radon levels under specific ambient conditions and to test the performance of radon monitoring equipment. Radon chambers are designed in various sizes ranging from small chamber at 0.01 $m^{-3}$ to very large chamber.

In this study, a homemade chamber made from Perspex material has been constructed and tested to determine the emanation rate of samples using radon monitoring system. The accumulated radon concentration in the closed airtight homemade chamber containing the sample is continuously monitored without any disturbance induced by outdoor gas.

## Materials and Methods

### Radon chamber design

The chamber was made from a clear perspex material of thickness 6 x $10^{-3}$ m. The total volume of the chamber was 0.07 $m^3$ with 0.5 m (length) x 0.4 m (width) x 0.35 m (height) of size. Silicone glue was used to join the pieces of perspex to ensure the chamber is airtight. The door was built with metal handle to pull the door out. To keep the door of chamber to be airtight, the plasticine was applied at the edge of the door and two metallic gasket keys acts as a lock keys to close the door to be tight. The setup of radon chamber is as shown in Figure 1.

### Measurement of the radon emanation and activity concentration

Radon measurements were performed using two diffused junction photodiode continuous radon monitor (Sun Nuclear: Model 1029). The measurement accuracy is + 25 % pr 1 pCi/l and the sensitivity of radon monitor is 5 cph/pCi/l. This instrument has recognised by Environmental Protection Energy (EPA) and calibrated yearly by the manufacturer. The measurement range of the detection is between 1 $Bq/m^3$ – 100 $kBq/m^3$. The radon concentration in the chamber is monitored at one hour interval for 96 hours. The continuous radon monitor can only detect the radon gas not the radon progenies gaseous hence the radon progenies are negligible. The sensitivity of radon monitor is dependent on the material and volume of homemade chamber, the position of continuous radon monitor in the radon chamber.

Experiments were performed to measure the emanation of radon gas in the homemade chamber as a function of time. To do this, a background counting is done by opening the chamber's door and allowing the chamber air to reach equilibrium with the ambient room air naturally [3]. The chamber's door then was closed with radon monitor inside; begin to allow the radon monitor to collect the data. Next, this step was used to count the Xenotime sample until one hour intervals for 96 hours measurements.

The leakage tests for homemade chamber were carried out before radon concentration was measured. The test was done by using the tap water added with blue dye. After that the blue dye of water was filled in the homemade chamber. Tissue was used to cover the outer walls of radon chamber to observe whether the condition of tissue.

After the test was done, the finding showed that all the tissue was not wet and still in a good condition. Even though water had larger molecule of particle compared with gaseous but it can be notified that there was no leakage showed when this practiced made.

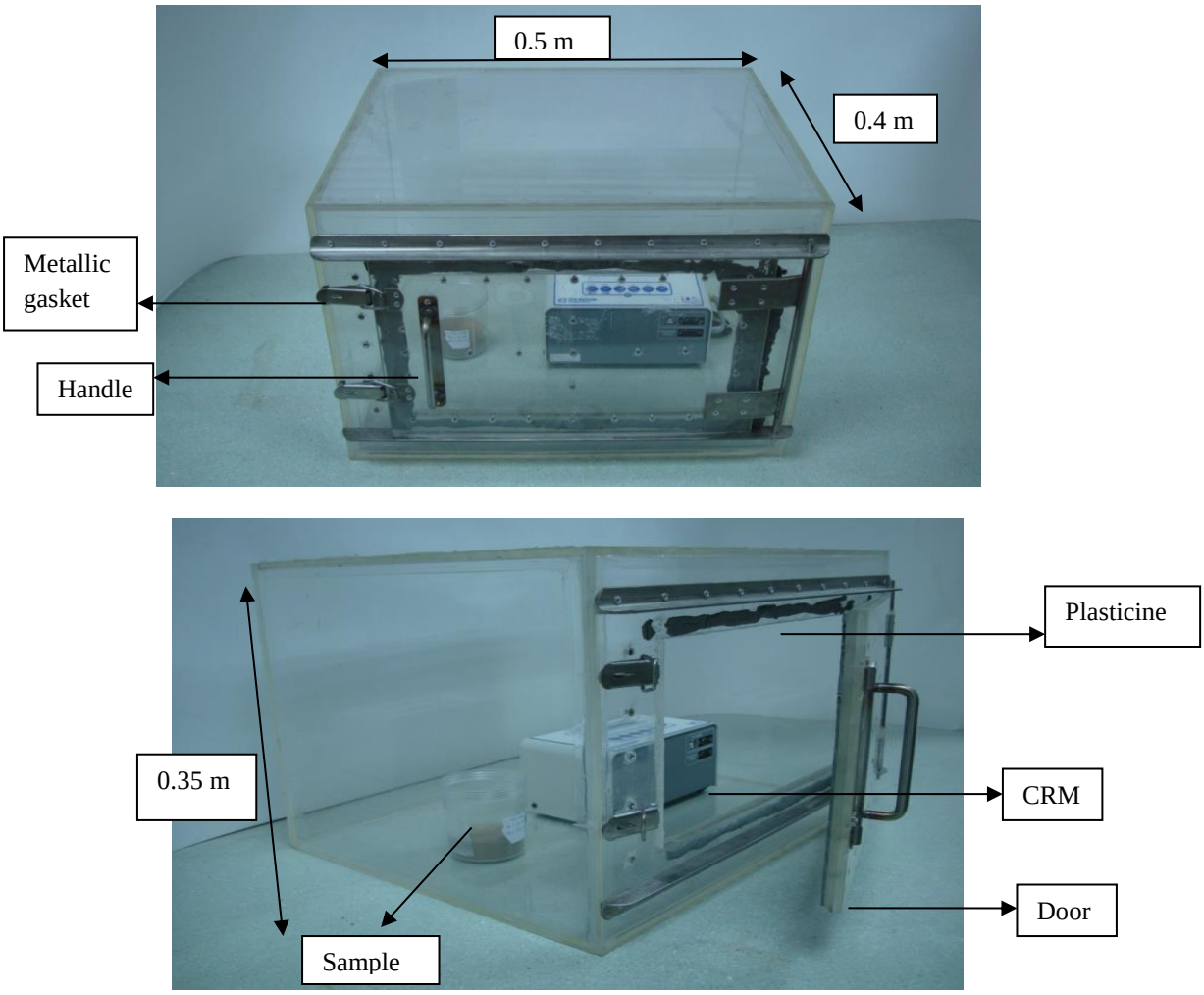



Figure 1. The radon chamber with radon monitor and samples

**Measurement of the radon emanation and activity concentration**

Radon measurements were performed using two diffused junction photodiode continuous radon monitor (Sun Nuclear: Model 1029) as shown in Figure 2. The measurement accuracy is + 25 % pr 1 pCi/l and the sensitivity of radon monitor is 5 cph/pCi/l. This instrument has recognised by Environmental Protection Energy (EPA) and calibrated yearly by the manufacturer. The measurement range of the detection is between 1 $Bq/m^3$ – 100 $kBq/m^3$. The radon concentration in the chamber is monitored at one hour interval for 96 hours. The continuous radon monitor can only detect the radon gas not the radon progenies gaseous hence the radon progenies are negligible. The sensitivity of radon monitor is dependent on the material and volume of homemade chamber, the position of continuous radon monitor in the radon chamber.

Experiments were performed to measure the emanation of radon gas in the homemade chamber as a function of time. To do this, a background counting is done by opening the chamber's door and allowing the chamber air to reach equilibrium with the ambient room air naturally [3]. The chamber's door then was closed with radon monitor inside; begin to allow the radon monitor to collect the data. Next, this step was used to count the Xenotime sample until one hour intervals for 96 hours measurements.

The leakage tests for homemade chamber were carried out before radon concentration was measured. The test was done by using the tap water added with blue dye. After that the blue dye of water was filled in the homemade chamber. Tissue was used to cover the outer walls of radon chamber to observe whether the condition of tissue. After the test was done, the finding showed that all the tissue was not wet and still in a good condition. Even though water had larger molecule of particle compared with gaseous but it can be notified that there was no leakage showed when this practiced made.

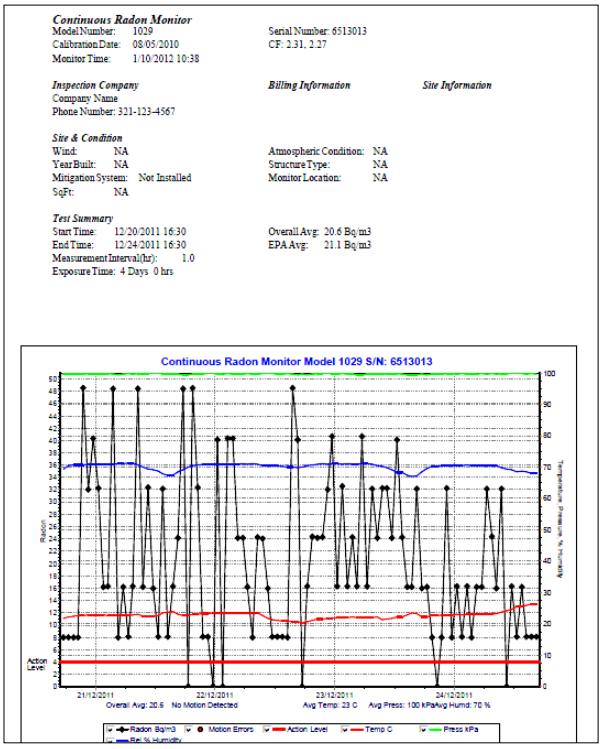



Figure 2. The report of radon concentration using radon monitor Sun Nuclear 1029

**Study sample**

Xenotime mineral has greater production of radon gas compared to the other minerals such as Ilmenite, Monazite, Struverite and Zircon. This is because the activity of radium-226 ($^{226}$Ra) in Xenotime mineral is higher than others and it is known that $^{226}$Ra is the parent of radon gas. That is why Xenotime mineral is chose to become the source of radon in this study. Xenotime mineral is collected from an amang processing plant located in Factory of Hup Lee Sdn. Bhd., Kampar, Perak, Malaysia with GPS coordinate 4$^{o}$ 39"N 100$^{o}$ 98" E .

**Treatment of samples**

The samples were oven dried at temperature of 105$^{o}$C for 24 hours until constant mass, then xenotime was sieved through > 500 µm mesh sieve and their bulk densities determined. All the samples had nearly the same densities (i.e. 1.0593 g cm$^{-3}$).

Each sample were weighed according to the selected portion of 150 g, 250 g and 500 g and put into counting container. Each prepared samples were labelled according to the code used in Table 1 below.

Table 1. Classification of samples and its code

| Code | Mass (g) |
|---|---|
| XE 1 | 150 |
| XE 2 | 250 |
| XE 3 | 500 |

**Concentration of radon**

Radon concentration for each samples studied, were measured using a radon monitor that was left for 96 hours at the homemade chamber. The reading of radon concentration (Bq $m^{-3}$) was obtained, recorded and classified according to study sample. The values were calculated by subtracting the average reading of first three readings since they were considered unstable and to permits the test environment to stabilize. The average reading at each sample were classified into a set of 24 hours, which the average concentration of radon readings taken accordingly in the range of 1-24 hours, 25-48 hours, 49-72 hours and 73-96 hours with a standard deviation calculated for each interval of 24 hours. The average radon concentration was determined using the following equation suggested by EPA [6]:

$$\text{Average Reading} = \frac{\text{Total reading 96 hours} - \text{3 first reading}}{\text{93 hours}} \quad (\text{Bq m}^{-3}\,\text{h}^{-1}) \qquad \text{(Eq. 1)}$$

## Results and Discussion

**Data analysis for background chamber**

Analysis for background counting was done by measuring the empty chamber using radon monitor for 96 hours. The results of radon concentration showed by the radon monitor system were deducted with the background radon concentration collected in empty radon chamber.

Table 2 showed the result of radon concentration for background counting in blank chamber. The average of radon concentration recorded for each interval for 1 to 24 hours showed 23.4 Bq $m^{-3}$, 24 to 48 hours showed 21.8 Bq $m^{-3}$, 48-72 hours showed 24.9 Bq $m^{-3}$ and 72-96 hours showed 14.1 Bq $m^{-3}$. The total radon concentration recorded was 21.0 ± 4.8 Bq $m^{-3}$ meanwhile EPA average showed 21.1 Bq $m^{-3}$. The total radon concentration were called as measured radon emanation while for EPA average was radon emanation that calculated automatically based on the system configuration of radon monitor and it appeared with the result of radon concentration. The EPA average was the average of total reading radon concentration without deducting the three first reading of radon concentration. The EPA was a guideline data for radon concentration's action level. The result of background counting was due to air that contained in the chamber.

**Data comparisons between Xenotime sample**

In this research, Xenotime sample were used to observe the radon emanation patterns in the radon chamber. The comparisons were made between the background counting and the different masses i.e 150 g, 250 g and 500 g of Xenotime as a manipulated variable. The results showed that increasing the sample, the higher concentration of radon will get. Table 3 indicated the radon concentration for each hour until 96 hours for XE 1 (150 g), XE 2 (250 g) and XE 3 (500 g).

Table 2. Background radon concentration

| Hour | Blank (Bq $m^{-3}$) | | | |
|---|---|---|---|---|
| | **1-24** | **24-48** | **48-72** | **72-96** |
| 1 | 8.0 | 48.4 | 0.0 | 16.0 |
| 2 | 8.0 | 0.0 | 16.3 | 16.1 |
| 3 | 8.0 | 48.5 | 24.4 | 8.0 |
| 4 | 8.0 | 32.4 | 24.1 | 0.0 |
| 5 | 48.5 | 8.1 | 24.3 | 8.0 |
| 6 | 32.0 | 8.1 | 32.0 | 32.3 |
| 7 | 40.3 | 0.0 | 40.7 | 8.0 |
| 8 | 32.3 | 40.2 | 16.3 | 16.3 |
| 9 | 16.1 | 0.0 | 32.5 | 8.1 |
| 10 | 16.3 | 40.3 | 16.3 | 16.3 |
| 11 | 48.4 | 40.3 | 24.3 | 8.0 |
| 12 | 8.0 | 24.1 | 16.3 | 16.0 |
| 13 | 16.1 | 24.1 | 40.7 | 16.1 |
| 14 | 8.1 | 16.1 | 16.3 | 32.1 |
| 15 | 16.3 | 8.0 | 32.1 | 24.4 |
| 16 | 48.4 | 24.3 | 24.1 | 16.0 |
| 17 | 16.1 | 24.0 | 32.3 | 32.1 |
| 18 | 32.4 | 16.0 | 32.3 | 0.0 |
| 19 | 16.0 | 8.1 | 24.1 | 16.3 |
| 20 | 8.1 | 8.1 | 40.2 | 8.1 |
| 21 | 32.1 | 8.1 | 24.3 | 16.1 |
| 22 | 8.1 | 8.0 | 16.1 | 8.1 |
| 23 | 16.3 | 48.5 | 16.1 | 8.1 |
| 24 | 24.1 | 40.2 | 32.1 | 8.1 |
| Total | 492.0 | 523.9 | 598.2 | 338.6 |
| Average | 23.4 | 21.8 | 24.9 | 14.1 |
| Radon concentration | 21.0 ± 4.8 | | | |

EPA average 21.1 Bq $m^{-3}$

Table 3 showed that the measured radon concentration for XE 1, XE 2 and XE 3 are 249.6 ± 119.1 Bq $m^{-3}$, 402.0 ± 187.6 Bq $m^{-3}$ and 2236.6 ± 213.8 Bq $m^{-3}$ respectively. EPA average are 252.1 Bq $m^{-3}$, 403.6 Bq $m^{-3}$ and 2239.0 Bq $m^{-3}$ respectively. The results determined the highest radon concentration was XE 3 while the lowest was XE 1. Furthermore, the radon activity also indicated that XE 3 showed the highest contribution on radon activity but XE 2 showed the lowest radon activity. The reasons why Xenotime sample were used in this research due to the high natural radioactivity of radium contained that produced radon as its decay product. Xenotime is one of tin tailing that contained high radioactivity. Other tin tailing are Monozite and Ilmenite were high natural radioactivity of thorium which not produced radon but thoron. In this case, the measured radon concentration from Xenotime

samples were assumed to be the maximum radon gas collected in this chamber. The chamber was airtight, sealed and not affected by the outdoor air. It was only from the sample that emanated the radon gas.

Table 3. Radon concentration for Xenotime sample at 150 g, 250 g and 500 g

| Sample | Radon concentration ($Bq\ m^{-3}$) | EPA Average ($Bq\ m^{-3}$) |
|---|---|---|
| **XE 1** | 249.6 ± 119.1 | 252.1 |
| **XE 2** | 402.0 ± 187.6 | 403.6 |
| **XE 3** | 2236.6 ± 213.8 | 2239.0 |

**Parameters studied**

There were three parameters to be studied in this research. The temperature, humidity and pressure were the parameters that give effects to radon concentration in the radon chamber. When the temperature cold, the radon gas will became inactive and due to their physical property which is radon is a heavy gas, it will assemble together closely [7]. Humidity gives effects on radon concentration by the presence of moist air. Pressure plays an important role to the production of radon concentration. When the pressure is high, the pressure may depress the radon flux from the Xenotime samples and the radon concentration may be decreased [8]. The EPA did not mention the standard range for temperature, humidity and pressure in radon studies to use it as a comparison reference value.

Table 4 showed the average true reading of radon concentration, temperature, humidity and pressure. The true reading was calculated based on measured radon concentration by the radon monitor. The value of temperature, humidity and pressure were measured automatically by the radon monitor 1029. This monitor was able to detect the parameters due to special specifications built in the monitor. With these parameters, the patterns of radon emanation can be observed and studied.

Table 4. The average true reading of radon concentration and all the parameters

| Samples | Radon concentration ($Bq\ m^{-3}$) | Temperature ($^oC$) | Humidity (%) | Pressure (Pa) |
|---|---|---|---|---|
| Empty chamber | 21.0 ± 4.8 | 23.0 | 69.0 | 996.5 |
| XE 1 | 249.6 ± 119.1 | 27.0 | 57.0 | 997.5 |
| XE 2 | 400.0 ± 187.6 | 29.0 | 59.0 | 998.0 |
| XE 3 | 2236.6 ± 213.8 | 22.5 | 60.0 | 998.5 |

Figure 3, 4 and 5 showed the graph of temperature, pressure and humidity against radon concentration for empty chamber, XE 1, XE 2 and XE 3. From the results, the temperature for empty chamber and for each xenotime sample showed in the range from 20 $^oC$ to 34 $^oC$. For pressure, the results showed in the range from 993 Pa to 1002 Pa and for humidity the results showed in the range from 54 % to 71 %. In this studied, all those parameters should be constant because the measurement was done in enclosed chamber without any disturbance from the outside surrounding. From this result, it showed that there is a variation occurred on temperature, pressure and humidity for each measurement but the deviation is still in a range.

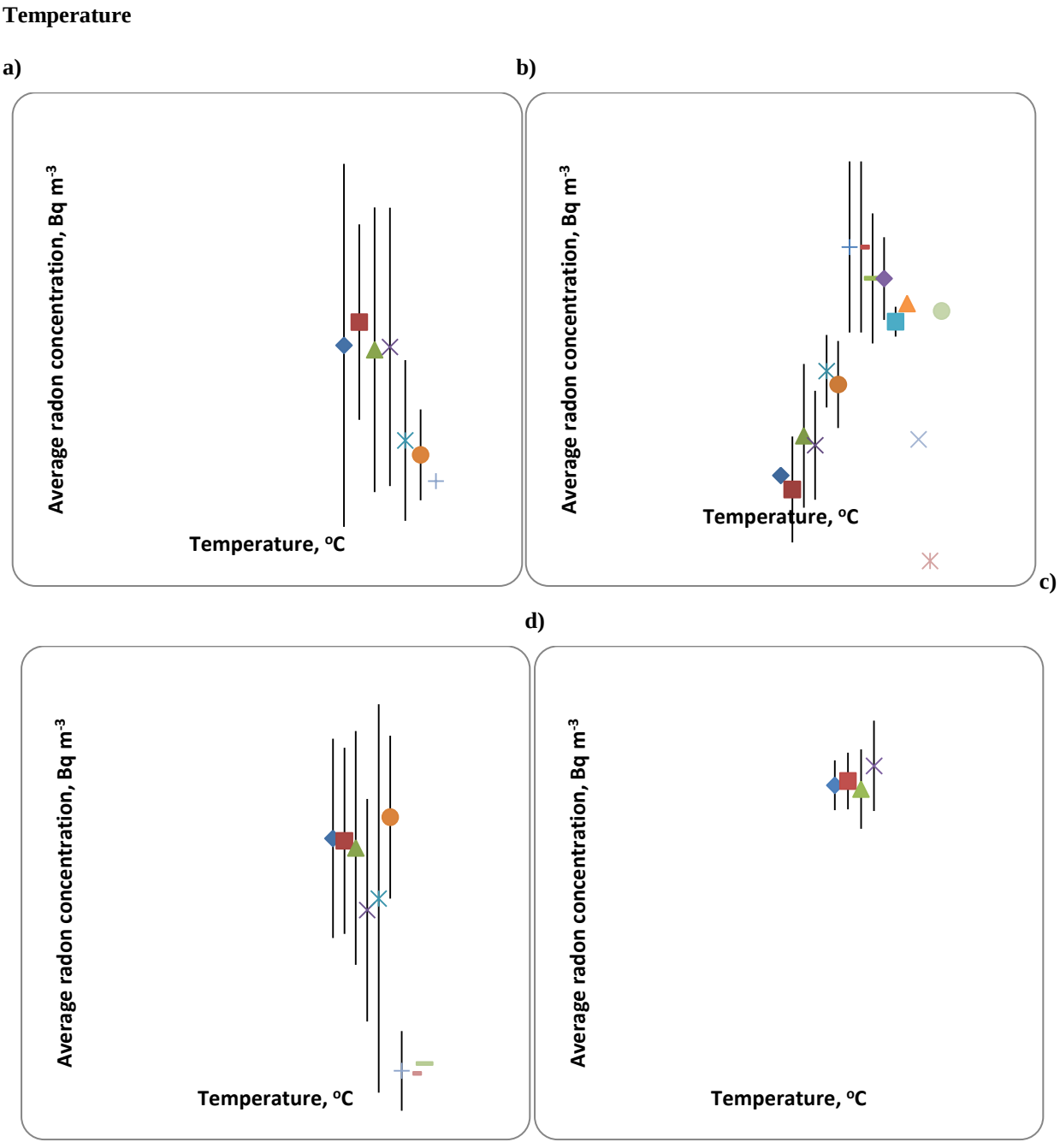



Figure 3. Variation of temperature against radon concentration for a) empty chamber b) XE1 c) XE2 d) XE3

**Pressure**

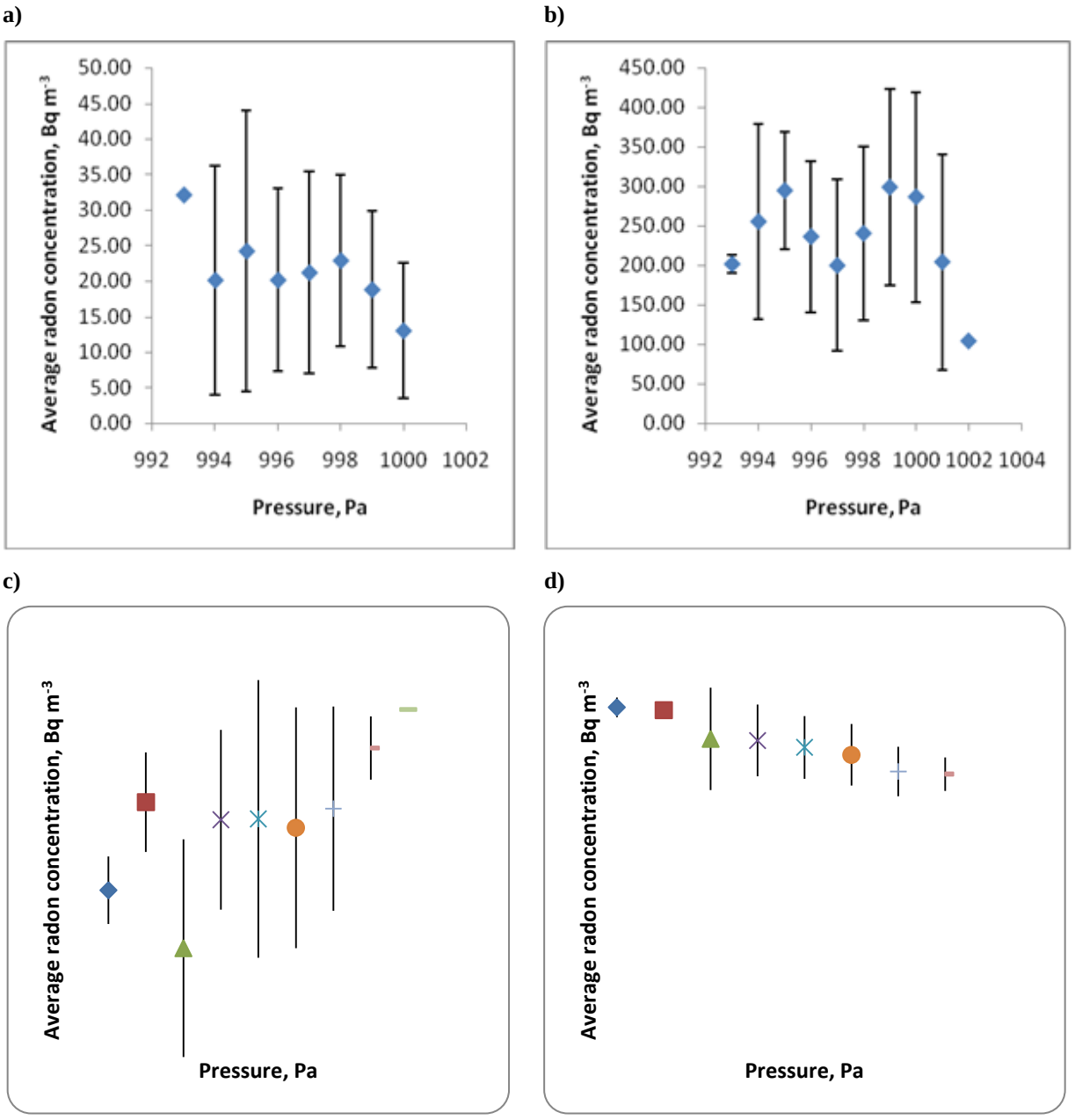



Figure 4. Variation of pressure against radon concentration for a) empty chamber b) XE1 c) XE2 d) XE3

**Humidity**

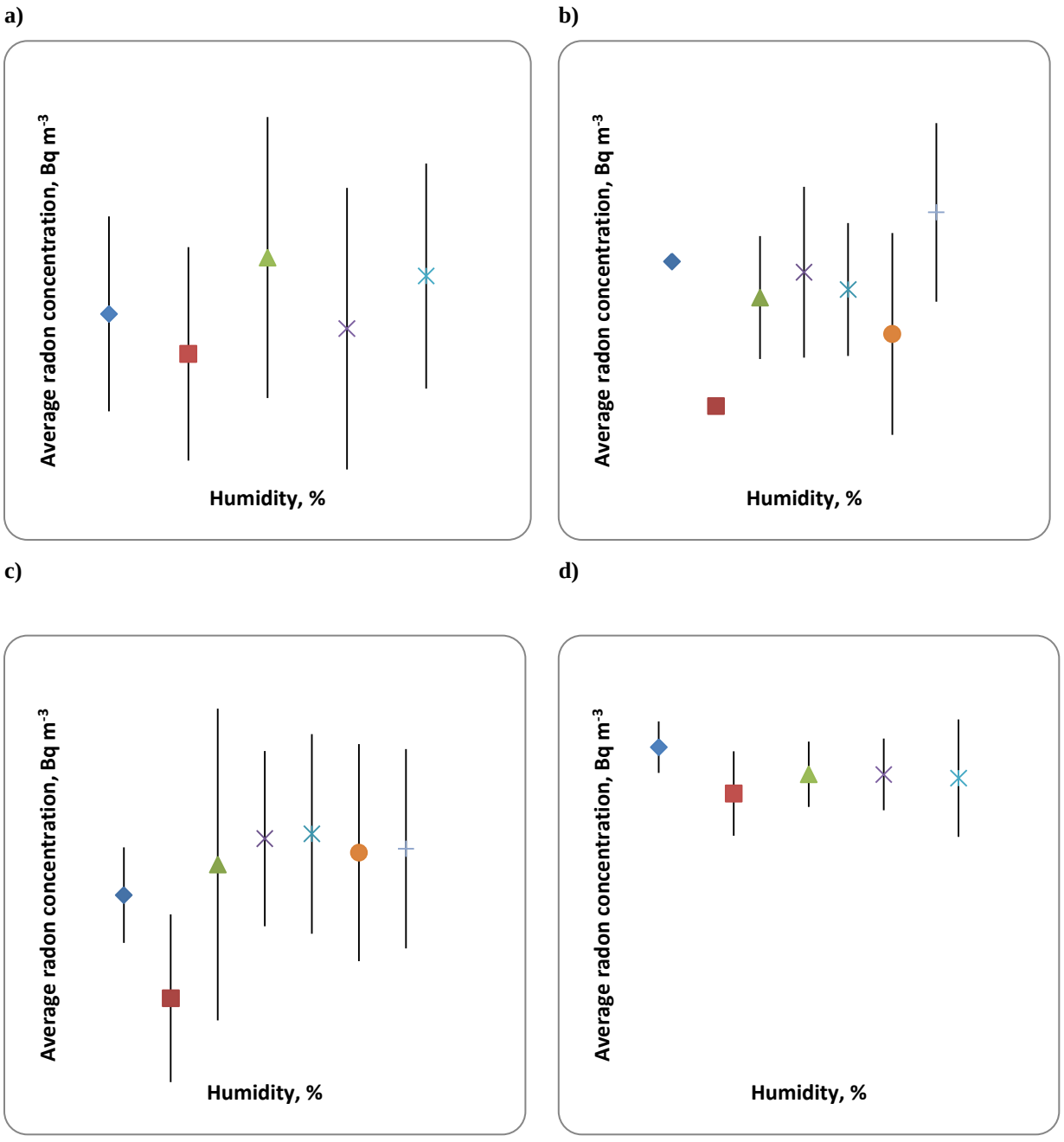



Figure 5. Variation of humidity against radon concentration for a) empty chamber b) XE1 c) XE2 d) XE3

## Conclusion

This chamber designed is unique because of its size, Perspex material, and airtight design. This paper describes an experimental method for determining radon concentration in homemade radon chamber using Xenotime sample as studied sample. The method proposed here is based on 96 hours accumulation technique. The radon concentration is measures using radon monitor Sun Nuclear Model 1029 directly in the chamber. This configuration allows the radon concentration increase to be monitored hourly without any disturbance induced by outdoor air. The effects of parameters on the radon concentration measurement are taken into account. Results showed that this homemade chamber can be used to determine the radon concentration, EPA average and radon activity using radon monitor.

## Acknowledgement

The authors would like to thank to Universiti Kebangsaan Malaysia for the project grant with reference number UKM-AP-PLW-04-2009/1 and UKM-GUP-2011-152 and to Nuclear Science Programme of UKM for their technical support throughout the research.

## References

1. NRC. 1999. *Health Effects of Exposure to Radon.* National Research Council, Biological Effects of Ionizing Radiation (BEIR) VI Report.
2. IARC. 2001. *IARC Monographs on the Evaluation of Carcinogenic Risks to Humans* 78, Part 2: Some Internally Deposited Radionuclides.
3. Moore, J.A. and Kearfott, K.J. 2005. A Simple Radon Chamber for Educational Use. *The Radiation Safety Journal* 89 (5):78-84
4. Moore, R. and Moore W.S. 1984. Mechanism of transport of U-Th series radioisotopes from solids into ground water. *Geochim.Cosmochim.*Acta 48: 395-399.
5. Greeman, D. J. and Rose, A.W. 1996. Factoscontrolling the emenation of radon and thoron in soils of the eastern U.S.A Chem. Geol. 129: 1-14.
6. EPA. Environmental Protection Agency. 2003. EPA Assessment of Risks from Radon in Homes. PA 402-R03-003. U.S.
7. Al-Ahmady, K. and Hintenlang, D.1994. Assessment of Temperature-Driven Pressure Differences with regard to Radon Entry and Indoor Radon Concentration. AARST International Radon Symposium
8. Nazaroff, W.W. and Sextro, R.G. 1989. Technique for Measuring the Indoor Rn 222 Source Potential of Soil. *Environmental Science and Technology* 23 (4): 451-458.

The Malaysian Journal of ANALYTICAL SCIENCES ISSN 1394-2506

# THE EFFECTIVENESS OF POLYDIMETHYLSILOXANE (PDMS) AND HEXAMETHYLDISILOXANE (HMDSO) AS COMPATIBILIZER ON THE PREPARATION OF BETEL NUT FIBER (BNF) AND POLYPROPYLENE (PP) /POLYSTYRENE (PS) WOOD COMPOSITES

## (Keberkesanan Polidimetilsiloksana (PDMS) dan Heksametildisiloksana (HMDSO) Sebagai Pengserasi Dalam Penyediaan Komposit Kayu Berasaskan Serabut Pinang dan Polipropilena (PP)/Polistirena (PS))

Nurul Izzaty Khalid, Azizah Baharum*,Siti Sarah Ramli, Siti Norhana Mohd Nor

*School of Chemical Science and Food Technology, Faculty of Science and Technology, Universiti Kebangsaan Malaysia, 43600 Bangi, Selangor, Malaysia.*

**Corresponding author: azeiss@ukm.edu.my*

**Abstract**

This research was carried out to investigate the effectiveness of polydimethylsiloxane (PDMS) and hexamethyldisiloxane (HMDSO) as compatibilizing agent in producing wood composites of betel nut fiber/polypropylene (BNF/PP) and betel nut fiber/polystyrene (BNF/PS). Wood composite was prepared by blending 40% of matrix polymer and 60% of treated and untreated BNF using internal mixer Brabender Plasticoder at 170˚C with 50 rpm rotor speed for 13 minutes. The treatment was done prior to blending the materials by immersing the BNF in PDMS and HMDSO solutions with 1%, 3% and 5% of concentrations for 24 hours. The effects of 1% HMDSO treatment on BNF/PP composite contributed to high flexure strength and impact strength which are 19.2 MPa and 7.9 kJ/M$^2$ respectively while the percentage of water absorption showed the minimum value of 6.7%. The impact strength of BNF/PS composite treated with 3% HMDSO showed maximum value that is 4.7 kJ/M$^2$ and minimum percentage of water absorption, 6.8%. However, the flexure strength of untreated BNF/PS composite is higher than treated BNF/PS composite with value of 4.7 MPa. The morphology of treated BNF/PP composites from SEM micrographs showed better interface interaction between fibers and matrices. FTIR spectra showed the presence of siloxane groups such as Si-O, Si-$CH_3$, Si-($CH_3$) and Si($CH_3$) as a result of HMDSO and PDMS treatment. Based on the characterization analysis, HMDSO treated composite of BNF/PP showed more effective interfacial interaction between BNF and matrices.

**Keywords:** polydimethylsiloxane, hexamethyldisiloxane, polypropylene, polystyrene, betel nut fiber, wood composite

**Abstrak**

Penyelidikan ini dijalankan untuk mengkaji keberkesanan polidimetilsiloksana (PDMS) dan heksadimetilsiloksana (HMDSO) sebagai agen pengserasi dalam penghasilan komposit kayu berasaskan serabut pinang/polipropilena (SP/PP) dan serabut pinang/polistirena (SP/PS). Komposit kayu disediakan dengan pengadunan 40% polimer matrik dan 60% SP terawat dan tak terawat menggunakan mesin pengadun dalaman *Brabender Plasticoder* pada suhu 170˚C dengan kadar pengadunan 50 rpm selama 13 minit. Rawatan ke atas SP dijalankan sebelum proses pengadunan dengan merendamkan SP selama 24 jam ke dalam larutan PDMS dan HMDSO yang mempunyai peratus kepekatan berbeza iaitu 1%, 3% dan 5 %. Kesan daripada rawatan 1% HMDSO ke atas komposit SP/PP telah menyumbang kepada peningkatan kekuatan lenturan dan hentaman dengan nilai masing-masingnya ialah 19.2 MPa dan 7.9 kJ/M$^2$, sementara peratus serapan air terhadap komposit ini menunjukkan nilai minimum iaitu sebanyak 6.7%. Kekuatan hentaman bagi komposit SP/PS yang dirawat dengan 3% HMDSO menunjukkan nilai maksimum sebanyak 4.7 kJ/M$^2$ dan peratus serapan air yang minimum iaitu 6.8%. Walaubagaimanapun, kekuatan lenturan bagi komposit SP/PS yang tak terawat lebih tinggi daripada komposit SP/PS yang terawat dengan bacaan kekuatan sebanyak 4.7 MPa. Morfologi komposit SP/PP yang terawat dapat dilihat daripada mikrograf mikroskop imbasan elektron yang mana ia menunjukkan interaksi antara muka yang lebih baik antara serabut dan matrik. Spektrum FTIR menunjukkan kehadiran kumpulan siloksana seperti Si-O, Si-$CH_3$, Si-($CH_3$) and Si($CH_3$) iaitu hasil daripada rawatan HMDSO dan PDMS. Berdasarkan

kepada analisis pencirian, komposit SP/PP yang dirawat dengan HMDSO menunjukkan interaksi antaramuka yang lebih berkesan antara SP dan matriks.

**Kata kunci:** polidimetilsiloksana, heksametildisiloksana, polipropilena, polistirena, serabut pinang, komposit kayu

## Introduction

Synthetic wood or wood composite is composite material produced from a mixture of plastic polymer and wood flour or wood fiber [1]. It is designed widely due to certain factors such as environmentally friendly and do not contribute to the waste of natural resources as most wood composite can be reprocessed [2]. The physical and mechanical properties of wood composites have been found to possess toughness and stiffness, the strength of stretching, resistance to impact and high resistance to weather where the properties are significantly important to determine the product's compatibility to be used in any applications [3-5]. The main components used in the production of wood composite are natural fiber and matrix polymer. Natural fiber is dispersed phase and can be categorized into three types, derived from animals, plants and minerals. Most of the natural fibers used in the production of wood composite are from the plant such as blast sugarcane, kenaf and rice husk depends on the suitability of a particular product to be produced.

In composite processing, increasing fiber composition potentially increases the mechanical properties of wood composites [6-7]. Natural fiber replaces fiberglass used in many applications because it showed a significant increase of the strength and flexibility as well as reduce weight composite products. Natural fiber used for this research is betel nut fiber (*Areca*) which is mostly derived from renewable and biodegradable resources [8]. It can be classified as short fiber as the average fiber length is in the range of 4 cm [9]. It contains certain components comprising lignin (13 - 24.6%), hemicellulose (35 - 64.8%), ash content (4.4%) and water (8-25%) [10]. It contained a large amount of very fine capillary found in the outer layer of fiber surface known as trichomes. Trichomes are able to improve the adhesion of the interface between fiber and matrix polymer [11]. Thermoplastic polymers used in this study are polypropylene (PP) and Polystyrene (PS), which is classified in group of polyolefins. PP consist of propene monomer ($C_3H_6$) covalently bound to each other. PP is a semi-crystalline polymer that will melt when heated and when frozen it will turn into a glassy state. PS ($C_8H_8$), is an aromatic polymer made from the aromatic monomer of styrene. The melting point of PP is at a temperature of 160-175°C, which allows it to be processed at a temperature lower than 200°C, a temperature that is used in the processing of wood composite [12]. Polystyrene is an amorphous polymer in nature, brittle and rigid materials with its melting point is at ~240°C. It is a thermoplastic material that is normally existed in a solid state at room temperature, melt when heated at temperatures above 100°C and will return solid when cooled. Najafi et al [13] states that any plastic or recycled plastic that can be melted and processed at temperatures below the degradation temperature of wood filler can be used for production of wood composite.

Problems often arise when comes to the processing of wood composites using natural fibers and thermoplastic matrix due to the different nature of fiber and matrix. Different nature of these two main components leads to incompatibility at the fiber-matrix interphase and producing non-homogenous dispersion of fiber within the matrix. Hydrophobic nature of the matrix has potential to protect the natural fiber from moisture. Therefore the fiber should be evenly distributed throughout the matrix or coated with the polymer matrix completely to prevent moisture absorption of composites produced [14]. Generally, additives or compatibilizing agent will increase compatibility between hydrophilic wood and hydrophobic plastic and allows the formation of a single phase to occur [15]. Thus, the siloxane group of polydimethylsiloxane (PDMS) and hexadimethylsiloxane (HMDSO) is used to modify the surface of the fiber. PDMS is used as compatibilizer between natural fibers and thermoplastic matrix to improve the physical and mechanical properties of wood composites and promote adhesion between two incompatible materials [16]. According to Hocker [17], the treatment was conducted using HMDSO can make a material having a smooth surface and a very high hydrophobicity effect of water contact angle.

The aim of this study was to investigate the effectiveness of polydimethylsiloxane (PDMS) and hexamethyldisiloxane (HMDSO) as compatibilizing agent in producing wood composites of betel nut fiber/polypropylene (BNF/PP) and betel nut fiber/polystyrene (BNF/PS).

## Materials and Methods

### Materials

The betel nut short fiber (BNF) used in this study was obtained from Faculty of Engineering and Built Environment, Universiti Kebangsaan Malaysia (UKM). The matrices selected for this study were polypropylene (PP) and polystyrene (PS) which was supplied by BDH Chemicals Ltd, Poole, England. The compatibilizing agent used was polydimethylsiloxane (PDMS) with a density of 0.965 g/cm$^3$ which was supplied by Acros Organics and hexamethyldisiloxane (HMDSO) which was obtained from Sigma Aldrich, Steinheim, Germany. The isopropyl alcohol used as solvent was supplied from Systerm, Shah Alam.

### Preparation of Fiber

The BNF was prepared by separating the skin and its fruit. The layer of its skin was peeled to get the fiber and cut into specific size within 0.5 – 1.0 cm. Then the fiber was dried under sunlight to remove moisture before being used.

### PDMS and HMDSO Treatment

The treatment was carried out by immersing the dried fiber in PDMS and HMDSO solution with different concentrations which were 1%, 3% and 5%, for about 24 hours at room temperature. The treated fiber were then left in fume hood to let the solvent evaporate, rinsed several times with distilled water and finally dried in an oven at 104$^o$C for 3 hours before being used.

### Preparation of Wood Composite (BNF/PP and BNF/PS)

The untreated and treated BNF were blended with PP or PS using an internal mixer Brabender Plasticoder Model PL 2000 with capacity of 60 cm$^3$and composition ratio of fiber to matrix of 60:40. The blending was carried out at 170$^o$C for about 13 minutes and mixing rate of 50 rpm. Then, the composites were compressed in mould with hotpress machine to produce specimen with 3 mm thickness for further testing and analysis.

### Fourier Transform Infra Red (FTIR) Analysis

The FTIR spectral analysis was done using Perkin Elmer Model BX machine at room temperature to determine the functional group present in untreated and treated wood composite. The specimens with weight around 0.5 – 1 gram were finely ground and mixed with potassium bromide (KBr) then pressed to form pellet for analysis.

### Scanning Electron Microscope (SEM)

Scanning electron microscope (SEM) model LEO 1450VP were used to examine the morphology of untreated and treated composites. Fractured specimen resulted from impact test were coated with gold in a hood Sputter model SC 500 to be analyzed. The scanning electron micrographs were then studied to define the fiber-matrix interphase before and after treatment.

### Impact Test

Unnotched Izod impact test were tested using a Digital Pendulum Machine model RR/MT (Ray Ran) with a 2.706 J pendulum. Eight specimens were cut into 65 mm x 12 mm x 3 mm according to ASTM D 4812 and the best five results were calculated to get an average impact value.

### Flexural Test

Flexural tests were performed using universal testing machine (Instron model 5567) according to ASTM D 790. Three point bending method with load cell 10 kN and speed of 1.3 mm/min were done on five duplicated samples, with dimensions of 120 mm x 12 mm x 3 mm, to determine average flexural value.

### Water Absorption Test

This test was conducted according to ASTM D 570 to determine the total water absorption by two duplicated samples for each composite in 24 hours. The specimens were oven dried at 104 ˚C for 2 hours prior to testing and then were put into desiccators to avoid moisture during cooling process. The weight of dry sample was taken before and after immersing the samples in 200 mL of water for 24 hours. Total of water uptake were determined using the following equation (1):

$$M_t(\%) = \frac{W_t - W_o}{W_o} X100 \quad (1)$$

where,
$M_t$ = Total water uptake at time t
$W_t$ = Weight of sample at time t
$W_o$ = Weight before immersion

## Results and Discussion

### Flexural Test

Flexural modulus is determined to know the stiffness of composite towards flexure. To analyze the data, each data represented treated composites compared to the untreated composites. Figure 1 shows better flexural modulus for BNF/PP composites treated with HMDSO where 1% HMDSO is the optimum concentration which gives a rise to 24.2% increment. Meanwhile the flexural modulus decreased around 9.9% and 30.3% for BNF/PP treated with 3% and 5% HMDSO respectively. This result reveals that only a small portion of compatibilizer needed to trigger an effective interphase reaction and improved the homogeneity of fiber and matrix. The concept can be applied to the use of PDMS compatibilizer where 1% PDMS led to an increase of 16.7% in flexural modulus. Even though PDMS contained the same functional group as HMDSO and acted as compatibilizer, the flexural modulus for BNF/PP treated with 3% and 5% PDMS is reduced due to agglomeration and entanglement of longer PDMS chain in treated fiber.

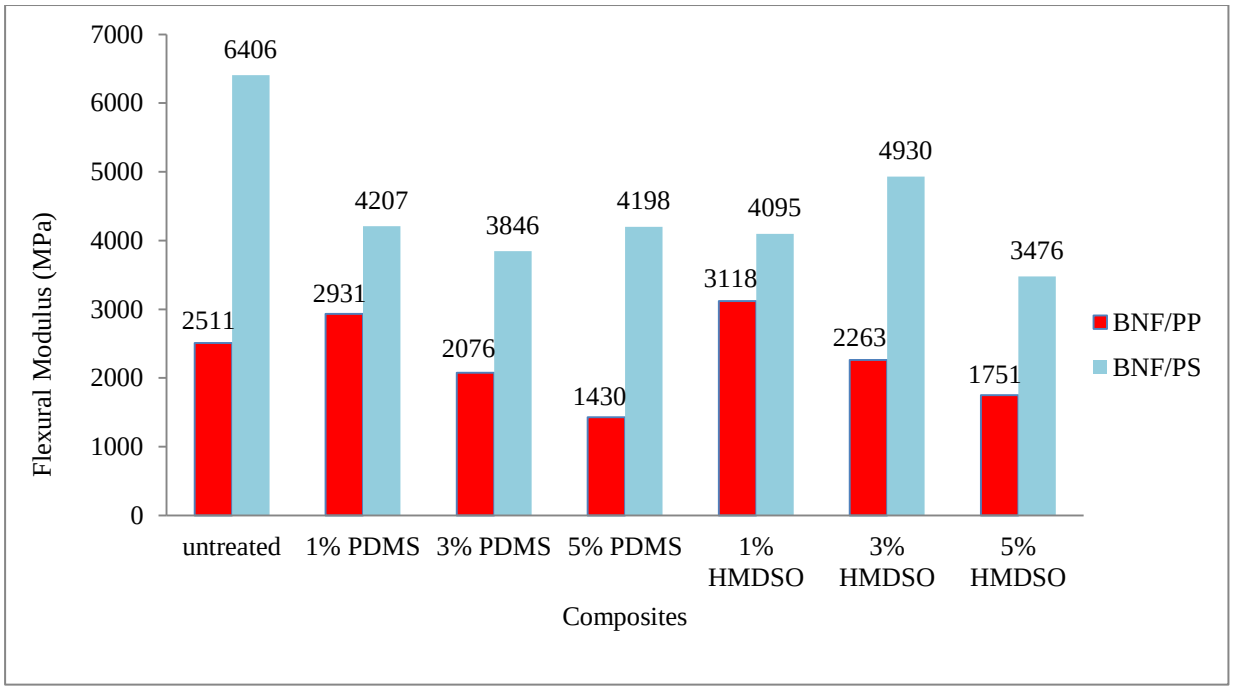



Figure 1. The effect of PDMS and HMDSO treatments with a series of concentration on the flexural modulus of BNF/PP and BNF/PS wood composites

Flexural strength of BNF/PP containing PDMS as compatibilizing agent for all concentrations is lower than untreated composites as shown in Figure 2. However, the flexural strength of BNF/PP treated with HMDSO at all testing concentrations depicts better reading than the untreated composites. The BNF/PP composites treated with 1% HMDSO increased the flexural strength by 18.5%. Based on the trend of flexural modulus and flexural strength of BNF/PP composites, it can be concluded that the modulus is proportional to flexural strength for both types of treatment. The trend shows decrement as the percentage of compatibilizer concentration increased.

As can be seen in Figure 1, the flexural modulus of untreated BNF/PS is much higher than untreated BNF/PP. However, the BNF/PS treated with PDMS and HMDSO both has reduced the flexural modulus around 35.6%. The trend also goes similarly with flexural strength of BNF/PS treated with PDMS and HMDSO with decrement around 41.7%. Untreated BNF has many small furry spaces which known as trichomes that stand out of fiber surface. The increment in the flexural result of untreated BNF/PS might be due to effective interaction between trichomes and PS matrices. After treatment, thin layer of PDMS and HMDSO that formed on surface of BNF in BNF/PS composite might reduce the interaction between trichomes and the PS matrices (Figure 9 (e) and (f)).

In particular, this research found that flexural strength of BNF/PP composites treated with HMDSO is higher than composites treated with PDMS while both HMDSO and PDMS treatments did not improved flexural properties of BNF/PS composites.

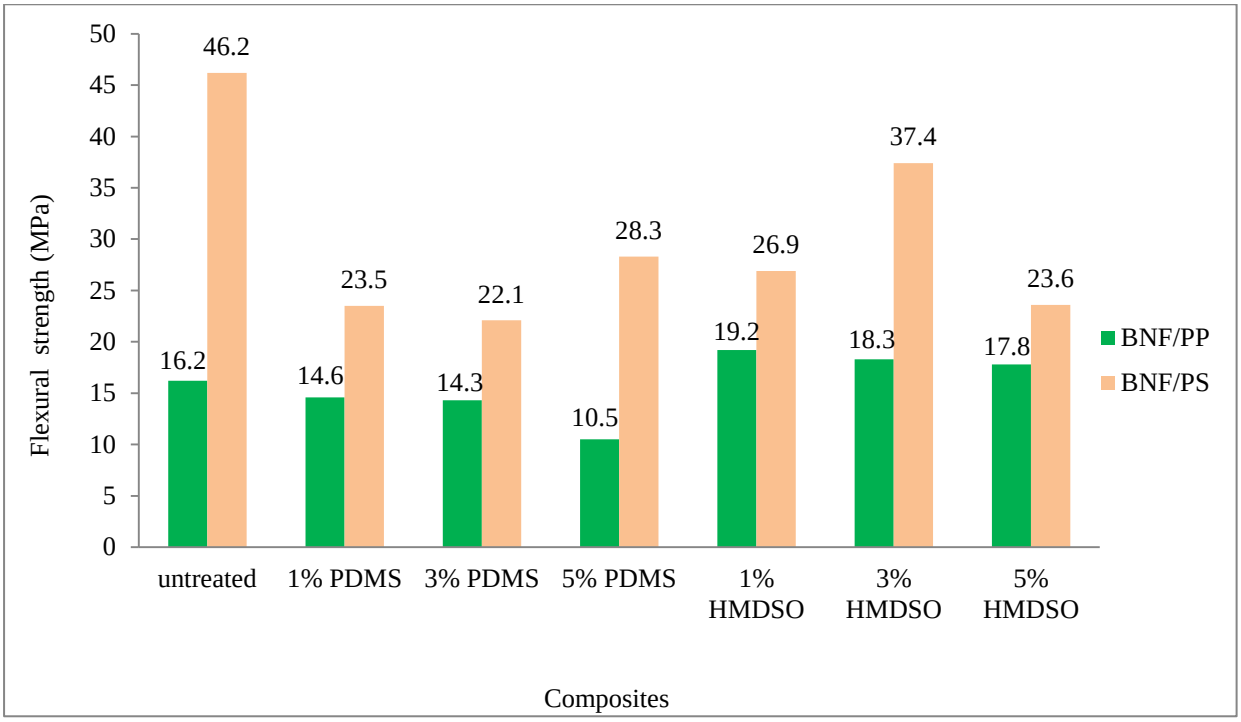



Figure 2. The effect of PDMS and HMDSO treatments with a series of concentration on the flexural strength of BNF/PP and BNF/PS wood composites

**Impact Test**

Figure 3 shows impact strength of composites. The impact strength of BNF/PP shows increment after treatment with PDMS but the impact strength decreased with the increase of concentration of HMDSO. BNF/PP with 1% HMDSO treatment has the highest impact strength with an increase at 70.3% compared to other treated composites. The higher the impact strength leads to higher rigidity of composite. Thus it requires high kinetic energy during

impact to initiate crack propagation until it breaks. The increase of impact strength for BNF/PP treated with increasing concentration of PDMS is due to the addition of long chain of PDMS which absorbed impact strength effectively. Weak interfacial interaction leads to the formation of micro spaces between fiber and matrix. When an impact is applied on samples, micro fracture will occur and lead to crack dispersion. As a result, the impact strength needed to fracture the sample is lower.

PS matrix in crystalline form exhibits low impact energy. As shown in Figure 3, BNF/PS treated with 3% of HMDSO increased the impact strength by 38.2%, more than other treated and untreated BNF/PS. This improvement could be related to flexible Si-O-Si chains from the compatibilizer. HMDSO and PDMS treatment on fiber improved the compatibility between fiber and matrix because it allows a better load transfer from matrix to fiber during impact due to strong bond of fiber-matrix.

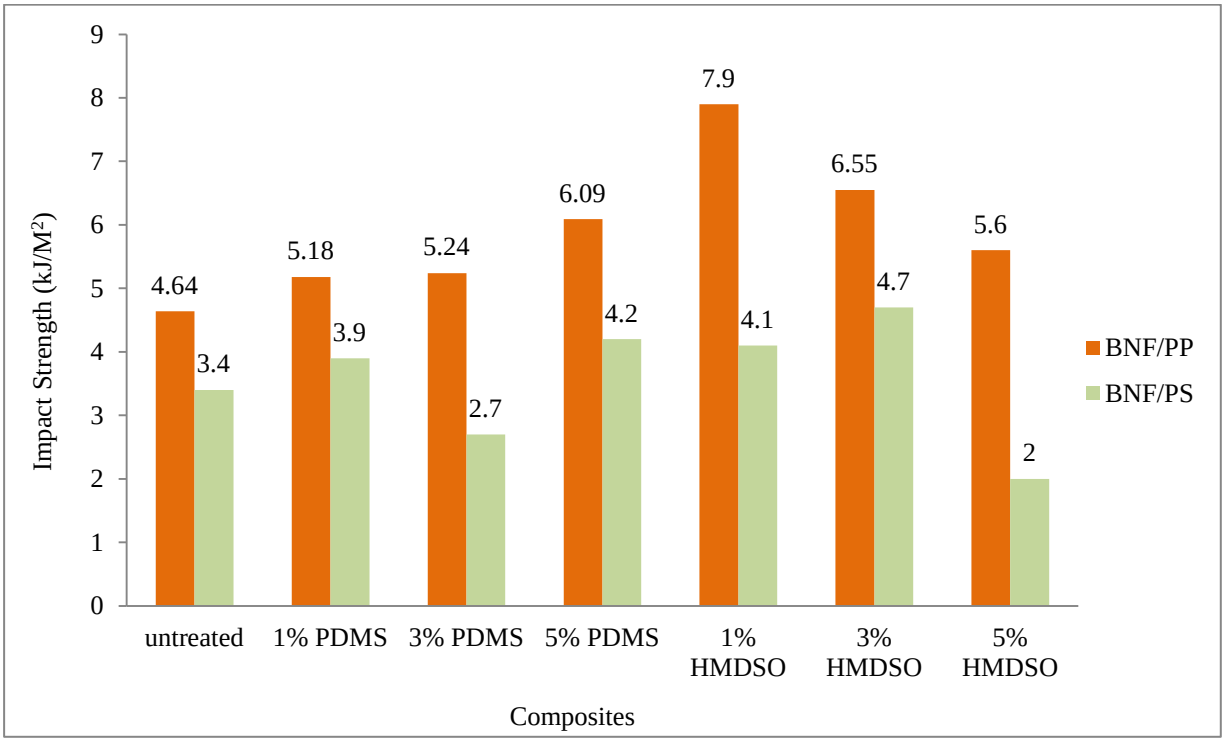



Figure 3. The effect of HMDSO and PDMS treatment with a series of concentration on the impact strength of BNF/PP and BNF/PS wood composites

**Water Absorption Test**

Generally, water absorption of treated BNF/PP composite shows lower value than untreated composite as proven in Figure 4. Main components in fiber such as hemicelluloses, cellulose and lignin are able to absorb water and moisture from environment. Based on past research by Agnantopoulou et al [18], they found that hemicelluloses is more hygroscopic element as it contains more hydroxyl group than lignin. The hollow cavity which known as lumen formed from fiber cell units are also available to generate more space or passage for water to seep into the fiber. Therefore, the treatment caused wood composite to become less hygroscopic due to the distribution and dispersion of compatibilizer which fulfill the wood cell wall space, in turn exhibiting hydrophobic properties. Diffusion of water and other molecules in the cell walls was also reduced because the compatibilizer has blocked micropores in the cell walls which resulting hygroscopic properties of wood composites to decrease.

However, the trend for BNF/PS composite is different with BNF/PP composite where only 3% HMDSO treatment showed improvement on water resistivity by an increment around 11.7%. The other treated BNF/PS composite shows higher water absorption than untreated composite probably due to poor fiber–matrix interaction in the composite. Additives treatment has possibility to increase or to decrease the percentage of water absorption as stated by Gnatowski [19].The treatment with 1% HMDSO on BNF/PP composite has decreased the percentage of water absorption by 61.9% due to the formation of hydrophobic layer on the fiber surface. HMDSO posses strong water resistivity to block water diffusion into voids of fiber. HMDSO treatment results in the smooth surface of fiber.

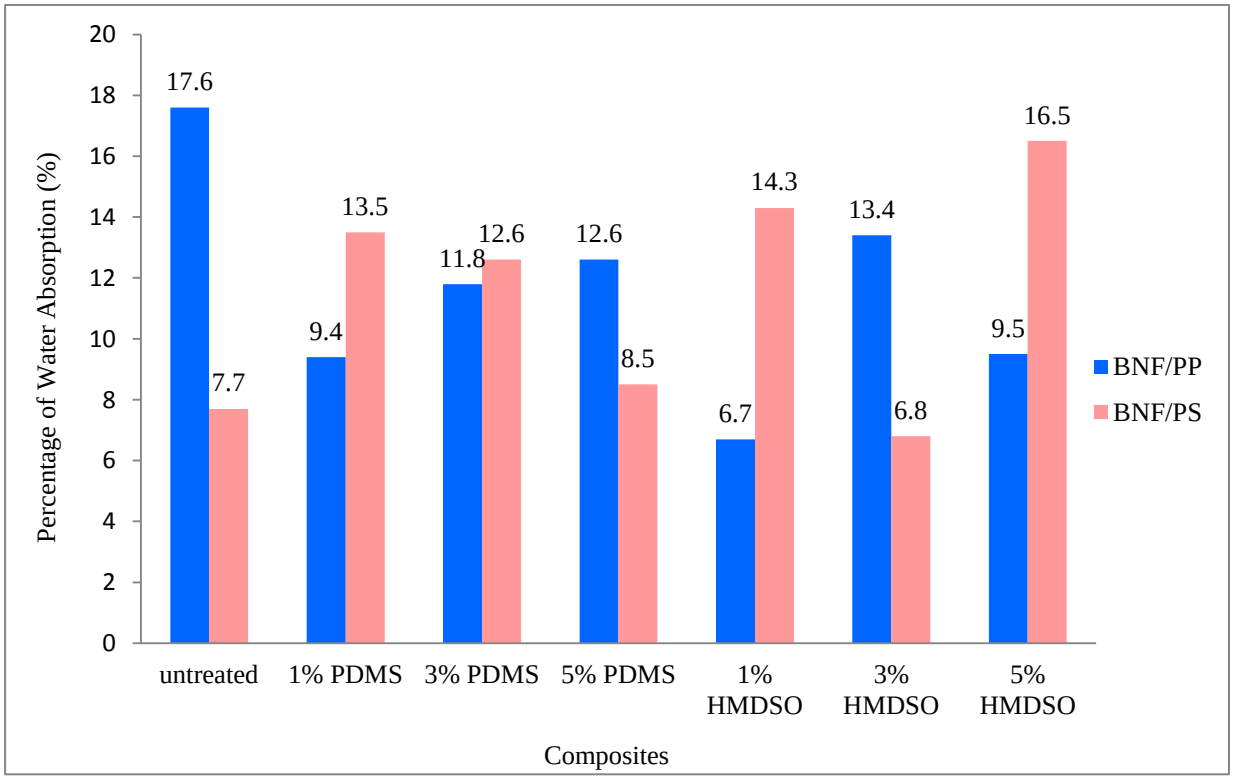



Figure 4. The effect of HMDSO and PDMS treatment with a series of concentration on the water absorption by BNF/PP and BNF/PS wood composites

**FTIR Spectra Analysis**

The FTIR spectral analysis of untreated and treated composites is shown in Table 1. For both untreated BNF/PP and BNF/PS, there were peaks at 3663 $cm^{-1}$ and 3433 $cm^{-1}$ respectively due to hydroxyl group (OH) of cellulose in fiber. In addition, other peaks were also present which belong to CH stretch, carbonyl (CO) and ether (C-O-C) groups in both untreated composites. Based on the spectrum of BNF/PP treated with HMDSO in Figure 6, OH and C-H stretching from cellulose fiber can be observed at 3305 $cm^{-1}$ and 2754 $cm^{-1}$ respectively. There were no peak presence for ether group from cellulose and lignin because of impurities such as dust or water molecule since it can resist the absorption of any peak on spectrum. PP matrix is identified at 2874$cm^{-1}$ for bent $CH_3$ group. FTIR spectrum of treated composites from both PP and PS showed several peaks at 785 $cm^{-1}$, 846 $cm^{-1}$ and 1202 $cm^{-1}$ which attributed to $Si(CH_3)$, Si-C stretching vibration and Si-O stretching respectively that occur due to the physical interaction of fiber and HMDSO. Theoretically, HMDSO formed a thin layer on the surface of fiber without experiencing any chemical reaction to form new chain. The presence of Si-O-Si chains in HMDSO structure with elasticity properties gives high flexibility in composites by increasing the flexural strength as shown by the flexural test results.

Table 1. FTIR analysis of untreated and HMDSO treated composite

| **Functional Group** | **Wavenumbers, $cm^{-1}$** | | | |
|---|---|---|---|---|
| | **Untreated BNF/PP** | **HMDSO treated BNF/PP** | **Untreated BNF/PS** | **HMDSO treated BNF/PS** |
| OH | 3663 | 3305 | 3433 | 3525 |
| CH | 2983 | 2754 | 2917 | 2920 |
| CO | 1060 | - | 1044 | 1035 |
| C-O-C | 1146 | - | 1149 | 1123 |
| $CH_3$ (symmetry and asymmetry) | 2983 | - | - | - |
| $CH_3$ (bent) | - | 2874 | - | - |
| C-H (aromatic stretching) | - | - | 3433 | 3060 |
| $Si(CH_3)$- | - | 785 | - | 746 |
| Si-C (vibration stretching at Si-$CH_3$ and $Si(CH_3)$-) | - | 846 | - | 844 |
| Si-O (stretching) | - | 1202 | - | 1071 |

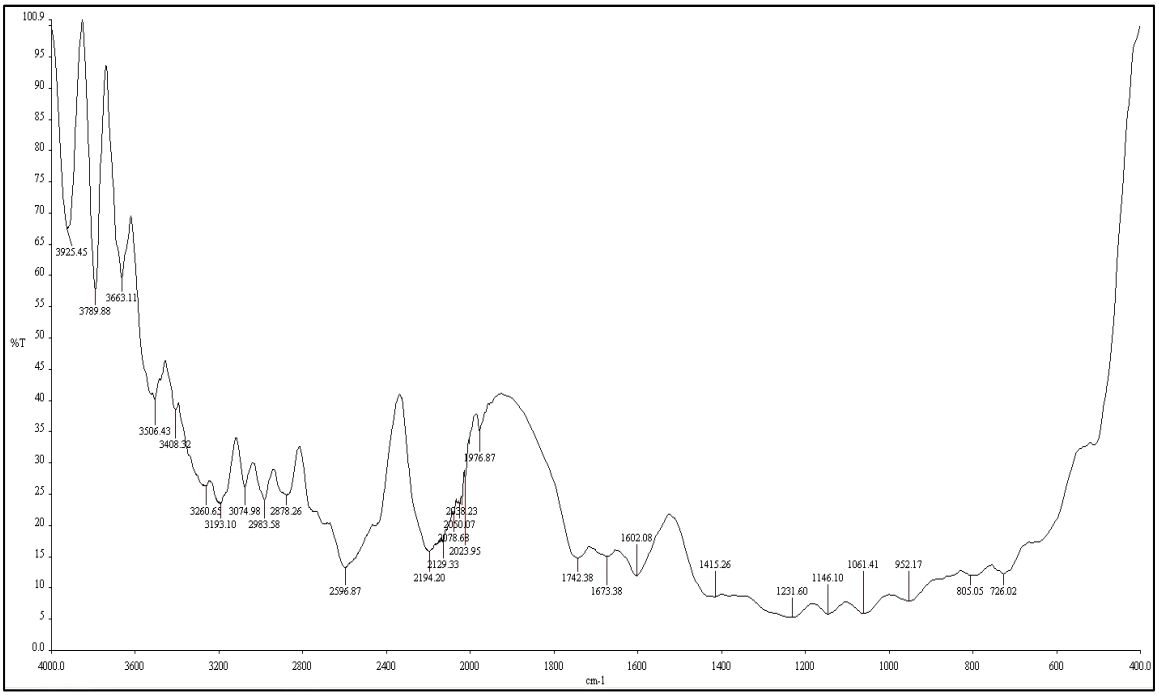



Figure 5. FTIR spectrum of untreated BNF/PP composite

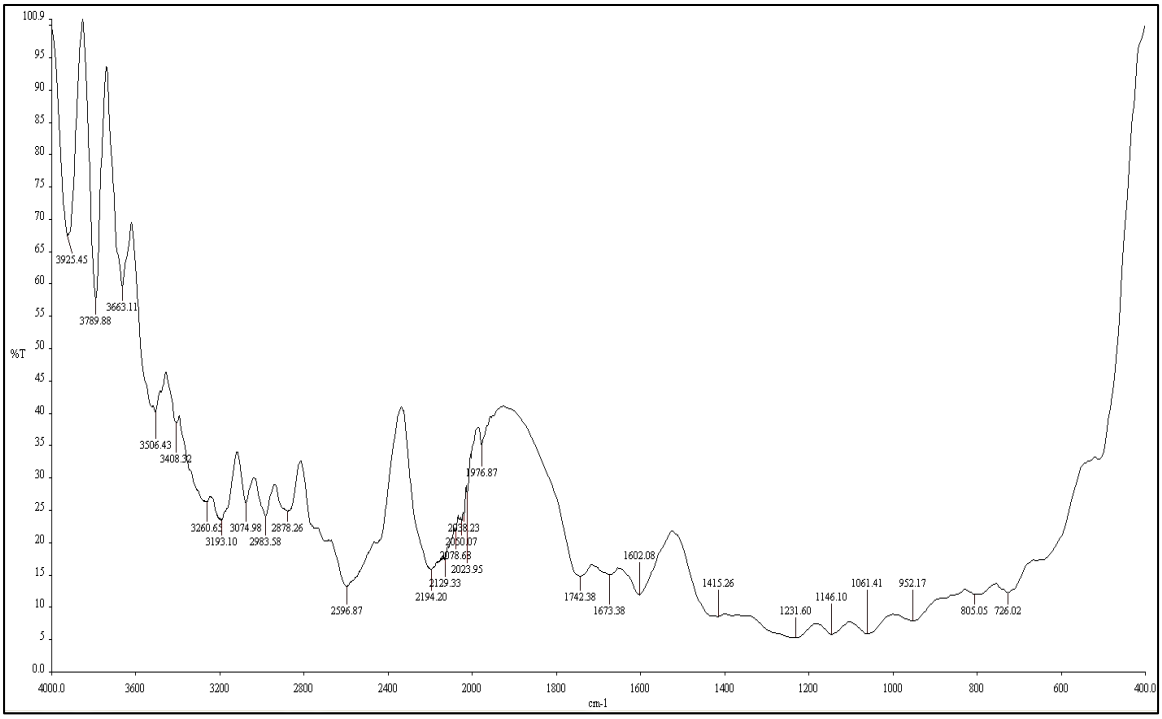



Figure 6. FTIR spectrum of BNF/PP treated with HMDSO

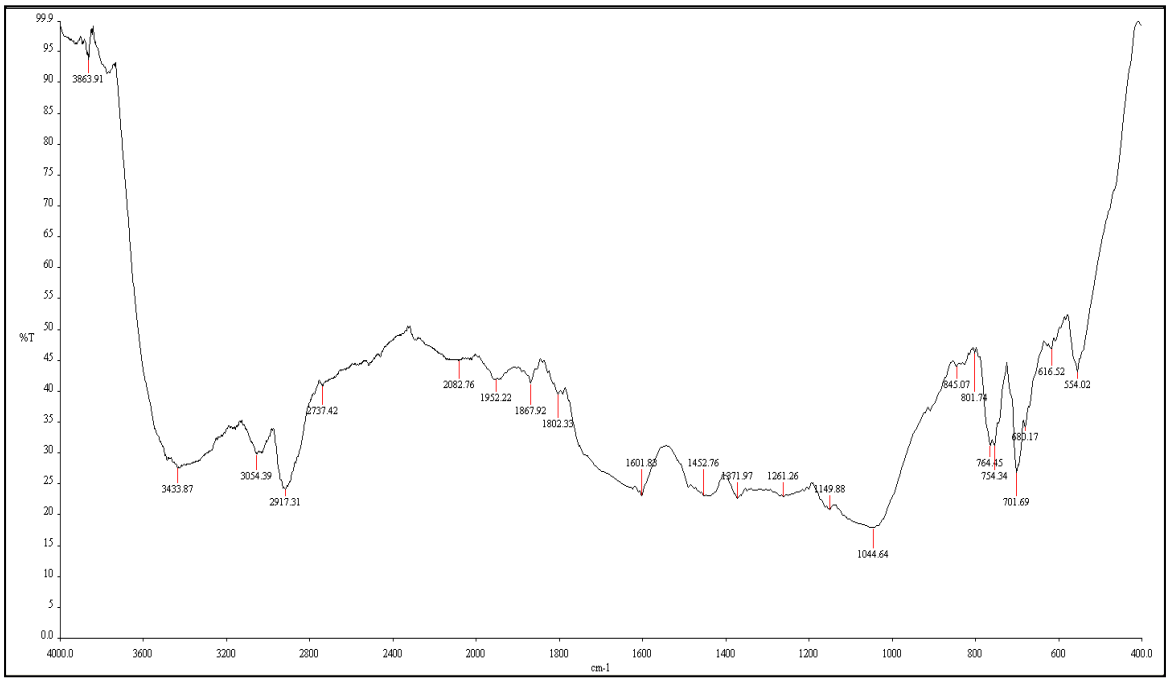



Figure 7. FTIR spectrum of untreated BNF/PS composite

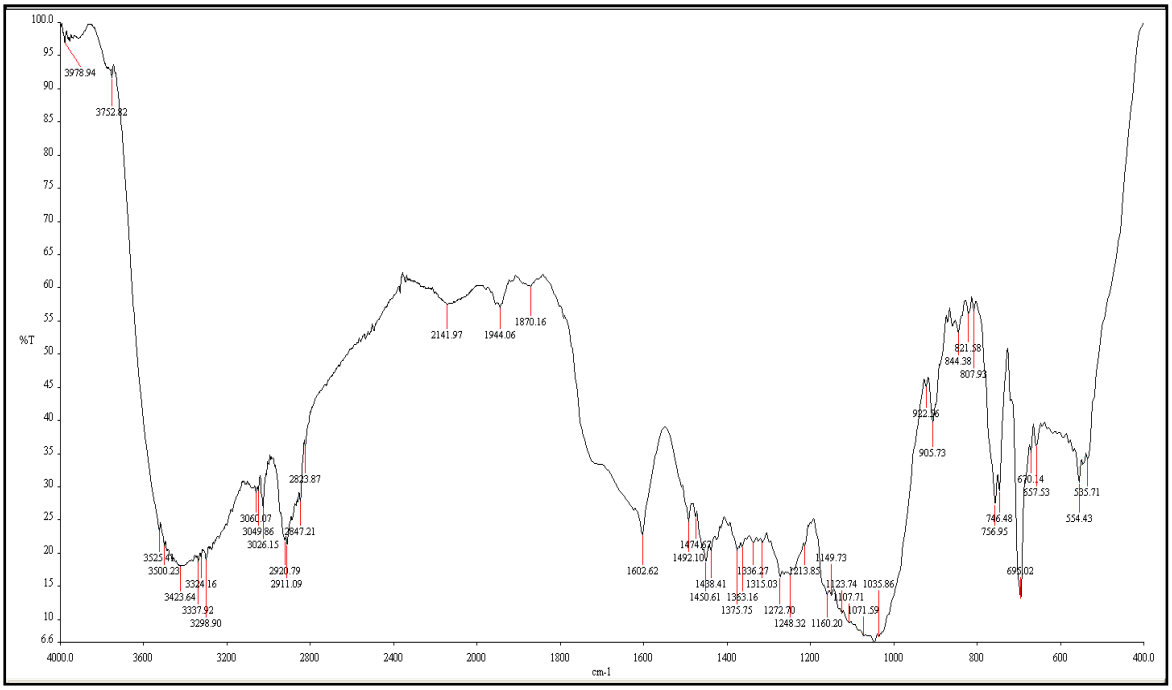



Figure 8. FTIR spectrum of BNF/PS treated with HMDSO

**Scanning Electron Microghraphs**

SEM micrograph from Figure 9(a) showed the presence of microvoids for untreated BNF/PP composite which mostly covered by trichomes as it is a major component in BNF. PP matrix can be seen binding at a random position due to the variation of fiber size from 0.5 – 1.0 cm. Besides, it is found that fiber pulled out occurred in the specimen because of weak adhesion interaction at fiber-matrix interphase. After 1% HMDSO treatment on BNF/PP composites, the HMDSO coated most of the trichomes on the fiber. Adhesion between treated BNF and PP matrix was found to be more compatible and showed fiber breakage at the fractured surface as in Figure 9(b) because of better interface and interphase interaction in the composite However, for 1% PDMS in the BNF/PP composite, both fiber pulled out and fiber breakage could be seen on the fractured surface compare to 1% HMDSO treated BNF/PP composite (Figure 9(c)).

Based on Figure 9(d), it is observed that BNF were tightly interacted within PS matrix due to trichomes on the surface of BNF, provides better adhesion of fiber–matrix interface which supported the flexural strength data of untreated BNF/PS in Figure 2. SEM micrographs from Figure 9(e) and 9(f) clearly show that, the fractured surface exhibited many voids as the fiber was pulled out from PS matrix after impact test. Treatment with 3% HMDSO provides better compatibility at fiber-matrix interphase than treatment with 3% PDMS and it resulted in fewer voids after the treatment. However, treated BNF/PS only increases the impact strength and water absorption.

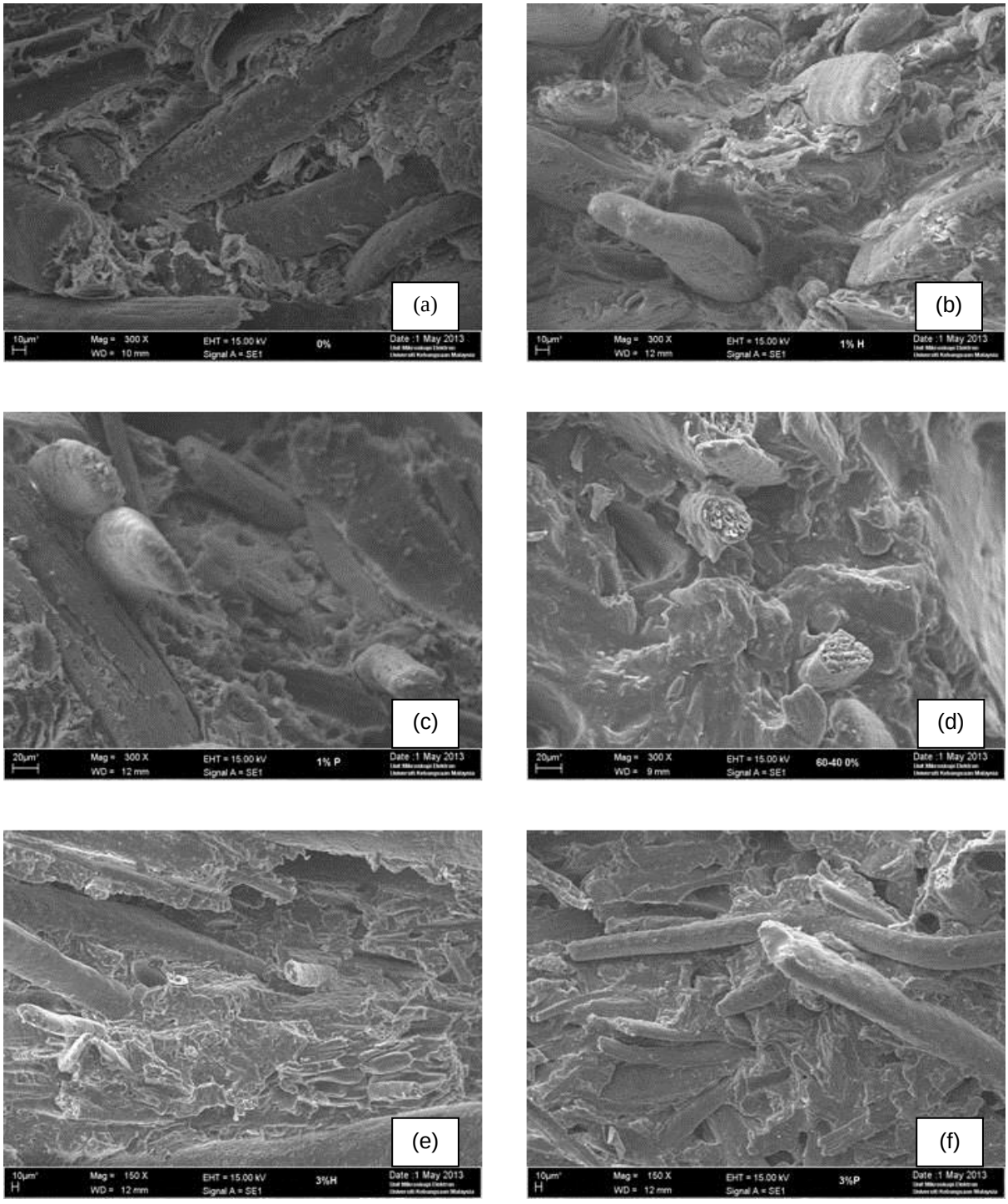



Figure 9. SEM micrographs of composites with magnification of 300x: (a) Untreated BNF/PP, (b) BNF/PP with 1% HMDSO, (c) BNF/PP with 1% PDMS, (d) Untreated BNF/PS, (e) BNF/PS with 3% HMDSO, (f) BNF/PS with 3% PDMS

## Conclusion

The effects of the HMDSO and PDMS treatments on the BNF/PP and BNF/PS were investigated in this study. Generally, treatment with HMDSO was better than PDMS and show that HMDSO acted better as compatibilizing agent in BNF/PP composite. This is due to simple structure of HMDSO resulting in homogeneity between fiber and matrices. SEM micrograph also revealed that the microvoids of BNF/PP and BNF/PS was reduced after HMDSO treatment and it is proved by FTIR spectral analysis which indicate peaks $Si(CH_3)$, Si-C stretching vibration and Si-O stretching that show physical interaction at fiber-matrix interphase. The results revealed 1% HMDSO as the optimum amount to be used as compatibilizer for BNF/PP composite where the compatibility of fiber-matrix interphase was significantly improved and contributed to the increment of flexural strength (18.5%), flexural modulus (24.2%), impact strength (70.3%) and percentage of water absorption (61.9%). PDMS and HMDSO are not effective as compatibilizers in BNF/PS composite and showed no significant improvement on their mechanical properties.

## Acknowledgement

The authors would like to thank the Department of Chemistry, Faculty of Science and Technology, National University of Malaysia and lab technicians for the technical support of this project.

## References

1. Matthew, F. L. & Rawlings, R. D. (1999). Composite Material: Engineering and Science. Imperial College of Science, U.K.
2. Mcdonough, W. & Braungart, M. (2002*). Cradle to Cradle: Remaking The Way We Make Things.* United States: North Point Press.
3. Sain, M. & Pervaiz, M. (2008). *Wood Polymer-Composites* Cambridge, England: Woodhead Publishing Limited and CRC Press LLC.
4. Bengtsson, M. & Oksman, K. (2006). Silane Crosslinked Wood Plastic Composites: Processing and Properties.*Composites Science and Technology*, 66: 2177-2186.
5. Winandy, J. E., Stark, N. M. & Clemons, C. M. (2004). Considerations in Recycling of Wood-Plastic Composites.*5th Global Wood and Natural Fibre Composites Symposium. Kassel, Germany,* April 27- 28.
6. Basiji, F., Safdari, V., Nourbakhsh, A. & Pilla, S. (2010). The Effects of Fiber Length and Fiber Loading on the Mechanical Properties of Wood Plastic (Polypropylene) Composites.*Turkish Journal of Agriculture and Forestry*, 34: 191 - 196.
7. Bouafif, H., Koubaa, A., Perre, P. & Cloutier, A. (2009). Effects of Fiber Characteristics on the Physical and Mechanical Properties of Wood Plastic Composites.*Composites Part A: Applied Science and Manufacturing*, 40 (12): 1975 – 1981.
8. Choudhury, S. U., Hazarika, S. B., Barbhuiya, A. H. & Ray, B. C. (2006). Natural Fibre Reinforced Polymer Biocomposites and Blends: Synthesis, Characterization and Applications. Department of Chemistry, Cotton College, Guwahati, Assam, India Department of Biochemistry, Regional College of Higher Education, Guwahati, India Jadavpur University, Kolkata, India.
9. Venkateshappa, S. C., Bennehalli, B., Kenchappa, M. G. & Ranganagowda, R. P. G. (2010). Flexural Behaviour of Areca Fibers Composites.*BioResources*, 5 (3): 1846 - 1858.
10. Kumar, G. C. M. (2008). A Study of Short Areca Fiber Reinforced PF Composites. *Proceedings of the World Congress on Engineering Vol II, London U.K*, 2 – 4 July 2008.
11. Nirmal, U., Jamil, N., Yousif, B. F., Rilling, D. & Brevern, P. V. (2010). The Potential of Using Treated Betel Nut Fibers as Reinforcement for Tribo-Bio Polymeric Composites Subjected to Dry/Wet Contact Conditions. *Second International Conference on Natural Polymers, Bio-Polymers, Bio- Materials, Their Composites, Blends, IPN'S and Gels Polyelectrolytes and Gels: Macro to Nano Scales.* Organized by Kottayam, Kerala, India, September 24-26.
12. Clemons, C. (2008). Wood Polymer Composites. Cambridge, England: Woodhead Publising Limited and CRC Press LLC.
13. Najafi, S. K., Mehdi, T. & Elham, H. (2007). Effect of Temperature, Plastic Type and Virginity on the Water Uptake of Sawdust/Plastic Composites.Holz RohWerkst, 65: 37 – 382.
14. Sobczak, L., Bruggemann, O. & Putz, R. F. (2012). Polyolefin Composites with Natural Fibers and Wood-Modification of the Fiber/Filler-Matrix Interaction.*Journal of Applied Science*, 127 (1): 1 - 17.

15. Wechsler, A., Hiziroglu, S. & Ballerini, A. A. (2008). Some of the Properties of Wood Plastic Composites.*Proceedings of the 51st International Convention of Society of Wood Science and Technology*, 1-10.
16. Botros, M. (2003). Development of New Generation Coupling Agents for Wood-Plastic Composites. Intertech Conference The Global Outlook for Natural and Wood Fiber Composites. Organized by New Orleans, LA, 3 - 5 December.
17. Hocker, H. (2002). Plasma Treatment of Textile Fibres.*Pure Applied Chemistry*, 74 (3): 423 - 427.
18. Agnantopoulou, E., Tserki, V., Marras, S., Philippou, J. & Panayiotou, C. (2012). Development of Biodegradable Composites Based on Wood Waste Flour and Thermoplastic Starch.*Journal of Applied Polymer Science*, 126 (1): 273 – 281.
19. Gnatowski, M. (2009). Water Absorption and Durability Composites. Ph.D., Research Director, Polymer Engineering Company Ltd. Burnaby, BC, Canada.

The Malaysian Journal of ANALYTICAL SCIENCES ISSN 1394-2506

# CHARACTERIZATION OF POLYLACTIC ACID/MICROCRYSTALLINE CELLULOSE/MONTMORILLONITE HYBRID COMPOSITES

## (Pencirian Komposit Polilaktik asid/Selulosa Mikrohablur/ Hibrid Montmorilonit)

Reza Arjmandi[1], Azman Hassan[1]*, M.K. Mohamad Haafiz[1, 2], Zainoha Zakaria[3], I. M. Inuwa[1]

[1]*Department of Polymer Engineering, Faculty of Chemical Engineering, Universiti Teknologi Malaysia, 81310 UTM Skudai, Johor, Malaysia*
[2]*School of Industrial Technology, Universiti Sains Malaysia, 11800 Penang, Malaysia*
[3]*Faculty of Science, Universiti Teknologi Malaysia, 81310 UTM Skudai, Johor, Malaysia*

**Corresponding author: azmanh@cheme.utm.my*

**Abstract**

The objective of this study is to investigate the effect of montmorillonite (MMT)/microcrystalline cellulose (MCC) hybrid fillers on mechanical properties and morphological characteristics of polylactic acid (PLA) composites. PLA/MMT nanocomposites and PLA/MMT/MCC hybrid composites were prepared by solution casting method. Morphology and tensile properties of PLA composites were investigated using Field emission scanning electron microscopy and Instron tensile testing machine. The maximum tensile strength of PLA/MMT nanocomposites was obtained with 5 phr contents of MMT, which corresponding to 30.75 MPa. Based on optimized formulation of PLA/MMT nanocomposites (5 phr MMT contents), various amounts of MCC (0 to 7 phr) were added into optimum formulation of PLA/MMT in order to produce PLA/MMT/MCC hybrid composites. Fourier transform infrared spectroscopy revealed some level of interaction between PLA and both MMT and MCC in the hybrid composites. However, the percent elongation at break of the hybrid composites was generally higher than PLA/MMT nanocomposites. Additionally, Young's modulus of the PLA/MMT/MCC hybrid composites increased gradually with increasing of MCC contents and was higher than PLA/MMT at all compositions. The present results are the first among a series of experiments that have been designed in order to probe the effect of MMT and MCC in the PLA.

**Keywords:** Hybrid composites, microcrystalline cellulose, polylactic acid, montmorillonite, solution casting

**Abstrak**

Objektif kajian ini adalah untuk mengkaji kesan pengisi hibrid montmorilonit (MMT)/selulosa mikrohablur (MCC) ke atas sifat mekanikal dan ciri-ciri morfologi komposit polilaktik asid (PLA). Nanokomposit PLA/MMT dan komposit hibrid PLA/MMT/MCC telah di sediakan menggunakan kaedah larutan beracun. Morfologi dan sifat regangan komposit PLA telah dikaji menggunakan mikroskop pengimbas electron kawasan terpancar (FESEM) dan mesin ujian regangan Instron. Kekuatan regangan maksimum nanokomposit PLA/MMT telah diperolehi dengan 5 bsg kandungan MMT, yang bersamaan dengan 30.75 MPa. Berdasarkan formulasi optimum nanokomposit PLA/MMT (5 bsg kandungan MMT), pelbagai jumlah MCC (0-7 bsg) telah ditambah ke dalam formulasi optimum PLA/MMT untuk menghasilkan komposit hibrid PLA/MMT/MCC. Spektroskopi inframerah transformasi fourier (FTIR) mendedahkan beberapa tahap interaksi di antara PLA dan kedua-dua MMT dan MCC dalam komposit hibrid. Walaubagaimanapun, peratusan terikan pada takat putus bagi komposit hibrid adalah lebih tinggi daripada nanokomposit PLA/MMT. Selain itu, modulus Young bagi komposit hibrid PLA/MMT/MCC meningkat secara beransur-ansur dengan peningkatan kandungan MCC dan ia adalah lebih tinggi daripada PLA/MMT pada semua komposisi. Keputusan ini adalah yang pertama dalam kalangan satu siri eksperimen yang telah direka untuk mengkaji kesan MMT dan MCC di dalam PLA.

**Kata kunci:** komposit hibrid, selulosa mikrohablur, polilaktik asid, montmorilonit, larutan beracun

## Introduction

In recent decades, the use of biopolymers materials has been attracting more interest in the public research due to the increasing in environmental concerns and diminishing petrochemical resources. One of the most promising biopolymers is polylactic acid (PLA). PLA is a linear aliphatic thermoplastic polyester which synthesized by ring-opening polymerization of the cyclic lactide dimer. PLA is a widely studied biodegradable polymers because of its high mechanical properties and the easy production from its monomer (i.e. lactic acid) [1]. The majority of lactic acid used for PLA production is produced by fermentation of agricultural products (e.g. corn). The high biocompatibility and biodegradability of PLA make it a good candidate to be used in biomedical and packaging applications. In spite of all these advantages, its range of application is still limited by its high production cost, its brittleness and its low thermal stability. PLA nanocomposites containing high aspect ratio fillers have been developed to further enhance the strength, stiffness and thermal stability while lowering the production cost [2, 3].

Montmorillonite (MMT) is the most familiar clay among the commonly used fillers. It consists of two fused silica tetrahedral sheets sandwiching an edge shared octahedral sheet of either magnesium or aluminum hydroxide [4]. MMT with nano-sized layered structure has a large surface area providing sufficient interfacial regions in polymer nanocomposites that offer tremendous improvement in wide range of physical and engineering properties for polymers. [3, 5]. Montmorillonite (MMT) is a suitable filler for PLA nanocomposites because it has the ability to fine-tune its surface chemistry through ion exchange reactions with organic and inorganic cations [3]. PLA/MMT nanocomposites have been most well studied [2, 6]. Despite the all benefits of MMT, ductility is detrimentally affected by the addition of MMT. The replacement of MMT with other renewable and biodegradable fillers like as cellulose could minimize the production costs of the polymer nanocomposites, enhance the biodegradability, mechanical and thermal behaviors of PLA [1, 7].

One of the most fascinating natural fillers is cellulose. Microcrystalline cellulose (MCC) is a kind of cellulose fillers, which used as a reinforcement in a polymer matrix [8, 9]. MCC is produced by combining mechanical (e.g., pressure homogenizing) and chemical (e.g., acid hydrolysis) processes of natural celluloses such as plant and wood. MCC possesses a relatively high specific surface area compared with other fillers such as natural fiber, glass fiber, talc, and mica [10, 11]. As a result, MCC have a great potential to be used as reinforcing agent in composites. Few studies have been done on PLA/MCC composites and it is shown that the stiffness of PLA/MCC composites improved with the addition of MCC [12]. However, the ductility and tensile strength decreased with the addition of MCC [13].

It would be interesting to study the combined effect of MCC and MMT on stiffness, strength and ductility of PLA. Therefore, the objective of this study is to compare the mechanical and morphological properties of PLA/MMT nanocomposites and PLA/MMT/MCC hybrid composites. To the best of our knowledge, no study has been reported on using of MMT/MCC hybrid filler in order to enhance the mechanical properties of PLA composites using solution casting method.

## Materials and Methods

### Materials

Polylactic acid (NatureWorkTM PLA 300ID) in pellet form was obtained from NatureWork® LLC, Minnetonka, MN USA. It has a density of 1.24 g $cm^{-3}$ and melt flow index (MFI) around 15 g/10 min (190 °C/2.16 kg). MCC was supplied by Sigma-Aldrich (Avicel; type PH-101). It was obtained from a cotton linter and had an average particle size of 50 μm. Organo-modified montmorillonite, Nanomer 1.30TC was obtained from Nanocor Inc. (Arlington Heights IL, USA) Nanomer 1.30TC is organically modified with around 30 wt.% of octadecylamine with mean dry particle size of 16–22 mm. The reagent used was chloroform secured from Merck, Malaysia.

### Preparation of PLA and PLA/MMT nanocomposites

10 g pellets of PLA were fully dissolved in 64 ml of chloroform and stirred in water bath for 2 hours at 60 °C [14]. The PLA solution was immediately casted on a clean glass plates and left to allow the solvent to evaporate at room temperature for 48 hours. The thickness of the casted film was approximately 100 μm.

The PLA/MMT nanocomposites were prepared by mixing the 10 g of PLA pellets with different MMT contents (1, 3, 5, and 7 phr) at 60 °C. The various mixtures were placed in 64 ml of chloroform and stirred with strong agitation for 2 hours at 60 °C until PLA pellets were dissolved. The suspension was then sonicated for 5 minutes and immediately casted on a clean glass plate to obtain the composite of ~100 μm thickness. The composites were designated as P/MT1, P/MT3, P/MT5, and P/MT7 are shown in Table 1.

**Preparation of PLA/MMT/MCC hybrid composites**

The PLA/MMT/MCC hybrid composites were prepared by mixing 10 g of PLA pellets with 5 phr of MMT and different MCC contents (1, 3, 5, and 7 phr) at 60 °C. The various mixtures were placed in 64 ml of chloroform and stirred with strong agitation for 2 hours at 60 °C until all the PLA pellets dissolved. The suspension were then sonicated for 5 minutes and were immediately casted on a clean glass plate to obtain the composite of ~100 μm. The hybrid composites were designated as P/MT5/MC1, P/MT5/MC3, P/MT5/MC5, and P/MT5/MC7 are summarized in Table 1.

Table 1. Polylactic acid composites formulation

| Designation | PLA (wt. %) | MMT (phr) | MCC (phr) |
|---|---|---|---|
| PLA | 100 | 0 | 0 |
| P/MT1 | 100 | 1 | 0 |
| P/MT3 | 100 | 3 | 0 |
| P/MT5 | 100 | 5 | 0 |
| P/MT7 | 100 | 7 | 0 |
| P/MT5/MC1 | 100 | 5 | 1 |
| P/MT5/MC3 | 100 | 5 | 3 |
| P/MT5/MC5 | 100 | 5 | 5 |
| P/MT5/MC7 | 100 | 5 | 7 |

phr = parts per hundred parts of polymer (PLA)

**Characterization**

***Fourier transform infrared***

Fourier transform infrared (FT-IR) analysis was performed on a Perkin Elmer 1600 Infrared spectrometer. FT-IR spectra of the samples were recorded by using Nicolet's AVATAR 360 at 32 scans with a resolution of 4 $cm^{-1}$ and within the wave number range of 4000 to 370 $cm^{-1}$.

***Mechanical testing***

Mechanical test was done using the Instron 4400 Universal Tester to measure the tensile strength at the point of breakage for each sample and Young's modulus. Tensile tests were carried out at room temperature, according to the ASTM D882 type V. A fixed crosshead rate of 10 mm/min was utilized in all cases and the results were taken as an average of 10 tests.

***Morphology analysis***

The morphology of samples was characterized by using Field emission scanning electron microscopy (FESEM). FESEM was conducted using a Carls Zeiss (Germany) Supra 35 VP and an extra high tension (EHT) of 8–10 kV. The samples were sputter-coated with gold prior to observation.

## Results and Discussion

**FT-IR spectroscopy analysis**

FT-IR spectroscopy was used to observe the interfacial interaction between PLA matrix and both MMT and MCC. FT-IR spectra of pure PLA, a P/MT5 nanocomposite and a P/MT5/MC1 hybrid composite are shown in Figure 1a-c, respectively. As can be seen from Figure 1a, the peak at 3508 $cm^{-1}$ was assigned to the -OH stretching vibration [15,

16]. The 2997 and 2948 $cm^{-1}$ absorption peaks attributed to the asymmetric stretching vibration of -CH [15, 17]. Stretching vibration of carbonyl groups (C=O) appeared at 1764 $cm^{-1}$ and the peak at 1089 $cm^{-1}$ indicate the stretching vibration of C-O. Similar results were reported by other studies [15-17]. The peaks at 1457 and 1049 $cm^{-1}$ are ascribed to the $–CH_3$ bending and –OH bending, respectively and stretching vibration of C-C single bond was situated at 868 and 920 $cm^{-1}$ [15-18].

Figure 1b and c revealed the character peaks of a P/MT5 nanocomposite and a P/MT5/MC1 hybrid composite, respectively. As shown in Figure 1b, the presence of new peaks at 465 and 520 $cm^{-1}$ for nanocomposites spectra were attributed to the absorption peak of $SiO_2$ and Si-O vibration, respectively [19]. As can be clearly observed from Figure 1b, the O-H (3508 $cm^{-1}$), C=O (1764 $cm^{-1}$) and C-O (1089 $cm^{-1}$) stretching peaks were shifted to lower wave numbers of 3502 $cm^{-1}$, 1760 $cm^{-1}$ and 1084 $cm^{-1}$, respectively. This was attributed to the strong polar interaction between the PLA and the MMT platelet surfaces and the hydroxyl groups of the ammonium surfactant in the organically modified clay [19]. Figure 1c illustrates that no new peak was created when MMT/MCC hybrid fillers were added into PLA matrix, because lower amount of fillers used to produce the hybrid composites and only physical interaction occurred between PLA and MMT/MCC hybrid fillers, instead of chemical interaction [13, 17]. On the other hand, the peak at 3502 $cm^{-1}$ for P/MT5/MC1 hybrid composite (Figure 1c) becomes broader as compared to P/MT5 nanocomposite (Figure 1b) when MCC filler was added. The broadness of the peak in the P/MT5/MC1 hybrid composite indicates the existence of good interaction between PLA and both MMT and MCC [20].

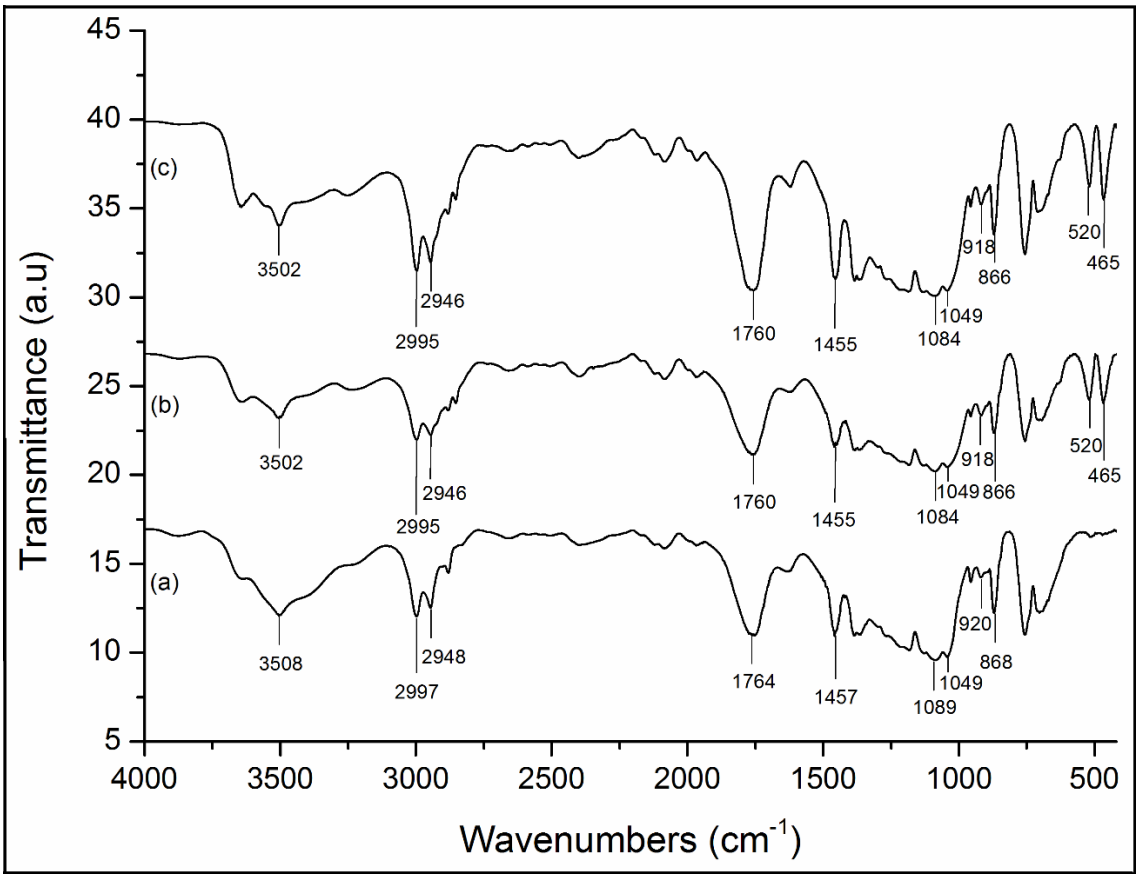



Figure 1. Typical FT-IR spectroscopy of (a) Pure PLA, (b) a P/MT5 nanocomposite and (c) a P/MT5/MC1 hybrid composite.

**Tensile properties**

Figure 2a demonstrates the effect of MMT contents on tensile strength and Young's modulus of PLA and PLA/MMT nanocomposites. The results revealed that the addition of MMT gradually increased the tensile strength and Young's modulus of the nanocomposites. The PLA/MMT nanocomposites exhibited approximately 63 % (at 5 phr MMT contents) increase in the tensile strength as compared to pure PLA. As the MMT contents further increased, the tensile strength decreased, which is attributed to the aggregation of MMT particles. Previous studies also reported that higher contents of MMT (>5 wt.%) in polymer can result in its agglomeration resulting in deprived mechanical performance compared to lower contents [21, 22]. The Young's modulus values of PLA/MMT nanocomposites increased steadily with increasing MMT contents. The PLA/MMT nanocomposites exhibited approximately 18 % increase in modulus as compared to the pure PLA. The improvement in modulus of PLA nanocomposites is due to the high rigidity exerted by the MMT as it does not deform and therefore the PLA's chain movement was suppressed by MMT particles [23]. This improvement in modulus may also be ascribed to the dispersion and alignment of MMT platelets within PLA and enhancement of the silicate interlayers incorporated into the polymer matrix. [2, 23].

Figure 2b displays the effect of MCC contents on the tensile strength and Young's modulus of PLA/MMT nanocomposites. It can be seen that, the addition of MCC give negative impact on the tensile strength. It is interesting to note that the Young's modulus of PLA/MMT/MCC hybrid composites increase gradually with increase in MCC contents and higher than PLA/MMT nanocomposites in all compositions (from 4.8 GPa to 5.25 GPa). This improvement in modulus of PLA/MMT/MCC hybrid composites is due to the increase in stiffening effect of the MCC [13, 24]. The tensile strength values of PLA/MMT/MCC hybrid composites however, decreased due to the presence of MCC. This could may be attributed to agglomeration of MCC due to Van der Waal's forces or there is practically no interfacial bonding between the reinforcing fillers and the polymer matrix [17, 20].

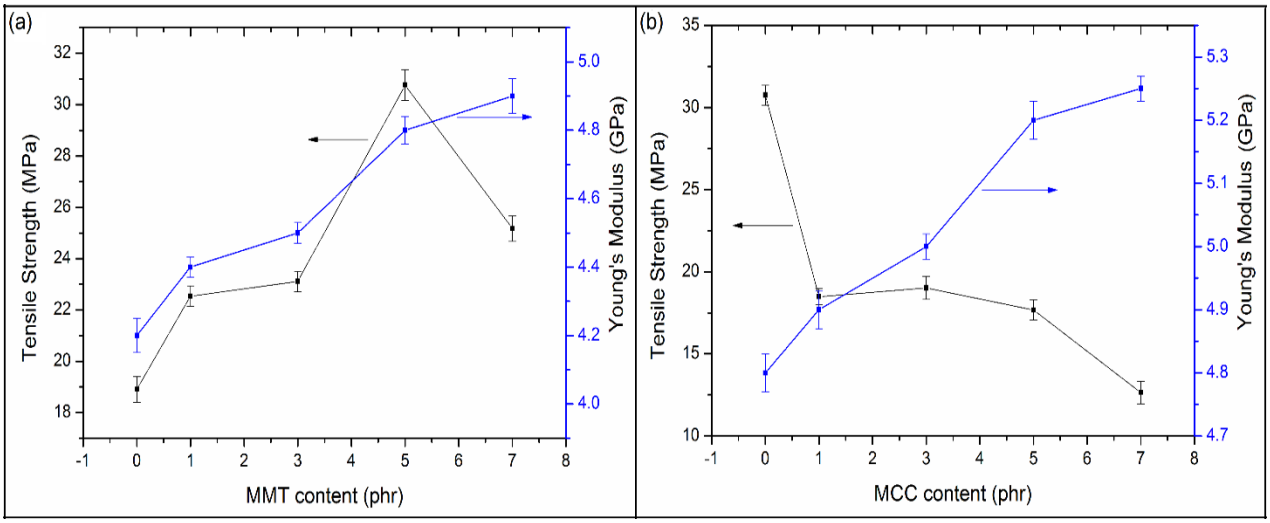



Figure 2. Tensile strength and Young's modulus of (a) PLA/MMT nanocomposites (b) and PLA/MMT/MCC hybrid composites.

The effect of MMT and MCC contents on the elongation at break of PLA/MMT nanocomposites and PLA/MMT/MCC hybrid composites was shown in Table 2 and Table 3, respectively. It can be clearly seen that, the elongation at break values of PLA/MMT/MCC hybrid composites (Table 3) increased with the presence of MCC in hybrid composites as compared to PLA/MMT nanocomposites (Table 2). The elongation at break values of the

PLA/MMT/MCC hybrid composites increased from ~10 to ~60 % in the presence of MCC. As the MCC contents further increased, the elongation at break decreased, which is ascribed to the aggregation of MCC particles. The initial increment in elongation at break with the presence of the MCC in PLA/MMT/MCC hybrid composites may be attributed to the interaction between reinforcements and matrix, which enhanced the interfacial bonds of MMT/MCC hybrid fillers and PLA matrix [2]. This results corroborates the observation made in the FT-IR analysis.

Table 2. Elongation at break of PLA/MMT nanocomposites

| **Designation** | **Elongation at break (%)** |
|---|---|
| PLA | 124.8±0.5 |
| P/MT1 | 55.0±0.3 |
| P/MT3 | 29.5±0.5 |
| P/MT5 | 10.6±0.4 |
| P/MT7 | 6.4±0.5 |

Table 3. Elongation at break of PLA/MMT/MCC hybrid composites

| **Designation** | **Elongation at break (%)** |
|---|---|
| P/MT5/MC1 | 60.0±0.5 |
| P/MT5/MC3 | 35.5±0.3 |
| P/MT5/MC5 | 11.0±0.4 |
| P/MT5/MC7 | 8.1±0.5 |

**Field emission scanning electron microscopy**

Figure 3 shows the field emission scanning electron microscopy (FESEM) images of fractured cross-sectional surfaces of pure PLA, a P/MT5 nanocomposites and a P/MT5/MC1 hybrid composites. Due to the lack of large scale plastic deformation, pure PLA showed a fairly smooth fracture surface (Figure 3a) [6]. It can be clearly seen from Figure 3b, MMT was dispersed uniformly throughout PLA matrix due to its finer particle size and the MMT was embedded within PLA matrix, as indicated by arrows. Figure 3c indicates the presence of MMT and MCC in the PLA matrix. However, adding the MCC has been resulting in agglomeration of MCC in the PLA matrix (as indicated by circle), and decreased the tensile strength of hybrid composites compared to the PLA/MMT nanocomposites. Due to the stiffening action of fillers in general, Young's modulus increased as compared to PLA/MMT nanocomposites.

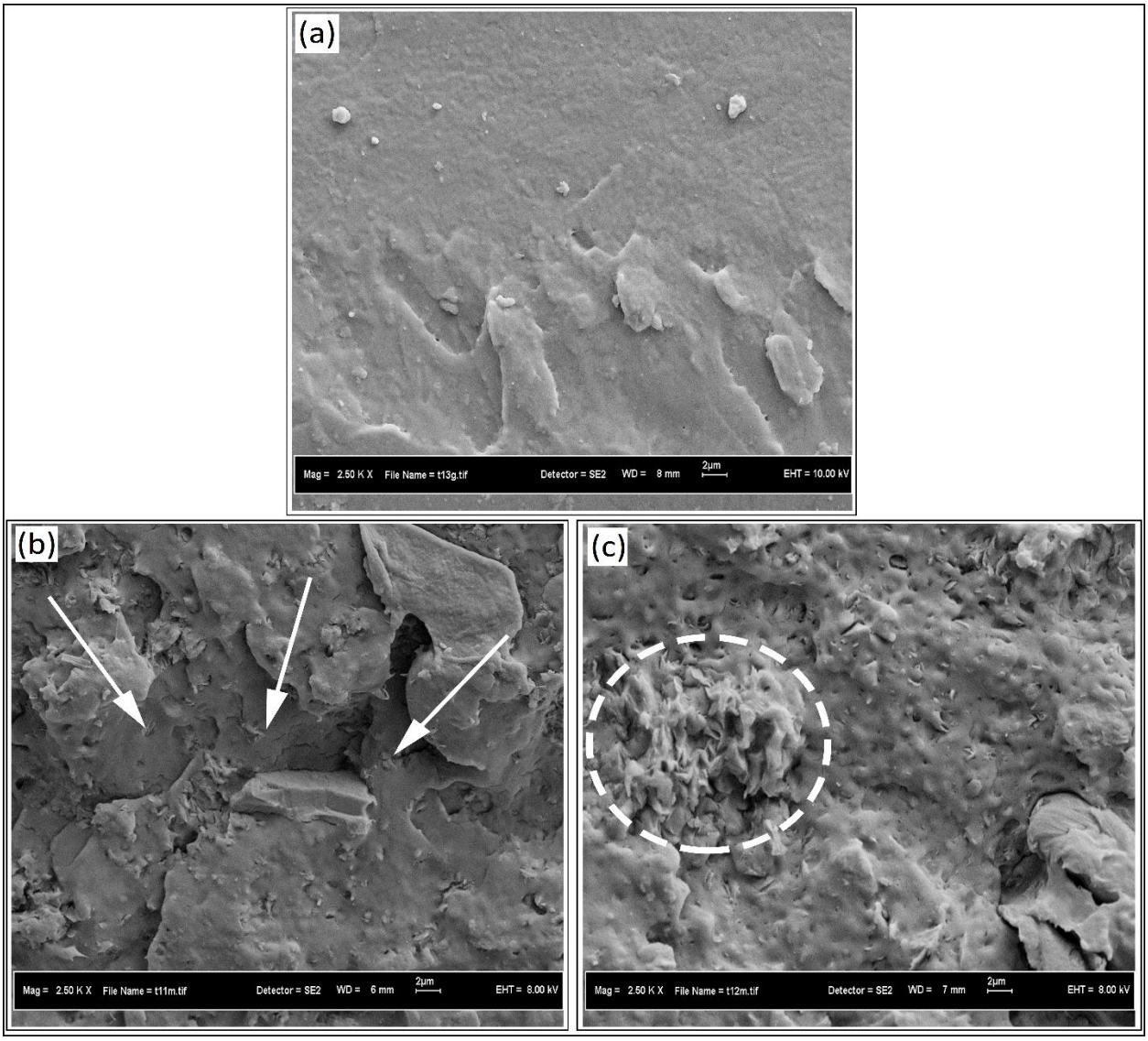



Figure 3. Field emission scanning electron micrographs of fractured cross-sections of (a) Pure PLA, (b) a P/MT5 nanocomposite and (c) a P/MT5/MC1 hybrid composite.

## Conclusion

PLA/MMT nancomposites and PLA/MMT/MCC hybrid composites were successfully prepared by solution casting technique. The FT-IR results indicated that good interaction between PLA and MMT occurred due to presence of new peaks. Only physical interaction in recorded between PLA and MMT/MCC hybrid fillers, due to absence of new peaks. Tensile properties of the PLA/MMT nanocomposites showed an increased in tensile strength up to 5 phr of MMT contents and increased Young's modulus with increasing MMT content due to the adequate dispersion and alignment of MMT platelets within PLA. However, Young's modulus and elongation at break of PLA/MMT/MCC hybrid composites increased due to the increased in stiffening effect of the MCC and interaction between MMT/MCC hybrid fillers and PLA polymer, respectively. The morphological observations using FESEM showed the uniformly dispersed MMT in PLA matrix and agglomeration of MCC by adding MCC in the hybrid composites.

The development of PLA/MMT/MCC hybrid composites is expected to play an important role in membrane technology and packaging.

**Acknowledgement**

The authors wish to acknowledge the Universiti Teknologi Malaysia (UTM) and Research University Grant 05H22, sub-code: Q.J130000.2509.05H22 for financial support.

**References**

1. Oksman, K., Skrifvars, M. & Selin, J. F. (2003). Natural fibres as reinforcement in polylactic acid (PLA) composites. *Composites science and technology*. *Composites Science and Technology*, 63(9): 1317–1324.
2. He, Y. N., Guo, K., Chen, J. Z., Niu, M. J., Wang, W. J. & Li, X. F. (2011). Preparation and Characterization of Poly(lactic acid)/Montmorillonite Nanocomposites via a Masterbatching Method. *Advanced Materials Research*, 335-336: 1493-1498.
3. Sinha Ray, S. & Okamoto, M. (2003). Polymer/layered silicate nanocomposites: a review from preparation to processing. *Progress in Polymer Science*, 28(11): 1539–1641.
4. Giannelis, E. P., Krishnamoorti, R. & Manias, E. (1999). Polymer-silicate nanocomposites: model systems for confined polymers and polymer brushes. *Polymers in confined environments*, 138: 107–147.
5. Zeng, Q. H., Yu, A. B., Lu, G. Q. M. & Paul, D. R. (2005). Clay-based polymer nanocomposites: research and commercial development. *Journal of Nanoscience and Nanotechnology*, 5(10): 1574–1592.
6. Jiang, L., Zhang, J. & Wolcott, M. P. (2007). Jiang, L., Zhang, J., & Wolcott, M. P. (2007). Comparison of polylactide/nano-sized calcium carbonate and polylactide/montmorillonite composites: reinforcing effects and toughening mechanisms. *Polymer*, 48(26): 7632–7644.
7. Petinakis, E., Yu, L., Edward, G., Dean, K., Liu, H. & Scully, A. (2009). Effect of matrix–particle interfacial adhesion on the mechanical properties of poly (lactic acid)/wood-flour micro-composites. *Journal of Polymers and the Environment*, 17(2): 83-94.
8. Chen, W., Yu, H., Liu, Y., Chen, P., Zhang, M. & Hai, Y. (2011). Individualization of cellulose nanofibers from wood using high-intensity ultrasonication combined with chemical pretreatments. *Carbohydrate Polymers*, 83(4): 1804–1811.
9. Iwatake, A., Nogi, M. & Yano, H. (2008). Cellulose nanofiber-reinforced polylactic acid. *Composites Science and Technology*, 68(9): 2103–2106.
10. Lu, J., Askeland, P. & Drzal, L. T. (2008). Surface modification of microfibrillated cellulose for epoxy composite applications. *Polymer*, 49(5): 1285–1296.
11. Lu, J., Wang, T. & Drzal, L. T. (2008). Preparation and properties of microfibrillated cellulose polyvinyl alcohol composite materials. *Composites Part A: Applied Science and Manufacturing*, 39(5): 738–746.
12. Mathew, A. P., Oksman, K. & Sain, M. (2005). Mechanical properties of biodegradable composites from poly lactic acid (PLA) and microcrystalline cellulose (MCC). *Journal of Applied Polymer Science*, 97(5): 2014–2025.
13. Haafiz, M. M. K., Azman Hassan, Zainoha Z., Inuwaa, I. M., Islam, M. S. & Jawaid, M. (2013). Properties of polylactic acid composites reinforced with oil palm biomass microcrystalline cellulose. *Carbohydrate Polymers*, 98(1): 139-145.
14. Sanchez-Garcia, M. D. & Lagaron, J. M. (2010). On the use of plant cellulose nanowhiskers to enhance the barrier properties of polylactic acid. *Cellulose*, *17*(5): 987-1004.
15. Kemala, T., Budianto, E. & Soegiyono, B. (2012). Preparation and characterization of microspheres based on blend of poly (lactic acid) and poly (ε-caprolactone) with poly (vinyl alcohol) as emulsifier. *Arabian Journal of Chemistry*, 5(1): 103-108.
16. Pamula, E., Blazeeicz, M., Paluszkiewiez, C. & Dobrzyǹ, ski. (2001). FTIR study of degradation products of aliphatic polyesters–carbon fibres composites. *Journal of Molecular Structure*, 596(1): 69-75.
17. Qu, P., Goa, Y., Wu, G. F. & Zhang, L. P. (2010). Nanocomposites of poly (lactic acid) reinforced with cellulose nanofibrils. *BioResources*, 5(3): 1811-1823.
18. Donald, G. (2001). A literature review of poly (lactic acid). *Journal of Polymers and the Environment*, 9(2): 63-84.
19. Chen, N. L., Feng, H. X., Guo, J. W., Luo, H. M. & Qiu, J. H. (2011). Biodegradable Poly (lactic Acid)/TDI-Montmorillonite Nanocomposites: Preparation and Characterization. *Advanced Materials Research*, 221: 211-

215.
20. Yew, G. H., Mohd Yusof, A. M., Mohd Ishak, Z. A. & Ishiaku, U. S. (2005). Water absorption and enzymatic degradation of poly (lactic acid)/rice starch composites. *Polymer Degradation and Stability*, 90(3): 488-500.
21. Lee, J., Sun, Q. & Deng, Y. (2008). Nanocomposites from regenerated cellulose and nanoclay. *Journal of Biobased Materials and Bioenergy*, 2(2): 162–168.
22. Wilkinson, A. N., Man, Z., Stanford, J. L., Matikainen, P., Clemens, M. L., Lees, G. C. & Liauw, C. M. (2007). Tensile properties of melt intercalated polyamide 6–Montmorillonite nanocomposites. *Composites Science and Technology*, 67(15): 3360–3368.
23. Yang, K. K., Wang, X. L. & Wang, Y. Z. (2007). Progress in nanocomposite of biodegradable polymer. *Journal of Industrial and Engineering Chemistry*, 13(4): 485–500.
24. Cheng, Q., Wang, S. & Rials, T. G. (2009). Poly (vinyl alcohol) nanocomposites reinforced with cellulose fibrils isolated by high intensity ultrasonication. *Composites Part A: Applied Science and Manufacturing*, *40*(2): 218-224.

The Malaysian Journal of ANALYTICAL SCIENCES ISSN 1394-2506

# EFFECT OF REINFORCED HYBRID PALM SHELLS ON MECHANICAL PROPERTIES OF POLYURETHANE-JUTE WOVEN/VINYL ESTER SANDWICH BOARD

## (Kesan Tenunan Hibrid Biji Kering Kelapa Sawit Terhadap Sifat-sifat Mekanikal Poliuretana-Jute Wooven/Ester Vinil Papan Sandwic)

Teo Siew Cheng, Nurul Ain binti Nanyan, Du Ngoc Uy Lan*, Teh Pei Leng

*School of Materials Engineering,*
*Universiti Malaysia Perlis,Taman Muhibah, Jejawi, 02600 Arau, Perlis,Malaysia*

**Corresponding author: uylan@unimap.edu.my*

**Abstract**

A natural fiber sandwich was constructed from palm shells/polyurethane core and jute woven/vinyl ester facesheets by the in-situ sandwich process (core and panel prepared simultaneously). The polyurethane sandwich core was reinforced by hybrid shell systems of dried palm shell (DPS) and palm kernel shell (PKS) (50P-50D, 25P-75D), and single shell system of PKS (100P) as well as 20phr empty fruit bunch (EFB) based on hundred part of polyurethane. The sandwich facesheets are prepared by using two jute woven layers and impregnated by vinyl ester. Interlocking between DPS and polyurethane matrix was formed, which hence enhanced the mechanical properties. The interfacial adhesion between DPS, PKS, and EFB with the polyurethane binder played the important role to achieve high mechanical properties. It was found that hybrid shells exhibited high reinforcement for sandwich's performance resulting better compression (50P-50D) and flexural (25P-75D) properties. The single shell 100P showed only improvement on flexural modulus.The fracture surface morphology of sandwich under mechanical test was performed by using optical microscopy.

**Keywords**: Interlocking, sandwich, palm shell, empty fruit bunch, jute woven

**Abstrak**

Sandwic serat semula jadi telah dibina dari biji kering kelapa sawit/ poliuretana teras dan jute anyaman /ester vinil melalui proses sandwic *in-situ* (bahagian teras dan lapisan luar disediakan pada masa yang sama). Sandwich teras poliuretana telah diperkukuhkan oleh sistem biji hibrid biji kering kelapa sawit (DPS) dan biji kelapa sawit (PKS) (50P-50D, 25P-75D), dan sistem biji tunggal PKS (100P) serta tandan buah kosong kelapa sawit (EFB) sebanyak 20phr berdasarkan bahagian per seratus poliuretena . The panel sandwich disediakan dengan menggunakan dua lapisan jute anyaman dan diimpregnat oleh vinil ester. Saling cantum antara DPS dan matriks poliuretana telah dibentuk, dimana sifat-sifat mekanikal telah dipertingkatkan. Pelekatan antaramuka antara DPS, PKS, dan EFB dengan pengikat poliuretana memainkan peranan penting untuk mencapai sifat-sifat mekanikal yang tinggi. Didapati bahawa hibrid biji menunjukkan pengukuhan yang tinggi bagi prestasi sandwich yang mengakibatkan sifat mampatan yang lebih baik (50P-50D) dan juga peningkatan dalam sifat-sifat kelenturan (25P-75D). 100P biji tunggal hanya menunjukkan peningkatan pada modulus kelenturan. Morfologi permukaan patah sandwic selepas ujian mekanikal telah dilakukan dengan menggunakan mikroskop optik.

**Kata kunci**: *Interlocking*, sandwic, biji kering kelapa sawit, tandan buah kosong kelapa sawit, jute wooven

## Introduction

Composite sandwiches fabricated from two thin and stiff surface facesheets with a lightweight and thick core have been widely used in the automotive, aerospace, land transport, marine and civil construction industrial applications. Their advantages from such applications are high specific bending stiffness, strength under distributed loads and good energy-absorbing capacity [1,2]. The behavior of sandwich board depends on the properties of core material, especially under mechanical loading. The flexibility of sandwich construction allows innovative structural developments and it is important to choose high-quality core material in the optimal design of sandwich board [2-4].

The sandwich core must provide the structure stiffness in the transverse direction in order to prevent the delamination of facesheets over each other. Honeycomb core architectures have been widely used in aerospace application and the major disadvantage is the water trapping in the hexagonal cells of the honeycomb, which corrodes the core material [5]**.** Besides, defection can be occurred easily during manufacturing or in-service conditions due to debonding at the small adhesive area between honeycomb cells and facesheets [6]. Balsa core is another type of sandwich wood core, which can provide good mechanical properties and can be processed with a lot of sandwich manufacturing techniques. However, balsa wood experience problems in water ingress which is important for penetrations through tank bulkheads or outer shells in marine application.In present,palm oil mills produce crude palm oil as their main product, and some residue such as mesocarp fibre, PKS and empty fruit bunch (EFB) [7]. The palm oil industry has to dispose of approximately 1.1 tons of EFB per every ton of palm oil produced [8]. This biomass is traditionally used as a thermal energy sources for boilers to provide process steam and to produce electricity [9]. Problems are associated with the burning of these solid fuels, about 5% by weight of ash was collected and stockpiled in open field have caused light particles of ash are easily carried away by the wind, resulting in smog and thus it had negative impact on environment [10].

Palm fruit loosens naturally off the bunches and falls on the palm fields, after drying naturally and then the mesocarp is peeled off, with the resulting waste product referred to as dried palm shell (DPS), which is considered as a natural macro-cenosphere due to elliptical shape and empty core (as seen in Figure 1a). The shell has high potential to be used as reinforcement shell for sandwich core. Moreover, binder could flow into DPS's core and form a macro interlock, which results in high mechanical properties. This research also chooses jute fibres to reinforce the panel of the sandwich, because it has 64.4% cellulose content and possess superior mechanical properties [11]. The potential to use recycled jute fibers is made possible by the rapid expansion of coffee industry with a 7% annual growth rate in restaurant industry [12]. This preliminary study centered on the effect of different contour of palm shell (spherical and flaky) on the mechanical properties (flatwise compression and three point bending).The economic utilization oil palm waste material as reinforced filler in sandwich core not only can reduce the environmental issue but exploit the possible value of palm shells for sandwich industry.

## Materials and Methods

### Materials

Polyol (PEG 400) and 4, 4 methylenebis (phenyl isocyanate) were obtained from Maskimi Polyol Sdn. Bhd, Selangor, Malaysia. Dried palm shell (DPS) from the Kepala Batas plantation in Penang with a diameter from 15 mm to 20 mm and a bulk density of 0.85 $gcm^{-3}$ (The shells are sealed their surface hold and measured byElectronic Densimeter MD-300S). Relative density of DPS is 1.4345 $gcm^{-3}$obtained by using Pynometer (Micromeritics Ltd, AccuPyc 1330). Empty fruit bunch (EFB) with a length ranging from 600 µm to 2.98 mm and palm kernel shells (PKS) with a density of 0.65 $gcm^{-3}$ were obtained from DST Technology Sdn. Bhd., These materials were used for core preparation. The vinyl ester jute woven (VEJW) panel was prepared using vinyl ester and methyl ethyl ketone peroxide (MEKP), which were obtained from PT. Kawaguchi Kimia Indonesia. Jute woven (JW) obtained from waste jute bags used for vegetable packaging and was washed and dried before use.

### Sandwich preparation

A wooden mould with dimensions of 260 mm × 220 mm × 25 mm was used, and was covered with a polypropylene film for demoulding. Two ply jute woven (JW) were placed inquasi isotropic arrangement in the mould.The mixture of DPS/PKS and EFB fibre was arranged into the mould. Polyol and MDI (1:1) were mixed at 250 rpm for 1 min using a stirrer and then cast into the palm shells and EFB. Lastly, the other two ply JW were place on the top of palm shell-EFB mixture. The mould was closed with a polypropylene film covered-steel plate and pressed at room temperature for 24 hours. The board was demoulded and the overflow of PU foam was trimmed.For facesheets finishing, mixture of vinyl ester resin and MEKP in the ratio 100:3 (stirring at 400 rpm for 1 min) was impregnated to the JW surfaceby hand lay-up method. The sandwich boards were allowed to cure at room temperature for 24 hours before testing. Table 1 represents the composition sandwich core; single shell system 100P was compared to hybrid palm shell system, 50P-50D and 25P-75D. It is noted that the volume fraction of hybrid system was below 50% compared to single system. This was due to the different size and density of PKS and DPS. Flaky PKS is the by-products after oil extraction using compression method, hence, PKS has smaller size, thinner wall, and lower density compared to DPS, which was used directly without any prior processing.

Table 1. Composition palm shell/polyurethane sandwich core

| Palm shells blend ratio | PKS (% by weight) | DPS (% by weight) | Palm shell volume fraction, vol % | Palm shells content | PU content | Core Density |
|---|---|---|---|---|---|---|
| 100P | 100 | 0 | 48.55 | 75wt% | 25wt% | 0.4295 |
| 50P-50D | 50 | 50 | 42.84 | | | 0.4272 |
| 25P-75D | 25 | 75 | 40.00 | | | 0.4213 |

*EFB was used 20 phr for all recipes, which is part per hundred weights of PU and MDI
*wt%=weight percent based on total weight of sandwich core

**Mechanical characterization**

A three point bending test was performed in accordance with ASTM C 393. Flexural specimens of sandwich (26 mm in thickness) were cut with bandsaw to the dimensions of 220 mm × 50 mm. A flat compression test was conducted according to ASTM C 365-11a with sandwich specimens of 50 mm × 50 mm × 26 mm. Five replicate specimens were tested in each test with a displacement rate of 5 mm/min.

## Results and Discussion

**Interlocking observation**

The interlocking between DPS and PU binder were formed in the sandwich system as depicted in Figure 1 (b). The cenospherical shape of DPS induces the formation of PU inside the DPS empty core so interlocking was obtained. There are two shell systems, sandwich 100P composed of single type of shell and hybrid shell DPS and PKS such as 50P-50D and 25P-50D. The cross surface of 50P-50D sandwich was shown in Figure 1 (c), which presented the distribution of palm kernel shells in sandwich core. Shell structure and volume have a significant influence on sandwich mechanical properties. In term of same weight percent, PKS has higher volume compared to DPS due to low density.In comparison, a single shell of DPS is stronger than PKS due to the cenospherical structure as well as the interlocking formation.

**Flexural properties of PU sandwich board**

Flexural strength and modulus of the sandwich are shown in Table 2 and depicted in Figure 2. The flexural strength of sandwich was enhanced by the increase of DPS ratio in DPS/PKS hybrid. Besides, single shell system of 100P exhibited quite similar flexural strength to 25P-75D. During flexural loading, the upper VEJW panel of the PU sandwich sample is undercompression, the lower VEJW panel is under tension and the palm shell-EFB core is under shear. Therefore, it could be said that one of the most important properties of a reinforced core are shear strength and stiffness. The VEJW facesheets are subjected to compression/tension and are largely responsible for the strength of the PU sandwich board [14]. Three points bending test more focus on localized load at roller transferring throughout the specimen [15]. Therefore, the interfacial adhesion between PU binder and palms shells (DPS/PKS) in sandwich system is a main factor imparts on flexural.

Table 2. Mechanical properties of PU sandwich board with 20phr EFB

| PU Sandwich | Flexural strength, Mpa | Flexural modulus, Mpa | Compression strength, MPa | Compression modulus, MPa |
|---|---|---|---|---|
| 100P | 2.826 | 97.907 | 5.580 | 28.360 |
| 50P-50D | 2.195 | 29.827 | 12.839 | 68.013 |
| 25P-75D | 2.865 | 24.517 | 9.654 | 45.353 |

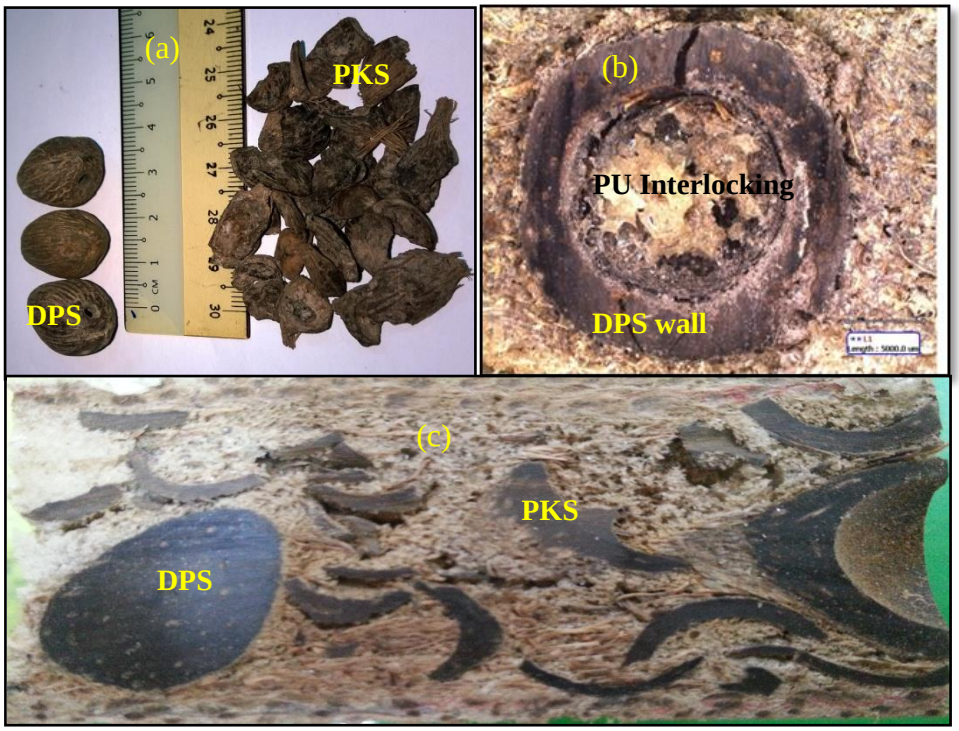



Figure 1. (a)The natural spherical shape of DPS and the flaky irregularly shape of PKS, (b) the cross section of interlocking between DPS and PU, (c) cross surface50P-50Dsandwich [13].

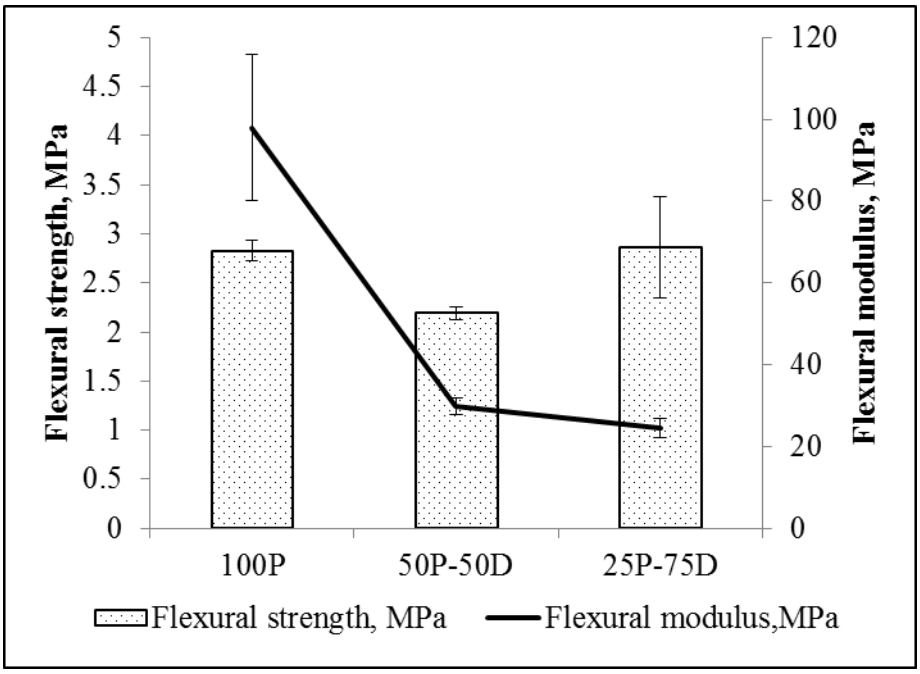



Figure 2. The effect of palm shell blend ratio on flexural properties of PU sandwich

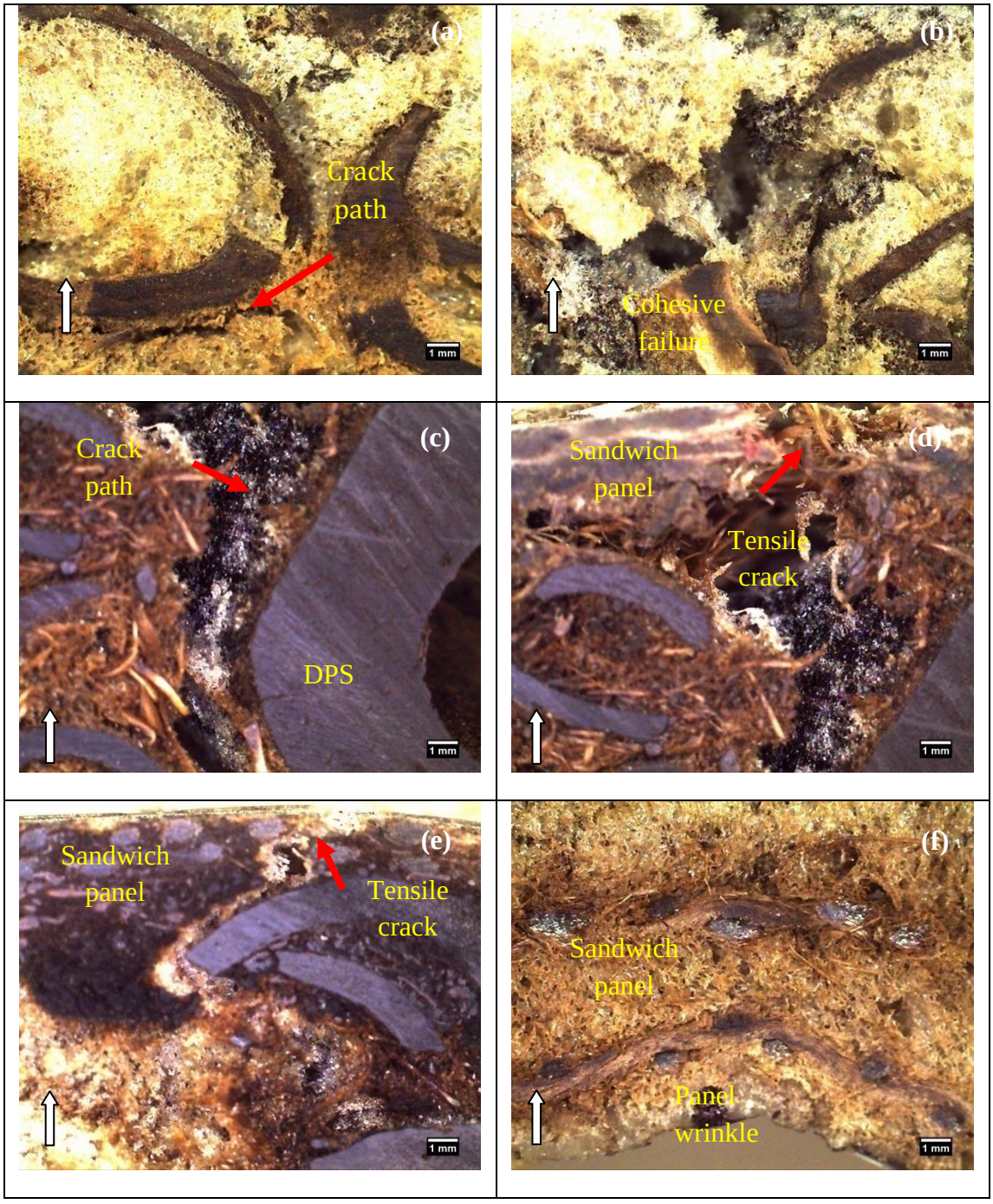



Figure 3. Fracture deformations of PU sandwiches after flexural test (a) Sandwich 100P: Crack path deflects by PKS; (b) Sandwich 100P: Shear core failure; (c) Sandwich 50P-50D: Crack path deflects by DPS caused cohesive failure; (d) Sandwich 50P-50D: Fractured of JWVE panel due to tensile crack; (e) Sandwich 25P-75D: Crack path from tensile crack deflect by PKS; (f) Sandwich 25P-75D: Panel wrinkle at loading roller; ⇑ : Flexure load direction

Flexural modulus depend not only on the hybrid composition, but also inpalm shell positions of in the core. A spherical shell of DPS could cause the sandwich be initially bent easier compared to the irregular shape of PKS under the localized load applied from the flexural rollers. More PKS dispersed throughout the samples due to its higher volume of the lighter density compared to DPS was also produced larger interface area so that the modulus of sandwich 100P was enhanced. A similar result was also founded in the modulus of 50P-50D over that of 25P-75D in hybrid shell system but with a slight effect.

In sandwich 100P, the large quantities of PKS allowed well connected with each other so that the bending load could transfer well. The arrangement of PKS with across each other entrapping PU binder between themselves has also imparted to the flexural strength. PKS in sandwich core are important in reflection of the crack path from its original path to increase the flexural strength as shown in Figure 3(a).In addition, high shear stresses are given across the core of the sandwich 100P and once the sandwich board failed by core shear, all the forces transfer to the bottom panel. The bottom panel carried the built up load and deflection and finally, it was failed, leading debonding occurred at the bottom panel as shown in Figure 3(b) [16,17].

In hybrid shell sandwich board, considerable interlocking formed between PU binder and DPS could enhance the strength of sandwich. This explains the higher flexural strength of sandwich 25P-75D than that of sandwich 50D-50P. However, both sandwiches 25P-75D and 50P-50D have common failure that is tensile crack occurred middle of the bottom VEJW panel as shown in Figures 3(c), (d) and Figures 3(e), (f) respectively. This is because of the applied stress exceeds the yield strength or buckling strength, the tensile panel or compressive panel will fail proving a good bond between facesheets and core in the sandwich [3].

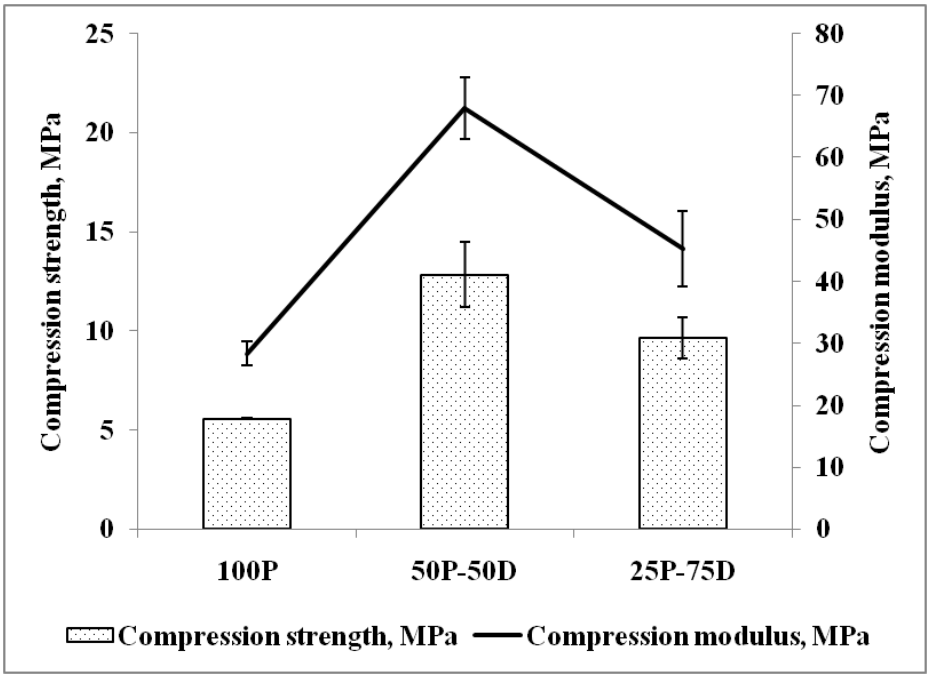



Figure 4. The compression strength and modulus of PU sandwich boards with different palm shell blend ratio

**Compression properties of PU sandwich board**

In terms of axial compressive load applied on PU sandwiches, sandwich 100P exhibited lower compressive strength compared to hybrid shell sandwiches 50P-50D and 25P-75D as depicted in Figure 4. These results are different from flexural results. The behaviour of sandwich 100P may be attributed to the intrinsic properties of PKS under compressive load. PKS was obtained after kernel extraction. Since PKS underwent mechanical pressing and crushed into irregular semi-ellipse shape, so PKS are weak compared to DPS, which does not bear any mechanical process before proven by DPS crystal structure morphology as shown in Figure 5. Furthermore, weak PU binder imparts common cohesive failure (Figure 6(a)) and bulking of sandwich core at the edge of sandwich are common failure in sandwich 100P. Significant improvement in compression strength was found in hybrid shell sandwich system. The enhancement was contributed from the intrinsically cenospherical structure of DPS. Naturally ellipse morphology is considered as the perfect shape in compressive resistance.However, more DPS does not enhance the compression resistance, where sandwich 50P-50D performed better compressive strength than sandwich 25P-75D. The reason could be originated from better shell arrangement based on the equivalent blend ratio of DPS and PKS, which is important in compression resistance as shown in Figure 6(b). DPS with presence of PU interlocking cracked under compression load at the edge of sandwich as shown in Figure 6(c). PU interlocking formed in DPS is damaged by the crack propagated while the DPS shell wall was ruptured by compression load. Sandwich with 25P-75D with large amounts of DPS contents confer crushed down of the DPS and the pullout of DPS shell at the cutting edge of 25P-75D sample as shown in Figure 6(d).

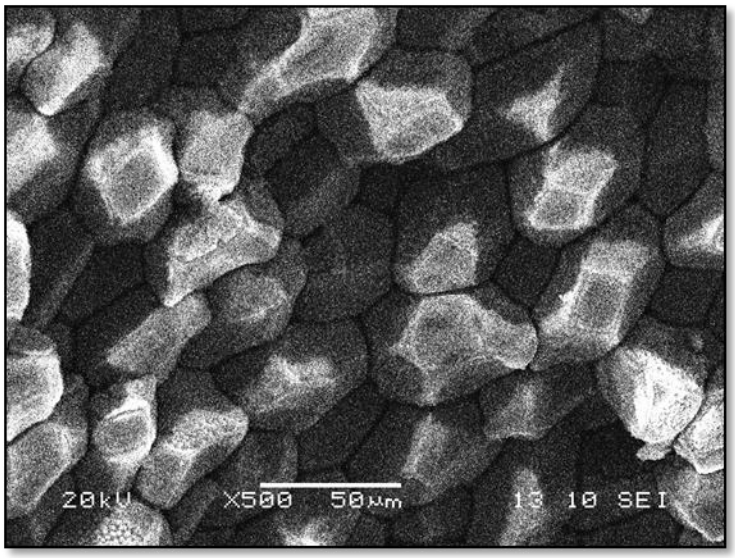



Figure 5. The crystalline arrangement morphologyof DPS wall exhibits strong mechanical properties

Correspondingly, compression modulus can be related to the stiffness of PU sandwich. Sandwich 50P-50D has highest compression modulus;this can be attributed to the equivalent blend ratio of DPS and PKS in sandwich core. The result is in agreement with flexural modulus. Based on the volume fraction of palm shell as tabulated in Table 1, sandwich 50P-50D has a large interfacial area than sandwich 25P-75D due to PKS content in sandwich core, which played important role in load transfer to strong DPS. Large quantitiesof PKS in sandwich 100P could cause inadequate of wetting of PKS and EFB by PU binder in sandwich core, thus100P sandwich performed a poor modulus compared to that of hybrid sandwich.

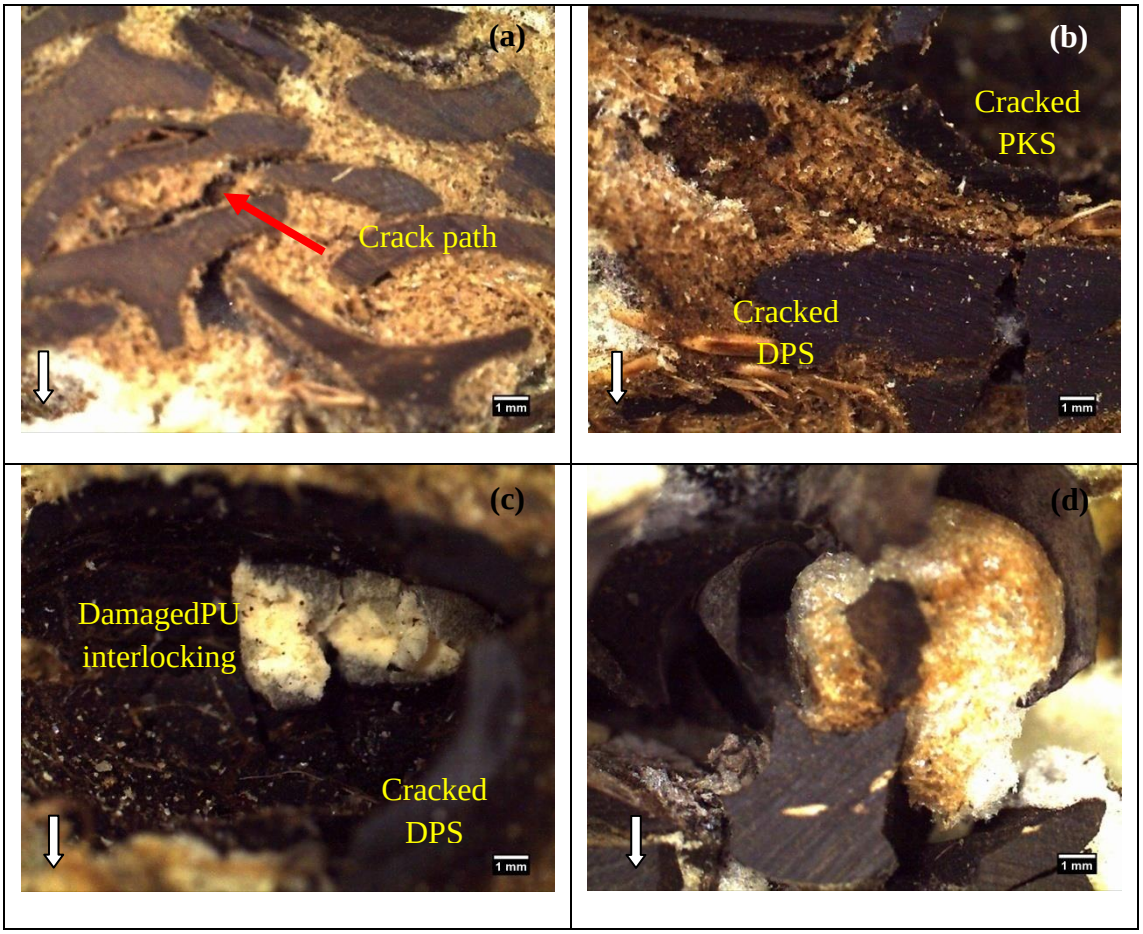



Figure 6. Fracture surfaces of PU sandwiches after compression test (a) Sandwich 100P: cohesive failure; (b) Sandwich 50P-50D: Crushed DPS and PKS; (c) Sandwich 50P-50D: PU Interlocking formed inside DPS; (d) Sandwich 25P-75D: Damaged PU interlocking in crushed DPS; ⇓ : Compression load direction

## Conclusion

Hybrid shell system imparts higher mechanical properties than a single shell system proven by the results of flexural strength of sandwich 25P-75D and compression strength of sandwich 50D50P. In the hybrid system, the blend ratio of DPS and PKS showed a significant effect on the stiffness of sandwich board due to the interlocking, crystal structure of the DPS's shell wall and the volume fraction of palm shell. Different deformation patterns are also observed depending on the interaction of PU binder with DPS, PKS and EFB. In details, the crack propagation occurred through the PU binder and caused cohesive failure between palm shells, while interlocking formation deflect the crack path was also observed. PKS was crushed under flexural and compression load. DPS tends to be cracked and crushed down under axial compression load, but maintain the sandwich's strength, which is considered as densification.

## Acknowledgement

The researchers would like to thank the Minister of Higher Education, Malaysia for providing the Fundamental Research Grant Scheme (FRGS) 9003-00326 that made this work possible.

**References**


1. Fleck, N.A. and Sridhar, I. (2002). End compression of sandwich columns. *Compos. Part A. Appl. Sci. Manuf.* 33: 353-359.
2. Yu, J.L., Wang, E.H., Li, J.R. and Zheng, Z.J. (2008). Static and low-velocity impact behavior of sandwich beams with closed-cell aluminum-foam core in three-point bending. *Int. J. Impact. Eng*. 35: 885–894.
3. Manalo, A.C., Aravinthan, T. and Karunasena, W. (2010). Flexural behaviour of glue-laminated fibre composite sandwich beams. *Compos. Struct*. 92: 2703–2711.
4. Daniel, I. M. (2009). Influence of core properties on the failure of composite sandwich beams *J. Mech. Mater. Struct*. 4(7-8): 1271-128.
5. Belouettar, S., Abbadi, A., Azari, Z., Belouettar, P. and Freres, P. (2009). Experimental Investigation of Static and Fatigue Behaviour of Composites Honeycomb Materials Using Four Point Bending Tests. *Compos. Struct*. 87(3): 265-273.
6. Burlayenko, N.V., Sadowski, T. (2009). Analysis of structural performance of aluminum sandwich plates with foam-filled hexagonal honeycomb core. *Comput. Mater. Sci*. 45(3): 658–662.
7. Husain, Z., Zainac, Z. and Abdullah Z. (2002). Briquetting of palm fibre and shell from the processing of palm nuts to palm oil. *Biomass. Bioener*.22: 505-509.
8. Karina, M., Onggo, H., Dawam Abudullah, A.H. and Syampurwadi, A. (2008). Effect of oil palm empty fruit bunch fiber on the physical and mechanical properties of fiber glass reinforced polyester resin composites. *J. Biol Sci*, 8(1):101-106.
9. Konsomboon, S., Pipatmanomai, S., Madhiyanon, T. and Tia, S. (2011). Effect of kaolin addition on ash characteristics of palm empty fruit bunch (EFB) upon combustion. *Appl. Energy*. 88(1): 298–305.
10. Tay, J.-H. (1991). Complete reclamation of oil palm wastes. *Resour. Conserv. Recy.* 5:383-392.
11. Bledzki, A.K. and Gassan, J. (1999). Composites reinforced with cellulose based fibres.*Prog. Polym. Sci.* 24: 221–274.
12. Du, Y., Yan, N. and Kortschot, M.T. 2012. Light-weight honeycomb core sandwich panels containing biofiber-reinforced thermoset polymer composite skins: Fabrication and evaluation.*Compos. Part B.* Eng. 43(7): 2875–2882.
13. Du, N.U.L. (2014). Malaysia Patent No.PI 2014700124. Selangor, Pintas IP Group Sdn.Bhd.
14. Jawid, M., Abdul Khalil, H.P.S. and Abu Bakar, A.( 2010). Mechanical performance of oil palm empty fruit bunches/jute fibres reinforced epoxy hybrid composites. *J. Mater. Sci. Eng. A.* 527: 7944-7949.
15. Feraboli, F. and Keyward, K.T. (2003). Four-point bend interlaminar shear testing of uni- and multi-directional carbon/epoxy composite systems. *Compos. Part A. Appl. Sci. Manuf*. 34(12): 1265-1271.
16. McCormack, T.M., Miller, R., Kesler, O. and Gibson, L.J. (2001). Failure of sandwich beams with metallic foam cores. *Int. J. Solids. Struct.* 38, 4901-4920
17. Awad, Z.K., Aravinthan, T. and Manalo, A. (2012). Geometry effect on the behaviour of single and glue-laminated glass fibre reinforced polymer composite sandwich beams loaded in four-point bending *Mater. Des*. 39: 93-103.

The Malaysian Journal of ANALYTICAL SCIENCES ISSN 1394-2506

# EFFECTS OF USING DIFFERENT HEALING AGENTS ON HEALING EFFICIENCY IN SOLID STATE SELF-HEALING SYSTEM

## (Kesan menggunakan Agen Pemulihan Berbeza ke atas Keberkesanan Pemulihan Sistem Swa-Pemulihan Keadaan Pepejal)

N. N Muhamad[1]*, S. M. Makenan[1], M. J. Mohd Suzeren[1], S. Abdullah[2], M.A.S Mat Lazim[1]

[1]*School of Chemical Science and Food Technology, Faculty of Science and Technology*
[2]*Department of Mechanical & Materials, Faculty of Engineering and Architecture Engineering*
*Universiti Kebangsaan Malaysia, 43600 UKM Bangi, Selangor, Malaysia*

**Corresponding author: msuzeren@gmail.com*

**Abstract**

Self-healing polymers possess the ability to heal in response to damage using resources inherently available to the system. The solid-state self-healing system was obtained by blending thermoplastic polymers into epoxy resin matrix. This study aimed to investigate the effect of polymer healing efficiency by using different thermoplastic polymers as healing agents which were poly (bisphenol-A-co-epichlorohydrin) (PDGEBA), polypropylene (PP) and polyethylene (PE). The bonding formed in the epoxy resins were characterized by means of Fourier transform infrared spectroscopy (FTIR). Healing was achieved by heating the fractured specimen to a specific temperature, above their glass transition temperature (Tg) to mobilize the polymeric chains of the healing agent. The Tg for each specimen was obtained from dynamic mechanical analysis (DMA). From the Izod impact test it was found that healable resin with PDGEBA has the highest healing efficiency followed by PP and PE, with 63%, 31% and 24% of average percentage healing efficiencies, respectively. These results were due to the different solubility parameters of the thermoset/network and thermoplastic polymer which led to the phase separation. The morphological properties and the fracture-healing process of the resins were then observed using optical microscope.

**Keywords:** Solid state self-healing; different healing agent; healing efficiency; impact test

**Abstrak**

Swa-pemulihan polimer memiliki keupayaan untuk memulihkan kerosakan menggunakan sumber yang telah tersedia di dalam sistem tersebut. Sistem swa-pemulihan keadaan pepejal disediakan dengan mengadunkan polimer termoplastik ke dalam matriks resin epoksi. Dalam kajian ini, kesan keberkesanan pemulihan telah dikaji dengan menggunakan polimer termoplastik yang berbeza sebagai agen pemulihan iaitu poli(bisfenol-A-ko-epiklorohidrin) (PDGEBA), polipropilena (PP) dan polietilena (PE). Pencirian ikatan yang terbentuk dalam resin epoksi telah dijalankan menggunakan spektroskopi inframerah (FTIR) Pemulihan telah dicapai dengan memanaskan spesimen yang patah menggunakan suhu spesifik, iaitu suhu di atas suhu peralihan kaca (Tg) matriks resin bagi membolehkan rantai polimer agen pemulihan bergerak. Suhu peralihan kaca bagi setiap spesimen telah diperolehi dari analisis mekanikal dinamik (DMA) Hasil daripada ujian hentaman Izod, resin pemulihan dengan agen pemulihan PDGEBA menunjukkan keberkesanan pemulihan yang tertinggi diikuti dengan agen pemulihan PP dan PE, dengan masing-masing memiliki purata peratusan keberkesanan pemulihan 63%, 31% dan 24%. Hasil ini adalah disebabkan oleh perbezaan parameter kelarutan polimer termoset dan termoplastik yang membawa kepada pemisahan fasa. Pencirian morfologi dan proses patah-pemulihan kemudiannnya dikaji menggunakan mikroskop optik.

**Kata kunci:** Swa-pemulihan keadaan pepejal; agen pemulihan berbeza; keberkesanan pemulihan; ujian impak

## Introduction

Polymers and structural composites are used in a variety of applications, which include transport vehicles, civil engineering, and electronics [1]. However, these polymeric materials are susceptible to damage in the form of cracking or micro cracking deep within the structure where detection and external intervention are difficult or impossible, resulting in a significant shortening of the service lifetime [1].

In response, the concept of self-healing polymeric materials was proposed in 1980s by [2] as a mean of healing invisible micro cracks. This self-healing concept is taken to be where the concept or basic mechanism of self-healing has been inspired by mimicking the biological systems [3]. A number of self-healing techniques have been employed to prepare self-healing materials. In early work by Dry [4], hollow fibers filled with reactive liquids were embedded in concrete. The concrete ruptured on failure and filled cracks to cause strength recovery. In different technique, White, Sottos [5] developed polymer composites that heal autonomously. In these systems, microcapsules filled with monomers are dispersed within a catalyst-containing matrix. Upon failure, the microcapsules rupture, releasing monomers that fill the crack site and react when exposed to the catalyst particles. Both mentioned techniques have demonstrated the design of systems that can heal autonomously at least once. However, the need to develop materials that can heal multiple times without substantial loss in strength is proven because once the filled inclusions are ruptured, the healing agent is depleted, leading to only a singular local healing event.

To date, new approaches have been demonstrated show promise as continuously rehealable material systems; intrinsic healing polymers [6, 7]. For intrinsic systems, the matrix is inherently self-healing, and sequestration of healing agents is no longer required, avoiding many of the problems with integration and healing-agent compatibility that arise in vascular and capsule-based self-healing materials [8]. However this system need an external stimulus; heat for healing occurred [1]. These systems rely on chain mobility and entanglement, reversible polymerizations, melting of thermoplastic phases, hydrogen bonding, or ionic interactions to initiate self-healing because each of these reactions is reversible, multiple healing events are possible. A solid-state healable system via the incorporation of linear polymer chains [9] was identified as an alternative technology for intrinsic system. This system employs a thermosetting resin as a matrix of which a thermoplastic is dissolved. In this system a linear polymer should be bonded into epoxy matrix through hydrogen bonding. Upon giving a stimulus, the hydrogen bonding would break allowed the linear polymer material mobilize and diffuse through the thermosetting matrix, with some chains bridging closing the cracks and thereby facilitating healing. Kim and Wool [10] also proposed a microscopic theory on the basis of the "Reptation model"; proposed by de Gennes [11] that describes the diffusion and randomization in polymer-polymer crack interfaces for strength recovery (Figure 1).

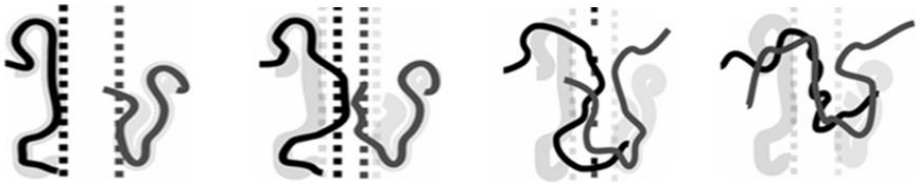



Figure 1. Schematic illustration of mechanisms involved in self-healing via molecular interdiffusion based on (a) Rearrangement of surface approach; (b) Wetting of the surface; (c) Low level diffusion between surface; and (d) Diffusion, equilibration and randomization process [1]

The work reported herein represents the crack-healing study of new linear polymers as healing agents in solid state self-healing using standard epoxy. The efficiency for healing damage of the healable resin of each linear polymer was examined.

## Materials and Methods

### Assessment of Matrix Healing Through Impact Testing

Testing of the ability of the matrix to heal was carried out using Izod impact testing machine, manual clamping vice with a specimen adapter for ASTM D256 (Standard Test Method for Determining the Izod Pendulum Impact Resistance of Plastics). Specimens have being prepared with the dimensions 64 mm x 13 mm x 4 mm. The specimens were lightly polished ensuring a regular rectangular shape. A notch was introduced using a motorized

notching cutter (Ray-Ran). This cuts a ASTM standard notch (3 mm) in a single pass which was sharp and reproducible. Room temperature Izod impact test was performed using an impact test of Ray-Ran Test Equipment RR/IMT (RR/MT/100).

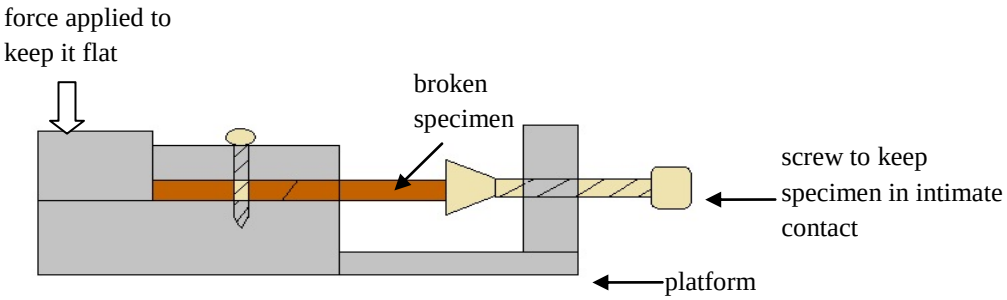



Figure 2. Schematic of the healing platform for the fractured Izod impact specimens

**Under** test, these specimens were fully fractured, with the two halves being immediately relocated and lightly clamped together using the healing platform shown in Figure 2. Gentle pressure was applied to ensure that the faces of the two halves were kept in alignment and intimate contact. The samples were healed at 160˚C for 6 hours. Samples were repeatedly healed and tested throughout the study, to examine the effect of repeated healings on the efficiency of impact strength recovery. Each sample was tested 3 times, making a total of 9 tests at each healing temperature. Considering the qualitative nature of the Izod impact test, the efficiency of impact strength recovery was calculated from the relative impact energies, Equation 1 [12],

$$R_E = \frac{100 \times E_{healed}}{E_{initial}}. \quad (1)$$

where $E_{healed}$ and $E_{initial}$ are the post-healing and initial impact energies, respectively. $R_E$ is the percentage recovery in impact strength. The resin healing efficiency ($H_E$) has been re-estimated from Equation 2, [12], where $R_E$ and $R^{\circ}_E$ are the recovery percentage of healable resin and residual healing effect of reference resin (containing no healing agent) respectively.

$$H_E = R_E - R_E^o \quad (2)$$

**Characterization**

FTIR spectra were recorded with Spectrum ASCII PEDS 400 ATR Spectrometer to determine the functional group in the resin system. All spectra were recorded at room temperature with the infrared spectra range of 4000 - 650 $cm^1$. Dynamical mechanical thermal analysis (DMTA) was performed on a TA Instruments Thermal Analysis DMA 2980 Dynamic Mechanical Analyzer operating in the single cantilever-bending mode at an oscillation frequency of 1Hz. Data were collected from room temperature to 180$^o$C at a scanning rate of 2$^o$C/min. The sample specimens were made in the form of rectangular bars of a nominal 35 mm x 15 mm x 5 mm. The morphology of the sample crack surfaces from Izod impact test were observed using optical range microscopy (Axiolab A45090 Image Analyzer) with Zeiss camera.

## Results and Discussion

**Infrared Analysis**

Interaction between functional group in epoxy resin was determined by infrared spectrum as shown in Figure 3. Throughout all resin system, there were peaks for hydroxyl (–OH) functional group in the range of 3300-3600 $cm^{-1}$ in the spectrum of reference resin (Figure 3b) and healable resins (Figures 3c, 3d, 3e). The peaks are quite broad and clear for almost cases, indicates the presence of hydroxyl group. For Figure 3a, the -OH stretching groups observed

at 3500 $cm^{-1}$ for DGEBA spectrum is due to the the presence of dimers or high molecular weight species [13]. The existence of hydroxyl groups in healable resins are very importance to introduce the self-healing mechanism at crack surface through hydrogen bonding physically. The reaction between anhydride and epoxy group was found in reference and healable resins. This reaction produced ester group with clear peak at 1730$cm^{-1}$. Due to the opening of epoxy ring from curing process, the reduction in the intensity of the epoxy ring band at 910$cm^{-1}$ was observed. The band at 915$cm^{-1}$ is assigned to the asymmetric stretching vibration of C-O-C (epoxy ring).

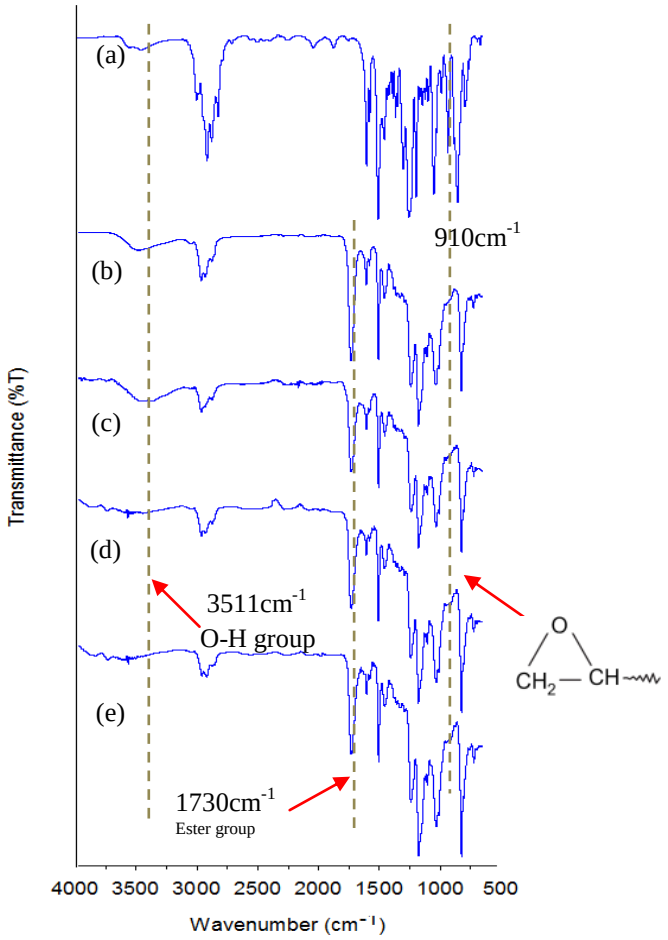



Figure 3. FTIR spectra of (a) DGEBA (b) reference resin, (c) healable resin containing PDGEBA, (d) healable resincontaining polypropylene and (e)healable resin containing polyethylene

**Glass Transition Temperature (*Tg*)**

The glass transition temperature (*Tg*) of reference and healable resins were determined by dynamic mechanical thermal analysis (DMTA). Figure 4 shows the DMTA curves for the reference and healable resins. The *Tg* for reference resin (DGEBA resin) appeared at 139˚C while for healable resins containing PDGEBA, PP and PE are 137˚C, 126˚C and 125˚C respectively. Determination of *Tg* for each sample are important so the minimal healing temperature can be determined. Solubility parameter of the network and thermoplastic polymer is the main factor for optimal repairing damage, which it provides directly indications of their solubility behaviors in the mixture. The solubility parameter of the healing agents and a model of the NMA-cured diglycidylether of bisphenol A were calculated using the group contribution methodology of Hoy [14] from The Hoy Solubility Parameter Software (from Computer Chemistry Consultancy, Germany). The values for polymeric matrix resin with repeat unit is 21.88

$(J/cm^3)^{1/2}$. This value is close to the solubility parameter value of 21.25 $(J/cm^3)^{1/2}$ for healing agent PDGEBA. The traces for reference and healable resins in addition of PDGEBA (Figure 4) are essentially identical demonstrating the solubility of the healing agent thus confirms that by closely matching the linear molecule to the cross-linked network, diffusional healing can be achieved [9]. While for healable resins containing PP and PE, the solubility parameter values are 16.69 $(J/cm^3)^{1/2}$ and 18.01 $(J/cm^3)^{1/2}$ respectively, which these values are slightly different compared to the polymeric matrix resin. The traces for both healable resins evident the incompability of PP and PE as healing agents in matrix. Therefore, linear polymer of PDGEBA has the potential to be soluble in the cured epoxy resins compared to PP and PE.

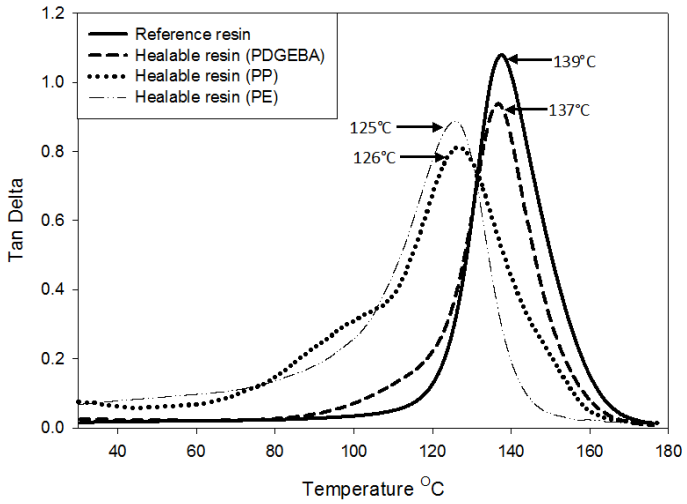



Figure 4. Dynamical mechanical thermal analysis (DMTA) traces for the NMA-cured bisphenol A epoxy resin of reference resin, healable resin containing PDGEBA, healable resin containing PP, and healable resin containing PE

**Healing Efficiency**

The healing efficiency of the resins matrix was investigated using Izod impact testing. Figure 5 shows the percentage recovery ($R_E$) and percentage of healing efficiency ($H_E$) in Izod impact strength after fracture as a function of the varying healing agent calculated from Equation 1 and 2. Data for three impact/heal cycles are shown to reveal the effect of multiple healing events on the healing performance.

Figure 5(a) shows that the reference resin can be thermally healed to a limited extent after 6 h at 160˚C. The graph shows a 19.5% recovery in impact strength for the reference resin after one healing event. The implication is that there is some post-cure of the samples in the curing schedule. To compensate for this, the healing efficiency ($H_E$) of healable resins was calculated using Equation 2. Thus, $H_E$ contribution to healing from the addition of the healing agent can be examined.

Figure 5(b) shows the healing efficiency across the range of varying healing agent. From this graph, it was found that healable resin with PDGEBA has higher healing efficiency followed by PP and PE, with 63%, 31% and 24% of average percentage healing efficiencies, which taken from the average of all three healing cycle. All three healing agents shows maximum healing efficiency of 38-65% with PDGEBA the highest in the first healing cycle followed by PP and PE. Subsequent healing cycles lead to significant healing efficiency in impact strength although at a lower level than for the first cycle, with 63, 23 and 20% for a second healing and with 60, 14 and 13% for the third cycle for each of healable resin. For the second and third healing cycles, it was observed that PDGEBA still achieved the highest healing efficiency followed by PP and PE. However, there are a reduction in the healing efficiency for all specimens especially healable resins of PP and PE after first healing event. These reductions are

possibly due to physical ageing effect. Physical ageing effect of epoxy resin can be explained by the molecular relaxation in which the epoxy network loses the mobility and the free volume during its approach towards the equilibrium glassy state [15, 16]. This effect in self-healing system was also reported by [12], Peterson, Kotthapalli [17]. The full detail study on the physical ageing effect will be explored in the future.

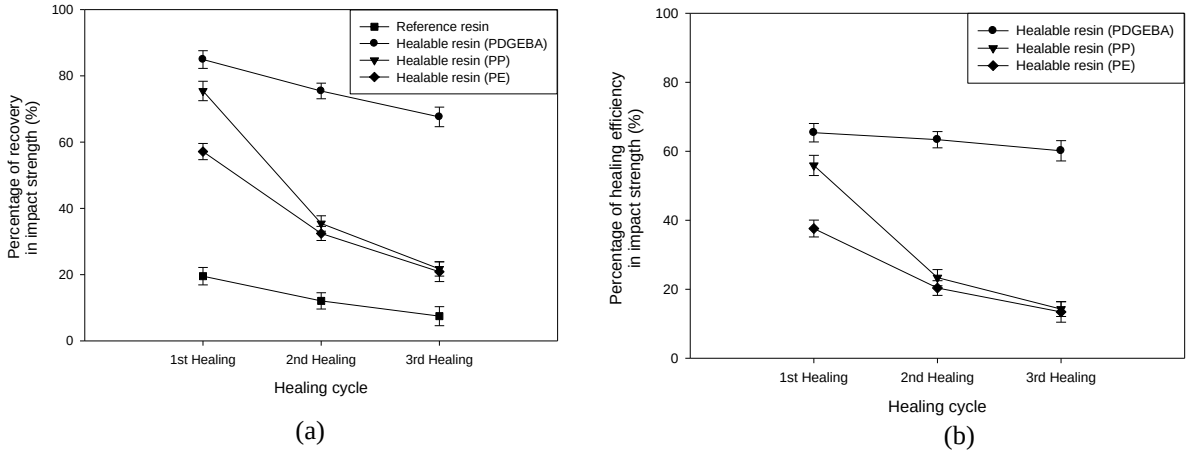



Figure 5. (a) The percentage recovery in Izod impact strength ($R_E$) of epoxy resin (b) The percentage of healing efficiency in Izod impact strength ($H_E$) of epoxy resin

Both Figures 5 (a) and (b) shows that PP and PE have a limited effect on healing efficiency compared to PDGEBA. An explanation could be that the healing agent is not completely dissolved in the thermosetting DGEBA matrix because the solubility parameter value of healing agents are not closely matched to the solubility parameter value of matrix. The solubility parameters are need to be matched so that the 'healing agent' remains uniformly dissolved in the matrix, without phase separation [9].

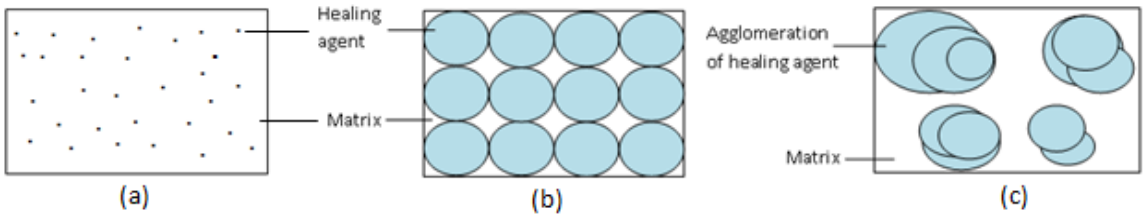



Figure 6. Visualisation of (a) miscible healing agent in matrix, (b) partially dissolved of healing agent in matrix and (c) agglomeration of healing agent in matrix

Healable resin containing PDGEBA as a healing agent shows a miscible system (Figure 6a) where all the PDGEBA dissolved in the resin, while for healable resin containing PP and PE show an immiscible systems where PP and PE were partially dissolved in the matrix. Using Hoy software, it was shown that the solubility parameter value of PP and PE are not matched to the solubility parameter value of the network. The surface morphology obtained (Figure 7 g-l), evident that these healable resins are phase separated as the PP and PE are not miscible to the matrix. Thus it can be postulated that the reduced healing efficiency appears to be due to its immobilization of linear polymer which is attributed from the phase separation.

The difference in solubility parameter also lead to the formation of agglomeration (Figure 6c). Since the mechanism of the healing is believed to be the diffusion of the soluble linear healing agent, it can be postulated that the less thermoplastics miscible with the epoxy, such that there is reduced capacity for molecular scale migration through unoccupied or free volume within the matrix resin for crack closure.

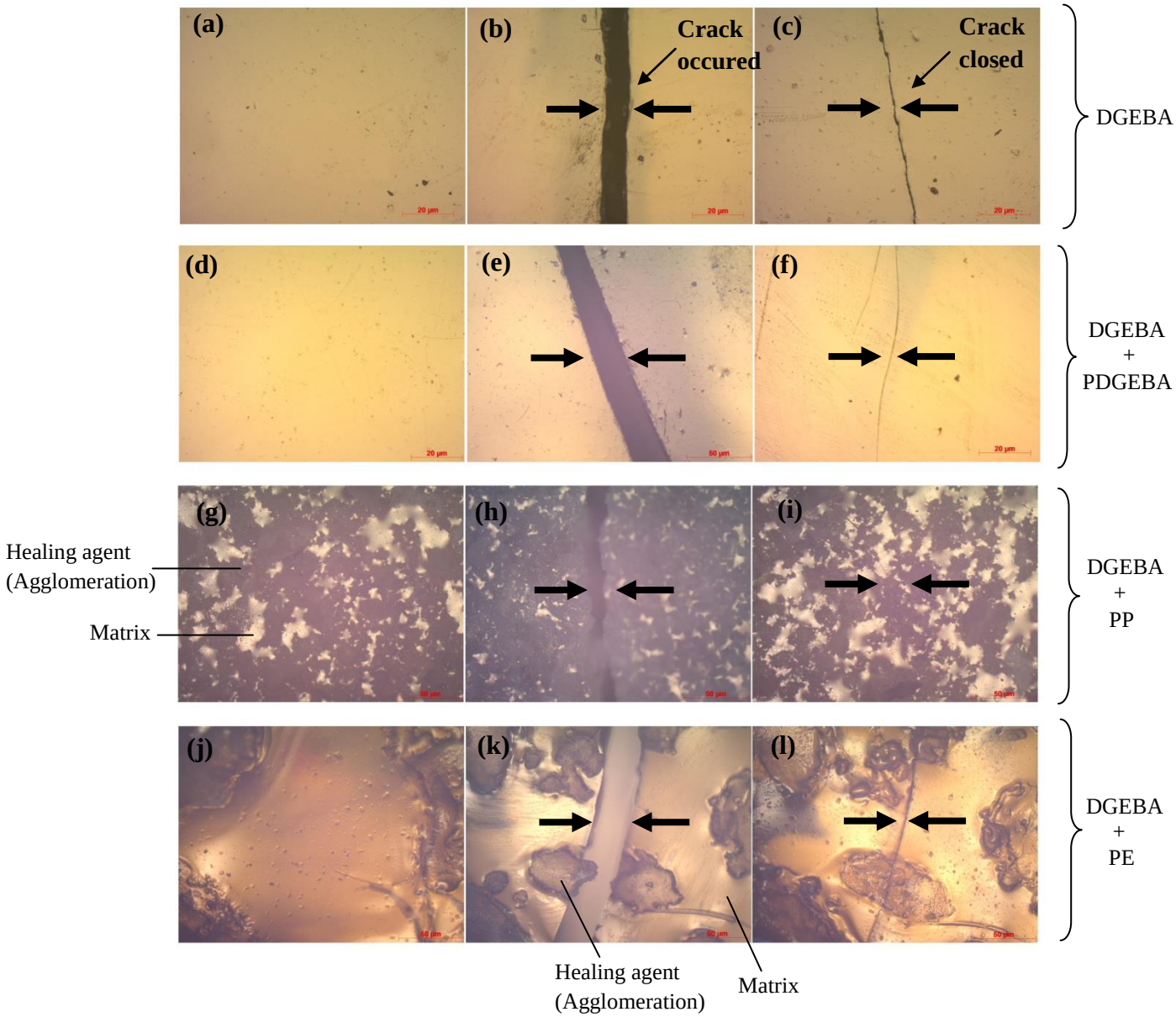



Figure 7. Visualization of the fracture-healing process for reference (a, b, c) and healable resin with PDGEBA (d, e, f), PP (g ,h ,i) and PE (j, k, l). Optical microscopy images of (a, d, g, j) the surface of the sample before fracture, (b, e, h, k) the crack on a completely fractured samples, (c, f, i, l) the cracked surface after thermal mending

The healing capability and the visualization of the fracture-healing process for healable resins were observed through the surface morphology using optical microscopy (Figure 7). The crack in the sample after fracture can be clearly seen in Figures 7 (b, e, h, k) with the magnification of 5x. After healing at $160^0$C for 6h, this crack is apparently healed as shown in Figures 7 (c, f, i, l). This phenomenon can be clearly observed in which the crack has been filled and the two fracture surfaces have been bonded together. The agglomeration and phase separation effect in healable resins of PP and PE also can be clearly verified in Figures 7 (g, h, i, j, k, l).

## Conclusion

The healing efficiency in a matrix resins by using different healing agents, which are PDGEBA, PP and PE is attempted. The addition of the three healing agents to a thermosetting epoxy resin has been shown to be a means of inducing self-healing but at different efficiency. From this study it was shown that PDGEBA is the most effective healing agent compared to PP and PE with 63%, 31% and 24% of average percentage healing efficiencies. The poor healing efficiencies of healable resins containing PP and PE are due to the existence of phase separation which can be clearly seen through the surface morphology study. Since the mechanism of the healing is believed to be the diffusion of the soluble linear healing agent, it can be concluded that there was a definite correlation between the solubility parameter value of the network and the healing agent with the kinetics of diffusion.

## Acknowledgement

The authors acknowledge the financial support of this study by Government of Malaysia through grant number of FRGS/1/2012/SE07/UKM/03/1, GGPM-2012-014 and ERGS/1/2012/TK04/UKM/03/3. The authors also wish to thank the National University of Malaysia for the support of this project.

## References

1. Wu, D. Y., Meure, S., & Solomon, D. (2008). Self-healing polymeric materials: A review of recent developments. *Progress in Polymer Science*, 33 (5): 479-522.
2. Jud, K., Kausch, H. H., & Williams, J. G. (1981). Fracture mechanics studies of crack healing and welding of polymers. *Journal of Materials Science*, 16 (1): 204-210.
3. Trask, R. S., Williams, H. R., & Bond, I. P. (2007). Self-healing polymer composites: mimicking nature to enhance performance. *Bioinspiration & Biomimetics*, 2 (1): 1-12.
4. Dry, C. (1994). Matrix cracking repair and filling using active and passive modes for smart timed release of chemicals from fibers into cement matrices. *Smart Materials and Structures*, 3 (2): 118.
5. White, S. R., Sottos, N. R., Geubelle, P. H., Moore, J. S., Kessler, M. R., Sriram, S. R., Brown, E. N., & Viswanathan, S. (2001). Autonomic healing of polymer composites. *Nature*, 409 (6822): 794-797.
6. Kalista, S. J. & Ward, T. C. (2007). Thermal characteristics of the self-healing response in poly(ethylene-co-methacrylic acid) copolymers. *Journal of The Royal Society Interface*, 4 (13): 405-411.
7. Murphy, E. B. & Wudl, F. (2010). The world of smart healable materials. *Progress in Polymer Science*, 35 (1–2): 223-251.
8. Blaiszik, B. J., Kramer, S. L. B., Olugebefola, S. C., Moore, J. S., Sottos, N. R., & White, S. R. (2010). Self-Healing Polymers and Composites. *Annual Review of Materials Research*, 40: 179 - 211.
9. Hayes, S. A., Jones, F. R., Marshiya, K., & Zhang, W. (2007 a). A self-healing thermosetting composite material. *Composites Part A: Applied Science and Manufacturing*, 38 (4): 1116-1120.
10. Kim, Y. H. & Wool, R. P. (1983). A theory of healing at a polymer-polymer interface. *Macromolecules*, 16 (7): 1115-1120.
11. De Gennes, P. G., *Scaling concepts in polymer physics*. 1979: Cornell university press.
12. Hayes, S. A., Zhang, W., Branthwaite, M., & Jones, F. R. (2007 b). Self-healing of damage in fibre-reinforced polymer-matrix composites. *Journal of The Royal Society Interface*, 4 (13): 381-387.
13. González, M. G., Cabanelas, J. C., & Baselga, J. (2012). Applications of FTIR on Epoxy Resins–Identification, Monitoring the Curing Process, Phase Separation and Water Uptake. *Infrared Spectroscopy–Materials Science, Engineering and Technology*.
14. Hoy, K. (1970). New values of the solubility parameters from vapor pressure data. *Journal of Paint Technology*, 42 (541): 76-118.
15. Hutchinson, J. M. (1995). Physical aging of polymers. *Progress in Polymer Science*, 20 (4): 703-760.

16. Kong, E. S.-W.(1986) *Physical aging in epoxy matrices and composites*, in *Epoxy Resins and Composites IV* Springer:125-171.
17. Peterson, A. M., Kotthapalli, H., Rahmathullah, M. A. M., & Palmese, G. R. (2012). Investigation of interpenetrating polymer networks for self-healing applications. *Composites Science and Technology*, 72 (2): 330-336.

The Malaysian Journal of ANALYTICAL SCIENCES ISSN 1394-2506

# IMPROVEMENT OF MECHANICAL PROPERTIES OF POLY(LACTIC ACID) BY ELASTOMER

## (Penambahbaikkan Sifat Mekanikal Poli(Asid Laktik) Oleh Elastomer)

Penwarat Sennan and Jantrawan Pumchusak*

*Department of Industrial Chemistry, Faculty of Science*
*Chiang Mai University Chiang Mai 50200, Thailand*

**Corresponding author: jantrawan@gmail.com*

**Abstract**

Poly(lactic acid), PLA is a biodegradable thermoplastic that has a limited application due to its brittleness. This study has tried to overcome this weakness by blending polybutadiene (BR) into PLA. In the beginning period of the investigation, the preparation of PLA film with the thickness of less than 0.2 mm was prepared using the solvent casting method. The BR contents of 3, 5, 10 and 20 wt% were investigated. Vibracell sonicator was applied to disperse and lessen the rubber particle size in the PLA matrix. It was found that the elongation at break of the samples improved from 11 % for neat PLA to 39 % by blending with 10 wt%BR. However, tensile strength decreased as the BR contents was increased. SEM imaging revealed that the rubber has played an important role in the increase of sample toughness.

**Keywords**: polylactic acid, polybutadiene, biodegradable

**Abstrak**

Poli(asid laktik) (PLA) merupakan termoplastik biourai yang mempunyai aplikasi yang terhad kerana sifat kerapuhannya. Kajian ini cuba untuk mengatasi kelemahan tersebut dengan mengadunkan polibutadiena (BR) bersama PLA. Pada peringkat awal, penyediaan filem PLA dengan ketebalan kurang daripada 0.2 mm telah disediakan dengan menggunakan kaedah percampuran pelarut. Kandungan BR sebanyak 3, 5, 10 dan 20% berat telah dikaji. Sonikator Vibracell telah digunakan untuk menyebarkan dan seterusnya mengurangkansaiz zarah getah dalam matriks PLA. Kajian mendapati bahawa pemanjangan pada takat putus meningkat daripada 11% untuk matriks PLA kepada 39% untuk adunan yang ditambahkan 10% berat BR. Walau bagaimanapun, kekuatan tensil menurun dengan peningkatan kandungan BR dalam adunan. Pemeriksaan SEM membuktikan bahawa kehadirangetah telah memainkan peranan penting dalam peningkatan keliatan sampel.

**Kata kunci:** poli(asid laktik), polibutadiena, biourai

## Introduction

It is known that environmental problems could cause by plastic bags made from petroleum. As a result, in recent years bioplastics or biopolymer have been of interest to be used to replace plastic. PLA is both bio-based and biocompostable, high strength and stiffness at room temperature that make it promising as a substitute for conventional petroleum-based polymers. However, there are serious limitations, notably brittleness and a low heat distortion temperature [1,2,3]. Several studies have reported to improve the physical and mechanical properties of PLA by blending with other polymers, such as low density poly (ethylene) [4]. poly(propylene glycol) and poly(ethylene glycol). [5,6]. However, most of these blends are incompatible; therefore, compatibilizers are required in order to attain the desired properties. Furthermore, there were some researches focused on the addition of rubber into PLA [7]. Rubber matrices have commonly been used as a second phase polymer to improve the toughness of brittle thermoplastic materials. The rubber particles behave as stress concentrators enhancing the fracture energy absorption of brittle polymers and ultimately result in a material with improved toughness. In order to improve the toughness of polymers, several criteria must be met: the rubber must be distributed as small domains in the polymer matrix; the rubber must have good interfacial adhesion to the polymer [8,9]. Liu reported that small rubber particles lead to increase in the impact strength of the polypropylene (PP) / ethylene-propylene rubber (EPR) blend. They

showed the toughening efficiency of very fine rubber particles [10]. This research aims to prepare PLA film blended with different amount of polybutadiene rubber and Vibracell sonicator was applied to lessen the size of rubber phase in PLA matrix. Mechanical properties especially elongation at break were investigated.

## Materials and Methods

The PLA resin was supplied by NatureWorks®, USA. The selected grade, PLA 2003D (MI = 5-7 g/10 min), is an extrusion grade. Polybutadiene was kindly supplied by Thai Hashi Corporation Co., Ltd. under the trade name of BR-AA or BR-BB (raw Mooney viscosity: ML (1+4) 100 °C). PLA film was prepared in the thickness of less than 0.2 mm by solvent casting method. The PLA resin was dried in a vacuum oven at 80 °C for 4 h to remove moisture before casting. PLA/BR was dissolved in chloroform to obtain a polymer blend solution. The mixtures were stirred at room temperature for 3 h. Moreover, the dispersion of rubber by Vibra-cell sonicator electric power between 150-750 watts was applied for about 1-5 minutes after the mechanical stirring. The blend solution was then casted on the glass plates. The films were dried for about 4 h at room temperature and 4 h at 80 °C in a vacuum dryer to remove the remain solvent. The BR content in the range of 0-20 wt% was studied. The tensile strength, elongation at break and Young's modulus of the PLA films were measured using a Lloyd Instruments LRX testing machine according to the ASTM standard method D882-88. Specimen samples were cut to the size of 10 cm×2.54 cm. Samples were conditioned for 48 h at 23±0.5 ◦C and 50% RH in a constant temperature and humidity chamber before the measurement. Initial grip separation and cross-head speed were set at 5 cm and 12.5 mm/min, respectively. The values presented were the average of five measurements. The surface morphology of the materials was observed using an optical microscope (OM) and scanning electron microscope (SEM). The specimen surfaces for the SEM were sputter coated with gold to avoid charging. The element analyzer was done by energy dispersive x-ray spectrometer (EDS).

## Results and Discussion

### Morphological Properties

The morphologies of the film surfaces were investigated by OM as presented in Figure 1. Neat PLA showed a smooth and uniform surface (Figure 1(a)). Figure 1(b) – (e) show the OM images of PLA/BR blends with 3, 5 10 and 20 wt% of BR, respectively. For these blends, the blend solutions were mechanical stirred at 400 rpm. The rubber droplets were well dispersed in all blends. The image J program was used to analyze the rubber droplet size and found that the rubber droplets were in the average size of 4.80, 4.45, 5.74, and 6.94 micrometer for the 3, 5, 10 and 20 wt% BR blends, respectively (Table 1). The higher rubber content gave the bigger rubber droplets.

Table 1. The rubber droplet size analysis of PLA/BR blends by image J program.

| Time / Watt | Particle size (μm) | | | |
|---|---|---|---|---|
| | **0** | **1** | **3** | **5** |
| 3%BR** | 4.80 | - | - | - |
| 5%BR** | 4.45 | - | - | - |
| 10%BR** | 5.74 | - | - | - |
| 20%BR** | 6.94 | - | - | - |
| 5%BR 150 watt | - | 6.06 | 4.35 | 2.77 |
| 5%BR 350 watt | - | 3.29 | 2.51 | 6.34 |
| 5%BR 650 watt | - | 1.40 | 1.21 | 1.33 |

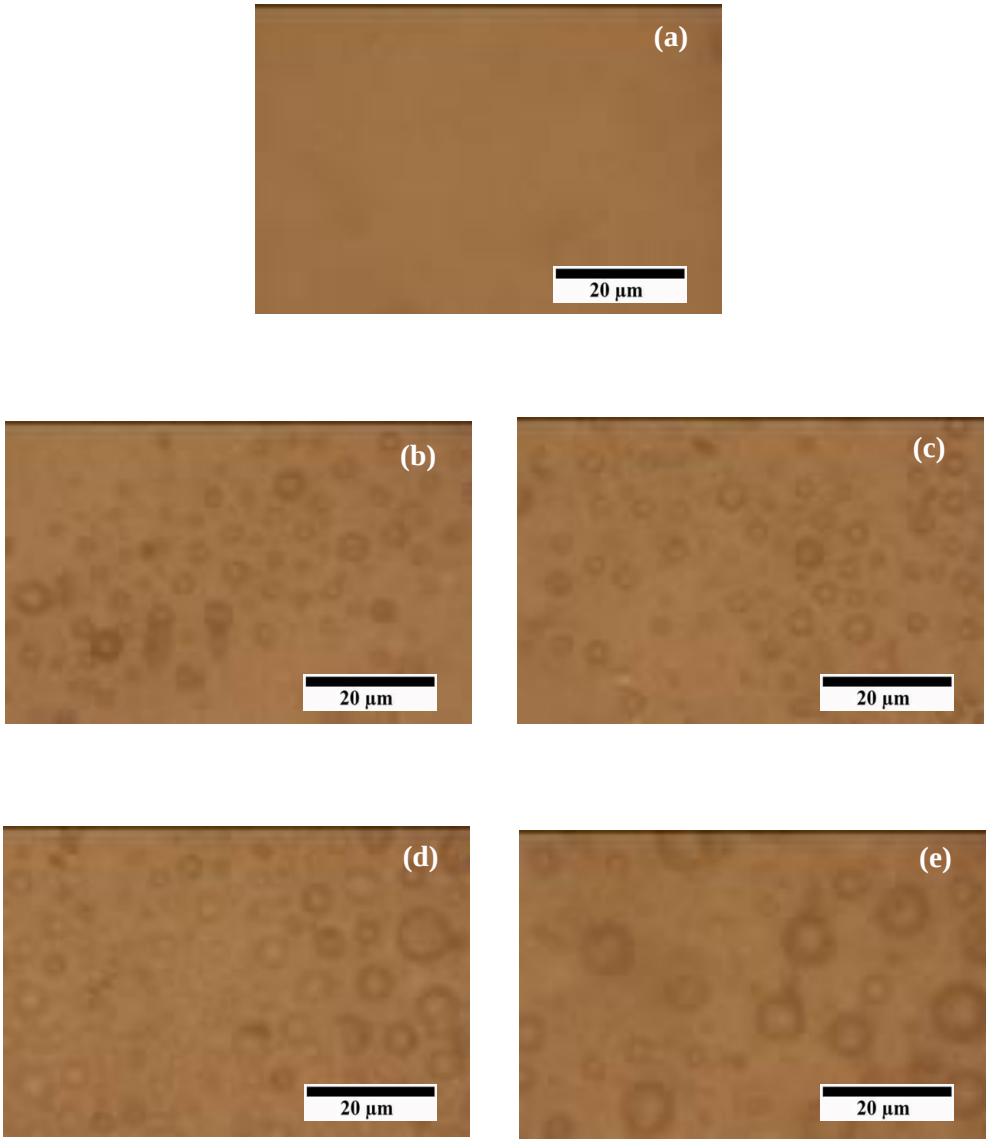



Figure 1. OM images of (a) neat PLA and PLA/BR blends at (b) 3 wt% (c) 5 wt% (d) 10 wt% (e) 20 wt%. The blend solutions were mechanical stirred at 400 rpm.

There was a greater tendency to form some rubber agglomerates when higher content of rubber was used [11]. Furthermore, Vibracell sonication was applied to the blend solution after mechanical stirring in order to reduce the size of rubber droplets. Figure 2 (a-d) show the OM images of the PLA/5 wt% BR blends which were sonicated by Vibracell sonicator at different watts and times. Table 1 shows the rubber droplet size of the blends. It can be seen that the higher watt provide the smaller droplet size, and 3 minutes application gave the smallest droplet size. The higher watt provided the higher vibration; therefore, small rubber droplets were obtained. However, during the sonication high amount of heat could be created (solution was warmer after sonication). This caused the solvent lost, which resulted the re-combination of the rubber particles, so the bigger particles were obtained when longer sonication was applied.

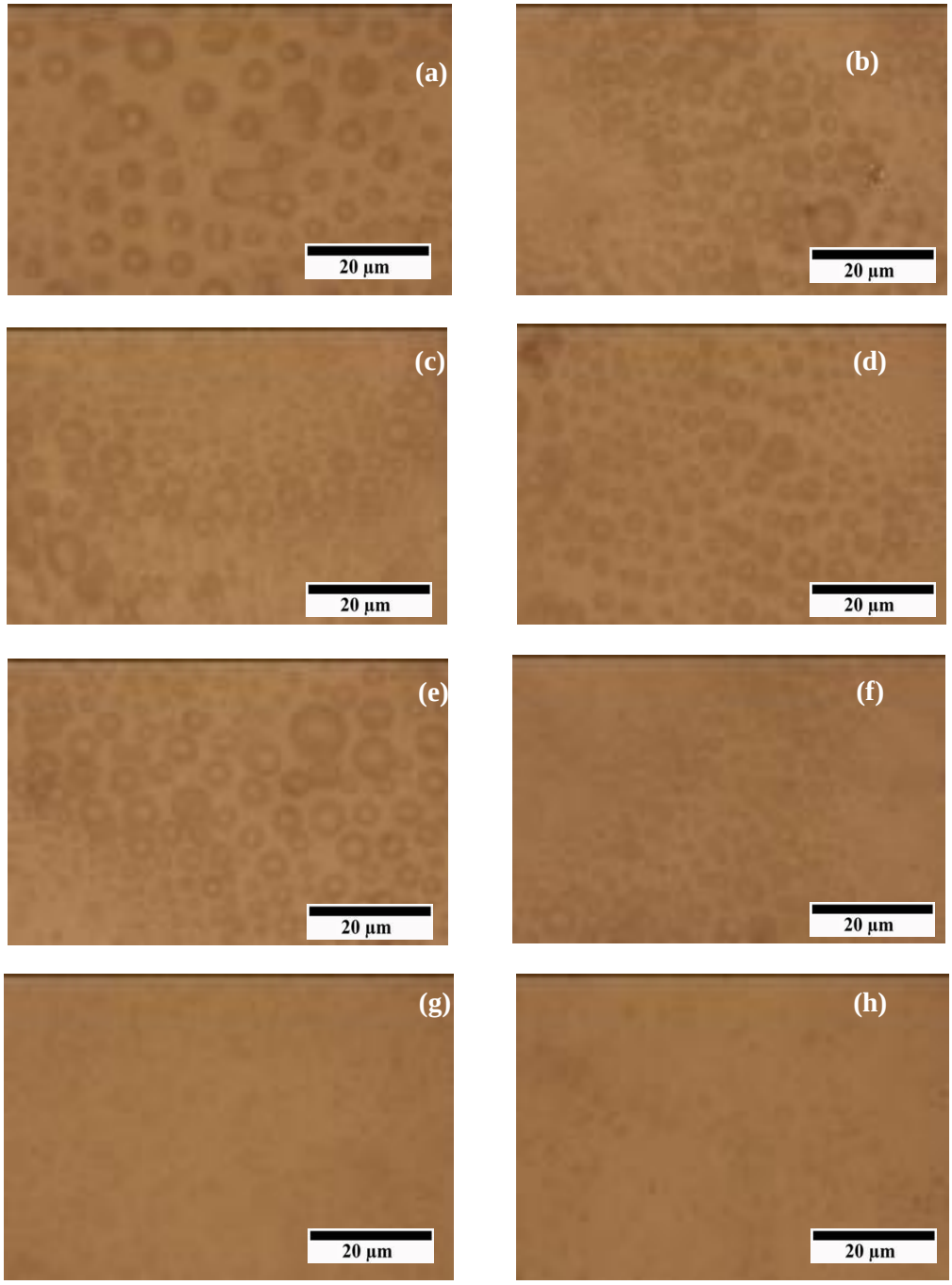



Figure 2. OM images of PLA/5 wt% BR blends at different watts and times of Vibracell sonicator application (a) 150 watt 1 min (b) 150 watt 3 mins (c) 150 watt 5 mins (d) 350 watt 1 min (e) 350 watt 3 mins (f) 350 watt 5 mins (g) 650 watt 1 min (h) 650 watt 3 mins.

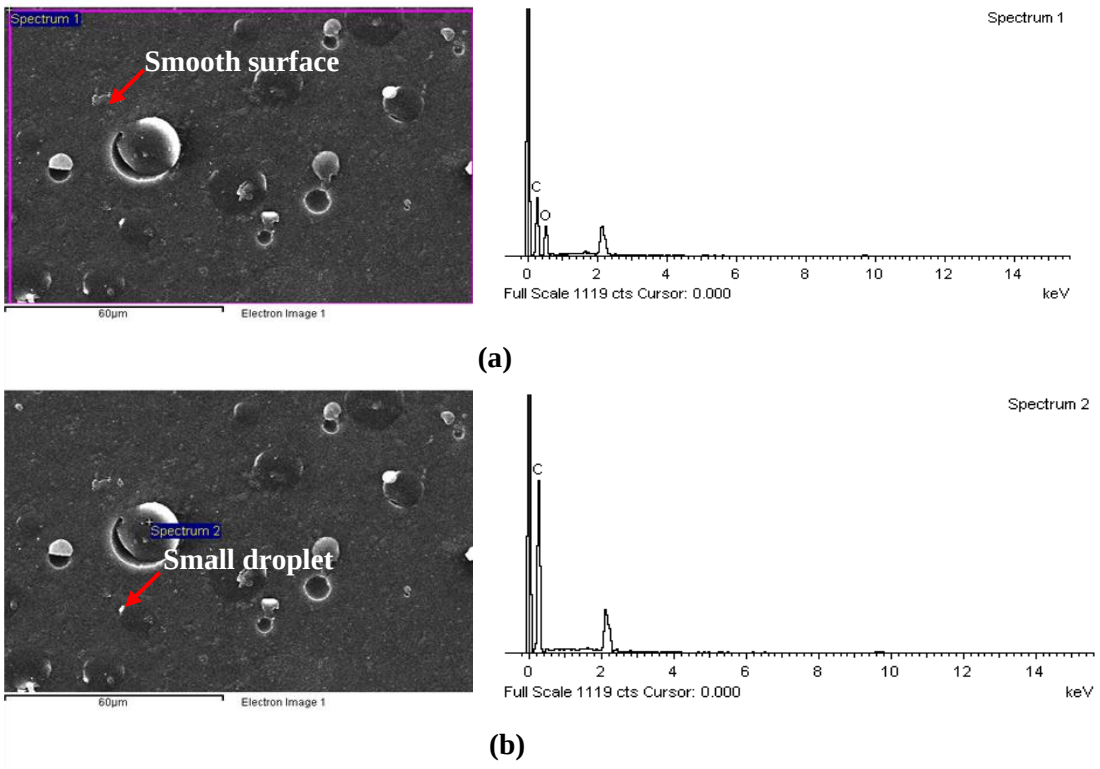



Figure 3. LV-SEM micrographs and EDS results of PLA/ 3 wt% BR blend. (a) smooth surface site (b) small droplet site.

Table 2.Tensile properties of PLA and PLA/BR blends

| | **Young's modulus (MPa)** | **Tensile strength (MPa)** | **Elongation at break (%)** |
|---|---|---|---|
| PLA neat | 421 ± 55 | 48± 10 | 11± 1 |
| 3 wt.%BR | 452 ± 29 | 40 ± 2 | 21 ± 1 |
| 5 wt.%BR | 441 ± 51 | 36 ± 1 | 21± 2 |
| 10 wt.%BR | 354 ± 34 | 32 ± 1 | 39± 3 |
| 20 wt.%BR | 317± 55 | 20 ± 3 | 30 ± 4 |
| 5%BR 650 watt 3 min. | 384± 72 | 33 ± 2 | 49± 4 |

**Mechanical Properties of PLA/BR Films**

Young's modulus, tensile strength and elongation at break are the important factors for studying mechanical properties of PLA film. Figure 4 compares the stress-strain curves of the neat PLA to the PLA/5 wt% BR (non-sonication) and PLA/5 wt % BR (with sonication). It is clearly stated that the addition of BR gave more ductile and

tougher materials. Moreover, the utilization of Vibracell sonicator, which provided the smaller rubber droplets, gave the tougher blends with the same rubber content. Table 2 exhibits the tensile properties of the neat PLA and PLA/BR blends. The elongation at break increased as the content of BR increased. PLA with 5 wt% BR and dispersion by Vibracell sonicator showed the highest elongation at break. However, the 20 wt% of BR blend revealed a lower elongation at break. In addition, the addition of BR decreased the strength of samples, and the high content of rubber decreased the Young's modulus of samples. This is because of the low tensile strength and Young's modulus of rubber. So the rigidity of PLA was lessen, which is good for the packaging application.

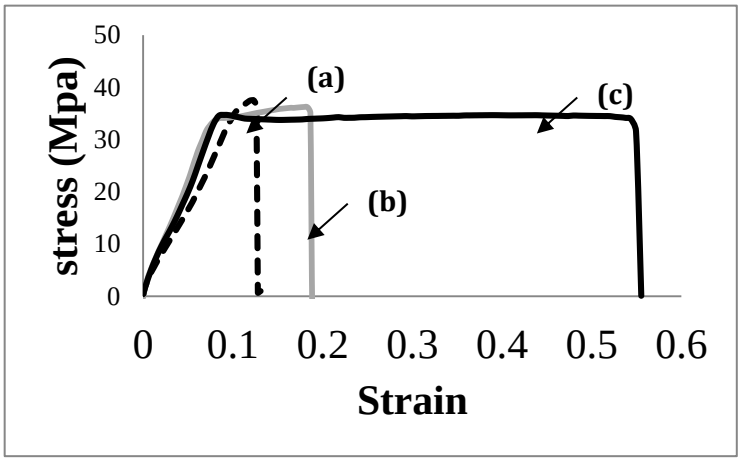



Figure 4. Stress-strain curves of the (a) PLA neat (b) PLA/ 5 wt.%BR non-sonication and (c) PLA/5 wt.%BR with sonication.

## Conclusion

The PLA/BR blends were prepared by solvent casting method. The higher content of BR provided the higher elongation at break and lower the strength and Young's modulus. The Vibra-cell sonicator was applied and found that it could lessen the rubber droplet size and provided the tougher materials.

## Acknowledgement

This research was financially supported by National Research University (NRU) and the Graduated School, Chiang Mai University.

## References

1. Kim, J. K., Park, D. J., Lee, M. S. & Ihn, K. J. (2001). Synthesis and crystallization behavior of poly (L-lactide) -block-poly (e-caprolactone) copolymer. *Polymer*, 42(17): 7429–41.
2. Martin, O. & Avérous, L. (2001). Poly (lactic acid): plasticization and properties of biodegradable multiphase s ystems. *Polymer*, 42(14): 6209–19.
3. Rasal, R. M., Janorkar, A. V. & Hirt, D. E. (2010). Poly(lactic acid) modifications. *Progress Polymer Science*, 35(3): 338–56.
4. Anderson, K.S., Lim, S.H. & Hillmyer, M.A. (2003). Toughening of polylactide by melt blending with linear lo w-density polyethylene. *Polymer Science*, 89: 3757–3768.
5. Piorkowska, E., Kulinski, Z., Galeski, A. & Masirek, R. (2006). Plasticization of semicrystalline poly(L-lactide ) with poly(propylene glycol). *Polymer*, 47: 7178–7188.
6. Hu, Y., Topolkaraev, V., Hiltner, A. & Baer, E. (2003). Crystallization and phase separation in blends of high st ereoregular poly (lactide) with poly (ethylene glycol). *Polymer*, 44: 5681–5689.
7. Ma, P., Hristova-Bogaerds, D.G., Goossens, J.G.P., Spoe;stra A.B., Zhang Y. & Lemstra P.J. (2012). Toughenin ng of poly(lactic acid) by ethylene-co-vinyl acetate copolymer with different vinyl acetate contents. *European*

*Polymer*, 48: 146-154.
8. Wu, S.H. (1985). Phase structure and adhesion in polymer blends: A criterion for rubber toughening. *Polymer*, 26: 1855–1863.
9. Kim, G.M. & Michler, G.H. (1998). Micromechanical deformation processes toughened and particle-filled sem icrystalline polymers-Part 1- Characterization of deformation processes in dependence on phase morphology. *P olymer*, 39: 5689–5697.
10. Liu, Y., Zhang, X., Gao, J., Huang, F., Tan, B., Wei, G. & Qiao, J. (2004). Toughening of polypropylene by c ombined rubber system of ultrafine full-vulcanized powdered rubber and SBS. *Polymer*, 45: 275-286.
11. Petchwattana, N., Covavisaruch, S. & Euapanthasate, N. (2012). Utilization of ultrafine acrylate rubber particle as a toughening agent for poly(lactic acid). *Material Science and Engineering*: 64-70.

The Malaysian Journal of ANALYTICAL SCIENCES ISSN 1394-2506

# BENZOFURAN GLYCOSIDES FROM *STYRAX BENZOIN*

## (Glikosida bezofuran daripada *Styrax benzoin*)

Hasliza Yusof, Laily B. Din, Wan A. Yaacob*

*School of Chemical Sciences and Food Technology, Faculty of Science and Technology, Universiti Kebangsaan Malaysia, 43600 UKM Bangi, Selangor D.E., Malaysia*

**Corresponding author: wanyaa@ukm.edu.my*

**Abstract**

Separation of methanol extracts of the fruits and stem bark of *Styrax benzoin* using various chromatography (vacuum liquid chromatography, column chromatography and preparative thin layer chromatography) gave four benzofuran glycosides namely egonol gentiobioside (**1**), egonol gentiotrioside (**2**), egonol glucoside (**3**) and masutakeside (**4**). The compounds were identified by spectroscopic analysis (NMR, mass and infra-red spectral data) and by comparison of the data with that of the literature. Isolation of compounds from this plant has never been reported before.

**Keywords**: *styrax benzoin*, styracaceae, egonol gentiobioside, egonol gentiotrioside, egonol glucoside, masutakeside

**Abstrak**

Pemisahan kromatografi ke atas ekstrak metanol buah dan kulit batang *Styrax benzoin* menggunakan pelbagai teknik kromatografi (kromatografi cecair vakum, kromatografi turus dan kromatografi lapisan thin preparatif) memberikan empat benzofuran glikosida yang bernama egonol gentiobiosida (**1**), egonol gentiotriosida (**2**), egonol glukosida (**3**) dan masutakesida (**4**). Sebatian ini telah dikenal pasti dengan analisis spektroskopi (data spektrum RMN, jisim dan infra merah) dan membandingkan data ini dengan data kepustakaan. Pemisahan sebatian daripada tumbuhan ini belum pernah dilaporkan sebelum ini

**Kata kunci**: *styrax benzoin*, styracaceae, egonol gentiobiosida, egonol gentiotriosida, egonol glukosida, masutakesida

## Introduction

Styracaceae is a family consisting of small trees and shrubs, mostly native to tropical and subtropical regions (Asia, Mediterranean, and North to South America) [1]. The genus *Styrax* is different from other genera of this family by the production of resinous material, usually secreted when the barks and trunks are injured by sharp objects [2, 3]. This resin was used by Romans, Egyptians, Phoenicians and Ionians as incense and in therapeutics [1]. Previous studies of this genus led to the isolation of saponins [4 - 7], terpenes [2, 8 -10], lignans [3, 10 - 12], benzofuran derivatives and their glycosides [2 - 4, 8, 9, 11, 13 - 16].

*Styrax benzoin* (locally known as Pokok Kemenyan) is fairly tall tree and distributed from Malay Peninsula to Sumatra and Western Java [17], where it grows to about 12 metres in maximum height. This species is cultivated as a main source of resin (Sumatra Benzoin or Gum Benjamin) in Indonesia and used as incense and medicine [18]. However, no chemical study on this plant has been reported. We report here the isolation and structural elucidation of four benzofuran glucosides from *S. benzoin*.

## Materials and Methods

### Plant Material

The fruits and stem bark of *Styrax benzoin* were collected in March 2010 from Teras Jernang, Bangi, Selangor, Malaysia. A voucher specimen (SM2104) is deposited at the Herbarium of Universiti Kebangsaan Malaysia (UKMB) and identified by Mr. Sani Miran.

**Extraction and Isolation**

The dried powder of fruits of *Styrax benzoin* (0.98 kg) was extracted consecutively at room temperature with EtOAc (3 x 2.5 L), each time for 3 days. After filtration and evaporation of the solvent under vacuum, 13.1 g (1.34 %) of EtOAc extract was obtained. The residue was then extracted with MeOH (3 x 2.5 L) to give 115.5 g (11.79%) of MeOH extract. The dried powder of stem bark (2.75 kg) was extracted similarly with EtOAc (3 x 8.0 L; yield 63.52 g, 2.31 %) and MeOH (3 x 8.0 L, produced 151.37 g, 5.50 %). The MeOH extracts of respective fruits (33.0 g) and stem bark (50.0 g) were fractionated separately by using vaccum liquid chromatography (VLC) eluted with increasing polarity of $CHCl_3$ and MeOH. The eluates that exibited similar profile on silica gel thin layer chromatography (TLC) (Merck 5554) were combined to give 6 fractions (A-F) each for the fruits and stem bark. Purification of fruits, fractions B (6.06 g) and E (5.03 g) by VLC, column chromatography (CC) and preparative TLC using EtOAc and MeOH (8.5:1.5; 7:3) gave compounds **1** (1.2022 g) and **2** (0.1128 g), respectively. Separation of stem bark, fractions D (5.45 g) and E (4.38 g) by VLC, CC and preparative TLC using EtOAc and MeOH (8.5:1.5; 7.5:2.5) afforded compounds **3** (0.0338 g) and **4** (0.0526 g), respectively.

Purification of fruits, fractions B (6.06 g) and E (5.03 g) by VLC, column chromatography (CC) and preparative TLC using EtOAc and MeOH (8.5:1.5; 7:3) gave compounds **1** (1.2022 g) and **2** (0.1128 g), respectively. Separation of stem bark, fractions D (5.45 g) and E (4.38 g) by VLC, CC and preparative TLC using EtOAc and MeOH (8.5:1.5; 7.5:2.5) afforded compounds **3** (0.0338 g) and **4** (0.0526 g), respectively.

**Egonol gentiobioside 1**

(1.2022 g): viscous yellow oil. $R_f$ (6:2:1, ethyl acetate-pyridine-water) = 0.83. ESI-MS (m/z) 673.2071 $[M+Na]^+$, $C_{31}H_{38}O_{15}$. FTIR (ATR) $cm^{-1}$: 3358, 2934, 1599, 1477, 1227, 1022, 928. $^1H$ and $^{13}C$ NMR data: see Table 1

**Egonol gentiotrioside 2**

(0.1128 g): white amorphous. $R_f$ (6:2:1, ethyl acetate-pyridine-water) = 0.62. ESI-MS (m/z): 835.2620 $[M+Na]^+$, $C_{37}H_{48}O_{20}$. $^1H$ and $^{13}C$ NMR data: see Table 1

**Egonol glucoside 3**

(0.0338 g): viscous yellow oil. $R_f$ (6:2:1, ethyl acetate-pyridine-water) = 0.93. ESI-MS (m/z): 527.1859 $[M+K]^+$, $C_{25}H_{28}O_{10}$. UV (MeOH) $\lambda_{max}$: 225, 311 nm. FTIR (ATR) $cm^{-1}$: 3394, 2941, 1601, 1515, 1485, 1141, 1023, 858. $^1H$ and $^{13}C$ NMR data: see Table 1

**Masutakeside 4**

(0.0526 g): viscous yellow oil. $R_f$ (6:2:1, ethyl acetate-pyridine-water) = 0.81. ESI-MS (m/z): 659.2262 $[M+K]^+$, $C_{30}H_{36}O_{14}$. UV (MeOH) $\lambda_{max}$: 224, 311 nm. FTIR (ATR) $cm^{-1}$: 3546, 3459, 2924, 1595, 1485, 1140, 1036 $^1H$ and $^{13}C$ NMR data: see Table 1.

## Results and Discussion

Compound **1** was isolated as viscous yellow oil. Its molecular formula was determined as $C_{31}H_{38}O_{15}$ from the molecular ion peak at m/z 673.2071 $[M+Na]^+$ in the ESI-MS. The IR spectrum showed the presence of many hydroxyl groups (3358 $cm^{-1}$). Comparison of the $^1H$ and $^{13}C$-APT NMR spectra of the compound suggested that it is egonol diglucoside. The $^{13}C$-APT NMR spectrum showed the location of twelve out of 31 signals which suggested that the compound is gentiobioside. This was supported by presence of the signals at $\delta_H$ 4.13 (*d*, *J* = 7.8 Hz, Glc-H-1') and 4.27 (*d*, *J* = 7.8 Hz, Glc-H-1") in the $^1H$ NMR spectrum, which could be assigned to two anomeric protons. Thus, the structure of **1** was determined as egonol gentiobioside previously isolated from *Styrax perkinsiae* [2, 11], *S. officinalis* [4] and *S. macranthus* [8].

Compound **2**, $C_{37}H_{48}O_{20}$ appeared as a white amorphous. The mass spectrum showed a molecular ion peak ESI-MS $[M+Na]^+$ at m/z = 835.2620 consistent with a molecular formula of $C_{37}H_{48}O_{20}$. Comparing the $^1H$ and $^{13}C$-APT NMR data of compound **2** with those of compound **1**, compound **2** has three signals at $\delta_H$ 4.13 (*d*, *J* = 7.8 Hz, Glc-H-1'), 4.22 (*d*, *J* = 7.8 Hz, Glc-H-1'") and 4.25 (*d*, *J* = 7.8 Hz, Glc-H-1") in the $^1H$ NMR spectrum, which could be assigned to three anomeric protons. Thus, compound **2** was elucidated as egonol gentiotrioside previously isolated from *Styrax perkinsiae* [2, 11], *S. officinalis* [4] and *S. macranthus* [8].

Compound **3** was obtained as viscous yellow oil. The molecular ion peak at m/z = 527.1859 $[M+K]^+$ in the ESI-MS provided a molecular formula of $C_{25}H_{28}O_{10}$. The UV spectrum absorptions in ethanol at 225 and 311 nm suggested that this compound has the egonol skeleton. The IR (3394 $cm^{-1}$) of compound **3** showed the presence of many hydroxyl groups. The $^1H$ NMR spectrum showed only one signal at $\delta_H$ 4.12 (*d*, *J* = 7.8 Hz, Glc-H-1') could be assigned to the anomeric proton. Compound **3** was confirmed as egonol glucoside previously isolated from *Styrax perkinsiae* [2, 11], *S. ferrugineus* [3], *S. officinalis* [4] and *S. macranthus* [8] and *S. obassia* [15].

Compound **4** was isolated as viscous yellow oil. The mass spectrum showed a molecular ion peak ESI-MS $[M+K]^+$ at m/z = 659.2262 consistent with a molecular formula of $C_{30}H_{36}O_{14}$. Compound **4** exhibited UV absorptions at 224 and 311 nm which suggested the egonol skeleton. The IR (3546 $cm^{-1}$) spectrum of the compound suggested the presence of hydroxyl groups. Comparing the $^1H$ and $^{13}C$-APT NMR data of compound **4** with those of compound **1**, compound **4** still has two signals at $\delta_H$ 4.12 (*d*, *J* = 7.8 Hz, Glc-H-1) and 4.21 (*d*, *J*_ = 7.8 Hz, Xyl-H-1), but compound **4** has less one signal proton and carbon. Thus spectroscopic data led to the structure of masutakeside previously isolated from *Styrax japonica* [9] and *S. perkinsiae* [11]. The structure of compounds **1**, **2**, **3** and **4** show in Figure 1.

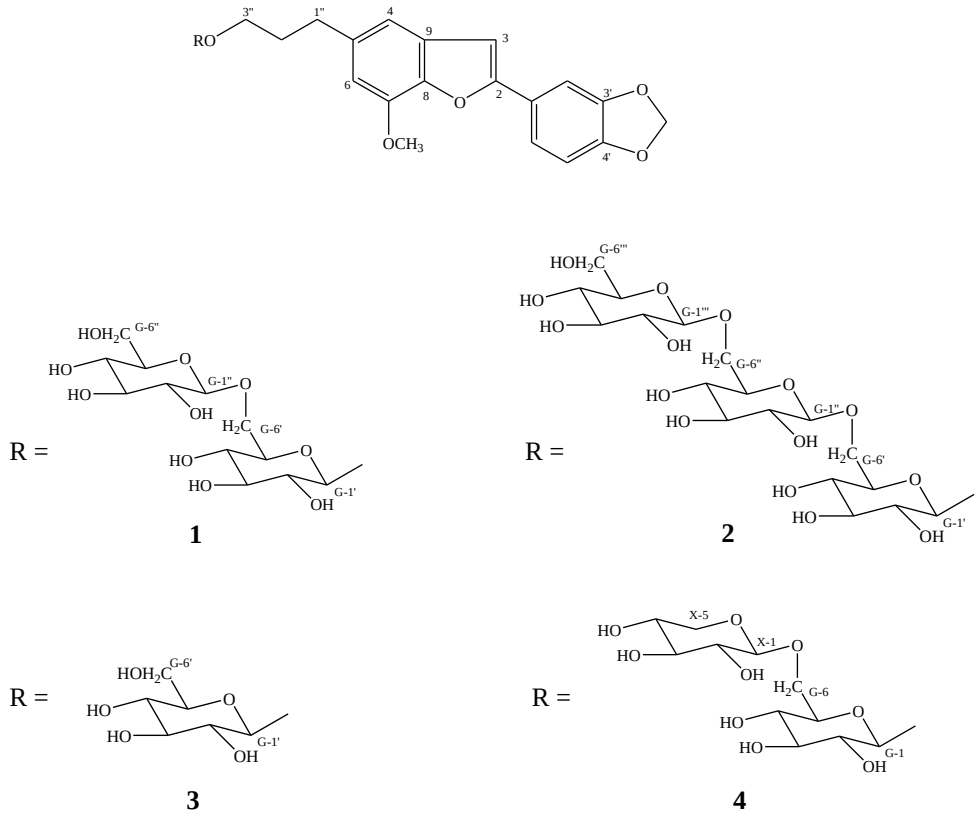



Figure 1. Structure of compounds **1**, **2**, **3** and **4**

Table 1. $^{1}$H NMR (600 MHz) spectral data of compounds 1-4 in DMSO-*d*

| Position | $\delta_H$ (multiplicity, *J* in Hz) | | | |
|---|---|---|---|---|
| | **Egonol gentiobioside 1** | **Egonol gentiotrioside 2** | **Egonol glucoside 3** | **Masutakeside 4** |
| 2 | - | - | - | - |
| 3 | 7.20 (1H, *s*) | 7.19 (1H, *s*) | 7.21 (1H, *s*) | 7.21 (1H, *s*) |
| 4 | 7.00 (1H, *d*, 0.9) | 7.00 (1H, *s*) | 7.00 (1H, *s*) | 7.01 (1H, *s*) |
| 5 | - | - | - | - |
| 6 | 6.78 (1H, *d*, 0.9) | 6.77 (1H, *s*) | 6.79 (1H, *d*, 0.6) | 6.78 (1H, *d*, 0.6) |
| 7 | - | - | - | - |
| 8 | - | - | - | - |
| 9 | - | - | - | - |
| 1' | - | - | - | - |
| 2' | 7.42 (1H, *d*, 1.6) | 7.40 (1H, *s*) | 7.43 (1H, *d*, 1.6) | 7.43 (1H, *d*, 1.6) |
| 3' | - | - | - | - |
| 4' | - | - | - | - |
| 5' | 7.03 (1H, *d*, 8.2) | 7.02 (1H, *d*, 9.0) | 7.03 (1H, *d*, 8.0) | 7.03 (1H, *d*, 8.2) |
| 6' | 7.40 (1H, *dd*, 1.6, 8.2) | 7.38 (1H, *dd*, 1.2, 9.0) | 7.40 (1H, *dd*, 1.6, 8.0) | 7.40 (1H, *dd*, 1.6, 8.2) |
| 1" | 2.71 (1H, *t*, 8.6)<br>2.73 (1H, *t*, 8.6) | 2.70 (1H, *t*, 9.6)<br>2.72 (1H, *t*, 9.6) | 2.72 (2H, *t*, 7.8) | 2.71 (1H, *t*, 7.8)<br>2.72 (1H, *t*, 7.8) |
| 2" | 1.87 (2H, *q*, 6.9) | 1.85 (2H, *q*, 6.9) | 1.87 (2H, *q*, 6.8) | 1.86 (2H, *q*, 6.9) |
| 3" | 3.44 (1H, *m*)<br>3.80 (1H, *dt*, 6.5, 9.6) | 3.44 (1H, *m*)<br>3.80 (1H, *dt*, 6.3, 9.6) | 3.42 (1H, *m*)<br>3.80 (1H, *dt*, 6.3, 9.3) | 3.43 (1H, *m*)<br>3.79 (1H, *dt*, 5.7, 9.3) |
| 7-$OCH_3$ | 3.95 (3H, *s*) | 3.94 (3H, *s*) | 3.95 (3H, *s*) | 3.95 (3H, *s*) |
| -$OCH_2O$- | 6.09 (2H, *s*) | 6.07 (2H, *s*) | 6.09 (2H, *s*) | 6.09 (2H, *s*) |
| G-1' | 4.13 (1H, *d*, 7.8) | 4.13 (1H, *d*, 7.8) | 4.12 (1H, *d*, 7.8) | 4.12 (1H, *d*, 7.8) |
| G-2' | 2.96 (1H, *br t*, 8.7) | 2.98 (1H, *m*) | 2.97 (1H, *dt*, 4.4, 8.3) | 2.96 (1H, *dt*, 3.4, 8.3) |
| G-3' | 3.13 (1H, *br t*, 9.0) | 3.13 (1H, *m*) | 3.08 (1H, *dt*, 1.8, 7.8) | 3.14 (1H, *br t*, 8.7) |
| G-4' | 3.06 (1H, *br s*) | 3.05 (1H, *t*, 3.0) | 3.04 (1H, *dt*, 4.4, 9.0) | 3.08 (1H, *br t*, 8.7) |
| G-5' | 3.30 (1H, *d*, 1.2) | 3.29 (1H, *br t*, 8.1) | 3.14 (1H, *dt*, 3.2, 8.2) | 3.27 (1H, br t, 7.8) |
| G-6' | 3.58 (1H, *dd*, 6.6, 11.4)<br>3.97 (1H, *dd*, 1.2, 11.4) | 3.97 (1H, *d*, 10.8)<br>- | 3.42 (1H, *m*)<br>3.66 (1H, *dd*, 4.8, 10.8) | 3.54 (1H, *dd*, 6.6, 11.4)<br>3.93 (1H, *dd*, 1.2, 11.4) |
| G-1" | 4.27 (1H, *d*, 7.8) | 4.25 (1H, *d*, 7.8) | - | - |
| G-2" | 2.99 (1H, *t*, 8.4) | 2.98 (1H, *m*) | - | - |
| G-3" | 3.08 (1H, *br t*, 10.2) | 3.13 (1H, *m*) | - | - |
| G-4" | 3.06 (1H, *br s*) | 3.13 (1H, *m*) | - | - |
| G-5" | 3.14 (1H, *br t*, 9.3) | 3.26 (1H, *br t*, 7.8) | - | - |
| G-6" | 3.44 (1H, *m*)<br>3.66 (1H, *br d*, 10.8) | - | - | - |

*(table continues)*

| Position | $\delta_H$ (multiplicity, *J* in Hz) | | | |
|---|---|---|---|---|
| | **Egonol gentiobioside 1** | **Egonol gentiotrioside 2** | **Egonol glucoside 3** | **Masutakeside 4** |
| G-2''' | - | 2.98 (1H, *m*) | - | - |
| G-3''' | - | 3.06 (1H, *br s*) | - | - |
| G-4''' | - | 3.13 (1H, *m*) | - | - |
| G-5''' | - | 3.13 (1H, *m*) | - | - |
| G-6''' | - | 3.44 (1H, *m*)<br>3.65 (1H, *m*) | - | - |
| X-1 | - | - | - | 4.21 (1H, *d*, 7.8) |
| X-2 | - | - | - | 2.97 (1H, *br t*, 10.6) |
| X-3 | - | - | - | 3.08 (1H, *br t*, 8.7) |
| X-4 | - | - | - | 3.27 (1H, *br t*, 7.8) |
| X-5 | - | - | - | 3.00 (1H, *t*, 10.8)<br>3.68<br>(1H, *dd*, 5.4, 11.4) |

Table 2. $^{13}$C-APT NMR (150MHz) spectral data of compounds 1-4 in DMSO-*d*

| Position | $\delta_C$ APT | | | |
|---|---|---|---|---|
| | **Egonol gentiobioside 1** | **Egonol gentiotrioside 2** | **Egonol glucoside 3** | **Masutakeside 4** |
| 2 | 155.6 | 155.6 | 155.6 | 155.6 |
| 3 | 101.6 | 101.6 | 101.6 | 101.6 |
| 4 | 112.6 | 112.6 | 112.6 | 112.6 |
| 5 | 138.4 | 138.4 | 138.3 | 138.3 |
| 6 | 108.3 | 108.3 | 108.3 | 108.3 |
| 7 | 144.8 | 144.7 | 144.8 | 144.7 |
| 8 | 142.1 | 142.0 | 142.0 | 142.0 |
| 9 | 130.9 | 130.9 | 130.9 | 130.9 |
| 1' | 124.5 | 124.5 | 124.5 | 124.5 |
| 2' | 105.4 | 105.4 | 105.4 | 105.4 |
| 3' | 148.4 | 148.4 | 148.4 | 148.4 |
| 4' | 148.3 | 148.2 | 148.3 | 148.3 |
| 5' | 109.3 | 109.3 | 109.3 | 109.3 |
| 6' | 119.2 | 119.2 | 119.2 | 119.2 |
| 1'' | 32.3 | 32.3 | 32.2 | 32.3 |
| 2'' | 32.0 | 32.0 | 31.9 | 31.9 |
| 3'' | 68.3 | 68.4 | 68.3 | 68.3 |
| 7-$OCH_3$ | 56.3 | 56.2 | 56.2 | 56.2 |
| -$OCH_2O$- | 101.9 | 101.9 | 101.9 | 101.9 |
| G-1' | 103.3 | 103.2 | 103.4 | 103.3 |

*(table continues)*

| Position | $\delta_C$ APT | | | |
|---|---|---|---|---|
| | Egonol gentiobioside 1 | Egonol gentiotrioside 2 | Egonol glucoside 3 | Masutakeside 4 |
| G-2' | 73.9 | 73.9 | 74.0 | 73.8 |
| G-3' | 77.2 | 77.0 | 77.3 | 77.0/ 77.1 |
| G-4' | 70.5 | 70.4 | 70.5 | 70.3 |
| G-5' | 76.3 | 76.0 | 77.2 | 76.2 |
| G-6' | 68.8 | 68.8 | 61.5 | 68.8 |
| G-1" | 103.8 | 103.6 | - | - |
| G-2" | 74.0 | 73.9 | - | - |
| G-3" | 77.4 | 77.0 | - | - |
| G-4" | 70.5 | 70.3 | - | - |
| G-5" | 77.1 | 76.1 | - | - |
| G-6" | 61.5 | 68.8 | - | - |
| G-1'" | - | 103.7 | - | - |
| G-2'" | - | 73.9 | - | - |
| G-3'" | - | 77.2 | - | - |
| G-4'" | - | 70.3 | - | - |
| G-5'" | - | 77.1 | - | - |
| G-6'" | - | 61.5 | - | - |
| X-1 | - | - | - | 104.5 |
| X-2 | - | - | - | 73.8 |
| X-3 | - | - | - | 77.0/ 77.1 |
| X-4 | - | - | - | 70.0 |
| X-5 | - | - | - | 66.1 |

## Conclusion

Four benzofuran glycosides namely egonol gentiobioside **1**, egonol gentiotrioside **2**, egonol glucoside **3** and masutakeside **4** were successfully isolated from the methanol extract of *Styrax benzoin*. This is the first reported phytochemical studies of this plant.

## Acknowledgement

This research was financially supported by UKM grant (UKM-GUP-2011-205, UKM-DLP-2012-033, UKM-DLP-2013-18). Special thanks to School of Chemical Sciences and Food Technology, Faculty of Science and Technology, UKM and Centre for Research and Innovation Management (CRIM) UKM for the technical support on NMR, LC-MSToF, UV and FTIR instrumentation and Mr. Sani Miran for the assistance in identifying plant material.

## References

1. Ng, F. S. P. (1992). *Manual of forest fruits, seeds and seedlings*. Vol. II. Forest Research Institute Malaysia
2. Li, Q. L., Li, B. G., Qi, H. Y., Gao, X. P. & Zhang, G. L. (2005). Four new benzofurans from seeds of *Styrax perkinsiae*. *Planta Medica*, 71: 847-851
3. Pauletti, P. M., Araujo, A. R., Young, M. C. M., Giesbrecht, A. M. & Bolzani, V. d. S. (2000). nor-Lignans from the leaves of *Styrax ferrugineus* (Styracaceae) with antibacterial and antifungal activity. *Phytochemistry*, 55: 597-601

4. Anil, H. (1980). Four benzofuran glycosides from *Styrax officinalis*, *Phytochemistry* 19: 2784-2786
5. Nakano, T., Hasegawa, M., Fukumaru, T & Tobinaga, S. (1967). The structure of jeposapogenol. *Tetrahedron Letters*, 4: 365-371
6. Segal, R., Govrin, H. & Zaitechek, D. V. (1964). A new type of saponin from *Styrax officinalis* L. *Tetrahedron Letters*, 10: 527-530
7. Yayla, Y., Caliskan, O. A., Anil, H., Bates, R. B., Stessman, C. C. & Kane, V. V. (2002). Saponins from *Styrax officinalis*. *Fitoterapia*, 73: 320-326
8. Lou, Y., He, Z. & Li, H. (2007). 2-aryl benzofurans and their derivatives from seeds of *Styrax macranthus*. *Fitoterapia*, 78: 211-214
9. Min, B. S., Oh, S. R., Ahn, K. S., Kim, J. H., Lee, J., Kim, D. Y., Kim, E. H. & Lee, H. K. (2004a). Anti-complement activity of norlignans and terpenes from the stem bark of *Styrax japonica*. *Planta Medica*, 70: 1210-1215
10. Min, B. S., Na, M. K., Oh, S. R., Ahn, K. S., Jeong, G. S., Lee, S. K., Joung, H. & Lee, H. K. (2004b). New furofuran and butyrolactone lignans with antioxidant activity from the stem bark of *Styrax japonica*. *Journal of Natural Product*, 67: 1980-1984
11. Feng, C. Q., Zhen, C. X., You, L. G., Chun, W. & Lin, Z. G. (2012). Two new 2-phenylbenzofurans from the bark of *Styrax perkinsiae*. *Chinese Journal of Natural Medicines*, 10: 92-97
12. Ulubelen, A., Saiki, Y., Lotter, H., Chari, V. M. & Wagner, H. (1978). Chemical components of *Styrax officinalis* L. - IV the structure of a new lignan styraxin. *Planta Medica*, 34: 403-407
13. Akgul, Y. Y. & Anil, H. (2003a). Benzofurans and another constituents from seeds of *Styrax officinalis*. *Phytochemistry*, 63: 939-943
14. Akgul, Y. Y. & Anil, H. (2003b). Benzofuran from seeds of *Styrax officinalis*. *Fitoterapia*, 74: 743-745
15. Takanashi, M. & Takizawa, Y. (1988). New benzofurans related to egonol from immature seeds of *Styrax obassia*. *Phytochemistry*, 27: 1224-1226
16. Takanashi, M. & Takizawa, Y. (2002). New egonol glycoside having D-xylose from immature seeds of *Styrax obassia* Sieb. et Zucc. *Journal of Oleo Science*, 51: 423-426
17. Burkill, I. H. (1966). *A dictionary of the economic products of the Malay Peninsula*. Vol II (I-Z). Kuala Lumpur: Ministry of Agriculture & Co-operatives
18. Ridley, H. N. (1967). *The flora of the Malay Peninsula*. Vol II. London: L. Reeve & Co.

The Malaysian Journal of ANALYTICAL SCIENCES ISSN 1394-2506

# FTIR ANALYSIS OF PHENOLIC COMPOUND AS PANCREATIC LIPASE INHIBITOR FROM INOCULATED *AQUILARIA MALACCENSIS*

## (Analisis Sebatian Fenolik daripada *Aquilaria malaccensis* yang di Inokulasi sebagai Perencat kepada Enzim Lipase Pankreas Menggunakan FTIR)

Nur Fahana Jamahseri*, Miradatul Najwa Mohd Rodhi, Nur Hidayah Zulkarnain, Nursyuhada Che Husain, Ahmad Fakhri Syahmi Masruddin

*Faculty of Chemical Engineering,*
*Universiti Teknologi MARA, 40450 Shah Alam, Selangor Darul Ehsan, Malaysia*

**Corresponding author: farah_hana90@ymail.com*

**Abstract**

This research aimed to discover the potential of inoculated *Aquilaria malaccensis* extract as a new and safe lipase inhibitor. The phenolic compounds in this plant are expected to promote inhibitory activity towards pancreatic lipase enzyme. Inoculated *Aquilaria malaccensis* was selected for this research, wherein the parts of this species (bark and leaves) were extracted via hydro distillation process. The extracts of this plant which are hydrosol, oil, and leaves were analyzed for phytochemical compound via Fourier Transform Infrared Spectroscopy (FTIR). FTIR analysis of the extracts of inoculated *Aquilaria malccensis* revealed the presence of hydroxyl functional group in both leaves and hydrosol extracts but absence in oil. This validate the presence of phenolic compound in hydrosol and leaves extract. Therefore, the leaves and hydrosol extracts have potential as an anti-obesity agent by inhibiting pancreatic lipase.

**Keywords:** *Aquilaria malaccensis*, phenolics, essential oil, hydrosol

**Abstrak**

Kajian ini dijalankan bertujuan mengenal pasti potensi ekstrak *Aquilaria malaccensis* yang diinokulasi sebagai inhibitor enzim lipase pankreas yang baru dan selamat. Sebatian fenolik dalam tumbuhan ini dipercayai akan dapat merencatkan aktiviti enzim lipase pankreas. Bahagian tumbuhan iaitu kayu dan daun telah diekstrak dengan menggunakan kaedah penyulingan hidro. Penyulingan hidro pada bahagian kayu tumbuhan menghasilkan minyak dan hidrosol.Ekstrak daripada kayu dan daun kemudian dianalisis untuk sebatian fitokimia menggunakan Spektrofotometer Inframerah Transformasi Fourier (FTIR). Melalui analisis FTIR, kumpulan berfungsi hidrosil didapati pada sampel ekstrak daun dan hidrosol namun tidak pada ekstrak minyak. Kajian ini mengesahkan kehadiran sebatian fenolik pada ekstrak daun dan hidrosol. Oleh itu, ekstrak daun dan hidrosol mempunyai potensi sebagai agen anti -obesiti dengan merencatkan aktiviti enzim lipase pankreas.

**Kata kunci:** *Aquilaria malaccensis*, fenolik, minyak, hidrosol

## Introduction

Obesity is a major contributor towards chronic diseases and disability including hypertension, stroke, diabetes, cardiovascular diseases and more. Ahn et al. defined obesity as abnormal or excessive fat accumulation with imbalance between levels of energy intake and expenditure [1]. Regarding obesity, The Star Malaysia (2013) reported that Malaysia is ranked at the sixth place among Asia-Pacific countries and tops the list of South-East Asia countries [2]. A review on article of Obesity and Overweight by the World Health Organization, WHO (2003) stated that the worldwide obesity has nearly doubled since 1980 with more than 1.4 billion adults were overweight which about 300 million women and more than 200 million men were obese in 2008 [3].

Obesity could be prevented by inhibiting pancreatic lipase in order to block fat absorption in the small intestine after being hydrolysed by pancreatic lipase. Another way is by disturbing adipocyte differentiation to inhibit fat

accumulation [1]. Pancreatic lipase (PL) is a primary enzyme that hydrolyses dietary fat molecules in digestive system by converting triglyceride to monoglyceride and free fatty acid [4]. The inhibition of PL is the key target to mediate obesity since this reaction reduced fat and nutrient absorption to the body. Orlistat is a drug designed to treat obesity in which it acts as lipase inhibitor. However, orlistat consumption has some serious side effects. Its consumption might damage liver and kidney, reduce the effectiveness of other medications including life-saving cancer treatment and also stimulate the multiplication of cancer cells [4].

At present, natural resources have been utilized as medicinal agent. Natural medicines are recognized as cost effective and safe with zero side effects at plausible dosage. It is found that natural resources have become one of the most vital approaches to treat obesity since it is rich with bioactive compounds [5]. Phytochemicals are natural bioactive compound that found in plants that work together with minerals, vitamins and fibre to promote good health. Currently, there are many researches are carried out to study the potential of phytochemical for anti-obesity treatment using various natural resources. According to Yun (2010), scientists have identified many phytochemicals that have potential to be used in obesity treatment by inhibiting PL. The phytochemicals identified are polyphenols, flavonoids, and saponin [4]. These compounds can be extracted from wide variety of plants such as soybean, grape seed extract, black tea, green tea, oak, broccoli, apple and many more [6]. In addition, Tucci et al. mentioned that polyphenol extract from plant such as apple or grape seed is able to inhibit PL. For example, polyphenol extracted from apple inhibits PL with $IC_{50}$ value of 1.4 μg/ml where $IC_{50}$ is defined as the sample concentration causing 50% inhibition of the pancreatic lipase activity [7]. This research will be focusing on identification of phenolic compound in inoculated *Aquilaria malaccensis* due to their significance on inhibiting PL.

*Aquilaria spp.* which also known as agarwood or 'gaharu' is one of the valuable forest products due to its high demand in various industries such as perfumery and pharmaceuticals. *Aquilaria malaccensis* is one of the Malaysian treasures that rich in phytochemicals contents in its resin. Hence, this research was attentive to discover the miracles of its phytochemicals content since at this present time there is no detailed documentation of phytochemicals compound presence in *Aquilaria spp.* [8]. In this research, inoculated *Aquilaria malaccensis* extracts are used as research materials to discover the new and safe pancreatic lipase inhibitor. The extracts of the plant which are hydrosol, oil and leaves taken from the hydro distillation process of inoculated *Aquilaria malaccencis*. Hydro distillation technique is used for extraction of phytochemical compound of inoculated *Aquilaria malaccencis* because it is safe to operate, eco-friendly and cost effective [9]. This study focused on the identification of phenolic compounds from inoculated *Aquilaria malaccensis* extract by using FTIR as potential PL inhibitor.

## Materials and Methods

### Collection of the plant materials

The bark, stem and leaves for compound extraction via hydrodistillation was collected from inoculated *Aquilaria malaccensis* planted in Jalan Kebun, Shah Alam, Selangor.

### Pre-treatment of inoculated *Aquilaria malaccensis* leaves

Inoculated *Aquilaria malaccensis* leaves collected were separated prior to washing. The leaves were very well selected where the damaged and diseased one were excluded. Then, those selected were washed and cleaned to remove the dirt and impurities before undergoing drying process. The drying process was conducted at 60 $^{o}$C for 24 hours inside an oven. Finally, the dried leaves were cooled at room temperature before they were ground and sieved into smaller particle size between 600 μm to <300 μm.

### Hydro distillation process of inoculated *Aquilaria malaccensis* leaves

The leaves sample was boiled with the distilled water in a round bottom flask where the temperature was maintained at 70 $^{o}$C. The water vapor from the hydro distillation process was collected. The water vapor consists of steamed and volatile compound that rises from the extractor and pass through to the condenser. The sample was then evaporated in rotary evaporation before undergoing the analysis for chemical compound presence via FTIR.

### Soaking and drying of grinded inoculated *Aquilaria malaccensis* bark and stem

The grinded inoculated *Aquilaria malaccensis* was soaked in distilled water for 7 days during the pre-treatment process. This treatment was carried out to promote the enlargement of the pore size [10]. This will enhance the

releasing of the phytochemicals compound from the wood. The soaking ratio of inoculated *Aquilaria malaccensis* to distilled water was 1:2 (kg/litre). This soaking method was a modification from A. Hakim et.al, (2013) [9]. The soaked samples were dried at outdoor condition.

**Hydro distillation of grinded inoculated *Aquilaria malaccensis* bark and stem**

The soaked inoculated *Aquilaria malaccensis* chips were boiled in hydro distiller vessels. Aluminium vessel was used for hydrodistillation. The hydro distillation process occurred at constant temperature of 100 $^{o}$C at atmospheric pressure. This process was carried out for five days. The resultant steam contained plant volatile compound is condensed and captured. The vapour consists of steam and volatile compounds rose from the extractor and went through the condenser. Two forms of heterogeneous liquid mixture were collected which are hydrosol (aromatic water) and essential oil. The liquid mixture was separated and hydrosol was collected for further analysis. This extraction method was obtained and modified from A.Hakim et al. [9].

**FTIR analysis**

The identifications of the active functional groups presence in inoculated *Aquilaria malaccensis* oil, hydrosol and leaves extracts was conducted by the aid of FTIR spectroscopy (Perkin Elmer Spectrum 2000). The investigation was performed within the wavelength ranging from 4000 to 400 $cm^{-1}$ where the spectrum takes about two minutes to be recorded. This range was selected because phenolic compounds functional groups will be identified at this wavelength. Lastly, comparison between the resultant spectrums with the standard for entirely functional groups was conducted [8].

## Results and Discussion

Pancreatic lipase is the enzyme that responsible for hydrolysis of 50-70% of triglycerides into monoglycerides and fatty acid, thus pancreatic lipase inhibition is a valuable pathway towards the treatment of obesity [11]. Several studies had reported the potential of phenolic compounds as pancreatic lipase inhibitor. Ahn et al. reported that flavonoid from *Nelumbo nucifera* is able to inhibit pancreatic lipase where the flavonoids, flavones without glucose inhibit pancreatic lipase whereas flavone glycosides did not [1].

FTIR was used for the identification of functional group presence in the leaves, hydrosol and oil inoculated *Aquilaria malaccensis*. Figure 1 - 3 show FTIR spectrum of leaves, hydrosol and oil extracts taken from inoculated *Aquilaria malaccensis* respectively. The functional groups which are present in the inoculated *Aquilaria malaccensis* extracts are further described in details [12].

O-H bond of hydrogen bonded alcohol/phenol (3600-3200 $cm^{-1}$) group frequency was present in leaves and hydrosol extract with 3323.61 $cm^{-1}$ and 3312.65 $cm^{-1}$ respectively. O-H bond of alcohol/ phenol functional group was absent in oil extract. A broad spectrum can be observed from Fig. 1 and Fig. 2 represent the availability O-H bond in the extracts. Both leaves and hydrosol extracts has strong H-bond since the lower the frequency, the stronger the H bond. This is the important part because presence of O-H bond indicates the existance of phenolic compound in the extracts. This finding is in agreement with Khalil et al. (2013) where presence of alcohol/phenol functional group was identified in Agarwood leaves with frequency of 3388 $cm^{-1}$ and 3384 $cm^{-1}$ for before and after inoculation process respectively[8]. Besides, Ahn et al., (2013) had reported *Nelumbo nucifera* leaves that consist IR spectrum of hydroxyl group (3338 $cm^{-1}$) was able to inhibit pancreatic lipase [1].

C-H bond of alkanes bonded with -$COCH_3$ (3100-2900 $cm^{-1}$) group frequency was identified in hydrosol extract with frequency of 2970.73 $cm^{-1}$. C-H bond of alkanes (2970-2850 $cm^{-1}$) group frequency was only exist in oil extract at frequency of 2853.03 $cm^{-1}$ assigned to the presence of unfunctionalised C-H stretching band of methylene (-CH2) and methyl (-CH3) groups. C-H bond of aromatic ring (690-900 $cm^{-1}$) group frequency was present in oil extract with frequency of 887.43 $cm^{-1}$ and 721.53 $cm^{-1}$. C≡C bond of Alkyne group frequency of 2260-2150 $cm^{-1}$ was present in both leaves and hydrosol extract with frequency of 2160.24 $cm^{-1}$ and 2154.55 $cm^{-1}$ respectively.

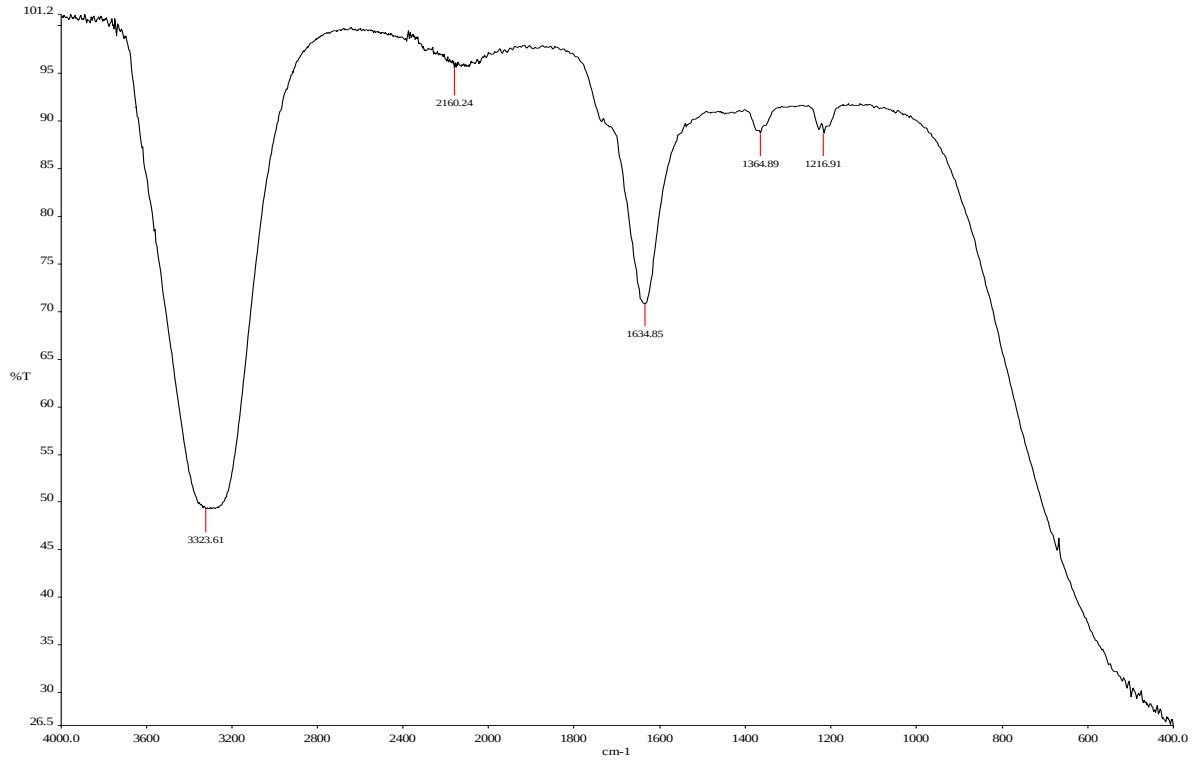



Figure 1. FTIR spectrum of inoculated *Aquilaria malaccensis* leaves extracts

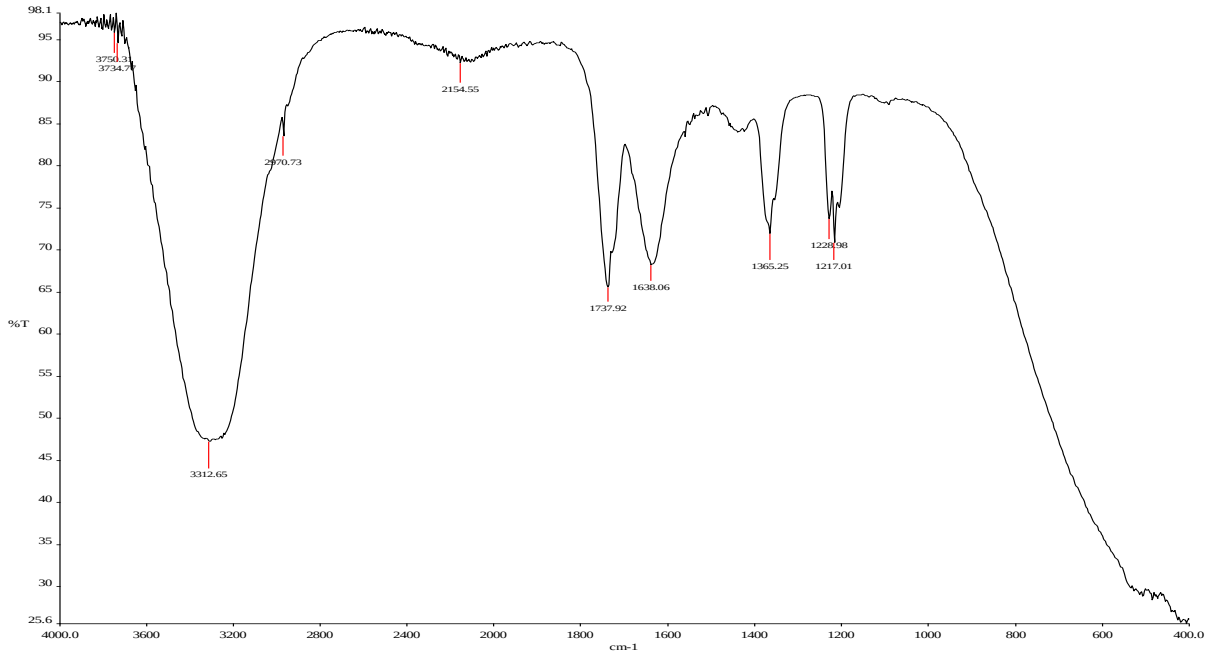



Figure 2. FTIR spectrum of inoculated *Aquilaria malaccensis* hydrosol extracts

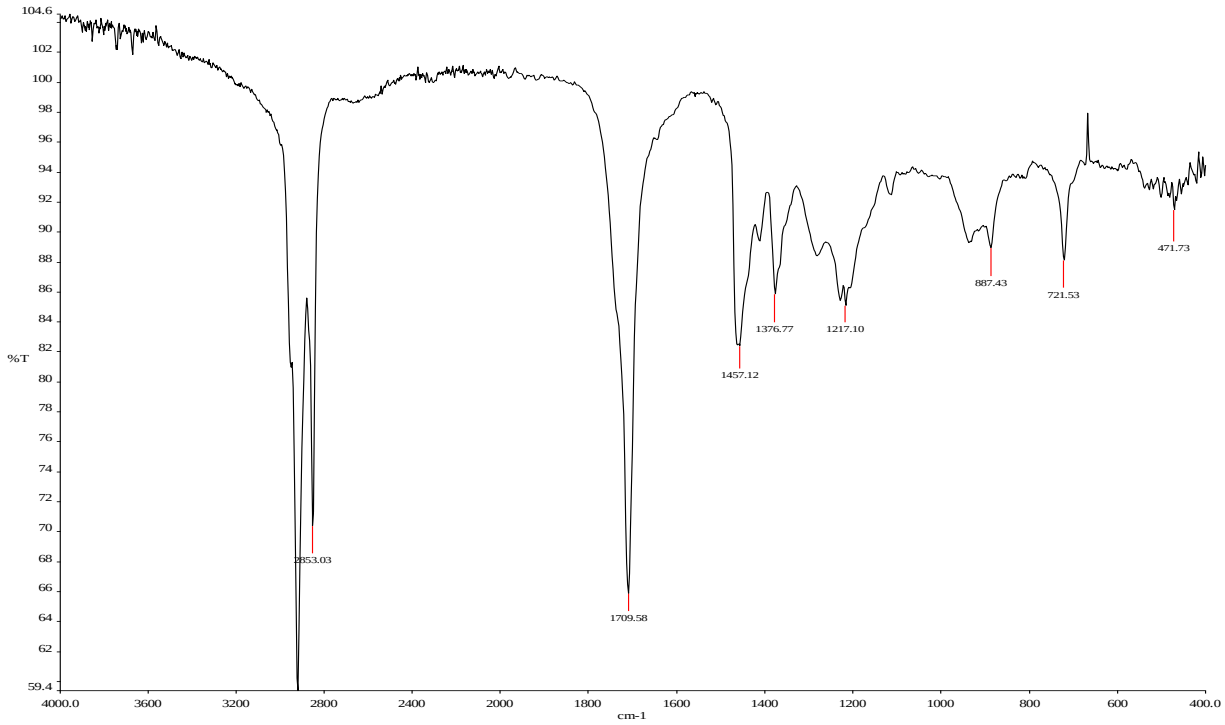



Figure 3. FTIR spectrum of inoculated *Aquilaria malaccensis* oil extracts

N-H bending of amides (1650-1560 $cm^{-1}$) group frequency was identified in both leaves and hydrosol extracts with frequency of 1634.85 $cm^{-1}$ and 1638.06 $cm^{-1}$ respectively. C-H stretching of amine (1250-1020 $cm^{-1}$) group frequency was also found in the hydrosol extract. C-H bond of Aromatic ring (690-900 $cm^{-1}$) group frequency were present in oil extract with frequency of 887.43 $cm^{-1}$ and 721.53 $cm^{-1}$. Leaves and hydrosol extracts were also containing C-O stretch of ether functional group (1300-1000 $cm^{-1}$) with frequency of 1216.91 $cm^{-1}$ and 1217.01 $cm^{-1}$ respectively. The presence of ester, ether and aromatic ring in all extracts explain the phenomenon of sweet and pleasant smell being produced during extraction process. Table 1 - 3 show the summary of the functional group of leaves, hydrosol and oil extracts from inoculated *Aquilaria malaccensis* respectively.

Table 1. Functional groups of inoculated *Aquilaria malaccensis* leaves extracts [13]

| **Wavenumber ($cm^{-1}$)** | **Bond** | **Functional Group** | **Group band ($cm^{-1}$)** |
|---|---|---|---|
| 3323.61 | H-bonded-OH | Alcohol/ Phenol | 3600-3200 |
| 2160.24 | C≡C-C | Alkyne | 2260-2110 |
| 1634.85 | N-H bending | Amide | 1650-1560 |
| 1364.89 | C-H bending vibration – OCOCH | Alkanes | 1370-1350 |
| 1216.91 | C-O stretch | Ether | 1300-1000 |

Table 2. Functional groups of inoculated *Aquilaria malaccensis* hydrosol extracts [13]

| Wavenumber ($cm^{-1}$) | Bond | Functional Group | Group band ($cm^{-1}$) |
|---|---|---|---|
| 3750.31 | Unknown | - | - |
| 3734.77 | Unknown | - | - |
| 3312.65 | H-bonded-OH | Alcohol/ Phenol | 3600-3200 |
| 2970.73 | C-H bonded-COCH3 | Alkane | 3100-2900 |
| 2154.55 | C≡C-C | Alkyne | 2260-2110 |
| 1737.92 | C=O stretching | Ester | 1750-1735 |
| 1638.06 | N-H bending | Amide | 1650-1560 |
| 1365.25 | C-H bending vibration –OCOCH | Alkanes | 1370-1350 |
| 1228.98 | C-H stretching | Amine | 1250-1020 |
| 1217.01 | C-O stretching | Ether | 1275-1200 |

Table 3. Functional groups of inoculated *Aquilaria malaccensis* oil extracts [13]

| Wavenumber ($cm^{-1}$) | Bond | Functional Group | Group band ($cm^{-1}$) |
|---|---|---|---|
| 2853.03 | C-H bond | Alkane | 2960-2850 |
| 1709.58 | C=O stretching | α,β-unsaturated aldehydes,ketones | 1710-1665 |
| 1457.12 | C-H bend | Alkane | 1470-1430 |
| 1376.77 | C-H bending vibration –OCOCH | Alkanes | 1370-1350 |
| 1217.70 | C-O stretching | Ether | 1275-1200 |
| 887.43 | C-H bond | Aromatic Ring | 900-690 |
| 721.53 | C-H bond | Aromatic Ring | 900-690 |
| 471.71 | S-S | Polysulfide | 500-470 |

From all extracts that were analyzed, it was found that hydrosols and leaves consist the alcohol/phenols functional groups that are very useful to prove the presence of phenolic compounds inside the hydrosol and leaves extract. Besides, the pattern of FTIR spectrum for both leaves and hydrosol extract were quite similar in which both spectrum did not show significance change of peaks compared to FTIR spectrum obtained from oil extract indicate their similar potential as pancreatic lipase inhibitor.

## Conclusion

The present study has revealed that leaves and hydrosols extracted from inoculated *Aquilaria malaccensis* hydrosol consist of phenolic compounds. This was due to the presence of alcohol/phenols group in the FTIR analysis. The active functional groups of hydrosol and leaves extract are alcohol/phenol, alkane, alkyne, ester and amide. Meanwhile, the functional groups of oil extract are alkane, aldehydes, ketones, ether, aromatic ring and polysulfide. Finally, this analysis had achieved its objective to identify the presence of phenolic compounds from inoculated *Aquilaria malaccensis.*

## Acknowledgement

We gratefully acknowledge the Ministry of Education for awarding research grant 600-RMI/RAGS 5/3 (68/2012) for financial support and to UiTM Shah Alam Malaysia for providing facilities to conduct this research.

**References**


1. Ahn J. H., Kim E. S., Lee C., Kim S., Cho S.-H., Hwang B. Y., and Lee M. K., (2013). Chemical constituents from *Nelumbo nucifera* leaves and their anti-obesity effects." *Bioorg. Med. Chem. Lett.* 23 (12): 3604.
2. Audrey E. Audrey, "Obesity a big problem now in Malaysia''The Star Online, 2013.
3. World Health Organization (2014). Obesity and Overweight, Online Available: http://www.who.int/mediacentre/factsheets/fs311/en/. [Accessed: 10-Jul-2014].
4. Yun J. W., (2010). Possible anti-obesity therapeutics from nature- A review. *Phytochemistry* 71 (14): 1625 - 1641
5. Park T. and Kim Y. (2011). Phytochemicals as Potential Agents for Prevention and Treatment of Obesity and Metabolic Diseases, Anti-obesity drug discovery and development. Bentham, Dubai, 150-185.
6. Sergent T., Vanderstraeten J., Winnand J., Beguin P., and Schneider Y. (2012). Phenolic compounds and plant extracts as potential natural anti-obesity substances, *Food Chem.* 135 (1): 68–73.
7. Tucci S. A., Boyland E. J., and Halford J. C. (2010). The role of lipid and carbohydrate digestive enzyme inhibitors in the management of obesity: a review of current and emerging therapeutic agents. *Diabetes. Metab. Syndr. Obese.* 3: 125–143.
8. Khalil K. B., Rahim A. S., Taha A. A., and Abdallah K. K. (2013). Characterization of Methanolic Extracts of Agarwood Leaves. *J. Appl. Ind. Sci.* 1(3): 78–88.
9. Hakim A., Ku K. H. and Rodhi, M. N. M. (2013). Extraction of Essential Oil from Biologically Inoculated Agarwood, *IEEE Business Engineering and Industrial Applications Colloquium (BEIAC)*: 889–892.
10. Fazila K. N. and Halim K. H. K. (2012). Effects of soaking on Yield and Quality of Agarwood Oil. *Journal of Tropical Forest Science* 24 (4): 557–564.
11. Liu S., Li D., Huang B., Chen Y., Lu X., and Wang Y. (2013). Inhibition of pancreatic lipase, α-glucosidase, α-amylase, and hypolipidemic effects of the total flavonoids from Nelumbo nucifera leaves. *J. Ethnopharmacol*. 149 (1): 263–269.
12. Pednekar P. A. and Raman B. (2013). The FTIR spectrometric studies of vibrational band of *Semercarpus anacardium* linn.f. Leaf, stems powder and extract. *Asian J. Pharm. Clin. Res.* 6 (3): 159 -168
13. Williams D. H. and Fleming Ian (2008). Spectroscopic Methods in Organic Chemistry: 48–61.

The Malaysian Journal of ANALYTICAL SCIENCES ISSN 1394-2506

# EFFECT OF ULTRASONIC-ASSISTED EXTRACTION ON PHENOLIC CONTENT OF AVOCADO

## (Kesan Pengekstrakan Bantuan Ultrasonik ke Atas Kandungan Komponen Phenolik Dalam Buah Avokado)

Rafidah Husen[1,3], Yoshito Andou[1]*, Amin Ismail[2], Yoshihito Shirai[1]

[1]*Department of Biological Functions and Engineering, Graduate School of Life Science and Systems Engineering, Kyushu Institute of Technology, 2-4 Hibikino, Wakamatsu-ku, Kitakyushu, Fukuoka, 808-0196, Japan*
[2]*Department of Nutrition and Dietetics, Faculty of Medicine and Health Sciences, Universiti Putra Malaysia, 43400 Serdang, Selangor, Malaysia*
[3]*Faculty of Applied Sciences, Universiti Teknologi MARA Sarawak, 94300 Kota Samarahan, Sarawak, Malaysia*

**Corresponding author: yando@life.kyutech.ac.jp*

**Abstract**

This study evaluate the effect of ultrasonic application in the extraction process on total phenolic content (TPC) of Hass avocado (*Persea americana* Mill) pulp. In this study, the solid/solvent ratio of 1/30 (wt/vol) and extraction temperature of 40°C gave higher TPC value. This ratio and temperature was applied in the ultrasonic-assisted extraction (UAE) of avocado pulp. This study then compared the TPC obtained from the avocado pulp extract without involving ultrasonic and the TPC obtained from the UAE. Results showed that the TPC value of avocado pulp was significantly higher in the UAE (235.77 mg GAE/100g dried sample) compared to the TPC in the non-UAE (166.32 mg GAE/100g dried sample). The increase in the TPC was between ~31% and ~41% when 5 to 20 min of ultrasonication applied in the extraction. Ultrasonication duration of 15 min gave the highest TPC where the value was significantly higher compared to the other duration.

**Keywords:** avocado pulp, ultrasonic-assisted extraction, total phenolic content

**Abstrak**

Kajian ini memperlihatkan kesan aplikasi ultrasonik dalam proses pengekstrakan ke atas jumlah kandungan komponen phenolik (TPC) dalam isi buah avokado (*Persea americana* Mill). Dalam kajian ini, nisbah pepejal/pelarut 1/30 (berat/isipadu) dan suhu pengekstrakan 40°C telah memberikan nilai TPC yang lebih tinggi. Nisbah dan suhu ini kemudiannya diaplikasikan dalam pengekstrakan bantuan ultrasonic (UAE) bagi isi buah avokado. Kajian ini kemudiannya membandingkan di antara nilai TPC dalam isi avokado yang telah diekstrak tanpa UAE dengan nilai TPC dalam ekstrak avokado yang telah melalui UAE. Keputusan telah menunjukkan bahawa nilai TPC adalah lebih tinggi (perbezaan bererti) dalam ekstrak isi avokado yang telah melalui UAE (235.77 mg GAE/100g sampel kering) berbanding ekstrak isi avokado tanpa UAE (166.32 mg GAE/100g sampel kering). Peningkatan dalam nilai TPC adalah di antara ~31% dan ~41% apabila 5 hingga 20 minit ultrasonik diaplikasikan. Tempoh ultrasonik 15 minit adalah tempoh yang memberikan nilai TPC yang paling tinggi (perbezaan bererti) berbanding tempoh lain yang digunakan.

**Kata kunci:** isi avokado; pengekstrakan bantuan ultrasonik; kandungan komponen phenolik

## Introduction

The avocado (*Persea Americana* Mill), belonging to the Lauraceae family is a tropical-subtropical fruit native to Mexico and Central America. They ripen after being harvested where the fruit depicts a green-skinned, fleshy body that resembles the shape of a pear [1]. Many studies have reported on the bioactive phytochemicals of this fruit. They include carotenoids, phenolic acids and flavonoids [2–4]. Antioxidant activities have also been reported in avocado [5]. It has been reported that avocado contains many different polyphenols including catechins,

hydroxybenzoic acids, hydroxycinnamic acids, procyanidins, flavanol, gentisic, chlorogenic, caffeic acids, laricitrin, aringenin, chrysin, kaempferide, protocatechuic, p-coumaric, ferulic, sinapic, and benzoic acids [4–6].

Avocado extract is usually obtained by solid-liquid extraction with different solvents. In research involving plants, various extraction methods have been developed for the extraction of phytochemicals in order to increase the extraction yield, shorten the extraction time as well as enhance the quality of extracts. Ultrasound-assisted extraction is among the methods used to enhance the process of extraction. It is inexpensive, simple and efficient alternative to conventional extraction techniques. Like soxhlet extraction, it can be used with any solvent for extracting a wide variety of natural compounds. In solid-liquid extraction, it offers advantages which include increased yield and faster kinetics. The apparatus is cheaper and easier to operate compared to other novel extraction techniques such as microwave-assisted extraction and supercritical fluid extraction [7].

Ultrasound-assisted extraction is widely used in the extraction of plant compounds. However, no information is available on the effect of ultrasound-assisted extraction on polyphenol content in avocado. This study is carried out to evaluate the usage of ultrasound in overcoming the limitation of conventional extraction of avocado fruit as well as its effect on the phenolic content of the fruit.

## Materials and Methods

Folin-Ciocalteu's phenol reagent and gallic acid ($C_7H_6O_5$) were purchased from Sigma-Aldrich, Germany. Sodium carbonate ($Na_2CO_3$) was purchased from Merck, Germany. All chemicals were of analytical grade.

### Sample preparation

Fresh avocado fruits (Hass avocado) were purchased from the local grocery store in Kitakyushu, Japan. Once ripened, all the fruits were cleaned, cut and peeled. The pulp of the fruit was dried using a freeze dryer (EYELA FDU-1200, Tokyo Rikakikai Co. Ltd Japan) and used in this study. The dried pulp was ground to fine powder using Waring commercial blender 8011S (Connecticut, USA) and kept at -40°C until further use.

### Sample extraction

One gram of powdered sample was extracted in 80% ethanol where ratio of solid/liquid were at 1/30 and 1/40 (wt/vol). Extraction was carried out at 400 rpm at the temperature of 30°C and 40°C for 2 hours using Heidolph Instrument Unimax 1010DT orbital shaker, Germany. The extracts were then filtered and analysed for total phenolic content. The solid/liquid ratio and temperature which gave better result was selected and applied in ultrasonic-assisted extraction.

### Ultrasonic-assisted extraction (UAE)

One gram of powdered sample in 80% ethanol was ultrasonicated for the duration of 5, 10, 15 and 20 min using a 37kHz ultrasonic generator (UT-106, SHARP, Japan). The mixture was then centrifuged at 400 rpm for 30 min using Heidolph Instrument Unimax 1010DT orbital shaker, Germany. The extracts were filtered and used for further analysis.

### Total Phenolic Content

Total phenolics were determined using a modified Folin-Ciocalteau colorimetric method [8,9]. A volume of 0.25ml of ethanolic extract was mixed with 1ml distilled water in a test tube. 0.25ml Folin-Ciocalteau reagent was added to the solution and allowed to react for 6 min. Then, 2.5ml of 7% sodium carbonate solution was added into the test tubes, and the mixture was diluted to 6ml with deionized water. Each sample was allowed to stand for 90 minutes, and the absorbance was measured at 760 nm using UV-Vis spectrophotometer UV1601 (Shimadzu Corporation, Australia). The measurement was compared to a standard curve of gallic acid concentrations and expressed as milligrams of gallic acid equivalents (GAE) per 100g dried sample.

### Statistical Analysis

Experiments were performed in triplicates. The results were expressed as mean ± standard deviation (S.D). The experimental data were analysed using analysis of variance (ANOVA). The mean values were considered at the 95% confidence level ($p = 0.05$). Statistical analysis was done using IBM SPSS Statistics (version 19).

## Results and Discussion

### Total phenolic content

In avocado, the pulp is consumed while the peel and seed are considered as wastes. It has been reported that the moisture content of avocado pulp was at ~74% [10,11]. In determining total phenolic content of avocado pulp, freeze dried material was prepared in this study. The total phenolic content of the pulp were estimated using the Folin-Ciocalteu method, which relies on the transfer of electrons from phenolic compounds to the Folin-Ciocalteu reagent in alkaline medium [12].

As recorded in Table 1, solid/liquid (wt/vol) ratio that gave a higher total phenolic content (TPC) reading was 1/30 at both temperatures used. Among the two temperatures, TPC was higher at the temperature of 40°C for both solid/liquid ratios. Thus, it was concluded that TPC was highest at solid/liquid ratio of 1/30 and at the temperature of 40°C. This condition gave the best result and it was taken as the best condition to perform further extraction.

Table 1. Total phenolic content of avocado pulp without UAE.

| | **Temperature** | | | |
|---|---|---|---|---|
| | **30°C** | | **40°C** | |
| Wt/Vol (g/ml) | mg GAE | ±S.D. | mg GAE | ±S.D. |
| 1/30 | 163.27 | 1.43 | 166.32 | 0.98 |
| 1/40 | 130.21 | 2.26 | 155.95 | 2.26 |

GAE, gallic acid equivalents per 100g dried sample. Mean ±S.D. n=3.

### Effect of UAE on total phenolic content

As indicated in Table 2, when extraction was repeated using UAE method, the TPC readings were higher compared to the extraction without UAE (166.32 mg GAE/100g dried sample extracted using 1/30 ratio at 40°C). The increase in TPC was at ~31% – 41% when 5 to 20 min of ultrasonication was applied. Among the four different durations used, the duration of 15 min gave the highest TPC reading at 235.77 mg GAE/100g dried sample. This TPC value was significantly higher when compared to the other duration.

Table 2. Total phenolic content for UAE of avocado pulp with different ultrasonication duration

| | **mg GAE** | **±S.D.** | **% Increase** |
|---|---|---|---|
| 5 min | 226.69 | 0.56 | 36.30 |
| 10 min | 219.19 | 0.28 | 31.79 |
| 15 min | *235.77 | 0.80 | *41.75 |
| 20 min | 222.44 | 0.85 | 33.74 |

GAE, gallic acid equivalents per 100g dried sample. Mean ±S.D. n=3. *$p < 0.05$.

Ultrasound-assisted extraction is an attractive alternative to conventional extraction techniques because it is easy, inexpensive and efficient. The main benefit of including ultrasound in an extraction procedure is that it increases yield and the extraction process can be done at a faster rate [7]. In this study, the usage of ultrasound has successfully enhanced the extraction process as indicated by the significantly higher TPC values and furthermore, has reduced the centrifuge time from 2 hours to 30 minutes (75% reduction).

This is made possible due to the propagation of ultrasound pressure waves through the solvent resulting in cavitation phenomena. The controlling mechanism of ultrasound-assisted extraction is generally attributed to mechanical, cavitation, and thermal effects which can result in disruption of cell walls, particle size reduction, and enhanced mass transfer across cell membranes, which lead to target compounds dissolving in the solvent, hence increasing yield with shorter time [13]. Research have found that ultrasonication is a critical pretreatment to obtain high yields of oils from almond, apricot and rice bran [14]. For extraction of saponin from ginseng assisted by ultrasound, the total yield and saponin yield increased by 15 and 30%, respectively [15]. The yield of oil extracted from soybeans also increased significantly when ultrasound was applied [16].

## Conclusion

The TPC of avocado pulp extracted with and without the application of ultrasonic were compared in this study. The results clearly indicated that the values of TPC were significantly higher when the extraction procedure included ultrasonic as assistance in the method. This study showed that avocado extraction can benefit from UAE especially by reducing the extraction time.

## Acknowledgement

This Work Has Been Supported By The Department of Nutrition and Dietetics, Faculty of Medicine and Health Sciences, Universiti Putra Malaysia.

## References

1. Chen H, Morrell P. L, Ashworth V. E. T. M, De La Cruz M and Clegg M. T. (2008). Tracing the Geographic Origins of Major Avocado Cultivars. *J Hered.* 100 (1):56–65.
2. Lu Q. Y, Arteaga J. R, Zhang Q, Huerta S, Go V. L. W. and Heber D. (2005). Inhibition of prostate cancer cell growth by an avocado extract: Role of lipid-soluble bioactive substances. *J Nutr Biochem.* 16(1): 23–30.
3. Rodríguez-Carpena J-G, Morcuende D, Andrade M-J, Kylli P, and Estévez M. (2011). Avocado (Persea americana Mill.) phenolics, in vitro antioxidant and antimicrobial activities, and inhibition of lipid and protein oxidation in porcine patties. *J Agric Food Chem.* 59(10): 5625–5635.
4. Kosińska A, Karamać M, Estrella I, Hernández T, Bartolomé B, and Dykes G. (2012). Phenolic compound profiles and antioxidant capacity of Persea americana Mill. peels and seeds of two varieties. *J Agric Food Chem.* 60(18): 4613–4619.
5. Wang W., Bostic T. R. and Gu L. (2010). Antioxidant capacities, procyanidins and pigments in avocados of different strains and cultivars. *Food Chem*. 122(4): 1193–1198.
6. Hurtado-Fernández E, Carrasco-Pancorbo A. and Fernández-Gutiérrez A. (2011). Profiling LC-DAD-ESI-TOF MS method for the determination of phenolic metabolites from avocado (Persea americana). *J Agric Food Chem.* 59(6): 2255–2267.
7. Wang L. and Weller C. L. (2006). Recent advances in extraction of nutraceuticals from plants. T*rends Food Sci Technol.* 17(6): 300–312.
8. Waterhouse A. L. (2002). *Determination of Total Phenolics.* Current Protocols in Food Analytical Chemistry. R.E., Wiley. p. I1.1.1–I1.1.8.
9. Wolfe K. L, Kang X, He X, Dong M, Zhang Q. and Liu R. H. (2008). Cellular antioxidant activity of common fruits. *J Agric Food Chem*. 56(18): 8418–8426.
10. David Klein. (1998). Avocado - the fruit that would make butter and meat obsolete. Living Nutrition Publications [Internet]. [cited 2014 Mar 25]; Available from: http://www.living-foods.com/articles/avocadoarticle.html
11. Husen R, Andou Y, Ismail A, Shirai Y. and Hassan M. A. (2014). Enhanced polyphenol content and antioxidant capacity in the edible portion of avocado dried with superheated-steam. *Int J Adv Res.* 2(8): 241–248.
12. Singleton V. L. and Rossi J. A. (1965). Colorimetry of Total Phenolics with Phosphomolybdic-Phosphotungstic Acid Reagents. *American Society for Enology and Viticulture.* 16(3): 144–158.
13. Shirsath S. R, Sonawane S. H. and Gogate P. R. (2012). Intensification of extraction of natural products using ultrasonic irradiations—A review of current status. *Chem Eng Process Process Intensif.* 53:10–23.
14. Sharma A. and Gupta M. N. (2004). Oil extraction from almond, apricot and rice bran by three-phase partitioning after ultrasonication. *Eur J Lipid Sci Technol.* 106(3):183–186.

15. Li H, Ohdaira E and Ide M. (1994). Effects of Ultrasound on Extraction of Saponin from Ginseng. *Jpn J Appl Phys.* 33(Part 1, No. 5B): 3085–3087.
16. Li H, Pordesimo L. and Weiss J. (2004). High intensity ultrasound-assisted extraction of oil from soybeans. *Food Res Int.* 37(7): 731–738.

The Malaysian Journal of ANALYTICAL SCIENCES ISSN 1394-2506

# HYDROTHERMAL OXIDATIVE DEGRADATION OF ORGANIC COMPOUNDS DERIVED FROM PRODUCED WATER

## (Penguraian Secara Pengoksidaan Hidrotermal Bahan Organik daripada Air Hasilan)

Ahmad Rafizan Mohamad Daud*, Mohd Zahid Marzuki, Mohd Muslim Abu Hassan

*Faculty of Chemical Engineering,*
*Universiti Teknologi Mara (UiTM), 40450 Shah Alam, Selangor, Malaysia*

**Corresponding author: ahmad2057@salam.uitm.edu.my*

**Abstract**

Produced water contains various hazardous organic compounds such as BTEX (benzene, toluene, ethyl benzene and xylene), phenolics and polycyclic aromatic hydrocarbons (PAHs). These compounds are stable and difficult to degrade by conventional wastewater treatment method. Aqueous based hydrothermal oxidative method is viewed as a promising approach for produced water treatment. The experiment was conducted in a micro-bomb reactor at subcritical water condition (200-300 $^{o}$C) and 30 minute reaction time. Hydrogen peroxide was used as an oxidant. The reaction products were analyzed using a Fourier Transform Infra-Red (FTIR) and a Gas Chromatography-Mass Spectroscopy (GC-MS). The hydrothermal treatment in the absence of an oxidant showed minimal degradation of organics for the temperature range investigated. With the presence of an oxidant, the organics degradation increased drastically to near completion within the 30 minute reaction time at 300 $^{o}$C. The results indicated that most of the organic compounds found in the produced water were successfully degraded using hydrothermal oxidative method.

**Keywords:** Produced water, organic, degradation, hydrothermal, oxidation

**Abstrak**

Air hasilan mengandungi pelbagai bahan organik berbahaya seperti BTEX (benzena, toluena, etil benzena dan xylene), fenol dan hidrokarbon polisiklik aromatik (PAHs). Bahan-bahan ini adalah stabil dan sukar untuk diuraikan dengan menggunakan kaedah rawatan air sisa buangan konvensional. Kaedah rawatan berasaskan air seperti pengoksidaan hidrotermal dilihat sebagai satu kaedah yang berpotensi untuk rawatan air hasilan. Eksperimen telah dijalankan menggunakan reaktor bom mikro pada keadaan air dibawah paras kritikal (200-300 $^{o}$C) dan masa tindakbalas 30 minit. Hidrogen peroksida telah digunakan sebagai ejen pengoksidaan. Hasil tindakbalas telah dianalisa menggunakan peralatan Fourier Transform Infra-Red (FTIR) dan Gas Chromatography-Mass Spectroscopy (GC-MS). Hasil kajian pada keadaan air dibawah paras kritikal mendapati rawatan secara hidrotermal tanpa sokongan ejen pengoksidaan tidak berupaya untuk menguraikan bahan organik. Penggunaan ejen pengoksida seperti hydrogen peroksida telah meningkatkan tahap penguraian bahan organic secara drastic menghampiri tahap penguraian sepenuhnya dalam jangkamasa 30 minit pada suhu 300 $^{o}$C. Hasil kajian juga menunjukkan kebanyakan bahan organik yang terdapat didalam air hasilan telah berjaya diuraikan menggunakan kaedah pengoksidaan hidrotermal.

**Kata kunci:** Air hasilan, penguraian, organik, hidrotermal, pengoksidaan

## Introduction

Increasing water production over oil is now a major environmental and economic challenge for the downstream and upstream industries. Lee et al. [1] reported that oil wells in the United States produced an average of more than 7 bbl of water for each barrel of oil. For crude oil wells nearing the end of their production life span, water can comprise as much as 98% of the material brought to the surface. Wells elsewhere in the world averages at 3 bbl of water for each barrel of oil produced [2].

Produced water (PW) is hazardous and requires specific disposal and handling care. It contains a broad range of organic as well as inorganic compounds including carboxylic acids, benzene, toluene, ethyl benzene, and xylene

(BTEX), polycyclic aromatic hydrocarbons (PAHs), inorganic nutrient such as ammonia, and heavy metals. Soluble organic compounds in PW or oily refinery waste discharges represent treatment problems for the industry. The organic components frequently recognized as high chain alkenes, phenolic categories, aromatic acids and also polycyclic aromatics are difficult to be eliminated with the conventional treatment processes. For instance, the organic compounds dissolved in the PW are simply not possible to be eliminated by physical separation alone. On the other hand, an aeration method usually resulted in massive amount of solid toxic sludge which requires further costly treatment such as incineration.

Considering that PW is highly aqueous in nature, hydrothermal oxidative treatment (oxidation in water at high pressure and temperature) is viewed as a promising alternative treatment approach. An oxidant such as hydrogen peroxide ($H_2O_2$) has been showed to enhance the degradation of organics under subcritical and critical condition [3]. This study aims to investigate the effect of hydrothermal oxidative reaction temperature on the degradation of organic compounds.

## Materials and Methods

### Material

The PW sample was obtained from a local oil refinery. Hydrogen peroxide, $H_2O_2$ (30% w/v) purchased from Merck Sdn. Bhd. was used as the oxidation agent. Dichloromethane (DCM) was used as a solvent for liquid-liquid extraction step.

### Experimental Procedure

Experiments were conducted in a micro-bomb reactor constructed by using a ½ inch stainless steel tubing. The volume of the reactor is 8 mL. The micro bomb reactor tubing is closed at both ends using stainless steel end caps whereby one of the ends was used for loading and unloading of reactants and reaction products. Typically, 5mL of liquid PW sample was filtered and loaded into the reactor. The reactor was heat up to the desired temperature using an electrical furnace and kept at the reaction temperature for 30 minutes. Next, the micro bomb reactor was quenched to a room temperature in a cold water bath to minimize the secondary reaction. The liquid organic product was extracted with the DCM solvent. The experiment was repeated with the addition of $H_2O_2$.

Extracted product was analyzed using a Perkin Elmer Spectrum One FTIR and an Agilent 7890A GC-MS. The GC-MS was equipped with a 30m x 0.25 mm ID fused silica capillary column bonded with 5 % methyl silicone (HP-5). The film thickness is 0.25-µm. The oven temperature program was set as follows: 40°C for 1 min, then heating at a 5°C $min^{-1}$ heating rate up to 260°C. The oven temperature was kept at the final temperature for 10 minutes.

## Results and Discussion

The fresh PW sample was analyzed with FTIR to determine the major organic classes present. Figure 1 shows the FTIR spectrum for the fresh PW sample. Three distinctive peaks at 3308, 2107 and 1635 $cm^{-1}$ wavenumber were observed. The 3308 $cm^{-1}$ is most likely corresponded to the alcohols or phenolic groups. Typically the 3400-3300 $cm^{-1}$ wavenumber represents the O-H bond [4]. The FTIR results also indicated the presence of alkynes or carboxylic acid (2250-2100 $cm^{-1}$) as well as alkenes group (1680-1600 $cm^{-1}$) in the fresh PW.

The PW sample was also analyzed using a GC-MS to identify the organic components present (Figure 2). Major compounds identified using the NIST library matching is presented in Table 1. They include hydroxyl, phenolic and carboxylic group compounds. Overall, the results were in agreement with the FTIR analysis.

Hydrothermal treatment of the fresh PW without an oxidant at 200, 250 and 300$^oC$ resulted in small degradation of its initial organics composition. Figure 3 indicates the various organics present in the hydrothermally treated PW at 300 $^oC$ as observed by the GC-MS analysis. Water at elevated temperature and pressure alone could not bring much effect on the degradation of organic compounds in the PW. This result is in line with the findings of Daud et al.[3] which found that minimum degradation of organics such as phenanthrene was observed under subcritical water condition. In this case, the role of the subcritical water is thought to be limited to being a reaction medium rather than a reactant or a catalyst for the reaction.

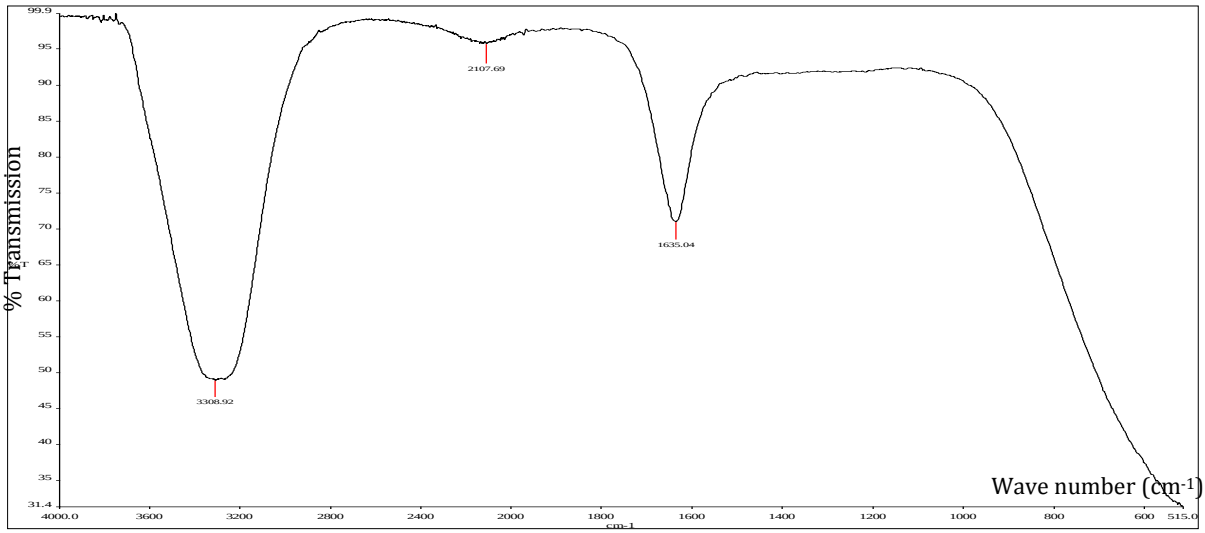



Figure 1. FTIR spectrum of fresh PW.

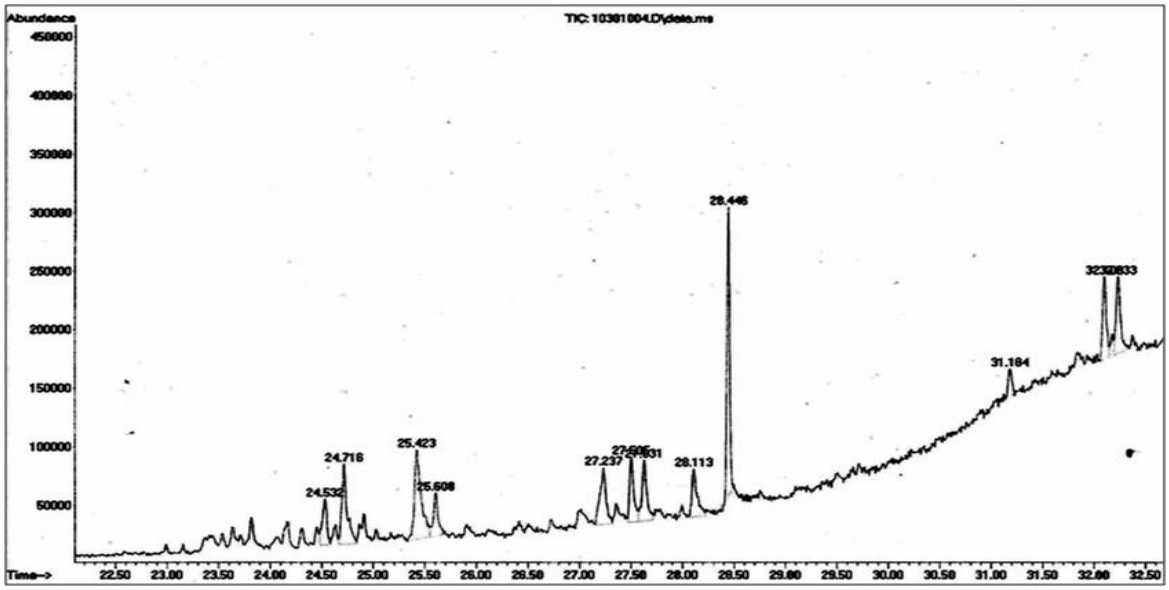



Figure 2. GC-MS chromatogram of fresh PW

Table 1. Major organic compounds present in the PW identified by GC-MS analysis

| Retention Times (min) | Major Compound Detected |
|---|---|
| 25.442 | Xaanthen-9-one,1-hydroxy-3,5,8-tri methoxy |
| | Decanamide- |
| | Hexadecanamide |
| 27.628 | 2,4-bis (1-phenyethyl)-phenol |
| 28.110 | 1,2-benzenedicarboxylic acid, diis ooctyl ester |
| | 9-Octadecenamide |
| 28.442 | 1,2-benzenedicarboxylic acid, mono (2-ethylhexyl) ester |
| | 2,4-bis (1-phenylethyl)-phenol |

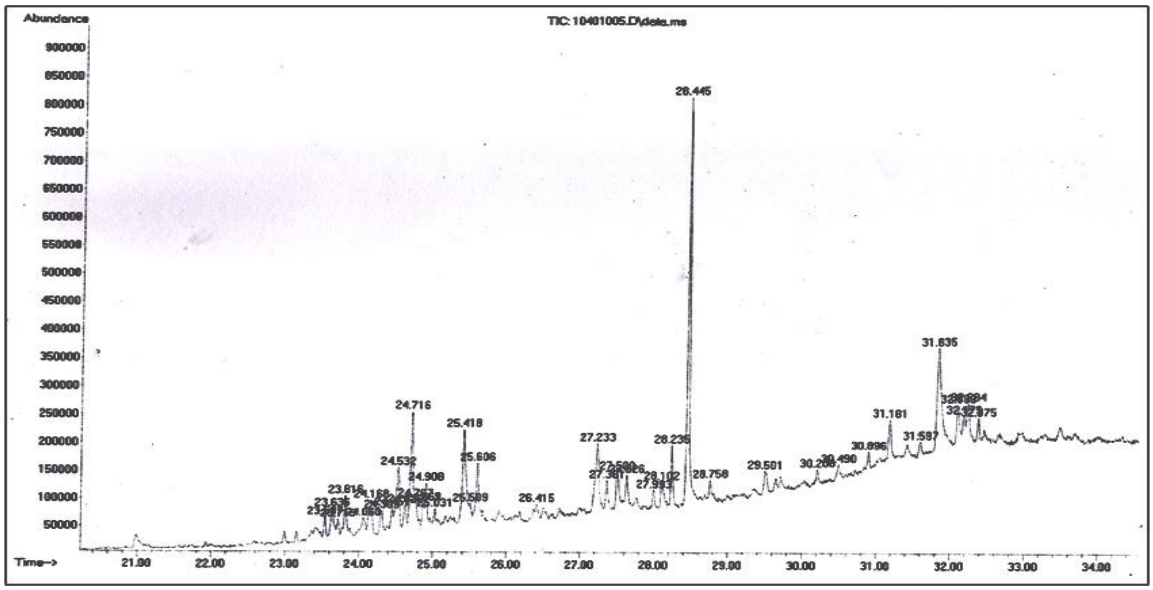



Figure 3. GC-MS chromatogram showing the organics distribution after hydrothermal treatment without an oxidant at 300ºC for 30 min reaction time.

The fresh PW was also subjected to hydrothermal oxidation treatment at 200, 250 and 300 $^{o}$C. With the addition of the $H_2O_2$ oxidant, the organics degradation was increased as the reaction temperature was raised from 200 to 300 $^{o}$C. Figure 4 shows the GC-MS result for the hydrothermal oxidation treatment at 300 ºC. It can be clearly observed that the addition of $H_2O_2$ has enhanced the degradation of the organics whereby major organic components such as phenolic, carboxylic acids and alkenes were fully decomposed into mostly water and carbon dioxide. Previous studies [3,5] have observed similar organics degradation pattern under subcritical and supercritical water conditions. The enhanced degradation of organics is most likely due to the presence of active radicals as a result of the $H_2O_2$ decomposition [6]. The dissociation pathways of $H_2O_2$ involved the formation of highly reactive $OH^{\bullet}$ and $HO_2^{\bullet}$ radicals. These radicals could in fact affect the organics degradation rate.

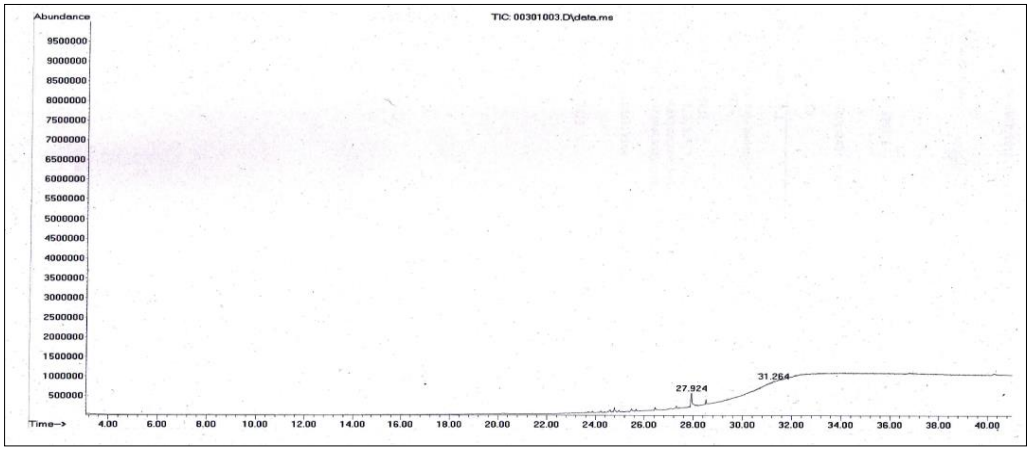



Figure 4. GC-MS chromatogram showing the destruction of organics under hydrothermal oxidation treatment at 300ºC and 30 min reaction time

## Conclusion

The fresh PW was found to contain mostly carboxylic, alkenes, phenolic and aromatics groups. These compounds were resistant to hydrothermal treatment alone whereby minimum degradation was observed up to 300˚C reaction temperature. However, with the presence of the $H_2O_2$ oxidant, the degradation of these compounds has proceeded to near completion largely due to the availability of $OH^{\bullet}$ and $HO_2^{\bullet}$ active radicals. It was found that almost all of the organics present in the sample were successfully degraded into mostly water and carbon dioxide at 300 $^{o}$C. This study established the influence of temperature and an oxidant in the degradation of organics derived from the PW under subcritical water conditions.

## Acknowledgement

The authors would like to thank the Ministry of Education Malaysia and Universiti Teknologi MARA for the financial support provided through research funds 600-RMI/FRGS 5/3(25/2013) and 600-RMI/DANA 5/3 RIF (131/2012) that has made this work possible.

## References

1. Lee, R., Seright, R., Hightower, M., Sattler, A., Cather, M., McPherson, B., Wrotenbery, L.,Martin, D. and Whitworth, M. (2002). Strategies for Produced Water Handling in NewMexico, Ground Water Protection Council Produced WaterConference, Colorado Springs, Oct. 16-17.
2. Khatib, Z.and Verbeek, P.(2003).Water to Value - Produced water management forfield development of mature and green fields,*Journal of PetroleumTechnology*.55(1):26-28.
3. Daud, A. R. M., Millan-Agorio, M., Hellgardt, K. And Kandiyoti, R. (2011). Partial Oxidative Cracking of Polycyclic Aromatic Compounds under Supercritical Water Conditions for Heavy Hydrocarbons Upgrading, Ph.D. Thesis,Imperial College London.
4. Lampman, G. M., Pavia, D. L., Kriz, G. S. and Vyvyan, J. R. (2009). Introduction to Spectroscopy. Fourth Edition, Brooks/Cole, Belmont, CA.
5. Onwudili, J. A. and Williams,P. T.(2007). Reaction mechanisms for the decomposition of phenanthrene and naphthalene under hydrothermal conditions,*The Journal of Supercritical Fluids*.39(3): 399-408.
6. Croiset, E., Rice, S.F. and. Hanush, R. G.(1997).Hydrogen peroxide decomposition in supercritical water, *AIChE Journal* 43(9): 2343-2352.

The Malaysian Journal of ANALYTICAL SCIENCES ISSN 1394-2506

# PRODUCTION OF BIOCHAR WITH HIGH MINERAL CONTENT FROM OIL PALM BIOMASS

## (Pengeluaran Biochar dengan Kandungan Mineral yang Tinggi dari Biomas Kelapa Sawit)

Juferi Idris[1,2,3], Yoshihito Shirai[1] , Yoshito Ando[1] , Ahmad Amiruddin Mohd Ali[1] , Mohd Ridzuan Othman[4] , Izzudin Ibrahim[4], Mohd Ali Hassan[4,5]*

[1]*Department of Biological Functions and Engineering, Graduate School of Life Science and Systems Engineering, Kyushu Institute of Technology, 2-4 Hibikino, Wakamatsu-ku, Kitakyushu, Fukuoka 808-0196, Japan.*
[2]*Faculty of Chemical Engineering, Universiti Teknologi MARA (UiTM) Sarawak, 94300, Kota Samarahan, Sarawak, Malaysia*
[3]*Faculty of Chemical Engineering, Universiti Teknologi MARA (UiTM) Malaysia, 40450, Shah Alam, Selangor, Malaysia.*
[4]*Department of Bioprocess Technology, Faculty of Biotechnology and Bimolecular Sciences,*
[5]*Department of Process and Food Engineering, Faculty of Engineering, Universiti Putra Malaysia, 43400 UPM Serdang, Selangor, Malaysia*

**Corresponding author: alihas@upm.edu.my*

**Abstract**

Carbonization of oil palm empty fruit bunch (OPEFB) biomass for the production of high mineral content biochar under an uncontrolled carbonization temperature and controlled air flow rate was studied using a pilot-scale brick carbonization reactor. The maximum temperature during the carbonization process was found to be in the range of 543 to 564 $^{o}$C at exhaust gas flow rate of 36 m$^3$/hr. All minerals (i.e P, K ,Mg, Ca, Na, Mn, Fe, Cr, AI) showed an increased from the feedstock concentration up to 300 %. The concentration of heavy metal extracted from OPEFB biochar was lower than listed ceiling permitted levels. This proposed system without electrical control and heating source is preferable to the industry due to its simplicity, ease of operation and low energy requirement making it suitable for OPEFB biochar production for mulching purposes with more than double the mineral content compared to raw OPEFB biomass.

**Keywords**: biochar, elemental, carbonization; oil palm empty fruit bunch; oil palm biomass

**Abstrak**

Karbonisasi kelapa sawit tandan kosong biomas untuk pengeluaran kandungan mineral yang tinggi biochar di bawah suhu karbonisasi yang tidak terkawal dan dikawal kadar aliran keluar asap telah dikaji menggunakan skala-pilot reaktor bata karbonisasi. Suhu maksimum semasa proses karbonisasi yang didapati dalam julat 543-564$^{o}$C pada kadar aliran asap pada 36 m$^3$/jam. Semua mineral (iaitu P, K, Mg, Ca, Na, Mn, Fe, Cr, AI) menunjukkan peningkatan dari kepekatan bahan mentah sehingga 300%. Kepekatan logam berat yang diekstrak daripada biochar adalah lebih rendah daripada paras siling dibenarkan disenaraikan. Sistem yang dicadangkan tanpa kawalan elektrik dan sumber pemanasan adalah lebih baik untuk industri karena kesederhanaan, kemudahan operasi dan keperluan tenaga yang rendah menjadikan ia sesuai untuk pengeluaran biochar kelapa sawit untuk tujuan mulsa dengan lebih daripada dua kali ganda kandungan mineral berbanding kelapa biomas mentah.

**Kata kunci** : biochar, unsur mineral, karbonisasi; kelapa sawit buah tandan kosong; biomas kelapa sawit

## Introduction

Biochar is a carbon-rich substance produced when biomass is heated at a certain temperature without any oxygen in a closed system [1]. The utilization of biochar give better improvement for soil fertility and reduce the use of chemical fertilizers as compared to raw biomass for the same purpose [2]. In addition, biochar from biomass can be used to prevent erosion and maintain soil moisture while reducing pollution to the environment [3]. Being one of the largest producer and exporter of palm oil, Malaysia palm oil industry is currently expanding rapidly and yields large

amount of poorly utilized waste biomass [4]. Malaysia has 362 palm oil mills, processing 71.3 million tons of fresh fruit bunch per year and producing an estimated 19 million tons of crop residues annually in the form of OPEFB, fibre and shell [5]. About 69,000 dry tons of OPEFB can be produced per year at a typical palm oil mill [6]. Currently, only mesocarp fibers and palm kernel shell are used as fuel to generate steam and electricity for palm oil mills requirement [7], while raw OPEFB is partly sold for mulching purpose [6].

Utilization of biomass-derived combustion fly ash comprises both char and inorganic ash component generated by biomass-based power plant for soil amendment are of recent interest [8]. The ash obtained from combustion with high inorganic content is useful for increasing the pH and providing nutrient [9]. Moreover, gaseous emission generated from power plant or incinerator has created pollution to the environment. In this study, we propose an uncontrolled carbonization to produce biochar with high mineral content and low heavy metal using biomass feedstock. Under uncontrolled carbonization, a sustained combustion process without an electrical control source is more preferable to the industry due to its simplicity, ease of operation and low energy requirement.

## Materials and Methods

Pressed-shredded OPEFB biomass particle size range 100-150 mm was obtained from Seri Ulu Langat Palm Oil Mill, Dengkil, Selangor, Malaysia. The carbonization was carried out in the 1m x 1m clay brick reactor with 30 kg capacity using portable propane burner where initial burning on top of the reactor for about 5-10 minutes before being completely closed with no oxygen entrance. The temperatures inside the reactor were monitored using three k-type thermocouples positioned at different heights from top to bottom of the reactor. The exhaust gas flow rate discharged from the reactor was set at 36 $m^3$/hr to ensure the circulation of hot air distributed uniformly from top to the bottom before being discharged through 3 meter chimney. The experiments were repeated at least two times to ensure reproducibility.

The main elements obtained from raw OPEFB biomass and OPEFB biochar samples was analyzed using inductive coupled plasma-optical effluent spectrophotometer (ICP-AES, model: Perkin Elmer 2100). About 1-2 gram of the samples was first placed in the furnace at temperature gradually to 300 $^oC$ until smoke ceased and was raised up to 500 $^oC$ and continued at this temperature until a white or greyish-white ash was obtained. The sample was then digested using concentrated hydrochloric acid (37% v/v) and nitric acid (20% v/v) [10].

## Results and Discussion

### Raw OPEFB elemental characteristic

Table 1 shows the main elementals obtained from the raw OPEFB biomass. All elemental found in this study is according to Wan Razali et al. [11] where the source of raw OPEFB biomass collected was from the same place (Seri Ulu Langat Palm Oil Mill, Dengkil, Selangor, Malaysia). High concentrations of potassium (K) and phosphorus (P) is due to usage of fertilizers which contain potassium nitrate ($KNO_3$) and phosphoric acid ($H_3PO_4$) [12].

### Effect of the OPEFB biomass on the carbonization temperature profile under uncontrolled temperatures

Figure 1 shows the average temperature profiles measured during carbonization of OPEFB biomass under uncontrolled carbonization temperatures. The experiment was repeated at least twice to ensure reproducibility of the process. The temperature in the reactor gradually increased moments after the fire was introduced from the top shown in Figure 1. The carbonization start time measured when the temperature reached 300 $^oC$, The maximum temperature for experiment 1 and 2 were found to be 564 and 543 $^oC$ respectively and were found maintained above 300 $^oC$ at average retention time 630 min for long period of carbonization process which was suitable for targeting char production [13]. Generally the temperatures increased as combustion moved from top towards the bottom of the reactor.

Table 1. Elemental analysis of EFB samples carried out by ICP-OES

| | Concentration ppm (%) | |
|---|---|---|
| **Elements** | **This study** | **Wan Razali et al [11]** |
| Phosphorus, P | 470 ±180 (0.05%) | 0.1% |
| Calcium, Ca | 1330 ±410 (0.13%) | 0.2% |
| Sulphur, S | 1730±210 (0.17%) | 0.1% |
| Iron, Fe | 561.57 ±131.64 (0.06%) | 0.1% |
| Potassium, K | 12200 ±2600 (1.22%) | 1.4% |
| Magnesium, Mg | 870 ±270 (0.09%) | 0.1% |
| Sodium, Na | 71.97 ±8.23 | - |
| Chromium, Cr | 2.03 ±0.12 | 39.1 ppm |
| Manganese, Mn | 21.47 ±4.18 | 26.4 ppm |
| Boron, B | 11.9 ±1.42 | 1.8 ppm |
| Cadmium, Cd | 0.2 ±0.14 | ND |
| Copper, Cu | 17.3 ±5.09 | 19.6 ppm |
| Nickel, Ni | 1.8 | ND |
| Lead, Pb | 1.13 ±0.21 | 0.2 ppm |
| Zinc, Zn | 16 ±5.9 | 22.4 ppm |
| Silicon, Si | 304.1 ±90.25 | - |

ND=Not detected

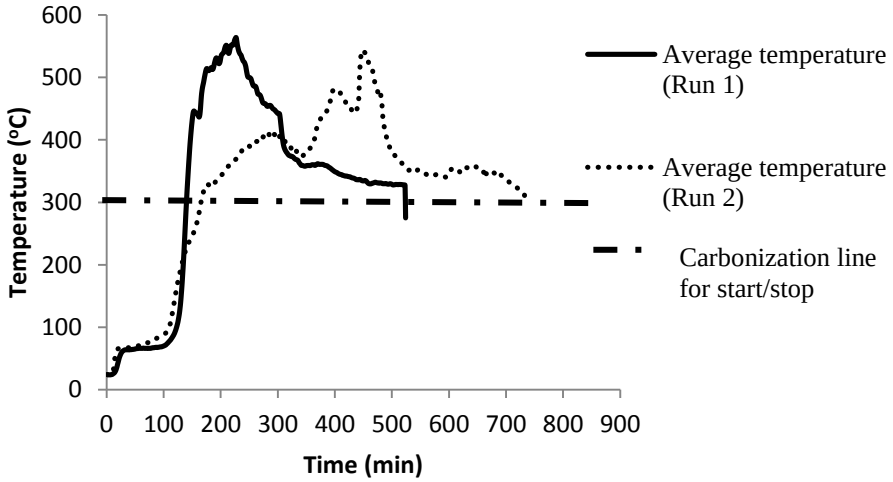



Figure 1. Temperature profiles of during carbonization of OPEFB biomass under uncontrolled carbonization temperatures and controlled air flow rates.

**Elemental content of OPEFB biochar at different particle size under uncontrolled carbonization temperature and controlled air flow rates**

Carbonization concentrated minerals of OPEFB biochar is shown in Figure 2. Being rich in minerals, OPEFB biochar may be better suited as alternative chemical fertilizer or at least reduced the usage of them. For example, P-content in OPEFB biochar increased tremendously from the raw OPEFB biomass concentration by 310 %. K-content also has high effect on the soil fertility increased by 286 %. Other mineral (i.e Mg, Ca, Na, Mn, Fe, Cr, AI) also showed increased from the feedstock concentration by 142-376 %. Although all minerals reported in this study were lower than fly ash but P and K content which were 1.46 and 34.85 g/kg respectively was comparable to Pan and Eberhardt (2011) which found in the range 2.44 and 20.33 g/kg respectively.

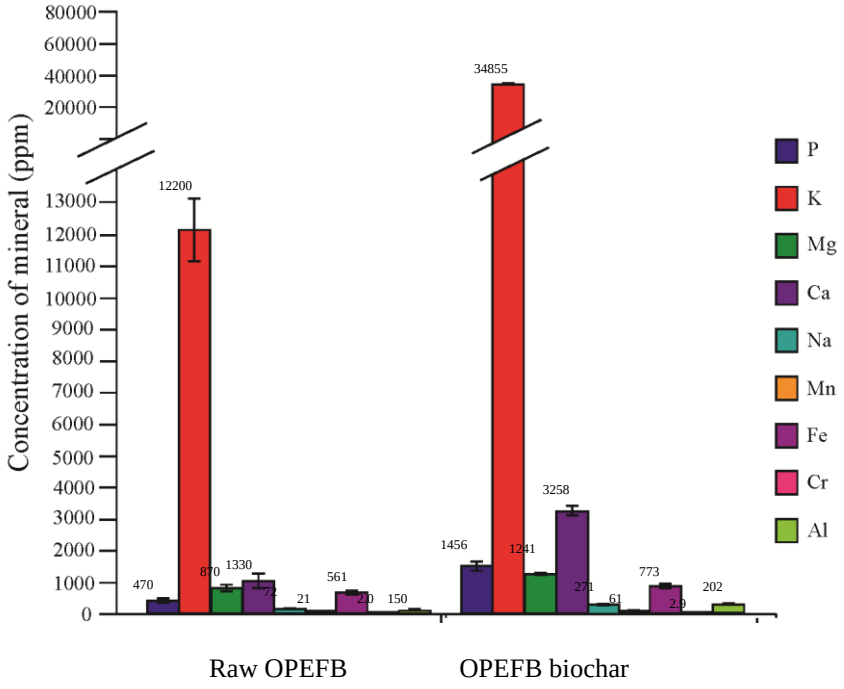



Figure 2. Comparison of mineral concentration between raw OPEFB and OPEFB biochar

Table 2. Heavy metal concentration of OPEFB biochar

| Heavy metal | Concentration (ppm) | |
|---|---|---|
| | This study | Pan and Eberhardt [8] |
| Cu | 28.53 (±4.27) | 37.25(3.64) |
| Zn | 55.93 (±8.80) | 345.45(5.05) |
| Cd | 0.40 (±0.20) | 4.39(0.09) |
| Pb | 23.7 (±2.97) | 11.83(0.17) |
| Ni | 2.53 (±1.17) | 47.29(3.27) |
| Mo | 8.27 (±3.63) | - |
| As | 71.4 (±23.19) | 10.06(10.90) |

The concentration of heavy metal (Table 2) extracted from OPEFB biochar were lower than standards for the use or disposal of sewage sludge listed ceiling concentration under 40 C.F.R §503 [14]. Lower concentration of Cd due to lost in gas oil phase at carbonization up to 400 $^{o}$C which was within temperature of this study however in contrast, Cd, Zn, and Cu did not exhibit losses to the same phase [15]. As compared to ash fly heavy metal reported by Pan and Eberhardt (2011), the concentration of heavy metal in this study were much lower, thus effect on the plant growth can be minimized.

## Conclusion

The application of uncontrolled carbonization in a pilot scale for the production of high mineral content biochar from OPEFB biomass successfully increased from the feedstock concentration by 300 % and phosphorus and potassium were comparable with other studies. Meanwhile heavy metals were found lower than listed ceiling concentration. This proposed system without electrical control and heating source is preferable to the industry due to its simplicity, ease of operation and low energy requirement.

## Acknowledgement

The authors would like to thank Kyushu Institute of Technology (Kyutech), Japan, Universiti Putra Malaysia (UPM), Malaysia, Universiti Teknologi MARA (UiTM), Malaysia and Universiti Teknologi MARA (UiTM) Sarawak for their financial and technical support towards this research.

## References

1. Gaunt, J. L. and Lehmann, J. (2008). Energy balance and emissions associated with biochar sequestration and pyrolysis bioenergy production. *Environ Sci Technol* 42: 4152–4158.
2. Abu Bakar, R., Darus, S. Z. and Kulaseharan, S. (2010). Jamaluddin N. Effects of ten year application of empty fruit bunches in an oil palm plantation on soil chemical properties. *Nutr Cycl Agroecosystems* 89:341–349.
3. Lim, K. C. and Zaharah, A. R. (2000). Decomposition and n & k release by oil palm empty fruit bunches applied under mature palms. *J Oil Palm Res* 12:55–62.
4. Malaysian palm oil council (MPOC). Oil palm plantation (2014). Oil palm plantation .http://www.mpoc.org.my/Overview.aspx. [aceessed 20.4.2014]
5. Sumathi, S., Chai, S. P. and Mohamed, A. R. (2008). Utilization of oil palm as a source of renewable energy in Malaysia. *Renew Sustain Energy Rev* 12: 2404–2421.
6. Yoshizaki, T., Shirai, Y., Hassan, M. A., Baharuddin, A. S., Raja Abdullah, N. M. and Sulaiman, A. (2013). Improved economic viability of integrated biogas energy and compost production for sustainable palm oil mill management. *J Clean Prod* 44:1–7.
7. Yusoff, S. (2006). Renewable energy from palm oil – innovation on effective utilization of waste. *J Clean Prod*, 14:87–93.
8. Pan, H. and Eberhardt, T.L. (2011). Characterization of the fly ash from the gasification of wood and assessment for its application as a soil amendment. *Bioresources* 6:3987–4004.
9. Odlare, M. and Pell, M. (2009). Effect of wood fly ash and compost on nitrification and denitrification in agricultural soil. *Appl Energy* 86:74–80.
10. Idris, J., Musa, M., Yin, C. Y. and Hamid, K. H. K. (2010). Recovery of nickel from spent catalyst from palm oil hydrogenation process using acidic solutions. *J Ind Eng Chem* 16:251–255.
11. Razali, W. A. W., Baharuddin, A. S., Talib, A. T., Sulaiman, A., Naim, M. N. and Hassan, M.A. (2012). Degradation of oil palm empty fruit bunches (OPEFB) fibre during composting process using in-vessel composter. *BioResources* 7:4786–805.
12. Razuan, R., Chen, Q., Finney, K. N., Russell, N. V., Sharifi, V. N. and Swithenbank, J. (2011). Combustion of oil palm stone in a pilot-scale fluidised bed reactor. *Fuel Process Technol* 92:2219–2225.
13. Spokas, K. A., Cantrell, K. B., Novak, J. M., Archer, D. W., Ippolito, J. A. and Collins, H. P. (2012). Biochar: a synthesis of its agronomic impact beyond carbon sequestration. *J Environ Qual* 41:973–89.
14. EPA. (2005). Title 40-Protection of environment. Standards for the use or disposal of sewage sludge. Code of federal regulations. Washington, D.C.
15. Lievens, C., Yperman, J., Vangronsveld, J. and Carleer, R. (2008). Study of the potential valorisation of heavy metal contaminated biomass via phytoremediation by fast pyrolysis: Part I. Influence of temperature, biomass species and solid heat carrier on the behaviour of heavy metals. *Fuel*, 87:1894–905.

The Malaysian Journal of ANALYTICAL SCIENCES ISSN 1394-2506

# THERMOGRAVIMETRIC ANALYSIS OF RICE HUSK AND COCONUT PULP FOR POTENTIAL BIOFUEL PRODUCTION BY FLASH PYROLYSIS

## (Analisa Thermogravimetrik Sekam Padi dan Pulpa Kelapa Untuk Mengkaji Potensi Penghasilan Minyak Bio Melalui Pirolisis Pantas)

Noorhaza Alias[1], Norazana Ibrahim[1]*, Mohd. Kamaruddin Abd. Hamid[2], Hasrinah Hasbullah[3], Roshafima Rasit Ali[4], Aziatul Niza Sadikin[4], Umi Aisah Asli[4]

[1]*UTM-MPRC Institute for Oil and Gas, Faculty of Petroleum and Renewable Energy Engineering,*
[2]*Process Systems of Engineering Centre, Faculty of Chemical Engineering,*
[3]*AMTEC, Faculty of Petroleum and Renewable Energy Engineering,*
[4]*Faculty of Chemical Engineering,*
*Universiti Teknologi Malaysia, 81310 UTM Johor Bahru, Johor, Malaysia*

**Corresponding author: norazana@petroleum.utm.my*

**Abstract**

The purpose of this paper is to study the characteristics and thermal degradation behavior of rice husk and coconut pulp for biofuel production via flash pyrolysis technology. The elemental properties of the feedstock were characterized by an elemental analyzer while thermal properties were investigated using thermogravimetric analyzer (TGA). The pyrolysis processes were carried out at room temperature up to 700°C in the presence of nitrogen gas flowing at 150 ml/min. The investigated parameters are particle sizes and heating rates. The particle sizes varied in the range of $dp_1 < 0.30$ mm and $0.30 \leq dp_2 < 0.50$ mm. The heating rates applied were 50°C/min and 80°C/min. It was shown smaller particle size produces 2.11-3.59% less volatile product when pyrolized at 50°C/min compared to 80°C/min. Higher heating rates causes biomass degrades in a narrow temperature range by 25°C. It also increases the maximum peak rate by 0.01 mg/s for rice husk at $dp_1$ and 0.02 mg/s at $dp_2$. In case of coconut pulp, the change is not significant for $dp_1$ but for $dp_2$ a 0.02 mg/s changes was recorded.

**Keywords:** rice husk, coconut pulp, thermogravimetric analyses, flash pyrolysis, biofuel

**Abstrak**

Tujuan kajian ini dijalankan adalah untuk mengenalpasti ciri-ciri serta corak degradasi therma sekam padi dan pulpa kelapa bagi tujuan penghasilan minyak bio melalui proses pirolisis pantas. Komposisi unsur ditentukan dengan menggunakan penganalisa unsur manakala ciri-ciri therma dikaji menggunakan penganalisa thermogravimetrik (TGA). Proses degradasi therma dijalankan pada suhu bilik sehingga mencapai 700°C, dengan aliran gas nitrogen pada kadar 150 ml/min. Dua pemboleh ubah telah dikenalpasti sebagai fokus kajian iaitu saiz partikel dan kadar pemanasan. Saiz partikel yang digunakan adalah $dp_1 < 0.30$ mm dan $0.30 \leq dp_2 < 0.50$ mm manakala kadar pemanasan ditetapkan pada suhu 50°C/min dan 80°C/min. Hasil kajian mendapati bahawa saiz partikel yang lebih kecil menghasilkan kurang produk meruap sebanyak 2.11 - 3.59% apabila diproses pada suhu 50°C/min. Kadar pemanasan yang tinggi menyebabkan kedua-dua sampel lupus pada jangka suhu yang lebih cepat iaitu sebanyak 25°C. Kadar degradasi maxima bagi sekam padi turut meningkat sebanyak 0.01 mg/s pada $dp_1$ dan 0.02 mg/s pada $dp_2$. Pulpa kelapa tidak mencatat sebarang perubahan yang signifikan pada $dp_1$ tetapi pada $dp_2$ peningkatan sebanyak 0.02 mg/s telah direkodkan.

**Kata kunci:** sekam padi, pulpa kelapa, analisa thermogravimetrik, pirolisis pantas, minyak bio

## Introduction

Biomass is defined as the products fraction of biologically degradable waste from agriculture which includes animal and vegetable materials, forestry and biologically degradable fraction of industrial and household waste [1]. In Malaysia, the amount of biomass generated from agricultural waste is 72, 962 kton/year and holds an annual potential electricity generation of 5863 GWh [2**]**. The technology of converting biomass into energy is a right option

since it is a renewable type of energy source that could dramatically improve the environment, economy and energy security. Fast pyrolysis is one of the most promising technologies of biomass utilization, and it is also the first stage of biomass thermochemical conversion. Under this process, biomass is converted into liquid oil, char and gases. Up to 50-75% of biomass can be converted into liquid oils, which can be directly used in combustion application or upgraded for high-end chemical recovery. In the absence of oxygen, the yields and compositions of pyrolysis products depends on the type of biomass, operating temperature, heating rates, type of reactors, particles size and co-reactant [3]. The objective of this study is to investigate the characteristic and thermal degradation behavior of rice husk and coconut pulp by using thermogravimetric analysis (TGA). This study will provide important information for potential biofuels production from these two types of biomass.

## Materials and Methods

### Materials Preparation and Characterization

Rice husk was obtained from Bernas factory in Sabak Bernam, Selangor while coconut pulp was obtained from local coconut milk producer in Johor Bahru, Johor. All feedstock were first milled and sieved into smaller particle size of <0.50 mm. The characterizations of rice husk and coconut pulp were performed in order to obtain its ultimate, proximate and high heating value (HHV). The ultimate analysis was carried by out using elemental analyzer (The PerkinElmer 2400 Series II) to determine the amount of carbon, hydrogen, nitrogen and sulphur in the feedstock. The proximate analysis was conducted by using thermogravimetry analyzers (TGA) (TA Instruments Q500) to analyze volatile matter (VM), fixed carbon (FC), moisture content and ash content in all samples. The HHV of rice husk and coconut pulp were determined by using bomb calorimeter (Suprashesh ABC-123).

### Experimental Procedures

TGA was carried out in the presence of nitrogen ($N_2$) at the flowing rate of 150 ml/min. Rice husk and coconut pulp samples between 0.5 and 1.0 g were pyrolyzed to a maximum temperature of 700°C. The samples were first heated to 110°C and kept at that temperature for 30 minutes to remove any moisture. After that, the samples were heated at the rate of 50°C/min and 80°C/min individually until it reaches the maximum temperature. The experiment was repeated for each type of biomass at different particle size as follows: $dp_1 < 0.30$ mm and $0.30 \leq dp_2 < 0.50$ mm.

## Results and Discussion

### Properties and Composition of Feedstock

From the analysis conducted, moisture contents for both types of biomass vary with 2.82%. Higher moisture content decreases the heating value of the coconut pulp, in this case by 0.88% because of some energy were needed to vaporize the moisture at the beginning of conversion process [4]. Rice husk contains high amount of ash due to the presence of silica that can constitute up to 90-97% in the final residue [5]. Coconut pulp contains higher volatile matter and fixed carbon content compared to rice husk by 5.22% and 7.37%, respectively. The elemental properties for both samples do not differ much as been reported. In general, coconut pulp contains higher amount of carbon and hydrogen but lower nitrogen and sulphur content. The properties of rice husk and coconut pulp used in this study are summarized in Table 1.

In general, the pyrolysis of any biomass can be divided into three phases which are drying and evaporation of light components (phase I), devolatilization of hemicellulose and cellulose (phase II) and decomposition of lignin (phase III). Phase I occurs at temperature below 150°C, phase II starts from 150°C to 450°C and finally phase III is attained at temperature above 450°C. From Fig. 1 (a), it was observed that the amount of residue left for $dp_1$ at higher heating rate (80°C/min) are 2.43% and 3.01% lower for rice husk and coconut pulp, respectively. When bigger particle size $dp_2$ is used however, the residue at higher heating rates is 1.99% and 1.18% more for rice husk and coconut pulp, respectively (see Fig.2 (a)). It is well agreed in the literature that larger particle sizes yields more residue because poor heat transfer to the inner surfaces leads to a low average particles temperature [6,7]. However, in this study it was shown that particle size does not provide a significant effect on thermal degradation of both rice husk and coconut pulp.

Table 1. Properties of rice husk and coconut pulp

| Analysis | | Rice husk | Coconut pulp |
|---|---|---|---|
| **Proximate analysis (db wt %)** | Moisture content | 6.73 | 9.55 |
| | Ash content | 17.06 | 0.45 |
| | Volatile matter | 62.61 | 67.83 |
| | Fixed Carbon | 14.96 | 22.30 |
| | High heating value (HHV) (MJ/Kg) | 17.91 | 17.03 |
| **Ultimate analysis (db wt %)** | Carbon (C) | 38.22 | 39.44 |
| | Hydrogen(H) | 5.88 | 6.14 |
| | Nitrogen (N) | 0.68 | 0.50 |
| | Sulphur (S) | 0.07 | 0.04 |

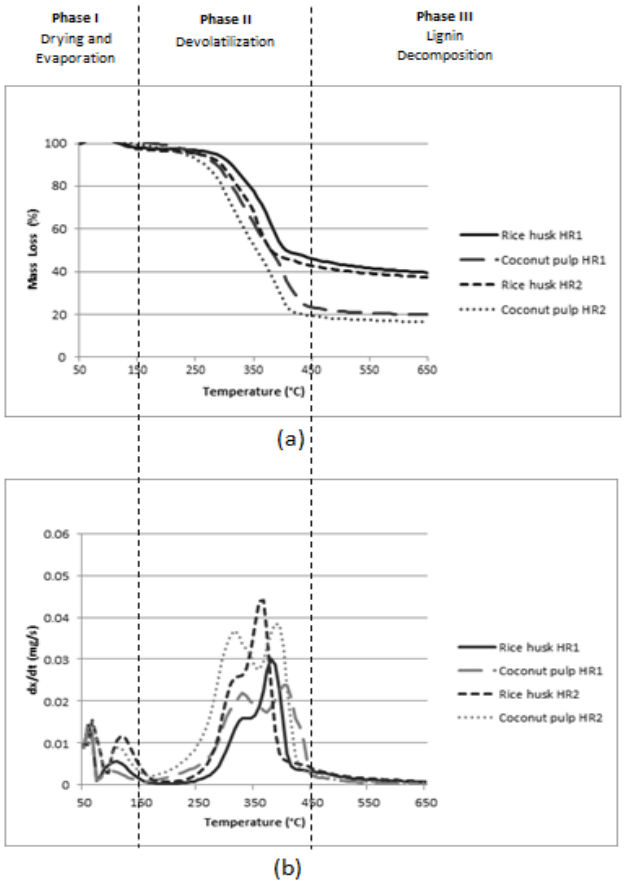



Figure 1. A plot of (a) TGA and (b) DTG for $dp_1$ at both heating rates, where HR1 = 50°C/min and HR2 = 80 °C/min

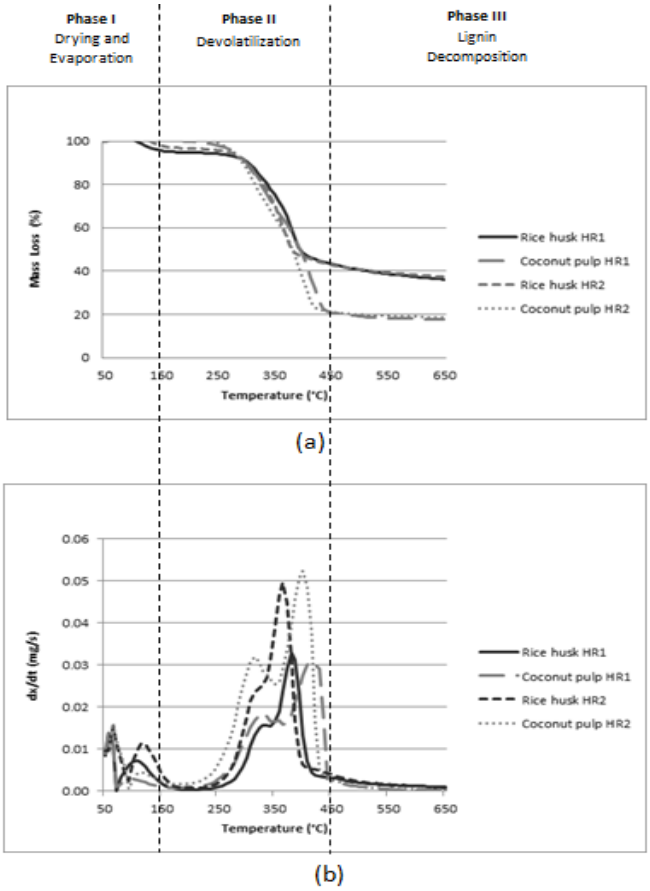



Figure 2. A plot of (a) TGA and (b) DTG for $dp_2$ at both heating rates, where HR1 = 50°C/min and HR2 = 80 °C/min

**Thermogravimetric Analysis**

Thermogravimetric results for all eight samples are plotted as a function of temperature as shown in Figure 1 and 2. Fig. 1 (b) and Fig. 2 (b) illustrate the effects of heating rates and particle sizes on degradation peak rates. It was observed that higher heating rates speed up the degradation process by 0.01 mg/s (at 370°C) for rice husk samples in $dp_1$, while $dp_2$ recorded almost a 0.02 mg/s difference (at 355°C). The peak in phase I corresponds to the moisture released from the biomass feedstock. There are two peaks in phase II: the first peak shows the degradation of lower molecular weights components (hemicellulose) from 180°C to 310°C and second peaks indicates cellulose degradation which occurs between 320°C and 410°C. Lignin gradually degrades over a range of temperature from 380°C to 700°C. It is noted that when the temperature reaches 650°C, the degradation rates are no longer significant as most volatiles had already been pyrolysed and the rest were converted into char and gases. Lower heating rates causes the biomass to decompose under a wider temperature range from 225°C to 450°C compared to 250°C to 450°C.

The peaks pattern in phase II for coconut pulp is not similar at different particle size. In Fig. 1 (b), both peak rates does not changes that much (0.002 mg/s difference from 325-410°C) but in Fig. 2 (b) the difference is 0.02 mg/s (at 330-425°C). In this study, the pyrolysis behavior for coconut pulp is very unpredictable and is not well understood since not much research had been conducted before. However, it produced a very high amount of volatile and proves to be a very favorable feedstock for biofuel production via flash pyrolysis. Due to high composition of lignin

(24.4%) [8], the amount of volatiles for rice husk is lower compared to coconut pulp (10.0 % lignin) [9]. Biomass with more cellulose and hemicellulose contents (i.e. herbaceous biomass) will produces more volatiles compared to woody biomasses [10]. Table 2 summarized the product yields for both type of feedstock at different particle size and heating rates:

Table 2. Pyrolysis product yeilds for rice husk and coconut pulp at heating rate 50° C/min and 80° C/min

| **Types of biomass** | **Product yields (%)** | **Heating rate (50°C/min)** | | **Heating rate (80°C/min)** | |
|---|---|---|---|---|---|
| | | $dp_1$ | $dp_2$ | $dp_1$ | $dp_2$ |
| Rice husk | Char | 39.09 | 35.50 | 37.47 | 37.49 |
| | Volatile matter | 60.91 | 64.50 | 62.53 | 62.51 |
| Coconut pulp | Char | 19.57 | 17.46 | 16.56 | 18.64 |
| | Volatile matter | 80.43 | 82.54 | 83.44 | 81.36 |

## Conclusion

There are many factors influencing the pyrolysis process. The main factors discussed in this research are the effect of particle size, heating rate and the properties of biomass itself. Smaller particle size produces 2.11-3.59% less volatile product when pyrolized at 50°C/min. At higher heating rate however, the amount of volatiles is 2.08% higher for $dp_1$. As such, it can be concluded that particle size has insignificant effect on pyrolysis of rice husk and coconut pulp. Higher heating rate however causes biomass to be degraded under a narrow temperature range by 25°C. It also increases the maximum peak rate by 0.01 mg/s for rice husk at $dp_1$ and 0.02 mg/s at $dp_2$. In case of coconut pulp, the change is not significant for $dp_1$ but for $dp_2$ a 0.02 mg/s changes were recorded. High lignin content in rice husk lowers the amount of volatiles produces which is in accordance to literature findings. Further studies need to be conducted to understand more on the behavior of coconut pulp pyrolysis since it provides a promising potential feedstock for biofuel production.

## Acknowledgement

The authors gratefully acknowledge the financial support from Universiti Teknologi Malaysia and Ministry of Higher Education (MOHE) of Malaysia (Q.J130000.2542.07H10 and R.J130000.7842.4L128).

## References

1. Patel, B. and Gami, B. (2012). Biomass Characterization and its Use as Solid for Combustion. *Iranica Journal of Energy and Environment*, 123-128.
2. Zafar, S., (2014). Bioenergy Developments in Malaysia. *Retrieved from http://www.bioenergyconsult.com/tag/biomass-resources-in-malaysia/*
3. Jahirul, M. I., Rasul, M. G., Chowdhury, A. A. & Ashwath, N. (2012). Biofuels Production through Biomass Pyrolysis - A Technological Review. *Energies 5: 4952-5001*.
4. Mansaray, K. G. and Ghaly, A. E. (1997). Physical and Thermochemical Properties of Rice Husk. *Energy Sources*, 27: 989-1004.
5. Chuayjuljit, S., Eiumnoh, S. and Potiyaraj, P. (2001). Using Silica from Rice Husk as a Reinforcing Filler In Natural Rubber. *Journal of Scientific Research Chulalongkorn University*, 26: 127-137.
6. Stenseng, M., Jensen, A. and Dam-Johansen, K. (2001). Investigation of Biomass Pyrolysis by Thermogravimetric Analysis and Differential Scanning Calorimetry. *Journal of Analytical and Applied Pyrolysis* 58-59: 765-780.

7. Stresov, V., Moghtaderi, B. and Lucas, J. (2003). Thermal Study of Decomposition of Selected Biomass Samples. *Journal of Thermal Analysis and Calorimetry*, 72: 1041-1048.
8. Wannapeera, J., Worasuwannarak, N. and Pipatmanomai, S. (2008). Product Yields and Characteristics of Rice Husk, Rice Straw and Corncob During Fast Pyrolysis in a Drop-Tube/Fixed-Bed Reactor. *Songklanakarin J. Sci. Technol*. 30 (3): 393-404.
9. Ho, Y.S., and Ofomaja, A.E. (2006). Biosorption Thermodynamics of Cadmium on Coconut Copra Meal as Biosorbent. *Biochemical Engineering Journal*, 30: 117–123.
10. Burhennea, L., Messmer, J., Aicher, T. and Laborie, M. (2013). The Effect of The Biomass Components Lignin, Cellulose and Hemicellulose on TGA and Fixed Bed Pyrolysis. *Journal of Analytical and Applied Pyrolysis*, 101: 177–184.

The Malaysian Journal of ANALYTICAL SCIENCES ISSN 1394-2506

# THERMAL CHARACTERIZATION OF MODIFIED *TACCA LEONTOPETALOIDES* STARCH AND NATURAL RUBBER BASED THERMOPLASTIC ELASTOMER

## (Pencirian Termal antara Modifikasi Kanji *Tacca leontopetaloides* dan Getah Semulajadi berasaskan Termoplastik Elastomer)

Ainatul Mardhiah Mohd Amin*, Nur Shahidah Ab Aziz, Nurul Shuhada Mohd Makhtar, Miradatul Najwa Mohd Rodhi, Suhaila Mohd Sauid

*Faculty of Chemical Engineering,*
*Universiti Teknologi MARA, 40450 Shah Alam, Selangor Darul Ehsan, Malaysia*

**Corresponding author: mardhiah.amin@yahoo.com*

**Abstract**

The purpose of this study is to identify the potential of *Tacca leontopetaloides* starch as bio-based thermoplastic elastomers, TPEs. Starch based polymer had been recognized to have highly potential in replace existing source of conventional elastomeric polymer. The modification process of blending starch with natural rubber, plasticizers, additives, and filler contribute to the enhancement and improvement for the properties of starch in order to produce biopolymers by approaching the properties of TPEs. Thermal properties of starch based thermoplastic was studied to evaluate the decomposition and degradation of the samples by using Thermogravimetric Analysis, TGA while the properties of endothermic reactions of the samples were thermally analyzed via Differential Scanning Calorimetry, DSC. From the analysis, it was found that the thermal properties of samples were revealed by recognizing GM-2 (green materials, GM) has high thermal resistance towards high temperature up to 480.06°C with higher amount of residue which is 4.97 mg compared to other samples. This indicates GM-2 comprises of superior combination of ratio between natural rubbers and glycerol (plasticizer) in purpose of approaching the properties of Thermoplastic Elastomers, TPEs.

**Keywords:** biopolymer, green material, *Tacca leontopetaloides*, thermal characterization

**Abstrak**

Kajian ini dijalankan bertujuan mengenal pasti potensi kanji *Tacca leontopetaloides* untuk dijadikan sebagai bahan asas bio yang akan digunapakai dalam pembuatan termoplastik elastomer, TPE. Kanji *Tacca* ini dikenalpasti mempunyai potensi yang tinggi dalam menggantikan sumber yang ada bagi pembuatan konvensional elastomerik polimer. Proses modifikasi antara adunan kanji, getah semulajadi, pemplastik, aditif dan bahan pengisi mampu menyumbang kepada penambahbaikan dan peningkatan ciri-ciri bahan asas bio untuk menghasilkan biopolimer sekaligus menepati sifat-sifat termoplastik elastomer, TPE. Sifat termal bagi sample modifikasi *Tacca* sebagai bahan asas bio dalam pembuatan termoplastik dikaji adalah untuk menilai kesan penghuraian dan degradasi dengan menggunakan Analisis Termogravimetri (TGA). Manakala alat Kalorimetri Imbasan Diferensial (DSC) digunakan untuk menganalisis tindak balas sample terhadap reaksi endotermik. Daripada analisa dan kajian yang dijalankan, sample GM-2 (bahan hijau, GM) didapati menepati ciri-ciri termal dalam menolak rintangan haba terhadap suhu yang tinggi sehingga mencecah 480.06 ° C dan meninggalkan jumlah sisa yang lebih tinggi iaitu sebanyak 4.97 mg berbanding sample-sample lain. Hal ini menunjukkan bahawa sample GM-2 memiliki kombinasi yang unggul antara nisbah getah asli dan gliserol (pemplastik) dalam menepati sifat-sifat termoplastik elastomer, TPEs.

**Kata kunci:** biopolymer, bahan hijau, *Tacca leontopetaloides*, pencirian termal

## Introduction

In the years ago, plastics are made from petrochemical polymer for various applications such as packaging, automobile, construction and consumer goods. The extensively used for these applications make plastics be demanding in market trade which gives high gross profit to the polymer industries. In the previous study, the

development of plastic was contributed by the involvement factor of the chemical structure and physical structure. Hence, this factor was led to the formation of differential and classification of plastics. The classification of plastics can be differentiated into thermoplastics, elastomers and thermosets [1]. Among these classes, elastomeric plastics or known as thermoplastic (TPE) shows highly importance in any production which could contributes to the higher total production capacity per year since in 30 years last decades starting from 1 million tons to more than 150 million tons per year [2]. Thermoplastic elastomers has superior characteristic because the characterization of elastomeric that present in TPE production has brought to the similar characteristic likes a rubber but it is durable [3]. TPE possess of elastomeric properties is because of the presence of amorphous and crystalline regions makes the product tends to be rubbery [4]. The production of thermoplastic elastomers, TPEs is relatively simple because the finishing period of TPEs is shorter and economical. TPEs is also creates the good mechanical properties in resist towards heat and humidity.

However, there is disadvantage appeared behind the favor of TPEs, much of end-use of TPE serves adverse effect to the ecological system as it is not easily degrade in nature [5]. Due to this drawback factor, bio-based polymer from selected starch, *Tacca* blended with several additives material has potentially being recognized to produce a potent thermoplastic starch, TPS. Hence, *Tacca* starch will be used as a main "tools" to produce bio-polymer because it has two major compositions needed to make a good thermoplastic in order to approach the characteristic similar with TPE. These two major compositions are amylose and amylopectin which can serve a good mechanical inherent similar with existing TPE. Although, *Tacca* starch should be mixed with other substituents or additives in order to enhance the properties of TPS [6]. TPS made from *Tacca* starch offers an excellent initiative to be a good biopolymer [7] because the composition of the starch contains about 28% of amylose [8]. In this study will identified either *Tacca leontopetaloides* starch has potentially can be one of the reliable raw material to be use in TPS making through blending or grafting process or vice versa [9]. In the meantime, the thermal properties of starch based TPS will be studied to evaluate the decomposition and degradation of samples using Thermogravimetric Analysis (TGA) and study the endothermic reaction using Differential Scanning Calorimetry (DSC).

## Materials and Methods

### Raw Materials

*Tacca leontopetaloides* starch used was collected from the East-Cost of Peninsular Malaysia; latex natural rubber was supplied by Malaysia Rubber Board (MRB); rice husks were collected from Bernas Rice Mill Tanjung Karang, Selangor and glycerol was purchased from Merck (M) Sdn Bhd. Other materials used were Calcium Chloride ($CaCl_2$), stearic acid and sulphur.

### Preparation of Green Materials

Green materials, GMs were produced by the use of *Tacca* starch and natural rubber was prepared by melt blending using a beaker and hot plate. 10 g of *Tacca* starch was added to 150 mL of distilled water in beaker with temperature range between 150 °C to 200 °C. *Tacca* starch solution was thoroughly mixed while 1 g of treated silica was added into blending solution. Glycerol with varies volume of 6%, 10%, 20% and 30% was added respectively into solution after 10 minutes blending by constantly stirred using magnetic stirrer at 150 rpm. At ambient temperature, natural rubber was mixed into blending solution by varying the volume from 40% to 60% while adding with $CaCl_2$ to stabilize the composition of GM. The composition of material was dried at 110˚C about 24 hours in an air-circulated oven to remove the moisture. The dried sample of GM was rolled at temperature of 50°C to 60°C by using two roll-mills. During compounding process, 0.2 mg of sulphur and stearic acid were mixed with sample until shape of GM form as a sheet with thickness of 3 mm. The sheet of GM was cut into smaller size for thermal analysis. The preparation composition of GMs was stated in Table 1.

### Fourier Transform Infrared (FT-IR)

Fourier Transform Infrared Spectrophotometer (FT-IR) (Perkin Elmer, Spectrum GX, UK) was used to analyze the functional group exhibit in the GMs formulated from varies range of natural rubber and glycerol between 400 cm-1 to 4000 cm-1 of infrared wave length by thermally compressing the samples into a thin film.

**Thermogravimetric Analysis (TGA)**

The thermal stability and decomposition of GMs were measured by using thermogravimetric analyzer. The samples of GMs with different ranges of natural rubber ranging from 40% to 60% and plasticizer in range of 6% to30% were analyzed. About ≤5 mg samples were placed in aluminium pans and were heated from room temperature to 600 ˚C at heating rate 10 °C/min under air flow condition. The mass loss and percent residue leaved for each GM samples were determined based on ASTM E 967.

Table 1. Compositions of green materials

| Sample | NR (%) | Glycerol (%) | Starch (g) | $dH_2O$ (ml) | RHS (g) | $CaCl_2$ (g) |
|---|---|---|---|---|---|---|
| **GM1** | 40 | 30 | 10 | 150 | 1 | 1 |
| **GM2** | 50 | 6 | 10 | 150 | 1 | 1 |
| **GM3** | 60 | 30 | 10 | 150 | 1 | 1 |
| **GM4** | 40 | 10 | 10 | 150 | 1 | 1 |
| **GM5** | 50 | 20 | 10 | 150 | 1 | 1 |

**Differential Scanning Calorimetry (DSC)**

Differential Scanning Calorimetry (DSC) analysis of GMs with different range of natural rubber which ranging from 40%, 50% and 60% and plasticizer in range of 6%, 10%, 20% to 30% were carried out under 10˚C/min of nitrogen flow by following the American Standard Method, ASTM D 3418-03. The samples of ≤ 5 mg were heated from 25°C to 500°C. The enthalpy of reaction (J/g) and the residual reaction heat were measured at point of under the DSC peaks. The mid-point temperature of the peak was considered as the melting temperature, $T_m$.

## Results and Discussion

**Fourier Transform Infrared (FTIR) Analysis**

The absorption peaks of GM1, GM2,GM3 GM4 and GM5 were detected at functional group of hydroxyl group, methyl group, C-H stretch, nitro group, ether stretch, and vinyl group, C-C=C asymmetric stretch [10].The assignment of each functional group present in sample of GM can be shown as Table 2.

Table 2. FTIR assignment of green material samples

| Wavenumber ($cm^{-1}$) | Functional Group |
|---|---|
| **3400-3450** | Hydroxyl group (O-H bond) |
| **2800-3000** | Methyl group (C-H stretch) |
| **1450-1600** | Nitro group |
| **1400-1500** | Vinyl group (C-C=C asymmetric stretch) |
| **1000-1300** | Ether stretch |

The absorbance bands in range 3400 – 3450 $cm^{-1}$ indicates the hydroxyl group due to covalent bond present between oxygen and hydrogen atom. After addition of starch into the composition of GMs, the absorbance band changes into 2800-3000 $cm^{-1}$ indicate the methyl group. The present of nitro group with absorbance band between 1450-1600 $cm^{-1}$ makes the sample more stable due to the present of natural rubber which causes H-bond directly increases proportionally with molecular weight and yield more rubbery effect to the sample. The addition of glycerol causes the functional group ester present in range of absorbance band between 1400-1500 $cm^{-1}$. As high

amount of glycerol added to the samples, the molecular weight increases as well as the bonding of ether increases which causes GMs samples more unstable become narrow and lower [11].

**Thermogravimetric Analysis (TGA)**

Figure 1 shows the TGA profile to investigate the effect of decomposition onto GM samples. According to the graph, there were two major steps of weight loss as temperature arose. The first neat of GM start to degrade at 260 °C to 390 °C to show the degradation of glycerol present while the second region of weight loss shows the natural rubber decomposed effect occurred at temperature range of 400 °C before completely end the degradation process at temperature 600°C [12]. As GMs composition contains lower blending of plasticizer, the higher decomposition temperature would require to thermally decompose of materials [13]. According to Table 3, the sample which has higher temperature of early and final stage of degradation was GM2 at temperature of 308.46 °C and 480.06 °C respectively. Meanwhile, when low blending of glycerol was added to material, lower temperature was required to increase the decomposition rate [14]. For example, GM2 has low amount of glycerol and require high decomposition rate at 2.09 $mgmin^{-1}$ with the highest residue, 4.97 mg compared to others.

Derivative Thermogravimetric (DTG) curves of GM samples as illustrated in Figure 2 shows three major peaks present during the thermal degradation. The first peak occurs at temperature range between 150 °C to 250 °C which indicates the degradation of glycerol. According to Susan et al., the temperature range of 250 °C to 400 °C is stages where most of plasticizer and oil contain in TPS were degraded. Meanwhile, the second peak was present at temperature range 250 °C to 270 °C to show the thermal degradation of *Tacca* starch in five samples while temperature range between 370 °C to 400 °C represent the decomposition phase of natural rubber [15]. Hence, the characteristic of thermal degradation and decomposition prove the sample of GM2 has superior bonding compared to other sample due to higher amount of natural rubber and small amount of plasticizer remarked GM2 toughen the green material from decomposed and degraded at elevated temperature.

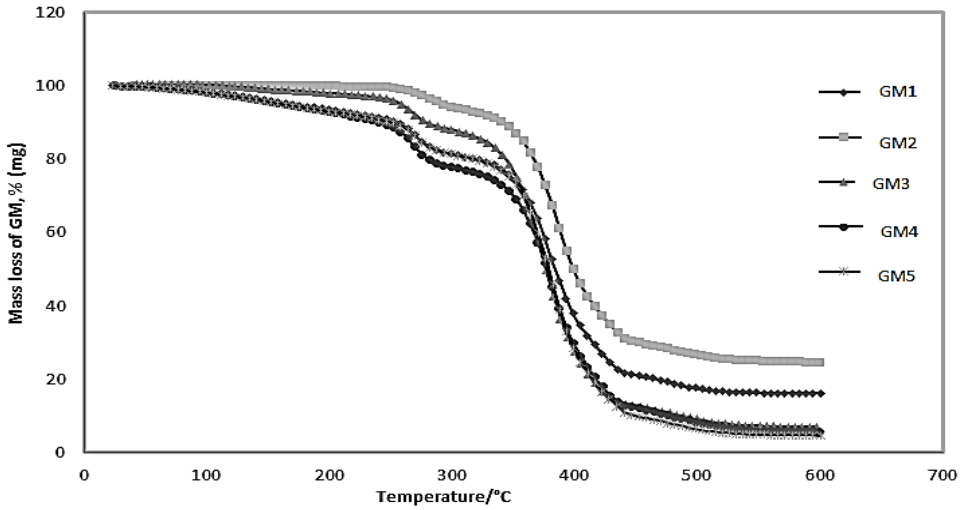



Figure 1. Thermogravimetric Analysis of GM1, GM2, GM3, GM4, and GM5

Table 3. Results of Thermogravimetric Analysis, TGA and DTG data of Green Materials

| Sample GM | Early stage of Decomposition Temperature ($^oC$) | Final stage of Decomposition temperature, $T_d$ ($^oC$) | Decomposition rate, $T_d$ ($mgmin^{-1}$) | Residue of GM (mg) |
|---|---|---|---|---|
| **GM1** | 307.06 | 466.06 | 3.65 | 3.26 |
| **GM2** | 308.46 | 480.06 | 2.09 | 4.97 |
| **GM3** | 304.88 | 479.53 | 1.42 | 1.42 |
| **GM4** | 304.65 | 472.06 | 1.19 | 1.19 |
| **GM5** | 306.02 | 473.02 | 0.97 | 0.97 |

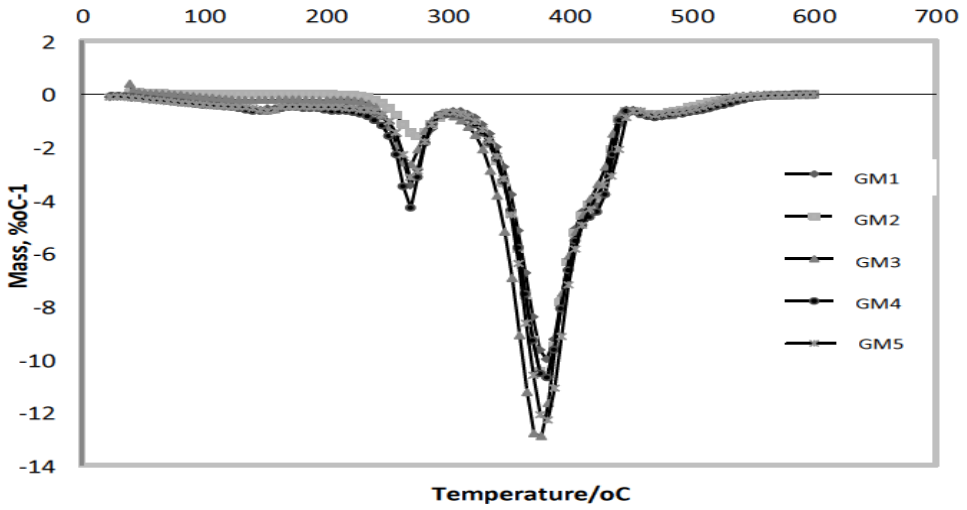



Figure 2. Derivative Thermogravimetric Analysis of GM1, GM2, GM3, GM4 and GM5

**Differential Scanning Calorimetry (DSC) Analysis**

The profile of thermal degradation by DSC to trace GM samples contain of *Tacca* starch, glycerol and natural rubber were illustrated as Fig. 3. The melting temperature, $T_m$ and the enthalpy involved during the process of thermal degradation was presented in Table 4. In this experiment, the temperature of glass transition, $T_g$ is initially considered in order to recognize the changes of calorific capacity during transition process of sample which started in solid form to shift into liquid phase. However, the temperature of $T_g$ was not detected due to difficulty to identify the midpoint temperature during the testing.

Based on thermal degradation, GMs reflect an endothermic slope due to increases of heat capacity with the increases of temperature [16]. According to Fig.3, the first curve shows on the degradation of glycerol in each sample. Through the result, the melting temperature was occurred between 100°C to 150°C which indicates the presence of plasticizer in the sample. For *Tacca* starch, the indication of the material occur when the melting temperature, $T_m$ was started at a range of 250°C to 300°C while temperature of 300°C to 500°C was corresponded to $T_m$for natural rubber content in GM samples. As in Table 4, it shows the sample of GM2 has high enthalpy, 76.74

J/g due to the present of low amount of plasticizer which about 6% in sample while GM5 has lowest enthalpy, 45.03 J/g due to high amount of plasticizer, 20%. This cause the $T_m$ of GM5 lower compared to GM2. As a result, the degradation process was easier for GM5 due to small amount heat absorb needed to degrade the sample [17]. Therefore, it was proven GM2 has high degree of degradability as it undergoes amorphous phase which made the sample was harden to degrade [18].

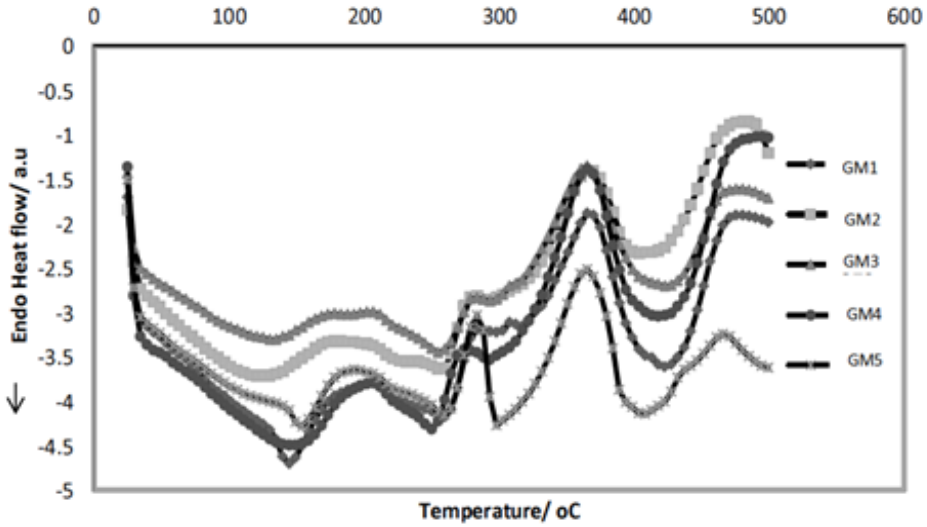



Figure 3. Differential Scanning Calorimetry Analysis of GM1, GM2, GM3, GM4 and GM5

Table 4. Data of Differential Scanning Calorimetry analysis.

| Sample GM | Enthalpy, $\Delta H_f, (J/g)$ | Melting temperature, $T_m$ of glycerol, ($^oC$) | Melting temperature, $T_m$ of *Tacca* starch, ($^oC$) | Melting temperature, $T_m$ of natural rubber, ($^oC$) |
|---|---|---|---|---|
| **GM1** | 112.36 | 144.47 | 260.76 | 423.06 |
| **GM2** | 76.74 | 118.52 | 258.62 | 417.16 |
| **GM3** | 80.66 | 131.87 | 256.13 | 422.13 |
| **GM4** | 104.53 | 141.31 | 251.42 | 423.27 |
| **GM5** | 45.03 | 153.81 | 260.92 | 404.53 |

## Conclusion

Blends of thermoplastic starch and natural rubber were obtained directly from the latex and granular *Tacca leontopetaloides* starch. The natural rubber was homogenously distributed with the aids of glycerol plasticizer. The complementation between natural rubber, *Tacca* starch and glycerol as a green material was responsible for a great improvement in the thermal properties of the biopolymer. Thermally, the sample requires low plasticizer and high natural rubber to be sustain in high temperature which are not easily degraded and decomposed. Thus, GM2 shows high resistance towards the higher temperature with the presence of high natural rubber content with low glycerol content.

**Acknowledgement**

The authors are thankful and grateful to Research Management Institute (600-RMI/RAGS5/3 (84/2013)) of Universiti Teknologi MARA Shah Alam, Malaysia for supporting and providing funds for the paper.

**References**

1. Chaudhary, P. T. (2009). Amylose content and chemical modification effects on thermoplastic starch from maize, Processing and characterisation using conventional polymer equipment. *Carbohydrates Polymer*, 917–925.
2. Bourtoom, T. (2008). Plasticizer effect on the properties of biodegradable blend film from rice starch-chitosan. *Science and Technology*, 149-165.
3. Mahallati, P., Arefazar, A., and Naderi, Gh. (2011). Thermal and morphological properties of thermoplastic elastomer nanocomposites based on PA6 / NBR. *Iranian Journal of Chemical Engineering* 8: 1 (Winter).
4. Long Yu, K. D. (2006). Polymer blends and composites from renewable resources. *Progress in Polymer Science*, 576–602.
5. Mondragón, M., Hernández, E. M., Rivera-Armenta, J. L., and Rodríguez-González, F. J. (2009). Injection molded thermoplastic starch/natural rubber/clay nanocomposites: morphology and mechanical properties. *Carbohydrate Polymers*, 77(1), 80-86.
6. Maurizio Avella, A. B. (2009). Eco-Challenges of Bio-Based Polymer Composites. *Materials*, 911-925.
7. Richard J. and Spontak, N. P. (2000). Thermoplastic elastomers: fundamentals and applications. *Colloids and Interface Science* 5(5): 334-340
8. Spennemann, D. H. (1992). *Notes on the occurrence, utilisation and importance of Polynesian Arrowroot (Taccaleontopetaloides) in the Marshall Islands.*
9. Prachayawarakorn, J., Sangnitidej, P. and Boonpasith, P. (2010). Properties of thermoplastic rice starch composites reinforced by cotton fiber or low-density polyethylene. *Carbohydrate Polymers*, 81(2): 425-433.
10. Curvelo, A. A. S., De Carvalho, A. J. F., and Agnelli, J. A. M. (2001). Thermoplastic starch–cellulosic fibers composites: preliminary results. *Carbohydrate Polymers*, 45(2): 183-188.
11. Alessandra L, D. R., Márcia, D. Z., Antonio, A.S.C., & Antonio J.F, C. (2011). Thermoplastic starch modified during melt processing with organic acids: The effect of molar mass on thermal and mechanical properties. *Industrial Crops and Products*, 33(1): 152-157.
12. Mohd Makhtar, N, S., Muhd Rodhi., M, N., Musa, M., & Ku Hamid, K, H. (2013). Thermal Behavior of Tacca leontopetaloides Starch-Based Biopolymer. *International Journal of Polymer Science* 3: 1-7.
13. Zhang F., Zhang J. and Sun D. (2009). Study on Thermal Decomposition of Intumescent Fire-Retardant Polypropylene by TG/Fourier Transform Infrared. *Thermoplastic Composite Materials*, 22: 681.
14. Taghizadeh, A., Sazarin, P., & Favis, B. D. (2013). High molecular weight plasticizers in thermoplastic starch/polyethylene blends. *Journal of Materials Science*, 48: 1799-1811.
15. Saikrasun, S., & Amornsakchai, T. (2012). Thermal decomposition behavior and mechanical properties of elastomeric composites based on polyolefinic thermoplastic elastomer and organomontmorillonite. *Journal of Polymer Research*, 19(1), 1-13.
16. Rodriguez, G. F. J., Ramsay, B. A., and Favis, B. D. (2004). Rheological and thermal properties of thermoplastic starch with high glycerol content. *Carbohydrate Polymers*, 58(2): 139-147.
17. Montoya, M., Tomba, J. P., Carella, J. M. and Gobernado-Mitre, M. I. (2004). Physical characterization of commercial polyolefinic thermoplastic elastomers. *European polymer journal*, 40(12), 2757-2766. *Differential Scanning Calorimetry (DSC)*. (n.d.). Retrieved from www1.chm.colostate.edu/Files/CIFDSC/dsc2000.pdf

The Malaysian Journal of ANALYTICAL SCIENCES ISSN 1394-2506

# STUDY ON THE STRUCTURE, TEXTURE AND THERMAL STABILITY OF $CeZrYO_2$ NANOPARTICLES SYNTHESIZED VIA MICROEMULSION METHOD

## (Kajian Terhadap Struktur, Tekstur dan Kestabilan Termal $CeZrYO_2$ Nanopartikel Disintesis Melalui Kaedah Microemulsi)

Abdul Hadi[1]*, M. Nazri Abu Shah[1], Noraakinah Hassan[1], S. Azurah Suliman[1], S. Hanim Md Nor[1], Mahidin[2], Kamariah Noor Ismail[1]

*[1]Faculty of Chemical Engineering,*
*Universiti Teknologi MARA, 40450 Shah Alam, Selangor, Malaysia*
*[2]Department of Chemical Engineering,*
*Syiah Kuala University, 23111 Banda Aceh, Indonesia*

**Corresponding author: hadi9598@salam.uitm.edu.my*

**Abstract**

The $CeZrYO_2$ (CZY) was synthesized via microemulsion method. Phase structure, texture, and thermal stability of CZY nanoparticles were characterized by X-ray diffraction (XRD), transmission electron microscopy (TEM), $N_2$ adsorption-desorption and thermogravimetric Analysis (TGA). XRD analysis confirmed the cubic phase and homogeneous solid solution of CZY nanoparticles formed. TEM micrograph also revealed the CZY nanoparticles well-defined crystallite, spherical shaped and nanoscale size in range of 5 – 10 nm. The surface area of CZY nanoparticles was 219.50 $m^2/g$ and isotherm profile was mesoporous type IV. It was also found that the synthesized CZY nanoparticles remain a good thermal stability, in the range of temperature more than 900$^oC$ according to thermo gravimetric analysis.

**Keywords:** $CeZrYO_2$, Yttrium, nanoparticles, microemulsion

**Abstrak**

$CeZrYO_2$ (CZY) telah disintesis melalui kaedah mikroemulsi. Struktur fasa, tekstur, dan kestabilan termal nanopartikel CZY dicirikan oleh pembelauan sinar-X (XRD), mikroskop elektron transmisi (TEM), $N_2$ penjerapan - desorpsi dan analisis termogravimetri (TGA). Analisis XRD mengesahkan fasa kubik dan homogen nanopartikel larutan pepejal terbentuk. TEM mikrograf juga mendedahkan nanopartikel CZY kristal terbentuk dengan jelas, berbentuk bulat, dan bersaiz nano dalam lingkungan 5 – 10 nm. Luas permukaan nanopartikel CZY adalah 219.50 $m^2/g$ dan isoterma profil adalah mesopori (Jenis IV). Ia juga mendapati bahawa nanopartikel CZY mempunyai kestabilan terma yang baik, dalam lingkungan suhu melebihi 900$^oC$ mengikut termogravimetri analisis.

**Kata kunci:** $CeZrYO_2$, Yttrium, nanopartikel, microemulsi

## Introduction

In recent years, the modification of ceria-zirconia that has bright potential in improvement of catalytic performance of three-way catalysts (TWCs) to eliminate the automotive emission has a great attention from researchers. It is due to the ceria-zirconia has limitation on the performance of oxygen storage and released during cold start emissions [1]. It is well known that the zirconia act as thermal stabilizer of ceria against the sintering phenomenon and it is not attributed to the oxygen mobility [2]. Therefore, the incorporation of ceria-zirconia has made the reduction of percentage composition of ceria as oxygen storage material in TWCs, resulting in the decrement of oxygen mobility rate under lower temperature.

Most researcher have suggested the modification of ceria-zirconia using rare earth metals such as the yttrium, Y to be a potential element to produce the efficient oxygen storage materials [3-5]. The addition of Y into ceria-zirconia provides two distinct properties: (i) high density of $Ce^{4+}$ ions on the surface, and (ii) high reactive surface area, facilitating the dispersion active catalysts and oxygen mobility [5, 6]. Wang, et al. [7] reported that the introduction of Y lead to remarkable increased of surface area, increase the dispersion of Pd and strong interaction of between Pd-catalysts and support, which resulted the catalysts exhibit high catalytic activity.

However, the preparation techniques also have great influence on the structural and textural properties, especially on the homogeneous solid solution and surface area. It is well known that the homogeneous solid solution can create better properties and the high surface area which can be helpful or even essential in attaining a significant reaction rate [8]. The smaller size particle can provide the high surface area and it can minimize the sintering impact of modified ceria-zirconia and provide more $Ce^{4+}$ ions to mobilize oxygen [9]. Therefore, water/oil microemulsion method have been proposed because it is able to produce the homogeneity of the mixed oxides formed, offering the nano-size range particles, high specific surface area and high metallic dispersion [10]. In this study, the $CeZrYO_2$ (CZY) nanoparticles were synthesized by water/oil microemulsion method. The effects of addition of yttrium into ceria-zirconia on the structure, texture and thermal stability were studied.

## Materials and Methods

### Synthesis

The CZY nanoparticle was synthesized using water/oil microemulsion method. The similar procedure was adapted from Hadi and Yaacob [11]. CTAB/Butanol/Octane/Water system was used in this work. CTAB, butanol, n-octane were obtained from Merck Malaysia and the metals nitrate were obtained from Sigma Aldrich. The first microemulsion containing the 21% metals nitrate solution (Ce, Zr and Y) was prepared by mixing the 13% CTAB, 13% butanol and 53% octane under continuous stirring at room temperature until the clear solution was obtained. Similar procedure was also applied for second microemulsion containing the reducing agent (NaOH). Both microemulsions were then mixed under vigorous agitation for 3 hours and the colloidal precipitates were formed. The colloidal precipitates were left at room temperature for 24 hours. Then, it was washed with ethanol and deionized water for three times using centrifuge at 10,000 rpm for 10 minutes. Finally, the samples were dried at $110^{o}$C for 24 hours.

### Characterization

The X-ray diffraction (Model: Rigaku Ultima IV) patterns were recorded on a Rigaku Ultima IV diffractometer with Cu Kα radiation (λ= 0.15418 nm) operating at 40kV and 20mA at a scanning rate 1.2°/min in the range 2θ is 20° to 70°. The crystallite phases were identified according to the reference data from the International Center Diffraction Data (ICDD). Transmission electron microscopy (Tecnai G2 20) examined the microstructure studies of sample. The surface areas of synthesized samples were determined using Autosorb-1 Quanta Chrome Instrument TUSA, $N_2$ adsorption isotherms at -196°C. For the thermogravimetric analysis (TGA) was performed (METLER TOLEDO TGA SDTA851) in a temperature range of 50 to 1000˚C to observe the thermal stability and degradation of the synthesized CZY nanoparticles.

## Results and Discussion

### X-ray Diffraction Analysis

Diffractogram pattern of the CZY nanoparticles is presented in Figure 1. It can be seen that the pattern obtained are correspond to pure ceria (ICDD: 021306). Based on previous studies, Abu Shah, et al. [12] reported that the peaks of commercial $CeO_2$ has a cubic phase, in which at 2θ = 28.51, 33.04, 47.43, 56.1 and 59.05 are assigned to the (111), (200), (220), (311) and (222) planes, respectively. A symmetrical diffractogram pattern of the CZY nanoparticles and pure ceria was observed. These findings suggest that the synthesized CZY nanoparticles are symmetrically phase with pure ceria, in which the cubic phase was formed even though the insertion of yttrium. It is also observe that the diffractogram patterns of yttrium are undetected. It may be attributed to well-defined homogeneous solid solution formed [13]. In addition, the diffractogram of the CZY nanoparticles show the crystallites pattern, even though the CZY nanoparticles do not undergo the heating treatment. It can be concluded that the microemulsion method can produce the CZY nanoparticles with their cubic phase at room temperature and it does not require the further heating treatment.

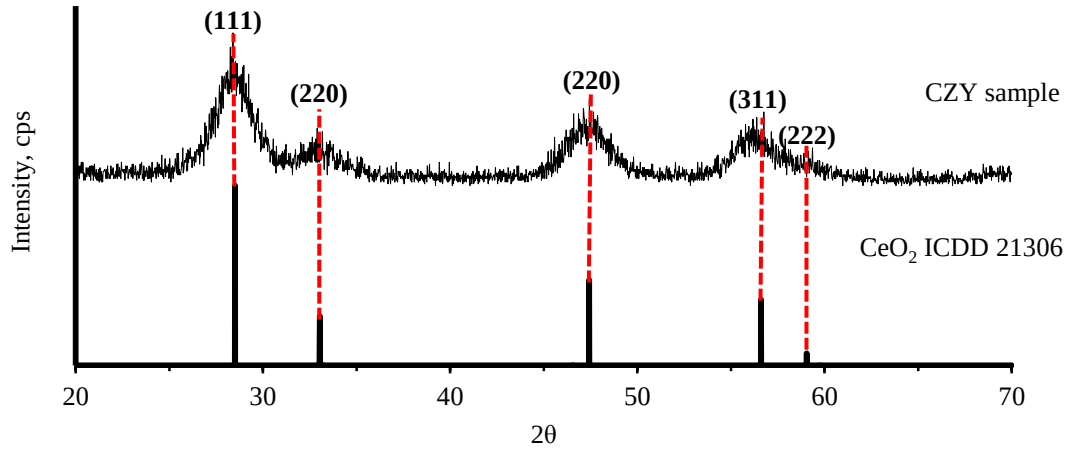



Figure 1. X-ray diffraction pattern of the CZY nanoparticles

**Transmission Electron Microscopy Analysis**

Figure 2 shows the transmission electron microscopy (TEM) of CZY nanoparticles. The micrograph of CZY nanoparticles reveals spherical shape of particles. This observation also reveals that the size particles of CZY in range of 5 – 10 nm. From other literature [14] also reported that the typical size of cerium-zirconia was obtained in range of 50 – 100nm, in which it is bigger than the CZY nanoparticles. It indicates that the CZY nanoparticle via microemulsion method able produced smaller size than the ceria-zirconia. The synthesized CZY also exhibits polycrystalline structure in which the existence of a bright diffraction rings in Figure 2 and clearly shows the lattice fringes with d spacing of 0.310 nm, which attribute to the plane (111). These findings may suggest that the well-defined crystalline of CZY nanoparticle was formed.

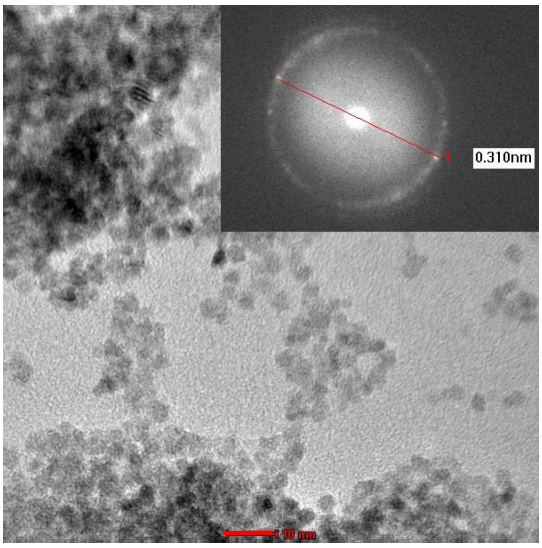



Figure 2.Transmission electron microscopy of CZY nanoparticles

**$N_2$ Adsorption-Desorption Analysis**

The specific surface area, total pore volume, and average pore size of CZY and commercial $CeO_2$ are listed in Table 1. The surface area of CZY nanoparticles is higher than the surface area of commercial $CeO_2$. This indicates that the microemulsion method able to produce high surface area particles. The isotherm profile of $CeO_2$-commercial clearly follows the type V, which have a weak adsorption and desorption. Instead, the CZY nanoparticles are follows the type IV which is mesoporous materials with a strong absorption and desorption as shown in Figure 3. It clearly proven that the narrow size of particles gives high surface area and strong substrate site. These results showed the potential characters of CZY nanoparticles are suitable to be applied in three-way catalyst.

Table 1.Textural property of commercial-$CeO_2$ and CZY nanoparticles

| Identity | Specific Surface Area, $m^2/g$ | Total Pore Volume, $(10^{-3})$ $cm^3/g$ | Average Pore Size, nm |
|---|---|---|---|
| $CeO_2$-commercial | 41.85 | 74.00 | 11.50 |
| CZY | 219.50 | 93.10 | 2.64 |

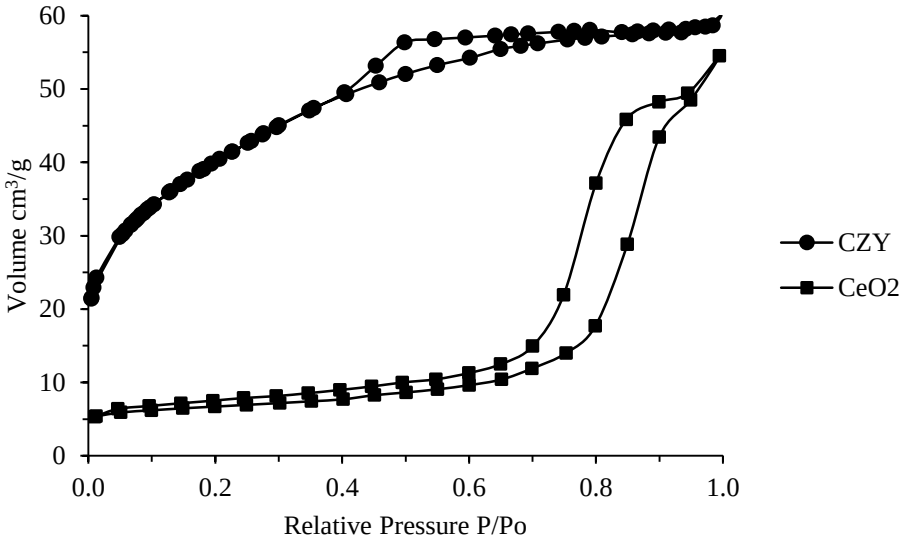



Figure 3. Isotherm profiles of CZY nanoparticles

**Thermogravimetric Analysis (TGA)**

The thermal stability of CZY nanoparticles are examined via TGA. In Figure 4, TGA and DTG profile show four (4) major peaks during the thermal course. Firstly, the initial point of the weight loss is shown at T < 100 ˚C. It indicates the removal of water molecule and excess of volatile compound during synthesis route. The second point of the weight loss is observed at range 200°C > T > 350˚C with a weight loss of 0.24 mg/min. It may be attributed to the transformation of degree crystallinity of CZY nanoparticles. According to the Toshiyuki Masui, et al. [15], the amorphous phase of the sample may change to a better crystallinity at temperature of 250°C. The third peak is observed at range 450°C > T > 700 °C with a weight loss of 0.12 mg/min. It indicates the reducibility transformation of $Ce^{4+} \rightarrow Ce^{3+}$ ions, which the removal of oxygen atom from ceria and makes the reduction of

weight of sample. Some literatures report that the reducibility of the modification ceria activate at temperature ~ 400-700 $^{o}$C [2, 6, 16, 17]. The last peak is observed at range 900°C > T > 1100 °C with a very small weight loss (0.05mg/min). It may due to the decomposition of ceria, which the changing of oxidation number ceria (+3 → 0) and indicating the chemical deactivation of CZY nanoparticles. The results also revealed that the peak 4 shows the lowest weight losses which of < 0.04 mg/min, indicating the CZY nanoparticles have a good thermal stability in the range of temperature more than 900$^{o}$C.

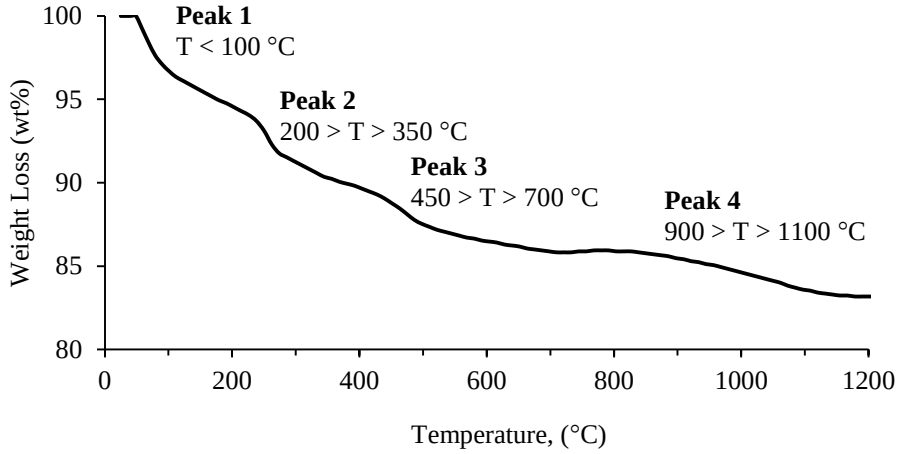



Figure 4(a). Thermogravimetric analysis (TGA) profile of CZY nanoparticles

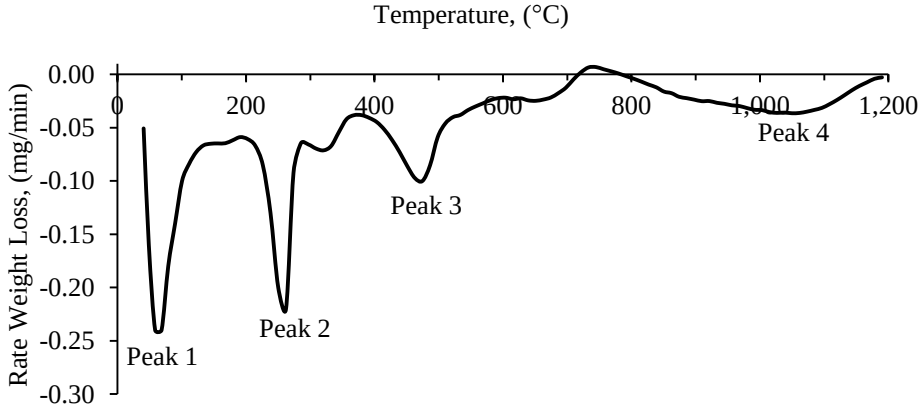



Figure 4(b). Derivative thermogravimetric analysis of CZY nanoparticles

## Conclusion

The CZY nanoparticle was successfully synthesized via microemulsion method under room temperature. These findings may suggests that the synthesized CZY nanoparticles via microemulsion method was produced a homogeneous solid solution and well-defined crystalline formed. The insertion of yttrium into ceria-zirconia structure formed the (fcc) cubic phase. The particle size of synthesized CZY was nanoscale in the range of 5 – 10 nm. The smaller size CZY nanoparticles provided the high surface area of CZY nanoparticles was 219.50 $m^2$/g. The

presence of yttrium in ceria-zirconia structure improved thermal stability of ceria-zirconia nanoparticles in the range of temperature more than 900$^{o}$C.

**Acknowledgement**

The authors would like to acknowledge e-Science Project No. 06-01-01SF0502 supporting by Ministry of Science, Technology and Innovation (MOSTI), Malaysia. We would also thank to Universiti Teknologi MARA (UiTM) for supporting the research.

**References**

1. Guillen – Hurtado N., Rico-Pérez V., García-García A., Lozano-Castelló D., and Bueno-López A. (2012), Three-way catalysts: Past, present and future," DYNA (Colombia) 79: 114-121.
2. Li H., Zhu Q., Li Y., Gong M., Chen Y., and Wang J. (2010). Effects of ceria/zirconia ratio on properties of mixed $CeO_2$-$ZrO_2$-$Al_2O_3$ compound. *J. of Rare Earths* 28: 79-83.
3. Shah M. N. A., Nor S. H. M., Ismail K. N., and Hadi A. (2014). Overview: Modification of Cerium Oxide in Three-Way Catalysts. *Applied Mechanics and Materials* 575: 97-102.
4. Cao H., Song W., Gong M., Wang J., Yan S. and Liu Z. (2009). $MnO_x/Al_2O_3/Ce_{0.45}Zr_{0.45}M_{0.10}Oy$ (M = Mn, Y, La) catalysts used for ethanol catalytic combustion. *J. of Natural Gas Chemistry* 18: 83-87.
5. Jiaxiu G., Zhonghua S., Dongdong W., Huaqiang Y., Maochu G. and Yaoqiang C. (2013). Study of Pt–Rh/$CeO_2$–$ZrO_2$–$M_xO_y$ (M=Y, La)/$Al_2O_3$ three-way catalysts. *Applied Surface Science* 273: 527-535.
6. Wang G., Dai H., Zhang L., Deang J., Liu C. and He H. (2010). CrOx/nano-$Ce_{0.60}Zr_{0.35}Y_{0.05}O_2$ catalysts that are highly selective for the oxidative dehydrogenation of isobutane to isobutene. *Applied Catalysis A: General* 375: 272-278.
7. Wang G., You R. and Meng M. (2013). An optimized highly active and thermo-stable oxidation catalyst Pd/Ce–Zr–Y/$Al_2O_3$ calcined at superhigh temperature and used for $C_3H_8$ total oxidation. *Fuel* 103: 799-804.
8. Fogler H. S. (1992) Elements of Chemical Reaction Engineering (Second Edition): Prentice Hall PTR.
9. Guo M.-N., Guo C.-X., Jin L.-Y, Wang Y.-J., Lu J.-Q. and Luo M.-F. (2010). Nano-sized $CeO_2$ with extra-high surface area and its activity for CO oxidation. *Materials Letters* 64: 1638-1640.
10. Laguna O. H., Centeno M. A., Boutonnet M. and Odriozola J. A. (2011). Fe-doped Ceria Solids Synthesized by the Microemulsion Method for CO Oxidation Reactions. *Applied Catalysis B: Environmental* 106: 621-629.
11. Hadi A.and Yaacob I. I. (2007). Novel synthesis of nanocrystalline $CeO_2$ by mechanochemical and water-in-oil microemulsion methods. *Materials Letters* 61: 93-96.
12. Abu Shah M. N., Md Nor S. H., Ismail K. N., and Hadi A. (2014). Study on the Structure and Morphology of $Ce_xZr_{(1-x)}O_2$ Mixed Oxides," Advanced Materials Research 938: 46-51.
13. Feng L G., Quiyan W., Bo Z., and Renxian Z. (2010). The promotional effect of transition metals on the catalytic behavior of model Pd/$Ce_{0.67}Zr_{0.33}O_2$ three-way catalyst. *Catalysis Today* 158: 385-392.
14. Martinez-Arias A., Fernandez-Garcia M., Ballesteros V., Salamanca L. N., Conesa J. C. and Otero C. (1999) Characterization of High Surface Area Zr-Ce (1:1) Mixed Oxides by a Microemulsion Method. *Langmuir* 15: 4796-4802.
15. Masui T., Fujiwara K., Peng Y., Sakata T., Machida Ken-ichi and Mori H. (1998). Characterization and catalytic properties of $CeO_2$–$ZrO_2$ ultrafine particles prepared by the microemulsion method. *J. of Alloys and Compounds* 269: 116 -122.
16. Radlik M., Adamowska M., Lamacz A., Krzton A., Costa P. D., and Turek W., (2013). Study of the surface evolution of nitrogen species on CuO/$CeZrO_2$ catalysts," *Reaction Kinetics, Mechanisms and Catalysis* 109: 43-56.
17. He H., Dai H. X., and Au C. T. (2004). Defective structure, oxygen mobility, oxygen storage capacity, and redox properties of RE-based (RE = Ce, Pr) solid solutions. *Catalysis Today* 90: 245-254.

The Malaysian Journal of ANALYTICAL SCIENCES ISSN 1394-2506

# PHYSICO-CHEMICAL CHARACTERIZATIONS OF SAWDUST-DERIVED BIOCHAR AS POTENTIAL SOLID FUELS

## (Pencirian Fizikal-Kimia bagi Biochar Diperoleh daripada Debu Kayu Sebagai Potensi Bahan Bakar Pepejal)

Wan Azlina Wan Ab Karim Ghani[1,2]*, Gabriel da Silva[2], Azil Bahari Alias[2,3]

[1]*Department of Chemical Engineering and Environmental Engineering, Faculty of Engineering, Universiti Putra Malaysia, 43400 Serdang, Selangor, Malaysia*
[2]*Department of Chemical and Biomolecular Engineering, The University of Melbourne, Victoria 3010, Australia*
[3]*Faculty of Chemical Engineering, University Teknologi MARA Malaysia,40450 Shah Alam, Selangor, Malaysia*

**Corresponding author: wanazlina@upm.edu.my*

**Abstract**

Characterization Malaysian rubber-wood sawdust derived biochar (MRWSB) produced in the fixed bed pyrolysis under different temperatures (450 to 850°C) were studied for its applicability as a solid fuel. A range of analyses were carried out, including biochar oxidation reactivity , inorganic species, oxygen and hydrogen contents in the biochars, release of heteroatoms in biochar as the gaseous product, and biochar structural evolution during pyrolysis process. The results show that the optimum temperature for carbonization to obtain a char having moderately high yield was found as 450 °C. Thermogravimetric analyses (TG) shows that temperatures induces a progressively more ordered carbonaceous structure and leads to a significant changes in the biochar reactivity. The process is coupled with the loss of heteroatoms, released as dominantly carbon dioxide ($C0_2$) and carbon dioxide (CO). In addition, the elemental study of wood-derived biochar shows the higher carbon content but with low H/C and 0/C ratio suggested this material was dominated by highly aromatic structures and this were revealed in the Fourier transform infra-red (FTIR). More importantly, insignificant amount of inorganic species is evidenced in the samples.

**Keywords:** biochar, sawdust, fixed-bed, pyrolysis, combustion, solid fuels

**Abstrak**

Pencirian biochar berasaskan habuk kayu getah Malaysia (MRWSB) yang dihasilkan melalui pirolisis reaktor tetap di bawah suhu yang berbeza (450 hingga 850 °C) telah dikaji untuk kesesuaian sebagai bahan bakar. Pelbagai analisis dilakukan, termasuk kereaktifan biochar pengoksidaan, spesies bukan organik, kandungan oksigen dan hidrogen dalam biochar, pelepasan heteroatom didalam biochar sebagai produk gas, dan evolusi struktur biochar semasa proses pirolisis. Hasil kajian menunjukkan bahawa suhu optimum untuk karbonisasi untuk mendapatkan arang dengan perolehan yang tinggi didapati pada suhu 450 °C. Analisis Termogravimetri (TG) menunjukkan bahawa suhu mendorong struktur karbon semakin lebih tersusun dan membawa kepada perubahan ketara dalam kereaktifan biochar ini. Proses ini ditambah pula dengan kehilangan heteroatom, dilepaskan sebagai karbon dominan dioksida ($C0_2$) dan karbon dioksida (CO). Di samping itu, kajian unsur biochar kayu yang diperolehi menunjukkan kandungan karbon lebih tinggi tetapi dengan rendah H/C dan nisbah 0/C menyarankan bahan ini dikuasai oleh struktur yang sangat aromatik dan ini telah diverifikasi di dalam transformasi Fourier infra-merah (FTIR). Lebih penting lagi, jumlah spesies bukan organik yang tidak ketara terbukti dalam sampel.

**Kata kunci**: biochar, habuk papan, reaktor tetap, pirolisis, pembakaran, bahan api pepejal

## Introduction

Biomass utilization for energy production is highly interesting possibilities for sustainable option to reduce dependency on fossil fuels. In Malaysia, major biomass resource is cheap and widely available especially in form agricultural residues namely palm oil residues, rice, forestry and others. More than 2 million tones agricultural

wastes generated annually and a primary energy equivalent of 108 PJ, are potentially an attractive feedstock for producing energy as it use contributes little or no net carbon dioxide to the atmosphere. However, their utilization is limited due to various reasons such seasonal issues, low value heating value (HV), high ash and mineral content. These issues may cause operational problem in the boiler such agglomeration, molten slag and others [1]. Biochar is a carbon rich (65 to 90%), fine-grained and porous substance obtained when biomass, such as wood, manure and leaves, is heated or natural burned under oxygen limited condition and at relatively low temperatures (<700°C) [2]. The feedstock which is favored for biochar was those with high carbon content. These may include abundant, available and low-cost agricultural by-products, including crop residues (including straw, nut shells and rice husks and rice hulls) [3], switch grass, organic wastes including distillers grain, bagasse from sugarcane industry and olive waste [4], chicken litter dairy manure [5], sewage sludge and paper sludge [6].

There are various technologies currently in use for biochar production namely pyrolysis, carbonisation and gasification. However, slow pyrolysis technology which is characterized by moderate heating rates (ca. 20- 100 °C min- 1 and maximum temperatures of around 600°C is the most often referred to the biochar production from various feedstock in the literatures [7-10]. Despite the range of feedstock and techniques available to produce biochar, relatively little work has reported the mechanistic understanding on correlations between biochar's physical and thermochemical properties with view to potential solid fuel in energy production. In the present work, a rubber-wood sawdust (Heveabrasiliensis) has been used as a feedstock. Rubber wood is one of the main plantation crops in South East Asia with an estimated plantation area of 1.82 million hectares in Malaysia alone which accounts for 20% of global plantations. To the of the authors knowledge, apart from as successful adsorbent (activated carbon precursor dye removal [11-13]), no publicly accessible reports are available to investigate the stability rubber-wood sawdust-derived biochar as solid fuel in energy production. Hence, the present work attempted to assess Rubber-wood sawdust- derived biochars properties suitability in fuel application.

## Materials and Methods

### Raw Material and Sample Preparation

Sawdust from rubber wood (Hevea brasilensis) is used in this study, was obtained from a local (Selangor, Malaysia) furniture manufacture. Sawdust samples were dried in crucibles in an oven at 110 °C for 24 hours. The samples were then ground and sieved to 2 to 3 mm particle sizes. The main characteristics of the raw sawdust are presented in Table 1.

Table 1. Main characteristics of the raw sawdust based on ASTM method D 5373

| **Proximate analyses ( wt% dry basis)** | | | **Ultimate analyses (wt% dry basis)** | | | | | |
|---|---|---|---|---|---|---|---|---|
| **Volatile** | **Fixed carbon** | **Ash** | **Carbon** | **Hydrogen** | **Oxygen*** | **Nitrogen** | **Sulfur** | **Calorific Value (MJ/kg)** |
| 51.39 | 14.29 | 22.67 | 53.4 | 6.7 | 36.8 | 3.1 | 0 | 18.3 |

*By difference

### Biochar Preparation

Pyrolysis to prepare the biochars was carried out using a specially designed fixed-bed stainless steel reactor, with an internal diameter of approximately 60 mm, housed vertically in an electrically heated furnace, under well-controlled conditions. The biomass sample (30 g) loaded into reactor and was heated at a slow-heating rate of 10 K $min^{-1}$ to a desired temperature (450 to 850 °C) and then held for under 200 mL min-1 ultrahigh-purity (UHP) nitrogen . At the end of the experiment, the reactor was lifted out of the furnace immediately to cool naturally to room temperature with a continuous flow of argon through the reactor. The biochar was then recovered for further characterization.

**Instrumental analysis**

Proximate and ultimate analyses were performed according to ASTM standard test method D 5373 using a CHNS0 analyser (Perkin Elmer 2400 series II). The biochar oxidation reactivity was measured using a Thermogravimetric analyser (Metler Toledo/TGA/ SDRA5le) operating under isothermal conditions. The tests were conducted in an atmosphere of 5% 02 'in nitrogen at a heating rate of 30°Cmin"1 for temperature range 30 to 900°C. The gas evolution the biochars during combustion were measured using evolved gas analysis (EGA) technique and Fourier transform infrared (FTIR) (Perkin-Elmer1600 series analyzer) spectroscopic for functional group analyses. Inorganic species such as AI, Ca,Fe,Mg,Si and Zn were analysed using inductively coupled plasma-atomic emission spectroscopy (ICP-AES).

## Results and Discussion

**Evolution of biochar and its reactivity**

Figure 1 shows the TG (primary y-axis) and DTG (secondary y-axis) curves for the studied biochars. The thermal events of the MRWSB generally follow the basic evolution of carbonaceous residue obtained when lignocellulosic biomass is thermally degraded under different temperatures conditions such cellulose, hemicellulose and lignin at distinctive thermal decomposition [6]. Hemicellulose is the first to decompose, beginning at 250°C and substantially completed by 300°C and followed by cellulose decomposition which may begin at temperatures as low as 300°C. Although lignin begins to decompose at 160°C, it is a slow, steady process extending to 900°C which described the lower peaks heights. However, different profiles were observed for biochar produced at higher temperatures. This suggested that these biochar is stabilized no further decompositions is occurred in their chemical structure.

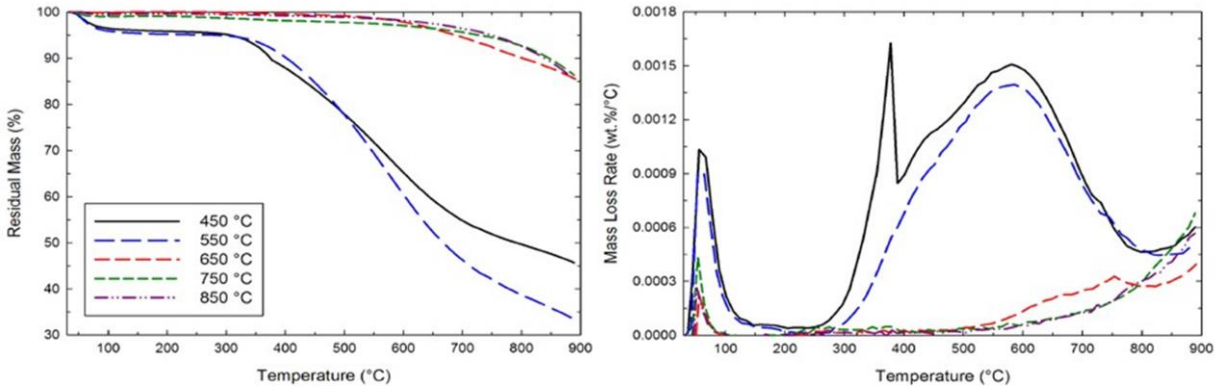



Figure 1. Thermogravimetric analysis of the pyrolysis of biochars at constant heating rate (10 °C $min^{-1}$) with $N_2$ sweep gas at 120 mL $min^{-1}$

Figure 2 shows the exit gas composition of raw sawdust, sawdust derived biochars samples at 450°C and 850°C, respectively. Gas evolution profiles for both samples, with the most notable difference being the releases of oxides of carbon over three distinct temperature regions compared one region to biochar samples. Raw sawdust primarily produced carbon dioxide and carbon monoxide during heating to 280, 380 and 440°C, respectively whereas for biochar samples, the gases evolved during heating between 400 and 450°C.The peaks obtained were due to decomposition of the original sawdust which suggesting that biochar has a homogeneous compound compared to raw sawdust.

This phenomenon explain the degree of aromaticity and the maturation and bonding arrangement of the biochar samples which is reflected in the FTIR spectrum analyses. This indicated that the most C is either directly bonded to a proton or connected through hydroxyl (OH) group. These information on the functionality of the biochars

suggested that the chemical characteristics can vary substantially to a significant extend by the degree of aromaticity.

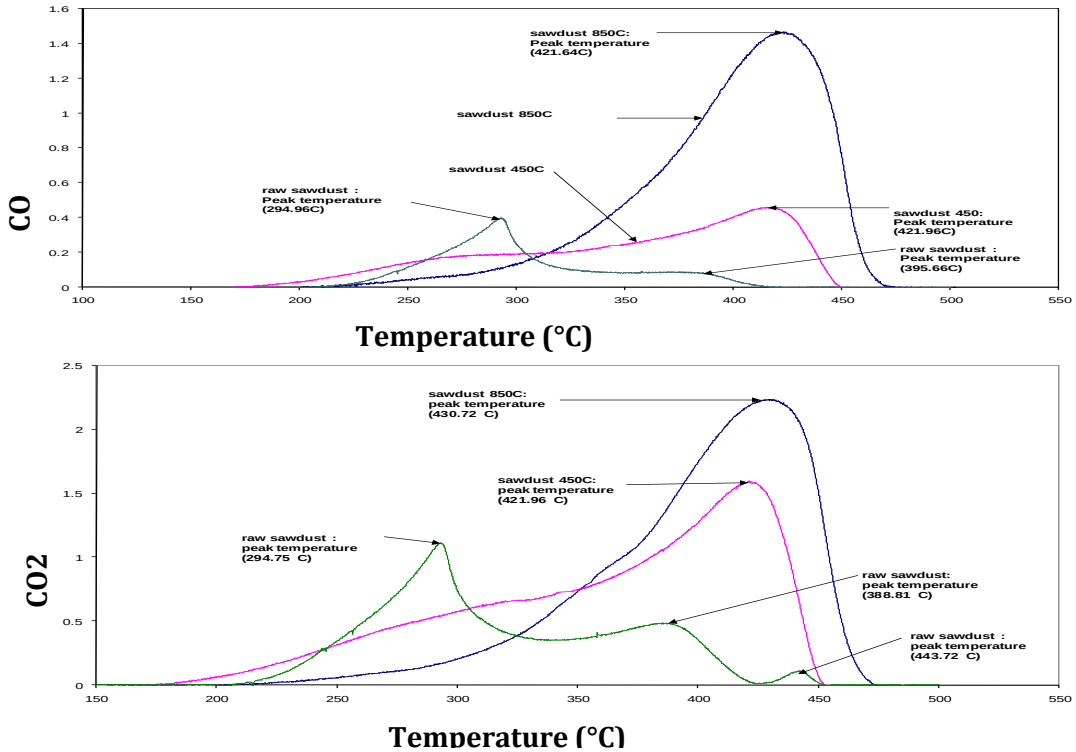



Figure 2. Gas evolution profiles during combustion runs of sawdust and sawdust-derived biochar at different temperatures

Table 2. Elemental contents of raw rubber wood sawdust and biochars. Results of elemental analysis are reported on a dry weight basis.

| | **Biochars** | | | | |
|---|---|---|---|---|---|
| | **450 °C** | **550 °C** | **650 °C** | **750 °C** | **850 °C** |
| H/C (mass/mass) | 0.039 | 0.028 | 0.019 | 0.011 | 0.010 |
| O/C (mass/mass) | 0.17 | 0.073 | 0.067 | 0.012 | 0.005 |
| Ash (%) | 14.5 | 16.3 | 17.8 | 19.5 | 20.0 |
| Yield (%) | 41.86 | 37.16 | 32.78 | 30.96 | 28.90 |
| Specific surface ($m^{2/}g$) | 10 | 50 | 100 | 200 | 200 |
| Heating value (MJ/kg) | 27.3 | 27.68 | 27.8 | 29.6 | 30.96 |

BDL – below instrumental detection limit.
[a] Results expressed as percentage of dry matter free of ash.
[b] Calculated by difference

**Effect of temperature on biochar yield, calorific value, carbon, oxygen and Hydrogen content**

Table 2 shows the biochar properties for various pyrolysis temperatures between 450 and 850°C. It can be seen that the biochar yield varied according to the reaction temperature. Biochar yield decreased with increasing temperature from 41.86% at 450°C to 28.90% at 850°C. The change in the solid and gas products due to thermal decomposition of the individual components of the original biomass. This phenomenon is likely to be explained by the combined decomposition of the lignin, cellulose and hemicelluloses in the biomass since the breakdown of these components has been shown to occur between 250 and 450°C [14-15]. Above 700°C, the cellulose and hemicelluloses components of the sawdust were evolved mainly in the gas products whereas lignin was mainly responsible for the char. On the other hand, the carbon (C) content showed an increased with increasing pyrolysis temperature, from 44 wt % at 450°C to 97% at 850°C and hence calorific values. This is a result of increased oxidation at higher temperatures, and reflects the conclusion drawn by the Schmidt and Noack on the characteristics of black carbon [16].

**Retention of Inorganic Species in Biochars**

Table 3 shows the contents of various inorganic species in the raw sawdust and sawdust-derived biochar sample. For the raw wood, the AI and Zn species, such are dominant species but traces amount were detected in the biochar samples.

Table 3. Elemental compositions ofbiochar samples from sawdust

| **Samples** | **AI** | **Ca** | **Fe** | **Mg** | **Si** | **Zn** |
|---|---|---|---|---|---|---|
| Raw sawdust | 13.89 | 12.72 | 8.35 | 0.35 | 8.78 | 19.32 |
| Biochar (450°C) | nd | 4.121 | 6.563 | nd | Nd | 12.93 |
| Biochar (550°C) | nd | 6.582 | 7.652 | nd | Nd | 3.128 |
| Biochar (650°C) | nd | 10.3 | 6.157 | nd | Nd | 7.256 |
| Biochar (750°C) | nd | 1.848 | 0.576 | nd | Nd | 2.299 |
| Biochar (850°C) | nd | 5.83 | 1.605 | nd | Nd | 4.626 |

nd -not detected

## Conclusion

The pyrolysis of MRSWB is characterized as carbon rich and reactive where pyrolysis temperature is found greatly influenced both their thermal and chemical properties. These characterizations suggested that these biochars is suitable for fuel purposes as well after processing like briquetting and in the form of char-liquid fuel and char-water slurries. This study shows that the sawdust can be a resource for biochar production. These findings will serve as a base for future systematic research on the same issue.

## Acknowledgement

The authors express their gratitude to the Ministry of Science, Technology and Innovation (MOSTI) of Malaysia, Academy Science of Malaysia and Ministry of Higher Education (MOHE) of Malaysia (FRGS 03-01-04-799FR/5523839 and RUGS 05-02-12-895RU/9346500) for financial support. Also kind acknowledgements to the Dept. of Chemical and Biomolecular, University of Melbourne, Australia for their combustion test facilities.

## References

1. Werther J., Saenger M. (2000). Combustion of agricultural residues. *Progress in Energy and Combustion Science*. 26:1-27.
2. Sohi S, Lopez-Cape E, Krull E and Bol R. (2009). Biochar, Climate change and soil: A review to guide future

research. CSIRO *Land and Water Science Report* 05/09.: 64-80.
3. Zhang T, Walawender WP, Fan T, Fan M, Daugaard D. and Brown R. C.(2004). Preparation of activate carbon from forest and agricultural residues through C02 activation. *Journal of Chemical Engineering* 105:53-59.
4. Sensoz S., Demirala I. and Ferdi G. H (2006). Olive bagasse (Olea europea L. Pyrolysis *Bioresource Technology* 97:429-436.
5. Das K.C., Garcia-Perez M., Bibens B., and Melear N(2008). Slow pyrolysis of poultry litter and pine woody biomass, Impact of chars and bio-oils on microbial growth. *J. of Environmental Science and Health: Part A* 43:714-724
6. Shinogi, Y., Yoshida H., Koizumi T., Yamaoka M. and Saito, T. (2002). Basic characteristics of low-temperature carbon products from waste sludge. *Advances in Environmental Research* 7:661-665.
7. Purevsuren B. Avid, Tesche B. and Davajaav (2003). A biochar from casein and its properties. *J. Material Science* 38:2347-2351.
8. Sensoz S. (2003). Slow pyrolysis of wood barks from Pinus brutia Ten and product Compositions *Bioresource Technology* 89:307-311.
9. Azargohar R and Dalai A. K (2008). Steam and KOH activation of biochar: Experimental and Modeling studies. *Microporous Mesoporous Material* ll0: 413-421.
10. Xinde C., Lena M., Bin G. and Willie H. (2009). Dairy-Manure derived biochar effectively sorbs lead and atrazine. *Environmental Science and Technology* 43:3285-3291.
11. Srinivasakannan and Mohamad Zailani Abu Bakar(2004), Production of activated carbon from rubber wood sawdust. *Biomass and Bioenergy* 27:89-96.
12. Prakash Kumar, B. G., Shivakamy, Lima Rose M. and Velan M. (2006). Preparation of steam activated carbon rubberwood sawdust (Hevea brasiliensis) and its adsorption kinetics. *J. of Hazardous Material* 136: 922-929.
13. Materazzi S., Gentili A. and Curini R. (2006). Application of evolved gas analysis Part 2: EGA by mass spectrometry, *Talanta*, 69:26-35.
14. Demirbas A. (2004). Effects of temperature and particle size on biochar yield from pyrolysis of agricultural residues. *J. of Analytical and Applied Pyrolysis* 72(2):243-248.
15. Van de Velden M, Baeyens J, Brems A, Janssens B. and Dewil R. (2010). Fundamentals, Kinetics and endothermicity of the biomass pyrolysis reaction. *Renewable Energy*, 35: 232-242.
16. Schmidt W. M. I and Noack A. G. (2000). Black carbon in soils and sediments: Analysis, Distribution, implications, and current challenges. *Global Biogeochemical* Cycles 14:777-793.

The Malaysian Journal of ANALYTICAL SCIENCES ISSN 1394-2506

# THERMOGRAVIMETRIC ANALYSIS (TGA) PROFILE OF MODIFIED SBA-15 AT DIFFERENT AMOUNT OF ALKOXYSILANE GROUP

## (Profil Thermografimetrik Analisis SBA-15 Berfungsi Pada Jumlah Kumpulan Alkoxysilane Yang Berlainan)

Norhasyimi Rahmat*, Nur Fathilah Mohd Yusof, Ezani Hafiza

*Faculty of Chemical Engineering,*
*Universiti Teknologi MARA, 40450 Shah Alam, Selangor, Malaysia*

**Corresponding author: norhasyimi@salam.uitm.edu.my*

**Abstract**

This study focused on mesoporous silica SBA-15 modified with alkoxysilane functional group; phenyltriethoxysilane (PTES) and vinyltriethoxysilane (VTES) using direct synthesis and post-grafting methods. By direct synthesis method, SBA-15 templated by triblock copolymer (P123) and functionalized with alkoxysilane groups at different amount of loadings were co-condensed with tetraethyl orthosilicate (TEOS) under acidic conditions. As for post-grafting method, different loadings of alkoxysilane groups were added after co-condensation of TEOS with P123 template. Both synthesis methods used calcination process to remove surfactant template at 550°C for 5 hours. The derivatized SBA-15 was characterized by thermogravimetric analysis to evaluate the profile at different loadings of alkoxysilane groups with different synthesis method. At temperature range of 300°C-800°C, post-grafting method displayed the highest weight loss of phenyl and vinyl groups. However, there was no significant difference of weight loss for different amount of organosilane groups. In this study, TGA has shown to be significant characterization means to determine the effects of different method used in synthesizing modified SBA-15. It was shown that different loading of phenyl and vinyl groups did not affect the efficiency of surfactant removal.

**Keywords:** characterization, thermogravimetric analysis, direct synthesis, post-grafting, modified SBA-15, mesoporous silica

**Abstrak**

Kajian ini ditumpukan kepada silika mesoporus, SBA-15, yang difungsikan dengan kumpulan alkoxysilane; phenyltriethoxysilane (PTES) dan vinyltriethoxysilane (VTES) menggunakan kaedah sintesis langsung dan pos-grafting. Melalui sintesis langsung, SBA-15 yang ditemplatkan oleh triblok kopolimer (P123) dan difungsikan oleh kumpulan alkoxysilane pada jumlah berlainan telah dikondensasikan bersama tetraethyl orthosilicate (TEOS) dalam keadaan berasid. Dengan kaedah pos-grafting pula, jumlah kumpulan alkoxysilane yang berlainan ditambahkan hanya selepas kondensasi TEOS pada templat P123. Kedua-dua kaedah ini menggunakan proses pembakaran untuk menyesarkan templat surfaktan pada suhu 550°C selama 5 jam. Derivatisasi SBA-15 telah diperincikan oleh thermografimetrik analisis untuk menilai profil pada jumlah kumpulan alkoxysilane yang berlainan bagi teknik yang berbeza. Pada rangkuman suhu 300°C-800°C, kaedah pos-grafting telah menunjukkan kehilangan berat kumpulan phenyl dan vinyl yang paling tinggi. Namun begitu, tiada perbezaan kehilangan berat yang ketara didapati pada jumlah kumpulan alkoxysilane yang berlainan. Dalam kajian ini juga, TGA telah membuktikan kepentingannya sebagai kaedah perincian untuk menentukan kesan teknik sintesis kefungsian SBA-15 yang berbeza. Telah dibuktikan juga bahawa jumlah kumpulan phenyl dan vinyl yang berlainan tidak memberi kesan terhadap efisiensi penyingkiran surfaktan.

**Kata kunci**: perincian, analisis thermografimetrik, sintesis langsung, pos-grafting, SBA-15 berfungsi, silika mesoporus

## Introduction

Santa Barbara Amorphous-15 (SBA-15) is one of the unique mesoporous structures that have uniform hexagonal array of pores with limited pore size distribution and pore diameter of between 5 and 15 nm [1]. The thickness of the framework walls is about 3.1 to 6.4 nm, which gives SBA-15 advantage on hydrothermal and mechanical stability. It also has high internal surface area of 400 to 900 $m^2$, which makes SBA-15 as a good choice for use in many applications [2]. Pure silica SBA-15 showed very limited catalytic activities due to the lack of lattice defect,

redox properties, basicity and acidity. There have been many ways to increase the active sites and improve the catalytic activity by introducing guests into the framework of SBA-15, in which the effect of surface modification has not been rigorously investigated. Specifically, there are two accesses to produce organic functionalization of SBA-15, which are (i) post grafting method and (ii) direct synthesis method [3].

Direct synthesis is a method used to functionalize SBA-15 which involves one-step co-condensation of tetraalkoxysilanes such as tetraethyl orthosilicate (TEOS) with organosilanes prepare under basic or neutral or near-neutral pH condition during functionalization [4] while post-grafting method consists of reaction of a organosilane with surface silanol groups using an appropriate solvent under reflux conditions. This method is actually the first method to be used to modify mesoporous silica materials. The silanol groups react with the organosilane to form a layer of covalently coupled surface functional groups [5].

The use of organosilanes organic groups gives the resulting materials many favorable features to broaden the application fields. In this regard, vinyl and phenyl functionalities are hypothesized to exhibit ample reactivity and display versatile precursor moieties for both subsequent organic transformations and metal incorporation reactions. Thus, the introduction of such reactive groups on the SBA-15 could keep a sufficiently large pore volume, makes the material very interesting for catalytic and sensing applications [6].

Thermogravimetric analysis or thermal gravimetric analysis (TGA) is a method of thermal analysis in which changes in physical and chemical properties of materials are measured as a function of increasing temperature (with constant heating rate), or as a function of time (with constant temperature and/or constant mass loss). Thermogravimetric analysis is a useful tool to determine the presence of material containing carbon, hydrogen, and oxygen on the surface of silica such as surfactants (in the case of templated silicas) and bonded alkyl groups. This method can also yield quantitative results as the weight loss is accurately measured by an internal microbalance, and the percent weight of a sample lost through thermal decomposition can be calculated [7]. This characterization technique has been used in various environmental, food, pharmaceutical and petrochemical applications [8].

Since the discovery of mesoporous materials, numerous studies on modified SBA-15 has been done due to its specialty to be used in various applications. However, study on TGA profile of alkoxysilane modified SBA-15 has yet to be widely explored. Thus, in this study, the characterization of modified SBA-15 using the TGA technique is employed for different methods of post-grafting and direct synthesis.

## Materials and Methods

### Materials

Pluronic 123 triblock copolymer [poly(ethylene oxide)$_{20}$–poly(propyleneoxide)$_{70}$–poly(ethylene oxide)$_{20}$] (P123), tetraorthosilicate (TEOS), 2M hydrochloric acid (HCl), phenyltriethoxysilane (PTES), toluene, *p*-toluenesulfonic acid (PTSA).

### Synthesis of Pure SBA-15

4g of P123 was dissolved in 125mL of 2M HCl at room temperature. After complete dissolution, the mixture was heated to 40°C on hotplate and 8.6g of TEOS was added. The solution was stirred for 20h and the temperature was maintained at 40°C. Then, the white precipitate was hydrothermally aged in oven at 100°C for 24h. The product was recovered and dried. The surfactant was removed by calcination in static air at 550°C for 5h using furnace.

### Synthesis of PTES-SBA-15 and VTES-SBA-15 using direct synthesis

4g of P123 was dissolved in 125mL of 2M HCl at room temperature. After complete dissolution, the mixture was heated to 40°C on hotplate and 8.6g of TEOS was added. PTES was added in TEOS: PTES molar ratio of 1: 5 and 1:15.The solution was stirred for 20h and the temperature was maintained at 40°C. Then, the white precipitate was hydrothermally aged at 100°C for 24h in oven. The product was recovered and dried. The surfactant was removed by calcination in static air using furnace at 550°C for 5 hours.

**Synthesis of PTES-SBA-15 and VTES-SBA-15 using post-grafting**

1g of SBA-15 and 150mL toluene were dissolved in 3 flask equipped with mechanical agitator. The dissolved mixture was stirred for 30 minutes at 50°C. 0.007g of PTSA and PTES were added in TEOS: PTES molar ratio of 1:5 and 1:15. After stirring for 2 hours, the sample was filtered and hydrothermally aged at 100°C for 24h in oven. Calcination was carried out in static air using furnace at 550°C for 5 hours.

**Characterization**

Characterization was conducted using TGA 4000 Brand Perkin Elmer in the presence of nitrogen as inert purge with flow of 100mL/min and heating rate of 10°C/min, heating from 20°C to 900°C.

## Results and Discussion

Direct synthesis of phenyl modified SBA-15. Figure 1 shows different loading of PTES-SBA-15 functionalizes using direct-synthesis. At starting temperature to 150$^{o}$C, a phenomenon of release of water formed from condensation process in silica is happened. At this range, the water loss varies from 16-21% for different type of samples.

Surfactant tends to be decomposed at temperature range of 150$^{o}$C to 300$^{o}$C. All samples show low percentage of surfactant decomposition, which indicates that surfactant have been efficiently removed during calcination. Further weight loss at temperature range 300$^{o}$C to 800$^{o}$C is due to the decomposition of organosilane groups as reported by Kruk et al. [2]. With this regard, sample both samples PTES:TEOS 5:1 and 15:1 have shown to have 2-2.5% weight loss of phenyl groups.

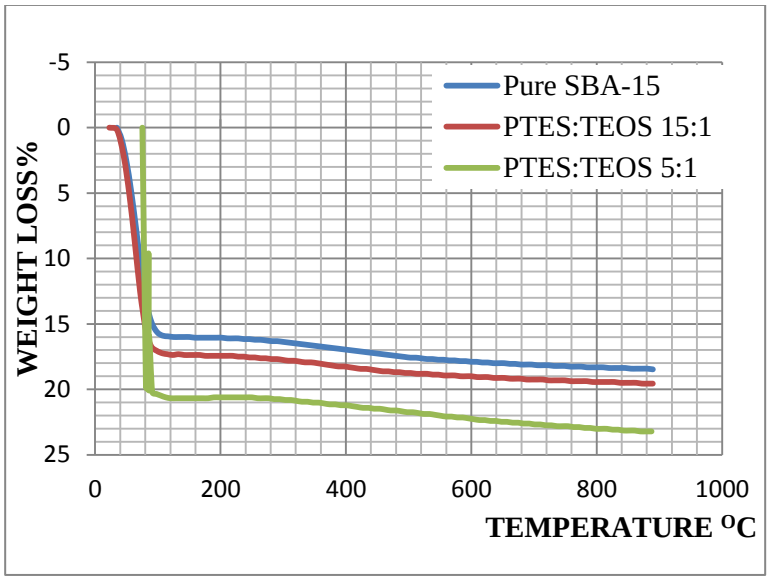



Figure 1. Different loading of phenyl group to synthesize modified SBA-15 using direct-synthesis method.

**Post-grafting of phenyl modified SBA-15**

Figure 2 shows the comparison of different loading of phenyl group functionalized with SBA-15 using post-grafting method. At temperature range of 25$^{o}$C to 150$^{o}$C, evaporation of water for pure SBA-15 is about 16.05%, which is the highest. Evaporation of water for PTES:TEOS 15:1 and PTES:TEOS 1:5 are about 10.40% and 5.13%, respectively.

Weight loss occurs for all samples after 150°C to 800°C due to decomposition of surfactant and organosilane groups. However, all samples show very least of surfactant weight loss at temperature 150°C to 300°C. This could be due to calcination condition that completely decompose and remove the templating surfactant from mesopore framework. Small difference of weight loss at range of 300°C and 800°C is observed between PTES:TEOS 5:1 and PTES:TEOS 15:1 which are at respective 6.34% and 6.9% weight loss.

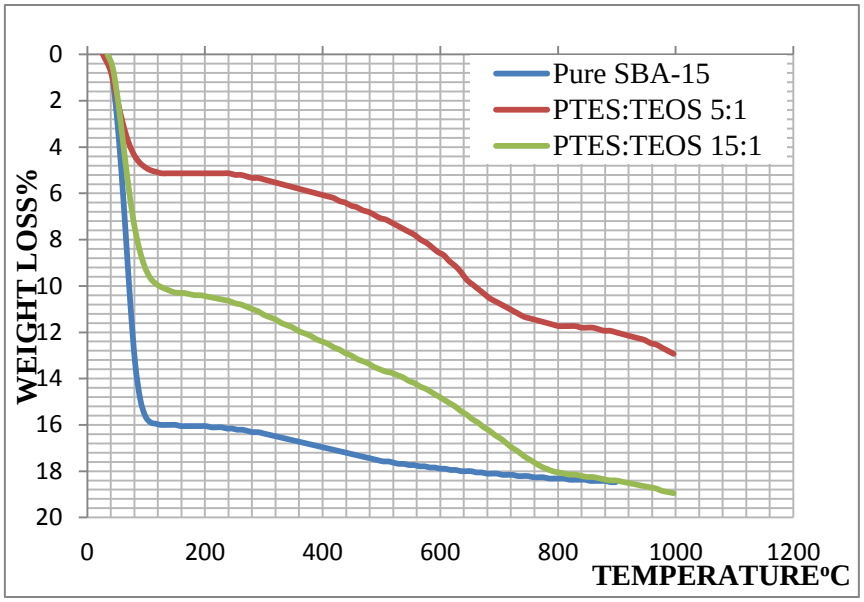



Figure 2. Different loading of phenyl group to synthesize modified SBA-15 using post-grafting method.

As shown in Figure 3, two sets of different methods were carried out to functionalize SBA-15. In the first set, SBA-15 was functionalized using direct-synthesis while the second set using post-grafting. Both sets of sample have same loading phenyl-group being attached in silica mesopores framework.

At temperature range of 300℃ to 800℃, sample of phenyl group functionalized by post grafting shows a higher weight loss compare to sample functionalized by direct synthesis. Sample post-grafting 15:1 has 6.8% while sample post-grafting 5:1 has 6.3% weight loss. Samples from direct synthesis 15:1 and 5:1 show only 2.1% and 2.6% weight loss. At this amount of phenyl group loading, it could be predicted that phenyl-group is efficiently incorporated into silica mesoporous framework using post-grafting compare to direct-synthesis method.

**Direct synthesis of vinyl modified SBA-15**

In comparison with pure SBA-15, VTES-SBA-15 (ratio 5:1) exhibit higher weight loss than pure SBA-15. The difference of weight loss of pure SBA-15 and VTES-SBA-15 is due to the amount of vinyl group incorporated.

The surfactant (P123) decomposes at temperature range from 150 to 300ºC. Kruk et al. [2] has shown similar pattern of result when analyzing the TGA profile of calcined SBA-15 [2]. It is claimed that major weight loss in this temperature range is due to desorption of surfactant template. Based on Figure 4, all three samples show the same trend in weight loss, which indicates that the decomposition of remaining surfactant in those three samples do not affected by different amount of vinyl group during calcination process.

In accordance with the work of Lim et al. [9], this study also displays decomposition of VTES group at temperature between 280 and 440ºC [9]. Small difference of weight loss is observed between VTES: TEOS 5:1 and VTES:TEOS 15:1 which are at 2.5% and 1.35% respectively.

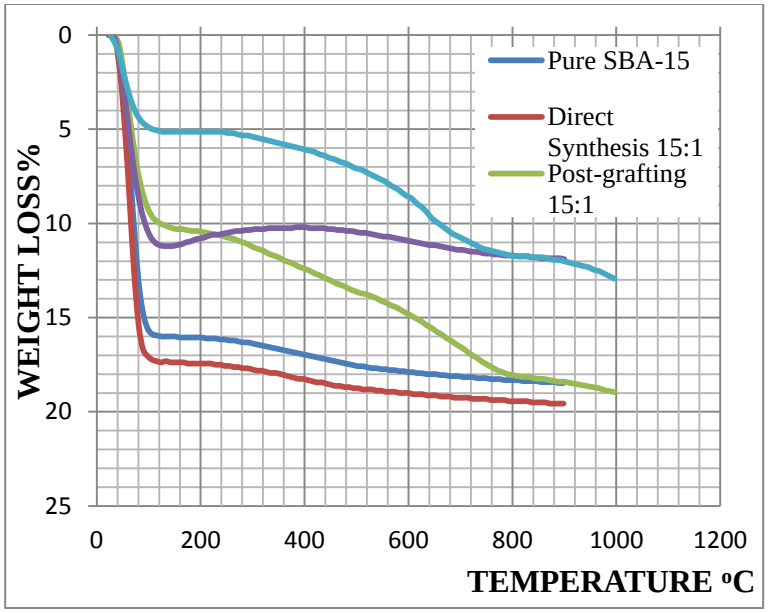



Figure 3. Different methods of synthesizing PTES-SBA-15

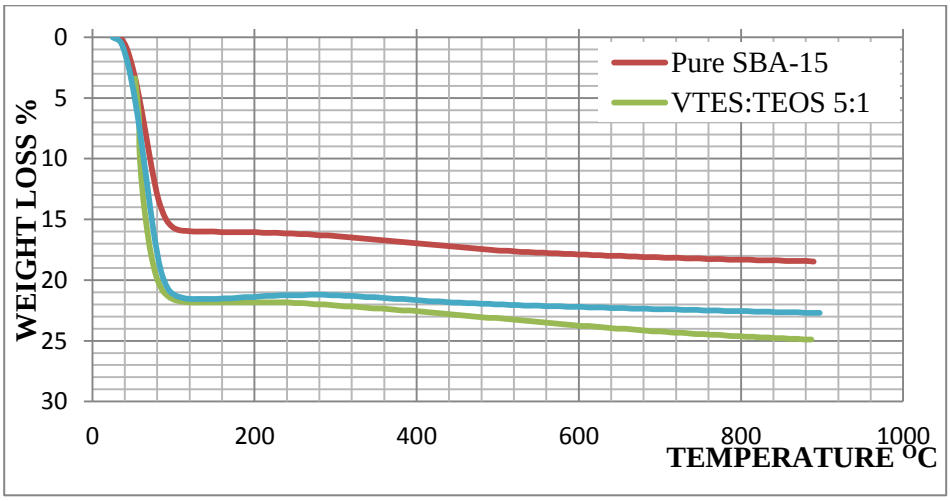



Figure 4. Different loading of vinyl group to synthesize modified SBA-15 using direct-synthesis method.

**The effects of methods on the functionalization of VTES-SBA-15**

Figure 5 shows the TGA profile of VTES-SBA-15 using different method of functionalization, which is direct synthesis and post-grafting. Both methods have gone through the same calcinations process at 550 $^{o}$C for 5 hours.

In the temperature range from 30 to 150$^{o}$C, sample VTES-SBA-15 prepared from direct synthesis method shows the highest weight loss as compared to VTES-SBA-15 by post grafting. This could be due to the amount of water adsorbed in the mesoporous structure during direct synthesis is higher compare to post-grafting method. For the temperature range between 150-280$^{o}$C, VTES-SBA-15 by direct synthesis shows equally the same weight loss with

VTES-SBA-15 by post-grafting, which is 0.5-0.64%. This shows that different methods do not affect the surfactant removal process.

At the range of 280-440°C, VTES-SBA-15 by post-grafting shows a higher value of weight loss than VTES-SBA-15 by direct synthesis due to higher amount of vinyl group decomposition. This also indicates that more triethoxyvinylsilane groups are attached to SBA-15 mesoporous structure by post-grafting method.

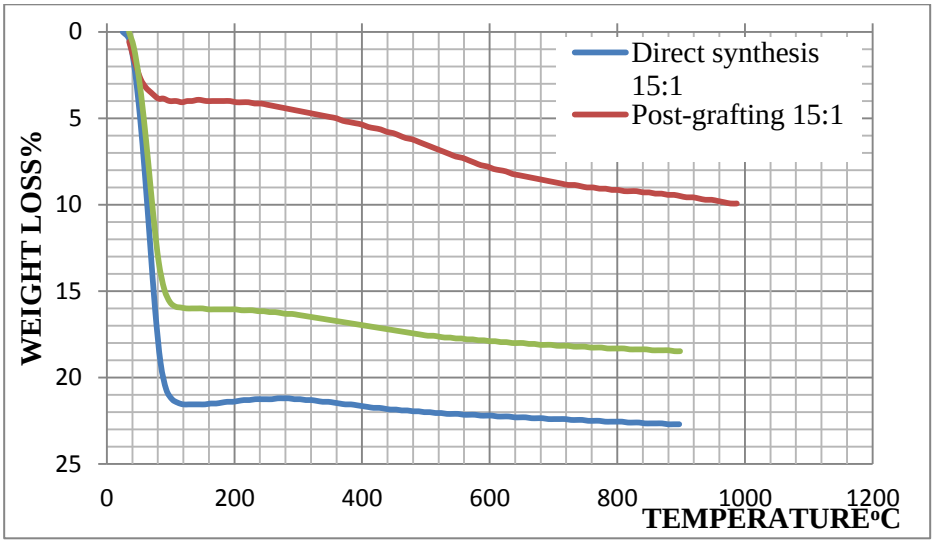



Figure 5. Different methods of synthesizing VTES-SBA-15

## Conclusion

In this study, direct-synthesis and post-grafting method used to synthesize different loading of phenyltriethoxysilane and vinyltriethoxysilane into SBA-15 mesoporous structure using TGA analysis has been successfully demonstrated. Both methods of synthesizing both types of organosilane functionalized SBA-15 do not influence the process of surfactant template removal. There is no significant weight loss observed for different amount functionalized with SBA-15 in this scope of work. However, TGA analysis displays a significant difference of weight loss on different methods used to functionalize SBA-15 for both PTES and VTES functional group.

## Acknowledgement

Appreciation goes to Ministry of Higher Education of Malaysia for funding this research project (FRGS). Special thanks to Research Management Institute of Universiti Teknologi MARA and technical personnel who helped to realize the execution of this research study.

## References

1. Van Grieken, R., Iglesias, J., Morales, V. and García, R.A. (2010). Synthesis and characterization of SBA-15 materials functionalized with olefinic groups and subsequent modification through oxidation procedures. *Microporous and Mesoporous Materials* 131, 321-330.
2. Kruk, M., Jaroniec, M., Ko, C.H. and Ryoo, R. (2000). Characterization of the Porous Structure of SBA-15. *Chemistry of Materials* 12, 1961-1968.
3. Maria Chong, A.S., Zhao, X.S., Kustedjo, A.T. and Qiao, S.Z. (2004). Functionalization of large-pore mesoporous silicas with organosilanes by direct synthesis. *Microporous and Mesoporous Materials* 72, 33-42.
4. Melero, J.A., Van Grieken, R., Morales, G. and Paniagua, M. (2007). Acidic mesoporous silica for the acetylation of glycerol: Synthesis of bioadditives to petrol fuel. *Energy Fuels* 21, 1782-1791.
5. Mercier, L. and Pinnavaia, T.J. (1999). Direct synthesis of hybrid organic-inorganic nanoporous silica by a

neutral amine assembly route: Structure-function control by stoichiometric incorporation of organosiloxane molecules. *Chemistry of Materials* 12, 188-196.
6. Chytil, S., Haugland, L. and Blekkan, E.A. (2008). On the mechanical stability of mesoporous silica SBA-15. *Microporous and Mesoporous Materials* 111, 134-142.
7. Kozlova, S.A. and Kirik, S.D. (2010). Post-synthetic activation of silanol covering in the mesostructured silicate materials MSM-41 and SBA-15. *Microporous and Mesoporous Materials* 133: 124-133.
8. Pyramides, G., Robinson, J.W. and William Zito, S. (1995). The combined use of DSC and TGA for the thermal analysis of atenolol tablets. *Journal of Pharmaceutical and Biomedical Analysis* 13, 103-110.
9. Lim, M.H. and Stein, A. (1999). Comparative studies of grafting and direct syntheses of inorganic-organic hybrid mesoporous materials. *Chemistry of Materials* 11, 3285-3295.

The Malaysian Journal of ANALYTICAL SCIENCES ISSN 1394-2506

# EFFECT OF MECHANICAL GRINDING AND IONIC LIQUID PRE-TREATMENT ON OIL PALM FROND

## (Kesan Pra-rawatan Pengisaran Mekanikal dan Cecair Ionik ke atas Pelepah Kelapa Sawit)

Siti Norsyarahah Che Kamarludin, Nor Sharliza Mohd Safaai*, Amizon Azizan , Hazimah Madzaki, Mimi Suhada Mamat, Niswah Hashina Zulkifli, Mohd Firdaus Zainuddin

*Faculty of Chemical Engineering,*
*Universiti Teknologi MARA, 40450 Shah Alam, Selangor, Malaysia*

**Corresponding author: sharliza972@salam.uitm.edu.my*

**Abstract**

The present study was set to investigate the chemical structural group of different particle size of Oil palm frond (OPF) after mechanical and Ionic liquid (IL) pretreatment by FTIR analysis. The particle sizes range of biomass used were 0-75, 75-125, 125-180, 180-250 and 250-355 µm which were prepared through mechanical grinding process by using an analytical mill. IL used in this experiment was 1-ethyl-3-methylimidazolium chloride [EMIM][Ac] with two different concentration of 1M and 3M. Pretreatment by IL was done on BioshakeIQ for 3 hours at 800 rpm and 85 ˚C. The pretreated OPF was then analyzed using FTIR spectroscopy in order to evaluate the performance of mechanical grinding and IL pretreatment based on the change observed in chemical structure through functional group existed. It was found that after size reduction through grinding process, the spectra between all particle sizes obtained did not differ much except for particle size range of 75-125 µm. The particle size range showed on much characteristics of cellulose due to the broad peak within the 3600-3100 cm-1 which stand for O-H bonding. However, when the FTIR spectra were compared between before and after IL pretreatments, there were some different in peaks trend which explained there were some chemical structure changes within the OPF samples. There were some appearances and disappearances of certain peak were observed after the IL pretreatment especially the peak at band near 1700 cm-1 and 1550 cm-1.

**Keywords:** Mechanical pretreatment, Ionic liquid, lignocellulosic biomass, bioethanol, cellulose, oil palm frond

**Abstrak**

Kajian ini dijalankan untuk mempelajari kumpulan struktur kimia dari pelepah kelapa sawit (OPF) selepas pra-rawatan mekanikal dan cecair ionik (IL) dengan menggunakan analisis FTIR. Julat saiz zarah biomas yang digunakan adalah 0-75, 75-125, 125-180, 180-250 dan 250-355 µm yang disediakan melalui proses pengisaran mekanikal. IL yang digunakan dalam penyelidikan ini adalah 1-etil-3-methylimidazolium asetat [Emim][Ac] dengan dua kepekatan berbeza iaitu 1M dan 3M. Pra-rawatan dengan IL dilakukan menggunakan BioshakeIQ selama 3 jam pada 800 rpm dan 85˚C. Selepas pra-perawatan, OPF dianalisis menggunakan spektroskopi FTIR bagi menilai potensi pra-rawatan berdasarkan perubahan yang diperhatikan melalui kumpulan struktur kimia yang wujud sebleum dan selepas pra-rawatan. Berdasarkan keputusan selepas pengurangan saiz melalui proses pengisaran, spectrum dari analisis FTIR antara semua saiz zarah yang diperolehi tidak banyak berbeza kecuali saiz 75-125 µm. Saiz tersebut menunjukkan banyak ciri-ciri selulosa berbanding saiz lain berdasarkan puncak yang luas dalam lingkungan 3600-3100 $cm^{-1}$ melibatkan ikatan OH. Apabila spektrum FTIR dibandingkan antara sebelum dan selepas pra-rawatan IL, perbezaan dapat dilihat antara puncak yang terbentuk di antara satu sama lain yang menjelaskan terdapatnya beberapa perubahan struktur kimia. Ada beberapa puncak yang sebelum dilakukan pra-rawatan menggunakan IL wujud tetapi, setelah pra-rawatan dijalankan hilang terutama yang terbentuk berhampiran 1700 $cm^{-1}$ dan 1550 $cm^{-1}$.

**Kata kunci**: Prarawatan mekanikal, Cecair ionik, biojisim lignoselulosa, bioetanol, selulosa, pelepah kelapa sawit

## Introduction

In recent years, non-renewable energy resources especially the petroleum are facing challenges in depleting reserves, increasing price and environmental issue. Therefore, it is critically important to explore new alternatives to replace the petroleum-based liquid transportation fuels. One such alternative is bioethanol produce from

lignocellulosic biomass (LB). The LB, second generation of biofuel which come from the woody biomass is a promising raw material for biofuel/bioethanol production. It is sustainable, relatively carbon neutral and readily available with a yearly supply of approximately 200 billion tons worldwide [1].

However, conversion of LB to bioethanol which comprising of hydrolysis, fermentation and separation processes is facing with chemical and physical barriers. More specifically, crystalline structure of cellulose, presence of lignin and covalent cross-linkages between hemicellulose and lignin which wrapped around the cellulose in cell wall interrupt the digestibility of cellulose during enzymatic hydrolysis to release sugar [2]. A high sugar yield in this processing step is important to the cost-effectiveness in production of cellulosic bioethanol. Hence, pretreatment is the key to unlock the recalcitrance of LB during the hydrolysis and downstream fermentation of the sugars released [1].

To date, several pretreatment approaches have been introduced to improve the LB accessibility to enzymatic hydrolysis including physical (milling, grinding etc.), chemical (organosolv, acid, alkali etc.), physico-chemical (wet oxidation, ammonia fiber explosion, steam explosion etc.) and biological pretreatment [3]. However, most of the conventional pretreatment methods suffer from one or more drawbacks like high energy consumption, costly, toxicity and instability in processing. As for example, pretreatment by dilute acid requires costly corrosion resistant equipment and also produce a significant amount of fermentation inhibitors during the processing step.

Recent attempts have been striving to make pretreatment methods cost effective, environmental friendly and more efficient. Among them, application of ionic liquid (IL) as a chemical solvent in pretreatment method has attracted much attention. IL is an organic salt comprising of cations and anions which melt below 100$^{o}$C [4]. The safety features of IL which is unique and only requires mild process condition during the pretreatment are regarded as the main advantages [4]. Furthermore, the biomass structure after pretreatment by IL has altered its native structure. It also resulted in higher saccharification with better digestibility compared to untreated biomass during the enzymatic hydrolysis [2]. Although the IL has ability to alter the biomass structure and able to dissolve the cellulose in the biomass, however, its effectiveness during the pretreatment processing step also will depends on the particles size of biomass. Previously study was stated that the smaller the particles size, the larger the total surface area, thus, more surface area contacted between biomass with IL solvent during the pretreatment. As a result, cellulose is easier to dissolve and its digestibility during the enzymatic hydrolysis step also will be enhanced [5].

In this study, Oil palm frond (OPF) was undergone some sort of mechanical grinding pretreatment to produce different particles size and then were pretreated using 1-ethyl-3-methylimidazolium acetate [EMIM][Ac] with two different molarity. Chemical structure of every particles size will be investigated before and after pretreatment in order to prove the contribution of particle size during the pretreatment by IL. Besides, the performance of IL also was evaluated based on the change observed in chemical structure of the biomass.

## Materials and Methods

### Materials

Oil palm frond (OPF) was supplied by Forest Research Institute of Malaysia (FRIM) located in Kepong, Kuala Lumpur. Ionic liquid (IL) used in this experiment was 1-ethyl-3-methylimidazolium acetate [EMIM][Ac] supplied by Sigma-Aldrich, Malaysia. The IL was in liquid form with 90% purity, molecular weight of 170.21 g/mol and density of 1.027 g/cm$^3$.

### Mechanical pretreatment (grinding)

The OPF was dried in a universal oven (ULE 400, Memmert) at 60 °C for 48 hours. The dried biomass then was placed in a desiccator and allowed to cool down to room temperature. The biomass then cut into smaller size before being grinded by a manual grinder machine (IKA A11 basic Analytical mill 115V, IKA Germany). The grinded samples were sieved by using a sieve shaker (Endecotss Octagon Digital) into different size range for 30 min. The sizes range used were 0-75, 75-125, 125-180, 180-250 and 250-355 µm.

**Ionic liquid pretreatment**

The samples biomass were pretreated with [EMIM][Ac] at 5 wt% by mixing 0.075 g of biomass and 1.5 g [EMIM][Ac] in 1.5 mL Eppendorf tube [6]. This step was done for all size range of the samples in triplicate. The Eppendorf tubes containing the mixture were then placed into a temperature controlled shaker (BioShakeiQ, Germany). The speed of the mixing was set to 800 rpm at a controlled temperature at 85 °C for 3 hours [7]. After 3 hours, the samples were left to cool in the room temperature. After cooling, the samples were placed into a mini centrifuge (Eppendorf Centrifuge 5415 R, USA). The samples were then centrifuge at 10,000 rpm and 4°C for 10 minutes. The precipitate was form. The liquid containing [EMIM] [Ac] was removed, and the precipitate was washed at least two times with additions of distilled water in order to ensure that excess ionic liquid had been removed [7]. The samples were then dried in the drying oven at 60 °C for 48 hours.

**FTIR analysis**

Fourier Transform Infrared (Spectrum One FT-IR Spectrometer, Perkin Elmer) analysis was conducted to observe the biomass structure before and after pretreatment for every different particles size. All spectra were recorded in the range of 4000-400 $cm^{-1}$ and were measured at a spectral resolution of 4 $cm^{-1}$ and 64 scans were taken per sample.

## Results and Discussion

**FTIR analysis on different particles size after mechanical grinding pretreatment**

FTIR analysis is a useful tool for obtaining rapid information about the functional group and chemical changes taking place in cellulose due to various pretreatments. Figure 1 shown FTIR spectra of OPF after the mechanical grinding process at different particles size of 0-75, 75-125, 125-180, 180-250 and 250-355 µm. From the figure, it was observed that the trends between all those particles sizes are quietly similar. The result obtained can be related to the type of grinder used which was hammer mill type. It was previously studied that the hammer mills give good size reduction without increasing the availability of cellulose or in other words it did not change the chemical structure of cellulose in sample biomass [8].

Although the trend obtained was practically quite similar, however, the absorption peak for smaller particles size of 75-125 µm was a little bit different compared to others. The O-H stretching vibration peak within the 3600-3100 $cm^{-1}$ for 75-125 µm become stronger and narrower than other larger particle size ranges. Generally, cellulose structure is packed with intermolecular and intra-molecular of O-H bonding. The strong band within the 3600-3100 $cm^{-1}$ can be concluded that there is high cellulose content for these particles size range.

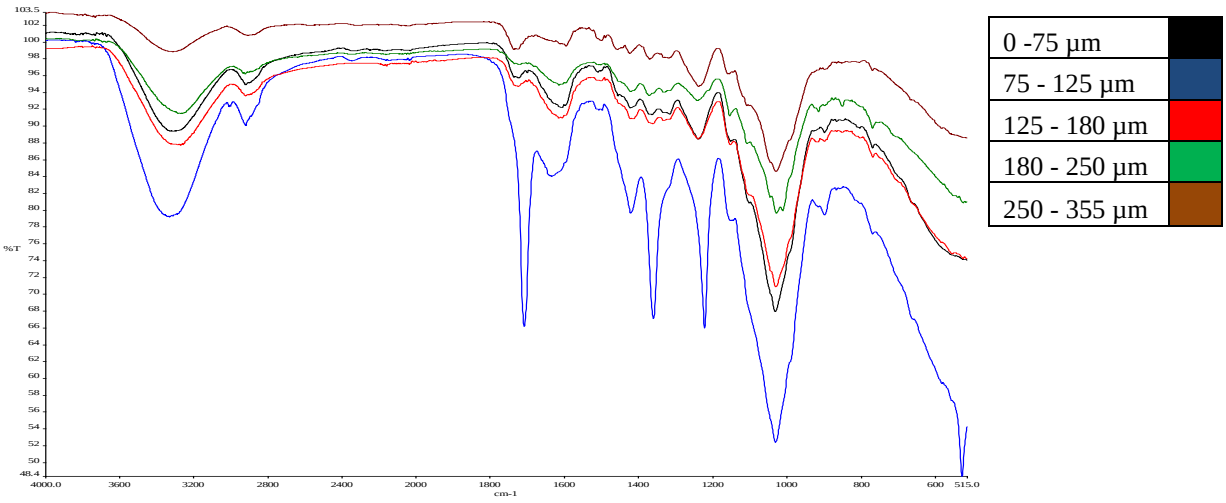



Figure 1. FTIR spectra of OPF with different particles size after mechanical grinding pretreatment

Besides, the band intensity of 1051 $cm^{-1}$ which is corresponding of C-O stretching vibration in cellulose/hemicellulose was more resolved in spectra of 75-125 µm indicating that the cellulose rich wood fibers are richer in carbohydrates [9]. In addition, there are strong peaks form near 1700 $cm^{-1}$ and around 1400-1300 $cm^{-1}$ with respectively correspond to bending or stretching vibrations of C=O and C-H group [10]. By the analysis between the different particles size, it can be said that the particle size range of 75-125 µm was the optimum size after mechanical pretreatment. Hence, this particles size range can be selected to conduct further pretreatment with IL which has high cellulose amount due to the commonly structure characteristics of cellulose shown in FTIR spectra analysis compared to other sizes.

**Comparison of FTIR analysis on different particles size before and after IL pretreatment**

The comparison between before and after pretreatment by FTIR analysis was investigated to confirm whether any new functional group was generated during the interaction of OPF with IL. Figure 2 shows the FTIR spectra of OPF for particle size 75-125 µm before IL pretreatment, and after pretreatment with 1 and 3 M of IL. It was observed that the spectra generated for samples pretreated by both concentration of IL show new formation of peaks compared to the original spectra before the IL pretreatment. The band at range of 800-900 $cm^{-1}$ which characterizes the C-O-C stretching at β-1,4-glycosidic linkage is appeared after the pretreatment. The intensity of this range is very sensitive to the amount of crystalline versus amorphous structure of cellulose. The broadening of this band illustrates the amount of disordered structure (amorphous) higher [11]. The disorder arrangement of cellulose structure is expected caused by the changes in angle around of β-1,4-glycosidic linkage and hydrogen bonding form between the sugar hydroxyl group in cellulose and ion of IL which loosen the original packing and ordered arrangement of cellulose. Besides, the band at range 1000-1200 also resolved after IL pretreatment for both concentration which the band referred to functional groups of C-O-C and C-OH [12].

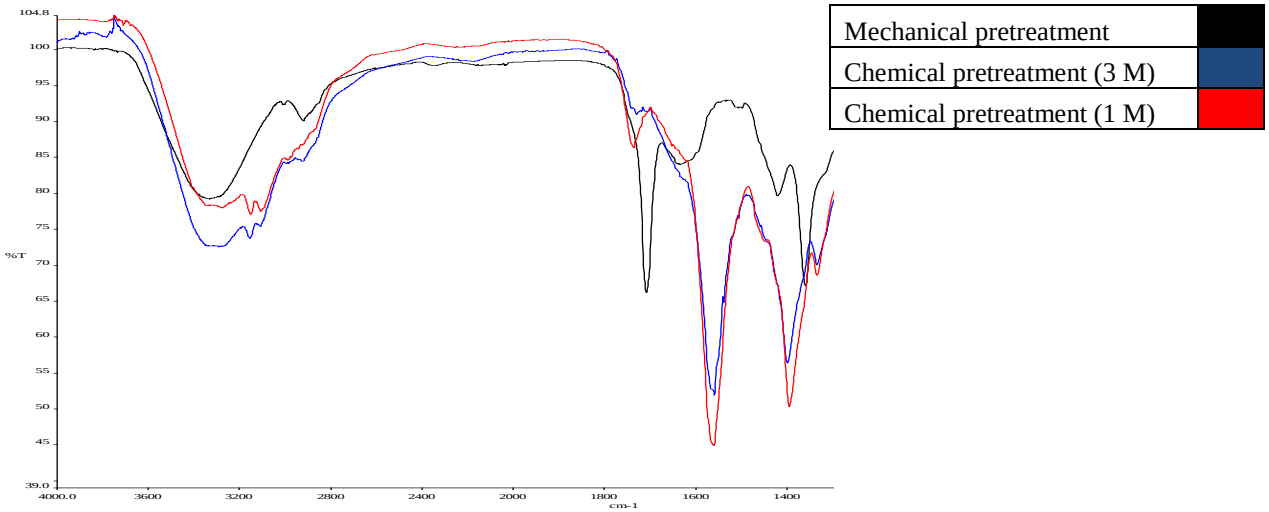



Figure 2. Comparison of FTIR spectra of OPF between before and after chemical pretreatment for size range 75-125 µm

Figure 2 also illustrated that after the mechanical pretreatment (before IL pretreatment), the sample shows the presence of cellulose groups at band around 1430 $cm^{-1}$ and hemicellulose at band near 1700 $cm^{-1}$. However, after the IL pretreatment for both 1M and 3M, it can be seen that the hemicellulose band of 1700 $cm^{-1}$ has decreased and shifted to the left. The weakening of peak at 1700 $cm^{-1}$ can be referred to the degradation of acetyl groups [12]. The peak at 1430 $cm^{-1}$ also was originally existed in spectra of untreated biomass. However after the treating with IL, the peak was totally disappeared. Sohrab and co-worker reported this band would be strong in crystalline cellulose

and weak in amorphous cellulose [2]. The disappearance of this band showing that by IL pretreatment, the crystalline structure of sample biomass is altered to be amorphous structure.

Furthermore, there was a new peak form within 1550 $cm^{-1}$ which relates to functional group exists in lignin. From the band formed, it can be said that by IL pretreatment, the dissolution was occurred and as a result the lignin bonding within the biomass structure was broken. Other difference characteristic which has been observed was at the band of O-H vibration, 3600-3100 $cm^{-1}$. The vibration band of the treated biomass with IL for both concentrations became sharper and lower in intensity. This is due to the scission of the intra-intermolecular of O-H bonding [13]. Furthermore, from the same figure of 3, the spectra of FTIR analysis between 1M and 3M concentration of IL were quietly similar and did not show any significant different.

## Conclusion

In conclusion, the particle size range of 75-125 µm is an optimum size to further pretreat with IL due to the characteristics of cellulose observed in FTIR spectra. The comparison between the cellulose structure of OPF between mechanical (before IL pretreatment) and chemical (after IL pretreatment) also has been studied. Based on the result, it shows that the chemical structure of cellulose was disrupted by formation of O-H bonding between the hydroxyl of cellulose and ion of IL during the dissolution time with IL. As a result, the cellulose network broken and less in crystalline structure. In bioethanol production from LB feedstock, the cellulose crystalline structure is a concern because it may affect the sugar yield during the enzymatic hydrolysis.

## Acknowledgement

The work is supported by the Fundamental Research Grant Scheme (FRGS) 600-RM1/FRGS 5/3 (32/2013) and Dana Kecemerlangan 600-RM1/DANA 5/3/RIF (745/2012) from the Ministry of Higher Learning Malaysia and Research Management Institute, Universiti Teknologi Malaysia, respectively. Appreciation is also given to the Faculty of Chemical Engineering, Universiti Teknologi Mara, Shah Alam.

## References

1. Fu D. and Mazza G. (2011). Aqueous ionic liquid pretreatment of straw. *Bioresour. Technol.* 102 (13): 7008–11.
2. Mood S. H., Golfeshan A. H., Tabatabaei M., Abbasalizadeh S., and Ardjmand M. Ardjmand (2013). Comparison of different ionic liquids pretreatment for barley straw enzymatic saccharification. *3 Biotech* 3 (5): 399–406.
3. Mosier N., Wyman C., Dale B., Elander R., Lee Y. Y., Holtzapple M., and Ladisch M. (2005). Features of promising technologies for pretreatment of lignocellulosic biomass. *Bioresour. Technol.* 96 (6): 673–86.
4. Tan H. T., Lee K. T., and Mohamed A. R.(2011). Pretreatment of lignocellulosic palm biomass using a solvent-ionic liquid [BMIM]Cl for glucose recovery: An optimisation study using response surface methodology. *Carbohydr. Polym.* 83 (4): 1862–1868.
5. Zhang Q., Zhang P., Pei Z. J., and Wang D. (2013). Relationships between cellulosic biomass particle size and enzymatic hydrolysis sugar yield: Analysis of inconsistent reports in the literature. *Renew. Energy* 60: 127–136.
6. Zhang H., Wu J., Zhang J., and He J. (2005). 1-Allyl-3-methylimidazolium Chloride Room Temperature Ionic Liquid: A New and Powerful Nonderivatizing Solvent for Cellulose. *Macromolecules* 38 (20): 8272–8277.
7. Li C., Knierim B., Manisseri C., Arora R., Scheller H. V., Auer M., Vogel K. P., Simmons B. A., and Singh S. (2010). Comparison of dilute acid and ionic liquid pretreatment of switchgrass: Biomass recalcitrance, delignification and enzymatic saccharification. *Bioresour. Technol.* 101 (13): 4900–6.
8. M. Mandels, L. Hontz, and J. Nystrom (1974). Enzymatic Hydrolysis of Waste Cellulose. *Biotechnology and Bioengineering*, 16: 1471–1493.
9. Moniruzzaman M., Ono T., Yusup S., Chowdhury S., and Bustam M. A. (2013). Improved biological delignification of wood biomass via Ionic liquids pretreatment: A one step process. *Journal of Energy Technologies and Policy* 3 (11): 144–152.
10. Cheng G., Varanasi P., Arora R., Stavila V., and Simmons B. A. (2012). Impact of Ionic Liquid Pretreatment Conditions on Cellulose. *J. Phys. Chem. B* 116: 10049−10054.

11. Proniewicz L. M., Paluszkiewicz C., Wesełucha-Birczyńska A., Majcherczyk H., Barański A., and Konieczna A. (2001). FT-IR and FT-Raman study of hydrothermally degradated cellulose. *J. Mol. Struct.* 596 (1–3): 163–169.
12. Lionetto F., Del Sole R., Cannoletta D., Vasapollo G., and Maffezzoli A. (2012). Monitoring Wood Degradation during Weathering by Cellulose Crystallinity. *Materials (Basel)*, 5 (12): 1910–1922.
13. Ciolacu D., Ciolacu F., and Popa V. I. (2011). Amorphous Cellulose – Structure And Characterization. *Cellulose Chemistry and Technology* 45 (1-2): 13–21.